Encyclopedia of
Complexity and Systems Science Series
Editor-in-Chief: Robert A. Meyers

SPRINGER
REFERENCE

Axel Hutt · Hermann Haken *Editors*

Synergetics

A Volume in the Encyclopedia of Complexity and Systems Science, Second Edition

Springer

Encyclopedia of Complexity and Systems Science Series

Editor-in-Chief

Robert A. Meyers

The Encyclopedia of Complexity and Systems Science Series of topical volumes provides an authoritative source for understanding and applying the concepts of complexity theory together with the tools and measures for analyzing complex systems in all fields of science and engineering. Many phenomena at all scales in science and engineering have the characteristics of complex systems and can be fully understood only through the transdisciplinary perspectives, theories, and tools of self-organization, synergetics, dynamical systems, turbulence, catastrophes, instabilities, nonlinearity, stochastic processes, chaos, neural networks, cellular automata, adaptive systems, genetic algorithms, and so on. Examples of near-term problems and major unknowns that can be approached through complexity and systems science include: the structure, history, and future of the universe; the biological basis of consciousness; the integration of genomics, proteomics, and bioinformatics as systems biology; human longevity limits; the limits of computing; sustainability of human societies and life on earth; predictability, dynamics, and extent of earthquakes, hurricanes, tsunamis, and other natural disasters; the dynamics of turbulent flows; lasers or fluids in physics; microprocessor design; macromolecular assembly in chemistry and biophysics; brain functions in cognitive neuroscience; climate change; ecosystem management; traffic management; and business cycles. All these seemingly diverse kinds of phenomena and structure formation have a number of important features and underlying structures in common. These deep structural similarities can be exploited to transfer analytical methods and understanding from one field to another. This unique work will extend the influence of complexity and system science to a much wider audience than has been possible to date.

More information about this series at https://link.springer.com/bookseries/15581

Axel Hutt • Hermann Haken
Editors

Synergetics

A Volume in the Encyclopedia of Complexity and Systems Science, Second Edition

With 223 Figures and 7 Tables

Springer

Editors
Axel Hutt
INRIA Grand Est
Strasbourg, France

Hermann Haken
Institut für Theoretische Physik 1
Universität Stuttgart
Stuttgart, Germany

ISBN 978-1-0716-0420-5 ISBN 978-1-0716-0421-2 (eBook)
ISBN 978-1-0716-0422-9 (print and electronic bundle)
https://doi.org/10.1007/978-1-0716-0421-2

Foreword

Almost all processes in our universe and even the whole can be regarded as complex systems. Because there are manifold crucial problems with such systems, this century is often called the century of complex systems science. It is important to emphasize that this discipline has already a rich history. It started in 1665 when Christiaan Huygens discovered synchronization of two pendulum clocks, what he called sympathy. Huygens understood that the key ingredient of this phenomenon is that both clocks are (weakly) coupled.

One of the most influential steps in the following evolution of this science has been the concept of *Synergetics* introduced about 50 years ago by Hermann Haken and substantially further developed by him and his school and later by many followers. He originally integrated various fields and created a new very successful perspective to study processes of self-organization. Important theoretical as well as applied advances of this new discipline were published in the Springer Series Synergetics founded and edited by Hermann Haken.

The time is now ripe to present an overview of recent advances as well as perspectives of Synergetics. Hermann Haken and Axel Hutt brought together 20 contributions covering basic aspects of theoretical studies by including basic principles and stochastic descriptions and different fields of applications, such as quantum optics, fluid dynamics, neuroscience, as well as socio-economics. They clearly demonstrate that this discipline is strongly evolving and is a fundamental part of complex systems science.

It is my hope that this book will provide valuable information and will induce various inspirations for further creative work in this discipline and various applications. I strongly recommend it to readers from physics and mathematics as well as from all scientific disciplines where complex systems are studied.

Berlin and Potsdam — Jürgen Kurths
June 2020

Series Preface

The Encyclopedia of Complexity and System Science Series is a multivolume authoritative source for understanding and applying the basic tenets of complexity and systems theory as well as the tools and measures for analyzing complex systems in science, engineering, and many areas of social, financial, and business interactions. It is written for an audience of advanced university undergraduate and graduate students, professors, and professionals in a wide range of fields who must manage complexity on scales ranging from the atomic and molecular to the societal and global.

Complex systems are systems that comprise many interacting parts with the ability to generate a new quality of collective behavior through selforganization, e.g., the spontaneous formation of temporal, spatial, or functional structures. They are therefore adaptive as they evolve and may contain self-driving feedback loops. Thus, complex systems are much more than a sum of their parts. Complex systems are often characterized as having extreme sensitivity to initial conditions as well as emergent behavior that are not readily predictable or even completely deterministic. The conclusion is that a reductionist (bottom-up) approach is often an incomplete description of a phenomenon.

This recognition that the collective behavior of the whole system cannot be simply inferred from the understanding of the behavior of the individual components has led to many new concepts and sophisticated mathematical and modeling tools for application to many scientific, engineering, and societal issues that can be adequately described only in terms of complexity and complex systems.

Examples of Grand Scientific Challenges which can be approached through complexity and systems science include: the structure, history, and future of the universe; the biological basis of consciousness; the true complexity of the genetic makeup and molecular functioning of humans (genetics and epigenetics) and other life forms; human longevity limits; unification of the laws of physics; the dynamics and extent of climate change and the effects of climate change; extending the boundaries of and understanding the theoretical limits of computing; sustainability of life on the earth; workings of the interior of the earth; predictability, dynamics, and extent of earthquakes, tsunamis, and other natural disasters; dynamics of turbulent flows and the motion of granular materials; the structure of atoms as expressed in the Standard Model and the formulation of the Standard Model and gravity into a Unified Theory; the structure of water; control of global infectious diseases; and also evolution and quantification of (ultimately) human cooperative behavior in politics, economics, business systems,

and social interactions. In fact, most of these issues have identified nonlinearities and are beginning to be addressed with nonlinear techniques, e.g., human longevity limits, the Standard Model, climate change, earthquake prediction, workings of the earth's interior, natural disaster prediction, etc.

The individual complex systems mathematical and modeling tools and scientific and engineering applications that comprised the *Encyclopedia of Complexity and Systems Science* are being completely updated and the majority will be published as individual books edited by experts in each field who are eminent university faculty members.

The topics are as follows:

Agent Based Modeling and Simulation
Applications of Physics and Mathematics to Social Science
Cellular Automata, Mathematical Basis of
Chaos and Complexity in Astrophysics
Climate Modeling, Global Warming, and Weather Prediction
Complex Networks and Graph Theory
Complexity and Nonlinearity in Autonomous Robotics
Complexity in Computational Chemistry
Complexity in Earthquakes, Tsunamis, and Volcanoes, and Forecasting and Early Warning of Their Hazards
Computational and Theoretical Nanoscience
Control and Dynamical Systems
Data Mining and Knowledge Discovery
Ecological Complexity
Ergodic Theory
Finance and Econometrics
Fractals and Multifractals
Game Theory
Granular Computing
Intelligent Systems
Nonlinear Ordinary Differential Equations and Dynamical Systems
Nonlinear Partial Differential Equations
Percolation
Perturbation Theory
Probability and Statistics in Complex Systems
Quantum Information Science
Social Network Analysis
Soft Computing
Solitons
Statistical and Nonlinear Physics
Synergetics
System Dynamics
Systems Biology

Each entry in each of the Series books was selected and peer reviews organized by one of our university-based book Editors with advice and consultation provided by our eminent Board Members and the Editor-in-Chief.

This level of coordination assures that the reader can have a level of confidence in the relevance and accuracy of the information far exceeding than that generally found on the World Wide Web. Accessibility is also a priority and for this reason each entry includes a glossary of important terms and a concise definition of the subject. In addition, we are pleased that the mathematical portions of our Encyclopedia have been selected by Math Reviews for indexing in MathSciNet. Also, ACM, the world's largest educational and scientific computing society, recognized our *Computational Complexity: Theory, Techniques, and Applications* book, which contains content taken exclusively from the *Encyclopedia of Complexity and Systems Science*, with an award as one of the notable Computer Science publications. Clearly, we have achieved prominence at a level beyond our expectations, but consistent with the high quality of the content!

Palm Desert, CA, USA
June 2020

Robert A. Meyers
Editor-in-Chief

Volume Preface

The laws of physics are fundamental to natural sciences and describe the system dynamics on multiple scales. In spite of their validity, descriptions of complex systems are difficult based just on the fundamental laws and different concepts of description are mandatory. Such concepts provide more abstract descriptions of natural phenomena and these concepts in fact reject fundamental mechanisms. For instance, quantum field theory description of the laser (Haken 1984) provides deep insights into dynamical features observed experimentally and also demonstrates that the laser exhibits self-organized behavior similar to fluid or biological systems (Haken 1983). This self-organization is a descriptive concept that rejects the system's underlying order mechanism. The similarity of the laser dynamics to weather chaos (Haken 1975) further demonstrates the common underlying mechanism of chaos in apparently different complex systems. Synergetics is the discipline that allows us to describe these underlying mechanisms in diverse natural systems.

Phase transitions are another macroscopic feature in nature and diverse natural systems may exhibit identical dynamics close to their stability threshold.

Examples are second-order phase transitions in lasers, fluids, animal populations, or the brain, whose dynamics obey the Ginzburg-Landau equations known from solid state physics. A more microscopic look at such phase transitions reveals a hierarchy of modes, e.g., on fast and slow time scales. Mathematical techniques describe such mode hierarchies in an abstract or even impenetrable way, whereas from a physics point of view some modes enslave other modes, i.e., force them to follow their own dynamics (slaving principle). This physical interpretation reformulates elegantly a purely mathematical description into a common sense notion. This reduction of descriptive complexity to an intuitive notion of slaving is a very powerful element in Synergetics, since it permits to translate underlying mechanisms in one system and research domain to a broad range of other scientific domains. The Introduction and Basic Concept chapters illustrate well the key ideas and their vast range of applications.

The idea of the book came up many years ago and was originally intended to collect scientific contributions of Hermann Haken's long-standing collaboration partners in the field of Synergetics. Then Axel Hutt came on board and proposed to combine these chapters with new, more recent work demonstrating that Synergetics is still practiced although it is not called like this. This

collaboration of H. Haken and A. Hutt has led to the current chapter collection providing a broad overview over applications of Synergetics. It is a solid collection of topics valuable for graduate students and researchers in complex systems theory and applied mathematics. The first chapters consider chaotic and turbulent spatio-temporal dynamics in physical systems, followed by more theoretical studies on quantum chaos and stochastic dynamics. Today, Synergetics has evolved primarily towards the description of non-physical systems, such as the brain, medical human diseases, and human behavior as shown in subsequent chapters. Finally, the last chapters focus on human cities, financial markets, and global industrial dynamics.

Strasbourg, France
Stuttgart, Germany
June 2020

Axel Hutt
Hermann Haken
Editors

Bibliography

Haken H (1984) Laser theory. Springer
Haken H (1983) Synergetics. Springer
Haken H (1975) Phys Lett A 53:77

Contents

Synergetics: An Introduction 1
Axel Hutt

Synergetics: Basic Concepts 5
Hermann Haken

Laser Dynamics and Delayed Feedback 31
Kathy Lüdge and Benjamin Lingnau

Fluid Dynamics, Pattern Formation 49
Michael Bestehorn

Patterns and Interfaces in Dissipative Dynamics 85
L. M. Pismen

Fluid Dynamics: Turbulence 107
Rudolf Friedrich, Joachim Peinke, and Oliver Kamps

Recent Advances in Quantum Chaos of Generic Systems 133
Marko Robnik

Linear and Nonlinear Fokker-Planck Equations 149
Till D. Frank

Additive Noise Tunes the Self-Organization in Complex Systems 183
Axel Hutt and Jérémie Lefebvre

Chaotic Dynamics in Neural Systems 197
Krishna Pusuluri, Huiwen Ju, and Andrey Shilnikov

Shilnikov Chaos in Epilepsy 211
Christian Uhl and Bastian Seifert

Phase Synchronization in Neural Systems 221
Andreas Daffertshofer and Bastian Pietras

Brain Pacemaker 235
Peter A. Tass, Christian Hauptmann, and Oleksandr V. Popovych

Self-Organization in Clinical Psychology 263
Günter Schiepek and Volker Perlitz

Movement Coordination 287
Armin Fuchs and J. A. Scott Kelso

Determinisms of Behavior and Synergetics 309
Till D. Frank

Intentionality: Steps Towards Naturalization on the Basis of Complex Dynamical Systems 343
Wolfgang Tschacher

Self-Organization and the City 357
Juval Portugali

Financial Market Dynamics: A Synergetic Perspective 405
Lisa Borland

Industrial Society's Natural Future 421
Hans G. Danielmeyer and Thomas Martinetz

Index 443

About the Editor-in-Chief

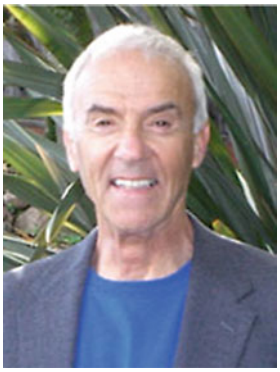

Robert A. Meyers
President: RAMTECH Limited
Manger, Chemical Process Technology, TRW Inc.
Post doctoral Fellow: California Institute of Technology
Ph.D. Chemistry, University of California at Los Angeles
B.A. Chemistry, California State University, San Diego

Biography

Dr. Meyers has worked with more than 20 Nobel laureates during his career and is the originator and serves as Editor-in-Chief of both the Springer Nature *Encyclopedia of Sustainability Science and Technology* and the related and supportive Springer Nature *Encyclopedia of Complexity and Systems Science*.

Education

Postdoctoral Fellow: California Institute of Technology
Ph.D. in Organic Chemistry, University of California at Los Angeles
B.A. Chemistry with minor in Mathematics, California State University, San Diego

Dr. Meyers holds more than 20 patents and is the author or Editor-in-Chief of 12 technical books including the *Handbook of Chemical Production Processes*, *Handbook of Synfuels Technology*, and *Handbook of Petroleum Refining Processes* now in 4th Edition, and the *Handbook of Petrochemical Production Processes*, now in its second edition, (McGraw-Hill) and the *Handbook of Energy Technology and Economics*, published by John Wiley & Sons; *Coal Structure*, published by Academic Press; and *Coal Desulfurization* as well as the *Coal Handbook* published by Marcel Dekker. He served as Chairman of the Advisory Board for *A Guide to Nuclear Power Technology*, published by John Wiley & Sons, which won the Association of American Publishers Award as the best book in technology and engineering.

About the Volume Editors

Axel Hutt is Directeur de Recherche at INRIA, France, and his work focuses on topics in mathematical and computational neuroscience. He received his Ph.D. in Theoretical Physics from the University of Stuttgart (2000) and had received the Schloessmann Fellowship of the Max Planck Society for his Ph.D. thesis. Axel gained his habilitation (HDR) at the University of Nice – Sophia Antipolis (2012) and was awarded an ERC Starting Grant on Mathematical Modeling of Anaesthesia in the same year. His current research interest is data assimilation and control of neural systems in the clinical context.

Hermann Haken was professor for Theoretical Physics at the University of Stuttgart from 1960–1995. He is acknowledged as one of the fathers of laser theory and as the founder of the discipline Synergetics.

Contributors

Michael Bestehorn Brandenburg University of Technology, Cottbus, Germany

Lisa Borland Cerebellum Capital, San Francisco, CA, USA

Andreas Daffertshofer Faculty of Behavioural and Movement Sciences, Amsterdam Movement Sciences and Institute for Brain and Behaviour Amsterdam, Vrije Universiteit Amsterdam, Amsterdam, The Netherlands

Hans G. Danielmeyer Institut für Neuro- und Bioinformatik, Universität zu Lübeck, Lübeck, Germany

Till D. Frank Department of Psychology and Department of Physics, University of Connecticut, Storrs, CT, USA

Rudolf Friedrich Institute for Theoretical Physics, University of Münster, Münster, Germany

Armin Fuchs Human Brain and Behavior Laboratory, Center for Complex Systems and Brain Sciences, Florida Atlantic University, Boca Raton, FL, USA

Department of Physics, Florida Atlantic University, Boca Raton, FL, USA

Hermann Haken Institut für Theoretische Physik, Universität Stuttgart, Stuttgart, Germany

Christian Hauptmann Institute of Neuroscience and Medicine – Neuromodulation (INM-7), Jülich Research Center, Jülich, Germany

Axel Hutt Deutscher Wetterdienst, Offenbach am Main, Germany

Huiwen Ju Neuroscience Institute, Georgia State University, Atlanta, GA, USA

Oliver Kamps Center for Nonlinear Science, Universität of Münster, Münster, Germany

J. A. Scott Kelso Human Brain and Behavior Laboratory, Center for Complex Systems and Brain Sciences, Florida Atlantic University, Boca Raton, FL, USA

Intelligent Systems Research Centre, School of Computing and Intelligent Systems, Ulster University, Derry Londonderry, Northern Ireland, UK

Jérémie Lefebvre Krembil Research Institute, Toronto, ON, Canada

Benjamin Lingnau Department of Physics, University College Cork, Cork, Ireland

Kathy Lüdge Institut für Theoretische Physik, Technische Universität Berlin, Berlin, Germany

Thomas Martinetz Institut für Neuro- und Bioinformatik, Universität zu Lübeck, Lübeck, Germany

Joachim Peinke Institute of Physics, Carl-von-Ossietzky University Oldenburg, Oldenburg, Germany

Volker Perlitz Klinik für Psychosomatik, Universitätsklinikum der RWTH Aachen, Aachen, Germany

Bastian Pietras Institute of Mathematics, Technische Universität Berlin and Bernstein Center for Computational Neuroscience Berlin, Berlin, Germany

L. M. Pismen Department of Chemical Engineering and Minerva Center for Nonlinear Physics of Complex Systems, Technion – Israel Institute of Technology, Haifa, Israel

Oleksandr V. Popovych Institute of Neuroscience and Medicine – Neuromodulation (INM-7), Jülich Research Center, Jülich, Germany

Juval Portugali ESLab (Environmental Simulation Lab), Department of Geography and the Human Environment, Tel Aviv University, Tel Aviv, Israel

Krishna Pusuluri Neuroscience Institute, Georgia State University, Atlanta, GA, USA

Marko Robnik CAMTP-Center for Applied Mathematics and Theoretical Physics, University of Maribor, Maribor, Slovenia

Günter Schiepek Institute of Synergetics and Psychotherapy Research, Paracelsus Medical University, Salzburg, Austria

Bastian Seifert Center for Signal Analysis of Complex Systems (CCS), Ansbach University of Applied Sciences, Ansbach, Germany

Andrey Shilnikov Neuroscience Institute, and Department of Mathematics and Statistics, Georgia State University, Atlanta, GA, USA

Peter A. Tass Institute of Neuroscience and Medicine – Neuromodulation (INM-7), Jülich Research Center, Jülich, Germany

Department of Neurosurgery, Stanford University, Stanford, CA, USA

Department of Neuromodulation, University of Cologne, Cologne, Germany

Wolfgang Tschacher University Hospital of Psychiatry and Psychotherapy, University of Bern, Bern, Switzerland

Freiburg Institute for Advanced Studies (FRIAS), University of Freiburg, Freiburg, Germany

Christian Uhl Center for Signal Analysis of Complex Systems (CCS), Ansbach University of Applied Sciences, Ansbach, Germany

Synergetics: An Introduction

Axel Hutt
Deutscher Wetterdienst, Offenbach am Main, Germany

How do complex systems organize? What are the underlying mechanisms in such systems that let emerge new phenomena that cannot be explained by isolated subsystems? Synergetics (after the Greek expression *synergeon*: science of cooperation) is an interdisciplinary research field that provides answers to these essential questions. The discipline Synergetics was founded by H. Haken about 50 years ago. Today, it covers a huge range of research fields ranging from natural sciences through medical sciences to economy and social sciences.

Complex systems are heterogenous and hierarchical in the sense that they are built up of interacting subsystems that are built up of subsystems themselves and so on. The various subsystems may be of different nature, e.g., may evolve on different spatial or temporal scales or may represent physical or more abstract entities. The interaction of subsystems may lead to emergent self-organization phenomena that cannot be explained by separated subsystems. An obvious example for a complex system is the brain that is built up of interacting brain areas, such as visual or motor areas, which in turn are built up of nerve cells and connecting fibers, which in turn exhibit complex substructures of interacting molecules. Synergetics asks about the general principles of self-organization of such complex systems, irrespective of the nature of the individual entities, cf. chapter ▶ "Synergetics: Basic Concepts."

To approach this goal, it is advantageous to focus on such situations where the macroscopic system state changes qualitatively. Indeed, it is an outstanding fact that few fundamental concepts allow us to cover a great variety of self-organization phenomena from a unifying point of view. Examples for such concepts are stability, instability, control parameters, order parameters, the slaving principle, and the circular causality.

Today Synergetics is a meeting place between bifurcation theory, the theory of stochastic processes, phase transition theory, and synchronization. In physics, it has become possible to start from first principles. For instance, in quantum optics, the coherence properties of laser light were derived in every detail based on Heisenberg equations of motion for operators. In the present book, K. Lüdge and B. Lingnau show their recent experimental and theoretical results on quantum dot and quantum well lasers in the presence of delayed feedback in the chapter ▶ "Laser Dynamics and Delayed Feedback." The authors reveal the bifurcation criteria for emerging chaotic dynamics. Another example is fluid dynamics where an energetically excited fluid may run through a hierarchy of spatio-temporal patterns with increasing degree of excitation. At comparatively low excitation levels, well-defined patterns evolve. While regular patterns stand in the foreground of the chapter ▶ "Fluid Dynamics, Pattern Formation" by M. Bestehorn, the chapter by L. Pismen ▶ "Patterns and Interfaces in Dissipative Dynamics" emphasizes defects and interfaces. At higher excitation levels, turbulence comes into play, cf. the chapter ▶ "Fluid Dynamics: Turbulence" of R. Friedrich and J. Peinke. The authors provide a broad overview of the corresponding research field while discussing both the deterministic chaotic and stochastic dynamics of turbulent systems.

In general, chaotic and stochastic processes are two descriptions to formulate mathematically seemingly rather irregular system behavior. Their relation and even coexistence is demonstrated nicely in chapter ▶ "Recent Advances in Quantum Chaos of Generic Systems" by M. Robnik. The author reviews the fundamental concepts of quantum chaos in Hamiltonian systems. In general, Synergetics applies classical mathematical tools to describe stochastic processes such as generalized Langevin equations, the FokkerPlanck equation and the density matrix equation. In the chapter ▶ "Linear and Nonlinear Fokker-Planck Equations," the author T. Frank

A. Hutt, H. Haken (eds.), *Synergetics*,
https://doi.org/10.1007/978-1-0716-0421-2_534

Originally published in
R. A. Meyers (ed.), *Encyclopedia of Complexity and Systems Science*, © Springer Science+Business Media LLC 2020
https://doi.org/10.1007/978-3-642-27737-5_534-2

follows up the method of the Fokker-Planck equation and provides a deep insight into self-organizing stochastic systems whose probability density obeys nonlinear Fokker-Planck equations. Stochastic processes may also induce phase transitions as demonstrated by A. Hutt and J. Lefebvre in chapter ▶ "Additive Noise Tunes the Self-Organization in Complex Systems." Here, the authors apply both a path-wise stochastic analysis and the probability-based Fokker-Planck analysis.

Although, historically, Synergetics had started by studies motivated by phenomena observed in physical systems, its concepts have been applied to diverse phenomena in other research fields. Bifurcation theory represents a valuable concept to describe chaotic dynamics in natural systems. For instance, neural information processing is based on brain cells and their network interactions. Each cell exhibits diverse dynamic operation modes, such as regular spiking, bursting, or chaotic behavior. In chapter ▶ "Chaotic Dynamics in Neural Systems," A. Pusuluri, H. Ju, and A. Shilnikov show detailed bifurcation analysis of various high-dimensional phase space models of brain cells. Brain networks may inherit the single cells behavior or show new emergent self-organized dynamic patterns that in turn again may exhibit chaotic dynamics. Macroscopic biological brain networks can be observed by several experimental techniques, such as electroencephalography (EEG). The authors C. Uhl and B. Seifert demonstrate in chapter ▶ "Shilnikov Chaos in Epilepsy" that experimental EEG may obey the dynamics of a chaotic attractor.

The concept of order parameter is a major feature in Synergetics. It represents the quantity that allows us to describe the essential dynamics of a system. This order parameter may be an amplitude variable or a synchronization measure. It is well established that the brain encodes and decodes information by synchronization and A. Daffertshofer and B. Pietras consider a phase synchronization measure as order parameter in brain models in chapter ▶ "Phase Synchronization in Neural Systems". They describe how such a measure provides deeper insight into the underlying brain mechanisms. Since synchronization represents a primary mechanism of neural information coding, P. Tass, G. Hauptmann, and C. Popovych consider external stimulation protocols in clinical patients to tune the synchronization between brain cells. Their chapter ▶ "Brain Pacemaker" explains that highly synchronized brain states may reflect a pathological state in certain brain areas and the authors demonstrate how external electrical stimulation may de-synchronize the brain state and thus alleviate the health situation of patients.

Going beyond the description of specific mesoscopic complex biological systems, such as brain cells or the brain signal EEG in the examples given above, Synergetics concepts have been applied to more macrosopic systems. As a first step, one may relate mesoscopic dynamics to macroscopic observations. For instance, self-organization in the brain may be observed as mental states, cognitive abilities, or behavior. Clinical psychology knows the concept of *Gestalt* that represents a certain pattern in perception, behavior, or social interactions. The chapter ▶ "Self-Organization in Clinical Psychology" by G. Schiepek and V. Perlitz bring together Gestalt theory and the Synergetics concepts of self-organized patterns. The chapter shows nicely how methods of mathematical analysis enter more and more the field of psychiatry and how this allows doctors to monitor the mental and behavioral state of patients.

Another macroscopic self-organized pattern observed in humans and animals is ▶ "Movement Coordination" as pointed out by A. Fuchs and S. Kelso. They can show how a large class of transitions in movement coordination can be described by the Synergetics concept of order parameter equations although humans and animals are highly complex systems.

More general, human and animal behavior consists of sequences of actions that are the results of free choices as to what kind of behavior the subject would like to perform next. These sequences are the result of internal, e.g., neurobiological, conditions and external circumstances. Since these conditions and circumstances in turn are the consequences of prior actions, behavior, and experiences, behavior is determined by laws. The chapter ▶ "Determinisms of Behavior and Synergetics" by T. Frank presents Synergetics as a mathematical and conceptual framework that

allows us to describe switches between actions and behavior in mathematical terms.

The latter studies consider quantifiable observations that can be modeled explicitly, such as index variables of behavior in clinical psychology, movement frequency, amplitude, and phase in movement coordination or determined behavioral motor actions. The situation is even more complex in cognition, where thought and behavioral patterns or intentions are hardly quantifiable. Nevertheless, W. Tschacher has been undertaking this challenge and shows in chapter ▶ "Intentionality: Steps Towards Naturalization on the Basis of Complex Dynamical Systems" how mental processes can be linked to material processes. Here, the author tackles the long-standing problem of intentionality and relates it to circular causality and self-organizing pattern formation which can be formalized by concepts of Synergetics.

Extending the view from the self-organization in single individuals to self-organization of a population of individuals, it is obvious that the same Synergetics concepts can be applied due to the hierarchical structure of complex systems. From this point of view, J. Portugali takes a closer look at cities. In the chapter ▶ "Self-Organization and the City," he discusses the interrelation between human individuals and their ability to form social groups as a process of self-organization. Another complex system built up of several different human populations is the financial market, cf. the chapter ▶ "Financial Market Dynamics: A Synergetic Perspective" by L. Borland. This system is highly complex due to the heterogeneity of human populations, their underlying market psychology, and their diverse financial interests. The traders represent the interacting subsystems, their actions, feed back into the financial market, and macroeconomic phenomena may contribute to the dynamics as well. The order parameters in such systems are traded quantities, such as the price of shares. The author relates the market dynamics to dynamics well-known from other Synergetic systems. At last, the even more global view of the world's ▶ "Industrial Society's Natural Future" presented by H.G. Danielmayer and T. Martinetz considers the subsystems industry, economy, human nature and finance, and their interactions. The authors follow the concept of Synergetics and provide a unified description of these four, until now, separated academic disciplines. They undergird the work's prediction by large datasets and hence, once again, demonstrate the power of Synergetics as discipline.

Synergetics: Basic Concepts

Hermann Haken
Institut für Theoretische Physik, Universität Stuttgart, Stuttgart, Germany

Article Outline

Glossary
The Role of Synergetics in Science
The Laser Paradigm
The Hierarchical Structure of Synergetics
Basic Equations
Method of Solution
A Remark on the Method of Solution of Evolution Eq. (1)
Quantum Theoretical Formulation
Quantum-Classical Correspondence
Regular Spatial and Spatio-Temporal Patterns
Infinite Boundaries
Theory, Representation Theory, Finite Boundaries
A Further Mathematical Tool: Shannon Information and the Maximum (Information) Entropy Principle
Phenomenological Synergetics
Semantic Synergetics
Some Selected Examples
History and Relations to Other Fields
Future Directions
Bibliography

Glossary

Attractor Region in the state vector space ("q-space") to which all neighboring states are attracted in the course of time.

Control parameter One or a set of (mostly externally) fixed parameters in the evolution equations.

Dynamical System System whose state vector changes in the course of time deterministically.

Evolution equations Determine the temporal evolution of the state vector. May be deterministic, stochastic or both.

Fixed point, stable Point in q space to which all neighboring trajectories converge in course of time.

Fluctuating forces Stochastic (random) forces appearing in evolution equations.

Fokker Planck equation Evolution equation for probability density function, based on drift and diffusion.

Generalized Langevin equation General evolution equations that contain both a deterministic and a stochastic part ("fluctuating forces").

Group Set of elements with specific multiplication rules (axioms).

Hamilton operator Classical Hamilton function, in which variables, e. g. position x and momentum p, are replaced by quantum mechanical operators.

Heisenberg picture in quantum mechanics The state vector is time-independent, while the operators are time-dependent and determined by Heisenberg equations of motion.

Instability Loss of stability.

Langevin equation Originally: evolution equation for velocity of a Brownian particle subject to damping and fluctuating force.

Limit cycle, stable A closed trajectory to which all neighboring trajectories converge.

Normal form Especially simple polynomial expression that still captures the essential features, e. g. of the right hand side of deterministic evolution equations.

Order parameters Collective variables that determine the macroscopic behavior of systems.

Pattern A pattern is essentially an arrangement. It is characterized by the order of the elements of which it is made rather than by the intrinsic nature of these elements (Norbert Wiener).

Probability distribution function Function that determines the probability of a random variable r to have fixed value $r = r_0$.

Quantum classical correspondence Establishes relation between quantum mechanical density

A. Hutt, H. Haken (eds.), *Synergetics*,
https://doi.org/10.1007/978-1-0716-0421-2_533

Originally published in
R. A. Meyers (ed.), *Encyclopedia of Complexity and Systems Science*, © Springer-Verlag 2009
https://doi.org/10.1007/978-3-642-27737-5_533

matrix and classical quasi-probability distribution.

Schrödinger picture of quantum mechanics In it operators are time-independent, while the wave-function ("state vector") is time-dependent and determined by the Schrödinger equation.

Self-organization Formation of spatio-temporal patterns (structures) and/or performance of functions without an "ordering hand".

Slaving principle A general theorem that allows the reduction of the variables of a system to order parameters (close to instability).

Spatial coordinate (vector x) In one, two or three dimensions.

$$\Delta \text{Laplace operator} (\text{in } 1, 2 \text{ or } 3 \text{ dimensions}).$$

$$\nabla \text{Vector} \left(\frac{\mathrm{d}}{\mathrm{d}x_1}, \frac{\mathrm{d}}{\mathrm{d}x_2}, \frac{\mathrm{d}}{\mathrm{d}x_3} \right) \text{ in } 1, 2 \text{ or } 3 \text{ dimensions}.$$

Spectrum Set of eigenvalues belonging to linear stability equations with boundary conditions.

Stability of a system System returns after a (small) perturbation of its state vector into original state.

State vector Set of time- or time-independent variables that characterize the state of a system.

Symmetry Invariance of a system against specific transformations (e. g. mirror symmetry).

Synergetics Science of cooperation.

Trajectory Smooth curve q(t) of solution of evolution equation in q-space.

The Role of Synergetics in Science

In science, we may essentially distinguish between two trends:

1. The accumulation of knowledge
2. Information reduction in the sense of finding general principles, common features.

In physics, such unifying approaches are well known: the unification of magnetism, electricity and, later on, weak and other interactions leading eventually to a unified field theory. General relativity unifies concepts of space, time and gravitation. While these unifications take place at a fundamental level, one may ask whether it is worthwhile to look also for unifications at say more macroscopic or phenomenological levels. One example is thermodynamics, another the theory of phase transitions of systems in thermal equilibrium by means of the renormalization group approach, or the concept of fractals, etc.

The main goal of Synergetics is the search for unifying principles for systems that are composed of many individual parts or components, and that may show the phenomenon of self-organization, i.e. the spontaneous formation of spatial, temporal, spatial-temporal or functional structures. The systems under discussion are, in the widest sense of the word, open physical systems whose states are maintained by an in- and outflux of energy, matter and /or information. A typical and well known example is that of a fluid in a pan that is uniformly heated from below. When the temperature difference between the lower and upper surface exceeds a critical value, the formerly homogeneous fluid develops roll or hexagonal patterns in which the fluid moves in a specific manner (Fig. 1).

As it turned out, the general principles originally elaborated in physics, can also be applied to many other systems, such as in biology, economy, ecology, sociology, management theory, psychology etc. In spite of the great variety of the

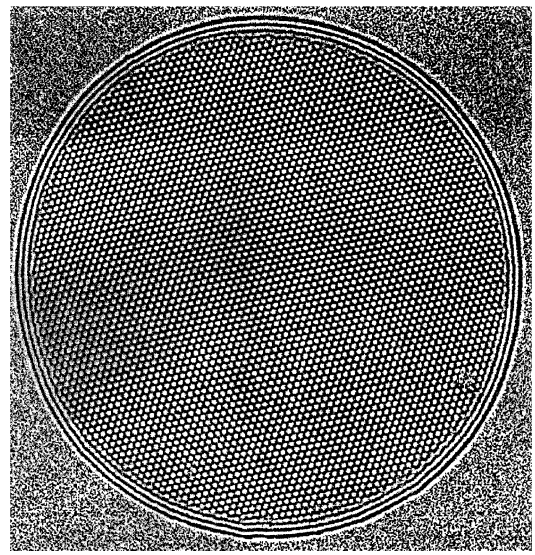

Synergetics: Basic Concepts, Fig. 1 Hexagonal pattern of a fluid (liquid helium) uniformly heated from below (Bodenschatz et al. 2000)

individual systems with their components quite different in nature, such principles apply to large classes of phenomena. This is achieved by restricting the study to situations where the systems undergo qualitative changes at macroscopic scales. Here macroscopic means "with time and length scales large compared to those of the individual components".

This leads to the definition of Synergetics as given in the preamble of the Springer Series in Synergetics: "An ever increasing number of scientific disciplines deal with complex systems. These are systems that are composed of many parts which interact with one another in a more or less complicated manner. One of the most striking features of many such systems is their ability to spontaneously form spatial or temporal structures. A great variety of these structures are found, in both the inanimate and the living world. In the inanimate world of physics and chemistry, examples include the growth of crystals, coherent oscillations of laser light, and the spiral structures formed in fluids and chemical reactions. In biology we encounter the growth of plants and animals (morphogenesis) and the evolution of species. In medicine we observe, for instance, the electromagnetic activity of the brain with its pronounced spatio-temporal structures. Psychology deals with characteristic features of human behavior ranging from simple pattern recognition tasks to complex patterns of social behavior. Examples from sociology include the formation of public opinion and cooperation or competition between social groups."

In recent decades, it has become increasingly evident that all these seemingly quite different kinds of structure formation have a number of important features in common. The task of studying analogies as well as differences between structure formation in these different fields has proved to be an ambitious but highly rewarding endeavor. The Springer Series in Synergetics provides a forum for interdisciplinary research and discussions on this fascinating new scientific challenge. It deals with both experimental and theoretical aspects. The scientific community and the interested layman are becoming ever more conscious of concepts such as self-organization, instabilities, deterministic chaos, nonlinearity, dynamical systems, stochastic processes, and complexity. All of these concepts are facets of a field that tackles complex systems, namely Synergetics.

The Laser Paradigm

This example elucidates central concepts used in Synergetics in a qualitative fashion. An example for the laser device (an acronym for light amplification by stimulated emission of radiation, originally called optical maser (Schawlow and Townes 1958)) is the gas laser in which gas atoms are enclosed in a tube at the end-faces of which mirrors are mounted. The mirrors serve the purpose of reflecting light running in axial direction sufficiently often so that the corresponding light wave stays for an extended period in this device and can interact intensely with the atoms. The atoms are excited from the outside, e. g. by a pump light source. After having been excited, each atom can spontaneously emit a light wave track. In the usual case of a *lamp*, these wave tracks are emitted independently of each other and the amplitudes are Gaussian distributed. When the pump intensity is increased beyond a critical value, the present state gives way to a single wave with *stable amplitude* on which small *amplitude fluctuations* and *phase diffusion* are superimposed (Haken 1964). The pump intensity serves as *control parameter.* At its critical value, the old state becomes *unstable.* The emerging coherent wave acts as *order parameter* that via stimulated emission forces the electrons of the gas molecules to emit light waves in a coherent fashion. This action of the order parameter on the individual parts of the system is called *slaving principle.* If the pump power is increased further, more instabilities can appear, and a variety of temporal but also spatio-temporal patterns of light waves may appear, such as laser light chaos (Haken 1975a) or ultrashort laser pulses. The first laser threshold shows the typical features of a phase transition of a system in thermal equilibrium, namely critical slowing down, critical fluctuations and symmetry breaking (DeGiorgio and

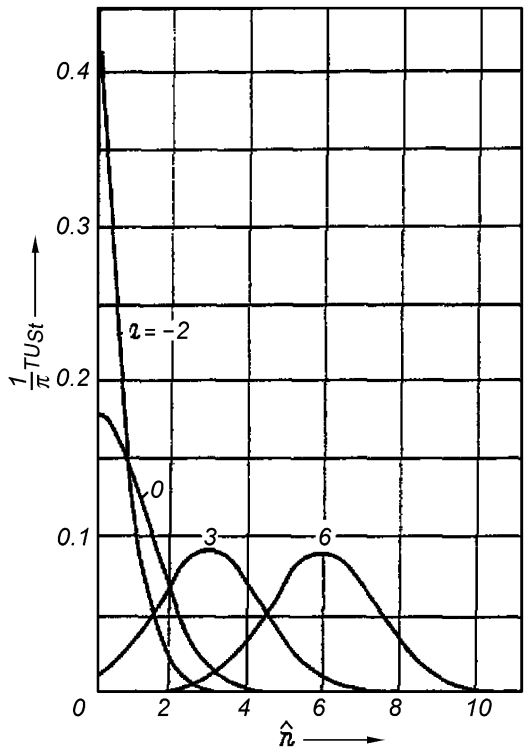

Synergetics: Basic Concepts, Fig. 2 The stationary distribution function of the laser light intensity as a function of the normalized intensity $\hat{n}$. The individual *curves* refer to different normalized pump power values *a*, where $a < 0$ below threshold, $a = 0$ at threshold, $a > 0$ above threshold. (After Risken 1965)

Scully 1970; Graham and Haken 1968; Haken 1964, 1985; Sargent et al. 1974), as well as the emergence of a c-number amplitude of the quantized light field (Fig. 2).

The Hierarchical Structure of Synergetics

Before I discuss the mathematical approach in detail and to provide the ground for farther reaching applications, I hint at the three levels of Synergetics:

1. *The microscopic theory*, based either on microscopic equations, such as in the laser example, those of quantum mechanics and quantum field theory, or in biology on mathematical models on the behavior of individual parts of a system. At this level, concepts, such as order parameters and enslavement (cf. section "The Laser Paradigm"), can be mathematically derived.
2. *Phenomenological Synergetics* directly starts from concepts, such as order parameters and enslavement, which then may be cast into mathematical relations.
3. *Semantic Synergetics* deals with cases where a mathematical formulation is (at present or in principle) not possible, but still formulations using concepts and relationships unearthed in Synergetics are applicable.

A general goal of Synergetics consists in elaborating relationships between levels 1, 2, 3.

In the present article I will mainly focus my attention on the mathematical formulation dealing with 1 and 2.

Basic Equations

The basic equations are classical or quantum mechanical evolution equations, in which the temporal evolution of the microscopic quantities under consideration is described by ordinary or partial differential equations. Since the systems are open, the inputs and outputs of energy, matter and/or information must be taken care of, which, quite often, appears in the form of coupling to heat baths in the sense of thermodynamics. In open systems, these heat baths must be kept at different temperatures, in order to maintain the non-equilibrium state of the system. The heat bath variables can be eliminated which gives rise to differential equations which contain "pumping" and "damping" terms as well as fluctuating (stochastic) forces. In the case of quantum mechanical equations the stochastic forces are operators. With the inclusion of stochastic forces, the classical or quantum mechanical equations acquire the character of stochastic differential equations which may be called "generalized Langevin equations".

Depending on the definition of the random forces, we may distinguish between the *I* to, the Statonovich and the Klimontovich approach (Haken 2004b; Îto 1969; Stratonovich 1963). As is well known in statistical physics, Langevin equations can be converted into equations for distribution functions, such as e. g. the Fokker–Planck equation.

A further approach, mainly used in quantum mechanics, but also in models on sociodynamics, is the master equation.

In order not to overload this article, I will focus my attention on the treatment of evolution equations.

This approach seems to be particularly suited for the treatment of phase transition- like phenomena, i.e. the transitions between qualitatively different states of a system. If noise is neglected and transients are not treated, these transitions are called bifurcations (Arnold et al. 1999; Chow and Hale 1982; Guckenheimer and Holmes 1983; Iooss and Joseph 1980; Kielhöfer 2004; Kuznetsov 1995; Ma and Wang 2005).

At the microscopic level the systems are described by a state vector q with components $q_1,\ldots, q_n$ which may also be space dependent, $q_j = q_j\ (x,\ t)$, where x is a one, two or three dimensional vector. The time dependence is described by evolution equations of the form of a vector equation.

$$\dot{q} = N(q, \nabla, \alpha) + F(q, \nabla, \alpha). \tag{1}$$

The dot˙ means time-derivative. N is a vector valued function that depends on q in a nonlinear fashion. ∇ indicates spatial derivatives (of any order) or non-local integrations e. g. of the form

$$\int K(x, x')q(x')\mathrm{d}x' \tag{2}$$

where K is a matrix.

α represents a set of fixed control parameters. If not otherwise stated, we explicitly treat only one control parameter. Equation (1) must be supplemented by appropriate boundary and initial conditions. F is a vector valued stochastic function of time with vanishing mean.

Method of Solution

We assume that for a certain control parameter value α_0 the state vector as solution of Eq. (1) is known, $q = q_0$. The following cases have been considered, see e. g. (Haken 2004b):

(a) q_0 is a stable fixed point (section "Instability of a Fixed Point")
(b) q_0 is a stable limit cycle (section "Instability of a Limit Cycle, $q_0(t)$ (Haken 2004b)")
(c) q_0 is a stable n-dimensional torus. (section "Instability of Tori (Haken 2004b)")

Now the control parameter value is changed and the stability of the system is checked by means of linear stability analysis (Hahn 1967).

Instability of a Fixed Point

We first elucidate our general procedure by means of the instability of an originally stable fixed point. This procedure differs from the classical approach of bifurcation theory (Lyapunov 1906; Schmidt 1908) in two important aspects:

1. The role of the fluctuating forces is fully taken into account in order to be able to make contact with the theory of phase transitions in the Landau sense (Landau and Lifshitz 1959).

2. The approach covers the surrounding of the fixed point in order to deal with relaxation processes towards the newly evolving stable states.

The hypothesis

$$q(t) = q_0 + W(t) \tag{3}$$

is inserted into (1) and the Eq. (1) with $F \equiv 0$ linearized with respect to *W(t),*

$$\dot{W} = LW \tag{4}$$

where L may be a linear differential (or integral) linear operator.

The solutions are of the form

$$W(x, t) = e^{\lambda_k t} \sum_{d=0}^{D} t^d v_{k,d}(x) \tag{5}$$

where $D > 0$ may happen if the corresponding eigenvalue λ_k is degenerate. In the following we consider $D = 0$ and $v_{k,d} = v_k$. The unstable modes $v_k \equiv v_u$ are connected with

$$\mathrm{Re}\,\lambda_k \geq 0, \tag{6}$$

the stable modes $v_k \equiv v_s$ with

$$\mathrm{Re}\,\lambda_k < 0. \tag{7}$$

It is assumed that $\mathrm{Re}\,\lambda_k < A < 0$, A fixed, if the eigenvalues are discrete.

We decompose the wanted solution to the original non-linear and stochastic equations into a super position of modes determined by the instability analysis whereby we distinguish between the unstable and stable modes. The amplitudes of the unstable modes are the order parameters. Inserting

$$q(t) = q_0 + \sum_u \xi_u(t) v_u(x) + \sum_s \xi_s(t) v_s(x) \tag{8}$$

into the Eqs. (1) and projecting both sides of the resulting equation on the stable and unstable modes, we obtain equations of the form

$$\begin{aligned} \dot{\xi}_u &= \lambda_u \xi_u + \widehat{N}_u(\{\xi_u\}, \{\xi_s\}) \\ &\quad + \widehat{F}_u(\{\xi_u\}, \{\xi_s\}) \qquad (9) \\ \dot{\xi}_u &= \lambda_s \xi_s + \widehat{N}_s(\{\xi_u\}, \{\xi_s\}) \\ &\quad + \widehat{F}_s(\{\xi_u\}, \{\xi_s\}). \qquad (10) \end{aligned}$$

λ_u, λ_s are the eigenvalues (6), (7), which are assumed to be discrete. By a suitable, in general nonlinear, transformation to new variables, $\tilde{N}(\{\xi_u\})$ can be cast into a particularly simple form ("normal form" theory (Murdock 2002; Nayfeh 1993), initiated by Poincaré (1960)).

If the eigenvalues λ_u, $0 > \mathrm{Re}\,\lambda_s > -|B|$ are a continuous function of an index, e. g. a wave number k, wave packets of $\xi_u(t)$ are used as new order parameter variables Ξ and $\lambda_u(k)$ is replaced by an operator $\Lambda_u\left(-i\frac{\mathrm{d}}{\mathrm{dx}}\right)$ in one space-dimension or, more generally, $\Lambda_u = (-i\nabla)$ (Haken 2004b). For a related approach in fluid dynamics cf. (Newell and Whitehead 1969).

The central idea of further procedure consists in eliminating the amplitudes of the stable modes. This is achieved by the *slaving principle* (Haken 1975b, 2004b; Haken and Wunderlin 1982; Wunderlin and Haken 1981) which allows us to express the amplitudes of the stable modes in terms of the unstable modes

$$\xi_s(t) = f_s(\{\xi_u(t)\}, t), \tag{11}$$

where ξ_s, ξ_u, are taken at the same time t. The explicit time-dependence of f_s stems exclusively from that of the fluctuating forces. f_s can be explicitly calculated in terms of a series expansion in powers of the order parameters. For practical purposes, in general only a few terms are needed. For a general discussion of the convergence of this series see (Haken 2004b). When noise is neglected, contact can be made with center manifold theory (Kelley 1967; Pliss 1964), which originally was a mere existence theory and was not constructive. For more recent developments, see books on bifurcation theory. A related approach is based on time-scale separation: The slowly damped or undamped modes serve as order parameters, which enslave the rapidly damped modes. A special case is adiabatic elimination.

Resulting Langevin Equations The enslaved mode amplitudes can be expressed by the order parameters and inserted in (9), so that closed equations for the order parameters alone result.

$$\dot{\xi}_u = \lambda_u \xi_u + \tilde{N}_u(\{\xi_u\}) + \tilde{F}_u(\{\xi_u\}, t) \tag{12}$$

where $\tilde{N}$ is a polynominal of $\xi(x, t)$ starting with at least second order. $\tilde{F}$ is a stochastic force. A simple, yet prototypical example is (with a single order parameter $\xi = \xi_u$)

$$\dot{\xi} = \lambda\xi + a\xi^2 - b\xi^2 + F(t), \quad b > 0 \tag{13}$$

$$\dot{\xi} = -\frac{\partial V(\xi)}{\partial \xi} + F(t), \tag{14}$$

with the potential

$$V = -\frac{\lambda}{2}\xi^2 - \frac{a}{3}\xi^3 + \frac{b}{4}\xi^4. \tag{15}$$

If λ_u, λ_s (6, 7) represent a continuous spectrum, (generalized) Ginzburg–Landau equations result (Haken 2004b). For example, the complex Ginzburg–Landau equation with fluctuating force reads (Aronson and Kramer 2002).

$$\begin{aligned} &(\xi(x,t) \equiv \xi_u, \text{complex order parameter}) \\ &\dot{\xi} = \lambda\xi + a\Delta\xi - c|\xi|^2\xi + F(t). \end{aligned} \tag{16}$$

A further example is given by the Swift–Hohenberg equation (Swift and Hohenberg

1977), see also (Cross and Hohenberg 1993) (which was derived differently, however)

$$\dot{\xi}(x,t) = (a - b\Delta)^2 \xi(x,t) + c\xi(x,t) - d\xi(x,t)^3. \quad (17)$$

The Eqs. (12, 13, 16, 17) allow for a great variety of solutions. In the case of real λ and a single order parameter, a nonequilibrium phase transition occurs (see below). In case of λ complex, and (at least) one complex order parameter, Landau-Hopf bifurcation (Hopf 1942, 1948), i.e. formation of a limit cycle may happen. In case of (at least) three order parameters and no noise, deterministic chaos may occur (Lorenz 1963; Ruelle and Takens 1971; Sparrow 1982) (in the presence of noise, mixed effects may occur).

Fokker–Planck Equation Below and above the instability point in control parameters space, in a first step the fluctuations can be neglected and then, in the next step, taken care of by means of lowest order perturbation theory. In order to cover the transition region, under well defined conditions a Fokker–Planck equation for the probability density function $f(\{\xi_u\})$ of the order parameters can be derived. For details see (Haken 2004b; Haken and Graham 1971) and the article by T. Frank, this volume.

The Fokker–Planck equation is of the general form

$$\dot{f}(\{\xi_u\}) = -\sum_u \frac{\partial}{\partial \xi_u}(\tilde{N}_u f) + \frac{1}{2}\sum_{uv} \frac{\partial^2}{\partial \xi_u \partial \xi_v}(Q_{uv} f). \quad (18)$$

It is assumed that $\tilde{F}_u$ in (12) is δ correlated in time,

$$\langle \tilde{F}_u(t)\tilde{F}_v(t')\rangle = Q_{uv}\,\delta(t-t'). \quad (19)$$

If $\tilde{F}_u$ depends on ξ_u, the $\hat{I}$ to, Stratonovich or Klimontovich procedure must be applied.

In the case of a single order parameter, where the Langevin equation (Langevin 1908), originally with $\tilde{N} = -\alpha\xi$) is given by

$$\dot{\xi} = \tilde{N}(\xi) + F(t),\ \langle F(t)F(t')\rangle = Q\,\delta(t-t'). \quad (20)$$

The steady state distribution function of (18) is given by (Haken 2004b; Risken 1965)

$$f(\xi) = N \exp\left(-2\int^{\xi} (\tilde{N}(\xi')/Q\mathrm{d}\xi') \equiv N\exp(-2V(\xi)/Q\right) \quad (21)$$

provided the boundary conditions are

$$f(\xi) \to 0 \text{ for } |\xi| \to \infty. \quad (22)$$

In the second Eq. (21), $Q =$ const. is assumed. N is a normalization constant. A generalization of (18) to continuous variables, $\xi_u(x, t)$, gives rise to a functional Fokker–Planck equation. An explicit solution of the Fokker–Planck equation in the case of several discrete or continuous order parameters can be found if the drift and diffusion coefficients obey the rules of detailed balance (Graham 1981; Graham and Haken 1971).

Nonequilibrium Phase Transition. Connection with Landau Theory The explicit form of the solution of the Fokker–Planck Eq. (21) allows us to make contact with the theory of phase transitions in the sense of the Landau theory (Landau and Lifshitz 1959) where

$$f(\xi) = N\exp(-F(\xi,T)/(kT)),$$
$$F(\xi,T) = F(0,T) + a(T-T_c)\xi^2 + \frac{\beta}{4}\xi^4. \quad (23)$$

In (21), V corresponds to the free energy F and the noise strength Q corresponds to *absolute* temperature T. T_c is the critical temperature, and (23) refers to a second order phase transition. In case of a first order phase transition, an additional term $\gamma\xi^3$ appears in (23).

An important difference between phase transitions at thermal equilibrium and in the present case of non-equilibrium should be mentioned, however. The decisive constants in the case of non-equilibrium (Haken 2004b) phase transitions are rate constants in contrast to thermodynamic quantities in (23). While non-equilibrium phase transitions described by (21) were experimentally very well verified for instance in the case of lasers (Risken 1965) (Fig. 1), in the case of thermal equilibrium the Landau theory can not be considered as a good approximation and had been replaced by the concept of critical exponents

etc. as dealt with by renormalization group theory (Kadanoff et al. 1967; Wilson and Kogut 1974). For a treatment of the time dependent Fokker–Planck equations see Risken (1989).

In a number of cases the drift- and diffusion coefficients of the Fokker–Planck equation are by themselves expectation values, defined on the probability density function so that the Fokker–Planck equation becomes non-linear. For more details see the article by T.D. Frank in this volume.

Instability of a Limit Cycle, $q_0(t)$ (Haken 2004b)
The instability is checked by linear stability analysis by means of the hypothesis

$$q(t) = q_0(t) + W(t), \tag{24}$$

where $q_0(t)$ is a time-periodic solution to (1) with $\alpha = \alpha_0$, $W(t)$ a small deviation.

Inserting (24) into (1) with $F \equiv 0$ and linearization leads to an equation of the form (4), where L because of $q_0(t)$ has become also a time-periodic function with the same period as $q_0(t)$. According to Floquet theory (Floquet 1883), the solutions to (4) with periodic $L(t)$ are given by

$$W(t) = e^{\lambda_f t} v_j(t) \tag{25}$$

(in the case of nondegeneracy), where $v_j(t)$ has the same period as q_0, i.e. L.

Depending on Re $\lambda_j \geq 0$ or < 0 we distinguish between unstable and stable modes (6, 7), respectively. One eigenvalue is $= 0$ and corresponds to an indeterminate phase shift, which in nonlinear analysis is taken care of by a phase $\phi(t)$ that acts as additional order parameter. In order to solve the fully nonlinear and stochastic equations, the hypothesis

$$\begin{aligned} q(t) = {} & q_0(t + \phi(t)) \\ & + \sum_u \xi_u(t) v_u(t + \phi(t)) \\ & + \sum_s \xi_s(t) v_s(t + \phi(t)) \end{aligned} \tag{26}$$

is inserted in the Eqs. (1). The subsequent procedure follows the lines outlined above and leads to order parameter equations of the form

$$\dot{\xi}_u = \lambda_u \xi_u + \widehat{N}_u(\{\xi_u\}, \phi) + \widehat{F}_u(\{\xi_u\}, \phi) \tag{27}$$

$$\dot{\phi} = M(\{\xi_u\}, \phi) + G(\{\xi_u\}, \phi) \tag{28}$$

where $\widehat{N}$, $\widehat{F}$, M, G are polynominals in $\{\xi_u\}$ and periodic functions of ϕ.

The novelty as compared to the case of an unstable fixed point consists in the introduction of a phase as order parameter.

When noise is neglected, the newly evolving, i.e. bifurcating solutions are either two (or several) limit cycles or tori. Also basically, depending on the system, also a "back bifurcation" to a stable focus can happen.

Instability of Tori (Haken 2004b)
The corresponding theory is rather complex so that a few words must suffice here. The basic idea (Haken 2004b) is based on an extension of (24, 26) where q_0 is chosen as a quasi periodic function

$$q_0 = q_0(\omega_1 t, \omega_2 t, \ldots, \omega_M t) \tag{29}$$

where the $\omega' s$ must be sufficiently irrational in the sense of the KAM (Kolmogorov (1954), Arnold (1963), Moser (1967)) theorem. Besides amplitudes as order parameters, also phases $\phi_1(t), \ldots, \phi_M(t)$ are introduced. For details cf. (Haken 2004b), and for alternative approaches (Chenciner and Iooss 1979; Sell 1979).

A Remark on the Method of Solution of Evolution Eq. (1)

In this article the central role of order parameters is stressed because this allows us to establish profound analogies between quite different systems. In practical applications it may be preferable, however, to apply other methods of solution, analytical, numerical or mixed, in order to derive the spatial, temporal or spatio-temporal patterns. In this way, the Springer Series in Synergetics have developed a "tool box" of models (Mikhailov 1993).

Quantum Theoretical Formulation

In a quantum theoretical treatment one deals with quantum mechanical Langevin equations which are Heisenberg equations of motion for operators to which pumping and damping terms as well as random noise sources are added. Here, according to quantum theory, the system's observables are represented by time-dependent quantum mechanical operators, Ω_j. For instance, by the position operator $\hat{x}$ and the momentum operator $\hat{p}$ of a particle, or, in quantum field theory, by creation and annihilation operators $\hat{b}^+$, $\hat{b}$, respectively. The quantum mechanical Langevin equations read (see, for instance (Haken 1970, 1985)):

$$\dot{\Omega}_j = \frac{i}{\hbar}\left[H, \Omega_j\right] + \text{damping} + F_j(t), \qquad (30)$$

where H is the Hamilton operator, and $F_j(t)$ are stochastic operators which usually are assumed to be δ-correlated in time. The quantum mechanical properties can be determined by the postulate of quantum mechanical consistency of Ω_j, (cf. (Haken 1970), appendix).

If the non-commutativity of operators is taken care of, the procedure to derive order parameter equations is formally the same as in the case of classical Langevin equations as indicated above. The Fokker–Planck equation, however, must be replaced by a density matrix equation, originally introduced as master equation (Pauli 1928). For nonequilibrium systems, such as the laser, see (Scully and Lamb 1967; Weidlich and Haake 1965), also (Haken 1970; Sargent et al. 1974). Using methods of quantum classical correspondence, this density matrix equation can be converted into a Fokker–Planck equation under specific conditions. The basic idea is this:

Quantum-Classical Correspondence

There are several ways to define quantum classical correspondence. In the case of position operator $\hat{x}$ and momentum operator $\hat{p}$ with the commutator $[\hat{p}, \hat{x}] = \frac{\hbar}{i}$ and the density matrix ρ, the Wigner distribution function $W(x, p)$ (Wigner 1932) is defined by

$$W(x,p) = \frac{1}{(2\pi)^2} \cdot \int \int_{-\infty}^{\infty} e^{-ikx-ilp} \cdot \mathrm{tr}\left(e^{ik\hat{x}+il\hat{p}}\rho\right) \mathrm{d}k\,\mathrm{d}l \qquad (31)$$

where "tr" means trace.

Thus a relation is established between the quantum mechanical density matrix and a classical quasi-density $W(x, p)$. Based on (31) or equation (34, 35, 36), a density matrix equation can be converted into a generalized Fokker–Planck equation (Haken 1964).

By the transformation of $\hat{x}$, $\hat{p}$ to creation and annihilation operators b^+, b by means of

$$\hat{b}^+ = \frac{1}{\sqrt{2\hbar}}(\hat{x} + i\hat{p}) \qquad (32)$$

$$\hat{b} = \frac{1}{\sqrt{2\hbar}}(\hat{x} - i\hat{p}) \qquad (33)$$

an alternative form to (32) is given by

$$P(\beta, \beta*) = \frac{1}{\pi^2} \int \int_{-\infty}^{\infty} e^{-i\beta k - i\beta* l} \cdot \mathrm{tr}\left(e^{ik\hat{b}^+ + il\hat{b}}\rho\right) \mathrm{d}\,k\,\mathrm{d}\,l. \qquad (34)$$

Because $\hat{b}^+$, $\hat{b}$ are noncommuting operators, $[\hat{b}^+, \hat{b}] = 1$, different "quasiprobability" distributions P result, if

$$e^{ik\hat{b}^+ + il\hat{b}}$$

is replaced by

$$e^{ik\hat{b}^+} e^{il\hat{b}} \qquad (35)$$

or

$$e^{ik\hat{b}} e^{il\hat{b}^+}. \qquad (36)$$

(35) gives rise to the Glauber–Sudarshan representation. For details and references see (Haken 1970).

Regular Spatial and Spatio-Temporal Patterns

One of the most striking features of non-equilibrium systems in physics, chemistry and biology is their capability of forming (more or less) regular spatial pattern (for explicit examples see below). (There is a rich literature on pattern formation in physics, especially fluids (Chandrasekhar 1961; Cross and Hohenberg 1993; Manneville 1990; Swinney and Gollub 1981), but also semiconductors (Schöll 2001) and nonlinear optics (Staliunas et al. 2003), chemistry (Epstein and Pojman 1998; Fife 1979; Kuramoto 1984) and biology (Babloyantz 1986; Meinhardt 1982, 1990; Murray 1989) and general (Horsthemke and Lefever 1983; Hoyle 2006; Mikhailov 1993; Nekorkin and Velarde 2002; Pismen 1999, 2006; Rabinovich et al. 2000; Vavilin et al. 1967). Furthermore, the patterns exhibit striking similarities in spite of the fact that the individual parts are quite different. The methodology of Synergetics (e. g. (Haken 2004b)) provides us with a basic insight into the causes of such analogies.

Pattern formation is determined by at least three causes:

1. internal mechanism, such as e. g. the interplay between reactions and diffusion in large scale chemical processes,
2. the influence of boundaries,
3. initial conditions.

Concerning (1) and (2) between two (limiting) cases can be distinguished.

1. dimensions of the internally evolving patterns are of the same or larger order as those of the boundaries. Here a strong influence of the boundaries must be expected.
2. dimensions of evolving patterns are small compared to those of the boundaries (boundaries $\rightarrow \infty$).

To bring out the essential features we consider that originally for a control parameter value α_0 the system is homogeneous and quiescent. The approach can, however, be extended to a space dependent reference state (which, e. g. resulted from a first bifurcation leading to $q_0 = q_0(x)$) and the cases of a limit cycle or torus. The space may be 1, 2 or three dimensional Euclidian or, e. g., a 2 or 3 sphere.

Infinite Boundaries

We start with 2 infinite boundaries, the medium is homogeneous and isotropic. We assume a continuous transition from the homogeneous to the "bifurcating" state. The evolving patterns are determined by the leading terms in (8) that we call the "mode skeleton"

$$q(x,t) = q_0 + \sum \xi_u(t) v_u(x) \tag{37}$$

and the order parameter Eq. (12). The functions $v_u(x)$ are *the space-dependent part of the* solutions to (4) where L is a differential (or integral) operator which is invariant against translation and rotation. Thus, e. g., L commutes with the displacement operator

$$\Omega_a : x \rightarrow x + a,\ a \text{ constant vector.}$$

Thus $v_u(x)$ can be chosen as eigenfunction to Ω_a,

$$\Omega_a v_u(x) = \Lambda v_u(x) \tag{38}$$

with

$$v_u = e^{ikx} \tag{39}$$

$$\Lambda = e^{ika} \tag{40}$$

i.e. plane waves. Which waves must be considered in (37) is determined by λ_u in (6) as well as by the order parameter Eq. (12).

The condition Re $\lambda_u(k) = 0$ defines $k = k_{\text{crit}}$. As was shown by means of many examples $k \approx k_{\text{crit}} \neq 0$. If the boundaries are finite, such a discrete k must be chosen which comes closest to k_{crit}. If the boundaries tend to infinity, a continuous set k is taken care of by (generalized)

Ginzburg–Landau equation (see above). If the boundaries are "narrow" in 1 or 2 dimensions, but large in the remaining dimensions, the wave vector k must be split into k_{II} and $k_{\perp}$ where k_{II} is practically continuous and $k_{\perp}$ discrete. Quite often only one $k_{\perp}$ (the most critical) needs to be considered. This leads to practically 2 (or 1) dimensional patterns connected with k_{II}. In the 2-dimensional case, the modes with $|k_{\text{II}}| = k_{\text{crit.}}$ are degenerate. This degeneracy can be lifted by a weak influence of boundaries (leading to roll patterns), by specific initial condition which (by chance) prefers a specific roll pattern, or by terms in the order parameter-equations that lead to specific combinations, e. g.

$$k_1 + k_2 + k_3 = 0, \tag{41}$$

where k_j, $j = 1, 2, 3$ belong to k_{II}.

This gives rise to the formation of hexagons. This is the case if the leading term of $\tilde{N}$ contains

$$\int v_{k_1} v_{k_2} v_{k_3} \, \mathrm{d}^2 x \neq 0. \tag{42}$$

In three dimensions this mechanism may lead to plane wave fronts stabilizing each other which gives rise to icosaeders, as observed in diatomea.

An important class of spatio-temporal patterns (in 2 dimensions) results when the system utilizes *rotation symmetry.* This can best be explained by the following example:

In many cases of practical interest, N in (1) and thus L in (4) contain the Laplace operator Δ When written in planar polar coordinates r, ϑ, solutions to (4) are of the general form

$$v \propto \mathrm{e}^{i(m\vartheta - kr - \omega t)} \tag{43}$$

(times a rotation symmetric function *g(r))* which represents *spirals.* $m = 0$ represents concentric rings, while an integer $m > 0$ represents the number of spiral arms. $\omega = 0$ represents standing spirals, $\omega \neq 0$ rotating spirals.

The mode skeleton (37) is composed of functions of the form (43). Which of the functions (43) appear in (37) depends on the competition Eqs. (12) for order parameters, which may also allow for a super position of counter rotating spirals (such as in the sunflower head). As group theory shows (see below), solutions (43) with different m's belong to different irreducible representations, and do not coexist in (37). This does not exclude the coexistence of differently rotating spirals in *different* regions of space, however.

The above results can be cast into the isomorphy principle:

While the "true" q is represented by (we omit the homogeneous q_0)

$$q = \sum_u \xi_u v_u(x) + \text{enslaved modes, with same symmetry.} \tag{44}$$

and v_u "true modes", its symmetry features can be replaced by a "representative" q'*:*

$$q' = \sum_k \xi_k R_k(x), \tag{45}$$

where R_k represent the "elementary" functions showing the symmetry under consideration. While the material significance and explicit form of q according to (44) may be quite different for different material substrates, q' (45) shows the *same* patterns for different systems.

These results can be deepened by invoking group theory, in which also the effect of the boundaries is taken into account.

Theory, Representation Theory, Finite Boundaries

Consider a set of transformations G_j of space variables $x \to x'$ so that

$$G_j q \to q' \tag{46}$$

Example 1 G_j induces the translation

$$x \to x + a \text{ so that } G_j q(x) = q(x + a). \tag{47}$$

The transformations must be so that they are compatible with the internal properties of the system (1) and the boundary conditions. Example: when

dealing with a problem on a 2-dimensional sphere, the transformed coordinates x must not leave the sphere.

Because of the symmetry of the problem, the transformations G_j form a group defined by

1. existence of unity E such

$$G_j E = G_j \text{ for all } j \tag{48}$$

2. the product of two group elements is again an element of the group,

$$G_j G_k = G_l \text{ for all } j,k \tag{49}$$

3. existence of an inverse G_j^{-1} for all j so that

$$G_j^{-1} G_j = E, \tag{50}$$

4. associative law

$$(G_k G_l) G_j = G_k \left(G_l G_j\right) \tag{51}$$

for all group elements.

In the following we first ignore random forces, i.e. we consider (1) with $F \equiv 0$.

$$\dot{q}(x,t) = N(q, \Delta, \alpha). \tag{52}$$

Jointly with the boundary conditions, (52) defines a function space S in which all functions to be considered must lie (i.e. can be represented by linear combinations of a complete set of (vector valued) basic functions of S; example: S is a Hilbert space)

Definition 1 The system is invariant against G_j if for all f ∈ S

$$G_j N\left(G_j^{-1} f\right) = N(f). \tag{53}$$

Example 2

$$G_j : x \to x + a, \tag{54}$$

$$N(f) = \Delta f + V(x) f + f^2. \tag{55}$$

Then

$$\begin{aligned} G_j \cdot N\left(G_j^{-1} f\right) &= \Delta G_j^{-1} f(x+a) \\ &\quad + V(x+a) G_j^{-1} f(x+a) \\ &\quad + \left(G_j^{-1} f(x+a)\right)^2 \end{aligned} \tag{56}$$

$$= \Delta f(x) + V(x+a) f(x) + f(x)^2 \tag{57}$$

$$\neq N(f) = \Delta f(x) + V(x) f(x) + f(x)^2 \tag{58}$$

unless $V(x+a) = V(x)$. If a in (54) is arbitrary, N is not invariant against (54).

Application of G_j to q in (52) leads to

$$\frac{\mathrm{d}}{\mathrm{d}t}\left(G_j q\right) = N\left(G_j q\right) \tag{59}$$

or because of (53), (with $f = G_j q$), to

$$\frac{\mathrm{d}}{\mathrm{d}t}\left(G_j q\right) = G_j N(q). \tag{60}$$

In the spirit of representation theory of groups the action of G_j on f can be understood as an abstract operation, but also as a matrix acting on the vector f in S- space.

By appropriate transformation of basis of q, and using the representation theory of symmetry groups, all matrices U_j belonging to all group elements j can simultaneously be decomposed into "irreducible" representations so that (in the example of 3 irreducible representations)

$$U_j = \begin{pmatrix} \square & \circ & \circ \\ \circ & \square & \circ \\ \circ & \circ & \square \end{pmatrix} \tag{61}$$

Each box □ is a matrix $U_j^{(k)}$ with dimension Dk, so that

$$D_1 + D_2 + \cdots + Dk = \text{dimension } U_j.$$

Example 3 Rotation group applied to 2-sphere (e. g. earth surface). Basis functions are spherical harmonics Y_m^l with "quantum numbers" l, m. Subspace l fixed, $m = 0, \ldots, l-1$. As a consequence, the mode skeleton reduces to (q_0 dropped)

$$q^l = \sum_m \xi_m(t) Y^l_m. \tag{62}$$

There is no coupling between different *ls,* which implies a low dimensional dynamics of ξ_m.

Generally, the original function space S is decomposed into subspaces forming the basis of each irreducible representation. This implies a symmetry reduction beyond bifurcation point, compared to the situation below bifurcation point, where

$$G_j\, q = q \text{ for all } j, \tag{63}$$

i.e. q fully symmetric under G.

In our example beyond the bifurcation point q is given by q^l where Y^l_m transforms according to the subgroup G^l, which leaves the space spanned by Y^l_m invariant. If, however, group elements not belonging to G^l are applied to q^l, this space is left. In other words, q^l is connected with a lower symmetry than q (63). By bifurcations, the symmetry of q is lowered and one speaks of "symmetry breaking instability". If fluctuating forces in (1), i.e. in (52) are taken into account, the full symmetry can be restored (under specific conditions on the fluctuating forces).

While group theory has found important and widespread applications to quantum theory, it is less frequently used in problems of Synergetics, though there it may lead to deep insights as pointed out above. (For an in-depth approach see (Golubitsky and Schaeffer 1988; Golubitsky et al. 1988; Sattinger 1980).)

On top of, or jointly with, regular patterns, a variety of defects as well as boundaries between different patterns may occur (cf. contribution by Pismen, this volume and (Pismen 1999, 2006)).

A Further Mathematical Tool: Shannon Information and the Maximum (Information) Entropy Principle

While evolution equations are the backbone of Synergetics, also other tools are invoked to deal with complex systems. Such a tool is Shannon information (Shannon and Weaver 1949) which is defined by

$$i = -\sum_j p_j \log_2 p_j \tag{64}$$

where p_j is the relative frequency of the event j or, in a different interpretation, the probability of finding the realization j in an experiment. The maximum (information) entropy principle as formulated by Jaynes (1957, 1967), for an earlier proposal see (Elsasser 1937)), allows one to make unbiased guesses on systems on which only incomplete data are known by maximizing the informations, i.e. (64) = max! or = extremum! under given constraints.

A simple example is provided by a gas composed of N particles, where the total kinetic energy $\mathrm{E}^{\mathrm{tot}}_{\mathrm{kin}}$ is fixed. Denoting the kinetic energy of a particle with mass m and velocity v_i by $f_i = (m/2)v_i^2$, the mean kinetic energy per particle is

$$\sum_i p_i f_i = \mathrm{E}^{\mathrm{tot}}_{\mathrm{kin}}/\mathrm{N} \tag{65}$$

To fix p_i, (64) must be maximized under the normalization condition

$$\sum_i p_i = 1 \tag{66}$$

and the constraint (65).

Using Lagrange multipliers, λ, λ_1, the result reads

$$p_i = \exp\left(-\lambda - \lambda_1 m v_i^2/2\right) \tag{67}$$

i.e. the Maxwell–Boltzmann distribution function. Also relations between the Lagrange multipliers λ, λ_1 can be established which, evidently, have fundamental thermodynamic significance.

This approach has been extended to the treatment of nonequilibrium phase transitions, i.e. determination of order parameters, enslaved modes and emerging patterns (Haken 2000). The crucial idea consists in the proper choice of constraints, as which the moments of the variables q_i are chosen:

$< \ldots >$ means average over the joint distribution function $f(q_1, q_2, \ldots, q_n)$ which replaces p_j and the vector $(q_1, \ldots, q_N)$ replaces j. The variables q_j may be discrete or continuous.

$$f_i = < q_i >, i = 1, 2, \ldots, N. \quad (68)$$

$$f_{ij} = < q_i q_j >. \quad (69)$$

$$f_{ijkl} = < q_i q_j q_k q_l >, i, j, k, l = 1, 2, \ldots, N. \quad (70)$$

The resulting distribution function is given by

$$q = \exp V(\lambda, q) \quad (71)$$

with

$$V(\lambda, q) = \lambda + \sum_i \lambda_i q_i + \cdots + \sum_{ijkl} \lambda_{ijkl} q_i q_j q_k q_l. \quad (72)$$

(71) is a starting point to make contact with the Landau or Ginzburg–Landau theory of phase transitions (Landau and Lifshitz 1959), and to guessing Fokker–Planck equations. The approach allows one to calculate the efficiency of self-organizing systems close to their instability points.

The method has been extended to the "unbiased modeling" of stochastic processes: how to guess path integrals, Fokker–Planck equations and Langevin-Îto equations (Haken 1996). The central quantity to be searched for is the probability density P_n of paths.

Let $q(t)$ be the state vector $q = (q_1, \ldots, q_n)$ at time t, then

$$P_n(t_n, t_{n-1}, \ldots, t_0) = P_n(q(t_n), t_n; q(t_{n-1}), t_{n-1}; \ldots; q(t_0), t_0), \quad t_n > t_{n-1} > \ldots > t_0. \quad (73)$$

This task is simplified if the Markov hypothesis on the process holds, i.e.

$$P_n(t_n, t_{n-1}, \ldots, t_0) = \widehat{P}(q(t_n), t_n | q(t_{n-1}) t_{n-1}) \cdot P_{n-1} \quad (74)$$

where $\widehat{P}$ is the transition probability so that only transition probabilities between subsequent states (with $\Delta t \to 0$) must be guessed in addition to P_0.

In the frame of the present approach, this task is fulfilled by use of the maximum information principle. The constraints to be used are essentially conditional first order moments and two-time correlation functions of the state vectors $q(t)$, $q(t')$.

Phenomenological Synergetics

In many fields of science, including medicine, the microscopic variables and their dynamics are not well-known or not known at all. Nevertheless, in quite a number of cases, namely where dramatic macroscopic changes of the system's behavior take place, general insights, gained by Synergetics, can be invoked. A paradigm for this procedure is the modeling of Kelso's finger experiments (Kelso 1981, 1995) (Fig. 3). He instructed subjects to move their index fingers in parallel which was accordingly performed. However, when the speed of the fingers was increased, the parallel movement was replaced by a symmetric movement quite involuntarily and spontaneously. In other words, a transition from a parallel to an anti-parallel phase takes place. In terms of Synergetics, the interpretation is simple: the control parameter consists in the prescribed frequency ω of the finger movement, whereas the macroscopic quantity, i.e. the order parameter that changes dramatically is provided by the relative phase of the two index fingers. According to the experience made in Synergetics, the order

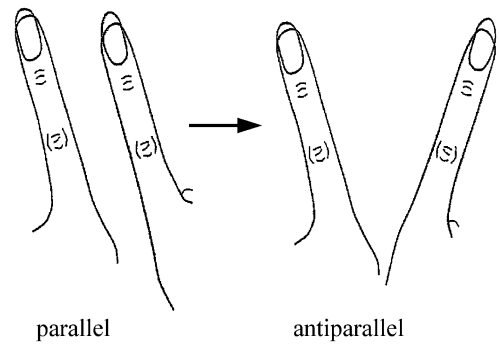

Synergetics: Basic Concepts, Fig. 3 Transition between finger movements from parallel to symmetric in Kelso's experiment (Haken et al. 1985)

parameter, here called ϕ obeys a typical order parameter equations of the form (Haken et al. 1985)

$$\dot{\phi} = -\frac{\partial V}{\partial \phi} + F(t), \tag{75}$$

where $V(\phi, \omega))is$ a potential function and F a fluctuating force. When the control parameter ω is changed, the potential runs through a series of forms as depicted in Fig. 4. As was shown in detail, at a critical value of ω, the transition from one potential minimum to another one occurs, as related to the change of the kind of finger movement. The mathematical analysis shows hysteresis, critical slowing down and critical fluctuations (Haken 1996) which reject the idea that the brain acts like a computer via a motor program but rather via self-organization.

Another application is made by the Synergetic computer (Haken 2004a) (Figs. 5 and 6), where to each pattern to be recognized a specific order parameter is attached. Pattern recognition is then achieved via a competition between order parameters. The competition equations are given by

$$\dot{\xi}_k = \frac{\partial V}{\partial \xi_k} V(\xi_1, \ldots, \xi_M)$$
$$= -\frac{1}{2}\sum_k \lambda_k \xi_k^2 + \beta \sum_{k,k'} \xi_k^2 \xi_{k'}^2 - C\sum_k \xi_k^4. \tag{76}$$

This approach may serve also for modeling of brain functions: both recognition as well as movements are governed by the establishing of order parameters which may wander from one quasi attractor to another one. Quasi attractors are defined as attractors that vanish after the task has been accomplished, e. g. after a pattern has been recognized or movement performed.

Based on the concept of order parameters, a learning procedure for Synergetic computers has been developed (Haken 2004a). Here the number of patterns to be recognized is prescribed and then a special functional must be minimized. In the case of the Synergetic computer, it is possible to make contact between the microscopic and the mesoscopic description, i.e. the microscopic variables are pixel values q_j, j pixel index, whereas the mesoscopic (or macroscopic) quantities are the order parameters ξ_k.

The relation between ξ_k, q_j is given by

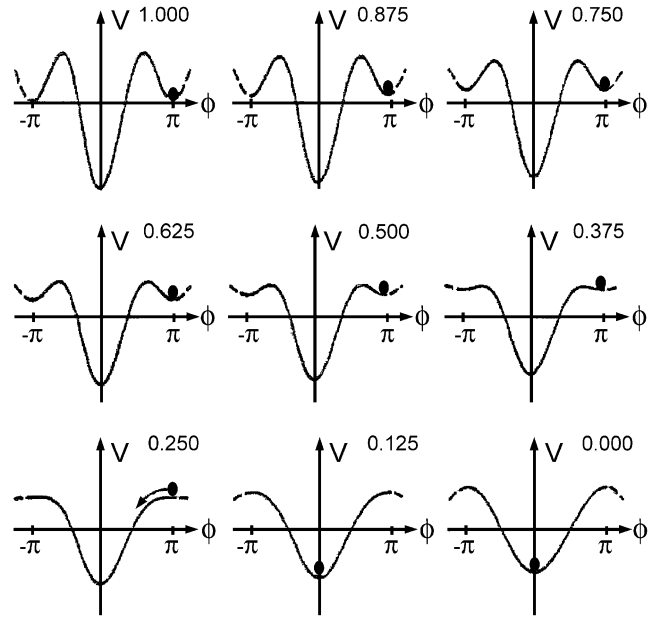

Synergetics: Basic Concepts, Fig. 4 Sequence of potential curves of the Haken–Kelso–Bunz model of Kelso's experiment (Haken et al. 1985)

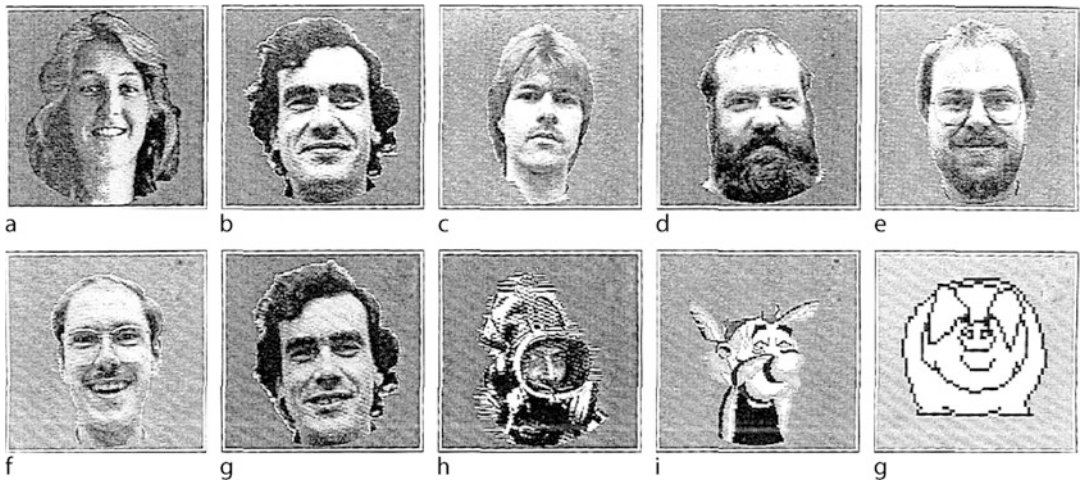

Synergetics: Basic Concepts, Fig. 5 Recognition of faces by the synergetic computer: stored or learned prototype patterns (Haken 2004a)

Synergetics: Basic Concepts, Fig. 6 Pattern recognition by the synergetic computer: recognition of a specific face of which initially only a subset of pixels is presented (Haken 2004a)

$$\xi_k = \sum_j v_j^{k+} q_j, \tag{77}$$

where v_j^{k+} are adjoint prototype patterns, with k pattern index, j pixel index.

The relation between prototype patterns v_j^k and their adjoints is given by

$$\sum_j v_j^{k+} v_j^{k'} = \delta_{kk'} \tag{78}$$

At the phenomenological level the order parameter concept allows us to interpret and model complex movement patterns, e. g. learning to ride on a pedalo (Haken 1996). In the experiments, LED's are fixed at the joints of the subject and their positions measured which gives rise to a series of time-dependent tracks. Then, in a first step, a principle component analysis is performed, in the next step, by means of a variational principle, the best fit is searched in terms of order parameters and their equations of motion, in order to mimic the actual tracks. While in the learning phase several order parameters are needed, at the end the whole movement is governed by a rather simple equation for a complex order parameter.

During the development of Synergetics it turned out that there are strong relations to gestalt theory (Köhler 1920) as well as to psycho physics. A typical example is provided by ambivalent figures where (Fig. 7) (Fisher 1967) shows an example. An observer may either perceive a young woman or an old woman, but not both simultaneously, rather the perception switches between these two percepts. In the mathematical modeling to each percept an order parameter is attached (Haken 2004a), which obeys the typical equations of Synergetics. The control parameter invoked

here is attention. According to an early suggestion by Wolfgang Köhler (1920), when a pattern is recognized, the corresponding attention fades away. This has been modeled mathematically based on a competition dynamics between two order parameters, when the control parameter (attention) of one pattern fades away, the other pattern gets the possibility of being perceived. Then in the next step the corresponding attention parameter fades away and the first pattern may re-appear (Fig. 8) (Haken 2004a). This model describes details of the observed phenomena, such as the dependence of the duration of the perception of one face as compared to that of the other face, dependent on the bias which face is recognized first. Also, one may distinguish between slow, medium and fast observers, depending on the individual parameters.

Quite generally, order parameters may have properties of gestalt in the sense that they are invariant against size, orientation and perception of objects in space.

In medicine, a syndrome has the characteristic features of an order parameter. On the one hand it is generated by the co-operation, or at least by the simultaneous presence of specific features, on the other hand once the syndrome (order parameter) is established, it acts on the individual parts of the system, where the slaving principle induces specific phenomena at the level of individual parts. Clearly, the concept of circular causality plays an important role here. It shows that the syndrome, at least in general, can not be cured by curing an individual symptom, but rather by curing a decisive majority of individual causes.

Synergetics: Basic Concepts, Fig. 7 Example of an ambivalent figure: young/or old woman? (Fisher 1967)

Semantic Synergetics

In soft sciences, but also in medicine and other fields, a mathematical modeling, even at the level of order parameters may not be possible. Nevertheless, Synergetics may provide us with qualitative insights into basic mechanisms. In psychology and psychiatry (Schiepek 1999), quite often specific mental states can be ascribed to a patient. For instance in bipolar patients a depressive phase or a manic phase may appear or in depressive patients a normal phase and a depressive phase. Another example is provided by patients with a compulsory action. In the spirit of Synergetics, as a theory of indirect control, one may ask, whether there are appropriate control parameters by means of which the behavior of a person can be changed. Let the two states be

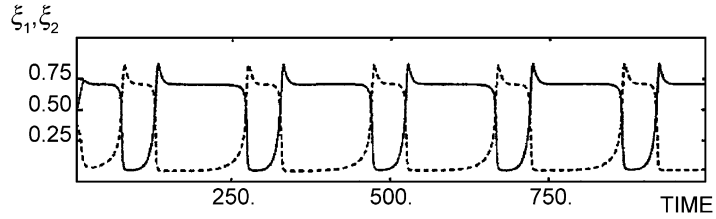

Synergetics: Basic Concepts, Fig. 8 Order parameter oscillations belonging to the recognition young woman/old woman with bias towards the young woman (Haken 1996)

represented by the positions of a ball in a landscape with two valleys. In this situation, direct control means to push the ball from the unwanted position to the wanted. Indirect control means to lower the potential hill between the two valleys so that the wanted transition may occur via self-organization. This may happen through interventions used in cognitive psychology, a change of environmental conditions, or/and by specific medication. The central issue here is that the patient is not directly influenced, e. g. by saying you must do this or that, but rather by a soft changing of his/her point of view. A number of successes have been reported about this method which is, to some extent, well known in psychiatry, but finds here a scientific theoretical basis. For more details see the article by G. Schiepek and V. Perlitz, this section, and in a somewhat related form (Hansch 2002).

Some Selected Examples

The study of nonlinear, self-sustained oscillations (Abraham and Marsden 1978; Andronov et al. 1966; Bogoliubov and Mitropolsky 1961) be it in radio-engineering, mechanics or other fields, has a long tradition. In the context of bifurcation theory, their origin was unearthed by Hopf (1942, 1948).

Nonlinear optics (Mills 1991) and, when quantum effects are important, quantum optics (Haken 1979; Meystre and Sargent 1990; Schleich 2001; Walls and Milburn 1994) provide us with a wealth of phenomena, in particular of the formation of coherent oscillations. A device, closely related to the laser, is the parametric oscillator (Graham 1970), in which, within a nonlinear crystal, incoming pumplight is split into a signal and an idler. Then, similar to the laser light, the signal light becomes amplified, and its generation can be described as that of a nonlinear quantum-mechanical oscillator. Fluid dynamics is rich of pattern formations (including chaos) (Bodenschatz et al. 2000; Busse 1972; Bénard 1900a, b; Fenstermacher et al. 1979; Gollup and Benson 1979; Lorenz 1963; Manneville 1990; Newell and Whitehead 1969; Rabinovich et al. 2000; Ruelle and Takens 1971; Segel 1969; Swift and Hohenberg 1977; Swinney and Gollub 1981), to mention just a few. In a fluid heated uniformly from below, with increasing temperature difference, several instabilities may occur for instance giving rise to stationary patterns, such as rolls, hexagons (Fig. 9) or squares. In the next step the rolls may start to show oscillations, and still more complex patterns may occur (Fig. 3). In the case of the Taylor instability (Taylor 1923), a liquid is placed in between two coaxial cylinders, where the outer one is rotating. With increasing rotation speed, a hierarchy of instabilities is reached, first the formation of roles, then oscillating rolls at one frequency, then oscillation of rolls at two frequencies, and finally weak turbulence, i.e. chaos occurs (Fig. 10) (Fenstermacher et al. 1979; Marx 1987). Important phenomena are the establishing of boundaries and of defects as described in the article by Pismen (1999, 2006) and other articles of this Encyclopedia. A rich variety of pattern formation may occur in semiconductors (Schöll 2001), where electrons and holes as well as currents form specific spatio-temporal patterns. In meteorology, atmospheric convection patterns and other instabilities are treated (Giaiotti et al. 2007). In chemistry, oscillations and large scale patterns arise by means of the interplay of chemical reactions and diffusions (Belousov 1959; Bray 1921; Epstein and Pojman 1998; Field et al. 1972; Fife 1979; Zaikin and Zhabotinsky 1970), e.g. concentric ring patterns, each starting from a center, which then annihilate each other when colliding. An important class is provided by spiral patterns which may have one to several arms (Fig. 11). In biology, specific models on morphogenesis were treated, such as the formation of stripe or spot patterns on animal furs or skins of fish (Fig. 12) or still more complicated patterns on sea shells (Gierer and Meinhard 1972; Haken 2004b; Meinhardt 1982; Meinhardt 1990; Murray 1989). The basic idea which can be traced back to Turing (Turing 1952) is this: originally unspecialized cells produce activator and inhibitor molecules which by reaction and diffusion form a prepattern, a morphogenetic field (Wolpert 1969). At positions of high

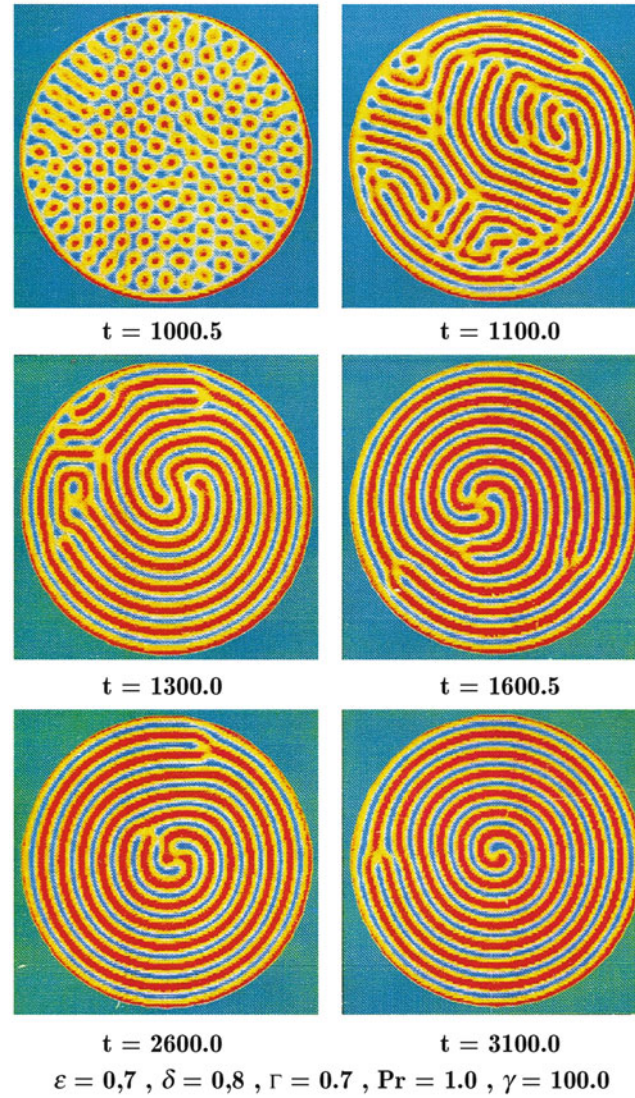

Synergetics: Basic Concepts, Fig. 9 Model calculation of the motion of a fluid in a circular pan uniformly heated from below. (After Fantz et al. 1993). Upper left corner: above a critical temperature difference between lower and upper surface of the fluid layer, a hexagonal pattern appears. If the boundary is also heated uniformly, a transition to the spiral pattern with one or several arms can be found (lower right corner)

activator concentration, genes are switched on which then leads to cell differention producing e. g. pigments. In aggregating slime mold, spiral or concentric ring patterns are observed (Bonner et al. 1972; Gerisch and Hess 1974). Mathematical models on prebiotic evolution (Eigen and Schuster 1977) study the competition between species of biomolecules and the "survival" of the fittest, where pronounced analogies with the dynamics of laser photons can be unearthed, fully in line with Synergetics (Haken 2004b). In the understanding of brain function, for instance, steering of movements, pattern recognition or decision making, the reduction of degrees of freedom of the numerous neurons to few order parameters is central (Haken 1996).

The concepts and principles of Synergetics shed new light on important relationships in economy, such as cooperation and competition between companies, the important role of indirect steering by means of control parameters, such as taxes, interest rates. It can be shown, that a fusion of companies does not necessarily lead to so called synergy effects, but rather critically

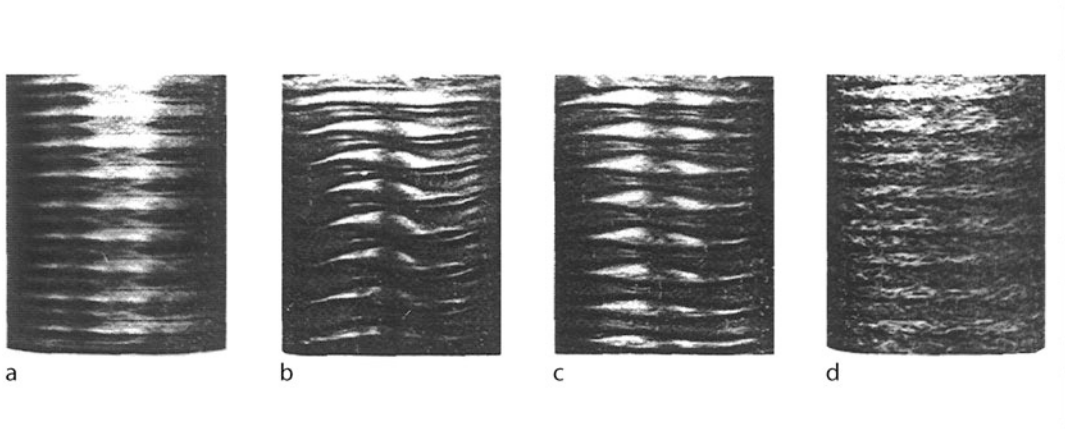

Synergetics: Basic Concepts, Fig. 10 Pattern hierarchy in the Taylor–Couette instability. A fluid in between two vertical coaxial cylinders of which the outer one rotates, shows no macroscopic movement pattern, if the movement of the outer cylinder is slow. When the rotation speed is increased, first a role pattern appears in which the fluid moves outwards at one height, and then inwards at another height. This movement pattern is periodic with respect to height (Taylor 1923). At a further critical rotation speed, the pattern shows oscillations which at a further speed transform into a motion with two frequencies until eventually chaotic motion appears. The experiments were done by (Fenstermacher et al. 1979), the modeling was done for the first transition (homogeneous to roles) and especially the second transition (roles to oscillating roles) by (Marx 1987)

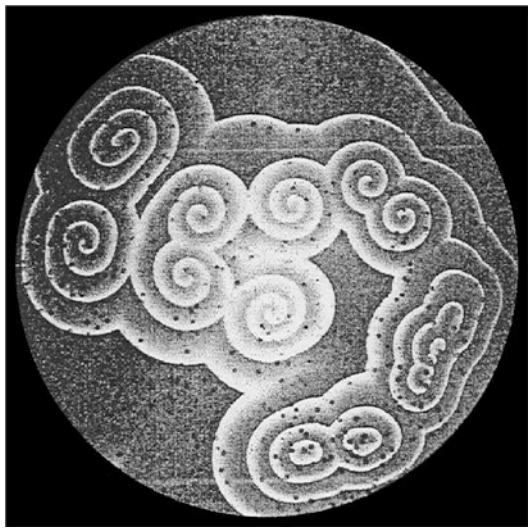

Synergetics: Basic Concepts, Fig. 11 Belousov–Shabotinsky reaction: the occurrence of spirals. (Courtesy A.T. Winfree). They may show one to several arms. The centers of the spirals may occur at different positions. Spirals hitting each other, annihilate each other

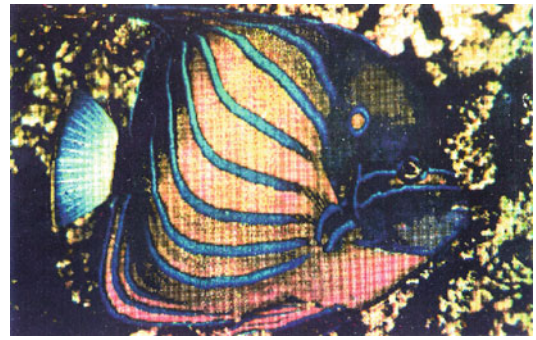

Synergetics: Basic Concepts, Fig. 12 Stripe pattern on a tropical fish

depends on initial conditions and details of the cooperation between the previously separated firms. Important insights are also gained into fundamental processes of climatology, as well as in ecology such as the by now well-known and publicly discussed effects that even small concentrations of chemicals in the atmosphere can change the climate dramatically. The same is true for lakes, in which beyond a critical pollution, fish population dies out entirely.

In this way, the numerous examples collected in the field of Synergetics, provide not only scientists but also the public with impressive examples of dramatic changes (instabilities) provoked by even a slight change of control parameters. Clearly, an important research subject of

Synergetics is a detailed study of which control parameters are critical and to which control parameters a system is rather insensitive. Sociology is an important field for the application of stochastic models (Bartholomew 1967). In particular, basic concepts of Synergetics have proven useful in the developing field of sociodynamics, where e. g. phase transition-like phenomena may occur (Weidlich 2000).

History and Relations to Other Fields

The term Synergetics was coined by H. Haken in 1969 in a lecture at University of Stuttgart. A first description of the goals of this field was given by H. Haken and R. Graham in 1971 (Haken and Graham 1971) where the unifying role of the concept of order parameters is outlined. A relationship exists to the general system theory due to von Bertalanffi (1950), which also aims at the exploration of analogies between different systems, but on the level of the individual elements rather than on the level of order parameters. Von Bertalanffi coined the term flux equilibrium (Fließgleichgewicht) in order to characterize homeostasis in active systems (von Bertalanffi 1953). A general mathematical frame for Synergetics is provided by dynamic systems theory (see, for instance, (Guckenheimer and Holmes 1983)) which, however, in the traditional approach ignores stochastic processes (mainly chance events) which are also of great relevance for Synergetics. Here the theory of Markov processes with their typical equations, such as Langevin equations, Fokker–Planck equations, Chapman–Kolmogorov equations, the Kramers–Moyal expansion etc. is important (see for instance (Stratonovich 1963) and Linear and Non-linear Fokker–Planck Equations by T. Frank).

A basic feature of Synergetics consists in dealing with nonlinearities in complex systems and studying, mainly quantitatively, qualitative changes at macroscopic scales. Qualitative changes of systems at macroscopic levels are studied also by catastrophe theory (Arnold et al. 1999; Thom 1975), which may be interpreted as a study of the surfaces of equilibrium points of few order parameters, where different cases are classified according to the (low) number of control and order parameters. Chaos theory studies the mostly irregular dynamics of deterministic low dimensional continuous (Lorenz 1963; Newhouse et al. 1978; Ruelle and Takens 1971; Sparrow 1982) or discrete dynamic systems (Collet and Eckmann 1980; Feigenbaum 1978; Grossmann and Thomae 1977; May 1976; Smale 1967), where the behavior is mainly characterized by so called Lyapounov exponents, various kinds of fractal dimensions and chaotic attractors. The slaving principle of Synergetics provides a basis for an application of chaos theory to multi-component systems in that Synergetics shows the possibility of reducing the degrees of freedom. Synergetics shares some of its topics with singularity theory (Arnold 1993; Golubitsky and Schaeffer 1988; Golubitsky et al. 1988), which applies to bifurcation points and their surrounding. Another point of contact is bifurcation theory (see the quotations in previous chapters), in which the branching of solutions of the dynamic system close to instability points is studied. The term dissipative structure was coined by Prigogine (Glansdorff and Prigogine 1971) to characterize evolving structures in systems away from thermal equilibrium where as in all such non-equilibrium systems dissipation occurs. A typical example is that of the convection instability. Prigogine tried to base his approach on thermodynamics, introducing concepts of entropy production and excess entropy production. As we now know, these concepts are, however, insufficient to deal with structure formation in such systems (Landauer 1975). Based on a fundamental idea of A. Turing (1952), Prigogine and Nicolis (1967), see also (Nicolis and Prigogine 1977), treated macroscopic pattern formation in a specific chemical reaction model. For more recent work see (Nicolis 1995).

Because of the fundamental importance of thermodynamics, we elucidate its relationship to Synergetics more closely.

Thermodynamics (see for instance (Callen 1960)) deals with systems in and out of thermal

equilibrium. A central concept is entropy. In a closed system, it tends to its maximum value. Thermal equilibrium is characterized by the equipartition theorem: each degree of freedom has an average energy of $1/2\ kT$, $k =$ Boltzmann constant, T absolute temperature. This may refer e. g. to gas atoms as well as to collective excitations in crystals. These systems are in thermal equilibrium with their surrounding (heatbaths, reservoirs).

Irreversible thermodynamics (Haase 1969) treats systems which are not in thermal equilibrium but close to it. It mainly deals with transport and relaxation processes. A central concept is entropy production.

In the domains of physics, chemistry, biology, Synergetics deals with systems far from (thermal) equilibrium. This state is caused and maintained by an in- and outflow of matter, energy and/or information. This is achieved by a coupling of the "proper system" to heat baths (reservoirs) at different temperatures. The former concepts of thermodynamics, in particular the first and second law, are still valid for the total system ("proper" plus reservoirs), but no more sufficient to deal with the kinetics of the proper system. Now the central concept is growth and decay rates. In systems far from thermal equilibrium, collective modes are formed. One or

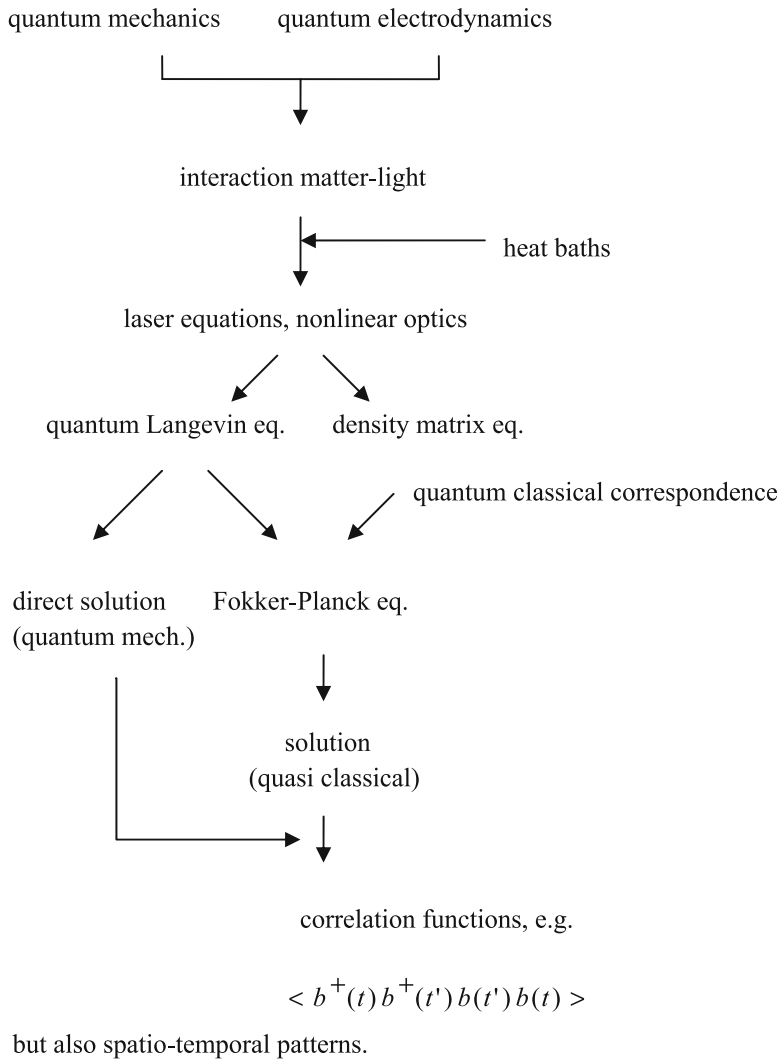

Synergetics: Basic Concepts, Scheme 1 Quantum optics, example laser. (After Haken 1970)

several of them compete best for the external supply of matter, energy, information and grow at the expense of all other degrees of freedom (or modes). Thus the equipartion theorem is no more valid. In general, the behavior of the system is governed by few degrees of freedom (order parameters). Incidentally, this "growth and competition" principle applies to a great variety of fields out of physics, chemistry and biology, where "modes" may not only be special physical structures, but may mean behavioral patterns, special functions etc. Quite often, a "mode" is initiated by a chance event (fluctuation). Clearly, a generalized Darwinian principle can be seen: The interplay between *mutations* (microscopic chance events) and *selection* (competition between mascropic modes) leads to macroscopic patterns (structures) in the widest sense of the word (Scheme 1).

In present days research, a new name is spreading, namely complexity or complexity theory. There seems to be no precise definition of this field available in the scientific community. Of what is known so far, we may conclude that this field has strong ties to the original field of Synergetics in that it searches also for general principles but, in addition, it allows the collection or accumulation of knowledge on all kinds of complex systems, as is witnessed in the excellent Complexity Digest, weekly edited by Gottfried Mayer. What "complexity" eventually might mean is reflected by the present encyclopedia.

Future Directions

Synergetics is surely not a closed scientific discipline but quite open to further research. On the one hand we may think of further applications of the principles of Synergetics that have been hitherto elaborated on, such as order parameters etc. Here a wide field of application is provided by robotics, construction of prostheses, automatic steering of cars etc. On the other hand, new ideas to endow systems with self-organizing properties are needed, e. g. groups of mobile agents for the execution of specific tasks. First steps have been done for instance by Kornienko (Kernbach 2008).

Bibliography

Basically, the individual volumes of the Springer Series in Synergetics and selected volumes of the Springer Series on Complexity provide further information. Here, because of lack of space, only a few basic papers can be quoted.

The number of books, reviews and original papers on the topic of the present article is enormous. I have tried to achieve a fair balance between original contributions and reviews/books. Nevertheless, my selection must remain – to some extent – arbitrary and incomplete.

Primary Literature

Abraham R, Marsden JE (1978) Foundations of mechanics. Benjamin/Cummings, Reading
Andronov A, Vitt A, Khaikin SE (1966) Theory of oscillators. Pergamon Press, London-Paris
Arnold VI (1963) Russ Math Surv 18:9
Arnold VI (1993) Dynamical systems VI singularity theory 1. Encyclopaedia of mathematical sciences, vol 6. Springer, Berlin
Arnold VI, Afrajmovich VS, Il'yashenko, Yu S, Shil'nikov Lf (1999) Bifurcation theory and catastrophe theory. Springer, Berlin
Aronson IS, Kramer L (2002) The world of the complex Ginzburg–Landau equation. Rev Mod Phys 74:99–143
Babloyantz A (1986) Molecules, dynamics and life: an introduction to self-organization of matter. Wiley, Indianapolis
Bartholomew DJ (1967) Stochastic models for social processes. Wiley, London
Belousov BP (1959) Sb Ref Radats Med, Moscow
Bénard H (1900a) Ann Chim Phys 7(23):62
Bénard H (1900b) Rev Gén Sci Pures Appl 11:1261–1309
Bodenschatz E, Pesch W, Ahlers G (2000) Annu Rev Fluid Mech 32:709
Bogoliubov NN, Mitropolsky YA (1961) Asymptotic methods in the theory of nonlinear oscillations. Hindustan Publ Corp, Delhi
Bonner JT, Barkley PS, Hall EM, Konjin TM, Mason JW, O'Keefe G, Wolfe PB (1972) Dev Biol 20:72
Bray CH (1921) J Am Chem Soc 43:1262
Busse FH (1972) J Fluid Mech 52:1–97
Callen HB (1960) Thermodynamics. Wiley, New York
Chandrasekhar S (1961) Hydrodynamic and hydromagnetic stability. Clarendon Press, Oxford
Chenciner A, Iooss G (1979) Arch Ration Mech Anal 69:109
Chow S-N, Hale JK (1982) Methods of bifurcation theory. Springer, Berlin

Collet P, Eckmann JP (1980) Iterated maps on the interval as dynamical system. Birkhäuser, Boston
Cross MC, Hohenberg P (1993) Rev Mod Phys 65:851
DeGiorgio V, Scully MO (1970) Phys Rev A 2:1170
Eigen M, Schuster P (1977) Naturwissenschaften 64:541, (1978) 65:7, 65:341
Elsasser W (1937) Phys Rev 52:987, (1968) Z Phys 171
Epstein IR, Pojman JA (1998) Introduction to nonlinear chemical dynamics. Oxford University Press, New York
Fantz M, Bestehorn M Friedrich R, Haken H (1993) Phys Lett A 174:48–52
Feigenbaum MJ (1978) J Stat Phys 19:25
Fenstermacher RP, Swinney HL, Gollub JP (1979) J Fluid Mech 94:103
Field RJ, Korös E, Noyes RM (1972) Am Chem Soc 49:8649
Fife PC (1979) Mathematical aspects of reacting and diffusing systems. Springer, Berlin
Fisher G (1967) Measuring ambiguity. Am J Psychol 80:541–547
Floquet G (1883) Sur les équations différentielles linéaires à coefficients périodiques. Ann Ècole Norm 2(12):47
Gardiner CW (1994) Handbook of stochastic methods. Springer series in synergetics, vol 13. Springer, Berlin
Gerisch G, Hess B (1974) Proc Natl Acad Sci (Wash) 71:2118
Giaiotti DB, Steinacker R, Stel F (2007) Atmospheric convection. Research and operational forecasting aspects, Cism International Centre for Mechanical Sciences Courses and Lectures. Springer, Wien
Gierer A, Meinhard H (1972) Kybernetika 12:30
Glansdorff P, Prigogine I (1971) Thermodynamic theory of structure, stability, and fluctuations. Willey, New York
Gollup J, Benson SV (1979) In: Haken H (ed) Pattern formation by dynamic systems and pattern recognition. Springer series in synergetics, vol 5. Springer, Berlin
Golubitsky M, Schaeffer D (1988) Singularities and groups in bifurcation theory I, vol 1. Springer, Berlin
Golubitsky M, Stewart I, Schaeffer D (1988) Singularities and groups in bifurcation theory, vol 2. Springer, Berlin
Graham R (1970) Quantum statistics of optical parametric oscillation. In: Kay SM, Maitland A (eds) Quantum optics. Academic, New York
Graham R (1981) Z Phys B 40:149
Graham R, Haken H (1968) Z Phys 213:420, (1970) 235, 237:31,166
Graham R, Haken H (1971) Z Phys 248:289
Grossmann S, Thomae S (1977) Z Naturforsch 32A:1353
Guckenheimer J, Holmes P (1983) Nonlinear oscillations, dynamical systems, and bifurcations of vector fields. Springer, Berlin
Haake F (1973) In: Springer tracts in modern physics, vol 66. Springer, Berlin, p 98
Haase R (1969) Thermodynamics of irreversible processes. Addison-Wesley, Reading
Hahn W (1967) Stability of motion. In: Die Grundlehren der mathematischen Wissenschaften in Einzeldarstellungen, Bd 138. Springer, Berlin
Haken H (1964) Z Phys 181:96
Haken H (1970) In: Encyclopedia of physics, vol XXV/2c: laser theory. Springer, Berlin
Haken H (1975a) Phys Lett 53A:77
Haken H (1975b) Z Phys B 21:105, B 22:69, B 23:388
Haken H (1979) Light. Elements of quantum optics, 1. North-Holland Physics Publishing, Amsterdam/New York
Haken H (1985) Light. Laser light dynamics, 2. North-Holland Physics Publishing, Amsterdam/New York
Haken H (1996) Principles of brain functioning. Springer, Berlin
Haken H (2000) Information and self-organization, 2. Springer, Berlin
Haken H (2004a) Synergetic computers and cognition, 2nd edn. Springer, Berlin
Haken H (2004b) Synergetics: an introduction and advanced topics. Springer, Berlin
Haken H, Graham R (1971) Umschau 6:191
Haken H, Wunderlin A (1982) Z Phys B 47:179
Haken H, Kelso S, Bunz H (1985) Biol Cybern 51:347
Hansch D (2002) Evolution und lebenskunst. Grundlagen der psychosynenergetik. Ein Selbstmanagement-Lehrbuch. Vandenhoeck und Ruprecht, Göttingen
Hopf E (1942) Abzweigung einer periodischen lösung eines differentialsystems. Berichte der Mathematisch-Physikalischen Klasse der Sächsischen Akademie der Wissenschaften zu Leipzig XCIV 1, Leipzig
Hopf E (1948) Commun Pure Appl Math 1:303
Horsthemke W, Lefever R (1983) Noise-induced transitions. Springer series in synergetics, vol 15. Springer, Berlin
Hoyle RG (2006) Pattern formation. Cambridge University Press, Cambridge
Iooss G, Joseph DD (1980) Elementary stability and bifurcation theory. Springer, Berlin
Îto K (1969) Stochastic processes. Universitet Matematisk Institut, Aarhus
Jaynes ET (1957) Phys Rev 106:4, 620, Phys Rev 108:171
Jaynes ET (1967) In: Delaware seminar in the foundations of physics. Springer, Berlin
Kadanoff LP, Götze W, Hamblen D, Hecht R Lewis EAS, Palcanskas VV, Rayl M, Swift J, Aspnes D, Kane J (1967) Rev Mod Phys 39:395
Kelley A (1967) In: Abraham R, Robbin J (eds) Transversal mappings and flows. Benjamin, New York
Kelso JAS (1981) Bull Psycon Soc 18:63
Kelso JAS (1995) Dynamic patterns: The self-organization of brain and behavior. MIT Press, Cambridge
Kernbach S (2008) Structural self-organization in multi-agent and multi-robotic systems. Thesis, Stuttgart University, Logos, Berlin
Kielhöfer, Hansjörg (2004) Bifurcation theory, an introduction with applications to PDES. Springer, Berlin
Köhler W (1920) Die physischen gestalten in ruhe und im stationären zustand. Vieweg, Braunschweig
Kolmogorov AN (1954) Dokl Akad Nauk USSR 98:527
Kuhn TS (1996) The structure of scientific revolutions, 3. University of Chicago Press, Chicago

Kuramoto Y (1984) Chemical oscillations, waves and turbulence. Springer, Berlin
Kuznetsov, Yuri A (1995) Elements of applied bifurcation theory. Springer, Berlin
Landau LD, Lifshitz IM (1959) In: Course of theoretical physics. Statistical physics, vol 5. Pergamon Press, London-Paris
Landauer R (1975) Phys Rev A 12:636
Langevin P (1908) Sur la théorie du movement brownien. CR Acad Sci Paris 146:530
Lorenz EN (1963) J Atmospheric Sci 20:130, 20:448
Lyapunov AM (1906) Sur la masse liquide homogène donnée d'un movement de rotation. Zap Acad Nauk St Petersburg 1:1
Ma, Tian, Wang, Shouhong (2005) Bifurcation theory and applications. World Scientific, Singapore
Manneville P (1990) Dissipative structures and weak turbulence. Academic, San Diego
Marx K (1987) Analytische und numerische behandlung der zweiten instabilität beim Taylor-Problem der flüssigkeitsdynamik, Thesis. Stuttgart University, Shaker, Aachen
May RM (1976) Nature 261:459
Meinhardt H (1982) Models of biological pattern formation. Academic, London
Meinhardt H (1990) The beauty of sea shells. Springer, Berlin
Meystre P, Sargent M (1990) Elements of quantum optics. Springer, Berlin
Mikhailov AS (1993) Foundations of synergetics. In: Distributed active systems, II (with AY Loskutov): complex patterns. Springer, Berlin
Mills DL (1991) Nonlinear optics basic concepts. Springer, Berlin
Moser J (1967) Math Ann 169:136
Murdock J (2002) Normal forms and unfoldings for local dynamical systems. Springer, New York
Murray JD (1989) Mathematical biology, 2nd edn 1993, 3rd edn 2002/2003. Springer, Berlin
Nayfeh, Ali H (1993) Method of normal forms. Wiley, New York
Nekorkin VI, Velarde MG (2002) Synergetic phenomena in active lattices. Patterns, waves, solitons, chaos. Springer, Berlin
Newell AC, Whitehead JA (1969) J Fluid Mech 38:279
Newhouse S, Ruelle D, Takens F (1978) Commun Math Phys 64:35
Nicolis G (1995) Introduction to nonlinear science. Cambridge University Press, Cambridge
Nicolis G, Prigogine I (1977) Self-organization in nonequilibrium systems. Wiley, New York
Pauli H (1928) Probleme der modernen physik. In: P Debye (ed) Festschrift zum 60. Geburtstag A Sommerfelds. Hirzel, Leipzig
Pismen LM (1999) Vortices in nonlinear fields. Clarendon Press, Oxford
Pismen LM (2006) Patterns and interfaces in dissipative dynamics. Springer, Berlin
Pliss VA (1964) Izv Akad Nauk SSSR, Mat Ser 28:1297
Poincaré H (1960) Les methods nouvelles de la méchanique céleste. Gauthier-Villars, Paris. Reprint 1892/99 Dover Publ, New York
Prigogine I, Nicolis G (1967) J Chem Phys 46:3542
Rabinovich MI, Ezersky AB, Weidmann PD (2000) The dynamics of patterns. World Scientific, Singapore
Risken H (1965) Z Phys 186:85
Risken H (1989) The Fokker Planck eq. Springer, Berlin
Ruelle D, Takens F (1971) Commun Math Phys 20:167
Sargent M, Scully MO, Lamb WE (1974) Laser physics. Addison-Wesley, Reading
Sattinger DH (1980) Group theoretic methods in bifurcation theory. Lecture Notes Math, vol 762. Springer, Berlin
Schawlow AL, Townes CH (1958) Phys Rev 112:1940
Schiepek G (1999) Die grundlagen der systemischen thérapie. Theorie-Praxis-Forschung. Vandenhoeck und Ruprecht, Göttingen
Schleich WP (2001) Quantum optics in phase space. Wiley-VCH, Weinheim
Schmidt E (1908) Zur theorie der linearen und nichtlinearen integralgleichungen, Teil 3. Math Ann 65:370
Schöll E (2001) Nonlinear spatio-temporal dynamics and chaos in semiconductors. Cambridge University Press, Cambridge
Scully M, Lamb WE (1967) Phys Rev 159:208, (1968) 166:246
Segel LA (1969) J Fluid Mech 38:203
Sell GR (1979) Arch Ration Mech Anal 69:199
Shannon CE, Weaver W (1949) The mathematical theory of communication. Univ of Illin Press, Urbana
Smale S (1967) Bull AMS 73:747
Sounders PT (1980) An introduction to catastrophe theory. Cambridge University Press, Cambridge
Sparrow CT (1982) The Lorenz equations: bifurcations, chaos and strange attractors. Springer, Berlin
Staliunas K, Sanchez-Morcillo V, Gaul LJ (2003) Transverse patterns in nonlinear optical resonators. Springer, Berlin
Stratonovich RL (1963) Topics in the theory of random noise, vol 1, 1967 vol II. Gordon Breach, New York/London
Swift J, Hohenberg PC (1977) Phys Rev A 15:319
Swinney HL, Gollub JP (eds) (1981) Hydrodynamic instabilities and the transition to turbulence, Topics Appl Phys, vol 45. Springer, Berlin
Taylor GI (1923) Philos Trans R Soc Lond A 223:289
Thom R (1975) Structural stability and morphogenesis. Benjamin, Reading
Turing AM (1952) Philos Trans R Soc Lond B 237:37
Vavilin VA, Zhabotinsky AM, Yaguzhinsky LS (1967) Oscillatory processes in biological and chemical systems. Moscow Science Publ, Moscow, p 181
von Bertalanffi L (1950) Br J Phil Sci 1:134
von Bertalanffi L (1953) Biophysik des Fließgleichgewichts. Vieweg, Braunschweig
Walgraef D (1997) Spatio-temporal pattern formation. Springer, New York
Walls DF, Milburn GJ (1994) Quantum optics. Springer, Berlin

Weidlich W (2000) Sociodynamics. A systematic approach to mathematical modelling in the social sciences. Harwood Academic Publishers, Amsterdam
Weidlich W, Haake F (1965) Z Phys 186:203
Wigner EP (1932) Phys Rev 40:749
Wilson KG, Kogut J (1974) Phys Rep 12 C:75
Wolpert L (1969) J Theor Biol 25:1
Wunderlin A, Haken H (1981) Z Phys B 44:135
Zaikin AN, Zhabotinsky AM (1970) Nature 225:535

Books and Reviews

Haken H (1977) Springer series in synergetics, vols 1–ca 100. Springer, Berlin

Laser Dynamics and Delayed Feedback

Kathy Lüdge[1] and Benjamin Lingnau[2]
[1]Institut für Theoretische Physik, Technische Universität Berlin, Berlin, Germany
[2]Department of Physics, University College Cork, Cork, Ireland

Article Outline

Glossary
Definition of the Subject
Introduction
Dynamic Timescales and Relaxation Oscillations
Optical Feedback (Class-B Lasers)
Optical Feedback of Class-C Lasers
Optical Feedback of Two-State QD Lasers
Future Directions
Bibliography

Glossary

Laser dynamics Time evolution of the laser light within the cavity as well as the time evolution of the charge-carriers that participate in the radiative emission process.

Constant wave emission (cw) Laser emission with a constant intensity.

Relaxation oscillations (RO) If a laser is perturbed from its steady state (constant wave emission), it will relax back performing a pure exponential decay (*Class-A* laser) or by performing damped oscillations (*Class-B* laser); damping rate and oscillation frequency are used to quantify the dynamics.

***Class-C* laser** A laser, for which the timescale of the induced material polarization inside the gain material is on the same order of magnitude as the electron and the photon lifetime. These lasers have to be modeled with Maxwell-Bloch equations in contrast to *Class A* and *Class B* lasers where laser rate-equations are sufficient for the modeling.

Bifurcation qualitative change in the system's behavior under parameter changes.

1D bifurcation diagram Unique extrema detected within a time series of the laser intensity, plotted as a function of one system parameter (bifurcation parameter) to detect bifurcations; e.g., suddenly occurring harmonic oscillations (Hopf bifurcation) or a sudden birth of new solutions (saddle node bifurcation).

2D bifurcation diagram Classification of the system dynamics in a 2D parameter space; bifurcations form the boundaries between parameter regions of qualitative different dynamics (e.g., chaotic pulsing and periodic oscillations).

External cavity mode (ECM) Optical mode that can exist in an optical resonator that is formed by a laser and an external cavity (laser with optical self-feedback); with increasing feedback strength the number of ECMs increases and their stability changes.

Definition of the Subject

The subject of investigating the laser dynamics under optical feedback is to characterize the changes in the light emission dynamics, i.e., unravel the bifurcation structure, when a laser is perturbed by its own back-reflections. Since optical feedback can happen due to unwanted reflections in every optical setup, it is important to note, at first, the tolerance of a stable laser to perturbations by optical feedback. Secondly, also complex pulsations and chaotic emission can be useful for applications and thus there is a need to understand the conditions for an emergence of complex laser dynamics. Mathematically the subject is interesting because the dynamics is modeled by delay differential equations, where the delay is given by the time the light needs to re-enter the cavity. In this entry, we will compare different semiconductor laser systems which are quantum dot (QD) and a quantum well

A. Hutt, H. Haken (eds.), *Synergetics*,
https://doi.org/10.1007/978-1-0716-0421-2_729

Originally published in
R. A. Meyers (ed.), *Encyclopedia of Complexity and Systems Science*, © Springer Science+Business Media LLC 2020
https://doi.org/10.1007/978-3-642-27737-5_729-1

(QW) lasers with one more wavelength emission as well as nanolaser systems with very short photon lifetimes (*Class – C* laser). We will learn the importance of internal timescales of the gain medium and give some general rules about how the internal degrees of freedom simplify the emerging light emission under optical feedback.

Introduction

The effect of delay has been investigated in various systems and recent progress in this field is documented for instance in focus issues on delay systems (Erneux et al. 2017; Otto et al. 2019). In this chapter, the focus lies on the laser dynamics when a control signal from the laser is fed back into it after a time delay. This includes setups such as external optical feedback, which can be realized, for example, by a simple mirror in some distance of the laser which feeds back the emitted light into the laser cavity. Another implementation is by an external electronic circuit which feeds back a delayed electric signal to the laser device depending on the output of the laser. In this context, the interaction between the laser and the feedback signal becomes increasingly complex when the feedback time is similar to the internal laser timescale. Since in real-world applications parasitic reflections off surfaces and optical interfaces can never be suppressed completely, time-delayed feedback arises naturally in nearly every laser setup. Immense effort has been put into improving the resistance of semiconductor lasers towards optical instabilities caused by feedback (Lenstra et al. 2019) in applications where a steady laser output is required. At the same time, the guided exploitation of feedback leads to novel applications harnessing the dynamical complexity of the system. In both cases, a thorough understanding of the underlying physical and dynamical processes is required.

The dynamical complexity of lasers with feedback is an extremely broad topic which has attracted much interest in the past and today. A lot has been done in order to understand the bifurcation structure of lasers with optical feedback and this entry does not aim to give a complete overview. The interested reader is referred to the pioneering works that can be found in Mørk et al. (1992), Sano (1994), Simmendinger and Hess (1996), Ye and Ohtsubo (1998), Ohtsubo (1999); Erneux et al. (2000), Pieroux et al. (2000, 2001), Wolfrum and Turaev (2002), Yanchuk and Wolfrum (2004), Radziunas et al. (2006), Rottschäfer and Krauskopf (2007). A variety of experimental data exists, see for example (Mørk et al. 1990a; Li et al. 1993; Heil et al. 2003; Wünsche et al. 2008; Kim et al. 2014; Locquet et al. 2017) or results on integrated devices (Kane et al. 2015; Karsaklian Dal et al. 2017) which support and still inspire theoretical analysis. See, e.g., (van Tartwijk and Agrawal 1998; Soriano et al. 2013; Ohtsubo 2013) for an overview. General properties of delay systems, like the recurrence of solutions (Yanchuk and Perlikowski 2009), play a crucial role to understand the response of a laser to delayed feedback.

In delayed feedback systems, the interplay with noise sources as they usually appear due to spontaneous photon emission can lead to a variety of dynamical effects and unforeseen behavior. This issue will only shortly be touched in the course of this entry and the interested reader is referred to the literature: The effect of noise was studied in Mørk et al. (1988a, 1990b) to explain mode hopping in multimode lasers with feedback, in Otto et al. (2014) to find coherence resonance, or in Oliver et al. (2015), Jüngling et al. (2018), Porte et al. (2014) to quantify the consistency properties of the laser output via the evaluation of the time delay signature (Rontani et al. 2007, 2009). Related to that the linewidth reduction with optical feedback has attracted recent interest as well (Agrawal 1984; Flunkert and Schöll 2007; Jaurigue et al. 2016; Brunner et al. 2017). The complex feedback induced dynamics that is the focus of this entry is usually detrimental to the linewidth (Li et al. 1993; Lenstra et al. 1985), but the bifurcation analysis that we present below can predict the regions where the feedback leads to a stabilization.

An important step towards improving the resistance of semiconductor lasers to optical feedback and other perturbations was the fabrication and subsequent employment of self-assembled semiconductor quantum dots (QDs) as the active medium in lasers (Bimberg et al. 1999; Bimberg

and Pohl 2011). In addition to their reduced threshold current and temperature stability, QD lasers are more robust against such perturbations (Otto et al. 2010, 2012a; Globisch et al. 2012; Lingnau et al. 2013; Duan et al. 2019; O'Brien et al. 2004; Huyet et al. 2004). As we will see later on, this robustness is facilitated by a change of the internal dynamical timescales due to the presence of the QDs.

In recent years there has been a steady push towards exploitation of complex dynamics induced by delayed feedback in laser systems. Right now those laser systems with delay find great attention in applications for information processing, i.e., all-optical reservoir computing (Argyris et al. 2018; Bueno et al. 2017; Kuriki et al. 2018; Nguimdo et al. 2017), as random number generators (Verschaffelt et al. 2017; Reidler et al. 2009; Oliver et al. 2011), in chaotic LIDAR systems (Lin and Liu 2004; Cheng et al. 2018), or in nanometric sensing (Choi et al. 2019).

This review article will discuss the interrelation between dynamic degrees of freedom within the laser gain medium and the stability of the laser if subjected to optical self-feedback. We will show that the response becomes less complex and more controllable with every additional timescale that is added to the system dynamics.

In the following, we will first introduce a rate equation model for nanostructured laser gain media in section "Dynamic Timescales and Relaxation Oscillations" and discuss the role of the charge carrier relaxation timescales that directly or indirectly participate in the laser process and, for their part, control the laser response to perturbations. Second, different semiconductor laser with complex gain media and their response to optical feedback will be compared in section "Optical Feedback (Class-B Lasers)" and the nonnegligible dynamic effect of a model reduction will be discussed. The effect of feedback on devices with nanoscale dimensions, where the photon lifetime starts to be on the same order of magnitude as the timescale of the microscopic polarization, will be discussed in section "Optical Feedback of Class-C Lasers" before we come to quantum dot lasers with simultaneous two-color emission and their response to feedback in section "Optical Feedback of Two-State QD Lasers."

Dynamic Timescales and Relaxation Oscillations

The response of dynamical systems towards perturbations depends sensitively on the internal dynamical timescales of the system itself. A universal example of this is a driven damped oscillator, showing resonance effects when driven close to its natural frequency, with the resonance overshoot depending on its damping. Most semiconductor lasers possess an intrinsic resonance frequency and associated damping due to the presence of relaxation oscillations (ROs) – oscillations in the energy exchange between the intracavity photons and the available gain. In the laser classification scheme due to Arecchi et al. (1984), such lasers are labeled *Class-B*. These intrinsic timescales can be readily observed in the laser response to delayed feedback. Most dynamical features occur at frequencies related to the RO frequency, and complex dynamics can be observed if the delay time is in the order of the RO frequency. The minimum feedback strength required to induce complex dynamics is closely related to the damping of the ROs, with stronger damping usually leading to a more robust system (Helms and Petermann 1990). It is therefore natural to assume that the introduction of additional timescales into a dynamical system that is subjected to delayed feedback changes its response. We want to illuminate this effect for two examples: At first, a QD laser that has more than one carrier type and thus an additional relaxation channel with an associated dynamic timescale. Secondly, a *Class-C* laser where the timescale of the induced material polarization plays a crucial role for the dynamics.

Quantum-dot lasers differ from conventional semiconductor lasers in the dimensionality of the active medium. Whereas in quantum-well lasers the active medium is quasi-two-dimensional, QDs are effectively zero-dimensional systems, embedded in a two-dimensional charge-carrier reservoir. The active optical transition is thus formed by deeper lying atom-like energy states which have to be gradually filled by surrounding charge-carriers, see Fig. 1a. This additional scattering pathway introduces an extra timescale in the dynamic laser system (Table 1).

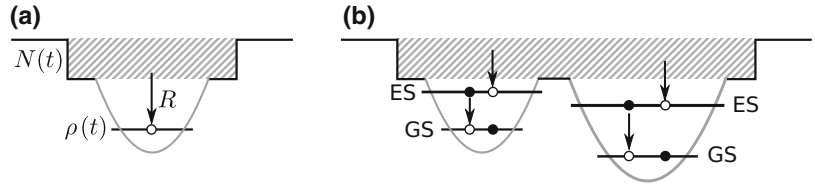

Laser Dynamics and Delayed Feedback, Fig. 1 (**a**) Sketch of the energy levels in the simplest quantum-dot (QD) laser. The QD occupation probability ρ increases due to inscattering of charge carriers from the reservoir states, N, with the scattering rate R. The QD transitions are the active optical transitions. (**b**) More realistic depiction of the quantum dot structure. Quantum dots with different sizes have different energy levels. In addition to the ground state (GS), one or more excited states (ES) can exist

The minimal model to describe a QD laser is thus at least three-dimensional, as we need to consider the dynamics of the charge-carrier number in the reservoir, $N(t)$, the occupation of the QD states, $\rho(t)$, and the amplitude of the cavity electric field, $E(t)$ (the intracavity photon number is proportional to $|E(t)|^2$):

$$\dot{N} = J - \frac{N}{T_1} - R\left(\rho^{\mathrm{th}} + d\left(N - N^{\mathrm{th}}\right) - \rho\right), \quad (1a)$$

$$\dot{\rho} = R\left(\rho^{\mathrm{th}} + d\left(N - N^{\mathrm{th}}\right) - \rho\right) - \frac{\rho}{T_{\mathrm{sp}}} - \left[g\left(\rho - \rho^{\mathrm{th}}\right) + \frac{1}{T_{\mathrm{ph}}}\right]|E|^2, \quad (1b)$$

$$\dot{E} = \frac{g}{2}(1 - i\alpha)\left(\rho - \rho^{\mathrm{th}}\right)E + \frac{K}{T_{\mathrm{ph}}}e^{-iC}E(t - \tau) \quad (1c)$$

The parameters entering the equations are explained in Table 1. In thermodynamic equilibrium, the in- and out-scattering processes between charge carrier states at different energies obey a detailed-balance relation, i.e., their ratio is given by a Boltzmann factor that determines the equilibrium occupation of the charge-carrier states. For the quasi-equilibrium within a pumped laser, this also applies and in the presented minimal QD laser model it enters via the coefficient d. The coefficient $d = \frac{\partial}{\partial N}\rho^{\mathrm{eq}}\big|_{\mathrm{th}}$ describes the change of the quasi-equilibrium QD occupation with respect to the normalized reservoir density close to the threshold. With increasing charge-carrier number in the reservoir, this balance is shifted towards higher occupation, which is included in the minimal QD laser model in a linearized fashion. An important feature of QD lasers is the imperfect clamping of charge-carriers above threshold (Lüdge and Schöll 2009; Röhm et al. 2015), i.e., the quantum dots can never be filled completely.

Laser Dynamics and Delayed Feedback, Table 1 Parameters used in this chapter and their meaning

Symbol	Meaning
J	Normalized pump current
T_1	Charge-carrier lifetime
T_2	Induced polarization lifetime
T_{ph}	Cavity photon lifetime
T_{sp}	QD lifetime
R	QD scattering rate
N^{th}	Threshold reservoir density
ρ^{th}	Threshold QD occupation probability
d	Detailed balance coefficient
g	Normalized gain coefficient
α	Amplitude-phase coupling parameter
K	Optical feedback strength
C	Feedback phase
τ	Feedback delay time

The delayed optical feedback enters the equations via the delayed optical field, $E(t - \tau)$ in Eq. (1c). This modeling approach was first proposed independently by Rosanov (1975), and Lang and Kobayashi (1980). Within this approach, only a single round-trip in the external cavity formed between the laser facet and the external mirror is taken into account. For strong external reflectivities, multiple round-trips become important and the treatment of the feedback field must be

extended (Schelte et al. 2019). The optical feedback is characterized by the feedback strength K, the time delay τ, and the feedback phase C. The effect of the feedback and the effect of α will be discussed in the next section. For now we set $K = 0$ which completely decouples the dynamics of the phase of the electric field and leaves the intensity $|E(t)|^2$ as the only important dynamic quantity for the field inside the cavity.

Depending on size and composition of the QDs, the effective charge-carrier scattering rate R can vary significantly. We therefore treat it as a free parameter and discuss its impact on the dynamic response of the QD laser in Fig. 2. This allows us to identify different dynamic regimes and the important dynamic timescales of a QD laser system, Eq. (1a–1c), as a function of R. The internal timescales and frequencies can be extracted from the Lyapunov exponents, which are the eigenvalues of the Jacobian of the right hand side of the differential equation system. Real and imaginary part of the dominating eigenvalue λ determine the respective intrinsic relaxation oscillation frequencies and damping rates, i.e., Im $\lambda = \omega_{RO}$ and Re $\lambda = \Gamma_{RO}$. Figure 2 shows their dependence on the scattering timescale R. As can be seen, the presence of the additional scattering process strongly influences the RO timescales. The most striking feature is the maximum of the RO damping and the vanishing RO frequency at values of $R \approx 10^{11}\ s^{-1}$. For these moderate scattering rates,

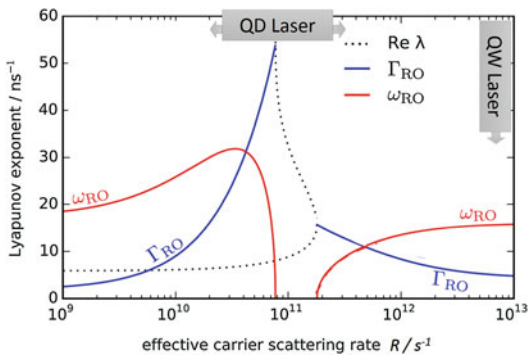

Laser Dynamics and Delayed Feedback, Fig. 2 Relaxation oscillation damping Γ_{RO} (blue) and frequency ω_{RO} (blue) determined from the minimal QD laser model given in Eq. (1a–1c). (Reproduced from Lingnau (2015) with permission from Springer)

the ROs are overdamped and the eigenvalues become purely real. For higher values, both charge-carrier types are closely coupled and the dynamics has only one effective degree of freedom in the charge-carrier dynamics. For much smaller values of R, the carrier reservoir N is only weakly influenced by the dynamics of ρ and remains nearly constant. Thus, it acts as a constant reservoir for the active charge-carriers and again the charge-carrier dynamics is effectively one-dimensional. In the intermediate range of R, where we cannot neglect the dynamics of either charge-carrier species, the internal gain dynamics is more complex but leads to a very simple dynamic response, i.e., without visible relaxation oscillations. At the same time, the RO damping is largest close to this parameter range, which explains the resilience of QD lasers towards external perturbations. This is usually known for *Class-A* lasers, which however do not have any independent degree of freedom of the carrier dynamics. While we have explicitly discussed the case of a QD laser, we note that in most cases an additional slow dynamic scattering or charge-carrier transport process will lead to dynamic equations similar to Eq. (1a–1c). The presence of such a slow dynamic charge-carrier process will thus lead to similar dynamic behavior.

As we will see, the laser response to delayed optical feedback is not as complex in QD lasers as in quantum-well (QW) lasers. QW lasers can be thought of to operate in the limit of $R \to \infty$, with only one type of charge-carriers present and a near-instant equilibration. In this limit, the minimal QD laser model reduces to the QW laser equations:

$$\dot{N} = J - \frac{N}{T_1} - \left[g\left(N - N^{th}\right) + \frac{1}{T_{\mathrm{ph}}}\right]|E|^2 \quad (2a)$$

$$\dot{E} = \frac{g}{2}(1 - i\alpha)\left(N - N^{th}\right)E + \frac{K}{T_{\mathrm{ph}}}e^{-iC}E(t-\tau) \quad (2b)$$

These equations are of Rosanov-Lang-Kobayashi-type, and they constitute the fundamental model for the description of *Class-B* lasers with weak time-delayed optical feedback.

Optical Feedback (Class-B Lasers)

As already mentioned in the last section, the most important timescale when it comes to the response of a laser gain medium to optical perturbations is the relaxation oscillation frequency and damping, as they describe how the laser relaxes to its steady state. While a *Class-A* laser just reacts with an exponential decay of its intensity, the so-called *Class-B* laser performs damped oscillations towards the steady state. We now illuminate three examples of semiconductor lasers: A conventional quantum well (QW) laser (*Class-B*) with one carrier type as given in Eq. (2a–2b); a quantum dot (QD) laser that has more than one carrier type and thus an additional dynamic degrees of freedom and is described by the minimal model in Eq. (1a–1c) and a QD laser that is described on a different more complex level of the laser modeling hierarchy.

The time-delayed feedback term introduced already in the last section will now be discussed in detail. A sketch of the setup is shown in Fig. 3. For coherent optical feedback, the response will depend on the phase of the electric field. The feedback phase C gives the optical phase shift accumulated over one feedback round-trip time and determines whether the light fed back into the laser interferes destructively or constructively with the cavity field. The dynamics under time delayed optical feedback has been shown to sensitively depend on the feedback phase, especially in the regime of short delays (Heil et al. 2003) which we assume in this entry. Short delay, in this context means that the roundtrip time in the external cavity τ is not larger than the RO period $T = 2\pi/\omega_{RO}$. The most general formulation of the dynamic equation of the electric field then reads (van Tartwijk and Agrawal 1998; Lingnau et al. 2012, 2013):

$$\dot{E}(t) = \left[G(\omega, t) - i\Delta\omega_0 - \frac{1}{2T_{\text{ph}}}\right]E(t) + \frac{K}{T_{ph}}e^{-iC}E(t-\tau), \tag{3}$$

where $K \in [0, 1]$ is the feedback strength, denoting the ratio of the light lost through the cavity mirrors that is coupled back into the cavity. The electric field is expressed in a rotating frame with frequency $\Delta\omega_0$, such that its phase velocity vanishes in the steady-state. The external cavity feedback time τ and the feedback phase C are in principle both determined from the optical path length of the feedback section, but since the feedback phase is much more sensitive to changes in τ, it is treated as an independent parameter (Heil et al. 2003). The gain $G(\boldsymbol{\omega}, t)$ is in general a complex valued function determined by the microscopic polarization of the gain medium. Its real part, $\text{Re}[G(\boldsymbol{\omega}, t)]$, describes the amplitude gain of the electric field, and $\text{Im}[G(\boldsymbol{\omega}, t)]$ is the change of the instantaneous electric field frequency due to carrier-induced refractive index changes. The modeling of $G(\boldsymbol{\omega}, t)$ can be performed on different levels of complexity. Very common is the introduction of an amplitude-phase coupling or Henry parameter, α, which describes the instantaneous coupling of the electric field frequency to the optical gain. The amplitude phase coupling factor α is defined as

$$\alpha = -\frac{\partial \text{Im}[G(\boldsymbol{\omega})]/\partial N}{\partial\, \text{Re}\,[G(\boldsymbol{\omega})]/\partial N} \tag{4}$$

and significantly simplifies the dependence of the complex gain $G = \text{Re}\ G + i\text{Im}\ G$ on the carrier density N. The simplified dynamic equation for the electric field then reads (van Tartwijk and Agrawal 1998; Ohtsubo 2013; Lingnau et al. 2013):

$$\dot{E}(t) = \left[\text{Re}\ G(\omega) - \frac{1}{2T_{\text{ph}}}\right](1 - i\alpha)E(t) + \frac{K}{T_{\text{ph}}}e^{-iC}E(t-\tau). \tag{5}$$

The amplitude phase coupling is an important parameter when discussing the sensitivity of the laser to optical feedback and for determining the

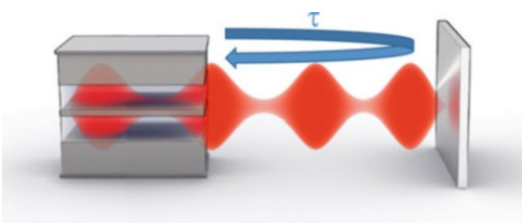

Laser Dynamics and Delayed Feedback, Fig. 3 Sketch of a semiconductor laser that is subjected to optical self-feedback with a delay length of τ

structure of the dynamical solutions. High values of α generally lead to highly complex dynamics. The general solution structure of the laser with delayed optical feedback is largely formed by the so-called external-cavity modes (ECMs). These modes denote the solutions of the combined system of the laser and the external cavity with constant intensity. The resonant frequencies of the isolated laser cavity and the external cavity are in general different. The presence of the feedback thus introduces a frequency shift of the laser output away from the free-running lasing frequency. The ECM solutions of the form $E(t) = E_0 e^{-\Omega t}$ are located on an ellipse in the phase space spanned by the optical gain ReG and the ECM frequency, Ω, as we will discuss further in section "Optical Feedback of Class-C Lasers." If the gain is assumed to be linear, i.e., Re $G = g(N - N^{th})$, which is a common and very good assumption for laser operation (van Tartwijk and Agrawal 1998; Ohtsubo 2013; Mørk et al. 1988a; Chow and Koch 1999), the charge-carrier number N and Ω can be used for the phase space projection of the ellipse.

The dynamics of the complex gain G in a QW laser with a gain medium consisting of only one carrier type (same dynamics as observed from the minimal QD laser model Eq. (1a–1c) for large R) can be closely described by a constant α. The induced frequency shift then proportionally and instantly follows the dynamics of the optical gain. In a QD laser with finite R, both resonant and nonresonant carriers within different states must be considered, and thus the gain dynamics are more complex due to the additional dynamic degrees of freedom. The minimal QD laser model takes the dynamics of the nonresonant carriers into account but still assumes an α-factor for the refractive index changes. Figure 4 compares the reaction to feedback for both laser types. There, the bifurcation diagram, i.e., the unique extrema found in a time series of the laser intensity for a given feedback strength K, is displayed as a function of K. Additionally, two timeseries are plotted as insets in Fig. 4b which illustrate the increase in complexity with K. Comparing both bifurcation diagrams of the QW and the QD laser, it can be seen that the differences in the charge-carrier dynamics directly influence the dynamics.

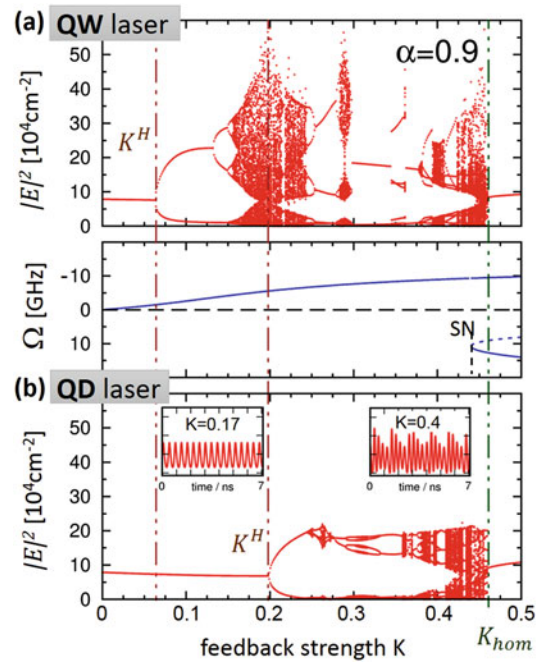

Laser Dynamics and Delayed Feedback, Fig. 4 1D-Bifurcation diagram of two different lasers if subjected to optical self-feedback. It shows the impact of different RO damping exemplarily for a QW laser (**a**) and a QD laser (**b**). Insets in (**b**) show time series of the QD laser for two K values. Vertical dash-dotted lines indicate the critical feedback strength K^H and the homoclinic bifurcation K_{hom}. *SN* indicates the saddle-node bifurcation where new ECM solutions (one stable and one unstable) are born. $C = \pi$, $\tau = 160$ ps. (Reproduced from Otto et al. (2010) with permission from Wiley)

The most significant difference is the value of the feedback strength K at which the laser starts to show intensity oscillations. This bifurcation point is the critical feedback strength. It is labeled K^H in Fig. 4. It is much larger for the QD laser, which means this laser can withstand a higher amount of feedback before it starts to show intensity oscillations. Instead, the point where the two lasers switch back to stable emission on the next ECM solution via a homoclinic bifurcation at K_{hom} only marginally depends on the gain model (vertical dash-dotted line in Fig. 4). The reason lies in the solution structure formed by the ECMs of the electric field equation which are also plotted as blue lines in Fig. 4 (center). At a K value of 0.45 two new ECM solutions appear: one stable (solid line) and one unstable (dashed). This bifurcation point is called saddle node bifurcation and

indicated with *SN* in Fig. 4 (center). The ECM solutions themselves are the same for both lasers, as long as they have the same α-factor, while the instability of the first solution (the Hopf bifurcation at K^H) strongly depends on the relaxation oscillation timescales and thus on the internal carrier dynamics. It can be analytically shown (Otto et al. 2012a, b; Globisch et al. 2012) that the critical feedback strength K^H, i.e., the Hopf bifurcation point at which the stable ECM with frequency Ω is destabilized, can be approximated via:

$$K^H = \frac{2\Gamma^{RO} T_{\mathrm{ph}}}{\sqrt{1+\alpha^2}\,(1-\cos(\omega^{RO}\tau))\cos(\pi - C - \Omega\tau + \arctan(\alpha))} \tag{6}$$

Here, ω^{RO} is the frequency of the relaxation oscillations and Γ^{RO} their damping rate. Similar equations for the critical feedback level have already been derived in Helms and Petermann (1990), Mørk et al. (1988b), Binder and Cormack (1989), however, without treating the dependence on the feedback phase. For long feedback delay, the phase is hard to control. It is therefore useful to estimate the smallest value of K^H (C) which is reached for $C = -\Omega\tau + \pi + \arctan\alpha \approx \pi + \arctan\alpha$ (see for example Fig. 5 for the evolution of the stability border, i.e., transition from blue to white, as a function of C). Thus, the laser is guaranteed to be stable for

$$K^H < K^H_m = \frac{\Gamma^{RO} T_{\mathrm{ph}}}{\sqrt{1+\alpha^2}}. \tag{7}$$

This stability condition was derived for a quantum-well laser by Mørk et al. (1992) and previously suggested by Helms and Petermann (1990) as a simple analytical criterion for tolerance with respect to optical feedback. If the laser operates at the minimum linewidth mode (Levine et al. 1995), a slightly different minimal critical feedback strength is derived from Eq. (6) and is given by $K^H_m = \Gamma^{RO} T_{\mathrm{ph}} \sqrt{1+\alpha^2}/(\alpha^2 - 1)$.

From Eqs. (6) and (7), it becomes clear that the less complex QW laser with its small RO damping is more susceptible to back reflections while a QD laser, engineered such that it shows very strong RO damping, has a very high feedback tolerance.

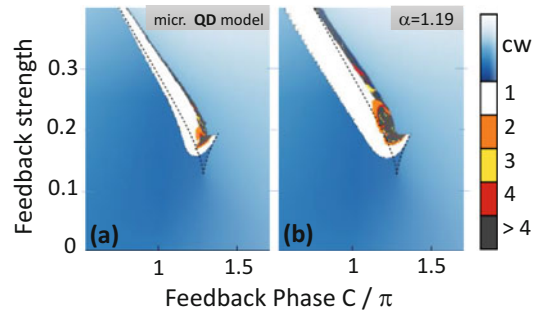

Laser Dynamics and Delayed Feedback, Fig. 5 Comparison of the feedback induced dynamics for a full microscopic QD laser model (Lingnau et al. 2013) with many degrees of freedom of the charge carriers (**a**) and the corresponding QD laser model that uses an effective α-factor description (**b**). The blue color encodes the intensity of the stable laser emission while other colors indicate the number of unique maxima observed in the pulsating time series. Dashed lines represent the saddle-node (SN) bifurcation along which a new ECM solution is born. $\tau = 100\ ps$

For the latter, all involved carriers relax on similar timescale and the number of dynamic degrees of freedom is higher.

The numerical and analytical results on the QD laser presented so far have been obtained for the minimal model shown in Eq. (1a–1c) with two carrier types, N and ρ. If a more sophisticated modeling approach is chosen, the equations can be extended to a more microscopic model with a higher number of degrees of freedom of the carriers. The details are discussed in Lingnau et al. (2013) and we just mention some important ingredients. Besides the pure existence of more confined carrier levels and thus more dynamic equations, this model also considers dynamic changes in the imaginary part of the material gain Im G, i.e., the refractive index can show dynamics on its own timescale. Surprisingly, the QD laser that is described by the much more complex model shows less complex response to optical feedback. This is visualized in Fig. 5a, b where the laser dynamics numerically obtained from the microscopic model and the minimal model with constant α-factor are compared. The dashed lines in Fig. 5 represent the saddle-node (SN) bifurcation along which a new ECM solution

is born. The critical feedback strength where the first ECM loses stability can be seen along the transition from blue (cw operation) to white areas (regular pulsations with one maximum). It can be seen that taking into account the contribution of the refractive index dynamics in (a) leads to a stabilization of the dynamics and consequently less regions with complex dynamics (orange and grey colors) occur. If the charge-carrier induced frequency shift is approximated by an α-factor as done in (b) (compare also Eqs. (3) and (5)), the separate time evolution of the imaginary part of the gain is neglected, and the gain dynamics becomes less complex. As a result, however, the dynamic response to optical feedback becomes more complex (Fig. 5b) and we instead observe a simplification of the dynamic response for the higher internal complexity (Fig. 5a). The effect of increasing the susceptibility to optical perturbations by a model reduction occurs to be rather general and has to be kept in mind.

At the borders between stable emission and regions with complex dynamics (between blue and grey in Fig. 5), bifurcations occur and the laser switches to emission at the next ECM, i.e., emission at a different wavelength. For the pump current chosen here this is a homoclinic bifurcation. This transition was already mentioned in Fig. 4 and marked with K_{hom}. It defines the point in parameter space where the laser re-stabilizes. Around this transition point where the laser just started to emit at the new frequency, the *cw* solution is only weakly stable and thus very susceptible to noise. To get an impression of the dynamics in phase space, Fig. 6a, b visualizes the trajectory after a noise perturbation in the vicinity of the homoclinic bifurcation. These noise-induced pulsations are no stable solutions of the delay differential equation but they follow parts of an attractor that has been stable before. As such the interspike interval between pulses, indicated by T_{ISI} in Fig. 6a, changes stochastically. Interestingly an optimal noise strength can be found, where the noise-induced pulsations occur most regularly, i.e., the distribution of interspike intervals T_{ISI} becomes relatively sharp. This effect – called coherence resonance – occurs due to the nonlinearity of the light-matter interaction and is a universal effect in excitable nonlinear systems in the presence of noise (Lindner et al. 2004). Experimentally, these kind of pulses have been observed, e.g., in Heil et al. (2003, 2001). Note that for higher laser pump currents, the bifurcation that causes the laser to start stable emission at the newly born ECM changes from a homoclinic bifurcation to a boundary crisis (Otto et al.

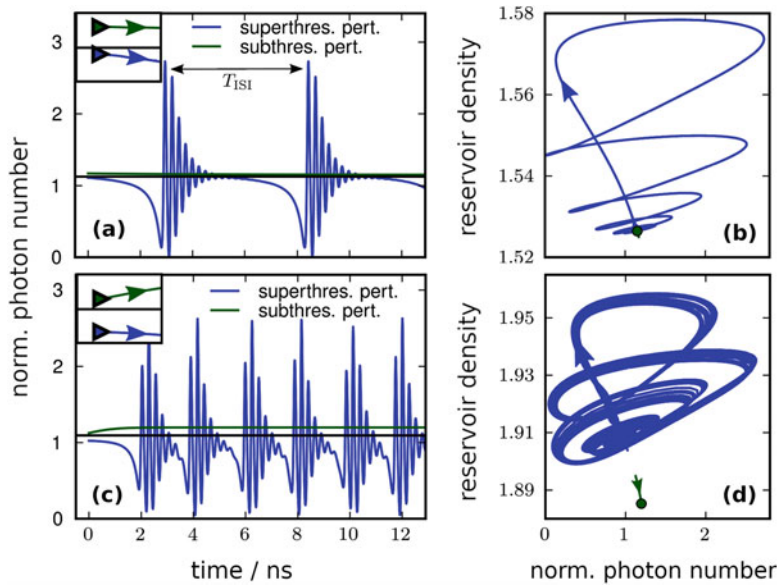

Laser Dynamics and Delayed Feedback, Fig. 6 Trajectories of a QD laser with optical feedback after noise excitation plotted as a function of time (**a**, **c**) and as a phase space projection (**b**, **d**). (**a**, **b**): close to the homoclinic bifurcation that was discussed in Fig. 4;(**c**, **d**): close to the boundary crisis that exists for higher pump currents. $C = \pi$, $\tau = 160\,ps$. (Reprinted with permission from Otto et al. (2014) ©The Optical Society)

2014). Nevertheless, coherence resonance can also be found here (Otto et al. 2014). Figure 6c shows the chaotic pulse packages induced by a superthreshold perturbation right after the boundary crisis of the chaotic attractor. The green circle in Fig. 6d indicates the stable ECM solution that is perturbed by the noise. The path of the trajectory along the former chaotic attractor can be seen in the phase space projection in Fig. 6d.

Optical Feedback of Class-C Lasers

So far the discussion was limited to *Class-B* lasers that were solely described by the carrier and photon dynamics. However, the light matter interaction is driven via the microscopic polarization within the medium. For the *Class-B* laser, the optical gain is assumed to instantaneously follow the available charge-carriers in the optically active transitions. The stimulated emission rate is assumed to adiabatically follow the charge-carrier and electric field dynamics and thus does not need to be explicitly considered as a dynamical variable. With the recent success and progress of semiconductor epitaxy and wafer processing, the realization of very small devices has become possible, down to lasers with cavity dimensions in the order of the wavelength of the laser light. Due to the small size of their cavity, those nanolasers have a strong spontaneous emission and relatively short photon lifetimes. While the stronger photon losses are compensated by an increase of the optical gain, the photon lifetime now is comparable to the lifetime of the induced material polarization. The active laser medium can thus no longer be treated as a simple source of instantaneous optical gain. Rather, the field emitted by stimulated emission of light becomes a dynamical variable itself. When all three timescales (electrons, polarization, photons) end up to be of a similar order of magnitude, the fundamental physics of the laser system change. These nanolasers, so-called *Class-C* lasers, exhibit special behavior like the second laser threshold (Haken 1986), after which self-pulsing of the laser emission occurs, but also react differently to optical feedback (Lingnau et al. 2019).

Class-C lasers can be described by the Maxwell-Bloch equations (MBEs), which explicitly include the dynamics of the induced material polarization (Chow and Koch 1999; Haken 1986). The delayed optical feedback extends the MBEs by an additional driving term in the electric field to include the effects of time-delayed optical feedback. Since we now want to focus on the effect of the polarization, a QW laser with just one carrier type N is modeled.

The normalized MBEs with delayed optical feedback are given by:

$$\dot{N} = \frac{1}{T_1}(J - N - 2c\,\mathrm{Re}\,[PE^*]), \tag{8}$$

$$\dot{P} = \frac{1}{T_2}[EN - (1 - i\alpha)P] - i\omega_0 P, \tag{9}$$

$$\dot{E} = \frac{1}{T_{\mathrm{ph}}}\left[cP - \frac{1}{2}E\right] - i\omega_0 E + \frac{K}{T_{\mathrm{ph}}}e^{-iC}E(t-\tau). \tag{10}$$

Here, the additional timescale T_2 of the induced polarization enters the equations. The stimulated emission is now given by cP, with a normalization constant $c = 1 + (2\alpha/(2 + T_2/T_{\mathrm{ph}}))^2$. The parameter α in Eq. (9) measures the frequency difference between the gain maximum and the cavity mode. For the case of very small T_2, when the MBE model reduces to the $Class - B$ laser model, it takes the role of the α-factor that we introduced in the last section.

The lifetime T_2 of the polarization plays a crucial physical role as it determines the gain bandwidth of the laser transition, with long lifetimes producing a sharp, narrow gain peak. Consequently, with increasing T_2 the gain bandwidth becomes narrower and the possible deviation of the lasing frequency from the transition frequency is limited. This reduces the number of possible ECMs in *Class-C* lasers with a single optical transition. It is depicted in Fig. 7 for four different values of the dephasing time T_2, which is the lifetime of the polarization. The rotating wave solutions of the above equation, i.e., the external cavity modes (ECMs), are shown as open circles in the plane of charge-carrier number, N, and ECM frequency, Ω. It underlines the impact of the additional dynamic equation and it can be seen that for $T_2 = 0$ we recover the case of a *Class-B* laser and

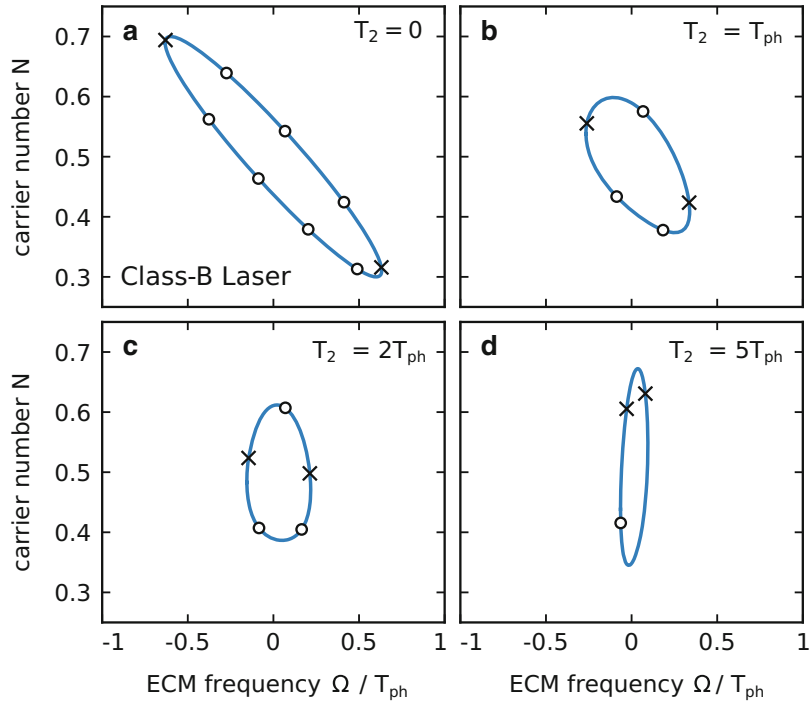

Laser Dynamics and Delayed Feedback, Fig. 7 External cavity solutions (ECMs) of a laser with optical self-feedback plotted as a function of ECM frequency Ω and carrier number *N*. (**a**) *Class-B* laser with dephasing times $T_2 = 0$, (**b**–**d**): *Class-C* laser $T_2 = T_{ph}$, $T_2 = 2T_{ph}$, and $T_2 = 5\ T_{ph}$. Solid closed lines denote all possible solutions in the (Ω, *N*)-plane while open circles denote solutions obtained for a specific feedback phase $C = \pi$. Crosses mark saddle node (SN) bifurcations where new solutions are born. The connection between the crosses separates the ellipse into regions where the solutions are born unstable (upper part) and stable (lower part). Other parameters: $K = 0.2$, $\tau = 20T_{ph}$, $\alpha = 3$. (Reprinted from Lingnau et al. (2019) with permission from Royal Soc)

observe the rotated ellipse in phase space on which the ECM solutions can exist. For larger values of T_2, the number of solutions (open circles) is decreased while they all move closer together. Furthermore, the effect of the amplitude-phase coupling α, which usually leads to a high aspect ratio of the ellipse for the *Class – B* laser, is reduced as can be seen by comparing the circles in Fig. 7. The possible ECM solutions appear in a more symmetric shape around $\Omega = 0$ for larger T_2 times.

The numerically obtained response of the *Class-C* laser to optical feedback is plotted in Fig. 8 for the four different dephasing times T_2. The number of unique maxima is encoded in the color and thus dark colors indicate complex dynamics and chaos. While a *Class-C* laser is usually known for its second laser threshold after which it emits chaotic light without any perturbations, it appears to be much more stable than a *Class-B* laser if it is subjected to optical feedback (compare Fig. 8a, d).

In the limit of $T_2 \to 0$ (Fig. 8a), the MBEs reduce to the conventional Lang-Kobayashi equations, which show well-known bifurcation cascades and eventually can produce optical chaos. For this case we also plotted the two bifurcations that organize the parameter space in Fig. 8a; the Hopf bifurcation at which the first ECM destabilizes, called critical feedback strength in section "Optical Feedback (Class-B Lasers)," is plotted in blue. The saddle node (SN) bifurcation where the next ECM is born (compare Fig. 4 (center) where the SN bifurcation is marked) is plotted in red. For higher values of T_2, the dynamical regions in the feedback parameter undergo a transformation.

Quite counter-intuitively, the addition of another dynamic dimension to the system can have a stabilizing effect on its dynamics. This

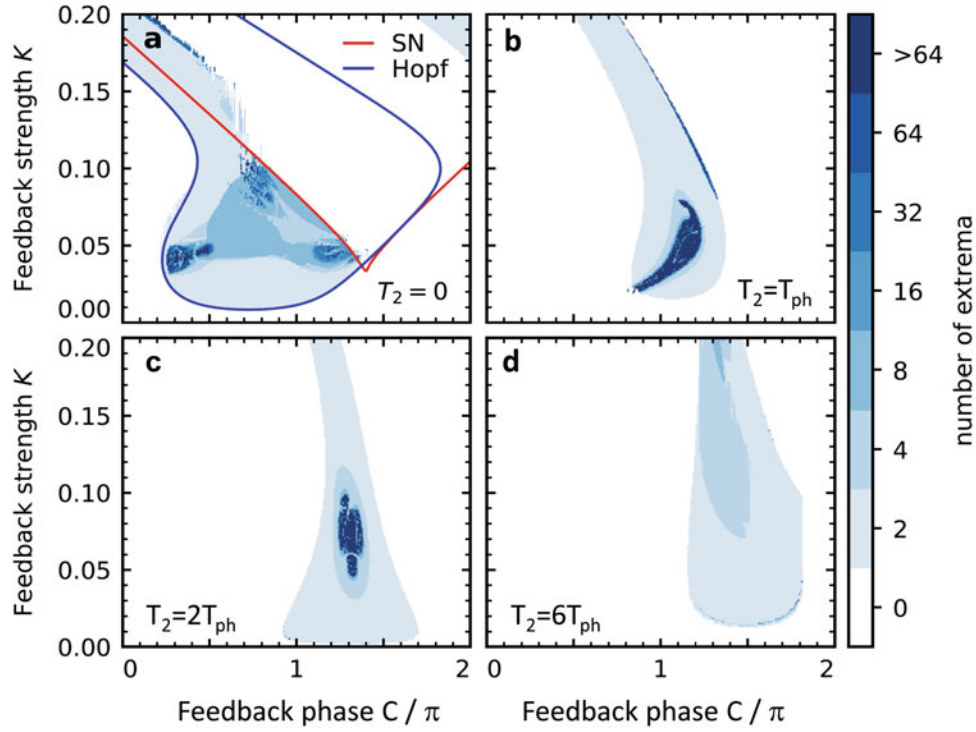

Laser Dynamics and Delayed Feedback, Fig. 8 Dynamics observed numerically in the laser emission for a small feedback delay time $\tau = 10T_{\mathrm{ph}}$ in the plane of feedback strength K and feedback phase C. (**a**): *Class-B* laser with $T_2 = 0$, (**b**–**d**): *Class-C* laser with $T_2 = T_{ph}$, $T_2 = 2T_{ph}$, and $T_2 = 6T_{ph}$. Shown are the number of unique intensity extrema (color-coded), where zero extrema correspond to CW operation, and nonzero values to periodic or complex dynamics. In panel (**a**), we show saddle-node (SN, red line) and Hopf (blue line) bifurcation curves of the first ECM, obtained by numerical path continuation. Other parameters: $J = 5$, $\alpha = 3$. (Adapted from Lingnau et al. (2019) with permission from Royal Soc)

can be seen for increasing values of T_2, for which the dynamics becomes strikingly less complex, and only small regions of chaos remain (see Fig. 8c, d). Following the arguments of the last sections, the explanation again lies in the increased dynamic degrees of freedom. Having the possibility for a dynamic response with independent polarization dynamics, a chaotic response becomes unlikely (Fig. 8d). Driving a dynamic system into chaos with external perturbations can thus be seen to become harder with higher phase space dimension which vary on a dynamic timescale similar to the rest of the system. This conclusion is found to be quite robust with respect to parameter changes.

To get some insights into the impact of the delay time τ, we visualize the dynamics of the $Class - C$ laser in another parameter plane spanned by T_2 and the delay time τ in Fig. 9a. Again the dark colors represent a high number of different maxima observed in the timeseries and thus more complex dynamics. As expected, small values of T_2 reproduce the dynamics of a *Class-B* laser and we find complex dynamics. Between $0.5\ T_{\mathrm{ph}} < T_2 < 2T_{\mathrm{ph}}$ only continuous wave or periodic emission is found, while dynamics with a higher number of unique maxima appears again for larger values of T_2. A high number of unique extrema is not sufficient to classify the dynamics into (quasi-)periodic or chaotic behavior. We therefore calculate the largest nontrivial Lyapunov exponent which gives us a value for the speed at which two adjacent trajectories diverge in time. A Lyapunov exponent with a positive value (plotted in red in Fig. 9b) indicates chaos (sensitive dependence on initial conditions), while negative values indicate stable dynamics. A value of zero is an indication for a periodic solution. We can thus conclude from

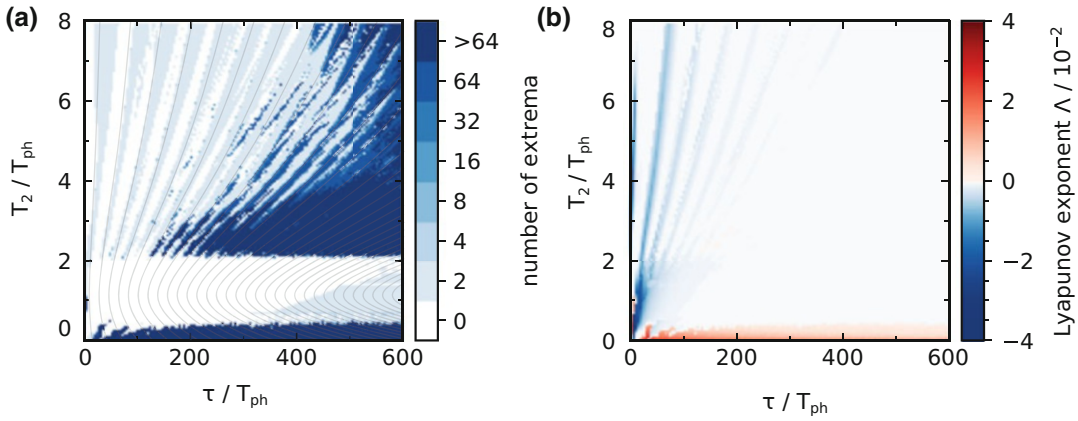

Laser Dynamics and Delayed Feedback, Fig. 9 Dynamics of a *Class-C* laser in dependence of the feedback delay time τ and the polarization dephasing time T_2. (**a**) Color code represents the number of unique extrema, thin grey lines show resonances of the relaxation oscillation frequency, $\tau = \left(n + \frac{1}{2}\right) \frac{2\pi}{|\mathrm{Im}\lambda|}$, with $n \in \mathbb{N}$. (**b**) largest Lyapunov exponent Λ. Other parameters: $J = 10$, $\alpha = 3$, $K = 0.1$, $C = \pi$. (Adapted from Lingnau et al. (2019) with permission from Royal Soc)

Fig. 9 that optical chaos only occurs for the *Class-B* laser case, mainly for high feedback delay times τ, while *Class-C* laser remain stable or, for large dephasing times, show quasi-periodic dynamics.

Optical Feedback of Two-State QD Lasers

Semiconductor lasers which are emitting on two distinct laser modes are a highly attractive application of laser dynamics due to the interaction of those modes. Prime examples of such laser systems include vertical-cavity surface emitting lasers (VCSELs), which due to their circular cavity symmetry support two orthogonally polarized modes (Olejniczak et al. 2009; Virte et al. 2012), or carefully designed laser cavity emitting on more than one wavelength (Osborne et al. 2009, 2012). Such two-mode lasers show a variety of complex dynamics related to the switching between the two laser modes in various setups including when subjected to time-delayed feedback (Osborne et al. 2012; Sciamanna et al. 2003). Their dynamics is governed by the energy exchange and gain competition between the two modes, which can be influenced by the external perturbation. Different realizations of two (or multi) mode emission will therefore show very similar properties, regardless of the exact system. We want to focus on two-mode emission with delayed optical feedback in this last section.

Quantum-dot lasers have shown two-state emission even without specially designed laser cavities. Due to the nonequlibrium carrier distribution among the different confined levels, simultaneous emission on two wavelengths is possible, namely, on the ground state (GS) and the first (or higher) excited state (ES) (Markus et al. 2003; Gioannini 2012; Röhm 2015). See Fig. 1 for a sketch of the energy band structure. In view of the discussion of the previous sections, the possibility for the QD laser to switch to an other optical transition also increases the dynamical degrees of freedom. Compared to single-color lasers, the presence of the second emission wavelength again stabilizes the laser output under delayed feedback. This can be seen in Fig. 10 where we show the dynamic response of the two-state QD laser to optical feedback. There the numerically obtained results for a two-state laser (panel (a)) and an otherwise identical single-color laser (panel (b)) are shown. The regions with pulsations are shown in blue and green, while the intensity of stable cw operation is encoded in orange. In the parameter plane of feedback strength K and feedback phase C, the optical feedback induces complex responses within larger parameter regions for the

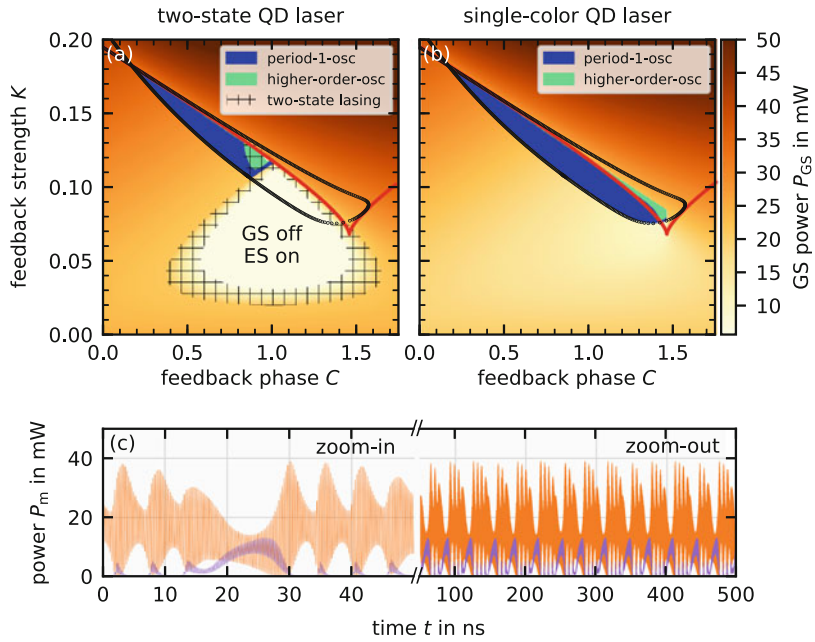

Laser Dynamics and Delayed Feedback, Fig. 10 2D Bifurcation diagram of (**a**): a two state and (**b**): a single color QD laser that is subjected to optical self-feedback. Orange shading indicates the intensity of stable ground state (GS) emission. Blue and green regions indicate regular pulsations and complex dynamics, respectively. Saddle node (SN) and Hopf bifurcations are plotted as red and black lines. (**c**) Time series of the complex dynamics found inside the green region in (**a**), orange and violet show the GS and ES intensity, respectively

single-color QD laser in Fig. 10b. In these parameter regions of complex emission, the two-color laser instead can turn to steady state emission on the excited state (Fig. 10a) and thus can partly suppress the pulsations. The green regions of complex dynamics that occur in the two-color laser are quasi-periodic pulsations that are born in a torus bifurcation. The time evolution of the intensities of the two states is shown in Fig. 10c. Those two-color bursting oscillations are found in regions where the single state QD laser emits chaotic pulse packages as discussed in Fig. 6 in the vicinity of the homoclinic bifurcation. From a dynamic system point of view, the behavior is very interesting as the existence of two-color emission allows for an additional bridge between subsequent ECM, connecting their solutions in parameter space.

Future Directions

The presence of time-delayed feedback in lasers offers a possibility to employ the rich dynamics of delay systems in technological applications. As we have seen, semiconductor lasers with delayed feedback offer a large variety of modes of operation by choice of proper external parameters. Depending on the desired laser behavior, the choice of active medium and cavity design allows control over the susceptibility towards delayed feedback. Only recently the periodic or chaotic dynamics induced by external perturbations such as optical feedback has been seen as an opportunity for novel applications, and not as a nuisance detrimental to the laser operation. A thorough understanding of the material and charge-carrier dynamics in the laser device is crucial for modeling and understanding the complex dynamics that can occur in these laser systems. With quantum-dot lasers and nanolasers, we have illuminated possible material systems for current and future technology where laser dynamics can be employed as an integral part providing the key functionality. Dynamical wavelength switching in QD lasers or the controlled dynamics of nanolasers will possibly allow novel applications in optical computing and data processing. Time-delayed feedback will provide a simple yet effective way of providing the necessary dynamics.

Bibliography

Agrawal GP (1984) Line narrowing in a single-mode injection-laser due to external optical feedback. IEEE

J Quantum Electron 20:468–471. https://doi.org/10.1109/jqe.1984.1072420
Arecchi FT, Lippi GL, Puccioni GP, Tredicce JR (1984) Deterministic chaos in laser with injected signal. Opt Commun 51(5):308–315. https://doi.org/10.1016/0030-4018(84)90016-6
Argyris A, Bueno J, Fischer I (2018) Photonic machine learning implementation for signal recovery in optical communications. Sci Rep 8(8487):1–13. https://doi.org/10.1038/s41598-018-26927-y
Bimberg D, Pohl UW (2011) Quantum dots: promises and accomplishments. Mater Today 14(9):388–397. https://doi.org/10.1016/s1369-7021(11)70183-3
Bimberg D, Grundmann M, Ledentsov NN (1999) Quantum dot heterostructures. Wiley, New York
Binder JO, Cormack GD (1989) Mode selection and stability of a semiconductor laser with weak optical feedback. IEEE J Quantum Electron 25(11):2255. https://doi.org/10.1109/3.42053
Brunner D, Luna R, Latorre ADI, Porte X, Fischer I (2017) Semiconductor laser linewidth reduction by six orders of magnitude via delayed optical feedback. Opt Lett 42(1):163–166. https://doi.org/10.1364/ol.42.000163
Bueno J, Brunner D, Soriano MC, Fischer I (2017) Conditions for reservoir computing performance using semiconductor lasers with delayed optical feedback. Opt Express 25(3):2401–2412. https://doi.org/10.1364/oe.25.002401
Cheng CH, Chen CY, Chen JD, Pan DK, Ting KT, Lin FY (2018) 3d pulsed chaos lidar system, Opt Express 26(9):12230–12241. https://doi.org/10.1364/oe.26.012230
Choi D, Wishon MJ, Viktorov EA, Citrin DS, Locquet A (2019) Nanometric sensing with laser feedback interferometry. Opt Lett 44(4):903–906. https://doi.org/10.1364/ol.44.000903
Chow WW, Koch SW (1999) Semiconductor-laser fundamentals. Springer, Berlin
Duan J, Huang H, Dong B, Jung D, Norman JC, Bowers JE, Grillot F (2019) 1.3-μ m reflection insensitive inas/gaas quantum dot lasers directly grown on silicon. IEEE Photon Technol Lett 31(5):345–348. https://doi.org/10.1109/lpt.2019.2895049
Erneux T, Rogister F, Gavrielides A, Kovanis V (2000) Bifurcation to mixed external cavity mode solutions for semiconductor lasers subject to optical feedback. Opt Commun 183(5–6):467–477. https://doi.org/10.1016/s0030-4018(00)00899-3
Erneux T, Javaloyes J, Wolfrum M, Yanchuk S (2017) Introduction to focus issue: time-delay dynamics. Chaos 27(11):114201. https://doi.org/10.1063/1.5011354
Flunkert V, Schöll E (2007) Suppressing noise-induced intensity pulsations in semiconductor lasers by means of time-delayed feedback. Phys Rev E 76:066202. https://doi.org/10.1103/physreve.76.066202
Gioannini M (2012) Ground-state quenching in two-state lasing quantum dot lasers. J Appl Phys 111:043108. https://doi.org/10.1063/1.3682574
Globisch B, Otto C, Schöll E, Lüdge K (2012) Influence of carrier lifetimes on the dynamical behavior of quantum-dot lasers subject to optical feedback. Phys Rev E 86:046201. https://doi.org/10.1103/physreve.86.046201
Haken H (1986) Laser light dynamics, vol II, 1st edn. North Holland, Amsterdam
Heil T, Fischer I, Elsäßer W, Gavrielides A (2001) Dynamics of semiconductor lasers subject to delayed optical feedback: the short cavity regime. Phys Rev Lett 87:243901. https://doi.org/10.1103/physrevlett.87.243901
Heil T, Fischer I, Elsäßer W, Krauskopf B, Green K, Gavrielides A (2003) Delay dynamics of semiconductor lasers with short external cavities: bifurcation scenarios and mechanisms. Phys Rev E 67:066214. https://doi.org/10.1103/physreve.67.066214
Helms J, Petermann K (1990) A simple analytic expression for the stable operation range of laser diodes with optical feedback. IEEE J Quantum Electron 26(5):833. https://doi.org/10.1109/3.55523
Huyet G, O'Brien D, Hegarty SP, McInerney JG, Uskov AV, Bimberg D, Ribbat C, Ustinov VM, Zhukov AE, Mikhrin SS, Kovsh AR, White JK, Hinzer K, SpringThorpe AJ (2004) Quantum dot semiconductor lasers with optical feedback. Phys Status Solidi B 201(2): 345–352. https://doi.org/10.1002/pssa.200303971
Jaurigue LC, Schöll E, Lüdge K (2016) Suppression of noise-induced modulations in multidelay systems. Phys Rev Lett 117:154101. https://doi.org/10.1103/physrevlett.117.154101
Jüngling T, Soriano MC, Oliver N, Porte X, Fischer I (2018) Consistency properties of chaotic systems driven by time-delayed feedback. Phys Rev E 97:042202. https://doi.org/10.1103/physreve.97.042202
Kane DM, McMahon C, Argyris A, Syvridis D (2015) Integrated semiconductor laser with optical feedback: transition from short to long cavity regime. Opt Express 23(14):18754. https://doi.org/10.1364/oe.23.018754
Karsaklian Dal A, Bosco S, Ohara N, Sato Y, Akizawa A, Uchida T, Harayama MI (2017) Dynamics versus feedback delay time inphotonic integrated circuits: mapping theshort cavity regime. IEEE Photon J 9(2):1. https://doi.org/10.1109/jphot.2017.2667883
Kim B, Locquet A, Li N, Choi D, Citrin DS (2014) Bifurcation-cascade diagrams of an external-cavity semiconductor laser: experiment and theory. IEEE J Quantum Electron 50(12):965–972. https://doi.org/10.1109/jqe.2014.2363568
Kuriki Y, Nakayama J, Takano K, Uchida A (2018) Impact of input mask signals on delay-based photonic reservoir computing with semiconductor lasers. Opt Express 26(5):5777–5788. https://doi.org/10.1364/oe.26.005777
Lang R, Kobayashi K (1980) External optical feedback effects on semiconductor injection laser properties. IEEE J Quantum Electron 16:347–355. https://doi.org/10.1109/jqe.1980.1070479
Lenstra D, Verbeek B, Den Boef A (1985) Coherence collapse in single-mode semiconductor lasers due to optical feedback. IEEE J Quantum Electron 21(6):674–679. https://doi.org/10.1109/jqe.1985.1072725
Lenstra D, van Schaijk TTM, Williams KA (2019) Toward a feedback-insensitive semiconductor laser. IEEE J Sel

Top Quantum Electron 25(6):1. https://doi.org/10.1109/jstqe.2019.2924139
Levine AM, van Tartwijk GHM, Lenstra D, Erneux T (1995) Diode lasers with optical feedback: stability of the maximum gain mode. Phys Rev A 52(5):R3436. https://doi.org/10.1103/physreva.52.r3436. (4 pages)
Li H, Ye J, McInerney JG (1993) Detailed analysis of coherence collapse in semiconductor lasers. IEEE J Quantum Electron 29(9):2421–2432. https://doi.org/10.1109/3.247700
Lin FY, Liu JM (2004) Chaotic LIDAR. IEEE J Sel Top Quantum Electron 10(5):991–997. https://doi.org/10.1109/jstqe.2004.835296
Lindner B, García-Ojalvo J, Neiman AB, Schimansky-Geier L (2004) Effects of noise in excitable systems. Phys Rep 392:321–424. https://doi.org/10.1016/j.physrep.2003.10.015
Lingnau B (2015) Nonlinear and nonequilibrium dynamics of quantum-dot optoelectronic devices. Springer Theses (Springer International Publishing), Cham. https://doi.org/10.1007/978-3-319-25805-8
Lingnau B, Lüdge K, Chow WW, Schöll E (2012) Failure of the α-factor in describing dynamical instabilities and chaos in quantum-dot lasers. Phys Rev E 86(6):065201(R). https://doi.org/10.1103/physreve.86.065201
Lingnau B, Chow WW, Schöll E, Lüdge K (2013) Feedback and injection locking instabilities in quantum-dot lasers: a microscopically based bifurcation analysis. New J Phys 15:093031. https://doi.org/10.1088/1367-2630/15/9/093031
Lingnau B, Turnwald J, Lüdge K (2019) Class-C semiconductor lasers with time-delayed optical feedback. Phil Trans R Soc A 377(2153):20180124. https://doi.org/10.1098/rsta.2018.0124
Locquet A, Kim B, Choi D, Li N, Citrin DS (2017) Initial-state dependence of the route to chaos of an external-cavity laser. Phys Rev A 95:023801. https://doi.org/10.1103/physreva.95.023801
Lüdge K, Schöll E (2009) Quantum-dot lasers – desynchronized nonlinear dynamics of electrons and holes. IEEE J Quantum Electron 45(11):1396–1403. https://doi.org/10.1109/jqe.2009.2028159
Markus A, Chen JX, Paranthoen C, Fiore A, Platz C, Gauthier-Lafaye O (2003) Simultaneous two-state lasing in quantum-dot lasers. Appl Phys Lett 82(12):1818. https://doi.org/10.1063/1.1563742
Mørk J, Tromborg B, Christiansen PL (1988a) Bistability and low-frequency fluctuations in semiconductor lasers with optical feedback: a theoretical analysis. IEEE J Quantum Electron 24(2):123–133. https://doi.org/10.1109/3.105
Mørk J, Christiansen PL, Tromborg B (1988b) Limits of stable operation of ar-coated semiconductor lasers with strong optical feedback. Electron Lett 24(17):1065. https://doi.org/10.1049/el:19880722
Mørk J, Mark J, Tromborg B (1990a) Route to chaos and competition between relaxation oscillations for a semiconductor laser with optical feedback. Phys Rev Lett 65(16):1999–2002. https://doi.org/10.1103/physrevlett.65.1999
Mørk J, Semkow M, Tromborg B (1990b) Measurement and theory of mode hopping in external cavity lasers. Electron Lett 26(9):609–610. https://doi.org/10.1049/el:19900400
Mørk J, Tromborg B, Mark J (1992) Chaos in semiconductor lasers with optical feedback-theory and experiment. IEEE J Quantum Electron 28:93–108. https://doi.org/10.1109/3.119502
Nguimdo RM, Lacot E, Jacquin O, Hugon O, Van der Sande G, de Chatellus HG (2017) Prediction performance of reservoir computing systems based on a diode-pumped erbium-doped microchip laser subject to optical feedback. Opt Lett 42(3):375. https://doi.org/10.1364/ol.42.000375
O'Brien D, Hegarty SP, Huyet G, Uskov AV (2004) Sensitivity of quantum-dot semiconductor lasers to optical feedback. Opt Lett 29(10):1072–1074. https://doi.org/10.1364/ol.29.001072
Ohtsubo J (1999) Feedback induced instability and chaos in semiconductor lasers and their applications. J Opt Rev 6:1–15. https://doi.org/10.1007/s10043-999-0001-z
Ohtsubo J (2013) Semiconductor lasers: stability, instability and chaos, 3rd edn. Springer, Berlin. https://doi.org/10.1007/978-3-642-30147-6
Olejniczak L, Sciamanna M, Thienpont H, Panajotov K, Mutig A, Hopfer F, Bimberg D (2009) Polarization switching in quantum-dot vertical-cavity surface-emitting lasers. IEEE Photon Technol Lett 21(14):1008–1010. https://doi.org/10.1109/lpt.2009.2021954
Oliver N, Soriano MC, Sukow DW, Fischer I (2011) Dynamics of a semiconductor laser with polarization-rotated feedback and its utilization for random bit generation. Opt Lett 36(23):4632–4634. https://doi.org/10.1364/ol.36.004632
Oliver N, Jüngling T, Fischer I (2015) Consistency properties of a chaotic semiconductor laser driven by optical feedback. Phys Rev Lett 114(123902):114. https://doi.org/10.1103/physrevlett.114.123902
Osborne S, Buckley K, Amann A, O'Brien S (2009) All-optical memory based on the injection locking bistability of a two-color laser diode. Opt Express 17(8):6293–6300. https://doi.org/10.1364/oe.17.006293
Osborne S, Heinricht P, Brandonisio N, Amann A, O'Brien S (2012) Wavelength switching dynamics of two-colour semiconductor lasers with optical injection and feedback. Semicond Sci Technol 27(9):094001. https://doi.org/10.1088/0268-1242/27/9/094001
Otto C, Lüdge K, Schöll E (2010) Modeling quantum dot lasers with optical feedback: sensitivity of bifurcation scenarios. Phys Status Solidi B 247(4):829–845. https://doi.org/10.1002/pssb.200945434
Otto C, Globisch B, Lüdge K, Schöll E, Erneux T (2012a) Complex dynamics of semiconductor quantum dot lasers subject to delayed optical feedback. Int J Bifurc Chaos 22(10):1250246. https://doi.org/10.1142/s021812741250246x
Otto C, Lüdge K, Viktorov EA, Erneux T (2012b) Quantum dot laser tolerance to optical feedback. In: Lüdge K (ed) Nonlinear laser dynamics – from quantum dots to cryptography. Wiley-VCH, Weinheim, pp 141–162

Otto C, Lingnau B, Schöll E, Lüdge K (2014) Manipulating coherence resonance in a quantum dot semiconductor laser via electrical pumping. Opt Express 22:13288. https://doi.org/10.1364/oe.22.013288

Otto A, Just W, Radons G (2019) Nonlinear dynamics of delay systems: an overview. Phil Trans R Soc A 377(2153):20180389. https://doi.org/10.1098/rsta.2018.0389

Pieroux D, Erneux T, Gavrielides A, Kovanis V (2000) Hopf bifurcation subject to a large delay in a laser system. SIAM J Appl Math 61(3):966–982. https://doi.org/10.1137/s0036139999360131

Pieroux D, Erneux T, Haegeman B, Engelborghs K, Roose D (2001) Bridges of periodic solutions and tori in semiconductor lasers subject to delay. Phys Rev Lett 87(19):193901. https://doi.org/10.1103/physrevlett.87.193901

Porte X, Soriano MC, Fischer I (2014) Similarity properties in the dynamics of delayedfeedback semiconductor lasers. Phys Rev A 89:023822. https://doi.org/10.1103/physreva.89.023822

Radziunas M, Wünsche HJ, Krauskopf B (2006) External cavity modes in Lang-Kobayashi and travelling wave models. M Wolfrum Proc SPIE 6184:61840X. https://doi.org/10.1117/12.663546

Reidler I, Aviad Y, Rosenbluh M, Kanter I (2009) Ultrahigh-speed random number generation based on a chaotic semiconductor laser. Phys Rev Lett 103:024102. https://doi.org/10.1103/physrevlett.103.024102

Röhm A (2015) Dynamic scenarios in two-state quantum dot lasers. BestMasters 2015. Springer Spektrum, Wiesbaden. https://doi.org/10.1007/978-3-658-09402-7

Röhm A, Lingnau B, Lüdge K (2015) Understanding ground-state quenching in quantum-dot lasers. IEEE J Quantum Electron 51(1):2000211. https://doi.org/10.1109/jqe.2014.2370793

Rontani D, Locquet A, Sciamanna M, Citrin DS (2007) Loss of time-delay signature in the chaotic output of a semiconductor laser with optical feedback. Opt Lett 32(20):2960–2962. https://doi.org/10.1364/ol.32.002960

Rontani D, Locquet A, Sciamanna M, Citrin DS, Ortin S (2009) Time-delay identification in a chaotic semiconductor laser with optical feedback: a dynamical point of view. IEEE J Quantum Electron 45(7):879–1891. https://doi.org/10.1109/jqe.2009.2013116

Rosanov NN (1975) Kinetics of a solid-state laser with an additional moving mirror. Sov J Quant Electron 4(10):1191–1193. https://doi.org/10.1070/qe1975v004n10abeh011629

Rottschäfer V, Krauskopf B (2007) The ECM-backbone of the Lang-Kobayashi equations: a geometric picture. Int J Bifurc Chaos 17(5):1575–1588. https://doi.org/10.1142/s0218127407017914

Sano T (1994) Antimode dynamics and chaotic itinerancy in the coherence collapse of semiconductor lasers with optical feedback. Phys Rev A 50(3):2719–2726. https://doi.org/10.1103/physreva.50.2719

Schelte C, Camelin P, Marconi M, Garnache A, Huyet G, Beaudoin G, Sagnes I, Giudici M, Javaloyes J, Gurevich SV (2019) Third order dispersion in time-delayed systems. Phys Rev Lett 123:043902. https://doi.org/10.1103/physrevlett.123.043902

Sciamanna M, Panajotov K, Thienpont H, Veretennicoff I, Mégret P, Blondel M (2003) Optical feedback induces polarization mode hopping in vertical-cavity surface-emitting lasers. Opt Lett 28(17):1543–1545. https://doi.org/10.1364/ol.28.001543

Simmendinger C, Hess O (1996) Controlling delay-induced chaotic behavior of a semiconductor laser with optical feedback. Phys Lett A 216:97. https://doi.org/10.1016/0375-9601(96)00269-1

Soriano MC, García-Ojalvo J, Mirasso CR, Fischer I (2013) Complex photonics: Dynamics and applications of delay-coupled semiconductors lasers. Rev Mod Phys 85:421–470. https://doi.org/10.1103/revmodphys.85.421

van Tartwijk GHM, Agrawal GP (1998) Laser instabilities: a modern perspective. Prog Quantum Electron 22(2):43–122. https://doi.org/10.1016/s0079-6727(98)00008-1

Verschaffelt G, Khoder M, Van der Sande G (2017) Random number generator based on an integrated laser with on-chip optical feedback. Chaos 27(11):114310. https://doi.org/10.1063/1.5007862

Virte M, Panajotov K, Thienpont H, Sciamanna M (2012) Deterministic polarization chaos from a laser diode. Nat Photonics 7(1):60–65. https://doi.org/10.1038/nphoton.2012.286

Wolfrum M, Turaev DV (2002) Instabilities of lasers with moderately delayed optical feedback. Opt Commun 212(1–3): 127–138. https://doi.org/10.1016/s0030-4018(02)01824-2

Wünsche HJ, Schikora S, Henneberger F (2008) Noninvasive Control of Semiconductor Lasers by Delayed Optical Feedback. In: Schuster HG, Schöll E (eds) Handbook of chaos control. Wiley-VCH, Weinheim. https://doi.org/10.1002/9783527622313.ch21. Second completely revised and enlarged edition

Yanchuk S, Perlikowski P (2009) Delay and periodicity. Phys Rev E 79(4):046221. https://doi.org/10.1103/physreve.79.046221

Yanchuk S, Wolfrum M (2004) Instabilities of stationary states in lasers with long-delay optical feedback. Rep Weierstrass Inst Appl Anal Stochastics 962:1–16

Ye SY, Ohtsubo J (1998) Experimental investigation of stability enhancement in semiconductor lasers with optical feedback. Opt Rev 5(5):280–284. https://doi.org/10.1007/s10043-998-0280-9

Fluid Dynamics, Pattern Formation

Michael Bestehorn
Brandenburg University of Technology, Cottbus, Germany

Article Outline

Glossary
Definition of the Subject
Introduction
The Basic Equations of Fluid Dynamics
Surface Waves
Instabilities
Instabilities
Order Parameter Equations
Conserved Order Parameter Fields
Future Directions
Bibliography

Glossary

Order parameter(s) (Field) variable(s) characterizing the spatio-temporal state of a system. Other state variables such as velocity, temperature, density, etc. can be computed if the order parameter(s) are known.

Control parameter(s) Parameters which are fixed and can be tuned from outside of the system under consideration.

Critical point, threshold, onset The points in control parameter space where new and qualitatively different solutions bifurcate from (usually simpler) ones.

Slaving principle Stated by H. Haken in 1975, the slaving principle allows for a huge reduction of degrees of freedom close to a critical point. It states that a very large number of linearly damped modes are slaved to and therefore completely determined by the few modes that grow in the vicinity of the critical point. The amplitudes of the growing modes are also called order parameters.

Natural patterns Spatial patterns showing a certain periodic (near) order, but also defects, grain boundaries etc.

Turing patterns Natural patterns that have a certain typical length scale and that show relaxation to a stationary state in the long term. Typical ingredients of Turing patterns are stripes, hexagons and squares.

Swift–Hohenberg equation Derived by Swift and Hohenberg in 1977 and nowadays established as the standard form for a scalar, real-valued order parameter equation showing Turing patterns at onset.

Coarsening The monotonic increase of the typical length scale of a structure in time. Often connected to spinodal decomposition, for example, of a binary mixture of non-mixing components such as water and oil. Small oil droplets in the beginning merge and finally form a large oil drop on the water surface. Coarsening slows down if the length scale increases.

Definition of the Subject

The state of a fluid is described by its velocity, density, pressure, and temperature. All these variables depend in general on space and time. Pattern formation refers to the situation where one or more of these variables are organized within a certain spatial and/or temporal order. This order has macroscopic length and time scales, that is, characteristic lengths and times are much larger than those of the atoms or molecules which constitute the fluid. Therefore a continuous description is appropriate.

Macroscopic fluid patterns may be encountered in nature as well as in technological applications for a large variety of different systems. Far from being complete, we mention some examples:

A. Hutt, H. Haken (eds.), *Synergetics*,
https://doi.org/10.1007/978-1-0716-0421-2_214

Originally published in
R. A. Meyers (ed.), *Encyclopedia of Complexity and Systems Science*, © Springer-Verlag 2009
https://doi.org/10.1007/978-3-642-27737-5_214

- Water waves caused by wind or by sea quakes and land slides (Tsunamis).
- Localized excitations of the surface of a fluid (solitons), such as that seen on shallow water channels.
- Shear instabilities in clouds or in multi-layer systems such as the Kelvin–Helmholtz instability or the Rayleigh–Taylor-instability.
- Surface deflections in the form of holes or drops of thin fluid films in coating or wetting processes.
- Convection instabilities in laboratory experiments, but also in the atmosphere, in the earth's interior or in stars.
- Creation and controlled growth of ordered structures in (nano-) technological applications.
- Biological applications: Behavior of liquid films on leaves or of the tear film on the cornea of the eye. Dynamics of thin blood layers, blood clotting.
- Films on the walls of combustion cells.
- Lubrication films in mechanical machines.

Fluid patterns may occur due to several mechanisms. One can distinguish between two main cases: Patterns excited and organized by some external forces or disturbances (such as Tsunamis) and those formed by instabilities. The latter may show the aspects of self-organization and will be the focus of the present contribution.

Introduction

Since the first observations of Michael Faraday almost 180 years ago (Faraday 1831) (Fig. 1), pattern formation in liquids or gases (*fluids*) has been subject to innumerable experimental (Bodenschatz et al. 2000; Schatz and Neitzel 2001; Van Dyke 1982), theoretical (Chandrasekhar 1961; Colinet et al. 2001; Getling 1998) and, later on, numerical work (Bestehorn 1993; Busse 1989; Pesch 1996). After the famous experiments by Henri Bénard around 1901 (Bénard 1901), convection in a single or later in multi-component fluids came into the focus of interest. The first theoretical studies were made by Lord Rayleigh (Lord 1915). Theoretical computations up to the early 1960s were restricted on the linearized basic equations and could explain the existence of critical points in parameter space as well as the observed length scales of the structures found experimentally (Block 1956; Palm 1960). In the meantime, Alan Turing (Turing 1952) showed in his famous paper of 1952 that similar patterns could emerge out of equilibrium in reaction-diffusion systems. It took almost 40 years for an experimental confirmation using the so-called CIMA reaction (Castets et al. 1990; Ouyang and Swinney 1991).

With the appearance and rapid development of computers, the field gained further momentum from the new discipline of nonlinear dynamics

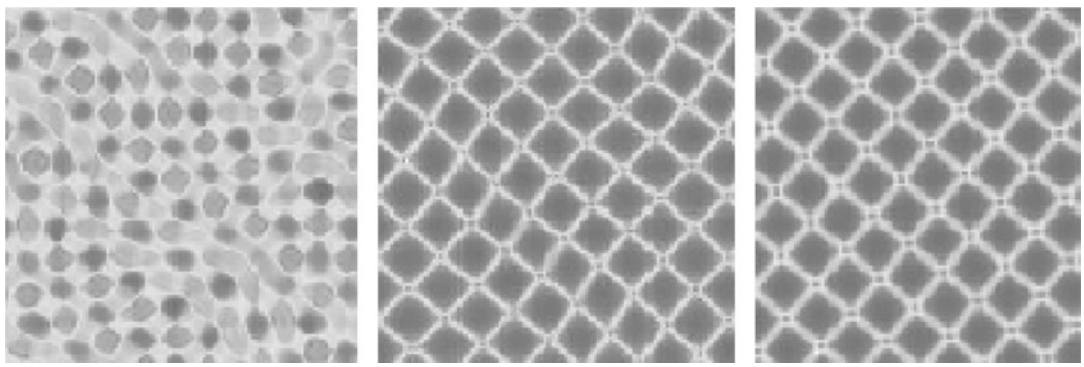

Fluid Dynamics, Pattern Formation, Fig. 1 Michael Faraday observed surface patterns on a liquid horizontal layer if the whole layer vibrated vertically with a certain amplitude and frequency. Very often, regular squares are found, as shown in the time series as a numerical result of the shallow water equations (see Section "Surface Waves")

and nonlinear system theory (Argyris et al. 1994; Guckenheimer and Holmes 2002; Haken 1975, 2004). Early computations in 1963 by Edward Lorenz of a system of three coupled ordinary differential equations derived by a crudely truncated mode expansion of the Navier–Stokes equations revealed the first chaotic attractor of a dissipative system (Lorenz 1963). Though the chaotic behavior seen in the Lorenz equations does not originate from hydrodynamic equations and has nothing to do with irregular fluid behavior, the Lorenz model now stands on its own as a paradigm for a relatively simple system showing low dimensional chaos (Sparrow 1982).

Patterns that emerge from an instability roughly pass through two phases. As long as amplitudes (or order parameters) are small, the behavior is often determined by the linear parts of the system and exponential growth of a certain part of the mode spectrum is found. In the second phase, nonlinearities come into play and may lead to saturation and selection of certain mode configurations, seen then as regular structures in configuration space (Fig. 2). The full mathematical description of hydrodynamic systems has been well known for a long time. Fluid motion is described by the Euler or Navier–Stokes equations, temperature fields by the heat equation and chemical concentrations by some nonlinear reaction-diffusion equations. The location and spatio-temporal evolution of surfaces or interfaces can be computed by the kinematic boundary conditions if the velocity of the fluid near the interface is known. All these equations can be coupled and provided with suitable boundary and initial conditions, resulting in rather complicated systems of nonlinear partial differential equations. Even today in the age of supercomputers, their further treatment, especially in three spatial dimensions, remains a challenge.

On the other hand, directly solving the basic equations, can be considered merely as another experiment. For these reasons and to get a deeper insight into the physics behind pattern formation, other methods have been devised. Very often one of the three spatial dimension is distinguished, either for physical reasons or simply due to the geometry of the system. A good example is surface waves on a water layer. Here, the behavior of the solutions in the vertical direction (z) is very different from those in the horizontal ones. For shallow water waves (wave length long compared to the layer depth) the velocities are more or less independent on z, where in the other limit of deep water waves, fluid motion takes only place along a small layer under the surface and decreases exponentially with depth. In both cases one may reduce the dimension of the basic problem by an expansion with respect to simple functions for the vertical dependence of the variables (Cohen and Kundu 2004). An analogue method can be applied describing thin film surface patterns (Oron et al. 1997). Also for convection cells, the vertical dimension plays a special role and the solution

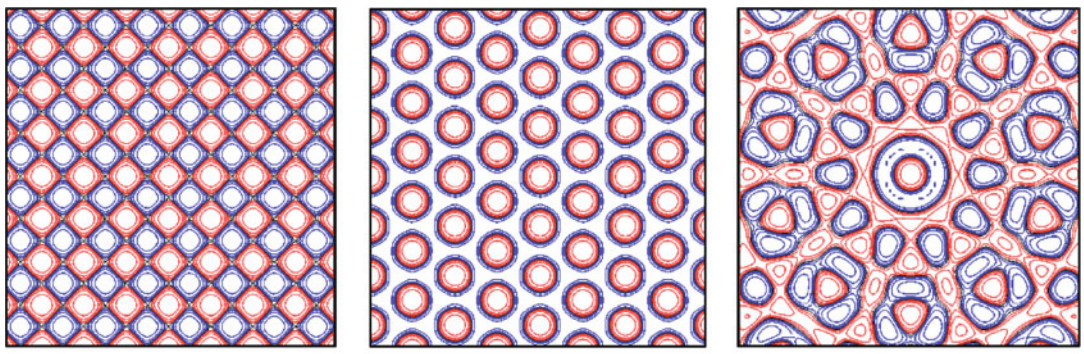

Fluid Dynamics, Pattern Formation, Fig. 2 The composition of plane waves with the same wave number but different orientation in 2D space results in regular patterns. For two modes ($N = 2$) one sees squares, for $N = 3$ hexagons and for $N > 3$ quasi periodic structures in space or Penrose tilings (Penrose 1974) are found

can be projected onto a few modes near the critical point (Busse 1967; Pesch 1996).

Another concept that reduces the number of dependent variables and equations is that of order parameters. The notion of the "order parameter" goes back to Landau (Landau and Lifshitz 1996) and refers originally to a variable that measures the order of a certain system. Rather a variable than a parameter, the order parameter normally depends on time and, in theories describing the formation of natural patterns, also on space (Newell and Whitehead 1969). Thus, the order parameter equation (abbreviated: OPE) is a partial differential equation with certain nonlinear terms that become important for pattern selection and saturation.

Theoretical methods developed by the Haken school (Haken 1983, 1975, 2004) starting in the 1970s allow for a systematic derivation of the OPEs (sometimes also called "generalized Ginzburg–Landau equations") for a great variety of nonequilibrium and open systems from physics, chemistry and biology. The key idea is to find a reduced description in terms of relevant or active modes close to a certain bifurcation point. The amplitudes of these active modes, the order parameters, now generalized to a nonequilibrium, pattern forming system, obey unified and simplified equations, namely the OPEs. It turns out that the structure of these equations depends not so much on the particular system under consideration as on the type of bifurcation. To each type of bifurcation a special "normal form" of OPE is related (Cross 1988). In deriving the OPEs, the slaving principle (Haken 2004) allows us to eliminate a huge number of slaved variables and express them by the active ones.

This contribution is concerned mainly with structures in fluids that originate from self-organized processes. It tries to bring together direct numerical solutions of hydrodynamic equations with the modern concepts of pattern formation. After introducing the basic equations (Section "The Basic Equations of Fluid Dynamics") of fluid dynamics, it presents a short section on waves and descriptions reduced by geometrical reasons. Several types of instabilities are discussed in Section "Instabilities", together with computer solutions for the different cases. Section "Order Parameter Equations" presents different types of two-dimensional order parameter equations. Finally, Section "Conserved Order Parameter Fields" is devoted to the special case of conserved order parameters.

The Basic Equations of Fluid Dynamics

Let the state of a fluid be described by its velocity, its density, its pressure, and its temperature field

$$\vec{v}\left(\vec{r},t\right),\ \rho\left(\vec{r},t\right),\ p\left(\vec{r},t\right),\ T\left(\vec{r},t\right). \qquad (1)$$

In this section we wish to specify the basic hydrodynamic equations that rule the spatio-temporal behavior of these seven variables. They have to be completed by suitable boundary conditions (abbreviated: b.c.) which we shall present later with the particular systems under consideration.

Continuity Equation

The conservation of mass yields the continuity equation

$$\partial_t \rho + \mathrm{div}\left(\rho\vec{v}\right) = \partial_t \rho + \left(\vec{v}\cdot\nabla\right)\rho + \rho\ \mathrm{div}\ \vec{v} = 0. \qquad (2)$$

In most cases, liquids are difficult to compress. One can usually assume that a volume element does not change its density while it moves with the fluid (Lagrangian description)

$$\partial_t \rho + \left(\vec{v}\cdot\nabla\right)\rho = 0.$$

From (2) one finds the condition of incompressibility

$$\mathrm{div}\ \vec{v}\left(\vec{r},t\right) = 0, \qquad (3)$$

or, in other words, the velocity field is free of sources and sinks. Equation (3) can be satisfied by the ansatz

$$\vec{v}\left(\vec{r},t\right) = \mathrm{curl}\,\vec{A}\left(\vec{r},t\right) \tag{4}$$

where $\vec{A}$ plays the role of a vector potential. In (4) one can use the particular decomposition (Bestehorn 1993; Chandrasekhar 1961)

$$\begin{aligned}\vec{v}\left(\vec{r},t\right) &= \mathrm{curl}(\Phi\hat{\mathrm{e}}_z) + \mathrm{curl}\,\mathrm{curl}(\Psi\hat{\mathrm{e}}_z)\\ &= \begin{pmatrix}\partial_y\Phi + \partial_z\partial_x\Psi\\ -\partial_x\Phi + \partial_z\partial_x\Psi\\ -\Delta_2\Psi\end{pmatrix}\end{aligned} \tag{5}$$

with the two independent scalar functions $\Phi\left(\vec{r},t\right)$ and $\Psi\left(\vec{r},t\right)$ and $\Delta_2 = \partial_{xx}^2 + \partial_{yy}^2$ as the 2D-Laplacian.

If the velocity field is irrotational, that is without vortices $\left(\mathrm{curl}\,\vec{v} = 0\right)$, it can be derived from a scalar potential

$$\vec{v} = \mathrm{grad}\,\phi. \tag{6}$$

For incompressible and irrotational flows, hydrodynamics is reduced to a boundary value problem, since the potential must fulfill the Laplace equation

$$\mathrm{div}\,\vec{v} = \Delta\phi = 0 \tag{7}$$

and the velocity field is solely determined by its boundary conditions.

Euler Equations

For a perfect fluid, a fluid with no viscosity, one derives the Euler equations from the law of conservation of momentum (Lai et al. 1993). They read

$$\begin{aligned}&\rho\left(\vec{r},t\right)\left[\partial_t\vec{v}\left(\vec{r},t\right) + \left(\vec{v}(\vec{r},t)\cdot\nabla\right)\vec{v}(\vec{r},t)\right] =\\ &-\mathrm{grad}\,p\left(\vec{r},t\right) + \vec{f}\left(\vec{r},t\right),\end{aligned} \tag{8}$$

where $\vec{f}$ denotes external volume forces. Together with a state equation of the form

$$p = p(\rho,T), \tag{9}$$

the continuity Eq. (2) and the temperature equations (to be shown below) (Subsection "Transport Equations") constitute the basic set for the seven state variables (1).

Incompressible Fluids For an incompressible fluid, a state equation of the form (9) makes no sense since pressure will not change with density. So p can be eliminated by forming the curl of (8)

$$\partial_t\vec{\Omega} = \mathrm{curl}\left(\vec{v}\times\vec{\Omega}\right) + \frac{1}{\rho}\mathrm{curl}\,\vec{f} \tag{10}$$

Where

$$\vec{\Omega} = \mathrm{curl}\,\vec{v} \tag{11}$$

denotes the vorticity. If p must be known, it can be computed from the divergence of (8) which yields

$$\nabla^2 p = \rho\left\{-\mathrm{Tr}\left[\left(\nabla\circ\vec{v}\right)\left(\nabla\circ\vec{v}\right)\right] + \mathrm{div}\,\vec{f}\right\}, \tag{12}$$

where $\circ$ is the dyadic product and Tr[. . .] the trace.

Incompressible Irrotational Fluids If, in addition, the flow is free of vortices, one may integrate the Euler equations and find the theorem of Bernoulli

$$\partial_t\phi = -\frac{1}{\rho}(p+U) - \frac{1}{2}(\nabla\phi)^2 \tag{13}$$

where U is the potential to $\vec{f}$ ($\vec{f}$ must be irrotational, too). For stationary solutions, the velocity potential ϕ is found from (7) and (13) can be used to determine the pressure.

Navier–Stokes Equations

Compressible Fluids In real fluids, shear stresses are a result of friction. They must be added to the balance of momentum and yield the Navier–Stokes equations. For a compressible Newtonian fluid they read

$$\begin{aligned}&\rho\left[\partial_t\vec{v} + \left(\vec{v}\cdot\nabla\right)\vec{v}\right]\\ &= -\mathrm{grad}\;\; p + \vec{f} + \eta\Delta\vec{v} + \left(\zeta + \frac{\eta}{3}\right)\mathrm{grad}\,\mathrm{div}\,\vec{v}\end{aligned} \tag{14}$$

where η denotes the first and ζ the second viscosity (Landau and Lifshitz 2004).

Incompressible Fluids The Navier–Stokes equations for incompressible fluids are simpler:

$$\rho\left[\partial_t \vec{v} + \left(\vec{v}\cdot\nabla\right)\vec{v}\right] = -\nabla p + \vec{f} + \eta\Delta\vec{v}. \tag{15}$$

Again, pressure can be eliminated by forming the curl. Taking the ansatz (5), the z-components of the curl and of the curl of the curl of (15), we have

$$\{\nu\Delta - \partial_t\}\,\Delta_2\Phi\left(\vec{r},t\right) = \left[\mathrm{curl}\left(\left(\vec{v}\cdot\nabla\right)\vec{v}\right)\right]_z + \frac{1}{\rho}\left(\partial_x f_y - \partial_y f_x\right) \tag{16a}$$

$$\{\nu\Delta - \partial_t\}\,\Delta\Delta_2\Psi\left(\vec{r},t\right) = \left[\mathrm{curl}\,\mathrm{curl}\left(\left(\vec{v}\cdot\nabla\right)\vec{v}\right)\right]_z + \frac{1}{\rho}\left(\Delta_2 f_z - \partial_x\partial_z f_x - \partial_y\partial_z f_y\right). \tag{16b}$$

Here we have introduced the kinematic viscosity $\nu = \eta/\rho$. We note that this decomposition is of particular interest if $f_x = f_y = 0$ as is the case in convection problems of a plane layer.

Incompressible Fluids with a Small Reynolds Number

For some applications it is convenient to use the Navier–Stokes equations in dimensionless form. With scaling with respect to a characteristic length L and velocity V_0:

$$\vec{r} = L\cdot\vec{r}', t = (L/V_0)\cdot t', \vec{v} = V_0\cdot\vec{v}', p' = \frac{L}{\eta V_0}\cdot p,$$

(15) turns into

$$R_e\left[\partial_t\vec{v}' + \left(\vec{v}'\cdot\nabla'\right)\vec{v}'\right] = -\nabla' p' + \Delta'\vec{v}'. \tag{17}$$

(We assumed a potential for $\vec{f}$ which can be confined into p.) The dimensionless quantity

$$R_e = \frac{LV_0}{\nu} \tag{18}$$

is the Reynolds number. If $R_e \ll 1$, the left hand side of (17) can be neglected and the Navier–Stokes equations become linear (primes omitted):

$$\Delta\vec{v} = \nabla p. \tag{19}$$

This is the Stokes equation, in which no time derivative of $\vec{v}$ occurs. Thus, as known from over-damped motion, the velocity field directly follows the pressure gradients.

Transport Equations

Scalar fields such as temperature or concentration of a mixture that may diffuse into and be transported with the fluid are ruled by the transport equation. Let $S\left(\vec{r},t\right)$ be the scalar field, then the transport equation reads

$$\partial_t S + \left(\vec{v}\cdot\nabla\right)S = D_s\Delta S, \tag{20}$$

where D_s is the appropriate diffusion coefficient.

Surface Waves

The only elastic forces in fluids are those coming from volume changes and may exist, therefore, only in compressible fluids. They give rise to longitudinal compression waves which usually have small amplitudes and behave linearly in a good approximation. A linear wave equation can be derived with a (space dependent) sound speed (Lai et al. 1993).

A transversal wave which is also possible in incompressible fluids can be formed along a deformable interface. Gravity and, for small wavelengths, surface tension provide the stabilizing mechanism of a flat surface, around which oscillations (gravity waves) may occur. If their amplitudes are big enough, nonlinearities may play an essential role for surface waves, as is clearly seen by solitons (Drazin et al. 1989; Nekorkin and Velarde 2002) and wave breaking (Dean and Dalrymple 2000). For this reason we shall discuss only surface waves in this section.

Gravity Waves

If one assumes an irrotational flow of a perfect and incompressible fluid on a flat substrate and with a free, deformable surface (Fig. 3), then the velocity

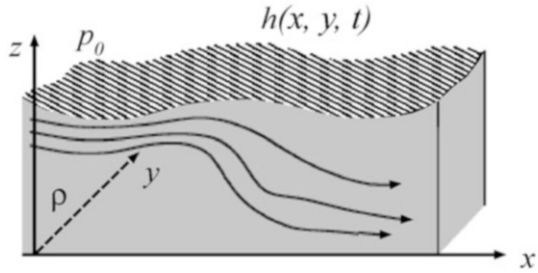

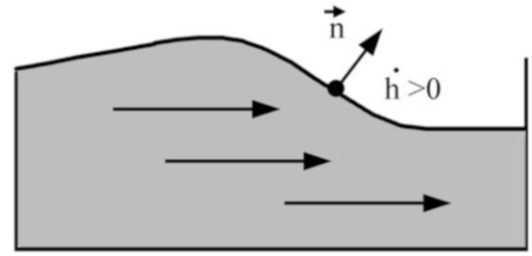

Fluid Dynamics, Pattern Formation, Fig. 3 *Left:* an (incompressible) fluid with a free and deformable surface located at $z = h(x, y, t)$, on which a constant external pressure p_0 is applied. *Right:* The location of a certain point of the surface changes if the fluid is in motion

is determined by the Laplace Eq. (7) which must be accomplished by boundary conditions at $z = 0$

$$v_z|_{z=0} = \partial_z \phi|_{z=0} = 0 \tag{21}$$

and at $z = h(x, y, t)$

$$\partial_t \phi\Big|_{z=h} = -gh - p(h)/\rho - \frac{1}{\rho}(\nabla\phi)^2 \tag{22}$$

where g denotes the gravitational acceleration. Equation (22) is nothing other than the Bernoulli Eq. (13) evaluated at the surface. The surface itself is determined by the so-called kinematic boundary condition that reads (see Fig. 3, right frame).

$$\begin{aligned}\partial_t h &= v_z\big|_{z=h} - v_x\big|_{z=h}\partial_x h - v_y\big|_{z=h}\partial_y h \\ &= \partial_z\phi\big|_{z=h} - (\partial_x h)(\partial_x\phi)_{z=h} - \big(\partial_y h\big)\big(\partial_y\phi\big)_{z=h}.\end{aligned} \tag{23}$$

Shallow Water Equations

For shallow water waves, one can introduce the small parameter

$$\delta = \mathrm{d}/l \tag{24}$$

which is the ratio of the water depth d and a typical horizontal scale (such as a wavelength) l. Then (7) can be solved iteratively; the result is a power series in δ^2 (Cohen and Kundu 2004; Dean and Dalrymple 2000):

$$\begin{aligned}&\phi\left(\vec{r}, t\right) = \Phi(x, y, t) \\ &+\delta^2\left[-\frac{z^2}{2}\Delta_2\Phi(x, y, t) + \varphi^{(1)}(x, y, t)\right] + O\left(\delta^4\right)\end{aligned} \tag{25}$$

with an arbitrary function φ_1. Inserting (25) into (23) and (22) yields up to the lowest order in δ the *shallow water equations*

$$\begin{aligned}\partial_t h = &-h\Delta_2\Phi - (\partial_x h)(\partial_x\Phi) \\ &- \big(\partial_y h\big)\big(\partial_y\Phi\big)\end{aligned} \tag{26a}$$

$$\begin{aligned}\partial_t\Phi = &-gh - p(h)/\rho - \frac{1}{2}(\partial_x\Phi)^2 \\ &- \frac{1}{2}\big(\partial_y\Phi\big)^2.\end{aligned} \tag{26b}$$

This is the first example of how to derive a two-dimensional system starting from three-dimensional fluid motion. Eq. (26) constitute a closed system of partial differential equations for the evolution of the two functions $h(x, y, t)$ and $\Phi(x, y, t)$. Using (25), one immediately finds from the latter the velocity field (up to the order δ^2).

Numerical Solutions

Figure 4 shows numerical solutions of the shallow water equations (left frame in one dimension, right frame in two dimensions). In one dimension, one sees clearly traveling surface waves which may run around due to the periodic boundary conditions in x. On the other hand, one can recognize a second wave with a smaller amplitude going to the left hand side. Both waves seem to penetrate each other without further interaction. The reason seems to be the smallness of the amplitude which results in a more or less linear behavior. In the two-dimensional frame, a snapshot of the temporal evolution of the surface is presented. The initial condition was chosen randomly. For numerical stability reasons, an additional damping of the form $\tilde{\nu}\Delta_2\Phi$ was added to the right hand side of (26b) which filters out the short wave lengths. This could be justified phenomenologically by friction and leads in the long term to a fluid at rest, if only gravity acts.

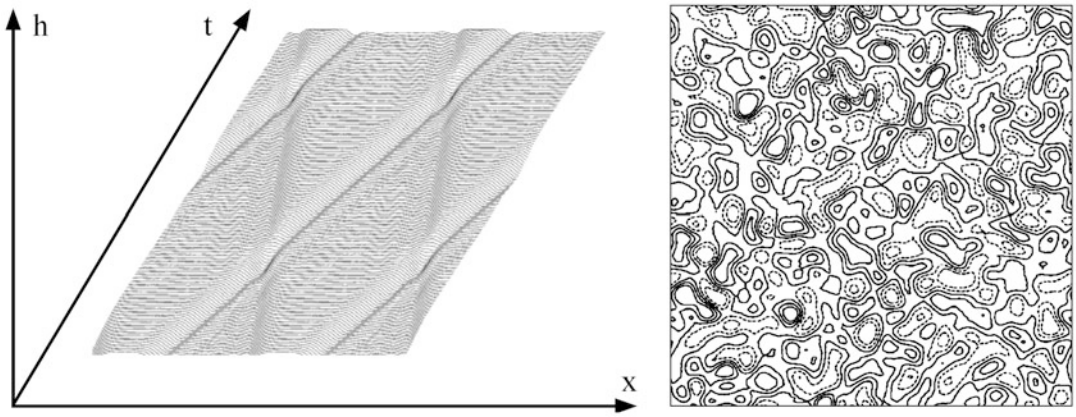

Fluid Dynamics, Pattern Formation, Fig. 4 Numerical solutions of the shallow water equations, *left frame* shows a temporal evolution in one dimension, *right frame* a snapshot in two dimensions. *Dashed contour lines* mark troughs, *solid ones* correspond to peaks of the sea

Instabilities

Laplace Pressure and Disjoining Pressure To discuss Eq. (26) further, we must elaborate a little on the dependence of the surface pressure on the depth $h(x, y, t)$ and on its curvature $-\Delta h$.

The length scale of the surface structures is proportional to the depth of the fluid layer. If the films are very thin, we expect to have scales in the range or even well below the capillary length $a = \sqrt{\Gamma/g\rho}$ where Γ denotes the surface tension. Then one has to take into account the additional pressure which originates from the curvature of the surface, the so-called *Laplace pressure* (Landau and Lifshitz 2004) $-\Gamma\Delta_2 h$. Thus we substitute in (26b)

$$p(h) = p_1(h) - \Gamma\Delta_2 h, \tag{27}$$

with a function p_1 (the disjoining pressure) that will be specified later (de Gennes 1985; Van Oss et al. 1988).

Linear Stability Analysis of the Flat Surface To see if the flat film $h = h_0$ is stable against small perturbations, one may perform a linear stability analysis. Inserting

$$(h - h_0, \Phi) = (a, b) \exp\,(\lambda t + ikx)$$

into (26) yields, after linearization with respect to a, b, a linear eigenvalue problem with the solvability condition

$$\begin{aligned}\lambda_{12}(k) &= -\frac{\tilde{\nu}k^2}{2} \\ &\pm i\,|k|\,\sqrt{h_0\left(g + p_1' + \Gamma k^2\right)/\rho - \tilde{\nu}^2 k^2/4},\end{aligned} \tag{28}$$

where

$$p_1' = \left.\frac{\mathrm{d}p_1}{\mathrm{d}h}\right|_{h=h_0}.$$

We assume that the artificial viscosity is small, $\tilde{\nu}^2 \ll \Gamma/\rho$. An instability occurs first at $k = 0$ if the expression under the integral can be negative, that is, for $p_1' + \rho g < 0$. This corresponds to the region of initial thickness h_0 where the generalized pressure

$$p_1(h) + \rho g h \tag{29}$$

has a negative slope. For that case, the real part of λ_1 starts at $k = 0$ at zero with positive slope, has a maximum at $k = k_c$ and decreases again to the value $-\nu k^2/2$. We shall revisit this instability in the next section and call it there, in a more systematic classification, a type II instability. How can (29) have a negative slope for a certain range of h_0? It is obvious that one has to assume that the pressure p_1 depends in some nonlinear nonmonotonic fashion on the value of h (Fig. 5). As we shall see later, this can be the case for very thin films where van der Waals forces between the solid support and the

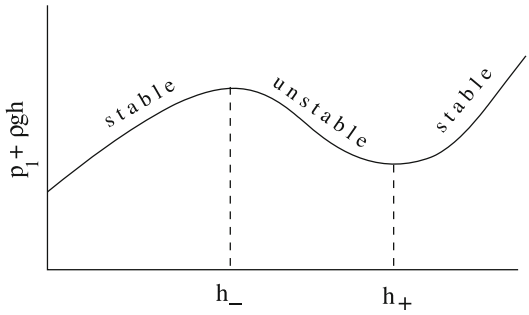

Fluid Dynamics, Pattern Formation, Fig. 5 If the pressure depends on h and has a certain region with a negative slope, the flat film is unstable in this region and pattern formation sets in

free surface come into play (de Gennes 1985; Israelachvili 1992; Van Oss et al. 1988). But also, in thicker films, this should be possible in non-isothermal situations, where the surface temperature, and therefore the surface tension, changes with the vertical coordinate (Marangoni effect, see Section "Instabilities", Fig. 8). If we take (for instance) as a model the polynomial

$$p_1 = c \cdot h \cdot (h - h_1) \cdot (h - h_2), c > 0, \qquad (30)$$

then the flat surface is unstable for h between the two spinodals

$$h_- < h < h_+$$

with $h_\pm$ being the roots of

$$3h^2 - 2h(h_1 + h_2) + h_1 h_2 + \rho g/c = 0.$$

Figure 6 shows a numerically determined time series of a random dot initial condition. The mean thickness h_0 was chosen in the unstable region. The formation shows traveling waves in the linear phase, followed by coarsening to a large scale structure, in this case one big region of depression, or a hole. This hole becomes more and more symmetric while the velocity decays due to the friction term. Finally, a steady state of a big circular hole remains.

Parametric Excitation of a Thin Bistable Fluid Layer

One way to replace the energy lost by damping (to "open" the system) is to accelerate the whole layer periodically in the vertical direction. This was done first in an experiment by Michael Faraday in 1831 (Faraday 1831). He obtained regular surface patterns normally in the form of squares, see Fig. 1.

Faraday patterns can be seen as a solution of the shallow water equations if the gravity constant g is modulated harmonically (Bestehorn 2006)

$$g(t) = g_0 + g_1 \cos \omega t. \qquad (31)$$

A linear stability analysis leads to a Mathieu Eq. (1). The flat film is unstable if frequency and amplitude fall into certain domains, the so-called *Arnold tongues*. There, one usually finds squares for not-too-supercritical values.

We conclude this section by showing a numerical solution of (26) with parameters as in Fig. 6, but now with an additional periodic excitation (Fig. 7). Coarsening is still present, but now oscillating drops emerge in the form of stars. No time stable structure is found in the long time limit.

Instabilities

Mechanisms of Instability in Fluids

We start with the specific case of a plane layer of a viscous fluid with a vertically applied, constant temperature gradient β (Fig. 11), where

$$\beta = (T_1 - T_0)/d \qquad (32)$$

and T_0, T_1 are the temperatures at the lower, upper side of the layer. We assume that a motionless stationary state exists as a (stable or unstable) solution of (15) and of an equation such as (20) for the temperature. The temperature and pressure distribution of that state can then be computed from (15, 20) by putting $\vec{v}$ and all time derivatives to zero:

$$\nabla p^0 = \vec{f} \qquad (33a)$$

$$\Delta T^0 = 0. \qquad (33b)$$

If an external force is provided by buoyancy, we may align the z-axis of the coordinate system along $\vec{f}$ which yields

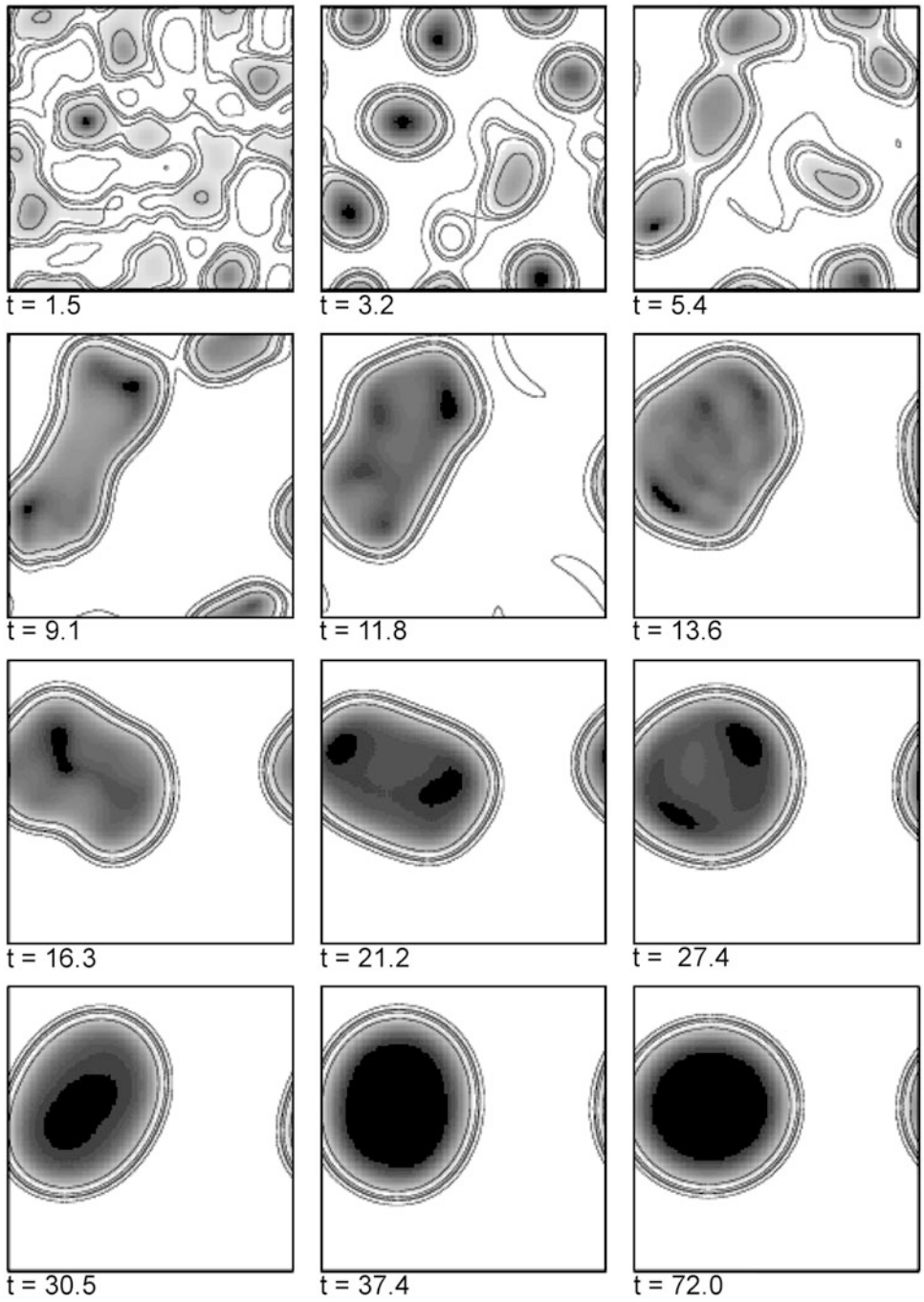

Fluid Dynamics, Pattern Formation, Fig. 6 Time series from a numerical solution of (26) with artificial damping and bistable pressure according to (30). Coarsening dominates the nonlinear evolution and eventually a stationary circular region of surface depression (a hole) remains. Periodic boundary conditions in both horizontal directions have been used

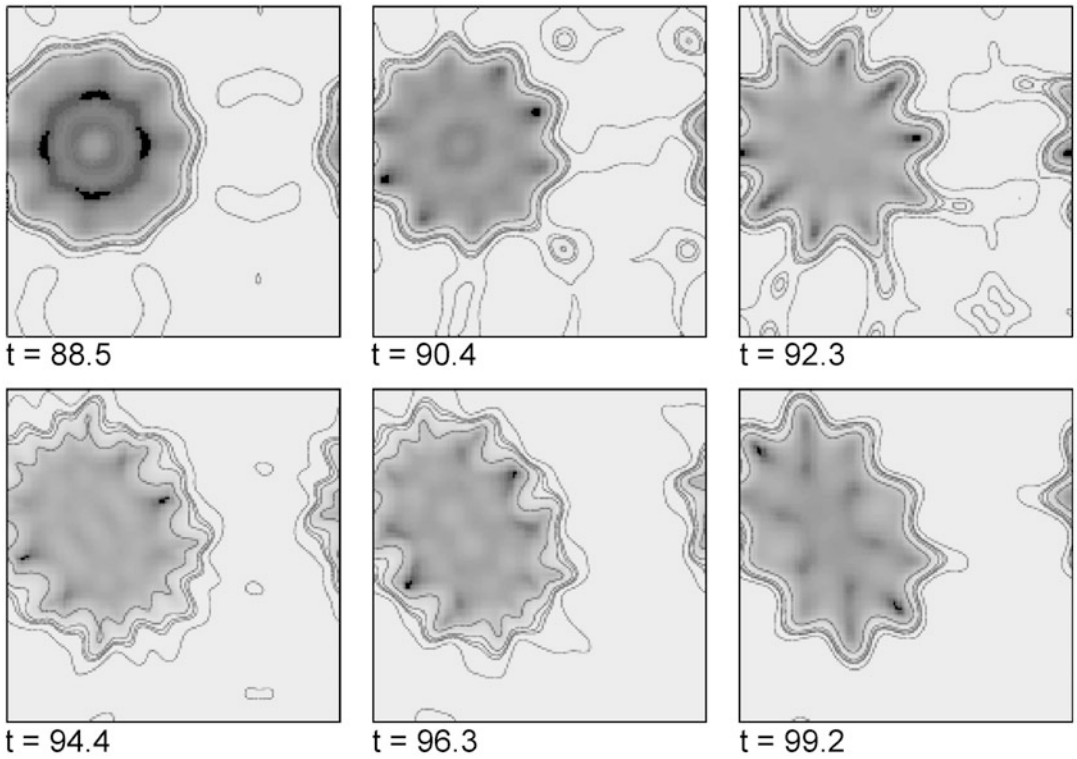

Fluid Dynamics, Pattern Formation, Fig. 7 Continuation of the series of Fig. 6, but with additional parametric excitation according to (30) switched on at $t = 72$. Instead of stationary patterns pulsating stars are found

$$\vec{f} = -g\,\rho\left(\vec{r}\right)\,\hat{\mathrm{e}}_z,$$

where g is the gravitational acceleration. Equation (33a) can be solved only if ρ does not depend on x and y. If one assumes that the density depends on temperature

$$\rho = \rho\left(T^0\right) \tag{34}$$

then T^0 can also depend only on z. Thus one finds from (33b)

$$T^0(z) = a + bz. \tag{35}$$

Taking a linear relation for (34)

$$\rho(T) = \rho_0[1 - \alpha(T - T_0)] \tag{36}$$

with the heat expansion coefficient $\alpha \equiv -\rho_0^{-1}\mathrm{d}\rho/\mathrm{d}T$ and ρ_0 as the density at the reference temperature T_0, one may integrate (33a) and find for the pressure of the motionless state (hydrostatic pressure)

$$p^0(z) = -g\int \rho \mathrm{d}z = -g\rho_0\left(z - \frac{1}{2}\alpha\beta z^2\right) \tag{37}$$

where we put $a = T_0$ and $b = \beta$, in agreement with (32).

A linear stability analysis (Chandrasekhar 1961) shows that the motionless, nonequilibrium state (35) can become unstable if the temperature gradient β exceeds a certain critical value, depending on the fluid properties and the geometry of the layer. There are two different mechanisms, if the fluid layer is heated from below:

(1) *Buoyancy:* Hot fluid particles (volume elements) near the bottom are lighter than colder ones and want to rise. Colder particles near the top want to sink. If the stabilizing forces of

thermal conduction and friction in the fluid are exceeded by the externally applied temperature gradient, patterned fluid motion sets in.

(2) *Surface tension:* If the upper surface of the fluid is free, that is, in contact with the ambient air, tangential surface tension normally increases with decreasing surface temperature (Fig. 8a–c). If a fluid particle near the surface moves by fluctuations, say, to the right, then warmer fluid is pulled up from the bottom, increasing the surface temperature locally. Due to laterally increasing surface tension with respect to the neighbored points, even more hot fluid is pumped up from the bottom and the fluid starts to move. This is called the Marangoni effect and works even without gravity, that is, in space experiments.

In both cases, the typical length of the structures which bifurcate from the motionless state is of the order of the layer depth. These instabilities are sometimes called *small scale instabilities.*

In the situation described above, the surface can be assumed to be flat and undeformable. Of course this is only an approximation, but valid for not-too-thin fluid layers and parameters not too far from threshold. If, on the other hand, the thickness of the fluid layer is less than a certain value which is on the order of 10^{-4} m for common silicone oils, another mechanism comes to the foreground. This mechanism is based on

Surface Deformation. If the surface is locally depressed by an arbitrary fluctuation, the depressed part is heated up due to the vertical temperature gradient. A lateral surface tension gradient is formed which pulls the liquid outside the depressed region (Fig. 8d). Since the continuity equation must hold, the surface becomes even more depressed and an instability occurs. The same mechanism leads to the growth of elevated parts of the surface, under which fluid is pumped in from adjacent regions (Golovin et al. 1997; Nepomnyashchy et al. 2002; Oron et al. 1997). The deformation mode belongs to the so-called *large-scale instability.* This means that the fastest growing modes have a wavelength that is very large compared to the layer depth. It is the depth of the layer which distinguishes which instability occurs first if the temperature gradient is increased from the sub-critical region (Fig. 9).

In ultra-thin films (depth of few 100 nm or less), other mechanisms are possible. Van der Waals forces between the free surface and the solid substrate then become important. They have a potential and can be expressed in the pressure by an extra term, *disjoining pressure,* as already shown in Section "Surface Waves". If that pressure increases with decreasing layer depth, fluid is pressed out of depressed regions and pumped into elevated regions and an instability occurs, even for isothermal cases (Fig. 10).

Pattern Formation – Examples

What happens if the critical value for the temperature gradient is exceeded? Since the famous experiments of Henri Bénard (Bénard 1901) in the beginning of the twentieth century, one knows that the fluid starts to move in form of hexagons if the surface is free and the layer is "thick" (Fig. 11). These kinds of experiments

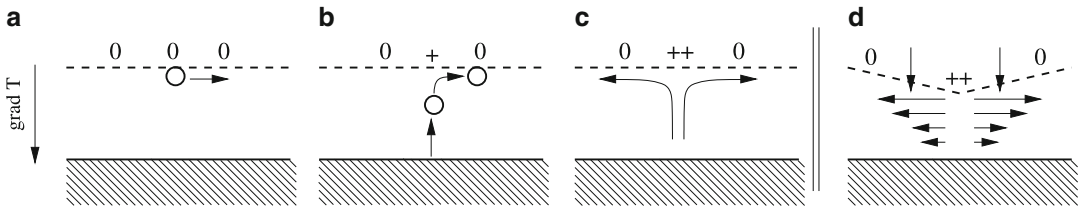

Fluid Dynamics, Pattern Formation, Fig. 8 **a-c** The Marangoni effect may destabilize a fluid layer at rest and may generate a (regular) fluid motion. The surface remains flat (to a good approximation). If the surface is deformable d, a large scale instability may occur as a consequence of the Marangoni effect and mass conservation. For both instabilities, it is sufficient to assume the surface tension as a linear function of temperature. (+/-/0) denote relative temperatures

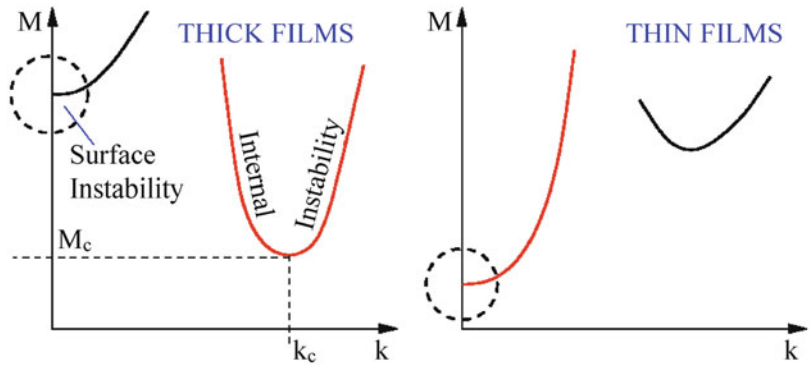

Fluid Dynamics, Pattern Formation, Fig. 9 The two cases "thick films" and "thin films" are defined by the instability that comes first when the temperature gradient is increased. The two instabilities differ in the wavelength Λ (wave number $k = 2\pi/\Lambda$) of the growing structures

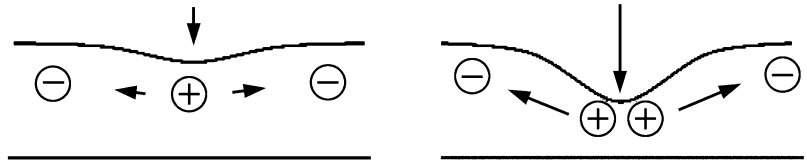

Fluid Dynamics, Pattern Formation, Fig. 10 In ultra-thin films (Reiter et al. 1999; Sharma and Khanna 1999; Vrij 1966), van der Waals forces between free surface and solid substrate may destabilize a plane fluid layer even without an external temperature gradient (+/− denote relative values of the disjoining pressure)

were repeated many times under excellent conditions, for free and closed surfaces, with different fluids, even under micro gravity conditions (Koschmieder 1993; Schwabe 2006).

Surprisingly, a secondary instability takes place for a larger external temperature gradient, which was not known before 1995, almost 100 years after Bénard. This instability shows the occurrence of rather regular squares and was discovered by Eckert and Thess in Dresden, Germany (Bestehorn 1996; Eckert et al. 1998; Nitschke-Eckert and Thess 1995) and, in the meantime but independently, by Schatz and Swinney in Austin, Texas (Schatz and Neitzel 2001; Schatz et al. 1999) (Fig. 12).

If the fluid is covered by a good thermal conductor (a sapphire plate, for instance), hexagons are not the typically found structure at onset, but rather stripes or rolls are encountered (Van Dyke 1982). This can be understood in the frame of reduced order parameter equations by simple symmetry arguments. We shall discuss this in more detail in Section "Order Parameter Equations". For small Prandtl numbers (the ratio between viscosity and thermal diffusivity of the fluid) more complicated

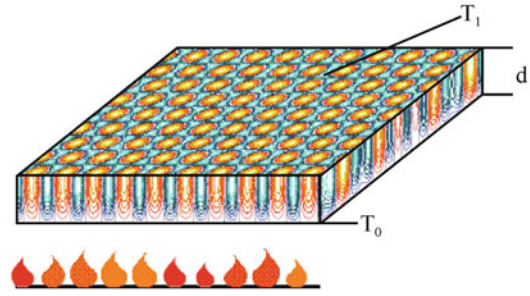

Fluid Dynamics, Pattern Formation, Fig. 11 Hexagonal motion of a fluid heated from below, found by computer solution. Shown are contour lines of the temperature field (after Bestehorn 1993)

and time dependent patterns are found in the form of spirals (Fig. 13) (Bestehorn et al. 1994; Morris et al. 1993; Pesch 1996).

The initial growth of patterns, with a certain horizontal length scale of the order of the depth of the fluid layer, is typical for pattern formation in thick films. In the long term, these structures can be stationary or time dependent, depending on several control and fluid parameters (temperature gradient, material properties, etc.). On the other

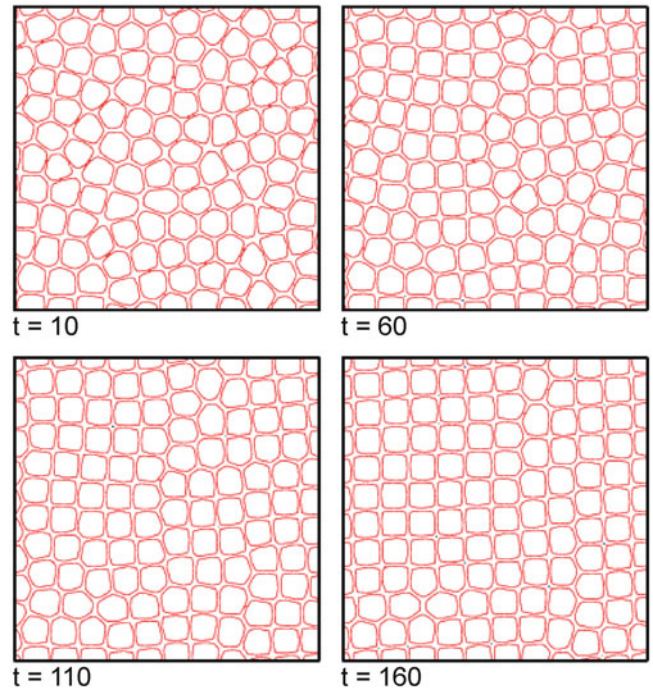

Fluid Dynamics, Pattern Formation, Fig. 12 Regular squares as a secondary instability of hexagons. Numerical solution of the basic Eq. (6)

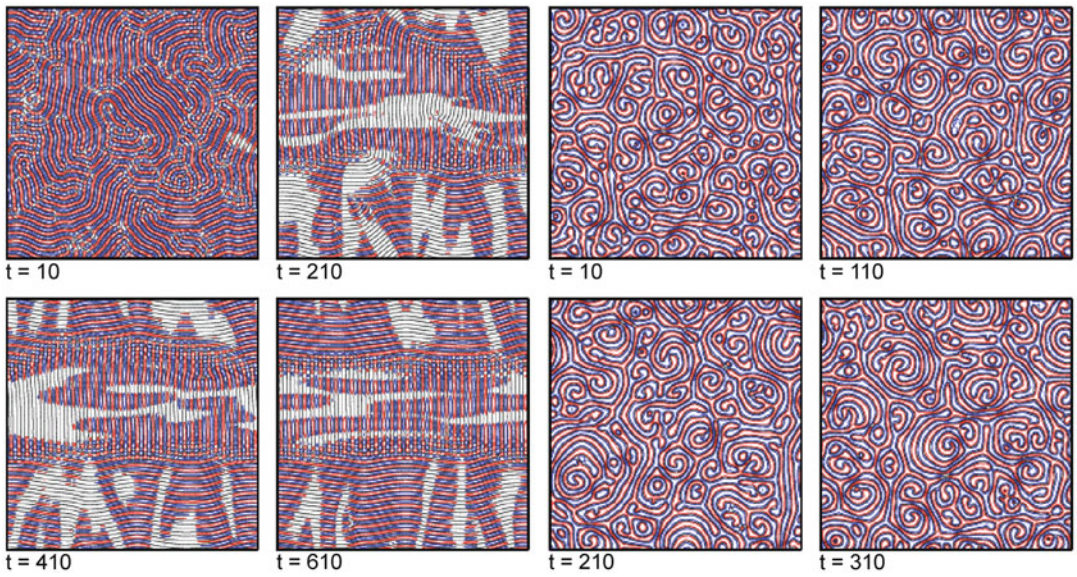

Fluid Dynamics, Pattern Formation, Fig. 13 *Left:* Rolls for high Prandtl number (Pr) fluids; *Right:* spirals for low Pr are found if the surface is covered by a good thermal conductor

hand, the spatio-temporal behavior is completely different for thin and ultra-thin films. Here one finds, after a rather short initial phase, the formation of larger and larger structures, known as *coarsening*. Eventually, the dynamics converge to a stationary state that consists of a single elevation (drop) or suppression (hole) on the surface (Fig. 14 left panel). This development can be interrupted by rupture of the film. Rupture is obtained if the surface touches the substrate and

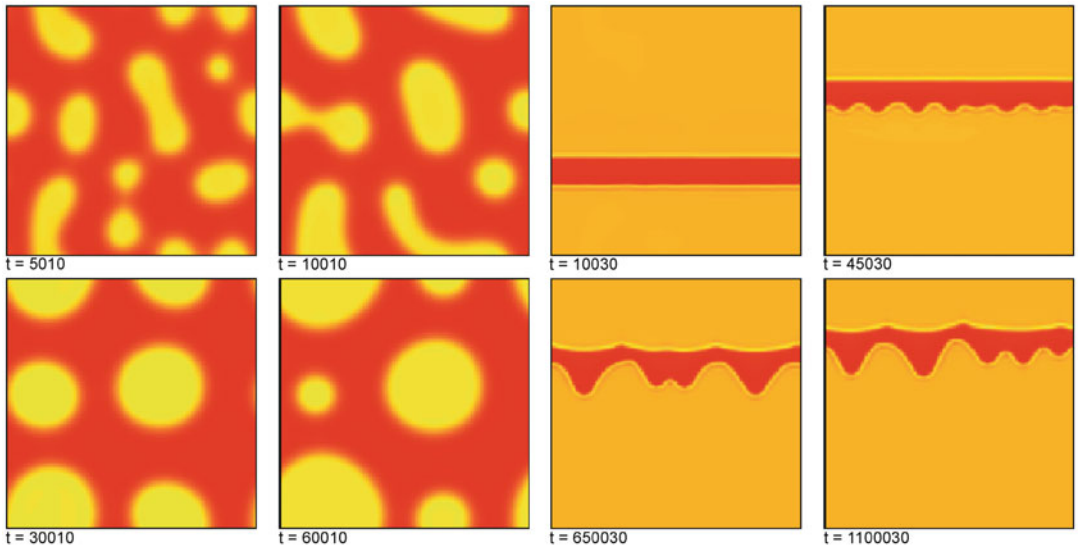

Fluid Dynamics, Pattern Formation, Fig. 14 Numerical solution of the thin film equation (see Section "Conserved Order Parameter Fields"), *red:* elevation, yellow: suppression. *Left:* Coarsening is the typical spatial behavior for a thin film. Finally, a stationary solution consisting of one single hole would survive. *Right:* If the layer is inclined, the motion of fronts and the development of front instabilities can be examined. From (Bestehorn et al. 2003)

the thickness reaches zero in certain domains. Rupture can be avoided by introducing a repelling disjoining pressure acting for a very small depth. In this situation, a completely dry region cannot exist but the substrate is, rather, covered by a so-called (ultra thin) precursor film (de Gennes 1985; Oron et al. 1997), already proposed by Hardy in 1919 (Hardy 1919).

If, in addition, horizontal forces are applied, that is, by inclining the fluid layer, interesting studies of falling films and front instabilities can be made in the frame of the thin film equation (Bestehorn and Neuffer 2001; Scheid et al. 2002). A typical example is shown in Fig. 14, right panel.

Types of Instabilities

Different types of instabilities can be classified according to their linear behavior at onset. Consider a mode having the complex eigenvalue

$$\lambda(k^2) = i\omega(k^2) + \sigma(k^2) \qquad (38)$$

with real valued frequency ω and real valued growth rate σ. Due to rotation symmetry with respect to the horizontal coordinates, all values depend only on the modulus of the wave vector of the unstable mode (assumed as a plane wave in horizontal direction).

According to (Cross and Hohenberg 1993), we use the following notions:

Type $\mathrm{III_s}$ "s" denotes stationary or monotonic and refers to the temporal behavior of the unstable mode close to onset. The type number specifies the spatial behavior of the modes. Type III means slowly varying or even constant in space ($k \approx 0$). The spatial structure beyond instability is then mainly dominated by the geometry and boundary conditions of the system under consideration. For (38) this means

$$\omega = 0 \text{ and } \left.\frac{\mathrm{d}\sigma}{\mathrm{d}k}\right|_{k=0} = 0,$$

See Fig. 15. A typical example for a type $\mathrm{III_s}$ instability is the real Ginzbur–Landau eq. A computer solution clearly showing the spatially (and temporally) slowly varying behavior can be seen in Fig. 16.

Type $\mathrm{III_o}$ "o" stands for oscillatory and denotes a non-vanishing imaginary part of (38) at threshold. This type includes Hopf-instabilities which have the same slow spatial behavior as $\mathrm{III_s}$. In (38) we have

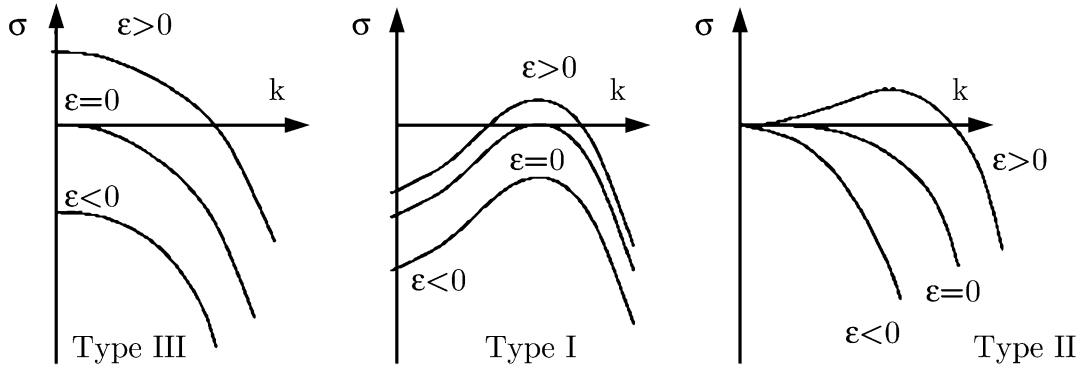

Fluid Dynamics, Pattern Formation, Fig. 15 Schematic drawing of the real part of the eigenvalue (38) as function of the wave vector for the three types of instabilities

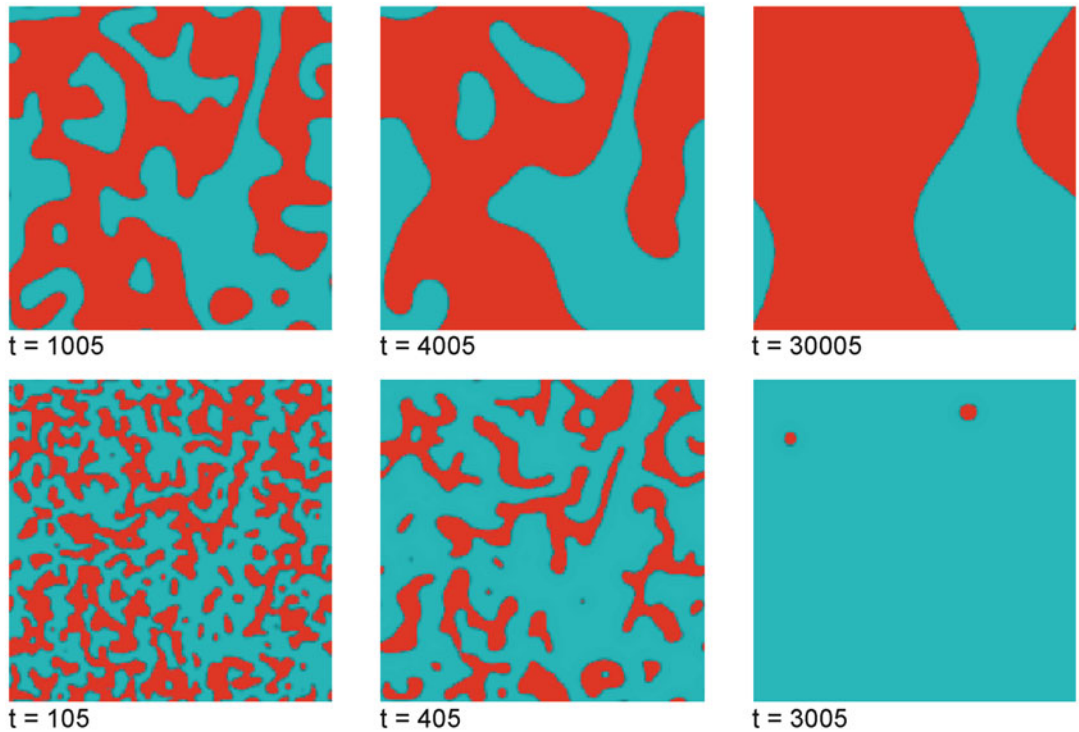

Fluid Dynamics, Pattern Formation, Fig. 16 Numerical solution (time series) of the real Ginzbur–Landau Eq. (39) which shows a III_s instability. The Ginzbur–Landau equation can be considered as a simple model for the magnetization of a ferro magnet. Then the two rows show the spatio-temporal evolution of the magnetization, *Top:* without external field, *Bottom:* with external field

$$\omega \neq 0 \text{ and } \left.\frac{\mathrm{d}\sigma}{\mathrm{d}k}\right|_{k=0} = 0.$$

For this kind of instability one needs at least two coupled diffusion equations. It is often encountered in reaction diffusion systems, as for instance the "Brusselator" (Prigogine and Levever 1968; Prigogine and Nicolis 1967).

Type I_s The short scale pattern forming instabilities shown in Figs. 11, 12 and 13 with periodicity

in space, $k_c \neq 0$ are of this type, see Fig. 15 middle frame. Again one needs at least two coupled diffusion equations to obtain such an instability. For the eigenvalue,

$$\omega = 0 \text{ and } \left.\frac{\mathrm{d}\sigma}{\mathrm{d}k}\right|_{k=k_c} = 0 \text{ with } k_c \neq 0$$

holds. Sometimes these kinds of patterns are called *Turing structures* or *Turing instabilities,* after the seminal work of Alan Turing, who predicted this patterns in skin, scales, or hair coating of certain animals (Turing 1952) (Fig. 17). For more details and pattern formation in biology see (Murray 1993).

Type $\mathbf{I_o}$ Denotes oscillating Turing structures, sometimes also called *wave instabilities.The* eigenvalue λ then has the form

$$\omega \neq 0 \text{ and } \left.\frac{\mathrm{d}\sigma}{\mathrm{d}k}\right|_{k=k_c} = 0 \text{ with } k_c \neq 0.$$

For this instability, the system must be described by at least three coupled diffusion equations. In fluid mechanics, this kind of instability can be encountered in binary mixtures and give rise to a very complicated, in general chaotic, spatio-temporal behavior just at onset (Bestehorn and Colinet 2000).

Type $\mathbf{II_s}$ This type is realized in the surface patterns of thin films, Fig. 14. Here, λ depends on k as shown in the right frame of Fig. 15. One has

$$\omega = 0 \text{ and } \left.\frac{\mathrm{d}\sigma}{\mathrm{d}k}\right|_{k=k_c} = 0 \text{ with } k_c \neq 0$$

and in addition

$$\sigma(k = 0) = 0.$$

From the last condition one sees that modes with $k = 0$, that is, those which are homogeneous in space, are marginally stable, meaning neither stable nor un stable. One may then add a constant to the order parameter (the mode amplitude)

$$\xi' = \xi + \text{const},$$

where ξ' is still a solution of the linear part of the order parameter equation. This property usually has its origin in a symmetry of the basic problem. We shall discuss this instability type in Section "Conserved Order Parameter Fields" on thin films. There, the symmetry corresponds to a global shift of the surface in vertical direction.

Type $\mathbf{II_0}$ The same as $\mathrm{II_s}$ but with an additional imaginary part $\omega \neq 0$. We mention this type only for the sake of completeness; there will be no further examples in this contribution.

Fluid Dynamics, Pattern Formation, Fig. 17 After a theory by A. Turing the painting on skin, scales, or coats of animals is organized by a nonequilibrium chemical reaction during the embryonal phase. *Left:* regular spots arranged in a hexagonal manner on the panther fish, *Right:* stripes with defects on the lion fish (pictures taken by the author in the Berlin Zoo)

Order Parameter Equations

Order Parameters

In this section, we wish to describe pattern formation in the weakly nonlinear regime. We shall mainly restrict ourselves to the case of monotonic (non-oscillatory) instabilities. For further references see (Bestehorn and Friedrich 1999; Bestehorn and Haken 1990; Cross and Hohenberg 1993; Haken 1983, 2004). Close to a bifurcation point to a new state, it is natural to expand nonlinearities with respect to small deviations from the old, unstable state. These deviations can be written as a composition of certain Galerkin functions or modes; the amplitudes of these modes are called *order parameters*. If the order parameters are functions only of time, the dynamics given by the order parameter equations (ordinary differential equations, abbreviated: ODE) are perfect patterns, for instance parallel stripes, squares (two order parameters) or hexagons (three order parameters). Natural patterns having defects and grain boundaries, as for instance the structures shown in Figs. 11, 12 and 13 can also be described in this frame. One then has to make the additional assumption that the order parameters also vary (slowly) in space and are ruled by partial differential equations (abbreviated: PDE).

The Ginzbur–Landau Eq.

A prominent (and historically the first) example of such a PDE order parameter equation is the Ginzbur–Landau equation (Aranson and Kramer 2002; Landau and Lifshitz 1996). In one spatial dimension it has the normal form

$$\partial_t \xi(x,t) = \varepsilon\,\xi(x,t) + q_0^2\,\partial_{xx}^2\,\xi(x,t) - c_3|\xi(x,t)|^2\xi(x,t) \tag{39}$$

and describes the spatio-temporal evolution of the complex order parameter field ξ. If ξ is the mode amplitude of a roll structure with a certain wave number, for example, the critical one, then stripes with defects are obtained if ξ varies (slowly) in space. If c_3 and q_0 are real valued, (39) is called the real Ginzbur–Landau equation. For complex values of the coefficients, an incomparably richer and much more complicated spatio-temporal behavior of the order parameter is encountered, for details we refer to (Aranson and Kramer 2002).

In the theory of nonequilibrium pattern formation, writing down an equation such as (39) is far from being purely phenomenological. It can be derived rather systematically from the basic hydrodynamic equations (Haken 1975; Newell and Whitehead 1969).

To give an idea of that, we do it briefly for the (two-dimensional) case of convection (the reader who is not interested in technical details can skip the rest of this section).

Starting point are the Eqs. (16) and (20) where in the latter, S stands for temperature T.

Scaling of independent $\left(\vec{r},t\right)$ and dependent $\left(\vec{v},T\right)$ variables allows the reduction of the numbers of parameters:

$$\begin{aligned}\vec{r} &= \vec{\tilde{r}}\cdot d, t = \tilde{t}\cdot\left(d^2/\kappa\right), \vec{v}\\ &= \vec{\tilde{v}}\cdot(\kappa/d), T = \tilde{T}\cdot\beta\cdot d,\end{aligned} \tag{40}$$

with the constant depth d and the externally applied temperature gradient (32). Note that if the liquid is heated from below, $\beta < 0$. Introducing the deviation Θ from the thermally conducting state

$$\begin{aligned}T\left(\vec{r},t\right) &= T^0(z) + \Theta\left(\vec{r},t\right)\\ &= T_0 + \beta z + \Theta\left(\vec{r},t\right)\end{aligned} \tag{41}$$

transforms (20) into

$$\begin{aligned}\{\Delta - \partial_t\}\,\Theta\left(\vec{r},t\right) &= -\Lambda_2\Psi\left(\vec{r},t\right)\\ &\quad + \left(\vec{v}\cdot\nabla\right)\Theta\left(\vec{r},t\right)\end{aligned} \tag{42}$$

and (16) into

$$\left\{\Lambda - \frac{1}{\mathrm{Pr}}\partial_t\right\}\Lambda_2\Phi\left(\vec{r},t\right) = -\frac{1}{\mathrm{Pr}}\left[\mathrm{curl}\left(\left(\vec{v}\cdot\nabla\right)\vec{v}\right)\right]_z \tag{43a}$$

$$\begin{aligned}&\left\{\Lambda - \frac{1}{\mathrm{Pr}}\partial_t\right\}\Lambda\Lambda_2\Psi\left(\vec{r},t\right)\\ &= -R\,\Lambda_2\,\Theta\left(\vec{r},t\right) - \frac{1}{\mathrm{Pr}}\left[\mathrm{curl}\,\mathrm{curl}\left(\left(\vec{v}\cdot\nabla\right)\vec{v}\right)\right]_z.\end{aligned} \tag{43b}$$

Two dimensionless numbers occurred. One is the material dependent *Prandtl number*

$$\mathrm{Pr} = \frac{\nu}{\kappa}, \tag{44}$$

which measures the ratio of the diffusion times of heat and momentum. The other one is called the *Rayleigh number* and turns out to be

$$R = -\frac{\beta g \alpha d^4}{\nu\kappa} \tag{45}$$

with α defined in (36). The system (42) and (43) constitutes the basic equations for the three scalar fields, Φ, Ψ, and Θ which describe convective motion and temperature of a plane fluid layer with a flat and undeformable surface onto a plane substrate. This can be further simplified by taking the large Prandtl number limes $1/\mathrm{Pr} = 0$ (good for fluids with high viscosity, oils, etc.). Then Φ vanishes everywhere and only two equations are left:

$$\Delta^2 \Psi\left(\vec{r},t\right) = -R\,\Theta\left(\vec{r},t\right) \tag{46a}$$

$$\{\Delta - \partial_t\}\Theta\left(\vec{r},t\right) = -\Delta_2 \Psi\left(\vec{r},t\right) + \left(\vec{v}\cdot\nabla\right)\Theta\left(\vec{r},t\right). \tag{46b}$$

A general nonlinear (2D) solution of Eqs. (46) may be expressed by

$$\begin{bmatrix}\Psi(x,z,t)\\ \Theta(x,z,t)\end{bmatrix} = \sum_l \int_{-\infty}^{\infty} \mathrm{d}k\,\xi_l(k,t)\begin{bmatrix} f_l\left(k^2,z\right)\\ g_l\left(k^2,z\right)\end{bmatrix} e^{-ikx} \tag{47}$$

and

$$\xi_l(k,t) = \xi_l^*(-k,t)$$

where f and g are eigenfunctions of the ODE eigenvalue problem

$$\begin{aligned}\left(d_z^2 - k^2\right) f_l + R\, g_l &= 0\\ \left(d_z^2 - k^2 - \lambda_l\left(k^2\right)\right) g_l - k^2 f_l &= 0.\end{aligned} \tag{48}$$

Here, l labels the different eigenfunctions. Equation (48) is obtained by inserting (47) with $\xi_l \sim \exp.(\lambda t)$ into (46) and keeping only linear terms. The functions f_l and g_l can be calculated numerically by a finite difference method in vertical direction where suitable boundary conditions must be implemented.

Inserting (47) into (46) yields, after multiplication with the adjoint function g_l^+ exp. (ikx) and integration over the spatial coordinates, the system:

$$\begin{aligned}\partial_t \xi_l(k,t) &= \lambda_l\left(k^2\right)\xi_l(k,t)\\ &-\sum_{l'l''}\int_{-\infty}^{\infty} \mathrm{d}k'\,\mathrm{d}k''\, c_{ll'l''}(kk'k'')\,\xi_{l'}(k',t)\,\xi_{l''}(k'',t)\\ &\qquad \delta(k-k'-k''),\end{aligned} \tag{49}$$

where the coefficients c are matrix elements that can be computed directly from the basic equations for any given set of control parameters:

$$\begin{aligned}&c_{ll'l''}(kk'k'')\\ &\equiv k'^2\int_0^1 \mathrm{d}z\, g_l^+\left(k^2,z\right) f_{l'}\left(k'^2,z\right)\partial_z g_{l''}\left(k''^2,z\right)\\ &-k'k''\int_0^1 \mathrm{d}z\, g_l^+\left(k^2,z\right) g_{l'}\left(k'^2,z\right)\partial_z f_{l''}\left(k''^2,z\right).\end{aligned} \tag{50}$$

Here we are still at the same level of complexity; the infinitely many degrees of freedom intrinsic in the basic partial differential equations are expressed by an infinite number of mode amplitudes $\xi_l(k, t)$. To eliminate the fast damped modes by the linearly growing ones, we divide the eigenmodes into two groups:

$$\lambda_l \to \begin{cases}\lambda_u\left(k^2\right) \approx 0 \Rightarrow \xi_u(k,t)\\ \qquad\qquad |\,k\,| \approx k_c, u = l = 1\\ \lambda_s\left(k^2\right) \ll 0 \Rightarrow \xi_s(k,t)\\ \quad s = l > 1 \text{ or } s = l = 1 \text{ but } |k| \neq k_c.\end{cases} \tag{51}$$

In the following we may therefore substitute the index l by u (unstable) or s (stable), depending on the values of l and $|k|$. Now we express the amplitudes of the enslaved modes invoking an adiabatic

elimination (k_c denotes the wave vector that maximizes λ_u). In this case, the dynamics of the enslaved modes are neglected, they follow instantaneously to the order parameters. This is a special case of the slaving principle of *synergetics,* which can be used in many other disciplines beyond hydrodynamics (Haken 1983).

The remaining equations for the order parameters ξ_u, the amplitude equations, read (here and in the following we suppress the index u at ξ and λ):

$$\begin{aligned}\partial_t \xi(k,t) &= \lambda\left(k^2\right)\xi(k,t)\\ &+\int \mathrm{d}k'\mathrm{d}k''\mathrm{d}k'''\, B\left(k,k',k'',k'''\right)\xi(k',t)\xi(k'',t)\\ &\quad \xi\left(k''',t\right)\delta\left(k-k'-k''-k'''\right)\end{aligned} \tag{52}$$

where $|k|, |k'|, |k''|, |k'''| \approx |k_c|$. Note that there are no quadratic expressions in ξ. This is because $k - k' - k''$ cannot vanish if all wave numbers have the same (nonzero) absolute value. In three spatial dimensions this is different. Three k-vectors can then form a resonant triangle, which is the reason why stable hexagons may occur.

The Landau coefficient B is directly related to the matrix elements (50):

$$\begin{aligned}B\left(k,k',k'',k'''\right) &= \sum_s \frac{1}{\lambda_s\left(\left(k''+k'''\right)^2\right)}\\ c_{suu}\left(k''+k''',k',k''\right)&\left[c_{uus}\left(k,k',k''+k'''\right)\right.\\ &\left.+c_{usu}\left(k,k''+k''',k'\right)\right]\end{aligned}$$

where the indices u and s are defined in (51).

To arrive at the Ginzbur–Landau equation, one must transform back to real space. If we express the δ-function in (52) as

$$\delta\left(k-k'-k''-k'''\right) = \frac{1}{2\pi}\int \mathrm{d}x\, \mathrm{e}^{i\left(k-k'-k''-k'''\right)x}$$

and assume, that the coefficient B does not depend much on k (it can be evaluated at $k = \pm k_c$), the cubic part of (52) takes the form

$$\begin{aligned}&\frac{\overline{B}}{2\pi}\int \mathrm{d}x \mathrm{e}^{ikx}\int \mathrm{d}k'\,\xi(k',t)\,\mathrm{e}^{-ik'x}\int \mathrm{d}k''\xi(k'',t)\\ &\mathrm{e}^{-ik''x}\int \mathrm{d}k'''\,\xi\left(k''',t\right)\mathrm{e}^{-ik'''x}\\ &\qquad = \frac{\overline{B}}{2\pi}\int \mathrm{d}x\, \mathrm{e}^{ikx}\Psi^3(x,t)\end{aligned} \tag{53}$$

where we have introduced the Fourier transform

$$\Psi(x,t) = \int \mathrm{d}k\,\xi(k,t)\,\mathrm{e}^{-ikx}. \tag{54}$$

Inserting (53) into (52), multiplying with $\mathrm{e}^{-ik\widetilde{x}}$ and integrating over k yields the order parameter equation in real space

$$\begin{aligned}\partial_t \Psi(\widetilde{x},t) &= \int \mathrm{d}k\lambda(k)\,\xi(k,t)\,\mathrm{e}^{-ik\widetilde{x}}\\ &\quad +\overline{B}\,\Psi^3(\widetilde{x},t).\end{aligned} \tag{55}$$

If we replace the k^2 -dependence of λ under the integral by $-\partial^2_{\widetilde{xx}}$ we may pull A out of the integral and write (55) in the form

$$\partial_t \Psi(x,t) = \lambda\left(-\partial^2_{xx}\right)\Psi(x,t) + \overline{B}\,\Psi^3(x,t). \tag{56}$$

The function $\Psi(x, t)$ can also be called an "order parameter", though it is not slowly varying in space compared to the small scale structure of the rolls, an idea which we shall work out in the following section. One big advantage can already be seen: the reduction of the number of space dimensions by one. We started with the hydrodynamic equations in two dimensions and get an order parameter equation in only one spatial dimension.

To find the form of the Ginzbur–Landau equation, we must introduce a slowly varying order parameter. This is done by recalling that the Fourier transform of W is mainly excited around $k = \pm k_c$. Then it is natural to make a "rotating wave approximation" with respect to x of the form

$$\Psi(x,t) = \xi(x,t)\,\mathrm{e}^{ik_c x} + \xi^*(x,t)\,\mathrm{e}^{-ik_c x}. \tag{57}$$

Inserting this into (56), multiplying by $\mathrm{e}^{-ik_c x}$ and integrating with respect to x over one period

$2\pi/k_c$ yields with the assumption of constant (slowly varying) ξ in this period

$$\partial_t \xi(x,t) = \lambda\left(-(\partial_x + ik_c)^2\right)\xi(x,t) + 3\overline{B}\,|\xi(x,t)|^2\xi(x,t).$$

The last approximation is concerned with the evaluation of the eigenvalue in form of a differential operator. Close to k_c, it has the form of a parabola, see Fig. 15 middle frame. Thus we may approximate

$$\lambda\left(k^2\right) = \varepsilon - q^2\left(k^2 - k_c^2\right)^2 \tag{58}$$

and also

$$\begin{aligned}\lambda\left(-(\partial_x + ik_c)^2\right) &= \varepsilon - q^2\left((\partial_x + ik_c)^2 + k_c^2\right)^2 \\ &= \varepsilon - q^2\left(\partial_{xx}^2 + 2ik_c\partial_x\right)^2 \\ &\approx \varepsilon + 4q^2k_c^2\partial_{xx}^2.\end{aligned} \tag{59}$$

For the last conversion, we neglect higher derivatives, which is justified due to the slowly varying spatial dependence of ξ. After scaling of ξ and the additional assumption $\overline{B} < 0$ we finally have derived the Ginzbur–Landau Eq. (39).

The Swift-Hohenberg Equation

In two spatial dimensions, the drawback of the Ginzburg-Landau equation is its lack of rotational symmetry. Therefore, it is better to pass on the rotating wave approximation (57) and to consider instead the fully space-dependent function Ψ as an order parameter, but now in two spatial dimensions. The resulting evolution equation in its lowest nonlinear approximation is the Swift-Hohenberg Eq. (88)

$$\dot{\Psi}\left(\vec{x},t\right) = \left[\varepsilon - (1+\Delta_2)^2\right]\Psi\left(\vec{x},t\right) - \Psi^3\left(\vec{x},t\right), \tag{60}$$

which we shall derive now.

Non-local Order Parameter Equations To this end we go back to (52) and write it down in two dimensions, now including the quadratic terms $\left(\vec{k} = (k_x, k_y)\right)$:

$$\begin{aligned}\partial_t\xi\left(\vec{k},t\right) &= \lambda\left(k^2\right)\xi\left(\vec{k},t\right) + \int \mathrm{d}^2\vec{k}'\,\mathrm{d}^2\vec{k}''\,A\left(\vec{k},\vec{k}',\vec{k}''\right) \\ &\cdot\xi\left(\vec{k}',t\right)\xi\left(\vec{k}'',t\right)\delta\left(\vec{k}-\vec{k}'-\vec{k}''\right) + \int \mathrm{d}^2\vec{k}'\,\mathrm{d}^2\vec{k}''\,\mathrm{d}^2\vec{k}''' \\ &\cdot B\left(\vec{k},\vec{k}',\vec{k}'',\vec{k}'''\right)\xi\left(\vec{k}',t\right)\xi\left(\vec{k}'',t\right)\xi\left(\vec{k}''',t\right) \\ &\cdot\delta\left(\vec{k}-\vec{k}'-\vec{k}''-\vec{k}'''\right).\end{aligned} \tag{61}$$

Introducing the (2D) Fourier transform $\left(\vec{x} = (x,y)\right)$,

$$\Psi\left(\vec{x},t\right) = \int \mathrm{d}^2\vec{k}\,\xi\left(\vec{k},t\right)\mathrm{e}^{-i\vec{k}\vec{x}}. \tag{62}$$

and transforming (61) to real space yields the integro-differential equation

$$\begin{aligned}&\partial_t\Psi\left(\vec{x},t\right) = \lambda(\Delta)\Psi\left(\vec{x},t\right) \\ &+\int\int \mathrm{d}^2\vec{x}'\,\mathrm{d}^2\vec{x}''\,G^{(2)}\left(\vec{x}-\vec{x}',\vec{x}-\vec{x}''\right)\Psi\left(\vec{x}',t\right)\Psi\left(\vec{x}'',t\right) \\ &+\int\int\int \mathrm{d}^2\vec{x}'\,\mathrm{d}^2\vec{x}''\,d^2\vec{x}'''\,G^{(3)}\left(\vec{x}-\vec{x}',\vec{x}-\vec{x}'',\vec{x}-\vec{x}'''\right) \\ &\Psi\left(\vec{x}',t\right)\Psi\left(\vec{x}'',t\right)\Psi\left(\vec{x}''',t\right)\end{aligned} \tag{63}$$

where the kernels are computed by the Fourier transforms:

$$\begin{aligned}&G^{(2)}\left(\vec{x},\vec{x}'\right) \\ &\quad= \frac{1}{16\pi^4}\int \mathrm{d}^2\vec{k}\,\mathrm{d}^2\vec{k}'\,A\left(\vec{k}+\vec{k}',\vec{k},\vec{k}'\right)\mathrm{e}^{-i\vec{k}\vec{x}}\,\mathrm{e}^{-i\vec{k}'\vec{x}'}, \\ &G^{(3)}\left(\vec{x},\vec{x}',\vec{x}'''\right) \\ &\quad= \frac{1}{64\pi^6}\int \mathrm{d}^2\vec{k}\,\mathrm{d}^2\vec{k}'\,\mathrm{d}^2\vec{k}''\,B\left(\vec{k}+\vec{k}'+\vec{k}'',\vec{k},\vec{k}',\vec{k}''\right) \\ &\qquad\cdot\mathrm{e}^{-i\vec{k}\vec{x}}\,\mathrm{e}^{-i\vec{k}'\vec{x}'}\,\mathrm{e}^{-i\vec{k}''\vec{x}''}.\end{aligned} \tag{64}$$

Gradient Expansion Although Eq. (63) has a rather general form, its further numerical treatment is not practicable, at least not in two dimensions. Each integral must be approximated somehow as a sum over mesh points. The cubic coefficients would result in a 6-fold sum with, if N is the number of mesh points, N^6 summands, which is, if N is around the size of 100, rather hopeless.

On the other hand, the excitation of ξ mainly close to k_c, in two dimensions on a (narrow) ring in Fourier space with radius k_c, makes it natural to expand Ψ under the integrals around $\vec{x}$. This works well if the kernels (64) have a finite (small) range with significant contribution only for $|\vec{x} - \vec{x}'| < \Lambda$ with $\Lambda = 2\pi/k_c$.

To save space we demonstrate the method only for the quadratic term of (63) and in one spatial dimension. A Taylor expansion of Ψ leads to

$$\int\int \mathrm{d}x'\mathrm{d}x'' G^{(2)}(x-x', x-x'') \sum_{m,n=0}^{\infty} \frac{1}{m!n!} \frac{\partial^m \Psi}{\partial x^m} \frac{\partial^n \Psi}{\partial x^n} (x-x')^m (x-x'')^n,$$

where the derivatives must be evaluated at x. They can be written in front of the integrals, yielding

$$\sum_{m,n=0}^{\infty} g^{(2)}_{m\,n} \frac{\partial^m \Psi}{\partial x^m} \frac{\partial^n \Psi}{\partial x^n} \tag{65}$$

with the moments

$$g^{(2)}_{mn} = \frac{1}{m!n!} \int\int \mathrm{d}x_1\, \mathrm{d}x_2\, G^{(2)}(x_1, x_2) x_1^m x_2^n).$$

A similar expression can be found for the cubic coefficient. A series of the form (65) is called *gradient expansion.* In this way, a local order parameter equation results, but which now has infinitely many nonlinear terms. It reads

$$\partial_t \Psi = \lambda(\Delta)\Psi + \sum_{m,n=0}^{\infty} g^{(2)}_{mn} \frac{\partial^m \Psi}{\partial x^m} \frac{\partial^n \Psi}{\partial x^n} + \sum_{l,m,n=0}^{\infty} g^{(3)}_{l\,m\,n} \frac{\partial^l \Psi}{\partial x^l} \frac{\partial^m \Psi}{\partial x^m} \frac{\partial^n \Psi}{\partial x^n} \tag{66}$$

with

$$g^{(3)}_{lmn} = \frac{1}{l!m!n!} \int\int\int \mathrm{d}x_1\, \mathrm{d}x_2\, \mathrm{d}x_3\, G^{(3)}(x_1, x_2, x_3) x_1^l x_2^m x_3^n.$$

For more details see (Bestehorn and Friedrich 1999).

Swift-Hohenberg-Haken Equation The series in (66) will converge rapidly if the kernels have a short range. Here we consider only the extreme case of δ-shaped kernels, now in two dimensions:

$$G^{(2)}\left(\vec{x}_1, \vec{x}_2\right) = A \cdot \delta\left(\vec{x}_1\right)\delta\left(\vec{x}_2\right),$$

$$G^{(3)}\left(\vec{x}_1, \vec{x}_2, \vec{x}_3\right) = B \cdot \delta\left(\vec{x}_1\right)\delta\left(\vec{x}_2\right)\delta\left(\vec{x}_3\right).$$

All coefficients vanish, except $g^{(2)}_{00}$ and $g^{(3)}_{000}$. Then (66) simplifies to

$$\partial_t \Psi\left(\vec{x}, t\right) = \lambda(\Delta)\Psi\left(\vec{x}, t\right) + A\,\Psi^2\left(\vec{x}, t\right) + B\,\Psi^3\left(\vec{x}, t.\right). \tag{67}$$

For the linear part we again use the expansion (58) and replace k^2 by $-\Delta$. After rescaling of length, time and V, (67) turns into the canonical form

$$\dot{\Psi}\left(\vec{x}, t\right) = \left[\varepsilon - (1 + \Delta_2)^2\right]\Psi\left(\vec{x}, t\right) + a\,\Psi^2\left(\vec{x}, t\right) - \Psi^3\left(\vec{x}, t\right) \tag{68}$$

With

$$a = \frac{A}{\sqrt{-B}}.$$

Equation (68) is the Swift–Hohenberg–Haken equation derived first using the theoretical methods of synergetics by Haken (Bestehorn and Haken 1983; Haken 1983).

Numerical solutions of (68) with $a = 0$ are shown in Fig. 18. Stripes as known from convection, but also from Turing instabilities, can be clearly seen. If $|a|$ exceeds a certain value which depends on $\sqrt{\varepsilon}$, hexagonal structures are found which agree qualitatively with those obtained in Bénard–Marangoni convection (Fig. 19). It can be shown that the symmetry break $z \to -z$ caused by the different vertical boundary conditions on top and bottom of the fluid gives rise to a (positive) quadratic coefficient. In the Swift–Hohenberg equation, this violates the symmetry $\Psi \to -\Psi$ and may stabilize two different sorts of hexagons, namely the already mentioned l - and g - hexagons. The first ones are found for large enough positive a, the latter for negative a.

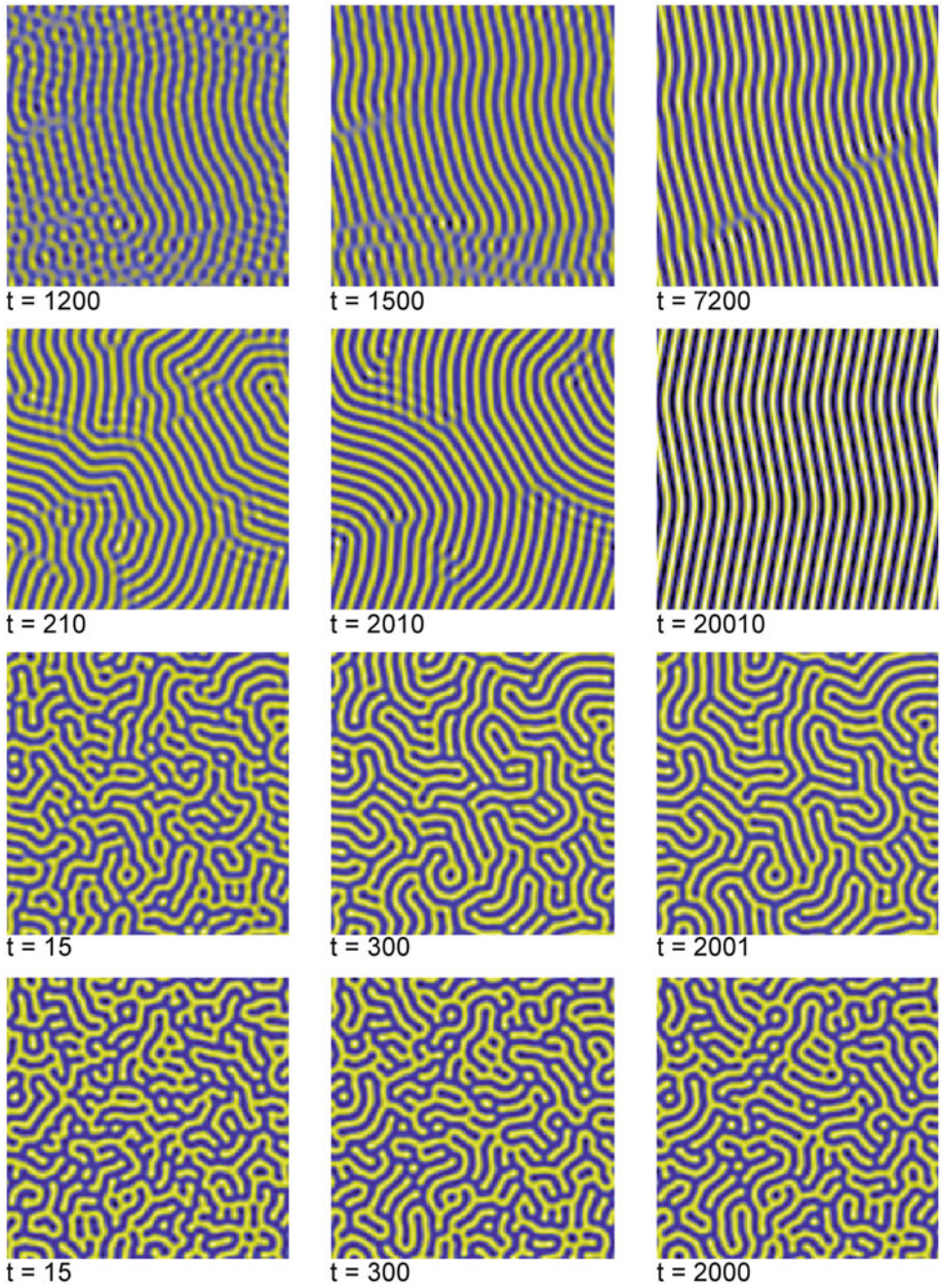

Fluid Dynamics, Pattern Formation, Fig. 18 Computer solutions of the Swift–Hohenberg Eq. (60) for several $\varepsilon = 0.01, 0.1, 1.0, 2.0$ (*top to bottom*). The evolution time scales with $1/\varepsilon$, the number of defects increases with ε

The Swift–Hohenberg equation can be considered as normal form of type I_s instabilities. The bifurcation scenario is general (Fig. 20): hexagons are the generic form at onset if symmetry breaking (quadratic) terms occur, which is normal. Even very small symmetry breaking effects lead to hexagons, although their stability region will decrease and finally shrink to the critical point

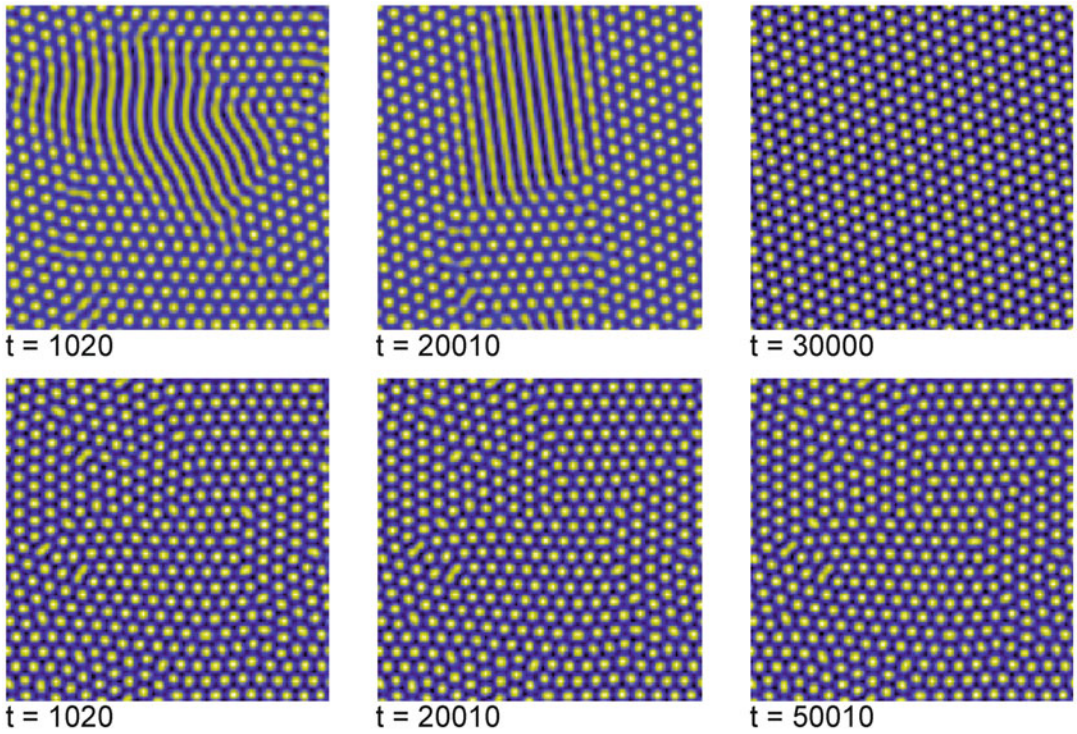

Fluid Dynamics, Pattern Formation, Fig. 19 Evolution of a random dot initial condition from (68) with $\varepsilon = 0.1$, $a = 0.26$ (*top*) and $a = 1.3$ (*bottom*). For a in the bistable region, top row, stripes and hexagons coexist for a long time until hexagons win. *Bottom:* for rather large a hexagons are formed soon showing many defects and grain boundaries. The defects survive for quite a long time

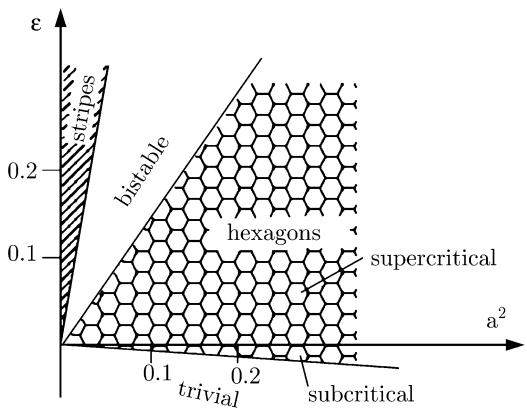

Fluid Dynamics, Pattern Formation, Fig. 20 Stability regions in the parameter plane of Eq. (68). Hexagons bifurcate subcritically from the trivial solution $\Psi = 0$. As a secondary instability, stripes emerge. The transition hexagons-stripes as well as trivial sol-hexagons both show hysteresis

$\varepsilon = 0$ if $a \to 0$. Well above threshold, stripes are expected – or squares.

Squares A linear stability analysis of the Swift–Hohenberg Eq. (68) shows that squares are always unstable in favor of rolls (or hexagons). Therefore there exists no stable square pattern as a solution. This can be changed including higher order terms in the gradient expansion (66), for details see (Bestehorn and Pérez-García 1992). In this spirit, the equation

$$\partial_t \Psi = \varepsilon \Psi - (\Delta + 1)^2 \Psi - b\, \Psi^3 - c\, \Psi \Delta^2 (\Psi^2) \tag{69}$$

has a stable square solution for $-32c/9 < b < 0$. In Fig. 21 we present numerical solutions of (69) for two different values of the parameter b.

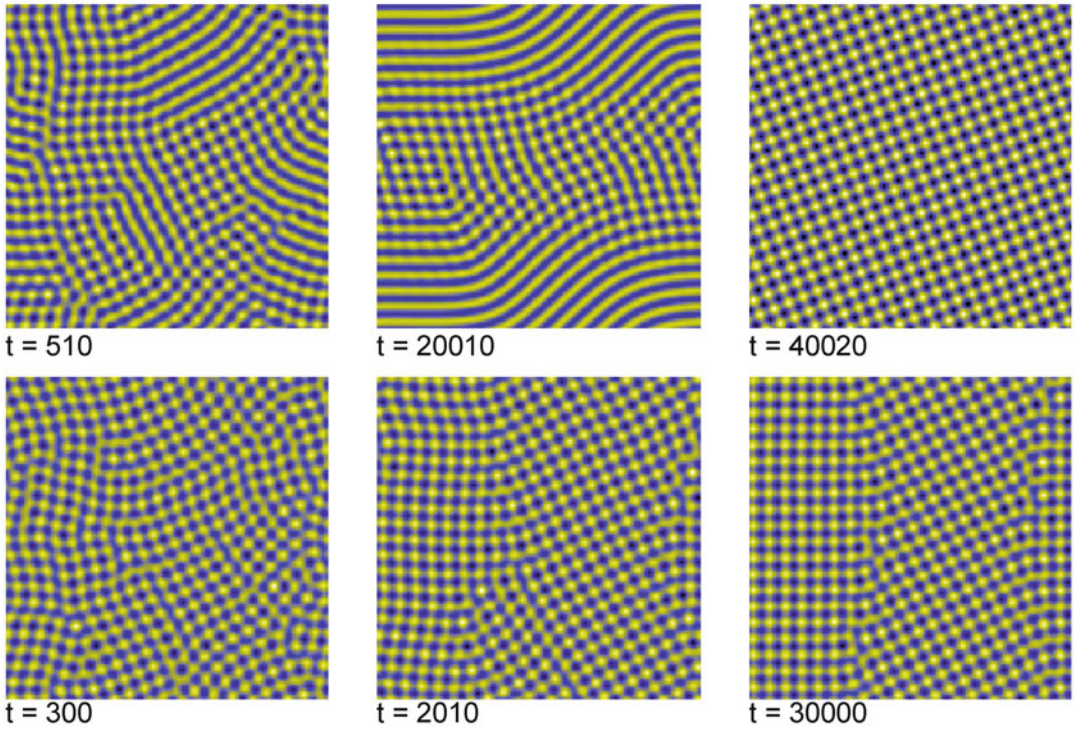

Fluid Dynamics, Pattern Formation, Fig. 21 Numerical solutions of (69) for e = 0.1, $c = 1/16$ and $b = 0$ (*top*), $b = -0.1$ (*bottom*). For $b = 0$ both squares and stripes are stable. After a longer time squares win the competition. *Bottom:* clearly in the square region of parameter space. Squares are formed soon having many defects and grain boundaries. Finally, a rather regular square pattern evolves

Regular squares are found in convection experiments with two poorly conducting top and bottom plates (Busse and Riahi 1980) or in binary mixtures with a certain mean concentration (Moses and Steinberg 1986). If the fluid viscosity is strongly temperature dependent (non-boussinesq effects), squares are also preferred, as shown in (Busse and Frick 1985). For all these cases, an equation of the form (69) can be approximately derived close to onset.

Conserved Order Parameter Fields

In the previous section, the OPE had the general form

$$\partial_t \xi\left(\vec{r}, t\right) = F(\xi, \nabla\xi, \Delta\xi) \tag{70}$$

with no further restrictions (except of boundary conditions) for the order parameter field ξ. However, there are many cases where the physical meaning of the order parameter is that of a density belonging to a conserved quantity such as total mass, volume or charge. Let ξ be such a density; then the mean value

$$M = \langle F \rangle \equiv \frac{1}{V} \int_V \mathrm{d}^3\vec{r}\, F(\xi, \nabla\xi, \Delta\xi) \tag{71}$$

should vanish, if $\langle\xi\rangle$ is a conserved quantity in the constant volume V. Then F can be written as

$$F(\xi, \nabla\xi, \Delta\xi) = -\mathrm{div}\ \vec{j}\left(\vec{r}, t\right) \tag{72}$$

if the total flow of the current density $\vec{j}$ through the surface A of V vanishes

$$\oint_{A(V)} \mathrm{d}^2\vec{f} \cdot \vec{j}\left(\vec{r}, t\right) = 0. \tag{73}$$

With (72), Eq. (70) takes the form of a continuity equation. In this section we wish to consider OPEs that fulfill (72) and (73).

Thin Films

Consider a fluid with a free and deformable surface located at $z = h(x, y, t)$ as already shown in Fig. 3. If the fluid is incompressible and there is no flow through the sidewalls, the total volume of the fluid layer

$$A \cdot \langle h \rangle = \int_A \mathrm{d}x\, \mathrm{d}y\, h(x, y, t) \tag{74}$$

is a conserved quantity, where A is the base area of the layer. As a consequence, the evolution equation for h must have the form

$$\partial_t h = -\mathrm{div}\ \vec{j} = -\partial_x j_x - \partial_y j_y. \tag{75}$$

Comparing (75) with the kinematic boundary conditions (23) and taking $v_z|_{z=h}$ from the integral of the incompressibility condition (3)

$$v_z|_{z=h} = -\int_0^h \mathrm{d}z\, \left(\partial_x v_x + \partial_y v_y\right) + v_z|_{z=0}$$

one finds with $v_z|_{z=0} = 0$

$$\vec{j} = \int_0^h \mathrm{d}z\, \vec{v}_H, \tag{76}$$

where $\vec{v}_H$ denotes the two horizontal velocity components.

The Lubrication Approximation To close the Eqs. (75), (76), it is necessary to compute $\vec{v}_H$ as a function of h. For thin films, the Reynolds number is small and the Stokes Eq. (19) determines the fluid velocity to a good approximation. Using scaling (Oron et al. 1997)

$$x = \tilde{x} \cdot l, y = \tilde{y} \cdot l, z = \tilde{z} \cdot \mathrm{d}, t = \tilde{t} \cdot \tau, h = \tilde{h} \cdot \mathrm{d}, \tag{77}$$

(19) turns into

$$\left(\delta^2\left(\partial^2_{\tilde{x}\tilde{x}} + \partial^2_{\tilde{y}\tilde{y}}\right) + \partial^2_{\tilde{z}\tilde{z}}\right)\vec{\tilde{v}}_H = \tilde{\nabla}_2 \tilde{P} \tag{78a}$$

$$\delta^2\left(\delta^2\left(\partial^2_{\tilde{x}\tilde{x}} + \partial^2_{\tilde{y}\tilde{y}}\right) + \partial^2_{\tilde{z}\tilde{z}}\right)\tilde{v}_z = \partial_{\tilde{z}}\tilde{P}. \tag{78b}$$

with the 2D-gradient $\nabla_2 = (\partial_x, \partial_y)$. In (78) we have introduced the dimensionless velocity and pressure

$$\vec{v}_H = \vec{\tilde{v}}_H \cdot \frac{l}{\tau}, v_z = \tilde{v}_z \cdot \frac{d}{\tau}, P = \tilde{P} \cdot \frac{\eta}{\delta^2 \tau}$$

and $\delta = d/l$ as a small parameter already defined in (24). In the limit $\delta \to 0$ it follows from (78b)

$$\partial_{\tilde{z}}\tilde{P} = 0 \text{ or } \tilde{P} = \tilde{P}(\tilde{x}, \tilde{y}).$$

Thus one can integrate (78a) twice over h and finds with the no-slip condition $\vec{\tilde{v}}_H(0) = 0$

$$\vec{\tilde{v}}_H(\tilde{x}, \tilde{y}, \tilde{z}) = \vec{f}(\tilde{x}, \tilde{y}) \cdot \tilde{z} + \frac{1}{2}\left(\tilde{\nabla}_2 \tilde{P}(\tilde{x}, \tilde{y})\right) \cdot \tilde{z}^2 \tag{79}$$

with a function $\vec{f}(\tilde{x}, \tilde{y})$ which can be determined by the boundary conditions. To this end we consider an inhomogeneous surface tension (caused, for example, by a temperature gradient) at the free surface, which yields the condition

$$\eta\, \partial_z \vec{v}_H|_{z=h} = \nabla_2 \Gamma|_{z=h}.$$

Inserting (79) there one finds

$$\vec{f} = \tilde{\nabla}_2 \tilde{\Gamma} - \left(\tilde{\nabla}_2 \tilde{P}\right) \cdot \tilde{h}$$

with the non-dimensional surface tension

$$\tilde{\Gamma} = \Gamma \frac{\tau d}{\eta l^2}.$$

Inserting everything into (76) and integrating by $\tilde{z}$ finally yields (all tildes omitted)

$$\partial_t h = -\nabla_2\left[-\frac{h^3}{3}\nabla_2 P + \frac{h^2}{2}\nabla_2 \Gamma\right]. \tag{80}$$

This is the basic equation for the evolution of the surface of a thin film in the so-called lubrication approximation (Ockendon and Ockendon 1995). Eq. (80) is sometimes denoted as the *thin film equation* (Oron et al. 1997; Vrij 1966).

The Disjoining Pressure for Ultra-thin Films Gravitation and surface tension can be included into the pressure P as already outlined in Section "Surface Waves". They both stabilize the flat film. On the other hand, an instability mechanism is encountered in very thin (ultra-thin) films where the thickness is some 100 nm or even less

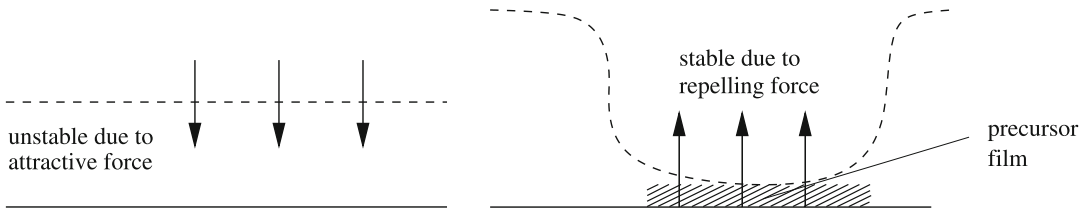

Fluid Dynamics, Pattern Formation, Fig. 22 Left: Thin flat films are unstable due to an attractive, long range van der Waals force between the free surface and the solid substrate of the fluid. *Right:* If the film is extremely thin (some nm), a repelling short range force acts as a stabilizer and the precursor film remains intact instead of rupturing

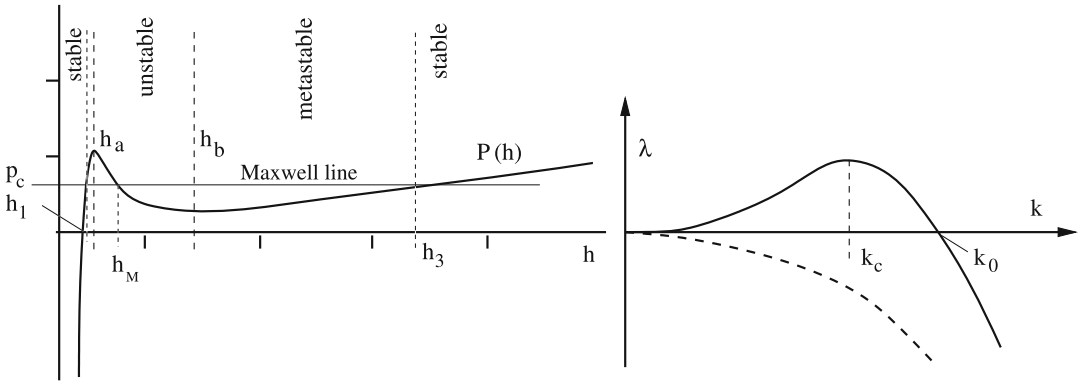

Fluid Dynamics, Pattern Formation, Fig. 23 *Left:* The disjoining pressure for a film with uniform thickness h including gravitation, $A_3 = 3$, $A_9 = 1$, $G = 0.1$. The region of unstable films is bounded by h_a and h_b. The critical pressure (depth) P_c (h_M) where drops turn into holes is determined by a Maxwell construction. *Right:* Growth rates of periodic disturbances of the plane surface with wave number k. The solid line corresponds to a film with a mean thickness in the unstable regime. Waves having a wave number $0 < k < k_0$ grow exponentially, the mode with $k = k_c$ has the largest growth rate (most dangerous mode). The instability is of type II

(Israelachvili 1992; Reiter et al. 1999; Sharma and Khanna 1998). Then, van der Waals forces between free surface and solid substrate can no longer be neglected (Israelachvili 1992). For an attractive force between surface and substrate one has

$$d_h P < 0.$$

But there can also exist a repelling van der Waals force with $d_h P > 0$ which stabilizes the flat surface. Attractive and repelling forces have different ranges. Usually, the repelling force is short range, the attractive one long range. Then, the initially "thick" film can be unstable due to attraction but rupture is avoided by repulsion. In this way completely dry regions cannot exist but the substrate always remains covered by an extremely thin film (some nm), called *precursor film,* Fig. 22 (Hardy 1919).

The complete expression for such an attractive/repulsive disjoining pressure including gravity and surface tension would be (Fig. 23)

$$P(h) = \frac{A_3}{h^3} - \frac{A_9}{h^9} + Gh - q\,\Delta_2\,h \qquad (81)$$

where A_3 and A_9 are material parameters, the Hamaker constants, and

$$G = \frac{d^3 g \tau}{l^2 \nu}, \quad q = \Gamma \frac{\tau d^3}{l^4 \eta}$$

denote the dimensionless gravitation number and the surface tension, respectively.

Spinodal Dewetting – Numerical Results If a thin liquid film is exposed to a non-or partially wetting substrate, a small perturbance is sufficient to destabilize the flat surface. The fluid then bubbles and many small drops are formed. This

phenomenon can be seen for instance if rain falls on a waxed cloth or on a well polished car roof. Such a process is called *spinodal dewetting* and refers to the unstable region of Fig. 23, (Bestehorn and Neuffer 2001; Seemann et al. 2001). As already explained in Section "Instabilities", an instability of the flat film occurs in the region where P has a negative slope. This instability is of type II, as is shown in Fig. 23, right frame, and has the growth rate (dispersion relation)

$$\lambda = \frac{1}{3}h_0^3\left(-D(h_0)k^2 - k^4\right) \tag{82}$$

with the "diffusion coefficient"

$$D(h) = d_h P.$$

(Here we restrict our further study to fluids with a uniform surface tension. For non-isothermal films with $\nabla_2 \Gamma \neq 0$ we refer to (Bestehorn et al. 2003; Oron 2000)). Next we wish to present numerical solutions of the fully nonlinear Eq. (80) with (81). To this end we used the parameters of Fig. 23 and several initial depths h_0. As initial condition a random distribution around the average depth h_0 was chosen.

In the early stage of the evolution (top line of Fig. 24), structures having a length scale of the critical wave length $\Lambda = 2\pi/k_c$, occur, were k_c is the wave number of the fastest growing mode

$$k_c = \sqrt{-\frac{D}{2}}.$$

This can be called "linear phase" since the amplitudes are still small and nonlinearities play no important role. The structure grows on the typical time scale

$$\tau = \lambda^{-1}(k_c) = \frac{12}{h_0^3 D^2} = \frac{12}{h_0^3}\left(P'(h_0)\right)^{-2},$$

which is inverse to the square of the slope of the disjoining pressure. This is the reason why pattern formation in thicker films takes much longer (right column in Fig. 24). As a consequence, the small scale (linear phase) structures are overlayed by holes created by certain seeds. After the linear phase, the position of h_0 with respect to the Maxwell point h_M (Fig. 23, left frame) is decisive. If $h_0 > h_M$, holes are formed, for $h_0 < h_M$, one finds drops. If $h_0 \approx h_M$, maze-like patterns are obtained in form of bent, rather irregular stripes (Fig. 24, middle column). In a last, strongly nonlinear phase, coarsening is observed. The final stationary structure (long term) is often a single entity in the form of one big drop or hole. The whole spatio-temporal evolution is transient and can be formulated as a gradient dynamics. The potential plays the role of a generalized free energy reaching its minimum in the steady end state (Bestehorn et al. 2003).

The flat film is unstable with respect to infinitesimal disturbances if h_0 is in the region between h_a and h_b. On the other hand, two meta-stable domains exist, where the flat film is stable, although the free energy could be lowered by pattern formation. Then, a finite disturbance is necessary, which can be caused by seeds coming, for instance, from impurities. Such a process is called *nucleation* and can be seen in the right column of Fig. 24. There, the seeds were provided by the random dot initial conditions and two holes are formed. Both processes (nucleation and wetting) converge in this region and it is a question of time scales which one emerges first. In experiments, the formation of holes by nucleation is seen quite often. The reason is that for a Lennard–Jones like disjoining pressure as (81), the meta-stable hole region is much larger compared to that of drops (Fig. 23, left frame).

Phase Field Models

In solidification processes, phase fields are introduced as additional variables to describe the state, here liquid or solid, of the system (Langer 1980). Phase fields depend on space and time and governing equations for the phase field variables must be stated or derived. If the phase field obeys an equation of the form of (70), it is called Model A, according to a classification given by Hohenberg and Halperin (Hohenberg and Halperin 1977).

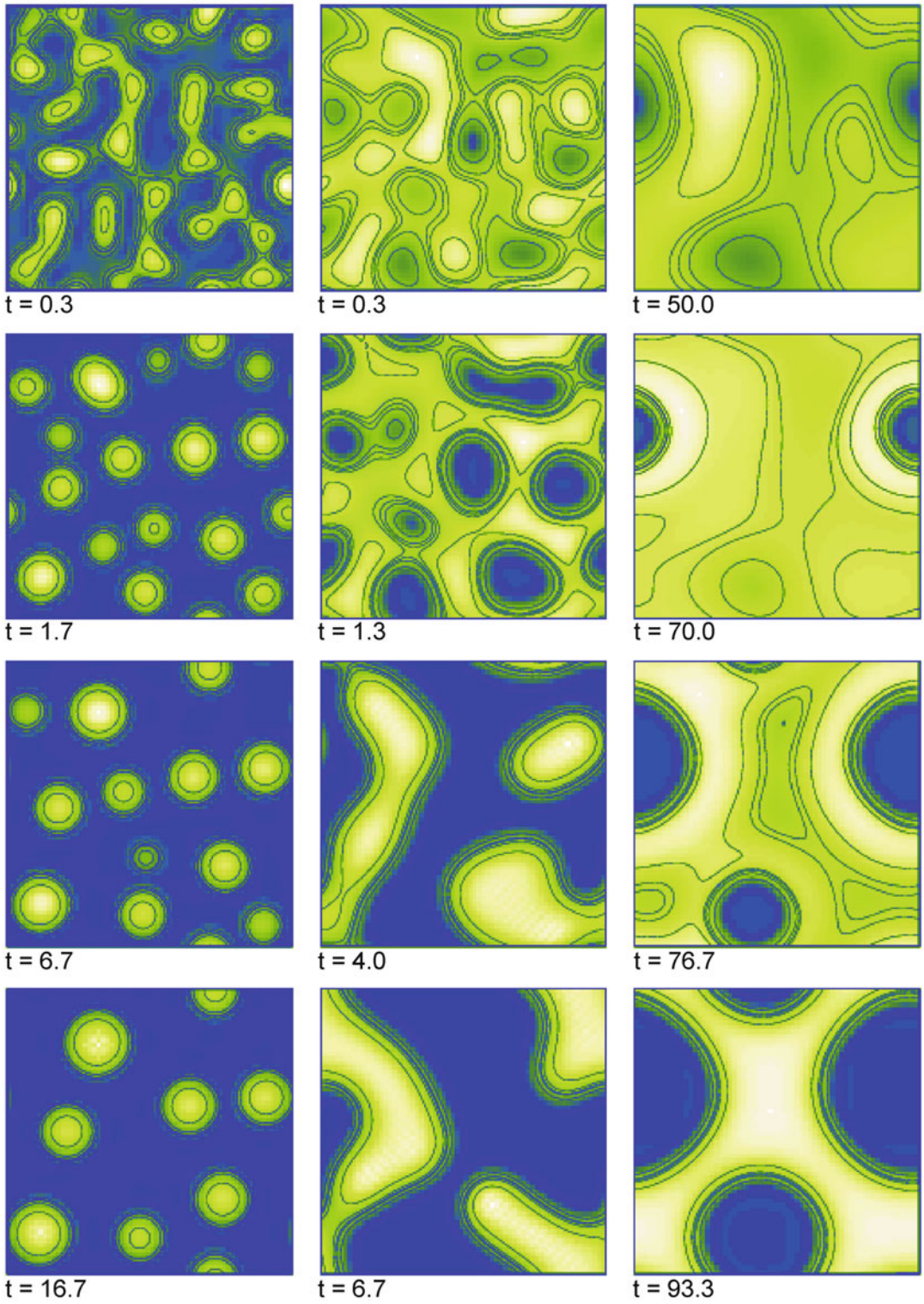

Fluid Dynamics, Pattern Formation, Fig. 24 Time series found by numerical integration of (80) for $h_0 = 1.2$ (*left column*), 1.862 (*middle*), and 2.8 (*right*). Light areas correspond to elevated regions of the surface (from Bestehorn 2007)

Model B Here, we are more interested in phase field equations belonging to Model B. The phase field (we call it Φ) is conserved and a continuity equation

$$\partial_t \Phi = -\mathrm{div}\ \vec{j} \tag{83}$$

must hold. As in nonequilibrium thermodynamics (Callen 1985) one assumes that the current density $\vec{j}$ is proportional to a generalized force $\vec{f}$

$$\vec{j} = Q(\Phi) \cdot \vec{f} \tag{84}$$

where Q stands for a non-negative mobility, which is normally a function of the phase field itself, but may also explicitly depend on space coordinates. If the force can be derived from a potential P (pressure)

$$\vec{f} = -\nabla P(\Phi) \tag{85}$$

which in turn can be written as functional derivative of another (thermodynamic) potential (free energy) F

$$P = \frac{\delta F}{\delta \Phi}, \tag{86}$$

we finally obtain a closed equation for (83) of the form

$$\partial_t \Phi = \mathrm{div}\left[Q(\Phi) \nabla \frac{\delta F}{\delta \Phi} \right]. \tag{87}$$

With (87) it is easy to show that $\mathrm{d}_t F \leq 0$.

The Cahn-Hilliard Equation As known from the Ginzbur–Landau equation, one may expand the free energy with respect to powers of the phase field. The surface term $(\nabla\Phi)^2$ penalizes phase field variations with respect to space by an increase of F:

$$F[\Phi] = \int_V d^3\vec{r} \left[\frac{D}{2} (\nabla\Phi)^2 + a_0 \Phi + \frac{a_1}{3} \Phi^2 + \frac{a_2}{3} \Phi^3 + \frac{a_3}{4} \Phi^4 + \ldots \right]. \tag{88}$$

Substituting this into (87) yields

$$\partial_t \Phi = \mathrm{div}[Q(\Phi) \nabla (-D\Delta\Phi + a_0 + a_1 \Phi) + a_2 \Phi^2 + a_3 \Phi^3]. \tag{89}$$

We further assume $a_2 = 0$ (this can be always obtained by a simple shift of Φ) and $a_1 < 0$, $a_3 > 0$. If we restrict us to the case of a constant mobility, we arrive from (89) after a suitable scaling at the Cahn-Hilliard Eq. [29]

$$\partial_t \Phi = -\Delta\Phi - \Delta^2 \Phi + \Delta(\Phi^3). \tag{90}$$

Equation (90) can be considered as a simple model for a conserved order parameter. A family of stationary solutions of (90) is given by $\Phi = \Phi_0 =$ constant. A linear stability analysis shows that these solutions are type II unstable if $\Phi_0^2 < \frac{1}{3}$ holds. Since (90) belongs to Model B, an infinitesimal disturbance can grow only in a way that keeps the mean value of $\Phi = \Phi_0$ constant. Therefore, spatially structured solutions are expected (Fig. 25).

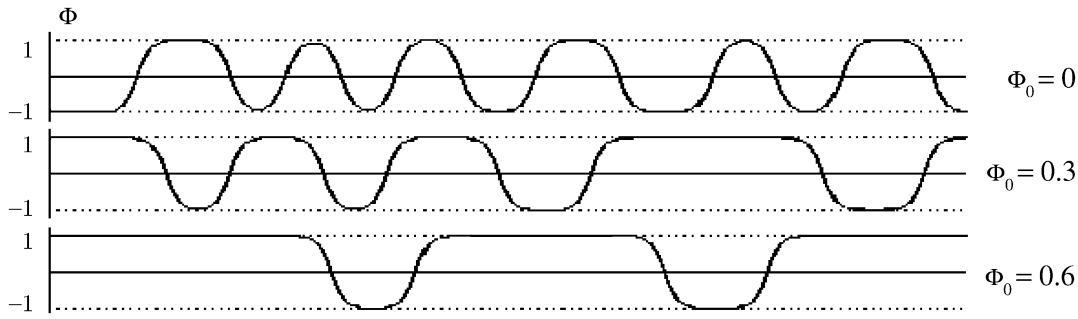

Fluid Dynamics, Pattern Formation, Fig. 25 Stationary solutions of the ID Cahn-Hilliard equation for several mean values Φ_0

The density of the free energy of a homogeneous solution reads

$$f(\Phi) = -\frac{\Phi^2}{2} + \frac{\Phi^4}{4} \tag{91}$$

and has its minima at $\Phi_m = \pm 1$. From Fig. 25 it becomes clear that the stationary pattern forming solutions are located between these two minima independently from the mean Φ_0. If the mean value is increased, the regions with $\Phi \approx 1$ grow at the cost of the regions with $\Phi \approx -1$ and vice versa. Taking (90) as a simple model for the phase transition from liquid to gas, the phase field defines the state of aggregation. The density can then be found from the linear relation

$$\rho\left(\vec{r},t\right) = \frac{1}{2}\left(\rho_f - \rho_g\right)\Phi\left(\vec{r},t\right) + \frac{1}{2}\left(\rho_f + \rho_g\right) \tag{92}$$

with ρ_g (ρ_f) as the density of the gaseous (liquid) state. Regions where $\Phi \approx -1$ are gaseous, those with $\Phi \approx +1$ liquid.

Equation (90) has no free parameters. On the other hand, the mean $\Phi_0 = \langle\Phi\rangle$ is a conserved quantity which influences the dynamics of pattern formation qualitatively and which can be considered as a control parameter. Integrating (92) over the volume, it turns out that Φ_0 is linked to the total mass M of the gas/liquid system

$$M = \frac{1}{2}\left(\rho_f - \rho_g\right)\Phi_0 \cdot V + \frac{1}{2}\left(\rho_f + \rho_g\right) \cdot V.$$

The stable homogeneous solutions $\Phi_0^2 > 1/3$ correspond to a pure gas phase ($\Phi_0 < 0$, small total mass), or to a pure liquid phase ($\Phi_0 > 0$, large total mass). In the unstable regime $\Phi_0^2 < 1/3$ the (homogeneous) system has a medium density; this corresponds either to an oversaturated vapor atmosphere ($\Phi_0 < 0$) or to a liquid with a temperature above its boiling point. In both cases, an infinitesimally small disturbance is sufficient to trigger pattern formation in the form of phase separation. In the first case, one observes drops in the gas atmosphere, in the latter, bubbles in the liquid. Figure 26 shows a numerical simulation of (90) in three dimensions.

The Fluid Density as Phase Field

Writing down an equation such as (87) and an expansion such as (88) seems to be rather ad hoc. However, for pure fluids it is evident to use the density itself as the phase field, if one is interested in the liquid/gas phase transition. Then, the continuity Eq. (2) may serve as a phase field equation in lieu of (87). Consequently, the fluid can no longer be considered incompressible.

The Model The Navier–Stokes equations for a compressible fluid (14) must be extended by a force term coming from spatial variations of the phase field (density). They read (Borcia and Bestehorn 2007; Jasnow and Vinals 1996)

$$\rho\left[\partial_t\vec{v} + \left(\vec{v}\cdot\nabla\right)\vec{v}\right] = -\mathrm{grad}\,p + \vec{f} + \eta\Delta\vec{v} + \left(\zeta + \frac{\eta}{3}\right)\mathrm{grad}\,\mathrm{div}\,\vec{v} + \mathcal{K}\rho\,\mathrm{grad}\,\Delta\rho. \tag{93}$$

The extra term at the end of (93) was first used by Korteweg in 1901 and is sometimes called Korteweg stress (Korteweg 1901). For (93) we assumed constant material parameters η, ζ and $\mathcal{K}$. Using the methods of thermodynamics, the pressure is related to the free energy density f (Anderson and Mc Fadden 1997; Davis and Scriven 1982)

$$p(\rho) = \rho\frac{\partial f(\rho)}{\partial\rho} - f(\rho) \tag{94}$$

and the free energy as a functional of ρ reads

$$F[\rho] = \int_V \mathrm{d}^3\vec{r}\left[\frac{\mathcal{K}}{2}(\nabla\rho)^2 + f(\rho)\right], \tag{95}$$

according to (88). Equations (93) with (94) and (2) form a closed system for the variables $\vec{v}$ and ρ. Wetting properties and contact angles at the walls depend on the boundary conditions $\rho = \rho_w$ along the wall (Pismen and Pomeau 2000). The choice $\rho_w = \rho_f$ corresponds to a completely wetting (hydrophilic) material, $\rho_w = \rho_g$ to a non-wetting (hydrophobic) boundary. The boundary condition for $\vec{v}$ can either be no-slip (along a wall), no flux, or periodic. It is straightforward to include evaporation and condensation effects into the model, which is studied in (Borcia and Bestehorn 2005).

Note that now the free energy (95) is not needed for determining the evolution of the

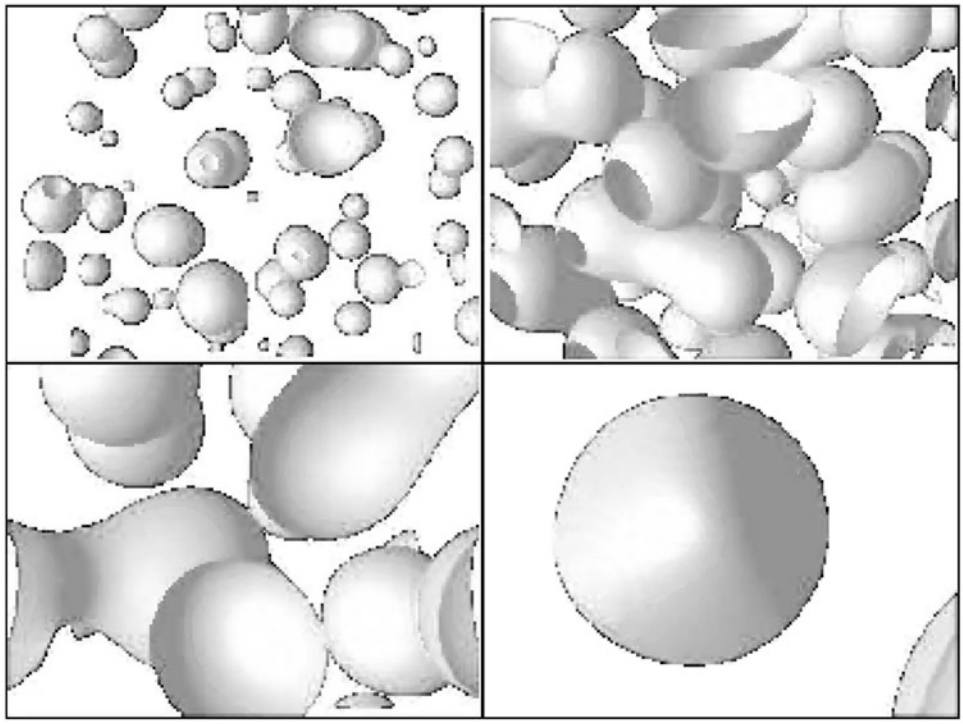

Fluid Dynamics, Pattern Formation, Fig. 26 Numerical solution of the Cahn-Hilliard Eq. (90) in three room dimensions. The time series (*top left to bottom right*) shows how liquid drops are formed in an oversaturated gas atmosphere. Finally they merge to one big drop by coarsening, a typical dynamic for a type II instability (from (Bestehorn 2006))

phase field by (*ad-hoc*) gradient dynamics. However, it can be shown that the free energy decreases monotonically in time.

Results Again, we wish to consider the formation of one state of aggregation on the background of the other. To account for the two stable states, liquid and gaseous, we take (for sake of simplicity we assume $\rho_g \approx 0$)

$$f(\rho) = \gamma\rho^2\left(\rho - \rho_f\right)^2. \qquad (96)$$

where y is a positive material constant. In Fig. 27 we show results of the breakup of a flat liquid film aligned along a rigid bottom plate. The layer is inclined by an angle φ and under vertical gravitation. Thus, an external force density of the form

$$\vec{f} = \rho g \begin{pmatrix} \sin\varphi \\ -\cos\varphi \end{pmatrix}$$

occurs in (93). The bottom material is assumed to be partially wetting ($\rho_w = 0.5\rho_f$) and the initial film is unstable under these conditions. Periodic disturbances grow along the fluid's surface. After rupture, bubbles separate and travel from left to right due to downhill force. Figure 28 shows final states of a sliding drop for two boundary values ρ_w. Clearly, the contact angles are different (Borcia et al. 2008a).

The phase field description goes far beyond the one based on the thin film equation of Section "Thin Films", since there the treatment was restricted to small contact angles and rupture was excluded from the beginning.

Future Directions

There is a huge number of applications in science, industry, and technology where the methods and models outlined in the present article can be used and developed further. In the field of patterns not

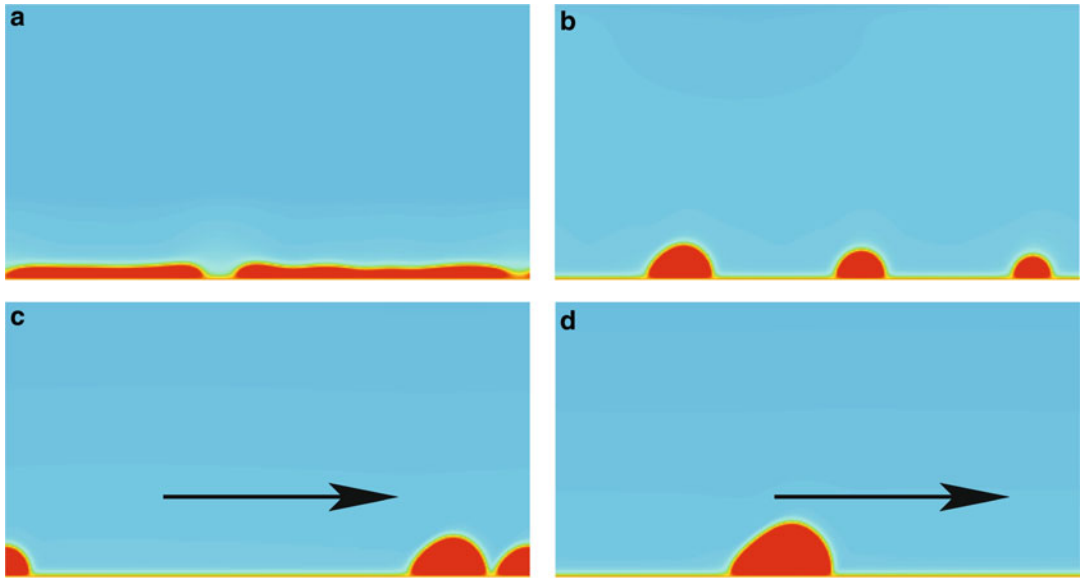

Fluid Dynamics, Pattern Formation, Fig. 27 Transition from a flat unstable liquid layer to a drop running down on an inclined substrate (arrows) under gravity effects. Numerical simulation (Borcia et al. 2008a) of (93) with (96) and the material parameters for water/vapor from (Burelbach et al. 1988) and $\rho_w = 0.5\rho_f$

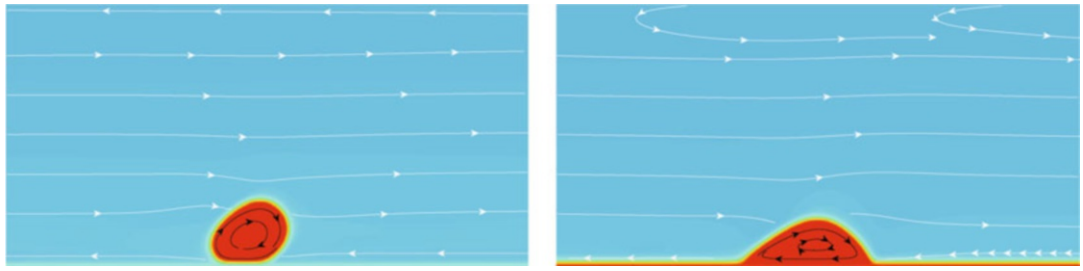

Fluid Dynamics, Pattern Formation, Fig. 28 Two final states showing a drop sliding down the inclined substrate with $\rho_w = 0.1\rho_f$ (left, almost hydrophobic) and $\rho_w = 0.8\rho_f$ (*right,* almost hydrophilic). The flow in the gas and in the liquid is indicated by *small arrows* (Borcia et al. 2008b)

formed by self-organized processes, but rather by external events such as tidal waves, storm surges or Tsunamis, a reduced and simplified description as discussed in Sections "Surface Waves" and "Order Parameter Equations" should allow for a better understanding of the underlying mechanisms and their effects. Highly involved problems, as for instance the flow, temperature, and concentration fields inside a combustion cell, could be tackled by such models, extended in a suitable way.

Self-organized fluid patterns (Section "Instabilities") are the focus of attention in many actual fields of quite different disciplines and scales. The conditions that lead to the creation and stabilization of hurricanes are not yet completely known. The rather high probability of the occurrence of freak waves in the open sea still waits for an explanation. On a planetary scale, convection problems are encountered in the interior of planets and stars and may give rise to the spontaneous formation of a magnetic field. Another problem of great interest for the geophysicist is that of a fluid (such as oil) in a porous medium. The equations for that case differ only a little from that discussed in Section "The Basic Equations of Fluid Dynamics" and could therefore be treated in the same spirit.

Understanding the mechanisms responsible for pattern formation can also help to control systems to avoid the occurrence of spatial patterns. In this way, the quality of products obtained from industrial processes, such as coating or solidification (crystal growth), might be improved.

On the micro-scale, fluid problems in general ruled by the Stokes equations discussed in Section "Conserved Order Parameter Fields" form a major issue, founding the new discipline of micro-fluidics. But even on the nanoscale, there are new applications in view. The self-organized growth of structures could be a promising tool in the conception and construction of nano-circuits.

An extension of the treatment to complex fluids such as mixtures and emulsions, or to non-Newtonian fluids using the phase field approach (Section "Conserved Order Parameter Fields"), is desirable. These fluids are important for biological applications.

Bibliography

Primary Literature

Abramowitz M, Stegun IA (1965) Handbook of mathematical functions. Dover, New York

Anderson DM, Mc Fadden GB (1997) A diffuse-interface description of internal waves in a near-critical fluid. Phys Fluids 9:1870–1879

Aranson IS, Kramer L (2002) The world of the complex Ginzbur–Landau equation. Rev Mod Phys 74:99–143

Argyris JH, Faust G, Haase M (1994) An exploration of chaos: an introduction for natural scientists and engineers. North-Holland, Amsterdam

Bénard H (1901) Les tourbillons cellulaires dans une nappe liquide. Ann Chim Phys 23:62–143

Bestehorn M (1993) Phase and amplitude instabilities for Bénard–Marangoni convection in fluid layers with large aspect ratio. Phys Rev 48:3622–3634

Bestehorn M (1996) Square patterns in Bénard–Marangoni convection. Phys Rev Lett 76:46–49

Bestehorn M (2006) Hydrodynamik und Strukturbildung. Springer, Berlin

Bestehorn M (2007) Convection in thick and thin fluid layers with a free interface. Eur Phys J Spec Top 146:391–405

Bestehorn M, Colinet P (2000) Bénard–Marangoni-convection of a binary mixture as an example of an oscillatory bifurcation under strong symmetry-breaking effects. Phys D 145:84

Bestehorn M, Friedrich R (1999) Rotationally invariant order parameter equations for natural patterns in non-equilibrium systems. Phys Rev E 59:2642–2652

Bestehorn M, Haken H (1983) A calculation of transient solutions describing roll and hexagon formation in the convection instability. Phys Lett A 99:265–268

Bestehorn M, Haken H (1990) Traveling waves and pulses in a two-dimensional large-aspect-ratio system. Phys Rev A 42:7195–7203

Bestehorn M, Neuffer K (2001) Surface patterns of laterally extended thin liquid films in three dimensions. Phys Rev Lett 87:046101

Bestehorn M, Pérez-García C (1992) Study of a model of thermal convection in cylindrical containers. Phys D 61:67–76

Bestehorn M, Neufeld M, Friedrich R, Haken H (1994) Comment on spiral-pattern formation in Rayleigh–Bénard convection. Phys Rev E 50:625

Bestehorn M, Pototsky A, Thiele U (2003) 3D Large scale Marangoni convection in liquid films. EurPhys J B 33:457

Block MJ (1956) Surface tension as the cause of Bénard cells. Nat (London) 176:650–651

Bodenschatz E, Pesch W, Ahlers G (2000) Recent developments in Rayleigh–Bénard convection. Annu Rev Fluid Mech 32: 709–778

Borcia R, Bestehorn M (2005) Phase-filed simulations for evaporation with convection in liquid-vapor systems. Eur Phys J B 44:101–108

Borcia R, Bestehorn M (2007) Phase-field simulations for drops and bubbles. Phys Rev E 75:056309

Borcia R, Borcia I, Bestehorn M (2008a) Phys Rev E (submitted)

Borcia R, Borcia I, Bestehorn M (2008b) Static and dynamic contact angles. Eur Phys J Spec Top (in print)

Burelbach JP, Bankoff SG, Davis SH (1988) Nonlinear stability of evaporating/condensing liquid films. J Fluid Mech 195:463

Busse FH (1967) The stability of finite amplitude cellular convection. J Fluid Mech 30:625–649

Busse FH (1989) In: Peltier WR (ed) Fundamentals of thermal convection. Taylor, 23–95

Busse FH, Frick H (1985) Square-pattern convection in fluids with strongly temperature-dependent viscosity. J Fluid Mech 150:451–465

Busse FH, Riahi N (1980) Nonlinear convection in a layer with nearly insulating boundaries. J Fluid Mech 96:243–256

Cahn JW, Hilliard JE (1958) Free energy of a nonuniform system. J Chem Phys 28:258–267

Callen HB (1985) Thermodynamics and an introduction to thermostatistics. Wiley, New York

Castets V, Dulos E, Boissonade J, De Kepper P (1990) Experimental evidence of a sustained standing Turing-type nonequilibrium chemical pattern. Phys Rev Lett 64:2953–2956

Chandrasekhar S (1961) Hydrodynamic and hydromagnetic stability. Dover, New York

Cohen IM, Kundu PK (2004) Fluid mechanics. Academic, Amsterdam

Colinet P, Legros JC, Velarde MG (2001) Nonlinear dynamics of surface tension driven instabilities. Wiley, Berlin

Cross MC (1988) Theoretical methods in pattern formation in physics, chemistry and biology. In:Garrido L (ed) Far from equilibrium phase transitions. Springer, Berlin
Cross MC, Hohenberg PC (1993) Pattern formation outside of equilibrium. Rev Mod Phys 65:851–1112
Davis HT, Scriven LE (1982) Stress and structures in fluid interfaces. Adv Chem Phys 49:357
de Gennes PG (1985) Wetting: statics and dynamics. Rev Mod Phys 57:827–863
Dean RG, Dalrymple RA (2000) Water wave mechanics for engineers and scientists. World Science, Singapore
Drazin PG, Johnson RS, Crighton DG (1989) Solitons: an introduction. Cambridge University Press, Cambridge
Eckert K, Bestehorn M, Thess A (1998) Square cells in surface tension driven Bénard convection: experiment and theory. J Fluid Mech 356:155–197
Faraday M (1831) On a peculiar class of acoustical figures and on certain forms assumed by groups of particles upon vibrating elastic surfaces. Philos Trans R Soc Lond 121:299
Getling AV (1998) Rayleigh–benard convection: structures and dynamics. World Scientific
Golovin AA, Nepomnyashchy AA, Pismen LM (1997) Nonlinear evolution and secondary instabilities of Marangoni convection. J Fluid Mech 341:317–341
Guckenheimer J, Holmes P (2002) Nonlinear oscillations, dynamical systems, and bifurcations of vector fields. Springer, Berlin
Haken H (1975) Cooperative phenomena in systems far from thermal equilibrium and in nonphysical systems. Rev Mod Phys 47:67–121
Haken H (1983) Advanced synergetics: instability hierarchies of self-organizing systems and devices. Springer, Berlin
Haken H (2004) Synergetics introduction and advanced topics. Springer, Berlin
Hardy W (1919) The spreading of fluids on glass. Philos Mag 38:49–55
Hohenberg PC, Halperin BI (1977) Theory of dynamic critical phenomena. Rev Mod Phys 49:435–447
Israelachvili JN (1992) Intermolecular and surface forces. Academic, London
Jasnow D, Vinals J (1996) Coarse-grained description of thermo-capillary flow. Phys Fluids 8:660–669
Korteweg DJ (1901) Sur la forme que prennent les équation du mouvements des fluides. Arch Néerl Sci Exact Nat Ser II 6:1
Koschmieder EL (1993) Bénard cells and Taylor vortices. Cambridge University Press, Cambridge
Lai WM, Rubin D, Krempl E (1993) Introduction to continuum mechanics. Pergamon, Oxford
Landau LD, Lifshitz EM (1996) Statistical physics. In: Course of theoretical physics, 5. Heinemann, Butterworth
Landau LD, Lifshitz EM (2004) Fluid dynamics. In: Course of theoretical physics, 6. Heinemann, Butterworth
Langer JS (1980) Instabilities and pattern formation in crystal growth. Rev Mod Phys 52:1–28
Lorenz EN (1963) Deterministic nonperiodic flow. J Atmos Sci 20:130–141
Morris SW, Bodenschatz E, Cannell DS, Ahlers G (1993) Spiral defect chaos in large aspect ratio Rayleigh–Bénard convection. Phys Rev Lett 71:2026–2029
Moses E, Steinberg V (1986) Competing patterns in a convective binary mixture. Phys Rev Lett 57:2018–2021
Murray JD (1993) Mathematical biology. Springer, Berlin
Nekorkin VI, Velarde MG (2002) Synergetic phenomena in active lattices. Patterns, waves, solitons, chaos. Springer, Berlin
Nepomnyashchy AA, Velarde MG, Colinet P (2002) Interfacial phenomena and convection. Chapman & Hall, Boca Raton
Newell AC, Whitehead JA (1969) Finite bandwidth, finite amplitude convection. J Fluid Mech 38:279–303
Nitschke-Eckert K, Thess A (1995) Secondary instability in surface tension driven Bénard convection. Phys Rev E 52: 5772–5775
Ockendon H, Ockendon JR (1995) Viscous flow. Cambridge University Press, Cambridge
Oron A (2000) Nonlinear dynamics of three-dimensional longwave Marangoni instability in thin liquid films. Phys Fluids 12:1633–1645
Oron A, Davis SH, Bankoff SG (1997) Long-scale evolution of thin liquid films. Rev Mod Phys 69:931–980
Ouyang Q, Swinney HL (1991) Transition from a uniform state to hexagonal and striped Turing patterns. Nature 352:610–612
Palm E (1960) On the tendency towards hexagonal cells in steady convection. J Fluid Mech 19:183–192
Penrose R (1974) Role of aesthetics in pure and applied research. Bull Inst Math Appl 10:266
Pesch W (1996) Complex spatiotemporal convection patterns. Chaos 6:348–357
Pismen LM, Pomeau Y (2000) Disjoining potential and spreading of thin liquid layers in the diffuse-interface model coupled to hydrodynamics. Phys Rev E 62:2480–2492
Prigogine I, Levever R (1968) Symmetry breaking instabilities in dissipative systems II. J Chem Phys 48:1695–1700
Prigogine I, Nicolis G (1967) On symmetry-breaking instabilities in dissipative systems. J Chem Phys 46:3542–3550
Rayleigh Lord (1915) On convection currents in a horizontal layer of fluid. Philos Mag 32:462–468
Reiter G, Sharma A, Casoli A, David M-O, Khanna R, Auroy P (1999) Thin film instability induced by long-range forces. Langmuir 15:2551–2558
Schatz MF, Neitzel GP (2001) Experiments on thermocapillary instabilities. Annu Rev Fluid Mech 33:93–127
Schatz MF, Van Hook SJ, Mc Cormick WD, Swift JB, Swinney HL (1999) Time-independent square patterns in surface-tension-driven Bénard convection. Phys Fluids 11:2577–2582
Scheid B, Oron A, Colinet P, Thiele U, Legros JC (2002) Nonlinear evolution of nonuniformly heated falling liquid films. Phys Fluids 14:4130–4151
Schwabe D (2006) Marangoni instabilities in small circular containers under microgravity. Exp Fluids 40:942–950

See the up to now 69 volumes of the Springer Series of Synergetics, especially the monographs by Haken H (1983) Synergetics. An introduction.; Advanced synergetics.; Information and self-organization (2006)
Seemann R, Herminghaus S, Jacobs K (2001) Dewetting patterns and molecular forces: a reconciliation. Phys Rev Lett 86:5534–5553
Sharma A, Khanna R (1998) Pattern formation in unstable thin liquid films. Phys Rev Lett 81:3463–3466
Sharma A, Khanna R (1999) Pattern formation in unstable thin liquid films under the influence of antagonistic short and long-range forces. J Chem Phys 110:4929–4936
Sparrow C (1982) The Lorenz equations. Springer, Berlin
Swift JB, Hohenberg PC (1977) Hydrodynamic fluctuations at the convective instability. Phys Rev A 15:319; Chem Phys 48:1695–1700
Turing AM (1952) The chemical basis of morphogenesis. Philos Trans R Soc Lond B237:37
Van Dyke M (1982) An album of fluid motion. Parabolic, Stanford
Van Oss CJ,Chaudhury MK, Good RJ (1988) Interfacial Lifshitz–van der Waals and polar interactions in macroscopic systems. Chem Rev 88:927–941
Vrij A (1966) Possible mechanism for the spontaneous rupture of thin, free liquid films. Disc Faraday Soc 42:23–33

Books and Reviews

Emmerich H (2003) The diffusive interface approach in material science. Springer, Berlin
Fletcher CAJ (1988) Computational techniques for fluid dynamics, 1,2. Springer, Berlin
Manneville P (1990) Dissipative structures and weak turbulence. Academic, London
Pismen LM (2006) Patterns and interfaces in dissipative dynamics. Springer, Berlin
Platten JK, Legros JC (1984) Convection in liquids. Springer, Berlin
Schlichting H, Gersten K (2000) Boundary-layer theory. Springer, Berlin
Simanovskii IB, Nepomnyashchy AA (1993) Convective instabilities in systems with interface. Gordon Preach, Yverdon

Patterns and Interfaces in Dissipative Dynamics

L. M. Pismen
Department of Chemical Engineering and Minerva Center for Nonlinear Physics of Complex Systems, Technion – Israel Institute of Technology, Haifa, Israel

Article Outline

Glossary
Definition of the Subject
Introduction
Stationary Patterns
Moving Interfaces
Wave Patterns
Future Directions
Bibliography

Glossary

Interface An interface separates domains where different stationary states or different patterns prevail. In the latter case, it is also called a domain wall. The interface typically has a finite thickness comparable to a characteristic intrinsic scale of the system but small compared to the overall system size.

Stationary pattern A stationary pattern is formed as a result of an instability to perturbations with a finite wavenumber. It may have any of various spatial structures (striped, square, hexagonal, or quasicrystalline in 2D, lamellar, crystalline or quasicrystalline in 3D) and may slowly evolve in time.

Wave pattern A wave pattern is formed by a combination of waves propagating in one or different directions.

Definition of the Subject

A *pattern* is an inhomogeneous state of a physical system that arises spontaneously under spatially homogeneous conditions. Spontaneous pattern formation has been first observed by Faraday (1831) in vibrated liquid layers and Bénard (1900) in fluids heated from below. Turing (1952) envisaged pattern formation as the mechanism of morphogenesis in living Nature. Some patterns can be described as a collection of patches or domains where one of alternative homogeneous states prevails, separated by relatively narrow *interfaces.* In their turn, moving interfaces may develop corrugation patterns. Patterns can be stationary or wavelike; they can be regular, interlaced by defects, or chaotic (turbulent). In the latter part of twentieth century, numerous pattern formation phenomena have been observed in chemistry, biology, fluid mechanics, granular media, nonlinear optics, and other applications, and common models describing these phenomena in physically dissimilar settings have been formulated and studied. Understanding pattern formation is important both for describing natural self-organization phenomena and for developing manufacturing processes based on self-organization.

Introduction

A typical setup of a non-equilibrium system that may undergo a symmetry-breaking transition is shown in Fig. 1. A non-equilibrium stationary state homogeneous in the "horizontal" plane is sustained by fluxes in the normal ("vertical") direction, along which an inhomogeneous "vertical structure" may be formed. This setup may be realized as a layer of fluid or granular matter; a chemically reacting system, such as an active layer or a catalytic surface; an area where different populations spread out and compete; a propagating interphase boundary, e.g. a

A. Hutt, H. Haken (eds.), *Synergetics*,
https://doi.org/10.1007/978-1-0716-0421-2_381

Originally published in
R. A. Meyers (ed.), *Encyclopedia of Complexity and Systems Science*, © Springer Science+Business Media LLC 2017
https://doi.org/10.1007/978-3-642-27737-5_381-2

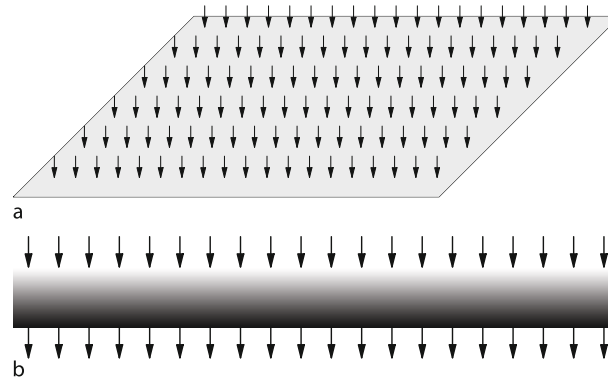

Patterns and Interfaces in Dissipative Dynamics, Fig. 1 An open system isotropic in two dimensions. A truly two-dimensional system (*above*) and a cut through a system with vertical structure (*below,* shown symbolically by *varied shading*). *Arrows* indicate the direction of external fluxes

melting or crystallizing solid; a slice of nonlinear optical medium, etc. Under certain conditions, most commonly, under increased driving, this homogeneous state may be destabilized, giving way to a stationary or moving pattern with a characteristic wavelength dependent on physical properties of the system as well as on external fluxes. In chemically reacting systems, three-dimensional patterns can be also formed when a sufficient amount of reactants is stored; such patterns may exist, of course, for a limited time until the original cache is depleted. Mathematically, a pattern typically emerges as an inhomogeneous solution of a (system of) partial differential equation(s) with space-independent coefficients in the absence of lateral fluxes.

Alternative states, corresponding to different phases, may exist also in equilibrium systems. Following a fast quench past a critical point, different states, separated by domain boundaries, would be approached at spatially removed locations. Typically, these domains would consequently slowly coarsen to minimize the extent of an interphase boundary and related energetic costs. A stationary pattern with a finite wavelength may exist, however, also at equilibrium, provided it minimizes the free energy of the system. Such patterns are realized as "mesoscopic crystals" in block-copolymers consisting of two kinds of mutually repelling units (Hamley 2003).

In fluid mechanics, inhomogeneous states, most often disordered but still retaining a measure of regularity, are commonplace, as anybody observing wavy sea and cloud patterns could have realized long before classical nineteenth century experiments of Faraday and Bénard. Wave patterns generated by oscillatory chemical reactions (which long considered to be impossible due to thermodynamic misconceptions) were demonstrated in 1960s (Burger and Field 1985), while controlled experiments demonstrating persistent stationary chemical patterns in reaction-diffusion systems had to wait till early 1990s (Ouyang and Swinney 1991). Shell growth patterns (Gierer and Meinhard 1972), striped and dotted animal skins (Murray 1981), and desert vegetation patterns (Gilad et al. 2007) have been always here for anybody to observe, before finding rational explanation in terms of the same nonlinear models. Corrugated interfaces were observed and described both as flame fronts in combustion theory (Zeldovich 1985) and as dendrite forms of growing crystals (Langer 1980). More recently, much attention has been drawn by nonlinear optical patterns – spontaneous images emerging in optical circuits and lasers (Arecchi 1999).

Stationary Patterns

Symmetry-Breaking Transitions

The most direct way to formation of stationary patterns is a symmetry-breaking bifurcation. It can be demonstrated in a straightforward way taking as an example a two-component reaction-diffusion system (RDS)

$$\partial_t u = D_1 \nabla^2 u + \gamma_1^{-1} f(u, v), \tag{1}$$

$$\partial_t v = D_2 \nabla^2 v + \gamma_2^{-1} g(u, v), \tag{2}$$

where $f(u, v)$, $g(u, v)$ are source functions depending on the variables u and v, D_1, D_2 are

diffusivities, and ∇^2 is the Laplace operator. We suppose that the system has a homogeneous stationary state (HSS) $u = u_s$, $v = v_s$ satisfying $f(u_s, v_s) = g(u_s, v_s) = 0$; the factors γ_1,γ_2 are introduced to scale the derivatives f_u, g_v computed at this HSS to unity. Stability analysis of the chosen HSS to infinitesimal perturbations $\tilde{u}, \tilde{v} \propto \exp(\mathrm{i}\boldsymbol{k} \cdot \boldsymbol{x})$ with a wave vector $\boldsymbol{k}$ shows that the most dangerous perturbations have the wavenumber

$$|\boldsymbol{k}|^2 \equiv k^2 = \frac{1}{2}\left(\frac{f_u}{\gamma_1 D_1} + \frac{g_v}{\gamma_2 D_2}\right). \quad (3)$$

This value should be positive, which is possible only in the presence of positive feedback, or, in chemical terms, when at least one of the species is "autocatalytic", say, $f_u > 0$ Breaking of spatial symmetry preempts Hopf bifurcation, which occurs at $\gamma_1^{-1} f_u + \gamma_2^{-1} g_v = 0$ and leads to homogeneous oscillations, provided only one of the species is autocatalytic, so that $g_v < 0$, and the autocatalytic species is less diffusive. Thus, for spatial symmetry breaking in a two-component system, one needs a combination of a slowly diffusing "activator" and a rapidly diffusing "inhibitor".

The development of a pattern can be understood qualitatively in the following way. A local upsurge of the activator concentration increases also the concentration of the inhibitor, which spreads out suppressing the activator at neighboring locations. This, in turn, suppresses the inhibitor locally and, through inhibitor diffusion, enhances the activator further along the line, so that the inhomogeneous state spreads out. This scheme works with the roles of an activator and an inhibitor played, respectively, by prey and predator in population dynamics, by growing plants and seeping moisture in ecology, or, rather less directly, by buoyancy and heat conduction in natural convection.

Pattern formation may also result from nonlocal interactions. For example, a nonlocal extension of the nonlinear Schrödinger equation (NLS) for a complex field u,

$$-i\partial_t u = \nabla^2 u - u(\boldsymbol{x}) \int U(\boldsymbol{x} - \boldsymbol{\xi}) |u(\boldsymbol{\xi})|^2 \mathrm{d}\xi, \quad (4)$$

generates a patterned state known as "supersolid", as compared and contrasted to superfluid solutions of the local NLS (Josserand et al. 2007). It might be possible to derive nonlocal equations from a local RDS. Thus, if in Eq. 2 $\gamma_2 << \gamma_1$, so that the inhibitor is fast as well as diffusive, the time derivative can be neglected; then, if the function $g(u, v)$ is linear in v, Eq. 2 can be resolved with the help of an appropriate Green's function, and substituting it in Eq. 1 yields a nonlocal activator equation.

Selection of Stationary Patterns

Symmetry breaking transitions in more than one dimension are degenerate due to spatial symmetries. In an isotropic system, an arbitrary number of differently directed modes with $k = |\boldsymbol{k}| = \text{idem}$ can be excited beyond the bifurcation point. A combination of these modes can give a variety of distinct *planforms*. Competition among the modes that determines the pattern selection is described by *amplitude equations* describing evolution of complex amplitudes a_j, which have a general form

$$\begin{aligned} \frac{\mathrm{d}a_j}{\mathrm{d}t} &= -\frac{\partial V}{\partial \overline{a}_j}, \\ V &= -\mu \sum |a_j|^2 + \sum v_{ijk} a_i a_j a_k \\ &\quad + \sum v_{ijkl} a_i a_j a_k a_l + \text{c.c.} \end{aligned} \quad (5)$$

Here the coefficient μ is proportional to the deviation from the bifurcation point; real coefficients v_{ijk}, v_{ijkl} characterize nonlinear interactions among the modes; the summation is carried out over all closed polygons formed by the wave vectors of extant modes. The product of the amplitudes $\overline{a}_j$, $\overline{a}_k$, etc. (where the overline denotes the complex conjugate) may appear in the equation for the amplitude a_j if the respective wave vectors add up to zero, $\boldsymbol{k}_i + \boldsymbol{k}_j + \boldsymbol{k}_k + \cdots = 0$. This condition ensures that the modes in question are in resonance. Otherwise, the product of these modes rapidly oscillates and is averaged out when the amplitude equation is derived using a multiscale expansion procedure. Stationary solutions, i.e. potential minima of Eq. 5 with one, two, three, or more non-vanishing modes with a symmetric star of wave vectors correspond, respectively, to a striped, square, hexagonal, or quasicrystalline pattern.

The cubic term in the potential (5) generates the lowest-order, hence, strongest nonlinear interactions. This term vanishes in the presence of inversion symmetry $a \rightarrow -a$, which exists, in particular, in the thoroughly studied case of buoyancy-driven convection in the Boussinesq approximation. Otherwise, it is dominant near the bifurcation point, causing (in 2D) a subcritical transition to a hexagonal pattern comprising modes forming a regular triangle. These three modes are in resonance, which means that their phases are not independent but bound by a linear relationship. The sum of phases always adjusts in such a way that interactions are destabilizing. The remaining two phase degrees of freedom correspond to translational symmetry in the plane.

In 3D, the preferred patterns, or crystalline structures, comprise wave vectors forming a regular polyhedron with triangular faces – tetrahedron, octahedron or dodecahedron (Alexander and McTague 1978). The former two correspond to a body- centered cubic (bcc), and the last one, to a quasicrystalline structure with fivefold symmetry. These lowest-order interactions cannot, however, stabilize the pattern at a finite amplitude, and next-order interactions generated by the quartic term in Eq. 5 are necessary to saturate the pattern. Depending on respective interaction coefficients, various structures can be chosen.

A greater variety of patterns may arise if planforms with different wavenumbers k are excited simultaneously. This can be achieved in a most natural way in two-layer systems where the wavelength of the excited pattern depends on the thickness of each layer, as in convection (Proctor and Jones 1988), or different diffusivities, as in a pattern-forming chemical system (Yang et al. 2002). More possibilities arise in nonlinear optics where spatial symmetry breaking may occur on different wavelengths at rather close values of a control parameter (Pampaloni et al. 1997). The resulting coupled amplitude equations can generate a variety of composite planforms, which may have a form of superstructures or quasicrystals. Lowest-order interactions can generate various resonances; no rigid fitting of wavenumbers is required for this, since resonant modes can form an isosceles triangle. Dynamics of mode interactions may be complicated (Pismen and Rubinstein 1999), since the gradient structure of Eq. 5 is, generally, lost.

Regular patterns may suffer various instabilities, which limit the range of admissible wavelengths or lead to a change of the planform through excitation of a non-collinear mode or decay of an extant mode. Wavelength changing instabilities, as a rule, do not saturate and lead to formation of defects.

Modulated and Distorted Patterns

Natural patterns seen both in experiment and simulations are never perfect: their amplitudes may be modulated at distances large compared to the basic wavelength, and they may have various defects: dislocations, disclinations, and domain walls. An example of an imperfect striped pattern is shown in Fig. 2. Variation of local wavelengths is possible because instability spreads out to a finite range of wavenumbers, scaled as the square root of the parametric deviation from the bifurcation point. Other imperfections are a consequence of the rotational symmetry of the system.

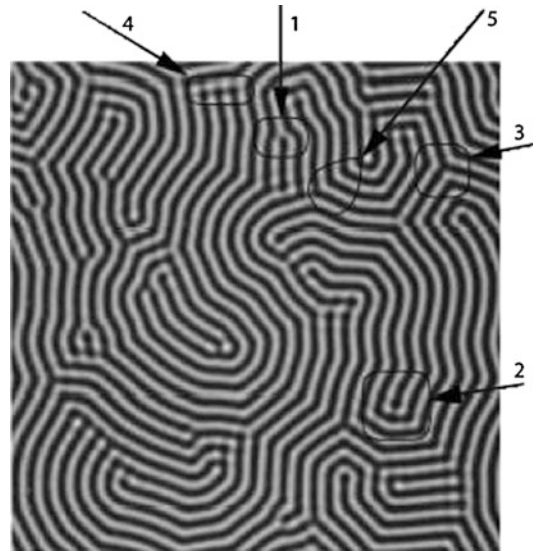

Patterns and Interfaces in Dissipative Dynamics, Fig. 2 Various forms of pattern defects. *1* – dislocation, *2* – concave disclination, *3* – convex disclination, *4* – amplitude domain wall, *5* – phase domain wall (Bowman and Newell 1998, reproduced with permission. Copyright by the American Physical Society)

Different orientations of stripes may be chosen at different locations, either randomly or under influence of boundary conditions or local inhomogeneities. The discrepancies of local orientations are reconciled through formation of disclinations and domain walls, while dislocations reconcile discrepancies of local wavelengths.

Weak distortions, which do not contain defects, can be described by means of either space-dependent amplitude equations applicable to small-amplitude patterns near the bifurcation point, or phase dynamics applicable also to finite-amplitude patterns but restricted to long-scale distortions.

The amplitude equation must have an anisotropic form in an isotropic system, the source of anisotropy being the direction of the wave vector itself. Modulations of this amplitude along and across the direction of the wave vector $\boldsymbol{k}$ should be scaled differently, since adding a small longitudinal component, say, ϵq_x changes $k = |\boldsymbol{k}|$ by $O(\epsilon)$, while adding a transverse component of the same magnitude ϵq_y changes k by $O(\epsilon^2)$ only; thus the stripes are bent far more easily than they are compressed or extended. This leads to the Newell-Whitehead-Segel (NWS) amplitude equation (Newell and Whitehead 1969; Segel 1969), which can be written in a rescaled universal form

$$\partial_t u = \left(\partial_x - \frac{i}{2k}\partial_y^2\right)u + u - |u|^2 u. \qquad (6)$$

The mixed-order differential operator entering this equation precisely accounts for the equivalence of all structures with identical wavenumbers, independently of the direction of the wave vector.

The NWS equation is ill-suited for computations, since the orientation of the coordinate axes depends on the local phase gradient, so that the differential operator is in fact strongly nonlinear. Most model computations of striped patterns are based on the Swift-Hohenberg (SH) equation

$$\partial_t u = -\left(1 + \nabla^2\right)u + u\left(\mu - u^2\right). \qquad (7)$$

In an *anisotropic* system where a certain direction of stripes is preferred, the situation is easier, and the amplitude equation can be reduced by rescaling to an *isotropic* real Ginzburg-Landau (RGL) equation

$$\partial_t u = \nabla^2 u + u - |u|^2 u. \qquad (8)$$

Phase Dynamics

The idea of phase dynamics (Pomeau and Manneville 1979) is to characterize a striped pattern by means of a single variable – phase θ, which changes by 2π over the period of the pattern or, more conveniently, by a rescaled phase $\Theta = \epsilon\theta$. The derivatives of the phase are the wave vector $\boldsymbol{k} = \nabla\theta$ and frequency $\omega = -\theta_t$, which vary on an extended scale exceeding the wavelength of the underlying structure by a factor $\epsilon^{-1} >> 1$. The general form of the phase equation in an isotropic system is determined by scaling and symmetry considerations alone:

$$\partial_T \Theta = D_1\left(\boldsymbol{n}\cdot\hat{\nabla}\right)^2\Theta + D_2\hat{\nabla}^2\Theta, \qquad (9)$$

where $\partial_T, \hat{\nabla}$ are derivatives with respect to slow time and extended spatial variables, $\boldsymbol{n}$ is the unit vector along $\boldsymbol{k}$, and D_1, D_2 are phase diffusivities that depend on a particular underlying problem and are, generally, functions of k. This equation can be also presented in an elegant gradient form (Cross and Newell 1984).

The phase equation (9) is, in fact, strongly nonlinear due to the dependence of both the diffusivities and the direction of the unit vector $\boldsymbol{n}$ on the local phase gradient. It can be linearized, yielding an anisotropic diffusion equation, only when deviations from a prevailing wave vector $\boldsymbol{k} = \boldsymbol{k}_0$ are arbitrary small. If the X- and Y-axes are drawn, respectively, along and across $\boldsymbol{k}_0$, (9) reduces to

$$\Theta_T = D_{||}(k_0)\Theta_{XX} + D_{\perp}(k_0)\Theta_{YY}, \qquad (10)$$

where $D_{||} = D_1 + D_2$ and $D_{\perp} = D_2$ are, respectively, the longitudinal and transverse phase diffusivities. The pattern with the wavenumber k_0 is stable to long-scale perturbations when both phase diffusivities are positive. Vanishing $D_{||}$ corresponds to the *Eckhaus* instability and vanishing $D_{\perp}$ to the *zigzag* instability. Eckhaus instability defines the upper limit of stable wavenumbers. It never

saturates, and usually leads to formation of defects effectively increasing the wavelength. Zigzag instability defines the upper limit of stable wavenumbers; it causes bending of stripes effectively decreasing the wavelength.

Dynamics of Defects

Dynamics of strongly distorted patterns is mostly governed by motion and interaction of defects. Defects are topological objects (Mermin 1979): a dislocation is characterized by circulation of the phase around any enclosing contour equal to an integer multiple of 2π, and a disclination, by circulation of the direction of the wave vector equal to an integer multiple of π. A single dislocation climbing across the direction of the wave vector of a striped pattern effects a change of the wavenumber over an extended region. The force driving the dislocation is due to the deviation from the optimal wavenumber. Eckhaus instability of a striped pattern leads to the formation of a dislocation pair. It is notable that, although the far field of dislocations can be described by phase equations, their interaction is determined by the dislocation core where these equations are inapplicable (Bodenschatz et al. 1988; Pismen and Rodriguez 1990).

Motion of dislocations in striped patterns is well understood and supported by experimental evidence (Braun and Steinberg 1991) for anisotropic patterns governed by Eq. 8. The structure of dislocations in isotropic systems described by Eq. 6 is more complicated, being strongly anisotropic (Nepomnyashchy and Pismen 1991). Disclinations pose more difficulties for the analysis, even on the topological level (Mermin 1979), see (Newell et al. 1996).

Paradoxically, defects enhance relaxation of the pattern to a state of minimum energy corresponding to an "optimal" wavelength. If a deviation of the control parameter from the symmetry breaking bifurcation point is of $O(\epsilon^2)$, the width of the band of excited modes is of $O(\epsilon)$, but the band width actually observed in a natural patterns containing defects is of $O(\epsilon^2)$ (Bowman and Newell 1998). The band shrinks due to motion of point defects and adjustments influenced by domain walls.

The structure and interaction of dislocations in a hexagonal pattern is strongly affected by the resonant character of interactions among the constituent modes. Dislocations in any two modes of the triplet forming a hexagonal pattern, created originally at arbitrary locations, are always attracted to each other (Bodenschatz et al. 2000; Rabinovich and Tsimring 1994), eventually forming an immobile bound pair corresponding to a penta-hepta defect (see Fig. 3).

Equations 6 and 8 are derivable from an energy functional that decreases monotonically in time until a stationary state of minimal energy is reached; this state may still contain defects necessary to satisfy boundary conditions in a confined region. In some cases, however, an additional field, besides the amplitude, is necessary to adequately describe a physical system even close to the symmetry-breaking bifurcation point. A well known example is Bénard convection in low Prandtl number fluids where the additional factor is mean flow generated by pattern distortions and

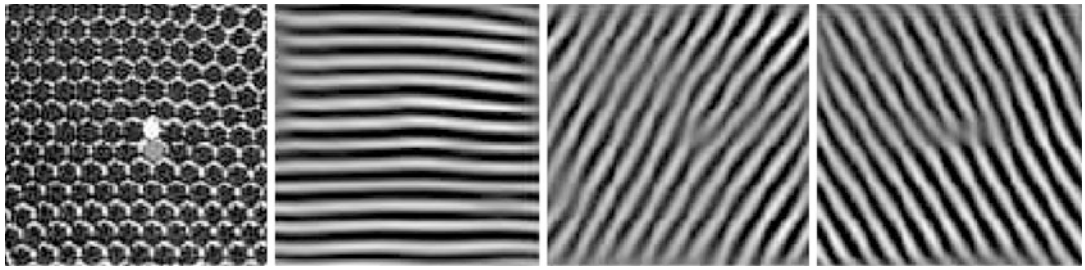

Patterns and Interfaces in Dissipative Dynamics, Fig. 3 Hexagonal pattern containing a penta-hepta defect (*left*) and its three constituent modes obtained by Fourier filtering of the initial image (Abou et al. 2000, reproduced with permission)

advecting the entire pattern. In this case, the patterns remains weakly turbulent indefinitely long, displaying labyrinthine structures, coexisting striped and hexagonal domains (Assenheimer and Steinberg 1993) or spiral defect chaos (Bodenschatz et al. 2000) (see Fig. 4). Chaotic non-stationary patterns also typically appear at higher amplitudes. In reaction-diffusion systems non-stationary and chaotic patterns become more likely when the inhibitor response is slowed down.

Moving Interfaces

Stationary and Propagating Fronts

Many physical systems, either at equilibrium or in a non-equilibrium steady state sustained by external fluxes, may exist in two or more alternative states. If different states are attained at different spatial locations, they are separated by an *interface,* carrying excess energy. The simplest model is a single "reaction-diffusion" equation

$$\partial_t u = D\nabla^2 u + f(u), \tag{11}$$

where D is diffusivity and the function $f(u) = -V'(u)$ (see Fig. 5) has three zeroes that correspond to two stable (with $f'(u) < 0$) and one unstable (with $f'(u) > 0$) HSS. This equation was first used in the context of phase equilibria (van der Waals 1894) as a model of gas-liquid interface, with u denoting density. It was later extended to the solidification problem, with u denoting a fictitious "phase field" assuming its two stable values $u = u_s^{\pm}$ in the liquid and solid phases (Cahn and Hilliard 1958). The coefficient D is interpreted in this context as *rigidity.* The "reaction-diffusion" interpretation applies to non-equilibrium systems, such as a catalytic

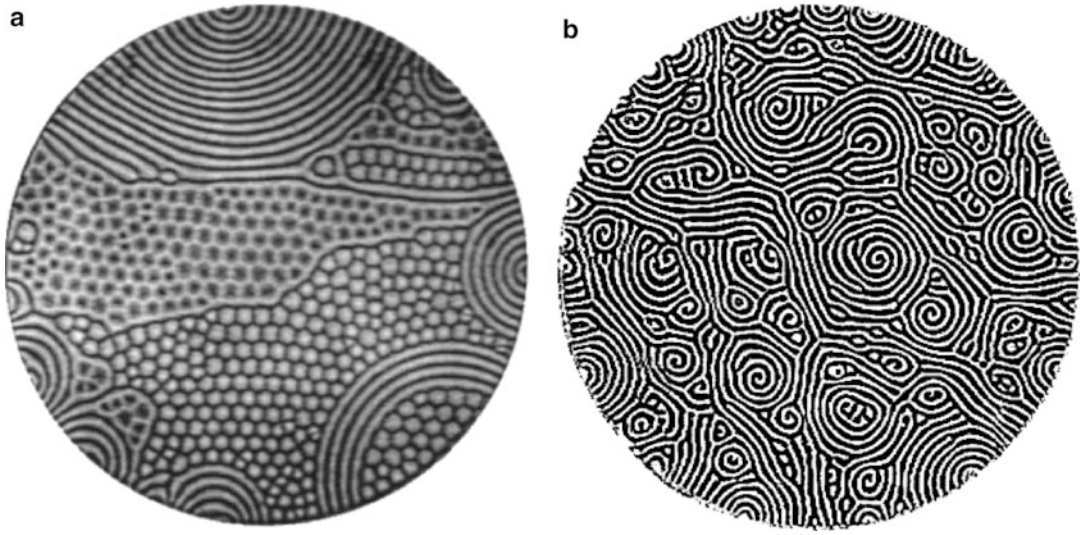

Patterns and Interfaces in Dissipative Dynamics, Fig. 4 (**a**) Coexisting domains; (**b**) Spiral defect chaos (Bodenschatz et al. 2000, reproduced with permission)

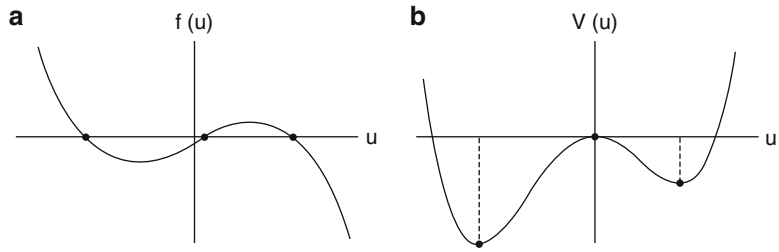

Patterns and Interfaces in Dissipative Dynamics, Fig. 5 A function $f(u)$ with three zeros (**a**) and the respective double-well potential (**b**)

surface or an ecological domain, with u denoting concentration and $f(u)$, the net production rate.
A straight-line or planar interface is stationary when the potentials $V\left(u_s^{\pm}\right)$ are equal. It carries then the interfacial energy

$$\sigma = D\int_{-\infty}^{\infty} u'(x)^2 \mathrm{d}x = \int_{u_s}^{u_s^+} -\sqrt{2DV(u)}\mathrm{d}u, \qquad (12)$$

which is identified with surface tension.

If the potentials are unequal, the front moves in the direction decreasing the total energy of the system. Assuming that the motion is stationary and directed along the x axis, (11) can be rewritten in the comoving frame propagating with the front velocity c. The steadily propagating solution depends on a single coordinate $\xi = x - ct$, and (11) reduces to an ordinary differential equation

$$cu'(\xi) + Du''(\xi) + f(u) = 0, \qquad (13)$$

subject to the boundary conditions $u = u_s^{\pm}$ at $\xi \to \pm\infty$.When both equilibria are stable, they are saddles when viewed as equilibria of (13). The front solution corresponds to a heteroclinic trajectory connecting the equilibria $u = u_s^{\pm}$. The heteroclinic connection exists only at unique value of c (see Fig. 6); thus, the propagation speed is determined uniquely by solving a nonlinear eigenvalue problem. Its value is proportional to the difference of potentials of the two HSS:

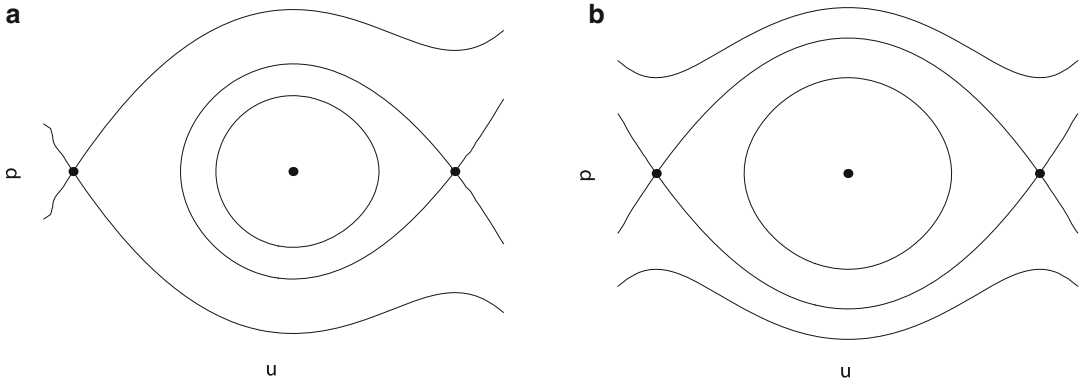

Patterns and Interfaces in Dissipative Dynamics, Fig. 6 Generic trajectories in the phase plane $u, p = u'(x)$ (**a**) and a nongeneric set of trajectories containing a heteroclinic orbit (**b**)

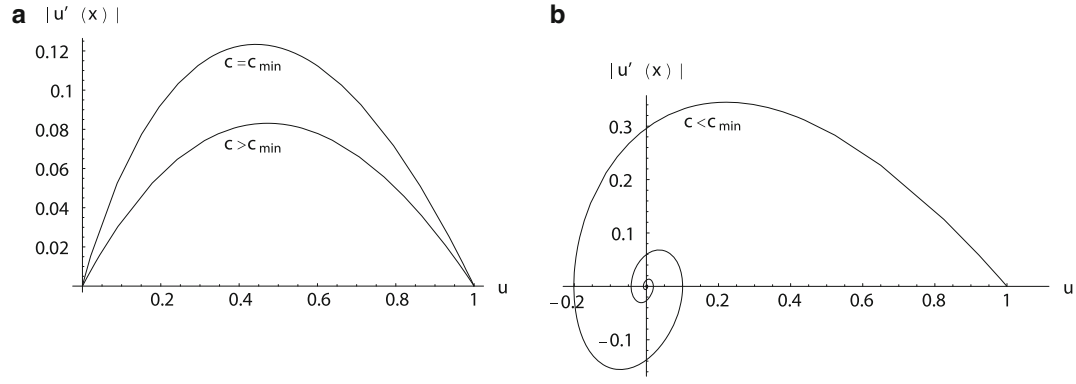

Patterns and Interfaces in Dissipative Dynamics, Fig. 7 Trajectories in the phase plane connecting a stable and an unstable equilibrium

$$c = \frac{D}{\sigma}\Delta V, \quad \Delta V = V\left(u_s^-\right) - V\left(u_s^+\right). \qquad (14)$$

The situation is different when the retreating state $u = u_s^0$ is unstable. This often happens in population dynamics: a state where a competitively advantageous specie is absent is formally unstable to infinitesimal perturbations but will be nevertheless preserved at any location until this specie is introduced there. An unstable state, viewed as an equilibrium point of (13), is a stable node at propagation speeds exceeding a certain threshold $c_{\min}$, Thus, a trajectory starting from the advancing stable HSS connects generically to u_s^0 at any $c > c_{\min}$ (see Fig. 7). Actual propagation speed is selected dynamically at the leading edge (Kolmogorov et al. 1937; van Saarloos 2003), and turns out to be equal to the minimum speed $c_{\min}$, which corresponds to the steepest front profile. Under certain conditions (when overshoots are allowed) a faster speed corresponding to a still steeper profile is selected nonlinearly (van Saarloos 2003). In the former case, the front is "pulled" by perturbations growing at the leading edge and described by linearized equations, while in the latter case, it is "pushed" by nonlinear interactions favoring the advancing state.

Interfacial Instabilities

The front solution is neutrally stable to translations along the x-axis. This neutral (Goldstone) mode is weakly perturbed when the translation is weakly nonuniform, so that the front becomes curvilinear but the curvature radius still far exceeds the characteristic front thickness.

Propagation of a weakly curved front is best understood in a coordinate frame aligned with its deformed shape. The nominal front position is defined by replacing a diffuse transitional region by a planar curve $\mathcal{C}$ drawn along some intermediate level of the variable u. The coordinate lines $x =$ const are obtained by shifting the curve along the normal by a constant increment, as shown in Fig. 8. This shift causes the length to increase on convex, and to decrease on concave side of the curve. Eventually, a singularity develops in the latter direction, but, when the curvature radius is much larger than the characteristic front thickness, this will happen far away within the region where one of the HSS is approached.

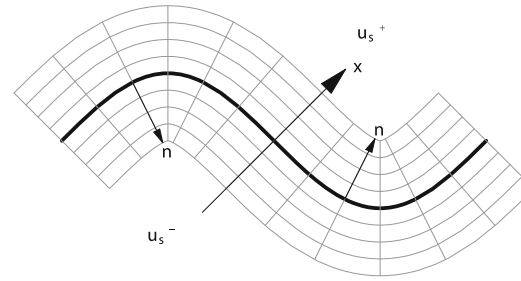

Patterns and Interfaces in Dissipative Dynamics, Fig. 8 Construction of the aligned coordinate frame. The coordinate lines are shown in *gray*. *Arrows* show the local directions of the normal **n** and the *x*-axis. Observe a singularity developing on the concave side

When (13) is rewritten in the aligned frame an expanded viewing the curvature as a small parameter, the local normal propagation speed of a curved front is expressed by the eikonal equation

$$c = c_0 - D\kappa = \frac{D}{\sigma}(\Delta V - \sigma\kappa), \qquad (15)$$

where c_0 is the speed of a planar front and k is the Gaussian curvature.

Since convex front segments propagate slower and concave segments faster, the front tends to flatten, provided c_0 is uniform everywhere. Instabilities may arise, however, when c_0 increases ahead of the front. This may happen in the presence of an externally imposed gradient, as in directional solidification (Langer 1980), but most commonly is caused by an additional "control" field. The control field responsible for the Mullins-Sekerka instability of solidification fronts (Langer 1980; Mullins and Sekerka 1963) is the concentration of a contaminant, which is rejected by the solid and slows down solidification by lowering the melting temperature. Since the contaminant diffuses away more easily from convex segments, they tend to propagate faster, which causes instability when the driving is strong enough to overcome surface tension.

Another example is instability of a combustion front, which separates hot burnt-out and cold fuel-rich domains (Zeldovich 1985). A thin front

structure arises in this case because combustion requires both fuel and sufficient temperature for its initiation, and both fuel concentration and temperature play the role of control variables. When heat transfer is the limiting factor, convex segments cool down and propagate slower, and the front is stable. When, on the opposite, propagation is limited by fuel supply, convex segments accelerate and instability sets on, leading to corrugated fronts.

Dynamics of weak deviations $\zeta(\boldsymbol{y})$ from a stable planar front spanned by a 2-vector y is described by expanding the normal propagation speed, front curvature and the control field in powers of a small parameter scaling both the deviation ζ and its transverse derivative $\nabla_{\mathbf{y}}$, as well as time. For stable fronts, the appropriate scaling is $\zeta = O(1)$, $\nabla_{\mathbf{y}} = O(\in)$, $\partial_t = O(\in^2)$, leading to the Burgers equation

$$\partial_t \zeta = D\nabla_{\mathbf{y}}^2 \zeta - \frac{1}{2} c_0 \left|\nabla_{\mathbf{y}} \zeta\right|^2. \tag{16}$$

The particular coefficients here correspond to (15), but also in other cases the same universal form can be obtained after the coefficients are removed by rescaling, provided the effective diffusivity D is positive. If the latter is negative but small, $|D| = O(\epsilon^2)$, the appropriate scaling is $\zeta = O(\in)$, $\nabla_{\mathbf{y}} = O(\in)$, $\partial_t = O(\in^4)$, and expanding to a higher order yields, after scaling away the coefficients, the Kuramoto-Sivashinsky equation (Sivashinsky 1977)

$$\partial_t \zeta + \nabla_{\mathbf{y}}^2 \zeta + \left(\nabla_{\mathbf{y}}^2\right)^2 \zeta + \frac{1}{2}\left|\nabla_{\mathbf{y}} \zeta\right|^2 = 0. \tag{17}$$

This equation, appearing also in phase dynamics (Kuramoto and Tsuzuki 1976), is a paradigm of weak turbulence.

Front Interactions and Coarsening

Fronts of opposite polarity in a one-dimensional system attract and eventually coalesce, thereby coarsening the distribution of domains, which may have been created initially in the process of phase separation or relaxation to alternative HSS. The interaction is, however, very weak, falling off exponentially with separation. In higher dimensions, the principal cause of coarsening, or Ostwald ripening, is the curvature dependence of the propagation speed, whereby small droplets with high curvature tend to shrink and eventually disappear. This is a manifestation of the Gibbs-Thomson effect relating the equilibrium conditions with the radius of a droplet.

Coarsening most often occurs under conditions when evolution is constrained by a conservation law, so that the integral $\int u(\mathbf{x})\mathrm{d}\mathbf{x}$ expressing the total amount of material in the system remains constant. Under these conditions, fronts cannot move independently from each other. The conservation law is accounted for when (11) is replaced by the Cahn-Hilliard equation (Cahn and Hilliard 1958)

$$\partial_t u = \nabla^2 \mu, \quad \mu = -\left[D\nabla^2 u + f(u)\right]. \tag{18}$$

The eikonal equation governing the front motion retains the form (15), but the value c_0 depends on chemical potential μ. The latter shifts in the course of coarsening in such a way that the value of the critical radius $R = \kappa^{-1}$ of a droplet that neither grows or shrinks, keeps growing as smaller droplets disappear. Analytical theory (Lifshitz and Slyozov 1958) predicts universal asymptotic droplet size distribution at late stages of coarsening.

Structures Built up of Fronts

Coarsening can be precluded when changes in an additional control field arrest growth of large and shrinking of small domains. This leads to formation of a variety of patterns and solitary structures. The paradigmal system for exploring these phenomena is the FitzHugh-Nagumo system, which has the form (1), (2) with the function $f(u, v)$ cubic in u and linear in v and a linear function $g(u, v)$. The rescaled form suitable for the analysis of stationary structures is

$$\in^2 \partial_t u = \in^2 \nabla^2 u + u - u^3 - \in v, \tag{19}$$

$$\tau^{-1} \partial_t v = \nabla^2 v - v - v + \mu u, \tag{20}$$

Here $\in = \sqrt{\gamma_1 D_1 / \gamma_2 D_2} << 1$ is the ratio of the characteristic lengths associated with the

activator and the inhibitor, $\tau = D_2/D_1$; the small coupling parameter ε in (19) ensures a balance between the effect of small interfacial curvature and weak symmetry breaking between the alternative HSS $u_s^{\pm} = \pm 1 + O(\in)$; the remaining parameters μ and ν regulate the coupling stress and bias.

Structures generated by the system (19), (20) are built up by assigning a region where the activator approaches one of the alternative HSS, computing the respective inhibitor distribution, and finding stationarity conditions for the fronts forming the boundaries of this region (Ohta et al. 1989). Possible stationary structures in two dimensions are a solitary band, a solitary disk, a striped pattern, or a hexagonal grid consisting of almost circular spots. The size of spots or stripes is determined by the parameters of the system, but there is a considerable leeway in choosing the general configuration. Under certain conditions, it even might be possible to store information by creating or extinguishing spots at chosen locations (Coullet et al. 2004). In other cases, splitting of a solitary spot initiates a multiplication cascade (Reynolds et al. 1994), leading eventually to a hexagonal pattern filling the plane.

Instabilities of stationary structures are studied with the help of the linearized eikonal equation (15) combined with the inhibitor equation (20) where the last term is expressed through a shift of the front position. Both solitary bands and disks can suffer zigzag (leading eventually to splitting), oscillatory and traveling instabilities. The latter two become prevalent as the parameter τ decreases, so that the inhibitor response to front displacements slows down. For example, a solitary band is destabilized in the zigzag mode at $\tau > 1$, while the traveling instability comes first at smaller τ (see Fig. 9). Oscillatory instability is always preceded by traveling one in this case, but may become relevant for a solitary disk.

Traveling instability indicates transition to various propagating structures and wave patterns. A solitary spot tends to either dissolve or spread out sidewise after being immobilized; in the latter case, a spiral structure starts to develop as the ends lag behind. A traveling spot can be, however, stabilized if a second inhibitor, both fast and long-range, is added (Or-Guil et al. 1998).

Various patterns of propagating fronts can be generated beyond this limit by the same FitzHugh-Nagumo system, which, however, should be scaled differently for this purpose. Unlike stationary or slowly evolving patterns where the characteristic length scale is set by the diffusional range of the long-scale inhibitor, the wavelength of a propagating pattern is tied to the propagation speed and remains finite even when the inhibitor is nondiffusive.

The long scale should be redefined therefore on the basis of the characteristic propagation speed of the activator front $c^* = \sqrt{D_1/\gamma_1}$ and the characteristic relaxation time of the inhibitor γ_2. Using this "advective" length unit, $L^* = \gamma_2\sqrt{D_1/\gamma_1}$ brings (1), (2) to the dimensionless form

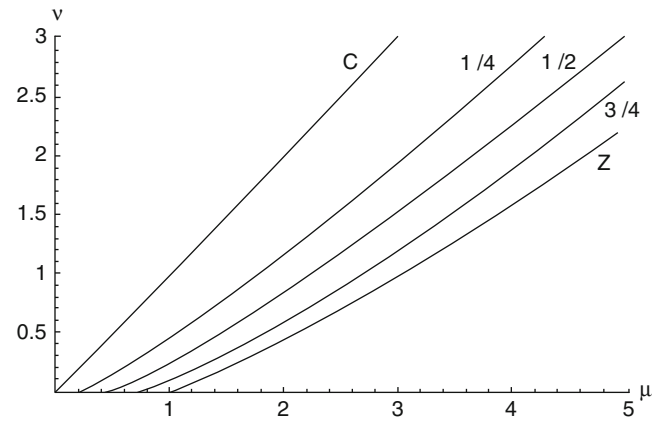

Patterns and Interfaces in Dissipative Dynamics, Fig. 9 Existence boundary (*C*) and loci of zigzag (*Z*) and traveling instability for a solitary band. The loci of traveling instability are marked by respective values of τ. A stable band exists between the line C and an applicable instability locus

$$\gamma \partial_t u = \gamma^2 \nabla^2 u + f(u, v), \tag{21}$$

$$\partial_t v = \delta^2 \nabla^2 v + g(u, v), \tag{22}$$

where $\gamma = \gamma_1/\gamma_2, \delta = \gamma/\in = \sqrt{\gamma D_2/D_1}$ .The "inner" scale of the transitional layer, where the system switches between the two alternative activator states, $u = u_s^{\pm}$, is now set exclusively by the capacitance ratio γ, independently of diffusivities, and, provided $\gamma \ll 1$, remains small even when the inhibitor is less diffusive than the activator. The parameters can be chosen in such a way that $\delta \ll 1$, so that the inhibitor diffusion is negligible, provided $\gamma \ll D_1/D_2$. Under these conditions, the inhibitor diffusion can be neglected, reducing (22) to $\partial_t v = g(u, v)$. Although this equation contains no mechanism for healing discontinuities in v, the inhibitor field should remain smooth in the course of evolution, barring freaky initial conditions or strongly localized perturbations. This opens the easiest way of constructing various wave patterns, including such exotic objects as chaotic wave trains (Elphick et al. 1988).

Interfaces of Patterns

Interfaces between different patterns or different pattern orientations (domain walls) can be described in the simplest way on the level of amplitude equations. This may give qualitatively correct results in static problems, even though changes across a domain wall in patterns generated in simulations and experiments are usually effected on a length comparable with the prevailing wavelength of the pattern. One can expect that a stationary solution exists only when the wavelengths are equal on both sides of the wall; otherwise, the wall would propagate in the direction decreasing the overall energy of the pattern. It turns out that an even stronger restriction is true, and both wavelengths should be optimal (Malomed et al. 1990). In this way, domain walls, alongside dislocations, enhance relaxation of the pattern to the optimal wavelength.

Dynamic problems are strongly influenced by detailed structure of the pattern, which is lost on the level of amplitude equations. When a pattern advances into an unstable uniform state, the wavelength selected at the leading edge is not identical to the wavelength of the full-grown pattern formed behind the front, and neither one coincides with the optimal wavelength (Ben-Jacob et al. 1985).

In the case when a stable homogeneous solution coexists with a stable periodic pattern, stable stationary fronts between the two states exist within a finite parametric interval (Pomeau 1986), rather than at a single point where the energies of both states are equal, as amplitude equations would predict. The motion of this front is affected by the discrete structure of the pattern, which causes self-induced pinning hindering the retreat of a metastable state. There are two depinning transitions, corresponding to "crystallization" or "melting" of the pattern, shown schematically by thick lines in Fig. 10. Between the two limits, various metastable stationary structures exist: a single cell ("soliton"), a finite patterned inclusion, sandwiched between semi-infinite domains occupied by a uniform state, or a semi-infinite pattern, coexisting with a uniform state. To the right of the crystallization threshold C, the pattern advances by a periodic nucleation process which creates new elementary cells at the interface (Aranson et al. 2000), while to the left of the melting limit M, the pattern recedes as elementary cells at the interface are destroyed. A different, far more efficient depinning mechanism works in two dimensions (Hagberg et al. 2006). It is initiated by a zigzag instability of the pattern followed by nucleation of disclinations, which further move toward the uniform state, as seen in Fig. 11. This generates stripes extending in the normal direction, turning eventually the original boundary into a domain wall separating striped patterns rotated by $\pi/2$.

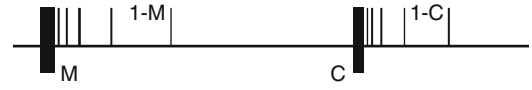

Patterns and Interfaces in Dissipative Dynamics, Fig. 10 A scheme of depinning transitions showing crystallization (*C*) and melting (*M*) thresholds for an infinite cluster, as well as the corresponding limits for clusters of different sizes, terminating in single-cell limits 1-C, 1-M

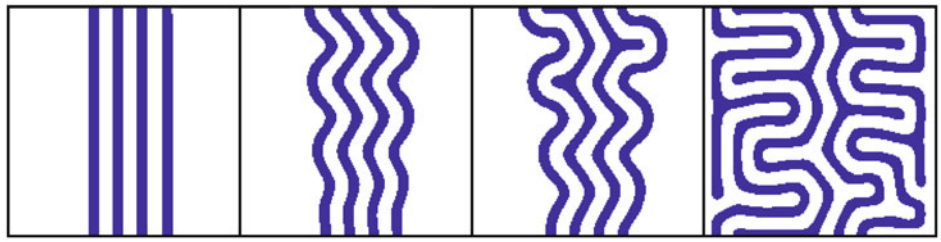

Patterns and Interfaces in Dissipative Dynamics, Fig. 11 Depinning of striped pattern initiated by a zigzag instability (Hagberg et al. 2006)

Wave Patterns

Plane Waves

A simplest propagating wave pattern is a periodic solution depending on a moving coordinate $\xi = x - ct$, where $c = \omega/k$ is phase velocity, ω is frequency and k is wavenumber. A waveform ~ exp. [i($kx - \omega t$)] may emerge directly by symmetry breaking bifurcation, but this is not the most common mechanism. It is impossible, in particular, in a two-component RDS (1), (2), where other scenarios lead to wave patterns. One of them, mentioned in the preceding section, is traveling instability of stationary structures. Another road to wave patterns, most amenable to analytical tools, starts in the vicinity of a Hopf bifurcation, where small-amplitude oscillations weakly modulated in space are described by the complex Ginzburg-Landau (CGL) equation. Its standard rescaled form is

$$\partial_t u = (1 + i\eta)\nabla^2 u + u - (1 + iv)|u|^2 u. \quad (23)$$

A plane wave solution of (23) with the wave vector $\boldsymbol{k}$ is

$$\begin{aligned} u &= \rho_0 \exp[i(\boldsymbol{k}\cdot\boldsymbol{x} - \omega t)], \\ \rho_0 &= \sqrt{1-k^2}, \quad \omega = v + (\eta - v)k^2. \end{aligned} \quad (24)$$

The waves are dispersive, and the group velocity is $\boldsymbol{v} = 2\,\boldsymbol{k}(\eta - v)$.

Instabilities of plane waves are studied most efficiently with the help of the phase dynamics approach, since the most dangerous perturbation modes can be viewed as long-scale distortions of neutrally stable translational modes. The longitudinal and transverse phase diffusivities are

$$D_{\|} = \frac{1 + v\eta - k^2(3 + v\eta + 2v^2)}{1 - k^2}, \quad D_{\perp} = 1 + v\eta. \quad (25)$$

Vanishing $D_{||}$ marks the threshold of Eckhaus instability, which limits the range of stable wavenumbers. Vanishing $D_{\perp}$ signals Benjamin-Feir (self-focusing) instability, independently of the wavelength. Both instabilities arising at the respective thresholds are convective, which means that growing perturbations are washed away with the prevailing group velocity. The absolute instability condition stipulating growth of perturbation at a particular location is less restrictive (see Fig. 12). Numerical simulations (Aranson and Kramer 2002) show that transition to turbulence occurs only when the absolute stability condition is violated, but the system is very sensitive to noise in the convectively unstable region.

Besides uniform wave trains, there is a variety of non-uniform one-dimensional solutions of the CGL equation with a constant frequency and spatially varying modulus and wavenumber, which are stationary in a frame propagating with a certain speed c and depend on the comoving coordinate $\xi = x - ct$ only. The solutions approaching asymptotically at $\xi \to \pm\infty$ either plane waves or the trivial state can be also viewed as defects separating domains where different uniform states prevail. Such solutions include pulses, approaching the trivial state at both extremes; nonlinear fronts, separating the trivial state from an invading wave train, and domain boundaries separating plane waves directed in the opposite

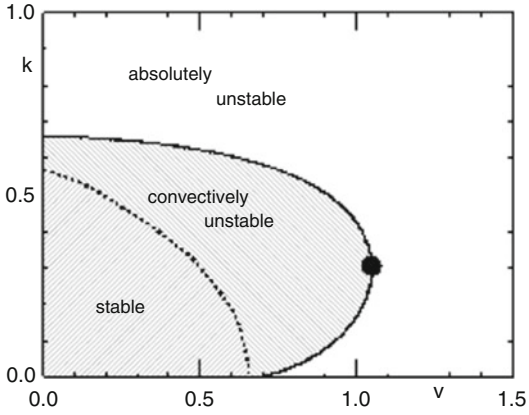

Patterns and Interfaces in Dissipative Dynamics, Fig. 12 Limits of convective and absolute instabilities in the plane (v, k) for $\eta = -3/2$. The *dot* marks the limit of convectively unstable waves (Aranson and Kramer 2002, reproduced with permission. Copyright by the American Physical Society)

sense and, possibly, having different wavelength (Aranson and Kramer 2002; van Saarloos and Hohenberg 1992). Interactions among various defects dominate chaotic dynamics beyond the self-focusing instability limit (Brusch et al. 2001).

Amplitude equations for wave patterns emerging directly from an HSS through a symmetry breaking bifurcation with $\omega \neq 0$, $k \neq 0$ should account for competition between waves with amplitudes $u^{\pm}$ propagating in the opposite directions, which may either suppress one another or combine to a standing wave. The normalized form of coupled equations for $u^{\pm}$ is

$$\begin{aligned}\partial_t u^{\pm} \pm c u_x^{\pm} &= (1+\mathrm{i}\eta) u_{xx}^{\pm} + u^{\pm} \\ &\quad - (1+\mathrm{i}v_+)\left|u^{\pm}\right|^2 u^{\pm} \\ &\quad - g(1+iv_-)|u^{\mp}|^2 u^{\pm}, \end{aligned} \tag{26}$$

where g is a coupling parameter. The orders of magnitude of all terms of these equations can be balanced only when the phase velocity $c = \omega/k$ is of the same $O(\epsilon)$ as $u^{\pm}$. Genetically, $c = O(1)$, and the advective term $cu_x^{\pm}$ is dominant. For a single wave, it can be removed by transforming to the comoving frame. When both waves are present, each wave, viewed in its own frame $\xi_{\pm} = x \mp ct$ samples the average amplitude of its counterpart propagating in this frame with a fast speed. The appropriate amplitude equations have then the form (Knobloch and de Luca 1990)

$$\begin{aligned}\partial_t u^{\pm} &= (1+\mathrm{i}\eta) u^{\pm}_{\xi_{\pm}\xi_{\pm}} + u^{\pm} \\ &\quad - (1-\mathrm{i}v_+)\left|u^{\pm}\right|^2 u^{\pm} \\ &\quad - g(1+\mathrm{i}v_-)|u^{\mp}|^2 u^{\pm}. \end{aligned} \tag{27}$$

These equations retain only global coupling carried by the spatial averages $\langle |u^{\mp}|^2 \rangle$.

In two dimensions, the amplitude equations also involve resonant interactions of pairs of waves propagating in the opposite directions. This makes possible complex dynamics even when the amplitudes are uniform and obey space-independent equations (Pismen 1986)

$$\begin{aligned}&\partial_t u_1^+ \\ &= u_1^+\left[\mu - v_+|u_1^+|^2 - v_-|u_1^-|^2 - \beta\left(|u_2^+|^2 + |u_2^-|^2\right)\right] \\ &\qquad + \overline{\gamma u_2^-}\, u_2^+ u_2^- . \end{aligned} \tag{28}$$

Spiral and Scroll Waves

A ubiquitous and extensively studied waveform is a rotating spiral wave. Its specific feature is the presence of a phase singularity. An n-armed spiral wave can be constructed as a circularly symmetric vortex solution of (23) with the topological charge n, i.e. phase circulation $2\pi n$. Unlike a symmetric defect in (8), the phase must also depend on the radial coordinate, so that the vortex radiates a wave with a certain uniquely selected asymptotic wavenumber k_∞. This solution is obtained (Hagan 1982) in polar cooordinates r, ϕ by assuming an *ansatz*

$$u = \rho(r)\mathrm{e}^{\mathrm{i}\theta}, \quad \theta = n\boldsymbol{\phi} + \psi(r) - \omega t. \tag{29}$$

Using this *ansatz* brings (23) to the form

$$\begin{aligned}&\rho''(r) + r^{-1}\rho'(r) \\ &\quad + \left(1 - k^2 - n^2/r^2 - \rho^2\right)\rho \\ &\quad = 0, \end{aligned} \tag{30}$$

$$\frac{1}{r\rho^2}\frac{\mathrm{d}}{\mathrm{d}r}\left(rk\rho^2\right) = q\left(\rho_\infty^2 - \rho^2\right), \tag{31}$$

where $k = \psi'(r)$ is the radial wavenumber. Stability analysis of plane waves applies also to far

regions of spiral waves; one could expect therefore a transition to a turbulent state to occur under conditions when the selected asymptotic wavenumber k_∞ falls into the range where the corresponding plane wave solution of (23) is unstable. The respective stability limits in the parametric plane (η, ν) are presented in Fig. 13.

Another approach to constructing rotating spiral waves exploits kinematics of fronts of opposite polarity described by RDS (21), (22) (Tyson and Keener 1988). The inhibitor diffusion can be neglected almost everywhere, except in the crucial tip region where the two fronts meet. Behavior of the spiral tip and its meandering instability has been elucidated analytically using a multiscale technique matching different approximations in overlapping regions (Hakim and Karma 1999). Complex dynamics of a meandering tip, which exhibit quasiperiodic and chaotic motion in some parametric domains, can be well described with the help of a simpler phenomenological model (Barkley 1994). A similar instability of spiral waves described by the CGL equation is the core acceleration instability (Aranson and Kramer 2002), which may serve as a trigger of transition to spatio-temporal chaos alternative to instability of radiated waves.

A special kind of spiral wave patterns arises when the underlying dynamical system undergoes a period doubling transition. The period doubling causes the appearance of synchronization defect (SD) lines, which serve to reconcile the doubling of the oscillation period with the period of rotation of the spiral wave (see Fig. 14a). These lines are defined as the loci of those points in the medium where the two loops of the period two orbit exchange their positions in local phase space. The period two oscillations on the opposite sides of a SD are shifted relative to each other by 2π (i.e., a half of the full period), so that the dynamics projected on the rotation direction is effectively of period one, while it is of period two locally at any point in the medium (Fig. 14b).

A three-dimensional extension of a rotating spiral is a rotating scroll wave. The core filament of a scroll wave is a line vortex. A scroll wave with a straight-line core directed along the z-axis has identical spiral waves in each cross-section. Even then, the structure can be nontrivial if the spiral phases are given a phase twist, i.e. are

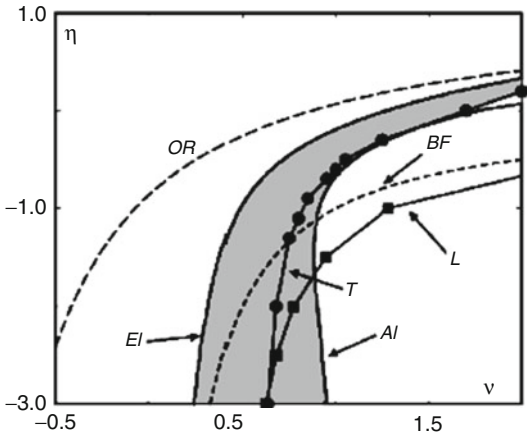

Patterns and Interfaces in Dissipative Dynamics, Fig. 13 Stability limits of a spiral wave solution in the parametric plane (η, ν). The curve *EI* shows the limit of convective instability and *AI*, of absolute instability for the waves emitted by the spiral; *OR* is the boundary of the oscillatory spatial decay for the emitted waves, $q = 0.845$ (bound states exist to the right of this line). *BF* indicates the Benjamin-Feir limit $\nu\eta = -1$, *L* is the limit of phase turbulence, and *T* corresponds to the transition to defect turbulence for random initial conditions (Aranson and Kramer 2002, based on Chaté and Manneville 1996; reproduced with permission. Copyright by the American Physical Society)

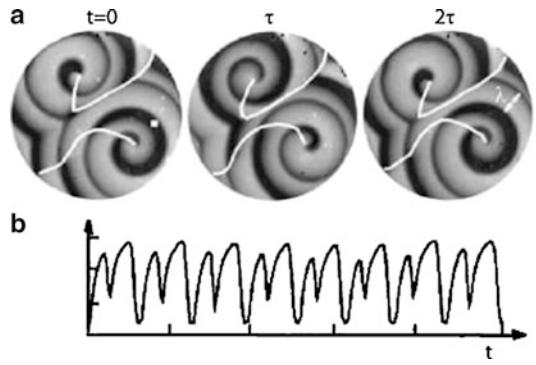

Patterns and Interfaces in Dissipative Dynamics, Fig. 14 (**a**) A pair of period two spiral waves with the fundamental period τ and the average wavelength λ. The *white solid lines* are the synchronization defects. (**b**) A period two time series measured at the point marked by the *white filled square* (Park and Lee 2002, reproduced with permission. Copyright by the American Physical Society)

shifted along the z-axis. A curved core filament may also close up into a ring or even form knots. A stable scroll structure evolves to decrease the filament curvature (Keener 1988). This kind of dynamics is similar to curvature-driven motion of interfaces, but may be reversed when the filament is unstable. The most dangerous perturbation modes are long-scale modes associated with meandering or translational core deformations (Henry and Hakim 2002). Meandering instability usually saturates as a distorted scroll wave with a twisted rotating core (Fig. 15). Instability in the translation mode, which causes spontaneous bending of the scroll axis, does not saturate, but gives rise to a scroll wave with a continuously extending core (Fig. 16a). This leads to a turbulent state visualized as a tangle of breaking wave fronts (Fig. 16b).

Spiral Patterns and Turbulence

Interaction of spiral waves is dominated by shocks – domain boundaries where waves emanating from different centers collide. The shocks effectively screen different spiral domains from radiation emitted by other spiral cores. A typical example of a spiral domain pattern in a stable parametric range obtained in a CGL simulation run starting from random initial conditions (Chaté and Manneville 1996) is shown in Fig. 17. At the initial stage, the system tends to relax locally to the stable state with unity real amplitude, but, as the phases are random, the relaxation is frustrated,

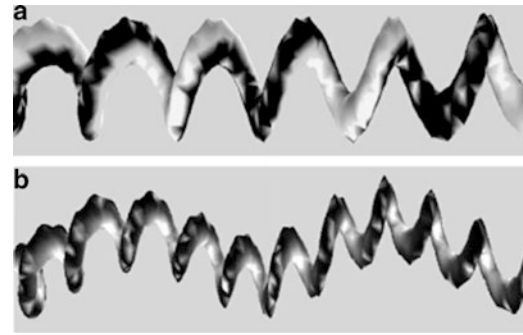

Patterns and Interfaces in Dissipative Dynamics, Fig. 15 (**a**) A restabilized helical vortex; (**b**) A doubly periodic "superhelix" Isosurfaces of the modulus $\rho = 0.6$ shaded by phase field are shown (CGL simulations (Rousseau et al. 1998), reproduced with permission. Copyright by the American Physical Society)

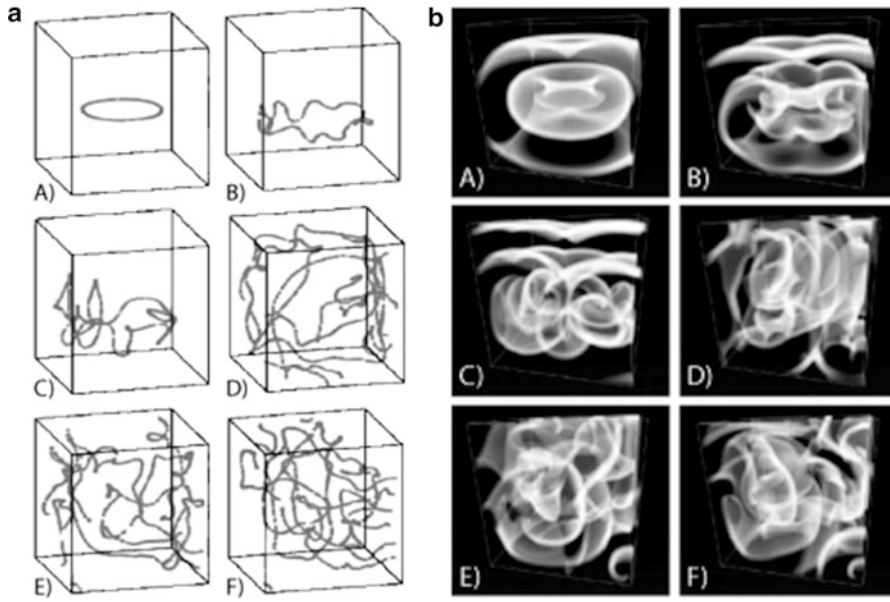

Patterns and Interfaces in Dissipative Dynamics, Fig. 16 Transition to turbulence due to core filament extension and breakup of scroll waves. (**a**) Snapshots of the core filament, starting from a closed loop. (**b**) Respective snapshots of wave patterns showing semitransparent visualization of the activator fronts (Alonso et al. 2004, reproduced with permission. Copyright by the American Physical Society)

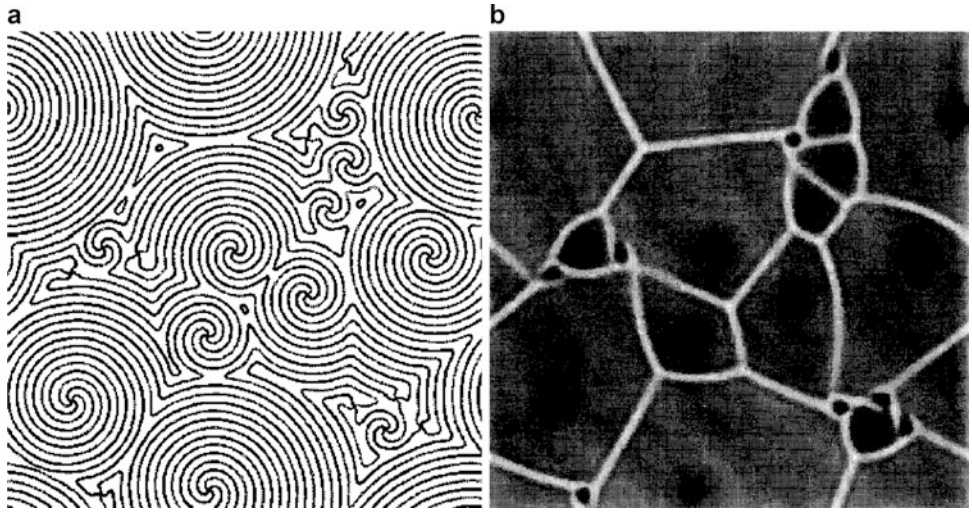

Patterns and Interfaces in Dissipative Dynamics, Fig. 17 Spiral domains. *Left:* levels of constant phase. *Right:* grayscale amplitude map showing enhanced amplitudes at the shocks (CGL simulations (Chaté and Manneville 1996), reproduced with permission from Elsevier Science)

and a large number of defects – vortices of unit charge – are formed. At the following coarsening stage, oppositely charged vortices annihilate, so that the density of defects decreases. The coarsening process, however, stops halfway, leaving a certain number of single-charged spiral vortices with either sense of rotation. Vortices that failed to conquer a sufficiently large domain are reduced to "naked cores", left to satisfy the topological condition of conservation of circulation. The resulting stable spiral domain pattern is called vortex glass. The waves always propagate outwards from the vortex cores, so that the entire domain structure is generated when local order spreads out from centers to the periphery. Perturbations, also traveling outwards with the prevailing group velocity, are absorbed at shocks, and therefore the pattern may survive beyond the convective instability threshold. The turbulent state takes over only when the emanated waves become absolutely unstable, i.e., when some perturbations grow locally in the laboratory frame.

The overall structure of the pattern changes in the range of oscillatory spatial decay of waves emanated by the spiral cores (below the line OR in Fig. 13). Under these conditions, formation of stable bound spiral pairs becomes possible (see Fig. 18). Unlike the monotonic range, spiral domains may have in oscillatory range a wide size distribution, since shocks can be immobilized at different separations.

"Frozen" glassy patterns actually evolve on a very long time scale, as revealed in very long simulation runs (Brito et al. 2003). In the monotonic range, spiral cores perform very slow diffusive motion; the apparent diffusivity increases with vortex density. In contrast, in the oscillatory range, spiral population spontaneously segregates after a very long transient into two distinct phases: large and almost immobile spirals and clusters of trapped small vortices. When the "liquid fraction" is small, the resulting pattern exhibits slow intermittent dynamics: bursts of activity separated by long quiescent intervals. The system keeps evolving on an extremely slow scale, which is consistent with exponentially weak repulsion between well separated spiral cores.

Another possibility, realized in a different parametric region, is a dynamic chaotic state that shows no persistent features. This state is attained under conditions when either spiral waves or vortex cores, or both, are unstable. One can distinguish between mild phase turbulence when no phase singularities occur, and defect chaos characterized by persistent creation and annihilation of vortex pairs. Phase turbulence may persist in the

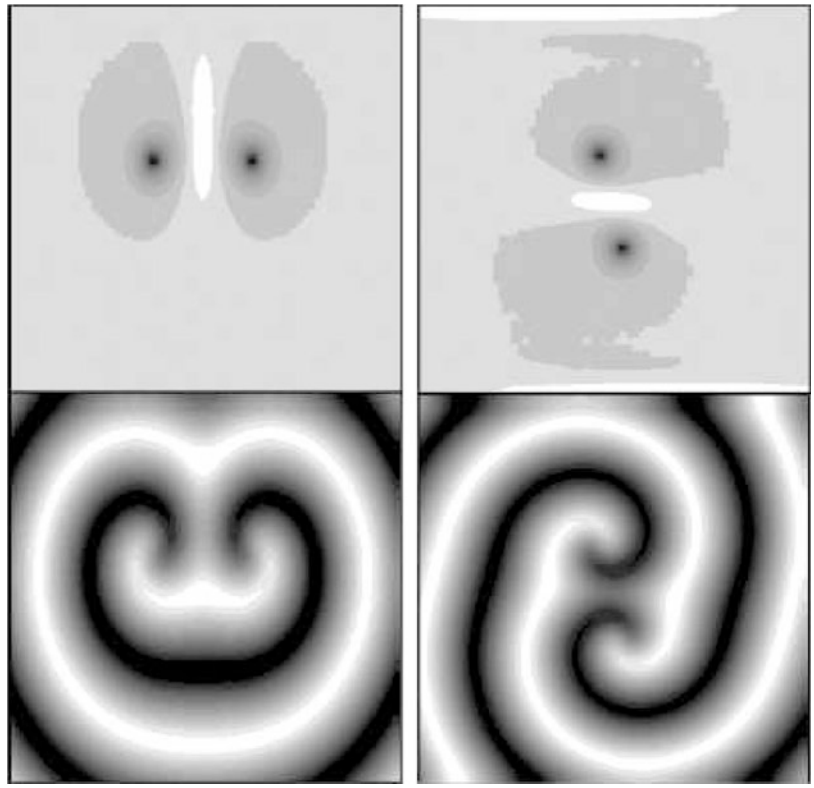

Patterns and Interfaces in Dissipative Dynamics, Fig. 18 Bound states of oppositely (*left*) and likely (*right*) charged spirals (CGL simulations, $\eta = 0$, $\nu = 1.5$). The images show the modulus $\rho(x, y)$ (*top*) and Re(u) (*bottom*) (Aranson and Kramer 2002, reproduced with permission. Copyright by the American Physical Society)

parametric region between the Benjamin-Feir line and the line L in Fig. 13 (Chaté and Manneville 1996). Beyond the line L, defects are created spontaneously, leading to defect chaos. Transition from vortex glass to defect turbulence in simulations starting from random initial conditions occurs at the numerically determined line T in Fig. 13 (Chaté and Manneville 1996). The transition occurs somewhat prior to the absolute instability limit determined by the linear stability analysis of plane waves emitted by spirals. This limit can be approached, however, by starting from carefully prepared initial conditions in the form of large spirals. Prior to the transition, one can observe transient defect turbulence which is unstable to spontaneous nucleation of spirals from the "turbulent sea", leading eventually to a vortex glass state.

Forced Systems

External forcing, including spatially as well as temporally variable inputs, can be used in a straightforward way to enhance or suppress spontaneously emerging patterns (Nepomnyashchy et al. 2004). Alternatively, it may enhance complexity by introducing additional spatial and temporal resonances, which may lead to formation of quasicrystalline structures (Pismen 1987). Resonant forcing of oscillatory systems may drastically change the structure of wave patterns through phase locking. This happens when the CGL equation is forced on a frequency ω_c commensurate with the basic frequency ω_0 at the Hopf bifurcation. For an integer ratio $\omega_c/\omega_0 = n$, the amplitude equation amending (23) can be written by adding the forcing term possessing the required symmetry:

$$\partial_t u = (1 + \mathrm{i}\eta)\nabla^2 u + (\mu + \mathrm{i}\omega)u - (1 - \mathrm{i}\nu)|u|^2 u + \gamma u^{-n-1}, \qquad (32)$$

where γ is the forcing amplitude and $\epsilon^2\omega$ is weak effective detuning, due to both parametric deviations from the Hopf bifurcation point and weak mismatch between ω_c/n and ω_0. The forcing term breaks the symmetry of the CGL equation to phase rotations, reducing it to discrete symmetry $u \to \mathrm{e}^{i\pi m}u$, $m = 1$, $\ldots$, $n - 1$. This changes

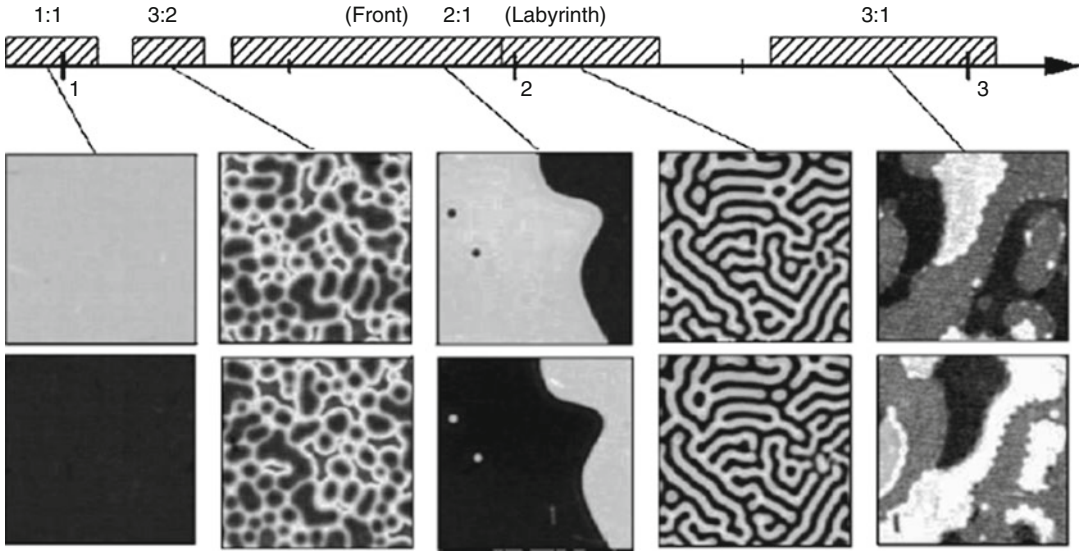

Patterns and Interfaces in Dissipative Dynamics, Fig. 19 Frequency-locked regimes (experiment with light-sensitive reaction under periodic optical forcing [*71*], reproduced with permission). The *axis above* shows the ratio of the forcing to basic frequency. Patterns are shown in pairs, one above the other, at times separated by the forcing period $2\pi/\omega_c$,except for the 1:1 resonance where the interval is π/ω_c

the character of defects: instead of vortices, one can observed fronts separating alternative phase states.

Various patterns at different forcing frequencies, which can be modeled by (32), were observed both in experiments and simulations (Petrov et al. 1997; Lin et al. 2004). Some typical patterns are shown in Fig. 19. For the case of strong resonance ($n = 1$), this system provides a convenient tool for studying transitions between stationary and propagating fronts (Coullet and Emilsson 1992), labyrinthine patterns (Yochelis et al. 2004), and solitary structures (Gomila et al. 2007). These structures are not unlike those observed in the FitzHugh-Nagumo system, although they represent standing waves with the alternative phases interchanging within each domain. Higher resonances create still more complex dynamics involving interactions of different kinds of fronts (Gallego et al. 2001).

Future Directions

The study of pattern formation is now a mature discipline based on well-established general theory and wealth of experimental evidence. The center of attention is turning to specific applications; among them, nonlinear optics and studies of granular media come to the forefront. Forcing and control of patterns, either enhancing or suppressing the complexity of behavior, are studied in detail. As a humble laptop turns into a supercomputer, more fascinating patterns, envy of abstract expressionists, are generated by model equations of increased complexity. Patterns showing dazzling mix of order and chaos are seen as well in various experimental setups.

The ultimate aim of controlled creation of self-organized structures still remains elusive, and new ideas are awaited as the new century comes of age. The study of pattern formation, dealing with ubiquitous problems of order and chaos, is bound to find its way into basic curricula and wealth of practical applications.

Bibliography

Primary Literature

Abou B, Wesfreid JE, Roux S (2000) J Fluid Mech 416:217
Alexander S, McTague J (1978) Phys Rev Lett 41:702

Alonso S, Kähler R, Mikhailov AS, Sagués F (2004) Phys Rev E 70:056201
Aranson IS, Kramer L (2002) Rev Mod Phys 74:99
Aranson IS, Malomed BA, Pismen LM, Tsimring LS (2000) Phys Rev E 62:R5
Arecchi FT (1999) Phys Rep 318:1
Assenheimer M, Steinberg V (1993) Phys Rev Lett 70:3888
Barkley D (1994) Phys Rev Lett 72:164
Bénard H (1900) Ann Chim Phys 7 (Ser 23) 62
Ben-Jacob E, Brand HR, Dee G, Kramer L, Langer JS (1985) Physica D 14:348
Bodenschatz E, Pesch W, Kramer L (1988) Physica D 32:135
Bodenschatz E, Pesch W, Ahlers G (2000) Annu Rev Fluid Mech 32:709
Bowman C, Newell AC (1998) Rev Mod Phys 70:289
Braun E, Steinberg V (1991) Europhys Lett 15:167
Brito C, Aranson IS, Chaté H (2003) Phys Rev Lett 90:068301
Brusch L, Torcini A, van Hecke M, Zimmermann MG, Bär M (2001) Physica D 160:127
Burger M, Field RJ (1985) Oscillations and traveling waves in chemical systems. Wiley, New York
Cahn JW, Hilliard JE (1958) J Chem Phys 28:258
Chaté H, Manneville P (1996) Physica A 224:348
Coullet P, Emilsson K (1992) Physica D 61:119
Coullet P, Riera C, Tresser C (2004) Chaos 14:193
Cross MC, Newell AC (1984) Physica D 10:299
Elphick C, Meron E, Spiegel EA (1988) Phys Rev Lett 61:496
Faraday M (1831) Philos Trans R Soc Lond 121:299
Gallego R, Walgraef D, San Miguel M, Toral R (2001) Phys Rev E 64:056218
Gierer A, Meinhard H (1972) Kybernetik 12:30
Gilad E, Shachak M, Meron E (2007) Theor Popul Biol 72:214
Gomila D, Colet P, San Miguel M, Oppo G-L (2007) Eur Phys J Spec Top 146:71
Hagan PS (1982) SIAM J Appl Math 42:762
Hagberg A, Yochelis A, Yizhak H, Elphick C, Pismen LM, Meron E (2006) Physica D 217:186
Hakim V, Karma A (1999) Phys Rev E 60:5073
Hamley IW (2003) Nanotechnology 14:R39
Henry H, Hakim V (2002) Phys Rev E 65:046235
Josserand C, Pomeau Y, Rica S (2007) Eur Phys J Special Topics 146:47
Keener JP (1988) Physica D 31:269
Knobloch E, de Luca J (1990) Nonlinearity 3:975
Kolmogorov A, Petrovsky I, Piskunov N (1937) Bull Univ Moscow. Ser Int Sec A 1:1
Kuramoto Y, Tsuzuki T (1976) Prog Theor Phys 55:356
Langer JS (1980) Rev Mod Phys 52:1
Lifshitz IM, Slyozov VV (1958) Zh Eksp Teor Fiz 35:479
Lin AL, Hagberg A, Meron E, Swinney HL (2004) Phys Rev E 69:066217
Malomed BA, Nepomnyashchy AA, Tribelsky MI (1990) Phys Rev A 42:7244
Mermin ND (1979) Rev Mod Phys 51:591
Mullins WW, Sekerka RF (1963) J Appl Phys 34:323
Murray JD (1981) J Theor Biol 88:161
Nepomnyashchy AA, Pismen LM (1991) Phys Lett A 153:427
Nepomnyashchy AA, Golovin AA, Gubareva V, Panfilov V (2004) Physica D 199:61
Newell AC, Whitehead JA (1969) J Fluid Mech 38:279
Newell AC, Passot T, Bowman C, Ercolani N, Indik R (1996) Physica D 97:185
Ohta T, Mimura M, Kobayashi R (1989) Physica D 34:115
Or-Guil M, Bode M, Schenk CP, Purwins H-G (1998) Phys Rev E 57:6432
Ouyang Q, Swinney HL (1991) Nature 352:610
Pampaloni E, Residori S, Soria S, Arecchi FT (1997) Phys Rev Lett 78:1042
Park J-S, Lee KJ (2002) Phys Rev Lett 88:224501
Petrov V, Ouyang Q, Swinney HL (1997) Nature 388:655
Pismen LM (1986) Dyn Stab Syst 1:97
Pismen LM (1987) Phys Rev Lett 59:2740
Pismen LM, Rodriguez JD (1990) Phys Rev A 42:2471
Pismen LM, Rubinstein BY (1999) Chaos Soliton Fractal 10:761
Pomeau Y (1986) Physica D 23:3
Pomeau Y, Manneville P (1979) J Phys Lett 40:L609
Proctor MRE, Jones CA (1988) J Fluid Mech 188:301
Rabinovich MI, Tsimring LS (1994) Phys Rev E 49:R35
Reynolds WN, Pearson JE, Ponce-Dawson S (1994) Phys Rev Lett 72:2797
Rousseau G, Chaté H, Kapral R (1998) Phys Rev Lett 80:5671
Sagués F, Sancho JM, García-Ojalvo J (2007) Spatiotemporal order out of noise. Rev Mod Phys 79:829
Segel LA (1969) J Fluid Mech 38:203
Sivashinsky GI (1977) Acta Astronaut 4:1177
Turing AM (1952) Philos Trans R Soc Lond Ser B 237:37
Tyson JJ, Keener JP (1988) Physica D 32:327
van der Waals JD (1894) Z Phys Chem 13:657
van Saarloos W, Hohenberg PC (1992) Physica D 56:303
van Saarloos W (2003) Phys Rep 386:29
Yang L, Dolnik M, Zhabotinsky AM, Epstein IR (2002) Phys Rev Lett 88:208303
Yochelis A, Elphick C, Hagberg A, Meron E (2004) Physica D 199:201
Zeldovich YB (1985) The mathematical theory of combustion and explosions. Consultants Bureau, New York

Books and Reviews

Cross MC, Hohenberg P (1993) Rev Mod Phys 65:851
Epstein IR, Pojman JA (1998) Introduction to nonlinear chemical dynamics. Oxford University Press, New York
Fife PC (1979) Mathematical aspects of reacting and diffusing systems. Springer, Berlin
Haken H (2004) Synergetics: introduction and advanced topics. Springer, Berlin
Hoyle R (2006) Pattern formation. Cambridge UP, Cambridge
Kuramoto Y (1984) Chemical oscillations, waves and turbulence. Springer, Berlin

Manneville P (1990) Dissipative structures and weak turbulence. Academic, San Diego
Mikhailov AS (1991) Foundations of synergetics i: distributed active systems II (with AY Loskutov): complex patterns. Springer, Berlin
Murray JD (1989) Mathematical biology. Springer, Berlin; 2nd edn 1993; 3rd edn 2002/2003
Pismen LM (1999) Vortices in nonlinear fields. Clarendon Press, Oxford
Pismen LM (2006) Patterns and interfaces in dissipative dynamics. Springer, Berlin
Rabinovich MI, Ezersky AB, Weidman PD (2000) The dynamics of patterns. World Scientific, Singapore
Walgraef D (1997) Spatio-temporal pattern formation. Springer, New York
Winfree AT (1987) When time breaks down. Princeton University Press, Princeton

Fluid Dynamics: Turbulence

Rudolf Friedrich[1], Joachim Peinke[2] and Oliver Kamps[3]
[1]Institute for Theoretical Physics, University of Münster, Münster, Germany
[2]Institute of Physics, Carl-von-Ossietzky University Oldenburg, Oldenburg, Germany
[3]Center for Nonlinear Science, Universität of Münster, Münster, Germany

Article Outline

Glossary
Definition of the Subject
Introduction
The Basic Hydrodynamic Equations
Vortex Solutions of the Navier-Stokes Equation
Patterns, Chaos, and Turbulence
Turbulence: Determinism and Stochasticity
Reynolds Equation and Turbulence Modeling
Phenomenological Theories of Turbulence
Multiscale Analysis of Turbulent Fields
Lagrangian Fluid Dynamics
Future Directions
Further Reading
Bibliography

Glossary

Basic equation of fluid dynamics Fluid motion is mathematically treated on the basis of a continuum theory. The fundamental evolution equations are the Euler equation for ideal fluids and the Navier-Stokes equation for Newtonian fluids.

Vortex motions Numerical calculations of turbulent flow fields show that the flows are dominated by coherent structures in the form of vortex sheets or tubelike vortices. The question, why vorticity tends to be condensed in localized objects, is one of the central issues of fluid dynamics. Regarding two-dimensional flows, there are attempts to approximate fluid motion by a collection of point vortices. This allows one to investigate properties of flows on the basis of a finite dimensional (Hamiltonian) dynamical system.

Turbulence modeling and large eddy simulations The evolution equation for the average velocity field of turbulent flows contains the Reynolds stresses, whose origin is the turbulent pulsations. Turbulence modeling consists of relating the Reynolds stresses to averaged quantities of the fluid motion. This allows one to perform numerical computations of large-scale flows without resolving the turbulent fine structure.

Phenomenological theories of the fine structure of turbulence Phenomenological theories play an important role in physics and are quite often formulated before a microscopic understanding of the physical problem has been achieved. Phenomenological theories have been developed for the fine structure of turbulence. Of great importance is the theory of Kolmogorov, which he formulated in the year 1941 and refined in 1962. The so-called K41 and K62 theories focus on the self-similar behavior of statistical properties of velocity increments, i.e., the velocity difference between two points with a spatial distance r. Recently, phenomenological theories have been developed that consider the joint probabilities of velocity increments at different scales. It is expected that multiple-scale analysis of turbulence will provide new insights into the spatiotemporal complexity of turbulence.

Turbulent cascades Fluid motions are dissipative systems. Stationary flows can only be maintained by a constant energy input in the form of shear flows or body forces. Usually, the length and time scales related to the energy input are widely separated from the ones on which energy is dissipated. A consequence is the establishment of an energy transport across

A. Hutt, H. Haken (eds.), *Synergetics*,
https://doi.org/10.1007/978-1-0716-0421-2_215

Originally published in
R. A. Meyers (ed.), *Encyclopedia of Complexity and Systems Science*, © Springer Science+Business Media LLC 2017
https://doi.org/10.1007/978-3-642-27737-5_215-5

scales. It is believed that this energy transport is local in scale leading to the so-called energy cascades. These cascades are related to the emergence of scaling behavior. There is a direct energy cascade in three dimensions from large to small scales and an inverse cascade of energy from small scales to large scales in two-dimensional flows.

Analytical theories of turbulence Analytical theories of turbulence try to assess the experimental results on turbulent flows directly from a statistical treatment of the basic fluid dynamical equations. Analytical theories rely on renormalized perturbation expansions and use methods from quantum field theory and renormalization group methods. However, no generally accepted theory has emerged so far.

Definition of the Subject

Fluid flows are open systems far from equilibrium. Fluid motion is sustained by energy injected at a certain scale, the so-called integral scale, and is dissipated by viscosity mainly in small-scale structures. If the integral scale and the dissipative scale are widely separated and the motions on the integral scale are sufficiently strong, the fluid develops a range of spatiotemporal structures. In three-dimensional flows, these structures steadily decay into smaller structures and are generated by the instability of larger structures. This leads to a cascading process which transports energy across scales. Turbulence appears if the fluid motion is driven far away from equilibrium. It develops through sequences of instabilities and processes of self-organization. From this respect, turbulence is a highly ordered phenomenon, whose spatiotemporal complexity, however, has still to be explored.

Introduction

Turbulence is one of the outstanding problems in the field of nonlinear dynamics and complex systems. Although the basic equations of ideal fluid dynamics were formulated by L. Euler 250 years ago and the equations for viscous flows, the so-called Navier-Stokes equation, were established about 150 years ago (Darrigol 2005), only a few analytical solutions have been found so far, because of the inherent nonlinear character of fluid flows. Furthermore, fluid motions are systems far from equilibrium. Their maintenance requires a constant input of energy, which is transformed by the viscous flow into heat. A measure for the distance from equilibrium, which corresponds to vanishing fluid velocity, is the Reynolds number

$$\mathrm{Re} = \frac{UL}{\nu} \tag{1}$$

where U is a characteristic velocity, L is a characteristic length scale, and ν is the kinematic viscosity. Flows with Reynolds numbers larger than $\mathrm{Re} = 1{,}000$ usually are turbulent. A turbulent field generated in a free jet experiment is exhibited in Fig. 1. By increasing the Reynolds number, one observes the occurrence of various types of instabilities resulting in time-dependent and chaotic patterns making these systems paradigms of self-organization. Whereas the flows generated by the first few instabilities can be treated satisfactorily, the transitions and properties of flows at higher Reynolds numbers are by far less understood. This lack of understanding hinders the scientific development in various fields, ranging from astrophysics and engineering to the life sciences.

Basic research on turbulence has always stimulated and contributed to the formulation of new scientific concepts like self-organization and pattern formation, chaos, and the theory of fractals. As a classical nonlinear field theory, the description of fluid motion has advanced the mathematical understanding of infinite dimensional nonlinear dynamical systems and the development of efficient

Fluid Dynamics: Turbulence, Fig. 1 Development of turbulent structures in a free jet experiment

computational tools. It is expected that combined experimental and theoretical efforts will lead to a satisfactory understanding of high Reynolds number flows in the near future.

The Basic Hydrodynamic Equations

Fluid motions are described in terms of a continuum theory. The basic ingredients of continuum theories are balance equations for a density $h(\mathbf{x}, t)$ of a physical quantity like mass or momentum defined at location $\mathbf{x}$ and time t:

$$\frac{\partial}{\partial t}h + \nabla \cdot [\mathbf{u}h + \mathbf{j}_h] = q. \tag{2}$$

Here, $\mathbf{u}$ denotes the fluid velocity, $\mathbf{j}_h$ denotes the current corresponding to the density h, and q denotes a source term (Chorin and Marsden 2000; Landau and Lifshitz 1981).

The balance equation for the mass density ρ reads

$$\frac{\partial}{\partial t}\rho + \nabla \cdot \rho\mathbf{u} = 0. \tag{3}$$

Since mass is conserved, the source term vanishes identically, $q = 0$.

Incompressible fluid motions are characterized by the condition

$$\nabla \cdot \mathbf{u} = 0. \tag{4}$$

In the present review, we shall mainly focus on incompressible fluids.

The balance equation for the density of momentum, $\rho\mathbf{u}(\mathbf{x}, t)$, takes the form

$$\frac{\partial}{\partial t}\rho u_i + \sum_j \frac{\partial}{\partial x_j} u_j \rho u_i = -\frac{\partial}{\partial x_i}p + \sum_j \frac{\partial}{\partial x_j}\sigma_{ij} + f_i, \tag{5}$$

where the momentum current $\mathbf{j}_h$ is expressed by pressure p and the viscous stress tensor σ_{ij}. External forces are summarized in f_i. A complete description requires the formulation of boundary conditions for the velocity field.

It is straightforward to derive the balance equation for the density of the kinetic energy, $\rho\mathbf{u}^2(\mathbf{x}, t)/2$, from the conservation law of momentum (5) for incompressible flows:

$$\frac{\partial}{\partial t}\frac{\rho}{2}\mathbf{u}^2 + \sum_j \frac{\partial}{\partial x_j}\left\{u_j\left[\frac{\rho}{2}\mathbf{u}^2 + p\right] - \sum_i \sigma_{ji}u_i\right\} = -\sum_{ij}\sigma_{ij}\frac{\partial u_i}{\partial x_j} + \sum_j u_j f_j. \tag{6}$$

This equation shows that energy is conserved provided the viscous stresses σ_{ij} vanish.

Ideal Fluids: Euler's Equation

For ideal fluid motions, the kinetic energy is conserved provided external forces are absent. The balance Eq. (6) shows that in this case the viscous stresses σ_{ij} have to vanish leading to the Euler equation for incompressible fluid motions:

$$\left[\frac{\partial}{\partial t} + \mathbf{u}.\nabla\right]\mathbf{u} = -\frac{1}{\rho}\nabla p + \frac{1}{\rho}\mathbf{f}. \tag{7}$$

The dynamics of ideal fluid motion is restricted by Kelvin's theorem. The circulation $\oint \mathbf{u}(\mathbf{x}, t)\mathrm{d}\mathbf{r}$ along closed curves going with the flow remains constant (Chorin and Marsden 2000; Landau and Lifshitz 1981).

Newtonian Fluids: Navier-Stokes Equation

Newtonian fluids are characterized by the presence of viscous stresses. They are assumed to be proportional to the strain matrix S_{ij}

$$\sigma_{ij} = \nu\rho S_{ij} = \nu\rho\frac{1}{2}\left[\frac{\partial u_i}{\partial x_j} + \frac{\partial u_j}{\partial x_i}\right]. \tag{8}$$

Assuming isotropic material properties of the fluid as well as incompressibility, one obtains the Navier-Stokes equation:

$$\left[\frac{\partial}{\partial t} + \mathbf{u}\cdot\nabla\right]\mathbf{u} = \nu\Delta\mathbf{u} - \nabla p + \mathbf{f}. \tag{9}$$

The kinematic viscosity ν characterizes different fluids. The local energy dissipation rate,

denoted by ϵ, is obtained from the balance equation of the density of kinetic energy (6):

$$\epsilon = \frac{\nu}{2} \sum_{ij} \left(\frac{\partial u_i}{\partial x_j} + \frac{\partial u_i}{\partial x_j} \right)^2 . \tag{10}$$

This quantity plays a crucial role for the understanding of turbulent fluid motions.

At first glance, the Navier-Stokes equation seems to be underdetermined due to the appearance of the gradient pressure term. However, as a result of incompressibility, the pressure is uniquely defined by the Poisson equation in connection with suitable boundary conditions:

$$\Delta p = -\sum_{ij} \frac{\partial u_i}{\partial x_j} \frac{\partial u_j}{\partial x_i} . \tag{11}$$

The pressure can be determined with the help of Green's function G of the Laplacian,

$$\Delta G(\mathbf{x} - \mathbf{x}') = -\delta(\mathbf{x} - \mathbf{x}'), \tag{12}$$

and yields the pressure as a functional of the velocity field:

$$p = \int d\mathbf{x}' G(\mathbf{x} - \mathbf{x}') \sum_{ij} \frac{\partial u_i}{\partial x_j'} \frac{\partial u_j}{\partial x_i'} . \tag{13}$$

This clearly demonstrates that incompressible fluid motions are governed by nonlinear, nonlocal interactions. The gradient pressure term can be regarded as a Lagrange parameter which guaranties the incompressibility of fluid motion.

Vorticity Formulation of Incompressible Fluid Dynamics

It is possible to formulate the basic fluid dynamic equations using the vorticity, $\boldsymbol{\omega}(\mathbf{x}, t) = \nabla \times \mathbf{u}(\mathbf{x}, t)$. Provided the vorticity is known, one can obtain the velocity field by the analogue of Maxwell's equation of magnetostatics:

$$\nabla \times \mathbf{u} = \boldsymbol{\omega}, \quad \nabla \cdot \mathbf{u} = 0. \tag{14}$$

The velocity field is determined by the analogy to Biot-Savart's law

$$\mathbf{u}(\mathbf{x}, t) = \int d\mathbf{x}' \boldsymbol{\omega}(\mathbf{x}', t) \times \mathbf{K}(\mathbf{x} - \mathbf{x}') + \nabla \Phi, \tag{15}$$

where $\mathbf{K}$ is related to Green's function $G(\mathbf{x})$ of the Laplacian $\mathbf{K}(\mathbf{x}) = \nabla G(\mathbf{x})$. The potential Φ has to fulfill $\Delta \Phi = 0$.

It is straightforward to derive an evolution equation for the vorticity:

$$\frac{\partial}{\partial t} \boldsymbol{\omega} + \mathbf{u} \cdot \nabla \boldsymbol{\omega} = \boldsymbol{\omega} \cdot \nabla \mathbf{u} + \nu \Delta \boldsymbol{\omega} + \mathbf{f}_\omega . \tag{16}$$

Here, an important difference between two- and three-dimensional fluid motions becomes evident. For two-dimensional flows, the vorticity only has a component perpendicular to the motion, and the so-called vortex stretching term $\boldsymbol{\omega} \cdot \nabla \mathbf{u}$ vanishes identically.

Lagrangian Formulation of Incompressible Fluid Dynamics

Up to now, we have treated fluid dynamics from the Eulerian point of view by considering fields defined at a fixed spatial location. There is an alternative approach to the description of fluid motion. This so-called Lagrangian treatment is based on the introduction of the Lagrangian velocity $\mathbf{U}(\mathbf{y}, t)$ and the Lagrangian path $\mathbf{X}(\mathbf{y}, t)$ of a point moving with the flow starting at time $t = 0$ at the location $\mathbf{y}$. For obvious reasons the quantity $\mathbf{X}(\mathbf{y}, \mathrm{t})$ is also denoted as *Lagrangian map*. The inverse map is denoted as $\mathbf{y}(\mathbf{x}, t)$. The basic fluid dynamical equations can also be formulated in this Lagrangian picture.

As an example we formulate the evolution equation for the Lagrangian vorticity for two-dimensional incompressible flows. To this end we introduce the Lagrangian vorticity $\boldsymbol{\Omega}(\mathbf{y}, t) = \boldsymbol{\omega}(\mathbf{X}(\mathbf{y}, t), t)$. The first equation defines the Lagrangian path and the second the evolution of the Lagrangian vorticity.

$$\begin{aligned} &\frac{\partial}{\partial t} \mathbf{X}(\mathbf{y}, t) = \int \mathrm{d}\mathbf{y}' \Omega(\mathbf{y}', t) \\ &\times \{ \mathbf{e}_z \times \mathbf{K}[\mathbf{X}(\mathbf{y}, t) - \mathbf{X}(\mathbf{y}', t)] \}, \\ &\frac{\partial}{\partial t} \Omega(\mathbf{y}, t) = \nu \left[\sum_{ijkl} \frac{\partial Y_l}{\partial x_i} \frac{\partial Y_k}{\partial x_i} \frac{\partial^2}{\partial y_l \partial y_k} + \sum_{li} \frac{\partial^2 Y_l}{\partial x_i \partial x_i} \frac{\partial}{\partial y_l} \right] \\ &\times \Omega(\mathbf{y}, t). \end{aligned} \tag{17}$$

For two-dimensional flows, the gradient of Green's function of the Laplacian takes the form

$\mathbf{K}(\mathbf{x}) = \frac{\mathbf{x}}{2\pi|\mathbf{x}|^2}$. It is immediately obvious that in the ideal fluid case, the two-dimensional vorticity is conserved along Lagrangian trajectories. A similar formulation exists for three-dimensional flows, where, however, the evolution equation for vorticity contains the vortex stretching term.

Recently, the Lagrangian formulation of fluid dynamics has become important due to the possibility to measure the path of passive tracer particles (La Porta et al. 2000; Mordant et al. 2001; Ott and Mann 2000). Its importance for the description of turbulence has already been emphasized by Taylor (1921) and Richardson (1926).

Existence and Smoothness Results

Although the Euler and the Navier-Stokes equations are of fundamental interest for various fields ranging from astrophysics to applied mechanics and engineering, their mathematical properties still remain puzzling. Especially for three-dimensional flows, results on the existence (or nonexistence) and smoothness of solutions could not yet be obtained. This topic is one of the millennium problems formulated by the Clay Mathematics Institute. As an introduction to the subject, we refer the reader to the webpage of the Clay institute with an outline of the mathematical problem due to Fefferman (http://www.claymath.org/millenium/), as well as the two monographs (Doering and Gibbon 1995; Foias et al. 2001).

Vortex Solutions of the Navier-Stokes Equation

Figure 2 shows a volume rendering of the absolute value of vorticity above a certain threshold obtained from a direct numerical solution of the vorticity equation. The field is characterized by the presence of elongated vortex structures (Jimenez et al. 1993). Whereas fully developed turbulent flows tend to be dominated by vortex-like objects, it seems that modest turbulent flows are characterized by the presence of sheetlike structures. There are several exact solutions of the Navier-Stokes equation, which seem to be related with the vortex structures observed in fully developed turbulence. They can be investigated using symmetry arguments and methods from group theory (Grassi et al. 2000).

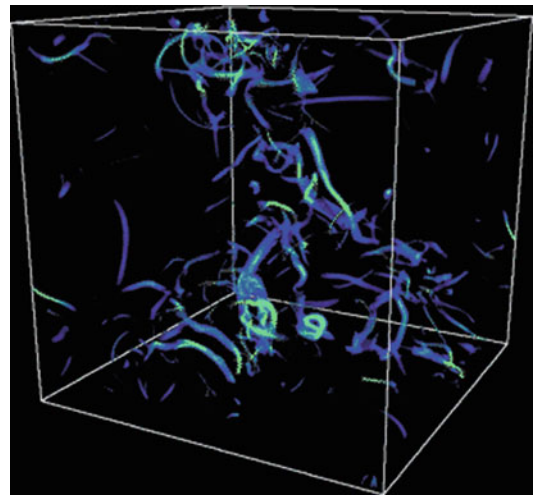

Fluid Dynamics: Turbulence, Fig. 2 Direct numerical calculation of the vorticity field of a turbulent fluid motion: Absolute value of vorticity above a given threshold. After (Wilczek)

Axisymmetric Vortices: Lamb-Oseen Vortex

An axisymmetric vorticity distribution $\boldsymbol{\omega} = \boldsymbol{\Omega}(r)\,\mathbf{e}_z$ generates a purely azimuthal velocity field. This fact has the consequence that in the vorticity equation, both, the convective term $\mathbf{u}\cdot\nabla\boldsymbol{\omega}$ and the vortex stretching term $\boldsymbol{\omega}\cdot\nabla\mathbf{u}$, identically vanish, leading to an equation which is the radially symmetric heat equation:

$$\frac{\partial}{\partial t}\Omega = \nu\frac{1}{r}\frac{\partial}{\partial r}r\frac{\partial}{\partial r}\Omega. \tag{18}$$

A solution is the so-called Lamb-Oseen vortex:

$$\Omega = \frac{\Gamma}{\pi r_{\mathrm{B}}^2}\mathrm{e}^{-r^2/r_{\mathrm{B}}^2}, \quad r_{\mathrm{B}}^2 = 4\nu t. \tag{19}$$

The corresponding velocity field is azimuthal and has the form

$$v_\varphi(r) = \frac{\Gamma}{2\pi r}\left[1 - \mathrm{e}^{-r^2/r_{\mathrm{B}}^2}\right]. \tag{20}$$

It decays like $\Gamma/2\pi r$ for large distances. Because of viscosity the velocity field at the origin vanishes identically.

The Lundgren Spiral

Another vortex solution in the form of a spiral vorticity distribution has been considered by Lundgren (1982). It is generated by a localized central, strong vorticity distribution whose velocity field drags surrounding, weaker vorticity distributions into spiral arms. In this way it is also possible to generate multiple-armed spirals. This process is depicted in Fig. 3. Recently the Lundgren spiral has been generated experimentally by the group of Petitjeans (Cuypers et al. 2003).

Stretched Vortices

A highly interesting class of solutions has been found by Lundgren. He considered the velocity field

$$\mathbf{u}(\mathbf{x},t) = \frac{a(t)}{2}[-x,\ -y, 2z] + [w_1(x,y,t), w_2(x,y,t), 0] \qquad (21)$$

and showed that the two-dimensional velocity field $\mathbf{w}(x, y, t)$ can be obtained from the velocity field $\mathbf{W}(\xi_1, \xi_2, \tau)$ by the *Lundgren transformation*

$$\begin{aligned} \mathbf{w}(x,y,t) &= A(t)\mathbf{W}[A(t)x, A(t)y, \tau(t)] \\ A(t) &= \mathrm{e}^{\int_0^t \mathrm{d}t' a(t')}, \quad \tau(t) = \int_0^t \mathrm{d}t' A(t')^2. \end{aligned} \qquad (22)$$

Thereby, the field $\mathbf{W}(\xi_1, \xi_2, \tau)$ obeys the two-dimensional Navier-Stokes equation.

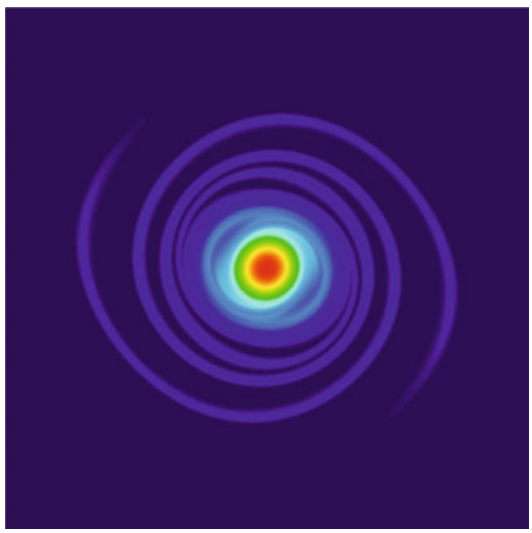

Fluid Dynamics: Turbulence, Fig. 3 Vorticity field of a two-armed Lundgren spiral

In the case of a time constant a, the decaying *Lamb-Oseen vortex*, Eq. (19) is changed into the *Burgers vortex* r_B, where it becomes constant, $r_\mathrm{B}^2 = \frac{4\nu}{a}$.

The corresponding two-dimensional velocity field is an azimuthal field, which for large values of r decays like $\frac{1}{r}$. In the limit $\nu \to 0$, the vorticity field approaches a delta-distribution.

Vorticity Alignment

Figure 2 exhibits the vorticity field obtained from a numerical simulation of the Navier-Stokes equation. Exhibited is a volume rendering of the absolute value of vorticity above a given value, and it is quite evident that Burgers-like vortices play a major role in the spatiotemporal organization of turbulence. Consequently, the Burgers vortices have been denoted as the *sinews of turbulence* (Moffat et al. 1994). Although the emergence of vortex-like objects as organization centers of turbulence has not yet been fully clarified, it is clear that it is related to the phenomenon of vorticity alignment (Galanti et al. 1997). It has been emphasized that locally the vorticity vector is predominantly aligned to the eigenvector of the intermediate eigenvalue λ_2 of the strain matrix S, Eq. (8). This matrix is symmetric and has three real eigenvalues $\lambda_1 \leq \lambda_2 \leq \lambda_3$. Vorticity alignment is still investigated intensively (Hamlington et al. 2008).

Vorticity alignment has also played a major role in the discussion of the possibility of finite-time singularities in Euler flows (Grafke et al. 2008; Grauer et al. 1998), a question which is fundamentally related to the question of the existence of solutions of the Euler and Navier-Stokes equations (Doering and Gibbon 1995; Foias et al. 2001).

Modeling Turbulent Fields by Random Vortex Distributions

There have been several attempts to model the fine structure of turbulent fields by statistically distributed vortex solutions of the Navier-Stokes equations. Townsend (1951) used a random arrangement of Burgers vortices. As already mentioned Lundgren (1982, 1993) considered the abovementioned spiral structures in a strain field.

He showed that suitable space-time average over a decaying Lundgren spiral leads to an energy spectrum predicted by Kolmogorov's phenomenological theory of turbulence. A cascade interpretation of Lundgren's model has been given by Gilbert (1993). Kambe (Hatakeyama and Kambe 1997) discussed randomly arranged Burgers vortices in a strain field and was able to model intermittency effects of Eulerian velocity increments.

Patterns, Chaos, and Turbulence

Pattern Formation and Routes to Chaos in Fluid Dynamics

Experiments on fluid dynamics in confined geometries like the Rayleigh-Bénard system or the Taylor-Couette experiment exhibit a variety of instabilities leading from stationary patterns to time-periodic structures and to chaotic motions. For an overview with further references on fluid instabilities, we refer the reader to the monograph of Manneville (2004). These flows are characterized by temporal complexity; however, the flow structures remain spatially coherent. The scale of energy injection and the scale of energy dissipation usually are not widely separated in these systems. This has the consequence that only few degrees of freedom are excited. Such types of flows can be successfully treated on the basis of the slaving principle of synergetics (Haken 1983, 1987). In mathematical terms, these types of flows are related to the existence of center or inertial manifolds (Temam 2007) in phase space. This allows explanation of the various *routes to chaos or routes to turbulence* observed in fluid motions, especially in confined geometries, on the basis of the theory of low-dimensional dynamical systems.

Point Vortex Motion

The *Lagrangian map* $\mathbf{X}(\mathbf{y}, t)$ of a two-dimensional ideal fluid motion is determined by the solution of the integrodifferential Eq. (17), where the Lagrangian vorticity $\mathbf{\Omega}(\mathbf{y}, t)$ is temporally constant. This integrodifferential equation can be reduced to a finite set of ordinary differential equations by considering fields with strongly localized vorticity

$$\mathbf{\Omega}(\mathbf{y}, t) = \sum_j \Gamma_j \delta\Big(\mathbf{y} - \mathbf{y}_j\Big). \tag{23}$$

Introducing the notation $\mathbf{X}(\mathbf{y}_j, t) = \mathbf{x}_j(t)$, we obtain the set of differential equations for the positions $\mathbf{x}_j(t)$ of the point vortices:

$$\dot{\mathbf{x}}_i = \sum_{j \neq i} \frac{\Gamma_j}{2\pi} \mathbf{e}_z \times \frac{\mathbf{x}_i - \mathbf{x}_j}{\left|\mathbf{x}_i - \mathbf{x}_j\right|^2}. \tag{24}$$

This set of equations for the vortex positions was already known by Kirchhoff (1883). Since then, there have been many studies of this problem (Aref 1983, 2007; Marchioro and Pulvirenti 1984; Newton 2001). We mention that the N-vortex problem of two-dimensional fluid motion shares many properties with the N-body problem of classical mechanics.

The Lagrangian motion of an arbitrary point $\mathbf{X}(\mathbf{y}, t)$ can be determined by the solution of the nonautonomous differential equation

$$\dot{\mathbf{X}}(\mathbf{y}, t) = \sum_{i=1}^{N} \frac{\Gamma_i}{2\pi} \mathbf{e}_z \times \frac{\mathbf{X}(\mathbf{y}, t) - \mathbf{x}_i(t)}{\left|\mathbf{X}(\mathbf{y}, t) - \mathbf{x}_i(t)\right|^2}, \tag{25}$$

where the point vortex positions $\mathbf{x}_i(t)$ are given by the evolution equations (24). The point vortex approximation, thus, allows one to study *mixing in two-dimensional flows* on the basis of sets of ordinary differential equations (Aref 1983; Ottino 1989; Sturman et al. 2006).

Since the point vortex system is obtained from the two-dimensional Euler equation, it is evident that the kinetic energy is conserved. In fact, introducing the Hamilton function

$$\begin{aligned} H &= -\frac{1}{4\pi} \sum_{i \neq j} \Gamma_i \ln\left|\mathbf{x}_i - \mathbf{x}_j\right| \Gamma_j \\ &= \frac{1}{2} \sum_{i \neq j} \Gamma_i G\left(\mathbf{x}_i, \mathbf{x}_j\right) \Gamma_j \end{aligned}, \tag{26}$$

we can rewrite the evolution equations in Hamiltonian form

$$\Gamma_i \dot{\mathbf{x}}_i = \mathbf{e}_z \times \nabla H. \tag{27}$$

There are further conserved quantities due to symmetry. The center of vorticity,

$$\mathbf{R} = \sum_i \Gamma_i \mathbf{x}_i, \tag{28}$$

as well as the quantity

$$I = \sum_i \Gamma_i \mathbf{x}_i^2 \tag{29}$$

are time constants.

The advantage of considering the motion of point vortices in two-dimensional ideal flows is the applicability of methods and notions from the theory of finite Hamiltonian systems. Explicitly, one can investigate the integrability of point vortex motions, i.e., the formation of time-periodic as well as quasiperiodic vortex motions and the emergence of chaotic motions. Because of the existence of the integrals of motions (26), (28), and (29), the motion of two vortices as well as three-point vortices is integrable leading to quasiperiodic motions in time. Furthermore, it has been shown that in the four vortex problem, in addition to quasiperiodic motions, chaotic motion is possible. We refer the reader to the review articles of Aref (1983, 2007) and the monograph of Newton (2001). Also the investigations of mixing by point vortex motion have revealed interesting insights into the geometry and the complexity of the mixing process. An example of the missing process by four point vortices is exhibited in Fig. 4. Similar concepts are expected to be applicable for general two- and three-dimensional turbulent flows.

Onsager's Statistical Theory of Two-Dimensional Turbulence

Onsager (1949) recognized the importance of two-dimensional vortex models for turbulent flows. Since the dynamics is Hamiltonian, one can perform a statistical treatment along the lines

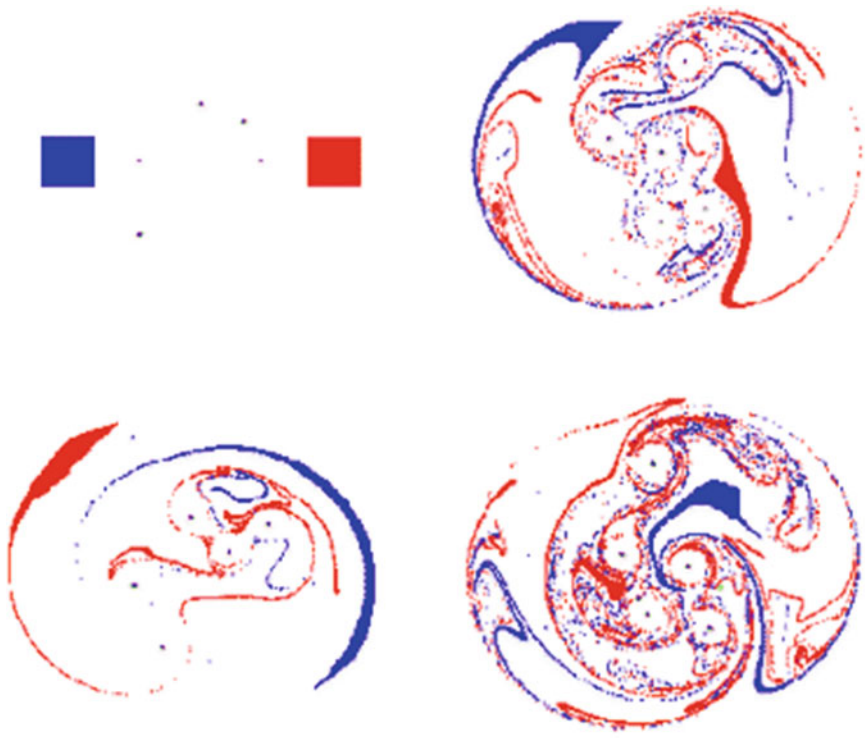

Fluid Dynamics: Turbulence, Fig. 4 Mixing induced by the motion of four point vortices

of equilibrium statistical mechanics. One can determine the corresponding probability distributions. If we focus onto the canonical ensemble, i.e., a point vortex system in connection with a heat bath, the probability distribution reads

$$f(\mathbf{x}_i) = Z^{-1}(\beta)\mathrm{e}^{-\beta\left[\frac{1}{2}\sum_{ij}\Gamma_i G(\mathbf{x}_i,\mathbf{x}_j)\Gamma_j\right]} = Z^{-1}(\beta)\mathrm{e}^{-\beta H}. \quad (30)$$

Onsager recognized that this probability distribution is normalizable both for negative and for positive values of β, which in statistical mechanics is related to temperature. A consequence of the existence of these *negative temperature states* is the tendency of the vortices to form large-scale flow structures. This property can be seen quite easily by recognizing that the probability distribution is the stationary probability distribution of the set of Langevin equations

$$\frac{\mathrm{d}}{\mathrm{d}t}\mathbf{x}_i = -\beta\nabla_{\mathbf{x}_i}H + \eta_j. \quad (31)$$

Here, η_j represents Gaussian white noise. For negative temperatures, the force between two point vortices is attractive for $\Gamma_i\Gamma_j > 0$ and repulsive in the other case. This leads to the formation of large-scale flows. We refer the reader to the recent review (Eyink and Sreenivasan 2006).

Extension to Three Dimensions

The extension of the philosophy of point vortex motion to three dimensions leads one to consider vortex filaments. The location of a single vortex filament is given by the local induction equation for the position $\mathbf{X}(s, t)$ of the filament as a function of arclength s and time t. This equation is again obtained from Biot-Savart's law assuming a filamentary vorticity distribution:

$$\frac{\partial}{\partial t}\mathbf{X}(s,t) = \frac{\partial}{\partial s}\mathbf{X}(s,t) \times \frac{\partial^2}{\partial s^2}\mathbf{X}(s,t) \quad (32)$$

It has been shown that the single filament equation is integrable. For a discussion we refer the reader to (Newton 2001).

Turbulence: Determinism and Stochasticity

It is evident that an understanding of the characteristics of turbulent fluid motions has to be based on the deterministic dynamics generated by the basic fluid dynamical equations in combination with methods of statistical physics. This has led to the field of *statistical hydrodynamics*, a topic which has been treated extensively by the Russian school founded by Kolmogorov (Monin and Yaglom 1971, 1975). A good overview can be found in (Frisch 1995; Lesieur et al. 2000).

Statistical Averages

In *statistical hydrodynamics* the Eulerian velocity field and related fields are treated as *random fields* in a probabilistic sense. To this end one has to define suitable averages, where usually *ensemble averages* are chosen. They are defined by specifying the statistics of the initial flow field by probability distributions, $f(\mathbf{u}_1, \mathbf{x}_1, t = 0)$, $f(\mathbf{u}_1, \mathbf{x}_1, t = 0; \ldots; \mathbf{u}_N, \mathbf{x}_N, t = 0)$ of the velocities $\mathbf{u}_i$ at positions $\mathbf{x}_i$ at initial time $t = 0$. The transition to a continuum of points requires one to consider a probability density functional $F[\mathbf{u}(\mathbf{x}), t = 0]$.

In practice, instead of ensemble averages, time averages are taken, provided the flow is stationary in a statistical sense.

The corresponding probability distributions at time t, which specify the temporal evolution of the considered statistical ensemble are given by

$$f(\mathbf{u}, \mathbf{x}, t) = \langle\delta(\mathbf{u} - \mathbf{u}(\mathbf{x}, t; \mathbf{u}_0))\rangle. \quad (33)$$

Here, $\mathbf{u}(\mathbf{x}, t; \mathbf{u}_0)$ is the solution of the fluid dynamic equation with the initial value of the velocity field at point $\mathbf{x}$: $\mathbf{u}(\mathbf{x}, t = 0;\mathbf{u}_0) = \mathbf{u}_0$. The brackets denote an ensemble average. Joint probability distributions and the probability functional $\boldsymbol{F}(\mathbf{u}(\mathbf{x}, t))$ are defined accordingly. Frequently, the characteristic functions, defined as the Fourier transform of the probability distributions, are used. The characteristic functional

$$Z(\alpha) = \left\langle \mathrm{e}^{i\int \mathrm{d}t \int \mathrm{d}^3\mathbf{x}\alpha(\mathbf{x},t)\cdot\mathbf{u}(\mathbf{x},t)} \right\rangle \quad (34)$$

is the functional Fourier transform of the probability functional. The ultimate goal of statistical

hydrodynamics is the determination of this functional, since it contains all information on the various correlation functions of the Eulerian velocity fields of the statistical ensemble.

Similar probability distributions can be defined for the Lagrangian description of fluid dynamics.

Hierarchy of Moment Equations

The temporal evolution of moments of the velocity field is determined by the basic fluid dynamical equations. For instance, an equation for the moment $\langle u_i(\mathbf{x}, t)u_j(\mathbf{x}', t)\rangle$ can be obtained in a straightforward manner from the Navier-Stokes equation

$$\begin{aligned}
&\frac{\partial}{\partial t}\left\langle u_i(\mathbf{x},t)u_j?(\mathbf{x}',t)\right\rangle \\
&\quad+\sum_k \frac{\partial}{\partial x_k}\left\langle u_k(\mathbf{x},t)u_i?(\mathbf{x},t)u_j?(\mathbf{x}',t)\right\rangle \\
&\quad+\sum_k \frac{\partial}{\partial x'_k}\left\langle u_k(\mathbf{x}',t)u_i?(\mathbf{x},t)u_j?(\mathbf{x}',t)\right\rangle = \\
&\quad-\frac{\partial}{\partial x_i}\left\langle p(\mathbf{x},t)u_j?(\mathbf{x}',t)\right\rangle \\
&\quad-\frac{\partial}{\partial x'_j}\left\langle p(\mathbf{x}',t)u_i?(\mathbf{x},t)\right\rangle \\
&\qquad+\nu[\Delta_x+\Delta_{x'}]\left\langle u_i(\mathbf{x},t)u_j?(\mathbf{x}',t)\right\rangle.
\end{aligned} \tag{35}$$

Similar equations can be formulated for the higher-order moments $\langle u_i(\mathbf{x}_1, t_1)u_j(\mathbf{x}_2, t_2)\ldots u_j(\mathbf{x}_N, t_N)\rangle$ using the Navier-Stokes equation. The equation for the average flow field $\langle \mathbf{u}(\mathbf{x}, t)\rangle$ has been considered by O. Reynolds (1883) (see the discussion below). The chain of evolution equations for the higher-order correlation functions are the so-called Friedmann-Keller equations.

The moment equations are not closed. The evolution equation containing the Nth order moment contains the $(N + 1)$-th order moment. This is the famous closure problem of turbulence. It is an immediate consequence of the nonlinearity of the Navier-Stokes equation. A mathematical discussion of the closure problem is given in (Fursikov 1999).

Evolution Equations for Probability Distributions

It is straightforward to derive evolution equations for the probability distributions from the Navier-Stokes equation. This has been emphasized by Lundgren (1969) and Ulinich and Lyubimov (1969). The evolution equation for $f(\mathbf{u}, \mathbf{x}, t)$ reads

$$\begin{aligned}
&\left[\frac{\partial}{\partial t}+\mathbf{u}\cdot\nabla_{\mathbf{x}}\right]f(\mathbf{u},\mathbf{x},t) \\
&\quad=-\nabla_{\mathbf{u}}\cdot\int \mathrm{d}\mathbf{u}'\mathrm{d}\mathbf{x}'\mathbf{K}(\mathbf{x}-\mathbf{x}') \\
&\qquad\times(\mathbf{u}'\cdot\nabla_{\mathbf{x}'})^2 f(\mathbf{u}',\mathbf{x}',t;\mathbf{u},\mathbf{x},t)-\nabla_{\mathbf{u}} \\
&\qquad\cdot\int \mathrm{d}\mathbf{u}'\mathrm{d}\mathbf{x}'\delta(\mathbf{x}-\mathbf{x}')\nabla_{\mathbf{x}'}\mathbf{u}' f(\mathbf{u}',\mathbf{x}',t;\mathbf{u},\mathbf{x},t).
\end{aligned} \tag{36}$$

(Here, $\mathbf{K}(\mathbf{x})$ is the gradient of Green's function $G(\mathbf{x})$ of the Laplacian.) The dynamics of the single-point probability distribution $f(\mathbf{u}, \mathbf{x}, t)$ is coupled to the two-point probability distribution $f(\mathbf{u}', \mathbf{x}', t; \mathbf{u}, \mathbf{x}, t)$ by the nonlocal pressure term and the dissipative term. Similar equations can be obtained for higher-order probability distributions. Again, the hierarchy shows clearly the closure problem of turbulence theory. The hierarchy is of considerable interest for the so-called Lagrangian pdf (probability density function) model approach advocated by S.B. Pope (1985, 2000). In this approach, the terms involving the two-point pdfs are modeled leading to a description of the turbulent velocity in terms of a stochastic process.

For the case of Burgers equation, which is the Navier-Stokes equation without the pressure term, it has been possible to solve the corresponding Lundgren hierarchy without approximation for a certain external forcing (Eule and Friedrich 2005).

Functional Equations

The Lundgren hierarchy of evolution equations arises due to the fact that the N-point probability distributions contain incomplete information on the evolution of the fluid continuum. A closed evolution equation is obtained for the characteristic functional (34). This equation is the famous Hopf functional equation (Hopf 1957), which forms a concise formulation of the statistical treatment of fluid motions. For a more detailed treatment, we refer the reader to the monograph of Monin and Yaglom (1975).

Path Integral Formulation

As has been emphasized by Martin et al. (1973), each classical field theory can be represented in terms of the path integral formalism. This is essentially true for a fluid motion driven by a fluctuating force, which is Gaussian and δ-correlated in time. The generating (MSR) functional has the following path integral representation

$$\boldsymbol{Z}(\alpha,\hat{\alpha}) = \int D\mathbf{u}D\hat{\mathbf{u}}\mathrm{e}^{S[\mathbf{u},\hat{\mathbf{u}}]+i\int \mathrm{d}\mathbf{x}\int \mathrm{d}t\boldsymbol{\alpha}(\mathbf{x},t)\cdot\mathbf{u}(\mathbf{x},t)+\hat{\boldsymbol{\alpha}}(\mathbf{x},t)\cdot\hat{\mathbf{u}}(\mathbf{x},t)}. \tag{37}$$

The functional $\boldsymbol{Z}(\alpha,\hat{\alpha}=0)$ is just the Hopf characteristic functional (34). The MSR action is defined according to

$$S = i\int \mathrm{d}\mathbf{x}\int \mathrm{d}t\hat{\mathbf{u}}(\mathbf{x},t) \cdot\left\{\dot{\mathbf{u}}(\mathbf{x},t)+\mathbf{u}(\mathbf{x},t)\cdot\nabla\mathbf{u}(\mathbf{x},t)-\nu\Delta\mathbf{u}(\mathbf{x},t) +\nabla p(\mathbf{x},t)\right\}-\frac{1}{2}\int \mathrm{d}t\int \mathrm{d}\mathbf{x}'\int \mathrm{d}\mathbf{x}\hat{\mathbf{u}}(\mathbf{x},t)Q(\mathbf{x}-\mathbf{x}')\hat{\mathbf{u}}(\mathbf{x}',t). \tag{38}$$

The MSR formalism is a convenient starting point for an analytical determination of correlation functions of the velocity field. A naive perturbation expansion of this functional yields the diagrammatic representation of the series by Wyld (1961). A renormalized perturbation expansion leads to the so-called direct interaction approximation (DIA) of Kraichnan and related analytical approximations. For an overview we refer the reader to the monographs of Lesieur (1997) and McComb (1990). Also the recent work by V. L'vov and I. Procaccia (L'vov and Procaccia) is based on this approach.

Reynolds Equation and Turbulence Modeling

O. Reynolds (1883) suggested to decompose a turbulent flow field $\mathbf{u}(\mathbf{x}, t)$ into a mean flow $\mathbf{u}$ and turbulent pulsations $\mathbf{w}(\mathbf{x}, t)$:

$$\mathbf{u}(\mathbf{x},t) = K\langle\mathbf{u}(\mathbf{x},t)\rangle + \mathbf{w}(\mathbf{x},t). \tag{39}$$

By averaging the Navier-Stokes equation, one ends up with the famous Reynolds's equation, which is the first equation of the hierarchy of moment equations (35):

$$\left[\frac{\partial}{\partial t}+\langle\mathbf{u}\rangle\cdot\nabla\right]\langle\mathbf{u}\rangle = -\nabla p-\sum_{ij}\frac{\partial^2}{\partial x_i\partial x_j}\langle w_i w_j\rangle+\nu\Delta\langle\mathbf{u}\rangle+\langle\mathbf{f}\rangle. \tag{40}$$

This equation contains the so-called Reynolds stress tensor $w_i\ w_j$, which cannot be neglected since the turbulent pulsations $\mathbf{w}$ can be larger than the averaged velocity $\mathbf{u}$. The turbulent pulsations w are closely linked to the *fine structures of turbulence*.

If the Reynolds stress tensor is known as a functional of the mean velocity field, the Reynolds equation is a closed evolution equation determining average flow properties. This makes numerical computations of the average flow quantities rather efficient since the *fine structures* or the *small-scale flow* has not to be resolved by numerical schemes.

The Reynolds stress tensor has been the subject of various investigations. Since a general theory determining the Reynolds stress tensor is lacking, engineers have developed the area of *turbulence modeling* in order to overcome the closure problem. Famous turbulence models are eddy viscosity models, which replace the Reynolds stress tensor by an effective damping term modeling the energy flux from the averaged flow into the turbulent pulsations, or the so-called $K-\epsilon$ models, which are based on the evolution equation for the local energy dissipation rate ϵ of the turbulent pulsations.

Turbulence modeling has to fulfill the *requirement of physical realizability* and should, for example, not lead to the development of negative kinetic energies. Furthermore, symmetry arguments should be taken into account (Oberlack 2000).

Turbulence modeling has led to the development of the field of *large eddy simulations* (LES), which has provided a variety of numerical, also commercially available, schemes for calculating the large-scale flows of applied fluid dynamical

problems. The LES approach, however, is limited by the fact that the properties of the Reynolds stresses cannot yet be derived from a physical treatment of the small-scale turbulent pulsations of flows, and the obtained numerical results have to be met with caution. For details we refer the reader to Piquet (1999), Jovanovic (2004), and the reviews of Métais and Leschziner in (Lesieur et al. 2000). Of considerable interest are the two articles of Johansson and Oberlack in (Oberlack and Busse 2002).

The Fine Structure of Turbulence

The fine structure of turbulence essentially influences the large-scale flows via the Reynolds stresses. Therefore, the investigation of the fine structure of turbulent flows is a central theme in turbulence research. It is commonly believed that the statistical characteristics of the turbulent fine structures are universal. A point emphasized by U. Frisch (1995) is that in the fine structures symmetries of the Euler equation of fluid dynamics are restored in a statistical sense. The symmetries of the Euler equations are translational symmetry, isotropy, and rescaling symmetry of space, time, and velocity. Although each of these symmetries is broken by the turbulent flows, the symmetries are restored for averaged quantities. If this hypothesis is true, then the turbulent fine structure is related with a universal state, which is called *fully developed stationary, homogeneous, and isotropic turbulence*.

Increments

The fine-scale structure of turbulence is evaluated by the introduction of the so-called velocity increment $\mathbf{v}_\mathbf{x}(\mathbf{r}, t)$

$$\mathbf{v}_\mathbf{x}(\mathbf{r}, t) = \mathbf{u}(\mathbf{x} + \mathbf{r}, t) - \mathbf{u}(\mathbf{x}, t). \tag{41}$$

Velocity increments are defined with respect to a reference point $\mathbf{x}$. A mean flow is eliminated by the definition of increments. Furthermore, one may consider velocity increments with respect to a moving reference point $\mathbf{x} = \mathbf{X}(\mathbf{y}, t)$. In the following we shall consider such moving increments.

The corresponding evolution equation for the incompressible velocity increment can easily be established using the definition (41) and the Navier-Stokes equation:

$$\begin{aligned}&\left[\frac{\partial}{\partial t} + \mathbf{v}(\mathbf{r}, t) \cdot \nabla_\mathbf{r}\right]\mathbf{v}(\mathbf{r}, t) = \\ &-\nabla_r p(\mathbf{r}, t) + \nu\Delta_r \mathbf{v}(\mathbf{r}, t) \\ &-\left[-\nabla_r p(\mathbf{r}, t) + \nu\Delta_r \mathbf{v}\left(\mathbf{r}, t\right)\right]_{\mathbf{r}=0}, \nabla \cdot \mathbf{v}_\mathbf{x}(\mathbf{r}, t) = 0.\end{aligned} \tag{42}$$

Length and Time Scales in Turbulent Flows

The Integral Scale

The integral scales are measures for a spatial distance L or a time interval T, across which the turbulent fluctuations become uncorrelated. The integral length scale is based on the velocity-velocity correlation function

$$\langle u(x + r, t)u(x, t)\rangle = \langle u(x, t)u(x, t)\rangle F\left(\frac{r}{L}\right), \tag{43}$$

which decays to zero as a function of the distance r. The integral length scale L is defined by the integral

$$L = \int_0^\infty \mathrm{d}r F\left(\frac{r}{L}\right). \tag{44}$$

Similarly, one can define temporal integral scales based on the decay of temporal correlations $\langle u(x, t + \tau)u(x, t)\rangle = \langle u(x, t)u(x, t)\rangle F\left(\frac{\tau}{T}\right)$ leading to the definition of the integral time scale T. An integral velocity scale can be formed quite naturally by the ratio

$$U_{\text{int}} = L/T. \tag{45}$$

The velocity field $u(x,t)$ describes the turbulent pulsations. A mean flow has already been subtracted. The correlation functions (43) actually are tensors. For flows which are nonisotropic in the statistical sense, it might be necessary to introduce different integral length scales.

The Kolmogorov Scales

The Navier-Stokes equation involves the kinematic viscosity ν as well as a measure of the excitation of turbulence, the mean local energy dissipation ϵ. It is convenient to form length and time scales from these two quantities and obtain the so-called Kolmogorov scales

$$\eta = \left(\frac{\nu^3}{\epsilon}\right)^{1/4}, \quad \tau_\eta = \left(\frac{\nu}{\epsilon}\right)^{1/2}, \quad u_\eta = \frac{\eta}{\tau_\eta} = (\epsilon\nu)^{1/4}. \tag{46}$$

On the basis of these quantities, one can define a Reynolds number which turns out to be unity, $\mathrm{Re} = \frac{\eta u_\eta}{\nu} = 1$. Therefore, the Kolmogorov scales have to be related with small-scale motions, which, due to dissipation, can be considered to be laminar on these scales.

Relation Between the Integral and the Kolmogorov Length Scale

One may find a relation between the integral length scale L and the Kolmogorov length scale η. This relation is based on the observation that the local energy dissipation rate ϵ can be dimensionally expressed in terms of the velocity at the integral scale, U_{int}, Eq. (45) via

$$\epsilon \approx \frac{U_{\mathrm{int}}^3}{L}. \tag{47}$$

This relation allows one to determine the ratio of the intergal scale L and the Kolmogorov scale η leading to a Reynolds number dependence

$$\frac{L}{\eta} \approx \mathrm{Re}^{3/4} = \left(\frac{U_{\mathrm{int}} L}{\nu}\right)^{3/4}. \tag{48}$$

The ratio increases with the Reynolds number. Typical length scales estimated from experimental data of a grid flow are shown in Fig. 5. It is seen that the estimate (48) can be confirmed experimentally.

From a dynamical point of view, the quantity $\left(\frac{L}{\eta}\right)^3 \approx \mathrm{Re}^{9/4}$ is a measure of the number of active degrees of freedom of the fluid motion.

The Taylor Length and the Taylor-Based Reynolds Number

A third length scale has been used to characterize a turbulent flow field. This is the so-called Taylor length, which frequently is denoted also as Taylor microscale, λ.

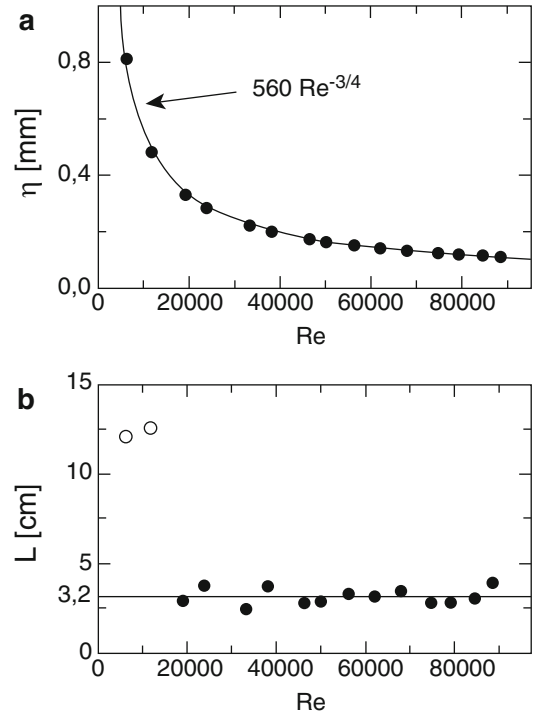

Fluid Dynamics: Turbulence, Fig. 5 Reynolds number dependence of the Kolmogorov scale (**a**) and the integral length scale (**b**) estimated from data of a grid experiment, (Lück et al. 2006)

It can be derived from the velocity u (here u denotes again the fluctuating part of a measured velocity signal) and the derivative as $\partial u/\partial x$

$$\lambda^2 = \lim \frac{\langle u^2 \rangle}{\left\langle (\partial u/\partial x)^2 \right\rangle}. \tag{49}$$

Aronson and Löfdahl (1993) suggested to estimate the Taylor length using the velocity increment $v(r) = u(x + r) - u(x)$:

$$\lambda^2 = \lim_{r \to 0} \frac{\left\langle u(x)^2 \right\rangle r^2}{\left\langle v(r)^2 \right\rangle}. \tag{50}$$

For the Taylor length, it is expected that $\frac{L}{\lambda} \approx \mathrm{Re}^{1/2}$ holds, which is also found experimentally; see Fig. 6a.

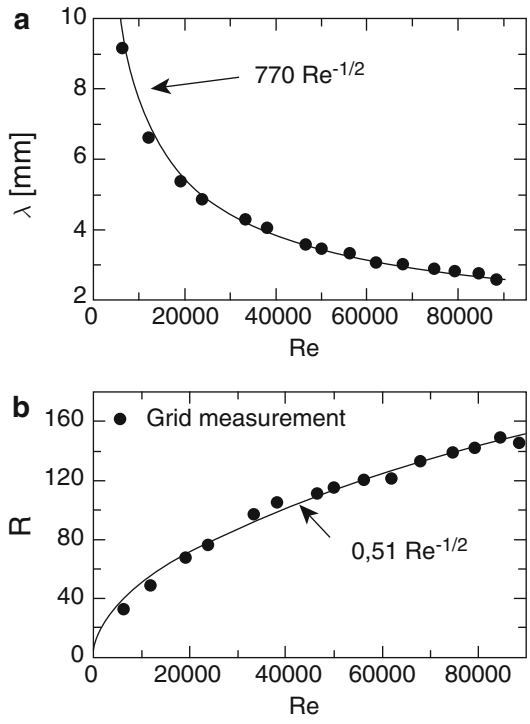

Fluid Dynamics: Turbulence, Fig. 6 Reynolds number dependence of the Taylor scale (**a**) and the Taylor length-based Reynolds number from data of a grid experiment (Lück et al. 2006)

On the basis of this Taylor length, it is also possible to define a new Reynolds number by the ratio of velocity times length scale and kinematic viscosity. The Taylor length-based Reynolds number R_λ should scale with the square of the usual Reynolds number; see Fig. 6b.

Statistics of Increments: Structure Functions

A great amount of work in turbulence research has been devoted to the so-called structure functions. In general, structure functions are equal the time moments of the velocity increments:

$$\left\langle v_i(\mathbf{r},t)v_j(\mathbf{r},t)\right\rangle, \quad \left\langle v_i(\mathbf{r},t)v_j(\mathbf{r},t)v_k(\mathbf{r},t)\right\rangle. \tag{51}$$

For stationary, homogeneous, and isotropic turbulence, the tensorial quantities can be considerably reduced by symmetry arguments. For homogeneous and isotropic turbulence, the second- and third-order moments can be related to the so-called longitudinal structure functions, i.e., the moments of the component of the velocity increment in the direction of $\mathbf{r}$, $\mathbf{e}_r \cdot \mathbf{v}(\mathbf{r}, t)$. They are defined according to

$$S^N(r) = \left\langle \left(\frac{\mathbf{r}}{r}\cdot \mathbf{v}(\mathbf{r},t)\right)^N \right\rangle. \tag{52}$$

For small values of r, the structure functions have to behave like $S^N \approx r^N$, since for small r the velocity increment can be expanded in a Taylor series.

The structure functions of different orders are related through the Navier-Stokes dynamics. The evaluation of the structure functions from the resulting hierarchy of evolution equations is one of the major theoretical challenges in turbulence research. However, it seems that so far only the lowest-order equations relating second- and third-order structure (the so-called Kolmogorov's 4/5 law) functions have been exploited rigorously.

Kolmogorov's 4/5 Law

Kolmogorov (c.f. (Frisch 1995; Monin and Yaglom 1975)) showed that the mean kinetic energy in an *eddy of scale r*, $\mathbf{v_x}(\mathbf{r},t)^2$, in a homogeneous, isotropic turbulent field is given by the equation

$$\frac{\partial}{\partial t}\left\langle \frac{\mathbf{v}_x(\mathbf{r},t)^2}{2}\right\rangle + \nabla_r \cdot \left\langle \mathbf{v}_x(\mathbf{r},t)\frac{\mathbf{v}_x(\mathbf{r},t)^2}{2}\right\rangle = \nu\Delta\left\langle \mathbf{v}_x(\mathbf{r},t)^2\right\rangle - \langle\epsilon\rangle, \tag{53}$$

where ϵ denotes the mean local energy dissipation rate

$$\langle\epsilon\rangle = \frac{\nu}{2}\sum_{ij}\left\langle \left(\frac{\partial u_i}{\partial x_j}+\frac{\partial u_j}{\partial x_i}\right)^2\right\rangle. \tag{54}$$

We formally consider the *turbulent limit* $\nu \to 0$. In this limit the mean local energy dissipation rate ϵ has to be constant. Thus, one can estimate that the gradients have to behave like

$$\frac{\partial u_i}{\partial x_j} \approx \frac{1}{\sqrt{\nu}}. \tag{55}$$

The relation (53) can be obtained as a balance equation for the density of the mean kinetic

energy from the evolution equation for the velocity increment (42) by scalar multiplication with **v** and subsequent averaging. The correlations involving the pressure term drop out due to homogeneity.

The resulting equation reads

$$S^3(r) - 6\nu\frac{\mathrm{d}}{\mathrm{d}r}S^2(r) = -\frac{4}{5}\langle\epsilon\rangle r. \tag{56}$$

This equation relates the second- and third-order structure functions and, at first glance, seems to be underdetermined. However, for small values of r, we can neglect the third-order structure function, since $S^3(r) \approx r^3$. The second-order structure function is then given by

$$S^2(r) = \frac{\langle\epsilon\rangle}{15\nu}r^2. \tag{57}$$

The range of validity of this law is denoted as the *dissipative range* and is close to the Kolmogorov length and smaller. It is dominated by viscous structures.

In the second regime, whose existence is inferred by the 4/5th law, the third-order structure function dominates, leading to

$$S^3(r) = \frac{4}{5}\langle\epsilon\rangle r. \tag{58}$$

This defines the so-called *inertial range* and is located between the Taylor length and the integral length. For data from a free jet experiment with high Reynolds numbers, we show in Fig. 7 the third-order structure function in different presentations, which clearly demonstrate the existence of the inertial range.

Phenomenological Theories of Turbulence

Kolmogorov's Theory K41: Self-Similarity in the Inertial Range

The inertial range is characterized by the decay of eddies, which can be assumed to be self-similar. As a consequence, the probability distribution of the longitudinal velocity increment v at scale r, $f(v, r)$, should have the form

$$f(v,r) = \frac{1}{\sqrt{\left\langle v(r)^2\right\rangle}}F\left(\frac{v}{\sqrt{\left\langle v(r)^2\right\rangle}}\right), \tag{59}$$

where $F(\xi)$ is a universal function in the range of scales $\lambda < r < L$. As a consequence, the nth order moments should have the form

$$\begin{aligned}\langle v^n(r)\rangle &= \int \mathrm{d}v\, v^n \frac{1}{\sqrt{\left\langle v(r)^2\right\rangle}}F\left(\frac{v}{\sqrt{\left\langle v(r)^2\right\rangle}}\right)\\ &= \left\langle v(r)^2\right\rangle^{n/2}\int \mathrm{d}w\, w^n F(w)\\ &= \left\langle v(r)^2\right\rangle^{n/2} V_n.\end{aligned} \tag{60}$$

Since the r-dependence of the third-order moment is known in the limit of high Reynolds number,

$$\left\langle v^3(r)\right\rangle = V_3\langle\epsilon\rangle r = \left\langle v(r)^2\right\rangle^{3/2} V_3, \tag{61}$$

we obtain

$$\left\langle v(r)^2\right\rangle = K(\langle\epsilon\rangle r)^{2/3}. \tag{62}$$

The K41 assumption of self-similarity of the velocity increment statistics in the inertial range leads to the following fractal scaling behavior of the nth order moments

$$\langle|\, v(r)^n\rangle = K_n(\langle\epsilon\rangle r)^{n/3}. \tag{63}$$

The corresponding probability distribution is entirely determined by the constants K_n. The scaling exponents $\zeta_n = N/3$ are linear functions of n.

Failure of K41: Intermittency

Kolmogorov's hypothesis on the self-similarity of the statistics in the inertial range has been tested experimentally as well as numerically. Figure 8 exhibits the probability distribution of the scaled variable $\tilde{v}$

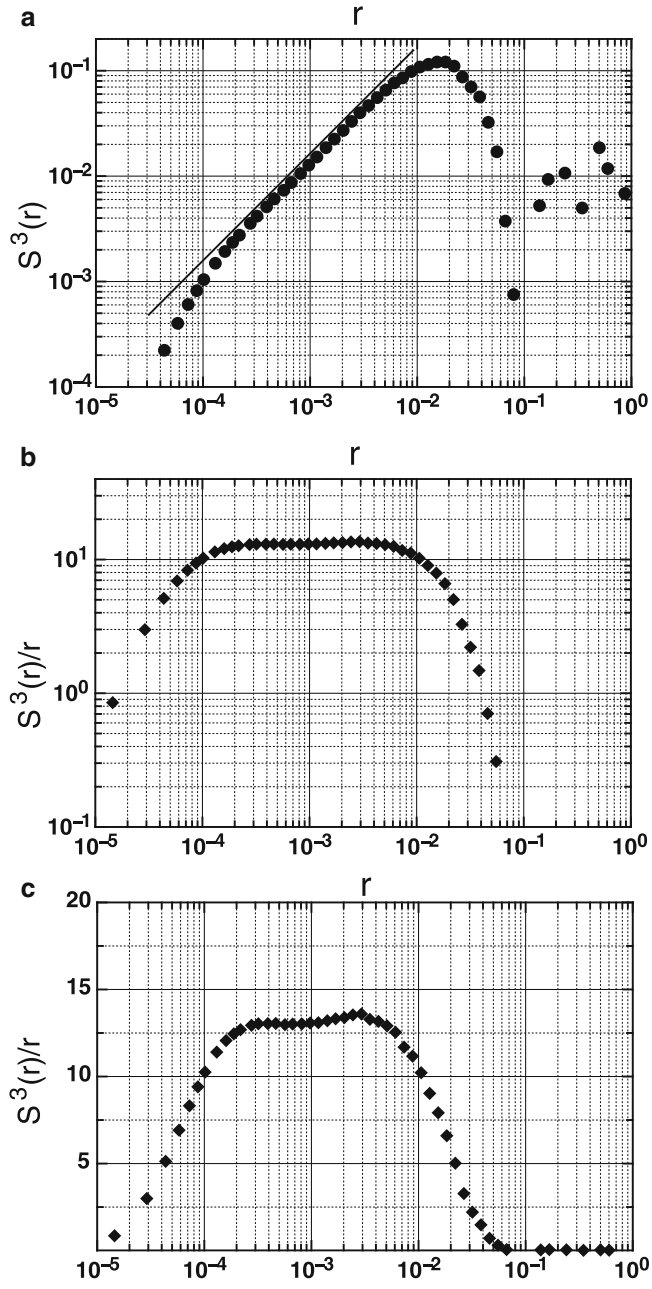

Fluid Dynamics: Turbulence, Fig. 7 Third-order structure function $S^3(r)$ (**a**) of cryogenic free jet measurements with Re = 210.000 and the compensated structure functions $S^3(r)/r$ in a semilogarithmic plot (**b**) and in a linear plot (**c**), showing in more detail the quality of the present scaling behavior (Note here we used the absolute values for $S^3(r)$; thus the values are all positive) (Chabaud)

$$\tilde{v} = \frac{v}{\sigma(r)} \text{with} \, \sigma(r) = \sqrt{\left\langle v(r)^2 \right\rangle}. \tag{64}$$

Because of K41 theory, all probability distributions should collapse for values of r taken from the inertial range. Both experimental and numerical results show clear deviations from this behavior. Although the scaling exponents of the second-order structure function are close to the K41 value **2/3**, a characteristic change of shape of the probability distribution can be detected. The change of the pdf with scale r in the inertial range is a signature of the phenomenon called *intermittency*. Consequently, the structure functions do not scale as suggested by the theory of Kolmogorov. This has been experimentally documented

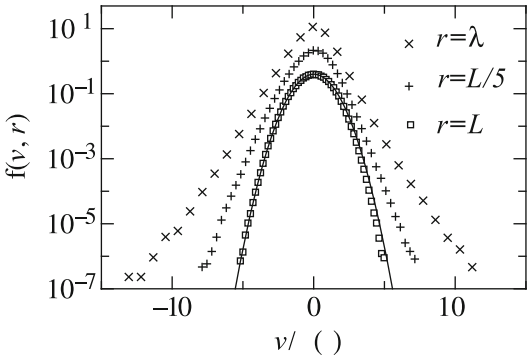

Fluid Dynamics: Turbulence, Fig. 8 Probability density functions (pdf) for velocity increments on three different length scales $r = L$, $L/5$, $L/30 \approx \lambda$. The pdfs are shifted along the ordinate for a better representation. On the largest scale L, a Gaussian distribution is fitted for comparison. Toward smaller scales, the deviations from the Gaussian form become obvious ($R_\lambda = 180$). For further details, see (Siefert and Peinke 2006)

by (Anselmet et al. 1984) and has been discussed by several groups.

Kolmogorov's Theory K62

In a famous note in the volume on hydrodynamics in his *Course on Theoretical Physics*, Landau (Landau and Lifshitz 1981) remarked that the formula of the K41 theory contains the mean value of the local energy dissipation rate, ϵ. However, this quantity is a strongly fluctuating quantity in space, due to the strong spatial variations of the velocity gradient, as can be seen from Fig. 9. According to Landau these fluctuations should show up in the structure functions.

Instead of the K41 result (63), he suggested the use of the following representation

$$\langle |\, v(r)^n \rangle = \tilde{K}_n \left\langle \epsilon_r^{n/3} \right\rangle r^{n/3} \tag{65}$$

where the quantity ϵ_r denotes the local energy dissipation rate averaged over a sphere of radius r. This reasoning leads to an extension of the K41 formula for the probability distribution in the form

$$f(v,r) = \int d\epsilon_r p\left(\epsilon_r, \frac{r}{L}\right) \frac{1}{(\epsilon r)^{2/3}} F\left(\frac{v}{(\epsilon_r r)^{2/3}}\right). \tag{66}$$

In 1962 Kolmogorov (1962) suggested the use of a lognormal distribution for the local energy

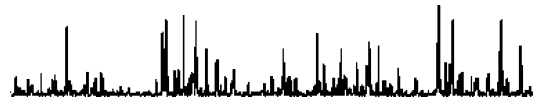

Fluid Dynamics: Turbulence, Fig. 9 Spatial distribution of the local energy dissipation rate. The quantity strongly fluctuates in space. Data is obtained from the experiment (Siefert and Peinke 2006)

dissipation rate ϵ_r, whose variance is $\mu \ln(L/r)$. As a result, the structure functions scale like

$$\langle |\, v(r)^n \rangle = \tilde{K}_n r^{n/3} (L/r)^{\mu n(n-3)}. \tag{67}$$

The experimental value for μ can be obtained from a fit of the K62 formula to experimental data. However, we note that the formula can only be valid for small values of n, since the scaling exponents ζ_n have to be a monotonously increasing function of the order n of the structure function.

The Multifractal Model

The multifractal model was introduced by U. Frisch and G. Parisi. For a detailed description, we refer the reader to Frisch (1995). The basic idea is to view a turbulent field to be composed of regions where the velocity increment field is assumed to be characterized by a scaling index h:

$$v(r,t) = \beta \left(\frac{r}{L}\right)^h. \tag{68}$$

The structure functions are then given by

$$S^N(r) = \beta_N \int \mathrm{d}h P(h,r) \left(\frac{r}{L}\right)^{Nh}, \tag{69}$$

where $P(r, h)\mathrm{d}h$ is the probability to find increments for a certain scale r with scaling exponent h. Assuming self-similarity, $P(h, r)$ should have the form

$$P(h,r) = \left(\frac{r}{L}\right)^{3-D(h)}. \tag{70}$$

Consequently, we have

$$S^N(r) = \beta_N \int \mathrm{d}h \left(\frac{r}{L}\right)^{Nh+3-D(h)} \approx r^{\zeta_N}, \tag{71}$$

where the evaluation of the integral with the method of steepest descend yields

$$\zeta_N = \mathrm{Min}[Nh + 3 - D(h)]. \tag{72}$$

The scaling indices ζ_N are related to the dimension $D(h)$ via a Legendre transform. Recently, an extension of the multifractal model has been presented by Chevillard et al. (2006). This approach is essentially based on the representation of the probability distribution due to (Castaing et al. 1990). They succeeded to obtain a model for the symmetric part of the probability function of the longitudinal velocity increment, which is valid both in the integral and the dissipative scale. This gives a reasonable approximation to the experimentally determined probability distribution $f(v, r)$.

As we have seen, the statistics of the longitudinal velocity increment for a single scale r can be modeled in various ways in order to describe the deviations from the fractal scaling behavior predicted by the phenomenological theory of Kolmogorov formulated in 1941. The major shortcoming of these approaches, however, is the fact that they contain no information on the joint statistics of the velocity fields at different scales and times. However, due to the presumed energy cascade, the velocity increments on different scales have to be correlated.

Multiscale Analysis of Turbulent Fields

The spatial correlation of the velocity of turbulent fields has been examined in two ways. From a field theoretic point of view, pursued by V. L'vov and I. Procaccia, the existence of so-called fusion rules has been hypothesized. For this approach we refer the reader to the survey (L'vov and Procaccia) and the work cited therein. A phenomenological approach has been performed by Friedrich and Peinke (1997a, 1997b). In this approach notions from the theory of stochastic processes have been used in order to characterize multiscale statistics of velocity increments. Relations to the fusion rule approach have been discussed in (Davoudi and Tabar 1999). In the following we shall discuss the phenomenological approach to multiscale statistics of turbulence.

Statistics Across Scales

In order to address the spatial signatures of the cascading process underlying stationary, homogeneous, and isotropic turbulence, it is necessary to consider the probability distributions for velocity increments at different scales:

$$f^N(\mathbf{v}_1, r_1; \mathbf{v}_2, r_2; \ldots; \mathbf{v}_N, r_N). \tag{73}$$

Thereby, the quantities $\mathbf{v}_i$ are velocity increments with respect to a common point of reference, $\mathbf{v}_i(\mathbf{r}_i, t) = \mathbf{u}(\mathbf{x} + \mathbf{r}_i, t) - \mathbf{u}(\mathbf{x}, t)$, and different distances $\mathbf{r}_i$.

In the following we shall consider the longitudinal velocity increments and locations $\mathbf{r}_i$ positioned along a straight line. These quantities are easily accessible from experimental data.

In case that the longitudinal velocity increments v_i of different scales r_i are statistically independent, the N-point probability distribution simply factorizes

$$\begin{aligned} &f^N(v_1, r_1; v_2, r_2; \ldots; v_N, r_N) \\ &= f^1(v_1, r_1) f^1(v_2, r_2) \ldots f^1(v_N, r_N). \end{aligned} \tag{74}$$

Because of the cascading process, which involves the dynamics of velocity increments at different scales, this relationship cannot hold true. However, provided the cascade is generated locally by the nonlinear interaction of velocity increments at neighboring scales, one may expect that the two scale probability distributions or the conditional probability distribution

$$p(v_1, r_1 | v_2, r_2) = \frac{f^2(v_1, r_1; v_2, r_2)}{f^1(v_2, r_2)} \tag{75}$$

contains the most important information on the N-scale probability distribution (73).

Markovian Properties

One may wonder whether the knowledge of the conditional probability distribution suffices to reconstruct the N-scale probability distribution (73) in the form

$$\begin{aligned} &f^N(v_1, r_1; \ldots; v_N, r_N) = p(v_1, r_1 | v_2, r_2) \\ &\times \ldots p(v_{N-1}, r_{N-1} | v_N, r_N) \cdot f(v_N, r_N). \end{aligned} \tag{76}$$

In this case, the probability distribution f^N defines a Markov chain.

The question, whether Markovian properties in scale exist for fully developed turbulence, has been pursued in several ways. First of all, a necessary condition for the existence of Markovian properties is the validity of the Chapman-Kolmogorov equation:

$$p(v_1, r_1 | v_3, r_3) = \int \mathrm{d}v_2 p(v_1, r_1 | v_2, r_2) \times p(v_2, r_2 | v_3, r_3). \quad (77)$$

This approach has been pursued in (Friedrich et al. 1998). Second, one can validate the Markovian properties by a direct inspection of the conditional probability distribution (75). Defining the conditional probability distribution

$$p(v_1, r_1 | v_2, r_2; v_3, r_3) = \frac{f^3(v_1, r_1; v_2, r_2; v_3, r_3)}{f^2(v_2, r_2; v_3, r_3)}, \quad (78)$$

the Markovian property can be assessed by comparing the conditional probability distributions

$$p(v_1, r_1 | v_2, r_2; v_3, r_3) = p(v_1, r_1 | v_2, r_2). \quad (79)$$

Summarizing the outcomes of the experimental investigations, one can state that the Markovian property can be empirically validated provided the differences of the scales, $r_1 - r_2$, $r_2 - r_3$, are not too small. This statement can be made even more precise. As has been shown in (Lück et al. 2006), the Markovian property breaks down provided the scale differences are smaller than the Taylor microscale [see Eq. (49)]. This finding attributes a statistical definition to the Taylor length scale. Because of the memory effect, we have now called this length Markov-Einstein coherence length L_{mar} (Lück et al. 2006).

Estimation of the Conditional Probability Distribution

Markov processes are defined through their conditional probability distributions. If one considers the statistics on scales larger compared to the Markov-Einstein length, one may perform the limit $L_{\mathrm{mar}} \to 0$ and consider the process to be continuous in scale r; the conditional probability distribution obeys a Fokker-Planck equation of the form

$$-\frac{\partial}{\partial r} p(v, r | v_0 r_0) = \left[-\frac{\partial}{\partial v} D^1(v, r) + \frac{\partial^2}{\partial v^2} D^2(v, r) \right] p(v, r | u_0 r_0), \quad (80)$$

where the statistics are determined by the drift function $D^1(v, r)$ and the diffusion function $D^2(v, r)$. We remind the reader that in the definition of $p(v, r|v_0, r_0)$, we have used $r_0 > r$, which leads to the minus sign in the Fokker-Planck equation.

The drift function and the diffusion function have been determined empirically using methods of data analysis of stochastic processes; for further details see (Renner et al. 2001). We also refer the reader to (Marcq and Naert 2001).

Path Integral Representation of the *N*-Scale Probability Distribution

Since the joint N-point probability distribution can be constructed by the conditional probability function due to the Markovian property, one can write down a path integral formula for the turbulent cascade in the form

$$F[v(r)] = Z^{-1} \exp\left[-\int \mathrm{d}r' \frac{\left[-\frac{dv(r')}{dr'} - D^1\left(v(r'), r'\right) \right]^2}{D^2(v(r'), r')} \right]. \quad (81)$$

This probability distribution is the analog to the Gibbs distribution describing the statistics of systems in thermodynamic equilibrium.

Statistics of Longitudinal and Transversal Components

Recently, an analysis of the joint statistics of the longitudinal and transversal components of the velocity increments has been performed (Siefert and Peinke 2004, 2006). The result is a Fokker-Planck equation of the form

$$-r\frac{\partial}{\partial r}p(\mathbf{u},t|\,\mathbf{u}_0,r_0) = \left\{-\frac{\partial}{\partial u_i}D_i^{(1)}(\mathbf{u},r)+\frac{\partial^2}{\partial u_i\partial u_j}D_{ij}^{(2)}(\mathbf{u},t)\right\} \cdot p(\mathbf{u},r|\,\mathbf{u}_0,r_0). \quad (82)$$

Here, $\mathbf{u}=(u_1,u_2)$ denotes the increment vector of the longitudinal and transversal components, respectively. As mentioned above and worked out in more detail in another contribution to this *Encyclopedia of Complexity and System Science* (Friedrich et al. 2008), both drift and diffusion terms $D^{(1)}$, $D^{(2)}$ can be estimated directly from given data.

Typical results are shown in Figs. 10 and 11. The drift terms turn out to be linear,

$$D_i^{(1)}(\mathbf{u},r)=d_i(r)u_i. \quad (83)$$

Furthermore, the diffusion matrix can be approximated by low-order polynomials

$$D_{ij}^{(2)}(\mathbf{u},r)=d_{ij}(r)+\sum_k d_{ij;k}u_k + \sum_{kl} d_{ij;kl}(r)u_k u_l. \quad (84)$$

Knowing the drift and diffusion coefficient, it is possible to solve the Fokker-Planck equation numerically, which can be taken as a self-consistent verification of the estimation procedure. In Fig. 12

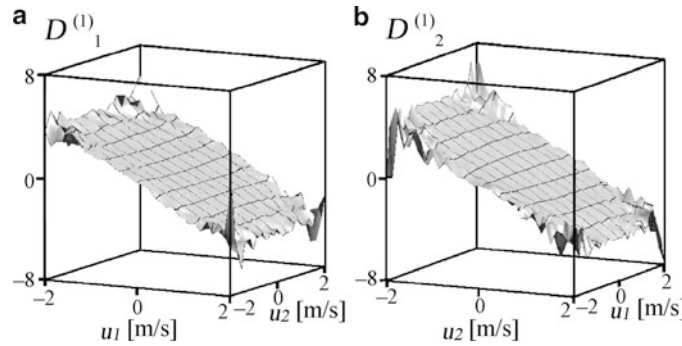

Fluid Dynamics: Turbulence, Fig. 10 The u_1 and u_2 dependence of the drift vector for the scale $r = L/4$. (**a**) The drift coefficient $D_1^{(1)}$ and (**b**) the drift coefficient $D_2^{(2)}$. Note that the vertical axis is rotated for better comparison between (**a**) and (**b**). Both coefficients are linear functions in $\mathbf{u}$ (Siefert and Peinke 2006)

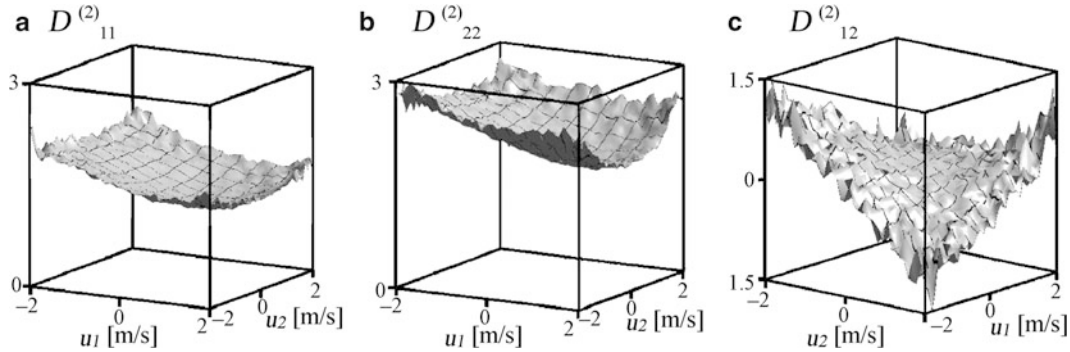

Fluid Dynamics: Turbulence, Fig. 11 The u_1 and u_2 dependence of the diffusion matrix for the scale $r = L/4$. (**a**) The coefficient $D_{11}^{(2)}$ and (**b**) the coefficient $D_{22}^{(2)}$. It can be seen that the diagonal coefficients are not constant but have a parabolic form, which is more pronounced for the $D_{22}^{(2)}$ coefficient (multiplicative noise). Both coefficients are symmetric under reflection with respect to $u_2 \to -u_2$, but not for $u_1 \to -u_1$. (**c**) The saddle-formed off-diagonal coefficient $D_{12}^{(2)}$ (Siefert and Peinke 2006)

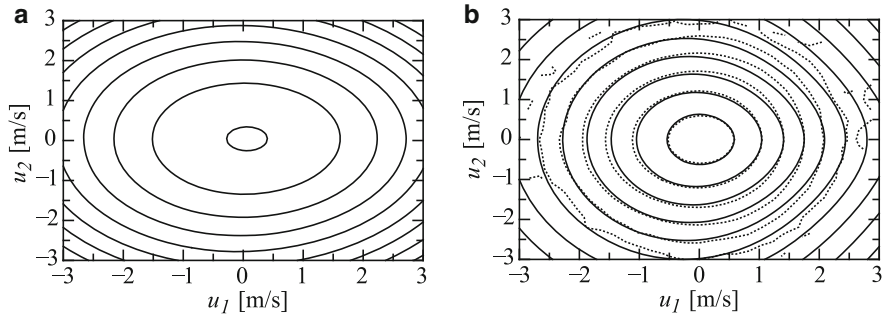

Fluid Dynamics: Turbulence, Fig. 12 Solution of the Fokker-Planck equation. (**a**) Contour plot of the initial condition in logarithmic scale. The simulation starts at the integral length $r = L$ with a Gaussian distribution fitted to the data. (**b**) The contour plots in logarithm scale of the simulated probability distribution on the scale $r = 2\lambda$. The distance between the contour lines is chosen in logarithmic scale and corresponds to a factor 10. *Dashed lines* indicate the probability distribution calculated directly from data; the *full lines* are the simulation ones. The simulation reproduces well the properties of the data (Siefert and Peinke 2006)

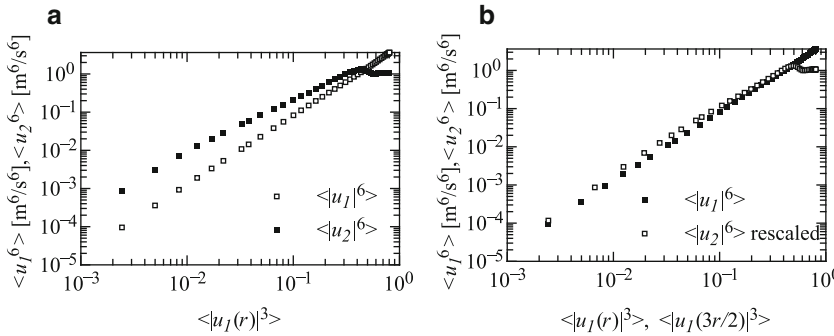

Fluid Dynamics: Turbulence, Fig. 13 The sixth-order longitudinal (*black squares*) and transversal (*white squares*) structure function in (**a**) ESS representation and (**b**) ESST representation (Siefert and Peinke 2006)

it is shown that the numerical solution of the Fokker-Planck equation reproduces the probability distribution directly obtained from the data quite well.

It is quite interesting to notice that the resulting moment equations reproduce Karman's equation, which is a relation between the longitudinal and transversal velocity increments

$$\left\langle u_2(r)^2 \right\rangle = \frac{1}{2r} \frac{\mathrm{d}}{\mathrm{d}r} r^2 \left\langle u_1(r)^2 \right\rangle. \qquad (85)$$

Karman's equation is a direct consequence of the incompressibility of the fluid motion. It can be interpreted as a low-order Taylor expansion of $\left\langle u_2(r)^2 \right\rangle = \left\langle u_1\left(\frac{3}{2}r\right)^2 \right\rangle$ which leads to the proposition that the complex structures of longitudinal and transversal velocity increments mainly differ in a different scale parametrization of the cascade, $r \to \frac{3}{2}r$.

Using these findings the different scaling exponents found for longitudinal and transversal increments can be explained. In Fig. 13 the longitudinal and transversal structure function are shown as a function of the third-order structure function, which should reveal the scaling behavior, too, as the third-order structure function is expected to depend linearly on r. (This presentation is called ESS – extended self-similarity (Benzi et al. 1993).) Most interestingly, the difference in the scaling exponents vanishes if the 3/2 rescaling is applied; see Fig. 13b. The result indicates that proper scaling behavior is not detected and can only be valid approximately.

The Markov analysis of turbulent velocity fields yields a closed phenomenological description of the spatial complexity of turbulence. We note that a similar multiscale analysis has been performed for a turbulent passive scalar field (Tutkun and Mydlarski 2004).

Lagrangian Fluid Dynamics

Because of experimental progress in the detection of the Lagrangian path of passive tracer particles (La Porta et al. 2000; Mordant et al. 2001), interest in the formulation of stochastic processes describing Lagrangian motion in turbulent fluids has been renewed. One of the first descriptions of such a process is due to Obukhov (1959), who suggested to model the Lagrangian acceleration as a white noise process. He formulated the corresponding evolution equation for the probability distribution $f(\mathbf{x}, \mathbf{u}, t)$ specifying the Lagrangian path in a form of a Fokker-Planck equation. The results, which can be derived from the Fokker-Planck equation, indicate scaling behavior for the Lagrangian velocity increments and the distance traveled by the particle during time t:

$$\begin{aligned} \left\langle (\mathbf{u}(t) - \mathbf{u}(0))^2 \right\rangle &= c\langle\epsilon\rangle t, \\ \left\langle (\mathbf{x}(t) - \mathbf{x}(0))^2 \right\rangle &= d(\langle\epsilon\rangle t)^3. \end{aligned} \tag{86}$$

This scaling behavior is inferred from dimensional considerations along the theory of Kolmogorov (K41). Therefore, it is not a surprise that the experimentally observed probability distributions deviate from the Gaussian shape required by the Obukhov model (Mordant et al. 2001). A modification of Obukhov's model has been suggested in (Friedrich 2003). Recently, Lagrangian particle statistics has been modeled on the basis of a simple vortex model (Wilczek et al. 2008), reproducing qualitatively the intermittent characteristics of Lagrangian velocity increments (Mordant et al. 2001).

The investigations of the Lagrangian statistics of turbulent flows have benefited a lot from the investigation of passive tracers in disordered flows. Especially the treatment of the Kraichnan model has led to considerable insights into the statistics of particles in flows. We refer the reader to the review article (Falkovich et al. 2001).

Future Directions

Although a fundamental understanding is still lacking, turbulence research has always led to new concepts and scientific ideas, which substantially have influenced the development of modern science. This will especially hold true for the future, where one may expect a major breakthrough due to combined efforts of experimental, numerical, and analytical work. The following points for future direction of research are only a rather subjective listing of the authors.

Fine Structure of Turbulence: A question which should be investigated experimentally in more detail is whether and how the fine structure is influenced by the mechanism of the generation of turbulence. This will also involve turbulent flows close to walls or in pipes. From the experimental side, high precision measurements are required.

Geometrical and Topological Aspects of Turbulence: There is a variational formulation of ideal hydrodynamics, emphasized by V.I. Arnold (Arnold and Khesin 1999). We expect that research based on topological and geometrical reasoning will yield further important insights into the spatiotemporal organization of fluid flow.

Statistical Properties of the Lagrangian Map: Topological and geometrical aspects are intimately related with the properties of the Lagrangian map. A further analysis of the trajectories of several Lagrangian particles is currently under consideration. A highly interesting question is whether the stochastic processes of the particle motion in the inertial range can be assessed.

Further Reading

For further reading we suggest the monographs and proceedings (Arnold and Khesin 1999; Darrigol 2005; Davidson 2004; Frisch 1995; Gyr

et al. 1999; Monin and Yaglom 1971, 1975; Pope 2000; Sreenivasan and Antonia 1997).

Acknowledgments We thank all members of our working groups for fruitful collaboration. We thank T. Christen and M. Wilczek for critically reading the manuscript.

Bibliography

Anselmet F, Gagne Y, Hopfinger EJ, Antonia RA (1984) High order structure functions in turbulent shear flows. J Fluid Mech 140:63

Antonia RA, Ould-Rouis M, Zhu Y, Anselmet F (1997) Fourth-order moments of longitudinal- and transverse-velocity structure functions. Europhys Lett 37:85

Aref H (1983) Integrable, chaotic, and turbulent vortex motion in two-dimensional flows. Ann Rev Fluid Mech 15:345

Aref H (2007) Vortices and polynomials. Fluid Dyn Res 39:5

Arnold VI, Khesin BA (1999) Topological methods in hydrodynamics. Springer, Berlin

Aronson D, Löfdahl LL (1993) The plane wake of a cylinder. Measurements and inferences on the turbulence modelling. Phys Fluids A 5:1433

Benzi R, Ciliberto S, Baudet C, Chavarria GR, Tripiccione R (1993) Extended self-similarity in the dissipation range of fully-developed turbulence. Europhys Lett 24:275

Castaing B, Gagne Y, Hopfinger EJ (1990) Velocity probability density functions of high Reynolds number turbulence. Phys D 46:177

Data provided by Chabaud B, Chanal O, CNRS Gernoble, France

Chevillard L, Castaing B, Lévêque E, Arneodo A (2006) Unified multifractal description of velocity increments statistics in turbulence: intermittency and skewness. Phys D 218:77

Chorin AJ, Marsden GE (2000) A mathematical introduction to fluid mechanics. Springer, Berlin

Cuypers Y, Maurel A, Petitjeans P (2003) Vortex burst as a source of turbulence. Phys Rev Lett 91:194502

Darrigol O (2005) Worlds of flow. Oxford University Press, Oxford

Davidson PA (2004) Turbulence. Oxford University Press, Oxford

Davoudi J, Tabar MRR (1999) Theoretical Model for Kramers-Moyal's description of Turbulence Cascade. Phys Rev Lett 82:1680

Doering CR, Gibbon JD (1995) Applied analysis of the Navier-Stokes equations. Cambridge University Press, Cambridge

Eule S, Friedrich R (2005) A note on a random driven Burgers equation. Phys Lett A 351:238

Eyink GL, Sreenivasan KR (2006) Onsager and the theory of hydrodynamic turbulence. Rev Mod Phys 78:87

Falkovich G, Gawedzki K, Vergassola M (2001) Particles and fields in fluid turbulence. Rev Mod Phys 73:797

Foias C, Rosa R, Manley O, Temam R (2001) Navier-Stokes equation and turbulence. Cambridge University Press, Cambridge

Friedrich R (2003) Statistics of Lagrangian velocities in turbulent flows. Phys Rev Lett 90:084501

Friedrich R, Peinke J (1997a) Description of a turbulent cascade by a Fokker-Planck equation. Phys Rev Lett 78:863

Friedrich R, Peinke J (1997b) Statistical properties of a turbulent cascade. Phys D 102:147

Friedrich R, Zeller J, Peinke J (1998) A Note in Three Point Statistics of Velocity Increments in Turbulence. Europhys Lett 41:153

Friedrich R, Peinke J, Tabar MRR (2008) Importance of fluctuations: complexity in the view of stochastic processes within this issue. Springer, Berlin

Frisch U (1995) Turbulence. The legacy of Kolmogorov. Cambridge University Press, Cambridge

Fursikov AV (1999) The closure problem of the Friedmann-Keller infinite chain of moment equations, corresponding to the Navier-Stokes system. In: Gyr A, Kinzelbach W, Tsinober A (eds) Fundamental problematic issues in turbulence. Birkhäuser, Basel

Galanti B, Gibbon JD, Heritage M (1997) Vorticity alignment results for the three-dimensional Euler and Navier-Stokes equations. Nonlinearity 10:1675

Gilbert AD (1993) A cascade interpretation of Lundgrens stretched spiral vortex model for turbulent fine structure. Phys Fluids A5:2831

Grafke T, Homann H, Dreher J, Grauer R (2008) Numerical simulations of possible finite time singularities in the incompressible Euler equations: comparison of numerical methods. Phys D 237:1932

Grassi V, Leo R, Soliani G, Tempesta P (2000) Vortices and invariant surfaces generated by symmetries for the 3D Navier-Stokes equations. Physica A 286:79

Grauer R, Marliani C, Germaschewski K (1998) Adaptive mesh refinement for singular solutions of the incompressible Euler equations. Phys Rev Lett 84:4850

Gyr A, Kinzelbach W, Tsinober A (1999) Fundamental problematic issues in turbulence. Birkhäuser, Basel

Haken H (1983) Synergetics, an introduction. Springer, Berlin

Haken H (1987) Advanced synergetics. Springer, Berlin

Hamlington PE, Schumacher J, Dahm WJA (2008) Local and nonlocal strain rate fields and vorticity alignment in turbulent flows. Phys Rev E 77:026303

Hatakeyama N, Kambe T (1997) Statistical laws of random strained vortices in turbulence. Phys Rev Lett 79:1257

Hopf E (1957) Statistical hydromechanics and functional calculus. J Rat Mech Anal 1:87

Jimenez J, Wray AA, Saffman PG, Rogallo RS (1993) The structure of intense vorticity in isotropic turbulence. J Fluid Mech 255:65

Jovanovic J (2004) The statistical dynamics of turbulence. Springer, Berlin

Kirchhoff G (1883) Vorlesungen über mathematische Physik, vol 1, 3rd edn. Teubner, Leipzig

Kolmogorov AN (1941a) Dissipation of energy in locally isotropic turbulence. Dokl Akad Nauk SSSR 32:19

Kolmogorov AN (1941b) The local structure of turbulence in incompressible viscous fluid for very large Reynold's numbers. Dokl Akad Nauk SSSR 30:301

Kolmogorov AN (1962) A refinement of previous hypotheses concerning the local structure of turbulence in a viscous incompressible fluid at high Reynolds number. J Fluid Mech 13:82

L'vov V, Procaccia I Hydrodynamic turbulence: a 19th century problem with a challenge for the 21st Centurs. arXiv:chao-dyn 96006015

La Porta A, Voth G, Crawford AM, Alexander J, Bodenschatz E (2000) Fluid particle acceleration in fully developped turbulence. Nature 409:1017

La Porta A, Voth G, Moisy F, Bodenschatz E (2001) Using cavitation to measure statistics of low-pressure events in large Reynolds-number turbulence. Phys Fluids 12:1485

Landau L, Lifshitz EM (1981) Lehrbuch der Theoretischen Physik, Bd. 6, Hydrodynamik. Akademie, Berlin

Langner M, Peinke J, Rauh A Langevin analysis with application to a Rayleigh-Benard convection experiment. Int J Nonlinear Dyn Syst Chaos (in press)

Lesieur M (1997) Turbulence in fluids. Kluwer Academic Publishers, Dordrecht

Lesieur M, Yaglom A, David F (2000) New trends in turbulence, LesHouches Summer School. Springer, Berlin

Lück S, Renner C, Peinke J, Friedrich R (2006) The Markov-Einstein coherence length: a new meaning for the Taylor length in turbulence. Phys Lett A 359:335

Lundgren TS (1969) Distribution functions in the statistical theory of turbulence. Phys Fluids 10:969

Lundgren TS (1982) Strained spiral vortex model for turbulent fine structure. Phys Fluids 25:2193

Lundgren TS (1993) A small-scale turbulence model. Phys Fluids A5:1472

Manneville P (2004) Instabilities, chaos and turbulence. Imperial College Press, London

Marchioro C, Pulvirenti M (1984) Vortex methods in two-dimensional fluid dynamics. Lecture Notes in Physics, Springer, Berlin

Marcq P, Naert AA (2001) Langevin equation for turbulent velocity increments. Phys Fluids 13:2590

Martin PC, Siggia ED, Rose HA (1973) Statistical dynamics of classical systems. Phys Rev A8:423

McComb WD (1990) The physics of fluid turbulence. Clarendon Press, Oxford

Moffat HK, Kida S, Ohkitani K (1994) Stretched vortices-the sinews of turbulence. J Fluid Mech 259:231

Monin AS, Yaglom AM (1971) Statistical fluid mechanics: Mechanics of turbulence, vol 1. MIT Press, Cambridge, MA

Monin AS, Yaglom AM (1975) Statistical fluid mechanics: Mechanics of turbulence, vol 2. MIT Press, Cambridge, MA

Mordant N, Metz P, Michel O, Pinton J-F (2001) Measurement of Lagrangian velocity in fully developed turbulence. Phys Rev Lett 87:214501

Newton PK (2001) The N-Vortex problem. Springer, New York

Oberlack M (2000) Symmetrie, Invarianz und Selbstähnlichkeit in der Turbulenz. Shaker, Aachen

Oberlack M, Busse FH (2002) Theories of turbulence. Springer, Wien

Obukhov AM (1959) Description of turbulence in terms of Lagrangian variables. Adv Geophys 6:113

Onsager L (1949) Statistical hydrodynamics. Suppl Nuovo Cimento 6:279

Ott S, Mann J (2000) An experimental investigation of the relative diffusion of particle pairs in three- dimensional turbulent flow. J Fluid Mech 402:207

Ottino JM (1989) The kinematics of mixing: Stretching, chaos, and transport. Cambridge University Press, Cambridge

Piquet J (1999) Turbulent flows, models and physics. Springer, Berlin

Pope SB (1985) Lagrangian PDF methods for turbulent flows. Annu Rev Fluid Mech 26:23

Pope SB (1994) Pdf methods for turbulent reactive flows. Prog Energy Combust Sci 11:119

Pope SB (2000) Turbulent flows. Cambridge University Press, Cambridge

Renner C, Peinke J, Friedrich R (2001) Experimental indications for Markov properties of small scale turbulence. J Fluid Mech 433:383

Renner C, Peinke J, Friedrich R, Chanal O, Chabaud B (2002) Universality of small scale turbulence. Phys Rev Lett 89:124502

Reynolds O (1883) An experimental investigation of the circumstances which determine whether the motion of water shall be direct or sinuous and the law of resistance in parallel channels Phil Trans R Soc 174:935–982

Richardson LF (1926) Atmospheric diffusion shown on a distance-neighbour graph. Proc R Soc Lond A 110:709

Siefert M, Peinke J (2004) Different cascade speeds for longitudinal and transverse velocity increments of small-scale turbulence. Phys Rev E 70:015302R

Siefert M, Peinke J (2006) Joint multi-scale statistics of longitudinal and transversal increments in small-scale wake turbulence. J Turbul 7:1

Sreenivasan KR, Antonia RA (1997) The phenomenology of small-scale turbulence. Annu Rev Fluid Mech 29:435–472

Sturman R, Ottino JM, Wiggins S (2006) The mathematical foundations of mixing the linked twist map as a paradigm in applications: micro to macro, fluids to solids series: cambridge monographs on applied and computational mathematics (No. 22). Cambridge University Press

Taylor GI (1921) Diffusion by continuous movement. Proc Lond Math Soc Ser 20(2):196

Temam R (2007) Infinite dimensional dynamical systems in mechanics and physics. Springer, Heidelberg
Townsend AA (1951) On the fine structure of turbulence. Proc R Soc Lond A 208:534
Tutkun M, Mydlarski L (2004) Markovian properties of passive scalar increments in grid-generated turbulence. New J Phys 6:49
Ulinich FR, Ya Lyubimov B (1969) Statistical theory of turbulence of an incompressible fluid at large Reynolds numbers. Zh Exper Teor Fiz 55:951
Wilczek M, Jenko F, Friedrich R (2008) Lagrangian particle statistics in turbulent flows from a simple vortex model. Phys Rev E 77:056301
Calculation performed by Wilczek M (Münster)
Wyld HW (1961) Formulation of the theory of turbulence in incompressible fluids. Ann Phys 14:143
http://www.claymath.org/millenium/

Recent Advances in Quantum Chaos of Generic Systems

Wave Chaos of Mixed-Type Systems

Marko Robnik
CAMTP-Center for Applied Mathematics and Theoretical Physics, University of Maribor, Maribor, Slovenia

Article Outline

Introduction
Quantum Properties of Classically Integrable Systems
Quantum Chaos of Classically Fully Chaotic (Ergodic) Systems
Quantum Chaos of Classically Generic (Mixed-Type) Systems
The Billiard Systems and Poincaré-Husimi Functions
The Localization Measures
Discussion and Conclusions
References

Keywords

Nonlinear dynamics · Chaotic systems · Quantum chaos · Wave chaos · Spectral statistics · Generic Hamilton systems · Quantum localization

Introduction

This entry is based on the recent review paper by the author (Robnik 2016), and other recent papers with coworkers (Batistić and Robnik 2010, 2013a, b; Batistić et al. 2018). The first part is an introduction to quantum chaos from the stationary point of view, where we shall describe the purely regular eigenstates versus purely chaotic eigenstates. In the second part, we shall address the problem of the mixed-type phase space of generic systems, where regular and chaotic eigenstates coexist. They are reflecting the complex mixed-type structure of the corresponding classical phase space, where regular classical motion on invariant tori exists for certain initial conditions, while the motion is chaotic for the complementary initial conditions. The books by Stöckmann (1999) and Haake (2010) offer an excellent introduction to quantum chaos. Stöckmann's book contains also many experimental applications of quantum chaos, most notably on microwave experiments he has been performing since 1990 up to date, addressing and realizing practically all important questions of quantum chaos. Most of the subjects of this entry can be found in the reviews (Robnik 1998, 2015, 2016).

Quantum chaos is the study of phenomena in the quantum domain which correspond to the classical chaotic behavior. Thus, we study the solutions of the Schrödinger equation of a point particle in the potential $V(\mathbf{q})$,

$$i\hbar\frac{\partial\psi}{\partial t} = \widehat{H}\psi = -\frac{\hbar^2}{2m}\Delta\psi + V(\mathbf{q})\psi, \qquad (1)$$

where $h = 2\pi\hbar$ is the Planck constant, $\psi(\mathbf{q}, t)$ the wave function depending on the N-dimensional space coordinate vector $\mathbf{q}$ and on time t, m the mass of the point particle moving under the influence of the potential $V(\mathbf{q})$, and $\Delta = \partial^2/\partial\mathbf{q}^2$ the N-dimensional Laplace operator. For example, in the case $N = 2$, we have

$$\Delta = \frac{\partial^2}{\partial x^2} + \frac{\partial^2}{\partial y^2}. \qquad (2)$$

In fact, in the following, when dealing with specific model systems, we shall restrict ourselves mainly to $N = 2$.

We investigate the solutions of the Schrödinger equation and try to relate them to the corresponding classical dynamics, for which obviously the limiting behavior $\hbar \to 0$ is of prime interest. The methods and approximations

A. Hutt, H. Haken (eds.), *Synergetics*,
https://doi.org/10.1007/978-1-0716-0421-2_730

Originally published in
R. A. Meyers (ed.), *Encyclopedia of Complexity and Systems Science*, © Springer Science+Business Media LLC 2019
https://doi.org/10.1007/978-3-642-27737-5_730-1

used to find approximate solutions for small $\hbar$ are known under the name *semiclassical mechanics*, which offers an important bridge between the classical and quantum mechanics, and is presented in detail in Stöckmann (1999) and Haake (2010). We also might think of this approximation as short wavelength approximation, which is in general applicable to all wave systems and their solutions.

In this entry, we shall restrict ourselves to the purely binding potential $V(\mathbf{q})$, such that the classical motion of the particle is bounded (finite) for all initial conditions, and also quantally the particle cannot escape to infinity (no ionization threshold). The energy spectrum of the Hamilton operator $\widehat{H}$ (1) is purely discrete and countable infinite. An example of such Hamiltonian system is a classical billiard system, where a point particle is moving freely inside a potential box with hard walls, experiencing an elastic collision when hitting the boundary.

Classically, in Hamiltonian systems, we can have regular, stable, quasiperiodic motion on invariant tori, or irregular, unstable, chaotic motion. The latter one is characterized by the property of the sensitive dependence on initial conditions, which is quantified by the existence of the positive Lyapunov exponents. In this case, two nearby orbits in the classical phase space diverge exponentially with time $\propto \exp(\lambda t)$, and the relevant exponent λ is called the largest positive Lyapunov exponent. In the example of billiard systems, the shape of the boundary determines what kind of dynamics the system exhibits. In quantum mechanics, the concept of an orbit and trajectory does not exist due to the Heisenberg uncertainty principle, according to which the product of uncertainties of position x, Δx, and the corresponding momentum p_x, Δp_x, satisfy the rigorous inequality $\Delta x \Delta p_x \geq \hbar/2$. This implies that also the divergence of nearby trajectories cannot be defined. Indeed, any attempt to define some kind of meaningful quantum analogue of the *asymptotic* Lyapunov exponent λ fails in the sense that it is always zero. Therefore, in quantum mechanics, the sensitive dependence on initial conditions does not exist, and the time evolution of the wave function $\psi(t)$ as the solution of the time-dependent Schrödinger equation (1) is stable, almost periodic, and reversible: integration of the classical chaotic motion for times much larger than Lyapunov time $\tau = 1/\lambda$ is fundamentally irreversible once the accuracy of integration is exhausted, while the corresponding quantum evolution of the wave function is still reversible. For details see Haake (2010). Therefore, quantum chaos in the sense of positive Lyapunov exponents does not exist. In this sense, in the time evolution, the correspondence of the classical and quantum chaos does not exist.

However, there is another, stationary, aspect of classical dynamics in Hamiltonian systems, namely the structure of the phase space, the so-called phase portrait, where the phase space is decomposed into the invariant components (regions), each one containing a dense orbit. In the case of classical integrability, to be defined in detail in the next section, all orbits wind quasi-periodically on N-dimensional invariant tori (N is the number of the degrees of freedom, that is the dimension of the configuration space), and the entire phase space is foliated into the family of invariant tori. The torus is uniquely labeled by the value of N classical canonical actions $\mathbf{I}$, and the position on the torus is uniquely specified by the N canonically conjugate angles θ. Integrable systems are very special and rare, but important, as we can entirely describe them analytically, and also understand what happens (to the phase portrait) if we slightly perturb them, by using a variety of perturbation methods. The opposite extreme is complete chaos, ergodicity, where almost each orbit is chaotic, the set of exceptions having measure zero, and the orbits visit arbitrarily small neighborhoods of any other point in phase space infinitely many times, as time goes to infinity. Therefore, the phase average of functions and the time average are equal. The entire phase space is just one chaotic invariant component. In between there are the mixed-type systems with extremely complex structure of the phase portrait, where regular islands of stability on the invariant tori coexist with chaotic sea surrounding them and which exhibit an infinite hierarchy of statistically selfsimilar structures. It is the fundamental KAM theorem which describes the slightly perturbed Hamiltonian systems. It states that most of the

invariant tori survive a perturbation, namely they do still exist after the perturbation with the same N frequencies of the quasiperiodic motion but are typically slightly distorted. However, the rational tori are destroyed, and in place of them, we get an even number of periodic orbits, half of them stable and half of them unstable, surrounded by chaotic region (Poincaré-Birkhoff theorem).

The analogue of the structure of the classical phase portrait in the quantum mechanics is the structure of the eigenfunctions, of their corresponding *Wigner functions in the quantum phase space* to be defined below, and of the properties of the corresponding energy spectra. As we shall see, in this stationary picture there is a very well-defined and rich correspondence between the classical and quantum chaos: The quantum signatures of classical chaos, as the title of Haake's book (Haake 2010) goes, are very well defined.

To start with, quantally, we have to solve the Schrödinger equation (1) for the eigenstates with sharply defined eigenenergies E_n, where $\psi(\mathbf{q}, t) \propto \psi_n(\mathbf{q})$ exp $(-iE_nt/\hbar)$ and the corresponding eigenfunctions ψ_n are satisfying the boundary conditions, always requiring the normalizability of ψ_n, namely $\int|\psi_n(\mathbf{q})|^2 d^N\mathbf{q} < \infty$. In billiards, we usually require the Dirichlet boundary conditions, $\psi = 0$ on the boundary, but other possibilities, e.g., the Neumann boundary conditions of vanishing normal derivative of ψ_n, might be interesting, depending on the circumstances.

The eigenstates are defined as the normalizable eigenfunctions of the Hamilton operator $\widehat{H}$, namely $\widehat{H}\psi_n = E_n\psi_n$. Thus, we have to solve the stationary (time-independent) Schrödinger equation,

$$\frac{\hbar^2}{2m}\Delta\psi_n + (E_n - V(\mathbf{q}))\psi_n = 0. \qquad (3)$$

In the following sections, we shall deal with this task, to characterize different types of solutions ψ_n and the associated energy spectra E_n.

In closing the introduction, let us make it clear that the time-dependent and time-independent Schrödinger equations, (1) and (3), are just special cases of some wave equations. From the mathematical point of view, they can be equivalent or similar to some other wave equations of mathematical physics, such as the wave equations describing electromagnetic, acoustic, elastic, seismic waves, water surface waves, etc., where precisely the same questions can be addressed, and the same conclusions can be reached. For details, see the books by Stöckmann (1999) and Haake (2010). Therefore, the terminology *quantum chaos* is much too narrow, and instead, we should speak of *wave chaos*. Nevertheless, the name quantum chaos is generally well established, but we should be aware of the wide spectrum of wave phenomena that can occur in almost all wave systems. Of course, understanding the wave chaos is also closely related to the opposite effects of the spontaneous formation of ordered structure in certain wave systems such as reaction-diffusion systems. It is necessary to understand under what conditions order or chaos can emerge, which is the central question of Haken's fundamental work on synergetics (Haken 2004).

Quantum Properties of Classically Integrable Systems

Integrable Hamiltonian systems are extremely rare but important, as explained above. The total energy is conserved if their Hamilton function does not depend on time (autonomous system). They are characterized by the existence of invariant N-dimensional tori everywhere in the classical phase space. Examples are centrally symmetric potentials where the angular momentum is conserved. In the domain of two-dimensional billiard systems, we have only the rectangle and the elliptic billiard. In the former case, the absolute value of the momenta p_x and p_y are conserved, while in the elliptic billiard (Berry 1981), the product of the angular momenta with respect to the two foci is the conserved quantity. In the special case of the circle (zero excentricity), the angular momentum is conserved.

What can we say about such systems? Do their eigenfunctions have some special structure, along with their energy spectra? Let us for a moment concentrate on the two-dimensional billiard systems. The general Schrödinger equation, when

using appropriate units, reduces to the simple two-dimensional Helmholtz equation

$$\frac{\partial^2\psi}{\partial x^2}+\frac{\partial^2\psi}{\partial y^2}+E\psi=0, \tag{4}$$

where we have suppressed the index (quantum number(s)) n, and let us assume the Dirichlet boundary conditions $\psi = 0$ on the boundary. The answer to the above question is yes. In both billiards, the eigenfunctions have an ordered structure, and in both cases, the solutions can be easily found, thanks to the separability of the systems. For the rectangle with horizontal width a and the vertical width b, it is easy to find the solution given by $\psi_{m,n}(x,y) = C \sin\frac{\pi mx}{a} \sin\frac{\pi ny}{b}$, where the constant C is determined by the normalization. Here, m and n are the two quantum numbers (positive integers), associated with and labeling the given eigenfunction. Indeed, the nodal lines defined by the vanishing of $\psi(\mathbf{q}) = 0$ are the horizontal straight lines $y = jb/n = \text{const.}$, where $j = 0, 1, \ldots, n$, and the vertical lines $x = ja/m = \text{const.}$, with $j = 0, 1, \ldots, m$.

In the circle billiard, the nodal lines are defined by the zeros of the radial Bessel functions, which are circles, and by the zeros of the angular trigonometric function, which are polar rays, straight lines, emanating from the center of the circle. If we perturb the two billiards, and solve the Helmholtz equation (4), this structure becomes immediately destroyed by a generic perturbation breaking the separability and integrability of the system. In fully chaotic systems, the nodal structure becomes entirely random.

How about the energy spectra E of the integrable billiards, determined by solving (4)? They are characterized by two quantum numbers. In the rectangle billiard with horizontal width a and the vertical width b, we find using the above eigenfunctions

$$E_{m,n}=\pi^2\left(\frac{m^2}{a^2}+\frac{n^2}{b^2}\right), \tag{5}$$

where m, n are the two quantum numbers (positive integers). Although this energy spectrum is simple and explicit, its statistical properties are not so simple. As we shall see, the statistical properties of energy spectra are deeply related to the dynamical nature of the underlying Hamiltonian system. If the system is integrable, the statistics is the Poissonian and characteristic of entirely uncorrelated energy levels, while in the case of fully chaotic (ergodic) systems, the statistics of the random matrix theory applies. This is to be explained in details in the next section.

Before the statistical analysis is performed, we must prepare the grounds for comparison of quite different systems. In order to achieve that, we must *unfold the spectrum*, which by definition means transformation of the actual energy spectrum E_n to *the unfolded energy spectrum* e_n, such that the mean spacing $\Delta e = \langle (e_{n+1} - e_n) \rangle$ of e_n is equal to unity everywhere (for all e). This can be done if we know the mean energy level spacing $\Delta E = 1/\rho(E)$, or the energy level density $\rho(E)$. Then, the unfolding is simply $e_n = E_n/\Delta E = E_n\rho(E_n)$. The density of states is known by the Thomas-Fermi rule of filling the classical phase space inside the energy surface $E = H(\mathbf{q}, \mathbf{p}) = const.$ with the Planck cells of volume $(2\pi\hbar)^N$. Namely, the cumulative number $\mathcal{N}$ of the energy eigenvalues below the energy E is given by

$$\mathcal{N}(E)=\frac{1}{(2\pi\hbar)^N}\int_{H(\mathbf{q},\mathbf{p})\le E} d^N\mathbf{q}\, d^N\mathbf{p}. \tag{6}$$

Therefore,

$$\rho(E)=\frac{d\mathcal{N}}{dE}=\frac{1}{(2\pi\hbar)^N}\int\delta\big(E-H(\mathbf{q},\mathbf{p})\big)d^N\mathbf{q}\, d^N\mathbf{p}, \tag{7}$$

where $\delta(x)$ is the Dirac delta function. For two-dimensional billiards with units defined by (4), we can get more than that, namely

$$\mathcal{N}(E)=\frac{\mathcal{A}E}{4\pi}-\frac{\mathcal{L}\sqrt{E}}{4\pi}+c.c. \tag{8}$$

where $\mathcal{A}$ and $\mathcal{L}$ are the area and the circumference of the billiard, while $c.c.$ are some small constants

(curvature and corner corrections) which for large E are unimportant. The first term in (8) results directly from (6), while the second one is the so-called perimeter correction. Asymptotically when $E \to \infty$, the leading term is important and dominant, and is known also as the Weyl formula, as Weyl was the first to derive it.

With the energy spectrum being unfolded, we start the statistical analysis. Rather than defining all the correlation functions, we shall consider only two statistical measures. The first one is the gap probability $\mathcal{E}(S)$, which is the probability that on an interval of length S there is no level (of the unfolded spectrum). The second one is the level spacing distribution $P(S)$: The probability to have a level spacing within the interval $(S, S + dS)$ is equal to $P(S)dS$. It turns out that they are related through $P(S) = d^2\mathcal{E}(S)/dS^2$ (see Haake 2010).

For the irrational rectangular billiard (a and b are not rationally connected), we find the Poissonian statistics, namely

$$\mathcal{E}(S) = \exp(-S), \qquad P(S) = \exp(-S). \tag{9}$$

There is no parameter involved in this formula, which is a hint that something similar should be observed in other integrable systems, like the elliptic billiard, of which the circle billiard is a special case. Indeed, this is the case, and we speak of *the universality class of the Poissonian spectral statistics of integrable systems*. There are some subleties around this problem, regarding the asymptotic behavior with increasing energy E, which were studied in Robnik and Veble (1998), but the major conclusion about the validity of the Poissonian statistics is confirmed. Intuitively, it is easy to understand: If a quantum energy spectrum is characterized by two or more quantum numbers, we will have generically a statistically independent superposition of infinitely many discrete number sequences. Independent of the properties of the individual number sequence, such a superposition always results in a Poissonian sequence.

In the general case of an N-dimensional classically integrable system defined by the Hamilton function $H(\mathbf{q}, \mathbf{p})$, we can perform the construction of such N quantum numbers in terms of the action-angle variables $(\mathbf{I}, \theta)$. In the semiclassical limit of small $\hbar$, the so-called EBK quantization (torus quantization) is based on the quantization of the classical actions $\mathbf{I}$. It is called after Einstein, Brillouin, and Keller. The phase space has $2N$ dimensions, the energy surface $E = H(\mathbf{q}, \mathbf{p}) = const.$ has $2N - 1$ dimensions, and by definition we have N integrals of motion $A_j, j = 1, \ldots, N$, of which A_1 is by convention the Hamilton function, the energy $E = H$. Then, the N-dimensional invariant surfaces labeled by $\mathbf{A}$ have the topology of N-dimensional tori. The actions – the generalized momenta – are defined by the N circuit integrals on a torus labeled by $\mathbf{A}$ or $\mathbf{I}$,

$$I_j = \frac{1}{2\pi}\oint_{C_j} \mathbf{p} \cdot d\mathbf{q} \tag{10}$$

The canonically conjugate angle variables θ_j are defined by using the action integral as a generating function of the underlying canonical transformation. For details, see, e.g., the references (Arnold 1980; Ott 1993). The Hamilton function $H(\mathbf{q}, \mathbf{p})$ becomes only a function of A_j values, and of $\mathbf{I}$, namely after inverting $A_j = A_j(I_k)$, it is a function of the actions alone, $A_1(\mathbf{q}, \mathbf{p}) = H(\mathbf{q}, \mathbf{p}) = H(\mathbf{I})$. We say that the angles θ_j are cyclic variables.

For sufficiently small $\hbar$, we obtain the so-called semiclassical torus quantization, or EBK quantization, because we quantize the actions of the tori,

$$\mathbf{I}_\mathbf{m} = \left(\mathbf{m} + \frac{\alpha}{4}\right)\hbar, \tag{11}$$

where $\mathbf{m}$ is an N-dimensional vector of nonnegative integers, and $\alpha = \alpha_1, \alpha_2, \ldots, \alpha_N$ are Maslov indices. The indices $\alpha_j, j = 1, 2, \ldots, N$ count the number of caustics (singularities of the wave function in configuration space) encountered in the configuration space while traversing round the fundamental circuit C_j. Thus, α_j depends on how the invariant torus lies in the phase space and on the structure of its projection singularities in the configuration space. The energy eigenvalues are then equal to the value of the Hamilton function at the quantized actions (11),

$$E_\mathbf{m} = H(\mathbf{I}_\mathbf{m}) = H\left(\left(\mathbf{m} + \frac{\alpha}{4}\right)\hbar\right). \tag{12}$$

The formula (12) with (11) is basically the higher dimensional generalization of the one-

dimensional semiclassical quantization, taking into account also the Maslov corrections, which Einstein, Brillouin, and Keller were not aware of. It is an approximate solution at small $\hbar$ of the Schrödinger eigenvalue problem (3). For further details, see Stöckmann (1999).

Now we can explain the origin of the Poissonian statistics for the quantal energy spectra of classically integrable systems: Having N quantum numbers $\mathbf{m} = (m_1, m_2, \ldots, m_N)$ means generically (in almost all cases, such where no pathological rationalities occur) statistical independent superposition of infinitely many level sequences, and this must result in a Poissonian sequence, unless there are some special and nongeneric rational relationships or correlations between the individual level sequences. For some discussions, see Robnik and Veble (1998), especially regarding the role of rational relationships in rectangle billiard.

Quantum Chaos of Classically Fully Chaotic (Ergodic) Systems

We now turn to the other extreme case of fully chaotic, ergodic systems. An example of fully chaotic ergodic motion with a positive Lyapunov exponent is the motion of a point particle in the well-known stadium billiard, defined as a rectangle with two semicircles on the two opposite sides, as introduced by Bunimovich (1974). Let us assume that the radius of the two semicircles is unity, while the width of the rectangle between them is ε. The billiard system is ergodic and chaotic at any nonzero value of ε, but the typical time for a chaotic trajectory to fill the entire phase space depends strongly on ε. The details of the diffusion-like motion have been recently studied by Lozej and Robnik (2018) and its consequences for quantum chaos in reference (Batistić et al. 2018). If $\varepsilon = 1$ this time, called diffusion time, or transport time t_T, is of order unity, while for very small ε it becomes very large. Thus, an initial small blob of initial conditions spreads diffusively very quickly in the classical phase space when $\varepsilon = 1$, while for small ε, t_T can become very large. As we shall see, this important time scale has to be compared with the important quantum time scale called *Heisenberg time* (or *break time*), defined by $t_H = 2\pi\hbar/\Delta E$, where ΔE is the mean energy level spacing of the corresponding quantum system $\Delta E = 1/\rho(E)$ determined by the Thomas-Fermi rule (7). Namely, empirically it is very well observed that the quantum diffusion follows the classical diffusion only up to the Heisenberg time (also called break time), and stops then due to the localization, which is a consequence of the destructive interference effects, and is called *dynamical localization* or *quantum localization*, first observed by Chirikov, Casati, Izrailev, and Ford in 1979 (Casati et al. 1979) in the context of time-periodic (Floquet) systems (quantum kicked rotator). If the semiclassical condition is satisfied that the Heisenberg time is larger than all important classical diffusion times in the given system, then we find the universal statistical behavior of the wave functions and of the energy spectra. Let us recall that according to Eq. (7) $\Delta E \propto (2\pi\hbar)^N$, and therefore as $\hbar \to 0$, for $N \geq 2$, t_H will eventually become larger than any t_T, the latter one being $\hbar$-independent. Thus, at some sufficiently small $\hbar$, in the ultimate semiclassical limit, the quantum localization effects disappear and we can expect the universality to be described in the following.

In contrast to the integrable billiard systems exemplified by the rectangle and the circle, the nodal lines of the stadium billiard with $\varepsilon = 1$ are entirely irregular, as found already by McDonald and Kaufman (1979). In fact, it has been proposed by Berry (1977) that the wave functions of classically fully chaotic billiards is a Gaussian random function, that is the probability amplitude $\psi_n(x, y)$ has a Gaussian distribution, and this has been widely confirmed (see Li and Robnik 1994). This indicates that we can expect again some kind of universal behavior. Regarding the unfolded energy spectrum of this billiard system, it has been shown by Bohigas, Giannoni, and Schmit in 1984 (Bohigas et al. 1984) that the level spacing distribution $P(S)$ is quite different from the Poissonian, and is approximately but

well described by the Wigner distribution (also called Wigner surmise) given by

$$P_W(S) = \frac{\pi S}{2} \exp\left(-\frac{\pi S^2}{4}\right), \qquad (13)$$

while the corresponding gap probability is

$$\mathcal{E}_W(S) = 1 - \mathrm{erf}\left(\frac{\sqrt{\pi}S}{2}\right) = \mathrm{erfc}\left(\frac{\sqrt{\pi}S}{2}\right) \qquad (14)$$

The important feature is the linear behavior of $P(S)$ at small S, starting from zero, meaning that the levels tend to be away from a degeneracy, and we speak of level repulsion phenomenon, in this case the linear level repulsion. This must be seen in the contradistinction to the Poissonian $P(S) = e^{-S}$, where the level repulsion is absent and the degeneracies are quite likely. Bohigas, Giannoni and Schmit went on, after numerical exploration of other fully chaotic ergodic billiards with short t_T, e.g., the Sinai billiard, by proposing what is now known as *Bohigas-Giannoni-Schmit (BGS) Conjecture*, namely that the statistical properties of the energy spectra of classically fully chaotic and ergodic systems are described by the random matrix theory (RMT), which is one of the fundamental cornerstones of quantum chaos. Some preliminary ideas were published already by Percival (1973), and in particular by Casati, Valz-Gris, and Guarneri (1980).

It has been widely numerically confirmed that the conjecture is correct, and the theoretical foundation has been laid down in the seminal paper by Berry in 1985 (Berry 1985). He has shown, using the semiclassical methods developed by Gutzwiller in a series of papers in late 1960s and early 1970s (Gutzwiller 1967), that the spectral autocorrelation function and its Fourier transform, the so-called spectral form factor, for small times indeed agree with the RMT. The subject is very difficult, and there was practically no theoretical progress until 2001, when Sieber and Richter (2001) extended Berry's work to the next order in power expansion for short times of the form factor. This line of research finally culminated in a series of papers starting in 2006 by Haake and his group (Haake 2010; Müller et al. 2009), who succeeded to show that the semiclassical form factor agrees with the RMT to all orders at least up to the Heisenberg time t_H, and beyond (very recently). Therefore, BGS Conjecture is proven and it is no longer a conjecture but a theorem. The mentioned method of Gutzwiller rests upon the semiclassical calculation of the quantum energy spectral density expressed in terms of a series expansion consisting of contributions stemming from classical periodic orbits. The so-called Gutzwiller trace formula is the stationary phase approximation of the relevant Feynman path integral, used to calculate the Green function. For an excellent introduction, see the book by Stöckmann (1999).

The RMT has been introduced and developed mainly by Wigner, Dyson, Mehta (Haake 2010; Mehta 1991), and others to describe statistical properties of the energy spectra of heavy complex nuclei. The main question is what are the statistical properties of the eigenvalues of appropriate ensembles of random matrices, that is matrices with random matrix elements each having a certain probability distribution. It was expected that a large complexity of the physical system results in some randomness. Therefore, it was a surprise that it applies also to low-dimensional dynamical systems, such as only two-degrees-of-freedom billiards, provided that they are fully chaotic (ergodic) and that the semiclassical condition $t_H > t_T$ is satisfied. The idea is that if we do not know the details of a complex system, and look at the representation of its Hamilton operator in some basis of the Hilbert space, the matrix elements will appear as random variables.

Due to the lack of space, we cannot go into the details of the RMT, and therefore touch only upon the main idea. RMT starts by assuming the Gaussian random distribution of the matrix elements, which are statistically independent of each other, and the distribution is invariant against the transformations that preserve the symmetry of the Hamilton matrices of the ensemble. In the case of real symmetric Hamilton matrices, the transformations are orthogonal transformations, and the ensemble of such random matrices is called Gaussian Orthogonal Ensemble (GOE). If H are complex Hermitian matrices, the group of symmetry preserving transformations are the unitary transformations, and the ensemble is called Gaussian Unitary Ensemble

(GUE). The central question, among others, is what are the statistical properties of the eigenvalues of such random matrix ensembles.

Rather than going into the full generality, we consider the case of just two-dimensional Gaussian random matrix ensembles, and derive the level spacing distribution for them.

Quite generally, for a Hermitian matrix

$$\begin{pmatrix} x & y+iz \\ y-iz & -x \end{pmatrix},$$

with x, y, z real, and $i^2 = -1$, the two eigenvalues are $\lambda = \pm\sqrt{x^2+y^2+z^2}$ and the level spacing is $S = \lambda_1 - \lambda_2 = 2\sqrt{x^2+y^2+z^2}$. Let us now assume that x, y, z have so far general distributions $g_x(x)$, $g_y(y)$, $g_z(z)$, correspondingly. The level spacing distribution is then

$$P(S) = \int_{R^3} dx\, dy\, dz\, g_x(x) g_y(y) g_z(z) \delta\left(S - 2\sqrt{x^2+y^2+z^2}\right). \tag{15}$$

The 2D GUE is obtained if we assume $g_x(u) = g_y(u) = g_z(u) = \frac{1}{\sigma\sqrt{\pi}} \exp\left(-\frac{u^2}{\sigma^2}\right)$, where we perform the necessary normalization $<S> = 1$, which fixes the σ. Using the spherical coordinates $r = \sqrt{x^2+y^2+z^2}$ and φ, θ, we can perform the integration, followed by the normalization $<S> = 1$, yielding 2D GUE formula

$$P(S) = \frac{32S^2}{\pi^2} \exp\left(-\frac{4S^2}{\pi}\right), \tag{16}$$

with quadratic level repulsion.

On the other hand, if we restrict the ensemble to the real symmetric class, where we must take $g_z(u) = \delta(u)$ while g_x and g_y remain unchanged Gaussian, and using the polar coordinates $r = \sqrt{x^2+y^2}$ and φ, we obtain the 2D GOE formula $P(S) = \frac{\pi S}{2} \exp\left(-\frac{\pi S^2}{4}\right)$, with the linear level repulsion, and indeed the result is identical to $P_W(S)$ from eq. (13).

One should be aware of the fact that there is a clear cut criterion for the GOE or GUE case: If in the system there exists an antiunitary symmetry exemplified by – but not limited to – the time reversal symmetry, then there exists a large and nontrivial basis in the Hilbert space where the representation of the Hamilton operator (matrix) is real symmetric, and GOE statistics applies. If there is no antiunitary symmetry, the system is a general complex Hermitian and the statistics is GUE (Mehta 1991; Robnik and Berry 1986; Robnik 1986).

Note that in both cases of the RMT, like in the Poissonian case of classical integrability, **there is no free parameter: Universality**. Thus, we speak of universality classes of spectral statistics. Hackenbroich and Weidenmüller (1995) have shown that the result applies also to a very large class of other random matrix ensembles, provided the limiting distribution of the eigenvalues is smooth and confined to a finite interval, which are quite mild conditions, thus showing that the universality classes are very robust. This has been numerically verified for a number of various non-Gaussian ensembles (Robnik et al. 2010). One elementary indication for the robustness of the linear level repulsion is demonstrated (Grossmann and Robnik 2007; Robnik et al. 2010) by using (15), assuming $g_z(u) = \delta(u)$, and for general g_x, g_y, using the polar coordinates for the integration over the (x, y) plane, we find:

$$P(S) = \frac{S}{4} \int_0^{2\pi} g_x\left(\frac{S}{2}\cos\varphi\right) g_y\left(\frac{S}{2}\sin\varphi\right) d\varphi, \tag{17}$$

and consequently for small S we obtain

$$P(S) = \frac{\pi S}{2} g_x(0) g_y(0), \tag{18}$$

showing, that if g_x, g_y at $x = 0$ and $y = 0$ are finite and nonzero, the level repulsion will be always linear, independent of the details of $g_x(x)$, $g_y(y)$. Indeed, for the Gaussian case, where the normalization $<S> = 1$ yields $\sigma = 1/\sqrt{\pi}$, we have $g_x(0) = g_y(0) = 1$ and see at once $P(S) = \pi S/2$ for small S, in agreement with (13). The result is easily generalized for the GUE case by using the general $g_z(z)$, deriving the quadratic level repulsion, and reproducing (16) for small S in the special case of Gaussian g_x, g_y, g_z.

Quantum Chaos of Classically Generic (Mixed-Type) Systems

Classically integrable and fully chaotic (ergodic) systems are exceptional. Typical – generic – classical Hamiltonian systems are of the mixed type,

with divided phase space. Typically they have extremely complex structure, with rare exceptions such as the mushroom billiards introduced by Bunimovich, where we have exactly one rigorously integrable (regular) component, and exactly one ergodic chaotic component.

In the general generic case, the regular regions consisting of N-dimensional invariant tori coexist in the phase space with chaotic regions. Typically there is an infinite hierarchy of statistically selfsimilar structure consisting of islands of stability surrounded by the chaotic sea, which by itself might comprise several disconnected invariant chaotic components. The phase portrait has a very rich structure and is difficult to describe in detail. The quantum mechanics of such systems is also difficult. In the semiclassical limit $\hbar \to 0$, the quantum mechanics of the stationary Schrödinger equation must somehow tend to the classical mechanics. It was the idea of Percival in 1973 (Percival 1973) who was the first to suggest, qualitatively, that one should distinguish between the *regular eigenstates* and the *chaotic eigenstates* (he called them irregular). However, the question is: *How*? It is rather obvious that we must introduce some kind of *the quantum phase space*, where the quantum structures can be compared with the classical ones. This can be achieved by introducing the Wigner functions of the quantum eigenstates.

Quantum Phase Space: The Wigner Functions

The Wigner functions of eigenstates, based on the stationary orthonormal wave functions $\psi_n(\mathbf{q})$ in configuration space, are defined in the *quantum phase space* $(\mathbf{q}, \mathbf{p})$ as follows:

$$W_n(\mathbf{q},\mathbf{p}) = \frac{1}{(2\pi\hbar)^N} \int d^N\mathbf{X} \exp\left(-\frac{i}{\hbar}\mathbf{p}.\mathbf{X}\right)\psi_n\left(\mathbf{q}-\frac{\mathbf{X}}{2}\right)\psi_n^*\left(\mathbf{q}+\frac{\mathbf{X}}{2}\right). \tag{19}$$

As one can easily see, they are real valued but **not positive definite**, and possess the following properties:

$(P1)$ $\int W_n(\mathbf{q}, \mathbf{p})d^N\mathbf{p} = |\psi_n(\mathbf{q})|^2$ (= probability density in configuration space)

$(P2)$ $\int W_n(\mathbf{q}, \mathbf{p})d^N\mathbf{q} = |\phi_n(\mathbf{p})|^2$ (= probability density in momentum space)

$(P3)$ $\int W_n(\mathbf{q}, \mathbf{p})d^N\mathbf{q}\ d^N\mathbf{p} = 1$ (normalization)

$(P4)$ $(2\pi\hbar)^N \int d^N\mathbf{q}\ d^N\mathbf{p} W_n(\mathbf{q}, \mathbf{p})W_m(\mathbf{q}, \mathbf{p}) = \delta_{nm}$ (orthogonality)

$(P5)$ $|W_n(\mathbf{q}, \mathbf{p})| \leq \frac{1}{(\pi\hbar)^N}$ (no singularities; Cauchy-Schwartz inequality)

$(P6 = P4)$ $\int W_n^2(\mathbf{q},\mathbf{p})d^N\mathbf{q}\ d^N\mathbf{p} = \frac{1}{(2\pi\hbar)^N}$ (divergence in the limit $\hbar \to 0$)

$(P7)$ $\hbar \to 0:\ W_n(\mathbf{q},\mathbf{p}) \to (2\pi\hbar)^N W_n^2(\mathbf{q},\mathbf{p}) > 0$ (positivity in the limit $\hbar \to 0$)

From this, one can conclude that in the semiclassical limit $\hbar \to 0$ the Wigner function becomes predominantly positive definite, that it is supported in a volume cell of size $(2\pi\hbar)^N$, and thus *condenses* in such a cell, and since the Wigner functions are orthogonal, they must "live" in disjoint supports and therefore become statistically independent of each other. The question is, what is the geometry/structure of such a cell.

Principle of Uniform Semiclassical Condensation (PUSC) of Wigner Functions of Eigenstates

The Principle of Uniform Semiclassical Condensation (PUSC) of Wigner functions of eigenstates, based on the papers by Percival (1973), Berry (1977), Shnirelman (1974), Voros (1979), Robnik (1998), and Veble, Robnik, and Liu (1999), states that the Wigner function $W_n(\mathbf{q}, \mathbf{p})$ condenses uniformly on a classical invariant component in the classical phase space, when $\hbar \to 0$ and if $t_H > t_T$. This can be an N-dimensional invariant torus, a chaotic component, or the entire energy surface in the case of classical ergodicity:

(C1) Invariant N-torus (integrable or KAM):

$$W_n(\mathbf{q},\mathbf{p}) = \frac{1}{(2\pi)^N}\delta(\mathbf{I}(q,p) - \mathbf{I}_n). \tag{20}$$

(C2) Uniform on topologically transitive (indecomposable invariant) chaotic region:

$$W_n(\mathbf{q},\mathbf{p}) = \frac{\delta(E_n - H(\mathbf{q},\mathbf{p}))\ \chi_\omega(\mathbf{q},\mathbf{p})}{\int d^N\mathbf{q}\ d^N\mathbf{p}\ \delta(E_n - H(\mathbf{q},\mathbf{p}))\ \chi_\omega(\mathbf{q},\mathbf{p})} \tag{21}$$

where $\chi_\omega(\mathbf{q}, \mathbf{p})$ is the characteristic function on the chaotic component indexed by ω

(C3) Ergodicity (microcanonical Wigner function):

$$W_n(\mathbf{q},\mathbf{p}) = \frac{\delta(E_n - H(\mathbf{q},\mathbf{p}))}{\int d^N\mathbf{q}\ d^N\mathbf{p}\ \delta(E_n - H(\mathbf{q},\mathbf{p})} \quad (22)$$

Here we also introduce the notation μ for the relative Liouville measure of the relevant classical invariant component indexed by ω:

$$\mu(\omega) = \frac{\int d^N\mathbf{q}\ d^N\mathbf{p}\ \delta(E_n - H(\mathbf{q},\mathbf{p}))\ \chi_\omega(\mathbf{q},\mathbf{p})}{\int d^N\mathbf{q}\ d^N\mathbf{p}\ \delta(E_n - H(\mathbf{q},\mathbf{p}))} \quad (23)$$

This principle turns out to have a great predictive power, as demonstrated and used, e.g., in Veble et al. (1999). However, it must be kept in mind that the condition for the uniformity of this semiclassical limit of chaotic states is the fulfillment of the semiclassical condition about the time scales: The Heisenberg time t_H must be larger than all relevant classical transport time scales t_T.

Spectral Statistics in the Mixed-Type Phase Space

From the PUSC it follows that in the semiclassical limit, the eigenstates can be clearly classified as regular and chaotic, just according to the criterion whether they overlap with an invariant N-dimensional torus or with a chaotic region. Using this criterion, one can separate the regular and chaotic eigenstates and perform the statistical analysis separately for each of them. Due to the nonoverlapping supports of the Wigner functions, they become statistically independent of each other. Therefore, also the corresponding energy level sequences become classified as regular and chaotic, where the regular ones obey the Poissonian statistics and the chaotic ones obey the RMT statistics, provided the semiclassical condition (of time scales) is satisfied. Then, the total spectrum can be represented as a statistically independent superposition of regular and chaotic level sequences. The regular ones can be lumped together in a single Poissonian sequence, simply because a statistically random superposition of Poissonian level sequences is a Poisson sequence again, while the chaotic sequences must be treated one by one, each of them associated with its relevant supporting classical chaotic region. In such a case, it becomes obvious that the gap probability $\mathcal{E}(S)$ factorizes: The probability of having no level on interval of length S is the product of probability of having no level of the regular type, times probability of having no level of the chaotic types. In the special case of just one chaotic sequence with the approximate gap probability $\mathcal{E}_W(S) = \mathrm{erfc}\left(\frac{\sqrt{\pi}S}{2}\right)$ and one Poissonian sequence with the gap probability $\mathcal{E}_P(S) = \exp(-S)$, we obtain

$$\begin{aligned}\mathcal{E}(S) &= \mathcal{E}_P(\mu_1 S)\ \ \mathcal{E}_W(\mu_2 S) \\ &= \exp(-\mu_1 S)\quad \mathrm{erfc}\left(\frac{\sqrt{\pi}\mu_2 S}{2}\right).\end{aligned} \quad (24)$$

Here μ_1 is the relative fraction of the phase space volume of the classical regular regions in the classical phase space, while $\mu_2 = 1 - \mu_1$ is the complementary relative Liouville measure of the chaotic component. Also, μ_1 is the mean relative density of the regular energy levels, while μ_2 is the mean relative density of the chaotic levels. Since the general relationship $P(S) = d^2\mathcal{E}(S)/dS^2$ applies, we derive at once the so-called Berry-Robnik level spacing distribution (Berry and Robnik 1984)

$$\begin{aligned}P_{BR}(S) = e^{-\mu_1 S}e^{-\frac{\pi\mu_2^2 S^2}{4}}\left(2\mu_1\mu_2 + \frac{\pi\mu_2^3 S}{2}\right) \\ + e^{-\mu_1 S}\mu_1^2\mathrm{erfc}\left(\frac{\sqrt{\pi}\mu_2 S}{2}\right).\end{aligned} \quad (25)$$

Of course, this probability distribution is normalized $<1> = 1$, and has the normalized first moment $<S> = 1$. It has been tested in many various billiard systems, and in order to see it, since the semiclassical condition (of the time scales) must be satisfied, it is very often necessary to reach the high-lying levels. Most notable confirmation has been achieved by Prosen and Robnik (1994, 1999), 10–15 years after its derivation. The generalization to many chaotic components is quite straightforward (Robnik 1998; Berry and Robnik 1984).

Dynamical Localization of the Chaotic Eigenstates

If the semiclassical condition of time scales $t_H > t_T$ is not satisfied, the Wigner functions of chaotic eigenstates do not spread out uniformly over the relevant

classical chaotic component, but are localized, which means that their effective support is smaller than the classically available chaotic region. For example, this is observed in the stadium billiard if ε is sufficiently small. It has been shown empirically quite recently (Batistić and Robnik 2010, 2013a, b; Batistić et al. 2013, 2018) that the aspects of dynamical localization in time-independent systems are quite analogous to the dynamical localization phenomena in time-dependent Floquet systems, specifically in quantum kicked rotator (Manos and Robnik 2013). Below we shall show examples of localized chaotic states.

If we neglect the tunneling effects (which couple regular and chaotic levels, breaking the statistical independence assumption), which we can do at high energies (small effective $\hbar$, because tunneling effects decrease exponentially with effective $1/\hbar$), but treat the dynamical localization effects, we observe empirically (Batistić and Robnik 2010, 2013a, b; Batistić et al. 2018; Prosen and Robnik 1994) that the level spacing distribution of the localized chaotic eigenstates is very well captured by the Brody distribution

$$P_B(S) = C_1 S^\beta \exp\left(-C_2 S^{\beta+1}\right), \qquad (26)$$

where the two parameters C_1 and C_2 are determined by the two normalizations $<1> = <S> = 1$, and the corresponding gap probability is

$$E_B(S) = \frac{1}{\alpha(\beta+1)} Q\left(\frac{1}{\beta+1}, (\alpha S)^{\beta+1}\right) \qquad (27)$$

where $\alpha = \Gamma\left(\frac{\beta+2}{\beta+1}\right)$ and $Q(a, x)$ is the incomplete Gamma function

$$Q(a,x) = \int_x^\infty t^{a-1} e^{-t} dt. \qquad (28)$$

Here the only parameter is β, the level repulsion exponent in (26), which measures the degree of localization of the chaotic eigenstates: if the localization is maximally strong, the eigenstates practically do not overlap in the phase space (of the Wigner functions) and we find $\beta = 0$ and Poissonian distribution, while in the case of maximal extendedness (no localization), we have $\beta = 1$, and the RMT statistics of levels applies. Thus, by replacing $E_W(S)$ with $E_B(S)$, we get the BRB (Berry-Robnik-Brody) distribution, which generalizes the Berry-Robnik distribution such that the localization effects are included (Batistić and Robnik 2010).

The Billiard Systems and Poincaré-Husimi Functions

Having established the formalism of Wigner functions as a kind of the quantum phase space, we now wish to actually look at the Wigner functions in mixed-type quantum systems, in order to separate the regular and the chaotic ones, by simply looking at whether the given eigenstate $W_n(\mathbf{q}, \mathbf{p})$ overlaps with a classical regular or classical chaotic region. Furthermore, the question arises whether the chaotic Wigner function is localized or extended on the classical chaotic component. The method and approach is general, but technically difficult to implement in general. Therefore, we have to choose some representative model system. The billiard systems are most suitable for such studies.

For a 2D billiard, the most natural coordinates in the phase space (s, p) are the arclength s round the billiard boundary, $s \in [0, \mathcal{L}]$, where $\mathcal{L}$ is the circumference, and the sine of the reflection angle, which is the component of the unit velocity vector tangent to the boundary at the collision point, equal to p, which is the canonically conjugate momentum to s. These are the Poincaré-Birkhoff coordinates. The bounce map $(s_1, p_1) \to (s_2, p_2)$ is area preserving (Berry 1981), and the phase portrait does not depend on the speed (or energy) of the particle. Quantum mechanically we have to solve the stationary Schrödinger equation, which in a billiard is just the Helmholtz equation $\Delta\psi + k^2\psi = 0$ with the Dirichlet boundary conditions $\psi|_{\partial\mathcal{B}} = 0$. The energy is $E = k^2$. The important quantity is the boundary function

$$u(s) = \mathbf{n} \cdot \nabla_{\mathbf{r}} \psi(\mathbf{r}(s)), \qquad (29)$$

which is the normal derivative of the wavefunction ψ at the point s ($\mathbf{n}$ is the outward unit normal vector). It satisfies the integral equation

$$u(s) = -2\oint dt\ u(t)\ \mathbf{n}\cdot\nabla_{\mathbf{r}}G(\mathbf{r},\mathbf{r}(t)), \qquad (30)$$

where $G(\mathbf{r},\mathbf{r}') = -\frac{i}{4}H_0^{(1)}(k|\mathbf{r}-\mathbf{r}'|)$ is the Green function in terms of the Hankel function $H_0(x)$. It is important to realize that boundary function $u(s)$ contains complete information about the wavefunction at any point $\mathbf{q}$ inside the billiard by the equation

$$\psi_j(\mathbf{r}) = -\oint dt\ u_j(t)\ G(\mathbf{r},\mathbf{r}(t)). \qquad (31)$$

Now we go over to the quantum phase space. We can calculate the Wigner functions based on $\psi_n(\mathbf{r})$ and perform the procedure developed in the previous section. However, in billiards, it is advantageous to calculate the Poincaré-Husimi functions. The Husimi functions are generally just Gaussian smoothed Wigner functions. Such smoothing makes them positive definite, so that we can treat them somehow as quasi-probability densities in the quantum phase space, and at the same time we eliminate the small oscillations of the Wigner functions around the zero level, which do not carry any significant physical contents, but just obscure the picture. Thus, following Tualle and Voros (1995) and Bäcker et al. (2004), we introduce (Batistić and Robnik 2013a) the properly $\mathcal{L}$-periodized coherent states centered at (q, p), as follows

$$c_{(q,p),k}(s) = \sum_{m\in\mathbf{Z}} \exp\{ikp(s-q+m\mathcal{L})\} \exp\left(-\frac{k}{2}(s-q+m\mathcal{L})^2\right). \qquad (32)$$

The Poincaré-Husimi function is then defined as the absolute square of the projection of the boundary function $u(s)$ onto the coherent state, namely

$$H_j(q,p) = \left|\int_{\partial\mathcal{B}} c_{(q,p),k_j}(s)\ u_j(s)\ ds\right|^2. \qquad (33)$$

In Fig. 1, we show examples of a regular and of a chaotic eigenstate for the billiard introduced in (Robnik 1983, 1984) with $\lambda = 0.15$.

Now the classification of eigenstates can be performed by their projection onto the classical surface of section. As we are very deep in the semiclassical regime, we do expect with probability one that either an eigenstate is regular or chaotic, with exceptions having measure zero, ideally. To automate this task, we have ascribed to each point on the grid a number $A_{i,j}$ whose value is either +1 if the grid point lies within the classical chaotic region or −1 if it belongs to a classical regular region. Technically, this has been done as follows. We have taken an initial condition in the chaotic region, and iterated it up to about 10^{10} collisions, enough for the convergence (within certain very small distance). Each visited cell (i, j) on the grid has then been assigned value $A_{i,j} = +1$, the remaining ones were assigned the value −1.

The Poincaré-Husimi function $H(q, p)$ (33) (normalized) was calculated on the grid points and the overlap index M was calculated according to the definition $M = \sum_{i,j} H_{i,j}\ A_{i,j}$. In practice, M is not exactly +1 or −1, but can have a value in between. There are two reasons: the finite discretization of the phase space (the finite size grid), and the finite wavelength (not sufficiently small effective Planck constant, for which we can take just $1/k_j$). If so, the question is,

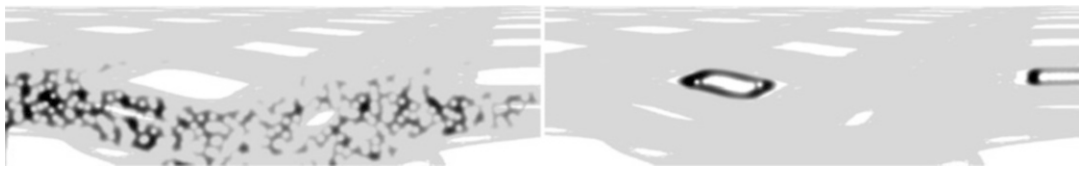

Recent Advances in Quantum Chaos of Generic Systems, Fig. 1 Examples of a chaotic (left) and a regular (right) state in the Poincaré-Husimi representation. k_j (M) are: chaotic: k_j (M) = 2000.0181794 (0.981); regular: k_j (M) = 2000.0777155 (−0.821). The gray background is the classically chaotic invariant component. We show only one quarter of the surface of section $(s, p) \in [0, \mathcal{L}/2] \times [0, 1]$, because due to the reflection symmetry and time-reversal symmetry, the four quadrants are equivalent

where to cut the distribution of the M-values, at the threshold value M_t, such that all states with $M < M_t$ are declared regular and those with $M > M_t$ chaotic.

There are two natural criteria: (i) *The classical criterion:* the threshold value M_t is chosen such that we have exactly μ_1 fraction of regular levels and $\mu_2 = 1 - \mu_1$ of chaotic levels. (ii) *The quantum criterion:* we choose M_t such that we get the best possible agreement of the chaotic level spacing distribution with the Brody distribution (26), which is expected to capture the dynamical localization effects of the chaotic levels.

Let us now separate the regular and chaotic eigenstates and the corresponding eigenvalues, after unfolding, according to our method, using the classical criterion (i). The corresponding threshold value of the index M is found to be $M_t = 0.431$. The level spacing distributions are shown in Fig. 2. As we see, we have perfect Brody distribution with $\beta = 0.444$ for the chaotic levels and almost pure Poisson for the regular levels.

The Localization Measures

After the success in separating the regular and chaotic eigenstates, we want to quantify the degree of localization of the chaotic eigenstates (Batistić and Robnik 2013b). We express the localization measures in terms of the discretized Husimi function. For the *entropy localization measure* denoted by A, we write $A = e^{<I>}/N_c$, where $I = -\int dq\, dp\, H(q,p) \ln((2\pi\hbar)^f H(q,p))$ is the information entropy and N_c is a number of cells on the classical chaotic domain. The mean $<I>$ is obtained by averaging I over a sufficiently large number of consecutive chaotic eigenstates. In the case of uniform distribution $H_{ij} = 1/N_C$ the localization measure is $A = 1$, while in the case of the strongest localization $I = 0$, and $A = 1/N_C \approx 0$.

For the *correlation localization measure* denoted by C, we first calculate the overlap (correlation matrix) $C_{nm} = \frac{1}{Q_n Q_m}\sum_{ij} H_{ij}^n H_{ij}^m$, where $Q_n = \sqrt{\sum_{ij}\left(H_{ij}^n\right)^2}$ is the normalizing factor. Then $C = \langle C_{nm}\rangle$, and the averaging is over all n, m and a large number of consecutive chaotic eigenstates.

Again we use the billiard like in section "The Billiard Systems and Poincaré-Husimi Functions" with $\lambda = 0.15$. For a good approximation of the localization measures A and C, it was sufficient to separate and extract about 1.500 consecutive chaotic eigenstates. The two localization measures are linearly equivalent as shown in Fig. 3. To get a good estimate of β, we need much more levels, and the separation of eigenstates is then technically too demanding. We have instead calculated

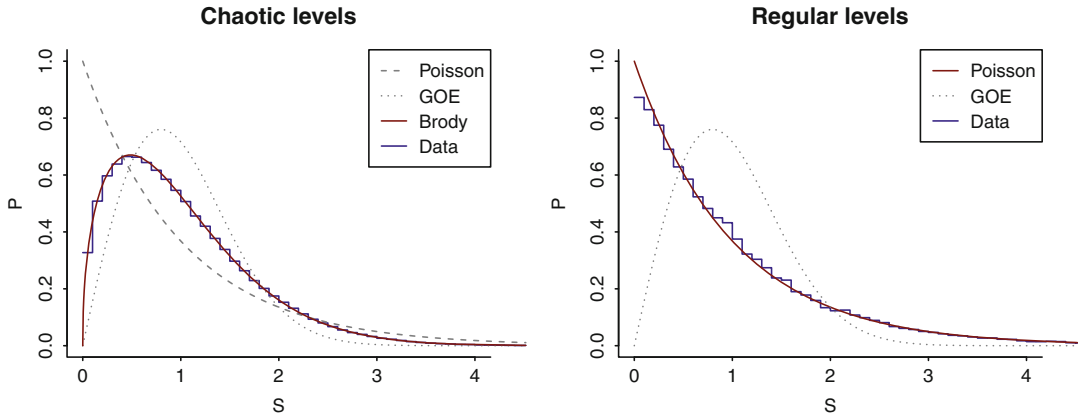

Recent Advances in Quantum Chaos of Generic Systems, Fig. 2 Separation of levels using the classical criterion $M_t = 0.431$. Left: The level spacing distribution for the chaotic subspectrum, after unfolding, in perfect agreement with the Brody distribution $\beta = 0.444$. Right: The level spacing distribution for the regular part of the spectrum, after unfolding, in excellent agreement with Poisson

spectra on small intervals around $k \approx 2000$ and $k \approx 4000$, about 100.000 consecutive levels (no separation), and obtained β by fitting the $P(S)$ by the BRB distribution derived in section "Dynamical Localization of the Chaotic Eigenstates" using the classical μ_1. The dependence of β on A is shown in Fig. 3. For aesthetic reasons, we have rescaled the measure $A \to A/A_{\max}$ such that it goes from 0 to 1. The maximal value of A, $A_{\max} = 0.68$, was estimated as $A_{\max} = e^{I_{\max}}/N_c$, where $I_{\max}$ is the maximum entropy of 1500 consecutive states of the almost fully chaotic $\lambda = 0.25$ billiard. Thus for fully chaotic systems, the procedure always yields $A = 1$. Namely, in real chaotic eigenstates, we never reach a perfectly uniform distribution $H(q, p)$, since they always have some oscillatory structure.

We clearly see that there is a functional relationship between A and β. By increasing k from 2000 to 4000, we increase the dimensionless Heisenberg time by factor 2; therefore, A must increase, but precisely in such a way, that the empirical points stay on the scaling curve, as it is observed and indicated by the arrows. We do not have yet a semiempirical functional description of the relationship $\beta(A)$ we found in Fig. 3. In the quantum kicked rotator, it is just almost linear (Batistić et al. 2013; Manos and Robnik 2013; Izrailev 1990). Similarly, it is found to be almost linear in the stadium of Bunimovich, as recently published in reference (Batistić et al. 2018) and shown in Fig. 4. Also, β is found to be a unique function of $\alpha = t_H/t_T$, well described empirically by the rational function

$$\beta = \beta_\infty \frac{s\alpha}{1 + s\alpha}, \tag{34}$$

as seen in Fig. 5. For details, see reference (Batistić et al. 2018). Nevertheless, one should observe some scattering of points around the mean value, noted already by Izrailev (1990) in the case of the quantum kicked rotator, which probably is due to the fact that the localization measure has a certain distribution rather than a sharp value, as has been observed recently in the kicked rotator by Manos and Robnik (2015).

Finally, there is a great lack in theoretical understanding of the physical origin of the relationship $\beta(A)$, even in the case of (the long-standing research on) the quantum kicked rotator, except for the intuitive idea, that energy spectral properties should be only a function of the degree of localization, because the localization gradually decouples the energy eigenstates and levels, switching the linear level repulsion $\beta = 1$ (extendedness) to a power law level repulsion

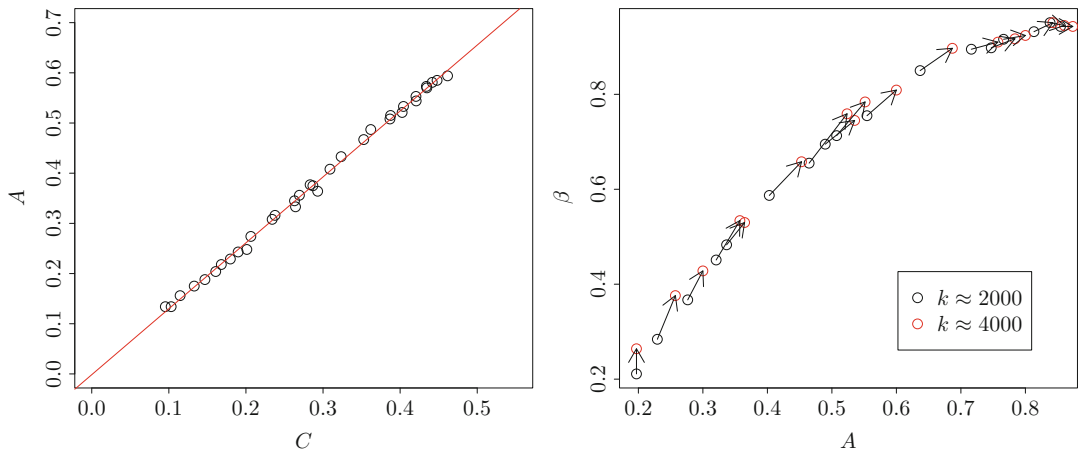

Recent Advances in Quantum Chaos of Generic Systems, Fig. 3 Left: Linear relation between the two entirely different localization measures, namely the entropy measure A and the correlation measure C, calculated for several different billiards at $k \approx 2000$ and $k \approx 4000$. Right: We show the functional relation between β and the localization measure A. Arrows connect points corresponding to the same λ at two different k

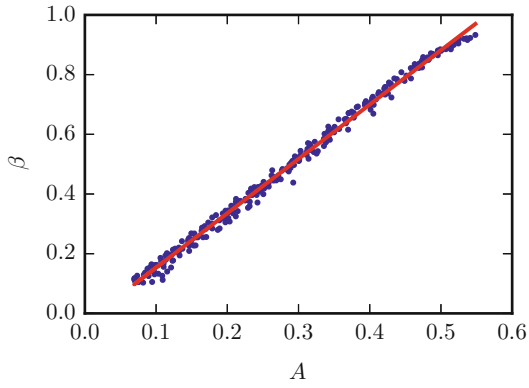

Recent Advances in Quantum Chaos of Generic Systems, Fig. 4 The level repulsion exponent β as a function of the entropy localization measure A for variety of stadia of different shapes ε and energies $E = k^2$

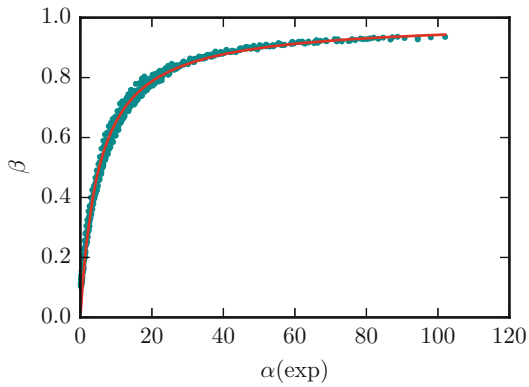

Recent Advances in Quantum Chaos of Generic Systems, Fig. 5 The level repulsion exponent β as a function of α fitted by the function (34), based on t_T from the exponential diffusion law, for variety of stadia of different shapes ε and energies $E = k^2$, as in Fig. 4. Here, $\beta_\infty = 0.98$ and $s = 0.20$

with exponent $\beta < 1$ (localization). The full physical explanation is open for the future.

Discussion and Conclusions

Quantum chaos, or wave chaos, is a study of the signatures of classical chaos of the underlying classical dynamical system, or more generally, of the ray dynamics of the limiting short-wavelength asymptotics. The time evolution of the bound quantum systems (with purely discrete spectrum) is always almost periodic, stable, and reversible in the sense of the absence of the sensitive dependence on intitial conditions, and thus it is quite diferent from the classically chaotic behavior exhibiting sensitive dependence on initial conditions, due to the positive Lyapunov exponents. In this sense, there is no quantum chaos. However, in the time-independent domain, when we look at the eigenstates of the stationary Schrödinger equation, we uncover a complexity of the solutions, fully revealed in the quantum phase space of the Wigner functions, which exactly correspond to the structure of the classical phase space. In the semiclassical limit of sufficiently small effective Planck constant, the Heisenberg time is larger than all classical transport (diffusion) time scales, and the chaotic eigenstates (their Wigner functions) are uniformly extended over the entire available chaotic region. Then the regular eigenstates "live" on invariant tori, while the chaotic ones are associated with the chaotic components. The energy spectra belong to the universality classes as for their statistical properties: the regular spectra obey Poissonian statistics, while the chaotic ones obey the statistics of the Gaussian random matrix theory. If the semiclassical condition on the time scales is not satisfied, the chaotic Wigner functions are localized due to the quantum (or dynamical) localization. The degree of localization (localization measures) can be defined in various ways, but different localization measures are found to be equivalent (linearly related). The degree of localization uniquely determines the Brody spectral parameter which enters in the level spacing distribution of localized chaotic eigenstates. Using the overlap criterion for the Wigner functions (or Husimi functions), one can separate the regular and chaotic states, and perform the statistical analysis separately. It is confirmed, in the sense of Percival (1973) and Berry and Robnik (1984), as generalized by Batistić and Robnik (2010–2013), that the regular levels are Poissonian, while the localized chaotic ones are Brody-like, where the Brody parameter is a unique function of the localization measure. When we go from the semiclassical limit to larger values of the effective Planck constant (in billiards it means to lower energies), we reveal the

tunneling (correlation) effects, where the regular and chaotic eigenstates start to overlap considerably, and thus no longer can be classified clearly as regular or chaotic. The picture becomes quite complex, and is subject of current research (Batistić and Robnik 2010; Gehler et al. 2015).

While the fully chaotic and regular eigenstates are generally very well understood, the description of the localized chaotic states, and of the mixed-type systems, is still open for further investigation. In particular, we need to derive a theory of dynamical localization of stationary chaotic eigenstates, including the derivation of the phenomenological Brody level spacing distribution of such localized chaotic eigenstates. Thus, quite a few fundamental questions of quantum chaos are open for the future.

Acknowledgment This work was supported by the Slovenian Research Agency ARRS under the grant J1-9112 "Quantum localization in chaotic systems."

References

Arnold VI (1980) Mathematical methods of classical mechanics. Springer, New York
Bäcker A, Fürstberger S, Schubert R (2004) Phys Rev E 70:036204
Batistić B, Robnik M (2010) J Phys A Math Theor 43:215101
Batistić B, Robnik M (2013a) J Phys A Math Theor 46:315102
Batistić B, Robnik M (2013b) Phys Rev E 88:052913
Batistić B, Manos T, Robnik M (2013) Europhys Lett 102:50008
Batistić B, Lozej Č, Robnik M (2018) Nonl Phen Compl Syst (Minsk) 21(1):225
Berry MV (1977) J Phys A Math Gen 10:2083
Berry MV (1981) Eur J Phys 2:91
Berry MV (1985) Proc Roy Soc Lond A 400:229
Berry MV, Robnik M (1984) J Phys A Math Gen 17:2413
Bohigas O, Giannoni MJ, Schmit C (1984) Phys Rev Lett 52:1
Bunimovich LA (1974) Func Anal Appl 8:254
Casati G, Chirikov BV, Izrailev FM, Ford J (1979) Lect Notes Phys 93:334
Casati G, Valz-Gris F, Guarneri I (1980) Lett Nuovo Cimento 28:279
Gehler S, Löck S, Shinohara S, Bäcker A, Ketzmerick R, Kuhl U, Stöckmann H-J (2015) Phys Rev Lett 115:104101, and references therein
Grossmann S, Robnik M (2007) Z Naturforsch 62a:471
Gutzwiller MC (1967) J Math Phys 8:1979; 10:1004 (1969); 11:1791 (1970); 12:343 (1971)
Haake F (2010) Quantum signatures of chaos. Springer, Berlin
Hackenbroich G, Weidenmüller HA (1995) Phys Rev Lett 74:4118
Haken H (2004) Synergetics. Springer, Berlin
Izrailev FM (1990) Phys Rep 196:299
Li B, Robnik M (1994) J Phys A Math Gen 27:5509
Lozej Č, Robnik M (2018) Phys Rev E 97(1):012206-1
Manos T, Robnik M (2013) Phys Rev E 87:062905
Manos T, Robnik M (2015) Phys Rev E 91:042904
McDonald SW, Kaufman AN (1979) Phys Rev Lett 42:1189; Phys Rev A 37:3067 (1988)
Mehta ML (1991) Random matrices. Academic, Boston
Müller S, Heusler S, Altland A, Braun P, Haake F (2009) New J Phys 11:103025, and references therein
Ott E (1993) Chaos in dynamical systems. Cambridge University Press, Cambridge
Percival IC (1973) J Phys B: At Mol Phys 6:L229
Prosen T, Robnik M (1994) J Phys A Math Gen 27:L459
Prosen T, Robnik M (1999) J Phys A Math Gen 32:1863
Robnik M (1983) J Phys A Math Gen 16:971
Robnik M (1984) J Phys A Math Gen 17:1049
Robnik M (1986) In: Seligman TH, Nishioka H (eds) Proceedings of the international conference quantum chaos and statistical nuclear physics, Cuernavaca, 1986. Lecture notes in physics, vol 263. Springer, Berlin, 1986, p 120
Robnik M (1998) Nonl Phen Compl Syst (Minsk) 1(1):1
Robnik M (2015) In: Aizawa Y, Miwa Y (eds) Proceedings of Waseda AICS symposium and the 14th Slovenia-Japan seminar, new challenges in complex systems science, 2014, vol B11, No. 3. Waseda University, Tokyo, pp 13–17
Robnik M (2016) Eur Phys J Spec Top 225:959
Robnik M, Berry MV (1986) J Phys A Math Gen 19:669
Robnik M, Veble G (1998) J Phys A Math Gen 49:4669
Robnik M, David HM, Vidmar G, Romanovski VG (2010) Nonl Phen Compl Syst (Minsk) 13(1):13
Shnirelman B (1974) Uspekhi Matem. Nauk 29:181. (in Russian)
Sieber M, Richter K (2001) Phys Scr T90:128
Stöckmann H-J (1999) Quantum chaos: an introduction. Cambridge University Press, Cambridge
Tualle JM, Voros A (1995) Chaos, Solitons Fractals 5:1085
Veble G, Robnik M, Liu J (1999) J Phys A Math Gen 32:6423
Voros A (1979) Lect Notes Phys 93:326

Linear and Nonlinear Fokker-Planck Equations

Till D. Frank
Department of Psychology and Department of Physics, University of Connecticut, Storrs, CT, USA

Article Outline

Glossary
Definition of the Subject
Introduction
Time-Dependent Solutions and First-Order Statistics
Markov Property: Second-Order and Higher-Order Statistics
Martingales
Examples
Summary and Future Directions
Bibliography

Glossary

Linear Here, linear with respect to a probability density.

Nonlinear Here, nonlinear with respect to a probability density.

Markov process Process for which it is sufficient to have information about the presence in order to make best predictions about the future. Additional information about the past will not improve the predictions.

Martingale process $\hat{Z}$ Process for which the future mean value $\langle Z(t+\Delta t)\rangle$ of a set of realizations $Z^{(i)}$ that is passing at presence t through a certain common state z is the state z: $z : \langle Z(t+\Delta t)\rangle_{Z(t)=z} = z$. Additional information about states z' visited at times t' prior to t is irrelevant.

Definition of the Subject

Let $\hat{X}$ denote a stochastic process defined on the space Ω and the time interval $[t_0, \infty]$, where t_0 denotes the initial time of the process. We assume that the process $\hat{X}$ can be described in terms of a random variable $X \in \Omega$. More precisely, let $X(t)$ denote the time-dependent evolution of the random variable X for $t \geq t_0$. Then, we assume that the process $\hat{X}$ can be described in terms of the infinitely large set of realizations $X^{(i)}(t)$ of $X(t)$ with $i = 1, 2, \ldots$. The realizations $i = 1, 2, \ldots$ constitute a statistical ensemble. At every time t the probability density P of the process $\hat{X}$ can be computed from the realizations $X^{(i)}(t)$, that is, from the ensemble by means of

$$P(x,t) = \langle \delta(x = X(t)) \rangle, \tag{1}$$

where $\langle\cdot\rangle$ denotes ensemble averaging and $\delta(\cdot)$ is the delta function. We assume that at time t_0 the process is distributed like u. That is, the function $u(x)$ describes the initial probability density of the random variable X and we have $P(x,t_0) = u(x)$. In general, the evolution of P depends on how the process is distributed at initial time t_0. In order to emphasize this point, we will use in what follows the notation $P(x,t;u)$. That is, we interpret Eq. (1) as a conditional probability density with the constraint given by the initial distribution u:

$$P(x,t;u) = \langle \delta(x = X(t)) \rangle_{\langle \delta(x - X(t_0)) \rangle = u(x)}. \tag{2}$$

We may also say that we study a family of stochastic processes (Frank 2005b). Each family member has a label or name which is given by u. For example, consider three experiments in which the evolution of dust particles in the air is observed for Gaussian, Lévy, and Cauchy initial distributions, respectively. It is known that dust particles perform a so-called Brownian random walk. So we would distinguish the three members $\hat{X}_1, \hat{X}_2, \hat{X}_3$ of our family of Brownian walk processes by the names of their initial distributions: Gauss, Lévy, and Cauchy.

Let us consider a stochastic process $\hat{X}$ whose evolution of its probability density P is defined by a partial differential equation of the form

A. Hutt, H. Haken (eds.), *Synergetics*,
https://doi.org/10.1007/978-1-0716-0421-2_311

Originally published in
R. A. Meyers (ed.), *Encyclopedia of Complexity and Systems Science*, © Springer Science+Business Media LLC 2017
https://doi.org/10.1007/978-3-642-27737-5_311-3

$$\frac{\partial}{\partial t}P(x,t;u) = \left[-\frac{\partial}{\partial x}D_1(x,t) + \frac{\partial^2}{\partial x^2}D_2(x,t)\right]P(x,t;u), \tag{3}$$

where D_1 and D_2 are functions of state x and time t. The functions D_1 and D_2 are referred to as drift and diffusion coefficients and constitute the Fokker-Planck operator

$$L^0(x,t) = -\frac{\partial}{\partial x}D_1(x,t) + \frac{\partial^2}{\partial x^2}D_2(x,t). \tag{4}$$

The evolution equation (3) is linear with respect to P. In this sense, Eq. (3) is a linear partial differential equation. Irrespective of this feature, the coefficients D_1 and D_2 may depend in a highly nonlinear fashion on the state x. For example, we may have $D_1 = -x + x^3$.

For appropriately chosen coefficients D_1 and D_2, Eq. (3) describes the probability density P of a Markov process. In this case, Eq. (3) is referred to as a Fokker-Planck equation. More precisely, if $\hat{X}$ is a Markov diffusion process whose probability density P is defined by Eq. (3), then Eq. (3) is called a Fokker-Planck equation. Note that roughly speaking, a Markov *diffusion* process is a Markov process characterized by a partial differential operator that can be truncated after the second-order partial derivative (see section "Kramers-Moyal Expansion"). In order to distinguish between linear and nonlinear Fokker-Planck equations, we will use the phrase "linear Fokker-Planck equation" instead of "Fokker-Planck equation."

Let us generalize Eq. (3) by assuming that the drift and diffusion coefficients depend on the probability density P. In this case, Eq. (3) becomes

$$\frac{\partial}{\partial t}P(x,t;u) = \left[-\frac{\partial}{\partial x}D_1(x,t,P(x,t;u)) + \frac{\partial^2}{\partial x^2}D_2(x,t,P(x,t;u))\right]P(x,t;u). \tag{5}$$

Likewise, the operator (4) is generalized to

$$L(x,t,P(x,t;u)) = -\frac{\partial}{\partial x}D_1(x,t,P(x,t;u)) + \frac{\partial^2}{\partial x^2}D_2(x,t,P(x,t;u)). \tag{6}$$

Equation (5) is nonlinear with respect to $P(x, t; u)$. Since the structure of the differential operator in the bracket of Eq. (5) is equivalent to the structure of the differential operator (4), evolution equations of the form (5) are frequently called nonlinear Fokker-Planck equations. In this context, it is important to realize that the phrase "nonlinear Fokker-Planck equation" does not necessarily imply that we are dealing with a Markov process. The phrase "nonlinear Fokker-Planck equation" simply means that we are dealing with a nonlinear partial differential equation involving a partial differential operator that exhibits the structure of a Fokker-Planck operator.

Note again that if an evolution equation of the form (3) is referred to as a Fokker-Planck equation, then it is tacitly assumed that there exists a stochastic process defined by that equation and that this process is a Markov process. Table 1 summarizes how to define linear and nonlinear Fokker-Planck equations by means of structure, existence of solutions, and Markov property.

Linear Fokker-Planck equations are an indispensable tool to describe stochastic processes in a variety of disciplines; see Fig. 1. The theoretical concept of Markov diffusion processes related to linear Fokker-Planck equations is well established. Researchers, applied scientist, technicians, research and development engineers in general, and financial engineers in particular are - usually aware that the particular linear Fokker-Planck model they are using belongs to the class of Markov models. That is, the world of linear Fokker-Planck equations is closed and connected.

Nonlinear Fokker-Planck equations are used in a variety of fields that are as diverse as the

Linear and Nonlinear Fokker-Planck Equations, Table 1 Definition of linear and nonlinear Fokker-Planck equations based on structure, existence of solutions, and Markov property

Fokker-Planck equations	Linear	Nonlinear
Structure	Eqs. (3)–(4)	Eqs. (5)–(6)
Solutions	Exist	Do not necessarily exist
Corresponding processes are Markov processes?	Yes	Maybe

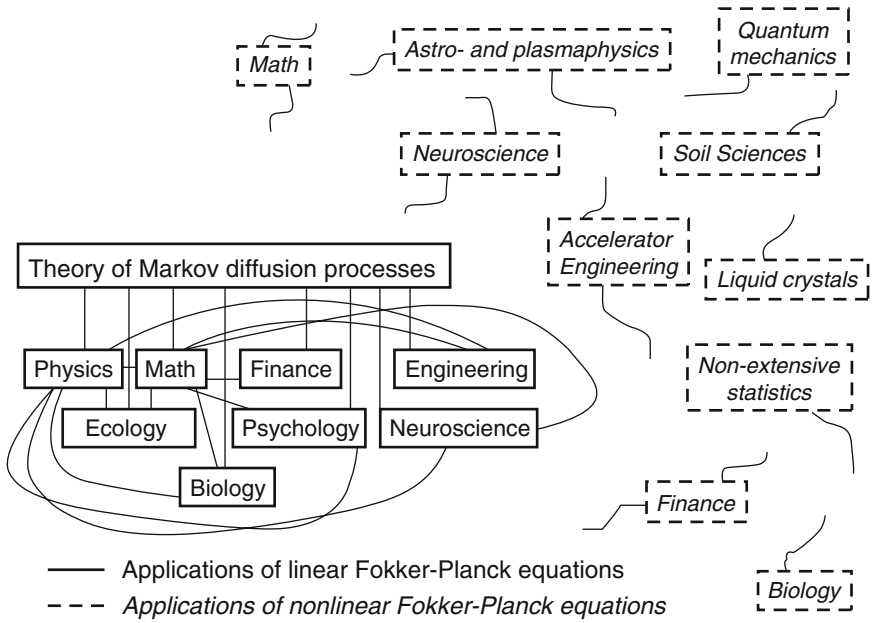

Linear and Nonlinear Fokker-Planck Equations, Fig. 1 Connected and disconnected applications of linear and nonlinear Fokker-Planck equations

application fields of linear Fokker-Planck equations. Unfortunately, so far, there is no well-established theory connecting all kinds of nonlinear Fokker-Planck equations. There is not even an academic consent about how to define them at all. This is why in Table 1 we used a very general and less constraining definition for nonlinear Fokker-Planck equations. Concepts of nonlinear Fokker-Planck equations are often developed for particular purposes and are not put into other contexts. That is, theoretical results and other achievements are often tailored to serve special needs and are not discussed in a larger framework. Even worse, so far, a well-established link between linear and nonlinear Fokker-Planck equations that applies to the variety of nonlinearities found in the literature does not exist. In sum, the world of nonlinear Fokker-Planck equations is disconnected. Different types of nonlinear Fokker-Planck equations and different application fields of nonlinear Fokker-Planck equations are often not related to each other and nonlinear Fokker-Planck equations are only loosely connected with their linear "relatives"; see Fig. 1.

Therefore, there is a need for developing a unifying approach to nonlinear Fokker-Planck equations that involves the concept of linear Fokker-Planck equations and applies to all types of nonlinearities and in doing so applies to all kinds of scientific disciplines. Some first efforts in this regard have been made previously (Acebron et al. 2005; Chavanis 2003, 2004; Frank 2001b, 2002a, b, 2005b; Frank and Daffertshofer 1999, 2001a, b; Kaniadakis 2001a; b; Shiino 2002b, 2003). In the following sections, we will review these efforts, present them in a consistent way, and in doing so make a further effort into this direction.

Introduction

Linear and nonlinear Fokker-Planck equations are widely used to describe stochastic phenomenon; see Fig. 1.

Linear Fokker-Planck equations (Gardiner 1997; Haken 2004; Risken 1989) have been introduced by Fokker (1914) and Planck (1917). In physics, linear Fokker-Planck equations have been used, for example, to describe Brownian motion, that is, the diffusion of dust particles in air or fluid layers (Reif 1965). Linear Fokker-Planck equations have been applied in engineering sciences, for example, to describe fluctuations in electronic circuits (Gardiner 1997). Linear

Fokker-Planck equations have been frequently used in chemistry to model stochastic aspects of chemical reactions (Hänggi et al. 1990; van Kampen 1981). In finance, one of the most important applications of the Fokker-Planck theory is option pricing by means of the so-called Black-Scholes model (Paul and Baschnagel 1999). Linear Fokker-Planck equations of biology systems (Goel and Dyn 1974) have been concerned, for example, with so-called Brownian motors (Hänggi et al. 2005; Reimann 2002). Population diffusion (Okubo and Levin 2001) and group behavior (Ebeling and Sokolov 2004; Mikhailov and Zanette 1999; Schweitzer 2003) in ecological systems and stochastic neuronal processing (Holden 1976) are further examples of application fields of linear Fokker-Planck equations. In psychology, linear Fokker-Planck models have been proposed for decision making (Bogacz et al. 2006; Ratcliff et al. 2004) and group behavior (Schwämmle et al. 2007b).

Many applications of nonlinear Fokker-Planck equation are related to several benchmark models: the Desai-Zwanzig model (Desai and Zwanzig 1978), the liquid crystal model (Doi and Edwards 1988; Hess 1976), the Kuramoto-Shinomoto-Sakaguchi model (Acebron et al. 2005; Kuramoto 1984; Strogatz 2000), the Vlasov model, and the nonlinear diffusion equation (Aronson 1986; Peletier 1981). Let us highlight some of these benchmark models.

Desai-Zwanzig Model

The Desai-Zwanzig model

$$\frac{\mathrm{d}}{\mathrm{d}t}P(x,t;u) = -\frac{\partial}{\partial x}\left[h(x) - \kappa \left(x - \int xP(x,t;u)\,\mathrm{d}x\right) + Q\frac{\partial}{\partial x}\right]P(x,t;u) \tag{7}$$

for κ , $Q > 0$ has been proposed by Desai and Zwanzig (1978) and Kometani and Shimizu (1975) to study collective phenomena in self-organizing systems.

- A Lyapunov functional approach to the Desai-Zwanzig model has been introduced by Shiino (1985, 1987) and since then has found several generalizations (Chavanis 2003, 2004; Dawson and Gärtner 1989; Frank 2001a, 2005b; Frank and Daffertshofer 2001b; Frank et al. 2001; Kaniadakis 2001a, b; Kharchenko and Kharchenko 2005; Schwämmle et al. 2007a; Shiino 2001, 2002a, b; 2003). With such a Lyapunov functional at hand, the stability of stationary probability densities, collective phenomena, and bifurcations can be studied by means of Lyapunov's direct method.
- The original Desai-Zwanzig model and various modifications of it have been discussed (Dawson 1983; Li et al. 1998; Lo 2005).
- The additive noise term in Eq. (7) has been replaced by a multiplicative noise term (Horsthemke and Lefever 1984) in order to study the interplay between the nonlinearity and the multiplicative noise (Birner et al. 2002; Müller et al. 1997; Zaikin et al. 2002).
- Fluctuation-dissipation theorems for stochastic processes described by the Desai-Zwanzig model have been derived (Drozdov and Morillo 1996; Frank 2004c; Morillo et al. 1995).
- The Desai-Zwanzig model has frequently been used as a mean field approximation of spatially distributed systems with diffusive coupling. By means of such a mean field approximation, analytical result has been derived and compared with numerical simulations (Garcia-Ojalvo et al. 1996; Garcia-Ojalvo and Sancho 1999; van den Broeck et al. 1994a, b, 1997).

Liquid Crystal Model

The nonlinear Fokker-Planck equation proposed by Hess (Hess 1976) and Doi and Edwards (1988) reads

$$\frac{\partial}{\partial t}P(\mathbf{x},t;u) = D_r\mathbf{L}\cdot\left\{\mathbf{L} + \frac{1}{kT}\left[\mathbf{L}\,e(\mathbf{x},P)\right]\right\}P(\mathbf{x},t;u) \tag{8}$$

with D_r , k , $T > 0$ and $\mathbf{L} = \mathbf{x} \times \partial/\partial\mathbf{x}$. The function $e(\mathbf{x}, P)$ describes the self-consistent potential of the Maier-Saupe mean field force. For processes $\hat{X}$ that exhibit cylindrical symmetry $e(\mathbf{x}, P)$ reads

$$e(\theta, P) = -U_0 kT \frac{3\cos^2\theta - 1}{2} \left\langle \frac{3\cos^2\theta - 1}{2} \right\rangle, \tag{9}$$

where θ is related to the unit vector $\mathbf{x}$ by $\mathbf{x} = (\sin\theta \cos\varphi, \sin\theta \sin\varphi, \cos\theta)$. Equation (8) and generalization of it have been extensively studied in the literature (Felderhof 2003; Fialkowiski and Hess 2000; Hütter et al. 2003; Ilg et al. 1999, 2005; Larson and Öttinger 1991) (see also Öttinger (1996) in general and Sect. 6.3.2 in Öttinger (1996) in particular). We will return to this model in section "Liquid Crystal Model."

Winfree and Kuramoto Model

Winfree's seminal studies on synchronization among animal populations (Winfree 1967, 2001) supported the interest in the nonlinear Fokker-Planck equation

$$\frac{\partial}{\partial t} P(x,t;u) = \left\{ -\frac{\partial}{\partial x} [h(x) - \kappa \cdot \int \sin(x-y) P(y,t;u)\, \mathrm{d}y \right] + Q \frac{\partial^2}{\partial x^2} \Big\} P(x,t;u), \tag{10}$$

that has been proposed by Kuramoto and co-workers (Kuramoto 1984). In Eq. (10), $h(x)$ is a 2π-periodic function and κ , $Q > 0$.

- While the Kuramoto-Shinomoto-Sakaguchi model involves an interaction term $\int a(x, y)P(y, t)\, \mathrm{d}y$, the model originally proposed by Winfree exhibits a coupling term of the form $\int a(y)P(y, t)\, \mathrm{d}y$. Models of this latter kind have also been addressed in Ariaratnam and Strogatz (2001), Li and Hänggi (2001), and Quinn et al. (2007).
- The Kuramoto-Shinomoto-Sakaguchi model describes an ensemble of phase oscillators. The eigenfrequencies of the phase oscillators do not occur in Eq. (10) because Eq. (10) describes an ensemble of phase oscillators exhibiting the same eigenfrequency ω. In this case, the common eigenfrequency ω can then be eliminated by means of a variable transformation into a rotating frame (Frank 2005b). However, in general, we may think of ensembles of coupled phase oscillators with different eigenfrequencies. In this context, the question arises as to what extent oscillators with different eigenfrequencies synchronize their behavior (Acebron et al. 1998; Arenas and Perez Vincente 1994; Bonilla et al. 1993; Crawford 1995; Kostur et al. 2002; Pikovsky et al. 2001; Sakaguchi 1988; Strogatz and Mirollo 1991).
- Coupled phase oscillator models of the form (10) have been used to describe associative memories (Yamana et al. 1999; Yoshioka and Shiino 2000).
- Just as for the Desai-Zwanzig model, the interplay between multiplicative noise and the nonlinearity of the Kuramoto-Shinomoto-Sakaguchi model has been investigated in several studies (Kim et al. 1997; Park and Kim 1996; Reimann et al. 1999a, b).
- The *sine*-coupling term in Eq. (10) has been replaced by higher-order coupling functions $\sin(2z)$, $\sin(3z)$, ... (Aonishi and Okada 2002; Daido 1996a, b; Hansel et al. 1993b; Kuramoto 1984). In this context, Daido proposed the so-called order function (Daido 1996a, b) that generalizes the notion of cluster phases and cluster amplitudes (Kuramoto 1984). This order function has also been related to experimental data (Zhai et al. 2005).
- The Kuramoto-Shinomoto-Sakaguchi has found clinical applications in the context of Parkinsonian disease (Tass 2001, 2003; 2006; see also Tass 1999).

Vlasov-Fokker-Planck Model

Vlasov-Fokker-Planck models frequently describe particle systems with electromagnetic interactions between charged particles. A typical example of a Vlasov-Fokker-Planck equation is shown here (Balescu 1975; Klimontovich 1986):

$$\frac{\partial}{\partial t} P(\mathbf{v}, t; u) = -\sum_{i=1}^{3} \frac{\partial}{\partial v_i} D_i(\mathbf{v}, P) P + \sum_{i,k=1}^{3} \times \frac{\partial^2}{\partial v_i \partial v_k} D_{ik}(\mathbf{v}, P) P. \tag{11}$$

Equation (11) involves the drift and diffusion coefficients

$$D_i(\mathbf{v},P) = a\frac{\partial}{\partial v_i}\int_\Omega \frac{P(\mathbf{v}',t;u)}{|\mathbf{v}-\mathbf{v}'|}|\mathrm{d}^3v',$$
$$D_{ik}(\mathbf{v},P) = b\frac{\partial^2}{\partial v_i v_k}\int_\Omega |\mathbf{v}-\mathbf{v}'|P(\mathbf{v}',t;u)\mathrm{d}^3v'. \quad (12)$$

Time-dependent solutions (Allen and Victory 1994; MacDonald et al. 1957; Nicholson 1983; Rosenbluth et al. 1957; Takai et al. 1981) for Eq. (12) and generalization of Eq. (12) that account for additional drift forces (Bychenkov et al. 1995; Epperlein et al. 1988) have been studied. In particular, numerical methods using short-time propagators (see section "Short-Time Propagator") have been developed for Vlasov-Fokker-Planck equations of the form (12) (Donoso and Salgado 2006; Donoso et al. 2005; Soler et al. 1992). Such nonlinear Vlasov-Fokker-Planck equations play important roles in plasma physics (Balescu 1975; Klimontovich 1986; Nicholson 1983) and astrophysics (Binney and Tremaine 1987; Lancellotti and Kiessling 2001). In general, astrophysical problems often require a stochastic description in terms of nonlinear Fokker-Planck equations (Chavanis et al. 2002; Shiino 2003; Sopik et al. 2006). Finally, note that Vlasov-Fokker-Planck models have been used in accelerator physics and accelerator engineering to examine instabilities in particle beams (Frank 2003a, 2006; Heifets 2001, 2003; Shobuda and Hirata 2001; Stupakov et al. 1997; Venturini and Warnock 2002).

Nonlinear Diffusion Equation, Nonextensive Thermostatistics, and Semiclassical Descriptions of Quantum Systems

The nonlinear diffusion equation (Aronson 1986; Peletier 1981) reads

$$\frac{\partial}{\partial t}P(x,t;u) = -\frac{\partial}{\partial x}h(x)P(x,t;u) + \frac{\partial^2}{\partial x^2}D(P(x,t;u)), \quad (13)$$

where $D(P)$ is a diffusion coefficient that depends on the probability density $P(x,t)$ of $X(t)$. In the original version of the nonlinear diffusion equation, the drift coefficient $h(x)$ vanishes, and the diffusion coefficient is proportional to a power of P. In general, there might be a more complicated dependence of D on P (Crank 1975; Daly and Porporato 2004).

- Since fluid flow through porous materials is an important application of the nonlinear diffusion equation, nonlinear diffusion plays a crucial role in soil sciences (Barenblatt et al. 1990). In biology, nonlinear diffusion equations of the form (13) seem to capture particular aspects of population diffusion (Gurtin and MacCamy 1977; Okubo and Levin 2001).
- The nonlinear diffusion Eq. (13) provides a link to stochastic processes subjected to nonextensive thermostatistics introduced by Tsallis (Abe and Okamoto 2001; Tsallis 1988, 1997, 2004). For $D(P) \propto P^q$, Eq. (13) becomes

$$\frac{\partial}{\partial t}P(x,t;u) = -\frac{\partial}{\partial x}h(x)P(x,t;u) + Q\frac{\partial^2}{\partial x^2}P^q(x,t;u). \quad (14)$$

Plastino and Plastino showed that stationary distributions of Eq. (14) correspond to canonical distribution that can be derived in a nonextensive framework (Plastino and Plastino 1995). Equation (14) has turned out to be a testbed for various analytical and numerical studies (Borland 1998; Chavanis 2003, 2004; Compte and Jou 1996; Drazer et al. 2000; Shiino 2003; Tsallis and Bukman 1996). Alternative nonlinear Fokker-Planck equations related to the Tsallis statistics have been derived from master equations in Curado and Nobre 2003 and Nobre et al. 2004. In addition, Eq. (14) has more recently discussed in finance in the context of a generalized Black-Scholes model for option pricing (Borland 2002, 2008; Borland and Bouchaud 2004; Vellekoop and Nieuwenhuis 2007) and fat tail distributions (Cortines and Riera 2007; Michael and Johnson 2003).

- The nonlinear diffusion Eq. (13) is also related to semiclassical descriptions of quantum

mechanical systems. For an appropriate choice of D, nonlinear Fokker-Planck equations for Fermi-Bose and Einstein-Dirac systems have been derived from Eq. (13) (Frank 2005b; Frank and Daffertshofer 1999). Alternative forms of nonlinear Fokker-Planck equations have been derived from quantum mechanical Boltzmann equations (Kaniadakis 2001a; Kaniadakis and Quarati 1993, 1994), on the basis of energy balance equations (Tsekov 1995, 2001), and by means of other techniques (Frank 2004b, 2005a; Kadanoff 2000; Sopik et al. 2006). We will return to semiclassical quantum mechanical descriptions in section "Semiclassical Description of Quantum Systems."

In addition, nonlinear Fokker-Planck equations have been turned out to be useful models to describe stochastic aspects of Josephson arrays (Hadley et al. 1988; Wiesenfeld et al. 1996), Landau damping (Strogatz et al. 1992), arrays of semiconductor lasers (Kozyreff et al. 2000), charge density waves (Bonilla 1987), and neurons coupled by Hodgkin-Huxley equations (Han et al. 1995; Hansel et al. 1993a).

Stochastic systems composed of different kinds of interacting subsystems or species have been modeled in terms of multivariate nonlinear Fokker-Planck equations (Dano et al. 2001; Gang et al. 1996; Ichiki et al. 2007). For example, the collective behavior of coupled relaxation oscillators has been studied (Yamaguchi and Shimizu 1984). Networks of neural oscillators as defined by the Wilson-Cowan model, (Schuster and Wagner 1990), the two-dimensional Morris-Lecar system (Han et al. 1995), the FitzHugh-Nagumo equations (Hasegawa 2003; Kanamaru et al. 2001; Park et al. 2004), and the Hindmarsh-Rose equations (Rosenblum and Pikovsky 2004) have been studied.

The dynamics of mean field coupled phase oscillators under the impact of inertia effects (Acebron and Spigler 1998) and related models have attracted considerable attention. Bridge vibrations induced by pedestrian walking have been discussed in this context recently (Eckhardt et al. 2007; Strogatz et al. 2005). Models for circadian rhythms have been examined (Daido 2001).

Solutions of the Kadar-Parisi-Zhang equation have been examined by means of nonlinear Fokker-Planck equations (Giada and Marsili 2000; Marsili and Bray 1996). In doing so, the growth of surfaces and roughening phenomena have been studied.

Wetting processes (de los Santos et al. 2003), interacting Brownian motors (Becker and Engel 2007; Savel'ev et al. 2003), and spatially distributed phase oscillators (Kawamura 2007; Kawamura et al. 2007) have been analyzed by means of the nonlinear Fokker-Planck perspective.

In the mathematical literature, a seminal study on nonlinear Fokker-Planck equations of the Burgers equation type was due to McKean Jr. (1969). In particular, the convergence of stochastic processes described by multivariate linear Fokker-Planck equations to processes described by nonlinear Fokker-Planck equations (Cepa and Lepingle 1997; Dawson 1983, 1993; Ding 1994; Djehiche and Kaj 1995; Fontbona 2003; Gärtner 1988; Greven 2005; Jourdain 2000; McKean 1969; Meleard 1996; Meleard and Coppoletta 1987; Oelschläger 1989; Overbeck 1996; Pilipenko 2005; Rogers and Shi 1993) and martingales of stochastic processes defined by nonlinear Fokker-Planck equations have been addressed (Djehiche and Kaj 1995; Fontbona 2003; Gärtner 1988; Graham 1990; Greven 2005; Jourdain 2000; Meleard 1996; Meleard and Coppoletta 1987; Overbeck 1996). Moreover, the propagation of molecular chaos has been studied (Bonilla 1987; Meleard 1996; Meleard and Coppoletta 1987). The convergence of transient solutions of nonlinear Fokker-Planck equations to stationary ones has been examined by means of functionals that are similar to the Lyapunov functionals introduced by Shiino (see above) (Arnold et al. 1996, 2000, 2001; Carillo et al. 2001, 2008). In addition, from a purely mathematical perspective, nonlinear Fokker-Planck equations should be considered as nonlinear parabolic partial differential equations that have been discussed in several textbooks (Friedman 1969).

In what follows, we will show that there is a common theoretical framework that unifies most of the aforementioned studies on nonlinear Fokker-Planck equations and includes the theory of linear Fokker-Planck equations as a special case. This

common theoretical framework is rooted in the notion of Markov processes and martingales.

Time-Dependent Solutions and First-Order Statistics

Linear Case

Equation (3) defines the evolution of P given an initial distribution $u(x)$. The norm of the probability density P equals unity for all times provided that the norm of $u(x)$ equals unity. That is, if $\int_\Omega u(x)\,\mathrm{d}x = 1$ holds, we have $\int_\Omega P(x, t; u)\,\mathrm{d}x = 1$ for $t \geq t_0$. We can see this by integrating Eq. (3) with respect to x. For appropriate boundary conditions, it can be shown by partial integration that the right-hand side vanishes which implies that $\mathrm{d}[\int_\Omega P(x, t; u)\,\mathrm{d}x]/\mathrm{d}t = 0$ holds. The formal solution of Eq. (3) reads

$$P(x,t;u) = \exp\left\{\int_{t_0}^{t} \mathrm{d}z\, L^0(x,z)\right\} u(x), \qquad (15)$$

where L^0 is defined in Eq. (4). Equation (15) can be used to solve Eq. (3) numerically (see Vol. 1, Sect. 6.5 in Haken 2004). Let t_n denote a discrete time point $t_n = t_0 + n\Delta t$ with $n = 0, 1, 2, \ldots$, where Δt is the interval of a single time step and should be small. Let us define $P_n(x; u) = P(x, t_n; u)$. Then, we have

$$P_{n+1}(x;u) = \left\{1 + \Delta t L^0(x,t_n)\right\} P_n(x;u) \qquad (16)$$

with $P_0 = u(x)$. If $\hat{X}$ corresponds to an autonomous processes, then the coefficient D_1 and D_2 do not depend on t. In this case, P_n can be expressed in terms of u as

$$P_n(x;u) = \left[1 + \Delta t L^0(x)\right]^n u(x). \qquad (17)$$

Numerical solutions converge to exact solutions in the limit $\Delta t \to 0$.

Nonlinear Case

For appropriately chosen drift and diffusion coefficients, Eq. (5) exhibits time-dependent solutions P. By analogy with the linear case, these solutions are normalized to unity provided that appropriate boundary conditions hold and that the initial probability density is normalized to unity. Solutions of Eq. (5) are formally defined by

$$P(x,t;u) = \exp\left\{\int_{t_0}^{t} \mathrm{d}z\, L(x,z,P(x,z;u))\right\} u(x). \qquad (18)$$

The time-dependent solutions P can be computed numerically by analogy to the linear case discussed above. That is, the probability densities $P_n(x; u) = P(x, t_n; u)$ on the discrete time grid t_0 , $t_0 + \Delta t$, $t_0 + 2\Delta t$, . . . can be computed from

$$P_{n+1}(x;u) = \left\{1 + \Delta t L(x,t_n,P_n(x;u))\right\} P_n(x;u) \qquad (19)$$

with $P_0 = u(x)$ and $n = 0$, 1 , 2 , ... If drift and diffusion coefficients do not explicitly depend on t, we find that the operator L still depends implicitly on t because it depends on the time-dependent solution P that in turn depends on t. Consequently, it is not trivial to generalize Eq. (17) to the nonlinear case. If the drift- and diffusion coefficients do not depend explicitly on time t and the process converges to a stationary one, then the nonlinear Fokker-Planck operator L does not depend on time. This implies that the stationary probability density P_{st} satisfies

$$P_{\mathrm{st}} = \left\{1 + \Delta t L(x, P_{\mathrm{st}})\right\} P_{\mathrm{st}} + O\left(\Delta t^2\right). \qquad (20)$$

Finally, note that we do not necessarily need to define the formal solution with respect to the initial probability density u as in Eq. (18). We can solve the nonlinear Fokker-Planck equation on the time interval $[t_0, t]$ by splitting the solution in two intervals $[t_0, t']$ and $[t', t]$. Then, we obtain

$$P(x,t;u) = \exp\left\{\int_{t'}^{t} \mathrm{d}z\, L(x,z,P(x,z;u))\right\} P(x,t';u). \qquad (21)$$

Equation (21) can be solved iteratively by means of Eq. (19) yielding a mapping $T_{\Delta t} : P(x,t;u) = T_{t-t'}[P(x,t';u)]$ with $\Delta t = t - t'$.

Markov Property: Second-Order and Higher-Order Statistics

Conditional Probability Densities

Let $p(x)$ define the probability density of the time-dependent random variable X at time t given that X assumed at earlier times t', t'', t''',... with $t \geq t' > t'' > t''' > \ldots$ particular values x', x'', x''',... Then p is defined by

$$p = \langle \delta(x - X(t)) \rangle_{X(t')=x', X(t'')=x'', X(t''')=x''', \ldots}. \tag{22}$$

In order to point out the information that we need to compute p, we write

$$p = p\left(x, t | x', t'; x'', t''; x''', t''', \ldots\right). \tag{23}$$

A conditional probability density is a relation that gives us estimates about future events and tells us what we need to know in order to be able to calculate these estimates. In our example given by Eq. (23), we see that we need the information of random values X at times $t' > t'' > t''' > \ldots$ in order to make a prediction about the statistics or probability density of X at time t. Alternatively, we may say that the conditional probability density depends on a list of variables. In the context of Markov processes, this alternative viewpoint however gives rise to a problem that will be discussed below.

If $\hat{X}$ is a Markov process, then the information about the stochastic process available at one particular time t' is sufficient to make predictions about the future $t \geq t'$. Adding more information about how the process evolved in the past before t' does not improve these predictions. That is, the information about the events at time t' is sufficient to make statistical estimates about events at time $t \geq t'$. An alternative definition of a Markov process is that a Markov process exhibits a conditional probability density $p\ (x,\ t\ |\cdot)$ that depends only on one time point prior to t. That is, according to the first definition, we look from time t' into the future, whereas according to the second definition, we look in the opposite direction: we look from time t into the past.

For example, in order to describe the probability density $p(T)$ of the temperature T in Boston (USA) on December 1st, 2007, given that on November 1st, 2007, the temperature was 2 °C and on October 1st, 2007, the temperature was 3 °C, we would define the conditional probability density $p(T,$ Dec 1st 2007$|\ T = 2,$ Nov 1st 2007; $T = 3,$ Oct 1st 2007). If the temperature T as a function of time t is a Markov process, it is sufficient to know the temperature at November 1st in order to compute the probability density $p(T)$ at December 1st. For example, we would obtain the same function $p(T)$ for the conditions (i) and (ii) with (i) $T = 2$ °C on Nov 1st and $T = 3$ °C on Oct 1st and (ii) $T = 2$ °C on Nov 1st and $T = 5$ °C on Oct 1st. That is, we would have

$$\begin{aligned} &p(T, \text{Dec 1st 2007} \mid T = 2, \text{Nov 1st 2007}; \\ &\qquad T = 3, \text{Oct 1st 2007}) \\ &= p(T, \text{Dec 1st 2007} \mid T = 2, \text{Nov 1st 2007}; \\ &\qquad T = 5, \text{Oct 1st 2007}) \\ &= p(T, \text{Dec 1st 2007} | T = 2, \text{Nov 1st 2007}. \end{aligned} \tag{24}$$

The information about the October temperature is irrelevant. In this sense, the conditional probability density would depend on the November temperature but would not depend on the October temperature.

A problem that arises in the context of the definition of Markov process is as follows. Suppose that there is a purely deterministic dynamical aspect involved in a stochastic process. In our example about Boston temperatures, we may think of the annual periodic changes of the temperature that are related to the annual changes in distance and declination angle between the earth and sun. Let us assume that distance and declination angle change periodically in a purely deterministic fashion such that the distance and declination angle at November 1st can be computed from the distance and declination angle at January 1st by a simple one-to-one mapping. Then the question arises: does the temperature in Boston on December 1st depend on the distance and declination angle of November 1st as suggested by $p(T,$ Dec 1st 2007 $\mid T = 25,$ Nov 1st 2007) or does it depend on the distance and declination angle of January 1st In the former case, we have a Markov conditional probability density. In the latter case, we would need to write p like

$$p(T, \text{Dec 1st 2007} | T = 25, \text{Nov 1st 2007}; \text{distance and angle, Jan 1st 2007})$$

indicated that we are dealing with a non-Markovian process. The situation becomes even worse if we take into consideration that the earth-sun distance and the declination angle at January 1, 2008, can be computed from the information known at November 1 using our simple one-to-one mapping. Therefore, we may say that the temperature estimate for December 1st, 2007, depends on a future event, namely, the earth-sun distance and declination angle given at January 1st, 2008. The conditional probability density would assume the form

$$p(T, \text{Dec 1st 2007} | T = 25, \text{Nov 1st 2007}; \text{distance and angle, Jan 1st 2008})$$

which would suggest again that we are dealing with a non-Markovian and – to a certain extent – noncausal process. We can solve this problem by realizing that purely deterministic relationships in time that represent external driving forces are irrelevant for the distinction between Markov and non-Markov processes. We can completely determine such an external driving force by a parameter set $\{t_0, A_1, A_2, \ldots\}$ that describes the initial state of the driving forces. Although this initial state is related to the initial time t_0 of the Markov process, the conditional probability density does not actually depend (i.e., it does not explicitly depend) on t_0. Likewise the conditional probability density does not actually depend on the parameters $\{A_1, A_2, \ldots\}$. The information that we have at time t' includes the information about the driving force at time t' and therefore the information about the driving force at all times $t \in [t_0, \infty)$. Consequently, the information at time t' is sufficient to predict how the driving force will evolve in the future at times $t \geq t'$. There is no need to assess information about events prior to t' or information about events that will happen in the future at times larger than in order to determine the evolution of the deterministic driving force.

Let us summarize. A stochastic process $\hat{X}$ is called a Markov process if information about the process at time t' is sufficient to make predictions about future events. This implies that the conditional probability density p defined in Eq. (23) can be simplified like

$$p\left(x, t | x', t' x'', t''; x''', t''', \ldots\right) = p(x, t | x', t'). \tag{25}$$

Note that we may say that p depends only on the state x' related to the time t' in the sense that the information at time t' is sufficient to predict how X will be distributed at time $t \geq t'$. We may say it is sufficient to best predict future events where best refers to the fact that adding additional information about the past does not improve our predictions. Let us illustrate this issue by another example. Let $p(x, t \mid X = \theta)$ denote the probability density of X at time t given that X equals the function θ in the interval $[t_0, t']$ with $t' \leq t$. If X describes a Markov process, we have

$$\begin{aligned} p(x, t | X = \theta) &= p(x, t | \theta(t'), t') \\ &= p(x, t | x', t') \end{aligned} \tag{26}$$

with $x' = \theta(t')$.

Linear Fokker-Planck Equations

As mentioned in section "Definition of the Subject," linear Fokker-Planck equations describe Markov processes (Gardiner 1997; Risken 1989). Markov processes related to linear Fokker-Planck equations of the form (4) have conditional probability densities defined by

$$\frac{\partial}{\partial t} p(x, t | x', t') = L^0(x, t) p(x, t | x', t') \tag{27}$$

with $\lim_{t \to t'} p(x, t | x', t') = \delta(x - x')$. The conditional probability density p is also called the fundamental solution or Green's function of the Fokker-Planck equation (3). In general, a stochastic process $\hat{X}$ is completely defined in terms of the joint probability density

$$\begin{aligned} P(x_n, t_n; x_{n-1}, t_{n-1}; \ldots; x_0, t_0) = \langle \delta(x_n - X(t_n)) \\ \cdot \delta(x_{n-1} - X(t_{n-1})) \cdots \delta(x_0 - X(t_0)) \rangle, \end{aligned} \tag{28}$$

where n can assume arbitrarily large integer numbers. In particular, if $\hat{X}$ is a Markov process, then this joint probability density can be computed from p and u like

$$\begin{aligned} P(\cdot) = p(x_n, t_n | x_{n-1}, t_{n-1}) \cdot p(x_{n-1}, t_{n-1} | x_{n-2}, t_{n-2}) \\ \cdots p(x_1, t_1 | x_0, t_0) u(x_0). \end{aligned} \tag{29}$$

Consequently, the linear Fokker-Planck equation (3) defines completely a Markov process via

the associated evolution equation (27) and the initial distribution u. In particular, the time-dependent probability densities $P(x, t; u)$ and $P(x, t'; u)$ with $t \geq t'$ are related to each other by means of a *linear* functional

$$P(x,t;u) = \int_{\Omega} p(x,t|\,x',t')P(x',t;u)\,\mathrm{d}x'. \quad (30)$$

That is, the Green's function p induces a functional that is linear with respect to $P(x', t'; u)$.

Langevin Equations of Linear Fokker-Planck Equations

The stochastic trajectories $X(t)$ of the Markov process $\hat{X}$ defined by Eq. (3) can be computed from the Ito-Langevin equation (Coffey et al. 2004; Gardiner 1997; Risken 1989)

$$\frac{\mathrm{d}}{\mathrm{d}t}X(t) = D_1(X(t),t) + \sqrt{D_2(X(t),t)}\Gamma(t), \quad (31)$$

where $\Gamma(t)$ denotes a Langevin force normalized to the delta function like $\langle \Gamma(t)\Gamma(t')\rangle = 2\delta(t - t')$ From the Langevin equation (31), it follows again that we are dealing with a Markov process. Information about one reference time t' is sufficient to compute the future behavior of the trajectory $X(t)$ with $t \geq t'$. On a discrete time grid the stochastic trajectories or realizations of $\hat{X}$ can be computed iteratively like (Kloeden and Platen 1992; Risken 1989)

$$X_{n+1} = X_n + \Delta t D_1(X_n, t_n) + \sqrt{\Delta t D_2(X_n, t_n)}\epsilon_n \quad (32)$$

with $X(t_n) = X_n$, $t_n = t_0 + n\Delta t$ and $n = 0, 1, 2, \ldots$ Here, ϵ_n are independent Gaussian distributed random numbers with vanishing mean and variance 2. That is, we have $\langle \epsilon_n \rangle = 0$ and $\langle \epsilon_n \epsilon_m \rangle = 2\,\delta_{nm}$, where δ_{nm} is the Kronecker symbol. Finally, the probability density W of ϵ_n at every step n is given by

$$W(\epsilon_n) = \frac{1}{\sqrt{4\pi}} \exp\left\{-\frac{\epsilon_n^2}{4}\right\}. \quad (33)$$

Note that we do not necessarily need to start the iteration iterative map at t_0. The Scheme (32) can be started at any time step n. Moreover, in order to compute the subsequent time steps, it is sufficient to have information about the random variable X at time t_n. Consequently, the sequence X_n, X_{n+1}, X_{n+2}, ... computed from Eq. (32) describes a trajectory of a Markov process.

Strongly Nonlinear Fokker-Planck Equations

In section "Definition of the Subject," we pointed out that there is some kind of inconsistency in the definition of linear and nonlinear Fokker-Planck equations. While a linear Fokker-Planck equation defines a stochastic process, a nonlinear Fokker-Planck equation defines at best the evolution of a probability density $P(x,t)$. That is, if solutions of Eq. (5) exist for $u \in U$, then Eq. (5) defines the evolution of first-order statistical properties of a stochastic process $\hat{X}$ such as the time-dependent probability density, the mean, and the variance of the process $\hat{X}$. In any case, Eq. (5) does not define second- and higher-order statistical quantities such as correlation functions and conditional probability densities (Frank 2004d). In particular, the time-dependent solutions P of Eq. (5) in general cannot be used to construct Green's functions of Markov processes because they do not necessarily correspond to Green's functions of Markov processes (Frank 2003b). Note that this is not a peculiarity of stochastic processes defined by nonlinear Fokker-Planck equations. In fact, time-dependent solutions P of linear Fokker-Planck equations Eq. (3) involving explicitly time-dependent coefficients D_1 and D_2 do not necessarily correspond to Green's functions. Mathematically speaking, let $P(x, t; u = \delta(x - x_0))$ denote the probability density of a process $\hat{X}$ defined by a nonautonomous linear Fokker-Planck equation or by a nonlinear Fokker-Planck equation and let $p(x, t|\,x', t')$ denote the conditional probability density of that process $\hat{X}$, then we have (Frank 2003b)

$$P(x,t;u = \delta(x - x'))_{t_0=t'} \text{ is not necessarily equivalent to } p(x,t|\,x',t'), \quad (34)$$

where $P(x,t;u = \delta(x - x'))_{t_0=t'}$ means that we take the time-dependent solution $P(x, t; u = \delta(x - x_0))$ and replace in this expression x_0 by x' and t_0 by t'.

Let us return to the issue how to define a stochastic process $\hat{X}$ on the basis of a nonlinear Fokker-Planck equation (5). In order to do so, we need to

define appropriate constraints such that out of all possible stochastic processes that exhibit a time-dependent probability density P defined by Eq. (5), one particular process is selected. In what follows, we will discuss one particular set of constraints (Frank 2004d). As we will see, the stochastic processes thus defined exhibit the Markov property.

Let U denote a set of initial probability densities u. That is, U is a set of functions or a space of functions. Let $P(x, t; u)$ denote the solution of the nonlinear Fokker-Planck equation

$$\frac{\partial}{\partial t}P(x,t,u) = L(x,t,P(x,t;u))P(x,t;u) \tag{35}$$

with

$$L(x,t,P(x,t;u)) = -\frac{\partial}{\partial x}D_1(x,t,P(x,t;u)) + \frac{\partial^2}{\partial x^2}D_2(x,t,P(x,t;u)) \tag{36}$$

for an initial distribution $u \in U$. Let us introduce the associated drift and diffusion coefficients $\tilde{D}_1$ and $\tilde{D}_2$ by

$$\begin{aligned}\tilde{D}_1(x,t;u) &= D_1(x,t;P(x,t;u)),\\ \tilde{D}_2(x,t;u) &= D_2(x,t;P(x,t;u)).\end{aligned} \tag{37}$$

That is, for any $u \in U$, Eq. (35) is solved analytically or by numerical iteration (19). The solution is substituted into the drift and diffusion coefficients D_1 and D_2. The coefficients thus obtained are the functions $\tilde{D}_1$ and $\tilde{D}_2$ associated to D_1 and D_2. Let us assume that for all $u \in U$, the evolution equation

$$\frac{\partial}{\partial t}p(x,t|x',t') = \left[-\frac{\partial}{\partial x}\tilde{D}_1(x,t;u) + -\frac{\partial^2}{\partial x^2}\tilde{D}_2(x,t;u)\right] \cdot p(x,t|x',t') \tag{38}$$

has a fundamental solution or Green's function. Then, this solution p and its corresponding initial distribution u define a Markov process. In (Frank 2004d) nonlinear Fokker-Planck equations that induce evolution equations (38) with fundamental solutions were called strongly nonlinear Fokker-Planck equations. Note that nonlinear Fokker-Planck equations (5) do not necessarily exhibit the property of being strongly nonlinear. Note also that in some applications, it might be worth to define carefully the set U of initial probability densities u such that a nonlinear Fokker-Planck equation under consideration becomes strongly nonlinear.

As indicated above, the time-dependent probability density P of a nonlinear Fokker-Planck equation depends on the initial distribution u. Likewise, the associated coefficients $\tilde{D}_1$ and $\tilde{D}_2$ depend on u. As a result, the conditional probability density $p(x, t|x', t')$ depends on u as well. For this reason, the notation $p(x, t|x', t'; u)$ has been suggested. Unfortunately, this notation is likely to cause confusion because one might think that p depends not only on the time t' but also on the initial time t_0 which seems to be incompatible with the notion of a Markov conditional probability density (Frank 2007; McCauley et al. 2006). In fact, this confusion results from the second alternative way to define Markov processes that has been discussed above. The evolution of the function $P(x, t; u)$ is a purely deterministic one. That is, $P(x, t; u)$ represents a deterministic driving force for the purpose of computing the conditional probability density. The distribution u is just a parameter which determines the initial value of this driving force. In this context, note again that the conditional probability density of a Markov process in general depends on parameters and in particular can depend on the initial time t_0 and other parameters $\{A_1, A_2, \ldots\}$ that define the initial state of a driving force. Consequently, the notation $p(x, t|x', t'; u)$ does not imply a contradiction with the notion of a Markov process. For example, the nonautonomous Langevin equation

$$\frac{\partial}{\partial t}X(t) = -\gamma X(t) - A\cos(\omega(t-t_0)) + \sqrt{Q}\Gamma(t) \tag{39}$$

with $\gamma, A, \omega, Q > 0$ defines a Markov process that is driven by a harmonic force $-A\cos(\omega(t - t_0))$. That is, the harmonic force has amplitude A at the beginning of the process. The conditional probability density of that process depends on the parameter γ, ω, Q but also on the parameters t_0 and A which correspond to the initial amplitude and time. We have (see Sect. 3.7.3 in Frank 2005b)

$$p = p(x,t|\,x',t',\gamma,\omega,Q,A,t_0). \tag{40}$$

Nevertheless, in what follows, we will develop a slightly different notation for conditional probability densities p of strongly nonlinear Fokker-Planck equations that is in line with the first definition of Markov processes discussed above and will be helpful to elucidate that the functions p reflect indeed Markov processes.

Let us exploit first the fact that if Eq. (35) is a strongly nonlinear Fokker-Planck equations, then time-dependent solutions $P(x, t; u)$ of Eq. (35) exist for $u \in U$ and are related to their initial probability densities u by a one-to-one mapping T_t. That is, for every t we have $P(x, t; u) = T_t[u(x)]$. For an explicit construction of the map T_t, see, for example, Eq. (18). Likewise, we have $P(x, t'; u) = T_{t'}[u(x)]$. Using the inverse of T, we can map u to P like $u(x) = T_{t'}^{-1}[P(x,t;u)]$. Substituting these expressions into $p(x, t|\,x',t'; u)$, we obtain $p(x,t|x',t';T_{t'}^{-1}[P(x,t';u)]$. This result demonstrates that the information about the stochastic process $\hat{X}$ at time t' is sufficient to predict the future at $t > t'$. We can regard the conditional probability density p as a function that does not depend explicitly on u, but it depends explicitly on the state of the driving force P at time t'. In line with this remark, we introduce conditional probability densities of the form $p\ (x,\ t\mid x',\ t',\ P(x',\ t';u))$.

Let us dwell on the interpretation of a conditional probability density $p\ (x, t \mid x', t', P(x', t'; u))$. To this end, we need to discuss briefly the notion of a particular conditional averaging that is important in this context and will become important later on as well. Let us assume that we make observations of realizations of a stochastic process $\hat{X}$ for which the following two conditions hold: (i) $X\ (t') = x'$ and (ii) the ensemble of all realization is distributed like P at time t'. Next, we average across all observations that we make under these conditions. In doing so, we average under the constraints

$$\begin{aligned} X(t') = x' \text{ and } &\langle \delta(x' - X(t'))\rangle \\ &= P(x',t';u). \end{aligned} \tag{41}$$

In order to indicate that such a structured constraint should hold, we will use the notation

$$\langle\cdot\rangle_{X(t')=x';\langle\delta(x'-X(t'))\rangle=P(x',t';u)}. \tag{42}$$

In words, Eq. (42) is the instruction to take out of an ensemble with probability density P at time t' only those realizations that assume the value x' at time t'. On the one hand, this constraint induces a trivial situation. We know for sure that $X(t') = x'$ and consequently can replace the random variable $X(t')$ by x'. On the other hand, the averaging procedure may involve the random variable $X(t)$ at a time point t different from t'. Although $X(t')$ is fixed at x', the random variable $X(t)$ can assume different values at t for different realizations of the process $\hat{X}$. The conditional probability density $p\ (x,\ t\mid x',\ t',\ P(x',\ t';\ u))$ is a special case in which the delta function is averaged under the constraint (41). We have

$$\begin{aligned} &p(x,t|\,x',t',P(x',t';u)) \\ &\quad = \langle\delta(x - X(t))\rangle_{X(t')=x';\langle\delta(x'-X(t'))\rangle=P(x',t';u)}. \end{aligned} \tag{43}$$

Summarizing the results we have derived so far, we see that strongly nonlinear Fokker-Planck equations define Markov processes whose

- Time-dependent probability densities $P(x, t; u)$ are defined by Eq. (35)
- Conditional probability densities $p\ (x,\ t|x',\ t',\ P(x',\ t';\ u))$ are defined by

$$\frac{\partial}{\partial t}p(x,t|\,x',t',P') = L(x,t,P)p(x,t|\,x',t',P') \tag{44}$$

with L given by Eq. (36), $P = P(x,\ t;\ u)$, and $P' = P(x',\ t';\ u)$. Note that by multiplying Eq. (44) with $P(x',\ t';\ u)$ and integrating with respect to x', we get Eq. (35) which in turn defines the evolution of $P(x,\ t;\ u)$. Consequently, Eq. (44) defines both the evolution of $P(x,\ t;\ u)$ and p-$(x,\ t|\ x',\ t',\ P')$. Note also that the solution of Eq. (44) formally reads

$$p(x,t|\,x',t',P(x',t';u)) = \exp\left\{\int_{t'}^{t} \mathrm{d}z\, L(x,z,P(x,z;u))\right\}\delta(x-x') \tag{45}$$

and depends on the evolution of $P(x, z; u)$ for $z \in [t', t]$. In fact, as indicated above, p depends only on $P(x', t', u)$. To see this recall that the formal solution (21) can be obtained by means of the iterative method (19) such that we can write $P(x, z; u) = T_{z-t'}[P(x, t'; u)]$. Substituting this solution into Eq. (45), we get

$$p(x,t|\,x',t',P(x',t';u)) = \exp\left\{\int_{t'}^{t} \mathrm{d}z\, L(x,z,T_{z-t'}\left[P(x,t';u)\right)\right\}\delta(x-x'). \tag{46}$$

In addition, we find that the solution (45) does not explicitly depend on u.

We arrive at the following conclusion: conditional probability densities $p(x, t|\cdot)$ of Markov processes described by strongly nonlinear Fokker-Planck equations depend only on the value of individual realizations at one prior time point $t' \leq t$ and on the probability density P defined by all realizations at the very same prior time point t'.

Equation (45) can be simplified for stationary Markov processes with operators L that do not depend explicitly on time t. Then the conditional probability density in the stationary case can be computed from

$$p(x,t|\,x',t',P_{\mathrm{st}}(x')) = \exp\{(t-t')L(x,P_{\mathrm{st}}(x))\}\,\delta(x-x'). \tag{47}$$

where $P_{\mathrm{st}}(x)$ denotes a stationary probability density out of a set of stationary probability densities defined by $LP_{\mathrm{st}} = 0$. Note that in this context, P_{st} plays the role of an initial distribution u.

Just as in the linear case, the conditional probability density p in combination with the initial distribution u completely defines the stochastic process $\hat{X}$. In particular, the joint probability density $P(x_n, t_n; x_{n-1}, t_{n-1}; \ldots x_0, t_0)$ can be computed from p and u like

$$\begin{aligned} P(\cdot) &= p(x_n,t_n|\,x_{n-1},t_{n-1},P_{n-1}) \\ &\cdot p(x_{n-1},t_{n-1}|\,x_{n-2},t_{n-2},P_{n-2})\cdots \\ &\cdots p(x_1,t_1|\,x_0,t_0,u)u(x_0), \end{aligned} \tag{48}$$

with $P_{n-1} = P(x_{n-1}, t_{n-1}; u)$, $P_{n-2} = P(x_{n-2}, t_{n-2}; u)$ and so on.

In particular, the time-dependent probability densities $P(x, t; u)$ and $P(x, t'; u)$ with $t \geq t'$ are related to each other by means of a *nonlinear* functional

$$P(x,t;u) = \int_{\Omega} p(x,t|\,x',t',P(x',t';u))P(x',t';u)\,\mathrm{d}x', \tag{49}$$

where p is defined by Eq. (46). That is, the Green's function p induces a functional that is nonlinear with respect to $P(x', t'; u)$.

Langevin Equations of Strongly Nonlinear Fokker-Planck Equations

The stochastic trajectories $X(t)$ of the Markov process $\hat{X}$ defined by Eq. (44) can be computed from two-layered Langevin equations (see Sect. 3.4 in Frank 2005b) or alternatively from the self-consistent Ito-Langevin equation

$$\frac{\mathrm{d}}{\mathrm{d}t}X(t) = D_1(X(t),t,P(X(t),t;u)) + \sqrt{D_2(X(t),t,P(X(t),t;u))}\,\Gamma(t), \tag{50}$$

where $\Gamma(t)$ denotes the Langevin force introduced earlier. Note that the expression $P(X(t), t; u)$ means that the function $P(x, t; u)$ is evaluated at the state x that is given by the random variable X at time t. That is, we may write $P(X(t), t; u) = P(x, t; u)|_{x=X(t)}$. From the Langevin equation (50), we can read off that we are dealing with a Markov process. Information about one reference time t' in terms of the state $X(t')$ of a realization and the distribution of the ensemble as given by the probability density $P(x, t'; u)$ is sufficient to compute the future behavior of the trajectory $X(t)$ with $t \geq t'$.

The Langevin equation (50) may be implemented on a computer using the iterative map

$$X_{n+1} = X_n + \Delta t D_1(X_n, t_n, P(X_n, t_n; u)) + \sqrt{\Delta t D_2(X_n, t_n, P(X_n, t_n; u))}\epsilon_n \quad (51)$$

with $X(t_n) = X_n$, $t_n = t_0 + n\Delta t$, $n = 0, 1, 2, \ldots$ and ϵ_n given as statistically independent Gaussian distributed random numbers with vanishing mean and variance 2 (see above). The expression $P(X_n, t; u)$ can be computed from the realizations generated by the iteration map (51). Let $X_n^{(i)}$ denote the ith realization at time step n. Then, the stochastic trajectories $X(t)$ can numerically be computed by simulating an ensemble of realizations $i = 1, \ldots, N$ like

$$X_{n+1}^{(i)} = X_n^{(i)} + \Delta t D_1\left(X_n^{(i)}, t_n, P_n\left(X_n^{(i)}\right)\right) + \sqrt{\Delta t D_2\left(X_n^{(i)}, t_n, P_n\left(X_n^{(i)}\right)\right)}\epsilon_n^{(i)}, \quad (52)$$

where $\epsilon_n^{(i)}$ are statistically independent Gaussian random numbers with respect to both indices n and i and P_n is computed from the set $\{X_n^{(1)}, \ldots, X_n^{(N)}\}$ of realizations using standard kernel estimators. For example, we may use

$$P_n(x) = \frac{1}{Ns\sqrt{2\pi}} \times \sum_{i=1}^{N} \exp\left\{-\frac{\left(x - X_n^{(i)}\right)^2}{2s^2}\right\}, \quad (53)$$

with $s = N^{-1/5}\sigma_e(t_n)$ where $\sigma_e(t_n)$ is the standard deviation of the empirical ensemble $\{X_n^{(1)}, \ldots, X_n^{(N)}\}$ (Frank 2005b, 2008; Silverman 1986). Just as in the case of Langevin equations of linear Fokker-Planck equations, the map (52) can be started at any time step n provided that we have information about P_n and X_n. In particular, if we start at a step $n > 0$, we see that the information about the initial distribution is irrelevant. Consequently, the sequence $X_n, X_{n+1}, X_{n+2}, \ldots$ computed from the time-discrete Langevin equation (52) related to the nonlinear Fokker-Planck equation (44) describes a trajectory of a Markov process.

Finally, note that self-consistent Langevin equations can be evaluated analytically in order to determine second-order statistical properties of a stochastic process defined by a strongly nonlinear Fokker-Planck equation (Borland 1998; Kharchenko and Kharchenko 2005).

Short-Time Propagator

The Green's function for short time intervals is frequently called the short-time propagator and can be derived from the time-discrete Ito-Langevin (51). Equation (51) relates the random variable ϵ_n that is distributed like $W(\epsilon_n)$ (see Eq. (33)) to the random variable X_{n+1}. In general, if X_{n+1} is a function of ϵ_n then the probability density $W'(x_{n+1})$ of X_{n+1} is given by

$$W'(x_{n+1}) = W(\epsilon_n)\frac{\mathrm{d}\epsilon_n}{\mathrm{d}x_{n+1}}. \quad (54)$$

In particular, if X_{n+1} is computed from ϵ_n for a particular value x_n and probability density P, then we obtain the short-time conditional probability density

$$p_s(x_{n+1}|\, x_n, P(x_n, t_n; u)) = W(\epsilon_n)\frac{\mathrm{d}\epsilon_n}{\mathrm{d}x_{n+1}}. \quad (55)$$

Equation (51) can be transformed into

$$\epsilon_n = \frac{X_{n+1} - X_n + \Delta t D_1(X_n, t_n, P(X_n, t_n; u))}{\sqrt{\Delta t D_2(X_n, t_n, P(X_n, t_n; u))}}. \quad (56)$$

Substituting Eq. (56) into Eq. (55), we obtain

$$p_s(x_{n+1}|\, x_n, P(x_n, t_n; u)) = \frac{\exp\left\{-\frac{[x_{n+1} - x_n + \Delta t D_1(x_n, t_n, P(x_n, t_n; u))]^2}{4\Delta t D_2(x_n, t_n, P(x_n, t_n; u))}\right\}}{\sqrt{4\pi\Delta t D_2(x_n, t_n, P(x_n, t_n; u))}}. \quad (57)$$

Using the time-continuous framework and the replacements $n \to t$, $x \to x$, $n+1 \to t = t + \Delta t$ $x \to x$ and likewise $P(x, t'; u) \to P(x', t'; u) = P'$, we obtain the short-time propagator (see Sect. 2.8.1 in Frank 2005b)

$$p_s(x,t|x',t',P') = \frac{\exp\left\{-\frac{[x-x'+\Delta t D_1(x',t',P')]^2}{4\Delta t D_2(x',t',P')}\right\}}{\sqrt{4\pi\Delta t D_2(x',t',P')}}. \tag{58}$$

The short-time propagator has originally been proposed by Wehner and Wolfer (1987) and can be used to solve nonlinear Fokker-Planck equations numerically (Donoso and Salgado 2006; Donoso et al. 2005; Soler et al. 1992). To this end, the short-time propagator is substituted into Eq. (48), and subsequently Eq. (48) is integrated over all variables $x_{n-1}, \ldots, x_0$. Thus we obtain $P(x, t_n; u)$ for $t_n = n\Delta t$. In the context of stochastic processes described by linear Fokker-Planck equations, the construction of solutions by means of short-time propagators is referred to as path integral approach (Gardiner 1997; Haken 2004; Risken 1989). We will return to a similar path integral approach in section "Semiclassical Description of Quantum Systems." Expectation values of functions f can be computed from (58) like

$$\langle f(X(t))\rangle_{X(t')=x';\langle\delta(x'-X(t'))\rangle=P(x',t';u)} = \int_\omega f(x) p_s(x,t|x',t',P')\mathrm{d}x, \tag{59}$$

which holds for small intervals $\Delta t = t - t'$. The short-time propagator illustrates again the Markov property of solutions of the strongly nonlinear Fokker-Planck equation (44). The information about x' and P' at time t' is sufficient to make predications in terms of expectation values that the stochastic process will assume at time $t = t' + \Delta t$.

Chapman-Kolmogorov Equation, Kramers-Moyal Expansion, and Drift-Diffusion Estimates

Linear Fokker-Planck equation can be derived using the Kramers-Moyal expansion of the Chapman-Kolmogorov equation (Gardiner 1997; Risken 1989). The definition of the expansion coefficients in turn can be used to estimate the Kramers-Moyal coefficients in general and the drift and diffusion coefficients of linear Fokker-Planck equations in particular from experimental data (Friedrich and Peinke 1997; Friedrich et al. 2000). We will show in this section that if a stochastic process defined by a nonlinear Fokker-Planck equation can be embedded into a Markov process using the concept of strongly nonlinear Fokker-Planck equations, then we can proceed as in the linear case. Taking a slightly different perspective, we may say that there are Markov processes that involve conditional probability densities of the form $p\,(x, t \mid x', t', P(x', t'; u))$ and can be characterized in terms of generalized Kramers-Moyal expansion coefficients.

Chapman-Kolmogorov Equation

Let $\hat{X}$ denote a stochastic Markov process with conditional probability density $p\,(x, t \mid x', t', P(x', t'; u))$. Then as discussed in the previous section, the joint probability $P(x, t; x', t'; x'', t''; u))$ can be expressed by

$$\begin{aligned} P(x,t;x',t';x'',t'';u) = {} & p(x,t|x',t',P(x',t';u)) \\ & \cdot p(x',t'|x'',t'',P(x'',t'';u))P(x'',t'';u). \end{aligned} \tag{60}$$

Integrating with respect to x' and dividing by $P(x'', t''; u)$ yields the generalized Chapman-Kolmogorov equation

$$\begin{aligned} & p(x,t|x'',t'',P(x'',t'';u)) \\ & = \int_\Omega p(x,t|x',t',P(x',t';u)) \\ & \quad \cdot p(x',t'|x'',t'',P(x'',t'';u))\,\mathrm{d}x'. \end{aligned} \tag{61}$$

Note that in what follows, we will use the notation

$$\begin{aligned} P &= P(x,t;u), \\ P' &= P(x',t';u), \\ P'' &= P(x'',t'';u). \end{aligned} \tag{62}$$

If we need to express probability densities P different from those listed in Eq. (62), we will write down if necessary their arguments explicitly.

For example, we will write $P(x, t'; u)$ to express the probability density $\langle \delta(x - X(t')) \rangle$ for a stochastic process $\hat{X}$ with initial distribution u.

Using the notation of Eq. (62), we can write the joint probability density (60) like

$$P(x,t;x',t';x'',t'';u) = p(x,t|x',t',P') \, p(x',t'|x'',t'',P'')P'' \tag{63}$$

and the generalized Chapman-Kolmogorov Eq. (61) becomes

$$p(x,t|x'',t'',P'') = \int_\Omega p(x,t|x',t',P')p(x',t'|x'',t'',P'')\,\mathrm{d}x'. \tag{64}$$

Kramers-Moyal Expansion

In this section, the Kramers-Moyal expansion for linear Fokker-Planck equations as discussed in Risken (1989) will be generalized to the nonlinear case. Consider the conditional probability density $p(x, t|x', t', P')$ for $t = t' + \Delta t$. Then, we have

$$p(x,t'+\Delta t|x',t',P') = \int_\Omega \delta(y-x)p(y,t'+\Delta t|x',t',P')\,\mathrm{d}y. \tag{65}$$

The variables x and x' denote arbitrary states in Ω. However, let us consider next states y that are close to x' such that is $\epsilon = y - x'$ small. Using $y - x = \epsilon + x' - x$, we obtain

$$\begin{aligned} p(x,t'+\Delta t|x',t',P') = &\int_\Omega \delta(x'-x+\epsilon) \\ &\cdot p(x'+\epsilon,t'+\Delta t|x',t',P')\,d\epsilon. \end{aligned} \tag{66}$$

Use

$$\begin{aligned} \delta(x'-x+\epsilon) = \delta(x'-x) + &\sum_1^\infty \\ &\times \frac{\epsilon^n}{n!}\left(\frac{\partial}{\partial x'}\right)^n \delta(x'-x). \end{aligned} \tag{67}$$

Then, Eq. (66) becomes

$$\begin{aligned} p(x,t'+\Delta t|x',t',P') = \delta(x'-x) + &\sum_1^\infty \int_\Omega d\epsilon \frac{\epsilon^n}{n!} \\ &\cdot p(x'+\epsilon,t'+\Delta t|x',t',P)\left(\frac{\partial}{\partial x'}\right)^n \delta(x'-x). \end{aligned} \tag{68}$$

Multiplying Eq. (68) with $p(x', t' \mid x'', t'', P'')$ and integrating with respect to x' yields on the left-hand side

$$\begin{aligned} \mathrm{LHS} = &\int_\Omega p(x,t'+\Delta t|x',t',P')p(x',t'|x'',t'',P'') \\ &\mathrm{d}x' = p(x,t'+\Delta t|x'',t'',P'') \end{aligned} \tag{69}$$

and on the right-hand side

$$\begin{aligned} &\mathrm{RHS} = p(x,t'|x'',t'',P'') \\ &+\sum_1^\infty \int_\Omega \mathrm{d}x' \int_\Omega d\epsilon \frac{\epsilon^n}{n!} p(x'+\epsilon,t'+\Delta t|x',t',P') \\ &\cdot p(x',t'|x'',t'',P'')\frac{\partial^n \delta(x'-x)}{\partial x'^n} \\ &\mathrm{RHS} = p(x,t'|x'',t'',P'') \\ &+\sum_1^\infty \int_\Omega \mathrm{d}x' \delta(x'-x)\frac{\partial^n}{\partial x'^n}(-1)^n \\ &\cdot \int_\Omega d\epsilon \frac{\epsilon^n}{n!} p(x'+\epsilon,t'+\Delta t|x',t',P')p(x',t'|x'',t'',P'') \\ &\mathrm{RHS} = p(x,t'|x'',t'',P'') \\ &+\sum_1^\infty \left(-\frac{\partial}{\partial x}\right)^n \int_\Omega d\epsilon \frac{\epsilon^n}{n!} p(x+\epsilon,t'+\Delta t|x,t',P(x,t';u)) \\ &\cdot p(x,t'|x'',t'',P''). \end{aligned} \tag{70}$$

Note that we used the Chapman-Kolmogorov Eq. (61) in order to evaluate the left-hand side (69) and we used Eq. (61) as well as partial integration in order to evaluate the right-hand side (70). Let us define the moments $M_n(x, t, \Delta t, P(x, t; u))$ by

$$M_n(x,t,\Delta t,P) = \int_\Omega d\epsilon \frac{\epsilon^n}{n!} p(x+\epsilon,t+\Delta t|x,t,P) \tag{71}$$

or using $\epsilon + x = z$ by

$$M_n(x,t,\Delta t,P) = \int_\Omega \mathrm{d}z \frac{(z-x)^n}{n!} p(z,t+\Delta t|x,t,P). \tag{72}$$

Combining the left- and right-hand sides given by Eqs. (69) and (70), respectively, we obtain

$$\begin{aligned} &p(x,t'+\Delta t|x'',t'',P'') \\ &\quad = p(x,t'|x'',t'',P'') + \sum_1^\infty \left(-\frac{\partial}{\partial x}\right)^n \\ &\qquad \cdot M_n(x,t',\Delta t,P(x,t';u))p(x,t'|x'',t'',P''). \end{aligned} \tag{73}$$

To improve readability, let us replace t' by t and subsequently t'' by t'. Thus, we obtain

$$p(x,t+\Delta t|x',t',P') = p(x,t|x',t',P' + \sum_{1}^{\infty}\left(-\frac{\partial}{\partial x}\right)^{n} \cdot M_n(x,t,\Delta t,P)p(x,t|x',t',P'). \tag{74}$$

This is the time-discrete version of the Kramers-Moyal expansion of the generalized Chapman-Kolmogorov Eq. (64). Note that M_n depends on $P(x, t; u)$, whereas p depends on $P(x', t'; u)$. Next, we define the Kramers-Moyal coefficients

$$D_n(x,t,P) = \lim_{\Delta t\to 0}\frac{M_n}{\Delta t}\lim_{\Delta t\to 0} \times \frac{1}{\Delta t}\int_{\Omega} \mathrm{d}x \frac{(z-x)^n}{n!} \cdot p(z,t+\Delta t|\,x,t,P). \tag{75}$$

Dividing Eq. (74) by Δt and taking the limiting case $\Delta t \to 0$, Eq. (74) becomes the time-continuous generalized Kramers-Moyal expansion

$$\frac{\partial}{\partial t}p(x,t|\,x',t',P) = \sum_{1}^{\infty}\left(-\frac{\partial}{\partial x}\right)^{n} D_n(x,t,P) \, p(x,t|\,x',t',P'). \tag{76}$$

Note that by generalizing the Kramers-Moyal expansion to the nonlinear case, we found immediately that the coefficients D_n depend on $P(x, t; u)$, whereas the conditional probability density p depends on $P(x', t'; u)$. Note also that in the special case $D_n = 0$ for $n \geq 3$, the Kramers-Moyal expansion (76) yields the nonlinear Fokker-Planck equation (44). Finally note that since we have $M_n(\Delta t = 0) = 0$ for all n, Kramers-Moyal coefficients can also be defined by

$$D_n(x,t,P) = \left.\frac{\partial M_n}{\partial \Delta t}\right|_{\Delta t=0} = \int_{\Omega}\mathrm{d}x\frac{(z-x)^n}{n!}\frac{\partial}{\partial u}p(z,u|\,x,t,P)\Big|_{u=t}. \tag{77}$$

Drift-Diffusion Estimates

The definition of the Kramers-Moyal coefficients can be exploited to extract the drift and diffusion coefficients of nonlinear Fokker-Planck equations from time series data. Accordingly, the drift coefficient D_1 and the diffusion coefficient D_2 are defined by

$$D_1(x,t,P) = \lim_{\Delta t\to 0}\frac{1}{\Delta t}\int_{\Omega}\mathrm{d}x(z-x)p(z,t+\Delta t|x,t,P),$$
$$D_2(x,t,P) = \lim_{\Delta t\to 0}\frac{1}{2\Delta t}\int_{\Omega}\mathrm{d}x\frac{(z-x)^2}{2}p(z,t+\Delta t|x,t,P). \tag{78}$$

The limiting case Δt may be approximated by the smallest time step that is available in the data set:

$$D_1(x,t,P) \approx \frac{1}{\Delta t}\int_{\Omega}\mathrm{d}x(z-x)p(z,t+\Delta t|\,x,t,P),$$
$$D_2(x,t,P) \approx \frac{1}{2\Delta t}\int_{\Omega}\mathrm{d}x\frac{(z-x)^2}{2}p(z,t+\Delta t|\,x,t,P), \tag{79}$$

where Δt denotes now the sampling interval between two data points. Note that on the basis of the alternative definition (77), higher-order approximations can also be defined (Patanarapeelert et al. 2006). The conditional averages can be approximated by empirical conditional averages computed from a finite set of realizations $X^{(1)}(t)$, $X^{(2)}(t)$, …, $X^{(N)}(t)$. Thus, we obtain

$$D_1(x,t,P) \approx \frac{1}{\Delta t}\frac{1}{\sum_{i\in I(t,x)}1}\cdot\sum_{i\in I(t,x)}\left[X^{(i)}(t+\Delta t)-X^{(i)}(t)\right],$$
$$D_2(x,t,P) \approx \frac{1}{2\Delta t}\frac{1}{\sum_{i\in I(t,x)}1}\cdot\sum_{i\in I(t,x)}\left[X^{(i)}(t+\Delta t)-X^{(i)}(t)\right]^2, \tag{80}$$

where $I(t,x)$ is the set of indices i for which $X^{(i)}(t) \approx x$. In the case of Markov processes described by linear Fokker-Planck equations, the argument P in the coefficients can be dropped and the above drift-diffusion estimates reduce to the estimates proposed in Friedrich and Peinke (1997) and Friedrich et al. (2000) that have recently found many applications (Bödeker et al. 2003; Jafari et al. 2002; Sura and Barsugli 2002; Waechter et al. 2004). For Markov processes described by nonlinear Fokker-Planck equations, we need to compute the conditional averages for different probability densities P. To this end, we may vary the initial distribution u of a stochastic process. For a stochastic process with a particular distribution of X at time t, we will obtain the coefficients D_1 and D_2 only for that particular distribution. Using the kernel estimate method mentioned above, we obtain

$$D_1\left(x,t,P\approx\frac{1}{Ns\sqrt{2\pi}}\sum_{i=1}^{N}\exp\left\{-\frac{\left(x-X^{(i)}(t)\right)^2}{2s^2}\right\}\right)$$
$$\approx\frac{1}{\Delta t}\frac{1}{\sum_{i\in I(t,x)}1}\times\sum_{i\in I(t,x)}\left[X^{(i)}(t+\Delta t)-X^{(i)}(t)\right] \tag{81}$$

and

$$D_2\left(x,t,P\approx\frac{1}{Ns\sqrt{2\pi}}\sum_{i=1}^{N}\exp\left\{-\frac{\left(x-X^{(i)}(t)\right)^2}{2s^2}\right\}\right)$$
$$\approx\frac{1}{2\Delta t}\frac{1}{\sum_{i\in I(t,x)}1}\times\sum_{i\in I(t,x)}\left[X^{(i)}(t+\Delta t)-X^{(i)}(t)\right]^2 \tag{82}$$

with $s = N^{-1/5}\sigma_e(t_n)$, where $\sigma_e(t_n)$ is the standard deviation of the empirical ensemble $\{X^{(1)}(t), \ldots, X^{(N)}(t)\}$. Note that in general the Kramers-Moyal coefficients of Markov processes induced by conditional probability densities of the form $p(x, t|x', t', P')$ can be estimated using

$$D_n\left(x,t,P\approx\frac{1}{Ns\sqrt{2\pi}}\sum_{i=1}^{N}\exp\left\{-\frac{\left(x-X^{(i)}(t)\right)^2}{2s^2}\right\}\right)$$
$$\approx\frac{1}{n!\Delta t}\frac{1}{\sum_{i\in I(t,x)}1}\times\sum_{i\in I(t,x)}\left[X^{(i)}(t+\Delta t)-X^{(i)}(t)\right]^n. \tag{83}$$

Alternatively, parametric estimate methods may be used. For example, we may be interested in estimating the exponent q of a Markov process defined by the Plastino-Plastino model (see section "Nonextensive Systems" below)

$$\frac{\partial}{\partial t}p(x,t|x',t',P')=\left[\frac{\partial}{\partial x}\gamma x+Q\frac{\partial^2}{\partial x^2}P(x,t;u)^{q-1}\right]p(x,t|x',t',P') \tag{84}$$

with γ, Q, $q > 0$. Then, the diffusion coefficient $D_2(P) = QP^{q-1}$ involves the parameter Q and q. Using Eq. (82) and taking the logarithm, we get

$$\ln Q+(q-1)\ln\left\{\frac{1}{Ns\sqrt{2\pi}}\sum_{i=1}^{N}\exp\left\{-\frac{\left(x-X^{(i)}(t)\right)^2}{2s^2}\right\}\right\}$$
$$\approx\ln\left\{\frac{1}{2\Delta t}\frac{1}{\sum_{i\in I(t,x)}1}\sum_{i\in I(t,x)}\left[X^{(i)}(t+\Delta t)-X^{(i)}(t)\right]^2\right\}. \tag{85}$$

For example, at a particular time t, Eq. (85) can be evaluated for different states x_i. In that case, Eq. (85) assumes the form $\ln Q + (q - 1) A_1(x_i) = A_2(x_i)$. Then, the expressions $\ln Q$ and $q - 1$ (and in doing so the parameters Q and q) can be estimated from a linear regression (Frank and Friedrich 2005).

Martingales

Let $Z(t)$ denote a functional of a stochastic process $\hat{X}$ defined for $t \geq t_0$. In what follows, we will put $t_0 = 0$. Then, Z is a martingale of $\hat{X}$ if

$$\langle Z(t)\rangle_{X=\theta} = Z(t') \tag{86}$$

holds for $t \geq t'$, where θ is a realization of the random variable X on the interval $[0,t']$ (see Sect. 1.3 in Karlin and Taylor 1975). That is, the constraint $X = \theta$ means $X(s) = \theta(s)$ holds for $s \in [0,t']$. That is, in the interval $[0,t']$ the trajectory X is fixed. Roughly speaking, a martingale is a random variable for which the best predictor of its future mean value is the present value. With regard to Eq. (86), the prediction of the future mean value is $\langle Z(t)\rangle$, whereas the present value of Z is $Z(t')$. Alternatively, we may say that the information at one time t' about the value of the martingale Z is sufficient to predict the mean value of the martingale Z for future times $t \geq t'$. Note that this alternative point of view is closely related with the first definition of Markov processes discussed in the previous section.

For linear Fokker-Planck equations, there is a close link between martingales and the Markov property. Accordingly, a stochastic process is a Markov process defined by a linear Fokker-Planck equation with drift and diffusion coefficients D_1

and D_2 if and only if a particular random variable Z that involves the Fokker-Planck operator is a martingale (see Sect. 15.1 in Karlin and Taylor 1981). In the mathematical literature, this link has also been studied in the context of nonlinear Fokker-Planck equations (Djehiche and Kaj 1995; Fontbona 2003; Gärtner 1988; Graham 1990; Greven 2005; Jourdain 2000; Meleard 1996; Meleard and Coppoletta 1987; Overbeck 1996).

Our aim in this section is to make the martingale approach more accessible to scientists working in physics, applied mathematicians, and related disciplines. To this end, we will in what follows illustrate this link between martingales and Markov processes defined by strongly nonlinear Fokker-Planck equation by means of standard techniques frequently used in physics.

Theorem 1 Let $\hat{X}$ be a stochastic process with initial probability density $u(x)$ and conditional probability density

$$p(x,t|\,x',t';P') = \langle \delta(x - X(t))\rangle_{X(t')=x';\langle\delta(x'-X(t'))\rangle=p(x',t';u)}. \quad (87)$$

Then, $\hat{X}$ is a Markov process defined by the nonlinear Fokker-Planck equation

$$\frac{\partial}{\partial t}p(x,t|\,x',t';P') = L(x,t,P)p(x,t|\,x',t';P') \quad (88)$$

with

$$L(x,t,P) = -\frac{\partial}{\partial x}D_1(x,t,P) + \frac{\partial^2}{\partial x^2}D_2(x,t,P) \quad (89)$$

if and only if $Z(t)$ defined by

$$Z(t) = f(X(t)) - \int_0^t L_B f[X(z),z,P]\,\mathrm{d}z \quad (90)$$

with

$$L_B(x,t,P) = D_1(x,t,P)\frac{\partial}{\partial x} + D_2(x,t,P)\frac{\partial^2}{\partial x^2} \quad (91)$$

is a martingale of X for smooth functions f. In the context of linear Fokker-Planck equations, the operator L_B is the Fokker-Planck backwards operator (Gardiner 1997; Risken 1989). Note that in our context, we refer to f as a smooth function if it has continuous second-order derivatives. Note also that above and in what follows, we will frequently use the notation (54). Note finally that in the above theorem the notion $L_B f[X(z), z, P]$ should be interpreted like

$$\begin{aligned} L_B f[X(z),z,P] &= L_B(X(z),z,P)f(X(z)) \\ &= \{L_B(x,t,P)f(x)\}_{x=X(z),\,t=z}. \end{aligned} \quad (92)$$

That is, first we carry out the differentiations defined by the operator L_B. Subsequently, we replace in the result the state variable x by the value of the random variable X at time z. Moreover we replace t by z. Let us prove the theorem in two parts.

From Strongly Nonlinear Fokker-Planck Equations to Martingales

Let us prove in this section that a Markov process defined by a strongly nonlinear Fokker-Planck equation exhibits the martingale Z. To this end, we first compute the conditional mean of the random variable Z defined in Eq. (90). Thus, we obtain

$$\begin{aligned} &\langle Z(t)\rangle_{X=\theta} \\ &= \langle f(X(t))\rangle_{X=\theta} - \int_0^t \mathrm{d}z\langle L_B f[X(z),z,P]\rangle_{X=\theta} \\ &= \langle f(X(t))\rangle_{X=\theta} - \int_{t'}^t \mathrm{d}z\langle L_B f[X(z),z,P]\rangle_{X=\theta} \\ &\quad - \int_0^{t'} \mathrm{d}s L_B f[\theta(s),s]. \end{aligned} \quad (93)$$

The Markov property implies that the constraints can be relaxed. That is, for every functional $g(t)$ of $X(t)$ with $t \geq t'$, we have $\langle g(t)\rangle_{X=\theta} = \langle g(t)\rangle_{X(t')=x';\,P'}$ where x' is given by $x' = \theta(t')$. We have indicated here that the average may depend on how the process is distributed at time t'. Consequently, Eq. (93) becomes

$$\begin{aligned} &\langle Z(t)\rangle_{X=\theta} = \langle f(X(t))\rangle_{X(t')=x';\langle\delta(x'-X(t'))\rangle=P'} \\ &- \int_{t'}^t \mathrm{d}z\langle L_B f[X(z),z,P]\rangle_{X(t')=x',\,\langle\delta(x'-X(t'))\rangle=P'} \\ &- \int_0^{t'} \mathrm{d}s L_B f[\theta(s),s,P]. \end{aligned} \quad (94)$$

Multiplying the Fokker-Planck equation (88) with $f(x)$ and integrating with respect to x, we obtain

$$\frac{\partial}{\partial t}\int_\Omega f(x)p(x,t|\,x',t';P')\,\mathrm{d}x = \int_\Omega f(x)L(x,t,P)p(x,t|\,x',t';P')\,\mathrm{d}x. \quad (95)$$

By means of partial integration, we find that $\int_\Omega f(x)L(x,\,t,\,P)p(x,\,t|\,x',\,t';\,P')\,\mathrm{d}x = \int_\Omega p(x,\,t|\,x',\,t';\,P')L_B(x,\,t,\,P)f(x)\,\mathrm{d}x$. As a result, Eq. (95) can be transformed into

$$\begin{aligned}&\frac{\partial}{\partial t}\int_\Omega f(x)p(x,t|\,x',t',P')\,\mathrm{d}x\\ &= \int_\Omega p(x,t|\,x',t',P')L_B(x,t,P)f(x)\,\mathrm{d}x\\ &= \langle L_B(x,t,P)f(x)\rangle_{X(t')=x';P'}.\end{aligned} \quad (96)$$

Using Eq. (96), we obtain

$$\begin{aligned}&\langle L_B f[X(z),z]\rangle_{X(t')=x';\langle\delta(x-X(t'))\rangle=P'}\\ &\quad = \frac{\partial}{\partial z}\int_\Omega f(x)p(x,t|\,x',t',P')\,\mathrm{d}x.\end{aligned} \quad (97)$$

Consequently, the following integral transformation holds

$$\begin{aligned}I &= \int_{t'}^{t}\mathrm{d}z\langle L_B f[X(z),z,P]\rangle_{X(t')=x';P'}\\ &= \int_{t'}^{t}\mathrm{d}z\frac{\partial}{\partial z}\int_\Omega \mathrm{d}x f(x)p(x,z|\,x',t',P')\\ &= \langle f(X(t)\rangle_{X(t')=x';P'} - f(x').\end{aligned} \quad (98)$$

Substituting Eq. (98) into Eq. (94), we get

$$\langle Z(t)\rangle_{X=\theta} = f(x') - \int_0^{t'}\mathrm{d}s L_B f[\theta(s),s,P]. \quad (99)$$

By definition, the function $Z(t')$ for $X(s) = \theta(s)$ given in $s \in [0,\, t']$ reads

$$Z(t') = f(x') - \int_0^{t'}\mathrm{d}s L_B f[\theta(s),s,P]. \quad (100)$$

Consequently, we have our final result

$$\langle Z(t)\rangle_{X=\theta} = Z(t') \quad (101)$$

and the proof is completed.

From Martingales to Strongly Nonlinear Fokker-Planck Equations

Let us prove next that the martingale (90) defines a Markov process of a strongly nonlinear Fokker-Planck equation. Evaluating Eq. (90) by analogy to Eq. (93) gives us

$$\begin{aligned}\langle Z(t)\rangle_{X=\theta} &= \langle f(X(t))\rangle_{X=\theta}\\ &\quad - \int_{t'}^{t}\mathrm{d}z\langle L_B f[X(z),z,P]\rangle_{X=\theta}\\ &\quad - \int_0^{t'}\mathrm{d}s L_B f[\theta(s),s,P].\end{aligned} \quad (102)$$

Substituting this result into Eq. (86) and substituting Eq. (100) into Eq. (86), we see that Eq. (86) becomes

$$\begin{aligned}f(X(t))\rangle_{X=\theta} &= f(x')\\ &\quad + \int_{t'}^{t}\mathrm{d}z\langle L_B f[X(z),z]\rangle_{X=\theta}.\end{aligned} \quad (103)$$

Equation (103) can equivalently be written as

$$\begin{aligned}&\int_\Omega f(x)p(x,t|\,X=\theta)\,\mathrm{d}x\\ &\quad = f(x') + \int_{t'}^{t}\mathrm{d}z\int_\Omega \mathrm{d}x p(x,z|\,X=\theta)L_B f[x,t,P]\end{aligned} \quad (104)$$

with $p(x,\,z|X=\theta) = \delta(x - X(z))_{X=\theta}$. Using partial integration, we can show that the operator L_B and the differential operator L are related to each other like

$$\begin{aligned}&\int_\Omega \mathrm{d}x p(x,z|\,X=\theta)\,L_B f[x,t,P]\\ &\quad = \int_\Omega \mathrm{d}x f(x)L(x,z,P)p(x,z|\,X=\theta).\end{aligned} \quad (105)$$

Substituting this result into Eq. (104) yields

$$\begin{aligned}0 = \int_\Omega \mathrm{d}x f(x)\{&p(x,t|X=\theta) - \delta(x-x') -\\ &\int_{t'}^{t}\mathrm{d}z L(x,z,P)p(x,z|X=\theta)\}.\end{aligned} \quad (106)$$

This holds for arbitrary smooth functions f. Since f is arbitrary, the expression in the brackets $\{\cdot\}$ of Eq. (106) must vanish, and we obtain

$$p(x,t|X=\theta)=\delta(x-x')+\int_{t'}^{t}\mathrm{d}z\,L(x,z,P)p(x,z|X=\theta). \tag{107}$$

Differentiating Eq. 107 with respect to t gives us

$$\frac{\partial}{\partial t}p(x,t|X=\theta)=L(x,t,P)p(x,t|X=\theta). \tag{108}$$

Multiplying with the probability density $P(X=\theta)$ and performing a functional integration with respect to the path θ, we obtain

$$\frac{\partial}{\partial t}P(x,t)=L(x,t,P)P(x,t). \tag{109}$$

The formal solutions of Eqs. (108) and (109) read

$$p(x,t|X=\theta)=\exp\left\{\int_{t'}^{t}\mathrm{d}z\,L(x,z,P)\right\}\delta(x-x') \tag{110}$$

and

$$P(x,t)=\exp\left\{\int_{t'}^{t}\mathrm{d}z\,L(x,z,P)\right\}P(x,t'). \tag{111}$$

We see that a solution of Eq. (108) under the initial condition $p(x,t|X=\theta)=\delta(x-x')$ for $t\to t'$ with $x'=\theta(t')$ only depends on $\theta(t')$ but does not depend on $\theta(s)$ for $s<t'$. Consequently, X is a Markov process. However, L depends on P. From Eq. (110), it is clear that the conditional probability density p depends on the time-dependent probability density P for $z\in[t',t]$. Since the probability density $P(x,t;u)$ for $t\geq t'$ can be computed from $P(x,t';u)$ as shown in Eq. (111), we conclude that p depends only on $P(x,t';u)$ and does not depend on the evolution of P on the whole interval $[t,t']$. Therefore, we have $p(x,t|X=\theta)=p(x,t|x',t',P')$. Substituting this result into Eq. (108), we see that Eq. (108) becomes a strongly nonlinear Fokker-Planck equation

$$\frac{\partial}{\partial t}p(x,t|x',t';P')=L(x,t,P)p(x,t|x',t';P'). \tag{112}$$

Examples

Shimizu-Yamada Model

The Shimizu-Yamada model (Shimizu 1974; Shimizu and Yamada 1972) corresponds to the Desai-Zwanzig model (7) for a linear single-particle force $h(x)=-\gamma x$. The evolution of the conditional probability density p is defined by

$$\frac{\partial}{\partial t}p(x,t|x',t',P')=\left[\frac{\partial}{\partial x}\gamma x+\kappa\left(x-\int_\Omega xP(x,t;u)\,\mathrm{d}x\right)+Q\frac{\partial^2}{\partial x^2}\right]\cdot p(x,t|x',t',P') \tag{113}$$

with $\Omega=\mathbb{R}$ and $\gamma,\kappa,Q>0$. Multiplying Eq. (113) with $P(x',t';u)$ and integrating with respect to x' yields the evolution equation for $P(x,t;u)$:

$$\frac{\partial}{\partial t}P(x,t;u)=\left[\frac{\partial}{\partial x}\gamma x+\kappa\left(x-\int_\Omega xP(x,t;u)\,\mathrm{d}x\right)+Q\frac{\partial^2}{\partial x^2}\right]\cdot P(x,t;u). \tag{114}$$

See also Frank (2004d) and Sect. 3.10 in Frank (2005b). From Eq. (114), it follows that the mean value $m(t)=\int_\Omega xP(x,t;u)\,\mathrm{d}x$ decays exponentially like

$$m(t)=m(t_0)\exp\{-\gamma(t-t_0)\} \tag{115}$$

with $m(t_0)=\int_\Omega xu(x)\,\mathrm{d}x$. Substituting Eq. (115) into Eqs. (113) and (114), we realize that a solution $P(x,t;u)$ and a Green's function p exists for any initial probability density $u(x)$. Therefore, the Shimizu-Yamada model is a strongly nonlinear Fokker-Planck equation and describes a Markov process.

It can be shown that the conditional probability density $p(x,t\mid x',t';u)$ reads (see Frank (2004d) and Sect. 3.10 in Frank (2005b))

$$p(x,t|x',t';u)=\frac{\exp\left\{-\dfrac{[x-g(t,t',t_0,u)-x'm(t,t')]^2}{2K(t,t')}\right\}}{\sqrt{2\pi K(t,t')}} \tag{116}$$

with

$$m(t,t')=\exp\{-(\gamma+\kappa)(t-t')\}, \tag{117}$$

$$K(t,t')=\frac{Q}{\gamma+\kappa}[1+\exp\{-2(\gamma+\kappa)(t-t')\}], \tag{118}$$

and

$$g = [\exp\{-\gamma(t-t_0)\} - \exp\{-(\gamma+\kappa)t + \gamma t_0 + \kappa t')\}] \cdot \int_\Omega xu(x)\,\mathrm{d}x. \tag{119}$$

The mean value $m(t)$ acts as a self-organized driving force of the stochastic process. Since there is a one-to-one mapping of $m(t)$ to $m(t')$ with $t' < t$, we can eliminate the parameter u in $p(x, t|x', t'; u)$ as argued in section "Strongly Nonlinear Fokker-Planck Equations." Substituting Eq. (115) into Eq. (119), we obtain

$$g(t,t',P(x,t';u)) = \exp\{-\gamma(t-t')\}\cdot [1-\exp\{-\kappa\,(t-t')\}]\int_\Omega xP(x,t';u)\,\mathrm{d}x \tag{120}$$

or

$$g(t,t',\langle X(t')\rangle)\exp\{-\gamma(t-t')\}\cdot [1-\exp\{-\kappa\,(t-t')\}]\,\langle X(t')\rangle. \tag{121}$$

Consequently, the conditional probability density $p(x, t|x', t', P')$ reads

$$p(x,t|x',t';P') = \frac{\exp\left\{-\frac{[x-g(t,t',\langle X(t')\rangle)-x'm(t,t')]^2}{2K(t,t')}\right\}}{\sqrt{2\pi K(t,t')}}. \tag{122}$$

Dynamic Takatsuji Model

The dynamic Takatsuji model for the conditional probability density p is defined by

$$\frac{\partial}{\partial t}p(x,t|\,x',t';P') = \left[\frac{\partial}{\partial x}(\gamma+c)x - \sqrt{c}\tanh\left(\sqrt{c}\int_\Omega xP(x,t;u)\,\mathrm{d}x\right) + Q\frac{\partial^2}{\partial x^2}\right]\cdot p(x,t|\,x',t';P') \tag{123}$$

with $x \in \Omega = \mathbb{R}$ and $c, Q > 0$ $\gamma \in \mathbb{R}$. Likewise, the probability density $P(x, t; u)$ satisfies

$$\frac{\partial}{\partial t}P(x,t;u) = \left[\frac{\partial}{\partial x}(\gamma+c)x - \sqrt{c}\tanh\left(\sqrt{c}\int_\Omega xP(x,t;u)\,\mathrm{d}x\right) + Q\frac{\partial^2}{\partial x^2}\right]\cdot P(x,t;u). \tag{124}$$

For details, see Frank (2004e) and Takatsuji (1975). From Eq. (124), it follows that the first moment $M_1(t) = X$ can be computed from

$$\frac{\mathrm{d}}{\mathrm{d}t}M_1(t) = -(\gamma+c)M_1 + \sqrt{c}\tanh\left[\sqrt{c}M_1(t)\right]. \tag{125}$$

For arbitrary initial distribution u, solutions of $M_1(t)$ exist and are smooth functions of t. Substituting these solutions into Eqs. (123) and (124), we see that solutions of Eqs. (123) and (124) in terms of Green's functions p and probability densities P exist as well. Consequently, the dynamic Takatsuji model belongs to the class of strongly nonlinear Fokker-Planck equations and describes a Markov process.

Since $p(x, t|x', t', P')$ depends on P', the expected mean value of $X(t)$ of realizations that assume the value x' at time t' depends on the distribution of the ensemble at time t'. Let us illustrate this issue. The conditional mean value under consideration reads

$$\langle X(t)\rangle_{X(t')=x',P'} = \int xp(x,t|\,x',t',P')\,\mathrm{d}x. \tag{126}$$

Multiplying Eq. (123) with x and integrating with respect to x, we obtain

$$\frac{\mathrm{d}}{\mathrm{d}t}\langle X(t)\rangle_{X(t')=x',P'} = -(\gamma+c)\langle X(t)\rangle_{X(t')=x',P'} + \sqrt{c}\tanh\left[\sqrt{c}M_1(t)\right]. \tag{127}$$

The solution reads

$$\langle X(t)\rangle_{X(t')=x',P'} = x'\exp\{-(\gamma+c)(t-t')\} + \sqrt{c}\int_{t'}^{t}\tanh\left[\sqrt{c}M_1(z)\right]\mathrm{d}z, \tag{128}$$

where $M_1(z)$ is the solution of Eq. (125) for the initial value $M_1(t') = \int_\Omega xP(x,t';u)\,\mathrm{d}x$. Let I denote the integral $I = \sqrt{c}\int_{t'}^{t}\tanh[\sqrt{c}M_1(z)]\,\mathrm{d}z$. Then, I depends on $M_1(t')$, c, γ, t' and t: $I = I(t, t', M_1(t'), c, \gamma)$. Consequently, Eq. (128) can be cast into the form

$$\langle X(t)\rangle_{X(t')=x',P'} = x'\exp\{-(\gamma+c)(t-t')\} + I\left(t,t',\int x'P(x',t';u)\,\mathrm{d}x',c,\gamma\right) \tag{129}$$

or

$$\langle X(t)\rangle_{X(t')=x',P'} = x'\exp\{-(\gamma+c)(t-t')\} + I(t,t',\langle X(t')\rangle,c,\gamma). \quad (130)$$

Equation (130) illustrates that in order to predict future conditional mean values of a Takatsuji process $\hat{X}$ at times t, it is sufficient to have at one time $t' \leq t$ information about the state value x' of a realization of $\hat{X}$ and the mean value $X(t')$ of all realizations of $\hat{X}$.

Note that the trajectories $Z(t)$ of martingale processes $\hat{Z}$ induced by the Takatsuji process $\hat{X}$ are given by

$$Z(t) = f(X) - \int_0^t \mathrm{d}s\{[-(\gamma+c)X(s) + \sqrt{c}\tanh\left(\sqrt{c}\langle X(s)\rangle\right)]\frac{\partial f}{\partial X(s)} + Q\frac{\partial^2 f}{\partial X^2(s)}\} \quad (131)$$

for arbitrary smooth functions f. We can exploit these martingale processes in order to compute conditional expectations. For example, for $f(y) = y$ from the martingale property (86), it follows that

$$\langle X(t)\rangle_{X(t')=x',P'} = x' - \int_{t'}^t \mathrm{d}s(\gamma+c)\langle X(s)\rangle - \sqrt{c}\tanh\left[\sqrt{c}\langle X(s)\rangle\right]. \quad (132)$$

Differentiating this relation with respect to t, we obtain Eq. (127) again and so we can compute the conditional expectation (130).

Liquid Crystal Model

Liquid crystals exhibit nematic-isotropic phase transitions (Chandrasekhar 1977; de Gennes and Prost 1993; de Jeu 1980). At high temperatures, the liquid crystal macromolecules exhibit an orientational disorder. The liquid crystal is said to be in the isotropic phase. Below a critical temperature, the macromolecules show some degree of orientational order. The degree of orientational order is often measured by the Maier-Saupe order parameter S (Maier and Saupe 1958).

A nonlinear Fokker-Planck equation that describes the stochastic behavior of the liquid crystal in the isotropic and nematic phases and to a certain extent also describes the order-disorder phase transition was proposed by Doi and Edwards (Doi and Edwards 1988) and Hess (Hess 1976) and is shown above in Eq. (8). Equation (8) describes the random walk of the orientation of liquid crystal molecules, where the orientation is given by a vector $\mathbf{x}$ that points to the surface of a unit sphere. If we are dealing with rod-like molecules, then the orientation corresponds to the primary axis of the molecules along the rod. In particular, for liquid crystals with an axial symmetry, the liquid crystal model can be simplified. The simplified model describes the random walk of the molecule alignment with the symmetry axis. The random variable is defined on $X \in \Omega = [0, 1]$. For sake of simplicity, we will extend the range of definition to the interval $\Omega = [-1, 1]$ and require that distributions are symmetric. For $X = 0$, the molecule has an orientation perpendicular to the symmetry axis. If $X = 1$ or $X = -1$, the molecule points exactly in the direction of the symmetry axis. In this symmetric case, the probability density P of X satisfies (Felderhof 2003)

$$\frac{\partial}{\partial t}P(x,t;u) = \frac{\partial}{\partial x}\left(1-x^2\right)\cdot\left[-\frac{9}{2}\kappa x\left(\int x^2 P(x,t;u)\,\mathrm{d}x - \frac{1}{3}\right) + D_r\frac{\partial}{\partial x}\right]P(x,t;u) \quad (133)$$

with κ, $D_r > 0$. Equation (133) as well as the original Eq. (8) are regarded as descriptions for an ensemble of macromolecules that perform rotational Brownian motion (Doi and Edwards 1988). Since Brownian motion is a Markov process, it is reasonable to construct on the basis of Eq. (133) a model for a many-body system that exhibits a Markov process. In line with our discussion in section "Markov Property: Second-Order and Higher-Order Statistics," we assume that the conditional probability density p satisfies (Frank 2005c)

$$\frac{\partial}{\partial t}p(x,t|x',t',P') = \frac{\partial}{\partial x}\left(1-x^2\right) \cdot \left[-\frac{9}{2}\kappa x\left(\int x^2 P(x,t;u)\,\mathrm{d}x - \frac{1}{3}\right) + D_r\frac{\partial}{\partial x}\right] \cdot p(x,t,|x',t',P'). \tag{134}$$

Note that the expression in the bracket $(\cdot)$ is related to the Maier-Saupe order parameter which reads in the symmetric case

$$S(t) = \frac{1}{2}\left(3\int x^2 P(x,t;u)\,\mathrm{d}x - 1\right). \tag{135}$$

Due to the boundary conditions $X \in [-1, 1]$, the order parameter S and consequently the bracket $(\cdot)$ is bounded. This implies that solutions P and p of Eqs. (133) and (134) exist and that the liquid crystal model (133)–(134) describes a Markov process. The self-consistent Ito-Langevin equation of this Markov process reads (Frank 2005c)

$$\frac{\mathrm{d}}{\mathrm{d}t}X(t) = \frac{9\kappa}{2}\left(1-X(t)^2\right)X(t)\left(\left\langle X(t)^2\right\rangle - \frac{1}{3}\right) - 2D_r X(t) + \sqrt{D_r\left(1-X(t)^2\right)}\Gamma(t). \tag{136}$$

Trajectories $Z(t)$ of martingale processes $\hat{Z}$ of the liquid crystal model are defined by (Frank 2007)

$$Z(t) = f(X(t)) - \int_0^t \mathrm{d}s[\cdot]f(X(s)) \tag{137}$$

with

$$[\cdot] = \left[\left(\frac{9\kappa}{2}\left(1-X(s)^2\right)X(s)\left(\left\langle [X(s)]^2\right\rangle - \frac{1}{3}\right) - 2D_r X(s)\right)\frac{\partial}{\partial X(s)} + D_r\frac{\partial^2}{\partial X^2(s)}\right]. \tag{138}$$

In the stationary case, the short-time autocorrelation function $C(\Delta t) = X(t)X(t+\Delta t)_{\mathrm{st}}$ reads (Frank 2005c)

$$C(\Delta t) = \frac{2S+1}{3} - \frac{2D_r(1-S)}{3}\Delta t + O\left(\Delta t^2\right), \tag{139}$$

where S denotes the order parameter (see above) in the stationary case. That is, we have $S = (3\ X^2_{\mathrm{st}} - 1)/2$. Consequently, C depends on S. This has important implications for the hysteresis loop of the nematic-isotropic phase transition. Let us assume that if we decrease the temperature of a liquid crystal, we find the transition from the isotropic to the nematic phase with $S = 0 \to S > 0$ at the critical temperature $T_{c,\mathrm{low}}$. In contrast, if we increase the temperature of a liquid crystal, we find the transition from the nematic to the isotropic phase with $S > 0 \to S = 0$ at the slightly higher critical temperature $T_{c,\mathrm{high}}$. Then, in the temperature interval $[T_{c,\mathrm{low}}, T_{c,\mathrm{high}}]$, the liquid crystal exhibits two autocorrelation functions

$$C_{\mathrm{isotrope}}(\Delta t) = \frac{1}{3} - \frac{2D_r}{3}\Delta t, \tag{140}$$

$$C_{\mathrm{nem}}(\Delta t) = \frac{2S(T)+1}{3} - \frac{2D_r(1-S(T))}{3}\Delta t \tag{141}$$

which hold up to terms of order Δt^2. Equations (140)–(141) illustrate that we are dealing with a system that exhibits two kinds of Markov processes that we may label "isotropic" and "nematic," respectively. The modeling approach by means of strongly nonlinear Fokker-Planck equations indicates that these Markov processes are just different members of a family of Markov processes that naturally emerge in the self-organized liquid crystal. That is, the two Markov processes are not related to two different systems but they represent two different "states" of the same self-organizing many-body system.

Let us compute the conditional mean value of molecules that are perpendicular to the symmetry axis. To this end, we consider the random walk of the orientation angle ϕ defined by $X(t) = \sin\phi(t)$. Using the Stratonovich-Langevin equation of Eq. (134) (see Frank 2005c), we obtain a self-consistent Langevin equation for ϕ:

$$\frac{\mathrm{d}}{\mathrm{d}t}\phi = \frac{9}{4}\kappa \sin(2\phi(t))\left(\left\langle \sin^2(\phi(t))\right\rangle - \frac{1}{3}\right) - D_r \tan\phi(t) + D_r\Gamma(t). \tag{142}$$

For short time intervals $\Delta t = t - t'$ and appropriate small noise amplitudes D_r, we assume that $\phi(t) \approx 0$ if $\phi(t') \approx 0$. Linearizing Eq. (142) at $\phi = 0$ yields

$$\frac{\mathrm{d}}{\mathrm{d}t}\phi(t) = \left\{\frac{9}{4}\kappa\left(\left\langle \sin^2(\phi(t))\right\rangle - \frac{1}{3}\right) - D_r\right\}\phi(t) + D_r\Gamma(t). \tag{143}$$

The conditional expectation value $\int \phi p(\phi, t|\phi', t', P)\mathrm{d}\phi$ for short time intervals Δt can then be computed from Eq. (143) by averaging both side of Eq. (143) under the constraint $\phi(t') = \phi'$ and $\phi(t')$ distributed like P'. Thus, we obtain

$$\langle\phi(t)\rangle_{\phi(t')=\phi',P'} = \phi'\left[1 + \Delta t\left\{\frac{9}{4}\kappa\left(\left\langle \sin^2(\phi(t'))\right\rangle - \frac{1}{3}\right) - D_r\right\}\right] \tag{144}$$

or

$$\langle\phi(t)\rangle_{\phi(t')=\phi',P'} = \phi'\left[1 + \Delta t\left\{\frac{3}{2}\kappa S(t') - D_r\right\}\right]. \tag{145}$$

These estimates hold for small intervals Δt, sufficiently small noise amplitudes D_r, and orientation angles $\phi' \approx 0$. Again, in line with our general discussion in the preceding sections, we see that the conditional expectation $\phi(t)_{\phi(t')=\phi',P'}$ can be computed provided that for $t' < t$ the distribution of $\phi(t')$ or at least the order parameter $S(t')$ is known and the angle ϕ' is selected.

Semiclassical Description of Quantum Systems

A stochastic treatment of semiclassical quantum systems by means of nonlinear Fokker-Planck equations that can be cast into the form of Eqs. (5) and (6) has been proposed and analyzed in several studies (Carrillo et al. 2008; Chavanis 2003; Frank and Daffertshofer 1999; Kadanoff 2000; Kaniadakis 2001a; Kaniadakis and Quarati 1993, 1994). Accordingly, a Fermi or Bose particle with mass 1 that moves in a one-dimensional space with velocity v exhibits in the stationary case a Fermi-Dirac or Bose-Einstein distribution of the kinetical energy $E_{\mathrm{kin}} = v^2/2$. The free diffusion of the particle can be described by the nonlinear Fokker-Planck equations (Frank and Daffertshofer 1999)

$$\frac{\partial}{\partial t}P(v,t;u) = \frac{\partial}{\partial v}\gamma v[1 \mp P(v,t,u)]P(v,t;u) + Q\frac{\partial^2}{\partial v^2}P(v,t;u), \tag{146}$$

where the upper sign holds for Fermi particles, the lower for Bose particles. The parameters γ and Q represent damping and fluctuation strength and are related to the temperature T by the fluctuation dissipation theorem $Q/\gamma = 1/(k_B T)$, where k_B is the Boltzmann constant. The stationary probability density $P_{\mathrm{st}}(v)$ of Eq. (146) reads

$$P_{\mathrm{st}}(v) = \frac{1}{\exp\{(E_{\mathrm{kin}} - \mu)/(k_B T)\} \pm 1}, \tag{147}$$

where μ is a normalization constant that can be interpreted as chemical potential. The transient solution $P(v, t; u)$ can be obtained by solving the integral equation (Frank 2007; Meleard and Coppoletta 1987)

$$P(v,t;u) = \int_\Omega \mathrm{d}v_0 G_B(t,t_0,v,v_0)u(v_0,t_0) + \int_{t_0}^{t}\mathrm{d}s \cdot \int_\Omega \mathrm{d}v' G_B(t,s,v,v')\gamma\frac{\partial}{\partial v'} \times [1 \mp P(v',s;u)]P(v',s;u) \tag{148}$$

with

$$G_B(t,t',v,v') = \frac{1}{\sqrt{2\pi Q(t-t')}}\exp\left\{-\frac{(v-v')^2}{2Q(t-t')}\right\}, \tag{149}$$

where G_B is the Gaussian propagator of Brownian motion. In the limit $t \to \infty$, the transient solution

$P(v, t; u)$ approaches $P_{\mathrm{st}}(v)$ (Frank and Daffertshofer 2001b; Kaniadakis 2001a). Equation (148) is a useful description for numerical approaches. Using partial integration, Eq. (148) can be written in the form

$$P(v,t;u) = \int_\Omega \mathrm{d}v_0 G_B(t,t_0,v,v_0)u(v_0,t_0) + \int_{t_0}^{t} \mathrm{d}s \int_\Omega \mathrm{d}v' G_B(t,s,v,v')\gamma \frac{v-v'}{Q(t-s)} \cdot [1 \mp P(v',s;u)]P(v',s;u). \tag{150}$$

This integral relation can be solved iteratively. In contrast to the iterative procedure discussed in section "Time-Dependent Solutions and First Order Statistics," there is no need to compute derivatives. That is, we are dealing with some kind of path integral approach here that is similar to the numerical path integral approach involving short-time propagators; see section "Short-Time Propagator."

In order to describe quantum particles that exhibits a Markov process, we may exploit the approach outlined in section "Markov Property: Second-Order and Higher-Order Statistics." Accordingly, the Markov conditional probability density of the quantum particle satisfies

$$\frac{\partial}{\partial t} p(v,t|v',t',P') = \left\{ \frac{\partial}{\partial v}\gamma v[1 \mp P(v,t;u)] + Q\frac{\partial^2}{\partial v^2} \right\} \cdot p(v,t|v',t',P'), \tag{151}$$

and the self-consistent Langevin equation reads

$$\frac{\mathrm{d}}{\mathrm{d}t} v(t) = -\gamma v(t)(1 \mp P(v(t),t;u)) + \sqrt{Q}\Gamma(t). \tag{152}$$

From a martingale perspective, we see that stochastic trajectories $v(t)$ induce for arbitrary smooth functions f the martingale $\hat{Z}$ with trajectories

$$Z(t) = f(v(t)) - \int_0^t \mathrm{d}s \cdot \left[-\gamma v(s)\left[1 \mp P(v(s),s;u)\right] \frac{\partial}{\partial v^2} + Q\frac{\partial^2}{\partial v^2} \right] f(v)|_{v=v(s)}. \tag{153}$$

Moreover, as far as the Markov short-time propagator is concerned, for small time intervals $t = t' + \Delta t$, the propagator reads

$$p(v,t|v',t',P') = \sqrt{\frac{1}{2\pi Q\Delta t}} \exp\left\{ -\frac{[v - v' + \Delta t\gamma v'[1 \mp P']]^2}{2Q\Delta t} \right\}, \tag{154}$$

and can be computed from the information about the distribution P' of $v(t')$ and the state v that was observed for particular realizations of the process $\hat{v}$. In the stationary case, the propagator p reads for small time intervals $\Delta t = t - t'$

$$p(v,t|v',t',P_{\mathrm{st}}(v')) = \sqrt{\frac{1}{2\pi Q\Delta t}} \exp\left\{ -\frac{[v - v' + \Delta t\gamma v'[1 \mp P_{\mathrm{st}}(v')]]^2}{2Q\Delta t} \right\} \tag{155}$$

with P_{st} defined by Eq. (147).

Nonextensive Systems

Nonextensive thermostatistical systems have been related to the Tsallis entropy (Abe and Okamoto 2001; Tsallis 1988)

$$S_q = \frac{1}{q-1}\int_\Omega [P(v)^q - P(v)]\,\mathrm{d}v, \tag{156}$$

where q measures the degree of nonextensivity. Diffusion processes in nonextensive thermostatistical systems can be regarded as generalized Ornstein-Uhlenbeck processes that satisfy the nonlinear Fokker-Planck equation (Plastino and Plastino 1995) (see also Borland 1998; Chavanis 2003, 2004; Compte and Jou 1996; Drazer et al. 2000; Frank and Daffertshofer 1999, 2000; Shiino 2003; Tsallis and Bukman 1996)

$$\frac{\partial}{\partial t} P(v,t;u) = \frac{\partial}{\partial v}\gamma v P(x,t;u) + Q\frac{\partial^2}{\partial v^2} P(v,t;u)^q, \tag{157}$$

where v is the velocity of a particle with mass 1 that moves in one spatial dimension. In the asymptotic domain $P(v, t; u)$ approaches, a stationary Tsallis distribution

$$P_{\mathrm{st}}(v) = \frac{D_{\mathrm{st}}}{\left[1 + \gamma(1-q)v^2/\left[2qQD_{\mathrm{st}}^{q-1}\right]\right]^{1/(1-q)}} \tag{158}$$

for $q \in (1/3, 1)$ with $D_{\mathrm{st}} = \left[\gamma/(2qQ)z_q^2\right]^{1/(1+q)}$ and $z_q = \sqrt{\pi/(1-q)}\Gamma[(1+q)/[2(1-q)]]/$

$\Gamma[1/(1-q)]$ (Frank and Daffertshofer 2000). The process described by Eq. (157) is said to evolve in a nonextensive thermodynamic framework because its stationary probability density (158) maximizing the entropy measure (156). As discussed in section "Markov Property: Second-Order and Higher-Order Statistics," the Markov conditional probability density p satisfies

$$\frac{\partial}{\partial t}p(v,t|\,v',t',P') = \frac{\partial}{\partial x}\gamma v p(v,t|\,v',t',P') + Q\frac{\partial^2}{\partial v^2}P(v,t;u)^{q-1}p(v,t|\,v',t',P'). \tag{159}$$

The self-consistent Langevin equation of the Markov diffusion process reads (see also Borland 1998)

$$\frac{\mathrm{d}}{\mathrm{d}t}v(t) = -\gamma v(t) + \sqrt{QP(v(t),t;u)^{q-1}}\Gamma(t). \tag{160}$$

Any stochastic path $v(t)$ computed from Eq. (160) yields for arbitrary smooth functions f the martingale

$$Z(t) = f(v(t)) - \int_0^t \mathrm{d}s\left[-\gamma v(s)\frac{\partial}{\partial v(s)} + QP(v(s),s;u)^{q-1}\frac{\partial^2}{\partial v(s)^2}\right]f(v(s)). \tag{161}$$

The autocorrelation $C = v(t)v(t')$ in the transient domain for $u(v_0) = \delta(v - v_0)$ reads (Frank 2004a)

$$C(t,t',v_0,t_0) = M_2(t',t_0,v_0)\exp\{-\gamma(t-t')\} \tag{162}$$

with

$$\begin{aligned} M_2(t',t_0,v_0) &= K(t',t_0) + M_1^2(t',t_0,v_0),\\ K(t',t_0) &= \frac{1}{3q-1}\left[\frac{2qQ\left[z_q\right]^{(1-q)}}{\gamma}\cdot(1-\exp\{-(1+q)\gamma(t-t_0)\})\right]^{2/(1+q)},\\ M_1(t',t_0,v_0) &= v_0\exp\{-\gamma(t'-t_0)\}. \end{aligned} \tag{163}$$

The autocorrelation function C depends on t_0. This is not in contradiction with the Markov property of the underlying process as discussed in section "Markov Property: Second-Order and Higher-Order Statistics." In particular, we may eliminating the initial condition. Then, Eq. (162) reads

$$C(t,t') = \langle u^2(t')\rangle\exp\{-\gamma(t-t')\}. \tag{164}$$

and holds for arbitrary initial probability densities u.

Linear Nonequilibrium Thermodynamics

Linear and nonlinear Fokker-Planck equations alike can be approached from the principles of linear nonequilibrium thermodynamics (de Groot and Mazur 1962; Glansdorff and Prigogine 1971; Kondepudi and Prigogine 1998). For stochastic processes to which linear nonequilibrium thermodynamics applies the probability density $P(x, t; u)$ of a process evolves such that the free energy functional $F[P]$ decreases as a function of time t. More precisely, following a study by Compte and Jou (Compte and Jou 1996), it has been proposed that P satisfies the nonlinear Fokker-Planck equations of the form (Chavanis 2004; Frank 2002a, 2005b; Scarfone and Wada 2007)

$$\frac{\partial}{\partial t}P = \frac{\partial}{\partial x}P\tilde{M}\frac{\partial}{\partial x}\frac{\delta F}{\delta P}, \tag{165}$$

where $\tilde{M}$ is an appropriately defined mobility coefficient and $\delta F/\delta P$ denotes the variational

derivative of F. Note that this thermodynamic approach is closely related to the GENERIC approach developed in Espanol et al. (1999), Jelic et al. (2006), Öttinger (2005, 2007), and Öttinger and Grmela (1997).

For example, the Desai-Zwanzig model (8) can be expressed in terms of Eq. (165) for $\tilde{M} = 1$ and (Frank 2005b; Shiino 1987)

$$F = \langle V \rangle + U_{\mathrm{MF}} - QS_{\mathrm{BGS}}. \tag{166}$$

Here, V is the potential of the force h (i.e., we have $V(x) = -\int h(x)\,\mathrm{d}x$, U_{MF} is the mean field energy given by $U_{\mathrm{MF}} = -\kappa\sigma^2/2$ (where σ^2 is the variance of the process), and S_{BGS} is the Boltzmann-Gibbs-Shannon entropy

$$S_{\mathrm{BGS}} = -\int_{\Omega} P(x,t;u)\ln P(x,t;u)\,\mathrm{d}x, \tag{167}$$

where we have put the Boltzmann constant equal to unity. The liquid crystal model (8) can be written as Eq. (165) with (Frank 2005c)

$$F = -\frac{\kappa}{2}S^2 - D_r S_{\mathrm{BGS}}, \tag{168}$$

where S is the Maier-Saupe order parameter (135). We have $\tilde{M} = 1 - x^2$. Moreover, the expression $-\kappa S^2/2$ is the Maier-Saupe mean field energy. The Kuramoto-Shinomoto-Sakaguchi model (10) can equivalently be expressed in terms of Eq. (165) with $\tilde{M} = 1$ (see Sect. 5.4 in Frank 2005b) using

$$F = \langle V \rangle - \frac{\kappa}{2}r^2 - QS_{\mathrm{BGS}}, \tag{169}$$

where r is the cluster phase defined by $r = |\exp.\{-iX(t)\}|$. Here, the expression $-\kappa r^2/2$ is a measure for the mean field energy among the phase oscillators described by the model. The Takatsuji model (124) involves a constant mobility coefficient $\tilde{M} = 1$ and the free energy functional (Frank 2005b)

$$F = \frac{\gamma + c}{2}\langle X^2 \rangle - \ln\cosh\left(\sqrt{c}\langle X \rangle\right) - QS_{\mathrm{BGS}}. \tag{170}$$

The Plastino-Plastino model (14) related to the nonextensive Tsallis entropy (156) is given by Eq. (165) and $\tilde{M} = 1$ with (Frank 2005b)

$$F = \langle V \rangle - QS_q, \tag{171}$$

where V is the potential of the gradient force h. For an appropriate choice of $\tilde{M}$, the quantum mechanical nonlinear Fokker-Planck equations (146) can be cast into the form Eq. (165) with

$$F = \langle V \rangle - QS_{\mathrm{FD,BE}}, \tag{172}$$

where $S_{\mathrm{FD,BE}}$ is the quantum mechanical entropy of the Fermi-Dirac or Bose-Einstein statistics and V is the potential of the function $h(x)$ again. For details, see Frank (2005b) and Frank and Daffertshofer (1999). From the perspective of linear nonequilibrium thermodynamics, linear and nonlinear Fokker-Planck equations can be distinguished by means of the thermodynamic flux (Compte and Jou 1996; Frank 2002a, 2005b, 2007)

$$J = -\tilde{M}P\frac{\partial}{\partial x}\frac{\delta F}{\delta P}. \tag{173}$$

Note that in this approach, the thermodynamic flux is equivalent to the probability current (Frank 2005b). As can be seen from Eq. (173), on the one hand, the flux is associated to the free energy F. On the other hand, from the evolution equation (165), it follows that

$$\frac{\partial}{\partial t}P = -\frac{\partial}{\partial x}J. \tag{174}$$

If J is linear with respect to P, then the corresponding Fokker-Planck equation is linear with respect to P as well. If J is nonlinear with respect to P, then we are dealing with a nonlinear Fokker-Planck equation. The question whether J is linear or not is answered by nature herself (Frank 2007). For the Brownian particle motion, we have $\tilde{M} = \gamma$ and

$$F = \frac{1}{2}\langle v^2 \rangle - QS_{\mathrm{BGS}}, \tag{175}$$

which yields

$$J = -\gamma v P - Q\frac{\partial}{\partial x}P. \tag{176}$$

J is linear and the corresponding Fokker-Planck equation is linear as well. For a self-

organizing system, frequently it is found that J is nonlinear because F involves a mean field energy term that is nonlinear with respect to P. For examples, see Eqs. (166), (168), (169), and (170). Likewise, for quantum and nonextensive systems, we find that J is nonlinear because F involves quantum and nonextensive entropies such as $S_{\mathrm{FD,BE}}$ and S_q. For examples, see Eqs. (171) and (172).

Summary and Future Directions

From the previous discussion in section "Linear Nonequilibrium Thermodynamics," it is clear that modeling approaches based on nonlinear Fokker-Planck equations are rooted in the theory of collective phenomena and self-organization, on the one hand, and in the theory of quantum mechanical and nonextensive systems, on the other. In contrast, linear Fokker-Planck equations are tailored to address the stochastic properties of systems composed of noninteracting subsystems when equating the material subsystem ensemble with the ensemble of statistical realizations. Note that – of course – linear Fokker-Planck equations can also be applied to discuss stochastic properties of self-organizing systems. However, in such cases, either the stochastic behavior of order parameters by means of low-dimensional linear Fokker-Planck equations is discussed (Haken 2004) or linear high-dimensional or even functional Fokker-Planck equations are involved (Gardiner 1997).

We showed in section "Markov Property: Second-Order and Higher-Order Statistics" that both linear and nonlinear Fokker-Planck equations exhibit Green's functions and Langevin equations. The fact that a nonlinear evolution equation can give rise to a Green's function may be counterintuitive because Green's functions are associated with linearity. In fact, the evolution equation of the Green's function p is linear with respect to p. The nonlinearity is in the evolution equation for the time-dependent probability density P but not in the evolution equation of the Green's function p. In this context, we would like to reiterate what we pointed out in section "Strongly Nonlinear Fokker-Planck Equations": time-dependent solutions P do not necessarily correspond to Green's function p (Frank 2003b).

In the mathematical literature, the theory of Markov processes that involve conditional probability densities of the form $p(x, t|x', t', P')$ has been discussed for several decades (see references in section "Definition of the Subject"). In line with these studies, we suggest to refer to Markov processes with conditional probability densities of the form $p(x, t|x', t', P')$ as *nonlinear* Markov processes or *nonlinear* families of Markov processes (Frank 2004d). Likewise, we suggest to refer to Markov processes whose conditional probability densities do not depend on P' as *linear* Markov processes or *linear* families of Markov processes. Using this terminology, we would say that strongly nonlinear Fokker-Planck equations describe nonlinear Markov diffusion processes, and vice versa nonlinear Markov diffusion processes can be expressed in terms of strongly nonlinear Fokker-Planck equations.

In physics and related disciplines, the relevance of nonlinear Markov processes has to be explored in the future. That is, except for research primarily reported in the mathematical literature, the theory of Markov processes constructed from conditional probability measures of the form $p(x, t|x', t', P')$ is still in its infancy. The Chapman-Kolmogorov equation and the Kramers-Moyal expansion presented in section "Markov Property: Second-Order and Higher-Order Statistics" provide promising departure points for future studies in this regard.

In the present study, we pointed out that there are a few overarching concepts that apply to linear and nonlinear Fokker-Planck equations alike: the concepts of Markov diffusion processes, martingales, and linear nonequilibrium thermodynamics. Therefore, future studies may change the state of the art illustrated in Fig. 1 into a scenario as shown in Fig. 2. In doing so, a closely connected world of linear and nonlinear Fokker-Planck equations that is governed by a small set of powerful principles could emerge.

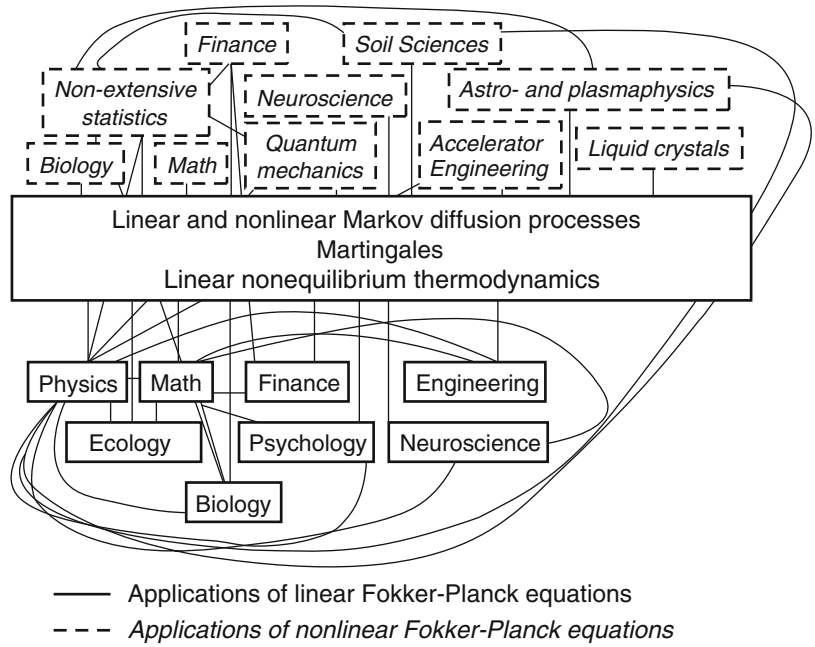

Linear and Nonlinear Fokker-Planck Equations, Fig. 2 Connected applications of linear and nonlinear Fokker-Planck equations

Bibliography

Abe S, Okamoto Y (2001) Nonextensive statistical mechanics and its applications. Springer, Berlin

Acebron JA, Spigler R (1998) Adaptive Frequency Model for Phase-Frequency Synchronization in Large Populations of Globally Coupled Nonlinear Oscillators. Phys Rev Lett 81:2229

Acebron JA, Bonilla LL, De Leo S, Spigler R (1998) Breaking the symmetry in bimodal frequency distributions of globally coupled oscillators. Phys Rev E 57:5287

Acebron JA, Bonilla LL, Vicente CJP, Ritort F, Spigler R (2005) The Kuramoto model: A simple paradigm for synchronization phenomena. Rev Mod Phys 77:137

Allen EJ, Victory HD Jr (1994) A computational investigation of the random particle method for numerical solution of the kinetic Vlasov-Poisson-Fokker-Planck equations. Physica A: Statistical Mechanics and its Applications 209:318

Aonishi T, Okada M (2002) Multibranch Entrainment and Slow Evolution among Branches in Coupled Oscillators. Phys Rev Lett 88:024102

Arenas A, Perez Vincente CJ (1994) Exact long-time behavior of a network of phase oscillators under random fields. Phys Rev E 50:949

Ariaratnam JT, Strogatz SH (2001) Phase Diagram for the Winfree Model of Coupled Nonlinear Oscillators. Phys Rev Lett 86:4278

Arnold A, Bonilla LL, Markowich P (1996) Transp Theor Stat Phys 25:733

Arnold A, Markowich P, Toscani G (2000) Transp Theor Stat Phys 29:571

Arnold A, Markowich P, Toscani G, Unterreiter A (2001) Commun Part Diff Eq 26:43

Aronson DG (1986) In: Dobb A, Eckmann B (eds) Nonlinear diffusion problems – lecture notes in mathematics, vol 1224. Springer, Berlin, pp 1–46

Balescu R (1975) Equilibrium and nonequilibrium statistical mechanics. Wiley, New York

Barenblatt GI, Entov VM, Ryzhik VM (1990) Theory of fluid flows through natural rocks. Kluwer Academic Publisher, Dordrecht

Becker V, Engel A (2007) Role of interactions in ferrofluid thermal ratchets. Phys Rev E 75:031118

Binney J, Tremaine S (1987) Galatic dynamics. Princeton University Press, Princeton

Birner T, Lippert K, Müller R, Kühnel A, Behn U (2002) Critical behavior of nonequilibrium phase transitions to magnetically ordered states. Phys Rev E 65:046110

Bödeker HU, Röttger MC, Liehr A, Frank TD, Friedrich R, Purwins HG (2003) Phys Rev E 67:056220

Bogacz R, Brown E, Moehlis J, Holmes P, Cohen JD (2006) The physics of optimal decision making: a formal analysis of models of performance in two-alternative forced-choice tasks. Psychol Rev 113:700

Bonilla LL (1987) Stable nonequilibrium probability densities and phase transitions for meanfield models in the thermodynamic limit. J Stat Phys 46:659

Bonilla LL, Vicente CJP, Rubi JM (1993) Stat J Phys 70:921

Borland L (1998) Microscopic dynamics of the nonlinear Fokker-Planck equation: A phenomenological model. Phys Rev E 57:6634

Borland L (2002) Option Pricing Formulas Based on a Non-Gaussian Stock Price Model. Phys Rev Lett 89:098701

Borland L (2008) Non-Gaussian option pricing. Successes, limitations and perspectives. In: Riccardi C, Roman HE

(eds) Anomalous fluctuations in complex systems: plasmas, fluids and financial markets. Special Review Book for Research Singpost, Transworld Research Network, KeralaMadison, pp 311–334
Borland L, Bouchaud JP (2004) A Non-Gaussian Option Pricing Model with Skew. Quantitative finance 4:499
Bychenkov VY, Rozmus W, Tikhonchuk VT (1995) Nonlocal Electron Transport in a Plasma. Phys Rev Lett 75:4405
Carillo JA, Jüngel A, Markowich PA, Toscani G, Unterreiter A (2001) Monatshefte für Mathematik 113:1
Carrillo JA, Rosado J, Salvarani F (2008) 1D nonlinear Fokker-Planck equations for fermions and bosons. Appl Math Letters 21:148
Cepa E, Lepingle D (1997) Diffusing particles with electrostatic repulsion. Probab Theory Relat Fields 107:429
Chandrasekhar S (1977) Liquid crystals. Cambridge University Press, Cambridge
Chavanis PH (2003) Generalized thermodynamics and Fokker-Planck equations: Applications to stellar dynamics and two-dimensional turbulence. Phys Rev E 68:036108
Chavanis PH (2004) Physica A 340:57
Chavanis PH, Rosier C, Sire C (2002) Thermodynamics of self-gravitating systems. Phys Rev E 66:036105
Coffey WT, Kalmykov YP, Waldron JT (2004) The Langevin equation. World Scientific, Singapore
Compte A, Jou D (1996) Non-extensive behavior of a stock market index at microscopic time scales. Phys J Math A Gen 29:4321
Cortines AAG, Riera R (2007) Physica A 377:181
Crank J (1975) The mathematics of diffusion. Clarendon Press, Oxford
Crawford JD (1995) Phys Rev Lett 74:4341
Curado EMF, Nobre FD (2003) Phys Rev E 67:021107
Daido H (1996a) Physica D 91:24
Daido H (1996b) Phys Rev Lett 77:1406
Daido H (2001) Phys Rev Lett 87:048101
Daly E, Porporato A (2004) Phys Rev E 70:056303
Dano S, Hynne F, De Monte S, d'Ovidio F, Sorensen PG, Westerhoff H (2001) Faraday Discuss 120:261
Dawson DA (1983) J Stat Phys 31:29
Dawson DA (1993) Lecture notes in mathematics 1541. In: Dawson DA, Maisonneuve B, Spencer J (eds) . Springer, Berlin, pp 6–16
Dawson DA, Gärtner J (1989) Large deviations, free energy functional and quasi-potential for a mean field model of interacting diffusions. American Mathematical Society, Providence
de Gennes P, Prost J (1993) The physics of liquid crystals. Clarendon Press, Oxford
de Groot SR, Mazur P (1962) Non-equilibrium thermodynamics. North-Holland, Amsterdam
de Jeu WH (1980) Physical properties of liquid crystalline materials. Gordon and Beach, New York
de los Santos F, Telo da Gamma MM, Munoz MA (2003) Phys Rev E 67:021607
Desai RC, Zwanzig R (1978) Stat J Phys 19:1
Ding X (1994) Adv Appl Prob 26:1022
Djehiche B, Kaj I (1995) Ann Probab 23:1414
Doi M, Edwards SF (1988) The theory of polymer dynamics. Clarendon Press, Oxford
Donoso JM, Salgado JJ (2006) J Phys A 39:12587
Donoso JM, Salgado JJ, Soler M (2005) J Phys A 38:9145
Drazer G, Wio HS, Tsallis C (2000) Phys Rev E 61:1417
Drozdov AN, Morillo M (1996) Phys Rev E 54:931
Ebeling W, Sokolov IM (2004) Statistical thermodynamics and stochastic theory of nonequilibrium systems. World Scientific, Singapore
Eckhardt B, Ott E, Strogatz SH, Abrams DM, McRobie A (2007) Phys Rev E 75:021110
Epperlein EM, Rickard GJ, Bell AR (1988) Phys Rev Lett 61:2453
Espanol P, Serrano M, Öttinger HC (1999) Phys Rev Lett 83:4542
Felderhof BU (2003) Physica A 323:88
Fialkowiski M, Hess S (2000) Physica A 282:65
Fokker AD (1914) Ann Phys 43:810
Fontbona J (2003) J Funct Analysis 200:198
Frank TD (2001a) Phys Lett A 280:91
Frank TD (2001b) Phys Lett A 290:93
Frank TD (2002a) Phys Lett A 305:150
Frank TD (2002b) Physica A 310:397
Frank TD (2003a) Phys Lett A 319:173
Frank TD (2003b) Physica A 320:204
Frank TD (2004a) Eur Phys J B 37:139
Frank TD (2004b) J Phys A 37:3561
Frank TD (2004c) Phys Lett A 329:475
Frank TD (2004d) Physica A 331:391
Frank TD (2004e) Physica D 195:229
Frank TD (2005a) Math Comput Mod 42:1057
Frank TD (2005b) Nonlinear Fokker-Planck equations: fundamentals and applications. Springer, Berlin
Frank TD (2005c) Phys Rev E 72:041703
Frank TD (2006) Phys Rev ST-AB 9:084401
Frank TD (2007) Physica A 382:453
Frank TD (2008) Physica A 387:773
Frank TD, Daffertshofer A (1999) Physica A 272:497
Frank TD, Daffertshofer A (2000) Physica A 285:351
Frank TD, Daffertshofer A (2001a) Physica A 292:392
Frank TD, Daffertshofer A (2001b) Physica A 295:455
Frank TD, Friedrich R (2005) Physica A 347:65
Frank TD, Daffertshofer A, Peper CE, Beek PJ, Haken H (2001) Physica D 150:219
Friedman A (1969) Partial differential equations. Holt, Rinehart and Winston, Inc., New York
Friedrich R, Peinke J (1997) Phys Rev Lett 78:863
Friedrich R, Siegert S, Peinke J, Lück S, Seifert M, Lindemann M, Raethjen J, Deuschl G, Pfister G (2000) Phys Lett A 271:217
Gang H, Haken H, Fagen X (1996) Phys Rev Lett 77:1925
Garcia-Ojalvo J, Sancho JM (1999) Noise in spatially extended systems. Springer, New York
Garcia-Ojalvo J, Parrondo JMR, Sancho JM, van den Broeck C (1996) Phys Rev E 54:6918
Gardiner CW (1997) Handbook of stochastic methods, 2nd edn. Springer, Berlin
Gärtner J (1988) Math Nachr 137:197

Giada L, Marsili M (2000) Phys Rev E 62:6015
Glansdorff P, Prigogine I (1971) Thermodynamic theory of structure, stability, and fluctuations. Wiley, New York
Goel NS, Dyn NR (1974) Stochastic models in biology. Academic Press, New York
Graham C (1990) Appl Math Optim 22:75
Greven A (2005) In: Deuschel J, Greven A (eds) Interacting stochastic systems. Springer, Berlin, pp 209–246
Gurtin ME, MacCamy RC (1977) Math Biosci 33:35
Hadley P, Beasley MR, Wiesenfeld K (1988) Phys Rev B 38:8712
Haken H (2004) Synergetics: introduction and advanced topics. Springer, Berlin
Han SK, Kurrer C, Kuramoto Y (1995) Phys Rev Lett 75:3190
Hänggi P, Talkner P, Borkovec M (1990) Rev Mod Phys 62:251
Hänggi P, Marchesoni F, Nori F (2005) Ann Phys 14:51
Hansel D, Mato G, Meunier C (1993a) Europhys Lett 23:367
Hansel D, Mato G, Meunier C (1993b) Phys Rev E 48:3470
Hasegawa H (2003) Phys Rev E 67:041903
Heifets S (2001) Phys Rev ST-AB 4:044401
Heifets S (2003) Phys Rev ST-AB 6:080701
Hess S (1976) Naturforschung Z A 31:1034
Holden AV (1976) Models of the stochastic activity of neurons, Lecture notes in biomathematics, vol 12. Springer, Berlin
Horsthemke W, Lefever R (1984) Noise-induced transitions. Springer, Berlin
Hütter M, Karlin IV, Öttinger HC (2003) Phys Rev E 68:016115
Ichiki A, Ito H, Shiino M (2007) Phys E 40:402
Ilg P, Karlin IV, Öttinger HC (1999) Phys Rev E 60:5783
Ilg P, Kröger M, Hess S (2005) Phys Rev E 71:051201
Jafari GR, Fazeli SM, Ghasemi F, Allaei SMV, Tabar MRR, Zad AI, Kavei G (2002) Phys Rev Lett 91:226101
Jelic A, Hütter M, Öttinger HC (2006) Phys Rev E 74:041126
Jourdain B (2000) Methodol Comput Appl Probab 2:69
Kadanoff LP (2000) Statistical physics: statics, dynamics and renormalization. World Scientific, Singapore
Kanamaru T, Horita T, Okabe Y (2001) Phys Rev E 64:031908
Kaniadakis G (2001a) Phys Lett A 288:283
Kaniadakis G (2001b) Physica A 296:405
Kaniadakis G, Quarati P (1993) Phys Rev E 48:4263
Kaniadakis G, Quarati P (1994) Phys Rev E 49:5103
Karlin S, Taylor HM (1975) A first course in stochastic processes. Academic Press, New York
Karlin S, Taylor HM (1981) A second course in stochastic processes. Academic Press, New York
Kawamura Y (2007) Phys Rev E 76:047201
Kawamura Y, Nakao H, Kuramoto Y (2007) Phys Rev E 75:036209
Kharchenko DO, Kharchenko VO (2005) Physica A 354:262
Kim S, Park SH, Ryu CS (1997) Phys Rev Lett 78:1616
Klimontovich YL (1986) Statistical physics. Harwood Academic Publ, New York
Kloeden PE, Platen E (1992) The numerical solution of stochastic differential equations. Springer, Berlin
Kometani K, Shimizu H (1975) J Stat Phys 13:473
Kondepudi D, Prigogine I (1998) Modern thermodynamics. Wiley, New York
Kostur M, Luczka J, Schimansky-Geier L (2002) Phys Rev E 65:051115
Kozyreff G, Vladimirov AG, Mandel P (2000) Phys Rev Lett 85:3809
Kuramoto Y (1984) Chemical oscillations, waves, and turbulence. Springer, Berlin
Lancellotti C, Kiessling M (2001) Astrophys J 549:L93
Larson RG, Öttinger HC (1991) Macromolecules 24:6270
Li JH, Hänggi P (2001) Phys Rev E 64:011106
Li JH, Huang ZQ, Xing DY (1998) Phys Rev E 58:2838
Lo CF (2005) Phys Lett A 336:141
MacDonald WM, Rosenbluth MN, Chuck W (1957) Phys Rev 107:350
Maier W, Saupe A (1958) Z Naturforschung A 13:564
Marsili M, Bray AJ (1996) Phys Rev Lett 76:2750
McCauley JL, Gunaratne GH, Bassler KE (2006) Physica A 382:445
McKean HP Jr (1969) In: Aziz AK (ed) Propagation of chaos for a class of nonlinear parabolic equations, Lectures in differential equations, vol II. Van Nostrand Reinhold Company, New York, pp 177–193
Meleard S (1996) Asymptotic behavior of some interacting particle systems: McKean-Vlasov and Boltzmann models. In: Graham C, Kurtz TG, Meleard S, Potter PE, Pulvirenti M, Talay D (eds) Probabilistic models for nonlinear partial differential equations. Springer, Berlin, pp 42–95
Meleard S, Coppoletta SR (1987) Stoch Process Appl 26:317
Michael F, Johnson MD (2003) Physica A 320:525
Mikhailov AS, Zanette DH (1999) Phys Rev E 60:4571
Morillo M, Gomez-Ordonez J, Casado JM (1995) Phys Rev E 52:316
Müller R, Lippert K, Kühnel A, Behn U (1997) Phys Rev E 56:2658
Nicholson DR (1983) Introduction to plasma theory. Wiley, New York
Nobre FD, Curado EMF, Rowlands G (2004) Physica A 334:109
Oelschläger K (1989) Probab Th Rel Fields 82:565
Okubo A, Levin SA (2001) Diffusion and ecological problems: modern perspectives. Springer, Berlin
Öttinger HC (1996) Stochastic processes in polymeric fluids. Springer, Berlin
Öttinger HC (2005) Beyond equilibrium thermodynamics. Wiley, New Jersey
Öttinger HC (2007) Phys Rev Lett 99:130602
Öttinger HC, Grmela M (1997) Phys Rev E 56:6633
Overbeck L (1996) Ann Probab 24(2):743
Park SH, Kim S (1996) Phys Rev E 53:3425

Park K, Lai YC, Liu Z, Nachman A (2004) Phys Lett A 326:391
Patanarapeelert K, Frank TD, Friedrich R, Beek PJ, Tang IM (2006) Phys Lett A 360:190
Paul W, Baschnagel J (1999) Stochastic processes: from physics to finance. Springer, Berlin
Peletier LA (1981) In: Amann H, Bazley N, Kirchgässner K (eds) Applications of nonlinear analysis in the physical science. Pitman Advanced Publishing Program, Boston, pp 229–241
Pikovsky A, Rosenblum M, Kurths J (2001) Synchronization: a universal concept in nonlinear sciences. Cambridge University Press, Cambridge
Pilipenko AY (2005) Urkainian Math J 57:1507
Planck M (1917) Sitzungsber. Preuss Akad Wissens, Berlin, p 324
Plastino AR, Plastino A (1995) Physica A 222:347
Quinn DA, Rand RH, Strogatz SH (2007) Phys Rev E 75:036218
Ratcliff R, Gomez P, McKoon G (2004) Psychol Rev 111:159
Reif F (1965) Fundamentals of statistical and thermal physics. McGraw-Hill Book Company, New York
Reimann P (2002) Phys Rep 361:57
Reimann P, Kawai R, Van den Broeck C, Hänggi P (1999a) Europhys Lett 45:545
Reimann P, Van den Broeck C, Kawai R (1999b) Phys Rev E 60:6402
Risken H (1989) The Fokker-Planck equation – methods of solution and applications. Springer, Berlin
Rogers LCG, Shi Z (1993) Probab Theroy Relat Fields 95:555
Rosenblum MG, Pikovsky AS (2004) Phys Rev Lett 92:114102
Rosenbluth M, MacDonald WM, Judd DL (1957) Phys Rev 107:1
Sakaguchi H (1988) Prog Theor Phys 79:39
Savel'ev S, Marchesoni F, Nori F (2003) Phys Rev Lett 91:010601
Scarfone MA, Wada T (2007) Physica A 384:305
Schuster HG, Wagner P (1990) Biol Cybern 64:77
Schwämmle V, Nobre FD, Curado E (2007a) Phys Rev E 76:041123
Schwämmle V, Gonzahles MC, Moreira AA, Andrade JS, Hermann HJ (2007b) Phys Rev E 75:066108
Schweitzer F (2003) Brownian agents and active particles. Springer, Berlin
Shiino M (1985) Phys Lett A 112:302
Shiino M (1987) Phys Rev A 36:2393
Shiino M (2001) J Math Phys 42:2540
Shiino M (2002a) J Math Phys 43:2654
Shiino M (2002b) J Phys Soc 40:1037
Shiino M (2003) Phys Rev E 67:056118
Shimizu H (1974) Prog Theor Phys 52:329
Shimizu H, Yamada T (1972) Prog Theor Phys 47:350
Shobuda Y, Hirata K (2001) Phys Rev E 64:067501
Silverman BW (1986) Density estimation for statistics and data analysis. Chapman and Hall, London
Soler M, Martinez FC, Donoso JM (1992) Stat J Phys 69:813
Sopik J, Sire C, Chavanis PH (2006) Phys Rev E 74:011112
Strogatz SH (2000) Physica D 143:1
Strogatz SH, Mirollo RE (1991) Stat J Phys 63:613
Strogatz SH, Morillo RE, Matthews PC (1992) Phys Rev Lett 68:2730
Strogatz SH, Abrams D, McRobie A, Eckhardt B, Ott E (2005) Nature 438:43
Stupakov GV, Breizman BN, Pekker MS (1997) Phys Rev E 55:5976
Sura P, Barsugli J (2002) Phys Lett A 305:304
Takai M, Akiyama H, Takeda S (1981) J Phys Soc Japan 50:1716
Takatsuji M (1975) Biol Cybern 17:207
Tass PA (1999) Phase resetting in medicine and biology – stochastic modelling and data analysis. Springer, Berlin
Tass PA (2001) Europhys Lett 55:171
Tass PA (2003) Biol Cybern 89:81
Tass PA (2006) Biol Cybern 94:58
Tsallis C (1988) Stat J Phys 52:479
Tsallis C (1997) Phys World 10(7):42
Tsallis C (2004) Physica D 193:3
Tsallis C, Bukman DJ (1996) Phys Rev E 54:R2197
Tsekov R (1995) J Phys A Math Gen 28:L557
Tsekov R (2001) Int J Mol Sci 2:66
van den Broeck C, Parrondo JMR, Armero J, Hernandez-Machado A (1994a) Phys Rev E 49:2639
van den Broeck C, Parrondo JMR, Toral R (1994b) Phys Rev Lett 73:3395
van den Broeck C, Parrondo JMR, Toral R, Kawai R (1997) Phys Rev E 55:4084
van Kampen NG (1981) Stochastic processes in physics and chemistry. North-Holland, Amsterdam
Vellekoop M, Nieuwenhuis H (2007) Quantitative finance 7:563
Venturini M, Warnock R (2002) Phys Rev Lett 89:224802
Waechter M, Riess F, Schimmel T, Wendt U, Peinke J (2004) Eur Phys J B 41:259
Wehner MF, Wolfer WG (1987) Phys Rev A 35:1795
Wiesenfeld K, Colet P, Strogatz SH (1996) Phys Rev Lett 76:404
Winfree AT (1967) Theor J Biol 16:15
Winfree AT (2001) The geometry of biological time, 2nd edn. Springer, Berlin
Yamaguchi Y, Shimizu H (1984) Physica D 11:213
Yamana M, Shiino M, Yoshioka M (1999) Phys J A Math Gen 32:3525
Yoshioka M, Shiino M (2000) Phys Rev E 61:4732
Zaikin AA, Garcia-Ojalvo J, Schimansky-Geier L, Kurths J (2002) Phys Rev Lett 88:010601
Zhai Y, Kiss IZ, Daido H, Hudson JL (2005) Physica D 205:57

Additive Noise Tunes the Self-Organization in Complex Systems

Axel Hutt[1] and Jérémie Lefebvre[2]
[1]Deutscher Wetterdienst, Offenbach am Main, Germany
[2]Krembil Research Institute, Toronto, ON, Canada

Article Outline

Glossary
Introduction
Slaving Principle and Center Manifold Theorem
Additive Noise in Low-Dimensional Models: Stochastic Center Manifold Theory
Additive Noise in Discrete Network Models
Future Directions
Bibliography

Glossary

Additive noise Random fluctuations that add to the phase space flow of model systems.

Center manifold theorem Mathematical theorem describing the slaving principle in complex systems.

Slaving principle Units in a complex system that interact nonlinearly with other units evolve on different time scales. Close to instability points, fast units obey the dynamics of slow units and are enslaved by them. Such units may be spatial modes in spatially extended systems or neural ensembles in neural populations.

Introduction

The dynamics of natural systems is complex, e.g., due to various processes and their interactions on different temporal and spatial scales. Several of such processes appear to be of random nature, i.e., they cannot be predicted by known laws. In this context, it is not necessary to know whether these processes are random in reality or whether we just do not know their deterministic law and they appear to be random. The insight that unknown laws of processes may be replaced or modelled by laws for random processes is helpful in modelling complex systems. Examples for such a replacement are manifold, and we mention model parametrization in meteorology (Noilhan and Planton 1989) and stimulus parametrization in biology (Doiron et al. 2004).

Considering random processes (or noise) in dynamical models, it is important how they are included. If the randomness is taken into account in multiplicative factors, e.g., parametrizing the unknown underlying dynamics of the factor, we call this *multiplicative* noise. Its effect has been studied extensively for the last decades in physics and mathematics, e.g., see the books of Horsthemke and Lefever (1984) and Garcia-Ojalvo and Sancho (1999). Conversely, *additive noise* is included in a model when the randomness is just added to the phase space flow. For instant, considering a model of differential equations in time additive noise is just added to the temporal deviation over time. For a long time, it has been known that multiplicative noise easily shifts the stability of systems, i.e., may shift bifurcations, whereas additive noise does not. This paradigm has been challenged recently in the studies of spatially extended systems (Hutt et al. 2007, 2008; Hutt 2008) and delayed systems (Lefebvre et al. 2012; Lefebvre and Hutt 2013; Hutt et al. 2012; Hutt and Lefebvre 2016). These studies show that additive noise may induce bifurcation shifts close to bifurcation points. This recent finding is illustrated and explained in a later section. Moreover, additive noise may not only affect the stability of systems close to instability points, but may also tune intrinsic time scales. We show in a later section that this effect occurs close and far from the bifurcation point.

Taking a close look at the complex systems subjected to additive noise, one learns that

A. Hutt, H. Haken (eds.), *Synergetics*,
https://doi.org/10.1007/978-1-0716-0421-2_696

Originally published in
R. A. Meyers (ed.), *Encyclopedia of Complexity and Systems Science*, © Springer Science+Business Media LLC 2018
https://doi.org/10.1007/978-3-642-27737-5_696-1

additive noise affects the coupling of the systems elements. Such elements may be spatial modes in spatially extended systems or microscopic elements, such as single neurons, whose interactions generate novel macroscopic order parameter modes, such as the macroscopic population dynamics. To illustrate such an interaction before we apply the concept to complex problems, we present briefly the major elements of the slaving principle in synergetics (Haken 1996, 2004) in the subsequent section and put it into relation to its mathematical equivalent, the center manifold theorem.

Slaving Principle and Center Manifold Theorem

We start with the illustration of the major concept of the center manifold theorem and finally put the concept into a physical context to explain the slaving principle.

For illustration, let us consider the dynamical system

$$\begin{aligned} \dot{x} &= \alpha x + ax^3 + xy - xy^2 \\ \dot{y} &= -y + bx^2 + x^2 y \end{aligned} \tag{1}$$

with $x, y, \alpha, a, b \in \mathcal{R}$. The stationary state is the fixed point $x = y = 0$. Linearizing about this fixed point shows that there are two eigenvalues $\lambda_1 = \alpha$, $\lambda_2 = -1$. Hence the node is asymptotically stable if $\alpha < 0$ and a saddle node for $\alpha > 0$.

At the Stability Threshold

For the moment, we assume $\alpha = 0$. Then close to the fixed point y evolves in the stable subspace spanned by the eigenvector $(0, 1)^t$ of the linearized system with corresponding eigenvalue $\lambda_2 < 0$ and x evolves in the center subspace. We observe that $x = 0$ is an invariant manifold which is a stable manifold of the origin since $dx/dt = 0$ and $dy/dt < 0$. Hence for initial points $(0, y_0)^t$ the system evolves on the stable manifold.

Now the question arises how one can find the invariant manifold for which the origin is neutrally stable corresponding to the eigenvalue $\lambda_1 = 0$, i.e., we want to find the center manifold. The center manifold theorem (Carr 1981) applies stating that $y = h(x)$ close to the origin, where $h(\cdot)$ is a nonlinear function with $h(0) = 0$, $dh(x)/dx = 0$ at $x = 0$. This stipulates

$$\begin{aligned} \dot{y} &= \frac{\partial h}{\partial x}\dot{x} \\ -y + bx^2 + x^2 y &= \frac{\partial h}{\partial x}\left(\alpha x + ax^3 + xy - xy^2\right) \\ -h(x) + bx^2 + x^2 h(x) &= \frac{\partial h}{\partial x}\left(\alpha x + ax^3 + xh(x) - xh^2(x)\right) \end{aligned}$$

Inserting the polynomial ansatz

$$h(x) = h_2 x^2 + h_3 x^3 + \cdots \tag{2}$$

and sorting by orders of x we gain $h_2 = b$, $h_3 = 0$, $h_4 = -b(2a - 1)$ and thus $y = bx^2 + b(2a - 1)x^4$ up to fourth order. Thus, for $\alpha = 0$, the system on the center manifold obeys

$$\dot{x} = (a + b)x^3 - \left(2ab - 1 + b^2\right)x^5 + O\left(x^6\right).$$

For $a + b < 0$, the origin is attractive, and the manifold is called a slow manifold close to the fixed point.

In physical terms, the variable x evolves on a much larger time scale than y since the time scales are inversely proportional to the corresponding eigenvalues of the linearized system. Moreover, the variable y obeys the slow variable x on the center manifold. In other words, the slow variable x enslaves the fast variable y and determines the dynamics of the full system. This prominent role of x is the reason why it is called an order parameter. Hence at bifurcation points, the slow variables enslave the fast variables. This slaving concept applies at all bifurcations that fulfil the rather general conditions of the center manifold and allows to describe most bifurcations observed in nature (Haken 1983), be oscillatory instabilities in the laser (Haken 1985) or human motor-coordination phase transitions in the brain (Fuchs et al. 1992; Jirsa et al. 1995). By virtue of the generality of this concept, it is called *slaving principle*. It is often formulated equivalently by an adiabatic approach in which the fast slaved variable decays rapidly and follows the slow order parameter dynamics (Haken 1996; Schanz and Pelster 2003; Schoener and Haken 1986).

About the Stability Threshold

Now we consider the case $\alpha \neq 0$, i.e., the system does not evolve necessarily at the bifurcation point. This is the more general case. To be still able to apply the center manifold theorem, we augment the phase space by the variable α and reformulate the model (1) as

$$\begin{aligned}\dot{\alpha} &= 0\\ \dot{x} &= \alpha x + ax^3 + xy - xy^2\\ \dot{y} &= -y + bx^2 + x^2 y.\end{aligned}$$

The linearized problem about the fixed point $(0,\ 0,\ 0)^t$ has the eigenvalues $\lambda_{1,2} = 0$ and $\lambda_3 = -1$, since now the term αx is treated as a nonlinear term. Now the variables $\alpha,\ x$ evolve in the center subspace while y is still enslaved by $y = h(\alpha,\ x)$. The center manifold is defined to obey $h(0,\ 0) = 0,\ \partial h/\partial\alpha = \partial h/\partial x = 0$ at $(\alpha,\ x)^t = (0,\ 0)^t$. With the ansatz

$$h(\alpha, x) = h_{2,1}\alpha^2 + h_{2,2}\alpha x + h_{2,3}x^2$$

we obtain $y = bx^2$ up to second order and the order parameter obeys

$$\dot{x} = \alpha x + (a+b)x^3 + O\left(x^4\right).$$

This solution extends naturally the case $\alpha = 0$.

The latter discussion assumes deterministic dynamics, while stochastic dynamics on center manifolds close to bifurcation points can be studied as well. This is shown in the subsequent section.

Additive Noise in Low-Dimensional Models: Stochastic Center Manifold Theory

The effects of additive noise emerge in multi-dimensional systems, e.g., in low-dimensional nondelayed systems or in infinite-dimensional delayed systems. The subsequent sections consider both cases.

Nondelayed Systems

Additive noise in systems close to the bifurcation point has been shown previously to trigger stochastic bifurcations (Boxler 1989; Arnold 1998; Schoener and Haken 1986). To see this, we consider here a reduced system of amplitude equations describing spatial modes of a stochastic Turing bifurcation (Hutt et al. 2007, 2008):

$$du_c = \left(\alpha_c u_c + 2\beta_c u_0 u_c + 2\gamma_c u_c^3\right)dt$$

$$du_0 = \left(\alpha_0 u_0 + 4\beta_0 u_c^2\right)dt + \eta dW(t)$$

with the slow order parameter u_c, the slaved fast mode u_0, constants $\alpha_c,\ \alpha_0,\ \beta_c,\ \beta_0,\ \gamma_c$, and noise level η. The control parameter α_c, the fast mode u_0, and the order parameter u_c are scaled as $\alpha \sim O(\varepsilon)$ and $u_0 \sim O(\varepsilon)$ and $u_c \sim O(\varepsilon^{1/2})$. The noise process $W(t)$ is a zero-mean Wiener process with $\langle dW(t)dW(\tau)\rangle = 2\delta(t-\tau)$. Here, amplitudes and noise levels are taken into account up to an order $O(\epsilon^{3/2})$. Applying the stochastic center manifold analysis (Boxler 1989; Xu and Roberts 1996; Hutt et al. 2007, 2008; Bloemker et al. 2005; Bloemker 2003) and an adiabatic Fokker-Planck approximation (Drolet and Vinals 1998, 2001; Hutt et al. 2007, 2008), we obtain for large times and scaled order parameter $\bar{u}_c$ and time T the Fokker–Planck equation (Hutt et al. 2008)

$$\frac{\partial P(\overline{u}_c, t)}{\partial T} = -\frac{\partial}{\partial \overline{u}_c}\left(\alpha\overline{u}_c + a\overline{u}_c^3\right)P(\overline{u}_c, T).$$

with new constants $\alpha,\ a$. We observe that the additive noise $dW(t)$ in the slaved fast mode u_0 has no effect on the order parameter $\bar{u}_c$.

For larger orders of amplitude and noise $O(\varepsilon^{5/2})$ in the same stochastic Turing bifurcation problem, amplitudes obey

$$du_c = \left(\alpha_c u_c + bu_0 u_c + 2\gamma_c u_c^3 + 3\gamma_c u_c u_0^2\right)dt$$

$$du_0 = \left(\alpha_0 u_0 + 4\beta_0 u_c^2 + \beta_0 u_0^2 + 2\gamma_0 u_0 u_c^2\right)dt + \eta dW(t).$$

After an adiabatic Fokker–Planck approximation, we obtain the Fokker–Planck equation for the order parameter (Hutt et al. 2008)

$$\frac{\partial P(\overline{u}_c, t)}{\partial T} = -\frac{\partial}{\partial \overline{u}_c}\left((\alpha - \alpha_{th}(\eta))\overline{u}_c + C\overline{u}_c^3 + D\overline{u}_c^5\right)P(\overline{u}_c, T). \tag{3}$$

with the control parameter shift $\alpha_{th}(\eta) \sim \eta^2$. Figure 1 shows this shift of the bifurcation by additive noise.

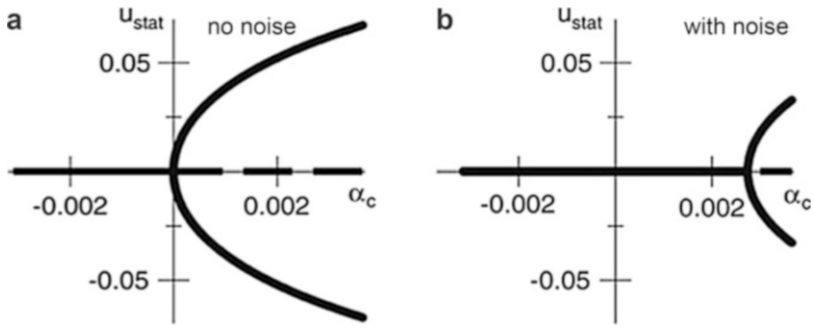

Additive Noise Tunes the Self-Organization in Complex Systems, Fig. 1 Additive noise shifts the bifurcation point. The stationary state u_{stat} is the state at the maximum of the stationary probability density of $P(\bar{u}_c, t)$ from Eq. (3). (**a**) $\eta = 0$. (**b**) $\eta = 0.02$ (Modified Fig. 9 in Hutt et al. 2008)

Equation (3) and Fig. 1 reveal that the bifurcation point of the order parameter u_c is shifted by additive noise in the slaved mode u_0. The underlying mechanism is known from multiplicative noise and can be understood as follows: the fast mode u_0 is stochastic and nonlinear coupling $u_c u_0^n$ with even order n yields an effective noise shift since $\langle u_0^n \rangle \neq 0$, whereas nonlinear coupling at odd order does not yield a shift since $\langle u_0^n \rangle = 0$. In sum, additive noise in a mode that is nonlinearly coupled at even order to the order parameter dynamics acts like multiplicative noise and hence tunes the bifurcation.

Delayed Systems

The nonlinear coupling of stochastic modes occurs in systems, where multiple elements couple nonlinearly. This occurs in high-dimensional systems, such as spatially extended systems (Hutt et al. 2008; Bloemker 2003) or delayed systems. To illustrate the corresponding stochastic effect in delayed systems, let us consider the stochastic delay differential equation (Hutt et al. 2012)

$$dx(t) = \big(-x(t) + \beta x(t-\tau) - \gamma x^3(t-\tau)\big)dt + \kappa dW(t) \tag{4}$$

with constants $\beta, \gamma > 0$, the noise level κ and the Wiener noise process $W(t)$. A stochastic center manifold analysis for delayed systems (Hutt and Lefebvre 2016; Lefebvre et al. 2012; Lefebvre and Hutt 2013; Hutt et al. 2012) permits to derive a delay-free stochastic order parameter equation on the center manifold. Applying an adiabatic approximation, the Fokker–Planck equation for the order parameter u reads up to a certain noise and magnitude order (Hutt et al. 2012)

$$\frac{\partial P(u,t)}{\partial t} = -\frac{\partial}{\partial u}\big(\big[A_1 + A_{1,\text{shift}}\big]u + \big[A_3 + A_{3,\text{shift}}\big]u^3 + A_5 u^5 + A_7 u^7 + A_9 u^9\big) \times P(u,t) + D\frac{\partial^2}{\partial u^2}P(u,t) \tag{5}$$

with $A_{1,\text{shift}}$, $A_{3,\text{shift}}$, $D \sim \kappa^2$ and constants A_1, A_3, A_5, A_7, A_9. We observe that additive noise in delayed systems induces a stochastic bifurcation and shifts the bifurcation point (Hutt and Lefebvre 2016; Lefebvre et al. 2012; Lefebvre and Hutt 2013; Hutt et al. 2012). Figure 2 shows the stationary probability functions of the original system (4) and the Fokker–Planck equation of the order parameter (5) for two different delay values. We observe that the stationary probability function of the order parameter $P_s(u)$ is in good accordance to the original probability density function $P_s(x)$ for small delays (a), while differences are visible for larger delays (b). In addition, increasing the noise level κ moves the magnitude of maxima to smaller values and hence shifts the bifurcation. This effect of additive noise is new and known for multiplicative noise only.

Additive Noise in Discrete Network Models

To extend the gained results of additive noise to large and more realistic systems, now we consider network models evolving far from bifurcation points.

Neural Mass Network

We consider a random network of N elements, whose elements with activity $u_n(t)$, $n = 1,\ldots, N$ evolve in time according to (Hutt et al. 2016)

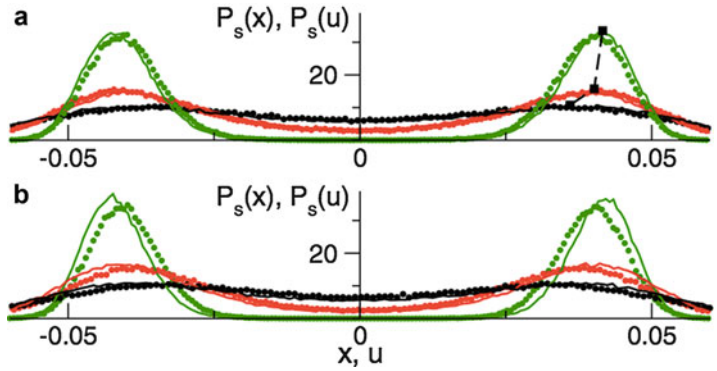

Additive Noise Tunes the Self-Organization in Complex Systems, Fig. 2 Stationary probability density functions of the original system $P_s(x)$ and the order parameter $P_s(u)$ as a solution of Eq. (5). The functions $P_s(u)$ (dotted line) and $P_s(x)$ (solid line) are computed for $\tau = 0.5$ (**a**) and $\tau = 1.0$ for noise level $\kappa = 0.005$ (green), $\kappa = 0.01$ (red), and $\kappa = 0.015$ (black) (Taken from Hutt et al. 2012 by permission)

$$\frac{1}{\alpha}\frac{du_n}{dt} = -u_n + \frac{1}{N}\sum_{m=1}^{N} w_{nm} f[u_m(t-\tau)] + I_n(t). \tag{6}$$

The network elements are delayed to each other by delay $\tau > 0$, $1/\alpha$ is the characteristic time scale of each element, w_{nm} is the random connection weight between elements n and m with

$$w_{nm} = g + s\eta_{nm} \tag{7}$$

and constants g, $s > 0$ and the statistically uncorrelated variables η_{nm} with

$$\sum_{n=1}^{N} \eta_{nm} = 0 \ \forall m = 1, \ldots, N \tag{8}$$

$$\sum_{m=1}^{N} \eta_{nm} = 0 \ \forall n = 1, \ldots, N \tag{9}$$

$$\frac{1}{N}\sum_{n=1}^{N} \eta_{nm}\eta_{ln} = \left[\frac{1}{N}\sum_{n=1}^{N}\eta_{nm}\right]\left[\frac{1}{N}\sum_{n=1}^{N}\eta_{ln}\right] \forall l, \quad m = 1, \ldots, N. \tag{10}$$

The last equation expresses the assumption that all columns and rows are statistically independent from each other.

The variable $I_n = I_0 + \xi_n(t)$ denotes the external noise driving each element with

$$\sum_{n=1}^{N} \xi_n(t) = 0, \quad \langle \xi_n \xi_m \rangle = 2D\delta_{n,m}, \tag{11}$$

where $\langle \cdot \rangle$ denotes the ensemble average, D is the noise intensity, and I_0 is a spatially constant stimulus bias.

In neural systems, the model (6) describes the spatially coarse-grained potential of N spatial patches subjected to afferent activity from other neural populations (Hutt et al. 2016). The function $f[\cdot]$ represents the activation or output function of each element, typically it is of sigmoidal shape. Figure 3 presents the topology of the network.

Analysis of the Global Synchronization

In the following, we study the degree of global synchronization in the network considering the network mean

$$\overline{u}(t) = u_n(t) - v_n(t) \tag{12}$$

with deviations $v_n(t)$ from the mean

$$\overline{u}(t) = \frac{1}{N}\sum_{n=1}^{N} u_n(t), \quad \sum_{n=1}^{N} v_n(t) = 0. \tag{13}$$

Then inserting (12) into (6) leads to

$$\frac{1}{\alpha}\frac{d}{dt}(\overline{u}(t) + v_n(t)) = -\overline{u}(t) - v_n(t) + \frac{1}{N}\sum_{m=1}^{N} w_{nm} f[\overline{u}(t-\tau) + v_m(t-\tau)] + I_0 + \xi_n(t). \tag{14}$$

Global Mode

After averaging Eq. (14) over all elements N one obtains the evolution equation of the spatial mean

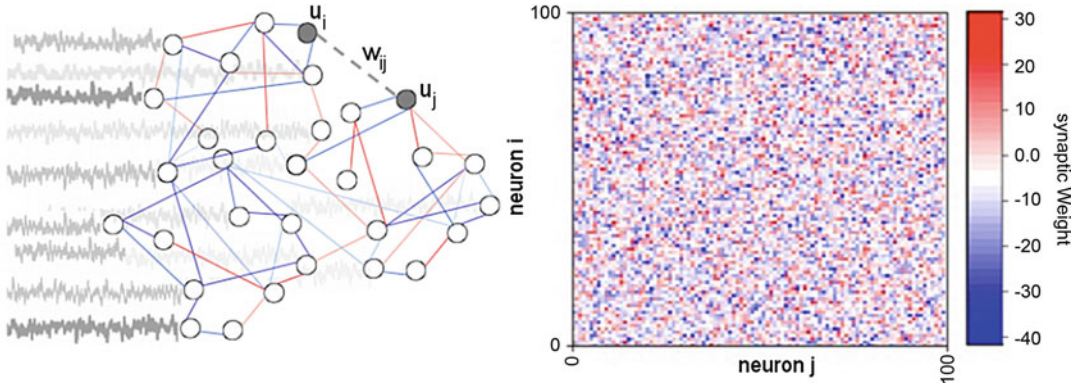

Additive Noise Tunes the Self-Organization in Complex Systems, Fig. 3 Simple spatial network topology

$$\frac{1}{\alpha}\frac{d}{dt}\overline{u}(t) = -\overline{u}(t) + \underbrace{\frac{1}{N^2}\sum_{n,m=1}^{N} w_{nm} f[\overline{u}(t-\tau)+v_m(t-\tau)]}_{=S_0} + I_0. \tag{15}$$

At first we note that with (8)

$$\frac{1}{N}\sum_{n=1}^{N} w_{nm} = g + s\frac{1}{N}\sum_{n=1}^{N}\eta_{nm} = g \quad \forall m = 1, \ldots, N. \tag{16}$$

Hence

$$S_0 = g\frac{1}{N}\sum_{m=1}^{N} f[\overline{u}(t-\tau)+v_m(t-\tau)] \tag{17}$$

If we denote $V_m = f[\bar{u}(t) + v_m(t)]$, we can write

$$\begin{aligned} S_0 &= gE[V] = \int_{-\infty}^{\infty} vp(v)dv \\ &= \int_{-\infty}^{\infty} f[\overline{u}(t)+v(t)]p(v,t)dv \end{aligned} \tag{18}$$

where $p(v, t)$ is the probability density function of the fluctuations $\{v_n\}$ at time instant t. Then

$$\frac{1}{\alpha}\frac{d}{dt}\overline{u}(t) = -\overline{u}(t) + \int_{-\infty}^{\infty} f[\overline{u}(t-\tau)+v(t-\tau)] \times p(v, t-\tau)dv + I_0. \tag{19}$$

Fluctuation Modes

Inserting Eq. (15) back into (14) yields

$$\frac{1}{\alpha}\frac{d}{dt}v_n(t) = -v_n(t) + \xi_n(t) + \frac{1}{N}\left[\underbrace{\sum_{m=1}^{N} w_{nm} f_m(t-\tau)}_{=S_1} - \underbrace{\frac{1}{N}\sum_{n,m=1}^{N} w_{nm} f_m(t-\tau)}_{=S_2}\right] \tag{20}$$

with $f_m(t) = f[\bar{u}(t) + v_m(t)]$. With the definition (7) and property (8), it is

$$\sum_{n=1}^{N} w_{nm} = Ng \,\forall_m = 1, \ldots, N \tag{21}$$

and hence

$$S_2 = \sum_{m=1}^{N} g f_m(t-\tau). \tag{22}$$

To calculate S_1, we note that

$$\sum_{m=1}^{N} w_{nm} f_m(t-\tau) = \sum_{m=1}^{N} g f_m(t-\tau) + s\sum_{m=1}^{N}\eta_{nm} f_m(t-\tau). \tag{23}$$

If $X_m = f_m$ and $Y_m = \eta_{nm}$ $\forall n$ are statistically independent from each other, then

$$\frac{1}{N}\sum_{m=1}^{N} X_m Y_m = \frac{1}{N}\sum_{k=1}^{N} X_k \frac{1}{N}\sum_{m=1}^{N} Y_m. \tag{24}$$

This assumption holds true in most cases, since η_{nm} are static and chosen independently from any dynamics and f_m evolves over time. Consequently,

$$\sum_{m=1}^{N} \eta_{nm} f_m(t-\tau) = \frac{1}{N} \times \sum_{k=1}^{N} \eta_{nk} \sum_{m=1}^{N} f_m(t-\tau). \tag{25}$$

and with condition (9)

$$\sum_{m=1}^{N} \eta_{nm} f_m(t-\tau) = 0 \tag{26}$$

and hence

$$S_1 = \sum_{m=1}^{N} g f_m(t-\tau). \tag{27}$$

Since $S_1 = S_2$, we obtain from Eq. (20)

$$\frac{1}{\alpha}\frac{d}{dt} v_n(t) = -v_n(t) + \xi_n(t) \tag{28}$$

and the fluctuations $v_n(t)$ are independent from the spatial mean, but the spatial mean depends on the $v_n(t)$, cf. Eq. (15).

If the external stimulus is random, uncorrelated and normal distributed with variance σ^2 about the mean I_0, then $v_n(t)$ is random as well and obeys an Ornstein–Uhlenbeck process. For large times, $v_n(t)$ approach a stationary state with the stationary probability density function

$$p_s(v_n) = \frac{1}{\sqrt{2\pi\alpha\sigma}} e^{-v_n^2/2\alpha\sigma^2}. \tag{29}$$

Merging Global and Fluctuation Dynamics

The global mode evolution (19) depends on the probability density function of the fluctuations $p(v, t)$. For large times, the fluctuations approach their stationary state much faster than the global mode evolves, i.e., $p(v, t) \to p_s(v)$ given in Eq. (29). Hence the global mode (19) evolves on a relative large time scale according to

$$\frac{1}{\alpha}\frac{d}{dt}\overline{u}(t) = -\overline{u}(t) + \frac{1}{\sqrt{2\pi\alpha\sigma}} \times \int_{-\infty}^{\infty} f[\overline{u}(t-\tau) + v]\, e^{-v^2/2\alpha\sigma^2} dv + I_0. \tag{30}$$

For illustration reasons, let us consider the special case of McCulloch–Pitts neurons, whose transfer function is a step function, i.e., $f[u] = \Theta(u - u_{th})$ with threshold u_{th}. Then the integral in Eq. (30) has a rather simple form and we gain (Hutt et al. 2016)

$$\frac{1}{\alpha}\frac{d}{dt}\overline{u}(t) = -\overline{u}(t) + \underbrace{\frac{g}{2}\left(1 + \mathrm{erf}\left[\frac{\overline{u}(t-\tau) - u_{th}}{\sqrt{2\alpha}\sigma}\right]\right)}_{=F[\overline{u}(t-\tau)]} + I_0 \tag{31}$$

with the error function erf(·). The transfer function $F[\bar{u}]$ has a sigmoidal shape and noise variance σ^2 determines its shape: weak noise, i.e., small σ, reflects a rather steep sigmoidal, whereas strong noise renders the sigmoidal function more flat.

From (30), we learn that F has always a sigmoidal shape if the single element transfer function $f(u)$ is a monotonically increasing function of u (Hutt and Buhry 2014). In the following, we assume the standard logistic sigmoidal function $F[u] = F_0/\left(1 + e^{-(u-u_{th})/c}\right)$. Here weak noise with low steepness parameter c reflects a steep step-like function whereas enhancing noise with increasing values of c flattens the sigmoid function. This is illustrated in Fig. 4.

Equation (30) describes the mean-field evolution of the global mode and permits to illustrate coherent structures. If $\bar{u} = 0$, then network elements are not coherent, whereas $\bar{u} \neq 0$ reflects coherent activity. In the following examples, we will see that coherence emerges in certain frequency bands dependent of the external noise level σ.

To gain some insights how coupling strength and noise strength modify the system dynamics, at first let us consider stationary solutions with $du_n/dt = 0$, i.e., $d\bar{u}(t)/dt = 0$. This yields

$$u_0 - I = F[u_0] \tag{32}$$

Figure 4 shows both sides of this equation and illustrates that increasing the coupling strength (increasing F_0) changes the stationary state u_0 and, even more important, the nonlinear gain $dF/d\bar{u}$ computed at $\bar{u} = u_0$. Linearizing about that stationary state yields for deviations x

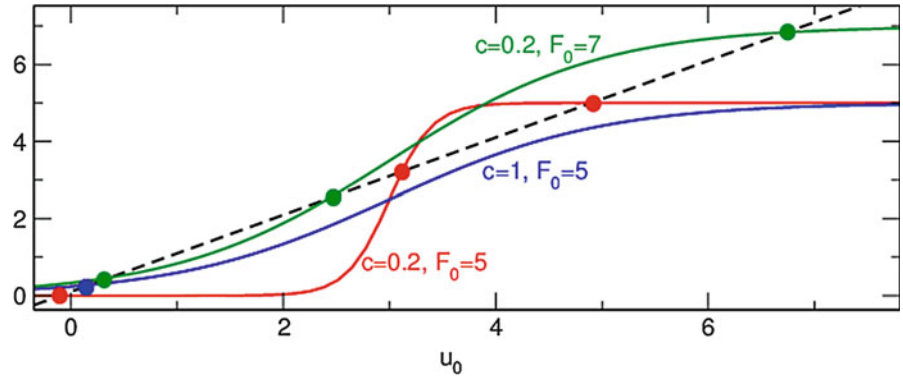

Additive Noise Tunes the Self-Organization in Complex Systems, Fig. 4 Illustration of the transfer function and the resulting stationary constant state. The dashed line denotes the left hand side of Eq. (32) and $u_{th} = 3$

$$\frac{1}{\alpha}\frac{dx(t)}{dt} = -x(t) + \gamma x(t-\tau), \quad \gamma = \frac{\partial F}{\partial \overline{u}}|_{\overline{u}=u_0}. \tag{33}$$

Hence the stability and timescale of solutions about the stationary state depends on the nonlinear gain. If the level of external noise increases (decreases), the transfer function becomes more flat (steep) and γ at upper and lower stationary state in Fig. 4 γ increases (decreases). In case of an oscillatory stable stationary state, the noise level determines the frequency of solutions (Hutt et al. 2016).

Coupling Induces Self-Organization in the Presence of Noise and Noise Affects System Frequency

To illustrate the network dynamic evolution subjected to noise, we simulate the full network of $N = 100$ elements that obeys (6) and increase the coupling strength between elements $\gamma = g/N$ continuously, cf. Fig. 5, lower panel. Synchronously, the noise level $\sigma = a\mu$, $a > 0$ is constant. This holds up to a certain time T.

We compute the time-dependent spectral power distribution and the phase-locking value (PLV) (Lachaux et al. 1999) in the course of time. The spectral power is computed by a windowed Fourier Transform with a 4s-window width, the PLV is computed as the circular variance of phases of 30 randomly chosen elements for each time-frequency pair. The phases result from a Morlet wavelet transform. The maximum value $PLV = 1$ reflects complete synchronization in the network, whereas the minimum value $PLV = 0$ reflects vanishing synchrony in the network. Figure 5 shows that the network elements do not synchronize at low coupling strengths since power and PLV are low. However, synchronization emerges with larger coupling expressed by large power and large PLV at $\nu = 45$ Hz. It is well-known that complex systems self-organize if the interaction between subunits are large enough. This is seen in our simple example. Analytically, the stationary state u_0 is a stable focus when power and PLV are low. When synchronization sets in at stronger coupling strength, the stable focus becomes unstable, the system oscillates along a limit cycle, and power is much stronger.

Until now, the noise level has been kept constant. Now removing the noise while retaining the coupling strength, cf. Fig. 5, lower panel for $t > T = 20$s, the PLV jumps to very high values while the maximum power jumps to lower values. Interestingly, the oscillation frequency with maximum power drops to $\nu = 40$ Hz that represents the systems endogenous oscillatory rhythm in the absence of noise. This drop clearly demonstrates that systems' frequency observed may depend heavily on the intrinsic noise level.

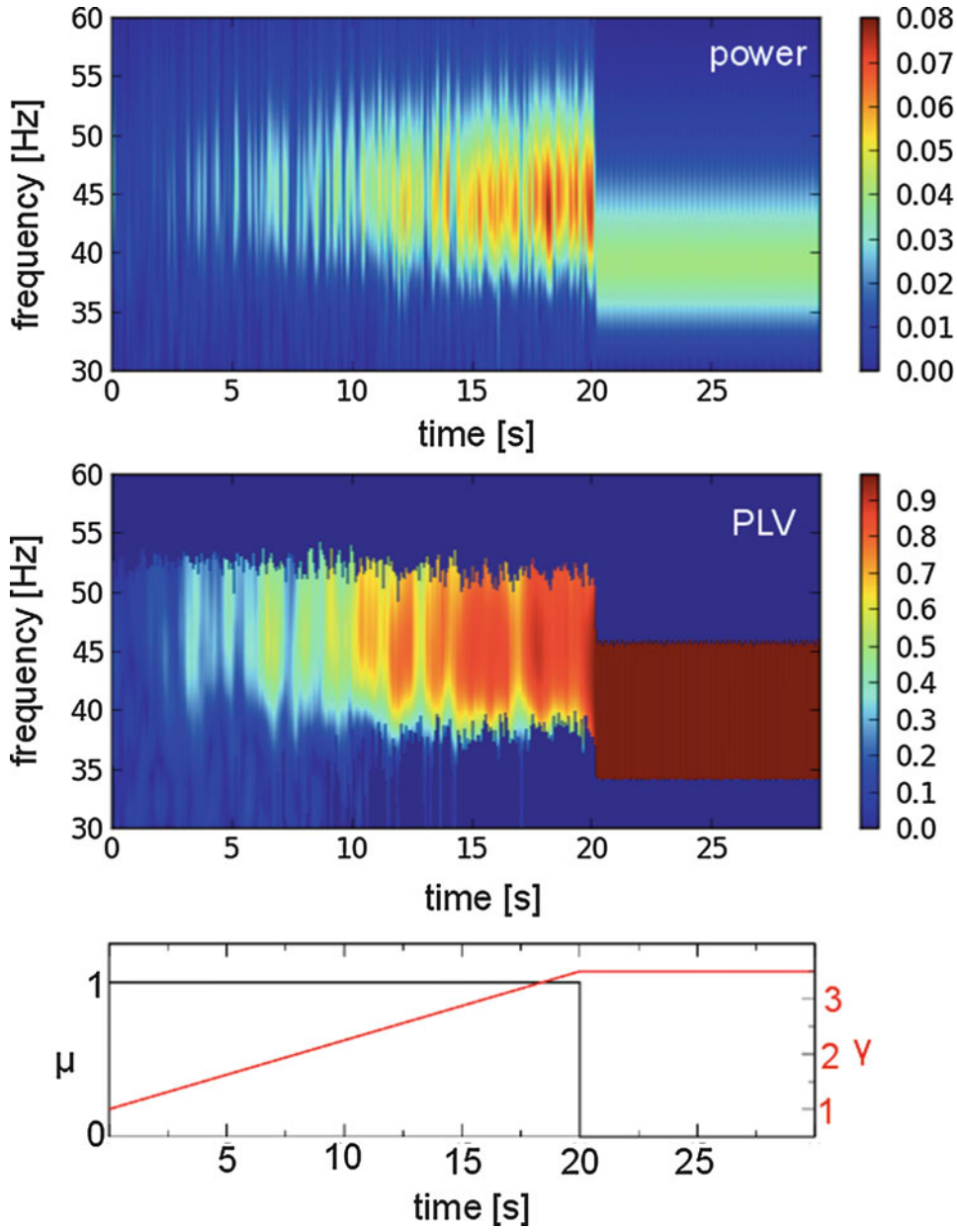

Additive Noise Tunes the Self-Organization in Complex Systems, Fig. 5 Spectral distribution and phase-locking value (PLV) in a simple spatial neural mass network subjected to varying noise and coupling strength. It is $\mu = \sqrt{60}\sigma$ and $T = 20$s, see text body

We learn that noise diminishes the synchronization between network elements and moves the system frequency. This is confirmed by Fig. 6 presenting epochs of single time series at low (left) and large coupling strength (center) at high noise levels and in the absence of any noise (right).

Analytically, this behavior can be understood by Eqs. (30) and (32) and Fig. 4: additive noise

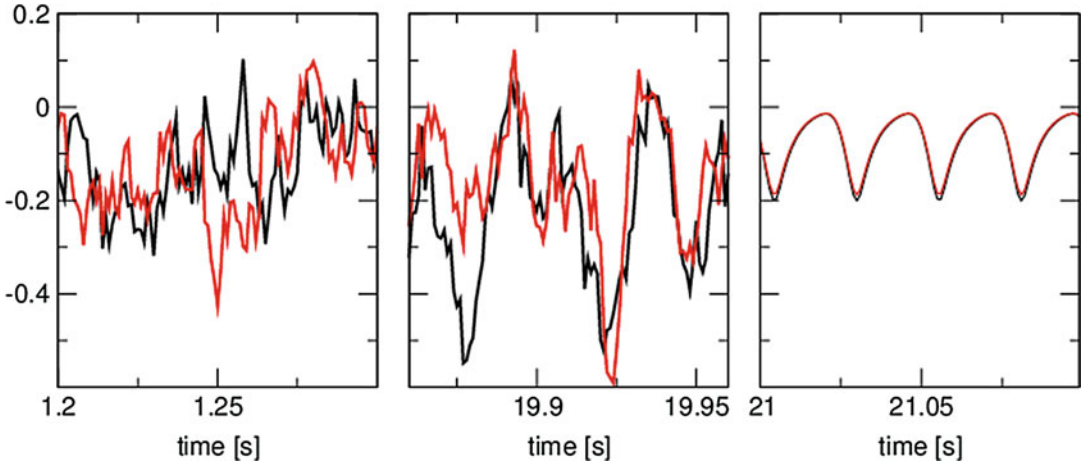

Additive Noise Tunes the Self-Organization in Complex Systems, Fig. 6 Activity at two spatial locations in simple spatial network. (Left panel) Weak coupling, with noise. (Center panel) Strong coupling, with noise. (Right panel) Strong coupling, no noise

tunes the effective transfer function, thus determines the stationary state and its stability and consequently the amplitude and frequency of the systems dynamics.

Noise Can Destruct Self-Organization While It Changes the System Frequency

The previous section shows that denoising enhances oscillatory power and shifts frequency of power peaks. Similarly, increasing the noise level may tune the systems' rhythmic activity and even destroy it at large enough noise levels. Figure 7 demonstrates that increasing noise level shifts the frequency of the system and, finally, destroys the oscillatory state. At large noise levels, the transfer function F is flat and a single stationary state exists. Hence increasing the noise level either makes the system jump from large values u_0 to low values of u_0 and/or its corresponding nonlinear gain renders the stationary state stable.

Synchronization in a Spiking Neural Network

To illustrate that the noise-induced change of synchronization also may occur in biologically more realistic networks, we study a spiking neural network of Poisson neurons (Lefebvre et al. 2017), cf. Fig. 8.

Figure 9 shows the average electric potential of cortical neurons (EEG) and their firing activity in a raster plot for two different noise levels D. We observe that denoising induces synchronization between neurons and enhances EEG power. A corresponding mean-field description of the spiking neural network, e.g., along the lines of the derivation shown in (Hutt and Buhry 2014), permits to describe the noise effect. Essentially, the mechanism is the same as the one shown in an above section and in previous studies (Hutt and Buhry 2014; Hutt et al. 2016; Lefebvre et al. 2015; Herrmann et al. 2016): increasing additive noise of network elements smoothens the effective transfer function, consequently shifts the stationary state and tunes its stability and may induce a transition to a new state.

Future Directions

Additive noise may have a strong impact on complex systems. The previous sections have shown

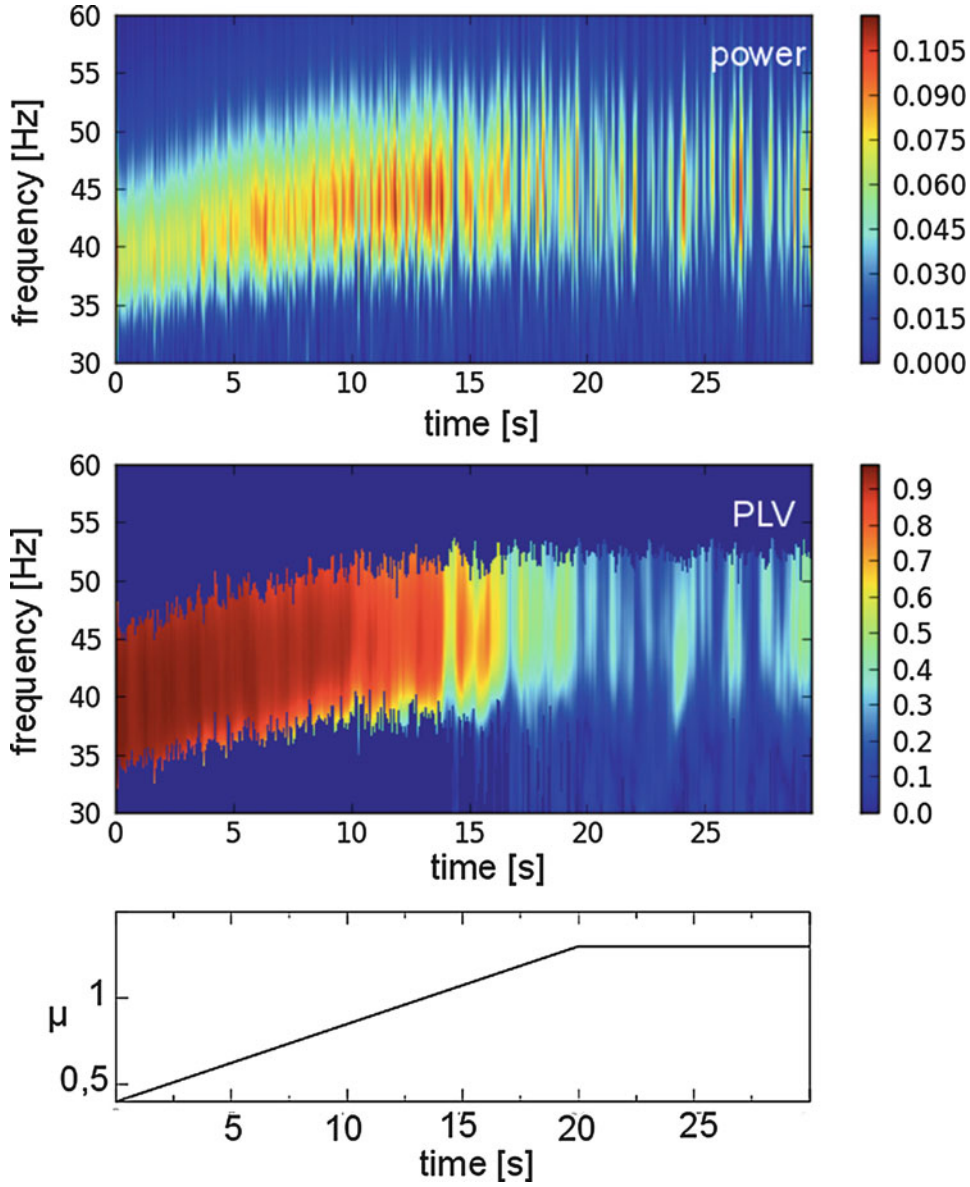

Additive Noise Tunes the Self-Organization in Complex Systems, Fig. 7 Time-frequency spectral power and global phase locking of simulations of the simple spatial neural mass network with increasing noise level

corresponding conditions and mathematical techniques. Additive noise may shift instability thresholds and tunes frequency and amplitude of rhythmic activity. We showed that additive noise in lower levels, e.g., in neurons or neural ensemble patches, may destroy synchronization in an upper level, e.g., in neural populations or populations of ensemble patches.

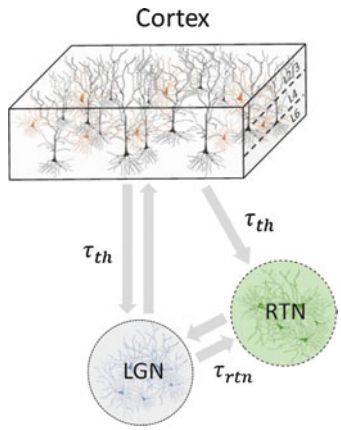

Additive Noise Tunes the Self-Organization in Complex Systems, Fig. 8 Network modeling the thalamocortical feedback circuit present in vertebrates. All neurons in the network receive spectral-white Gaussian noise with zero mean and finite variance

The insight, that additive noise affects endogenous brain activity, indicates impact of electric brain stimulation on the behavior of subjects. Corresponding experiments have been performed in the last decades, both for rhythmic stimulation (Herrmann et al. 2013) and noise stimulation (Terney et al. 2008). Perceptual learning under noise stimulation has been shown (Fertonani et al. 2011) to improve considering high-frequency noise (>100 Hz). Understanding how noise stimulation affects neural activity and how it enhances the perceptual learning is one of the great challenges in future years.

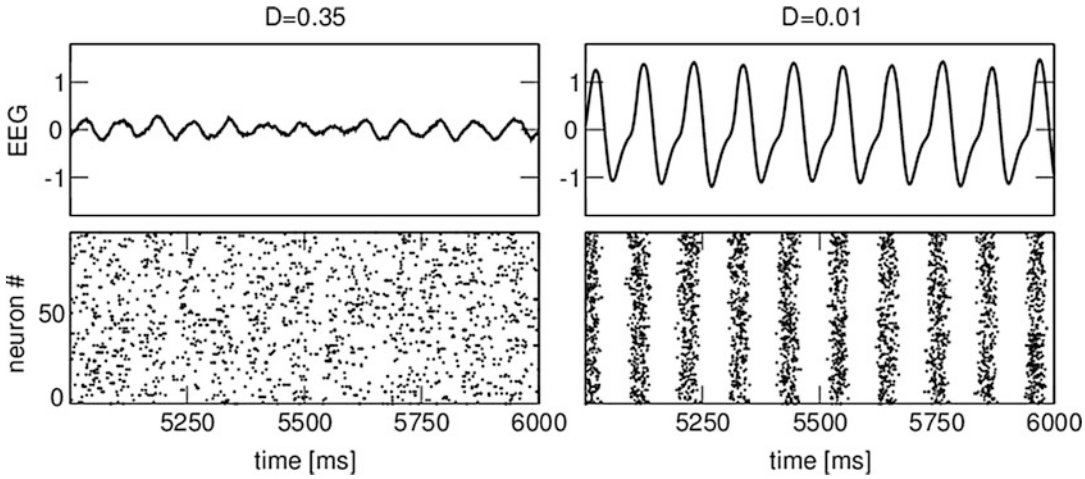

Additive Noise Tunes the Self-Organization in Complex Systems, Fig. 9 Noise reduction induces synchronization of spiking neurons. (Top panel) *EEG*(*t*) is the average electric potential of cortical neurons. (Bottom panel) Firing activity of neurons in the network

Bibliography

Arnold L (1998) Random dynamical systems. Springer, Berlin

Bloemker D (2003) Amplitude equations for locally cubic non-autonomous nonlinearities. SIAM J Appl Dyn Syst 2(2):464–486

Bloemker D, Hairer M, Pavliotis GA (2005) Modulation equations: stochastic bifurcation in large domains. Commun Math Phys 258:479–512

Boxler P (1989) A stochastic version of the center manifold theorem. Probab Theory Relat Fields 83:509–545

Carr J (1981) Applications of center manifold theory. Springer, Berlin

Doiron B, Lindner B, Longtin A, Maler L, Bastian J (2004) Oscillatory activity in electrosensory neurons increases with the spatial correlation of the stochastic input stimulus. Phys Rev Lett 93:048101

Drolet F, Vinals J (1998) Adiabatic reduction near a bifurcation in stochastically modulated systems. Phys Rev E 57(5):5036–5043

Drolet F, Vinals J (2001) Adiabatic elimination and reduced probability distribution functions in spatially extended systems with a fluctuating control parameter. Phys Rev E 64:026120

Fertonani A, Pirulli C, Miniussi C (2011) Random noise stimulation improves neuroplasticity in perceptual learning. J Neurosci 31(43):15416–15423

Fuchs A, Kelso J, Haken H (1992) Phase transitions in the human brain: spatial mode dynamics. Int J Bifurcation Chaos 2(4):917

Garcia-Ojalvo J, Sancho J (1999) Noise in spatially extended systems. Springer, New York

Haken H (1983) Advanced synergetics. Springer, Berlin

Haken H (1985) Light II – laser light dynamics. North Holland, Amsterdam

Haken H (1996) Slaving principle revisited. Phys D 97:95–103

Haken H (2004) Synergetics. Springer, Berlin

Herrmann C, Rach S, neuling T, Strüber D (2013) Transcranial alternating current stimulation: a review of the underlying mechanisms and modulation of cognitive processes. Front Hum Neurosci 7:279

Herrmann CS, Murray MM, Ionta S, Hutt A, Lefebvre J (2016) Shaping intrinsic neural oscillations with periodic stimulation. J Neurosci 36(19):5328–5339

Horsthemke W, Lefever R (1984) Noise-induced transitions. Springer, Berlin

Hutt A (2008) Additive noise may change the stability of nonlinear systems. Europhys Lett 84(34):003

Hutt A, Buhry L (2014) Study of GABAergic extrasynaptic tonic inhibition in single neurons and neural populations by traversing neural scales: application to propofol-induced anaesthesia. J Comput Neurosci 37(3):417–437

Hutt A, Lefebvre J (2016) Stochastic center manifold analysis in scalar nonlinear systems involving distributed delays and additive noise. Markov Process Relat Fields 22:555–572

Hutt A, Longtin A, Schimansky-Geier L (2007) Additive global noise delays Turing bifurcations. Phys Rev Lett 98:230601

Hutt A, Longtin A, Schimansky-Geier L (2008) Additive noise-induced Turing transitions in spatial systems with application to neural fields and the Swift–Hohenberg equation. Phys D 237:755–773

Hutt A, Lefebvre J, Longtin A (2012) Delay stabilizes stochastic systems near an non-oscillatory instability. Europhys Lett 98:20004

Hutt A, Mierau A, Lefebvre J (2016) Dynamic control of synchronous activity in networks of spiking neurons. PLoS One 11(9):e0161488. https://doi.org/10.1371/journal.pone.0161488

Jirsa V, Friedrich R, Haken H (1995) Reconstruction of the spatio-temporal dynamics of a human magnetoencephalogram. Phys D 89:100–122

Lachaux JP, Rodriguez E, Martinerie J, Varela F (1999) Measuring phase synchrony in brain signals. Hum Brain Mapp 8:194–208

Lefebvre J, Hutt A (2013) Additive noise quenches delay-induced oscillations. Europhys Lett 102:60003

Lefebvre J, Hutt A, LeBlanc V, Longtin A (2012) Reduced dynamics for delayed systems with harmonic or stochastic forcing. Chaos 22:043121

Lefebvre J, Hutt A, Knebel J, Whittingstall K, Murray M (2015) Stimulus statistics shape oscillations in nonlinear recurrent neural networks. J Neurosci 35(7):2895–2903

Lefebvre J, Hutt A, Frohlich F (2017) Stochastic resonance mediates the statedependent effect of periodic stimulation on cortical alpha oscillations. eLife 6:e32054

Noilhan J, Planton S (1989) A simple parameterization of land surface processes for meteorological models. Mon Weather Rev 117:536–549

Schanz M, Pelster A (2003) Synergetic system analysis for the delay-induced Hopf bifurcation in the Wright equation. SIAM J Appl Dyn Syst 2:277–296

Schoener G, Haken H (1986) The slaving principle for Stratonovich stochastic differential equations. Z Phys B 63:493–504

Terney D, Chaieb L, Moliadze V, Antal A, Paulus W (2008) Increasing human brain excitability by transcranial high-frequency random noise stimulation. J Neurosci 28(52):14147–14155

Xu C, Roberts A (1996) On the low-dimensional modelling of Stratonovich stochastic differential equations. Phys A 225:62–80

Chaotic Dynamics in Neural Systems

Krishna Pusuluri[1], Huiwen Ju[1] and Andrey Shilnikov[2]
[1]Neuroscience Institute, Georgia State University, Atlanta, GA, USA
[2]Neuroscience Institute, and Department of Mathematics and Statistics, Georgia State University, Atlanta, GA, USA

Article Outline

Introduction
Neuronal Activities and Transition Mechanisms
Chaos in Neuron Models
Appendix
Bibliography

Introduction

Several basic mechanisms of chaotic dynamics in phenomenological and biologically plausible models of individual neurons are discussed. We show that chaos occurs at the transition boundaries between generic activity types in neurons such as tonic spiking, bursting, and quiescence, where the system can also become bi-stable. The bifurcations underlying these transitions give rise to period-doubling cascades, various homoclinic and saddle phenomena, torus breakdown, and chaotic mixed-mode oscillations in such neuronal systems.

Neurons exhibit various activity regimes and state transitions that reflect their intrinsic ionic channel behaviors and modulatory states. The fundamental types of neuronal activity can be broadly defined as quiescence, subthreshold, and tonic spiking oscillations, as well as bursting composed of alternating periods of spiking activity and quiescence. A single neuron can endogenously demonstrate various bursting patterns, varying in response to the external influence of synapses, or to the intrinsic factors such as channel noise. The co-existence of bursting and tonic spiking, as well as several different bursting modes, have been observed in modeling (Cymbalyuk et al. 2002; Bertram 1993; Canavier et al. 1993; Butera 1998; Frohlich and Bazhenov 2006) and experimental (Hounsgaard and Kiehn 1989; Lechner et al. 1996; Turrigiano et al. 1996) studies. This complexity enhances the flexibility of the nervous and locomotive systems (Rabinovich et al. 2006).

The functional role of chaotic behaviors, and the dynamical and bifurcational mechanisms underlying their onset at transitions between neural activity types like spiking, bursting, and quiescence, has been the focus of various theoretical and experimental studies. Bursting is a manifestation of multiple timescale dynamics, composed of repetitive fast tonic spiking and a slow quiescent phase. It has been observed in various fields of science as diverse as food chain ecosystems (Rinaldi and Muratori 1992), nonlinear optics (DeShazer et al. 2003), medical studies of the human immune system (Shochat and Rom-Kedar 2008), and neuroscience (Steriade et al. 1990). Various bursting patterns, whether regular or chaotic, endogenous, or as emergent network phenomena, are the natural rhythms generated by central pattern generators (CPG) (Briggman and Kristan 2008; Kopell 1988; Marder and Calabrese 1996; Katz 2008; Shilnikov et al. 2008). CPGs are neural networks made up of a small number of constituent neurons that often control various vital repetitive locomotive functions (Marder and Calabrese 1996) such as walking and respiration of humans, or the swimming and crawling of leeches (Kristan et al. 2005; Kristan and Katz 2006; Briggman and Kristan 2006). Polyrhythmic bursting dynamics have also been observed in multifunctional CPG circuits that produce several coexisting stable oscillatory patterns or bursting rhythms, each of which is associated with a particular type of locomotor activity of the animal

A. Hutt, H. Haken (eds.), *Synergetics*,
https://doi.org/10.1007/978-1-0716-0421-2_738

Originally published in
R. A. Meyers (ed.), *Encyclopedia of Complexity and Systems Science*, © Springer Science+Business Media LLC 2020
https://doi.org/10.1007/978-3-642-27737-5_738-1

(Jalil et al. 2013; Alacam and Shilnikov 2015; Wojcik et al. 2014). Bursting has also been frequently observed in pathological brain states (Steriade et al. 1993; Rubin and Terman 2004), in particular, during epileptic seizures (Bazhenov et al. 2000; Timofeev et al. 2002). Neurons in bursting modes differ in their ability to transmit information and respond to stimulation from those in tonic spiking mode and therefore play an important role in information transfer and processing in normal states of the nervous system.

Understanding and modeling the generic mechanisms regulating the neuronal connectivity and the transitions between different patterns of neural activity, including global bifurcations occurring in neuron models and networks, pose fundamental challenges for mathematical neuroscience, with a number of open problems (Guckenheimer 1996). The range of bifurcation and dynamical phenomena underlying bursting *transcends* the existing state of the theory (Belykh et al. 2000; Shilnikov and Cymbaluyk 2004; Doiron et al. 2002; Laing et al. 2003; Rowat and Elson 2004; Shilnikov and Cymbalyuk 2005; Shilnikov et al. 2005a; Channell et al. 2007a; Cymbalyuk and Shilnikov 2005; Shilnikov and Kolomiets 2008; Kramer et al. 2008): This includes the blue sky catastrophe (Shilnikov et al. 2005b, 2014), torus-canard formation and breakdown, and homoclinic inclination/orbit-flip bifurcations, all of which can occur on the transition route to bursting in most square-wave and elliptic bursters. Studies of bursting require nonlocal homoclinic bifurcation analysis, which is often based on the Poincaré return mappings (Shilnikov et al. 1998/2001). Return mappings have been employed for computational neuroscience in Shilnikov and Rulkov (2003, 2004), Chay (1985), and Medvedev (2005). A drawback of mappings constructed from time series is sparseness, as they reflect only the dominating attractors of a system. In some cases, feasible reductions to one or two dimensional mappings can be achieved through slow-fast scale decomposition of the phase variables for the system (Griffiths and Pernarowski 1917–1948). A new, computer assisted method for constructing a complete family of *onto* mappings for membrane potentials, for a better understanding of simple and complex dynamics in neuronal models, both phenomenological and of the Hodgkin–Huxley type (Hodgkin and Huxley 1952), was proposed in Channell et al. (2007b). With this approach, one can study, for example, the spike-adding transitions in the leech heart interneuron model, and how chaotic dynamics in between is associated with homoclinic tangle bifurcations of some threshold saddle periodic orbits (Channell et al. 2009). Qualitative changes in a system's activity at transitions often reveal the quantitative information about changes of certain biophysical characteristics associated with the transition. This approach has proven to be exemplary in neuroscience for understanding the transitions between silence and tonic-spiking activities (Rinzel and Ermentrout 1989). Moreover, knowledge about the bifurcation (transition) predicts cooperative behavior of interconnected neurons of the identified types (Ermentrout 1993).

In this entry, we discuss nonlocal bifurcations in generic, representative models of neurodynamics, described by high order differential equations derived through the Hodgkin-Huxley formalism. We consider a number of neuroscience-related applications to reveal a multiplicity of causes and their bifurcation mechanisms leading to the onset of complex dynamics and chaos in these models.

Neuronal Activities and Transition Mechanisms

This entry deals with neuronal models, both biologically plausible and phenomenological, that can produce complex and distinct dynamics such as tonic spiking, bursting, quiescence, chaos, and mixed-mode oscillations (MMOs) representing fast spike trains alternating with subthreshold oscillations. MMOs are typical for many excitable systems describing various (electro)chemical reactions, including the famous Belousov-Zhabotinky reaction, and models of elliptic bursters (Wojcik and Shilnikov 2011). Geometrical configurations of slow-fast neuron models for bursting were pioneered in Wang and Rinzel (1995), Rinzel (1985), Rinzel and Ermentrout (1989) and further

developed in Bertram et al. (1995), Izhikevich (2000, 2007). Dynamics of such singularly perturbed systems are determined by and centered around the attracting pieces of the slow motion manifolds. These are composed of equilibria and limit cycles of the fast subsystem (Tikhonov 1948; Pontryagin and Rodygin 1960; Fenichel 1979; Mischenko and Rozov 1980; Andronov et al. 1966; Mischenko et al. 1994; Jones and Kopell 1994; Arnold et al. 1994) that in turn constitute the backbones of bursting patterns in a neuronal model. Using the geometric methods based on the slow-fast dissection, where the slowest variable becomes a control parameter, one can detect and follow the branches of equilibria and limit cycles in the fast subsystem. The slow-fast decomposition allows for drastic simplification, letting one clearly describe the dynamics of a singularly perturbed system. A typical Hodgkin-Huxley model possesses a pair of such manifolds (Rinzel 1985; Jones and Kopell 1994): quiescent and tonic spiking, respectively. The slow-fast dissection has been proven effective in low-order mathematical models of bursting neurons far from the bifurcation points. However, this approach does not account for the reciprocal, often complex interactions between the slow and fast dynamics, leading to the emergence of novel dynamical phenomena and bifurcations that can *only* occur in the whole system. Near such activity transitions, the bursting behavior becomes drastically complex and can exhibit deterministic chaos (Shilnikov and Cymbaluyk 2004; Shilnikov et al. 2005a; Cymbalyuk and Shilnikov 2005; Terman 1992; Holden and Fan 1992; Wang 1993; Feudel et al. 2000; Deng and Hines 2002; Elson et al. 2002).

Slow-Fast Decomposition

Many Hodgkin-Huxley type models can be treated as a generic slow-fast system

$$\mathbf{x}' = \mathbf{F}(\mathbf{x}, z) \quad z' = \mu G(\mathbf{x}, z, \alpha), \qquad (1)$$

where $0 < \mu \ll 1, \mathbf{x} \in R^n, n \geq 2$ and z is a scalar or can be a vector in R^2 (as in the extended Plant model with two slow variables below); α is a control parameter shifting the slow nullcline, given by $G(\mathbf{x}, \alpha) = 0$, in the phase space. In the singular limit $\mu = 0$, the z-variable becomes a parameter of the fast subsystem to detect and continue the equilibrium state (ES), given by $\mathbf{F}(\mathbf{x}, z) = 0$, and the limit cycles (LC) of the fast subsystem. As long as they (ES/LC) remain exponentially stable, by varying z one can trace down the smooth invariant manifolds in the phase space of (1) such as M_{eq} with the distinct Z-shape typical for many Hodgkin-Huxley type models (see Fig. 1), while the limit cycles form a cylinder-shaped surface M_{lc}. Locally, either is a center manifold for (1) persisting in a closed system, in virtue of (Tikhonov 1948; Pontryagin and Rodygin 1960; Fenichel 1979). The stable upper and lower branches of M_{eq} correspond to the de- and hyperpolarized steady states of the neuron, respectively. Folds on M_{eq} correspond to the saddle-node equilibrium states of the fast subsystem. The unstable de-polarized branch of M_{eq} can be enclosed by the tonic-spiking manifold M_{lc} typically emerging through an Andronov-Hopf bifurcation and terminating through a homoclinic bifurcation, which are the key features of the fast-subsystem of the square-wave bursters (Shilnikov 2012), like the Hindmarsh-Rose model (Barrio et al. 2014) and the Chay model (Chay 1985) (discussed below).

Poincaré Mappings

To elaborate on the nature of complex oscillations like bursting and their evolutions, one needs to examine nonlocal bifurcations that often require the use of Poincaré return maps (Shilnikov and Rulkov 2003, 2004; Chay 1985; Holden and Fan 1992; Deng 1999; Hutt and Beim Graben 2017; Beim Graben et al. 2016; Beim Graben and Hutt 2013, 2015). An obvious drawback of maps constructed from voltage time series is in their sparseness, as they can typically reveal some point-wise attractors of the system that trajectories fast converge to, unless there is a noise or small perturbations are added to get a more complete picture of the underlying structure. In some cases, a feasible reduction to low-dimensional mapping can be achieved through slow–fast scale decomposition of slow phase variables (Shilnikov et al. 1998/2001, 2005b; Griffiths and Pernarowski 1917–1948). We proposed and developed a new

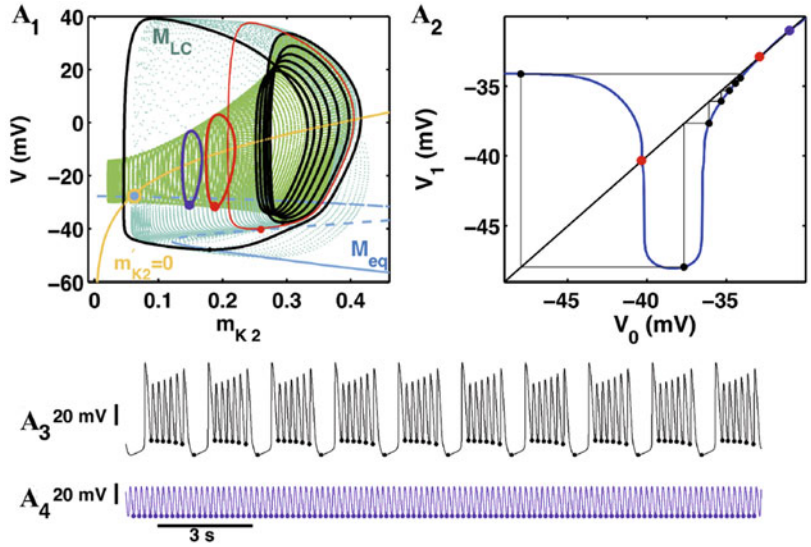

Chaotic Dynamics in Neural Systems, Fig. 1 ($\mathbf{A_1}$) Bistability of the coexisting tonic-spiking and bursting in the 3D phase space of the leech heart interneuron model (3). Inset ($\mathbf{A_2}$) depicts the shape of the corresponding 1D Poincaré map with stable fixed point corresponding to the tonic spiking periodic orbit (purple) with a single voltage minima, and period-7 bursting orbit, and 2 unstable fixed points (red): the right one separates attraction basins of tonic-spiking ($\mathbf{A_4}$) and bursting ($\mathbf{A_3}$) activities, whereas the left one causes chaotic dynamics at spike adding transitions, see Fig. 2

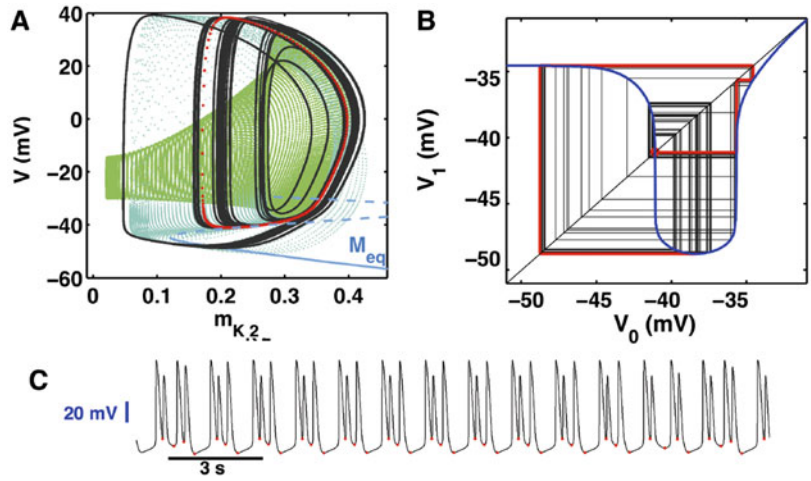

Chaotic Dynamics in Neural Systems, Fig. 2 (**A**) Chaotic bursting in the phase space of the leech heart interneuron model (3) and the corresponding map (**B**) at a transition between two and three spikes per burst in the voltage trace (**C**) due to proximity of the primary homoclinic orbit of the repelling fixed point (red) corresponding to a single minimum of the saddle periodic orbit (red) in (**A**)

computer assisted algorithm for constructing a dense family of *onto* mappings for membrane potentials in a Hodgkin–Huxley type neuronal model (Channell et al. 2007a). Such maps let us find and examine both the stable and unstable solutions in detail; moreover, unstable points are often the primary organizing centers globally governing the dynamics of the model in question. The construction of such a map begins with the localization of the tonic spiking manifold M_{lc} in the model, using the parameter continuation technique or the slow-fast dissection, see Fig. 1. Then, a curve on M_{lc} is defined, which corresponds to minimal (maximal) voltage values, denoted, say, by V_0. By construction, the 1D map M takes all V_0 (outgoing solutions integrated numerically) on this curve back onto itself, after a single turn around M_{lc}, i.e., M: $V_0 \rightarrow V_1$ for a selected value of the parameter. Two such maps are depicted in Figs. 1 and 2. One can see that these

are noninvertible (Mira 1987; Mira and Shilnikov 2005), unimodal maps with a single critical point (Devaney 1992; Sharkovsky et al. 1997), which happens to be a universal feature of many other square-wave bursters in neuroscience applications. With such maps, one can fully study the attractors, the repellers, and their bifurcations, including saddle-nodes, homoclinic orbits, spike-adding, and period-doubling. We note that detection of homoclinics of a saddle periodic orbit in the phase space of a model is in general *state-of-the art* and the Poincaré map technique allows us to locate them with ease.

Classifications of Bursting

The existing classifications (Wang and Rinzel 1995; Rinzel 1985; Rinzel and Ermentrout 1989; Bertram et al. 1995; Izhikevich 2000, 2007) of bursting are based on the bifurcation mechanisms of dynamical systems in a plane, which initiate or terminate fast trajectory transitions between the slow motion manifolds in the phase space of the slow-fast neuronal model. These classifications allow us to single out the classes of bursting by subdividing mathematical and realistic models into the following subclasses: elliptic or Hopf-fold subclass (FitzHugh-Rinzel (Wojcik and Shilnikov 2011) and Morris-Lecar models), square-wave bursters or fold-homoclinic subclass (Hindmarsh-Rose model (Shilnikov and Kolomiets 2008; Barrio and Shilnikov 2011), models of pancreatic β-cells, cells in the pre-Botzinger complex, as well as intrinsically bursting and chattering neurons in neocortex); parabolic or circle-circle subclass (model of R15 cells in the abdominal ganglion of the mollusk Aplysia (Butera 1998; Alacam and Shilnikov 2015), the reduced leech interneuron model at certain parameter values); and fold-fold subclass, or top hat models (Best et al. 2005), including the reduced heart interneuron model (3) discussed below.

Transition Routes

The current description of the transition routes between tonic spiking and bursting activities is incomplete and remains a fundamental problem for both neuroscience and the theory of dynamical systems. The first theoretical mechanism revealed in Terman (1992) explained chaos in the so-called square wave bursters (Rinzel 1985) emerging between tonic-spiking and bursting. Later, two global bifurcations that occur at the loss of stability of a tonic spiking periodic orbit through quite novel homoclinic saddle-node bifurcations were discovered and explained. The first transition, reversible and continuous, found in the reduced model of the leech heart interneuron (Shilnikov and Cymbaluyk 2004, 2005) and in a modified Hindmarsh-Rose model of a square-wave burster (Shilnikov and Kolomiets 2008; Shilnikov et al. 1998/2001), is based on the blue sky catastrophe (Shilnikov et al. 1998/2001; Turaev and Shilnikov 1995; Shilnikov and Turaev 1997, 2000; Gavrilov and Shilnikov 2000). This was proven in Shilnikov et al. (2005b) to be a typical bifurcation for slow-fast systems. This striking term (Abraham 1985), the *blue sky catastrophe,* stands for a novel bifurcation of a saddle-node periodic orbit with a 2D unstable manifold returning to the orbit making infinitely many revolutions. After the bifurcation, this homoclinic connection transforms into a long bursting periodic orbit with infinitely many spikes. The burst duration of the orbit near the transition is evaluated by $1/\sqrt{\alpha}$, where $0 < \alpha \ll 1$ is a bifurcation parameter. The second transition mechanism is due to a saddle-node periodic orbit with noncentral homoclinics (Lukyanov and Shilnikov 1978). An important feature of this transition is the bi-stability of co-existing tonic spiking and bursting activities in the neuron model, see Fig. 1. In this case, the burst duration towards the transition increases as fast as $|\ln(\alpha)|$. Another feature of this bifurcation is the transient chaos where the neuron generates an unpredictable number of burst trains before it starts spiking tonically. This phenomenon is a direct consequence of the Smale horseshoe finite shift dynamics in the system (Gavrilov and Shilnikov 1972), which is a rather atypical phenomenon for such slow-fast systems.

Chaos in Neuron Models

In this section, we present the basic mechanisms and routes to chaos in a variety of biophysically realistic neuronal models exhibiting rich and complex dynamics including tonic spiking, bursting,

and quiescence. A bifurcation describing a transition between neuronal activities typically occurs near saddle (unstable) orbits and results from reciprocal interactions involving the slow and fast dynamics of the model. Such interactions lead to the emergence of new dynamical phenomena and bifurcations that can occur only in the full model, but not in either of the slow or the fast subsystem. Chaotic dynamics can be characterized by unpredictable variations in the number of spikes during the active phases of bursting and/or the subthreshold oscillations. This phenomenon of chaotic dynamics is generally atypical in slow–fast systems as it occurs within narrow parameter windows only near the transition boundaries. Indeed, robust and regular dynamics of slow–fast neuron models contrast those of real bursting neurons exhibiting a phenomenal time dependent variability of oscillatory patterns.

Leech Heart Interneuron Model: Period Doubling Cascades and the Blue Sky Catastrophe

We first illustrate and discuss the onset of chaotic dynamics in the reduced (3D) model of the leech heart interneuron (see Eq. (3) of Appendix). This is a *typical* slow-fast Hodgkin-Huxley type (HH) model describing the dynamical interplay of a single slow variable – persistent potassium current, I_{K2}, and two fast variable – the sodium current, I_{Na} and the membrane voltage V that can be recast in this generic form (Shilnikov and Cymbalyuk 2005; Shilnikov et al. 2005a; Shilnikov 2012; Neiman et al. 2011):

$$CV_i' = -\sum_j I_j - \sum_i I_i^{\text{syn}},\ \tau_h h' = f_\infty(V) - h, \quad (2)$$

where C is a membrane capacitance, V is a transmembrane voltage, I_j stands for various in/outward currents including synaptic ones, $0 \leq h \leq 1$ stands for a gating (probability) variable, f_∞ is a sigmoidal function, and τ_h is a timescale, fast or slow, specific for specific currents.

This model shows a rich set of dynamics and can produce various types of complex chaotic and bistable behaviors, including the period-doubling cascade *en a route* from tonic spiking through bursting (Shilnikov and Cymbaluyk 2004; Cymbalyuk and Shilnikov 2005), as well as various types of homoclinic chaos. Following the period-doubling cascade, the model demonstrates a terminal phase of chaotic tonic spiking that coexists alongside another periodic tonic spiking activity. For a different set of parameter values compared to the period doubling cascade, the model can also exhibit the blue sky catastrophe as a continuous and reversible mechanism of the transition between bursting and tonic spiking. Figure 1 explains the nature of bi-stability in this model as it exhibits the co-existing tonic-spiking and bursting oscillations corresponding to the stable fixed point (FP) (purple) and the period-7 orbit in the 1D map, whose basins are separated by an unstable FP representing a saddle periodic orbit (red) on the 2D manifold M_{lc} in the 3D phase space. The role of the other unstable (red) FP is revealed by Fig. 2. It is shown that the spike-adding in bursting is accompanied with an onset of chaotic dynamics orchestrated by the homoclinic orbits and bifurcations involving the other saddle orbit, see more details in Shilnikov et al. (2014), Channell et al. (2009), Wojcik and Shilnikov (2011), Shilnikov (2012), Barrio et al. (2014), Barrio and Shilnikov (2011), and Neiman et al. (2011). Figure 3 shows the bifurcation diagram of the system constructed as a parametric sweep using our previously developed symbolic toolkit called the *Deterministic Chaos Prospector* (Pusuluri et al. 2017; Pusuluri and Shilnikov 2018, 2019) to process symbolic sequences extracted from wave-form traces and analyze activity types and underlying bifurcations. This bifurcation diagram identifies the regions of quiescence, tonic spiking, as well as bursting with spike adding cascades. The noisy regions near the boundaries of spike addition reveal the occurrence of chaos. In addition, the blue sky catastrophe takes place at the noisy region near the boundary between bursting and tonic spiking.

Period-Doubling in the Chay Model

The Chay model is a simple, realistic biophysical model for excitable cells, producing endogenous chaotic behavior (see its Eq. (5) of Appendix). The model transitions from tonic spiking to

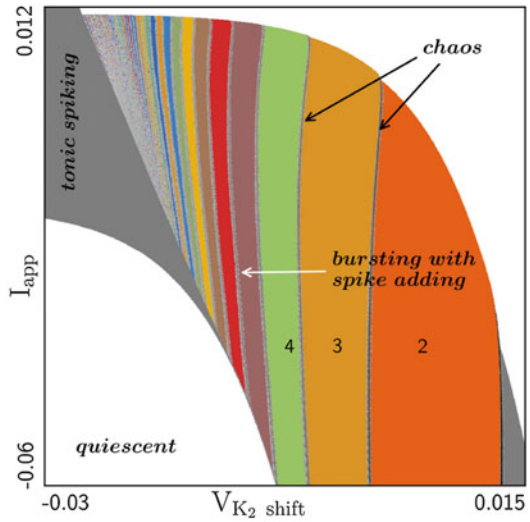

Chaotic Dynamics in Neural Systems, Fig. 3 Bi-parametric sweep of the leech heart interneuron model (3) using the symbolic toolkit *Deterministic Chaos Prospector* (Pusuluri et al. 2017; Pusuluri and Shilnikov 2018; Pusuluri and Shilnikov 2019) to process wave-form traces and to reveal regions of quiescent behavior, tonic spiking, as well as bursting activity with spike adding cascades: from 2 spikes (orange zone) to 3 spikes (yellowish zone), next to 4 spikes (light green zone) and so forth. The noisy regions near the boundaries of spike addition reveal the occurrence of chaos, while the noisy boundary between tonic spiking and bursting portrays the blue sky catastrophe (Shilnikov and Cymbaluyk 2004) corresponding to infinitely long bursting

bursting via period-doubling bifurcations, whereby chaotic dynamics can also arise. Figure 4 shows the 2D (*V*, *Ca*)-phase space projection of the Chay model with a period-4 orbit and a chaotic bursting orbit, along with the corresponding Poincaré return map. The model goes through a period-doubling cascade and then immediate chaotic bursting, before regular bursting as the bifurcation parameter $g_{K,c}$ increases.

Torus Breakdown in the Bull Frog Hair Cell Model

Next, we consider the hair cell model based on experimental studies of basolateral ionic currents in saccular hair cells in bullfrog (Hudspeth and Lewis 1988; Catacuzzeno et al. 2003, 2004; Rutherford and Roberts 2009). This is a further extension of the model of the Hodgkin-Huxley type developed in Catacuzzeno et al. (2004) that includes 12 coupled nonlinear ordinary differential equations, see Neiman et al. (2011) for its detailed description. In this model, the transition from bursting to tonic spiking is due to a torus bifurcation (TB) that leads to onset of quasi-periodic dynamics (Ju et al. 2018). Closer to this bifurcation the torus breaks down causing the onset of chaotic bursting in the system. In case of a supercritical TB, through which a stable torus emerges at the fold of the tonic spiking manifold M_{LC} (like one in Fig. 1), its development, growth and breakdown can be well studied using the Poincaré return maps. For example, Fig. 5a depicts that, right after the supercritical TB in the hair cell model, a stable torus (invariant circle) emerges from a stable tonic-spiking periodic orbit and grows from smooth and ergodic to non-smooth to resonant as the bifurcation parameter g_{K1} increases. Later, when the torus breaks down (starting at $g_{K1} = 29.213$ nS), bursting becomes chaotic as shown in the Poincaré map (Fig. 5b). Figure 5c illustrates the route from tonic spiking to bursting with chaotic dynamics at the torus breakdown.

Chaotic Mixed-Mode Oscillations in the Extended Plant Model

The conductance-based Plant model of endogenous parabolic bursters was originally developed to model the R15 neuron in the abdominal ganglion of the slug Aplysia Californica (Butera 1998). This was later extended and adapted to model the swim CPG of the sea slug *Melibe Leonina*, see Alacam and Shilnikov (2015) for details of the model and the equations. This model can produce chaotic bursting activity, as shown in Fig. 6a near the boundary between tonic spiking and bursting activity. In addition, the model exhibits complex chaotic *mixed mode oscillations* (MMOs) near the transition between bursting and the co-existing hyper-polarized quiescence state. Figure 6b illustrates the model generating spike-varying bursts and small amplitude subthreshold oscillations. Such chaotic MMOs coexist with a hyperpolarized quiescent state resulting in bistability due to a subcritical Andronov-Hopf bifurcation that gives rise to a saddle periodic orbit whose stable manifold

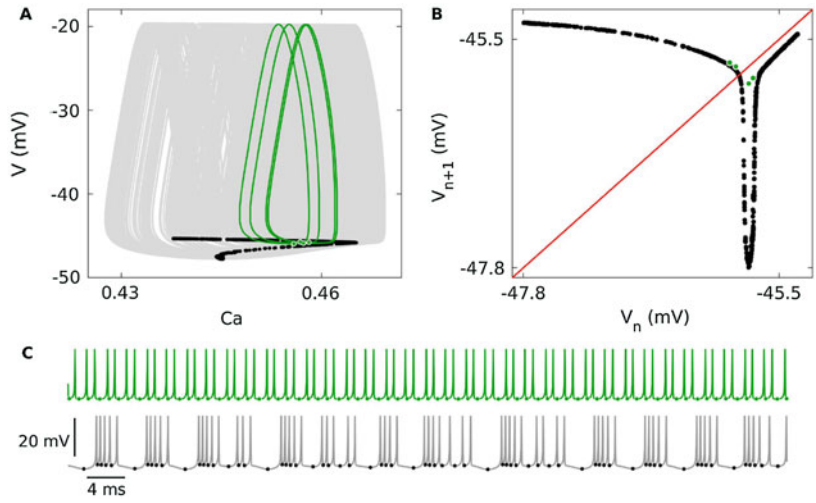

Chaotic Dynamics in Neural Systems, Fig. 4 (**A**) The (*V*, *Ca*) phase space projection overlaying a period-4 orbit (green, $g_{\underline{K},c} = 11.12$) and a chaotic bursting trajectory (grey, $g_{\underline{K},c} = 11.5$) generated by the Chay model. Here V_{min} – minimal values, labeled with green and black dots in the voltage traces (**C**), are used to generate 1D Poincaré return maps: $V_{min}^{(n)} \rightarrow V_{min}^{(n+1)}$ in Inset (**B**)

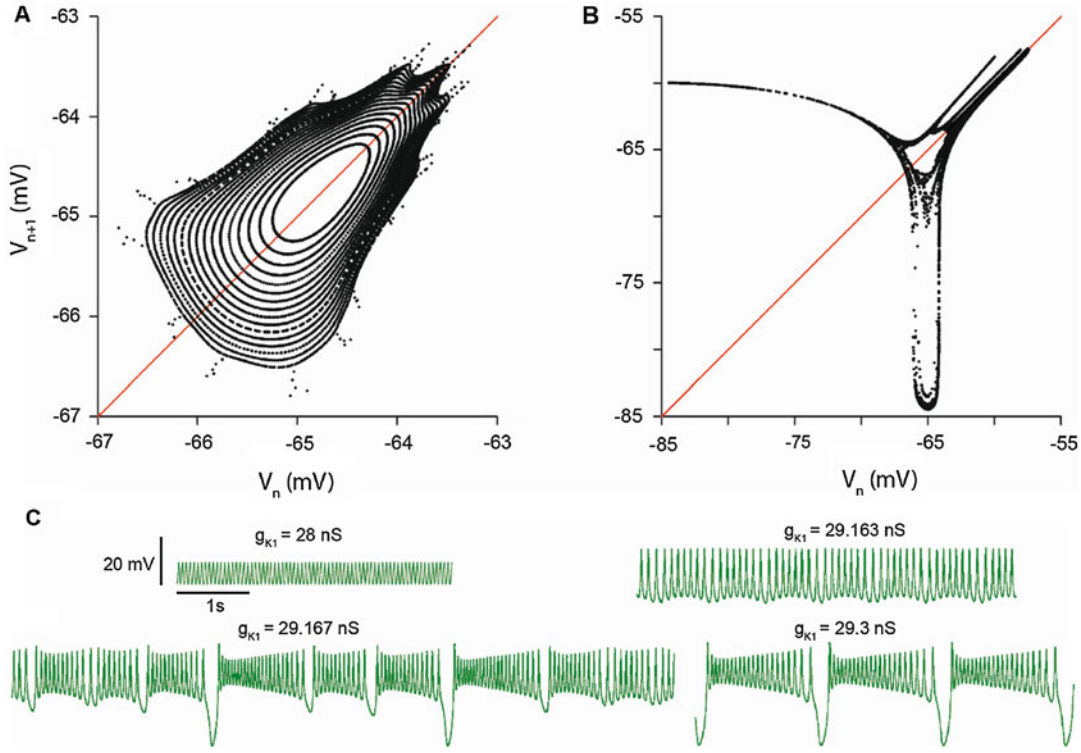

Chaotic Dynamics in Neural Systems, Fig. 5 Poincare return map, $V_{min}^{(n)} \rightarrow V_{min}^{(n+1)}$, for the consecutive V_{min}-values in voltage traces generated by the hair cell model. (**A**) Evolution of stable invariant circles (IC) from ergodic to resonant with further nonsmooth torus breakdown as the g_{K1} parameter is increased from 29.185 through 29.2073 nS. (**B**) Chaotic bursting after the torus breakdown at $g_{K1} = 29.213$ nS. The flat, stabilizing section of the map corresponds to hyperpolarized quiescence, while multiple sharp folds reveal a ghost of the nonsmooth IC in the depolarized range. (**C**) En route from tonic spiking to regular bursting, the voltage trace undergoes quasi-periodicity and chaotic bursting. (This figure is adapted from Ju et al. (2018))

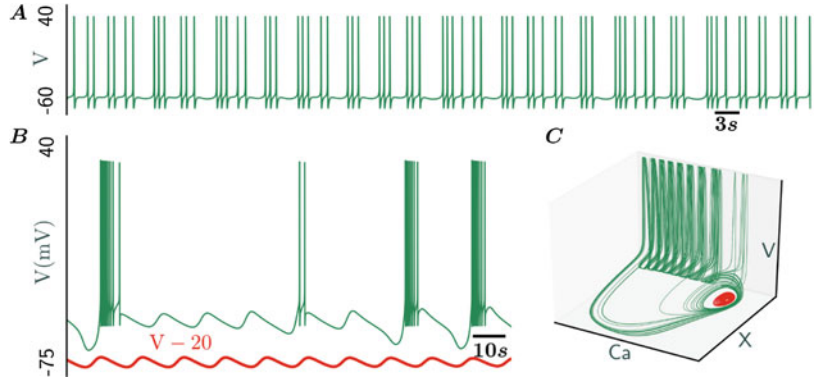

Chaotic Dynamics in Neural Systems, Fig. 6 The extended Plant model can exhibit chaotic bursting near the boundaries of tonic spiking and bursting with spike-adding (**A**) as well as bistability with chaotic mixed mode oscillations (green) and hyperpolarized quiescence (red) near the transitions between bursting with spike-adding and hyperpolarized quiescence (**B**). The corresponding phase space projection of the bistable states of (**B**) is shown in (**C**). Following a subcritical Andronov-Hopf bifurcation, a saddle periodic orbit (not seen) separates the chaotic mixed mode bursts (green) from the hyperpolarized quiescent state with spiral convergence (red)

separates the chaotic bursting activity (green) from the stable (spiraling) hyperpolarized quiescent state (red) as shown in Fig. 6c. As the parameters are varied, gradually the system transitions from this bistable state to the monostable hyperpolarized quiescence, or vice versa, to a dominant bursting activity.

Acknowledgments This work was funded in part by the NSF grant IOS-1455527 and the RSF grant 14-41-00044 at Lobachevsky University of Nizhny Novgorod. We thank the Brains and Behavior initiative of Georgia State University for providing pilot grant support and the doctoral fellowships of K. Pusuluri and H. Ju. We acknowledge the support of NVIDIA Corporation with the Tesla K40 GPUs used in this study. Finally, we are grateful to all the current and past members of the Shilnikov NeurDS lab for productive discussions.

Appendix

Leech Heart Interneuron Model

The reduced leech heart model is derived using the Hodgkin-Huxley formalism:

$$\begin{aligned} CV' &= -I_{\mathrm{Na}} - I_{\mathrm{K2}} - I_{\mathrm{leak}} + I_{\mathrm{app}}, \\ \tau_{\mathrm{Na}} h'_{\mathrm{Na}} &= h^{\infty}_{\mathrm{Na}}(V) - h, \\ \tau_{\mathrm{K2}} m'_{\mathrm{K2}} &= m^{\infty}_{\mathrm{K2}}(V) - m_{\mathrm{K2}}, \end{aligned} \tag{3}$$

with

$$\begin{aligned} I_{leak} &= 8(V + 0.046), \\ I_{\mathrm{K2}} &= 30 m^2_{\mathrm{k2}}(V + 0.07), \\ I_{\mathrm{Na}} &= 200 \left[m^{\infty}_{\mathrm{Na}}(V)\right]^3 h_{\mathrm{Na}}(V - 0.045), \end{aligned}$$

and where V is the membrane potential, $C = 0.5$; h_{Na} is a fast ($\tau_{\mathrm{Na}} = 0.0405$ sec) activation of I_{Na}, and m_{K2}; I_{L} describes the slow ($\tau_{\mathrm{K2}} = 0.25$ sec) activation of I_{K2}, I_{app} is an applied current. The steady states $h^{\infty}_{\mathrm{Na}}(V)$, $m^{\infty}_{\mathrm{Na}}(V)$, $m^{\infty}_{\mathrm{K2}}(V)$, of the of the gating variables are given by the Boltzmann equations given by

$$\begin{aligned} h^{\infty}_{\mathrm{Na}}(V) &= [1 + \exp(500(0.0333) + V))]^{-1}, \\ m^{\infty}_{\mathrm{Na}}(V) &= [1 + \exp(-150(0.0305) + V))]^{-1}, \\ m^{\infty}_{\mathrm{K2}}(V) &= \left[1 + \exp\left(-83(0.018) + \mathrm{V}^{\mathrm{shift}}_{\mathrm{K2}} + V\right)\right)]^{-1}. \end{aligned} \tag{4}$$

The bifurcation parameter $\mathrm{V}^{\mathrm{shift}}_{\mathrm{K2}}$ of the model is a deviation from the experimentally determined voltage $\mathrm{V}_{1/2} = 0.018$ V corresponding to the half-activated potassium channel, i.e., to $m^{\infty}_{\mathrm{k2}}(0.018) = 1/2$. In its range, $\mathrm{V}^{\mathrm{shift}}_{\mathrm{K2}}$ is $[-0.025; 0.0018]$V the upper boundary corresponds to the hyperpolarized quiescent state of the neuron, whereas the model produces spiking oscillations at the lower end $\mathrm{V}^{\mathrm{shift}}_{\mathrm{K2}}$ values and bursts in between.

Chay Model

The 3D Hodgkin-Huxley type Chay model reads as follows:

$$\begin{aligned} V' &= -g_I m_\infty^3 h_\infty (V - V_I) - g_{K,V} n_\infty^4 (V - V_K) \\ &\quad -g_{K,C} \frac{C}{1+C} (V - V_K) - g_L (V - V_L), \\ n' &= (n_\infty[V] - n)/\tau_n[V], \\ C' &= \rho \{ m_\infty^3 h_\infty (V_C - V) - k_C C \}, \end{aligned} \tag{5}$$

where n represents the gating variable of the voltage-sensitive K^+ channel and C represents the intracellular free calcium concentration. See (Chay 1985) for the detailed description.

Bibliography

Abraham RH (1985) Chaostrophes, intermittency, and noise, in Chaos, fractals, and dynamics, Conf. Univ. Guelph/Can. 1981 and 1983. Lect Notes Pure Appl Math 98:3–22

Alacam D, Shilnikov A (2015) Making a swim central pattern generator out of latent parabolic bursters. J Bifurcat Chaos 25(7):1540003

Andronov AA, Vitt AA, Khaikin SE (1966) Theory of oscillations. International series of monographs in physics. Pergamon Press, Oxford

Arnold VI, Afrajmovich VS, Ilyashenko YS, Shil'nikov LP (1994) Bifurcation theory, dynamical systems v. encyclopedia of mathematical sciences. Springer. https://www.springer.com/gp/book/9783540181736

Barrio R, Shilnikov A (2011) Parameter-sweeping techniques for temporal dynamics of neuronal systems: case study of hindmarsh-rose model. J Math Neurosci 1(1):6

Barrio R, Angeles Martínez M, Serrano S, Shilnikov A (2014) Macro-and micro-chaotic structures in the Hindmarsh-Rose model of bursting neurons. J Chaos 24(2):023128

Baxter DA, Lechner HA, Canavier CC, Butera RJ, Franceschi AA, Clark JW, Byrne JH (1999) Coexisting stable oscillatory states in single cell and multicellular neuronal oscillators. In: Levine DS, Brown VR, Shirey VT (eds) Oscillations in neural systems. Lawrence Erlbaum Associates, Mahwah, pp 51–78

Bazhenov M, Timofeev I, Steriade M, Sejnowski TJ (2000) Spiking-bursting activity in the thalamic reticular nucleus initiates sequences of spindle oscillations in thalamic networks. J Neurophysiol 84:1076–1087

Beim Graben P, Hutt A (2013) Detecting metastable states of dynamical systems by recurrence-based symbolic dynamics. Phys Rev Lett 110:154101

Beim Graben P, Hutt A (2015) Detecting event-related recurrences by symbolic analysis: applications to human language processing. Philos Trans Royal Soc A 373:20140089

Beim Graben P, Sellers KK, Frohlich F, Hutt A (2016) Optimal estimation of recurrence structures from time series. Europhys Lett 114(3):38003

Belykh I, Shilnikov A (2008) When weak inhibition synchronizes strongly desynchronizing networks of bursting neurons. Phys Rev Lett 101(7):078102

Belykh VN, Belykh IV, Colding-Joregensen M, Mosekilde E (2000) Homoclinic bifurcations leading to bursting oscillations in cell models. Eur Phys J 3:205

Bem T, Rinzel J (2004) Short duty cycle distabilizes a half-center oscillator, by gap junctions can restabilize the anti-phase pattern. J Neurophysiol 91:693–703

Bertram R (1993) A computational study of the effects of serotonin on a molluscan Burster neuron. Biol Cybern 69:257–267

Bertram R, Butte MJ, Kiemel T, Sherman A (1995) Topological and phenomenological classication of bursting oscillations. Bull Math Biol 57(3):413–439

Best J, Borisyuk A, Rubin J, Terman D, Wechselberger M (2005) The dynamic range of bursting in a model respiratory pacemaker network. SIAM J Appl Dyn Syst 4(4):1107–1139

Briggman KL, Kristan WB (2008) Multifunctional pattern-generating circuits. Annu Rev Neurosci 31:271–294

Briggman KL, Kristan WB Jr (2006) Imaging dedicated and multifunctional neural circuits generating distinct behaviors. J Neurosci 26(42):10925–10923

Butera R (1998) Multirhythmic bursting. J Chaos 8:274–282

Canavier CC, Baxter DA, Clark L, Byrne J (1993) Nonlinear dynamics in a model neuron provide a novel mechanism for transient synaptic inputs to produce long-term alterations of postsynaptic activity. J Neurophysiol 69:2252

Canavier CC, Baxter DA, Clark JW, Byrne JH (1999) Control of multistability in ring circuits of oscillators. Biol Cybern 80:87–102

Catacuzzeno L, Fioretti B, Franciolini F (2003) Voltage-gated outward K-currents in frog saccular hair cells. J Neurophysiol 90(6):3688–3701

Catacuzzeno L, Fioretti B, Perin P, Franciolini F (2004) Spontaneous low-frequency voltage oscillations in frog saccular hair cells. J Physiol 561:685–701

Channell P, Cymbalyuk G, Shilnikov AL (2007a) Origin of bursting through homoclinic spike adding in a neuron model. Phys Rev Lett 98:134101

Channell P, Cymbalyuk G, Shilnikov AL (2007b) Applications of the Poincare mapping technique to analysis of neuronal dynamics. Neurocomputing 70:10–12

Channell P, Fuwape I, Neiman AB, Shilnikov AL (2009) Variability of bursting patterns in a neuron model in the presence of noise. J Comp Neurosci 27(3):527

Chay TR (1985) Chaos in a three-variable model of an excitable cell. Phys D 16(2):233–242

Cymbalyuk GS, Calabrese RL (2001) A model of slow plateau-like oscillations based upon the fast Na^+ current in a window mode. Neurocomputing 38:159–166

Cymbalyuk G, Shilnikov AL (2005) Co-existent tonic spiking modes in a leech neuron model. J Comp Neurosci 18(3):255–263
Cymbalyuk GS, Nikolaev EV, Borisyuk RM (1994) In-phase and anti-phase self-oscillations in a model of two electrically coupled pacemakers. Biol Cybern 71:153160
Cymbalyuk GS, Gaudry Q, Masino MA, Calabrese RL (2002) Bursting in leech heart interneurons: cell autonomous and network based mechanisms. J Neurosci 22:10580–10592
Deng B (1999) Glucose-induced period-doubling cascade in the electrical activity of pancreatic β-cells. Math Biol 38(1):28
Deng B, Hines G (2002) Food chain chaos due to Shilnikov's orbit. J Chaos 12(3):533–538
DeShazer DJ, Garcia-Ojalv J, Roy R (2003) Bursting dynamics of a fiber laser with an injected signal. Phys Rev E 67(3):036602
Devaney R (1992) A first course in chaotic dynamical systems. Westview Press. https://www.taylorfrancis.com/books/9780429503481
Doiron B, Laing C, Longtin A (2002) Ghostbursting: a novel neuronal burst mechanism. J Comp Neurosci 12:5
Elson RC, Selverston AI, Abarbanel HDI, Rabinovich MI (2002) Dynamic control of irregular bursting in an identified neuron of an oscillatory circuit. J Neurophysiol 88:1166
Ermentrout B (1993) Type I membranes, phase resetting curves, and synchrony, neural computation 8, 979–1001, 1996. Phys D 62(1–4):338–346
Fan YS, Holden AV (1995) Bifurcations bursting, chaos and crises in the Rose-Hindmarsh model for neuronal activity. Chaos Solitons Fractals 3:439–449
Fenichel N (1979) Geometric singular perturbation theory for ordinary differential equations. J Diff Eqns 31:53–98
Feudel U, Neiman A, Pei X, Wojtenek W, Braun H, Huber M, Moss F (2000) Homoclinic bifurcation in a Hodgkin-Huxley model of thermally sensitive neurons. J Chaos 10(1):231–239
Frohlich F, Bazhenov M (2006) Coexistence of tonic firing and bursting in cortical neurons. Phys Rev E 74(3):031922–031929
ftp://ftp.cwi.nl/pub/CONTENT
Gavrilov NK, Shilnikov LP (1972) On three-dimensional dynamical systems close to systems with a structurally unstable homoclinic curve. I Math USSR-Sb 17(4): 467–484
Gavrilov N, Shilnikov A (2000) Example of a blue sky catastrophe, in Methods of qualitative theory of differential equations and related topics. Dedicated to the memory of E.A. Leontovich-Andronova. Am Math Soc Trans II Ser 200:99–105
Getting PA (1989) Emerging principles governing the operation of neural networks. Annu Rev Neurosci 12:185–204
Glass L (2005) Multistable spatiotemporal patterns of cardiac activity. Proc Natl Acad Sci U S A 102:10409
Glendenning P, Hall T (1996) Zeros of the kneading invariant and topological entropy for Lorenz maps. Nonlinearity 9:999–1014
Golomb D, Rinzel J (1993) Clustering in globally coupled inhibitory neurons. Phys Rev E 48:4810
Griffiths RE, Pernarowski MC (1917–1948) Return map characterizations for a model of bursting with two slow variables. SIAM J Appl Math 66(6):2006
Guckenheimer J (1996) Towards a global theory of singularly perturbed systems. Progr Nonlinear Diff Eqns Appl 19:214–225
Hill A, Lu J, Masino M, Olsen O, Calabrese RL (2001) A model of a segmental oscillator in the leech heartbeat neuronal network. J Comput Neurosci 10:281–302
Hodgkin AL, Huxley AF (1952) A quantitative description of membrane current and its application to conduction and excitation in nerve. J Physiol 117(4):500–544
Holden AV, Fan YS (1992) From simple to simple bursting oscillatory behavior via intermittent chaos in the Rose-Hindmarsh model for neuronal activity. Chaos Solutions Fractals 2(3):221–0236
Hounsgaard J, Kiehn O (1989) Serotonin-induced bistability of turtle motoneurones caused by a nifedipine-sensitive calcium plateau potential. J Physiol 414:265
Hudspeth A, Lewis R (1988) Kinetic analysis of voltage- and ion-dependent conductances in saccular hair cells of the bull-frog, *Rana catesbeiana*. J Physiol 400: 237–274
Hutt A, Beim Graben P (2017) Sequences by metastable attractors: interweaving dynamical systems and experimental data. Front Appl Math Stat 3:11
Izhikevich EM (2000) Neural excitability, spiking and bursting. Int J Bifurc Chaos 10(6):1171–1266
Izhikevich EM (2007) Dynamical systems in neuroscience. The geometry of excitability and bursting. MIT Press, Cambridge
Jalil S, Allen D, Youker J, Shilnikov A (2013) Toward robust phase-locking in melibe swim central pattern generator models. J Chaos 23(4):046105
Jones CKRT, Kopell N (1994) Tracking invariant manifolds with differential forms in singularly perturbed systems. J Diff Eqns 108:64–88
Ju H, Neiman A, Shilnikov A (2018) Bottom-up approach to torus bifurcation in neuron models. J Chaos 28: 106317
Katz PS (2008) Tritonia. Scholarpedia 2(6):3504
Kopell N (1988) Toward a theory of modeling central pattern generators. In: Cohen AH, Rossignol S, Grillner S (eds) Neural control of rhythmic movements in vertebrates. Wiley, New York, p 23
Kopell N, Ermentrout GB (2002) Mechanisms of phase-locking and frequency control. In: Fiedler B (ed) Handbook of dynamical systems, vol 2. Elsevier, Amsterdam, pp 3–54
Kopell N, Ermentrout GB (2004) Chemical and electrical synapses perform complementary roles in the synchronization of interneuronal networks. Proc Natl Acad Sci U S A 101:15482
Kramer MA, Traub RD, Kopell NJ (2008) New dynamics in cerebellar Purkinje cells: torus canards. Phys Rev Lett 101(6):068103
Kristan WB, Katz P (2006) Form and function in systems neuroscience. Curr Biol 16:R828–R831

Kristan WB, Calabrese RL, Friesen WO (2005) Neuronal control of leech behavior. Prog Neurobiol 76(5): 279–327
Kuznetsov YA (1998) Elements of applied bifurcation theory. Applied mathematical sciences, vol 112, 2nd edn. New York, Springer
Laing CR, Doiron B, Longtin A, Noonan L, Turner RW, Maler L (2003) Type I burst excitability. J Comput Neurosci 14:329
Lechner H, Baxter D, Clark C, Byrne J (1996) Bistability and its regulation by serotonin in the endogenously bursting neuron R15 in Aplysia. J Neurophysiol 75:957
Lukyanov V, Shilnikov L (1978) On some bifurcations of dynamical systems with homoclinic structures. Soviet Math Dokl 19(6):1314–1318
Marder E, Calabrese RL (1996) Principles of rhythmic motor pattern generation. Physiol Rev 76:687–713
Marder E, Kopell N, Sigvardt K (1998) How compuation aids in understanding biological networks. In: Stein PSG, Selverston A, Grillner S (eds) Neurons, networks, and motor behavior. MIT Press, Cambridge, pp 139–150
Medvedev GM (2005) Reduction of a model of an excitable cell to a one-dimensional map. Phys D 202(1–2): 87–106
Milnor J, Thurston W (1988) On iterated maps of the interval. In: Dynamical systems, Lecture notes in mathematics, vol 1342. Springer, Berlin, p 465563
Mira C (1987) Chaotic dynamics from the one-dimensional endomorphism to the two-dimensional diffeomorphism. World Scientific, Singapore
Mira C, Shilnikov AL (2005) Slow and fast dynamics generated by non-invertible plane maps. J Bifurc Chaos 15(11):3509–3534
Mischenko EF, Rozov NK (1980) Differential equations with small parameters and relaxation oscillations. Plenum Press, New York
Mischenko EF, Kolesov YS, Kolesov AY, Rozov NK (1994) Asymptotic methods in singularly perturbed systems. Monographs in contemporary mathematics. Consultants Bureau, New York
Neiman AB, Dierkes K, Lindner B, Han L, Shilnikov AL (2011) Spontaneous voltage oscillations and response dynamics of a Hodgkin-Huxley type model of sensory hair cells. J Math Neurosci 1(1):11
Pontryagin LS, Rodygin LV (1960) Periodic solution of a system of ordinary differential equations with a small parameter in the terms containing derivatives. Sov Math Dokl 1:611–661
Pusuluri K, Shilnikov A (2018) Homoclinic chaos and its organization in a nonlinear optics model. Phys Rev E 98(4):040202
Pusuluri K, Shilnikov A (2019) Symbolic representation of neuronal dynamics. In: Advances on nonlinear dynamics of electronic systems. World Scientific, Singapore, pp 97–102
Pusuluri K, Pikovsky A, Shilnikov A (2017) Unraveling the chaos-land and its organization in the Rabinovich system. In: Advances in dynamics, patterns, cognition. Springer, pp 41–60. https://doi.org/10.1007/978-3-319-53673-6_4
Rabinovich M, Varona P, Silverston AL, Abarbanel HD (2006) Dynamics principles in neuroscience. Rev Mod Phys 78(4):1213–1265
Rinaldi S, Muratori S (1992) Slow-fast limit cycles in predator-prey models. Ecol Model 61:287
Rinzel J (1985) Bursting oscillations in an excitable membrane model, in ordinary and partial differential equations. Lect Notes Math 1151:304
Rinzel J, Ermentrout B (1989) Analysis of neural excitability and oscillations. In: Koch C, Segev I (eds) Methods of neural modeling: from synapses to networks. MIT Press, Cambridge, pp 135–169
Rowat PF, Elson RC (2004) State-dependent effects of Na-channel noise on neuronal burst generation. J Comp Neurosci 16:87–0112
Rubin J, Terman D (2002a) Synchronized activity and loss of synchrony among heterogeneous conditional oscillators. SIAM J Appl Dyn Sys 1:146
Rubin J, Terman D (2002b) Geometric singular perturbation analysis of neuronal dynamics. In: Fiedler B (ed) Handbook of dynamical systems, vol 2. Elsevier, Amsterdam, pp 93–146
Rubin J, Terman D (2004) High frequency stimulation of the subthalamic nucleus eliminates pathological thalamic rhythmicity in a computational model. J Comput Neurosci 16:211
Rutherford M, Roberts W (2009) Spikes and membrane potential oscillations in hair cells generate periodic afferent activity in the frog sacculus. J Neurosci 29(32):10025–10037
Sharkovsky AN, Kolyada SF, Sivak AG, Fedorenko VV (1997) Dynamics of one dimensional maps. Mathematics and its applications, vol 407. Kluwer, Dordrecht
Sherman A (1994) Anti-phase, asymmetric, and aperiodic oscillations in excitable cells I. Coupled bursters. Bull Math Biol 56:811–835
Shilnikov A (2012) Complete dynamical analysis of a neuron model. J Nonlinear Dyn 68(3):305–328
Shilnikov A, Cymbaluyk G (2004) Homoclinic saddle-node orbit bifurcations en a route between tonic spiking and bursting in neuron models, invited paper. Regul Chaot Dyn 3(9):281–297
Shilnikov A, Cymbalyuk G (2005) Transition between tonic-spiking and bursting in a neuron model via the blue-sky catastrophe. Phys Rev Lett 94:048101
Shilnikov AL, Kolomiets ML (2008) Methods of the qualitative theory for the Hindmarsh-Rose model: a case study – a tutorial. Int J Bifurc Chaos 18(7):1–32
Shilnikov AL, Rulkov NF (2003) Origin of chaos in a two-dimensional map modeling spiking-bursting neural activity. J Bifurc Chaos 13(11):3325–3340
Shilnikov AL, Rulkov NF (2004) Subthreshold oscillations in a map-based neuron model. Phys Lett A 328:177–184
Shilnikov LP, Turaev DV (1997) On simple bifurcations leading to hyperbolic attractors. Comput Math Appl 34:441–457
Shilnikov L, Turaev D (2000) A new simple bifurcation of a periodic orbit of blue sky catastrophe type, in methods

of qualitative theory of differential equations and related topics. AMS Trans Ser II 200:165–188
Shilnikov LP, Shilnikov AL, Turaev DV, Chua L (1998/2001) Methods of qualitative theory in nonlinear dynamics. Volumes I and II. World Scientific, Singapore
Shilnikov AL, Shilnikov LP, Turaev DV (2004) Mathematical aspects of classical synchronization theory: a tutorial. J Bifurc Chaos 14(7):2143–2160
Shilnikov A, Calabrese R, Cymbalyuk G (2005a) Mechanism of bi-stability: tonic spiking and bursting in a neuron model. Phys Rev E 71(1):205
Shilnikov A, Shilnikov L, Turaev D (2005b) Blue sky catastrophe in singularly perturbed systems. Moscow Math J 5(1):205–218
Shilnikov AL, Gordon R, Belykh I (2008) Polyrhythmic synchronization in bursting network motifs. J Chaos 18:037120
Shilnikov LP, Shilnikov AL, Turaev DV (2014) Showcase of blue sky catastrophes. J Bifurc Chaos 24(8):1440003
Shochat E, Rom-Kedar V (2008) Novel strategies for granulocyte colony-stimulating factor treatment of severe prolonged neutropenia suggested by mathematical modeling. Clin Cancer Res 14:6354–6363
Somers D, Kopell N (1993) Rapid synchronization through fast threshold modulation. Biol Cybern 68:393
Steriade M, Jones EG, Llinás RR (1990) Thalamic oscillations and signaling. Wiley, New York
Steriade M, McCormick DA, Sejnowski TJ (1993) Thalamocortical oscillations in the sleeping and aroused brain. Science 262:679–685
Terman D (1991) Chaotic spikes arising from a model of bursting in excitable membranes. SIAM J Appl Math 51(5):1418–1450
Terman D (1992) The transition from bursting to continuous spiking in an excitable membrane model. J Nonlinear Sci 2:133–182
Terman D, Kopell N, Bose A (1998) Dynamics of two mutually coupled slow inhibitory neurons. Phys D 117:241
Tikhonov AN (1948) On the dependence of solutions of differential equations from a small parameter. Mat Sb 22(64):193–204
Timofeev I, Bazhenov M, Sejnowski T, Steriade M (2002) Cortical hyperpolarization-activateddepolarizing current takes part in the generation of focal paroxysmal activities. Proc Natl Acad Sci USA 99(14):9533–9537
Tobin A-E, Calabrese RL (2006) Endogenous and half-center bursting in morphologically-inspired models of leech heart interneurons. J Neurophysiol 96:2089–2109
Turaev DV, Shilnikov LP (1995) Blue sky catastrophes. Dokl Math 51:404–407
Turrigiano G, Marder E, Abbott L (1996) Cellular short-term memory from a slow potassium conductance. J Neurophysiol 75:963–966
Wang XJ (1993) Genesis of bursting oscillations in the Hindmarsh-Rose model and homoclinicity to a chaotic saddle. Phys D 62:263–274
Wang X-J, Rinzel J (1992) Alternating and synchronous rhythms in reciprocally inhibitory model neurons. Neural Comput 4:84
Wang XJ, Rinzel J (1995) Oscillatory and bursting properties of neurons. In: Arbib M (ed) The handbook of brain theory and neural networks. MIT Press, Cambridge, pp 686–691
Wojcik J, Shilnikov A (2011) Voltage interval mappings for activity transitions in neuron models for elliptic bursters. Phys D 240(14–15):1164–1180
Wojcik J, Schwabedal J, Clewley R, Shilnikov AL (2014) Key bifurcations of bursting polyrhythms in 3-cell central pattern generators. PLoS One 9(4):e92918
Yang Z, Qishao L, Li L (2006) The genesis of period-adding bursting without bursting-chaos in the Chay model. Chaos Solitons Fractals 27(3):689–697

Shilnikov Chaos in Epilepsy

Christian Uhl and Bastian Seifert
Center for Signal Analysis of Complex Systems (CCS), Ansbach University of Applied Sciences, Ansbach, Germany

Article Outline

Introduction
Synergetics: Bottom-up Approach of Dimensionality Reduction
DSBM: Data-Driven Method for Dimensionality Reduction
Epileptic Seizures and Shilnikov Chaos
Shilnikov Chaos in Case of Epileptic Seizures?
Summary and Outlook
Bibliography

Introduction

Epilepsy is a widespread neurological disorder. Approximately 5% of the population suffer from at least one epileptic seizure. Recurring epileptic seizures are observed in about 0.5–1% of the population. An important tool to diagnose epilepsy is electroencephalographic recordings (EEG), a technique introduced nearly a century ago (Berger 1929) but still an important tool due to the high temporal resolution of this measurement.

Epileptic seizures can be viewed as emerging patterns of a complex system (the brain) with a huge amount of microscopic elements (the neurons). Since synergetics (Haken 2012; 1983) deals with self-organizing complex systems, first concepts have been developed in the 1980s to link synergetics with brain science (Başar et al. 1983) which has generated a wide range of studies and theories in that context (see, e.g., Kelso 1997; Uhl 1999; Tass 1999; Fuchs and Jirsa 2008; Hutt 2011). An alternative approach to the typical bottom-up approach of synergetics, starting with microscopic interactions leading to macroscopic patterns in the vicinity of instabilities, is in general given by dynamical systems theory. Like Lorenz (1963) introduced a set of differential equations aiming at describing atmospheric convections, brain scientists have tried to model EEG signals by dynamical systems theory (e.g., Da Silva et al., 2003). In this context we will present a method (DSBM – dynamical systems based modeling) to obtain a low-dimensional model of the high-dimensional multielectrode EEG signals. In the case of a special type of epileptic seizures, so-called absence seizures, the dynamics of the signal can be described by a set of differential equations leading to a type of trajectories which resemble Shilnikov attractors. This was first observed in Friedrich and Uhl (1996), underpinned by theoretical work (van Veen and Liley 2006; Sohanian Haghighi and Markazi 2017) and recently investigated with a larger set of EEG data (Seifert et al. 2018a).

We will present the bottom-up approach of synergetics in section "Synergetics: Bottom-up Approach of Dimensionality Reduction" and dynamical systems based modeling (DSBM) in section "DSBM: Data-Driven Method for Dimensionality Reduction." The background of Shilnikov chaos is briefly discussed in section "Epileptic Seizures and Shilnikov Chaos," followed by the results of our investigations (section "Shilnikov Chaos in Case of Epileptic Seizures?") and concluded with summary and outlook in section "Summary and Outlook."

Synergetics: Bottom-up Approach of Dimensionality Reduction

Low-dimensional spatiotemporal patterns can emerge from high-dimensional open systems close to instabilities. This general observation was first rigorously described in the context of laser theory. The underlying concept leads to the

A. Hutt, H. Haken (eds.), *Synergetics*,
https://doi.org/10.1007/978-1-0716-0421-2_728

Originally published in
R. A. Meyers (ed.), *Encyclopedia of Complexity and Systems Science*, © pringer Science+Business Media LLC 2019
https://doi.org/10.1007/978-3-642-27737-5_728-1

interdisciplinary research field of synergetics (Haken 2012, 1983) and could be applied to a wide range of different scientific fields, reflected, e.g., by a whole series of books (Haken 1977).

The typical approach of synergetics is bottom-up, based on a state variable q depending, e.g., on time t and location r, $q = q(r,\ t)$. By introducing a state vector $\boldsymbol{q}(t) \in \mathbb{R}^N$, the spatial dependence can be represented by its vector components:

$$q(r,\ t) \quad \Rightarrow \quad \boldsymbol{q}(t) \in \mathbb{R}^N$$

If the dynamics of the underlying microscopic or mesoscopic level is known,

$$\dot{\boldsymbol{q}}(t) \ = \boldsymbol{f}(\varepsilon,\ \boldsymbol{q}(t)) \tag{1}$$

with ε representing a control parameter of the system, the state vector can be decomposed in the vicinity of an instability $\varepsilon \simeq \varepsilon_c$ in n unstable and $N - n$ stable "modes" (vectors) $\boldsymbol{v}_i^{(u)}$ and $\boldsymbol{v}_i^{(s)}$ and corresponding amplitudes $x_i^{(u)}(t)$ and $x_i^{(s)}(t)$ with $n \ll N$:

$$\boldsymbol{q}(t) = \sum_{i=1}^{n} x_i^{(u)}(t) \cdot \boldsymbol{v}_i^{(u)} + \sum_{i=1}^{N-n} x_i^{(s)}(t) \cdot \boldsymbol{v}_i^{(s)} \tag{2}$$

Since the modes $\boldsymbol{v}_i$ do not need to be orthogonal $\left(\boldsymbol{v}_i^{\top}\boldsymbol{v}_j \neq \delta_{ij}\right)$, a set of biorthogonal modes $\boldsymbol{p}_i$ with $\boldsymbol{p}_i^{\top}\boldsymbol{v}_j = \delta_{ij}$ can be introduced by inverting the matrix $V = (\boldsymbol{v}_1,\ \boldsymbol{v}_2,\ \ldots,\ \boldsymbol{v}_n)$. These biorthogonal modes can be utilized to obtain the amplitudes $x_i(t)$ by projecting $\boldsymbol{q}(t)$ onto these vectors:

$$x_i(t) \ = \boldsymbol{p}_i^{\top}\boldsymbol{q}(t) \tag{3}$$

The so-called slaving principle leads to a relaxation of the stable amplitudes onto the center manifold representing a reduction of dimensionality. The dynamics of the amplitudes is governed by the dynamics of the unstable amplitudes:

$$x_i^{(s)}(t) = x_i^{(s)}\left[x_i^{(u)}(t)\right] \tag{4}$$

The set of differential equations describing the amplitudes of the unstable modes and therefore – due to the slaving principle – describing the dynamics of the whole system are the order parameter equations:

$$\dot{x}_i^{(u)}(t) \ = g_i\left(x_1^{(u)},\ x_2^{(u)}, \ldots,\ x_n^{(u)}\right) \tag{5}$$

It can be shown that the order of magnitude of the contribution of the stable modes to the state vector is significantly smaller than the contribution of the unstable modes. As a first approximation the contribution of the stable modes can be disregarded, and we can summarize the dimension reduction in terms of the bottom-up approach of synergetics (neglecting (u) in the notation):

- Low-dimensional signal representation

$$\boldsymbol{q}(t) \ \simeq \sum_{i=1}^{n} x_i(t) \cdot \boldsymbol{v}_i, \text{ with } \boldsymbol{q}(t) \ \in \mathbb{R}^N \text{ and } n \ \ll N, \tag{6}$$

- With dynamics governed by a set of differential equations

$$\dot{x}_i(t) \ = g_i(x_1,\ x_2, \ldots, x_n) \tag{7}$$

- And the amplitudes obtained by projection

$$x_i(t) \ = \boldsymbol{p}_i^{\top}\boldsymbol{q}(t) \tag{8}$$

In the case of temporal discretization $(t \ = t_1,\ \ t_2,\ \ldots t_T)$, Eqs. (6) and (8) can be written in matrix notation:

$$Q \simeq VX = VP^{\top}Q \tag{9}$$

with

$$Q \in \mathbb{R}^{N\times T},\ \ V \in \mathbb{R}^{N\times n},\ \ X \in \mathbb{R}^{n\times T} \text{ and } P \in \mathbb{R}^{N\times n} \tag{10}$$

In the following section, we will discuss how this description can be modeled by DSBM, and the results of its application will be presented in section "Shilnikov Chaos in Case of Epileptic Seizures?"

DSBM: Data-Driven Method for Dimensionality Reduction

Dynamical systems based modeling (DSBM) is an approach to approximate a multivariate time-dependent signal $\boldsymbol{q}(t) \in \mathbb{R}^N$ by a low-dimensional signal representation (6) with corresponding amplitudes (8) being governed by a set of differential equations (7). First concepts of this approach are presented in Uhl et al. (1993, 1995) and have been applied to epilepsy data (Friedrich and Uhl 1996) and data of event-related potentials (Uhl et al. 1998, 2001; Hutt and Riedel 2003).

The number n of interacting modes is assumed to be known as well as the model of the set of differential equations $g_i(x_1, x_2, \ldots, x_n)$. We represent the functions g_i by parameter vectors $\boldsymbol{a}_i$ and assumed basis functions $\boldsymbol{\xi}_i$ depending on the amplitudes $x_1, x_2, \ldots, x_n$:

$$g_i = \boldsymbol{a_i}^{\top} \boldsymbol{\xi}_i(x_1, \ldots, x_n) \tag{11}$$

To obtain an approximation of Eqs. (6), (7), and (8), we minimize a least-square cost function

$$D(P, a) = \sum_{i=1}^{n} \frac{\left\langle \left(\boldsymbol{p}_i^{\top} \dot{\boldsymbol{q}} - \boldsymbol{a}_i{}^{\top} \boldsymbol{\xi}_i\right)^2 \right\rangle_t}{\left\langle \left(\boldsymbol{p}_i^{\top} \dot{\boldsymbol{q}}\right)^2 \right\rangle_t}, \tag{12}$$

over projections $P = (\boldsymbol{p}_1, \boldsymbol{p}_2, \cdots, \boldsymbol{p}_n) \in \mathbb{R}^{N \times n}$ and parameters $\boldsymbol{a} = (\boldsymbol{a}_1, \boldsymbol{a}_2, \ldots, \boldsymbol{a}_n)$ with $\langle \ldots \rangle_t$ denoting the time average. Introducing the autocorrelation matrix

$$Q_i = \langle \boldsymbol{\xi_i} \otimes \boldsymbol{\xi_i} \rangle_t \tag{13}$$

and the vector of correlation between the projected data and the basis functions

$$\boldsymbol{b_i} = \left\langle \left(\boldsymbol{p}_i^{\top} \dot{\boldsymbol{q}}\right) \boldsymbol{\xi_i} \right\rangle_t, \tag{14}$$

one can show that the coefficients describing the dynamics are given by

$$\boldsymbol{a_i} = Q_i^{-1} \boldsymbol{b_i}. \tag{15}$$

Hence the cost function D depends on the projection P, only.

$$D = D(P) \tag{16}$$

In the case of polynomial functions $\boldsymbol{\xi_i}$, the cost function is invariant with respect to linear transformations of P and therefore only dependent on the subspace spanned by the projection P. Thus one has to consider a global optimization problem on the compact Grassmannian manifold $\mathrm{Gr}(n, N)$. This can be utilized in the search of the global minimum of the cost function D: The calculation of Q_i^{-1} in (15) is numerically critical due to Q_i possibly containing entries outside of machine precision. To diminish this difficulty, the projection matrix P is replaced in each iteration by a different representative of the equivalence class of the Grassmannian manifold.

The matrix $V = (\boldsymbol{v}_1, \ldots, \boldsymbol{v}_n)$ of Eqs. (6) and (10) can be approximated by calculating a pseudo-inverse of the projection P. This pseudoinverse can be obtained by minimizing the quadratic error with respect to the signal representation

$$V = \underset{V \in \mathbb{R}^{N \times n}}{arg\,\min} \left\langle \| \boldsymbol{q} - VP^{\top} \boldsymbol{q} \| \right\rangle_t. \tag{17}$$

Varying this optimization problem with respect to the pseudoinverse V, an analytic description of V is obtained as follows. Denote the autocorrelation matrix of the projected signal by

$$M = \left\langle P^{\top} \boldsymbol{q} \otimes P^{\top} \boldsymbol{q} \right\rangle_t \tag{18}$$

and the correlation of the projected with the original signal by

$$B = \left\langle P^{\top} \boldsymbol{q} \otimes \boldsymbol{q} \right\rangle_t. \tag{19}$$

The pseudoinverse V can then be calculated by

$$V = M^{-1} B. \tag{20}$$

Epileptic Seizures and Shilnikov Chaos

An Ansatz to Model EEG Signals of Absence Seizures

Generalized spike-wave patterns are characteristic for absences, one special kind of epileptic

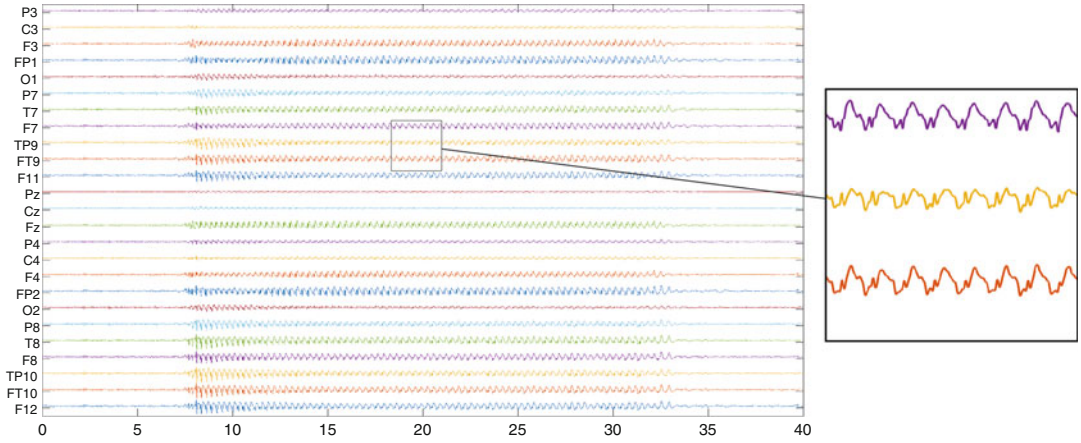

Shilnikov Chaos in Epilepsy, Fig. 1 Typical spike-wave pattern in the EEG signal of an absence seizure. The electrodes are positioned and labeled by the 10–20 system (Jasper 1958)

seizures, as shown in Fig. 1. The ictal signal (signal of the seizure) is between 8 and 33 s showing the spike-wave pattern generalized over all electrodes with a typical frequency of 3Hz.

Former studies of EEG signals of epileptic seizures showed chaotic behavior with a drop of the correlation dimension of the ictal signal (Babloyantz and Destexhe 1986; Lehnertz and Elger 1995). Friedrich and Uhl (1996) suggested that this pattern can be modeled by a dynamical system leading to a linear spiral component (spike behavior) and nonlinear components allowing a recurrence (wave) of the trajectory in phase space. This can be achieved by a set of ordinary differential equation of the form

$$\begin{aligned} \dot{x}_1 &= x_2 \\ \dot{x}_2 &= x_3 \\ \dot{x}_3 &= f(x_1,\ x_2,\ x_3). \end{aligned} \tag{21}$$

with a polynomial function $f(x_1,\ x_2,\ x_3)$. This set of differential equation can yield so-called Shilnikov chaos which will be discussed in the following subsection.

Our top-down approach to model the ictal signal with the ansatz (21) showing Shilnikov type of behavior is underpinned by a mesoscopic (bottom-up) model of the human cortex introduced by Van Veen and Liley (2006). Analyzing the bifurcation diagram, the authors showed that Shilnikov chaos can occur for some parameter combinations.

Shilnikov Chaos

One route to deterministic chaos is given by the Shilnikov bifurcation, where the homoclinic orbit of a saddle-focus breaks leading to a chaotic behavior of the system (Shilnikov 1965). We will briefly discuss the concept of stationary points and its linear stability analysis and thereby illustrate the characteristics of a saddle-focus.

To describe the behavior of a dynamical system

$$\dot{x} = F(x) \tag{22}$$

in the neighborhood of equilibrium points, one uses linear stability analysis. An equilibrium point x^* is called hyperbolic if all eigenvalues of the Jacobi matrix $\jmath(F)(x^*)$ at that point have non-vanishing real part. If an equilibrium point is hyperbolic, one can use the Hartman-Grobman theorem (1960) to investigate the behavior of F in the neighborhood of x^*. The theorem states that for any hyperbolic equilibrium point, there exists a neighborhood $U(x^*)$, in which the solutions of $\dot{x} = F(x)$ can be mapped homeomorphically to solutions of the linear system

$$\dot{y} = \jmath(F)(x^*)y. \tag{23}$$

For three-dimensional systems, the behavior at a hyperbolic equilibrium point depends on the signs of the eigenvalues only. The possible

behaviors are summarized in Table 1. If there exists a saddle-focus with the eigenvalues $\lambda_1 = \gamma$ and $\lambda_{2/3} = \rho \pm i\omega$, both either with a one-dimensional unstable ($\gamma > 0$) or a two-dimensional unstable ($\rho > 0$) eigenmanifold, Shilnikov chaos can occur. In Fig. 2 the two variants of saddle-foci are illustrated: on the left-hand side, the trajectory spirals out of the stationary point, and on the right-hand side, the trajectory spirals in.

The Shilnikov theorem (Shilnikov 1965) states two conditions to be fulfilled leading to a chaotic attractor:

(I) $|\gamma| > |\rho|$
(II) There has to be homoclinic orbit based at the equilibrium point.

Under these conditions the dynamical system can be mapped onto the topological Smale horseshoe (1967), proofing the existence of dynamical chaos.

Shilnikov Chaos in Case of Epileptic Seizures?

In a recent study (Seifert et al. 2018a), we investigated if EEG signals of absence seizures can be modeled by (21) and if Shilnikov chaos can be observed. In this section we largely present results of this investigation.

Data

We investigated ten EEG data sets from two different sources: (A) eight records provided by the Epilepsy Centre at the Department of Neurology Erlangen and (B) two records from the Temple University Hospital EEG Data Corpus (Obeid and Picone 2016). All data were sampled by 25 electrodes using the 10–20 system (Jasper 1958) with sampling rates 256 Hz (A) and 250 Hz (B), respectively. The data sets were filtered by a zero-phase bandpass with cutoff frequencies at 0.5 and 30 Hz. Windowing the ten data sets with windows of 2 seconds length, we ended up with

Shilnikov Chaos in Epilepsy, Table 1 Behavior of 3D systems near hyperbolic equilibrium points with Jacobi matrix having either three real eigenvalues λ_i or two complex eigenvalues $\lambda_{2/3} = \rho \pm i\omega$ and a real eigenvalue $\lambda_1 = \gamma$

λ_1	λ_2	λ_3	Type	γ	ρ	Type
−	−	−	Stable node	−	−	Stable focus node
+	+	+	Unstable node	+	+	Unstable focus node
+	−	±	Saddle	±	±	Saddle-focus

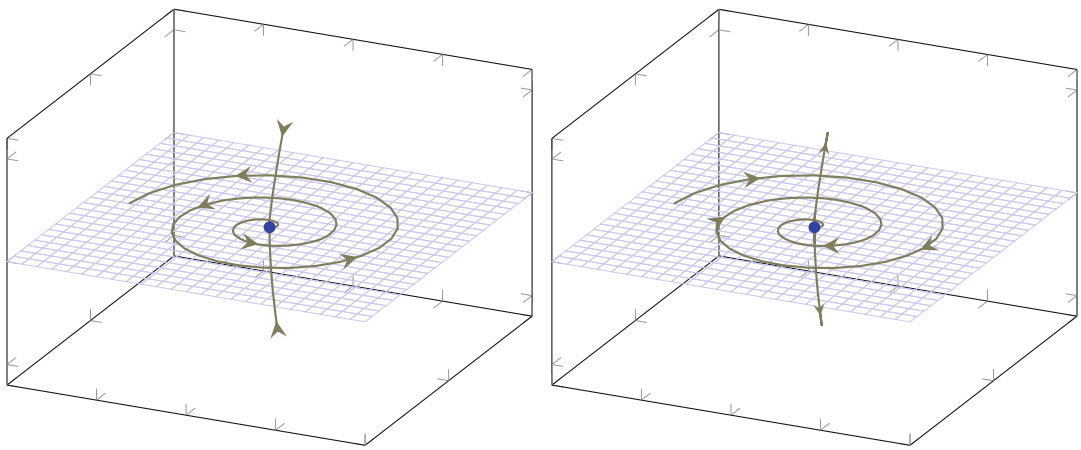

Shilnikov Chaos in Epilepsy, Fig. 2 Two types of saddle-foci: on the left the two-dimensional eigenmanifold is unstable, and the one-dimensional eigenmanifold is stable, while on the right, it is vice versa

139 windowed EEG data sets (epochs) with 65 ictal and 74 pre- and postictal signals.

Dynamics Representation

The application of DSBM on the windowed signals leads to a minimal value of the cost function (16) and an optimal projection for each window. The value of the cost function is plotted in Fig. 3 for the epochs of one data set to illustrate the results. In the background of the figure, the recording of one electrode (F4) is shown to allow a comparison of the values of the cost function with the original signal: A distinct drop of the value is observed during the ictal phases of the signal. The low value of the cost function (the least-square error) indicates that the ansatz (21) works well to describe the dynamics of the signal of absence seizures.

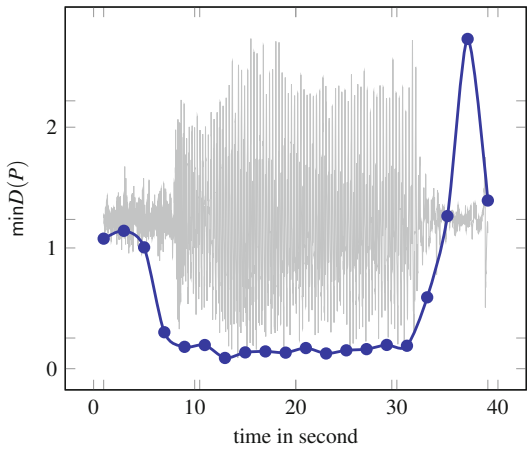

Shilnikov Chaos in Epilepsy, Fig. 3 Drop of cost function in ictal signal, background: signal of F4 electrode. (Reproduced by permission from Seifert et al. 2018a)

By defining a threshold, ictal phases can be separated from non-ictal phases. We calculated an optimal threshold on a training set and calculated the detection rate on the remaining evaluation set. The procedure is reiterated for all combinations of changing training set and evaluation set. This so-called leave-one-out cross-validation leads to following characteristic values with respect to seizure detection.

1. Specificity (true negative rate): 84%
2. Sensitivity (true positive rate): 75%

That is, 84% of all non-ictal phases and 75% of all ictal phases were correctly detected.

The optimal projection $P = (\boldsymbol{p}_1, \boldsymbol{p}_2, \boldsymbol{p}_3)$ representing the global minimum of the cost function (12) leads by (8) to amplitudes $(x_1(t), x_2(t), x_3(t))$. Figure 4 shows on the right-hand side the trajectory of these amplitudes in phase space. A quite stationary signal is observed with a distinct geometry. This becomes even more evident if we compare the DSBM results with conventional techniques of dimensionality reduction like principal component analysis (PCA) (Pearson 1901) and independent component analysis (ICA) (Hyvaerinen et al. 2001). Figure 4 shows on the left-hand side the amplitudes of the first three principal components as a trajectory in phase space. The central phase portrait shows the trajectory of the three "best" (in terms of the obtained geometry) independent components. The benefit of using DSBM instead of PCA and ICA is

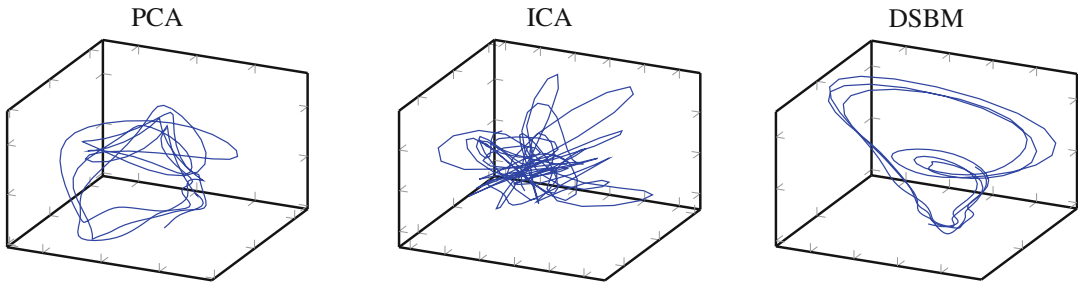

Shilnikov Chaos in Epilepsy, Fig. 4 Trajectories of projected signals in three-dimensional phase space. Projections obtained by (**a**) PCA, (**b**) ICA, (**c**) DSBM. (Reproduced by permission from Seifert et al. 2018a)

obvious, and the obtained structure of DSBM shows a spiral behavior in connection with a recurrence of the trajectory. Since this resembles a Shilnikov type of behavior, we investigate in the following if the dynamics obtained by DSBM fulfill Shilnikov theorem.

Shilnikov Condition

We consider only the epochs where the ansatz (21) well fitted the data. This is achieved by taking only EEG epochs into account with dynamics representation of above 90%, i.e., $D(P) < 0.3$ since $D(P = 0) = 3$ is the maximal value of the cost function. The dynamics of the windowed signals is estimated by (15). Stationary points and the eigenvalues of the Jacobi matrix can be calculated characterizing the linear behavior in the vicinity of the fixed point. 69% of all investigated epochs fulfill the first Shilnikov condition ($|\gamma| > |\rho|$ (compare section "An Ansatz to Model EEG Signals of Absence Seizures").

The second condition (II) is harder to investigate since a homoclinic trajectory is difficult to verify. Therefore we visually investigated the phase portraits of the projected signals. Figure 5 exemplarily shows obtained trajectories. The phase portrait of the epoch shown on the left-hand side is considered to be connected with an homoclinic orbits, whereas the example on the right-hand side does not show the expected homoclinic behavior and is therefore considered not to fulfill Shilnikov condition (II). In 79% of all investigated epochs, a homoclinic was visually detected. The fourfold cases fulfilling condition (I) and (II) are presented in Table 2.

Summary and Outlook

We showed that the ansatz (21) is a good choice to model – in accordance with the concept of synergetics – the low-dimensional behavior of

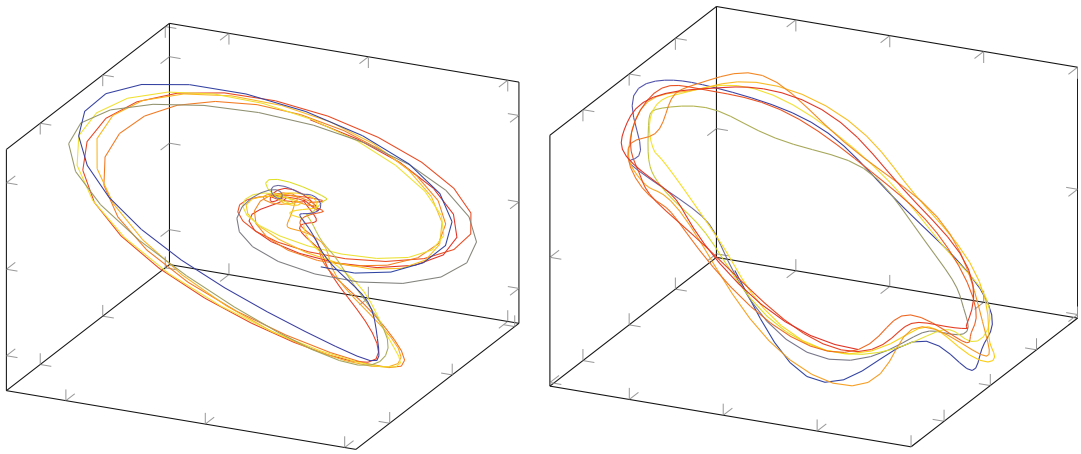

Shilnikov Chaos in Epilepsy, Fig. 5 Trajectories (**a**) confirming by visual inspection the second Shilnikov condition (homoclinic orbit), (**b**) not confirming the condition. (Reproduced by permission from Seifert et al. 2018a)

Shilnikov Chaos in Epilepsy, Table 2 Fourfold table evaluating Shilnikov conditions (I) and (II) in investigated data epochs

		Shilnikov condition (I)		
		Fulfilled	Not fulfilled	Sum
Shilnikov condition (II)	Observed	53%	26%	79%
Homoclinic orbit	Not observed	16%	5%	21%
Sum		69%	31%	100%

the high-dimensional EEG signal of absence seizures. Based on this ansatz, the DSBM method leads to stationary trajectories with distinct geometries. The theoretical concept of Shilnikov chaos was fulfilled in 53% of the investigated epochs. This number of 53% sounds weak for physicists and mathematicians but is impressive in the context of such complex biological systems like the brain.

We do not want to conceal that the global search of the optimum of the cost function, the central part of DSBM, is numerically challenging. The obtained parameters describing the dynamics might be unsecure in some cases especially combined with a linear stability analysis of calculated stationary points.

To circumvent the numerical challenges of DSBM, we developed a new algorithm called dynamical component analysis (DyCA) (Seifert et al. 2018b). Thereby projections are calculated solving a generalized eigenvalue problem of correlation matrices of the signal and its derivative based on certain constraints to the underlying dynamics. First results are promising, and we hope that this approach might also yield deeper insights in the future analyses of EEG signals of the human brain and on the long run might help to treat patients with brain diseases such as epilepsy.

Acknowledgments This work is dedicated to the memory of Rudolf Friedrich, scientific mentor of one of the authors (CU), the original initiator of this research, and with whom we would have loved to discuss the presented results. We acknowledge funding by the European Regional Development Fund (ERDF) and the support by the Bayerische Forschungsstiftung within the project Nilpherd. We thank the Epilepsy Centre at the Department of Neurology, Universitätsklinikum Erlangen for provided data, and BESA GmbH and Epilepsy Centre for helpful and interesting discussions.

Bibliography

Babloyantz A, Destexhe A (1986) Low-dimensional chaos in an instance of epilepsy. Proc Natl Acad Sci 83(10):3513–3517

Başar E, Flohr H, Haken H, Mandell AJ (eds) (1983) Synergetics of the brain. Springer, Berlin

Berger H (1929) Uber das Elektrenkephalogramm des Menschen. Archiv f Psychiatrie 4(9):973–977

Da Silva FL, Blanes W, Kalitzin SN, Parra J, Suffczynski P, Velis DN (2003) Epilepsies as dynamical diseases of brain systems: basic models of the transition between normal and epileptic activity. Epilepsia 44(s12):72–83

Friedrich R, Uhl C (1996) Spatio-temporal analysis of human electroencephalograms: petit mal epilepsy. Phys D 98:171–182

Fuchs A, Jirsa V (eds) (2008) Coordination: neural, behavioral and social dynamics. Springer, Berlin

Haken H (ed) (1977) Springer series in synergetics. Springer, Berlin

Haken H (1983) Advanced synergetics. Springer, Berlin

Haken H (2012) Synergetics: an introduction, 3rd edn. Springer, Berlin

Hartman P (1960) A lemma in the theory of structural stability of differential equations. Proc Am Math Soc 11:610–620

Hutt A (ed) (2011) Sleep and anesthesia. Springer, Dordrecht

Hutt A, Riedel H (2003) Analysis and modeling of quasi-stationary multivariate time series and their application to middle latency auditory evoked potentials. Phys D 177:203–232

Hyvaerinen A, Karhunen J, Oja E (2001) Independent component analysis. Wiley, Hoboken

Jasper H (1958) Report of the committee on methods of clinical examination in electroencephalography: 1957. Electroencephalogr Clin Neurophysiol 10(2):370–375

Kelso S (1997) Dynamic patterns: the self-organization of brain and behavior. MIT Press Ltd, Cambridge

Lehnertz K, Elger CE (1995) Spatio-temporal dynamics of the primary epileptogenic area in temporal lobe epilepsy characterized by neuronal complexity loss. Electroencephalogr Clin Neurophysiol 95(2):108–117

Lorenz EN (1963) Deterministic nonperiodic flow. J Atmos Sci 20(2):130–141

Obeid I, Picone J (2016) The temple university hospital EEG data corpus. Front Neurosci 10:196

Pearson K (1901) On lines and planes of closest fit to a system of points in space. Lond Edinb Dublin Philos Mag J Sci 6(2):559–572

Seifert B, Adamski D, Uhl C (2018a) Analytic quantification of Shilnikov chaos in epileptic EEG data. Front Appl Math Stat 4:57

Seifert B, Korn K, Hartmann S, Uhl C (2018b) Dynamical component analysis (DyCA): dimensionality reduction for high-dimensional deterministic time-series. In: 2018 IEEE 28th international workshop on machine learning for signal processing (MLSP)

Shilnikov LP (1965) A case of the existence of a denumerable set of periodic motions. Sov Math Dokl 6(2):163–166

Smale S (1967) Differentiable dynamical systems. Bull Am Math Soc 73:747–817

Sohanian Haghighi H, Markazi AHD (2017) A new description of epileptic seizures based on dynamic analysis of a thalamocortical model. Sci Rep 7:13615

Tass P (1999) Phase resetting in medicine and biology. Springer, Berlin

Uhl C (ed) (1999) Analysis of neurophysiological brain functioning. Springer, Berlin

Uhl C, Friedrich R, Haken H (1993) Reconstruction of spatio-temporal signals of complex systems. Z Phy B 92:211

Uhl C, Friedrich R, Haken H (1995) Analysis of spatio-temporal signals of complex systems. Phy Rev E 51:3890

Uhl C, Kruggel F, Opitz B, von Cramon DY (1998) A new concept for EEG/MEG signal analysis: detection of interacting spatial modes. Hum Brain Mapp 6:137–149

Uhl C, Hutt A, Kruggel F (2001) Improvement of source localization by dynamical systems based modeling (DSBM). Brain Topogr 13:219–225

van Veen L, Liley DTJ (2006) Chaos via Shilnikov's saddle-node bifurcation in a theory of the electroencephalogram. Phys Rev Lett 97:208101

Phase Synchronization in Neural Systems

Andreas Daffertshofer[1] and Bastian Pietras[2]
[1]Faculty of Behavioural and Movement Sciences, Amsterdam Movement Sciences and Institute for Brain and Behaviour Amsterdam, Vrije Universiteit Amsterdam, Amsterdam, The Netherlands
[2]Institute of Mathematics, Technische Universität Berlin and Bernstein Center for Computational Neuroscience Berlin, Berlin, Germany

Article Outline

Glossary
Definition of the Subject
Introduction
Micro- and Macroscopic Views
Correlated Behavior and Phase Synchronization
From Single Cell Dynamics to Neural Masses: Synchronization in a Neural Population
Synchronization Between Neural Populations: Coupled Neural Masses
Predicting Effects of Phase Synchronization
Final Notes
Summary
Bibliography

Glossary

Neural spikes Discrete events as proxy for action potentials in single neurons.

Firing rate Population activity measured at each instant in time as the fraction of neurons that fire a spike within a certain time window.

Membrane potential Common state variable of a single neuron that induces a spike/an action potential once it has crossed a certain threshold.

Stable limit cycle A periodic orbit along which rhythmic activity emerges and that attracts all neighboring trajectories in its vicinity.

Neural oscillator A single neuron, a population of similar neurons, or a pair of excitatory and inhibitory neural populations that exhibit rhythmic activity.

Phase oscillator Reduced description of an oscillator with sole focus on the evolution of its phase.

Phase reduction Technique to identify the state of a (high-dimensional) oscillator through its phase on or in the immediate vicinity of the stable limit cycle.

Order parameters Common variables describing the (dis)order of a large system of many components.

Neural mass model Description of a neural population by means of its density, often parametrized by the mean and/or variance.

Definition of the Subject

Oscillatory neural activity is abound on all temporal and spatial scales. One can observe this on the microscopic level of neuronal circuits as well as on mesoscopic and macroscopic levels of neural populations. The latter give rise to brain rhythms that, dependent on their spectral properties, adhere to different function. A disruption of the interplay of this oscillatory activity is often deemed a signature of pathology (Schnitzler and Gross 2005; Uhlhaas and Singer 2006; Hutt and Buhry 2014). All the more it is important to understand the underlying mechanisms how these neural oscillations emerge and evolve and how oscillations of different populations interact and influence each other. Synchronous firing of individual neurons can give rise to large-scale oscillatory activity of a population, and the phase synchronization between populations is key for communication between them.

Introduction

The functioning of the brain dwells on coordinated and coherent coactivity of a multitude of

A. Hutt, H. Haken (eds.), *Synergetics*,
https://doi.org/10.1007/978-1-0716-0421-2_693

Originally published in
R. A. Meyers (ed.), *Encyclopedia of Complexity and Systems Science*, © Springer Science+Business Media LLC 2020
https://doi.org/10.1007/978-3-642-27737-5_693-1

neurons. Perceptual, cognitive, and motor functions are believed to require an orchestration of distributed neuronal processes. If spike discharges of a large number of neurons exhibit correlated behavior in different areas of the brain, their (large-scale) integration allows for sensory integration, the generation of motor commands, and cognitive processing. Unraveling these integration processes poses a challenge in itself and is often referred to as the *binding problem* (Singer 2007). Binding by convergence results in the grouping of specialized neurons that encode a particular fixed constellation of contextual features. Dynamic binding, by contrast, assembles individual neurons dynamically to generate and represent particular patterns at particular points in time (Nunez 2000). A neuron can participate in the representation of one pattern in one moment, but an instant later, it is involved in encoding another one. Synchronization of neuronal discharges at millisecond scale can yield sequences of subsequently active assemblies, which can effectively encode complex information to be exchanged among neuronal networks. And, this temporal organization of neuronal activity capitalizes on self-organized information retention and local-global integration. The ability to preserve and store information is equally important as integrating distributed local processes into globally ordered states and controlling local computations through global brain activity. Both are likely maintained by a hierarchy of brain rhythms (Buzsaki 2006). The temporal coordination of distributed brain activity, hence, strongly – if not solely – relies on the synchronization of neural oscillations (Gray 1994; MacKay 1997).

On macroscopic scales, brain rhythms and oscillatory population activity are the dominant observables. There are numerous approaches to unravel the orchestration of intertwined neural processes, both experimental and theoretical. Bridging the gap between experiments and theory, however, has only been achieved in very restrictive cases and mainly on very small spatial and temporal scales. An overall and generic picture linking these two sides of the same coin is still being sought for. Neuroimaging techniques such as magneto- and electroencephalography (M/EEG) reflect voltage fluctuations resulting from ionic currents in the neurons. Given the noninvasive nature of these techniques, the recorded data display synchronous activity of several thousands of interacting neurons rather than the dynamics of a single neuron. The population dynamics, or mean field behavior, has often very little in common with what happens on the microscopic scale.

An urgent challenge in theoretical neuroscience is to deduce macroscopic dynamics from activity on these much smaller scales (Haken 2006; Deco et al. 2008; Coombes 2010; Siettos and Starke 2016; Breakspear 2017). Yet, the plenitude of findings provide valuable guidelines for our understanding of neural synchronization processes on both micro- and macroscopic scales; see Fig. 1 for an example.

Micro- and Macroscopic Views

When characterized as rhythmic changes in, e.g., local field potentials, neural oscillations set a recurrent temporal reference frame. The ups and downs in fluctuating local field potentials reflect high and low degrees of synchronization of neuronal currents within a certain brain area. That is why synchronization and neural oscillations are often used interchangeably to express coherent activity of a population of neurons. However, there is a subtle difference between the two phenomena (Singer 1993). Oscillatory activity can be induced on a population level through single oscillatory neurons, so-called pacemaker cells. It may also manifest as an emergent property of the underlying network architecture when a particular dynamic circuit motif is activated. Such a motif comprises the physical circuit structure, its electrophysiological signature, and the corresponding computational function (Womelsdorf et al. 2014). Synchronization, on the other hand, can also occur in the absence of oscillations. Two cells may always discharge simultaneously but at irregular intervals when driven by common noise. Or, a presented stimulus induces simultaneous bursting of neural populations. This is a typical signature of response synchronization. Synchronization

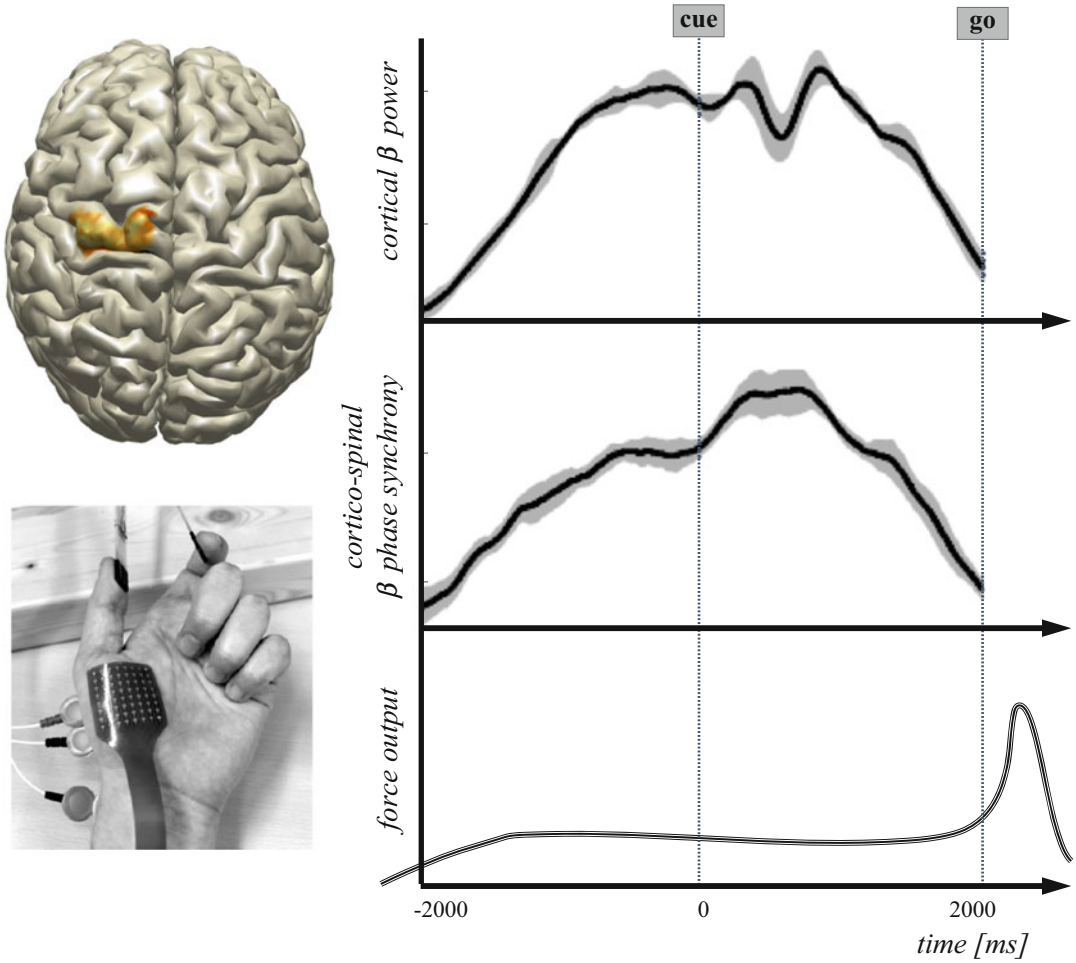

Phase Synchronization in Neural Systems, Fig. 1 Beta-range oscillatory activity measured via EEG over (here left) motor cortex and beta synchrony between cortex and spinal cord are up- or downregulated in anticipation of movement initiation. The temporal changes in local synchronization in motor cortex (top right panel: spectral power around 15–30 Hz) reflect a precision grip being produced with the right hand that ought to be changed after receiving a go-signal (lower right panel: force level). The corticospinal synchronization (middle right panel: phase synchronization between EEG-electromyographic signals of finger and thumb flexors) also follows that pattern although pre-cueing (cue-signal) 2 s ahead of movement initiation is seemingly not propagated along the corticospinal tract; see Van Wijk et al. (2008) for more details.

may lead to oscillations, and oscillations may facilitate synchronization, but, in general, they are "just" indicative for synchrony.

While oscillatory population activity can be related to synchronous interactions of individual cells – we provide an example below – one must be careful when relating single cell responses to synchronous network activity. There is a micro-macro dichotomy with respect to the transition from individual neuronal dynamics to the collective behavior of a neural population. It may happen that individual discharges of a neuron are perfectly time-locked with the oscillating field potential while, e.g., the lagged autocorrelation of the discharges does not show any sign of oscillatory activity. The seminal work by Brunel and Hakim offered a theoretical account of a collection of experimental studies hinting at sparse synchronization of neuronal networks (Brunel and Hakim 1999). By contrast, regular spiking activity

of single neurons does not necessarily result in (regular) oscillations on the population level but may yield collective chaos (Pazó and Montbrió 2016). Likewise, asynchronous network states may emerge despite a considerable amount of shared input (Renart et al. 2010).

Correlated Behavior and Phase Synchronization

Discernible neural population activity depends on correlated activity of a large number of neurons (Wang 2010). When considering time series of experimental or synthetic data, synchronization can be identified through a variety of measures. They range from correlation coefficients to coherence, from phase coherence to Granger causality, from phase locking values to Kullback-Leibler information divergence, and from state space-based measures to stochastic event synchrony (Dauwels et al. 2010). Some of these measures show a strong correlation among one another, whereas others do not, but all of them have in common that they seek to quantify the degree to which firing rates of neurons are related (Golomb 2007).

When it comes to neural oscillations, focus is on the oscillations' amplitudes and frequencies. For a given frequency, one can define the period as the duration of time of one cycle of oscillation. In between a cycle, one can further define the *phase* of oscillation, which continuously increases between 0 and 2π. Phase and amplitude thus become the main (time-resolved) determinants of the state of oscillation. Phase synchronization measures aim at quantifying the closeness of the phases when mapped on the unit circle (Jean-Philippe et al. 1999). Phase synchronization measures are particularly suited for cases in which oscillatory units are weakly coupled because in that case dynamically changing amplitudes can be largely ignored. In the following, we concentrate on such cases. As we will show, phase synchronization is paramount for functional connectivity of the brain and communication between neural populations in general (Varela et al. 2001; Sauseng and Klimesch 2008; Thut et al. 2012).

From Single Cell Dynamics to Neural Masses: Synchronization in a Neural Population

A plethora of modeling approaches exists to link single cell dynamics to the dynamics of neural populations. Modeling boomed in the 1970s. It was Walter Freeman who introduced the notion of neural mass models, which are in essence descriptions of the dynamics of neural population densities (Deco et al. 2008; Freeman 1975). Many of these models are arguably heuristic in nature (Lopes da Silva et al. 1974; Amari 1977; Jansen and Rit 1995) and/or involve debatable approximations. Here we illustrate a proper deduction of population or neural mass dynamics starting at a well-defined single cell level.

We follow a recent study by Montbrió et al. (2015) and consider a large population of identical quadratic integrate-and-fire (QIF) neurons with the ultimate goal to derive the dynamics of the population's mean membrane potential V. The neurons are coupled with each other electrically via gap junctions of strength G and/or through chemical synapses of strength J with activation function S, as detailed below. We denote the individual membrane potentials by v_j with $j = 1,\ldots, N \gg 1$ and assume that they follow the dynamics

$$\tau \dot{v}_j = v_j^2 + n_j + G\big(V - v_j\big) + J\tau S, \qquad (1a)$$

where τ represents the membranes' time constant and η_j is an external input current flowing into neuron j. To model action potentials, or spikes, as sketched in Fig. 2 (upper panel), the continuous dynamics (1a) is accompanied by the following discrete fire and reset rule:

$$\begin{aligned} &\text{if } v_j \text{ reaches } +\infty \text{ then neuron } j \text{ emits a spike} \\ &\quad \text{and its membrane potential } v_j \text{ resets to } -\infty. \end{aligned} \qquad (1b)$$

In the absence of any coupling between neurons, i.e., if $J = G = 0$ holds, the neurons are either quiescent or oscillate dependent on their individual, external input $\eta_j < 0$ or $\eta_j > 0$, respectively. More realistic, however, is the case in which the

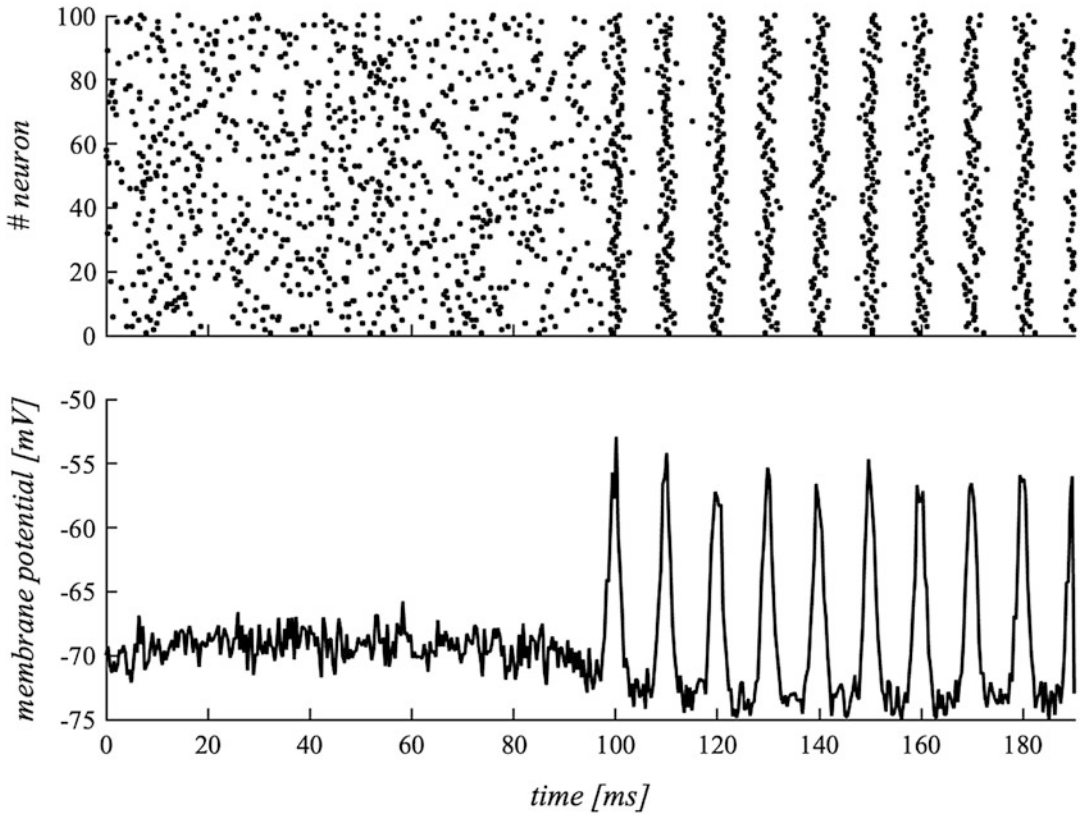

Phase Synchronization in Neural Systems, Fig. 2 Simulated spike trains of a population of 100 neurons (upper panel). At the beginning, spikes are emitted randomly causing the resulting mean-field potential (~local field potential) to weakly fluctuate around the resting potential of about −70 mV (lower panel). At around 100 ms, the neurons spontaneously synchronize their phases yielding a mean membrane potential that oscillates at about 100 Hz. The frequencies in local field potentials are usually higher than those observed in encephalographic recordings – cf. Fig. 1. To generate the figure, we used a stochastic extension of the Kuramoto model (7) and defined spike events via Poincaré sections of the phase oscillators' trajectories (Deschle et al. 2019). At around $t \approx 90$ ms, the coupling strengths κ was increased beyond the critical value κ_c, and, after a brief transient period, the population fires in synchrony at a rate given by the mean of the oscillators natural frequencies. Note that the mean membrane potential simply resembles the population density of spikes as a function of time, here adjusted to mimic standard values of action and reversal potentials (Kandel et al. 2013). The figure was inspired by Masquelier et al. (2009).

neurons are coupled to one another (Pietras et al. 2019). For coupling through chemical synapses, we adopt an obvious synaptic activation function

$$S(t) = \frac{1}{N}\sum_{j=1}^{N}\frac{1}{\tau_S}\int_{t-\tau_s}^{t}\sum_{k}\delta\left(t' - t_j^k\right)dt' \qquad (1c)$$

i.e., a summation of incoming spikes; t_j^k denotes the time of the k-th Dirac delta-spike of the j-th neuron and τ_S is a synaptic time constant. The synaptic strength J can be positive or negative implying the chemical synapses are excitatory or inhibitory, respectively. For electric coupling, we assume that it is diffusively modulated by the population's mean membrane voltage

$$V = \frac{1}{N}\sum_{j=1}^{N} v_j. \qquad (1d)$$

As it will turn out, electrical coupling tends to balance the membrane potentials v_j and may,

hence, facilitate synchronization between neurons. Yet, if a sufficiently large portion of neurons in the population is inactive, gap junctions can suppress oscillations and desynchronize neuronal activities (Connors 2017; Alcamí and Pereda 2019).

Following Montbrió et al. (2015) and Luke et al. (2013), we consider the thermodynamic limit $N \to \infty$ and define a density function ρ such that $\rho(v|\eta,\, t)\, dv$ denotes the fraction of neurons with membrane potentials between v and $v + dv$ at time t and external current η. For the sake of simplicity, we consider the external currents to be distributed according to a Lorentzian $\frac{\Delta}{\pi} / \left[(\eta - \overline{\eta})^2 + \Delta^2\right]$ centered around $\overline{\eta}$ with half-width Δ.

We further assume a clear separation of time scales in that the time scale of synaptic processing is much smaller than that of the membrane potentials. In fact, in the limit $\tau_S \to 0$, the synaptic interaction (1c) reduces to $S(t) = R(t)$ with $R(t)$ being the population's mean firing rate. At first glance, assuming instantaneous synaptic responses appears a limitation to our model since synaptic time scales are often considered to be longer than those of the cell membrane. However, synaptic time constants can be as small as 1.7 ms (Häusser and Roth 1997), much in the range of typical time scales of the membrane dynamics, which renders our approximation acceptable. Introducing finite time scales, e.g., via exponential or a synapse, can be realized by using the corresponding Green's functions (Haken 2006; Byrne et al. 2017). Effectively, this will cause a synaptic delay enriching the dynamical spectrum by far; see Devalle et al. (2018) for details. Here, however, we seek to highlight the effects of electric couplings as in our model they turn out to be the major ingredient for the emergence of neural oscillations.

All things considered, we find that the mean-field dynamics of the population of electrically and chemically coupled QIF neurons evolves according to

$$\begin{aligned} \tau \dot{R} &= \frac{\Delta}{\tau\pi} + 2RV - GR, \\ \tau \dot{V} &= V^2 + \overline{\eta} - (\pi\tau R)^2 + J\tau R. \end{aligned} \tag{2}$$

The common variables R and V are the already introduced mean firing rate and mean membrane potential of the population, respectively. Together they determine the total time-dependent voltage density of the population Eq. (1), which turns out to be a Lorentzian $\tau r(t)/\{[v - V(t)]^2 + [\pi\tau R(t)]^2\}$ centered at $V(t)$ with half-width $\pi\tau R(t)$. Electrical coupling leads to a narrowing of the voltage distribution ρ by decreasing the firing rate R as in (2). That is, it balances the neurons' membrane potentials and may promote synchrony, leading to their synchronized firing activity as anticipated before, and oscillations of the population firing rate can emerge. By contrast, chemical coupling merely shifts ρ through the voltage dynamics in (2). Figure 3 briefly summarizes the corresponding bifurcation scheme, but we refer to Montbrió et al. (2015) and Pietras et al. (2019) for the in-depth analysis.

Writing about neural mass modeling must not let the neural mass model by Wilson and Cowan (1972, 1973) be unnoticed. Like the neural mass model (2), it provides a comprehensive link toward a macroscopic description of the aforementioned cell assemblies (Kilpatrick 2015). The Wilson-Cowan neural mass model represents the interdependent collective neuronal dynamics in terms of the mean firing rates of the excitatory and inhibitory parts of the population, i.e., $R \to (E,\, I)$. It exhibits rich dynamic behavior as

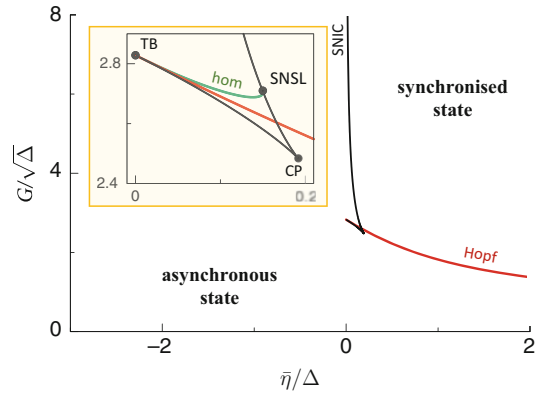

Phase Synchronization in Neural Systems, Fig. 3 Bifurcation diagram of the dynamics (2) for electrical coupling only ($J = 0$) is characterized by the presence of codimension-2 points (*TB* Takens-Bogdanov; *SNSL* saddle-node separatrix loop, Cusp) at $\overline{\eta} \geq 0$. The region of synchronization, i.e., oscillatory population activity, is limited by supercritical Hopf (red), SNIC (black), and homoclinic (green) bifurcations. Inset: Enlargement of the region near the three codimension-2 points. SN – saddle-node bifurcation; see Pietras et al. (2019) for details

well as different transitions to oscillatory dynamics (Hoppensteadt and Izhikevich 1997; Borisyuk and Kirillov 1992). This makes it also exemplary for a neural oscillator model. We will exploit some of these features when addressing coupled neural masses in the parts to come.

We consider N_e excitatory and N_i inhibitory neurons and denote by e_n and i_n the firing rate of a single excitatory and inhibitory neuron, respectively. The respective mean firing rates can be given by the averages $E = \frac{1}{N_e}\sum_{n=1}^{N_e} e_n$ and $I = \frac{1}{N_i}\sum_{n=1}^{N_i} i_n$. Every neuron receives inputs from all other neurons within the population and every excitatory neuron receives an external input η_j, whose average is given by $\overline{\eta} = \frac{1}{N_e}\sum_{n=1}^{N_e}\eta_n$. Once the sum of all inputs exceeds a certain threshold θ_n, a neuron elicits a spike. For a particular distribution of threshold values across the population, one can assign a sigmoidal activation function $\mathcal{S}[x] = 1/(1+e^{-x})$ with population-specific threshold values by Θ_E and Θ_I for the excitatory and inhibitory part, respectively. Then, the population dynamics follows

$$\begin{aligned}\tau_E\dot{E} &= -E(t) + [1 - r_E E]\times \\ &\quad \times\mathcal{S}[a_E(c_{EE}E - c_{IE}I - \Theta_E + \overline{\eta})] \\ \tau_I\dot{I} &= -I(t) + [1 - r_I I]\times \\ &\quad \times\mathcal{S}[a_I(c_{EI}E(t) - c_{II}I - \Theta_I)],\end{aligned} \tag{3}$$

with c_{kj} with $k, j \in \{E, I\}$ indicating the strength of interaction between the different parts within the population, and a_E, a_I define the slopes of the transfer function. The expressions $[1 - r_E E]$ and $[1 - r_I I]$ represent the refractory dynamics of the excitatory and inhibitory subpopulations, respectively, that we here ignore by setting $r_E = r_I = 0$ (Pinto et al. 1996). Like model (2) also the dynamics (3) can exhibit self-sustained oscillations and multi-stability (Wilson and Cowan 1972; Hoppensteadt and Izhikevich 1997; Borisyuk and Kirillov 1992); the bifurcation diagram is depicted in Fig. 4.

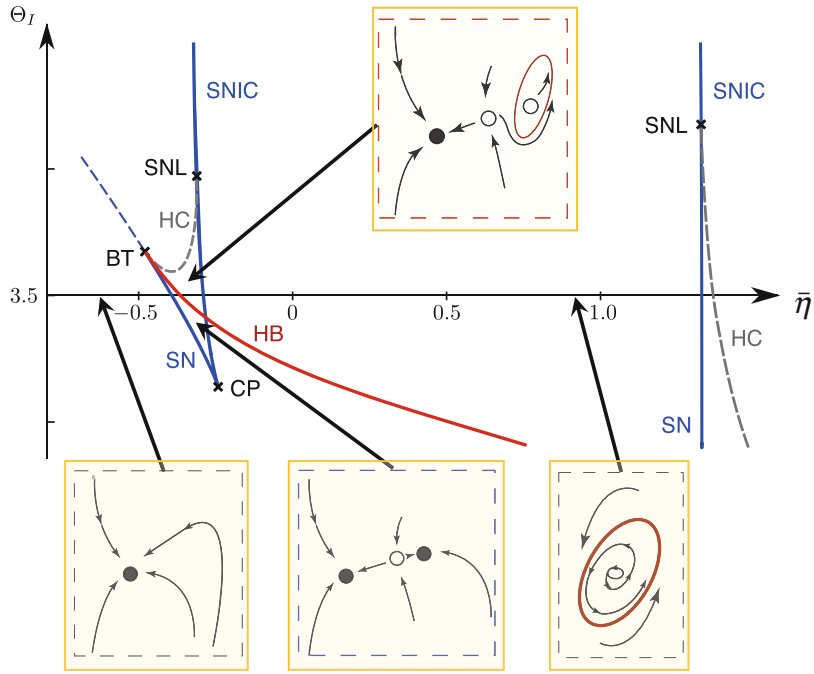

Phase Synchronization in Neural Systems, Fig. 4 Bifurcation diagram of the uncoupled Wilson-Cowan model (4). By increasing $\overline{\eta}$, one can identify four different dynamical regimes (see insets) that are separated by bifurcation boundaries; filled/empty dots, stable/unstable fixed points; red, stable limit cycle. In the lower right inset, the limit cycle is the unique attractor of the dynamics. *SN* saddle-node bifurcation, *HB* Hopf bifurcation, *HC* homoclinic bifurcation, *BT* Bogdanov-Takens point, *CP* cusp point, *SNL* saddle-node loop bifurcation, *SNIC* saddle node on invariant cycle bifurcation; see Pietras and Daffertshofer (2019) for more details

Synchronization Between Neural Populations: Coupled Neural Masses

The Wilson-Cowan model may be considered a generic description of a densely connected neural population as in a particular cortical region (Breakspear 2017; Daffertshofer and van Wijk 2011). Hence we use it to build a cortical network model. For this, we connect N different populations of excitatory and inhibitory neurons in a region (E_j, I_j) via their excitatory parts (Daffertshofer and van Wijk 2011; Schuster and Wagner 1990; Daffertshofer et al. 2018) – this creates a network of $j = 1,\ldots, N$ nodes; see Fig. 5 for illustration.

In line with (3), we assume the locally averaged fire rates at every node to obey the dynamics

$$\begin{aligned}\tau_E \dot{E}_j &= E_j + \mathcal{S}\Big[a_E\big(c_{EE}E_j - c_{IE}I_j - \Theta_E + \overline{\eta}_j + \\ &\quad + \frac{\kappa}{N}\sum_{k=1}^{N} C_{jk}\big(E_k - E_k^0\big)\Big)\Big] \\ \tau_I \dot{I}_j &= -I_j + \mathcal{S}\big[a_I\big(c_{EI}E_j - c_{II}I_j - \Theta_I\big)\big],\end{aligned} \tag{4}$$

where E_k^0 is the unstable fixed point solution of neural mass (E_k, I_k) in the absence of coupling. Importantly, $0 \le \kappa \ll 1$ denotes the overall coupling strength, $C = \{C_{jk}\}$ is an adjacency matrix resembling structural connectivity between cortical regions $(j, k) = 1,\ldots, N$, and the population specific average input fjj may differ across the different cortical regions.

Limit-cycle oscillations emerge in general through a bifurcation, which – and also whose type – can be revealed by looking at the eigenspectrum of the linearized dynamics. In the case of a Hopf bifurcation, oscillatory dynamics evolve on a stable limit cycle around an unstable fixed point. We therefore expect that for an uncoupled (E_j, I_j) node, the Jacobian of the Wilson-Cowan dynamics (4) evaluated at the unstable fixed point (E_j^0, I_j^0) has a pair of complex conjugate eigenvalues with negative real part, which corresponds to the distance $\mu := \overline{\eta}_j - \overline{\eta}_H$ to the Hopf bifurcation point. One typically expresses the dynamics in terms of the deviations $\boldsymbol{x}_j = \big(E_j - E_j^0(\mu), I_j - I_j^0(\mu)\big)$ around the unstable fixed points. Approximating the sigmoidal activation function S up to third order and applying some laborious algebraic transforms (Pietras and Daffertshofer 2019), one can derive a fairly generic form of the dynamics (4) that reads

$$\begin{aligned}\dot{\boldsymbol{x}}_j &= \boldsymbol{L}\boldsymbol{x}_j + \boldsymbol{T}^{-1}\boldsymbol{f}\big(\boldsymbol{T}\boldsymbol{x}_j;\mu\big) + \\ &\quad + \kappa\boldsymbol{T}^{-1}\sum_{k=1}^{N}\boldsymbol{g}\big(\boldsymbol{T}\boldsymbol{x}_j, \boldsymbol{T}\boldsymbol{x}_k\big).\end{aligned} \tag{5}$$

Here $\boldsymbol{L}$ is the Jordan real form of the dynamics' Jacobian $\boldsymbol{J}$, $\boldsymbol{T}$ the matrix containing the

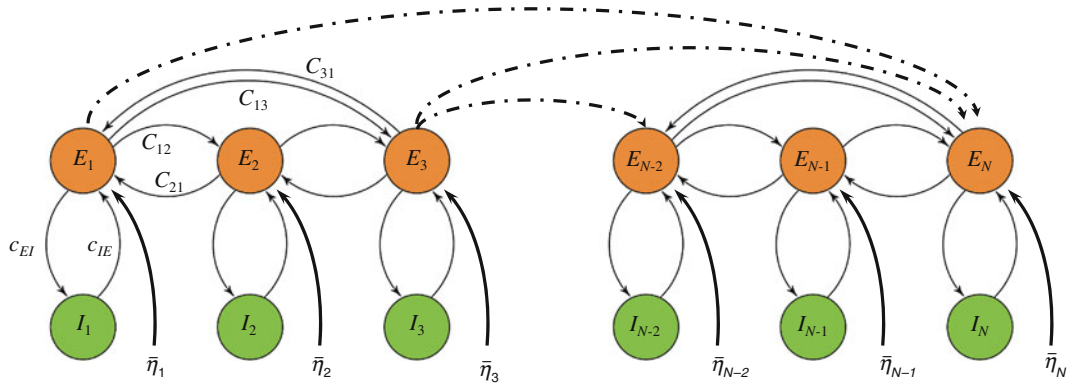

Phase Synchronization in Neural Systems, Fig. 5 Network of coupled Wilson-Cowan neural masses. Each neural population k contains excitatory and inhibitory units (E_j and I_j), which are internally coupled with strengths c_{nm}, $n, m \in \{E, I\}$. The populations receive external inputs $\overline{\eta}_j$. Interaction between two neural masses j, k occurs via their respective excitatory parts only, where C_{jk} denotes the connectivity whether node j receives input from node k.

eigenvectors of J. The function $\boldsymbol{f}$ includes all components within node j that contribute to its dynamical change, and $\boldsymbol{g}$ covers all the between-node interaction, i.e., the last term of the right-hand side of the $\dot{E}_j$ dynamics in (4) now given as coupling between the nodes $\boldsymbol{x}_j$ and $\boldsymbol{x}_k$. The dynamics (5) exhibits qualitatively the same behavior as (4), but due to the Jordan real form, a circular symmetry of the limit cycle is imposed on the full dynamics.

In the immediate vicinity of the Hopf bifurcation point, one can exploit the separation of time scales of phase and amplitude dynamics and readily transform (5) into $\boldsymbol{x}_j = (x_j, y_j) = (R_j \cos(\theta_j), R_j \sin(\theta_j))$, where R_j and $\theta_j = \Omega t + \phi_j$ are amplitude and phase (deviations) of the oscillations at node j, which are slowly varying with respect to the (mean) frequency Ω (Haken 2004), here defined over the eigenvalues at the Hopf point, $\Omega = \omega(0)$. Near the onset of oscillations through a supercritical Hopf bifurcation, $R_j \ll 1$ is small and, thus, the right-hand side of (5) is at least of order $\mathcal{O}(R_j)$. Given the slower time scales of R_j and $\phi_j = \theta_j - \Omega t$, one can average over one cycle $T = 2\pi/\Omega$. In line with Daffertshofer et al. (2018), this direct averaging of the dynamics (5) yields the phase model

$$\dot{\theta}_j = \omega_j + \sum_{k=1}^{N} D_{jk} \sin\left(\theta_k - \theta_j + \Delta_{jk}\right) \qquad (6)$$

with coupling $D_{jk} = \frac{\kappa}{2N} a_E S'_E \Lambda_j C_{jk} \left(R_k/R_j\right)$ and finite phase lag $\Delta_{jk} = \arctan(\rho_j) - \Omega\tau_{jk}$. Here we abbreviated $\Lambda_j^2 = 1 + \rho_j^2$ with $\rho_j = \frac{\kappa}{\omega_j} \times \left(a_E c_{EE} S'_E + a_I c_{II} S'_I\right)$ as well as $\omega_j = a_E a_I c_{IE} c_{EI} S'_E S'_I - \frac{1}{4}\left(a_E c_{EE} S'_E + a_I c_{II} S'_I\right)^2$; and, $S'_{E/I}$ denotes the first derivative of sigmoid $\mathcal{S}$ evaluated at the fixed points E_j^0/I_j^0 of (4). We would like to note that we included some time delays τ_{jk} between nodes $\boldsymbol{x}_j$ and $\boldsymbol{x}_k$ in the coupling function $\boldsymbol{g}(\boldsymbol{x}_j, \boldsymbol{x}_k) \to g(\boldsymbol{x}_j(t), \boldsymbol{x}k(t - \tau_{kj}))$; see Pietras and Daffertshofer (2019) and Daffertshofer et al. (2018) for more details. The dynamics (6) resembles the Kuramoto-Sakaguchi model with phase lag $|\Delta_{jk}| \leq \frac{\pi}{2}$.

Importantly, a transition to full synchronization occurs if the coupling strength κ exceeds a critical value κ_c as illustrated in Fig. 6. There we used the case in which the dynamics can be rewritten as

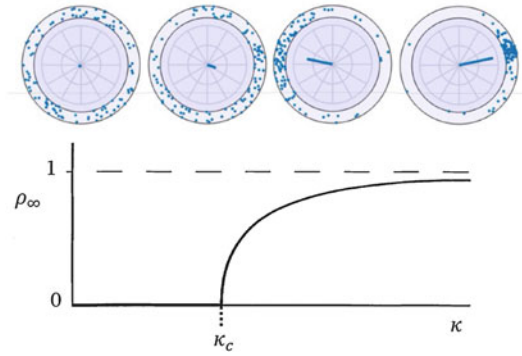

Phase Synchronization in Neural Systems, Fig. 6 Phase oscillators and phase synchronization. The distribution of phases θ_j of the neural oscillators is plotted as points $e^{i\theta_j}$ on the complex unit circle for increasing coupling strength κ. Their average over the population is the Kuramoto order parameter z, shown within the unit circle (top panels from left to right). The phase divergence $\rho = |z|$ describes the degree of synchronization and undergoes a pitchfork bifurcation from asynchrony, $\rho_\infty = 0$, to partial synchrony, $\rho_\infty > 0$, at a critical coupling strength $\kappa_c = 2\Delta$, with Δ being the half-width of the (Lorentzian) density of the oscillators' natural frequencies; see also Kuramoto (1984). Lower panel shows the asymptotic solution of (12)

$$\dot{\theta}_j = \omega_j + \frac{\kappa}{N} \sum_{k=1}^{N} \sin\left(\theta_k - \theta_j\right) \qquad (7)$$

which, in fact, is the seminal Kuramoto model (Kuramoto 1984); see also below.

Using more general phase reduction techniques may generate phase oscillator models that contain higher harmonics (Pietras and Daffertshofer 2019). The absence of higher harmonics hampers, e.g., clustering effects. In any case, however, the network dynamics of (weakly) coupled Wilson-Cowan neural masses can be expressed in terms of a corresponding phase model

$$\dot{\theta}_j = \omega_j + \frac{\kappa}{N} \sum_{k=1}^{N} C_{jk} H\left(\theta_j - \theta_k\right), \qquad (8)$$

$$\rho_\infty = \rho(t \to \infty) = \left\{ 0 \text{ for } \kappa < 2\Delta, \sqrt{1 - \frac{2\Delta}{\kappa}} \text{ otherwise} \right\}.$$

where the phase interaction function $H(\psi)$ admits a "simple" representation as a Fourier series

$$H(\psi) = \sum_{n\geq 0} \alpha_n \cos(n\psi) + \beta_n \sin(n\psi). \quad (9)$$

With such an expression at hand, one can seek to estimate the Fourier amplitudes α_n, β_n that readily provide crucial information about global synchronization of the full neural network or whether clustering of only a subset of network nodes occurs; see Pietras and Daffertshofer (2019) for more details.

Predicting Effects of Phase Synchronization

Mathematical theory and computational modeling go hand in hand with experimental neuroscientific research. Modeling helps to unravel the mechanisms underlying complex behavior. Not only can it provide proper and robust quantitative descriptions, but it also helps to formulate hypotheses and predict future outcome of experimental research. Many physiologically motivated neuronal models have been put forward to investigate synchronization properties in neural systems. Given their inherent complexity, a thorough analysis can be challenging even despite ever-increasing computational capacities. In some cases, the dynamics of neural systems can be simplified to *coupled phase oscillators models*, which often takes on a modified form of a network of seminal Kuramoto oscillators (7) (Daffertshofer and van Wijk 2011; Schuster and Wagner 1990; Rodrigues et al. 2016; Breakspear et al. 2010; Ton et al. 2014; Cabral et al. 2014; Tasseff et al. 2014; Sadilek and Thurner 2015; Schmidt et al. 2015). For the Kuramoto model, there exists a rigorous theory to describe the state of the network with very few macroscopic variables. Following either the Watanabe-Strogatz (Watanabe and Strogatz 1994) or the Ott-Antonsen theory (Ott and Antonsen 2008), the time evolution of these macroscopic variables can be derived exactly under some quite generic conditions. It thus becomes possible to study low-dimensional behavior of the collective dynamics in a straightforward way.

We use the Kuramoto model to illustrate this. In brief, given the model (7) of a population of phase oscillators θ_j with $j = 1,\ldots, N$, one introduces the Kuramoto *order parameter* (Kuramoto 1984)

$$z = \frac{1}{N}\sum_{j=1}^{N} e^{i\theta_j} \quad (10)$$

to describe the population's common dynamics. This order parameter can be expressed via the population density $p(\theta, t; \omega)$. The density contains both frequencies and phases $p(\theta, t; \omega) = q(\omega) f(\theta, t; \omega)$, where the phase density, in general, has the Fourier series $f(\theta, t; \omega) = \frac{1}{2\pi}\sum_{n=-\infty}^{\infty} f_n(t; \omega) e^{in\theta}$. Substituting this into (7) motivates the ansatz $f_n = \alpha^{|n|}$ with $\alpha = f_1 = z^*$. Considering a Lorentzian frequency density $q(\omega) = \frac{\Delta}{\pi} / \left[(\omega - \omega_0)^2 + \Delta^2\right]$, the exact solution of (7) for $N \to \infty$ yields the *order parameter dynamics*

$$\dot{z} = \left(i\omega_0 - \Delta + \frac{\kappa}{2}\right) z - \frac{\kappa}{2}|z|^2 z. \quad (11)$$

Accordingly, the *phase divergence* $\rho = |z|$ follows the well-established equation of motion

$$\dot{\rho} = -\left(\Delta - \frac{\kappa}{2}\right)\rho - \frac{\kappa}{2}\rho^3 \quad (12)$$

while the mean phase $\psi = \sphericalangle(z)$ follows $\dot{\psi} = \omega_0$. The explicit solution of (12) can be given by

$$\rho(t) = \sqrt{\frac{\Delta - \frac{\kappa}{2}}{\left(\Delta - \frac{\kappa}{2}\left(1 - \rho_0^2\right)\right) e^{(2\Delta - \kappa)t} - \frac{\kappa}{2}\rho_0^2}}\,\rho_0 \quad (13)$$

quantifying (one minus) the width of the density of phases

$$f(\theta, t; \omega) = \frac{1 - \rho^2}{1 - 2\rho\cos\theta + \rho^2}. \quad (14)$$

Hence, for some initial condition ρ_0, the dynamics' relaxation time becomes

$$\tau = \frac{1}{2\Delta - \kappa} \ln \left[\frac{2\Delta + \kappa\left(\rho_\tau^2 - 1\right)}{2\Delta + \kappa\left(\rho_0^2 - 1\right)} \cdot \frac{\rho_0^2}{\rho_\tau^2} \right] \qquad (15)$$

with $\rho(\tau) = \rho_\tau$. The value ρ_τ can be determined using the asymptotic solution as we set $\rho_\tau = \rho_0 - \gamma(\rho_0 - \rho_\infty)$ with, e.g., $\gamma = 99.9\%$.

Many studies speculated about the relevance of the (finite) time it takes for a population of neural oscillators to approach synchrony or to desynchronize, often in the context of the binding problem outlined in the introductory paragraph. Already by looking at Fig. 2, it becomes apparent that the local field potential of a group of neurons can only be of significant value if their phase density is sufficiently narrow. At larger scale, classic experimental paradigms for investigating relaxation times of phase synchronization involve event- or moton-related responses as sketched in Fig. 7.

Final Notes

Phase oscillator models help to explain how changes in the local dynamics affect functional connectivity, how neural synchronization can be achieved, and how functional clusters or modules are generated through remote synchronization. These models have also been used to investigate the interplay between structure (anatomy) and function, including effects of cortical lesions on the overall brain dynamics (Honey and Sporns 2008; Vása et al. 2015). Given their mathematical ease, they are particularly suited to explore the emergence of (de-)synchronized states per se and the corresponding relationship between them, but also to tackle even more generic characteristics such as self-organized criticality.

The use of phase oscillator models, however, is not without a risk: the reduction of a (network) dynamics to a phase oscillator model requires great care (Pietras and Daffertshofer 2019). Any (heuristic) approximation of an oscillatory neural network via a network of phase oscillators has to withstand comparison with the "original" dynamics and starting-off with "just" the phase oscillator network may lose contact with biophysical or physiological reality.

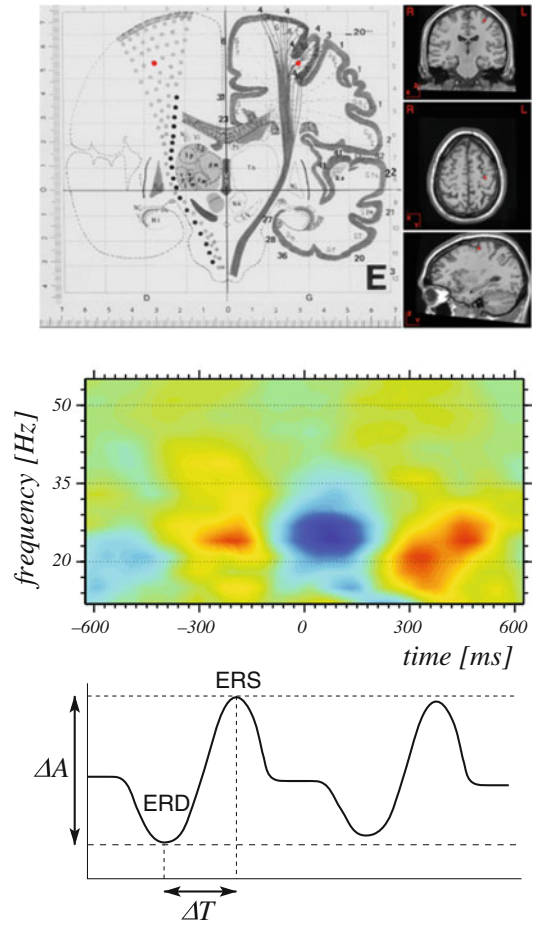

Phase Synchronization in Neural Systems, Fig. 7 Rhythmic motor performance is accompanied by a rhythmic modulation of beta-range oscillatory activity in primary motor cortices; cf. Fig. 1. The middle panel displays the time-dependent changes of the spectral power of a movement cycle as assessed via MEG (Houweling et al. 2010). The beta activity displays event-related synchronization and de-synchronization (ERS and ERD, i.e., red and blue patches, respectively). If the movement cycle is too short, ERS and ERD cannot develop due to the finite relaxation time of the underlying phase dynamics, and motor performance can no longer be timed.

Summary

Rhythmic behavior of a neural population implies an oscillatory dynamics of one or more macroscopic variables. The corresponding phase space exhibits a limit cycle that, if stable, attracts the population dynamics. If this attraction is sufficiently fast, the dynamics away from the limit

cycle can be approximated by the dynamics on the limit cycle. We illustrated this for the case of a single population. In such a case, the high-dimensional dynamics of neuronal oscillators can be uniquely identified by a one-dimensional phase variable. The phase reduction becomes especially useful when studying a network of interacting neural oscillators as we showed for the case of coupled Wilson-Cowan neural mass models. The resulting phase models can, in general, be analyzed along well-established techniques for networks of coupled phase oscillators. The resulting findings on synchronization properties can mimic oscillatory activity in neural masses as observed in experiments. They also help understanding effects of changes in synchronization for the macroscopic functioning of the nervous system.

Acknowledgments We would like to thank Federico Devalle, Ernest Montbrió, and Alex Roxin for the many discussions about interacting QIF neurons. Peter Beek, Sanne Houweling, Peter Praamstra, and Bernadette van Wijk provided the material that here served to illustrate some recent experimental findings on the phase dynamics in the human motor system. This work received financial support via ITN COSMOS funded by the EU Horizon 2020 research and innovation program under the Marie Skłodowska-Curie Grant Agreement No. 642563.

Bibliography

Alcamí P, Pereda AE (2019) Beyond plasticity: The dynamic impact of electrical synapses on neural circuits. Nat Rev Neurosci 20(5):253–271

Amari SI (1977) Dynamics of pattern formation in lateral-inhibition type neural fields. Biol Cybern 27(2):77–87

Borisyuk RM, Kirillov AB (1992) Bifurcation analysis of a neural network model. Biol Cybern 66(4):319–325

Breakspear M (2017) Dynamic models of large-scale brain activity. Nat Neurosci 20(3):340–352

Breakspear M, Heitmann S, Daffertshofer A (2010) Generative models of cortical oscillations: Neurobiological implications of the Kuramoto model. Front Hum Neurosci 4:190

Brunel N, Hakim V (1999) Fast global oscillations in networks of integrate-and-fire neurons with low firing rates. Neural Comput 11(7):1621–1671

Buzsaki G (2006) Rhythms of the brain. Oxford University Press

Byrne Á, Brookes MJ, Coombes S (2017) A mean field model for movement induced changes in the beta rhythm. J Comput Neurosci 43(2):143–158

Cabral J, Kringelbach ML, Deco G (2014) Exploring the network dynamics underlying brain activity during rest. Prog Neurobiol 114(Supplement C):102–131

Connors BW (2017) Synchrony and so much more: Diverse roles for electrical synapses in neural circuits. Dev Neurobiol 77(5):610–624

Coombes S (2010) Large-scale neural dynamics: Simple and complex. NeuroImage 52(3):731–739

Daffertshofer A, van Wijk B (2011) On the influence of amplitude on the connectivity between phases. Front Neuroinform 5:6

Daffertshofer A, Ton R, Pietras B, Kringelbach ML, Deco G (2018) Scale-freeness or partial synchronization in neural mass phase oscillator networks: Pick one of two? NeuroImage 180:428–441

Dauwels J, Vialatte F, Musha T, Cichocki A (2010) A comparative study of synchrony measures for the early diagnosis of Alzheimer's disease based on EEG. NeuroImage 49(1):668–693

Deco G, Jirsa VK, Robinson PA, Breakspear M, Friston K (2008) The dynamic brain: From spiking neurons to neural masses and cortical fields. PLoS Comput Biol 4(8):e1000092

Deschle N, Daffertshofer A, Battaglia D, Martens EA (2019) Directed flow of information in chimera states. Front Appl Math Stat 5:28

Devalle F, Montbrió E, Pazó D (2018) Dynamics of a large system of spiking neurons with synaptic delay. Phys Rev E 98(4):042214

Freeman WJ (1975) Mass action in the nervous system. Academic Press, New York

Golomb D (2007) Neuronal synchrony measures. Scholarpedia 2(1):1347

Gray CM (1994) Synchronous oscillations in neuronal systems: Mechanisms and functions. J Comput Neurosci 1(1–2):11–38

Haken H (2004) Synergetics: introduction and advanced topics. Springer, Berlin

Haken H (2006) Brain dynamics: synchronization and activity patterns in pulse-coupled neural nets with delays and noise. Springer, Berlin

Häusser M, Roth A (1997) Estimating the time course of the excitatory synaptic conductance in neocortical pyramidal cells using a novel voltage jump method. J Neurosci 17(20):7606–7625

Honey CJ, Sporns O (2008) Dynamical consequences of lesions in cortical networks. Hum Brain Mapp 29(7):802–809

Hoppensteadt FC, Izhikevich EM (1997) Weakly connected neural networks. Springer, New York

Houweling S, Beek PJ, Daffertshofer A (2010) Spectral changes of interhemispheric crosstalk during movement instabilities. Cereb Cortex 20(11):2605–2613

Hutt A, Buhry L (2014) Study of GABAergic extra-synaptic tonic inhibition in single neurons and neural populations by traversing neural scales: application to propofol-induced anaesthesia. J Comput Neurosci 37(3):417–437

Jansen BH, Rit VG (1995) Electroencephalogram and visual evoked potential generation in a mathematical

model of coupled cortical columns. Biol Cybern 73(4):357–366
Jean-Philippe L, Eugenio R, Jacques M, Varela FJ (1999) Measuring phase synchrony in brain signals. Hum Brain Mapp 8(4):194–208
Kandel ER, Schwartz JH, Jessell TM et al (2013) Principles of neural science, vol 5. McGraw-Hill, New York
Kilpatrick ZP (2015) Wilson-Cowan Model. In Encyclopedia of computational neuroscience, ed. by D. Jaeger, R. Jung (Springer, New York, 2015), pp. 3159–3163
Kuramoto Y (1984) Chemical oscillations, turbulence and waves. Springer, Berlin
Lopes da Silva F, Hoeks A, Smits H, Zetterberg L (1974) Model of brain rhythmic activity. Biol Cybern 15(1):27–37
Luke TB, Barreto E, So P (2013) Complete classification of the macroscopic behavior of a heterogeneous network of theta neurons. Neural Comput 25(12):3207–3234
MacKay WA (1997) Synchronized neuronal oscillations and their role in motor processes. Trends Cogn Sci 1(5):176–183
Masquelier T, Hugues E, Deco G, Thorpe SJ (2009) Oscillations, phase-of-firing coding, and spike timing-dependent plasticity: An efficient learning scheme. J Neurosci 29(43):13484–13493
Montbrió E, Pazó D, Roxin A (2015) Macroscopic description for networks of spiking neurons. Phys Rev X 5(2):021028
Nunez PL (2000) Toward a quantitative description of large-scale neocortical dynamic function and EEG. Behav Brain Sci 23(3):371–398
Ott E, Antonsen TM (2008) Low dimensional behavior of large systems of globally coupled oscillators. Chaos 18(3):037113
Pazó D, Montbrió E (2016) From quasiperiodic partial synchronization to collective chaos in populations of inhibitory neurons with delay. Phys Rev Lett 116:238101
Pietras B, Daffertshofer A (2019) Network dynamics of coupled oscillators and phase reduction techniques. Phys Rep 819:1–105
Pietras B, Devalle F, Roxin A, Daffertshofer A, Montbrió E (2019) Exact firing rate model reveals the differential effects of chemical versus electrical synapses in spiking networks. Phys Rev E 100:042412
Pinto DJ, Brumberg JC, Simons DJ, Ermentrout GB, Traub R (1996) A quantitative population model of whisker barrels: re-examining the Wilson-Cowan equations. J Comput Neurosci 3(3):247–264
Renart A, de la Rocha J, Bartho P, Hollender L, Parga N, Reyes A, Harris KD (2010) The asynchronous state in cortical circuits. Science 327(5965):587–590
Rodrigues FA, Peron TKD, Ji P, Kurths J (2016) The Kuramoto model in complex networks. Phys Rep 610:1–98
Sadilek M, Thurner S (2015) Physiologically motivated multiplex Kuramoto model describes phase diagram of cortical activity. Sci Rep 5:10015
Sauseng P, Klimesch W (2008) What does phase information of oscillatory brain activity tell us about cognitive processes? Neurosci Biobehav Rev 32(5):1001–1013
Schmidt R, LaFleur KJR, de Reus MA, van den Berg LH, van den Heuvel MP (2015) Kuramoto model simulation of neural hubs and dynamic synchrony in the human cerebral connectome. BMC Neurosci 16(1):54
Schnitzler A, Gross J (2005) Normal and pathological oscillatory communication in the brain. Nat Rev Neurosci 6(4):285–296
Schuster H, Wagner P (1990) A model for neuronal oscillations in the visual cortex. Biol Cybern 64(1):77–82
Siettos C, Starke J (2016) Multiscale modeling of brain dynamics: From single neurons and networks to mathematical tools. Wiley interdisciplinary reviews: Biol Med 8(5):438–458
Singer W (1993) Synchronization of cortical activity and its putative role in information processing and learning. Annu Rev Physiol 55:349–374
Singer W (2007) Binding by synchrony. Scholarpedia 2(12):1657
Tasseff R, Bheda-Malge A, DiColandrea T, Bascom CC, Isfort RJ, Gelinas R (2014) Mouse hair cycle expression dynamics modeled as coupled mesenchymal and epithelial oscillators. PLoS Comput Biol 10(11):1–21
Thut G, Miniussi C, Gross J (2012) The functional importance of rhythmic activity in the brain. Curr Biol 22(16):R658–R663
Ton R, Deco G, Daffertshofer A (2014) Structure-function discrepancy: Inhomogeneity and delays in synchronized neural networks. PLoS Comput Biol 10(7):e1003736
Uhlhaas PJ, Singer W (2006) Neural synchrony in brain disorders: Relevance for cognitive dysfunctions and pathophysiology. Neuron 52(1):155–168
Van Wijk B, Daffertshofer A, Roach N, Praamstra P (2008) A role of beta oscillatory synchrony in biasing response competition? Cereb Cortex 19(6):1294–1302
Varela F, Lachaux JP, Rodriguez E, Martinerie J (2001) The brainweb: Phase synchronization and large-scale integration. Nat Rev Neurosci 2(4):229–239
Vása F, Shanahan M, Hellyer PJ, Scott G, Cabral J, Leech R (2015) Effects of lesions on synchrony and metastability in cortical networks. NeuroImage 118-(Supplement C):456–467
Wang XJ (2010) Neurophysiological and computational principles of cortical rhythms in cognition. Physiol Rev 90(3):1195–1268
Watanabe S, Strogatz SH (1994) Constants of motion for superconducting Josephson arrays. Physica 74D(3):197–253
Wilson HR, Cowan JD (1972) Excitatory and inhibitory interactions in localized populations of model neurons. Biophys J 12(1):1–24
Wilson HR, Cowan JD (1973) A mathematical theory of the functional dynamics of cortical and thalamic nervous tissue. Kybernetika 13(2):55–80
Womelsdorf T, Valiante TA, Sahin NT, Miller KJ, Tiesinga P (2014) Dynamic circuit motifs underlying rhythmic gain control, gating and integration. Nat Neurosci 17(8):1031

Brain Pacemaker

Peter A. Tass[1,2,3], Christian Hauptmann[1] and Oleksandr V. Popovych[1]
[1]Institute of Neuroscience and Medicine – Neuromodulation (INM-7), Jülich Research Center, Jülich, Germany
[2]Department of Neurosurgery, Stanford University, Stanford, CA, USA
[3]Department of Neuromodulation, University of Cologne, Cologne, Germany

Article Outline

Glossary
Definition of the Subject
Introduction
Standard High-Frequency Stimulation
Coordinated Reset Stimulation
Multisite Linear Delayed Feedback
Nonlinear Delayed Feedback
Proportional–Integro–Differential Feedback
Plasticity
Closed-Loop DBS
Summary
Bibliography

Glossary

Coordinated reset stimulation Coordinated reset (CR) stimulation is an effectively desynchronizing control technique, where a population of synchronized oscillators is stimulated via several stimulation sites in such a way that spatially and timely coordinated phase reset is achieved in subpopulations assigned to each of the stimulation sites. This method is suggested for the counteraction of abnormal neuronal synchronization characteristic for several neurological diseases and amelioration of their symptoms. It has successively been verified in a number of experimental and clinical studies.

Deep brain stimulation Electrical deep brain stimulation (DBS) is the standard therapy for medically refractory movements disorders, e.g., Parkinson's disease and essential tremor. It requires a surgical treatment, where depth electrodes are chronically implanted in target areas like the thalamic ventralis intermedius nucleus or the subthalamic nucleus. For standard DBS electrical high-frequency (>100 Hz) stimulation is permanently delivered via depth electrodes. More sophisticated deep brain stimulation techniques are in the process of being established for clinical use.

Delayed feedback Delayed feedback is a method for the creation of a closed-loop forcing, where a portion of the measured output signal of a system is time delayed, linearly or non-linearly processed, and fed back into the system. This approach is often used to control the dynamic behavior of complex systems. In this article delayed feedback is used to control synchronization in ensembles of coupled oscillators, e.g., neurons.

Order parameter The order parameter is a quantity characterizing a phase transition or phase change in the transformation of a complex system from one phase (state) to another. The order parameter is convenient for characterizing the onset and extent of synchronization in larger ensembles: Perfect phase synchronization corresponds to a large value of the order parameter, whereas an incoherent (desynchronized) state is associated with a small value of the order parameter. In synergetics it has been shown that the dynamics of complex systems may be governed by only a few order parameters.

Synchronization Synchronization (from Greek *syn* = the same, common and *chronos* = time) means the adjustment of rhythms of self-sustained oscillators due to their weak interaction. The interacting oscillators can be regular (periodic) or chaotic. There are several different forms of synchronization including phase,

A. Hutt, H. Haken (eds.), *Synergetics*,
https://doi.org/10.1007/978-1-0716-0421-2_42

Originally published in
R. A. Meyers (ed.), *Encyclopedia of Complexity and Systems Science*, © Springer Science+Business Media LLC 2018
https://doi.org/10.1007/978-3-642-27737-5_42-2

complete, generalized, and lag synchronization, etc. In this article we focus on phase synchronization. In the simplest form, the oscillators, rotating with the same frequency, become phase synchronized (phase locked) to each other, if they tend to oscillate with the same repeating sequence of relative phase angles. Put otherwise, the oscillators adjust their rhythms, while their amplitude dynamics need not be correlated.

Definition of the Subject

A brain pacemaker is a medical device that is implanted into the brain with the purpose to stimulate nervous tissue with electrical signals. Brain pacemakers are used for the therapy of patients suffering, for example, from Parkinson's disease, epilepsy or mental disorders. Brain stimulation is either called deep brain stimulation (DBS) if structures deeply inside the brain are targeted or cortical stimulation (intracortical or epicortical), if the electrical contacts of the stimulator are positioned within the cortex or on its surface. Apart from direct brain stimulation, other targets may also be used, such as spinal cord (e.g., for the treatment of pain) or the vagus nerve (for the treatment of epilepsy). The electrical stimulation of the nervous system has a long history which goes back to the nineteenth century where first tests with cortical stimulation were documented (Gildenberg 2005). The first intraoperative deep brain stimulation was performed by Spiegel et al. in 1947 in a patient suffering from Huntington's chorea, and in the eighties DBS was introduced as a treatment for motor disorders (Brice and McLellan 1980; Benabid et al. 1987). DBS was approved by the Food and Drug Administration (FDA) as a treatment for essential tremor in 1997, for Parkinson's disease in 2002, and dystonia in 2003. The treatment of severe neurological and psychiatric diseases with brain pacemakers is a rapidly growing and promising field. Novel, model-based approaches, which use methods from synergetics, nonlinear dynamics, and statistical physics, to specifically restore brain function and connectivity, demonstrate how insights into the dynamics of complex systems contribute to the development of novel therapies.

Introduction

Self-organization processes are abundant in numerous fields of the natural sciences (Haken 1977, 1983). For instance, the nervous system elegantly utilizes self-organization principles for motor control purposes (Haken et al. 1985; Schöner et al. 1986; Haken 1996; Kelso 1995). A classical example of a self-organization process is synchronization of populations of interacting oscillators, which is widely observed in physics (Haken 1970, 1983; Pikovsky et al. 2001; Strogatz 2003), chemistry (Kuramoto 1984), biology (Winfree 1980), neuroscience (Steriade et al. 1990; Haken 2002), and medicine (Elble and Koller 1990; Milton and Jung 2003; Tass 1999). In the nervous system synchronization processes are important, e.g., in the context of information processing (Singer 1989) and motor control (Andres and Gerloff 1999). However, pathological, excessive synchronization strongly impairs brain function (Elble and Koller 1990; Milton and Jung 2003). In fact, pathological synchronization processes are the hallmark of several neurological diseases like Parkinson's disease (PD) or essential tremor (Alberts et al. 1969; Nini et al. 1995). For example, Parkinsonian resting tremor appears to be caused by a pacemaker-like population of neurons which fires in a synchronized and periodical manner (Alberts et al. 1969; Smirnov et al. 2008). In contrast, under healthy conditions these neurons fire in an uncorrelated, i.e. desynchronized manner (Nini et al. 1995).

Permanent deep brain stimulation (DBS) at high frequencies ($>$100 Hz) is the standard therapy for medically refractory patients suffering from Parkinson's disease and essential tremor (Benabid et al. 1991, 2002; Blond et al. 1992), see Fig. 1. High-frequency (HF) DBS has been developed empirically, mainly based on experimental results and clinical observations. The mechanism of HF DBS is still a matter of debate (Benabid et al. 2005). Clinical studies showed that

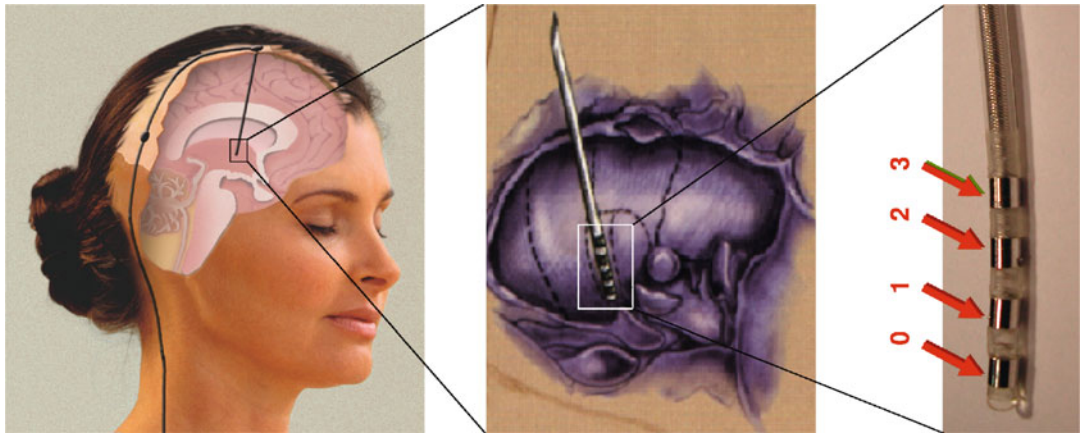

Brain Pacemaker, Fig. 1 Standard DBS setup. A depth electrode is implanted into the target structure (e.g., the *subthalamic nucleus*). The electrode is subcutaneously connected with the generator of the high-frequency stimulation signal (not shown in this image). The stimulation signal is delivered through one or more of the four stimulation contacts labeled from 0 to 3

HF DBS essentially has similar effects as observed after tissue lesioning. Compared to lesioning, DBS is reversible and has a lower rate of side effects (Tasker 1998; Schuurman et al. 2000). However, in spite of many beneficial effects, in some patients DBS may not help, or may cause side effects, or the therapeutic effects may disappear over time (Tasker 1998; Volkmann 2004; Rodriguez-Oroz et al. 2005; Deuschl et al. 2006). With the objective of finding better tolerated and more effective DBS techniques, a model-based development of novel stimulation methods has been initiated (Tass 1999, 2002a, c, 2003b; Hauptmann et al. 2005a, b, c, 2007b; Tass et al. 2006; Popovych et al. 2005, 2006a, b), see Fig. 2. In these studies, relevant neuronal target populations were modeled mathematically and stimulation techniques have been developed utilizing principles from nonlinear dynamics and statistical physics (Tass 1999).

One goal of this approach is to control the pathological neural dynamics appropriately in order to achieve a mild and efficient relief of symptoms (Tass 1999). The second, more ambitious goal is to stimulate in a way that the formerly affected neuronal populations unlearn their pathological connectivity and, hence, their tendency to produce pathological synchronization (Tass and Majtanik 2006). Put otherwise, the very goal of this approach is to induce long-lasting therapeutic effects which outlast the cessation of stimulation (Tass and Majtanik 2006; Tass and Hauptmann 2007; Hauptmann and Tass 2007). To this end, stimulation algorithms have been developed and optimized to exploit dynamic self-organization principles and plasticity rules (Tass and Majtanik 2006; Tass and Hauptmann 2006, 2007; Hauptmann and Tass 2007; Hauptmann et al. 2007b).

Several novel stimulation techniques have computationally been developed in the past. In this article four of these control methods will be presented in detail: coordinated reset (CR) stimulation (Tass 1999, 2002a, c, 2003b), multisite linear delayed feedback (MLDF) stimulation (Hauptmann et al. 2005a, b, c), nonlinear delayed feedback (NDF) stimulation (Popovych et al. 2005, 2006a, b; Popovych and Tass 2010), and proportional–integro–differential feedback (PIDF) stimulation (Pyragas et al. 2007). These techniques have the common objective of reducing the synchronized activity of the target population by reestablishing a normal desynchronized physiological activity in a highly synchronized population of neurons. For other stimulation methods we refer to Rosenblum and Pikovsky (2004a), Tukhlina et al. (2007), Kiss et al. (2007), Luo et al. (2009), Danzl et al. (2009), and Nabi and Moehlis (2011).

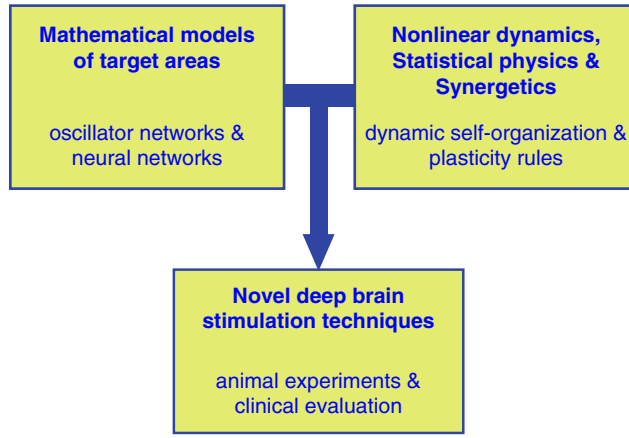

Brain Pacemaker, Fig. 2 Model-based development of novel deep brain stimulation techniques: Along the lines of a top-down approach target areas for deep brain stimulation are modeled by means of oscillator networks and physiology- and anatomy-based neural networks. Methods from nonlinear dynamics, statistical physics, and synergetics are employed to develop stimulation techniques which specifically utilize dynamic self-organization principles and plasticity rules. Experimental feedback from both animal experiments and clinical evaluation serves to validate, falsify or modify theoretical assumptions and predictions. This iterative approach aims at steadily improving the mathematically designed stimulation techniques and, hence, at establishing superior therapies

CR stimulation, in its original realization, uses short electrical pulse trains to subsequently reset sub-populations of the neuronal network, which induces a desynchronized state (Tass 1999, 2002a, c, 2003b). The stimulation is applied through a small number of stimulation sites which are equally spaced within the neuronal population. CR stimulation induced desynchronization is achieved by utilizing self-organization principles, in particular, the slaving principle induced by the pathological neuronal interactions (i.e., interactions which have the potential to induce a pathological synchronization) (Tass 2002a, c, 2003b). MLDF (Hauptmann et al. 2005a, b, c) and NDF (Popovych et al. 2005, 2006a, b; Popovych and Tass 2010) stimulation use delayed feedback for stabilizing a desynchronized state which is intended to be as close to the physiological mode of action as possible. Here, the local field potential (LFP) of the target population is measured, amplified, delayed, and fed back into the ensemble. The PIDF feedback (Pyragas et al. 2007) utilizes an instantaneous LFP and is designed for a particularly difficult situation characterized by a separate registration and stimulation setup.

It has been shown experimentally, that synaptic plasticity enhances pathological synchronization (Nowotny et al. 2003). From the kindling phenomenon in the context of epilepsy it is well known that neural networks may learn pathological strong interactions (Speckmann and Elger 1991; Morimoto et al. 2004). The novel desynchronizing stimulation protocols are designed to invert this pathological process, so that the affected neuronal populations unlearn their pathological connectivity, and physiological neuronal activity is re-established on a long-term basis. In a nutshell, the novel stimulation techniques aim at a well-directed employment of fundamental principles of dynamic brain action to induce long-lasting therapeutic effects.

Standard High-Frequency Stimulation

High-frequency (HF) deep brain stimulation (DBS) is the standard therapy for patients suffering from medically refractory PD or essential tremor (Benabid et al. 1991, 2002). To this end, depth electrodes are chronically implanted in the thalamic ventralis intermedius nucleus or the subthalamic nucleus (Benabid et al. 1991, 2002) and a permanent HF ($>$100 Hz) periodic pulse train stimulation is applied (Fig. 1). HF DBS has been

developed empirically, mainly based on intraoperative observations. HF DBS strongly alters the neuronal firing and mimics the effect of tissue lesioning, e.g., by suppressing neuronal firing, which, in turn, suppresses the peripheral tremor (Benabid et al. 2002; Filali et al. 2004; McIntyre et al. 2004b; Volkmann 2004). However, as yet, the mechanism of HF DBS is not sufficiently understood (McIntyre et al. 2004b).

During stimulation HF DBS seems to induce a regular bursting mode (Beurrier et al. 2002). After a reduction of stimulation artifacts, robust bursting activity in subthalamic nucleus (STN) neurons was observed in slices from naive or resperine-treated rats. After offset of stimulation, blockade of activity, i.e., a non-specific suppression of the neuronal activity in the target structures through a depolarization blockade which did not require synaptic transmission was observed (Beurrier et al. 2001).

Other hypotheses are that HF DBS applied to a PD patient mimics the effect of tissue lesioning and appears to block neuronal activity in relevant target areas during stimulation (Benabid et al. 2002). In single-compartment conductance-based biophysical models of isolated STN neurons the HF stimulation may cause a suppression of neuronal activity on an elementary membrane level, where a neuron's resting state or low-amplitude subthreshold oscillations can get stabilized (Pyragas et al. 2013). The obtained theoretical results resemble the clinically observed relations between stimulation amplitude and stimulation frequency required to suppress Parkinsonian tremor (Benabid et al. 1991). The most probable hypothesis was offered by Benabid et al. (2005), in which a mixture of different mechanisms was discussed. The contributing mechanisms resulting in the observed effects of HF DBS might be membrane inhibition, jamming, excitation of excitatory and inhibitory afferents, excitation of efferents and plasticity (Benabid et al. 2005). In particular, HF stimulation of afferent axons projecting to STN can account for a therapeutic effect of HF DBS within STN (Gradinaru et al. 2009).

To precisely evaluate the contribution of these different mechanisms, spatially extended multicompartment neuron models were used to demonstrate the effects of extracellular stimulation on the different structures of the stimulated neuronal population (Grill and McIntyre 2001). Depending on the stimulation amplitude and the shape of the stimulation pulses, either the cells were activated directly or fibers mediating excitatory or strong inhibitory action were activated (Grill and McIntyre 2001). Modeling studies indicate that already at the level of single neurons, the activation of a larger number of structures can take place with different and possibly conflicting impacts on the single neuron dynamics (Grill and McIntyre 2001). The collective dynamics of neuronal populations further adds aspects which are important for the creation of synchronized activity: cells responding differently to external inputs like somatosensory stimulation or stimulation due to active movements are present in the target tissue together with so called no-response cells (Lenz et al. 1994). HF stimulation has a complex impact on these structures (Benabid et al. 2002; Shen et al. 2003).

Experimental and modeling studies also indicate that the *globus pallidum interior* (GPi) – one structure of the basal ganglia – might be strongly involved in the mechanisms of DBS (Hashimoto et al. 2003; Garcia et al. 2005; McIntyre et al. 2004a; Rubin and Terman 2004; Miocinovic et al. 2006). The results of modeling studies indicate that under parkinsonian conditions the rhythmic inhibition from GPi to the thalamus compromises the ability of thalamocortical relay cells to respond to depolarizing inputs, such as sensorimotor signals. HF stimulation of STN regularizes GPi firing, and this restores the responsiveness of the thalamus (Rubin and Terman 2004). In such a way, one may distinguish between local and non-local effects of HF DBS. Locally, in the vicinity of the stimulation electrode, the axons rather than cell bodies (somas) get activated (McIntyre et al. 2004a), while the latter can even be effectively inhibited by the HF stimulation (Beurrier et al. 2001; Benabid et al. 2002; Welter et al. 2004; Meissner et al. 2005). The stimulation-induced axonal activity propagates antidromically and orthodromically (Hammond et al. 2008) and can change the firing

in the output structures downstream to the neuronal target population. The pathological discharge patterns there can be replaced by a HF spiking or suppressed depending on whether the efferent fibers of the stimulated nucleus are excitatory or inhibitory, respectively (Hashimoto et al. 2003; Anderson et al. 2003; McIntyre et al. 2004b). In other words, local and non-local effects of HF DBS may differ considerably.

HF DBS is reversible and has a much lower rate of side effects than lesioning with thermocoagulation (Schuurman et al. 2000). Although HF DBS is the golden standard for the therapy of medically refractory movement disorders, there are still limitations of HF DBS: On the one hand HF DBS may cause adverse effects like dysarthria, dysesthesia, cerebellar ataxia, and memory decline (Volkmann 2004; Rodriguez-Oroz et al. 2005; Freund 2005). On the other hand HF DBS may be ineffective or its therapeutic effect may wear off over time (Kumar et al. 2003; Rodriguez-Oroz et al. 2005). For instance, 11–15% of PD patients have unsatisfactory outcomes although their depth electrodes are properly placed (Limousin et al. 1999).

Coordinated Reset Stimulation

To study the impact of pulsatile stimuli on single oscillators and, in particular, populations of oscillators in a biologically more realistic setting, it was necessary to take into account random forces (Tass 1996a, b, 1999). To this end, a stochastic concept of phase resetting has been developed for populations of non-interacting (Tass 1996a, b) as well as interacting (Tass 1999) oscillators in the presence of noise. In this approach limit cycle oscillators were approximated by phase oscillators (Hansel et al. 1993b), so that the pulsatile stimulation only affects the oscillators' phases. If a single pulse of the right intensity and duration is delivered to the population in the stable synchronized state, it causes an at least temporary desynchronization provided it hits the population at a vulnerable phase. Theoretically, single pulse stimulation has also been studied in more complex networks, for instance, networks of coupled phase oscillators with inertia, modeling dendritic dynamics (Dolan et al. 2005; Majtanik et al. 2006). Based on the stochastic phase resetting theory and utilizing a phase oscillator as a model for a single neuron (Hansel et al. 1993b), demand-controlled single pulse deep brain stimulation has been suggested for the therapy of movement disorders like Parkinson's disease or essential tremor (Tass 1999, 2000).

However, there are drawbacks to single-pulse stimulation which decisively limit its applicability (Tass 2001b; Zhai et al. 2005): First, if the mutual coupling is not weak, the vulnerable phase range we have to hit in order to cause an effective desynchronization is only a small fraction (e.g., 5%) of a period of the collective oscillation. Second, the critical stimulation parameters required to achieve a good desynchronization depend on the initial dynamical state of the population. Thus, different stimulation parameters have to be used if the cluster is not in its stable synchronized state.

To overcome the limitations of single pulse stimulation, double pulse (Tass 2001a, b) stimulation has been proposed: Two qualitatively different stimuli are successively delivered. The first, stronger pulse resets (restarts) the collective oscillation irrespective of the initial state of the population. The second, weaker pulse is applied after a fixed time delay, where it hits the cluster in its vulnerable state and, hence, causes a desynchronization. There are different variants of double pulse stimulation, depending on the type of stimuli used to achieve a reset or a desynchronization (Tass 2001c, 2002a, b, c). For instance, the first resetting pulse can be replaced by a brief high-frequency pulse train (Tass 2001c) or by a softly resetting low-frequency pulse train (Tass 2002a, b).

Although double pulse stimulation causes a desynchronization irrespective of the initial dynamical state at which this stimulus is delivered, there are still limitations which may hinder an application to a biological system (Tass 2003a, b): On the one hand, double pulse stimulation requires a calibration. On the other hand, double pulse stimulation is only effective if the system parameters are reasonably stable. The required quasi-stationarity of the system parameters

combined with the possibly time consuming calibration may cause problems when applied to a real biological system, where fluctuations of model parameters are inevitable.

To provide a stimulation technique which is robust with respect to system parameters and which does not require calibration, coordinated reset (CR) stimulation has been developed (Tass 2003a, b). The idea behind this approach is to abstain from achieving a perfect desynchronization by a well-calibrated stimulus. Rather, by means of a robust and comparably mild stimulus the stimulated population is shifted into a dynamical state which is not the desired desynchronized state, but sufficiently close to it. Close in the sense that due to the pathologically strong coupling the population automatically relaxes into the desired desynchronized state. This approach essentially exploits the pathological tendency of the neuronal population to establish a synchronized state. Accordingly, CR stimulation is in a way comparable to Asian martial arts, where ideally a minimal amount of energy (i.e., CR stimulation) is invested to control the adversary by utilizing the adversary's own energy (i.e., the neurons' pathological strong coupling).

The scheme of the stimulation setup is presented in Fig. 3a. Several stimulation sites are placed within the target network and weak resetting stimulation signals are administered via these stimulation sites. In this way the oscillatory population is divided into several sub-populations, where each of them is assigned to the corresponding stimulation site and receiving the stimulation signal mostly from that stimulation site. CR stimulation means that a synchronized population of neurons is stimulated with a sequence of brief resetting stimuli (typically brief HF stimulus trains) via the different sites. The delay between the subsequent resetting stimuli can be chosen as $\tau = T/n$ with respect to that at the preceding site, where n is the number of stimulation sites, and T approximates the mean period of the collective dynamics of synchronized oscillators (Tass 2003a, b).

The subsequent reset of the different subpopulations induces a so-called cluster state, i.e., the whole population is divided into n subpopulations which differ with respect to their

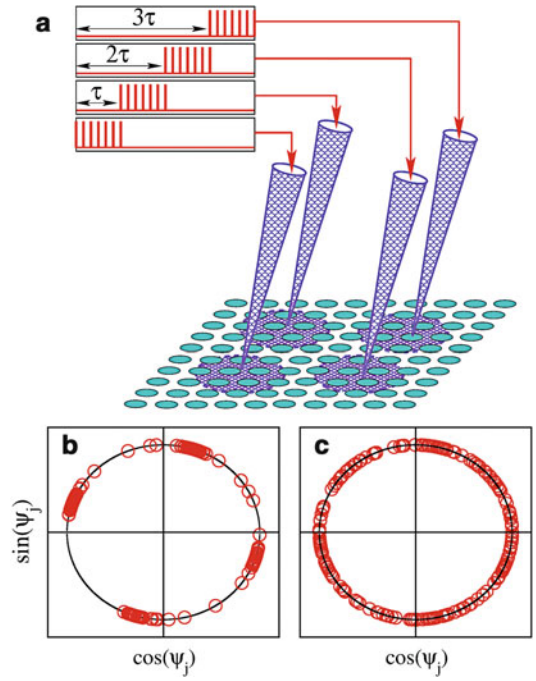

Brain Pacemaker, Fig. 3 Stimulation setup of CR stimulation method. (**a**) Brief and mild resetting stimuli are administered at different sites at subsequent times and effectively divide the stimulated population into several sub-populations such that (**b**) their phases ψ_j form phase clusters equidistantly (or close to that) distributed over the unit circle. (**c**) Nearly uniform distribution of the oscillator phases during the post-stimulation transient

mean phase. This effect is illustrated in Fig. 3b where a snapshot of the distribution of the phases ψ_j of stimulated oscillators is shown in the (cos(ψ_j),sin(ψ_j))-plane after CR stimulation. The phases of the population of oscillators stimulated via, e.g., four sites form four phase clusters distributed equidistantly (or close to that) over the unit circle. To estimate the extent and type of synchronization of the whole population of N oscillators, the cluster variables

$$Z_m(t) = R_m(t)\, e^{i\Psi_m(t)} = \frac{1}{N}\sum_{j=1}^{N} e^{i\, m\psi_j(t)}, \qquad (1)$$

can be used. $R_m(t)$ and $\Psi_m(t)$ are the corresponding real amplitude and real mean phase, where $0 \leq R_m(t) \leq 1$ for all time t (Daido 1992; Tass 1999). Cluster variables are convenient for characterizing synchronized states of

different types: Perfect in-phase synchronization corresponds to $R_1 = 1$, whereas an incoherent state, with uniformly distributed phases, is associated with $R_m = 0$, $m = 1, 2, 3, \ldots$ Small values of R_1 combined with large values of R_m are indicative of an m-cluster state consisting of m distinct and equally spaced clusters, where all oscillators within the same cluster have similar phases. In Fig. 3b, for instance, $R_1 \approx 0.02$, whereas $R_4 \approx 0.87$, indicating a four-cluster state induced by CR stimulation administered via four stimulation sites as in Fig. 3a.

From the cluster state the neurons typically relax to a uniformly desynchronized state (Fig. 3c) before they revert back to the in-phase synchronized state, if left unperturbed. To understand how a stimulus-induced clustering leads to an effective desynchronization, the dynamics of the leading modes $Z_1, Z_2, \ldots$, can be considered. When the coupling among oscillators becomes sufficiently large, e.g., it exceeds a certain critical value, Z_1 from (Eq. 1) becomes an *order parameter* (Kuramoto 1984), which according to the slaving principle (Haken 1983) governs the dynamics of the other stable modes Z_m ($m = 2, 3, \ldots$) on the center manifold (Pliss 1964): The order parameter Z_1 acts on a slow time scale, whereas the stable modes Z_m act on a fast time scale and relax to values given by the order parameter Z_1 (Wunderlin and Haken 1975; Haken 1983). In a system with a large number of oscillators this relationship reads (Tass 1999):

$$R_m \propto R_1^v \quad \text{with} \quad v \geq 2, \qquad m = 2, 3, 4, \ldots \tag{2}$$

Hence, to maintain a desynchronized neuronal firing, CR stimuli have to be administered repetitively.

CR stimulation exploits transient responses which are due to the oscillators' (pathologically strong) interactions. The general stimulation protocol of the intermittent CR stimulation is illustrated in Fig. 4. Here, the collective dynamics is

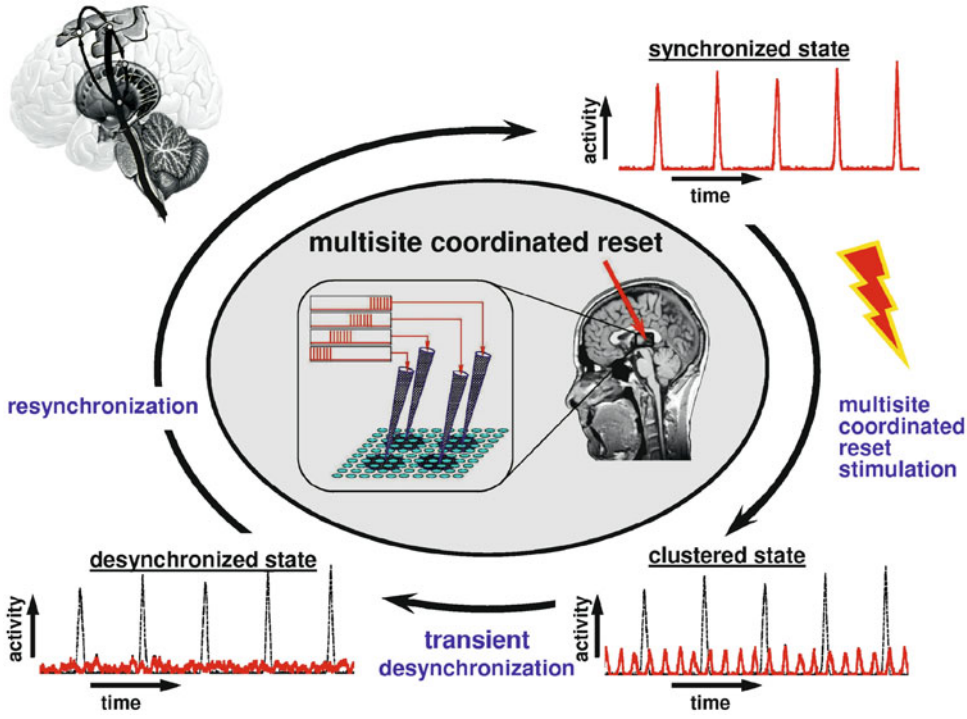

Brain Pacemaker, Fig. 4 A general scheme of the intermittent CR stimulation. Desynchronized firing of neurons is maintained by repetitive administration of CR stimuli intermingled with epochs of no stimulation

visualized by considering the collective firing of the neurons. A single firing/bursting model neuron fires/bursts whenever its phase is close to zero (modulo 2π) (Kuramoto 1984; Ermentrout and Kopell 1991; Grannan et al. 1993; Hansel et al. 1993a; Tass 1999). The collective firing can be illustrated with the *relative number of neurons producing an action potential or burst* at time t given by

$$n_{\mathrm{fire}}(t) = \frac{\text{number of neurons with } \cos\psi_j > 0.99}{N}. \tag{3}$$

$0 \leq n_{\mathrm{fire}}(t) \leq 1$ for all t. $n_{\mathrm{fire}}(t) = 0$ means that no neuron fires/bursts, while all neurons fire/burst at time t if $n_{\mathrm{fire}}(t) = 1$. Varying the threshold parameter 0.99 in a reasonable range does not change the results. As shown in Fig. 4, stimulation starts when the neurons are synchronized and the collective firing demonstrates high-amplitude rhythmic oscillations (upper-right insert in Fig. 4). After a few periods of stimulation the oscillatory population is set to a cluster state (bottom-right insert in Fig. 4). Then the stimulation is switched off and the ensemble returns to a synchronized state, on this way running through a uniformly desynchronized state (bottom-left insert in Fig. 4). And the procedure is repeated such that the ensemble is kept in a transient desynchronized state. The relaxation to a clustered state is due to the system being attracted by the center manifold as characterized by Eq. 2. By imposing a cluster state, the stimulation does only half of the desynchronizing work. The rest, namely approaching a uniformly desynchronized state, is done by the system itself. In this way the coupling, which causes the synchronization, is used for improving the desynchronizing effect. In the course of the post-stimulus transient R_1 and according to Eq. 2 also R_2, R_3, ... recover again. The system finally reaches its stable in-phase synchronized state again. In summary, by shifting the system into an unstable cluster state, the system reacts by automatically running through a desynchronized state. Finally, the system reverts back to the synchronized state, if left unperturbed.

The effectively desynchronizing intermittent CR stimulation can be used to block the resynchronization. For this, the repetitive stimulus administration can be organized either regardless of the state of the stimulated ensemble (open-loop control) or in a demand-controlled way (closed-loop control), where the following three different control strategies can be utilized:

(i) *Periodic administration of CR stimuli*: The most simple, open-loop type of stimulation is a periodic administration of CR stimuli. Here the time intervals of fixed length of CR stimulation (ON cycles) alternate with time intervals of fixed length where the stimulation is switched off (OFF cycles).

(ii) *Demand-controlled timing of the administration of identical stimuli*: Whenever the population tends to resynchronize, the same stimulus is administered (Fig. 5). The stronger synchronization among the neurons is, the more often a stimulus has to be administered to maintain an uncorrelated firing. In addition, for an ideal performance in an experimental application one has to observe the synchronized oscillation during a sufficiently long period of time in order to perform a frequency analysis which yields the period T of the population in the absence of stimulation and, thus, the critical stimulation parameter τ (the time delay between the two successive HF pulse trains administered via different stimulation sites, see Fig. 3). Moreover, instead of performing such a calibration of, pre-set values of can be used by adapting the latter to the typical frequency range of the pathological oscillation (see, e.g., Tass et al. 2012b).

(iii) *Periodically administered HF pulse trains of demand-controlled length*: The stimuli are periodically administered with offset times $t_k = kvT$, where $k = 0, 1, 2, 3, \ldots$ is the index labeling the different stimuli, $T = \tilde{T} + \varepsilon$ is a time interval in the range of the period $\tilde{T}$ of the population without stimulation, and v is a small integer such as 2 or 3. This means that a 1:v entrainment of the four sub-populations is performed, where the spontaneous

frequency of the neurons is approximately v times larger compared to the frequency of stimulus administration. The smaller $|\varepsilon|$, the smaller is the stimulation strength necessary to achieve an entrainment.

The closed-loop variants (*ii*) and (*iii*) require that the ensemble's activity or at least a quantity representing the extent of synchronization can be measured appropriately. Here, either the start times of identical CR stimuli or the length of periodically administered stimuli are calculated from the values of R_1. For example, in the case (*ii*) the stimulation is started if R_1 becomes larger than a certain threshold (Fig. 5, upper two plots), whereas in the case (*iii*) the stimulation period is longer for larger values of R_1 measured at the onset of the stimulation (Fig. 5, bottom two plots). In the latter case the length of the HF pulse trains increases linearly between a minimal value $M_{\min}$ and a maximal value $M_{\max}$ of single-pulses (except for rounding), where the latter is initially used for desynchronizing the fully synchronized population. R_1 is measured at (or, in practice, close to) times $t'_k = t_k - t_{\max}$ where $t_{\max}$ the maximal duration of a HF pulse train (containing $M_{\max}$ single-pulses). $R_1(t'_k)$ determines the number of pulses of the HF pulse trains administered via each of the stimulation sites of the kth stimulus according to

$$M_k = \min\left\{\left[\frac{R_1(t'_k)(M_{\max} - M_{\min})}{R_1(t_0)}\right]_{\mathbb{Z}} + M_{\min}, M_{\max}\right\}, \tag{4}$$

where $k = 0, 1, 2, 3, \ldots$, $[x]_{\mathbb{Z}}$ stands for rounding x to the nearest integer, and min $\{x_1, x_2\}$ stands for the minimum of $\{x_1, x_2\}$. The kth stimulus ends precisely at time $t_k = kvT$, whereas it starts somewhere between t'_k (for $M_k = M_{\max}$) and t_k (for $M_k = M_{\min} = 0$), depending on its duration. If the suppression of R_1 is not sufficient one may (i) choose a larger intensity of

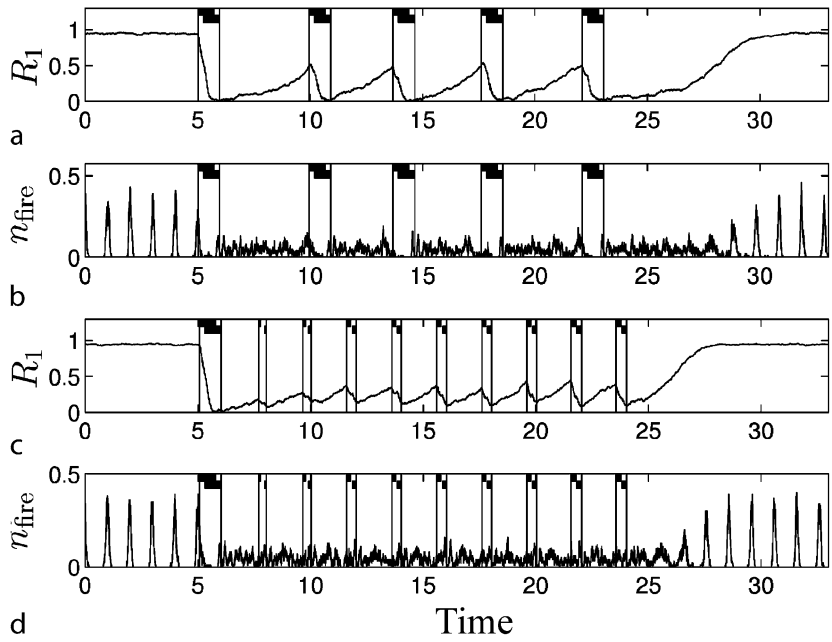

Brain Pacemaker, Fig. 5 Desynchronizing effect of the demand-controlled intermittent CR stimulation. Time course of R_1 from Eq. 1 (**a** and **c**) and of n_{fire} from Eq. 3 (**b** and **d**) during different types of stimulation. *Demand-controlled timing of stimulus administration* (**a** and **b**): As soon as the amplitude R_1 of the recovering order parameter reaches the value of 0.5, the stimulus is administered again. *Periodical stimulation with demand-controlled length of HF pulse train* (**c** and **d**): The stimulus is administered periodically, where the length of the HF pulse trains is adapted to R_1 according to Eq. 4 with $M_{\max} = 15$ and $M_{\min} = 0$. First published in Tass (2003b)

stimulation, (ii) increase $M_{\min}$, (iii) administer the stimuli at a higher rate, i.e. decrease ν, so that the inter-stimulus interval $t_{k+1} - t_k = \nu T$ gets smaller, (iv) increase the duration of each single pulse of the pulse trains and/or increase the intra-burst frequency of the pulse trains (i.e., bursts). The feedback value of R_1 can also be evaluated before time t'_k, especially in case of a slow order parameter dynamics (i.e., when the synchronization is weak with respect to the noise). One could also use the mean of R_1 in a period of evaluation.

Applying the standard, permanent HF stimulation (Benabid et al. 1991; Blond et al. 1992) (in a first approximation) corresponds to stimulating each neuron with the same HF pulse train. During a permanent HF stimulation a high-frequency entrainment of the order parameter Z_1 captures Z_1 in a small portion of the complex plane (Tass 2001c), so that the individual neurons' firing is stopped, but no desynchronization occurs. In contrast, during stimulation R_1 can be even larger compared to its pre-stimulus level, and after stimulation the synchronous firing continues immediately. To suppress the firing with such a simple pulse train persistently, it has to be administered permanently. The number of single pulses used to suppress the firing in the case of the standard permanent HF pulse train stimulation is about five to eight times larger than that used for blocking the resynchronization in Fig. 5a–d, respectively. This illustrates the effectiveness of the demand-controlled CR stimulation. The latter can effectively desynchronize stimulated oscillators with a significantly smaller amount of stimulation current compared to the standard permanent HF pulse-train stimulation.

The efficacy of CR stimulation can further be improved by an optimal choice of stimulation parameters. Several computational studies on neuronal models of different complexity have addressed this problem and showed that the intermittent m: n ON–OFF CR stimulation, where m cycles with stimulation ON are recurrently followed by n cycles with stimulation OFF, is most effective for a weak stimulation intensity and short ON intervals (Lysyansky et al. 2011a). The stimulation-induced cluster state leads to the longest desynchronizing post-stimulation transient which can further be prolonged for non-uniform timing of the stimuli onsets (Luecken et al. 2013). The number of stimulation sites is another important stimulation parameter, and its optimal choice essentially depends on the properties of the neuronal tissue (Lysyansky et al. 2013). For a weak (strong) spatial decay rate of the stimulation current with distance to the stimulation site, CR stimulation can optimally be delivered via small (large) number of stimulation sites.

The theoretical findings on the properties of CR stimulation have been verified experimentally. The resetting impact and the induced transient desynchronization of an electrical short-pulse stimulation, on which the CR technique is based, have been reported *in vivo* for coupled neuronal bursters in paddle fish (Neiman et al. 2007). Taking into account the spike timing-dependent synaptic plasticity (see section "Plasticity"), the long-lasting desynchronizing effects of CR stimulation have been investigated in detail in theoretical studies (Tass and Majtanik 2006; Tass and Hauptmann 2006, 2007; Hauptmann and Tass 2007), and the results have been confirmed experimentally *in vitro* in rat hippocampal slice (Tass et al. 2009). The beneficial therapeutic long-lasting aftereffects of weak CR stimulation have been observed in the 1-methyl-4-phenyl-1,2,3,6-tetrahydropyridine (MPTP)-treated macaque monkeys in contrast to a stronger CR stimulation and to the standard HF DBS (Tass et al. 2012b).

Modeling shows that CR stimulation can be effective for a number of stimulation setups and demonstrate a great applicability. Based on a computational study, CR stimulation has been suggested for counteraction of cerebral hypoactivity, in particular, to activate hypo-active or inactive neuronal populations found in a number of diseases without promoting pathological synchronization by a multi-frequency and phase-shifted activation of the stimulated neuronal networks (Lysyansky et al. 2011b). Other computational studies showed that CR stimulation can be effective in inducing desynchronization for direct somatic stimulation and as well as for excitatory or inhibitory synaptically meditated stimulation (Popovych and Tass 2012). The latter stimulation

setup might correspond to stimulation of afferent or efferent fibers or sensory stimulation where the stimulation signals arrive at the neural target population as post-synaptic potentials. Sensory CR stimulation has been suggested for suppression of the neural synchrony underlying tinnitus (Tass and Popovych 2012) and successively verified in a clinical proof of concept study in tinnitus patients treated with non-invasive acoustic CR stimulation (Tass et al. 2012a; Silchenko et al. 2013; Adamchic et al. 2013).

Multisite Linear Delayed Feedback

Similarly as in the case of CR stimulation, multisite linear delayed feedback (MLDF) (Hauptmann et al. 2005a, b, c, 2007a) is administered via several stimulation sites, e.g., via four sites as illustrated in Fig. 3a. The individual stimulation signals $S_m(t)$ of each of the stimulation sites are however derived from the delayed mean field $Z(t)$ of the stimulated ensemble using different time delays for different stimulation signals. The mean field characterizes the collective macroscopic dynamics of the oscillators and can be viewed as the ensemble average of the signals $z_j(t)$, $j = 1, \ldots, N$, of individual oscillators, $Z(t) = N^{-1} \sum_{j=1}^{N} z_j(t)$.

For n stimulation sites, the stimulation signals are calculated as $S_m(t) = KZ(t - \tau_m)$, $m = 1, \ldots, n$, where K is the amplification parameter, and the values of delay τ_m, for example, for $n = 4$ are calculated from the following relation:

$$\tau_m = \frac{11 - 2(m-1)}{8}\tau, \quad m = 1, 2, 3, 4. \qquad (5)$$

The delays τ_m are symmetrically distributed with respect to the main delay τ, where the smallest time delay between neighboring stimulation sites is chosen as $\tau/4$. In the case $\tau = T$ (mean period of the ensemble), the delays τ_m are uniformly distributed over the mean period T. In another realization, instead of four delays τ_m, $m = 1, \ldots, 4$ one can use only two of them, e.g., τ_1 and τ_2. One can put $\tau_3 = \tau_1$ and $\tau_4 = \tau_2$, where the polarity of the stimulation signals $S_3(t)$ and $S_4(t)$ is reversed: $S_3(t) = -S_1(t)$ and $S_4(t) = -S_2(t)$. Assuming that the mean field of the ensemble uniformly oscillates with period $T = \tau$, the alternating polarity of the signal corresponds to a shift in time by half a period. Therefore, under this condition the stimulation signal $S_3(t) = -S_1(t) = -KZ(t - \tau_1)$ approximates the stimulation signal $S_1(t + \tau/2)$ which is shifted in time by half of the period, which, in turn, is equal to $KZ(t - \tau_3)$, where τ_3 is calculated according to Eq. 5. Analogous arguments are applicable to the stimulation signal $S_4(t) = -S_2(t) = -KZ(t - \tau_2)$.

If the phase $\Psi(t)$ of the mean field $Z(t)$ (see also Z_1 from Eq. 1) uniformly rotates with a constant frequency $\Omega = 2\pi/\tau$, the phases $\Phi_m(t) = \Psi(t - \tau_m)$ of the stimulation signals $S_m(t)$ are distributed uniformly over the unit circle as illustrated in Fig. 6a. Then the phases $\psi_j(t)$ of the stimulated neuronal subpopulation assigned to the stimulation site m are attracted to the phase $\Psi(t - \tau_m)$ of the corresponding stimulation signal. Hence, the phases of all oscillators stimulated with MLDF become symmetrically redistributed on the circle $(0, 2\pi)$ in a cluster state. The order parameter $R_1(t)$ thus gets minimized. Depending on the value of delay τ, the stimulation can induce different clustered states in the stimulated ensemble, where the corresponding order parameter R_m attains large values.

As shown in Fig. 6b, c, the in-phase synchronization in the stimulated ensemble is effectively suppressed (for time $t > 200$, where both coupling and stimulation are switched on), where the order parameter $R_1 = |Z_1(t)|$ from Eq. 1 attains small values (Fig. 6b, c, *red curve*). This indicates a symmetrical redistribution of the oscillator phases $\psi_j(t)$ over the unit circle. For the parameter τ close to the mean period T of the stimulation-free ensemble a four cluster state is induced by the stimulation, where the order parameters R_1 and R_2 are small, whereas R_4 is relatively large (Fig. 6b). In the subplot, where four trajectories from each of the stimulated subpopulations are depicted, the emerging four-cluster state induced by MLDF is illustrated. For τ closer to, for example, $2T$ the stimulation

induces a two-cluster state, where R_1 is small, whereas R_2 and R_4 are large (Fig. 6c). The oscillators thus split into two clusters, which is also illustrated in the subplot in Fig. 6c.

MLDF robustly suppresses the in-phase synchronization as shown in Fig. 7a, where the time-averaged order parameter $\langle R_1 \rangle$ attains small values for a broad range of parameters τ and K. On the other hand, depending on system and stimulation parameters, MLDF can induce either a two-cluster state, where the second order parameter R_2 attains relatively large values (e.g., for $\tau \approx 2T$, see Fig. 7b), or a four-cluster state, where R_2 becomes small and the fourth order parameter R_4 increases (e.g., for $\tau \approx T$, see Fig. 7c). Therefore, the whole stimulated population is divided into two or four distinct sub-populations. Within the phase clusters the individual oscillators have phases close to each other, while the different phase clusters are equidistantly distributed within the cycle. Hence, depending on the values of the parameters τ and K, MLDF with four stimulation sites may cause either a two-cluster state, where R_1 is close to zero and R_2 is large, or a four-cluster state, where both R_1 and R_2 are small, but R_4 is large. The cluster states become less pronounced and the phases redistribute on the circle even more uniformly if a local coupling as well as spatially decaying profile of the current spread is taken into account (Hauptmann et al. 2005a).

In Fig. 7d a similar two-parameter diagram for the averaged order parameter $R_1(t)$ is presented for a *single-site linear delayed feedback* (SLDF) suggested for synchronization control in references (Rosenblum and Pikovsky 2004a, b). The stimulation is performed via one stimulation electrode in such a way that all oscillators of the

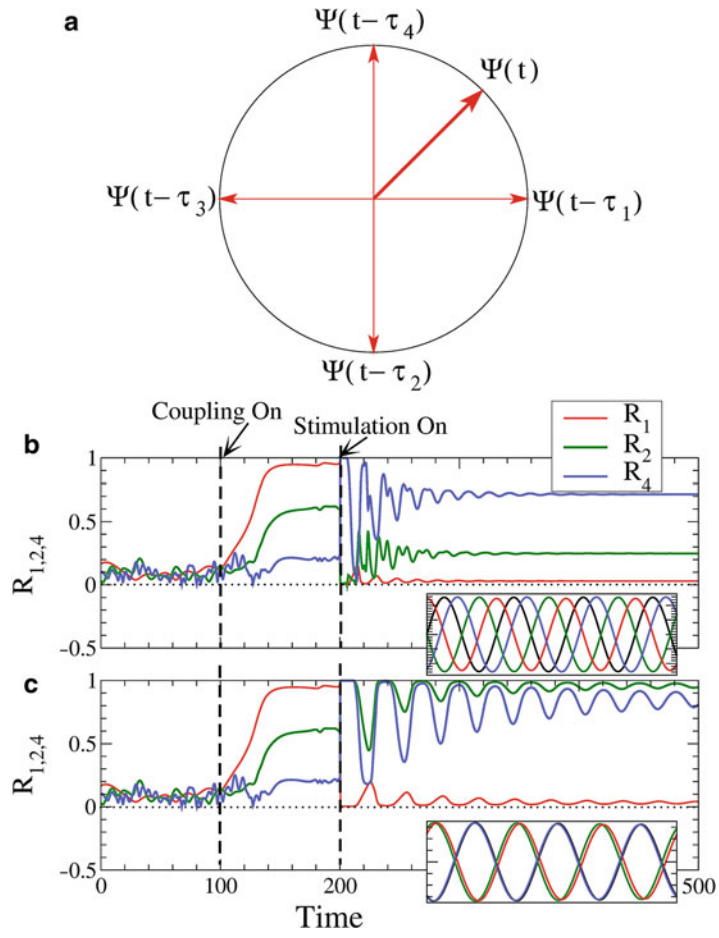

Brain Pacemaker, Fig. 6 Control of synchronization by multisite linear delayed feedback (MLDF) stimulation. (**a**) Distribution of the phases $\Phi_m(t)$ of the stimulation signals $S_m(t)$ administered via four stimulation sites (as in Fig. 3a), which are the delayed mean phase, $\Phi_m(t) = \Psi(t - \tau_m)$, with delays τ_m from Eq. 5 for $\tau = T$. (**b** and **c**) Time courses of the amplitudes of the cluster variables (Eq. 1), the order parameters R_1, R_2 and R_4. In the subplots four trajectories from each of four stimulated sub-populations assigned to each of four different stimulation sites are shown for $t \in (320,340)$. Parameter $\tau = T$ in (**b**) and $\tau = 2T$ in (**c**)

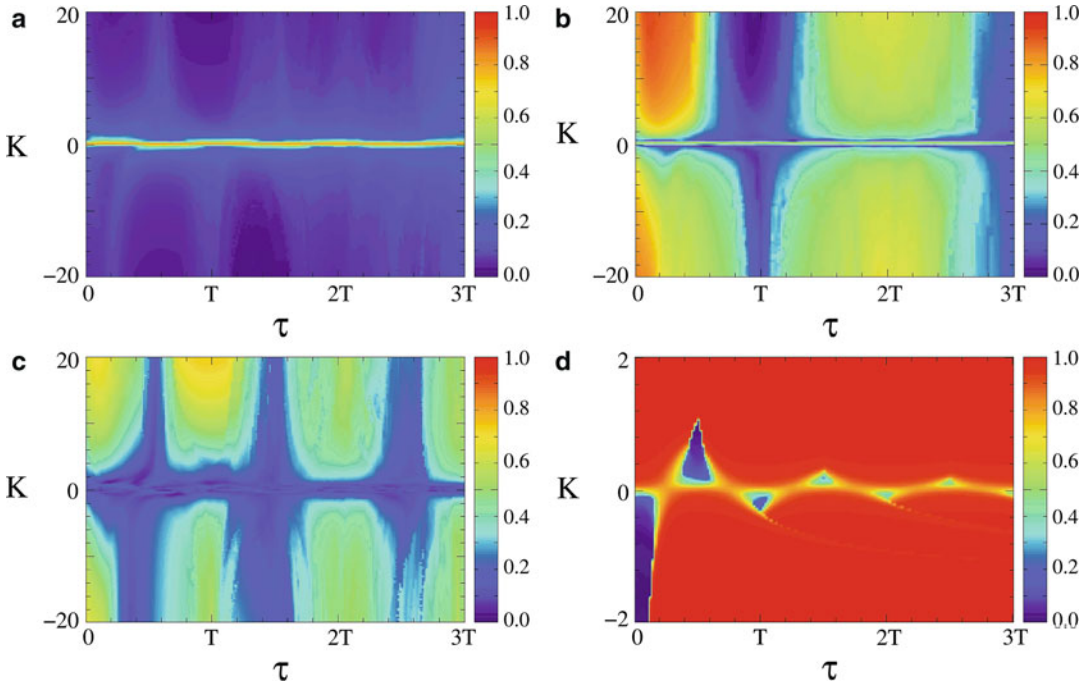

Brain Pacemaker, Fig. 7 Impact of the MLDF stimulation versus parameters τ and stimulus amplification K. The time-averaged order parameters $\langle R_1 \rangle$, $\langle R_2 \rangle$, and $\langle R_4 \rangle$ are depicted in plots (**a–c**), respectively, and encoded in color ranging from 0 (*blue*) to 1 (*red*). In plot (**d**) the impact of the single-site linear delayed feedback (SLDF) on the oscillatory population is illustrated, where the values of the order parameter $\langle R_1 \rangle$ are depicted in color versus parameters τ and K (First published in Popovych et al. (2006a))

ensemble (in the first approximation) receive the same stimulation signal $S(t)$. In this case the stimulation signal $S(t)$ attains the form $S(t) = KZ(t - \tau)$. For the stimulation with SLDF, in the corresponding two-parameter diagram (Fig. 7d) islands of perfect desynchronization are complemented by areas of stimulation-enhanced synchronization. In the limit $N \to \infty$ the order parameter $R_1 = 0$ in the desynchronization regions, where the phases are uniformly distributed on the circle $(0, 2\pi)$ (Rosenblum and Pikovsky 2004a, b). This is the state of complete desynchronization, where the stimulated oscillators rotate with different frequencies indicating an absence of any clustered state whatsoever. The island-like structure of desynchronization regions in parameter space of SLDF (Fig. 7d) was also experimentally confirmed for arrays of coupled electrochemical oscillators (Zhai et al. 2008).

The important property of the stimulation with the multi- and single-site linear delayed feedback is the inherit demand-controlled character of the methods. As soon as the desired desynchronized state is achieved, the values of the order parameter $R_1(t)$, i.e., the amplitude of the mean field become small. Along with the order parameter, in the desynchronized state the amplitude of the stimulation signal $S(t)$ vanishes as well. The stimulation with multi- and single-site linear delayed feedback thus represents noninvasive control methods for desynchronization of coupled oscillators. The stimulated ensemble is then subjected to a highly effective control at a minimal amount of stimulation force.

Nonlinear Delayed Feedback

As for the case of the single-site linear delayed feedback, for the stimulation with nonlinear delayed feedback (NDF) only one registering and one stimulating site is required, see Fig. 8a. All stimulated oscillators receive the same stimulation signal $S(t)$ which is constructed from the

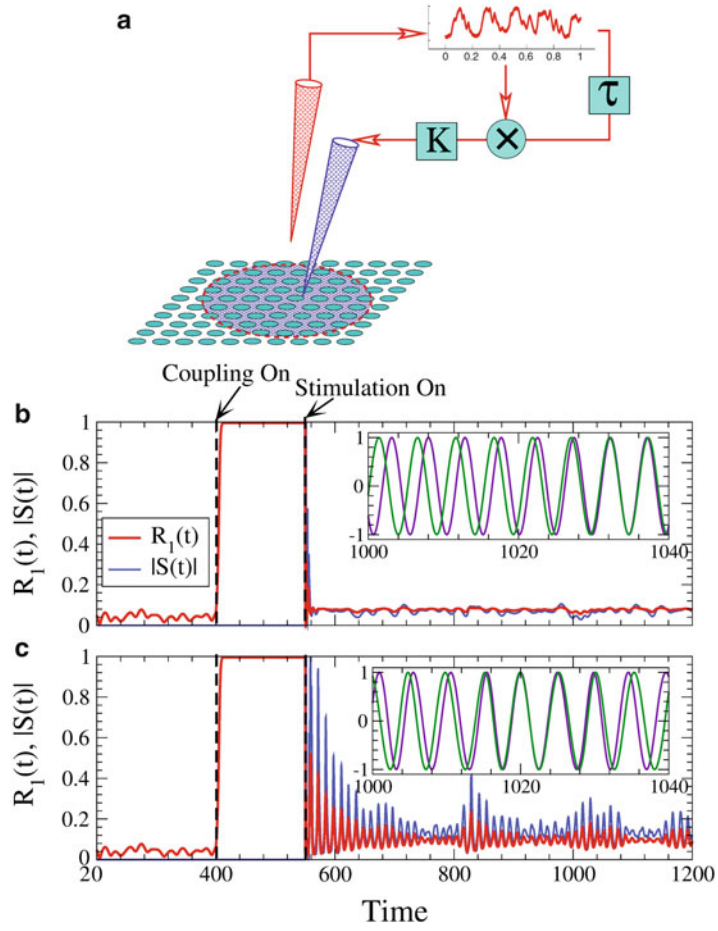

Brain Pacemaker, Fig. 8 Control of synchronization by nonlinear delayed feedback (NDF) stimulation. (**a**) The macroscopic activity (mean field) of the controlled population is measured, delayed, nonlinearly combined with the instantaneous mean field, amplified, and fed back via a single stimulation site. (**b** and **c**) Desynchronization of strongly synchronized oscillators by NDF. Time courses of the order parameter $R_1(t)$ (*red curves*) and the amplitude of the stimulation signal $|S(t)|$ (*blue curves*) are plotted for delay (**b**) $\tau = T/2$ and (**c**) $\tau = T$, where T is the mean period of the stimulation-free ensemble. In the subplots trajectories of two selected oscillators are depicted in the stimulated regime (First published in Popovych et al. (2008))

measured mean field of the ensemble. It is assumed that the measured mean field $Z(t)$ of the ensemble has the form of a complex analytic signal $Z(t) = X(t) + iY(t)$, where $X(t)$ and $Y(t)$ are the real and imaginary parts of $Z(t)$, respectively. If only a real part $X(t)$ of the mean field is measured, the imaginary part can be calculated, e.g., with the help of the Hilbert transform (Pikovsky et al. 2001). The stimulation signal is then constructed by a nonlinear combination of a delayed complex conjugate mean field with the instantaneous mean field (Popovych et al. 2005, 2006a, b; Tass et al. 2006),

$$S(t) = KZ^2(t)Z(t-\tau), \tag{6}$$

where K is a stimulus amplification parameter, τ is a time delay, and the asterisk denotes complex conjugacy.

The desynchronizing effect of the stimulation with NDF is illustrated in Fig. 8b, c. The onset of stimulation at $t = 550$ results in desynchronization of the stimulated oscillators and the order parameter $R_1(t)$ reaches the values of approximately the same order of magnitude as in the uncoupled regime ($t < 400$). This indicates a high level of desynchronization. The stimulation does not destroy the normal oscillatory activity of the individual oscillators. In the insets in Fig. 8b, c individual trajectories of two selected oscillators of stimulated ensemble are plotted. The stimulated oscillators rotate with different individual frequencies just as in the coupling- and stimulation-free regime.

As soon as a desynchronized state is achieved, the stimulation force declines and the stimulated system is subjected to a highly effective control with a minimal amount of stimulation force. Also,

as soon as a resynchronization occurs, the mean field starts to exhibit large-amplitude oscillations and the stimulation signal increases its amplitude and brings the ensemble back to a desynchronized state. This demand-controlled character of the nonlinear delayed feedback is illustrated in Fig. 8c where the onsets of resynchronization (increase of $R_1(t)$, *red curve*) at times around $t \approx 850$, 1,050, and 1,200 lead to an increase of the amplitude of the stimulation signal $|S(t)|$ (*blue curve*), which in turn results in a suppression of the resynchronization.

The impact of the nonlinear delayed feedback on the stimulated oscillators is twofold. On one hand, the stimulation can effectively desynchronize even strongly interacting oscillators for a large range of the stimulus amplification K, see Fig. 9a. This effect is very robust with respect to the variation of the delay τ and, as a result, with respect to the variation of the mean frequency Ω of the stimulated ensemble. On the other hand, in a weakly coupled ensemble the stimulation can induce synchronization in island-like regions of small values of the stimulus amplification K complemented by domains of desynchronization, see Fig. 9b.

An increase of the stimulus amplification parameter K results in a gradual decay of the order parameter R_1 for both strongly and weakly coupled oscillators, which indicates an onset of desynchronization in the stimulated ensemble. Simultaneously, the amplitude of the stimulation signal $|S(t)|$ decays as well, indicating the demand-controlled character of the nonlinear delayed feedback stimulation. For a fixed delay $\tau > 0$ the order parameter and the amplitude of the stimulation signal decay as $|K|$ increases according to the following power law (Fig. 10a):

$$R_1 \sim |K|^{-1/2}, \qquad |S| \sim |K|^{-1/2}. \tag{7}$$

The desynchronization transition for increasing K also manifests itself in a sequence of frequency-splitting bifurcations, where the observed individual frequencies $\overline{\omega}_j = \left\langle \dot{\psi}_j \right\rangle$ of the stimulated oscillators split, one after another from the mean frequency Ω as K increases (Fig. 10b) and approach the natural frequencies of the unperturbed oscillators (Fig. 10b, *blue diamonds*). For large values of K all stimulated oscillators rotate with different frequencies close to the natural frequencies ω_j. The oscillators thus exhibit a uniform desynchronous dynamics without any kind of cluster states. In addition, depending on the values of the delay τ, the nonlinear delayed feedback can significantly change the mean frequency Ω, i.e., the frequency of the mean field $Z(t)$ of the stimulated ensemble (Popovych et al. 2005, 2006a). The macroscopic dynamics can thus be either accelerated or slowed down, whereas the individual dynamics remains close to the original one. This opens an approach for the frequency control of the oscillatory population stimulated with the nonlinear delayed feedback.

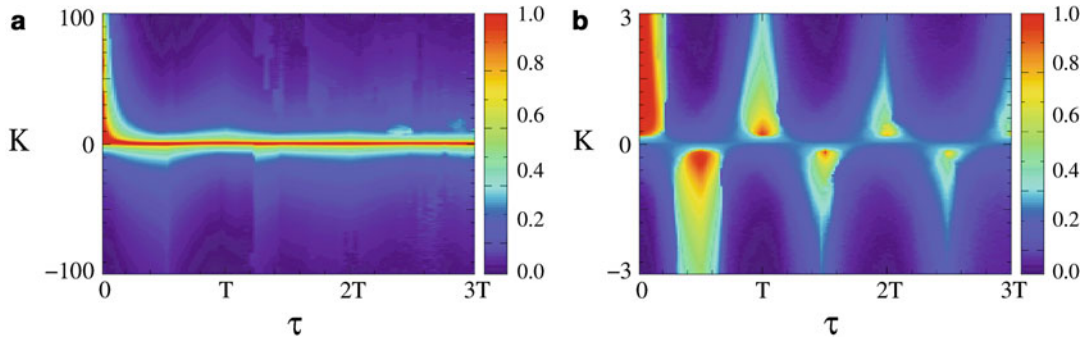

Brain Pacemaker, Fig. 9 Robustness of the NDF effects. (**a**) Stimulation-induced desynchronization and (**b**) stimulation-induced synchronization in ensembles of (**a**) strongly coupled and (**b**) weakly coupled oscillators. The time-averaged values of the order parameter R_1 are encoded in color ranging from *red* (synchronization) to *blue* (desynchronization) versus delay τ and stimulus amplification K

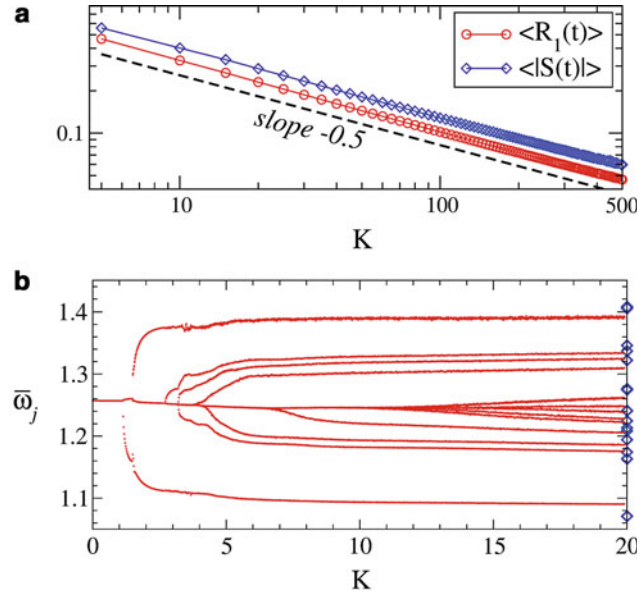

Brain Pacemaker, Fig. 10 Impact of NDF as the stimulus amplification K increases. (**a**) Log–log plot of the time-averaged order parameter R_1 and amplitude of the stimulation signal $|S(t)|$ versus K. The *dashed line* has the slope −0.5 and is given for comparison. (**b**) The observed individual frequencies $\overline{\omega}_j$ of the stimulated oscillators versus K. *Blue diamonds* at the right vertical axis depict values of the natural frequencies of the oscillators (First published in Popovych et al. (2006a))

Mixed Nonlinear Delayed Feedback

The NDF method can also be applied for desynchronization and decoupling of two (or more) interacting oscillator populations. For this, the mixed NDF can be used (Popovych and Tass 2010), see Fig. 11a. For a drive-response coupling scheme, the coupling within population 2 is assumed to be weak, so that, being isolated from population 1, no synchronization emerges in population 2. In contrast, the coupling in population 1 is strong enough to cause synchronization within population 1. It then drives the second population, which synchronizes because of the driving and sends a response signal back to population 1. The second ensemble is stimulated with signal $S(t)$, which is constructed from the mixed mean field Z_ε according to the rule of NDF from Eq. 6. The mixed mean field $Z_\varepsilon = \varepsilon W_1 + (1 - \varepsilon)W_2$ is a linear combination of the mean fields W_1 and W_2 of populations 1 and 2, respectively.

The level of mixing of the mean fields W_1 and W_2 within the stimulation signal is given by the parameter ε. Depending on it the mixed NDF can have different desynchronizing effects on populations 1 and 2.

- *Small* ε: mostly population 2 contributes to the stimulation signal. The mixed NDF desynchronizes the driven and stimulated population 2 (Fig. 11b), but the driving ensemble 1 remains unaffected and exhibits strongly synchronized dynamics (Fig. 11c). The populations get effectively decoupled from each other.
- *Intermediate* ε: both populations equally contribute to the stimulation signal. Both ensembles remain synchronized (Fig. 11b, c).
- *Large* ε: mostly population 1 contributes to the stimulation signal. Both ensembles are effectively desynchronized by the mixed NDF (Fig. 11b, c).

In the latter case the desynchronization induced by the mixed NDF in the driven and stimulated population 2 propagates to the drive population 1 which is not directly stimulated. This is indicative of an indirect control of synchronization by the mixed NDF.

Proportional–Integro–Differential Feedback

For a particularly difficult situation, where the measurement and stimulation are not possible at the same time and at the same place, there is another control method which is based on a proportional–integro–differential feedback (PIDF). The scheme of this stimulation protocol is sketched in Fig. 12a, see also Fig. 11a for $\varepsilon = 1$ except for the

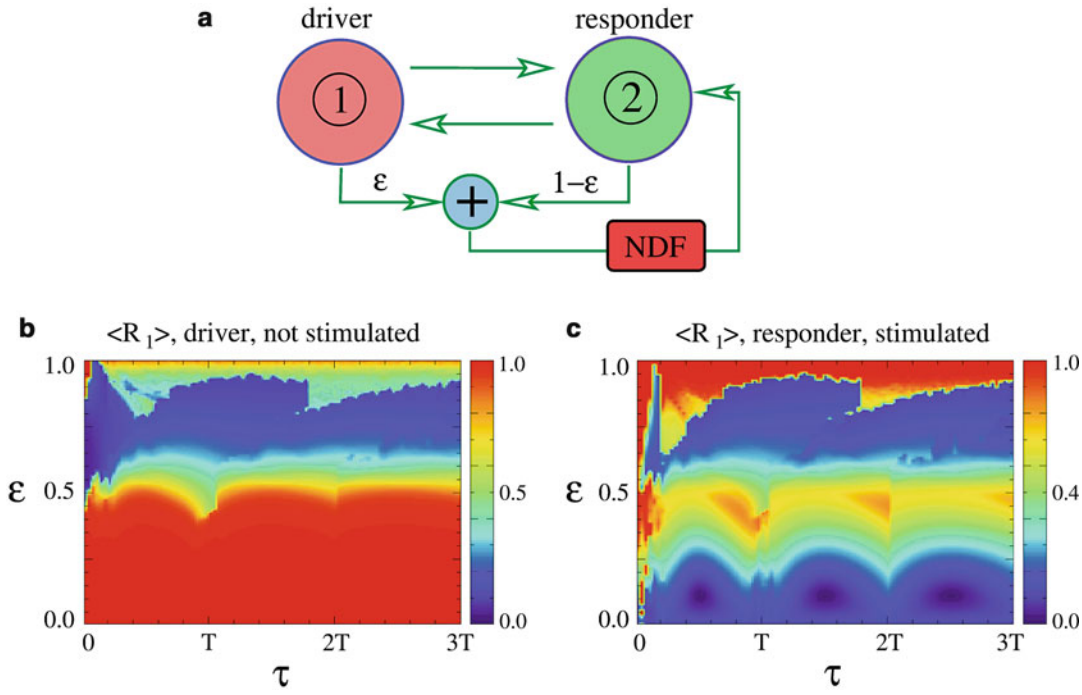

Brain Pacemaker, Fig. 11 Desynchronization and decoupling of interacting populations by the mixed NDF. (**a**) Stimulation setup: The measured mean fields of populations 1 and 2 is linearly combined into a mixed mean field, processed by the NDF algorithm (Eq. 6), and fed back to the target population 2. (**b** and **c**) Time-averaged order parameter R_1 of (**b**) intrinsically synchronized, drive population 1 and (**c**) stimulated population 2 driven to synchronization by population 1 versus time delay τ and mixing parameter ε. The *color coding* as in Fig. 9 (First published in Popovych and Tass (2010). Copyright (2010) by the American Physical Society)

measured signal being processed by a PIDF algorithm. The controlled ensemble of N coupled oscillators is divided into two separate sub-populations of N_1 and $N_2 = N - N_1$ oscillators, one being exclusively measured and the other being exclusively stimulated. In this way a separate stimulation-registration setup is realized, where the recording and stimulating sites are spatially separated and the measured signal is not corrupted by stimulation artifacts. The observed signal is considered to be the mean field W_1 of the measured sub-population. Below the main attention will be paid to the proportional-differential (PD) feedback only (for more details, see Pyragas et al. (2007)). Then, the stimulation signal $S(t)$ administered to the second, stimulated sub-population is constructed as

$$S(t) = PW_1(t) + D\dot{W}_1(t), \qquad (8)$$

where the parameters P and D define the strength of the proportional and differential feedback, respectively. The effect of the stimulation with PD feedback is illustrated in Fig. 12b. As the strength of the feedback (parameters P and D) increases the stimulation results in a complete desynchronization of the whole ensemble. The threshold of the onset of desynchronization depends on the relative splitting $N_1 : N_2$ of the oscillators between sub-populations and on the mean frequency Ω: The threshold is larger for smaller number of oscillators N_2 in the stimulated populations or for larger frequency Ω. The later dependence can be eliminated if an integral component is included in the stimulation signal, see Pyragas et al. (2007). Moreover, if the coupling in the ensemble is rather weak, the desynchronization can be achieved by applying the proportional feedback only. In contrast, in the case of strong coupling the stimulation signal additionally requires the differential feedback for robust desynchronization. As illustrated in the two-parameter diagrams in Fig. 12c, d, there exists a certain threshold in parameters P and D values, where the stimulation with PIDF

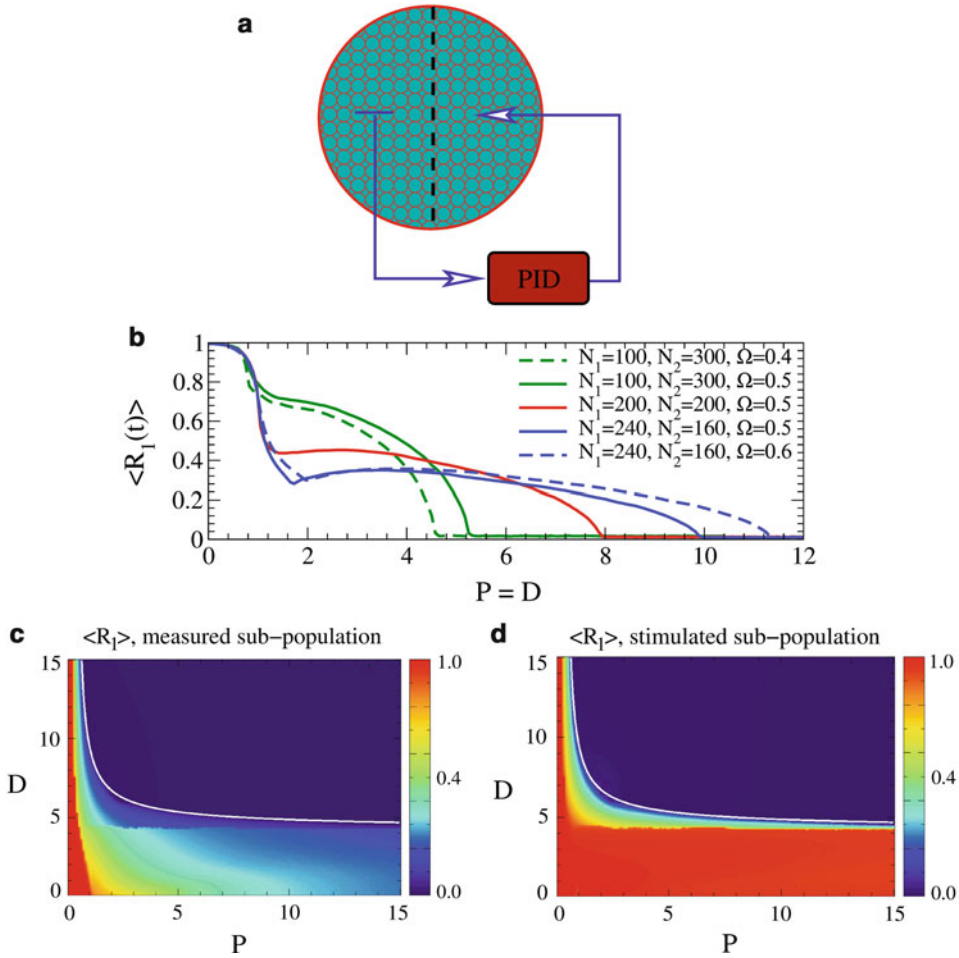

Brain Pacemaker, Fig. 12 PIDF control: (**a**) The mean field is measured in one part of the controlled ensemble and, after processing according to proportional–integro–differential feedback (PIDF) algorithm, is administered to the other part of the ensemble. (**b**) The time-averaged order parameter R_1 of the whole ensemble versus the strength of the PD feedback (with $P = D$) for different splitting $N_1 : N_2$ and different mean frequencies Ω. (**c** and **d**) The time-averaged order parameters R_1 (encoded in *color*) of (**c**) the measured sub-population and (**d**) stimulated sub-population versus stimulation parameters P and D. The *white curve* is the parameter threshold for the onset of desynchronization in the sub-populations (First published in Pyragas et al. (2007). Used with permission from EPL)

desynchronizes both sub-populations in the target ensemble: stimulated sub-population (Fig. 12c) and also measured, non-stimulated sub-population (Fig. 12d). In this sense the PIDF stimulation method appears to be very effective even for a complicated stimulation protocol with a separate stimulation-registration setup.

Plasticity

Plasticity is a fundamental property of the nervous system: In order to learn and to adapt to sensory inputs, neurons continuously adapt the strength of their synaptic connections in relation to the mutual timing properties of their firing or bursting (Hebb 1949; Gerstner et al. 1996; Markram et al. 1997; Debanne et al. 1998; Kilgard and Merzenich 1998; Abbott and Nelson 2000; Feldman 2000; Song et al. 2000; van Hemmen 2001; Zhou et al. 2003). However, plasticity may not only lead to desired learning and optimization processes. Rather neuronal populations can learn pathologically strong interactions which may lead, e.g., to the emergence of epilepsies

(Morimoto et al. 2004; Speckmann and Elger 1991). This is well-known from the so-called kindling phenomenon (Goddar 1967), where preparatory stimulation induces the spontaneous production of epileptic seizures without gross morphological changes (Morimoto et al. 2004).

The impact of plasticity on synaptic weights and collective neuronal dynamics has been accounted for by several theoretical studies on desynchronizing stimulation methods (Tass and Majtanik 2006; Hauptmann and Tass 2007; Tass and Hauptmann 2007; Maistrenko et al. 2007). They have initiated an approach which aims at unlearning pathologically strong synaptic interactions by desynchronizing brain stimulation and which has further been developed in latter papers (Hauptmann and Tass 2009, 2010; Tass and Popovych 2012; Popovych and Tass 2012). This approach exploits plasticity in two different ways: On the one hand, due to plasticity desynchronizing stimulation may decrease the strength of the neurons' synapses by decreasing the rate of coincidences. On the other hand, neuronal networks with synaptic plasticity may exhibit bi- or multistability (Seliger et al. 2002; Tass and Majtanik 2006; Hauptmann and Tass 2007; Tass and Hauptmann 2007; Maistrenko et al. 2007). Accordingly, by decreasing the mean synaptic weight, desynchronizing stimulation may shift a neuronal population from a stable synchronized (pathological) state to a stable desynchronized (healthy) state, where the neuronal population remains thereafter, if left unperturbed. In Fig. 13 an exemplary simulation of a model neural network is displayed, for further details concerning the mathematical model we refer to references (Hauptmann and Tass 2007; Tass and Hauptmann 2007). Induced by appropriate stimulation protocols a switching between the different stable states is realizable. Starting from a desynchronized state, associated with a physiological model dynamics, low-frequency

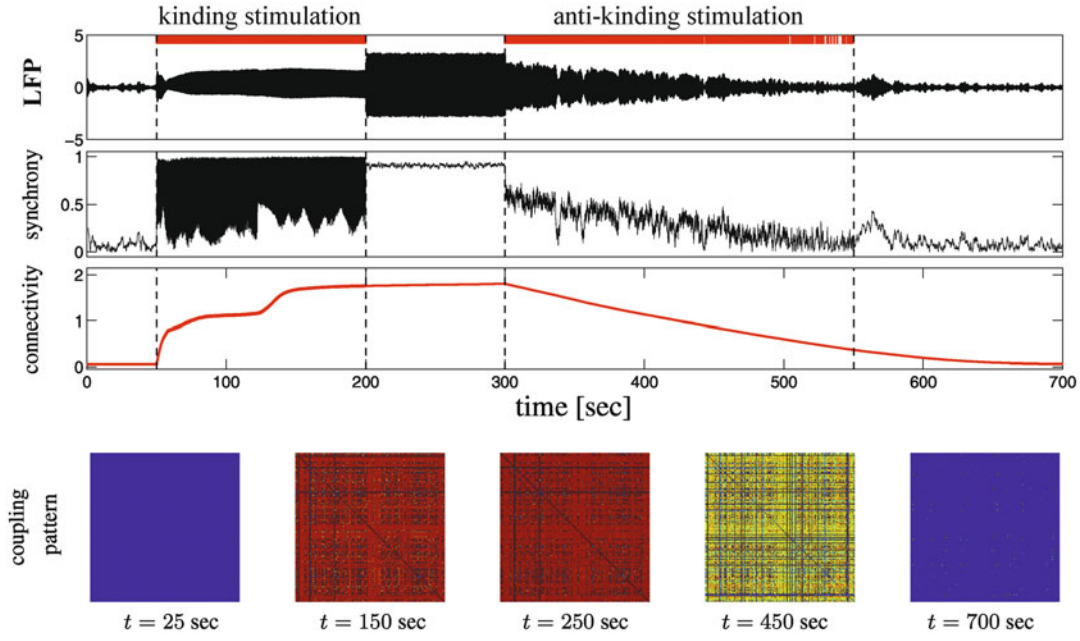

Brain Pacemaker, Fig. 13 Effects of kindling and anti-kindling stimulation on a population of model neurons. Low frequency stimulation is applied between 50 and 200 s, and CR stimulation (see section "Coordinated Reset Stimulation") is applied between 300 and 550 s. The local field potential, the level of synchronization within the network and the mean connectivity is plotted (from top to bottom). Five patterns representing the coupling topology of the network at different times are plotted below. *Blue* (*red*) colors represent low (high) values of the interneuronal connectivity

stimulation can induce a kindling of the synaptic connectivity and causes a stabilization of the synchronized state. After stimulation offset, the system remains in the pathological state (Fig. 13). In contrast, desynchronizing CR stimulation (see section "Coordinated Reset Stimulation") results in an anti-kindling of the pathological connectivity and, finally, the physiological weakly coupled and desynchronized state is reestablished (Fig. 13).

From a mathematical point of view, in a first approximation this situation may be illustrated by considering a double well potential, where each minimum corresponds to a stable attractor, surrounded by a basin of attraction (Fig. 14). The strongly synchronized state (*Pathol.* in Fig. 14) serves as a model for a disease state, whereas the uncorrelated or weakly synchronized state (*Healthy* in Fig. 14) is used as a model for a healthy state. As soon as the system, i.e., the neuronal population (illustrated by the *ball* in Fig. 14), enters a particular basin of attraction, it gets attracted by the corresponding attractor, so that it relaxes towards the corresponding minimum of the potential.

Appropriate stimulation protocols may shift the neuronal population from one state to another. Kindling stimulation of appropriate duration shifts the neuronal population from a desynchronized state close to a strongly synchronized state or at least into the basin of attraction of such a state (Fig. 14a, *red trajectory* from *Healthy* to *Pathol.*). Conversely, anti-kindling can be achieved by means of a desynchronizing stimulation which shifts the neuronal population close to the desynchronized state (Tass and Majtanik 2006; Hauptmann and Tass 2007, 2009, 2010; Tass and Hauptmann 2007; Tass and Popovych 2012; Popovych and Tass 2012) (Fig. 14b, *red trajectory* from *Pathol.* to *Healthy*). However, with respect to the long-term anti-kindling outcome, it is even sufficient to move the neuronal population from the synchronized state just into the basin of attraction of the desynchronized state (Fig. 14c, *red trajectory* from *Pathol.* to the intermediate state). After stimulus offset there may still be pronounced synchrony, but being captured within the basin of attraction of the desynchronized state, without further intervention the neuronal population spontaneously relaxes to the desynchronized state (Fig. 14c, *blue trajectory* from the intermediate state to *Healthy*). Note the short as well as the long desynchronizing stimulation in this schematic illustration have the same long-term anti-kindling outcome.

In PD neuronal populations of the basal ganglia are strongly synchronized (Beurrier et al. 2002; Schnitzler et al. 2006; Timmermann et al. 2007) and synaptic plasticity results in a further

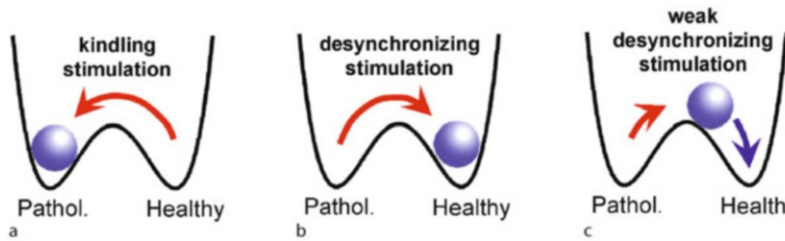

Brain Pacemaker, Fig. 14 Kindling and anti-kindling stimulation can move the neuronal population from one attractor to another: Schematic plot of the attractors symbolizing pathological (*Pathol.*) or healthy (*Healthy*) dynamical model states. (**a**) Periodic, kindling stimulation (*red trajectory*) shifts the population from a healthy, desynchronized state (*Healthy*) to a pathological, synchronized state (*Pathol.*). (**b**) Conversely, desynchronizing stimulation shifts the population from a pathological state (*Pathol.*) to the healthy uncorrelated state (*Healthy*). This anti-kindling is achieved by a desynchronizing stimulation of sufficient duration, so that after stimulus offset the population is close to the healthy state (*red trajectory*). (**c**) Alternatively, the same long-term anti-kindling effect can be achieved with a brief desynchronizing stimulation, which shifts the population to an intermediate state (*red trajectory*), which may still be connected with pronounced synchrony. However, since the intermediate state (*blue ball*) lies within the basin of attraction of a healthy state (*Healthy*) the population spontaneously relaxes to the healthy state without any further intervention (*blue trajectory*)

amplification of the synchronized activity by a strengthening of the synaptic connections (Nowotny et al. 2003). Properly designed electrical stimulation may be used to break this vicious circle and to induce an anti-kindling (Tass and Majtanik 2006; Hauptmann and Tass 2007, 2009, 2010; Tass and Hauptmann 2007; Tass and Popovych 2012; Popovych and Tass 2012), which finally might reestablish the normal level of connectivity, associated with a mostly uncorrelated neuronal activity. In this way a sustained long-lasting desynchronization can be achieved, and therapeutic after-effects can be expected after the cessation of desynchronizing stimulation as predicted computationally (see references above). In parkinsonian MPTP monkeys it was shown that unilateral CR stimulation delivered to the subthalamic nucleus (STN) for only 2 h per day during 5 days leads to significant and sustained therapeutic aftereffects for at least 30 days, while standard 130 Hz DBS has no aftereffects (Tass et al. 2012b).

Closed-Loop DBS

The standard setup of HF DBS assumes an open-loop stimulation protocol, where, after the corresponding parameter calibration, a permanent HF electrical pulse train is administered to the target nucleus without relation to the ongoing neuronal activity (Benabid et al. 1991; Volkmann 2004). Both, clinical studies and modeling studies systematically investigated the influence of stimulation parameters and focused on the optimization of the standard HF DBS via an appropriate parameter calibration (Rizzone et al. 2001; Moro et al. 2002; Rubin and Terman 2004) including a closed-loop optimization setup (Feng et al. 2007a, b).

In monkeys rendered parkinsonian with the neurotoxin MPTP a closed-loop DBS has been tested under acute conditions (Rosin et al. 2011). To this end, a short train (comprising seven pulses at 130 Hz) was delivered through a pair of electrodes located in the GPi at a predetermined, fixed latency (80 ms) following each action potential recorded through an electrode placed in the primary motor cortex (M1). This type of stimulation caused a strong decrease of the firing rate of the pallidal neurons together with a pronounced decrease of the oscillatory neuronal activity at tremor frequency (4–7 Hz) and at double tremor frequency (9–15 Hz) along with an amelioration of the MPTP-induced akinesia. After cessation of this type of closed-loop DBS the initial firing pattern reverted back, i.e., pallidal firing rate and pallidal oscillatory activity attained pre-stimulus levels (Rosin et al. 2011). In contrast, standard continuous 130 Hz DBS caused a less pronounced decrease of the pallidal firing rate, the oscillatory neuronal activity and the amelioration of the akinesia (Rosin et al. 2011).

Another study (Little et al. 2013) confirmed the efficacy of the closed-loop adaptive DBS (aDBS) in PD patients, where the onsets and offsets of HF stimulation were triggered by a threshold crossing by LFP in beta band measured via the same stimulation electrode implanted in STN. The stimulation trigger threshold for the LFP amplitude was heuristically determined in such a way that a reduction of the stimulation time of approximately 50% was achieved while maintaining clinical effect. The onset of HF stimulation was delayed by 30–40 ms after the crossing of the threshold by LFP, and the stimulation was sustained until beta amplitude fell below the threshold again (Little et al. 2013). For the same stimulation intensity and stimulation frequency (130 Hz), the aDBS can be about 30% more effective than standard continuous HF DBS, while less than 50% of the total electrical energy is delivered in the aDBS mode as compared to continuous HF DBS. Moreover, despite of the used fixed beta threshold, the triggered stimulation duration (per 10-s block) progressively drops over time during stimulation in the aDBS mode, which suggests that aDBS may lead to positive adaptive effects in pathological Parkinsonian networks (Little et al. 2013).

Summary

High-frequency deep brain stimulation is the golden standard for the treatment of medically refractory movement disorders (Benabid et al. 1991; Volkmann 2004).

Apart from the empirically developed standard DBS protocols (Benabid et al. 1991; Volkmann 2004), new stimulation approaches were successfully tested in pre-clinical and early clinical settings. For instance, a closed-loop neurostimulation controlled by beta-band activity showed a better performance than classical DBS in reducing motor signs as well as pallidal firing rate and oscillatory activity in parkinsonian nonhuman primates and PD patients (Rosin et al. 2011; Little et al. 2013).

Another approach, i.e., the model-based development of novel deep brain stimulation techniques, especially targets the pathological neuronal synchrony associated with Parkinson's disease (Tass 1999). This approach bases on dynamic neuronal self-organization principles and fundamental plasticity rules of the nervous system (Fig. 15) (Tass and Majtanik 2006; Tass and Hauptmann 2006, 2007; Hauptmann and Tass 2007, 2009, 2010; Tass and Popovych 2012; Popovych and Tass 2012).

The control methods discussed in this article differ to each other with respect to the stimulation setup and stimulation effects as well as other properties such as robustness and applicability. For example, CR stimulation in an open-loop protocol uses standard stimulation pulses (as used for HF stimulation) applied in a dedicated pattern and its technical realization was proven to be feasible (Hauptmann et al. 2009; Tass et al. 2012b). CR does not require sophisticated calibration and effectively causes transient desynchronization of the stimulated oscillators via a stimulation-induced cluster state. As mentioned in section "Coordinated Reset Stimulation," a number of computational, experimental and pre-clinical studies confirmed the applicability and efficacy of CR stimulation under different stimulation modalities.

Other smart feedback methods are more difficult to realize conceptually and technically and await experimental proof of concept, see sections "Multisite Linear Delayed Feedback," "Nonlinear Delayed

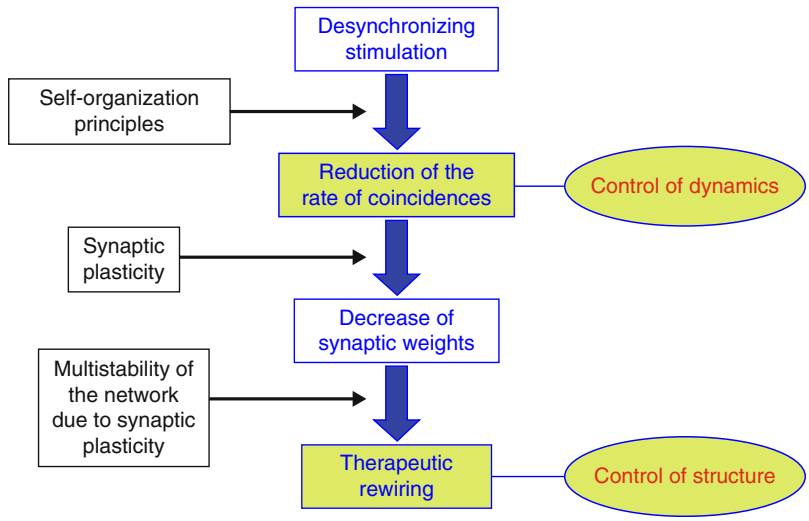

Brain Pacemaker, Fig. 15 Schematic illustration of unlearning of pathological connectivity by desynchronizing stimulation. The latter reduces the overall rate of coincidences in the neuronal population. This is effectively achieved by using dynamic self-organization principles. The reduction of the rate of coincidences, in turn, reduces the synaptic weights and shifts the stimulated network in a weakly coupled state. Because of the multistability, not only strongly coupled and synchronized states, but also weakly coupled and weakly synchronized states are stable. Accordingly, the neuronal population stably remains in a desynchronized or weakly synchronized state, after having been shifted into the basin of attraction of that state by means of desynchronizing stimulation. Hence, a suitable control of the dynamics of the network can lead to long-lasting changes of its connectivity and dynamics (First published in Tass and Hauptmann (2007). Used with permission from the *International Journal of Psychophysiology*)

Feedback," and "Proportional–Integro–Differential Feedback." In modeling studies they effectively result in a sustained desynchronized regime. The feedback methods can be applied under a variety of conditions, and possess an intrinsic demand-controlled character, where the stimulation signal is significantly reduced or even vanishes as soon as desynchronization is achieved. The experimental and clinical realization of these methods is a challenging task, first of all, from the technical side, since stimulation signals have to fulfill all safety aspects like charge density limits. These limits strongly affect the applicability of the slow feedback signals, i.e., slow compared to the timescales of HF and CR pulses. In this way, the application conditions of the methods have to be handled with care, and stimulation setups and effects have to clearly be distinguished for different feedback methods. Otherwise, one can come up with misleading conclusions and erroneous interpretations of the efficacy of feedback methods, see the computational study (Dovzhenok et al. 2013) where nonlinear and linear techniques were not properly distinguished. To this end, only an experimental proof of concept can finally assess the applicability and performance of the control methods.

In forthcoming studies the mathematical modeling needs to be refined to incorporate further anatomical and physiological details, for instance, the contributions of glial cells (Silchenko and Tass 2008). By the same token, control techniques have to be optimized and further developed. As currently done for CR stimulation (Tass et al. 2012b), clinical studies are necessary to evaluate the therapeutic effects of the novel stimulation techniques under real conditions. This interdisciplinary endeavor might finally provide superior therapies for patients with neurological or psychiatric diseases.

Bibliography

Abbott L, Nelson S (2000) Synaptic plasticity: taming the beast. Nat Neurosci 3:1178–1183

Adamchic I, Toth T, Hauptmann C, Tass PA (2013) Reversing pathologically increased electroencephalogram power by acoustic coordinated reset neuromodulation. Hum Brain Mapp 35(5):2099–2118

Alberts WW, Wright EJ, Feinstein B (1969) Cortical potentials and parkinsonian tremor. Nature 221:670–672

Anderson ME, Postupna N, Ruffo M (2003) Effects of high-frequency stimulation in the internal globus pallidus on the activity of thalamic neurons in the awake monkey. J Neurophysiol 89(2):1150–1160

Andres F, Gerloff C (1999) Coherence of sequential movements and motor learning. J Clin Neurophysiol 16(6):520–527

Benabid A, Pollak P, Louveau A, Henry S, de Rougemont JJ (1987) Combined (thalamotomy and stimulation) stereotactic surgery of the VIM thalamic nucleus for bilateral Parkinson disease. Appl Neurophysiol 50(1-6):344–346

Benabid AL, Pollak P, Gervason C, Hoffmann D, Gao DM, Hommel M, Perret JE, de Rougemount J (1991) Long-term suppression of tremor by chronic stimulation of ventral intermediate thalamic nucleus. Lancet 337:403–406

Benabid AL, Benazzous A, Pollak P (2002) Mechanisms of deep brain stimulation. Mov Disord 17:73–74

Benabid A-L, Wallace B, Mitrofanis J, Xia R, Piallat B, Chabardes S, Berger F (2005) A putative gerneralized model of the effects and mechanism of action of high frequency electrical stimulation of the central nervous system. Acta Neurol Belg 105:149–157

Beurrier C, Bioulac B, Audin J, Hammond C (2001) High-frequency stimulation produces a transient blockade of voltage-gated currents in subthalamic neurons. J Neurophysiol 85(4):1351–1356

Beurrier C, Garcia L, Bioulac B, Hammond C (2002) Subthalamic nucleus: a clock inside basal ganglia? Thalamus Relat Syst 2:1–8

Blond S, Caparros-Lefebvre D, Parker F, Assaker R, Petit H, Guieu J-D, Christiaens J-L (1992) Control of tremor and involuntary movement disorders by chronic stereotactic stimulation of the ventral intermediate thalamic nucleus. J Neurosurg 77:62–68

Brice J, McLellan L (1980) Suppression of intention tremor by contingent deep-brain stimulation. Lancet 1(8180):1221–1222

Daido H (1992) Order function and macroscopic mutual entrainment in uniformly coupled limit-cycle oscillators. Prog Theor Phys 88:1213–1218

Danzl P, Hespanha J, Moehlis J (2009) Event-based minimum-time control of oscillatory neuron models. Biol Cybern 101(5–6):387–399

Debanne D, Gahweiler B, Thompson S (1998) Long-term synaptic plasticity between pairs of individual CA3 pyramidal cells in rat hippocampus slice cultures. J Physiol 507:237–247

Deuschl G, Schade-Brittinger C, Krack P, Volkmann J, Schäfer H, Bötzel K, Daniels C, Deutschländer A, Dillmann U, Eisner W, Gruber D, Hamel W, Herzog J, Hilker R, Klebe S, Kloß M, Koy J, Krause M, Kupsch A, Lorenz D, Lorenzl S, Mehdorn H, Moringlane J, Oertel W, Pinsker M, Reichmann H, Reuß A, Schneider G-H, Schnitzler A, Steude U, Sturm V, Timmermann L, Tronnier V,

Trottenberg T, Wojtecki L, Wolf E, Poewe W, Voges J (2006) A randomized trial of deep-brain stimulation for Parkinson's disease. N Engl J Med 355:896–908
Dolan K, Majtanik M, Tass P (2005) Phase resetting and transient desynchronization in networks of globally coupled phase oscillators with inertia. Physica D 211:128–138
Dovzhenok A, Park C, Worth RM, Rubchinsky LL (2013) Failure of delayed feedback deep brain stimulation for intermittent pathological synchronization in Parkinson's disease. PLoS One 8(3):e58264
Elble RJ, Koller WC (1990) Tremor. John Hopkins University Press, Baltimore
Ermentrout B, Kopell N (1991) Multiple pulse interactions and averaging in systems of coupled neural assemblies. J Math Biol 29:195–217
Feldman D (2000) Timing-based LTP and LTD at vertical inputs to layer II/III pyramidal cells in rat barrel cortex. Neuron 27:45–56
Feng X, Greenwald B, Rabitz H, Shea-Brown E, Kosut R (2007a) Toward closed-loop optimization of deep brain stimulation for Parkinson's disease: concepts and lessons from a computational model. J Neural Eng 4(2): L14–L21
Feng XJ, Shea-Brown E, Greenwald B, Kosut R, Rabitz H (2007b) Optimal deep brain stimulation of the subthalamic nucleus – a computational study. J Comput Neurosci 23(3):265–282
Filali M, Hutchison W, Palter V, Lozano A, Dostrovsky JO (2004) Stimulation-induced inhibition of neuronal firing in human subthalamic nucleus. Exp Brain Res 156:274–281
Freund H-J (2005) Long-term effects of deep brain stimulation in Parkinson's disease. Brain 128:2222–2223
Garcia L, D'Alessandro G, Fernagut P-O, Bioulac B, Hammond C (2005) Impact of high-frequency stimulation parameters on the pattern of discharge of subthalamic neurons. J Neurophysiol 94:3662–3669
Gerstner W, Kempter R, van Hemmen J, Wagner H (1996) A neuronal learning rule for sub-millisecond temporal coding. Nature 383:76–78
Gildenberg P (2005) Evolution of neuromodulation. Stereotact Funct Neurosurg 83:71–79
Goddar G (1967) Development of epileptic seizures through brain stimulation at low intensity. Nature 214:1020–1021
Gradinaru V, Mogri M, Thompson KR, Henderson JM, Deisseroth K (2009) Optical deconstruction of parkinsonian neural circuitry. Science 324(5925):354–359
Grannan ER, Kleinfeld D, Sompolinsky H (1993) Stimulus-dependent synchronization of neuronal assemblies. Neural Comput 5:550–569
Grill WM, McIntyre CC (2001) Extracellular excitation of central neurons: implications for the mechanisms of deep brain stimulation. Thalamus Relat Syst 1:269–277
Haken H (1970) Laser theory, vol XXV/2C. Encyclopedia of physics. Springer, Berlin
Haken H (1977) Synergetics. An introduction. Springer, Berlin
Haken H (1983) Advanced synergetics. Springer, Berlin
Haken H (1996) Principles of brain functioning. A synergetic approach to brain activity, behavior, cognition. Springer, Berlin
Haken H (2002) Brain dynamics. Synchronization and activity patterns in pulse-coupled neural nets with delays and noise. Springer, Berlin
Haken H, Kelso J, Bunz H (1985) A theoretical model of phase transitions in human hand movements. Biol Cybern 51:347–356
Hammond C, Ammari R, Bioulac B, Garcia L (2008) Latest view on the mechanism of action of deep brain stimulation. Mov Disord 23(15):2111–2121
Hansel D, Mato G, Meunier C (1993a) Phase dynamics of weakly coupled Hodgkin–Huxley neurons. Europhys Lett 23:367–372
Hansel D, Mato G, Meunier C (1993b) Phase reduction and neural modeling. Concepts Neurosci 4(2):193–210
Hashimoto T, Elder C, Okun M, Patrick S, Vitek J (2003) Stimulation of the subthalamic nucleus changes the firing pattern of pallidal neurons. J Neurosci 23(5):1916–1923
Hauptmann C, Tass PA (2007) Therapeutic rewiring by means of desynchronizing brain stimulation. Biosystems 89:173–181
Hauptmann C, Tass PA (2009) Cumulative and after-effects of short and weak coordinated reset stimulation: a modeling study. J Neural Eng 6(1):016004
Hauptmann C, Tass PA (2010) Restoration of segregated, physiological neuronal connectivity by desynchronizing stimulation. J Neural Eng 7:056008
Hauptmann C, Popovych O, Tass PA (2005a) Delayed feedback control of synchronization in locally coupled neuronal networks. Neurocomputing 65–66:759–767
Hauptmann C, Popovych O, Tass PA (2005b) Effectively desynchronizing deep brain stimulation based on a coordinated delayed feedback stimulation via several sites: a computational study. Biol Cybern 93:463–470
Hauptmann C, Popovych O, Tass PA (2005c) Multisite coordinated delayed feedback for an effective desynchronization of neuronal networks. Stochastics Dyn 5(2):307–319
Hauptmann C, Omelchenko O, Popovych OV, Maistrenko Y, Tass PA (2007a) Control of spatially patterned synchrony with multisite delayed feedback. Phys Rev E 76:066209
Hauptmann C, Popovych O, Tass P (2007b) Desynchronizing the abnormally synchronized neural activity in the subthalamic nucleus: a modeling study. Expert Rev Med Devices 4(5):633–650
Hauptmann C, Roulet JC, Niederhauser JJ, Doll W, Kirlangic ME, Lysyansky B, Krachkovskyi V, Bhatti MA, Barnikol UB, Sasse L, Buhrle CP, Speckmann EJ, Gotz M, Sturm V, Freund HJ, Schnell U, Tass PA (2009) External trial deep brain stimulation device for the application of desynchronizing stimulation techniques. J Neural Eng 6(6):066003
Hebb D (1949) The organization of behavior. Wiley, New York

Kelso J (1995) Dynamic patterns: the self-organization of brain and behavior. MIT Press, Cambridge, MA

Kilgard M, Merzenich M (1998) Cortical map reorganization enabled by nucleus basalis activity. Science 279:1714–1718

Kiss IZ, Rusin CG, Kori H, Hudson JL (2007) Engineering complex dynamical structures: sequential patterns and desynchronization. Science 316(5833):1886–1889

Kumar R, Lozano A, Sime E, Lang A (2003) Long-term follow-up of thalamic deep brain stimulation for essential and parkinsonian tremor. Neurology 61:1601–1604

Kuramoto Y (1984) Chemical oscillations, waves, turbulence. Springer, Berlin/Heidelberg/New York

Lenz F, Kwan H, Martin R, Tasker R, Dostrovsky J, Lenz Y (1994) Single unit analysis of the human ventral thalamic nuclear group. Tremor-related activity in functionally identified cells. Brain 117:531–543

Limousin P, Speelman J, Gielen F, Janssens M (1999) Multicentre European study of thalamic stimulation in parkinsonian and essential tremor. J Neurol Neurosurg Psychiatry 66(3):289–296

Little S, Pogosyan A, Neal S, Zavala B, Zrinzo L, Hariz M, Foltynie T, Limousin P, Ashkan K, FitzGerald J, Green AL, Aziz TZ, Brown P (2013) Adaptive deep brain stimulation in advanced Parkinson disease. Ann Neurol 74(3):449–457

Luecken L, Yanchuk S, Popovych OV, Tass PA (2013) Desynchronization boost by non-uniform coordinated reset stimulation in ensembles of pulse-coupled neurons. Front Comput Neurosci 7:63

Luo M, YJ W, Peng JH (2009) Washout filter aided mean field feedback desynchronization in an ensemble of globally coupled neural oscillators. Biol Cybern 101(3):241–246

Lysyansky B, Popovych OV, Tass PA (2011a) Desynchronizing anti-resonance effect of m: n on–off coordinated reset stimulation. J Neural Eng 8(3):036019

Lysyansky B, Popovych OV, Tass PA (2011b) Multifrequency activation of neuronal networks by coordinated reset stimulation. Interface Focus 1(1):75–85

Lysyansky B, Popovych OV, Tass PA (2013) Optimal number of stimulation contacts for coordinated reset neuromodulation. Front Neuroeng 6:5

Maistrenko Y, Lysyansky B, Hauptmann C, Burylko O, Tass P (2007) Multistability in the Kuramoto model with synaptic plasticity. Phys Rev E 75:066207

Majtanik M, Dolan K, Tass P (2006) Desynchronization in networks of globally coupled neurons with dendritic dynamics. J Biol Phys 32:307–333

Markram H, Lübke J, Frotscher M, Sakmann B (1997) Regulation of synaptic efficacy by coincidence of postsynaptic APs and EPSPs. Science 275:213–215

McIntyre C, Grill W, Sherman D, Thakor N (2004a) Cellular effects of deep brain stimulation: model-based analysis of activation and inhibition. J Neurophysiol 91:1457–1469

McIntyre CC, Savasta M, Goff KKL, Vitek J (2004b) Uncovering the mechanism(s) of action of deep brain stimulation: activation, inhibition, or both. Clin Neurophysiol 115:1239–1248

Meissner W, Leblois A, Hansel D, Bioulac B, Gross CE, Benazzouz A, Boraud T (2005) Subthalamic high frequency stimulation resets subthalamic firing and reduces abnormal oscillations. Brain 128:2372–2382

Milton J, Jung P (eds) (2003) Epilepsy as a dynamics disease. Springer, Berlin

Miocinovic S, Parent M, Butson C, Hahn P, Russo G, Vitek J, McIntyre C (2006) Computational analysis of subthalamic nucleus and lenticular fasciculus activation during therapeutic deep brain stimulation. J Neurophysiol 96:1569–1580

Morimoto K, Fahnestock M, Racine R (2004) Kindling and status epilepticus models of epilepsy: rewiring the brain. Prog Neurobiol 73:1–60

Moro E, Esselink RJA, Xie J, Hommel M, Benabid AL, Pollak P (2002) The impact on Parkinson's disease of electrical parameter settings in STN stimulation. Neurology 59(5):706–713

Nabi A, Moehlis J (2011) Single input optimal control for globally coupled neuron networks. J Neural Eng 8(6):065008

Neiman A, Russell D, Yakusheva T, DiLullo A, Tass PA (2007) Response clustering in transient stochastic synchronization and desynchronization of coupled neuronal bursters. Phys Rev E 76:021908

Nini A, Feingold A, Slovin H, Bergmann H (1995) Neurons in the globus pallidus do not show correlated activity in the normal monkey, but phase-locked oscillations appear in the MPTP model of parkinsonism. J Neurophysiol 74:1800–1805

Nowotny T, Zhigulin V, Selverston A, Abarbanel H, Rabinovich M (2003) Enhancement of synchronization in a hybrid neural circuit by spike-timing dependent plasticity. J Neurosci 23:9776–9785

Pikovsky A, Rosenblum M, Kurths J (2001) Synchronization, a universal concept in nonlinear sciences. Cambridge University Press, Cambridge

Pliss V (1964) Principal reduction in the theory of stability of motion. Izv Akad Nauk SSSR Math Ser 28:1297–1324

Popovych OV, Tass PA (2010) Synchronization control of interacting oscillatory ensembles by mixed nonlinear delayed feedback. Phys Rev E 82(2):026204

Popovych OV, Tass PA (2012) Desynchronizing electrical and sensory coordinated reset neuromodulation. Front Hum Neurosci 6:58

Popovych OV, Hauptmann C, Tass PA (2005) Effective desynchronization by nonlinear delayed feedback. Phys Rev Lett 94:164102

Popovych OV, Hauptmann C, Tass PA (2006a) Control of neuronal synchrony by nonlinear delayed feedback. Biol Cybern 95:69–85

Popovych OV, Hauptmann C, Tass PA (2006b) Desynchronization and decoupling of interacting oscillators by nonlinear delayed feedback. Int J Bif Chaos 16(7):1977–1987

Pyragas K, Popovych OV, Tass PA (2007) Controlling synchrony in oscillatory networks with a separate stimulation-registration setup. Europhys Lett 80:40002

Pyragas K, Novicenko V, Tass P (2013) Mechanism of suppression of sustained neuronal spiking under high-frequency stimulation. Biol Cybern 107(6):669–684

Rizzone M, Lanotte M, Bergamasco B, Tavella A, Torre E, Faccani G, Melcarne A, Lopiano L (2001) Deep brain stimulation of the subthalamic nucleus in Parkinson's disease: effects of variation in stimulation parameters. J Neurol Neurosurg Psychiatry 71(2):215–219

Rodriguez-Oroz M, Obeso J, Lang A, Houeto J, Pollak P, Rehncrona S, Kulisevsky J, Albanese A, Volkmann J, Hariz M, Quinn N, Speelman J, Guridi J, Zamarbide I, Gironell A, Molet J, Pascual-Sedano B, Pidoux B, Bonnet A, Agid Y, Xie J, Benabid A, Lozano A, Saint-Cyr J, Romito L, Contarino M, Scerrati M, Fraix V, Blercom NV (2005) Bilateral deep brain stimulation in Parkinson's disease: a multicentre study with 4 years follow-up. Brain 128:2240–2249

Rosenblum MG, Pikovsky AS (2004a) Controlling synchronization in an ensemble of globally coupled oscillators. Phys Rev Lett 92:114102

Rosenblum MG, Pikovsky AS (2004b) Delayed feedback control of collective synchrony: an approach to suppression of pathological brain rhythms. Phys Rev E 70:041904

Rosin B, Slovik M, Mitelman R, Rivlin-Etzion M, Haber SN, Israel Z, Vaadia E, Bergman H (2011) Closed-loop deep brain stimulation is superior in ameliorating parkinsonism. Neuron 72(2):370–384

Rubin JE, Terman D (2004) High frequency stimulation of the subthalamic nucleus eliminates pathological thalamic rhythmicity in a computational model. J Comput Neurosci 16(3):211–235

Schnitzler A, Timmermann L, Gross J (2006) Physiological and pathological oscillatory networks in the human motor system. J Physiol Paris 99(1):3–7

Schöner G, Haken H, Kelso J (1986) A stochastic theory of phase transitions in human hand movement. Biol Cybern 53:247–257

Schuurman PR, Bosch DA, Bossuyt PM, Bonsel GJ, van Someren EJ, de Bie RM, Merkus MP, Speelman JD (2000) A comparison of continuous thalamic stimulation and thalamotomy for suppression of severe tremor. N Engl J Med 342:461–468

Seliger P, Young S, Tsimring L (2002) Plasticity and learning in a network of coupled phase oscillators. Phys Rev E 65:041906

Shen K, Zhu Z, Munhall A, Johnson SW (2003) Synaptic plasticity in rat subthalamic nucleus induced by high-frequency stimulation. Synapse 50:314–319

Silchenko A, Tass P (2008) Computational modeling of paroxysmal depolarization shifts in neurons induced by the glutamate release from astrocytes. Biol Cybern 98:61–74

Silchenko AN, Adamchic I, Hauptmann C, Tass PA (2013) Impact of acoustic coordinated reset neuromodulation on effective connectivity in a neural network of phantom sound. NeuroImage 77:133–147

Singer W (1989) Search for coherence: a basic principle of cortical self-organization. Concepts Neurosci 1:1–26

Smirnov DA, Barnikol UB, Barnikol TT, Bezruchko BP, Hauptmann C, Buhrle C, Maarouf M, Sturm V, Freund H-J, Tass PA (2008) The generation of parkinsonian tremor as revealed by directional coupling analysis. Europhys Lett 83(2):20003

Song S, Miller K, Abbott L (2000) Competitive Hebbian learning through spike-timing-dependent synaptic plasticity. Nat Neurosci 3(9):919–926

Speckmann E, Elger C (1991) The neurophysiological basis of epileptic activity: a condensed overview. Epilepsy Res Suppl 2:1–7

Steriade M, Jones EG, Llinas RR (1990) Thalamic oscillations and signaling. Wiley, New York

Strogatz SH (2003) Sync: the emerging science of spontaneous order. Hyperion Books, New York

Tasker RR (1998) Deep brain stimulation is preferable to thalamotomy for tremor suppression. Surg Neurol 49:145–154

Tass PA (1996a) Phase resetting associated with changes of burst shape. J Biol Phys 22:125–155

Tass PA (1996b) Resetting biological oscillators – a stochastic approach. J Biol Phys 22:27–64

Tass PA (1999) Phase resetting in medicine and biology: stochastic modelling and data analysis. Springer, Berlin

Tass PA (2000) Stochastic phase resetting: a theory for deep brain stimulation. Prog Theor Phys Suppl 139:301–313

Tass PA (2001a) Desynchronizing double-pulse phase resetting and application to deep brain stimulation. Biol Cybern 85:343–354

Tass PA (2001b) Effective desynchronization by means of double-pulse phase resetting. Europhys Lett 53:15–21

Tass PA (2001c) Effective desynchronization with a resetting pulse train followed by a single pulse. Europhys Lett 55:171–177

Tass PA (2002a) Desynchronization of brain rhythms with soft phase-resetting techniques. Biol Cybern 87:102–115

Tass PA (2002b) Effective desynchronization with a stimulation technique based on soft phase resetting. Europhys Lett 57:164–170

Tass PA (2002c) Effective desynchronization with bipolar double-pulse stimulation. Phys Rev E 66:036226

Tass PA (2003a) Desynchronization by means of a coordinated reset of neural sub-populations – a novel technique for demand-controlled deep brain stimulation. Prog Theor Phys Suppl 150:281–296

Tass PA (2003b) A model of desynchronizing deep brain stimulation with a demand-controlled coordinated reset of neural subpopulations. Biol Cybern 89:81–88

Tass PA, Hauptmann C (2006) Therapeutic rewiring by means of desynchronizing brain stimulation. Nonlinear Phenom Complex Syst 9(3):298–312

Tass P, Hauptmann C (2007) Therapeutic modulation of synaptic connectivity with desynchronizing brain stimulation. Int J Psychophysiol 64:53–61

Tass PA, Majtanik M (2006) Long-term anti-kindling effects of desynchronizing brain stimulation: a theoretical study. Biol Cybern 94:58–66

Tass PA, Popovych OV (2012) Unlearning tinnitus-related cerebral synchrony with acoustic coordinated reset stimulation: theoretical concept and modelling. Biol Cybern 106:27–36

Tass PA, Hauptmann C, Popovych OV (2006) Development of therapeutic brain stimulation techniques with methods from nonlinear dynamics and statistical physics. Int J Bif Chaos 16(7):1889–1911

Tass PA, Silchenko AN, Hauptmann C, Barnikol UB, Speckmann EJ (2009) Long-lasting desynchronization in rat hippocampal slice induced by coordinated reset stimulation. Phys Rev E 80(1):011902

Tass P, Adamchic I, Freund H-J, von Stackelberg T, Hauptmann C (2012a) Counteracting tinnitus by acoustic coordinated reset neuromodulation. Restor Neurol Neurosci 30:367–374

Tass PA, Qin L, Hauptmann C, Doveros S, Bezard E, Boraud T, Meissner WG (2012b) Coordinated reset has sustained aftereffects in parkinsonian monkeys. Ann Neurol 72:816–820

Timmermann L, Florin E, Reck C (2007) Pathological cerebral oscillatory activity in Parkinson's disease: a critical review on methods, data and hypotheses. Expert Rev Med Devices 4(5):651–661

Tukhlina N, Rosenblum M, Pikovsky A, Kurths J (2007) Feedback suppression of neural synchrony by vanishing stimulation. Phys Rev E 75:011918

van Hemmen J (2001) Theory of synaptic plasticity. In: Moss F, Gielen S (eds) Handbook of biological physics, vol 4. Elsevier, Amsterdam, pp 771–823

Volkmann J (2004) Deep brain stimulation for the treatment of Parkinson's disease. J Clin Neurophysiol 21:6–17

Welter ML, Houeto JL, Bonnet AM, Bejjani PB, Mesnage V, Dormont D, Navarro S, Cornu P, Agid Y, Pidoux B (2004) Effects of high-frequency stimulation on subthalamic neuronal activity in parkinsonian patients. Arch Neurol 61(1):89–96

Winfree A (1980) The geometry of biological time. Springer, Berlin

Wunderlin A, Haken H (1975) Scaling theory for non-equilibrium systems. Z Phys B 21:393–401

Zhai Y, Kiss IZ, Tass PA, Hudson JL (2005) Desynchronization of coupled electrochemical oscillators with pulse stimulations. Phys Rev E 71:065202

Zhai Y, Kiss IZ, Hudson JL (2008) Control of complex dynamics with time-delayed feedback in populations of chemical oscillators: desynchronization and clustering. Ind Eng Chem Res 47(10):3502–3514

Zhou Q, Tao H, Poo M (2003) Reversal and stabilization of synaptic modifications in a developing visual system. Science 300:1953–1957

Self-Organization in Clinical Psychology

Günter Schiepek[1] and Volker Perlitz[2]
[1]Institute of Synergetics and Psychotherapy Research, Paracelsus Medical University, Salzburg, Austria
[2]Klinik für Psychosomatik, Universitätsklinikum der RWTH Aachen, Aachen, Germany

Article Outline

Definition of the Subject
Introduction
Dynamic Diseases
Self-Organized Synchronization Patterns in Peripheral Physiological Systems
Nonlinear Dynamics in the Communication of Patient and Therapist
Self-Organization in Human Change Processes
The Concept of Self-Organization Promotes New Information Technologies in Clinical Psychology – The Synergetic Navigation System
The Self-Organizing Brain
Future Directions
Bibliography

Definition of the Subject

Clinical psychology is a sub-discipline of psychology engaged in the description, classification, explanation, and treatment of mental disorders. The primary focus is on psychological methods, models, and topics such as behavior, cognition, emotion, and social interaction with substantial overlap with related areas in psychiatry, psychosomatics, or behavioral medicine. Yet, the main stream in clinical psychology views the etiology of mental disorders, their time courses and susceptibility to psychological treatment still through the magnification glass of linear input-output philosophy of human functions. Owing to this paradigm, linear combinations of variables (as inner conflicts, irrational cognitions, or stressors) trigger the development of psychiatric diseases or disorders in genetically predisposed individuals. Therefore, linear multivariate regression models are assumed be able to predict the probability of falling ill or suffering from disorders. As an important field in clinical psychology, psychotherapy research defines randomized controlled trials as the golden standard of outcome research. Here, patients randomly assigned to different treatment modalities are being compared with respect to the outcome of different tests. In this regard, the input (treatment) is thought to determine the outcome (treatment effects).

Contrary, or rather, supplementing this line of research is the scientific paradigm of self-organization, i. e. the functioning of complex nonlinear systems with circular causality at its center. Gestalt psychology, traditionally concerned with patterns ("Gestalts") in perception, human behavior and interaction (e. g., those prevalent in group dynamics, Lewin Koch et al. 2002) focuses on such self-organization processes. Gestalt psychologists like Wolfgang Köhler (e. g. Köhler 1947), Wolfgang Metzger, Max Wertheimer, Kurt Lewin and others can be seen as direct predecessors of modern complexity researchers in psychology (Stadler and Kruse 1990). Another root of this development is Jean Piaget's equilibration theory of action-cognition patterns (schemata) describing assimilation-accommodation-cycles of these schemata (Piaget 1976). During these processes, input from the inner and outer environment assumes the role of disturbing stimulation of individual system dynamics. A third important line of thinking in circular causality comes from anthropological medicine. The "Gestaltkreis" integrates feedback loops between sensorial and actional systems on the one side, and individual and environmental systems on the other side (ecosystemic approach) (von Uexküll and Wesiack 1996).

A. Hutt, H. Haken (eds.), *Synergetics*,
https://doi.org/10.1007/978-1-0716-0421-2_472

Originally published in
R. A. Meyers (ed.), *Encyclopedia of Complexity and Systems Science*, © Springer-Verlag 2009
https://doi.org/10.1007/978-3-642-27737-5_472

Introduction

During the past decades in clinical psychology, it was particularly the transdisciplinary approach of *synergetics* (Haken 1990a) which inspired a specific nonlinear and complexity research on cognition (Haken 1990b; Tschacher and Dauwalder 1999), social interaction (Nowak and Vallacher 1998; Tschacher 1997), etiology and dynamics of mental diseases (e. g., Schiepek et al. 1992; Tschacher and Kupper 2002), and psychotherapy (for an overview see Haken and Schiepek 2006). Synergetics describes, measures, and explains the autonomous processes of pattern formation and pattern transitions in complex nonlinear systems. Founded on Haken's fundamental discovery that these processes do not depend of the matter of the systems they occur in, synergetics became one of the most important inspirations to many scientific fields and topics. Especially, Haken early transferred synergetics to brain research (e. g., Basar et al. 1983), since the brain is an outstanding example of a complex, self-organizing system. Today, it is widely accepted that the brain and a serial computer not only differ profoundly, but there is almost nothing they share: No wonder in light of the more than 10^{11} nonlinear interconnected neurons forming a dynamic mega-network of neural networks with essential features like arrays of emerging and submerging synchronizations, its flexibility and ever changing pattern formation, working at the edge of chaos, or realizing combined (activating and inhibiting) feedback mechanisms following the principles set forth by synergetics which describes the laws of self-organizing systems (Haken 1996, 2002).

Taking a closer look at most of the phenomena clinical psychology is concerned with it becomes obvious that they appear to be of dynamic nature. Human development processes, human change and learning processes, the dynamics and prognosis of mental disorders, problems mani-festing in social systems like couples, families, teams, or the question of how psychotherapy works: Self-organization is a ubiquitous entity.

Dynamic Diseases

Mental disorders are characterized by specific dynamic patterns, mirroring "endogenous" and common features of a disorder (like the repetitive phases of unipolar major depression or the bipolar phases of bipolar disorders, oscillating between mania and depression), as well as the effects of an individual life-style including individual coping and treatment efforts. Mental disorders can be conceived as highly structured and coherent states which enslave and thus impair the individual's mental and social functioning. Following the "enslaving principle", emerging order parameters reduce the degrees of freedom in the behavior of the single parts of a system. There is phenomenal evidence that this is the case in many mental disorders. Obsessive-compulsive disorder patients coerced to repeat unwished thoughts or rituals are just but one most impressive example. On the brain level, such pathological states correspond with abnormal synchronization in specific neural networks impairing brain functions. In obsessive-compulsive disorders, cortico-striato-thalamo-cortical feedback-loops are thought to be at the center of the dysfunctional network (Saxena and Rauch 2000; Schiepek et al. 2007), while abnormal synchronization in highly similar neural populations is the source of Parkinsonian resting tremor (Lenz et al. 1994; Pare et al. 1990).

At times, transitions between different pathological states or between states of health and disease are linear and balanced, at other times they are discontinuous and abrupt, such as in nonlinear phase transitions accompanied by critical fluctuations described by synergetics to occur in physical systems. Such transitions have been reported for unipolar or bipolar cyclic depression (e. g., Heiden 1992), and also for schizophrenia (Strauss 1989). The usefulness of the concept of attractors in psychopathology is best reflected by the final common pathway of different disorders with similar phenomenology and syndromal patterns. Different initial conditions and different qualities and degrees of stressors and vulnerability factors may result in similar pathological end-states on the one hand. But on the other hand, small fluctuations within the intrapsychic or

environmental conditions or small differences of some boundary or threshold conditions may result quite different disorders or may decide between health and disease (for a dynamical simulation of major depression see Schaub and Schiepek 1992). The encouraging message synergetics delivers is that while the structure of a generic system may stay unchanged, small changes in control parameters, threshold conditions, and internal or external fluctuations are able to trigger dramatic changes in the behavior of the system. As a consequence, therapy exerting changes of these parameters is thus able to trigger return of the system to a healthy state.

For illustrative purposes we present results of a computer simulation of different chronic courses of schizophrenia (Schiepek et al. 1992). A qualitative network model of five macroscopic variables was transformed into a set of nonlinear difference equations, with each equation describing and determining the change rate of each variable from t to $t + 1$. The empirical references of the simulation model were empirical studies of the chronic course of schizophrenic patterns, mostly mixed psychotic episodes, healthy functioning, and chronic states. For example, (Ciompi and Müller 1976) report on eight different patterns in the long-term evolution of schizophrenia, most of them reproduced by our model. These patterns result from various combinations of slow vs. acute onset, acute episodes vs. progressive deterioration, and remission vs. chronic end-state.

Variables taken into account were chosen from reviews in psychiatric and psychological schizophrenia research (e. g., Böker and Brenner 1996, 1989; Ciompi 1989). Selected were (1) degree of cognitive disorders, (2) emotional and interpersonal stress, (3) withdrawal and social isolation, (4) degree of expressed (negative) emotions in the social environment of the patient, and (5) positive symptoms like delusions and hallucinations. The parameters mediating the nonlinear interplay of these macroscopic variables or order parameters were (a) diffuseness of affective-cognitive schemata as a central long-term vulnerability of mental functioning, (b) dopamine and serotonin metabolism, (c) social deficits and lack of competencies, (d) genetic risk for schizophrenia, and (e) some parameters mediating mixed feedback processes, especially the negative feedback responsible for antipsychotic damping effects of the pathology. Results of the simulation runs are indicated in Fig. 1. The simulation reproduces most precisely (a) episodic patterns with prodromal symptoms and acute onset, (b) acute onset, but continuous evolution with chronic end-state, and (c) slow and smooth onset with chronic long-term course (see also Tretter and Scherer 2006).

Other simulation models are effective on the microscopic level of neural networks. Kruse et al. (Kruse et al. 1997) introduced a model focusing on the coupling dynamics between neurons processing brain correlates of social experiences. If unable to learn from cues delivered by the relevant environment, this system will fail to establish adaptive and coherent structures. When inducing fluctuations which promote re-learning and self-healing processes, the neural network causes incoherent and chaotic behavior. Most current models of schizophrenia take into account the neural circuits of relevant brain regions (cortical areas, basal ganglia like striatum and pallidum, thalamic areas, brain stem centers) and particularly the equilibria between different neurotransmitters and neuromodulators (e. g. Carlsson 2006). The complicated local balances and their (non-) equilibria states are in the focus of the strongly evolving field of computational or systems neuroscience (Friston et al. 2003; Penny et al. 2004).

Not only central neuroscience has benefitted from concepts introduced by synergetics, however, but also physiology studying the effects of the autonomic nervous system (ANS) activities on peripheral systems, such as the cardiovascular, the respiratory, or the microcirculation system. Such activities are most prominent as the ANS engages in the mediation of emotions.

Self-Organized Synchronization Patterns in Peripheral Physiological Systems

For decades, the study of the ANS involvement in emotional arousal and its impact on the cardiovascular system has attracted clinical and scientific

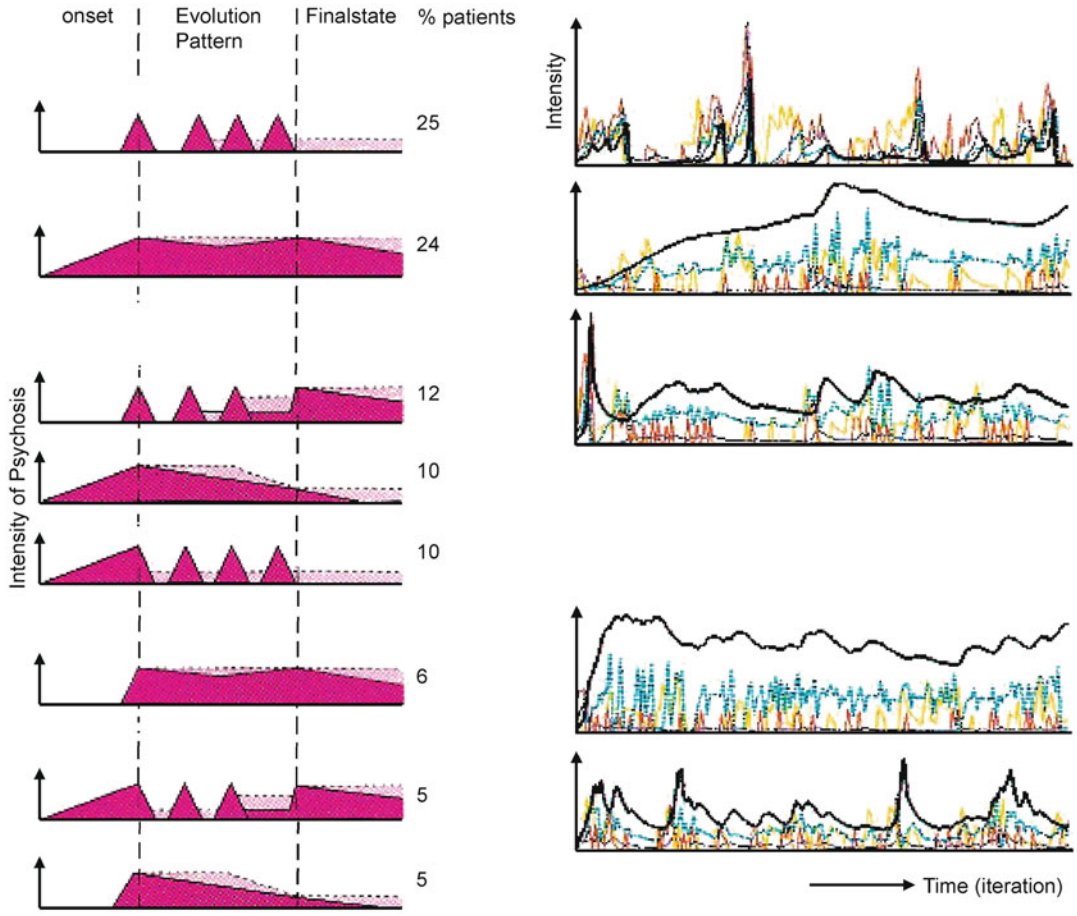

Self-Organization in Clinical Psychology, Fig. 1 Different patterns of the long-term evolution of schizophrenia (empirical data from a study by Ciompi and Müller 1976) *(left)* were reproduced by simulations based on a set of five coupled nonlinear difference equations with different parameter values (Schiepek et al. 1992) *(right)*

attention in psychology and psychophysiology (e. g. Sinha et al. 1992). Ever since the seminal findings of W. B. Cannon (1915) and H. Selye (1936) on the general adaptation syndrome, colloquially condensed as stress, the clinical relevance of emotional responses became ultimately clear. This obvious clinical relevance is thwarted by the fact that direct observations of ANS activity in humans are restricted not only because of ethical constraints but also because of the fear to provoke what they strive to detect. Therefore, the study of the ANS in humans had to rely for a long time preferably on indirect measures, such as the power spectral density (PSD), a linear computation method. Based on the fast Fourier transform (FFT) which extracts periodic components in the frequency domain, the PSD was favored by many researchers due to its computational ease to analyze frequencies inherent in the two branches of the ANS, the parasympathetic (PNS) and the sympathetic nervous system (SNS). This allowed to divide the effects of the PNS and SNS activity on variations of the heart rate, the so-called heart rate variability (HRV), into three major variance components, the very low frequency (VLF) band below 0.04 Hz, the low frequency (LF) band between 0.04–0.15 Hz, and the high frequency (HF) band between 0.15–0.45 Hz. While the origin of both VLF and the HF bands is not debated, controversy reigns whether the origin of the LF band is attributable to SNS activity or whether it represents a mixture of SNS and PNS activity.

Subsequently, some authors propose calculating the LF to HF ratio assumed to reflect the sympatho-vagal balance (for an overview see Task Force of the European Society of Cardiology and the North American Society of Pacing and Electrophysiology 1996). There has been growing discontent and criticism as to the validity of such drawer style classifications based on the consideration that the PSD, or FFT resp., as a linear routine is only able to detect linear properties, that are to some extent included in most physiological signals (Kettunen and Keltikangas-Järvinen 2001; Yuru et al. 2006). That, however, should restrict and limit its use since an increasing body of scientific evidence is demonstrating the obvious: In times of adaptation and rapid changes – a hallmark of life and its living systems – healthy ANS activity exhibits nonlinear dynamics necessary to mediate responses appropriate to those change processes. This is particularly the case for emoting as one of the most volatile change patterns.

However, this is not only true for discrete emotion transitions but also for a process crucial for the maintenance of health, namely psychophysical relaxation. Contrary to the rigid scheme depicted above, Perlitz and coworkers have introduced a relaxation model which takes into account adaptive, self-organizing characteristics of the central and peripheral subsystems involved in the psychophysical relaxation process. They scrutinized the physiological conditions and interactions observed with the emergence of a frequency at ca. 0.15 Hz, which in terms of the classical scheme is attributed to the transition between parasympathetic and sympathetic nervous activity. This frequency prevailed at different amplitudes in HRV, blood pressure and respiration, but foremost in the microcirculation of the forehead skin. Using several nonlinear methods, such as wavelet time frequency distributions (TFD) or post-event-scan (PES) analysis, this 0.15 Hz frequency band (range 0.12–0.18 Hz) emerged or erupted with amplified oscillations and periods of 6–7 s in all time series of subsystems under study. The emergence clearly depended on psychomotor drive reduction which can be either reduced by taking naive relaxation maneuvers (such as closing the eyes), or be enhanced using auto-suggestive means, such as autogenic training. Their zest to elaborate the origin of this frequency was supported by invasive observations with anesthetized dogs made by Lambertz and colleagues who had presented their findings earlier. They found a rhythm at a similar frequency which originated in reticular brainstem neurons of freely breathing dogs when administering narcotics to reduce drive. Followed by the emergence in those unspecific reticular neurons, this frequency also emerged in arterial blood pressure, HRV, and respiration (Lambertz et al. 2000; Perlitz et al. 2004b, c). This reticular rhythm, termed retR, was unaffected by changes in the frequency of respiration or arterial blood pressure which could both be presumed to exert distinct influences owing to linear models. Rather, in these experiments respiration and HRV were entrained to the 0.15 Hz band at 1:1, 2:1 and 1:2 integer number ratios which are, according to Bethe (Bethe 1940), an outflow of central-peripheral order–to–order transitions. With regard to parallels in frequency and dynamics observed in man and dog, Perlitz and coworkers suggested that also in humans the 0.15 Hz band most likely originates from reticular neurons of the lower brainstem network (Perlitz et al. 2004a, b, c).

In summary, the findings presented in Fig. 2 underpin the theory of synergetics, since there is reason to regard the ca. 0.15 Hz frequency as an order parameter and the level of mental drive as control parameter. The ca. 0.15 Hz frequency is a prominent example of biological pattern formation lacking external or macroscopic control.

Nonlinear Dynamics in the Communication of Patient and Therapist

As mentioned above, psychotherapy is usually conceptualized as the application of psychological treatments to patients in order to change their problem states and diseases. However, as different research programs revealed during the last decades, psychological change processes show all important features of nonlinear systems – like deterministic chaos, nonstationary phase transitions, and nonlinear coupling between patient

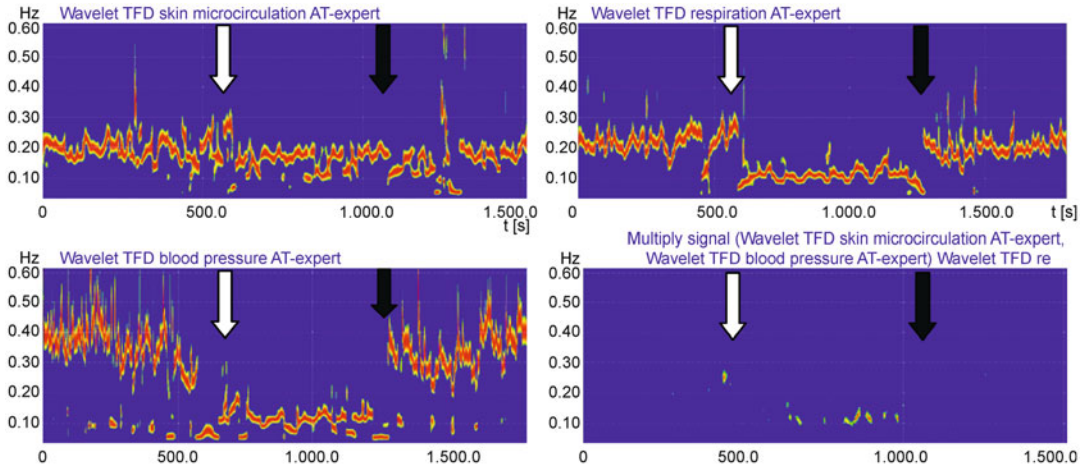

Self-Organization in Clinical Psychology, Fig. 2 Wavelet time frequency distributions (TFD) of peripheral noninvasively obtained recordings of a female expert in autogenic training (AT, 56 yrs., healthy, non-smoker, 15 yrs practice AT). *Top left:* TFD of glabella skin microcirculation photoplethysmography; *top right:* TFD of chest respiration related movements; *bottom left:* TFD of peripheral systemic arterial blood pressure; *bottom right:* So-called "joined TFD" of PPG-, respiration-and blood pressure-TFD, a novel method by Besting and colleagues (2005) (multiplying TFDs yielding only frequencies prominent at identical times and identical frequencies, used to compute the intersection of TFD time series. *White arrows* mark the start of AT, *black arrows* mark the end of AT. In the TFD of PPG, the main frequency is at ca. 0.21 Hz prior to the onset of AT and is clearly stabilized at ca. 0.18 Hz with the start of AT, with signs of dissociation when terminating AT. The TFD of respiration supplies ample evidence of an order-order transition triggered by the practice of AT: The main frequency plummets from ca. 0.25 to 0.15 and 0.07 Hz to be maintained at ca. 0.12 Hz. With termination of AT, the main frequency skips back to frequencies shown beforehand. The TFD of systemic arterial blood pressure exhibits an intersection of approx. 90% during the AT section, but also few minor intersections before and after AT (data not shown); the joined TFD intersection shows merely few frequency "spots" at ca. 0.12 Hz during AT

and therapist. Physiological synchronization appears to be realized at an interpersonal level (between therapist and patient) as well as between different phenomenological levels of the interpersonal system (speech qualities and psychophysiological variables). In a study of Villmann et al. (2008) heart rate, respiratory frequency, muscular tension, and skin conductivity were measured from both, therapist and patient, during 37 therapy sessions. Speech production was analyzed by the Mergenthaler model focusing on emotional feeling and cognitive referential activity/abstraction (Mergenthaler 1998). Physiological data were analyzed by an artificial neural network approach (growing self-organizing map), which uses a kernel smoothing for improved data density estimation. It was possible to generate an entropy model of psychophysiological variability detecting emotionally instable phases during the therapy process. The entropy reflecting psycho-physiological and emotional variability was related to the dramatic value of speech analysis according to the cycle model of Mergenthaler.

Empirical evidence exists also for synchronized chaoto-chaotic phase transitions in the brains of therapist and patient during a therapeutic interview, measured by local largest Lyapunov exponents in the EEGs of both interaction partners (Rockstroh et al. 1997).

Taking into account the importance of the therapeutic relationship for the treatment outcome the attention of a study realized by Schiepek and co-workers focused on the interactional process between therapist and patient (Kowalik et al. 1997; Schiepek et al. 1997). The authors used the method of sequential plan analysis, which is a development of the hierarchical plan analysis proposed by Grawe and Caspar (e. g. 1996). Plans in this sense are verbally or non-verbally

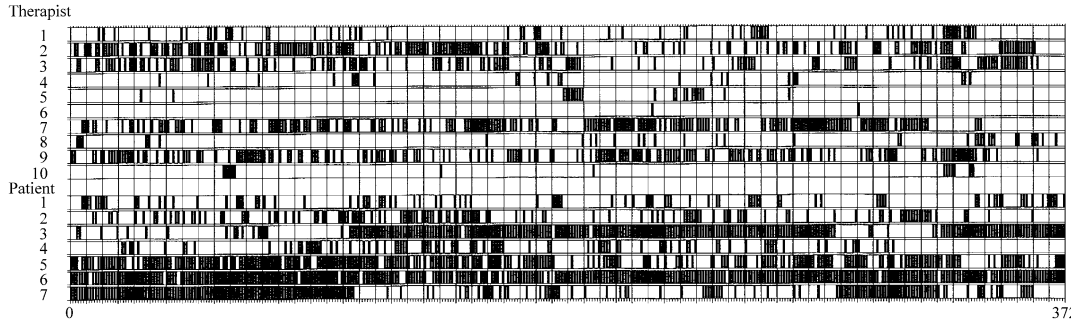

Self-Organization in Clinical Psychology, Fig. 3 Nominal sequences of interactional plans of the therapist *(top)* and the patient *(bottom)* during a psychotherapy session. The sampling rate is 10 s. Different plans can be realized simultaneously. The pattern looks like a music score with the plans representing the different instruments of an orchestra. A sonification of the score of plans coded from a 13-session psychotherapy is recorded on a DVD added to the textbook of Hakenand Schiepek 2006

Self-Organization in Clinical Psychology, Table 1 Second-order plans and categories of self-presentations as identified by the hierarchical plan analysis of a complete 13-session psychotherapy. Encoding of therapist and patient. Plans and categories are used as ideographic observation categories for the sequential plan analysis

	Second-order plans	Categories of self-presentation
Therapist	1 show competence 2 encourage a trusting relationship 3 show understanding 4 motivate her	I encourage trust/create a secure atmosphere
	5 encourage her to reflect on her patterns of thinking 6 confront her with her avoidance and problem behavior	II confrontation/exposing to insecurity
	7 activate her 8 show her that she is responsible	III encourage self-responsibility of the patient
	9 guide her focus of attention 10 give her structure	IV activate structuring work
Patient	1 demonstrate strength and competence 2 make it clear that things are or have been difficult 3 be a good patient/create a good relationship to the therapist	I search for sympathy/appreciation/good relationship
	4 show that your suffering is strongly influenced by external causes 5 ask for help from the therapist	II externalization/demonstration of helplessness
	6 show interest and willingness in solving your problems 7 protect yourself from threatening changes	III problem-oriented work (self-relatedness vs. avoidance)

communicated intentions of self-presentation in a social situation. Patient's and therapist's interactional behavior was analyzed on the basis of video recordings. Two complete therapies (13 and 9 therapy sessions, resp.) were encoded with a sampling rate of 10 s (Fig. 3). The construction of an inclusive hierarchical plan-analysis leads to an ideographic categorical system for the observation of the client–therapist interaction (Table 1).

The first hints of order in the dynamics came from the distribution of simultaneous configurations (on-off-patterns) of plans in the scores. This distribution follows a power law ($1/f^{\alpha}$) demonstrating a distinct structure order within the data (Fig. 4). Following Bak et al. (1989), power law-distributions as demonstrated in Fig. 4 emerge from self-organized criticality within dynamic systems.

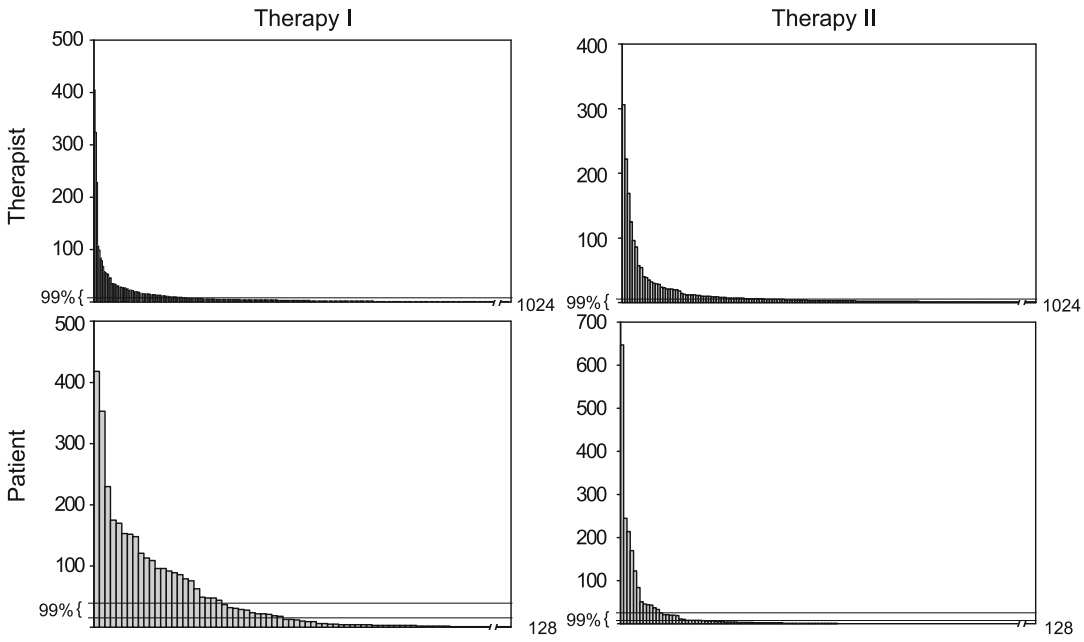

Self-Organization in Clinical Psychology, Fig. 4 Empirical frequencies of constellations of interactional plans realized by therapists (10 plans) and patients (7 plans) within two psychotherapies (therapy I: 13 sessions, therapy II: 9 sessions). *X*-axis: Number of all possible configurations of plans (therapist: $2^{10} = 1024$, patient: $2^7 = 128$) ordered by the frequency of their realization. *Y*-axis: Frequencies of plan configurations. The distributions follow a power-law ($\mathbf{1}/f^{\alpha}$) distribution

Further data analysis was based on the time series of the highest-level categories, the so-called categories of self-presentation (see Table 1). Since in the hierarchical system of the plan analysis the operators at the lowest observation level were quantified by intensity ratings, the plans and the self-presentation categories at the top level integrating the lower level categories were also quantified. The time series were analyzed by methods which are sensitive to the nonlinearity as well as the nonstationarity of the time series (Haken and Schiepek 2006; Kowalik et al. 1997; Schiepek et al. 1997; Strunk and Schiepek 2006). Nonlinearity was proofed by surrogate data tests (Rapp et al. 1994) using random surrogates and FFT-based phase-randomized surrogates (Strunk 2004). Whereas fractal dimensionalities of the empirical time series (based on the correlation dimension D2 as well as mean Pointwise D2 (Skinner et al. 1994)) saturated at finite values (convergence to a fractal dimensionality of about 6), random and FFT-surrogates did not. The methods of PD2 (Skinner et al. 1994) and of the local largest Lyapunov exponents (algorithm from Rosenstein et al. 1993) were used to identify phase-transition like discontinuities. Following the evolution of PD2 dimensionalities, both therapies realized nonstationarities, and both therapies showed periods of strongly synchronized (with correlations from 0.80 to 1.00) and anti-synchronized PD2-processes (with correlations from –0.80 to –1.00) between patient and therapist. Quite similar and even more pronounced dynamical jumps were to be seen in the development of the local largest Lyapunov exponents (Fig. 6), representing changes in the chaoticity of a time signal (Kowalik et al. 1997). An important part of the discontinuities of the LLLE were exactly synchronized between patient and therapist. Obviously both persons create a dynamic self-organizing communication system, which allows for the individual change processes of the patient.

These results get support from nonlinear coupling measures between the time series of the interaction partners. Pointwise transinformation as well as pointwise coupling conditional divergence (Lambertz et al. 2003; Vandenhouten 1998) were applied to the data, and both indicate changing and time-dependent coupling strengths between the time series of the interaction partners. There is no priority to the therapist's influence on the patient, which contradicts the classical idea that input from the therapist should determine the client's output. The other way round is also true and both constitute the circular causality of psychotherapeutic self-organization.

In other studies, sequential plan analysis was applied to the microdynamics of group interaction (Haken and Schiepek 2006). In a group of five persons a creativity and problem solving task was to be solved within 2,5 h (creation of ideas, rules, and physical handicraft realization of a prototype board game from different materials). Similar to the psychotherapy study the sampling rate was 10 s. The superordinate plans which could be identified for all five persons were (1) spontaneity and emotional engagement vs shyness, restricted behavior, and orientation to social norms, (2) engagement in the group interaction and in positive social climate, (3) task orientation. Length of time series was about 810 coding points (= intervals). D2 as well as mean PD2 estimates saturated at a fractal dimensionality of about 5 for all categories. The embedding of the time series was realized by two ways: (1) The phase space was constituted by the three dimensions of superordinated plans with five trajectories representing the five group members, or (2) the phase space was constituted by the five persons with three trajectories representing the time course of the three plans (additional embedding dimensions result from time delay coordinates). In both cases PD2 results show an evolving pattern of quasi-attractors with changing complexity and LLLEs (algorithm from Rosenstein et al. 1993) portray chaoto-chaotic phase transitions with clear-cut and interpersonally synchronized jumps – similar to the dyadic interaction of the psychotherapy study.

Self-Organization in Human Change Processes

A quite different approach to human change processes focuses on inpatient treatments at a hospital of psychosomatics. In a study by Schiepek and coworkers (results in Haken and Schiepek 2006) 94 change processes were investigated, realized by 91 inpatients with different diagnoses (depression, anxiety disorders, posttraumatic stress disorders, eating disorders, somatoform disorders, and others). The time series data was produced by patients' self-ratings which were completed once a day in the evening. For this purpose a 53-item rating sheet was developed (*Therapy Process Questionnaire [TPQ],* Haken and Schiepek 2006) whose factor analysis resulted in a solution of seven factors defining the subscales of the questionnaire (Table 2). The ratings combined seven-step Likert scales and visual analogue scales especially for ratings of emotions. TPQ measurements reflect important aspects of the patient's experience of progress and goal attainment, emotional involvement, self-efficacy, therapeutic relationship, social relations with other inpatients, and the ward atmosphere.

The inclusive outcome criterion integrated the following measures: Inventory of Interpersonal Problems (IIP), Gießener Beschwerdebogen (GBB), Hospital Anxiety and Depression Scale (HADS), Questionnaire for Social Support (F-SOZU), a life-quality questionnaire (Münchener Lebensqualitäts-Dimensionenliste), a self-efficacy questionnaire (Fragebogen zur Generalisierten Kompetenzerwartung), the Sense-of-Coherence Questionnaire, and an interview-based assessment of personal resources. Additionally, therapists and patients scored the overall treatment effectiveness and treatment quality.

Results confirmed synergetic conceptualizations of how psychotherapy works and corroborated hypotheses drawn from this model. Here therapy is supposed to provide support for the patient's own self-organization processes, which should be characterized by cascades of order-to-order transitions accompanied by critical instabilities of the process. Pathological and restrictive order should be transformed into more flexible and adaptive patterns of behavior, and the

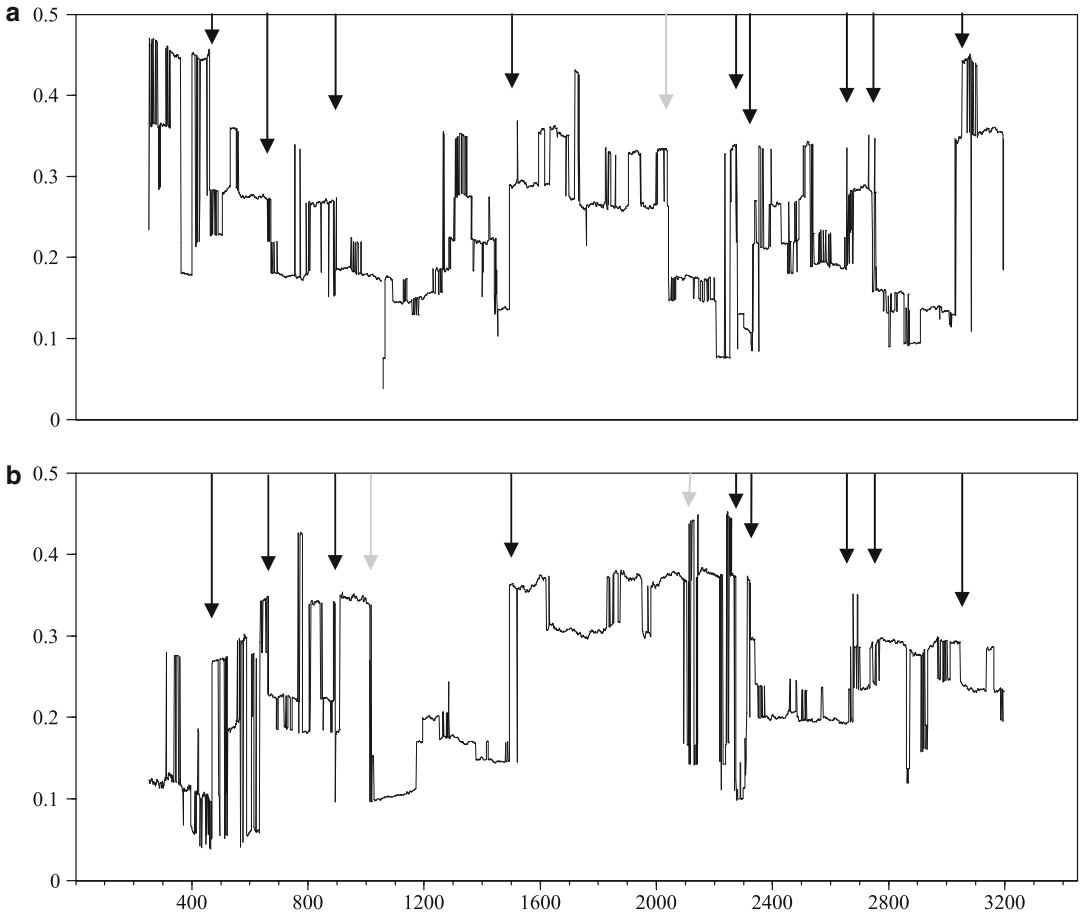

Self-Organization in Clinical Psychology, Fig. 5 Synchronized jumps in the dynamics of local largest Lyapunov exponents *(black arrows). Grey arrows* indicate not clearly synchronized changes. (**a**) Therapist, (**b**) Patient

synchronization of the different aspects of the patient's experience should undergo some transformations. Exactly this could be observed.

Significant correlations exist between the local maxima of critical fluctuations and the outcome of psychotherapy. The local maxima were defined by the difference between the mean dynamic complexity of the whole psychotherapy process and the maximum of the complexity which was observed during the process. Correlations were –0.455 (second-order factor I: "Change involvement" of the TPQ, $p = 0.002$), –0.431 (second-order factor 2: "Relationship/social climate", $p = 0.003$), and –0.572 (second-order factor 3: "Emotionality", $p = 0.000$) (compare Table 2). Negative correlations result from the fact that increased local maxima of dynamic complexity correspond to reduced problems, symptoms, and impairment.

The *dynamic complexity* combines a fluctuation index with a distribution index. The fluctuation index measures the frequency and amplitude of the change rates of a time series between the reversals of the development within a scanning window gliding over the whole time series. For analysis purpose a window width of seven measurement points (= days) was introduced. The distribution index measures the scattering of realized values within a given scanning window. The more scores are restricted to only narrow intervals of the available scale range, the smaller the distribution index becomes. The score of this index

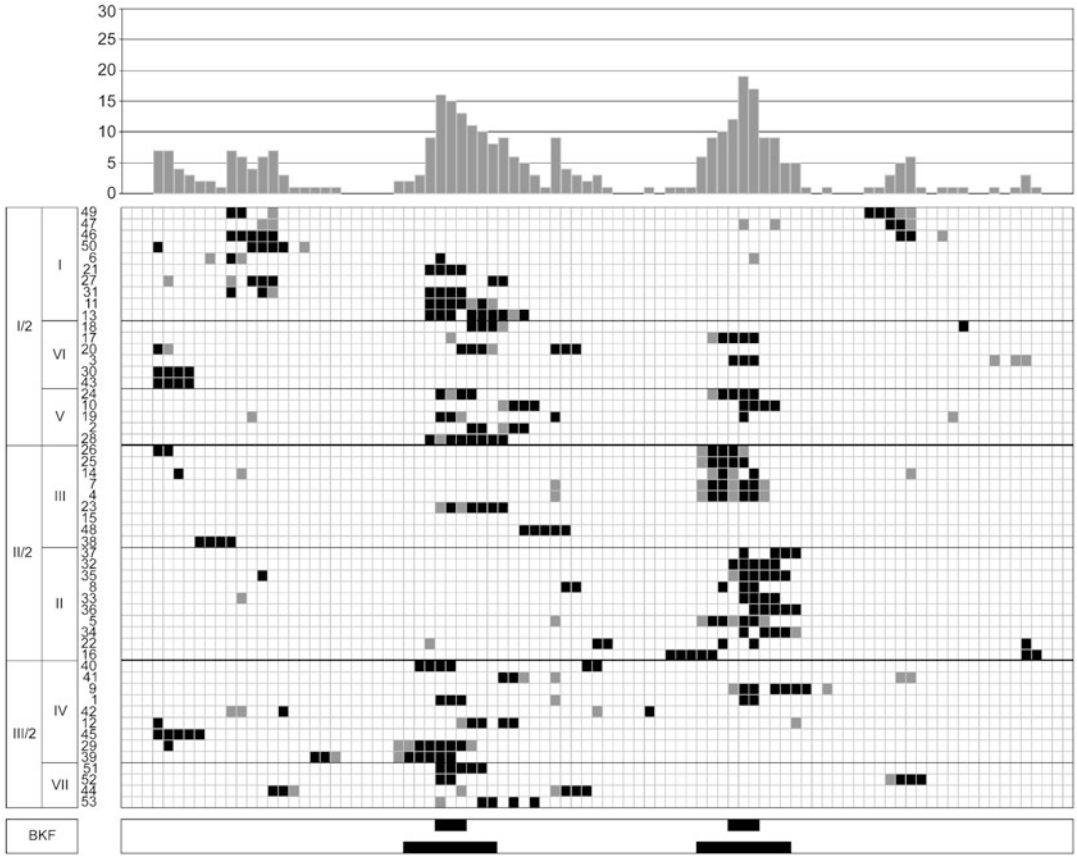

Self-Organization in Clinical Psychology, Fig. 6 Complexity resonance diagram of a psychotherapy process. Such diagrams portray the threshold exceeding dynamic complexities of a process encoded by the 53 items of the Therapy Process Questionnaire (TPQ). *Gray dots:* 5% threshold of significance; *black dots:* 1% threshold of significance. *X*-axis: Days of hospital stay, *Y*-axis: Items of the TPQ arranged by the order of the factors as reported in Table 2. Window width for the calculation of dynamic complexities is 7. Column-like structures indicate phases of critical instabilities during the process

Self-Organization in Clinical Psychology, Table 2 Factors (principal component analysis) of the Therapy Process Questionnaire (TPQ). Factor analysis was based on 94 therapy processes (mean stay = 66 days, daily ratings). Seven first-order factors *(right)* are related to three second-order factors *(left)*. Numbers behind the first-order factors indicate factor loadings on second-order factors (for details see Haken and Schiepek 2006)

I(2) Change involvement	I Therapeutic progress/confidence in treatment effects/self-efficacy (.571) VI Intensity of therapeutic work/motivation to change (.596) V Opening of perspectives/personal innovations (.649)
II(2) Relationship/Social climate	III Quality of the therapeutic relationship/openness/confidence in the therapist (.705) II Ward atmosphere, social relationship to other inpatients (.692)
III(2) Emotionality	IV Dysphoric emotions/self-relatedness (.732) VII Impairment by symptoms and problems

increases as the interval filled by the realized values grows. The algorithm solves the problem of value distribution independently of the scale resolution, the width of the scanning window, and of any combination of these parameters.

In order to answer the question if the observed intensities of dynamic complexity reach critical values, intraitem calibration procedures were used in order to define adequate thresholds fitting to the actual dynamics. The time series of dynamic complexity were standardized by *z*-transformations, providing significance thresholds of 5% or 1%. Applying this threshold method to all items of the TPQ reduces the quantitative complexity signals of each time series to a three-step signal (not significant, complexity exceeds a 5% threshold, complexity exceeds a 1% threshold). A synopsis of these qualitative signals referring to all items of the TPQ gives an impression of the localization of critical fluctuations during the whole process. Dynamic complexities seem to be synchronized over many items and factors of the TPQ, resulting in the structure of columns of grey ($< 5\%$) or black ($< 1\%$) dots. In a large part of the investigated therapies such column-like structures could be identified. In an item-by-time synopsis they indicate phases of intensified as well as synchronized fluctuations and entropies of quite different aspects of the process. Consequently, these item-by-time synopses are called *complexity resonance diagrams* (Fig. 6).

In order to confirm the structures found within the complexity-resonance-diagrams, surrogate tests were realized based on random as well as on FFT-based surrogates of the time series. The empirical patterns are impressively different from the surrogate-based patterns (all realized comparisons with $p = 0.000$). Further support for phase-transition like phenomena in the change processes came from recurrence plots representing similarities and dissimilarities of dynamic segments of a whole time series (Eckmann et al. 1987; Vandenhouten 1998; Webber and Zbilut 1994). This method is based on the embedding of time series into a phase space constructed by timedelay coordinates, a method which is also crucial in the algorithms for the estimation of dimensional complexity or chaoticity (e. g., Kolmogorov–Sinai-Entropy, Lyapunov Exponents). Neighbors in the time-delay phase space represent similar dynamic segments and are plotted by a dot in the recurrence plot. Dissimilarities are represented by empty columns in the recurrence plots, which in many cases exactly correspond to the columns of dots in the complexity-resonance diagrams. The overall correlation is –0.45, if small shifts (lags of + or –3 measurement points at maximum) will be allowed. This means that periods of critical instability correspond to transient dynamics outside of the quasi-attractors established by the self-organizing system under consideration. These different ways to identify critical phase transitions are further validated by the time frequency distribution (TFD) of the time series. The TFD method uses wavelet spectra in order to scan the evolution of the frequency distributions within a signal (Lambertz et al. 2003; Vandenhouten 1998). It is a dynamic counterpart to the static fast Fourier transformation and allows for the identification of pronounced frequency amplitudes or changes in the frequency distributions. In the data set of the referred study these often appear exactly during the phase transitions which can be identified by other methods (see the synoptical representations of different time series analysis methods on the DVD in the textbook of Haken and Schiepek 2006).

An overall result of the study is shown in Fig. 7. It portrays the evidence that in order to bring forth change processes within self-organizing systems at least two conditions should be realized. The first condition: The degree of the control parameter energizing the system and pushing it away from its actual equilibrium state should exceed a certain intensity level. With respect to psychotherapies this control parameter could be the patient's motivation to change including his engagement into the therapeutic work. Second condition: The degree of instability the system attains during its change process. This instability during emerging symmetries and symmetry breaking transitions is given by the local maximum of dynamic complexity during the hospital stay. The interaction of both conditions results in treatment effectiveness. A third important condition is not represented in Fig. 7: It is the experienced stability of the outer environment (context at the ward or therapeutic bond) or of the inner environment (as self-esteem,

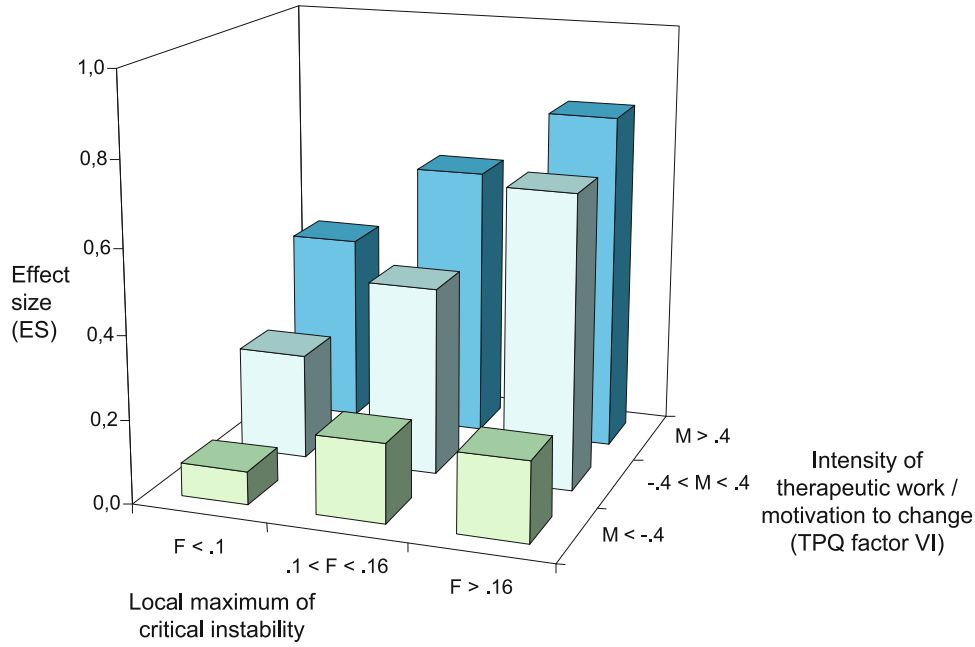

Self-Organization in Clinical Psychology, Fig. 7 The effect size (ES) (mean ES of all outcome measures introduced in the study, see text) of inpatient psychotherapy is produced by an interaction between the local maximum of critical fluctuations and the intensity of the control parameter realized during the change process. The local maxima of fluctuations were defined by the difference between the mean dynamic complexity of the whole therapy process and the maximum of the complexity observed during the process. The diagram is based on the mean of the local maxima of all items. The control parameter was defined by the overall mean of the TPQ factor VI: Intensity of therapeutic work/motivation to change

self-confidence, or activated resources). This context of stability is a prerequisite for a system to undergo critical instabilities.

The Concept of Self-Organization Promotes New Information Technologies in Clinical Psychology – The Synergetic Navigation System

Since self-organization and nonlinear dynamics seem to be ubiquitous in human change processes, it should be helpful to go beyond the diagnostics of steady states to an assessment of dynamics. Practitioners should get information on the therapy and its features *during* the ongoing process in order to use this information for an adequate placement of interventions and a control of the dynamics. "Controlling" self-organization processes in psychotherapies means the generation and co-creation (together with the patient) of adequate boundary conditions, the decision to do or to retain certain interventions, and to support the dynamics which the system is creating by itself. The patient takes an active and cooperative role in this understanding of data-based and co-creative change processes. Another important motivation for the development of real-time assessment comes from the evidence that most of the empirically identified specific and non-specific factors driving therapeutic change processes are connected with specific persons (the concrete therapist who meets a concrete patient in a concrete setting) and evolve by its nonlinear interactions in specific systems. These factors are (i) personal features of the patient like his motivation to change, his premorbid adaptation and degree of social functioning, personality integration, ego-strength, or comorbidities, (ii) personal and professional features of the therapist like his own personality integration, social and professional competencies, allegiance to his approach of doing therapy, stress-resistance, and so on, and (iii) factors of the professional and social context (see the so-called generic model of psychotherapy

Lambert and Ogles 2004; Orlinsky et al. 2004). In consequence, *evidence-based treatments* should be based on the evidence of concrete data mirroring the ongoing change process and on the professional decisions reflecting this insight.

Real-time monitoring actually uses internet-based presentations (including PDA or cell phone technology) of outcome and process questionnaires. Data are sent to a server, where they are stored and analyzed. Professionals and patients can inspect the results whenever they want. Experiences with real-time feedback to therapists (based on an outcome questionnaire the patient fills out during the therapy sessions in an ambulatory or outpatient context) are encouraging. Lambert and co-workers (e. g., Lambert et al. 2002) were able to identify processes on the way of getting difficult or unsuccessful ("not on track" therapies, compared to more promising "on track" therapies), and helped therapists to correct these not-on-track dynamics by specific interventions. By this, threatening drop-outs could be avoided, bad results could be corrected, and on-track processes could be optimized and even shortened.

More sophisticated than the distinction between "on-track" and "not-on-track" courses is the feedback on self-organization features realized by a system based on synergetics (Haken and Schiepek 2006). The *Synergetic Navigation System* uses the therapy process questionnaire for daily ratings and applies methods from nonlinear time series analysis in order to identify important qualities of the change process. This are:

- Stability or instability of the dynamics as represented by the subscales (factors) of the TPQ (see Table 2), which is measured by the dynamic complexity
- Recurrence plots indicating transitions or repeating patterns
- Intensity of synchronization and time-dependent synchronization patterns between the items and the factors of the TPQ (realized by the cross-correlations of all items of the TPQ, calculated within a running window).

Figure 8 shows a synopsis of these analysis methods applied to a specific change process. Preceding the inspection of all analysis results the raw data series of the items and the time courses of the factors (z-transformed values) are available. Additionally patients can write an electronic diary after filling out the questionnaire. The diary entries can be presented within a gliding tip-tool running over the time series. By this, corresponding qualitative and quantitative information completes the picture.

The Self-Organizing Brain

The human brain is one of the most outstanding examples of a complex nonlinear system producing self-organized patterns of functioning. Since function corresponds to structure and vice versa, structural changes (changes of intersynaptic coupling strengths and network configurations, (re-) wiring patterns following the synchronized coactivity of neurons) can be explained by functional self-organization of neural populations. Perception, action and transition of action patterns, decision making, and cognitive, behavioral, as well as emotional learning are psychological functions following the principles of self-organization (Haken and Schiepek 2006). At a neural level they correspond to and are based on nonlinear brain dynamics. The emergence of order parameters and the occurrence of phase transitions can be described and measured on a psychological as well as on a neural level.

One of the phenomena modeled by synergetics is Gestalt perception – the construction of percepts and the switching of ambiguous visual patterns (e. g., Necker cube or stroboscopic alternative motion). These processes of Gestalt perception constitute the link between Gestalt psychology and actual mathematical modeling in synergetics (Haken 1990b). The binding of different perceptual features or components to coherent structures or "qualia" seems to be due to synchronization processes of extended brain regions and converging integrative areas (Singer and Gray 1995). Pattern perception corresponds to pattern formation – as H. Haken puts it into pointed words. Tallon-Baudry et al. (Tallon-Baudry and Bertrand 1999; Tallon-Baudry et al. 1997) measured enhanced gamma-band activity (30–50 Hz) in the EEG of the primary and secondary visual

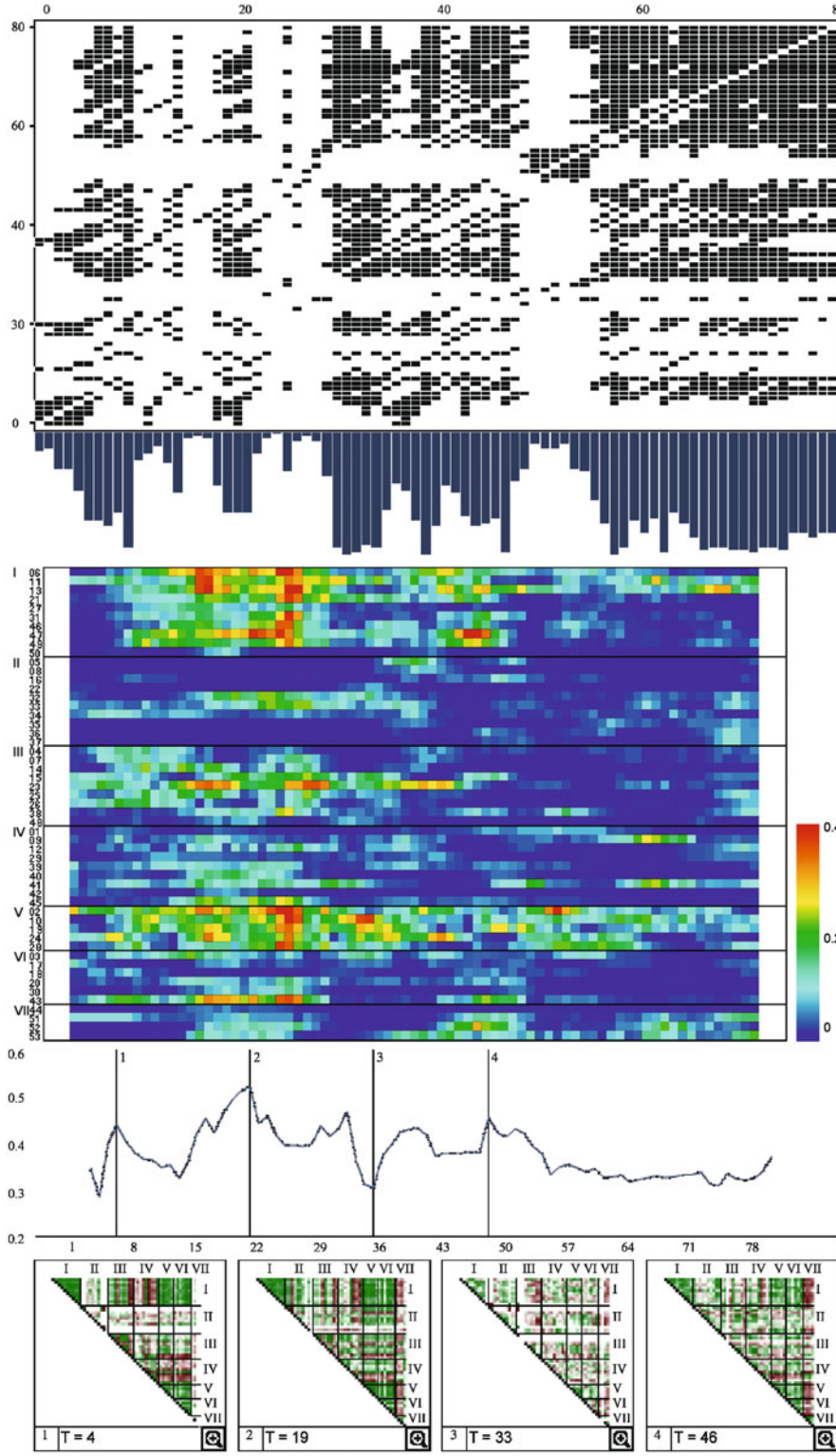

Self-Organization in Clinical Psychology, Fig. 8 Synopsis of a psychotherapy process as monitored by the Synergetic Navigation System. The time course of the inpatient treatment of a patient with eating disorders

cortex while subjects identified a triangle within the offered stimulus material. This could be a fingerprint of corresponding neural synchronization processes. This activity occurred when subjects saw a real object (triangle) as well as a figural illusion of the object (Kanizsa triangle), but not if geometrical components could not be composed to a true Gestalt. The research group of Basar–Eroglu and Stadler (Basar-Eroglu et al. 1996) measured significant gamma-band activity in EEG during states of perceptual switching triggered by stroboscopic alternative motions. In summary: Perception of multistability is one of the multifold cognitive processes giving rise to 40 Hz enhancement in the cortex, and coherent oscillations reflect an important mechanism of feature linking in the visual cortex which corresponds to the emergence of a neural order parameter. Changing order parameter dynamics during different cognitive activities was shown by Schupp et al. (Schupp et al. 1994). Mental imagery of an object could be differentiated from its concrete perception. The dimensional complexity of prefrontal EEG was increased during sensory imagery compared to the real perception of the same object (compare Lutzenberger et al. 1992).

The well-known movement coordination paradigm modeled by Haken et al. (Haken et al. 1985) was used to demonstrate neural correlates of instability and symmetry breaking processes in the motor brain. The order parameter in this finger movement experiment is the relative phase of the index fingers of both hands. Metronome-pacing – with movement frequency as the control parameter – triggers the system from parallel (out-of-phase) to mirror (inphase) movement. Meyer-Lindenberg et al. (2002) showed that the emergence of patterns in open, nonequilibrium systems like the brain is governed by their stability in response to small disturbances. Transitions could be elicited by interference at the neural level. Functional neuroimaging (PET) identified premotor (PMA) and supplementary motor (SMA) cortices as having neural activity linked to the degree of behavioral instability, induced by increasing frequency of the finger movement. These regions then were transiently disturbed with graded transcranial magnetic stimulation (TMS), which caused sustained and macroscopic behavioral transitions from the less stable out-of-phase to the stable in-phase movement, whereas the stable pattern could not be affected. Moreover, the strength of the disturbance needed (a measure of neural stability) was linked to the degree of the control parameter (movement frequency) and thereby to the behavioral stability of the system.

Synergetic research in clinical psychology is now reaching the brain level. The aim of an actual fMRI-study (Schiepek et al. 2008) is the investigation of phase transitions of brain activity and related subjective experiences of patients during their psychotherapy process. Repeated fMRI scans are related to the degree of stability or instability of the ongoing dynamics (measured by the dynamic complexity of daily TPQ-ratings) as well as to the therapy outcome. Realtime monitoring by the *Synergetic Navigation System* allows for the identification of stable or unstable periods and by this for a decision on the appropriate moments of fMRI acquisitions. Three or four scans are realized during each of the psychotherapy processes of 15 patients. The study includes only patients with obsessive-compulsive disorder (OCD) of the washing/contamination fear subtype (DSM IV: 300.3), without any

Self-Organization in Clinical Psychology, Fig. 8 (continued) portrays a clear cut phase-transition associated with critical instabilities. *Top:* Recurrence plot of the item "Today I was successful to do steps towards my personal goals". *Dots* represent recurrent segments of the time series, empty spaces represent transitions. *Middle:* Complexity resonance diagram of all items of the TPQ. Different from Fig. 6, the intensities of the dynamic complexity of each item is transformed into colors. Items are arranged by the order of the first-and second-order factors of TPQ. *Bottom:* Mean of all interitem correlations irrespective of the sign (absolute values). This is a measure of the overall synchronisation of the patient's experiences as represented by the items of the TPQ. The correlation structure is shown at four measurement points (days) of the psychotherapy process ($t = 4$, $t = 19$, $t = 33$, $t = 46$). Intensity of green represents positive correlations, intensities of red represents negative correlations

medication or comorbid psychiatric or somatic diagnoses. Patients are matched to healthy controls. (This research is a multi-center study of the Ludwig-Maximilians-University Munich, Institute of Psychology (Prof. Dr. Günter Schiepek, head of the project), and Clinic of Psychiatry (PD Dr. Oliver Pogarell, Dipl. Psych. Susanne Karch, Dr. Christoph Mulert), Hospital of Psychosomatic Medicine Windach/Ammersee and Day Treatment Centre Munich/Westend (Dr. Igor Tominschek, cand. Psych. Stephan Heinzel, Prof. Dr. Michael Zaudig), University Hospital Vienna/Astria, Clinic of Psychiatry (Prof. Dr. Martin Aigner, Prof. Dr. Gerhard Lenz, cand. med. Markus Dold, Dr. Annemarie Unger), MR Centre of Excellence, Medical University Vienna/Austria (Prof. Dr. Ewald Moser, Dr. Christian Windischberger).

OCD seems to be an appropriate model system for synergetic studies in clinical psychology, since the pathological order parameter is phenomenologically quite evident, the disease has an obvious and quite stable time course, and therapeutic phase transitions – if they do occur at all – are easy to be observed. OCD-specific functional neuroanatomy is partially known: Friedlander and Desrocher (Friedlander and Desrocher 2006) report on an executive dysfunction model corresponding to the cortico-striato-thalamo-cortical feedback-loops involved in perseverations and compulsions, and on a modulatory control model involved in the pathological mechanisms of anxiety and distress provoking obsessions.

The visual stimulation paradigm of the study uses symptom provoking, disgust provoking, and neutral pictures. The disgust and the neutral pictures are taken from the International Affective Picture System, whereas the OCD-related pictures are photographed in the home setting of the patients, showing specific and individualized symptom provoking stimuli.

For illustrative purposes we report on the results of a single case. It is a female patient, whose fMRI scans were taken three times during the 59 days of their hospital stay at days 9, 30, and 57. The healthy control was also scanned three times at identical time intervals as the patient. The second acquisition was done after an intensive period of critical instability of the TPQ-based time series, but just before the flooding was started. (Flooding or response prevention is an essential therapy technique in the treatment of OCD, where patients are confronted with symptom provoking stimuli but abstain from performing compulsive rituals.) The instability of the patient's process was the precursor of an important personal decision to divorce from her husband. (It should be noted that the development of her OCD symptoms was in the context of a long-lasting marital conflict.) This decision was the essential phase transition of the therapy.

Indeed, the most pronounced changes in brain activity occurred from the first to the second fMRI scan, whereas BOLD response differences from the second to the third session were only slight. They perhaps represent the neural correlates of an important personal phase transition related to the resolution of a severe personal conflict. Because these changes occurred before the flooding procedure was started, this can be seen as indicator of an early rapid response in the therapy (Lambert and Ogles 2004). Additionally, marked alternations in brain activity were to be observed before or during symptom reduction took place (measured by the Y-BOCS), not afterwards.

Alternations in brain activity involved widespread areas, e. g. the medial frontal brain regions including anterior cingulate cortex, superior and middle frontal gyrus, inferior frontal and precentral gyrus, superior temporal gyrus, superior parietal lobe, cuneus, thalamus and caudate nucleus in both hemispheres, as well as the right fusiform gyrus (see Fig. 9 for a OCD to disgust contrast). Thalamic and basal ganglia activation is part of the dorsolateral-caudate-striatum-thalamus circuitry of OCD. Especially the caudate nucleus takes a role within the executive dysfunction model of compulsions, and its activity has been found to be reduced after treatment (Nakao et al. 2005).

The function of the anterior cingulate cortex is interesting with regard to synergetics. The cingulate cortex comprises various functions like somatosensoric integration, mediation of affective and cognitive processes, control of attention, and processing of painful stimuli. Additionally, it plays an important role as conflict monitoring system: It is sensitive to ambiguous or conflicting

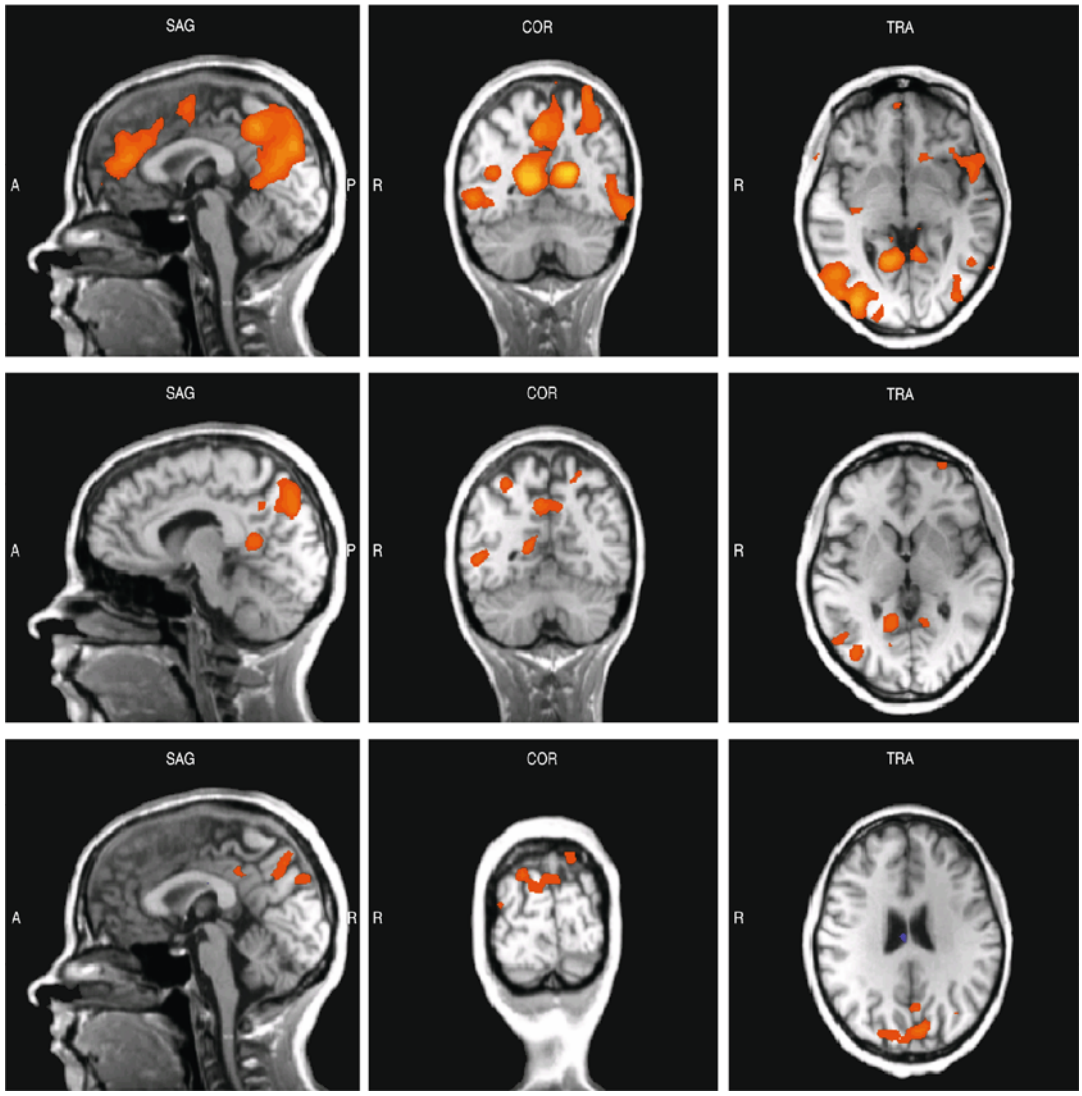

Self-Organization in Clinical Psychology, Fig. 9 Brain activation patterns of a patient with OCD during psychotherapy. BOLD signals from a 1.5 Tesla fMRI scanner. *Top:* First scan (9th day of hospital stay; $x = 0, y = -55, z = -2$; p(uncor) < 0.001). *Middle:* Second scan (30th day of hospital stay; $x = 8, y = -54, z = 5$; p (uncor) < 0.001). *Bottom:* The third scan (57th day of hospital stay; $x = 0, y = -85, z = 26$; p(uncor) < 0.001). Activations during the presentation of OCD-related pictures compared to activations during the presentation of neutral pictures (OCD > disgust)

information (van Veen and Carter 2002a, b), is involved in decision making (King-Casas et al. 2005; Sanfey et al. 2003), and its activation is predictive to treatment outcome in depression (e. g. Mayberg et al. 1997). This is true especially for the dorsal (cognitive) structures of the ACC. It could be an indicator of symmetry states of brain functioning, which is characterized by two or more dynamic patterns or attractors in competition. In the present case, the ACC activation at the beginning of the therapy could be either part of the pathology or could be indicative for the critical instability of the cognitive-affective system of the patient, preparing her important decision. The second fMRI measure was conducted during a local minimum of critical fluctuations. If the impressive

change in cingulate activation could be attributed to a changed critical symmetry state of the neural self-organization before vs. after the phase-transition or to changes in symptom severity cannot be decided within a single case study, but seems to be an interesting question to further research. Perhaps the fact that during the second fMRI measure the Y-BOCS score was nearly on the same level as during the first measure – only 14% reduction, compared to 50% reduction in dynamic complexity – could be a first argument in favor of the instability hypothesis.

The paradigm of self-organization is a very promising approach to clinical as well as other fields of psychology. Its interdisciplinary is due to the fact that the laws and principles of self-organization are true for neural, mental, and behavioral processes (and the corresponding data qualities). Interdisciplinary cooperation is underpinned by the unifying terminology as well as by the unifying formalism and modeling tools of synergetics. This opens new perspectives for basic and applied research, but also for the treatment of mental disorders. New developments in the real-time monitoring of human change processes based on synergetics and nonlinear science have been mentioned. Another field of encouraging developments is deep brain stimulation (DBS), which apply to neurological diseases as Parkinsonian or essential tremor, but also to psychiatric disorders as OCD or mayor depression (Tass et al. 2003). The difference between new technologies (applying the mathematical instruments and concepts of synergetics as well as methods from stochastic phase resetting) and classical electrical deep brain stimulation is that normal DBS at high frequencies has a blocking effect on the stimulated target and mimics the effect of tissue lesioning. New technologies are demand-controlled, working with low stimulation frequencies, and avoid the suppression of neurons' firing. Its effect is a desynchronization of pathologically synchronized populations of neurons, using multi-site coordinated reset stimulation (Tass and Hauptmann 2007) or nonlinear delayed feedback stimulation (Popovych et al. 2006). Both methods counteract abnormal interactions and detune the macroscopic frequency of the collective oscillators – that is the abnormally established order parameters of neural synchronization. Thereby they restore the natural frequencies of the individual oscillatory units. Neurons get in the range of physiological functioning and can engage in changing and varying synchronization patterns. If altered synchronization patterns also change the coupling strength connecting synapses, a rewiring of neural nets could be reached. Changed function triggers the emergence of healthy attractors and by this changes the structure of neural networks. Perhaps in the future technologies of DBS or even non-invasive brain stimulation could be combined with psychotherapy and psychological navigation instruments developed to optimize self-organizing change processes.

Future Directions

The future developments of self-organization and complexity research in clinical psychology and psychotherapy will be interconnected to its acceptance in practice and training. Perhaps this sounds paradoxically, since in most other scientific fields the future depends on the investigations to basic research and to new technologies. Of course this holds also for synergetics and its applications to clinical psychology. However, it should be noted that complexity research and nonlinear dynamics are done since more than two decades in European academic psychology with poor impact to mainstream science. So, the future will depend on a greater number of new arriving and highly qualified students in this topic who do not avoid the touch with mathematics. Self-organization and complexity research including its mathematical backgrounds should become part of the training curricula in psychology and psychotherapy. Since the Synergetic Navigation System waits for its broad application in clinical and psychotherapeutic practice, a new decade of practice-based research can be started. But these developments depend on its acceptance by practitioners because of the competencies required for the widespread use of sophisticated methods. This integration of

science with practice will open huge sources and new dimensions of data gathering on dynamic systems. An important database for outcome and time series data (including biomarkers) of human change processes is actually prepared.

Another stream of development is concerning the integration of psychological and biological/physiological data. Since human self-organization takes place on synchronized mental, social, and biological system levels, all of them should be taken into account in further research. One research paradigm was suggested in this chapter: The investigation of individual and social processes by the Synergetic Navigation System, and in parallel repeated brain scans using fMRI technology or other methods to get insight into brain dynamics (EEG, gene expression markers Koch et al. 2002, immune or endocrine markers Schubert and Schiepek 2003, or others). Two final remarks: First, future developments of synergetic-based minimal invasive DBS could be combined with psychotherapy and psychological interventions – as pharmacological and psychological treatments are combined nowadays. Second, the nonlinear networks underlying psychological as well as neural self-organization will not be understood without applying appropriate mathematical tools, giving raise to a new systemic psychology and neuroscience.

Bibliography

an der Heiden U (1992) Chaos in health and disease – phenomenology and theory. Tschacher W, Schiepek G, Brunner EJ (eds) Self-organization and clinical psychology. Springer, Berlin, 55–87

Bak P, Chen K, Creutz M (1989) Self-organized criticality and the 'game of life'. Nature 342:780–782

Basar E, Flohr H, Haken H, Mandell AJ (1983) Synergetics of the brain. Springer series in synergetics, 23. Springer, Berlin

Basar-Eroglu C, Strüber D, Kruse P, Basar E, Stadler M (1996) Frontal gamma-band enhancement during multistable visual perception. Int J Psychophysiol 24:113–125

Bethe A (1940) Die biologischen Rhythmusvorgänge als selbständige und erzwungene Kippvorgänge betrachtet. Pflugers Arch 244:1–42

Böker W, Brenner HD (eds) (1989) Schizophrenie als systemische Störung. Huber, Bern

Böker W, Brenner HD (1996) Stand systemischer Modellvorstellungen zur Schizophrenie und Implikationen für die Therapieforschung. In: Böker W, Brenner HD, Genner RM (eds) Integrative Therapie der Schizophrenie. Huber, Bern, pp 17–32

Cannon WB (1915) Bodily changes in pain, hunger, fear, and rage: an account of recent researches into the function of emotional excitement. Appleton, New York

Carlsson A (2006) The neurochemical circuitry of schizophrenia. Pharmacopsychiatry 39(Suppl 1):S10–S14

Caspar F (1996) Beziehungen und Probleme verstehen. Eine Einführung in die psychotherapeutische Plananalyse. Huber, Bern

Ciompi L (1989) Zur Dynamik komplexer biologisch-psychosozialer Systeme: Vier fundamentale Mediatoren in der Langzeitentwicklung der Schizophrenie. In: Böker W, Brenner HD (eds) Schizophrenie als systemische Störung. Huber, Bern, pp 27–38

Ciompi L, Müller C (1976) Lebensweg und Alter der Schizophrenen. Springer, Berlin

Eckmann JP, Oliffson Kamphorst S, Ruelle D (1987) Recurrence plots of dynamical systems. Europhys Lett 4:973–977

Friedlander L, Desrocher M (2006) Neuroimaging studies of obsessive-compulsive disorder in adults and children. Clin Psychol Rev 26:32–49

Friston KJ, Harrison L, Penny WD (2003) Dynamic causal modelling. NeuroImage 19:1273–1302

Haken H (1990a) Synergetics - an introduction. Non-equilibrium phase transitions in physics, chemistry, and biology. Springer, Berlin. (first edition 1977)

Haken H (1990b) Synergetics as a tool for the conceptualization and mathematization of cognition and behavior – How far can we go? In: Haken H, Stadler M (eds) Synergetics of cognition. Springer, Berlin, pp 2–31

Haken H (1996) Principles of brain functioning. A synergetic approach to brain activity, behavior, and cognition. Springer, Berlin

Haken H (2002) Brain dynamics. Springer, Berlin

Haken H (2004) Synergetics. Introduction and advanced topics. Springer, Berlin

Haken H, Schiepek G (2006) Synergetik in der Psychologie. Selbstorganisation verstehen und gestalten. Hogrefe, Göttingen

Haken H, Kelso JAS, Bunz H (1985) A theoretical model of phase transition in human hand movements. Biol Cybern 51:347–356

Kettunen J, Keltikangas-Järvinen L (2001) Intraindividual analysis of instantaneous heart rate variability. Psychophysiology 38:659–668

King-Casas B, Tomlin D, Anen C, Camerer CF, Quartz SR, Montague PR (2005) Getting to know you: reputation and trust in a two-person economic exchange. Science 308:78–83

Koch JM, Kell S, Hinze-Selch D, Aldenhoff JB (2002) Changes in CREB-phosphorylation during recovery from major depression. J Psychiatr Res 36:369–375

Köhler W (1947) Gestalt psychology. Liveright, New York

Kowalik ZJ, Schiepek G, Kumpf K, Roberts LE, Elbert T (1997) Psychotherapy as a chaotic process II: the application of nonlinear analysis methods on quasi time series of the client-therapist-interaction: a non-stationary approach. Psychother Res 7:197–218

Kruse P, Carmesin HO, Stadler M (1997) Schizophrenie als Korrespondenzproblem plastischer neuronaler Netze. In: Schiepek G, Tschacher W (eds) Selbstorganisation in Psychologie und Psychiatrie. Vieweg, Braunschweig, pp 171–190

Lambert MJ, Ogles BM (2004) The efficacy and effectiveness of psychotherapy. In: Lambert MJ (ed) Bergin and Garfield's handbook of psychotherapy and behavior change. Wiley, New York, pp 139–193

Lambert MJ, Whipple JL, Smart DW, Vermeersch DA, Nielsen SL, Hawkins EJ (2001) The effects of providing therapists with feedback on patient progress during psychotherapy: are outcomes enhanced? Psychother Res 11:49–68

Lambert MJ, Whipple JL, Vermeersch DA, Smart DW, Hawkins EJ, Nielsen SL, Goates M (2002) Enhancing psychotherapy outcomes via providing feedback on client progress: a replication. Clin Psychol Psychother 9:91–103

Lambertz M, Vandenhouten R, Grebe R, Langhorst P (2000) Phase transitions in the common brainstem and related systems investigated by nonstationary time series analysis. J Auton Nerv Syst 78:141–157

Lambertz M, Vandenhouten R, Langhorst P (2003) Transiente Kopplungen von Hirnstammneuronen mit Atmung, Herzkreislaufsystem und EEG: Ihre Bedeutung für Ordnungsübergänge in der Psychotherapie. In: Schiepek G (ed) Neurobiologie der Psychotherapie. Schattauer, Stuttgart, pp 302–324

Lenz F, Kwan H, Martin R, Tasker R, Dostrovsky J, Lenz Y (1994) Single unit analysis of the human ventral thalamic nuclear group. Tremor-related activity in functionally identified cells. Brain 117:531–543

Lewin K (1951) Field theory in social psychology. Harper, New York

Lutzenberger W, Elbert T, Birbaumer N, Ray WJ, Schupp H (1992) The scalp distribution of the fractal dimension of the EEG and its variation with mental tasks. Brain Topogr 5:27–34

Mayberg HS, Brannan SK, Mahurin RK, Jerabek PA, Brickman JS, Tekell JL, Silva JA, McGinnis S, Glass TG, Martin CC, Fox PT (1997) Cingulate function in depression: a potential predictor of treatment response. Neuroreport 8:1057–1061

Mergenthaler E (1998) Cycles of emotion-abstraction patterns: a way of practice oriented process research? Br Psychol Soc – Psychother Sect Newsl 24:16–29

Meyer-Lindenberg A, Ziemann U, Hajak G, Cohen L, Faith Berman K (2002) Transitions between dynamical states of differing stability in the human brain. PNAS USA 99:10948–10953

Nakao T, Nakagawa A, Yoshiura T, Nakatani E, Nabeyama M, Yoshizato C, Kudoh A,Tada K, Yoshioka K, Kawamoto M,Togao O, Kanba S (2005) Brain activation of patients with obsessive-compulsive disorder during neuropsychological and symptom provocation tasks before and after symptom improvement: a functional magnetic resonance imaging study. Biol Psychiatry 57:901–910

Nowak A, Vallacher RR (1998) Dynamical social psychology. Guilford, New York

Orlinsky DE, Ronnestad MH, Willutzki U (2004) Fifty years of psychotherapy process-outcome research: Continuity and change. In: Lambert MJ (ed) Bergin and Garfield's handbook of psychotherapy and behavior change. Wiley, New York, pp 307–389

Pare D, Curro'Dossi R, Steriade M (1990) Neuronal basis of the parkinsonian resting tremor: a hypothesis and its implications for treatment. Neurosci 35:217–226

Penny WD, Stephan KE, Mechelli A, Friston KJ (2004) Modelling functional integration: a comparison of structural equation and dynamic causal models. NeuroImage 23(Suppl 1):264–274

Perlitz V, Cotuk B, Haberstock S, Kahn N, Grebe R, Petzold ER, Schmid-Schönbein H (2003) Differentiation of cutaneous haemo-and neurodynamics using multiscale Time-frequency-distribution portrays. In: Blazek V, Schultz-Ehrenburg U (eds) Proceedings of the 10th international symposium CNVD 2001 at Aachen

Perlitz V,Cotuk B, Lambertz M, Grebe R, Schiepek G, Petzold ER, Schmid-Schönbein H, Flatten G (2004a) Coordination dynamics of circulatory and respiratory rhythms during psychomotor relaxation. Auton Neurosci 115(1–2):82–93

Perlitz V, Cotuk B, Schiepek G, Sen A, Haberstock S, Schmid-Schönbein H, Petzold ER, Flatten G (2004b) Synergetik der hypnoiden Relaxation. Psychother Psych Med 54:250–258

Perlitz V, Lambertz M, Cotuk B, Grebe R, Vandenhouten R, Flatten G, Petzold ER, Schmid-Schönbein H, Langhorst P (2004c) Cardiovascular rhythms in the 0.15 Hz band: common origin of identical phenomena in man and canine in the reticular formation of the brain stem? Pflugers Arch - Eur J Physiol 448(6):579–592

Piaget J (1976) Die Äquilibration der kognitiven Strukturen. Klett-Cotta, Stuttgart

Popovych OV, Hauptmann C, Tass PA (2006) Control of neural synchrony by nonlinear delayed feedback. Biol Cybern 95:69–85

Rapp PE, Albano ME, Zimmerman ID et al (1994) Phase-randomized surrogates can produce spurious identifications of non-random structure. Phys Lett A 192:27–33

Rockstroh B, Watzl H, Kowalik ZJ, Cohen R, Sterr A, Müller M, Elbert T (1997) Dynamical aspects of the EEG in different psychopathological states in an interview situation. A pilot study. Schizophr Res 28:77–85

Rosenstein MT, Collins JJ, de Luca CJ (1993) A practical method for calculating Largest Lyapunov Exponents from small data sets. Physica D 65:117–134

Sanfey AG, Rilling JK, Aronson JA, Nystrom LE, Cohen JD (2003) The neural basis of economic decision-

making in the Ultimatum Game. Science 300:1755–1758
Saxena S, Rauch SL (2000) Functional neuroimaging and the neuroanatomy of obsessive-compulsive disorder. Psychiatr Clin North Am 23:563–586
Schaub H, Schiepek G (1992) Simulation of psychological processes: Basic issues and an illustration within the etiology of a depressive disorder. In: Tschacher W, Schiepek G, Brunner EJ (eds) Self-organization and clinical psychology. Springer, Berlin,pp 121–149
Schiepek G, Schoppek W, Tretter F (1992) Synergetics in psychiatry: Simulation of evolutionary patterns of schizophrenia on the basis of nonlinear difference equations. In: Tschacher W, Schiepek G, Brunner EJ (eds) Self-organization and clinical psychology. Springer, Berlin, pp 163–194
Schiepek G, Kowalik ZJ, Schütz A, Köhler M, Richter K, Strunk G, Mühlnickel W, Elbert T (1997) Psychotherapy as a chaotic process I. Coding the client-therapist-interaction by means of sequential plan analysis and the search for chaos: a stationary approach. Psychother Res 7:173–194
Schiepek G, Tominschek I, Karch S, Mulert C, Pogarell O (2007) Neurobiologische Korrelate der Zwangsstörungen – Aktuelle Befunde zur funktionellen Bildgebung. Psychother Psych Med 57:379–394
Schiepek G, Tominschek I, Karch S, Lutz J, Mulert C, Born C, Pogarell O (2008) A controlled single case study with repeated fMRI measures during the treatment of a patient with obsessive-compulsive disorder: testing the nonlinear dynamics approach to psychotherapy. World J Biol Psychiatry doi:https://doi.org/10.1080/15622970802311829
Schubert C, Schiepek G (2003) Psychoneuroimmunologie und Psychotherapie: Psychosozial induzierte Veränderungen der dynamischen Komplexität von Immunprozessen. In: Schiepek G (ed) Neurobiologie der Psychotherapie. Schattauer, Stuttgart, pp 485–508
Schupp HAT, Lutzenberger W, Birbaumer N, Miltner W, Braun C (1994) Neurophysiological differences between perception and imagery. Cogn Brain Res 2:77–86
Selye HA (1936) Syndrome produced diverse nocuous agents. Nature 138:32
Singer W, Gray CM (1995) Visual feature integration and the temporal correlation hypothesis. Annu Rev Neurosci 18:555–586
Sinha R, Lovallo WR, Parsons OA (1992) Cardiovascular differentiation of emotions. Psychosom Med 54:422–435
Skinner JE, Molnar M, Tomberg C (1994) The point correlation dimension: performance with nonstationary surrogate data and noise. Integr Physiol Behav Sci 29:217–234
Stadler M, Kruse P (1990) The self-organization perspective in cognition research. Historical remarks and new experimental approaches. In: Haken H, Stadler M (eds) Synergetics of cognition. Springer, Berlin, pp 32–52
Strauss JS (1989) Intermediäre Prozesse in der Schizophrenie: Zu einer neuen dynamisch orientierten Psychiatrie. In: Böker W, Brenner HD (eds) Schizophrenie als systemische Störung. Huber, Bern, pp 39–50
Strunk G (2004) Organisierte Komplexität. Mikroprozess-Analysen der Interaktionsdynamik zweier Psychotherapien mit den Methoden der nichtlinearen Zeitreihenanalyse. Dissertation, Universität Bamberg
Strunk G, Schiepek G (2006) Systemische Psychologie. Eine Einführung in die komplexen Grundlagen menschlichen Verhaltens. Spektrum Akademischer Verlag, Heidelberg
Tallon-Baudry C, Bertrand O (1999) Oscillatory gamma activity in humans and its role in object representation. Trends Cogn Sci 3:151–162
Tallon-Baudry C, Bertrand O, Wienbruch C, Ross B, Pantev C (1997) Combined EEG and MEG recordings of visual 40 Hz resonses to illusory triangles in human. Neuroreport 8:1103–1107
Task Force of the European Society of Cardiology and the North American Society of Pacing and Electrophysiology (1996) Heart rate variability. Standards of measurement, physiological interpretation, and clinical use. Eur Heart J 17:354–381
Tass P, Hauptmann C (2007) Therapeutic modulation of synaptic connectivity with desynchronizing brain stimulation. Int J Psychophysiol 64:53–61
Tass PA, Klosterkötter J, Schneider F, Lenartz D, Kouluosakis A, Sturm V (2003) Obsessive-compulsive disorder: development of demand-controlled deep brain stimulation with methods of stochastic phase resetting. Neuropsychopharmacology 28:S27–S34
Tretter F, Scherer J (2006) Schizophrenia, neurobiology, and the methodology of systemic modelling. Pharmacopsychiatry 39(Suppl 1):S26–S35
Tschacher W (1997) Prozessgestalten. Hogrefe, Göttingen
Tschacher W, Dauwalder JP (1999) Situated cognition, ecological perception, and synergetics: A novel perspective for cognitive psychology? In: Tschacher W, Dauwalder JP (eds) Dynamics, synergerics, autonomous agents. World Scientific, Singapore, pp 83–104
Tschacher W, Kupper Z (2002) Time series models of symptoms in schizophrenia. Psychiatry Res 113:127–137
van Veen V, Carter CC (2002a) The anterior cingulate as a conflict monitor: fMRI and ERP studies. Physiol Behav 77:477–482
van Veen V, Carter CC (2002b) The timing of action-monitoring processes in the anterior cingulate cortex. J Cogn Neurosci 14:593–602
Vandenhouten R (1998) Analyse instationärer Zeitreihen komplexer Systeme und Anwendungen in der Physiologie. Shaker, Aachen

Villmann T, Liebers C, Bergmann B, Gumz A, Geyer M (2008) Investigation of psycho-physiological interactions between patient and therapist during a psychodynamic therapy and their relation to speech in terms of entropy analysis using a neural network approach. New Ideas Psychol 26:309–325

von Uexküll T, Wesiack W (1996) Wissenschaftstheorie: Ein bio-psycho-soziales Modell. In: Adler RH, Herrmann JM, Köhle K, Schonecke OW, von Uexküll T, Wesiack W (eds) Thure von Uexküll. Psychosomatische Medizin. Urban Schwarzenberg, München, pp 13–52

Webber CL, Zbilut JP (1994) Dynamical assessment of physiological systems and states using recurrence plot strategies. J Appl Physiol 76:965–973

Yuru Z, Jan KM, Ju KH, Chon KH (2006) Quantifying cardiac sympathetic and parasympathetic nervous activities using principal dynamic modes analysis of heart rate variability. Am J Physiol Heart Circ Physiol 291:H1475–H1483

Movement Coordination

Armin Fuchs[1,2] and J. A. Scott Kelso[1,3]
[1]Human Brain and Behavior Laboratory, Center for Complex Systems and Brain Sciences, Florida Atlantic University, Boca Raton, FL, USA
[2]Department of Physics, Florida Atlantic University, Boca Raton, FL, USA
[3]Intelligent Systems Research Centre, School of Computing and Intelligent Systems, Ulster University, Derry Londonderry, Northern Ireland, UK

Article Outline

Glossary
Definition of the Subject
Introduction
The Basic Law of Coordination: Relative Phase
Stability: Perturbations and Fluctuations
The Oscillator Level
Breaking and Restoring Symmetries
Conclusions
Extensions of the HKB Model
Future Directions
Bibliography

Glossary

Control parameter A parameter of internal or external origin that when manipulated controls the system in a nonspecific fashion and is capable of inducing changes in the system's behavior. These changes may be a smooth function of the control parameter or abrupt at certain critical values. The latter, also referred to as phase transitions, are of main interest here as they only occur in nonlinear systems and are accompanied by phenomena like critical slowing down and fluctuation enhancement that can be probed for experimentally.

Haken-Kelso-Bunz (HKB) model First published in 1985, the HKB model is the best-known and probably most extensively tested quantitative model in human movement behavior. In its original form, it describes the dynamics of the relative phase between two oscillating fingers or limbs under frequency scaling. The HKB model can be derived from coupled nonlinear oscillators and has been successfully extended in various ways, for instance, to situations where different limbs like an arm and a leg, a single limb and a metronome, or even two different people are involved.

Order parameter Order parameters are quantities that allow for a usually low-dimensional description of the dynamical behavior of a high-dimensional system on a macroscopic level. These quantities change their values abruptly when a system undergoes a phase transition. For example, density is an order parameter in the ice to water or water to vapor transitions. In movement coordination, the most-studied order parameter is relative phase, i.e., the difference in the phases between two or more oscillating entities.

Phase transition The best-known phase transitions are the changes from a solid to a fluid phase like ice to water or from fluid to gas like water to vapor. These transitions are called first-order phase transitions as they involve latent heat, which means that a certain amount of energy has to be put into the system at the transition point that does not cause an increase in temperature. For the second-order phase transitions, there is no latent heat involved. An example from physics is heating a magnet above its Curie temperature at which point it switches from a magnetic to a nonmagnetic state. The qualitative changes that are observed in many nonlinear dynamical systems when a parameter exceeds a certain threshold are also such second-order phase transitions.

Definition of the Subject

Movement coordination is present all the time in daily life but tends to be taken for granted when it

A. Hutt, H. Haken (eds.), *Synergetics*,
https://doi.org/10.1007/978-1-0716-0421-2_341

Originally published in
R. A. Meyers (ed.), *Encyclopedia of Complexity and Systems Science*, © Springer Science+Business Media LLC 2017
https://doi.org/10.1007/978-3-642-27737-5_341-3

works. One might say it is quite an arcane subject also for science. This changes drastically when some pieces of the locomotor system are not functioning properly because of injury, disease, or age. In most cases, it is only then that people become aware of the complex mechanisms that must be in place to control and coordinate the hundreds of muscles and joints in the body of humans or animals to allow for maintaining balance while maneuvering through rough terrains, for example. No robot performance comes even close in such a task.

Although these issues have been around for a long time, it was only during the last quarter century that scientists developed quantitative models for movement coordination based on the theory of nonlinear dynamical systems. Coordination dynamics, as the field is now called, has become arguably the most developed and best tested quantitative theory in the life sciences.

More importantly, even though this theory was originally developed for modeling of bimanual finger movements, it has turned out to be universal in the sense that it is also valid to describe the coordination patterns observed between different limbs, like an arm and a leg, different joints within a single limb, like the wrist and elbow, and even between different people that perform movements while watching each other.

Introduction

According to a dictionary definition, *coordination* is the act of coordinating, making different people or things work together for a goal or effect.

When we think about *movement coordination*, the "things" we make work together can be quite different like our legs for walking; fingers for playing the piano; mouth, tongue, and lips for articulating speech; body expressions; and the interplay between bodies in dancing and ballet, tactics, and timing between players in team sports and so on, not to forget other advanced skill activities like skiing or golfing.

All these actions have one thing in common: they look extremely easy if performed by people who have learned and practiced these skills, and they are incredibly difficult for novices and beginners. Slight differences might exist regarding how these difficulties are perceived, for instance, when asked whether they can play golf, some people may say: "I don't know, let me try," and they expect to outdrive Tiger Woods right away; there are very few individuals with a similar attitude toward playing the piano.

The physics of golf as far as the ball and the club are concerned is almost trivial: hit the ball with the highest possible velocity with the club face square at impact, and it will go straight and far. The more tricky question is how to achieve this goal with a body that consists of hundreds of different muscles, tendons, and joints, and, importantly, their sensory support in joint, skin, and muscle receptors (proprioception), in short, hundreds of degrees of freedom. How do these individual elements work together, and how are they coordinated? Notice that the question is not how do we coordinate them? None of the skills mentioned above can be performed by consciously controlling all the body parts involved. Conscious thinking sometimes seems to do more harm than good. So how do they/we do it? For some time, many scientists sought the answer to this question in what is called *motor programs* or, more recently, *internal models*. The basic idea is straightforward: when a skill is learned, it is somehow stored in the brain like a program in a computer and simply can be called and executed when needed. Additional learning or training leads to skill improvement, interpreted as refinements in the program. As intuitive as this sounds and even if one simply ignores all the unresolved issues like how such programs gain the necessary flexibility or in what form they might be stored in the first place, there are even deeper reasons and arguments suggesting that humans (or animals for that matter) do not work like that. One of the most striking of these arguments is known as motor equivalence: everybody who has learned to write with one of their hands can immediately write with the foot as well. This writing may not look too neat, but it will certainly be readable and represents the transfer of a quite complex and difficult movement from one end effector (the hand) to another (the foot) that is controlled by a completely different set of muscles and joints. Different degrees of freedom and redundancy in

the joints can still produce the same output (the letters) immediately, i.e., without any practice.

For the study of movement coordination, a most important entry point is to look at situations where the movement or coordination pattern changes abruptly. An example might be the well-known gait switches from walk to trot to gallop that horses perform. It turns out, however, that switching among patterns of coordination is a ubiquitous phenomenon in human limb movements. As will be described in detail, such switching has been used to probe human movement coordination in quantitative experiments.

It is the aim of this article to describe an approach to a quantitative modeling of human movements, called coordination dynamics, that deals with quantities that are accessible from experiments and makes predictions that can and have been tested. The intent is to show that coordination dynamics represents a theory allowing for quantitative predictions of phenomena in a way that is unprecedented in the life sciences. In parallel with the rapid development of noninvasive brain imaging techniques, coordination dynamics has even pointed to new ways for the study of brain functioning.

The Basic Law of Coordination: Relative Phase

The basic experiment, introduced by one of us (Kelso 1981, 1984), that gave birth to coordination dynamics, the theory underlying the coordination of movements, is easily demonstrated and has become a classroom exercise for generations of students: if a subject is moving the two index fingers in a so-called anti-phase, i.e., one finger is flexing while the other is extending, and then the movement rate is increased, there is a critical rate where the subject switches spontaneously from the anti-phase movement to in-phase , i.e., both fingers are now flexing and extending at the same time. On the other hand, if the subject starts at a high or low rate with an in-phase movement and the rate is slowed down or sped up, no such transition occurs.

These experimental findings can be translated or mapped into the language of dynamical systems theory as follows (Haken et al. 1985):

- At low movement rates, the system has two stable attractors, one representing anti-phase and one for in-phase – in short, the system is bistable.
- When the movement rate reaches a critical value, the anti-phase attractor disappears, and the only possible stable movement pattern remaining is in-phase.
- There is strong hysteresis: when the system is performing in-phase and the movement rate is decreased from a high value, the anti-phase attractor may reappear, but the system does not switch to it.

In order to make use of dynamical systems theory for a quantitative description of the transitions in coordinated movements, one needs to establish a measure that allows for a formulation of a dynamical system that captures these experimental observations and can serve as a phenomenological model. Essentially, the finger movements represent oscillations (as will be discussed in more detail in subsection. "Oscillators for Limb Movements") each of which is described by an amplitude r and a phase $\varphi(t)$. For the easiest case of harmonic oscillations, the amplitude r does not depend on time, and the phase increases linearly with time at a constant rate ω, called the angular velocity, leading to $\varphi(t) = \omega t$. Two oscillators are said to be in the in-phase mode if the two phases are the same, or $\varphi_1(t) - \varphi_2(t) = 0$, and in anti-phase if the difference between their two phases is 180° or π radians. Therefore, the quantity that is most commonly used to model the experimental findings in movement coordination is the phase difference or *relative phase*:

$$\begin{aligned}\phi(t) &= \varphi_1(t) - \varphi_2(t) \\ &= \begin{cases} \phi(t) = 0 & \text{for in - phase} \\ \phi(t) = \pi & \text{for anti - phase.} \end{cases}\end{aligned} \tag{1}$$

The minimal dynamical system for the relative phase that is consistent with observations is

known as the Haken-Kelso-Bunz (or HKB) model and was first published in a seminal paper in 1985 (Haken et al. 1985):

$$\dot{\phi} = -a \sin \phi - 2b \sin 2\phi \quad \text{with} \quad a, b \geq 0. \tag{2}$$

As is the case for all one-dimensional first-order differential equations, Eq. 2 can be derived from a potential function:

$$\begin{aligned} \dot{\phi} &= -\frac{dV(\phi)}{d\phi} \quad \text{with} \\ V(\phi) &= -a \cos \phi - b \cos 2\phi. \end{aligned} \tag{3}$$

One of the two parameters a and b that appear in Eqs. 2 and 3 can be eliminated by introducing a new time scale $\tau = \alpha t$, a procedure known as scaling and commonly used within the theory of nonlinear differential equations, leading to

$$\begin{aligned} \dot{\phi}(t) = \frac{d\phi(t)}{dt} &\rightarrow \frac{d\phi\left(\frac{\tau}{\alpha}\right)}{d\frac{\tau}{\alpha}} \\ &= -a \sin \phi\left(\frac{\tau}{\alpha}\right) - 2b \sin 2\phi\left(\frac{\tau}{\alpha}\right) \\ \alpha \frac{d\widetilde{\phi}}{d\tau} &= -a \sin \widetilde{\phi}(\tau) - 2b \sin 2\widetilde{\phi}(\tau) \end{aligned} \tag{4}$$

where $\widetilde{\phi}$ has the same shape as ϕ; it is just changing on a slower or faster time scale depending on whether α is bigger or smaller than one. After dividing by α and letting the so far undetermined $\alpha = a$ Eq. 4 becomes

$$\frac{d\widetilde{\phi}}{d\tau} = -\underbrace{\frac{a}{\alpha}}_{=1} \sin \widetilde{\phi} - 2\underbrace{\frac{b}{\alpha}}_{=k} \sin 2\widetilde{\phi}. \tag{5}$$

Finally, by dropping the tilde ~, Eqs. 2 and 3 can be written with only one parameter $k = \frac{b}{a}$ in the form

$$\begin{aligned} \dot{\phi} &= -\sin \phi - 2k \sin 2\phi = -\frac{dV(\phi)}{d\phi} \\ &\text{with } V(\phi) = -\cos \phi - k \cos 2\phi. \end{aligned} \tag{6}$$

The dynamical properties of the HKB model's *collective* or *coordinative* level of description are visualized in Fig. 1 with plots of the phase space ($\dot{\phi}$ as a function of ϕ) in the top row, the potential landscapes $V(\phi)$ in the second row, and the bifurcation diagram at the bottom. The control parameter k, as shown, is the ratio between b and a, $k = \frac{b}{a}$, which is inversely related to the movement rate: a large value of k corresponds to a slow rate, whereas k close to zero indicates that the movement rate is high.

In the phase space plots (Fig. 1 top row) for $k = 0.75$ and $k = 0.5$, there exist two stable fixed points at $\phi = 0$ and $\phi = \pi$ where the function crosses the horizontal axis with a negative slope, marked by solid circles (the fixed point at $-\pi$ is the same as the point at π as the function is 2π–periodic). These attractors are separated by repellers, zero crossings with a positive slope and marked by open circles. For the movement rates corresponding to these two values of k, the model suggests that both anti-phase and in-phase movements are stable. When the rate is increased, corresponding to a decrease in the control parameter k down to the critical point at $k_c = 0.25$, the former stable fixed point at $\phi = \pi$ collides with the unstable fixed point and becomes neutrally stable indicated by a half-filled circle. Beyond k_c, i.e., for faster rates and smaller values of k, the anti-phase movement is unstable and the only remaining stable coordination pattern is in-phase.

The potential functions, shown in the second row in Fig. 1, contain the same information as the phase space portraits as they are just a different representation of the dynamics. However, the strong hysteresis is more intuitive in the potential landscape than in phase space and can best be seen through an experiment that starts out with slow movements in anti-phase (indicated by the gray ball in the minimum of the potential at $\phi = \pi$) and increasing rate. After passing the critical value $k_c = 0.25$, the slightest perturbation will put the ball on the downhill slope and initiate a switch to in-phase. If the movement is now slowed down again, going from right to left in the plots, even though the minimum at $\phi = \pi$ reappears, the ball cannot jump up and occupy it but will stay in the deep minimum at $\phi = 0$, a phenomenon known as hysteresis.

Finally, a bifurcation diagram is shown at the bottom of Fig. 1, where the locations of stable

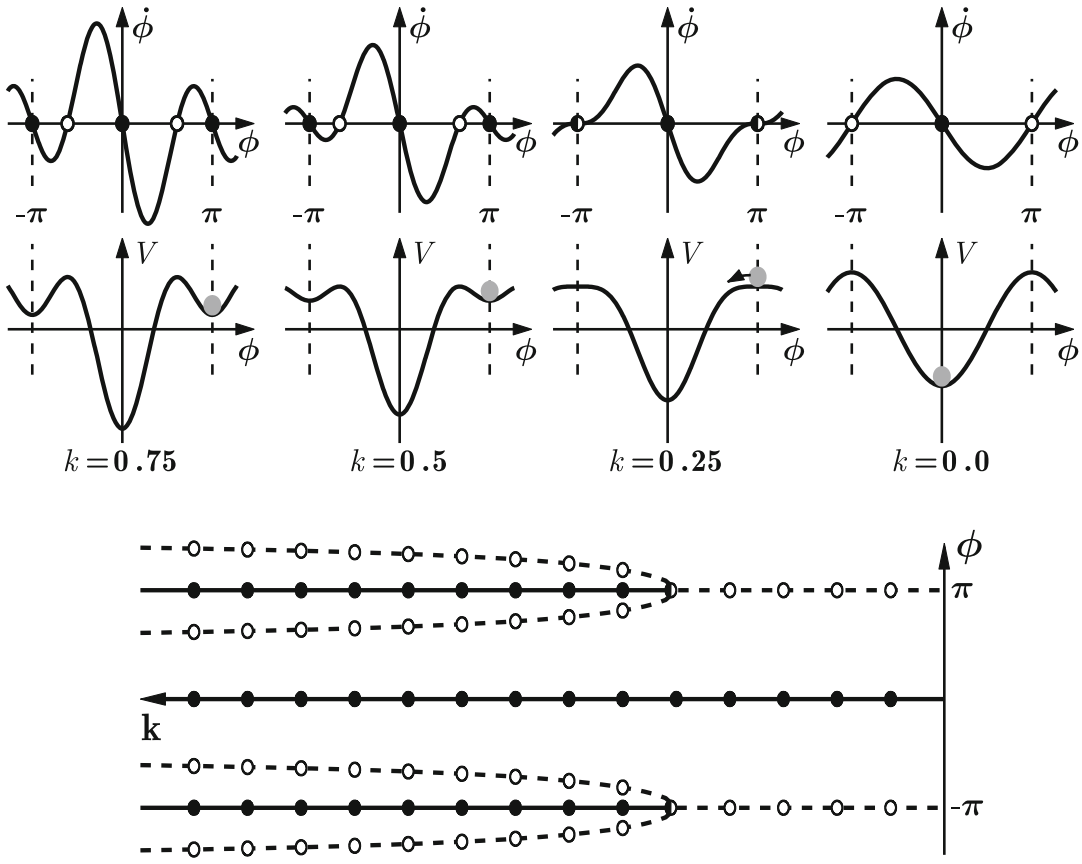

Movement Coordination, Fig. 1 Dynamics of the HKB model at the coordinative, relative phase (ϕ) level as a function of the control parameter $k = \frac{b}{a}$. *Top row*: Phase space plots $\dot{\phi}$ as a function of ϕ. *Middle*: Landscapes of the potential function $V(\phi)$. *Bottom*: Bifurcation diagram, where *solid lines* with *filled circles* correspond to stable fixed points (attractors) and *dashed lines* with *open circles* denote repellers. Note that k increases from right ($k = 0$) to left ($k = 0.75$)

fixed points for the relative phase ϕ are plotted as solid lines with solid circles and unstable fixed points as dashed lines with open circles. Around $k_c = 0.25$, the system undergoes a subcritical pitchfork bifurcation. Note that the control parameter k in this plot increases from right to left.

Evidently, the dynamical system represented by Eq. 2 is capable of reproducing the basic experimental findings listed above. From the viewpoint of theory, this is simply one of the preliminaries for a model that have to be fulfilled. In general, any model that only reproduces what is built into it is not of much value. More important are crucial experimental tests of the consequences and additional phenomena that are predicted when the model is worked through. Several such consequences and predictions will be described in detail in the following sections. It is only after such theoretical and experimental scrutiny that the HKB model has come to qualify as an elementary law of movement coordination.

Stability: Perturbations and Fluctuations

Random fluctuations, or noise for short, exist in all systems that dissipate energy. In fact, there exists a famous theorem that goes back to Einstein, known as the dissipation-fluctuation theorem, which states that the amount of random fluctuations in a system is proportional to its dissipation of energy. There are effects from random noise on the dynamics of

relative phase that can be predicted from theory both qualitatively and quantitatively, allowing for the HKB model's coordination level to be tested experimentally. Later the individual component level will be discussed.

An essential difference between the dynamical systems approach to movement coordination and the motor program or internal model hypotheses is most distinct in regions where the coordination pattern undergoes a spontaneous qualitative change as in the switch from anti-phase to in-phase in Kelso's experiment. From the latter point of view, these switches simply happen, very much like in the automatic transmission of a car: whenever certain criteria are fulfilled, the transmission switches from one gear to another. It is easy to imagine a similar mechanism to be at work and in control of the transitions in movements: as soon as a certain rate is exceeded, the anti-phase program is somehow replaced by the in-phase module, which is about all we can say regarding the mechanism of switching. On the other hand, by taking dynamic systems theory seriously, one can predict and test phenomena accompanying second-order phase transitions. Three of these phenomena, namely, critical slowing down, enhancement of fluctuations, and critical fluctuations, will be discussed here in detail.

For a quantitative treatment, it is advantageous to expand $\dot{\phi}$ and $V(\phi)$ in Eq. 6 into Taylor series around the fixed point $\phi = \pi$ and truncate them after the linear and quadratic terms, respectively:

$$\begin{aligned}
\dot{\phi} &= -\sin\phi - 2k\sin 2\phi \\
&= -\{-(\phi-\pi)+\ldots\} - 2k\{2(\phi-\pi)+\ldots\} \\
&\approx (1-4k)(\phi-\pi) \\
V(\phi) &= -\cos\phi - k\cos 2\phi \\
&= -\left\{-1+(\phi-\pi)^2+\ldots\right\} \\
&\quad -k\left\{1-4(\phi-\pi)^2+\ldots\right\} \\
&\approx 1-k-(1-4k)(\phi-\pi)^2.
\end{aligned} \tag{7}$$

A typical situation that occurs when a system approaches and passes through a transition point is shown in Fig. 2. In the top row, the potential function for $\phi \geq 0$ is plotted (dashed line) together with its expansion around the fixed point $\phi = \pi$ (solid). The bottom row consists of plots of time series showing how the fixed point is or is not approached when the system is initially at $\phi = \pi + \Delta$. The phenomena accompanying second-order phase transitions in a system that contains random fluctuations can be best described by Fig. 2.

Critical slowing down corresponds to the time it takes the system to recover from a small perturbation Δ. In the vicinity of the fixed point, the dynamics can be described by the linearization of the nonlinear

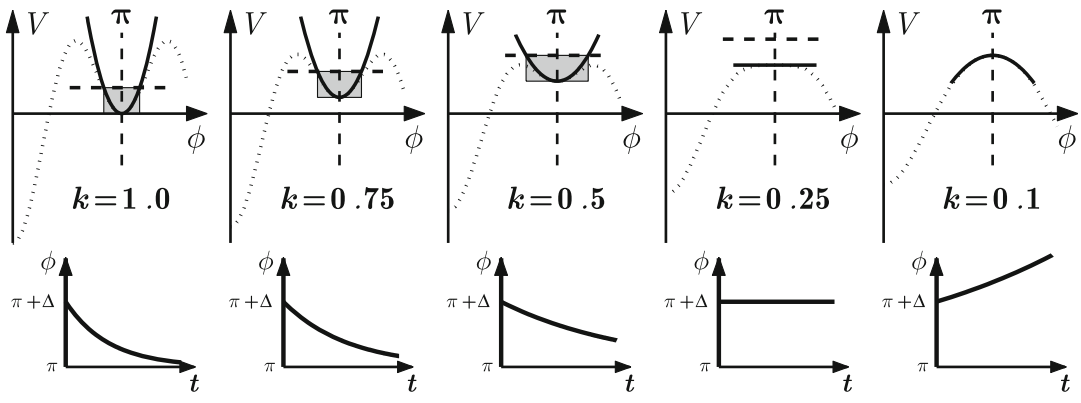

Movement Coordination, Fig. 2 Hallmarks of a system that approaches a transition point: enhancement of fluctuations, indicated by the increasing size of the *shaded area*; critical slowing down shown by the time it takes for the system to recover from a perturbation (*bottom*); critical fluctuations occur where the top of the shaded area is higher than the closest maximum in the potential, initiating a switch even though the system is still stable

equation around the fixed point Eq. 7. Such a linear equation can be readily solved leading to

$$\phi(t) = \pi + \Delta e^{(1-4k)t}.$$

As long as k is larger than its critical value $k_c = 0.25$, the exponent is negative and a perturbation will decay exponentially in time. However, as the system approaches the transition point, this decay will take longer and longer as shown in the bottom row in Fig. 2. At the critical parameter $k = 0.25$, the system will no longer return to the former stable fixed point, and beyond that value, it will even move away from it. In the latter parameter region, the linear approximation is no longer valid. Critical slowing down can be and has been tested experimentally by perturbing a coordination state and measuring the relaxation constant as a function of movement rate prior to the transition. The experimental findings (Kelso et al. 1987; Scholz and Kelso 1989; Scholz et al. 1987) are in remarkable agreement with the theoretical predictions of coordination dynamics (Schöner et al. 1986).

Enhancement of fluctuations is to some extent the stochastic analog to critical slowing down. The random fluctuations that exist in all dissipative systems are a stochastic force that kicks the system away from the minimum and (on average) up to a certain elevation in the potential landscape, indicated by the shaded areas in Fig. 2. For large values of k, the horizontal extent of this area is small but becomes larger and larger when the transition point is approached. Assuming that the strength of the random force does not change with the control parameter, the standard deviation of the relative phase is a direct measure of this enhancement of fluctuations and will be increasing when the control parameter is moving toward its critical value. Again experimental tests are in detailed agreement with the stochastic version of the HKB model (Kelso et al. 1986; Schöner et al. 1986; Scholz and Kelso 1989).

Critical fluctuations can induce transitions even when the critical value of the control parameter has not been reached. As before, random forces will kick the system around the potential minimum and up to (on average) a certain elevation. If this height is larger than the hump it has to cross, as in the case illustrated in Fig. 2 for $k = 0.5$, a transition will occur, even though the fixed point is still classified as stable. In excellent agreement with theory, such critical fluctuations were observed in the original experiments by Kelso and colleagues (1986) and have been found in a number of related experimental systems (Kelso et al. 1987; Schöner and Kelso 1988).

All these hallmarks point to the conclusion that transitions in movement coordination are not simply a switching of gears but take place in a well-defined way via the instability of a former stable coordination state. Such phenomena are also observed in systems in physics and other disciplines where in situations far from thermal equilibrium macroscopic patterns emerge or change, a process termed self-organization. A general theory of self-organizing systems, called synergetics (Haken 1983; Haken et al. 1985), was formulated by Hermann Haken in the early 1970s.

The Oscillator Level

The foregoing description and analysis of bimanual movement coordination takes place on the coordinative or collective level of relative phase. Looking at an actual experiment, there are two fingers moving back and forth, and one may ask whether it is possible to find a model on the level of the oscillatory components from which the dynamics of the relative phase can then be derived. The challenge for such an endeavor is at least twofold: first, one needs a dynamical system that accurately describes the movements of the individual oscillatory components (the fingers). Second, one must find a coupling function for these components that leads to the correct relation for the relative phase Eq. 2.

Oscillators for Limb Movements

In terms of oscillators, there is quite a variety to choose from as most second-order systems of the form

$$\ddot{x} + \gamma\dot{x} + \omega^2 x + N(x,\dot{x}) = 0 \qquad (8)$$

are potential candidates. Here ω is the angular frequency, γ is the linear damping constant, and $N(x,\dot{x})$ is a function containing nonlinear terms in x and $\dot{x}$.

Best known and most widely used are the harmonic oscillators, where $N(x,\dot{x}) = 0$, in particular

for the case without damping $\gamma = 0$. In the search for a model to describe human limb movements, however, harmonic oscillators are not well suited, because they do not have stable limit cycles. The phase space portrait of a harmonic oscillator is a circle (or ellipse), but only if it is not perturbed. If such a system is slightly kicked off the trajectory, it is moving on, and it will not return to its original circle but continue to move on a different orbit. In contrast, it is well known that if a rhythmic human limb movement is perturbed, this perturbation decreases exponentially in time, and the movement returns to its original trajectory, a stable limit cycle, which is an object that exists only for nonlinear oscillators (Kay et al. 1987, 1991).

Obviously, the amount of possible nonlinear terms to choose from is infinite, and at first sight, the task to find the appropriate ones is like looking for a needle in a haystack. However, there are powerful arguments that can be made from both theoretical reasoning and experimental findings that restrict the nonlinearities, as we shall see, to only two. First, we assume that the function $N(x,\dot{x})$ takes the form of a polynomial in x and $\dot{x}$ and that this polynomial is of the lowest possible order. So the first choice would be to assume that N is quadratic in x and $\dot{x}$ leading to an oscillator of the form

$$\ddot{x} + \gamma\dot{x} + \omega^2 x + ax^2 + b\dot{x}^2 + cx\dot{x} = 0. \tag{9}$$

How do we decide whether Eq. 9 is a good model for rhythmic finger movements? If a finger is moved back and forth, that is, performs an alternation between flexion and extension, then this process is to a good approximation symmetric: flexion is the mirror image of extension. In the equations, a mirror operation is carried out by substituting x by $-x$, and, in doing so, the equation of motion must not change for symmetry to be preserved. Applied to Eq. 9 this leads to

$$\begin{aligned} &-\ddot{x} + \gamma(-\dot{x}) + \omega^2(-x) + a(-x)^2 + b(-\dot{x})^2 \\ &+ c(-x)(-\dot{x}) = 0 \\ &-\ddot{x} - \gamma\dot{x} - \omega^2 x + ax^2 + b\dot{x}^2 + cx\dot{x} = 0 \\ &\ddot{x} + \gamma\dot{x} + \omega^2 x - ax^2 - b\dot{x}^2 - cx\dot{x} = 0 \end{aligned} \tag{10}$$

where the last equation in Eq. 10 is obtained by multiplying the second equation by -1. It is evident that this equation is not the same as Eq. 9. In fact, it is only the same if $a = b = c = 0$, which means that there must not be any quadratic terms in the oscillator equation if one wants to preserve the symmetry between flexion and extension phases of movement. The argument goes even further: $N(x,\dot{x})$ must not contain any terms of even order in x and $\dot{x}$ as all of them, like the quadratic ones, would break the required symmetry. It is easy to convince oneself that as far as the flexion-extension symmetry is concerned, all odd terms in x and $\dot{x}$ are fine. There are four possible cubic terms, namely, $\dot{x}^3, \dot{x}x^2, x\dot{x}^2$, and x^3 leading to a general oscillator equation of the form

$$\ddot{x} + \gamma\dot{x} + \omega^2 x + \delta\dot{x}^3 + \varepsilon\dot{x}x^2 + ax^3 + bx\dot{x}^2 = 0. \tag{11}$$

The effects that these nonlinear terms exert on the oscillator dynamics can be best seen by rewriting Eq. 11 as

$$\ddot{x} + \dot{x}\underbrace{\{\gamma + \varepsilon x^2 + \delta\dot{x}^2\}}_{\text{damping}} + x\underbrace{\{\omega^2 + ax^2 + b\dot{x}^2\}}_{\text{frequency}} = 0 \tag{12}$$

which shows that the terms $\dot{x}^3$ and $\dot{x}x^2$ are position- and velocity-dependent changes to the damping constant γ, whereas the nonlinearities x^3 and $x\dot{x}^2$ mainly influence the frequency. As the nonlinear terms were introduced to obtain stable limit cycles and the main interest is in amplitude and not frequency, we will let $a = b = 0$, which reduces the candidate oscillators to

$$\ddot{x} + \dot{x}\{\gamma + \varepsilon x^2 + \delta\dot{x}^2\} + \omega^2 x = 0. \tag{13}$$

Nonlinear oscillators with either $\delta = 0$ or $\varepsilon = 0$ have been studied for a long time and have been termed in the literature as van-der-Pol and Rayleigh oscillators, respectively.

Systems of the form Eq. 13 only show sustained oscillations on a stable limit cycle within certain ranges of the parameters, as can be seen easily for the van-der-Pol oscillator, given by Eq. 13 with $\delta = 0$:

$$\ddot{x} + \dot{x}\underbrace{\{\gamma + \epsilon x^2\}}_{\widetilde{\gamma}} + \omega^2 x = 0. \qquad (14)$$

The underbraced term in Eq. 14 represents the effective damping constant, $\widetilde{\gamma}$, now depending on the square of the displacement, x^2, a quantity which is nonnegative. For the parameters γ and ϵ, one can distinguish the following four cases:

$\gamma > 0, \epsilon > 0$ The effective damping $\widetilde{\gamma}$ is always positive. The trajectories are evolving toward the origin, which is a stable fixed point.

$\gamma < 0, \epsilon < 0$ The effective damping is $\widetilde{\gamma}$ always negative. The system is unstable and the trajectories are evolving toward infinity.

$\gamma > 0, \epsilon < 0$ For small values of the amplitude x^2, the effective damping $\widetilde{\gamma}$ is positive leading to even smaller amplitudes. For large values of x^2, the effective damping $\widetilde{\gamma}$ is negative leading to a further increase in amplitude. The system evolves either toward the fixed point or toward infinity depending on the initial conditions.

$\gamma < 0$, $\epsilon > 0$, For small values of the amplitude x^2, the effective damping $\widetilde{\gamma}$ is negative leading to an increase in amplitude. For large values of x^2, the effective damping is positive and decreases the amplitude. The system evolves toward a stable limit cycle.

The main features for the van-der-Pol oscillator are shown in Fig. 3 with the time series (left), the phase space portrait (middle), and the power spectrum (right). The time series is not a sine function but has a fast rising increasing flank and a more shallow slope on the decreasing side. Such time series are called relaxation oscillations. The trajectory in phase space is closer to a rectangle than to a circle, and the power spectrum shows pronounced peaks at the fundamental frequency ω and its odd higher harmonics (3ω , 5ω , . . .).

In contrast to the van-der-Pol case, the damping constant $\widetilde{\gamma}$ for the Rayleigh oscillator, the case $\epsilon = 0$ in Eq. 13, depends on the square of the velocity $\dot{x}^2$. Arguments similar to those above lead to the conclusion that the Rayleigh oscillator shows sustained oscillations for parameters $\gamma < 0$ and $\delta > 0$.

As shown in Fig. 4, the time series and trajectories of the Rayleigh oscillator also exhibit relaxation behavior but in this case with a slow rise and fast drop. As for the van-der-Pol, the phase space portrait is almost rectangular, but the long and short axes are switched. Again the power spectrum has peaks at the fundamental frequency and contains odd higher harmonics.

Evidently, taken by themselves, neither the van-der-Pol nor Rayleigh oscillators are good models for human limb movement for at least two reasons, even though they fulfill one requirement for a model: they have stable limit cycles. First, human limb movements are almost sinusoidal, and their trajectories have a circular or elliptical shape. Second, it has also been found in experiments with human subjects performing rhythmic limb movements that when the movement rate is increased the amplitude of the movement decreases linearly with frequency (Kay et al. 1987). It can be shown that for the van-der-Pol oscillator, the amplitude is independent of frequency, and for the Rayleigh it decreases proportional to ω^{-2}, both in disagreement with the experimental findings.

It turns out that a combination of the van-der-Pol and Rayleigh oscillator, termed the hybrid oscillator of the form Eq. 13, fulfills all the

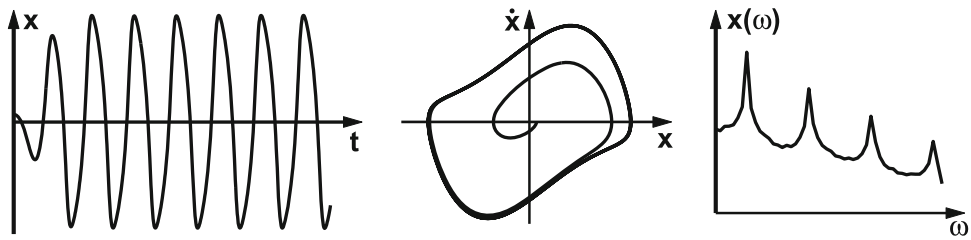

Movement Coordination, Fig. 3 The van-der-Pol oscillator: time series (*left*), phase space trajectory (*middle*), and power spectrum (*right*)

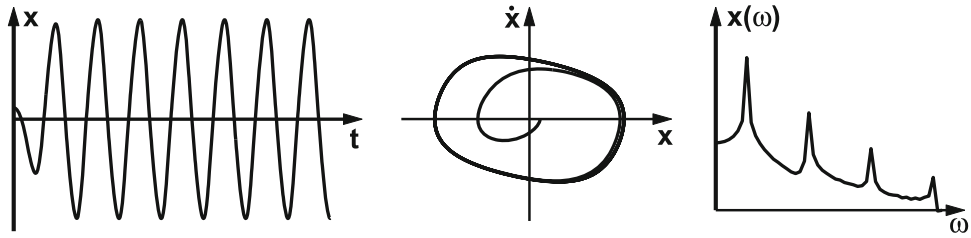

Movement Coordination, Fig. 4 The Rayleigh oscillator: time series (*left*), phase space trajectory (*middle*), and power spectrum (*right*)

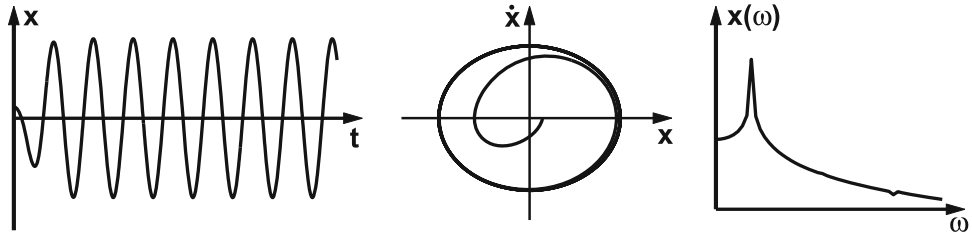

Movement Coordination, Fig. 5 The hybrid oscillator: time series (*left*), phase space trajectory (*middle*), and power spectrum (*right*)

above requirements if the parameters are chosen as $\gamma < 0$ and $\epsilon \approx \delta > 0$.

As shown in Fig. 5, the time series for the hybrid oscillator is almost sinusoidal and the trajectory is elliptical. The power spectrum has a single peak at the fundamental frequency. Moreover, the relation between the amplitude and frequency is a linear decrease in amplitude when the rate is increased as shown schematically in Fig. 6. Taken together, the hybrid oscillator is a good approximation for the trajectories observed experimentally in human limb movements.

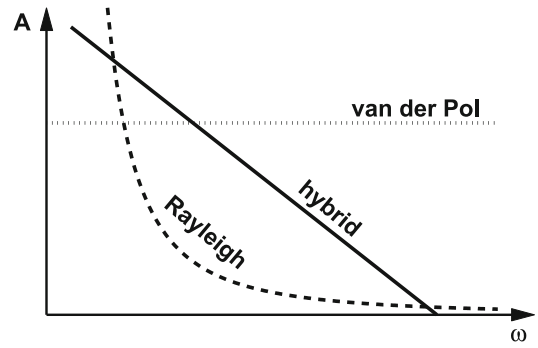

Movement Coordination, Fig. 6 Amplitude-frequency relation for the van-der-Pol (*dotted*), Rayleigh ($\sim\omega^{-2}$, *dashed*), and hybrid ($\sim-\omega$, *solid*) oscillator

The Coupling

As pointed out already, in a second step, one has to find a coupling function between two hybrid oscillators that leads to the correct dynamics for the relative phase Eq. 2. The most common realization of a coupling between two oscillators is a spring between two pendulums, leading to a force proportional to the difference in locations $f_{12} = k[x_1(t) - x_2(t)]$. It can easily be shown that such a coupling does not lead to the required dynamics on the relative phase level. In fact, several coupling terms have been suggested that do the trick, but none of them is very intuitive. The arguably easiest form, which is one of the possible couplings presented in the original HKB model (Haken et al. 1985), is given by

$$f_{12} = (\dot{x}_1 - \dot{x}_2)\left\{\alpha + \beta(x_1 - x_2)^2\right\}. \qquad (15)$$

Combined with two of the hybrid oscillators, the dynamical system that describes the transition from anti-phase to in-phase in bimanual finger movements takes the form

$$\ddot{x}_1 + \dot{x}_1\left(\gamma + \varepsilon x_1^2 + \delta \dot{x}_1^2\right) + \omega^2 x_1 = (\dot{x}_1 - \dot{x}_2)\left\{\alpha + \beta(x_1 - x_2)^2\right\}$$

$$\ddot{x}_2 + \dot{x}_2\left(\gamma + \varepsilon x_2^2 + \delta \dot{x}_2^2\right) + \omega^2 x_2 = (\dot{x}_2 - \dot{x}_1)\left\{\alpha + \beta(x_2 - x_1)^2\right\}. \quad (16)$$

A numerical simulation of Eq. 16 is shown in Fig. 7. In the top row, the amplitudes x_1 and x_2 are plotted as a function of time. The movement starts out in anti-phase at $\omega = 1.4$, and the frequency is continuously increased to a final value of $\omega = 1.8$. At a critical rate ω_c, the anti-phase pattern becomes unstable and a transition to in-phase takes place. At the bottom a continuous estimate of the relative phase $\phi(t)$ is shown calculated as

$$\phi(t) = \varphi_1(t) - \varphi_2(t) = \arctan\frac{\dot{x}_1}{x_1} - \arctan\frac{\dot{x}_2}{x_2}. \quad (17)$$

The relative phase changes from a value of π during the anti-phase movement to $\phi = 0$ when the in-phase pattern has been established.

To derive the phase relation Eq. 2 from Eq. 16 is a little lengthy but straightforward by using the ansatz (hypothesis)

$$x_k(t) = A_k(t)e^{i\omega t} + A_k^*(t)e^{-i\omega t} \quad (18)$$

then calculating the derivatives and inserting them into Eq. 16. Next a slowly varying amplitude approximation ($\dot{A}(t) \ll \omega$) and rotating wave approximation (neglect all frequencies ω) are applied. Finally, introducing the relative phase $\phi = \varphi_1 - \varphi_2$ after writing $A_k(t)$ in the form

$$A_k(t) = re^{i\varphi_k(t)} \quad (19)$$

leads to a relation for the relative phase ϕ of the form Eq. 2 from which the parameters a and b can be readily found in terms of the parameters that describe the oscillators and their coupling in Eq. 16:

$$a = -\alpha - 2\beta r^2, \quad b = \frac{1}{2}\beta r^2$$
$$\text{with} \quad r^2 = \frac{-\gamma + \alpha(1 - \cos\phi)}{\epsilon + 3\delta\omega^2 - 2\beta(1 - \cos\phi)^2}. \quad (20)$$

Breaking and Restoring Symmetries

Symmetry Breaking Through the Components

For simplicity, the original HKB model assumes on both the oscillator and the relative phase level that the two coordinating components are identical, like

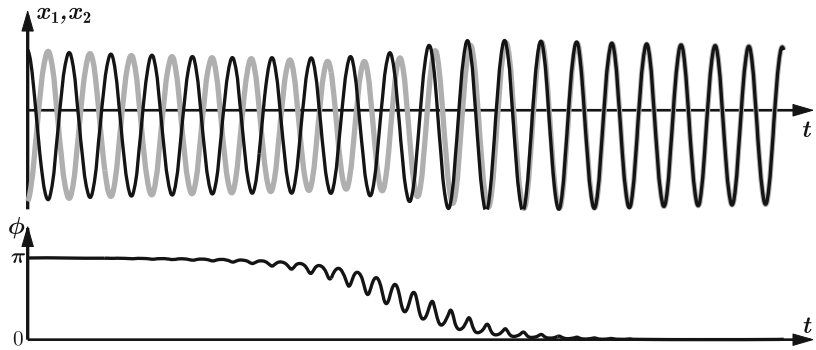

Movement Coordination, Fig. 7 Simulation of Eq. 16 where the frequency ω is continuously increased from $\omega = 1.4$ on the left to $\omega = 1.8$ on the right. *Top*: Time series of the amplitudes x_1 and x_2 undergoing a transition from anti-phase to in-phase when ω exceeds a critical value. *Bottom*: Continuous estimate of the relative phase ϕ changing from an initial value of π during anti-phase to zero when the in-phase movement is established. Parameters: $\gamma = -0.7$, $\epsilon = \delta = 1$, $\alpha = -0.2$, $\beta = 0.2$, and $\omega = 1.4$ to 1.8

two index fingers. As a consequence, the coupled system Eq. 16 has a symmetry: it stays invariant if we replace x_1 by x_2 and x_2 by x_1. For the coordination between two limbs that are not the same like an arm and a leg, this symmetry no longer exists – it is said to be broken. In terms of the model, the main difference between an arm and a leg is that they have different eigenfrequencies, so the oscillator frequencies ω in Eq. 16 are no longer the same but become ω_1 and ω_2. This does not necessarily mean that during the coordination the components oscillate at different frequencies; they are still coupled, and this coupling leads to a common frequency Ω, at least as long as the eigenfrequency difference is not too big. But still, a whole variety of new phenomena originates from such a breaking of the symmetry between the components (Carson et al. 2000; Jeka et al. 1993a, b; Kelso and Jeka 1992; Park and Turvey 2008).

As mentioned in subsection. "The Coupling," the dynamics for the relative phase can be derived from the level of coupled oscillators Eq. 16 for the case of the same eigenfrequencies. Performing the same calculations for two oscillators with frequencies ω_1 and ω_2 leads to an additional term in Eq. 2, which turns out to be a constant, commonly called $\delta\omega$. With this extension, the equation for the relative phase reads

$$\begin{aligned} \dot{\phi} &= \delta\omega - a\sin\phi - 2b\sin 2\phi \\ \text{with} \quad \delta\omega &= \frac{\omega_1^2 - \omega_2^2}{\Omega} \approx \omega_1 - \omega_2. \end{aligned} \tag{21}$$

The exact form for the term $\delta\omega$ turns out to be the difference of the squares of the eigenfrequencies divided by the rate Ω the oscillating frequency of the coupled system, which simplifies to $\omega_1 - \omega_2$ if the frequency difference is small. As before Eq. 21 can be scaled, which eliminates one of the parameters, and $\dot{\phi}$ can be derived from a potential function:

$$\begin{aligned} \dot{\phi} &= \delta\omega - \sin\phi - 2k\sin 2\phi = -\frac{dV(\phi)}{d\phi} \\ \text{with } V(\phi) &= -\delta\omega\,\phi - \cos\phi - k\cos 2\phi. \end{aligned} \tag{22}$$

Plots of the phase space and the potential landscape for different values of k and $\delta\omega$ are shown in Figs. 8 and 9, respectively. From these figures, it is

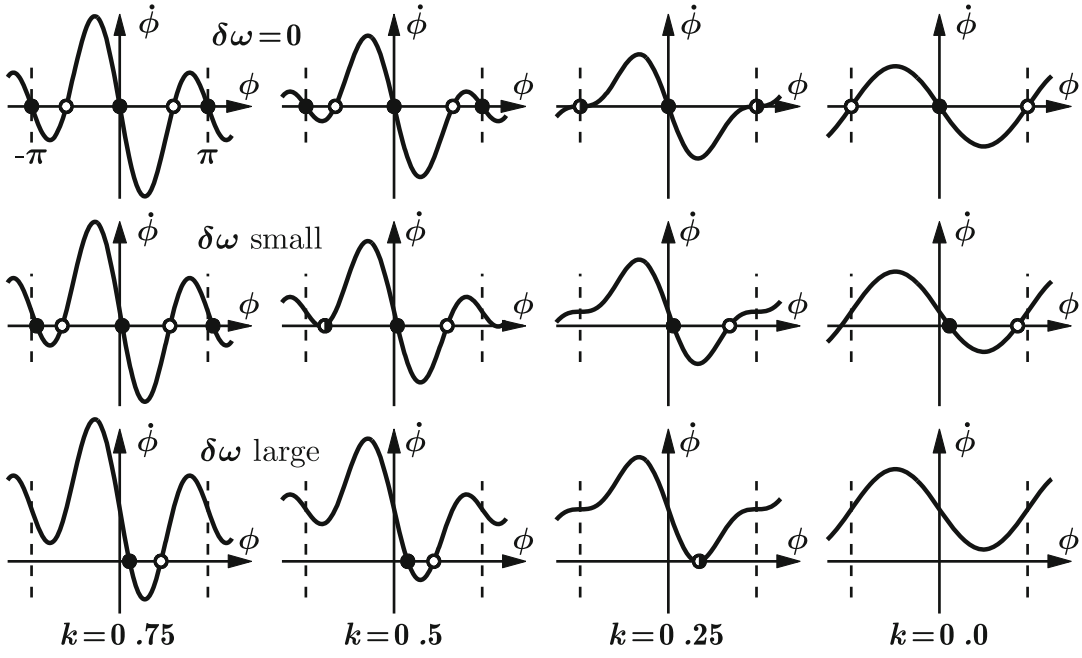

Movement Coordination, Fig. 8 Phase space plots for different values of the control parameters k and $\delta\omega$. With increasing asymmetry (*top* to *bottom*), the functions are shifted more and more upward leading to an elimination of the fixed points near $\phi = -\pi$ and $\phi = 0$ via saddle node bifurcations at $k = 0.5$ for small $\delta\omega$ and $k = 0.25$ for $\delta\omega$ large, respectively

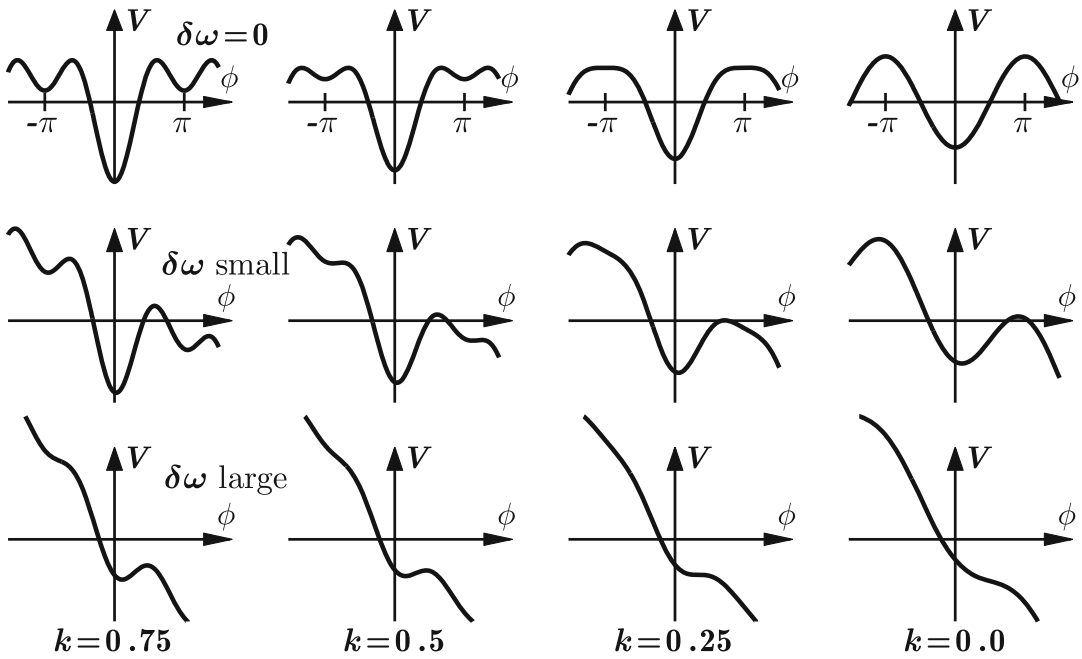

Movement Coordination, Fig. 9 Potential landscape for different values of the control parameters k and $\delta\omega$. With increasing asymmetry (*top* to *bottom*), the functions get more and more tilted, destabilizing the system up to a point where there are no fixed points left on the *bottom right*. However, remnants of the fixed point can still be seen as changes in the curvature of the potential

obvious that the symmetry breaking leads to a vertical shift of the curves in phase space and a tilt in the potential functions, which has several important consequences for the dynamics. First, for a nonvanishing $\delta\omega$, the stable fixed points for the relative phase are no longer located at $\phi = 0$ and $\phi = \pm\pi$ but are now shifted (see Fig. 8). The amount of this shift can be calculated for small values of $\delta\omega$, and new locations for the stable fixed points are given by

$$\phi^{(0)} = \frac{\delta\omega}{1+4k} \quad \text{and} \quad \phi^{(\pi)} = \pi - \frac{\delta\omega}{1-4k}. \tag{23}$$

Second, for large enough values of $\delta\omega$, not only the fixed point close to $\phi = \pi$ becomes unstable, but also the in-phase pattern loses stability undergoing a saddle node bifurcation as can be seen in the bottom row in Fig. 8. Beyond this point, there are no stable fixed points left, and the relative phase will not settle down at a fixed value anymore but exhibits phase wrapping. However, this wrapping does not occur with a constant angular velocity, which can best be seen in the plot on the bottom right in Fig. 9. As the change in relative phase $\dot{\phi}$ is the negative derivative of the potential function, it is given by the slope. This slope is large and almost constant for negative values of ϕ, but for small positive values, where the in-phase fixed point was formerly located, the slope becomes less steep indicating that ϕ changes more slowly in this region before the dynamics picks up speed again when approaching π. So even as the fixed point has disappeared, the dynamics still shows reminiscence of its former existence.

The dynamics of relative phase for the case of different eigenfrequencies from a simulation of Eq. 22 in shown in Fig. 10. Starting out at a slow movement rate on the left, the system settles into the fixed point close to $\phi = \pi$. When the movement rate is continuously increased, the fixed point drifts upward. At a first critical point, a transition to in-phase takes place, followed by another drift, this time for the fixed point representing the in-phase movement. Finally, this state also loses stability and the relative phase goes

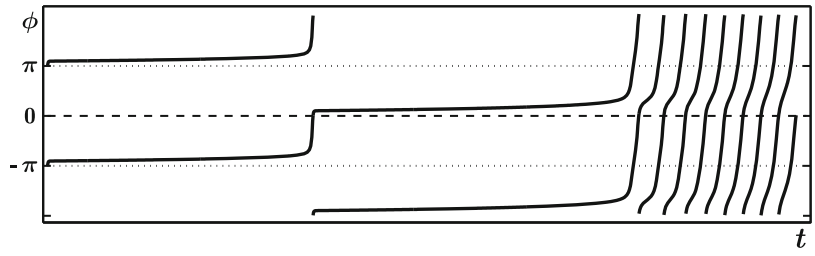

Movement Coordination, Fig. 10 Relative phase ϕ as a function of time. Shown is a 4-π plot of a simulation of Eq. 22 for $\delta\omega = 1.7$ where the control parameter k is continuously decreased from $k = 2$ on the left to $k = 0$ on the right. The system settles close to anti-phase, and the fixed point drifts as k is decreased (corresponding to a faster period of oscillation). At a first critical value, a transition to in-phase takes place followed by another fixed point drift. Finally, the in-phase fixed point disappears and the phase starts wrapping

into wrapping. Reminiscence in the phase regions of the former fixed point is still visible by a flattening of the slope around $\phi \approx \ > 0$. With a further increase of the movement rate, the function approaches a straight line.

The third consequence of this symmetry breaking is best described using the potential function for small values of $\delta\omega$ compared to the symmetric case $\delta\omega = 0$. For the latter, when the system is initially in anti-phase $\phi = \pi$ and k is decreased through its critical value a switch to in-phase takes place as was shown in Fig. 1 (middle row). However, the ball there does not necessarily have to roll to the left toward $\phi = 0$ but with the same probability could roll to the right ending up in the minimum that exists at $\phi = 2\pi$ and also represents an in-phase movement. Whereas the eventual outcome is the same because due to the periodicity $\phi = 0$ and $\phi = 2\pi$ are identical, the two paths can very well be distinguished. The curve in Fig. 7 (bottom), showing the continuous estimate of the relative phase during a transition, goes from $\phi = \pi$ down to $\phi = 0$, but could, in fact with the same probability, go up toward $\phi = 2\pi$. In contrast, if the eigenfrequencies are different, also the points $-\pi$ and π, and 0 and 2π are no longer the same. If the system is in anti-phase at $\phi = \pi$ and k is decreased, it is evident from the middle row in Fig. 9 that a switch will not take place toward the left to $\phi \approx 0$, as the dynamics would have to climb over a potential hill to do so. As there are random forces acting on the dynamics, a switch to $\phi \approx 0$ will still happen from time to time, but it is not equally probable to a transition to $\phi \approx 2\pi$, and it becomes even more unlikely with increasing $\delta\omega$.

These consequences, theoretically predicted to occur when the symmetry between the oscillating components is broken, can and have been tested and have been found to be in agreement with the experimental results (Jeka and Kelso 1995; Kelso and Jeka 1992) (see also Kelso et al. 1990; Schmidt et al. 1991).

Asymmetry in the Mode of Coordination

Even though Eq. 16 is symmetric in the coordinating components, it can only describe a transition from anti-phase to in-phase but not the other way around. Equation 16 is highly asymmetric with respect to coordination mode. This can be seen explicitly when we introduce variables that directly reflect modes of coordination:

$$\psi_+ = x_1 + x_2 \quad \text{and} \quad \psi_- = x_1 - x_2 \,. \tag{24}$$

For an in-phase movement, we have $x_1 = x_2$ and ψ_- vanishes, whereas for anti-phase $x_1 = -x_2$ and therefore $\psi_+ = 0$. We can now derive the dynamics in the variables ψ_+ and ψ_- by expressing the original displacements as

$$x_1 = \frac{1}{2}\left(\psi_+ + \psi_-\right) \quad \text{and} \quad x_2 = \frac{1}{2}\left(\psi_+ - \psi_-\right) \tag{25}$$

and inserting them into Eq. 16, which leads to

$$\ddot{\psi}_+ + \epsilon\dot{\psi}_+ + \omega^2\psi_+ + \frac{\gamma}{12}\frac{d}{dt}\left(\psi_+^3 + 3\psi_+\psi_-^2\right) + \frac{\delta}{4}\left(\dot{\psi}_+^3 + 3\dot{\psi}_+\dot{\psi}_-^2\right) = 0$$

$$\ddot{\psi}_- + \epsilon\dot{\psi}_- + \omega^2\psi_- + \frac{\gamma}{12}\frac{d}{dt}\left(\psi_-^3 + 3\psi_-\psi_+^2\right) + \frac{\delta}{4}\left(\dot{\psi}_-^3 + 3\dot{\psi}_-\dot{\psi}_+^2\right) = 2\dot{\psi}_-\left(\alpha + \beta\psi_-^2\right). \quad (26)$$

The asymmetry between in-phase and anti-phase is evident from Eq. 26, as the right-hand side of the first equation vanishes and the equation is even independent of the coupling parameters α and β. This is the reason that the original HKB model only shows transitions from anti-phase to in-phase and not vice versa.

Transitions to Anti-phase

In 2000 Carson and colleagues (Carson et al. 2000) published results from an experiment in which subjects performed bimanual pronation-supination movements paced by a metronome of increasing rate (see also Buchanan and Kelso 1993). In this context, an anti-phase movement corresponds to the case where one arm performs a pronation while the other arm is supinating. Correspondingly, pronation and supination with both arms at the same time represent in-phase. In their experiment, Carson et al. used a manipulandum that allowed for changing the axis of rotation individually for both arms as shown in Fig. 11a. With increasing movement rate, spontaneous transitions from anti-phase to in-phase, but not vice versa, were found when the subjects performed pronation-supination movements around the same axes for both arms. In trials where one arm was rotating around the axis above the hand and the other around the one below, anti-phase was found to be stable and the in-phase movement underwent a transition to anti-phase as shown for representative trials in Figs. 12 and 13.

It is evident that the HKB model in neither its original form Eq. 2 nor the mode formulation Eq. 26 is a valid model for these findings. However, Fuchs and Jirsa (2000) showed that by starting from the mode description Eq. 26 it is straightforward to extend HKB such that, depending on an additional parameter σ, either the in-phase or the anti-phase mode is a stable movement pattern at high rates. The additional parameter corresponds to the relative locations

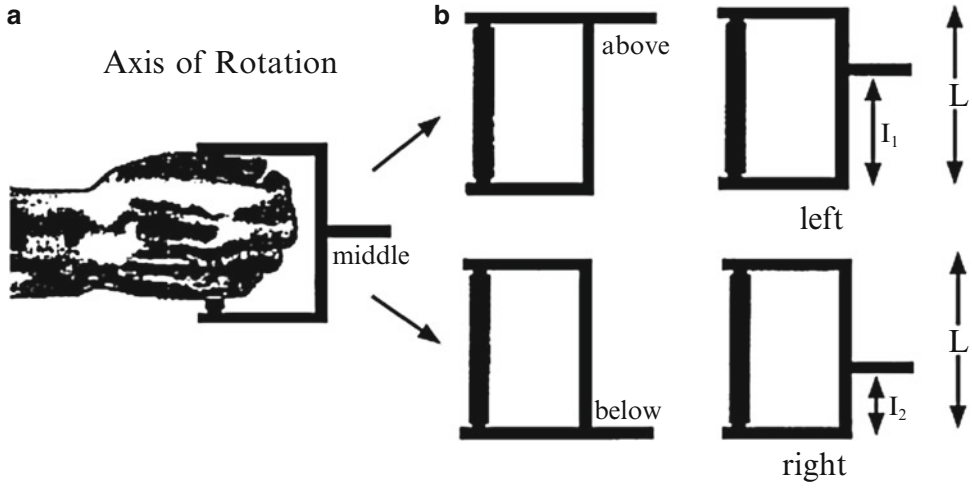

Movement Coordination, Fig. 11 Manipulandum used by Carson and colleagues (Carson et al. 2000). (**a**) The original apparatus that allowed for variation in axis of rotation above, below, and in the middle of the hand. (**b**) The axis of rotation can be changed continuously, allowing us to introduce a parameter σ as a quantitative measure for the relative locations of the axes

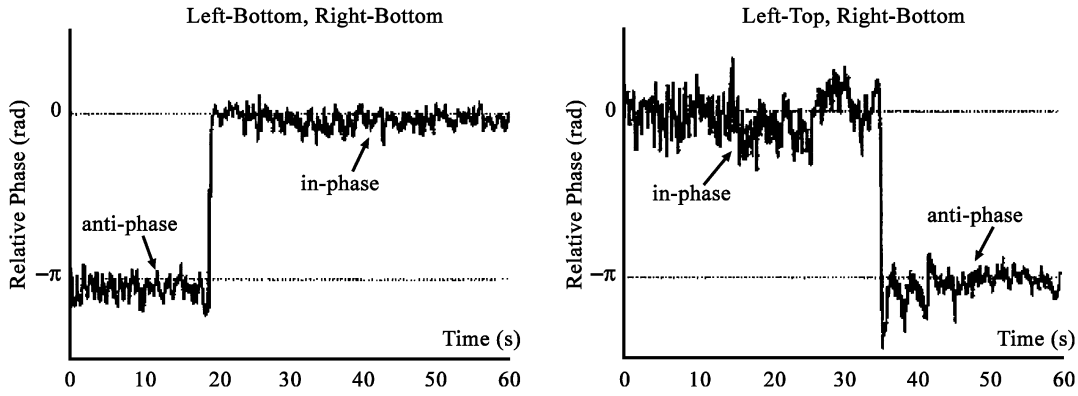

Movement Coordination, Fig. 12 Relative phase over time for two representative trials from the Carson et al. experiment. *Left*: the axis of rotation is below the hand for both arms and a switch from anti-phase to in-phase occurs as the movement speeds up. *Right*: with one axis above and the other below the hand, the in-phase movement becomes unstable at higher rates leading to a transition to anti-phase

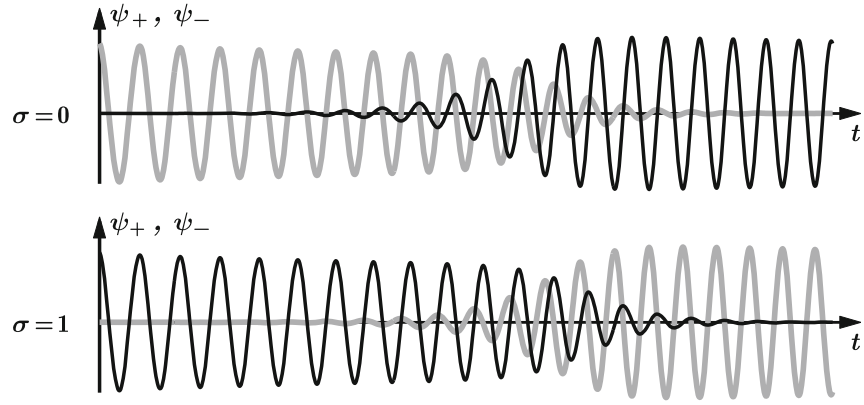

Movement Coordination, Fig. 13 Simulation of Eq. 28 for $\sigma = 0$ (*top*) and $\sigma = 1$ (*bottom*) where the frequency ω is continuously increased from $\omega = 1.4$ on the left to $\omega = 1.8$ on the right. Time series of the mode amplitudes ψ_+ (*black*) and ψ_- (*gray*) undergoing transitions from anti-phase to in-phase (*top*) and from in-phase to anti-phase (*bottom*) when ω exceeds a critical value. Parameters: $\gamma = -0.7$, $\epsilon{=}\delta = 1$, $\alpha = -0.2$, $\beta = 0.2$, and ω=1.4 to 1.8

of the axes of rotation in the Carson et al. experiment which can be defined in its easiest form as

$$\sigma = \frac{|l_1 - l_2|}{L} \tag{27}$$

where l_1, l_2, and L are as shown in Fig. 11b. In fact, any monotonic function f with $f(0){=}0$ and $f(1){=}1$ is compatible with theory, and its actual shape has to be determined experimentally.

By looking at the mode Eq. 26, it is clear that a substitution $\psi_+ \rightarrow \psi_-$ and $\psi_- \rightarrow \psi_+$ to the left-hand side of the first equation leads to the left-hand side of the second equation and vice versa. For the terms on the right-hand side representing the coupling, this is obviously not the case. Therefore, we now introduce a parameter σ and additional terms into Eq. 26 such that for $\sigma = 0$ these equations remain unchanged, whereas for $\sigma = 1$ we obtain Eq. 26 with all + and − subscripts reversed:

$$\ddot{\psi}_+ + \epsilon\dot{\psi}_+ + \omega^2\psi_+ + \frac{\gamma}{12}\frac{d}{dt}\left(\psi_+^3 + 3\psi_+\psi_-^2\right) + \frac{\delta}{4}\left(\dot{\psi}_+^3 + 3\dot{\psi}_+\dot{\psi}_-^2\right) = 2\sigma\dot{\psi}_+\left(\alpha + \beta\psi_+^2\right)$$
$$\ddot{\psi}_- + \epsilon\dot{\psi}_- + \omega^2\psi_- + \frac{\gamma}{12}\frac{d}{dt}\left(\psi_-^3 + 3\psi_-\psi_+^2\right) + \frac{\delta}{4}\left(\dot{\psi}_-^3 + 3\dot{\psi}_-\dot{\psi}_+^2\right) = 2(1-\sigma)\dot{\psi}_-\left(\alpha + \beta\psi_-^2\right). \quad (28)$$

From Eq. 28 it is straightforward to go back to the representation of the limb oscillators:

$$\begin{aligned}\ddot{x}_1 + \ldots &= \frac{1}{2}\left(\ddot{\psi}_+ + \ddot{\psi}_-\right) + \ldots \\ &= \dot{\psi}_-\left(\alpha + \beta\psi_-^2\right) + \sigma\left\{\dot{\psi}_+\left(\alpha + \beta\psi_+^2\right) - \dot{\psi}_-\left(\alpha + \beta\psi_-^2\right)\right\} \\ \ddot{x}_2 + \ldots &= \frac{1}{2}\left(\ddot{\psi}_+ - \ddot{\psi}_-\right) + \ldots \\ &= -\dot{\psi}_-\left(\alpha + \beta\psi_-^2\right) + \sigma\left\{\dot{\psi}_+\left(\alpha + \beta\psi_+^2\right) + \dot{\psi}_-\left(\alpha + \beta\psi_-^2\right)\right\}\end{aligned} \quad (29)$$

where the left-hand side which represents the oscillators has been written only symbolically as all we are dealing with is the coupling on the right. Replacing the mode amplitudes ψ_+ and ψ_- in Eq. 29 using Eq. 24, one finds the generalized coupling as a function of x_1 and x_2:

$$\begin{aligned}\ddot{x}_1 + \ldots &= \left(\dot{x}_1 - \dot{x}_2\right)\left\{\alpha + \beta(x_1 - x_2)^2\right\} \\ &+2\sigma\left\{\alpha\dot{x}_2 + \beta\left[\dot{x}_2\left(x_1^2 + x_2^2\right) + 2\dot{x}_1x_1x_2\right]\right\} \\ \ddot{x}_2 + \ldots &= \left(\dot{x}_2 - \dot{x}_1\right)\left\{\alpha + \beta(x_2 - x_1)^2\right\} \\ &+2\sigma\left\{\alpha\dot{x}_1 + \beta\left[\dot{x}_1\left(x_1^2 + x_2^2\right) + 2\dot{x}_2x_1x_2\right]\right\}.\end{aligned} \quad (30)$$

Like the original oscillator Eqs. 16 and 30 is invariant under the exchange of x_1 and x_2 but in addition allows for transitions from in-phase to anti-phase coordination if the parameter σ is chosen appropriately ($\sigma = 1$, for instance), as shown in Fig. 14.

As the final step, an equation for the dynamics of relative phase can be obtained from Eq. 30 by performing the same steps as before, which leads to a modified form of the HKB Eq. 2

$$\dot{\phi} = -(1-2\sigma)a\sin\phi - 2b\sin 2\phi \quad (31)$$

and the corresponding potential function

$$\dot{\phi} = -\frac{dV(\phi)}{d\phi}$$
$$\text{with} \quad V(\phi) = -(1-2\sigma)a\cos\phi - b\cos 2\phi. \quad (32)$$

Both equations can be scaled again leading to

$$\begin{aligned}\dot{\phi} &= -(1-2\sigma)\sin\phi - 2k\sin 2\phi \\ &= -\frac{dV(\phi)}{d\phi} \quad \text{with} \\ V(\phi) &= -(1-2\sigma)\cos\phi - k\cos 2\phi.\end{aligned} \quad (33)$$

The landscapes of the potential for different values of the control parameters k and σ are shown in Fig. 15. The left column exhibits the original HKB case which is obtained for $\sigma = 0$. The functions in the most right column,

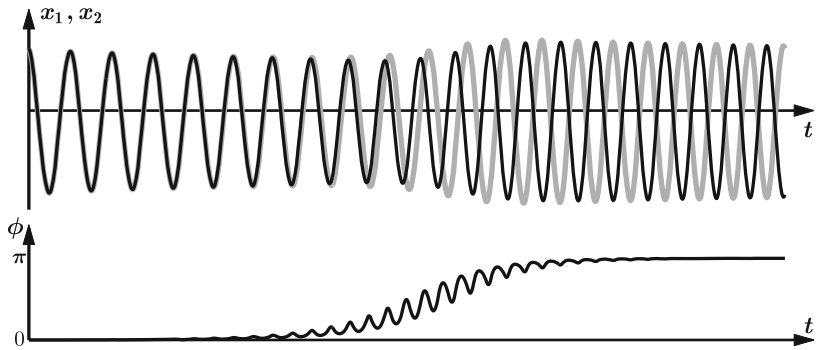

Movement Coordination, Fig. 14 Simulation of Eq. 30 where the frequency ω is continuously increased from $\omega = 1.4$ on the left to $\omega = 1.8$ on the right. *Top*: Time series of the amplitudes x_1 and x_2 undergoing a transition from in-phase to anti-phase when ω exceeds a critical value. *Bottom*: Continuous estimate of the relative phase ϕ changing from an initial value of zero during the in-phase to π when the anti-phase movement is established. Parameters: $\gamma = -0.7$, $\epsilon = \delta = 1$, $\alpha = -0.2$, $\beta = 0.2$, $\sigma = 1$ and $\omega = 1.4$ to 1.8

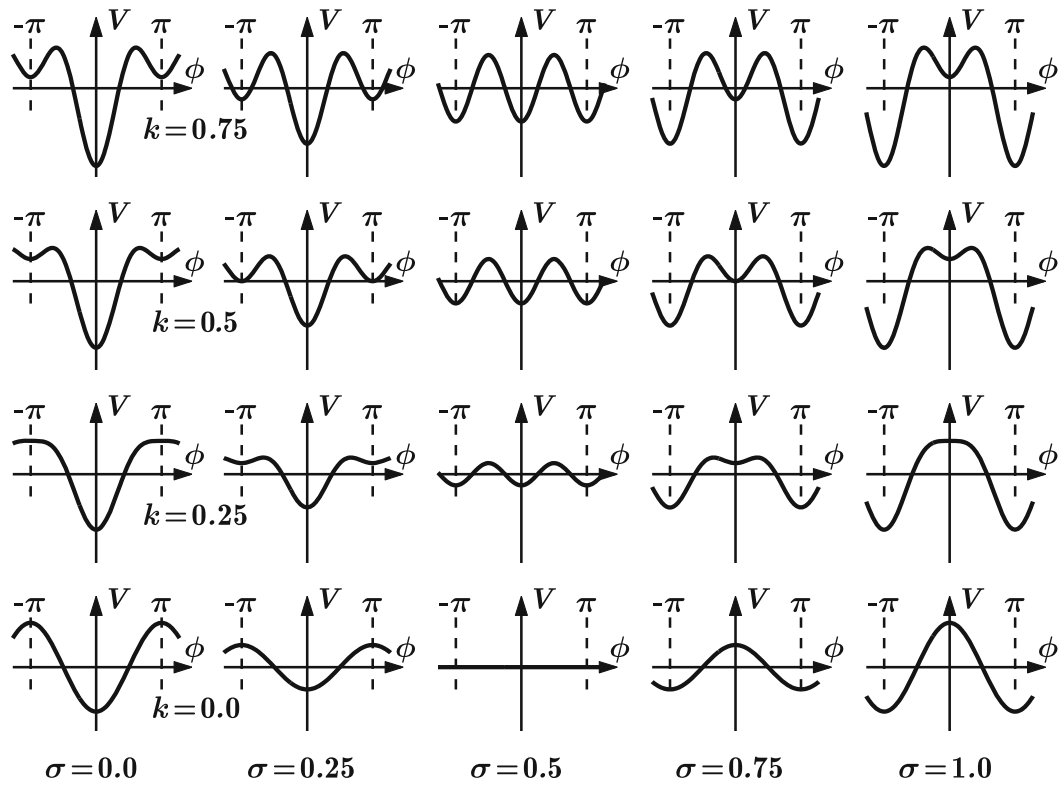

Movement Coordination, Fig. 15 Potential landscape for different values of the control parameters k and σ

representing the situation for $\sigma = 1$, are identical in shape to the $\sigma = 0$ case, simply shifted horizontally by a value of π. These two extreme cases are almost trivial and were the ones originally investigated in the Carson et al. experiment with the axes of rotation either on the same side or on opposite sides with respect to the hand. As the corresponding potential functions are shifted by π with respect to each other, one could assume that for an intermediate value of σ between zero and one the functions are also shifted, just by a smaller amount. Such horizontal translations lead to fixed point drifts, as has been seen before for oscillation components with different eigenfrequencies. The theory, however, predicts that this is not the case. In fact, for $\sigma = 0.5$, theory predicts that the two coordination modes in-phase and anti-phase are equally stable for all movement rates. The deep minima for slow rates indicate high stability for both movement patterns and as the rate increases, both minima become more and more shallow, i.e., both movement patterns become less stable. Eventually, for high rates at $k = 0$, the potential is entirely flat, which means that there are no attractive states whatsoever. Pushed only by the stochastic forces in the system, the relative phase will now undergo a random walk. Note that this is very different from the phase wrapping encountered before where the phase was constantly increasing due to the lack of an attractive state. Here the relative phase will move back and forth in a purely random fashion, known in the theory of stochastic systems as Brownian motion. Again experimental evidence exists from the Carson group that changing the distance between the axes of rotation gradually leads to the phenomena predicted by theory.

Conclusions

The theoretical framework outlined above represents the core of the dynamical systems approach

to movement coordination. Rather than going through the large variety of phenomena that coordination dynamics and the HKB model have been applied to, emphasis has been put on a detailed description of the close connection between theoretical models and experimental results. Modeling the coordination of movement as dynamical systems on both the mesoscopic level of the component oscillators and the macroscopic level of relative phase allowed for quantitative predictions and experimental tests with an accuracy that is virtually unprecedented in the life sciences, a field where most models are qualitative and descriptive.

Extensions of the HKB Model

Beyond the phenomena described above, the HKB model has been extended in various ways. Some of these extensions (by no mean exhaustive) are listed below with very brief descriptions; the interested reader is referred to the literature for details:

- The quantitative description of the influence of noise on the dynamics given in section "Stability: Perturbations and Fluctuations" can be done in a quantitative fashion by adding a stochastic term to Eq. 2 (Post et al. 2000; Schöner et al. 1986) or its generalizations Eqs. 21 and 31 (Fuchs and Jirsa 2000) and treating them as Langevin equations within the theory of stochastic systems (see, e.g., Gardiner (1985) for stochastic systems). In this case, the system is no longer described by a single time series for the relative phase but by a probability distribution function. How such distributions evolve in time is then given by the corresponding Fokker-Planck equation and allows for a quantitative description of the stochastic phenomena such as enhancement of fluctuations and critical fluctuations. An important quantity that can be derived in this context and is also related to the critical fluctuations is the mean-first-passage time, which is the time it takes (on average) to move over a hump in the potential function.
- When subjects flex a single finger between the beats of a metronome, i.e., syncopate with the stimulus, and the metronome rate is increased, they switch spontaneously to a coordination pattern where they flex their finger on the beat, i.e., synchronize with the stimulus. This so-called syncopation-synchronization paradigm introduced by Kelso and colleagues (Kelso et al. 1990) has been frequently used in brain-imaging experiments.
- A periodic patterning in the time series of the relative phase was found experimentally in the case of broken symmetry by Schmidt et al. (Schmidt 1991) and successfully derived from the oscillator level of the HKB model (Fuchs and Kelso 1994; Fuchs et al. 1996).
- The metronome pacing can be explicitly included into (2) and its generalizations (Jirsa et al. 2000). This so-called parametric driving allows us to explain effects in the movement trajectory known as anchoring, i.e., the variability of the movement is smaller around the metronome beat compared to other regions in phase space (Fink et al. 2000). With parametric driving, the HKB model also makes correct predictions for the stability of multifrequency coordination, where the metronome cycle is half of the movement cycle, i.e., there is a beat at the points of maximum flexion and maximum extension (Assisi et al. 2005). There are also effects from more complicated polyrhythms that have been studied (Peper and Beek 1998; Peper et al. 1995; Sternad et al. 1999; Kelso and DeGuzman 1988; DeGuzman and Kelso 1991).
- The effect of symmetry breaking has been studied intensively in experiments where subjects were swinging pendulums with different eigenfrequencies (Collins et al. 1996; Park and Turvey 2008; Sternad et al. 1995).
- Transitions are also found in trajectory formation, for instance, when subjects move their index finger such that they draw an "8" and this movement is sped up the pattern switches to a "0" (Buchanan et al. 1996, 1997; DeGuzman et al. 1997).

Future Directions

One of the most exciting applications of movement coordination and its spontaneous transitions

in particular is that they open a new window for probing the human brain, made possible by the rapid development of brain-imaging technologies that allow for the recording of brain activity in a noninvasive way. Electroencephalography (EEG), magnetoencephalography (MEG), and functional magnetic resonance imaging (fMRI) have been used in coordination experiments since the 1990s to study the changes in brain activations accompanying (or triggering?) the switches in movement behavior (Fuchs et al. 1992; Kelso et al. 1992, 1998). Results from MEG experiments reveal a strong frequency dependence of the dominating pattern with the contribution of the auditory system being strongest at low metronome/movement rates, whereas at high rates the signals from sensorimotor cortex dominate (Fuchs et al. 2000; Mayville et al. 2001). The crossover point is found at rates around 2 Hz, right where the transitions typically take place.

In two other studies, the rate dependence of the auditory and sensorimotor system was investigated separately. In an MEG experiment, Carver et al. (2002) found a resonance-like enhancement of a brain response that occurs about 50 ms after a tone is delivered, again at a rate of about 2 Hz. In the sensorimotor system, a nonlinear effect of rate was shown as well. Using a continuation paradigm, where subjects moved an index finger paced by a metronome which was turned off at a certain time while the subjects were to continue moving at the same rate, Mayville et al. (2005) showed that a certain pattern of brain activation drops out when the movement rate exceeds about 1.5 Hz. Even though their contribution to behavioral transitions is far from being completely understood, it is clear that such nonlinear effects of rate exist in both the auditory and the sensorimotor system in parameter regions where behavioral transitions are observed.

Using fMRI, brain areas have been identified that show a dependence of their activation level as a function of rate only, independent of coordination mode, whereas activation in other areas strongly depends on whether subjects are syncopating or synchronizing regardless of how fast they are moving (Jantzen and Kelso 2007).

Taken together, these applications of coordination dynamics to brain research have hardly scratched the surface so far, but the results are already very exciting as they demonstrate that the experimental paradigms from movement coordination may be used to prepare the brain into a certain state where its responses can be studied. With further improvement of the imaging technologies and analysis procedures, many more results can be expected to contribute significantly to our understanding of how the human brain works.

Acknowledgment Work reported herein was supported by NINDS Grant 48299, NIMH Grants 42900 and 80838, and the Pierre de Fermat Chair to J.A.S.K.

Bibliography

Primary Literature

Assisi CG, Jirsa VK, Kelso JAS (2005) Dynamics of multifrequency coordination using parametric driving: theory and Experiment. Biol Cybern 93:6–21

Buchanan JJ, Kelso JAS (1993) Posturally induced transitions in rhythmic multijoint limb movements. Exp Brain Res 94:131–142

Buchanan JJ, Kelso JAS, Fuchs A (1996) Coordination dynamics of trajectory formation. Biol Cybern 74:41–54

Buchanan JJ, Kelso JAS, DeGuzman GC (1997) The self-organization of trajectory formation: I. Experimental evidence. Biol Cybern 76:257–273

Carson RG, Goodman D, Kelso JAS, Elliott D (1995) Phase transitions and critical fluctuations in rhythmic coordination of ipsilateral hand and foot. J Mot Behav 27:211–224

Carson RG, Rick S, Smethrust CJ, Lison JF, Biblow WD (2000) Neuromuscular-skeletal constraints upon the dynamics of unimanual and bimanual coordination. Exp Brain Res 131:196–214

Carver FW, Fuchs A, Jantzen KJ, Kelso JAS (2002) Spatiotemporal analysis of neuromagnetic activity associated with rhythmic auditory stimulation. Clin Neurophysiol 113:1909–1920

Collins DR, Sternad D, Turvey MT (1996) An experimental note on defining frequency competition in intersegmental coordination dynamics. J Mot Behav 28:299–303

DeGuzman GC, Kelso JAS (1991) Multifrequency behavioral patterns and the phase attractive circle map. Biol Cybern 64:485–495

DeGuzman GC, Kelso JAS, Buchanan JJ (1997) The self-organization of trajectory formation: II. Theoretical model. Biol Cybern 76:275–284

Fink P, Kelso JAS, Jirsa VK, Foo P (2000) Local and global stabilization of coordination by sensory information. Exp Brain Res 134:9–20

Fuchs A, Jirsa VK (2000) The HKB model revisited: how varying the degree of symmetry controls dynamics. Hum Mov Sci 19:425–449

Fuchs A, Kelso JAS (1994) A theoretical note on models of Interlimb coordination. J Exp Psychol Hum Percept Perform 20:1088–1097

Fuchs A, Kelso JAS, Haken H (1992) Phase transitions in the human brain: spatial mode dynamics. Int J Bifurc Chaos 2:917–939

Fuchs A, Jirsa VK, Haken H, Kelso JAS (1996) Extending the HKB-Model of coordinated movement to oscillators with different eigenfrequencies. Biol Cybern 74:21–30

Fuchs A, Mayville JM, Cheyne D, Weinberg H, Deecke L, Kelso JAS (2000) Spatiotemporal analysis of neuromagnetic events underlying the emergence of coordinative instabilities. NeuroImage 12:71–84

Gardiner CW (1985) Handbook of stochastic systems. Springer, Heidelberg

Haken H (1977) Synergetics, an introduction. Springer, Heidelberg

Haken H (1983) Advanced synergetics. Springer, Heidelberg

Haken H, Kelso JAS, Bunz H (1985) A theoretical model of phase transition in human hand movements. Biol Cybern 51:347–356

Jantzen KJ, Kelso JAS (2007) Neural coordination dynamics of human sensorimotor behavior: a review. In: Jirsa VK, McIntosh AR (eds) Handbook of brain connectivity. Springer, Heidelberg

Jeka JJ, Kelso JAS (1995) Manipulating symmetry in human two-limb coordination dynamics. J Exp Psychol Hum Percept Perform 21:360–374

Jeka JJ, Kelso JAS, Kiemel T (1993a) Pattern switching in human multilimb coordination dynamics. Bull Math Biol 55:829–845

Jeka JJ, Kelso JAS, Kiemel T (1993b) Spontaneous transitions and symmetry: pattern dynamics in human four limb coordination. Hum Mov Sci 12:627–651

Jirsa VK, Fink P, Foo P, Kelso JAS (2000) Parametric stabilization of biological coordination: a theoretical model. J Biol Phys 26:85–112

Kay BA, Kelso JAS, Saltzman EL, Schöner G (1987) Space-time behavior of single and bimanual rhythmic movements: Data and limit cycle model. J Exp Psychol Hum Percept Perform 13:178–192

Kay BA, Saltzman EL, Kelso JAS (1991) Steady state and perturbed rhythmical movements: dynamical modeling using a variety of analytic tools. J Exp Psychol Hum Percept Perform 17:183–197

Kelso JAS (1981) On the oscillatory basis of movement. Bull Psychon Soc 18:63

Kelso JAS (1984) Phase transitions and critical behavior in human bimanual coordination. Am J Physiol Regul Integr Comp 15:R1000–R1004

Kelso JAS, DeGuzman GC (1988) Order in time: how the cooperation between the hands informs the design of the brain. In: Haken H (ed) Neural and synergetic computers. Springer, Berlin

Kelso JAS, Jeka JJ (1992) Symmetry breaking dynamics of human multilimb coordination. J Exp Psychol Hum Percept Perform 18:645–668

Kelso JAS, Scholz JP, Schöner G (1986) Nonequilibrium phase transitions in coordinated biological motion: critical fluctuations. Phys Lett A 118:279–284

Kelso JAS, Schöner G, Scholz JP, Haken H (1987) Phase locked modes, phase transitions and component oscillators in coordinated biological motion. Phys Scr 35:79–87

Kelso JAS, DelColle J, Schöner G (1990) Action-perception as a pattern forming process. In: Jannerod M (ed) Attention and performance XIII. Erlbaum, Hillsdale, pp 139–169

Kelso JAS, Bressler SL, Buchanan S, DeGuzman GC, Ding M, Fuchs A, Holroyd T (1992) A phase transition in human brain and behavior. Phys Lett A 169:134–144

Kelso JAS, Fuchs A, Holroyd T, Lancaster R, Cheyne D, Weinberg H (1998) Dynamic cortical activity in the human brain reveals motor equivalence. Nature 392:814–818

Mayville JM, Fuchs A, Ding M, Cheyne D, Deecke L, Kelso JAS (2001) Event-related changes in neuromagnetic activity associated with syncopation and synchronization timing tasks. Hum Brain Mapp 14:65–80

Mayville JM, Fuchs A, Kelso JAS (2005) Neuromagnetic motor fields accompanying self-paced rhythmic finger movements of different rates. Exp Brain Res 166:190–199

Park H, Turvey MT (2008) Imperfect symmetry and the elementary coordination law. In: Fuchs A, Jirsa VK (eds) Coordination: neural, behavioral and social dynamics. Springer, Heidelberg, pp 3–25

Peper CE, Beek PJ (1998) Distinguishing between the effects of frequency and amplitude on interlimb coupling in tapping a 2:3 polyrhythm. Exp Brain Res 118:78–92

Peper CE, Beek PJ, van Wieringen PC (1995) Frequency-induced phase transitions in bimanual tapping. Biol Cybern 73:303–309

Post AA, Peeper CE, Daffertshofer A, Beek PJ (2000) Relative phase dynamics in perturbed interlimb coordination: stability and stochasticity. Biol Cybern 83:443–459

Schmidt RC, Beek PJ, Treffner PJ, Turvey MT (1991) Dynamical substructure of coordinated rhythmic movements. J Exp Psychol Hum Percept Perform 17:635–651

Scholz JP, Kelso JAS (1989) A quantitative approach to understanding the formation and change of coordinated movement patterns. J Mot Behav 21:122–144

Scholz JP, Kelso JAS, Schöner G (1987) Nonequilibrium phase transitions in coordinated biological motion: critical slowing down and switching time. Phys Lett A 8:90–394

Schöner G, Kelso JAS (1988) Dynamic pattern generation in behavioral and neural systems. Science 239:1513–1520

Schöner G, Haken H, Kelso JAS (1986) A stochastic theory of phase transitions in human hand movements. Biol Cybern 53:442–453

Sternad D, Collins D, Turvey MT (1995) The detuning factor in the dynamics of interlimb rhythmic coordination. Biol Cybern 73:27–35

Sternad D, Turvey MT, Saltzman EL (1999) Dynamics of 1:2 coordination: generalizing relative phase to n:m rhythms. J Mot Behav 31:207–233

Books and Reviews

Fuchs A, Jirsa VK (eds) (2007) Coordination: neural, behavioral and social dynamics. Springer, Heidelberg

Haken H (1996) Principles of brain functioning. Springer, Heidelberg

Jirsa VK, Kelso JAS (eds) (2004) Coordination dynamics: issues and trends. Springer, Heidelberg

Kelso JAS (1995) Dynamics pattern: the self-organization of brain and behavior. MIT Press, Cambridge

Tschacher W, Dauwalder JP (eds) (2003) The dynamical systems approach to cognition: concepts and empirical paradigms based on self-organization, embodiment and coordination dynamics. World Scientific, Singapore

Determinisms of Behavior and Synergetics

Till D. Frank
Department of Psychology and Department of Physics, University of Connecticut, Storrs, CT, USA

Article Outline

Glossary
Definition of Subject
Introduction
Skinner and Determinism
Synergetics, Amplitude Equations, and Behavior
Application 1: Grasping of Objects with Different Sizes
Application 2: Walk-Run Transitions
Application 3: Action Chains and Child Play
General Aspects of the Modeling Framework
Conclusions
Future Directions
Bibliography

Glossary

Amplitude equations of BAB patterns Equations that define how amplitudes of BAB patterns evolve (in time). If an amplitude of a particular BAB pattern becomes finite while all other amplitudes approach values close to zero, then the corresponding BAB pattern has emerged and the human being under consideration performs the corresponding behavior.

Brain activity and body (BAB) patterns Patterns associated with human behaviors that can feature various components such as spatiotemporal patterns of brain activity, neural activity in descending pathways to muscles, neural activity in ascending pathways from peripheral sensors, muscle activity, and limb movements. In fact, the patterns may include aspects of the environment of a human being under consideration.

Determinism Behavioral activities are determined by laws. The laws correspond to if-then relationships. If a human actor is in a particular state (characterized by internal variables describing the human and external variables describing the environment including stimuli in experimental research), then the human actor will perform a certain behavior. Each state can be mapped to a behavior or behavioral response.

Free will The notion that a human can be the cause of his or her decisions and behaviors. In other words, a human is under control of his or her behavior. Decisions can be made irrespective of the past behaviors and experiences of the human.

Synergetics A theory of self-organization that puts emphasis on the emergence of patterns due to self-organization and describes the emergence and disappearance of patterns as well as transitions between patterns by means of dynamical systems such as amplitude equations.

Definition of Subject

Human and animal behavior consists of sequences of actions. For example, a student may study a textbook for a while. Subsequently, the student will do something else. It seems that the human individual or an animal under consideration has a choice as to what kind of behavior he/she or it would like to perform next. However, the concept of determinism states that actions and behaviors performed by humans and animals are the result of the internal (e.g., neurobiological) conditions and external circumstances characterizing the individual or animal under consideration. These conditions and circumstances in turn are the consequences of prior actions, behaviors, and experiences. As a result of this kind of causal chain, all behaviors are determined by laws. Therefore, determinism negates the concept of free will. A theoretical, mathematical framework

A. Hutt, H. Haken (eds.), *Synergetics*,
https://doi.org/10.1007/978-1-0716-0421-2_695

Originally published in
R. A. Meyers (ed.), *Encyclopedia of Complexity and Systems Science*, © Springer Science+Business Media LLC 2018
https://doi.org/10.1007/978-3-642-27737-5_695-1

that supports these claims of determinism is the theory of self-organization, in general, and synergetics, in particular. Synergetics is a theory of self-organization and pattern formation that puts emphasis on amplitude equations. With the help of amplitude equations, synergetics allows to describe the aforementioned switches between actions and behaviors in mathematical terms and consequently provides a framework for scientists to formulate mathematical laws for human and animal behavior.

Introduction

Human behavior is a complex and interdisciplinary research field. An aspect of human behavior that is not only of interest for researchers and applied scientists but is also of interest for the general public is the question whether human behavior is determined by laws or is the product of free will or at least involves an element of free choice.

Based on behavioral experiments with animals that showed that rats and pigeons can be trained to show various types of behaviors in response to various types of stimuli, Skinner concluded that behavior is the result of learned associations and free will is an illusion (Skinner 1953). Although attempts have been made to mathematize the laws underlying such associations, what is missing is a framework that is rooted in a mechanistic and microscopic perspective of human and animal behavior and at the same time is sufficiently broad such that it can qualitatively and quantitatively address a range of findings from research on human and animal behavior.

Taking a scientific perspective and introducing the framework of a science-based determinism for human behavior, it will be shown below that synergetics can describe human behavior in a deterministic, law-based manner without the need to introduce an element of free will. Moreover, it will be argued that synergetics is located between mechanistic, microscopic approaches, on the one hand, and widely applicable top-down approaches, on the other hand. As far as the latter issue is concerned, various types of human behavior have indeed been studied by taking advantage of top-down approaches based on synergetics. That is, synergetics has a broad scope of applications that will be reviewed briefly below. In detail, the application of synergetics to human behavior in the context of the debate about free will and determinism will be demonstrated for human grasping movements, gait transitions between walking and running, and transitions between playful activities of children during child play.

Skinner and Determinism

In what follows a small set of definitions will be given and conclusions will be drawn. The terminology used in what follows is open for debate. In fact, the author believes that any terminology would do more or less the same job. Therefore, the phrases used in the following definitions are not considered to be crucial for the statements to be made. Let us illustrate this point with an example from mathematics. We may define the numbers “one,” “two,” and “three” in the usual way. In addition, we may define the meaning of the addition operation “plus” and the meaning of the comparison “is equal to” in the usual way. If so, with these definitions at hand, we can arrive at the conclusion “One plus two is equal to three.” However, we may use a completely different terminology involving different phrases. For example, in German the numbers “one,” “two,” and “three” are called “eins,” “zwei,” and “drei.” The addition operation is written as “plus” again but pronounced differently from the English phrase “plus.” The “is equal to” comparison is called “ist gleich.” In summary, we may define the numbers “eins,” “zwei,” “drei” rather than “one,” “two,” “three,” the operation “plus” using German pronunciation rather than “plus” as pronounced in English, and the operation “ist gleich” rather than “is equal to.” If so, we arrive at the conclusion “Eins plus zwei ist gleich drei.” The two conclusions “One plus two is equal to three” and “Eins plus zwei ist gleich drei” formally use different phrases and a different kind of terminology but in fact they have the same

meaning. In this sense, the author believes that terminology does not play a primary role in the arguments that will be made below. The reader may use his or her own terminology rather than the one suggested by the author.

The author distinguishes between the scientific perspective of the universe and various nonscientific perspectives of the universe. In this context, no value is attached to any of those perspectives. For example, the scientific perspective is not regarded superior to any of the nonscientific perspectives. No statement is made that the scientific perspective is the true or correct perspective. For the author the distinction between different perspectives is not about finding the truth. It is about defining a starting point that can be used to draw conclusions. The scientific perspective of the universe is all-encompassing and consequently includes human behavior as a special case. Having said that, the application of the scientific perspective is limited in the sense anticipated above when talking about the truth. The scientific perspective only makes statements within the framework of the scientific perspective. Although this seems to be a triviality, in fact, it is important to be clear about this issue. For example, the scientific perspective does not make any statements about the existence or nonexistence of supernatural entities like God, Allah, etc. It does not speak in favor or against the existence of a human soul. As we will see in a moment, the scientific perspective can do without the notion of godlike entities, a human soul, free will, responsibility, and the past. To reiterate, this does not mean that it negates any of these because the scientific perspective does not make a statement about alternative, nonscientific perspectives that may claim that all of the above (godlike entities, the human soul, free will, responsibility and the past) do exist.

Let us define the scientific perspective of the universe as the perspective that states that everything that happens in the universe is determined by the first principles of physics. Accordingly, the universe is completely described by the Schrödinger equation and the four fundamental forces (i.e., the gravitational force, the electromagnetic force, and the strong and weak forces). The Schrödinger equation is taken from quantum mechanics and can be used to define the evolution of a probability function that describes the state of the particles (which are assumed to be countable) of the universe. First of all, the state of the universe at any given time point (including the current time point under which a particular human behavior is observed) can serve as initial condition for the evolution equation. Therefore, whether there exists a past or not is irrelevant for the scientific perspective. If a past exist, the past itself would be irrelevant for the evolution of the probability function describing the universe. Second, the evolution equation for the probability function is deterministic. There is no arbitrariness about the solution of the equation.

The definition of the scientific perspective of the universe allows us to define some related concepts: science-based lawfulness, science-based determinism, and psychology as a science. Let us define psychology as a science as the discipline in which all phenomena studied in psychology including human behavior are approached from the above-defined scientific perspective. These has implications for researchers in the field of psychology and anybody else who wants to apply the scientific perspective to human behavior. As already mentioned above, the scientific perspective takes the Schrödinger equation as a departure point. In this equation there are no expressions that could be regarded as reflecting a human soul or free will. Therefore, psychology as a science must do without the notion of a human soul and free will. This in turn implies that the notion that a human being is able to control his or her life should be disregarded in psychology (when conducting psychology as a science). Likewise, the concept of responsibility should not be used.

Let us return to the notion of free will. A precise definition is difficult to achieve. If so, how can we state that the scientific perspective, and, in particular, the Schrödinger equation, does not take free will into consideration? The reason for this is that any common-sense description of free will can be found to be in contradiction with the scientific perspective defined above. For example, Chisholm (1964, p. 32) states that if

we have free will "we cause certain events to happen, and nothing – or no one – causes us to cause these events to happen." This is in contradiction with the scientific perspective according to which the condition of the universe at an arbitrary reference point can be regarded as an initial condition and determines the future states of the universe. What happens in the future is caused by the conditions of the reference state (and the four fundamental forces and the quantum mechanical law captured by the Schrödinger equation). Likewise (when using the notion of a past for a moment), the behavior of a human observed at a particular point in time is a consequence of the state of affairs given at an arbitrarily selected, earlier point in time.

Let us define science-based lawfulness as the application of the scientific perspective in its general form to human behavior. Accordingly, there are laws that can be formulated at least in terms of evolution equations for probabilities that describe human behavior. In particular, the current state of affairs of a human being and the surrounding environment (which might be the whole universe) determines the probabilities of all possible future behaviors of that human being. We may compare the situation with the forecast of a tornado. Scientists may calculate for an emerging tornado the most likely path that it will take and, in addition, alternative, less-likely paths that the tornado may take. Importantly, the fact that the path of the tornado is described in a probabilistic sense does not mean that the tornado has free will. Likewise, when we arrive at the conclusion that the definition of science-based lawfulness implies there are laws of human behavior that are probabilistic in nature, then this does not mean that those by-chance-elements reflect any form of free will (when free will is defined in one of the ways it is usually done). Of course, an advocate, say Mr. Smith, may define free will in the sense that human behavior involves a by-chance element (put aside that this is not the common understanding of free will). If so, from the scientific perspective introduced above and from the aforementioned discussion it follows that this by-chance element is of quantum mechanical nature. However, any electron spinning around an atom exhibits this kind of quantum mechanical by-chance element. Consequently, if advocate Smith defines free will in terms of the presence of a by-chance element, then within the scientific perspective we would conclude that any electron possess the same kind of free will power. In fact, according to quantum mechanics, everything is determined by the quantum mechanical, probabilistic laws and consequently, everything would exhibit free will as defined by Mr. Smith. The scientific perspective is inconsistent with the notion that the free will defined by Mr. Smith is reserved to humans only – which is a claim that free will advocates like Mr. Smith typically want to make.

The Schrödinger equation is a quantum mechanical concept and comes with a fundamental physical constant: the Planck constant. Roughly speaking, the constant determines a spatial scale of observation or a time scale of observation on which quantum mechanical, probabilistic effects are relevant. The Planck constant is very small. Consequently, for many applications quantum effects are irrelevant. For example, in order to describe a hand-sized ball rolling down a slope, quantum effects typically can be neglected. When quantum effects are negligible, the Schrödinger equation can be used to derive various kinds of deterministic equations that adequately describe the evolution of subsystems of the universe. Let us define science-based determinism as the scientific perspective applied to human behavior assuming that quantum effects can be neglected. Consequently, science-based determinism is a special case of science-based lawfulness. Science-based determinism states that all human behaviors in principle can be described by deterministic evolution equations. According to those deterministic evolution equations, current states of affairs cause future states of affairs in a deterministic sense without any arbitrariness. If we place a hand-sized ball at the top of slope (e.g., a ramp with a particular incline), it will roll down the slope due to gravitational forces pulling the ball downwards. The dynamics of the ball is determined by certain evolution equations (e.g., Newton's equation of classical mechanics). At every point in time, we

may consider the current state of the ball on the slope as an initial condition of the ball that determines the future states. According to science-based determinism, human behavior is determined in just the same way as the ball dynamics. Of course, the equations that determine human behavior are in general different from those determining the dynamics of a ball on a slope. As we will discuss below, the mathematical equations provided by synergetics, a theory of self-organization, are promising candidate equations to describe human behavior.

Let us illustrate the consequence of science-based determinism with an example. Let us consider a person who is leaving for work and has to decide which pair of shoes he or she should put on. For sake of simplicity, we assume that there are only two pairs of shoes available that are labeled with A and B. Panel A of Fig. 1 illustrates this situation from a nonscientific perspective that assumes the existence of free will. At issue is to make a choice between A and B. The person under consideration is at a choice point. He or she makes a decision reflecting free will and chooses either pair A or pair B. Panel B of Fig. 1 illustrates the situation from the perspective of science-based determinism. The deterministic equations that can be derived from the Schrödinger equation do not involve any choice points. Therefore, according to science-based determinism, the notion that there is a unique situation that can either lead to the choice of pair A or the choice of pair B is a misconception. Rather, events that enfold in time are characterized by if-then relationships as illustrated in Panel B of Fig. 1. According to Panel B, a closer look at the person confronted with the question, what pair of shoes to wear, will reveal that in fact there are two different situations or cases. First, there is the case A in which the person asks himself or herself what shoes he or she should put on and in which the initial conditions are such that he or she will choose pair A. Second, there is the case B in which the person asks himself or herself what shoes he or she should put on – like in case A – and in which the initial conditions are different from case A, namely, such that he or she will choose pair B. We will return to this example below and will present there a deterministic mathematical description of the shoe-choosing problem based on synergetics.

Skinner has supported in various publications an overall deterministic point of view of human behavior (e.g., Skinner 1953). This point of view was motivated by research on animal behavior conducted by Skinner and his coworkers. Rats were trained to press a lever in order to obtain a food reward. Likewise, pigeons were trained to pick against a sensor to obtain food. Importantly, the animals were trained to show the food-rewarding behavior in response to various stimuli such as a light that was switched on. For example, when the light was switched on and the animal performed the lever-pressing or sensor-picking behavior then a food reward was given. When the lever was pressed or the sensor was picked while the light was off no reward was given. Using this experimental procedure, the animals learned to recognize the stimulus. Rats pressed the lever and pigeons picked the sensor when the light was switched on. Skinner generalized the insights obtained from those animal experiments to human behavior. According to Skinner, when we grow up we learn to behave in certain ways in

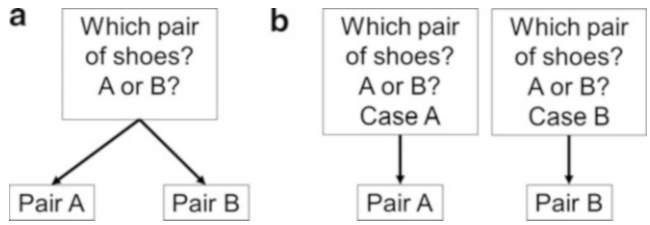

Determinisms of Behavior and Synergetics, Fig. 1 Decision making according to the free will perspective (Panel **A**) and the scientific perspective (Panel **B**). Illustration for the shoe-choosing problem

response to certain stimuli. All human behavior is understood as situation-specific learned response mechanisms. In other words, any observed behavior is the effect of a cause that can be found in the past.

In the context of the shoe-choosing example illustrated in Fig. 1, from Skinner's perspective, the person of interest has learned to put on the pair A when he or she is in the situation of choice-making described by case A. Whereas the person has learned to put on pair B when he or she is in the situation of choice-making described by case B. Skinner's point of view agrees by-and-large with the concept of science-based determinism introduced above. In particular, Skinner highlights that the concept of free will is an illusion. However, while Skinner focused on the impact of the environment to establish learned behavior, science-based determinism takes a neutral position in this regard. Both the conditions external to a human being and the state of the human being may be relevant to explain observed behavior. In particular, the framework of synergetics has its own take on the debate whether internal or external circumstances and likewise whether nature-related factors (e.g., genes) or nurture-related factors (e.g., education) are of relevance for the behavior to be discussed. We will return to this issue below.

In closing these considerations, we would like to reiterate that the scientific perspective introduced above and science-based determinism as derived from the scientific perspective do not make statements about the universe as such or the truth. While Skinner negates the existence of a free will, the scientific perspective states that there is no free will within the framework of the scientific perspective. No statement is made about different, nonscientific perspectives of the universe that may suggest that free will exists.

In the philosophical literature Skinner's point of view as well as science-based determinism may be seen as two examples of hard determinism. Hard determinism makes basically two statements. First, human behavior is determined by deterministic laws. Second, from the lawfulness of the human behavior it follows that there is no free will.

Synergetics, Amplitude Equations, and Behavior

According to the synergetics' perspective of human and animal behavior, behavior is a pattern formation process (Haken 1991, 1996). The pattern might be a rhythmic walking or running pattern of a human, a reaching and grasping action, or a complex activity such as being engaged in a small-talk conversation with somebody else or playing a game of chess. While in experimental studies typically only certain aspects of a pattern are observed (e.g., the limb movements during running), the boundaries of a pattern are not obvious (Frank submitted). For example, the relevant pattern describing a human on a run might include the limb movements, the associated brain activity, the descending neural signals to the muscles, and the ascending neural signals from the peripheral system providing feedback. However, even the rhythmic changes in the running shoes might contribute to the pattern. Moreover, if the runner is jogging with a friend, the limb movements of the friend (or the visual information about those movements) might belong to the pattern since it is known that humans have the tendency to couple their own rhythmic movements with those of others (Frank and Richardson 2010; Schmidt et al. 1990). For the sake of simplicity, the pattern will be referred to as a brain activity and body (BAB) pattern (Frank submitted). We may say that the pattern formation processes takes place "in" a human being.

A more rigorous point of view of the synergetics' perspective is that a human being represents processes that are about the formation of BAB patterns. That is, a human being performing a particular behavior "is" a pattern that emerged or is emerging from a pattern formation process – just like a hexagonal cloud pattern is a pattern that shapes itself due to a self-organization process. In cases in which the BAB extends the commonly defined physical boundaries of a human under consideration (e.g., when the person of interest goes for a walk together with somebody else), the human may be considered as part of a pattern formation process.

BAB patterns can be temporal, spatial, or spatiotemporal. For example, participants who swing a pendulum with one hand produce a temporal pattern describing the oscillatory dynamics of the swinging hand (Beek et al. 1995; Dotov and Frank 2011; Dotov et al. 2015; Kay et al. 1987; Kim et al. 2015). Likewise, rhythmic finger movements may be considered on the level of the finger movements as temporal patterns. However, when focusing on the associated brain activity that oscillates with the frequency of the finger movements, then spatial patterns of brain activity related to rhythmic finger movements can be identified by means of electroencephalography (EEG) measurements (Kelso 1995) and magnetoencephalography (MEG) measurements (Frank et al. 2000; Frank 2002, 2005; Kelso 1995).

Temporal patterns that describe an oscillatory (i.e., rhythmic) activity can conveniently be characterized by a measure that is either time-independent or varies slowly relative to the oscillatory changes: the amplitude of the oscillation. Taking half of the difference between the maximum and minimum value of the observed activity defines the amplitude of the oscillation. The amplitude may be defined for every individual oscillation period. If the oscillatory activity as a whole varies little over an extended period of time, then the amplitude varies only little from period to period. In contrast, if, for example, a participant initially performs pendulum swinging movements by varying the hand angle relative to an arbitrary reference angle only to a small amount and subsequently increases the amount to which the hand angle is varied during a swinging cycle, then the amplitude is initially small and subsequently increases over time. In this manner, the amplitude may change over time by 10%, 100%, or more of its initial value. Nevertheless, it is possible that the increase takes place on a slow time scale relative to the oscillatory activity. In what follows, it is assumed that this is the case. In fact, only if the amplitude changes relatively slow, then the amplitude can be introduced and defined as above. In other cases, more sophisticated approaches are required to define properly an oscillation amplitude. Given the notion of a well-defined amplitude of a temporal pattern, the emergence of the temporary pattern can be adequately described in terms of the increase of the amplitude from a small value towards a saturation value (which is also referred to as stationary value).

The concept of an amplitude also holds for spatial patterns and the emergence of spatial patterns as a result of a self-organization process. Panel A of Fig. 2 shows a hypothetical pattern of brain activity measured by an array of nine EEG sensors. The pattern can mathematically be described in terms of a vector with nine components that describes the strength of the brain activity in each sensor on a relative scale. The relative scale is chosen such that any pattern of brain activity measured by these nine sensors can be represented by a set of nine vectors expressed in the relative scale. These nine vectors are referred to as normalized vectors, eigenvectors (Haken 1991), normalized patterns, prototype patterns, or elementary patterns (Frank et al. 2015; Frank 2015a). In order to relate the relative scale to the actual measured brain activity, a pattern is multiplied with a proportionality factor. This factor is referred to as amplitude (Frank et al. 2015; Frank 2015a; Haken 1996; Hutt and Riedel 2003; Jirsa et al. 1995). For example, let us assume panel A of Fig. 2 displays an elementary pattern. If the amplitude is larger than one, then all activity scores are amplified and the observed pattern would look qualitatively as shown in Panel B. In contrast, if the pattern amplitude is equal to zero, then all components of the normalized vector (the elementary pattern) are multiplied by zero and the result is a pattern that shows no activity at all, as illustrated in panel C of Fig. 2. The emergence of a particular pattern of brain activity may be described in terms of an appropriately defined elementary pattern and its amplitude. The amplitude is initially close to zero and subsequently increases to a relative large value given by the saturation value (or stationary value).

In summary, the concept of an amplitude applies not only to temporal patterns but also to spatial patterns (Frank 2015a; Haken 2004). The emergence of temporal and spatial patterns can be described in terms of the dynamics of appropriately defined amplitudes. As we will argue below,

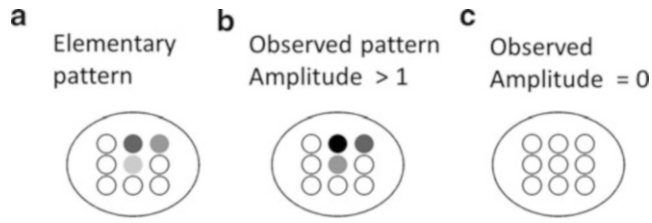

Determinisms of Behavior and Synergetics, Fig. 2 Schematic illustration of the distinction between a pattern and its amplitude for spatially distributed brain activity measured by means of electroencephalography using an array of nine sensors. All three panels **A**, **B**, **C** show top views of the head of a test person, the nine recording sites of sensors, and the activities in the recording sites. Color code: brain activity measured in arbitrary units increases with darkness (white: zero activity; black: high activity). Panel **A** shows brain activity as described by an elementary pattern. Panels **B** and **C** show brain activity patterns that would be observed when the elementary pattern has a finite amplitude larger than one (Panel **B**) and equal to zero (Panel **C**)

not only the emergence of patterns, also the disappearance of patterns and transitions between BAB patterns associated with different human behaviors can be described with the help of the time-evolution of amplitudes. Finally, note that the concept of amplitudes even applies to patterns that vary in time and extent in space, that is, to spatiotemporal patterns (Frank et al. 2015; Frank 2012a, 2015a; Haken 2004). In general, the dynamics of amplitudes is determined by a particular kind of mathematical equations: the amplitude equations. They are frequently given in terms of coupled, nonlinear, first-order differential equations. Note that synergetics distinguishes between two types of amplitudes: the order parameter amplitudes and amplitudes of a different kind. In order to keep this presentation short, in what follows, we will not make advantage of this distinction. For details on the order parameter concept, the reader is referred to Haken (2004).

Using so-called bottom-up approaches, amplitude equations can be derived from miscoscopic descriptions of self-organizing system (Haken 2004). In physics this has been demonstrated for roll patterns and other types of patterns emerging in hydrodynamic and gas systems by heating the systems from below (Bestehorn et al. 1989; Bestehorn and Haken 1991; Cross and Hohenberg 1993; Segal 1962, 1965; Newell and Whitehead 1969). Amplitude equations have been derived from reaction-diffusion equations for chemical and biochemical systems in which spatial patterns emerge as a result of pattern formation (Haken 2004; Wollkind and Stephenson 2000). In this context, amplitude equations describing pattern formation at so-called Turing instabilities have been determined for various model systems (Dufiet and Boissonade 1996; Dutt 2010; Pena and Perez-Garcia 2000). Reaction-diffusion models for the spread of epidemic diseases have been suggested in order to describe the emergence of spatial patterns of disease occurrences and the corresponding amplitude equations have been derived (Wang et al. 2011). Likewise, reaction-diffusion models for the emergence of patterns that describe the propagation of signals in cells have been suggested and the corresponding amplitude equations have been determined (Rattanakul et al. 2009; Stephenson and Wollkind 1995). In the field of human perception and behavior amplitude equations have been derived from Wilson-Cowan-like models of brain activity in order to explain the emergence of drug-induced hallucination patterns (Bressloff et al. 2001, 2002) and to provide a framework to discuss the performance of multiple consecutively performed tasks (Frank 2016a).

Although the methodology to derive amplitude equations from microscopic descriptions is well-developed (e.g., Haken 2004), for a given self-organizing system or a human actor performing a particular task an appropriate microscopic description might not be available or the derivation might be mathematically involved. In this case, it has been suggested to use a top-down approach that involves a general type of amplitude

equation (Lopresti-Goodman et al. 2011). While in bottom-up approaches the parameters occurring in amplitude equations are expressed in terms of the parameters of the corresponding microscopic models, in top-down approaches the model parameters are unknown. They might be fitted to experimental data (Frank 2014a, 2015b, 2016b, c; Kim and Frank 2016; Lopresti-Goodman et al. 2011, 2013).

In the field of human perception, there is a substantial literature on top-down approaches utilizing amplitude equations. Face and pattern recognition (Daffertshofer and Haken 1994; Frank 2011, 2012a; Frischholz et al. 1994; Haken 1991; Shimizu and Yamaguchi 1987; Yudashkin 1996) in particular in the context of associative memory have been studied by means of amplitude equations introduced in a top-down fashion. Selective attention (Fuchs and Haken 1988) and negative impacts of attention on object function perception within the functional fixedness paradigm (Frank 2015a) have been discussed. A series of studies has been devoted to study the oscillatory perception of ambiguous figures and ambiguous dynamic visual stimuli (Ditzinger and Haken 1989; Frank 2014a; Shao et al. 2008) and multistable (time-varying) perception of multistable acoustic stimuli (Ditzinger et al. 1997) by means of amplitude equations. Further studies on perception using the amplitude equation approach of synergetics have addressed how judgments for grasping opportunities (Frank 2016b; Kim and Frank 2016; Lopresti-Goodman et al. 2013) and opportunities for upright standing on tilted surfaces (Frank et al. 2015) are guided by visual information. Moreover, recently topics such as figure-ground perception (Kim and Frank in press) and perception under schizophrenia (Frank 2014a; Frank submitted) have been addressed.

In the field of human behavior, a few topics have been addressed that will be reviewed in detail below, namely, grasping (Frank et al. 2009, 2010; Lopresti-Goodman et al. 2011), gait transitions (Frank 2015b, 2016b), and action chains in rituals (Frank 2014b, c) and child play (Frank 2014b, d). Note however that the distinction between human behavior (here understood as a human performing an action) and perception is not that clear in any case. For example, when an experimenter presents a particular (e.g., relatively small) object to a participant and asks the participant whether he or she would grasp it with one or two hands, then the goal is to test how the participant perceives the object and in particular the opportunity to grasp the object without allowing the participant to perform the action. The task might be considered as a perceptual task. However, such experiments frequently require the participant to provide a response to the experimenter (e.g., the participant verbally responses with a "one" or "two" to indicate he or she would grasp the object with one or two hands, respectively). This response involves an action. To make a distinction between behavioral versus purely perceptual self-organizing processes more clearly participants may not be asked to provide a response. Rather, one might record task-related brain activity. In fact, studies aiming in this direction have been conducted (e.g., Kleinschmidt et al. 2002).

Application 1: Grasping of Objects with Different Sizes

Humans tend to grasp small objects, like a pen, with one hand. Bigger objects, like a chair, are typically grasped with two hands. Medium sized objects, like a book, may be grasped with one hand or two hands. Such objects of medium size are a particular challenge to theoretical modeling and to the claim that human behavior is determined by laws and is not based on free will. If medium sized objects are sometimes grasped with one hand and at other times the very same objects are grasped with two hands, then how can we identify a law that determines human grasping behavior? Interestingly, sophisticated experimental investigations of that matter discovered that in the domain of medium sized objects a phenomenon occurs that is well known in physics and allows to construct simple deterministic behavioral rules: the phenomenon of hysteresis. Let us first review an experimental study that has investigated grasping behavior and hysteresis in this

context. Subsequently, let us show how the aforementioned top-down amplitude equation approach of synergetics can contribute to a mechanistic understanding of grasping and allows us to simulate, reproduce, and – in this sense – predict human grasping behavior.

Various experiments on the different ways to grasp objects of different sizes have been reported in the literature (Cesari and Newell 1999, 2000; Lopresti-Goodman et al. 2009; Newell et al. 1989, 1993; Richardson et al. 2007; van der Kamp et al. 1998). In what follows, we consider the experimental study conducted by Lopresti-Goodman et al. (2011) and we focus on the control condition of Experiment 2 reported therein. Participants were shown wooden planks of different sizes. In total there were 41 rectangular-shaped planks that ranged in length from 4.5 to 24.5 cm and differed in length by 0.5 cm from plank to plank. Participants were asked to grasp the planks at the end sides either with one hand or with two hands. Planks were presented one at a time. There were two conditions. In the ascending condition, the shortest plank of the set of planks was presented first and subsequently longer planks were presented. In the descending condition, the longest plank was presented first and subsequently shorter planks were presented. Panel A in Fig. 3 illustrates the two experimental conditions. In line with our comment made at the beginning of this section, participants typically grasped the relatively short planks with one hand and the relatively long planks with two hands. In this context, it should also be noted that the mean hand span of the participants was 21.32 cm. Therefore, a great portion of the participants was physically not able to grasp the longest plank (i.e., the plank with 24.5 cm in size) at the two end sides with a single hand because the length of the longest plank exceeded their hand span. They had to grasp the longest plank with two hands. Consequently, it does not come as a surprise that in both experimental conditions participants typically switched from one grasping type to another while planks were presented (i.e., participants typically showed grasping transitions). Panel B in Fig. 3 illustrates the grasping behavior of a representative participant. In the ascending condition, planks of size 4.5 cm up to 15 cm were grasped with one hand. Planks longer than 15 cm up to the longest plank with 24.5 cm were grasped with two hands. There was a grasping transition (i.e., a transition between two different grasping types) at a plank length of 15 cm. Note that to make the transition point more clearly visible, in Panel B solid, continuous lines are used to represent the participant's behavior. In fact, responses were made only at the discrete values of planks sizes shown in Panel A. In this regard, the continuous character of the response line is somewhat misleading. In addition to the ascending condition, Panel B of Fig. 3 presents the responses of the representative

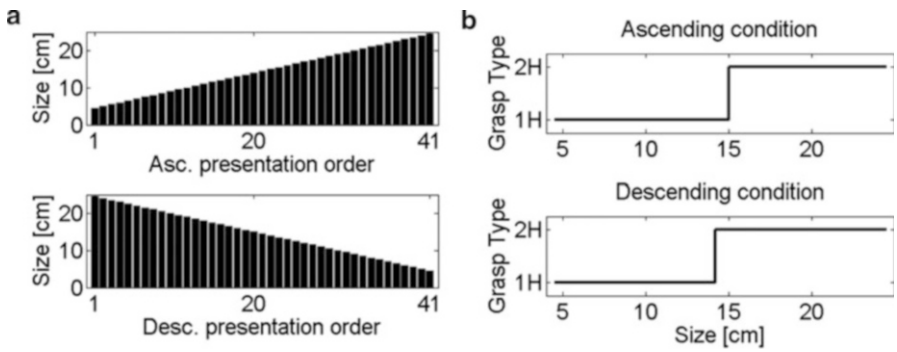

Determinisms of Behavior and Synergetics, Fig. 3 Experimental design and results reported by Lopresti-Goodman et al. (2011). Panel **A** shows the sequences of planks used in the experiment in the ascending (top subpanel) and descending (bottom subpanel) conditions. Panel **B** shows for a representative participant (see text for details) the grasping behavior in the ascending (top subpanel) and descending (bottom subpanel) conditions. For the descending condition, the horizontal axis should be read from right to left

participant in the descending condition. For the longest plank down to the plank with a size of 14 cm, planks were grasped with two hands. Planks shorter than 14 cm down to the shortest plank of 4.5 cm were grasped with one hand. Panel B reveals that the short and the long planks were grasped in a unique way, the medium sized planks in the range between 14 and 15 cm were grasped both with one hand and with two hands. While this might be at first sight suggest that there is some arbitrariness in the grasping behavior, a closer look makes clear that the grasping type was dependent on the experimental condition. Planks in the medium range of 14–15 cm were grasped with one hand in the ascending condition, while the very same planks were grasped with two hands in the descending condition. This also implies that the switching values at which the representative participant changed the grasping behavior from one- to two-handed grasping or, vice versa, from two-handed to one-handed grasping were not identical. The switching value in the ascending condition was larger than the switching value in the descending condition. Such a history dependency of switching values is known in physics as hysteresis (Haken 1996). For example, certain lasers that exhibit two different states of laser activity show hysteretic switching between these states when the pumping current is gradually increased and decreased (Barbay et al. 2000; Nagler et al. 2003). Finally, note that the representative participant that was introduced above and will be discussed below is a hypothetical participant that represents the sample mean values reported by Lopresti-Goodman et al. (2011) for the control condition of their Experiment 2.

The hysteresis observed in the control condition of Experiment 2 of the study by Lopresti-Goodman et al. (2011) was not statistically significant. However, in the study by Lopresti-Goodman et al. (2011) three alternative conditions were used in which participants were put in a more stressful scenario (by asking them to count back numbers in steps of 1, 3, and 7, respectively). Taken all four conditions together, hysteresis was observed as described above. Hypothesis testing showed that when taking all four conditions together the hysteresis (i.e., the difference between the switching values) was statistically significant, $F(2,56) = 36.37$, $p < 0.001$. Likewise, in Experiment 2 reported by Lopresti-Goodman et al. (2009) that involved both a counting back condition and performance speed manipulations during plank grasping, hysteresis was found and hypothesis testing revealed that the hysteresis when averaged across all experimental manipulations was statistically significant, $F(1,40) = 44.94$, $p < 0.01$. Moreover, in Experiment 2 reported by Richardson et al. (2007), which also involved plank grasping by one hand or two hands, a significant hysteresis was found, $F(1,11) = 11.07$, $p < 0.05$. In summary, there is experimental support that switching between grasping types in plank grasping experiments is subjected to hysteresis. But there are some conditions (like the control condition in Experiment 2 of Lopresti-Goodman et al. 2011) for which the amount of hysteresis seems to be relatively small such that hypothesis testing methods do not have the power to identify the hysteresis as statistically significant.

An amplitude equation model for describing the hysteretic transitions between one-handed and two-handed grasping has been proposed by Frank et al. (2009) and has been fitted to data in the study by Lopresti-Goodman et al. (2011). The amplitude equation model is a simplified version of the so-called synergetic computer introduced by Haken (1991). Let us refer to the amplitude equation model proposed by Frank et al. (2009) as grasping transition (GT) model. According to the GT model, there are two competing BAB patterns describing the one-handed grasping and two-handed grasping movements. Each pattern is characterized by a pattern amplitude (see above). If the amplitude of the pattern associated with one-handed grasping reaches its saturation value, while the amplitude of the other pattern (i.e., the pattern of two-handed grasping) approaches zero, then the pattern of one-handed grasping has emerged and the participant under consideration performs a one hand grasp. By analogy, two-handed grasping can be modeled.

A natural departure point to understand the GT model is to consider the symmetric case that occurs in the domain of medium sized planks. In

the symmetric case, there is no bias towards one of the two grasping types. The question arises how can we determine quantitatively the circumstances under which the symmetric case occurs?

In the experiment described above plank size was manipulated. Accordingly, a naïve approach would be to hypothesize that for each individual participant there was a particular plank length in the domain of medium sized planks for which the self-organizing system was completely unbiased. In fact, to some extent this is the correct point of view. However, in this context, the question arises if plank size is the most suitable variable to characterize a participant confronted with a particular plank. More precisely, from a dynamical systems perspective, we are looking for an appropriate control parameter (Haken 2004). Heuristically, a control parameter is a variable that varies with the experimental manipulation under consideration, on the one hand, and can be assumed to induce a transition from one behavior to another behavior, on the other hand. From a modeling perspective, transitions (or bifurcations) are induced by changes in the so-called eigenvalues (or Lyapunov exponents) that in what follows will be referred to as growth parameters (Frank 2009, 2015a; Frank et al. 2015). Any model parameter that can be manipulated by the experiment and that affects the growth parameters (eigenvalues) such that a transition is induced can be regarded as control parameter. Not only individual model parameters, but functions composed of several model parameters (in particular ratios of model parameters) are useful control parameters. For example, in fluid and gas dynamical systems that are heated from below roll patterns can emerge under appropriate circumstances. It has been shown that for pattern formation systems of this kind a useful control parameter is the so-called Rayleigh number, which is proportional to the temperature difference between the bottom and top layers of the systems divided by the diffusion constant of the systems. Consequently, for this kind of systems, the control parameter is a ratio. Studies on human motor behavior and perception have identified similar ratios to describe on what kind of variable human behavior depends upon. For example, if participants are shown a fleet of stairs and are asked to decide whether they can climb up the stairs, then it has been shown that participants do not base their decisions primarily on the stair step height. Rather, participants make their decisions based on the ratio of the stair step height over their leg length (Warren 1984). Likewise, for grasping behavior the relevant variable that determines human behavior is not the size of the objects to be grasped but the size of the objects relative to the hand size of the person that is grasping the objects (see e.g., Kim and Frank 2016). Therefore, in what follows, we will define relative plank size as the size of a plank divided by the hand span of a participant under consideration. With this definition at hand, we will use relative plank size rather than absolute plank size as control parameter.

Let us return to the issue of the symmetric case. From the GT model proposed by Frank et al. (2009) and the experimental data reported in Lopresti-Goodman et al. (2011) it follows that under the control conditions of Experiment 2 of Lopresti-Goodman et al. (2011) the symmetric case occurs at a relative plank size of 0.6850. For example, a participant with a hand span of 20 cm would act like a symmetric pattern formation system for a plank that is 13.70 cm long, while a participant with a hand span of 18 cm would perform like a symmetric pattern formation system for a plank that is 12.33 cm long. In the symmetric case, a participant regarded as a pattern formation system behaves similar to a square-shaped two-dimensional chemical system in which stripe patterns can emerge. As shown in Fig. 4 (panels A and B), at the transition point when a stripe pattern emerges there are two different stripe patterns that can emerge, which follows from the symmetric geometric of the square. If the conditions are such that a stripe pattern in one direction (e.g., the horizontal direction shown in panel A) can emerge, then the conditions are also such that a stripe pattern in the other direction (i.e., the vertical direction shown in panel B) can emerge. There is no bias towards one of the two possible stripe patterns. Let us return to the grasping experiment. As mentioned already, in the symmetric case, more explicitly, for planks with a relative plank size of 0.6850, participants behaved

like a symmetric pattern formation system. This implies that the grasping patterns illustrated in panels C and D of Fig. 4 of one-handed and two-handed grasping can both emerge and there is no bias towards one of them.

Although in the symmetric case, there is no bias towards one of the two grasping types, this does not imply that there is arbitrariness about the human behavior. That is, we do not need to introduce the notion of a free will. In the symmetric case, the initial conditions determine which pattern emerges. More precisely, the pattern emerges that exhibits initially (that is at the time point of the presentation of the plank to the participant) a higher amplitude. This can be illustrated by simulations of the GT model. Figure 5 shows two simulations for the symmetric case. In panel A, the case is shown when the amplitude of the one hand grasping pattern is initially larger than the amplitude of the two hands grasping pattern. Over the course of time, the amplitude of the one hand grasping pattern converges to its finite saturation value, while the other amplitude vanishes. Vice versa, panel B shows the case when the two hands grasping pattern initially dominates over the one hand grasping pattern and, consequently, the two hands grasping pattern emerges while the one hand grasping pattern "dies out."

Determinisms of Behavior and Synergetics, Fig. 4 Impact of symmetry on pattern formation systems. An analogy between chemical systems exhibiting stripe patterns and human grasping is drawn. Panels **A** and **B** show two stripe patterns emerging in a chemical system with a squared boundary exhibiting symmetry with respect to the horizontal and vertical axes. If one of the patterns can emerge, then the other can emerge as well. Panels **C** and **D** show two grasping patterns (one-handed and two-handed grasping) for a human actor tested under symmetric conditions. If one grasping behavior can emerge, then the other behavior can emerge as well

The symmetric case can be considered as a reference point to discuss the asymmetric case. Relatively long and relatively short planks are grasped in a unique way, either one-handed or two-handed. In order to account for this bias, it has been suggested to assume that the growth parameters of the two BAB patterns assume different values in the case of relatively long or short planks (Frank et al. 2009). More precisely, the GT model assumes that the growth parameters depend in a linear fashion on the control parameter, that is, relative plank size. The growth parameter of the amplitude of the one hand grasping pattern decays linearly with relative plank size, whereas the growth parameter of the amplitude of the two hands grasping pattern increases linearly with

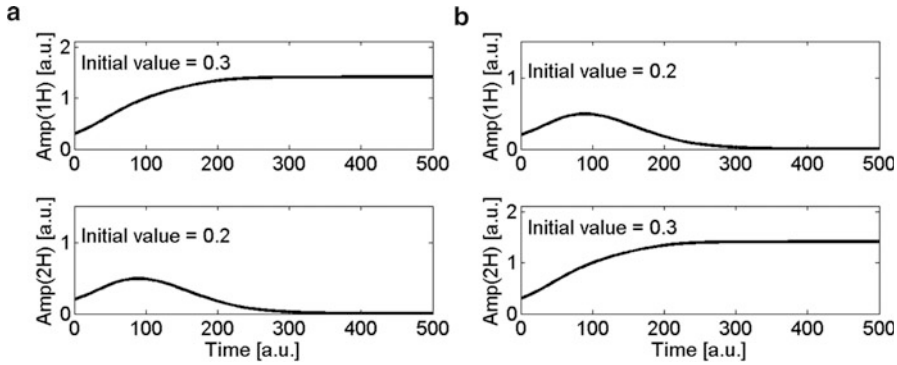

Determinisms of Behavior and Synergetics, Fig. 5 Simulation results of the GT model obtained for the symmetric condition. Panels **A** and **B** show the evolution of the amplitudes of the one-handed (top subpanels) and two-handed (bottom subpanels) grasping behavior for two different initial conditions. Panel **A**: The one-handed grasping amplitude dominates initially. Panel **B**: The two-handed grasping amplitude dominates initially. Parameters: both growth parameters were equal to 2 units, coupling parameter was equal to 2 units. For mathematical details see Frank et al. (2009)

relative plank size. Figure 6 illustrates the growth parameters as functions of relative plank size for the model parameters of the aforementioned representative participant. The vertical dotted line indicates the symmetric case (occurring at a relative plank size of 0.685). For planks shorter than 0.685 (as measured in relative length) the growth parameter for one-handed grasping is larger than the growth parameter for two-handed grasping. Likewise, for planks longer than 0.685 the growth parameter for two-handed grasping is larger than the growth parameter for one-handed grasping. Note that in the literature, the symmetric case is also referred to as the case of a homogeneous spectrum of growth parameters, whereas the asymmetric case is referred to as the case of an inhomogeneous spectrum of growth parameters (Frank 2009). We will address the V-shaped dotted line shown in Fig. 6 somewhat later.

The symmetric case does not allow us to discuss transitions between different grasping types because as illustrated in Fig. 4 in the symmetric case, there is no bias towards a pattern. In contrast, the asymmetric case (or inhomogeneous case) can be used to understand grasping transitions.

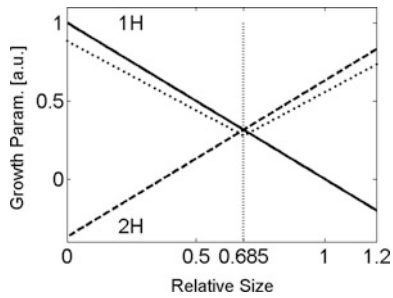

Determinisms of Behavior and Synergetics, Fig. 6 Growth parameters as functions of the relative plank size. Solid decaying line: One-handed grasping growth parameter. Dashed increasing line: Two-handed grasping growth parameter. Vertical dotted line indicates the symmetric condition. V-shaped dotted line is the lower bound of the stability band. Parameters are those of the representative participant of the study by Lopresti-Goodman et al. (2011) introduced in the text. For mathematical details see Frank et al. (2009) and Lopresti-Goodman et al. (2011). Accordingly, the growth parameter of the two-handed grasping amplitude has an offset value at zero plank size of −0.37 units. Coupling parameter equals 1.13 units

A detailed mathematical analysis (Frank 2009; Frank et al. 2010) shows that there exists a stability band for the growth parameters of the GT model. If a growth parameter belongs to the stability band, then the corresponding pattern emerges provided the initial conditions are appropriate. From a dynamical systems perspective, the reason for this is that within the framework of the GT model a grasping pattern exhibits an asymptotically stable fixed point if and only if the corresponding growth parameter belongs to the stability band. This implies that if a growth parameter does not belong to the stability band, then the corresponding grasping pattern cannot emerge (because the fixed point of the corresponding pattern amplitude is not asymptotically stable; it does not exist or is unstable). The stability band can be constructed as follows. The upper bound of the band is given by the largest growth parameter. The lower bound is given by the largest growth parameter divided by the coupling constant of the GT model. The coupling constant in turn describes the strength of the inhibitory interactions between the patterns. Figure 7 shows two exemplary cases of a growth parameter spectrum (composed of only two growth parameters) and the corresponding stability band. In panel A, we consider a plank with relative plank size of 0.685 (i.e., the symmetric case). From Fig. 6, we can read off the two growth parameters and plot them as a bar graph. The growth parameters are both 0.315 units large. Accordingly, the upper boundary of the stability band is 0.315 (top horizontal solid line in panel A). For the representative participant of Experiment 2 reported by Lopresti-Goodman et al. (2011) the coupling constant is 1.13. Therefore, the lower bound of the stability band is 0.315 units divided by 1.13 which equals 0.28 units (shown as bottom horizontal solid line in panel A). We see that the growth parameters of the one hand and two hands grasping patterns both belong to the stability band. Accordingly, the representative participant can grasp planks of relative size 0.685 with one hand or two hands. Just as in the symmetric case, the initial conditions determine what kind of grasping type actually will be performed. Panel B illustrates the case for a plank with relative size 0.7042. From Fig. 6, it

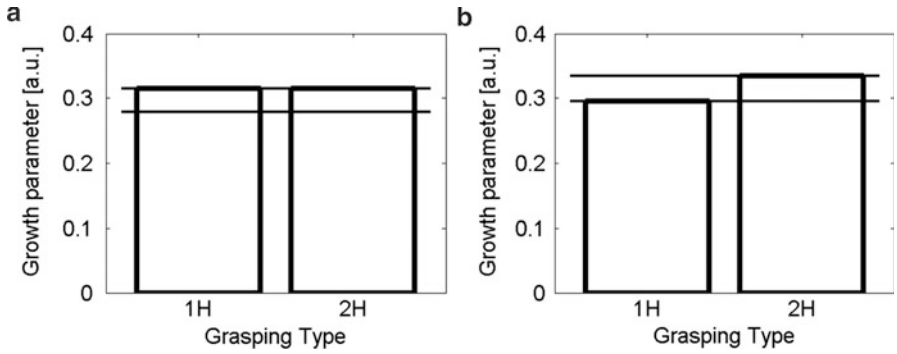

Determinisms of Behavior and Synergetics, Fig. 7 Growth parameter spectrum in the case of the two growth parameters of the GT model. Panels **A** and **B** show the growth parameters of the one-handed (left) and two-handed (right) grasping behaviors for the symmetric case (Panel **A**) and the critical asymmetric case of the ascending condition (Panel **B**). The two horizontal lines in Panels **A** and **B** indicate the stability band. In the critical ascending condition the growth parameter of the one-handed grasping amplitude drops out of the stability band

follows that the growth parameters are 0.2958 units (one hand grasping pattern) and 0.3342 units (one hand grasping pattern). The upper boundary is at 0.3342 (top horizontal solid line in panel B). The lower boundary of the stability band is 0.3342 units divided by 1.13, which equals 0.2958 units (bottom horizontal solid line in panel B). That is, this is the critical case at which the lower boundary corresponds to the smaller growth parameter. Accordingly, the growth parameter of the one hand grasping pattern drops out of the stability band and, consequently, the pattern can no longer emerge. The participant can no longer grasp the plank with one hand. If we take panels A and B together, we see how the GT model explains the transition from a one-handed grasping to two-handed grasping. Let us assume the representative participant is tested under the ascending condition and grasps a plank with relative plank size of 0.6850 with one hand. Subsequently, plank size is increased from 0.6850 to 0.7042 (measured in relative units). The growth parameter spectrum and the stability band change from panel A to panel B. The growth parameter of the one hand grasping pattern drops out of the stability band. The representative participant cannot grasp the plank with 0.7042 relative length with one hand even if the amplitude of the one hand grasp is relatively large (because this was the previous action performed by the participant). Consequently, the participant grasps the plank with two hands. The experimenter observes a switching from one hand grasping to two hands grasping.

We are now in the position to understand the hysteresis phenomenon in terms of the amplitude equation model. To this end, let us return to Fig. 6. The V-shaped dotted line in Fig. 6 represents the lower bound of the stability band as a function of relative plank size. That is, it represents the value of the larger of the two growth parameters divided by the coupling parameter (which is 1.13 units as mentioned above for the representative participant under consideration). In the ascending case, we follow the horizontal axis (the axis of relative plank size) from the left to the right. The growth parameter of the two hands grasping pattern (dashed line) increases, whereas the growth parameter of the one hand grasping pattern decreases (solid line). As discussed above in the context of Fig. 7 and as can be seen also from Fig. 6, at a value slightly above 0.685, namely, at 0.7042 the growth parameter of the one hand grasping pattern "hits" the lower boundary (the V-shaped line) and drops out of the stability band. According to the GT model, the participant switches from one-handed grasping to two-handed grasping. In the descending case, we follow the horizontal axis from the right to the left. The growth parameter of the two hands grasping pattern (dashed line) decreases, whereas the growth parameter of the one hand grasping pattern

increases (solid line). At a value slightly below 0.685, namely, at 0.6658 the growth parameter of the one hand grasping pattern "hits" the lower boundary (the V-shaped line) and drops out of the stability band. At this point, the participant switches from two-handed grasping to one-handed grasping. We see that the two switching values differ: 0.7042 in the ascending case versus 0.6658 in the descending case. The model predicts hysteresis.

Having discussed aspects of the GT model, let us show by a numerical simulation that the GT model – as a special case of an amplitude equation model proposed within the framework of synergetics – can reproduce and – in this sense – predict human behavior and in particular the hysteresis phenomenon observed in grasping transition experiments. To this end, we solved the amplitude equations of the GT model numerically for the model parameters of the representative participant. The model equations can be found in Frank et al. (2009) and Lopresti-Goodman et al. (2011). The result of the simulation is shown in Fig. 8. Panel A shows simulation results for the ascending case. The top panel shows the relative plank size of the planks presented to the participant and the order of presentation. The relative plank size increased from presentation to presentation. Note again that the use of continuous lines in Fig. 8 is somewhat misleading. According to the stimulation, the participant was tested in 41 discrete events. However, using continuous rather than dotted lines improves the visual clarity of the graphs. The second top panel shows the growth parameters of the one hand grasping pattern (solid line) and the two hands grasping pattern (dashed line) as functions of relative plank size. This second top panel is identical to Fig. 6 (except for the starting point of the horizontal axis which is 0 in Fig. 6, whereas it equals 4.5 cm divided by the hand span of the representative participant in Fig. 8). The third panel from the top shows the saturation values (or stationary values) of the amplitudes of the one hand grasping pattern (solid line) and two hands grasping pattern (dashed line). For example, in Fig. 5 the saturation values are those values observed at the end of the simulation period. From Fig. 8, we see that the amplitude of the one hand grasping pattern assumed a finite value in the range from the shortest plank up to planks of relative size 0.68, whereas the amplitude of the two hands grasping pattern vanished. This indicates that according to the GT model in this range of planks, the representative participant behaved like a pattern formation system in which a BAB pattern associated with one-handed grasping emerges. The amplitude dynamics exhibited a switch between 0.68 and 0.70 consistent with the discussion around Figs. 7 and 8. For planks with relative size 0.70 up to the longest plank the amplitude of the two hands grasping pattern was finite, whereas the amplitude of the one hand grasping pattern was equal to zero. That is, the GT model predicted the

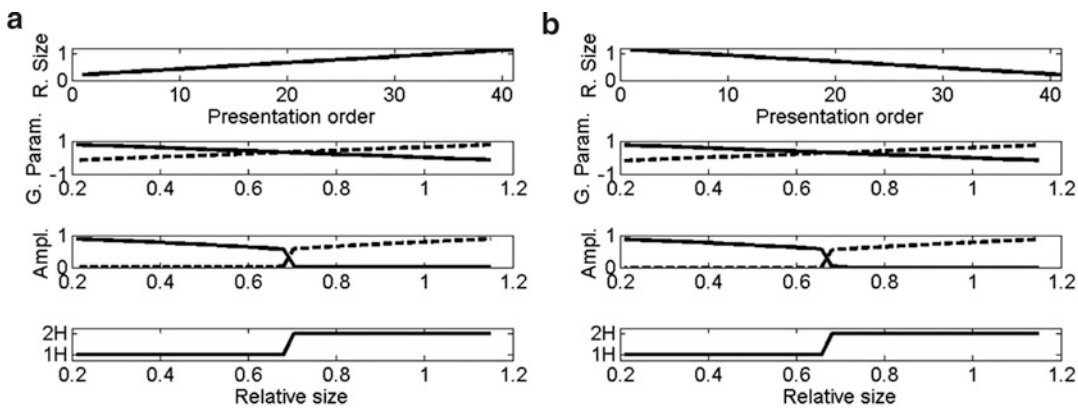

Determinisms of Behavior and Synergetics, Fig. 8 Simulation results for the representative participant of the study by Lopresti-Goodman et al. (2011) obtained from the GT model. See text for details. Parameters as in Fig. 6

emergence of a BAB pattern associated with two hands grasping at a value of 0.70. The bottom panel illustrates the behavioral response as function of the relative plank size. For planks that induced in the ascending condition the emergence of a BAB pattern associated with a one hand grasping pattern, the simulated participant grasped the planks with one hand. By analogy, the computer-simulated participant performed two-handed grasping when a two hand BAB pattern was present. The bottom panel is identical with the top panel of Fig. 3B expect for the scale on the horizontal axis. While in the top panel of Fig. 3B the behavioral response as function of absolute plank size is shown, in Fig. 8 relative plank size is used.

Panel B of Fig. 8 shows the simulation results for the descending case. The top panel shows again the relative plank size of the planks presented to the participant and the order of presentation. The relative plank size decreased from presentation to presentation. The second top panel shows the growth parameters of the one hand grasping pattern (solid line) and the two hands grasping pattern (dashed line) as functions of relative plank size. The panel is identical with the second top panel on the left. However, we need to read the horizontal axis from the right to the left. In the descending case, long planks with large values of relative size were presented first and subsequently shorter planks were presented. The third panel from the top shows the saturation values of the amplitudes of the one hand grasping pattern (solid line) and two hands grasping pattern (dashed line). Again the figure should be read from the right to the left. The amplitude of the two hands grasping pattern assumed a finite value in the range from the longest plank down to planks of relative size 0.68, whereas the amplitude of the one hand grasping pattern vanished. For planks with relative size 1.2 down to 0.68 the representative participant behaved like a pattern formation system in which a BAB pattern of two-handed grasping emerged. The amplitude dynamics exhibited a switch between 0.68 and 0.66 consistent with our discussion above of Fig. 6. For planks with relative size 0.66 down to the shortest plank, the amplitude of the one hand grasping pattern was finite, whereas the amplitude of the two hands grasping pattern was zero. In this range, the BAB pattern of one hand grasping emerged. The bottom panel is identical with the bottom panel of Fig. 3B expect for the scale on the horizontal axis. Comparing the switching points in panels A and B, we see that the simulation predicted that the switches occurred at different values. Note that they do not exactly correspond to the theoretical values of 0.7042 and 0.6658. This is due to the fact that in the simulation relative planks size was increased and decreased not in a continuous way but in discrete steps. Overall, the numerical simulation of the GT model is able to reproduce and predict the experimentally observed hysteresis phenomenon.

The GT model reviewed above involves some key components that are summarized in Fig. 9.

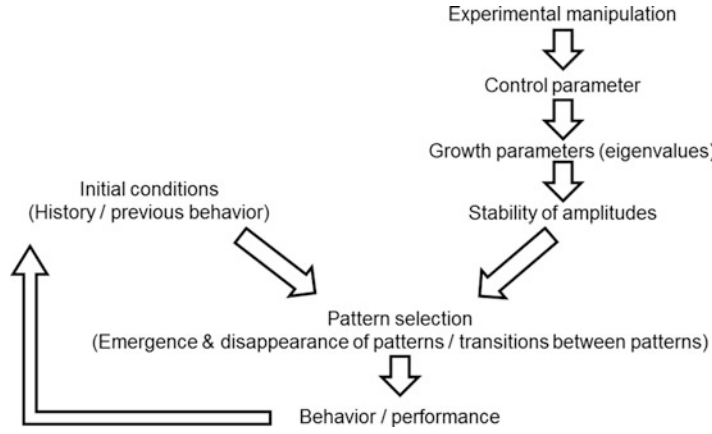

Determinisms of Behavior and Synergetics, Fig. 9 Components of the amplitude equations models of human behavior as discussed within the framework of synergetics

Since the GT model is a special case of an amplitude equation model, in general, amplitude equation models as discussed with the framework of synergetics feature elements identical or similar to those shown in Fig. 9. First of all, the GT model applies to grasping transition experiments in which the experimental manipulation is given by the systematic variation of the size of the to-be-grasped planks. As far as the experimental design of grasping transition experiments is concerned, plank size is regarded as the primary independent variable. The primary independent variable gives rise to a control parameter that depends on the independent variable but is also affected by other model parameters. In the case of the GT model, the control parameter is the plank size divided by hand span. The control parameter in turn affects the growth parameters (which correspond to the eigenvalues or Lyapunov exponents in the theory of dynamical systems) of the two BAB grasping patterns: the one hand and two hands grasping patterns. Bottom-up approaches would allow to derive explicitly the functional relationships between the growth parameters and the control parameter. We followed the top-down approach suggested by Frank et al. (2009) and Lopresti-Goodman et al. (2011) in which it was assumed for the sake of parsimony that the two growth parameters depend in a linear fashion on the control parameter. From dynamical systems theory it is well-known that the growth parameter (alias eigenvalues) determine the stability of the fixed points of a dynamical system. Likewise, the growth parameters of the GT model determine the stability of fixed points of the amplitudes. These fixed points describe the saturation values (or stationary values) of the amplitudes. The stability properties of the fixed points in combination with the initial conditions of the self-organizing system under consideration determine which pattern is selected. In the context of a sequence of grasping actions, the initial conditions are determined by the history given in terms of the behavior that was previously performed. In fact, such previously performed actions would determine the initial conditions of the amplitudes. The pattern selection process in general involves the emergence of a pattern. It might also involve the disappearance of another pattern and/or a transition between two patterns. Finally, the emergent BAB pattern exhibits a component that reflects the behavior or the actual performance of the participant.

Application 2: Walk-Run Transitions

Humans have various ways of locomotion such as crawling, hopping (or jumping), walking and running. We may refer to these different ways of locomotion as gaits. The aim of a gait is to allow him or her to move from one position to another. As far as walking and running are concerned, the key difference between these gaits is that during walking at any time there is at least one foot in contact with the ground, while during running there is a flight (or aerial) period. Contact with the ground is lost during the flight period. Typically, at low speeds of locomotion humans tend to walk, whereas at high locomotion speeds running is the preferred gait (see below). Walk-run and run-walk transitions are gait transitions in which humans switch from one gait to the other.

The transition from walk to run and vice versa from run to walk can be studied conveniently by asking participants to move on a treadmill and manipulating the treadmill speed. For example, Diedrich and Warren (1995) changed treadmill speed continuously from about 1 m/s to about 4 m/s and back to 1 m/s and observed walk-to-run and run-to-walk gait transitions at a treadmill speed of 2.07 m/s (when averaging walk-to-run and run-to-walk transition speeds). In a related study, Diedrich and Warren (1998) found transitions speeds of 2.19 m/s (for the control conditions in Experiments 1 and 2). Similarly, Hreljac (1995) reports a transition speed of 2.05 m/s for a sample of 28 participants. After data cleaning by removing two outliers, a reanalysis of the data by Hreljac (1995) yields a slightly higher value at 2.06 m/s for the corrected sample of 26 participants. Finally, Li (2000) determined walk-to-run and run-to-walk transitions using various treadmill acceleration conditions. Overall the transition speeds were found to fall into the range of 2.2–2.4 m/s (see Fig. 3 of Li 2000).

Just as for grasping transition experiments, in the context of gait transition experiments the questions arises whether speed as such is an appropriate control parameter. Based on theoretical considerations, it has been suggested that transition speed should increase with leg length. Accordingly, a rescaled parameter, the so-called Froude number, which is a dimensionless variable and defined by the speed squared divided by leg length, and the earth gravitational constant (Alexander 1992) should yield transition values that are independent of the leg length of participants. Therefore, the Froude number is generally considered to be a more appropriate control parameter. Let us illustrate this issue by means of the data reported for male participants in the study by Hreljac (1995). Panel A of Fig. 10 shows the scatter plot for the transition speeds and leg length scores of the male participants (excluding the two aforementioned outliers). Here speed is measured in meter per seconds and thigh length is used as a proxy for leg length. The data are taken from Table 1 of Hreljac (1995). The scatter plot reveals a positive correlation. The correlation coefficient equals 0.58 and is statistically significant, $r(9) = 0.58$, $p = 0.03$ (one-tailed). The regression line is shown in panel A as well. Let us express next the transition scores as Froude numbers rather than speed scores. Using again thigh length rather than leg length, we computed pseudo Froude numbers for all male participants. Panel B of Fig. 10 shows the scatter plot for the pseudo Froude numbers and leg length scores (again given in terms of thigh length measures). Comparing the scatter plots of panels A and B, visual inspection reveals that while for transition speed scores a linear relationship with leg length scores can be identified, for transition Froude numbers (which produced a correlation coefficient of −0.09) such a relationship is not obvious. Rather panel B suggests that participants change their gaits at more or less the same Froude number irrespective of their leg length. In fact, hypothesis testing (two-tailed) showed that the correlation coefficient was not statistically significant. Therefore, the experimental data taken from Hreljac (1995) support the aforementioned theoretical claim that the Froude number is a more appropriate control parameter than locomotion speed.

Diedrich and Warren (1995) found that gait transitions (averaged over walk-to-run and run-to-walk) occurred at a Froude number of 0.49. In their Experiments 1 and 2 reported in Diedrich and Warren (1998) they report slightly higher values, namely, transition Froude numbers of 0.54 and 0.55 for the respective control conditions. Frank (2016b) reports from a treadmill experiment with a control condition in which participants showed a transition Froude number of 0.43 both for walk-to-run and run-to-walk transitions.

So far the focus was on studies that reproduced walk-run transitions known from everyday life in

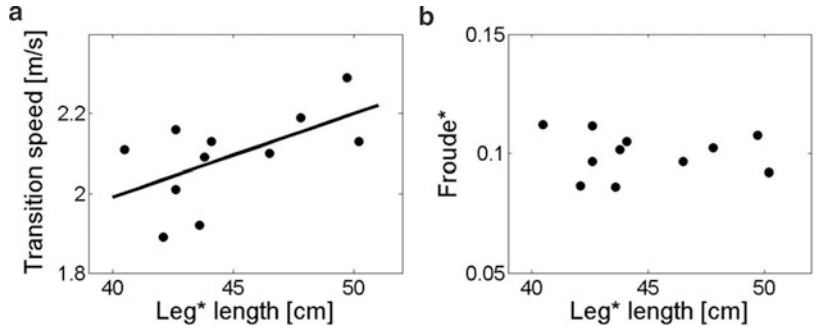

Determinisms of Behavior and Synergetics, Fig. 10 Scatter plots for transition scores observed in walk-run and run-walk gait transitions versus leg length of the participants. The scatter plots are shown in two different scales. Panel **A** shows transitions speeds in m/s on the vertical axis. Panel **B** shows Froude numbers (which are dimensionless scores) on the vertical axis. Transition speeds show a positive correlation with leg length as indicated by the regression line in Panel **A**. Such a correlation does not exist for the Froude numbers (Panel **B**) (Data taken from Hreljac (1995), see text)

a laboratory setting and characterized quantitatively the transition points either by means of a transition speed values or transition Froude numbers. In view of the hysteresis phenomenon reported for grasping transitions, it is worthwhile to examine whether the direction of change (walk-to-run versus run-to-walk) has an impact on the transition point. In fact, there are a few studies that report from gait transitions that showed hysteresis. Diedrich and Warren (1995) found for walk-to-run transitions a transition speed of 2.09 m/s and a corresponding transition Froude number of 0.5. In contrast, for run-to-walk transitions the scores were lower: the transition speed was 2.05 m/s and the corresponding transition Froude number was 0.48. The difference was statistically significant, $F(1,74) = 10.02$, $p < 0.01$. In Experiment 2 of Diedrich and Warren (1998), the impact of the slope of the walking belt on transition scores was examined (using two slope conditions: zero slope and nonzero slope). When averaged across the two slope conditions, Diedrich and Warren (1998) found that transition scores showed hysteresis with a walk-to-run transition speed of 2.12 m/s versus a run-to-walk transition speed of 2.07 m/s. The difference was statistically significant when taking participants into account as a factor, $F(1,83) = 18.04$, $p < 0.001$. Note that this observation has to be interpreted with caution because when ignoring the participant factor (i.e., when not taking participants into account as a factor) then the hysteresis turned out not to be statistically significant. Hreljac et al. (2007) studied gait transitions under three different slope conditions (zero slope, medium slope, and large slope). The transition speed values for walk-to-run and run-to-walk transitions ranged from 1.6 to 2.0 m/s (see Fig. 2 of Hreljac et al. 2007). Importantly, for all conditions the walk-to-run transition speeds were higher by about 0.07 m/s than the run-to-walk transition speeds. These differences were statistically significant. Finally, Li (2000) found for relatively high acceleration and de-acceleration values of treadmill speed that the walk-to-run transition speeds were larger than the run-to-walk transition speeds (see Fig. 3 of Li 2000). At relative low acceleration and de-acceleration values, the transition scores were the same or the effect was even reversed. This observation is reminiscent of the observation (reviewed above) made in the study by Lopresti-Goodman et al. (2011) on grasping transitions, namely, that the degree of hysteresis was relatively large when participants were put in a stressful situation, whereas under the control condition the degree of hysteresis was relatively small.

The GT model has been modified to account for walk-run transitions (Frank 2015b, 2016b, c). Let us refer to the modified model as walk-run-transition (WRT) model. The model describes two BAB patterns, walking and running, in terms of the respective amplitudes. Just like the GT model, the WRT model is composed of the elements shown in Fig. 9. In the context of walk-run transitions, the experimental manipulation is the variation of the treadmill speed. The control parameter is the Froude number introduced above. That is the Froude number replaces relative plank size. The WRT model features two growth parameters and two pattern amplitudes, which are the growth parameters and amplitudes of the walking and running patterns. Finally, if the amplitude of the walking pattern is finite, whereas the amplitude of the running pattern is close to zero, the BAB pattern associated with walking has emerged and the participant settles down in a walk. In contrast, if the amplitude of the running pattern is finite, whereas the amplitude of the walking pattern is close to zero, the BAB pattern of running has emerged and the participant is running.

In order to show that the WRT model can capture the experimentally observed hysteresis phenomenon, we solved the amplitude equations of the WRT model numerically. The model equations can be found in Frank (2015b, 2016c). The result of the simulation is shown in Fig. 11. Figure 11 is organized just like Fig. 8. The simulation results describe the representative participant number 2 of the study by Diedrich and Warren (1995). This participant has also been discussed in detail in Frank (2016c). Panel A of Fig. 11 shows simulation results when treadmill speed is increased. The top panel shows the Froude numbers of the simulation and the order in which the Froude number were used in the simulation. The

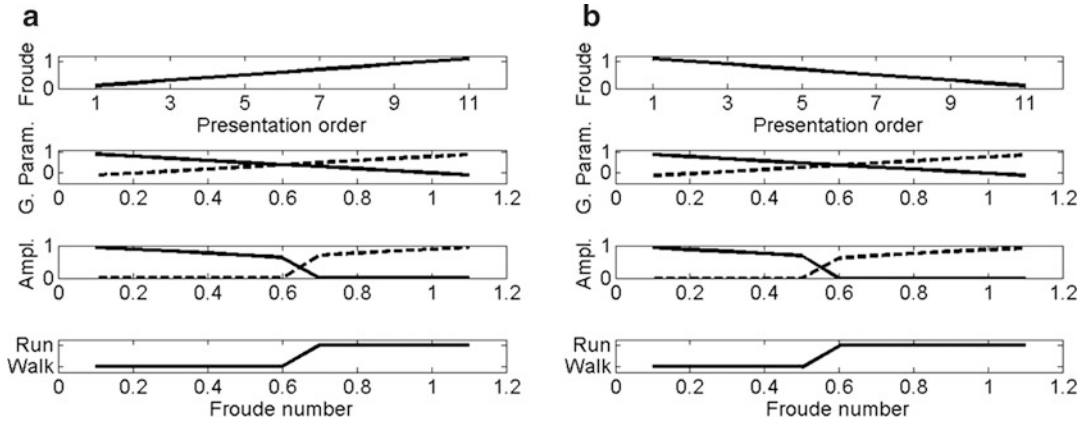

Determinisms of Behavior and Synergetics, Fig. 11 Simulation results for participant 2 of the study by Diedrich and Warren (1995) obtained from the WRT model. See text for details

Froude numbers were increased in 11 steps from 0.l to 1.1. The second top panel shows the growth parameters of the walking pattern (solid line) and the running pattern (dashed line) as functions of the Froude number. The third panel from the top shows the saturation values (or stationary values) of the amplitudes of the walking (solid line) and running (dashed line) patterns. The amplitude of the walking pattern assumed a finite value for Froude numbers from 0.1 to 0.6. In this range, the amplitude of the running pattern vanished for the increasing speed condition. Consequently, in this range of Froude numbers (relative treadmill speed values) the computer-simulated participant behaved like a pattern formation system in which a BAB pattern of walking emerged. The amplitude dynamics exhibits a switch between 0.6 and 0.7. In fact, Diedrich and Warren (1995) report for participant 2 a transition Froude of 0.66. For Froude numbers from 0.7 to 1.1 the amplitude of the running pattern was finite, whereas the amplitude of the walking pattern was equal to zero. The WRT model predicted the emergence of a BAB pattern of running. The bottom panel illustrates the behavioral response as function of the Froude number. For Froude numbers that induced in the increasing speed condition the emergence of a BAB pattern of walking, the computer-simulated participant was walking on the treadmill. When the BAB pattern of running emerged, then the participant was running on the treadmill.

Panel B of Fig. 11 shows the simulation results for decreasing treadmill speed. The top panel shows again the Froude numbers used in the simulation and the order in which they were used in the simulation. The Froude number decreased from presentation to presentation. The second top panel shows the growth parameters of the walking (solid line) and running (dashed line) patterns and is identical with the second top panel on the left. However, again, the horizontal axis should be read from the right to the left. In the case of the simulated treadmill speed de-acceleration, the treadmill speed was initially high and subsequently was reduced step by step. The third panel from the top shows the saturation values of the amplitudes of the walking (solid line) and running (dashed line) patterns. Again the figure should be read from the right to the left. The amplitude of the running pattern assumed a finite value in the range of Froude numbers from 1.1 down to 0.6. At a Froude number of 0.6 a switch happened. The amplitude of the running pattern jumped to zero, whereas the amplitude of the walking pattern increased and assumed a finite saturation value. In particular, for Froude numbers from 0.5 down to 0.1 the amplitude of the walking pattern was finite. The transition between Froude numbers of 0.6 and 0.5 mimics the experimentally observed transition reported in Diedrich and Warren (1995) for participant 2, which happened at 0.55 in the treadmill speed decreasing condition.

The bottom panel of Fig. 11B presents the performance of the simulated participant in the condition of decreasing treadmill speed. Comparing the switching points shown in the bottom panels of Fig. 11A, B, we see that the switches occurred at different values. The WRT model reproduced or predicted the experimentally observed hysteresis phenomenon.

Application 3: Action Chains and Child Play

So far we have discussed a circular causality mechanism leading to hysteresis, see Fig. 9: a performed action sets the initial conditions for the upcoming action. In the context of Fig. 9, we argued that action selection depends not only on the stability of the BAB patterns of a human being under consideration but also on the initial conditions of the pattern formation process taking place "in" that human being. The eventually performed behavior in turn sets the initial conditions for the subsequently performed behavior. Therefore, in the ascending condition of grasping transition experiments under which participants begin trials by grasping small planks with one hand, participants continue to grasp planks with one hand for a larger range of plank sizes as compared to trials of the descending condition. Likewise in the descending condition when participants begin trials by grasping large planks with two hands, participants continue to grasp planks with two hands for a larger range of planks sizes as compared to trials of the ascending condition. The same kind of argument holds for the hysteresis of walk-run transitions.

However, behavior performed at a certain moment in time may not only determine the initial conditions of pattern formation processes related to subsequently performed actions. Rather, it has been hypothesized that behavior can affect the control and growth parameters, as shown in Fig. 12. This working hypothesis (Frank et al. 2015; Frank 2015a) and similar hypotheses that have been made in the literature (Ditzinger and Haken 1989; Haken 1996; Tschacher and Dauwalder 1999) state that in general self-organization processes can act back on the circumstances under which they emerged in the first place. Let us point out the conceptually novel aspect of hypotheses of this kind. The synergetic approach discussed above allows us to understand the emergence of BAB patterns in terms of the dynamics of pattern amplitudes defined by amplitude equations. Importantly, BAB patterns emerge as part of pattern formation processes when externally controlled parameters (e.g., control parameters manipulated by an experimenter) exceed certain critical values. The synergetic approach does not take the possibility into

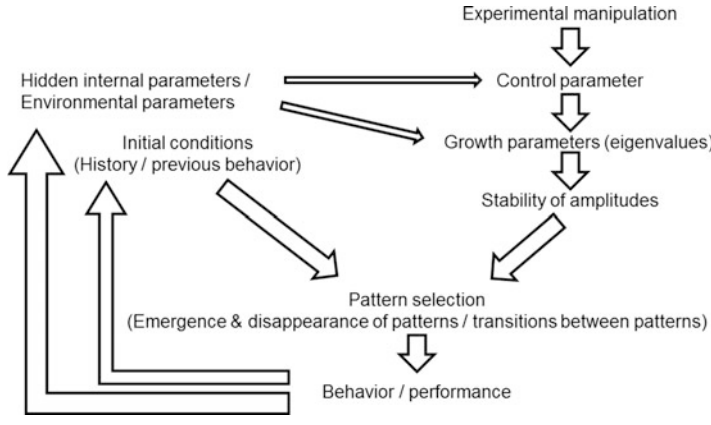

Determinisms of Behavior and Synergetics, Fig. 12 Components of models of human behavior (and perception) as formulated in the framework of extended synergetics and quasi-attractor theory. These models take into account the possibility that parameters are self-regulated by the performed behavior. Accordingly, in Fig. 12 the scheme shown in Fig. 9 is extended by an additional feedback loop

account that the pattern formation processes may affect parameters of the system that then act as control parameters and trigger secondary pattern formation processes. In doing so, action chains or the flow of actions can be explained.

This possibility of a self-regulation (Frank et al. 2015; Frank 2015a) of system parameters by self-organizing processes has been addressed in the context of the quasi-attractor theory by Haken and coworkers in order to explain selective attention (Fuchs and Haken 1988) and to study oscillatory perceptual processes induced by ambivalent figures and ambivalent acoustic stimuli (Ditzinger and Haken 1989; Ditzinger et al. 1997; Frank 2014a; Haken 1996). Recently, this notion has been discussed within the framework of extended synergetics to address negative impacts of attention on object function perception (Frank 2015a) and perceptual processes showing hysteresis of a different kind as discussed above (Frank et al. 2015; Frank 2016b; Kim and Frank 2016; Lopresti-Goodman et al. 2013). Priming (Frank 2009, 2012b), retrieval-induced forgetting (Frank 2012b), and the relapse of bipolar disorder due to medication nonadherence (Frank 2014e) have been studied in this context as well. Moreover, sequences of actions as observed during rituals (Frank 2014b, c) and child play (Frank 2014b, d) have been discussed. Let us review the studies on child play in more detail.

We consider a child who has a number of preferred leisure activities. For sake of simplicity, we restrict ourselves to consider three activities. However, the model can be generalized to account for any number of activities. Following Frank (2014b, d) the three activities are coloring, reading, and TV watching. Each activity is associated with a BAB pattern. The emergence of each pattern is determined by the corresponding pattern amplitude. If one of the three pattern amplitudes is at its finite saturation value, while the other two amplitudes are close to zero, then the BAB pattern exhibiting the finite amplitude has emerged and the child is engaged in the corresponding leisure activity. Importantly, it is assumed that performing a certain activity acts back in an inhibitory way on the pattern formation process that supported the emergence of that activity. We may think of an effect of an activity on external circumstances that are relevant for maintaining the activity. For example, when a child is coloring a picture, after a certain amount of time the picture may be completely colored. The motivation to color a second picture may be lower than the motivation that the child had in the first place. If so, we may interpret this drop in motivation to say that after discrete episodes in time of coloring (where each episode reflects that the child has completed a picture) the tendency becomes weaker and weaker that the pattern formation process leading to coloring is maintained. This is similar to the decay in the tendency to grasp planks with one hand when plank size is increased. In the context of grasping transition, the decay in the tendency to perform one-handed grasping has been modeled by a growth parameter for one-handed grasping that decays with increasing planks size, see Fig. 6 (solid line). Therefore, in the context of child play it has been assumed (Frank 2014b, d) that – roughly speaking – the growth parameter of coloring decays over time. More precisely, it is not time as such that makes the growth parameter to become smaller and smaller. Rather, what matters is the coloring activity of the child. That is, the decay of the growth parameter is a function of the duration of the coloring activity. The same argument can be made for reading and TV watching. Reading a short picture book naturally will make that the child finishes the book in a particular amount of time. Watching a TV show implies that there will be an end of the show. In doing so, reading and TV watching affect external circumstances. We consider here the case where such changes have inhibitory effects on the currently performed activity.

Having argued that the performance of an activity may change external circumstances relevant for the performance of that activity, in general, it has been hypothesized that performed activity can also affect internal parameters such that the performed activity is inhibited (Frank 2014b, d). This hypothesis is motivated by theoretical work on the oscillatory perception of ambivalent figures (Ditzinger and Haken 1989; Frank 2014a; Haken 1996; Shao et al. 2008) that explains the emergence of oscillations as an effect of negative feedback from higher cognitive

levels to lower levels of the visual perceptual system. In this case, only internal parameters of the perceptual self-organizing process are concerned. The external circumstances of the stimulus and its presentation are not altered in any way. In summary, as illustrated in Fig. 12, it is assumed that when a child performs a particular activity, then the activity itself affects external or internal circumstances that in turn result in a reduction of the growth parameter of the performed activity.

In the context of the postulated self-inhibition mechanism, we would like to remind the reader about the stability band for the pattern formation system under consideration (see above and Fig. 7 in particular). When the growth parameter of a given performed activity falls below the lower boundary of the stability band, then – from a dynamical systems perspective – the activity becomes unstable. Applied to the modeling of child play, this implies that the child will stop performing the current activity and will switch to another activity that has a stable fixed point (i.e., exhibits a growth parameter which belongs to the stability band). In our case, there might be two alternative activities available that exhibit stable fixed points. If so, the initial conditions given in terms of the amplitude values at the time point when the current activity becomes unstable determine which of the two alternative BAB patterns will emerge and, consequently, which alternative activity will be performed by the child.

Let us illustrate these issues by means of a computer simulation. The mathematical details can be found in Frank (2014b, d). The simulation parameters are given in Frank (2014d). In what follows, we consider the case A of Frank (2014d) but neglect the modeling of internal and external noise on the dynamics of the growth parameters (i.e., we put the corresponding noise parameter equal to zero). Moreover, unlike the simulation conducted in Frank (2014d), we assume that at the initial time point of the simulation the amplitude of the reading activity assumes the largest value of all three amplitudes.

The result of the simulation (that took the two aforementioned modifications into account) is shown in Fig. 13. Panel A shows the amplitudes as functions of time. Panel B provides the growth parameter dynamics. Panel C indicates which activity is performed over the course of time. All growth parameters were initially at the baseline level, see Panel B. In contrast, as mentioned above, initially the amplitude of the reading activity was larger than the amplitudes of the two other activities.

As a consequence of the initial amplitude bias, the amplitude of the reading activity was the "winner" in the competition process between the three amplitudes (reflecting the competition process between the three corresponding BAB patterns). The amplitude equation model converged to a fixed point given by a finite saturation value for the amplitude of the reading activity and zero saturation values for the amplitudes of the two alternative activities, see Panel A. Subsequently, the growth parameter of the reading activity decayed as a result of the postulated self-inhibitory impact of the reading activity, see Panel B. In contrast, the growth parameters of the two other activities stayed at constant levels. At about 20 time units the growth parameter of the reading activity dropped out of the stability band and the reading activity – roughly speaking – became unstable.

There was a competition process between the coloring and the TV watching activity. This competition processes can be seen in Panel A as the temporary increase of both amplitudes (see top and bottom subpanels) at about 20 time units. Due to the initial conditions at that point of 20 time units the coloring activity was the winner of the competition. The amplitude equation model converged to the fixed point given by a finite saturation value for the amplitude of the coloring activity and zero saturation values for the amplitudes of the two alternative activities, see Panel A. A self-inhibitory feedback process started again – that time with respect to the coloring activity. That is, the growth parameter of the coloring activity decayed (roughly speaking) as a function of time, see Panel B. In contrast, the growth parameter of the reading activity relaxed back to its baseline level, see Panel B again. At about 46 time units the growth parameter of the coloring activity dropped out of the stability band and the coloring activity became unstable.

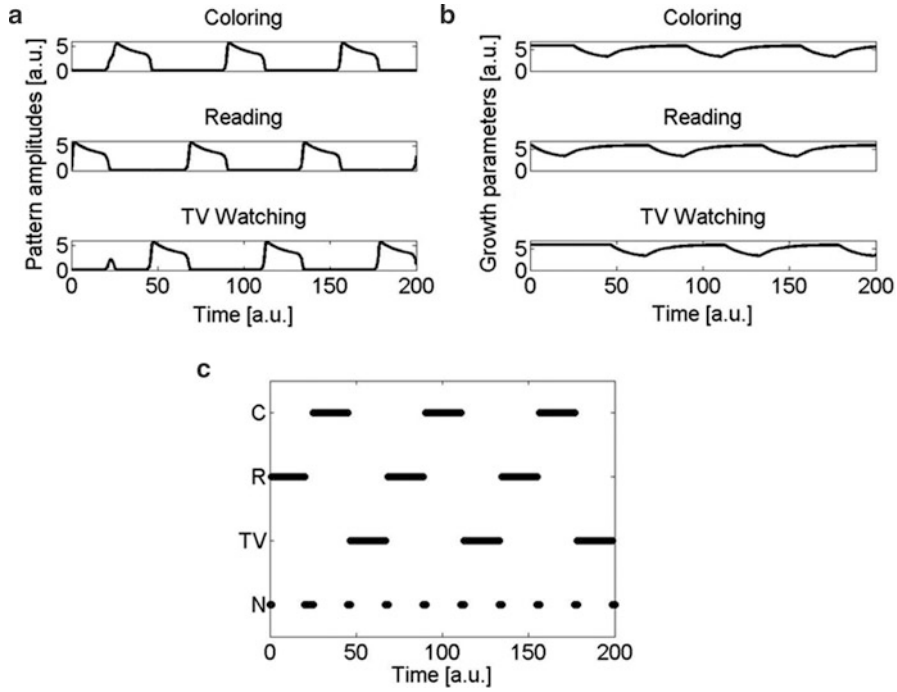

Determinisms of Behavior and Synergetics, Fig. 13 Simulation results of the amplitude equation model for child play. The model does not only describe the evolution of amplitudes (Panel **A**) of behavioral patterns but also describes the evolution of the growth parameters related to the behavioral patterns (Panel **B**). Panel **C** shows the performed activities as functions of time (C: coloring, R: reading, TV: TV watching, N: the child is undecided and in this sense is doing "nothing")

There was a competition between reading and TV watching. As can be seen from Panel B, the growth parameter of the reading activity did not yet reach the same baseline value as the growth parameter of the TV watching activity. As such, initial conditions in addition to the growth parameter values determine which activity wins a competition process. For the simulation shown in Fig. 13 these two factors were such that the TV watching amplitude won the competition process. Once the TV watching activity was established (i.e., the amplitude dynamics converged to a fixed point given by a finite saturation value for the amplitude of the TV watching activity and zero saturation values for the amplitudes of the two alternative activities, see Panel A), the self-inhibitory process for the TV watching activity took place and the growth parameter of the TV watching BAB pattern decayed as a function of time – more precisely as a function of the duration of the performed TV watching activity, see Panel B. The growth parameter of the coloring activity relaxed back to the baseline value. At about 67 time units the growth parameter of the TV watching activity dropped out of the stability band and TV watching – when regarded as a BAB pattern – became unstable.

The pattern formation system switched to the BAB pattern associated with reading and the three-activities cycle that we have just discussed started again.

Panel C is derived from Panel A. An activity was performed when the corresponding amplitude was at a finite saturation value, while the amplitudes of the alternative activity patterns were close to zero. Note that the finite saturation values of the amplitudes changed on a slow time scale due to the fact that the growth parameters decayed on an assumed slow time scale (for more details about that issue see Frank 2014d). According to the model suggested by Frank (2014d), the absolute value of the amplitude is not the primary criterion

that determines whether or not an activity is performed. Rather, the question arises whether or not an amplitude is close to its finite saturation value. During the slowly changing periods shown in Panel A, the amplitudes were close to their respective saturation value. In contrast, at the instability points (i.e., at 20, 46, and 67 time units) the respective amplitudes dropped relatively quickly to zero (see Panel A). During these short periods the amplitudes were not close to their respective finite saturation values. This also implies that there were short periods between two performed activities in which the child was undecided what to do. These periods are indicated with the label "N" for "nothing" in Panel C.

As already pointed out by Frank (2014d), the suggested amplitude equations model for child play eventually settles down in a periodic temporal pattern characterized by a three-activities cycle. In the example shown in Fig. 13, the three-activities cycle is given by the sequence: reading, coloring, TV watching. The observation of this three-activities cycle helps our understanding of the amplitude equations model for child play. However, in the real world a child is likely to perform only a single three-activities cycle. After having performed all three activities, the child will probably not repeat them again. Rather, the child will do something else (e.g., play with a friend or sibling, play with the family cat – if there is one, eat something, etc.). Consequently, only the first cycle might be of interest when modeling real data. In this context, we would like to reiterate that the model can be generalized for an arbitrary number of activities. Accordingly, the first cycle can be composed of as many activities as we would like to consider and can describe the whole day of a school child from getting up in the morning to getting to bed and falling asleep at the end of the day.

General Aspects of the Modeling Framework

We have reviewed a theory of human behavior based on synergetics. We focused on the issue how humans switch between different behaviors. According to the synergetics' perspective, behaviors correspond to brain activity and body (BAB) patterns. Each pattern comes with its own amplitude. Although in this chapter the focus was on behavior, for states of perception a similar assumption has been frequently made: each pattern of perception comes with its own amplitude (Haken 1991). For exceptions to this assumption in the field of vision see, for example, Bressloff et al. (2001). The emergence, the disappearance and the transitions between BAB patterns is determined by amplitude equations that describe the evolution of the pattern amplitudes over time.

First, we considered a human actor for whom it seems from the outside as if he or she would choose in a single event between two possible behaviors. We focused on the symmetric case in which both behaviors and likewise both BAB patterns associated with the behaviors have the same tendency to emerge. Interestingly, as we showed above, it is possible to determine by experimental research the circumstances under which the symmetric case holds. This can be done on an individual basis, that is, for each test person separately. At first sight, the symmetric case seems to open the possibility that behavior is selected due to free will. That is, it seems as if the participant tested under the symmetric case makes a decision towards a behavior based on his or her free will. However, taking a second look, we showed that the initial conditions determine uniquely the behavior that emerges.

In this context, let us return to the shoe-choosing example illustrated in Fig. 1. Let us assume that there is no bias towards the "choice" of one of the two pairs of shoes. That is, we consider the symmetric case from the scientific perspective illustrated in Panel B of Fig. 1. "Choosing" pair A is considered as a BAB pattern. Likewise, "choosing" pair B is considered as an alternative BAB pattern. Both patterns compete with each other for emergence. The dynamics of the self-organization process in which the patterns emerge is described in terms of the competition between the corresponding pattern amplitudes as defined by the GT model, when reinterpreting the components of the GT model in the context of the "shoe-choosing" scenario.

Figure 14 shows simulation results obtained from the GT model applied to the "shoe-choosing" problem. Panels A and B correspond to Panels A and B of Fig. 5 interpreted in the context of the "shoe-choosing" scenario. Panel A shows the case A in which a person is confronted with the problem to "choose" between two pairs of shoes and in which the initial conditions are such that he or she "chooses" pair A. While the top and middle subpanel of Panel A display the amplitudes of the two BAB patterns as functions of time, the bottom subpanel shows the behavior. During a transient period, the person under consideration is "undecided," which is indicated by the behavioral state "N" (where "N" stands again for "nothing"). At a certain point in time, the amplitude of the pattern for "choosing" pair A is sufficiently close to its finite saturation value and consequently the BAB pattern of "choosing": pair A has emerged. The behavior switches from "being undecided" to "choosing" pair A, see bottom subpanel. Panel B of Fig. 14 illustrates the same issues for the case B in which the participant is again confronted with the question about wearing shoes A or B. In contrast to case A, in case B the initial conditions are such that the person under consideration "chooses" the pair B of shoes. Note that panels A and B present the result of a mechanistic model for the two if-then relationships sketched in Fig. 1 of the science-based determinism perspective.

Panel C of Fig. 14 shows the flow field of the dynamics in the space of the two amplitudes related to the two BAB patterns. In order to draw Fig. 14, the amplitude equation model (i.e., the GT model) was simulated for different initial conditions and the amplitudes of "choosing" pair A and "choosing" pair B were plotted against each other for all simulated time points. Time is

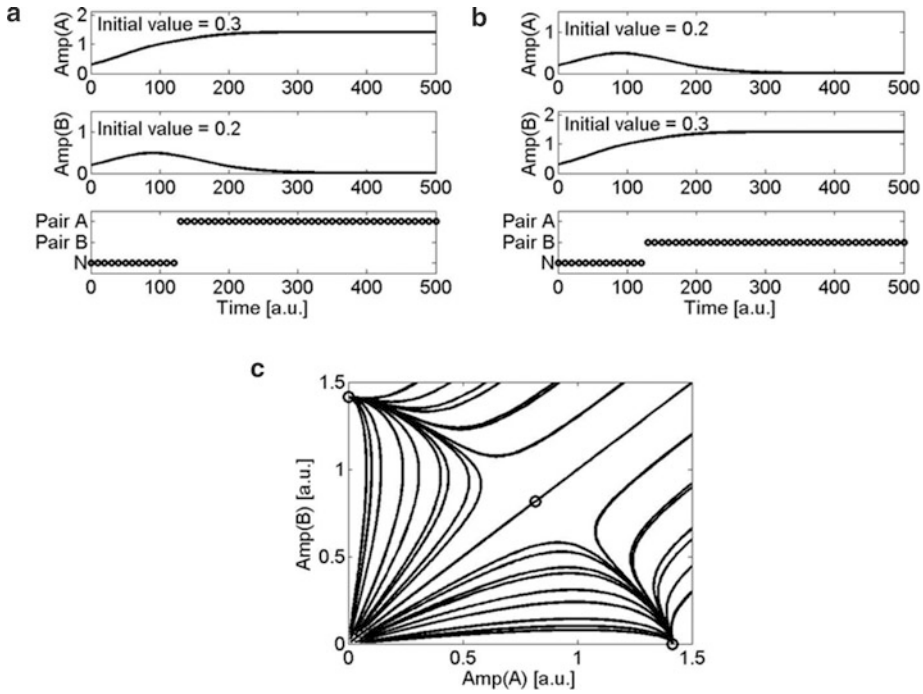

Determinisms of Behavior and Synergetics, Fig. 14 Simulation of the scientific perspective of the shoe-choosing problem sketched in Fig. 1B obtained by an appropriate reinterpretation of the GT model. The symmetric condition is considered. Panel **A** shows the case in which the amplitude of choosing pair A dominates. Panel **B** shows the corresponding situation for pair B. In Panels **A** and **B** the top and middle subpanels show the evolution of the amplitudes of the BAB patterns associated with choosing pair A (top) or pair B (middle). The bottom subpanels show the decision or performed behavior. Panel **C** illustrates the flow field obtained from the GT model. Circles indicated end points (i.e., fixed points) of the model dynamics. Parameters as in Fig. 5

not shown explicitly in Panel C. Rather, the reader has to follow one of the graphs from an arbitrary point to one of the three end points marked by the circles. In order to see how the amplitudes evolve in time, we would need to follow a graph and vary the speed. At some points the dynamics would be fast, at other points it would be slow. The speed information is not given in the plot shown in Fig. 14C and is irrelevant for the purposes of such a plot. Rather, the point that one wants to make is that we can image that for any initial point in the space spanned by the two amplitudes there is a graph that will go in a unique way to one of the three end points. When the dynamics reaches the end point with the finite BAB amplitude for "choosing" pair A (at a value of about 1.4 on the horizontal axis) and a zero BAB amplitude of "choosing" pair B, then the BAB pattern associated with the choice of pair A or the action of putting on pair A has emerged and the person under consideration chooses or puts on pair A. Likewise, when the dynamics has converged to the end point with a finite amplitude for "choosing" pair B (at a value of about 1.4 again on the vertical axis) and a zero amplitude for "choosing" pair A, then the BAB pattern for "choosing" B has emerged and the person puts on the pair B. These two end points correspond to the fixed points of the amplitude equations model to which solutions can converge over time in the symmetric case. The third end point on the diagonal can only be reached for unlikely initial conditions. These are initial conditions for which both amplitudes initially exhibit exactly the same value. These initial conditions are considered as unlikely because they rarely happen. Importantly, if the two amplitudes deviate from each other only slightly at a given (initial) point in time, then the amplitudes will not converge to the end point on the diagonal. Rather, they will end up at an end point located on one of the two axes. Most importantly, the flow field shown in Fig. 14 illustrates that there are no choice points. For this reason – from the perspective of science-based determinism – the verb "choosing" represents a misleading concept and has been put between quotation marks in this paragraph. There are only if-then relationships. In fact, there are infinitely many if-then relationships. We can prepare the two amplitudes values such that they fall onto an arbitrary point in the plane of Panel C, then from that initial point there is a unique graph that goes to one of the two fixed points located on the two axes. The diagonal separates the two regions of attraction (which are also called basins of attraction). All of these infinitely many if-then relationships are described by the amplitude equations of the GT model (whose mathematical details may be found in Frank et al. 2009 or Lopresti-Goodman et al. 2011) here applied to the "shoe-choosing" problem.

We have argued that the symmetric case can be used as a departure point to consider various asymmetric cases. For example, small objects are typically grasped with one hand, while large objects are typically grasped with two hands. At low speeds humans tend to walk; at high speeds we tend to run. We can account for asymmetries that capture a preference towards a behavior by introducing growth parameters for BAB patterns (or pattern amplitudes) that differ in magnitude. In particular, when one growth parameter dominates all other growth parameters such that they fall out of the stability band, then only the behavior corresponding to the dominant growth parameter can be performed. Let us return in this context to the "shoe-choosing" example. Let us assume there is a pair of black shoes and a pair of white shoes available. Let us consider a person born and grown up in a western country and culture. The person has to decide which shoes he or she should put on for attending a funeral, on the one hand, and a summer garden party, on the other hand. Panel A of Fig. 15 illustrates this scenario from a nonscientific perspective involving the notion of free will. The person may take a short while to think about pros and cons to put on black or white shoes for a funeral or a summer garden party. Eventually, he or she will then decide to wear the black shoes for a funeral and the white shoes for a summer garden party. This decision may reflect his or her free will. Panel B of Fig. 15 describes the situation within the framework of science-based determinism using the amplitude equations of synergetics (here: the GT model). The questions are considered as two separate questions that are related to two different

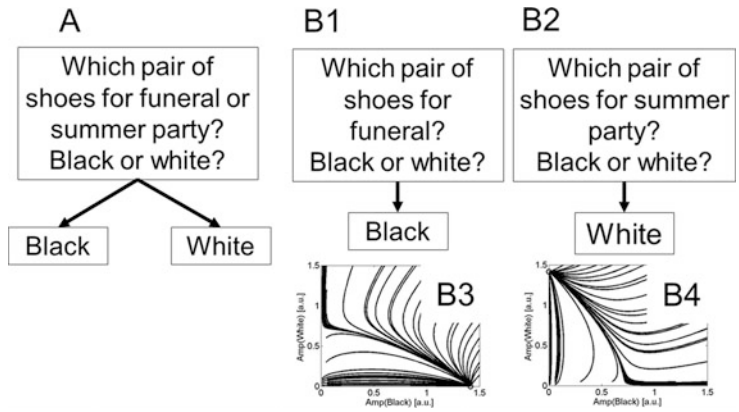

Determinisms of Behavior and Synergetics, Fig. 15 Illustration of a nonscientific perspective involving free will (Panel **A**) and the scientific perspective (Panels **B1**, **B2**, **B3**, **B4**) of the problem what kind of shoes to choose for a funeral and a summer garden party. Panels **B3** and **B4** show the flow fields obtained from the GT model applied to the shoe-choosing problem in the case of asymmetric growth parameters. Circles indicate end points. Parameters for **B3**: growth parameter for choosing black equals 2 units; growth parameter for choosing white equals 0.5 units; coupling parameter equal to 2. Consequently, the growth parameter for choosing white is out of the stability band and for any initial condition the dynamics converges to the end point related to the decision to choose the black shoes. Parameters for **B4**: growth parameter for choosing black equals 0.5 units; growth parameter for choosing white equals 2 units; coupling parameter equal to 2. Consequently, the growth parameter for choosing black is out of the stability band, which, in turn, implies that irrespective of the initial conditions the dynamics converges to the end point associated with the decision to choose the white shoes

situations labeled B1 and B2. When asking the question about the funeral (B1) the growth parameter of the amplitude that describes the selection of the black shoes dominates the alternative growth parameter. Accordingly, the flow field of the model exhibit only one end point (i.e., fixed point) in the plane spanned by the two amplitudes, see panel B3. Irrespective of the initial conditions, the amplitude dynamics converges to this unique fixed point. For this unique fixed point the amplitude of the BAB pattern related to the selection of the black shoes is finite (and assumes a value of about 1.4 units on the horizontal axis), whereas the alternative amplitude equals zero. Consequently, the person under consideration "chooses" the black shoes for a funeral. Likewise, the question what shoes to take for the summer garden party (B2) creates a situation that is characterized by a dominant growth parameter of the BAB pattern for putting on the white shoes. Consequently, the flow field of the amplitude equations model looks as shown in Panel B4. All graphs converge to a unique end point (located at about 1.4 units on the vertical axis) with a finite amplitude for the BAB pattern reflecting the decision to put on the white shoes.

Importantly, taking Skinner's point of view, it is plausible to assume that the growth parameters in these two situations assume large values because of the way the person grew up in the western culture. That is, we assume that initially (at a time point in the maturation of the person where it makes sense to talk about dressing for a funeral or a summer garden party) the growth parameters for putting on black and white shoes assumed the same value. Due to the various interactions of the person with the environment (here: parents, siblings, friends, media, etc.) the growth parameters became context-dependent such that for the adult person in the context of funerals the black-shoes growth parameter became large, whereas in the context of summer garden parties the white-shoes growth parameter became large.

We may compare the situation with the experiment by Skinner and coworkers in which pigeons were trained to distinguish between two signs on which different words were written. For the first sign, the pigeons were trained to turn around

themselves. For the second sign, the pigeons were trained to peck somewhere (the specific location did not matter). Although the words as such did not matter (what matters was just the fact that they were different), Skinner and coworkers used the phrases "turn" and "peck" in their experiment. This "peck and turn" experiment can be explained in complete analogy to the aforementioned "shoe-choosing" problem. The two behaviors in the Skinner experiment are turning around and pecking. The two contexts are the two different signs. For the "turn" sign the pigeons (when regarded as pattern formation systems) exhibited a growth parameter of the turning around BAB pattern that dominated all other growth parameters and, consequently, the turning around BAB pattern emerged and the pigeons turned around. For the "peck" sign the growth parameter of the pecking BAB pattern dominated all other growth parameters and, consequently, the pecking BAB pattern emerged and the pigeons were pecking against something. Our suggestion that the "peck and turn" experiment can be explained just like the hypothetical funeral and summer-garden-party "shoe-choosing" problem supports the suggestion that growth parameters of BAB patterns in human and animals vary due to learning and various forms of interactions with the environment. Since these interactions often involve behavior (e.g., in Skinner's experiments the animals had to do something), we are back again at Fig. 12 that suggest that there is a feedback loop from behavior to internal hidden parameters.

Conclusions

Having discussed single events in which a person (or animal) performs a behavior out of a repertoire of possible behaviors, we discussed sequences of likewise actions. We discussed experiments in which participants were asked to grasp objects repeatedly for slightly different sizes and in which participants were asked to move on a treadmill and in doing so moved their legs in a repetitive fashion while the treadmill speed was varied. In this context, we explained the phenomenon of hysteresis using the amplitude equation model. A key issue for understanding hysteresis is that in the symmetric case and in asymmetric cases that only exhibit a small degree of asymmetry we have two fixed points (end points) to which the amplitude dynamics can converge. That is, the flow field qualitatively looks as shown in Panel C of Fig. 14. Which fixed point and, consequently, which behavior is selected depends again on the initial conditions. For these sequences of actions, however, performing an action sets the initial conditions for the subsequent action. Therefore, in the context of sequences of behaviors it becomes obvious that human behavior can be understood as a chain of cause-and-effect relationships or if-then relationships, where the "then" part of an action determines the "if" part for the subsequent action.

Finally, we generalized our considerations for sequences of different types of actions. As an illustrative example we considered child play. From a theoretical point of view, the novel aspect was to consider the possibility that actions do not only determine initial conditions for subsequent action but may affect neurophysiological parameter that are captured in the amplitude equations model in terms of growth parameters, see Fig. 12. Recall that in the context of the funeral versus summer-garden-party example we assumed that the growth parameters become context-dependent on a relatively slow time scale of social learning and exposure to cultural norms and conventions. In contrast, we entertained in the context of the child play example the idea that on relatively short time scales the growth parameter of a behavior is down-regulated.

The flow of action, in principle, can be understood in terms of flow fields similar to those shown in Panel C of Fig. 14 and in Panels B3 and B4 of Fig. 15. However, the space of interest is not limited to the amplitudes. In order to adequately describe the flow field, we need to consider a higher dimensional space spanned by amplitudes and growth parameters. For example, if we consider three leisure activities of a child (as we did above), then we need a six dimensional space to capture the graphs that illustrate the child behavior. For example, the graphs in the three subpanels in Fig. 13A in combination with the

graphs in the three subpanels in Fig. 13B constitute a single graph in a six-dimensional space. Let us imagine we generate by computer simulations a variety of such graphs for different initial conditions and plot them all together in the six-dimensional space, then we would obtain the flow field of the child play model.

Due to this extension of the amplitude space, the theoretical framework that takes the growth parameter dynamics into account has been referred to as extended synergetics (Frank 2014c, d; Kim and Frank 2016). Likewise, when we imagine how the flow fields would look like in these higher dimensional spaces, we can see that in the subspace that is only spanned by the amplitudes we have pseudo end points like the end points shown in Panel C of Fig. 14 and Panels B3 and B4 of Fig. 15. The end points – which are also called fixed point or in more general terms attractors – are actually slowly drifting in time due to their dependency on the slowly evolving growth parameter dynamics (see Panel A of Fig. 13). Therefore, they have been referred to as quasi-attractors and the theoretical framework taking the growth parameter dynamics into account has also been referred to as quasi-attractor theory (Haken 1996). Extended synergetics and quasi-attractor theory include the original theoretical framework of synergetics as a special case. Therefore, extended synergetics and quasi-attractor theory provide a comprehensive tool to formulate laws of behavior that describe sequences of likewise behaviors and sequences of different behaviors from a scientific perspective and within the framework of science-based determinism.

Future Directions

Grasping, walking, and child play are only a few applications of a variety of possible applications of the theoretical framework outlined above. While the author is writing this chapter, the general public has become aware of seemingly unjustified violent actions of US police officers towards unarmed suspects. To perform violent and even fatal actions as a police officer against a suspect is an issue that should be addressed from the scientific perspective introduced above. In fact, research on violence using quantitative modeling and laboratory studies has been conducted in the past. As far as the amplitude equations approach is concerned, only a preliminary study has been conducted to understand the decision making process of law enforcement offices to use violence with likely fatal consequences (Frank 2016d). More detailed work in this regard is needed. In particular, in view of the fact that parameters of amplitude equations models can be estimated for individuals (see above), the top-down amplitude equations modeling approach seems to be a promising tool to characterize individuals. For example, the question arises whether or not model parameters are correlated to the degree to which police officers hold prejudices against certain ethnic groups. Moreover, while the simulations demonstrated above for grasping and walking transitions primarily are used to reproduce observed behavior and only in this sense predictions have been made, when applying modeling on an individual level simulations may be used to predict the probability of individuals to perform violent unjustified actions in the future. Such simulations of future behaviors could serve as a basis for interventions that aim to prevent unjustified violence from happening.

Bibliography

Alexander RM (1992) Exploring biomechanics: animals in motion. W.H. Freeman, New York

Barbay S, Giacomelli G, Marin F (2000) Stochastic resonance in vertical cavity surface emitting lasers. Phys Rev E 61:157–166

Beek PJ, Schmidt R, Morris A et al (1995) Linear and nonlinear stiffness and friction in biological rhythmic movements. Biol Cybern 73:499–507

Bestehorn M, Haken H (1991) Associate memory of a dynamical system: an example of the convection instability. Z Phys B 82:305–308

Bestehorn M, Friedrich R, Haken H (1989) Two dimensional traveling wave patterns in nonequilibirum systems. Z Phys B 75:265–274

Bressloff PC, Cowan JD, Golubitsky M et al (2001) Geometric visual hallucinations, Euclidean symmetry and

the functional architecture of striate cortex. Philos Trans R Soc Lond B 356:299–330
Bressloff PC, Cowan JD, Golubitsky M et al (2002) What geometric visual hallucinations tell us about the visual cortex. Neural Comput 14:473–491
Cesari P, Newell KM (1999) Body-scaled transitions in human grip configuration. J Exp Psychol Hum Percept Perform 26:1657–1668
Cesari P, Newell KM (2000) Body scaling of grip configurations in children aged 6–12 years. Dev Psychobiol 36:301–310
Chisholm R (1964) Human freedom and the self. The Lindley Lectures, Department of Philosophy, University of Kansas. Reprinted in Watson 2003
Cross MC, Hohenberg PC (1993) Pattern formation outside of equilibrium. Rev Mod Phys 65:851–1112
Daffertshofer A, Haken H (1994) A new approach to recognition of deformed patterns. Pattern Recogn 27:1697–1705
Diedrich FJ, Warren WH (1995) Why change gaits? Dynamics of the walk-run transition. J Exp Psychol Hum Percept Perform 21:183–202
Diedrich FJ, Warren WH (1998) The dynamics of gait transitions: effect of grade and load. J Mot Behav 30:60–78
Ditzinger T, Haken H (1989) Oscillations in the perception of ambiguous patterns: a model based on synergetics. Biol Cybern 61:279–287
Ditzinger T, Tuller B, Haken H et al (1997) A synergetic model for the verbal transformation effect. Biol Cybern 77:31–40
Dotov GD, Frank TD (2011) From the W-method to the canonical-dissipative method for studying uni-manual rhythmic behavior. Mot Control 15:550–567
Dotov GD, Kim S, Frank TD (2015) Non-equilibrium thermodynamic description of rhythmic motion patterns of active systems: a canonical-dissipative approach. Biosystems 128:26–36
Dufiet V, Boissonade J (1996) Dynamics of Turing pattern monolayers close to onset. Phys Rev E 53:4883–4892
Dutt AK (2010) Turing pattern amplitude equations for a model glycolytic reaction-diffusion system. J Math Chem 48:841–855
Frank TD (2002) On a mean field Haken-Kelso-Bunz model and a free energy approach to relaxation processes. Nonlinear Phenom Complex Syst 5:332–341
Frank TD (2005) Nonlinear Fokker-Planck equations: fundamentals and applications. Springer, Berlin
Frank TD (2009) On a multistable competitive network model in the case of an inhomogeneous growth rate spectrum: with an application to priming. Phys Lett A 373:4127–4133
Frank TD (2011) New perspectives on pattern recognition algorithm based on Haken's synergetic computer network. In: Fournier MD (ed) Perspectives on pattern recognition. Nova Publishers, New York, pp 153–172
Frank TD (2012a) Multistable pattern-formation systems: candidates for physical intelligence? Ecol Psychol 24:220–240
Frank TD (2012b) Psycho-thermodynamics of priming, recognition latencies, retrieval-induced forgetting, priming-induced recognition failures and psychopathological perception. In: Hsu N, Schutt Z (eds) Psychology of priming. Nova Publishers, New York, pp 175–204
Frank TD (2014a) Multistable perception in schizophrenia: a model-based analysis via course-grained order parameter dynamics and a comment on the 4th law. Univers J Psychol 2:231–240
Frank TD (2014b) Secondary bifurcations in a Lotka-Volterra model for N competitors with applications to action selection and compulsive behaviors. Int J Bifurcat Chaos 24:article 1450156
Frank TD (2014c) Action flow in obsessive-compulsive disorder rituals: a model based on extended synergetics and a comment on the 4th law. J Adv Phys 5:845–853
Frank TD (2014d) A nonlinear physics model based on extended synergetics for the flow of infant actions during infant-mother face-to-face communication. Int J Sci World 2:62–74
Frank TD (2014e) From systems biology to systems theory of bipolar disorder. In: Marinda F (ed) Systems theory perspective, applications and development. Nova Publishers, New York, pp 17–36
Frank TD (2015a) On the interplay between order parameter and system parameter dynamics in human perceptual-cognitive-behavioral systems. Nonlinear Dynamics Psychol Life Sci 19:111–146
Frank TD (2015b) Domains of attraction of walking and running attractors are context-dependent: illustration for locomotion on tilted floors. Int J Sci World 3:81–90
Frank TD (2016a) Formal derivation of Lotka-Volterra-Haken amplitude equations of task-related brain activity in multiple, consecutively performed tasks. Int J Bifurcat Chaos 26:article 1650164
Frank TD (2016b) Perception adapts via top-down regulation to task repetition. A Lotka-Volterra-Haken modeling analysis of experimental data. J Integr Neurosci 15:67–79
Frank TD (2016c) A synergetic gait transition model for hysteretic gait transitions from walking to running. J Biol Syst 24:51–61
Frank TD (2016d) A self-organization perspective of non-cooperative subject behavior leading to fatal shooting by law enforcement officers. In: Proceedings of the fifth international conference on advances in economics, social science and human behavior study, Bangkok, September 2016. Institute of Research Engineers and Doctors, New York, p 16
Frank TD (submitted). Visual and acoustic perception under schizophrenia: a theoretical account based on synergetics, a theory of self-organization. Submitted to Medical Hypotheses
Frank TD, Richardson MJ (2010) On a test statistics for the Kuramoto order parameter of synchronization: an illustration for group synchronization during rocking chairs. Phys D 239:2084–2092
Frank TD, Daffertshofer A, Peper CE et al (2000) Towards a comprehensive theory of brain activity: coupled oscillator systems under external forces. Phys D 144:62–86
Frank TD, Richardson MJ, Lopresti-Goodman SM et al (2009) Order parameter dynamics of body-scaled

hysteresis and mode transitions in grasping behavior. J Biol Phys 35:127–147
Frank TD, van der Kamp J, Savelsbergh GJP (2010) On a multistable dynamic model of behavioral and perceptual infant development. Dev Psychobiol 52:352–371
Frank TD, Profeta VLS, Harrison HS (2015) Interplay between order-parameter and system parameter dynamics: considerations on perceptual-cognitive-behavioral mode-mode transitions exhibiting positive and negative hysteresis and on response times. J Biol Phys 41:257–292
Frischholz RW, Boebel FG, Spinnler KP (1994) Face recognition with the synergetic computer. In: Proceedings of the first international conference on applied synergetic and synergetic engineering. Fraunhofer Institute IIS, Erlangen, pp 100–106
Fuchs A, Haken H (1988) Pattern recognition and associative memory as dynamical processes in a synergetic system. I. Translational invariance, selective attention, and decomposition of scene. Biol Cybern 60:17–22
Haken H (1991) Synergetic computers and cognition. Springer, Berlin
Haken H (1996) Principles of brain functioning. Springer, Berlin
Haken H (2004) Synergetics: introduction and advances topics. Springer, Berlin
Hreljac A (1995) Effects of physical characteristics on the gait transition speed during human locomotion. Hum Mov Sci 14:205–216
Hreljac A, Imamura R, Escamilla RF et al (2007) Effect of changing protocol, grade, and direction on the preferred gait transition speed during human locomotion. Gait Posture 25:419–424
Hutt A, Riedel H (2003) Analysis and modeling of quasi-stationary multivariate time series and their application to middle latency auditory evoked potentials. Phys D 177:203–232
Jirsa VK, Friedrich R, Haken H (1995) Reconstruction of the spatio-temporal dynamics of a human magnetoencephalogram. Phys D 89:100–122
Kay BA, Kelso JAS, Saltzman EI et al (1987) Space-time behavior of single and bimanual rhythmic movements: data and limit cycle model. J Exp Psychol Hum Percept Perform 13:178–192
Kelso JAS (1995) Dynamic patterns. MIT Press, Cambridge
Kim S, Frank TD (2016) Body-scaled perception is subjected to adaptation when repetitively judging opportunities for grasping. Exp Brain Res 234:2731–2743
Kim S, Frank TD (in press). Correlations between hysteretic categorical and continuous judgements of perceptual stimuli supporting a unified dynamical systems approach to perception. Perception
Kim S, Gordon JM, Frank TD (2015) Nonequilibrium thermodynamic state variables of human self-paced rhythmic motions: canonical-dissipative approach, augmented Langevin equation, and entropy maximization. Open Syst Inf Dyn 22:article 1550007
Kleinschmidt A, Buchel C, Hutton C et al (2002) The neural structures expressing perceptual hysteresis in visual letter recognition. Neuron 34:659–666
Li L (2000) Stability landscapes of walking and running near gait transition speed. J Appl Biomech 16:428–435
Lopresti-Goodman SM, Richardson MJ, Baron MJ et al (2009) Task constraints on affordance boundaries. Mot Control 13:69–83
Lopresti-Goodman SM, Turvey MT, Frank TD (2011) Behavioral dynamics of the affordance graspable. Atten Percept Psychophys 73:1948–1965
Lopresti-Goodman SM, Turvey MT, Frank TD (2013) Negative hysteresis in the behavioral dynamics of the affordance graspable. Atten Percept Psychophys 75:1075–1091
Nagler B, Peeters M, Albert J et al (2003) Polarization-mode hopping in single-mode vertical-cavity surface-emitting lasers: theory and experiment. Phys Rev A 68: article 013813
Newell AC, Whitehead JA (1969) Finite bandwidth, finite amplitude convection. J Fluid Mech 38:279–303
Newell KM, Scully DM, Tenenbaum F et al (1989) Body-scale and the development of prehension. Dev Psychobiol 64:469–475
Newell KM, McDonald PV, Baillargeon R (1993) Body-scale and infant grip configurations. Dev Psychobiol 26:195–205
Pena B, Perez-Garcia C (2000) Selection and competition of Turing patterns. Europhys Lett 51:300–306
Rattanakul C, Lenbury Y, Wollkind DJ et al (2009) Weakly nonlinear analysis of a signal transduction pathway. Nonlinear Anal 71:e1620–e1625
Richardson MJ, Marsh KL, Baron RM (2007) Judging and actualizing interpersonal and intrapersonal affordances. J Exp Psychol Hum Percept Perform 33:845–859
Schmidt RC, Carello C, Turvey MT (1990) Phase transitions and critical fluctuations in the visual coordination of rhythmic movements between people. J Exp Psychol Hum Percept Perform 16:227–247
Segal LA (1962) The nonlinear interaction of two disturbances in thermal convection problem. J Fluid Mech 14:97–114
Segal LA (1965) The nonlinear interaction of a finite number of disturbances to a layer of fluid heated from below. J Fluid Mech 21:359–384
Shao J, Gao J, Zhang X et al (2008) Research on synergetic perception of ambiguous and multivocal model. In: Guo M, Zhao L, Wang L (eds) Proceedings of the fourth international conference on natural computation. IEEE Computer Society, Washington, DC, pp 198–202
Shimizu H, Yamaguchi Y (1987) Synergetic computer and holonics. Information dynamics of a semantic computer. Phys Scr 36:970–985
Skinner BF (1953) Science and human behavior. The Free Press, New York
Stephenson LE, Wollkind DJ (1995) Weakly nonlinear analysis of one-dimensional Turing pattern formation in activator-inhibitor/immobilizer model system. J Math Biol 33:771–815
Tschacher W, Dauwalder JP (1999) Situated cognition, ecological perception, and synergetics: a novel perspective for cognitive psychology? In: Tschacher W, Dauwalder JP (eds) Dynamics, synergetics, autonomous agents. World Scientific, Singapore, pp 83–104

van der Kamp J, Savelsbergh GJP, Davis WE (1998). Body-scaled ratio as a control parameter for prehension in 5- to 9-year old children. Development Psychobiology 33: 351–361

Wang W, Lin Y, Wang H et al (2011) Pattern selection in an epidemic model with self and cross diffusion. J Biol Syst 19:19–31

Warren WH (1984) Perceiving affordances: visual guidance of stair climbing. J Exp Psychol Hum Percept Perform 10:683–703

Watson G (ed) (2003) Free will. Oxford University Press, Oxford

Wollkind DJ, Stephenson LE (2000) Chemical Turing pattern formation analysis: comparison of theory with experiment. SIAM J Appl Math 61:387–431

Yudashkin AA (1996) Bifurcations of steady-state solutions in the synergetic neural network and control of pattern recognition. Autom Remote Control 57:1647–1653

Intentionality: Steps Towards Naturalization on the Basis of Complex Dynamical Systems

Wolfgang Tschacher
University Hospital of Psychiatry and Psychotherapy, University of Bern, Bern, Switzerland
Freiburg Institute for Advanced Studies (FRIAS), University of Freiburg, Freiburg, Germany

Article Outline

Glossary
Definition of the Subject
Introduction
Intentionality and Representation
Synergetics
Discussion: A Structural Science Concept of Intentionality
Future Directions
Bibliography

Glossary

Cognition A general concept of psychology referring to all processes and structures of the mind. These comprise the processing of stimulus "input" (i.e., perception) and the internal processing of represented information (e.g., memory functions, thinking, problem solving); the latter processes presuppose intentional features of the mind. Cognitive structures are knowledge, categories, memory, attitudes, schemata, etc., again intentional concepts.

Dynamical systems theory A system is any set of things (components, elements) that stand in relation to one another. If a rule or description exists that defines how the system changes over time (such as a differential equation or a mapping algorithm), the system is a dynamical system.

Intentionality A characterizing property of the mind. In contrast to physical systems, mental states have content, i.e., they "are about something" in the sense that they contain a reference to an object, or the representation of an object. In addition to such aboutness, intentionality demands a *functional* reference to the intentional object.

Mind-body problem The philosophical question if and how mind and brain/body are linked. Analogously, the question whether mental processes and physical processes are ontologically different or not.

Naturalization Explaining mental phenomena using concepts and models derived from the natural sciences. Naturalization efforts may be viewed as tools by which (computer) simulation models of mental processes can be developed.

Structural science Several sciences do not fit into the two established groups of scientific disciplines, the natural sciences and the humanities. Such structural sciences, e.g., mathematics, dynamical systems theory, cybernetics, or synergetics, are abstract in the sense that they are not restricted by ontology, and thus may be applied to material and nonmaterial issues.

Definition of the Subject

In the philosophical and psychological tradition, intentionality is viewed as a characterizing property of mental (cognitive) acts. Mental acts have content, i.e., they "are about something." This something is called the intentional object. Intentionality may take the form of a desired state (as in, "I wish it were Friday") or a goal (e.g., my plan for a weekend trip to the mountains). When viewing the constituents of the mind (the cognitive system) in this intentionalist manner, we stand in stark contrast to scientific descriptions of physical systems. These latter systems are material things, which are sufficiently described without reference to objects they would "be about," or to states they

A. Hutt, H. Haken (eds.), *Synergetics*,
https://doi.org/10.1007/978-1-0716-0421-2_290

Originally published in
R. A. Meyers (ed.), *Encyclopedia of Complexity and Systems Science*, © Springer Science+Business Media LLC 2018
https://doi.org/10.1007/978-3-642-27737-5_290-4

might desire to realize. Therefore, are mental and physical systems qualitatively different with respect to intentionality? If yes, we are confronted with a dualist or dual-aspect view of the mind-body problem. If no, a solution is demanded that can elucidate how mental phenomena may be explained avoiding intentional language or, conversely, how physical systems may show or mimic the features of intentionality. The former project is the conceptualization of intentionality, the latter project may be named the naturalization of intentionality.

Clarifying the problem of intentionality is important in several respects. First, psychology and other cognitive sciences are conceptually divided into two approaches: the phenomenological (first-person) approach and the behavioral and/or biological (third-person) approach. The frequent conflation of first-person and third-person concepts is a serious impediment to theorizing in psychology and cognitive neuroscience. Second, modern societies have a growing demand for machines and software that can function in "intelligent" ways. Therefore, engineers of artificial knowledge-based systems need to know how intentionality may be implemented in physical information-processing machines. Third, the problem of intentionality is one of the foundational problems of philosophy of mind and of consciousness research. Any, even if partial, solution to this problem that may be derived is therefore welcomed.

The phenomenology of intentional acts is well known; phenomenology yields the features of intentionality, which can indicate how closely a formal-mathematical or physical model of intentionality approximates an understanding of the problem. These features are

- *Aboutness*, the intentional system's state must be about something in the system's environment (even about something fictitious)
- *Functionality*, intentional states should be functional or instrumental with respect to what they are about
- *Mental-likeness*, in the sense that apart from being intentional these model systems should have properties that resemble the properties of mental states. Especially, an interpreter (homunculus) who may account for missing links in the explanation of intentional mental states must not be allowed.

Introduction

If mind and matter are qualitatively different things, what is the nature of their difference? This is an elementary question of philosophy and of scientific disciplines addressing the mind. This question and the potential answers to it, referred to as the mind-body problem, have a long history. What is the relationship between mind and body? If there is no essential difference between the two, or only a superficial difference, one may reach a monistic understanding of the problem. Monism may be idealistic, positing that mind creates its world. The contrary monism would be materialism i.e., the assumption that the mind can be reduced to matter (e.g., Churchland 1986). If, on the other hand, a real difference between mind and body exists, we enter dualistic notions (e.g., Popper and Eccles 1977). Dualism is confronted with intricate questions of how we may conceive of the interaction between mind and body. In the interest of the specific discussion of intentionality in this entry, we will refrain from giving an account of the many philosophical theories of how mind and body may be associated in general.

Apart from presenting a core problem to the philosophy of mind, the mind-body problem is of interest to a wide range of contemporary scientific disciplines, especially psychology, neuroscience, and computer science (artificial intelligence). In recent decades, a novel approach to cognitive science has appeared combining dynamical systems theory with cognitive science. This "dynamical approach to cognition" addresses mind-body topics more or less explicitly. We will sketch this approach here because it provides the background for our ensuing structural treatment of intentionality.

The dynamical approach to cognition is founded on a number of studies and empirical paradigms. In various perceptual and behavioral

tasks, researchers have observed a set of signatures of cognitive and motor systems. These signatures were typically related to temporal patterns observed in the systems, especially asymptotic stability, and in many paradigmatic cases, multistability. Asymptotic stability means that a system's pattern of behavior is stable – in the face of an external disturbance, the system returns asymptotically to this same pattern. Multistability means that several such patterns may coexist in the behavioral space of a single system.

Movement coordination has been at the center of several applications. Haken et al. (1985) provided a model of the coordination of two limbs (e.g., the hands, or the forefingers, of a person) using equations from dynamical systems theory. The rhythmic movement of the limbs generally becomes synchronized after a short time; these synchronous movement patterns are stable with respect to external inputs, i.e., they usually return to synchrony after externally induced disruptions of movement. Furthermore, they have been shown to undergo phase transitions depending on the values of the control parameter (in the Haken-Kelso-Bunz system, a control parameter is the velocity of movements prescribed by a metronome). Characteristic phenomena were observed in the context of phase transitions, such as hysteresis and critical fluctuations. Analogous findings were reported in animal locomotion. Here, especially multistability has attracted the attention of researchers because in certain regions of control parameter space two qualitatively different limb coordination patterns may occur. For instance, a horse may either gallop or trot at a given velocity.

In the seemingly unrelated field of visual perception, very similar signatures of dynamical systems were found in ambiguous stimuli (Haken 1996; Leopold and Logothetis 1999). This research on perceptual organization may be viewed as a continuation of the tradition of Gestalt psychology (Köhler 1920; Tschacher 1997). For example, apparent motion (i.e., perception of motion in the absence of real motion of the stimuli) can be induced by presenting stimuli, e.g., black disks, alternately at different positions of the visual field. Certain spatial configurations of the disks induce perception of qualitatively different kinds of apparent motion, although identical stimuli are presented. Hence, this and related paradigms create cognitive multistability. Again, the signatures of self-organizing dynamical systems can be found in the phase transitions between the different apparent motion perceptions.

The dynamical hypothesis in cognitive science (van Gelder 1998; Tschacher and Dauwalder 2003) therefore proposes that cognitive agents may be modeled as dynamical systems (instead of, as physical symbol systems, Newell 1980). A common denominator in these dynamical approaches is to start from elementary perception-action cycles, an idea that was introduced by the concept of embodied cognition (Varela et al. 1991). Clark (1997) elaborated three bridging assumptions by which the numerous empirical findings can be integrated in the theory of dynamical systems. First, the assumption of continuity refers to cognition as continuous with its developmental foundations (Thelen and Smith 1994). Second, "off-line" reasoning and thinking is viewed as continuous with on-line motor control strategies. Therefore, abstract cognition may be decoupled from the actual environment but may still be working on the same dynamical principles; thinking is accordingly understood as "enacted" by emulated sensorimotor loops of perception-action cycles. Third, due to the dynamical hypothesis, pattern is provided not by programs but is "soft-assembled" by a continuing process of self-organization. This latter assumption was initially formulated in the interdisciplinary framework of theories of complex systems (especially Haken's synergetics: Haken 1977; and the theory of dissipative systems: Nicolis and Prigogine 1977). The self-organization approach was successively introduced to cognitive science (Haken and Stadler 1990; Kelso 1995). Historically, Gestalt psychology has developed a theoretical framework of cognition and action that was very much akin to the current dynamical systems approach (especially Köhler 1920 and Lewin 1936).

Cognitive science, especially its computational mainstream after behaviorist psychology had turned cognitive in the 1960s, has had a tendency to start with "higher" cognitive functions such as

goals, beliefs, and, in the context of goal-directed behavior, plans. The dynamical approach has avoided the problem of symbol grounding (Harnad 1990) that arises in a computational framework, and has therefore proceeded in a bottom-up fashion instead. Higher cognition is assumed to emerge from a basis of elementary sensorimotor loops. Rather than focusing on symbol grounding, the dynamical view addresses symbol emergence that occurs depending on control parameters. These control parameters comprise the ecological embedding of cognition, i.e., the context and environment of the cognitive agent. Therefore, the dynamical approach views cognition predominantly with reference to its embedding, and in this perspective, cognition is seen as embodied (Tschacher and Bergomi 2011), extended (Clark and Chalmers 1998), and situated (Greeno and Moore 1993).

Intentionality and Representation

The dynamical view in cognitive science thus naturally leads to the concepts of embodied, extended, and situated cognition. Consequently, intentionality of mental acts can be discussed anew under these premises. Rather than searching, in a top-down fashion, for a fundament of experienced intentionality of the mind, the dynamical systems heuristic can be formulated differently: If the mind is conceptualized as arising from self-organization processes, is there a way by which emergent mental acts can be conceptualized as *being about something*?

Intentionality was introduced as a characterizing property of mental acts by Franz von Brentano, a philosopher and early psychologist. In the late nineteenth century, Brentano was professor at the University of Vienna, where Edmund Husserl, Sigmund Freud, Carl Stumpf, and other later protagonists of philosophy and psychology counted among his students. According to Brentano (1874), mental phenomena are always directed towards an object (the intentional object). In other words, mental states contain within themselves something else ("*intentionale Inexistenz*," i.e., intentional existence within). No physical phenomenon has such intentional content, therefore according to Brentano intentionality constitutes the distinctive feature of the mind. Many concepts of contemporary cognitive psychology are in this sense intentional. The basic concepts *goal*, *wish*, *plan*, and *intention* of volitional psychology (Gollwitzer and Bargh 1996; Kuhl and Beckmann 1994) obviously have intentional content. The same applies to *achievement*, *valence*, and *need* within motivation psychology (McClelland et al. 1953). *Affects* and *emotions* are also commonly about something and are thus intrinsically intentional concepts.

It should be noted, however, that intentionality may not provide a sufficient and necessary condition for a state or process to be mental. Not all mental states are intentional; some emotional states (e.g., moods such as a pervasive feeling of melancholy or of serenity) do not necessarily possess intentional content because they are not about something; yet they are undoubtedly experienced mental states. Furthermore, intentionality is likely not the only property that distinguishes mental from physical systems. Many current philosophers of mind suggest that in addition to intentional content, the phenomenal content of mental states must be considered (Nagel 2012). This immediately leads to the topic of consciousness, which however cannot be addressed here.

A concept closely related to intentionality is *representation*. Representation plays a central role in cognitive psychology (as schema: Neisser 1976), in the philosophy of mind (as language of thought: Fodor 1975) and in artificial intelligence (as physical symbol system: Newell 1980). In all of these fields, representation of knowledge is a foundational concept, yet at the same time constitutes a core problem. If a cognitive agent is to have representational knowledge of its environment, the obvious idea is that there must be some kind of mental map or mental model of the environment "inside" the agent. On the basis of information thus represented, the agent would then perform cognitive actions such as memory functions, manipulations for problem solving, and the like. One may note the close analogy of representation with Brentano's intentional object.

The naive, folk-psychological intuition of an inner map or depiction of the environment, on which cognitive functions can then be performed, is however unsatisfactory (Bickhard and Terveen 1995; Clancey 1993). The map concept per se is not explanatory. The reason for this is simply put: if the problem of some information-processing agent is to make sense of its physical environment, the solution to this problem will not be alleviated at all by representation alone; the agent's task of making sense of the *represented* environment is just as demanding. The theory of direct perception (Gibson 1979) has therefore proposed that information pick-up must occur right at the moment of perception, without any representational interlude. For analog reasons, the "storehouse metaphor" of memory has been rejected by researchers of cognitive science (Glenberg 1997). Memory is likely not a passive store out of which represented items, some hypothetical memory engrams, can be retrieved at a later time, but a more active, constructive process (neural reuse: Anderson 2014). Psychological eyewitness research (e.g., the "false memory syndrome": Loftus 2003) has emphasized how modifiable and adaptive the represented contents of memory actually are. Representation-as-mapping has therefore been criticized as merely providing a pseudo solution to a deeper problem, which is likely the very conceptualization of intentionality.

Synergetics

We have proposed that cognitive phenomena have attributes of dynamical systems and that higher functions and more complicated mental processes are constructed bottom-up from simpler components by a process of self-organization. Both dynamical systems theory and self-organization theory are *structural sciences* that have been elaborated for interdisciplinary applications in diverse fields of science. It is the goal of our line of argument to show that intentionality can be conceptualized using a structural framework. The final step prior to our formulation of intentionality in terms of structural science is to introduce self-organization theory.

Here we will rely largely on the interdisciplinary modeling approach of synergetics. Synergetics deals with complex systems, i.e., systems composed of multiple components (Haken 1977, 1996, 2000). By way of their interactions, these components can produce new qualitative features on macroscopic scales. Synergetics focuses on the emergence of these new qualities and proposes that general principles govern the behavior of complex systems whenever such qualitative changes occur. This has been shown for a large class of systems – they are accessible to unifying mathematical and conceptual approaches, which characterizes a structural science approach. A paradigmatic physical system is the Bénard system (e.g., Bianciardi and Ulgiati 1998), which is comprised of a layer of fluid heated with temperature T_2 from below. The temperature at the upper surface of the fluid is T_1. Beyond a critical value of $\Delta T = T_2 - T_1$ extended coordinated motion of the components of the fluid system emerge. Compared to the erratic Brownian motion of the single components, these patterns are an example of the emergence of the new qualities.

Synergetics puts the focus on context – the behavior of complex systems is strongly determined by their environmental context. Context may be given by constant material constraints (e.g., the shape of solid walls that confine fluid systems such as the Bénard system) and by further environmental conditions that energize the systems (e.g., the heat source that drives the Bénard system). In the mathematical approach, these latter driving forces are expressed by control parameters. In many cases, control parameters take the form of externally applied gradients, which are imposed upon the system from outside, such as the difference in temperature ΔT of the Bénard system. The general strategy in synergetics sets out from a state of a system that is already known under a certain control parameter value. When the control parameter is changed, this system can become unstable and show a tendency to modify its state to develop a new type of behavior. The system in question is described by the states of its individual components, by means of a state vector q. The individual components in the Bénard

system, for example, are the motions of single fluid molecules; components may also be, with respect to applications in psychology, the attributes of members within a social group, or the activity of neurons in the brain (Atmanspacher and beim Graben 2007).

Synergetics shows that the behavior of the system close to instability points is described and determined by few quantities, namely the order parameters. In the case of a single order parameter n of a complex system, a typical equation reads

$$dn/dt = cn \tag{1}$$

where c is the "effective" control parameter.

For $c > 0$, n increases exponentially,

$c < 0$, n decreases exponentially,

$c = 0$, n remains constant.

As was mentioned, c denotes the control parameter, a relevant parameter imposed on the system from outside, i.e., from the environment of the system. The generally few order parameters enslave, i.e. entrain, the behavior of the many individual components. This implies an enormous information compression, because the description of the order parameters alone, rather than that of each component, suffices. In the case of the Bénard system, description of the coordinated motion yields a much more parsimonious description of system behavior than the description of all molecular movements in the Brownian motion state of the fluid. This information compression is the hallmark of self-organization.

While they are being determined by the order parameters, it is the individual components that react on the order parameters and, by so doing, even generate the latter. The relationship between order parameters and components is, therefore, founded on *circular causality*, which can explain the generally avalanche-like onset of, and transition between, macroscopic states. In other words, synergetic theory favors neither top-down nor bottom-up modeling but claims that both processes are entangled. Order parameters, after they have been generated in this fashion, quite often exhibit very simple behavior, for instance, asymptotic stability.

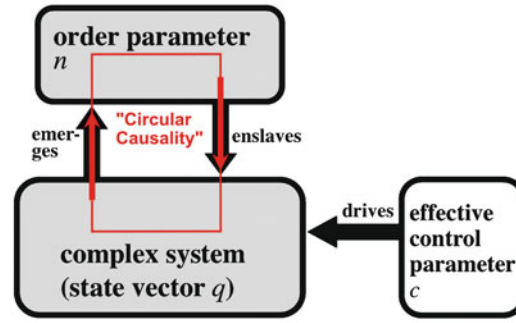

Intentionality: Steps Towards Naturalization on the Basis of Complex Dynamical Systems, Fig. 1 Schematic illustration of circular causality as viewed by synergetics

Obviously, the system depicted in Fig. 1 is an open system. Self-organizing systems are invariably open systems in that they depend on control parameters. In terms of thermodynamics, they are nonequilibrium systems.

Let us however first focus on closed systems, in other words, systems in thermal equilibrium. Classical thermodynamics deals with closed systems throughout. The probability of all configurations of components within the (closed) system can be estimated. When dealing with a complex system consisting of a multitude of components, many possible realizations of the state vector q exist, namely the number of all combinations W of the states of components. Only a small fraction of these realizations will manifest as regular, well-organized patterns. The vast majority of realizations, however, will represent a state of mixture. Should ordered patterns exist as an initial condition, it is far more probable that the temporally consecutive system states will be characterized by less order, owing to the statistical fact that the majority of possible consecutive states will be states with less order rather than states with the same, or even a higher degree, of order. Within a thermodynamics context, this touches on the concept of entropy S (disorder) in accordance with Boltzmann's statistical approach, in which S is directly related to the number of combinations W. The second law of thermodynamics states that any real closed system can only proceed in the direction of increasing entropy, thus following

a maximum entropy principle. Hence, the spontaneous generation of order is highly improbable as indeed a spontaneous generation of *dis*order is to be expected. In other words, the emergence of pattern from a state of mixture requires explanation; the explanation is that the phenomenon of self-organization is driven by an external source, so that the premises of closed systems do not apply. Since the concept of entropy is defined only for equilibrium or close-to-equilibrium systems, one may base the discussion of self-organizing systems on the concept of information (Haken 2000; Tschacher and Haken 2007).

Some authors have applied the laws of thermodynamics in order to allow the study of self-organizing systems. The "restated second law" of thermodynamics (Schneider and Kay 1994; Schneider and Sagan 2005) addresses non-equilibrium systems, i.e., systems that are forced away from equilibrium by the application of gradients. The degree to which a system is moved away from equilibrium is measured by the gradients imposed on the system. As soon as such gradients dwell in the system's environment, the system will, as a consequence of the restated second law, "(...) utilize all avenues available to counter the applied gradients. As the applied gradients increase, so does the system's ability to oppose further movement from equilibrium" (Schneider and Kay 1994). Schneider and Kay's restatement of the second law avoids some of the problems of defining entropy and entropy production by focusing on the destruction of gradients instead.

It should be kept in mind that this "destruction of gradients" is only virtual (in analogy to the principle of virtual work in mechanics), because in open systems gradients are generally maintained by the environment. If, however, the self-organizing system and its *finite* environment act as a closed system, the gradient reduction becomes real. In other words, the effective control parameter c depends on the order parameter n,

$$c = c_0 - \alpha n \tag{2}$$

where c_0 is the control parameter prescribed from the outside and α a constant. The effective control parameter (2) obeys the differential equation

$$dc/dn = -dV/dc \tag{3}$$

where

$$V = \alpha c \tag{4}$$

is a potential and thus the right-hand side of Eq. 3 a gradient.

Discussing the time-evolution of n and c according to Eqs. 1 and 2, we assume that, initially, $n = n(0)$ is close to zero and $c \approx c_0 > 0$.

Thus, according to Eq. 1, n increases exponentially. As a consequence, according to Eq. 2, c decreases, and the exponential increase of n slows down. This process goes on until $c = 0$ and n reaches a time-independent, i.e. steady, state. In practice, the transition to the new state is completed while the gradient has been reduced. In the Bénard example, the coordinated motion patterns have consumed the applied temperature difference and have reduced ΔT to 0. Then the motion patterns subside and steady state remains. This relationship between emergent pattern and control parameter is thus in line with the notion of gradient destruction. The reduction of c by n establishes a second kind of *circular causality*, which is schematically illustrated in Fig. 2.

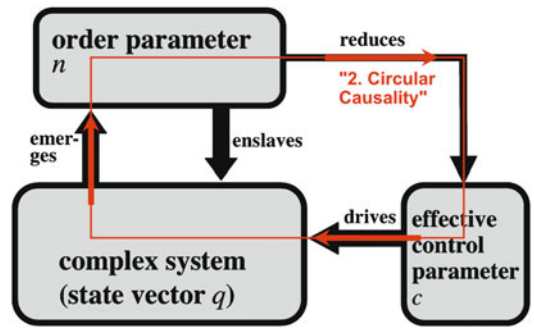

Intentionality: Steps Towards Naturalization on the Basis of Complex Dynamical Systems, Fig. 2 Schematic illustration of the relationship between control parameter and order parameter ("second circular causality")

Discussion: A Structural Science Concept of Intentionality

The steps above have put us in a position where a novel conceptualization of intentionality comes within reach. We propose that this can be achieved on the basis of the properties of self-organizing complex systems (Tschacher and Haken 2007; Haken and Tschacher 2010). In this section, we will therefore discuss to what extent the features of intentionality (listed in section "Definition of the Subject") can be approximated by such systems – the structural science of synergetics is used for the conceptualization of intentionality.

Aboutness

Intentionality implies that a system state is about something else, namely the intentional object. In terms of cognitive psychology, this process is called representation, by which a "cognitive map" of the object is generated, particularly during perceptual or memory processes.

For being capable of intentionality and representation, a minimum requirement is that the intentional system must be an open system. Many open systems can provide representations in the sense of mappings of environmental impacts. The silver particles of a light-sensitive surface of a photographic film can "represent" the objects in front of the lens, however in a trivial, weak sense. As has been shown in the previous section, a self-organizing system can likewise "represent" and thus generate the feature of being about something. In the latter system, the order parameter is a component in the loop labeled "second circular causality" (Fig. 2). Within this loop the complex system "represents" an external object by the generation of an order parameter. The intentional object in this case is the external control parameter c. The environmental context described by control parameters is what self-organized patterns are about.

The mechanisms of representation are clearly divergent in these two systems, as is the nature of the intentional objects. In the photographic system, the mapping of the environmental objects onto the representing system is unidirectional, whereas in the self-organizing system there is continuous interaction between environmental objects and system. This circularity is illustrated in Fig. 2 and provides an important and desirable aspect of the kind of aboutness realized by self-organizing systems – circularity guarantees that an intentional system is capable of exerting a retrograde effect back on what has been represented. This effect is generally a reduction of the gradient that was quantified by the control parameter.

Functionality

Intentionality must be functional in order to make representation explanatory, i.e., make representation more than just a mapping of environmental states onto the system's state. The functionality of open systems has previously been approached from the angle of thermodynamics. Schneider and Sagan (2005) pointed out that self-organizing systems maintain and increase their levels of organization by dissipating nonequilibrium gradients. If the gradient is to be kept constant, the demand on free energy (so-called exergy) that must be provided by an external source increases as the system becomes more organized. Alternatively, the efficiency of the system can be defined as the ratio of the change of work and the change of the gradient driving the system. This can be shown by findings in simple physical systems that generate patterns; e.g., mentioned Bénard cells reduce the temperature gradient more efficiently as soon as they have generated ordered convection structures. Efficiency has thus increased in the self-organized convection regime in comparison to the linear conduction regime of the fluid. Analogous relationships are found in further self-organizing systems such as the laser when output power is plotted against input power (Haken 1977). In other words, pattern formation in these open systems is in the service of gradient reduction. The association of pattern formation with gradient reduction makes pattern formation "functional."

In situations of multistability, several patterns are possible, so that each of these can be functional in reducing the gradients imposed on the system. These alternative patterns can be associated with different efficiencies. It is theoretically

suggestive that the two circular loops pointed out in Figs. 1, and 2 interact and thereby create a Darwinistic scenario in which a competition between microscopic modes q arises; the environmental forces c exert a selective impact on this competition of modes. From a mathematical modeling point of view, it is not however clear whether the optimal pattern is necessarily selected, nor under which circumstances the optimal pattern will be chosen. In some systems, such as quadruped movement coordination, it was empirically found that the specific pattern providing the most efficient behavior (measured by the metabolic cost of transport of the animal) will be realized by the system (Hoyt and Taylor 1981). The generalizability of such findings of optimality is not yet established.

Mental-Likeness

In this discussion, we have so far found that the aboutness of intentionality and representation can be modeled by open systems. A subclass of open systems additionally provides functional representations – especially self-organizing nonequilibrium systems appear to show both the features of aboutness and of functionality.

It is obviously useful to reserve the predicate "intentional" for mental systems alone. Thus, even though some physical self-organizing systems may show circular causality loops and thus stand the tests of aboutness and functionality, we would still not categorize systems such as lasers, Bénard cells as mental. We may say that such self-organizing physical systems behave "as if they were intentional," i.e., they are proto-intentional systems. Let us finally investigate under which conditions self-organizing nonequilibrium systems may also show mental features and, with this, we address the possible naturalization of intentionality. This final step is basically a discussion of the validity of the statement that physical self-organizing systems can show intentionality.

- *Complexity reduction* is a core hallmark of mental processes. The ability of a system to simplify, group, and coordinate environmental information is a necessary premise for any system to be mental. This property of information compression is addressed in the circular causality concept of synergetics illustrated in Fig. 1. With respect to complexity reduction, physical self-organizing systems are mental-like.
- *Stability* together with related signatures of stability (e.g., hysteresis, critical fluctuations) is a further mental property, which is empirically well founded especially in the psychology of perception. Again, the emergent order parameters of physical self-organizing systems generally show this property.
- *Autonomy* is required of intentional mental systems, i.e., mental systems must be able to function in the absence of external agents. This ability addresses the "homunculus-problem" that has already been introduced together with the feature of functionality. We may say that generally self-organizing systems do not require external supervision for producing order parameters (therefore, *self*-organizing). This does not rule out that several autonomous systems may be nested inside one another (cf. Minsky's (1985) society of mind, or the notion of subsumption architecture of Brooks' (1991) robotic agents). Thus, physical self-organizing systems are also autonomous.
- Is the nature of the *intentional content* mental-like, and which aspect of the environment is being represented by self-organizing systems? Order parameters are intentional with respect to those environmental parameters that drive the system. In other words, the intentional content is generally connected to what energizes the system. This is a satisfactory model in all those instances where mental intentionality is of a motivational character, resembling a psychological "drive" (Freud 1923). In the introduction, we named wishes, desires, affects, intentions, goals, and the like as intentional. Such intentional states can be directly modeled by self-organizing systems that act to reduce the driving parameters (in Freudian terms, drive reduction). The self-organization model, however, is less applicable whenever intentionality is of a language-like, propositional type (Fodor 1975). It would be not straightforward to model, for instance, the intentionality

inherent in the belief that "there is a unicorn grazing in the garden," using simple physical self-organizing systems. Therefore, the discussion of mental-likeness of self-organizing systems remains restricted to nonlinguistic intentionality.

- The only mental systems known to date, despite the efforts of several decades of artificial intelligence research, are linked with *neuronal networks* hosted by biological organisms. Therefore, can the argumentation above be applied to brain dynamics and to pattern formation in neural networks? One may then associate the gradient of c with intentionality in a neurocognitive sense. Haken (2002) has discussed synchronization, i.e., self-organization, of neural nets using various mathematical frameworks. Friston (2012) has applied a free-energy principle to brain dynamics. Haken and Tschacher (2010) have specifically addressed the reduction of the effective control parameter on the basis of the Wilson-Cowan equations describing cortical dynamics (Wilson and Cowan 1972). They suggested that the general findings on circular causality in the relationship between order parameter and control parameter can be readily applied to neural networks.
- Contrary to von Brentano's supposition, mental phenomena are intentional as well as *phenomenal-experiential*. Conscious mental states are characterized, from a first-person perspective, by a specific quality, by "what it is like" to experience this state (Nagel 1974). The qualia and "what-it-is-likeness" of phenomenal consciousness is not modeled by our present conceptualization. This comes as no surprise, as it relates to the "hard problem" (Chalmers 1996) of consciousness. Thus a constitutive ingredient of many mental processes, the phenomenal-experiential qualities, are not generated by physical self-organizing systems.

In conclusion, we have argued that a formulation of intentionality is feasible on the basis of the theory of complex dynamical systems. When such systems are removed from thermodynamical equilibrium, they acquire the capability of producing self-organized patterns. Pattern formation consequently puts the systems in a specific relationship to environmental parameters, the contexts of these systems. Owing to the accompanying circular loops, these systems show aboutness, the defining property of intentionality, as well as functionality, which is essential for making the aboutness of intentional states explanatory. We find, however, that this structural conceptualization of intentionality is not entirely mental-like because the phenomenal and experiential aspects of conscious cognition cannot be addressed by it.

Future Directions

We may conclude that nonexperiential intentionality can be conceptualized to a considerable extent using nonequilibrium complex systems. The limitations that have turned up during the above discussion may provide points of departure for future research.

First, it is as yet unclear whether the resulting self-organized patterns obey an optimization principle. In some empirically described systems showing multistability, it could be shown that the more optimal pattern wins the competition among order parameters, but the generality of such findings is yet to be corroborated. Correspondingly, Haken and Tschacher (2010) have discussed "second circular causality" in the case of only one order parameter. A mathematical model comprising $m > 1$ order parameters would be a desirable next step.

Second, we found that conceptualization, and even naturalization, of intentional states is achievable when these states comprise motivation, goals, intentions, or drives; these may be viewed as basic intentional states related to behavioral strivings. At the moment, however, the intentionality problem appears intractable when intentional states are of a symbolic and propositional nature. The difficulties of modeling Fodor's *language* of thought do indeed complicate the modeling of intentionality beyond its basic form (cf. Churchland 2002, p. 304). At the present time, we may consider nonlinguistic intentionality as one of two problems of a conceptualization of

intentionality, which in fact seems accessible. The more fundamental problem is however the second, the intentionality of an experiencing, conscious, linguistic agent. Structural conceptualization from a complex systems point of view addresses solely the basic aspect of intentionality, yet not the phenomenal nature of intentionality. This limitation points to a failure of the naturalization of conscious intentionality altogether. In a strict sense, naturalization is the explanation of mental phenomena by physical phenomena, and we have encountered serious obstacles of this approach. Eliminative physicalism, i.e., the totality of all possible naturalizations, is likely not a tenable program. As a future direction, one may have to further develop the structural science solution and, in philosophical approaches, contemplate dual-aspect theories (Atmanspacher 2017).

Third, the topic of intentionality has numerous implications beyond the philosophy of mind and theoretical psychology. In psychiatry and psychotherapy research, intentionality is a topic of considerable significance because intentional mental acts and states are often characteristically altered or disturbed during a mental disorder. Many such psychopathological conditions are found especially among the symptoms of schizophrenia, such as disorders of formal thought as well as of thought content, disorders of perception, and ego disorders. The symptoms are heterogeneous and manifold. A majority of these symptomatic alterations, however, involve changes in the cognitive coordination of the patients (Tschacher et al. 2017). Recent schizophrenia research has shown that a considerable portion of variance of psychotic symptoms can be explained by cognitive coordination measures (e.g., Tschacher et al. 2008). While no generally accepted encompassing theory of schizophrenia exists, a theory of intentionality may have the potential to contribute to progress in psychopathology. It may help to link the phenomenology and neurobiology of schizophrenia and other psychiatric disorders by introducing a dynamical systems perspective.

Fourth, artificial intelligence is a completely different field but is also confronted with intentionality as a core problem. During recent decades, the computational approach to machine intelligence has failed to a large extent; especially, no mental-like intelligence could be generated. Consequently, the field has turned to the more basic tasks of designing autonomous agents and robots with rudimentary adaptivity in the real world (Braitenberg 1986; Pfeifer and Bongard 2006). In this framework, intelligence is expected to be closely associated with embodiment (hence, embodied intelligence, mind-body coevolution), rather than with symbol manipulation and the programming of symbol systems. The latter constituted the classical approach to artificial intelligence. One of the novel directions of development is using emergence principles for the design of intelligent agents or multi-agent systems; this is closely related to the structural view on intentionality proposed here. The engineering approach of embodied agent design and the dynamical systems proposal of intentionality have the potential of subserving each other in artificial intelligence research.

Bibliography

Primary Literature

Anderson MA (2014) After phrenology. Neural reuse and the interactive brain. MIT Press, Cambridge

Atmanspacher H (2017) Contextual emergence in decompositional dual-aspect monism. Mind Matter 15:111–130

Atmanspacher H, beim Graben P (2007) Contextual emergence of mental states from neurodynamics. Chaos Complexity Lett 2:151–168

Bianciardi C, Ulgiati S (1998) Modelling entropy and exergy changes during a fluid self-organization process. Ecol Model 110:255–267

Bickhard M, Terveen L (1995) Foundational issues in artificial intelligence and cognitive science. North-Holland, Amsterdam

Braitenberg V (1986) Künstliche Wesen: Verhalten kybernetischer Vehikel. Vieweg, Braunschweig

Brooks R (1991) Intelligence without representation. Artif Intell 47:139–159

Chalmers D (1996) The conscious mind. Oxford University Press, Oxford

Churchland P (1986) Neurophilosophy: toward a unified science of the mind-brain. MIT Press, Cambridge

Churchland P (2002) Brain-wise: studies in neurophilosophy. MIT Press, Cambridge

Clancey WJ (1993) Situated action. A neurophysiological interpretation response to Vera and Simon. Cogn Sci 17:87–116

Clark A (1997) Being there: putting brain, body, and world together again. MIT Press, Cambridge
Clark A, Chalmers D (1998) The extended mind. Analysis 58:7–19
Fodor J (1975) The language of thought. Crowell, New York
Freud S (1923) Das Ich und das Es [published in English (1949) The Ego and the Id. The Hogarth Press Ltd, London]
Friston KJ (2012) A free energy principle for biological systems. Entropy 14:2100–2121
Gibson JJ (1979) The ecological approach to visual perception. Houghton Mifflin, Boston
Glenberg A (1997) What memory is for. Behav Brain Sci 20:1–19
Gollwitzer PM, Bargh GA (eds) (1996) The psychology of action: linking cognition and motivation to behavior. Guilford, New York
Greeno J, Moore J (1993) Situativity and symbols: response to Vera and Simon. Cogn Sci 17:49–59
Haken H (1977) Synergetics – an introduction. Non-equilibrium phase-transitions and self-organization in physics, chemistry and biology. Springer, Berlin
Haken H (1996) Principles of brain functioning: a synergetic approach to brain activity, behavior, and cognition. Springer, Berlin
Haken H (2000) Information and self-organization: a macroscopic approach to complex systems. Springer, Berlin
Haken H (2002) Brain dynamics. Synchronization and activity patterns in pulse-coupled neural nets with delays and noise. Springer, Berlin
Haken H, Stadler M (eds) (1990) Synergetics of cognition. Springer, Berlin
Haken H, Tschacher W (2010) A theoretical model of intentionality with an application to neural dynamics. Mind Matter 8:7–18
Haken H, Kelso J, Bunz H (1985) A theoretical model of phase transitions in human hand movements. Biol Cybern 51:347–356
Harnad S (1990) The symbol grounding problem. Physica D 42:335–346
Hoyt DT, Taylor CR (1981) Gait and the energetics of locomotion in horses. Nature 292:239–240
Kelso JAS (1995) Dynamic patterns: the self-organization of brain and behavior. MIT Press, Cambridge
Köhler W (1920) Die physischen Gestalten in Ruhe und in stationärem Zustand. Vieweg, Braunschweig
Kuhl J, Beckmann J (1994) Volition and personality. Action versus state orientation. Hogrefe and Huber Publishers, Göttingen
Leopold DA, Logothetis NK (1999) Multistable phenomena: changing views in perception. Trends Cogn Sci 3:254–264
Lewin K (1936) Principles of topological psychology. McGraw-Hill, New York
Loftus EL (2003) Our changeable memories: legal and practical implications. Nat Rev Neurosci 4:231–234
McClelland DC, Atkinson JW, Clark RA, Lowell EL (1953) The achievement motive. Van Nostrand, Princeton
Minsky M (1985) Society of mind. Simon & Schuster, New York
Nagel T (1974) What is it like to be a bat? Philos Rev 83:435–450
Nagel T (2012) Mind and cosmos: why the materialist neo-Darwinian conception of nature is almost certainly false. Oxford University Press, New York
Neisser U (1976) Cognition and reality. Principles and implications of cognitive psychology. Freeman, San Francisco
Newell A (1980) Physical symbol systems. Cogn Sci 4:135–183
Nicolis G, Prigogine I (1977) Self-organization in non-equilibrium systems. Wiley, New York
Pfeifer R, Bongard JC (2006) How the body shapes the way we think. A new view of intelligence. MIT Press, Cambridge
Popper K, Eccles J (1977) The self and its brain. Springer, Berlin
Schneider ED, Kay JJ (1994) Life as a manifestation of the second law of thermodynamics. Math Comput Model 19:25–48
Schneider ED, Sagan D (2005) Into the cool. Energy flow, thermodynamics and life. University of Chicago Press, Chicago
Thelen E, Smith LB (1994) A dynamic systems approach to the development of cognition and action. MIT Press, Cambridge
Tschacher W (1997) Prozessgestalten [Processual gestalts]. Hogrefe, Göttingen
Tschacher W, Bergomi C (eds) (2011) The implications of embodiment: cognition and communication. Imprint Academic, Exeter
Tschacher W, Dauwalder J-P (eds) (2003) The dynamical systems approach to cognition. World Scientific, Singapore
Tschacher W, Haken H (2007) Intentionality in non-equilibrium systems? The functional aspects of self-organized pattern formation. New Ideas Psychol 25:1–15
Tschacher W, Dubouloz P, Meier R, Junghan U (2008) Altered perception of apparent motion in schizophrenia spectrum disorder. Psychiatry Res 159:290–299
Tschacher W, Giersch A, Friston KJ (2017) Embodiment and schizophrenia: a review of implications and applications. Schizophr Bull 43:745–753
van Gelder T (1998) The dynamical hypothesis in cognitive science. Behav Brain Sci 21:615–628
Varela F, Thompson E, Rosch E (1991) The embodied mind. MIT Press, Cambridge
von Brentano F (1874) Psychologie vom empirischen Standpunkte. Duncker & Humblot, Leipzig
Wertheimer M (1912) Experimentelle Studien über das Sehen von Bewegungen [Experimental studies on the perception of motion]. Z Psychol 61:165–292

Wilson HR, Cowan JD (1972) Excitatory and inhibitory interactions in localized populations of model neurons. Biophys J 12:1–24

Books and Reviews

Beckermann A (2001) Analytische Einführung in die Philosophie des Geistes. de Gruyter, Berlin
Carter R (2002) Consciousness. Weidenfeld & Nicolson, London
Chaisson EJ (2001) Cosmic evolution. The rise of complexity in nature. Harvard University Press, Cambridge
Chalmers D (ed) (2002) Philosophy of mind: classical and contemporary readings. Oxford University Press, Oxford
Clark A (2013) Whatever next? Predictive brains, situated agents, and the future of cognitive science. Behav Brain Sci 36:181–253
Dennett DC, Kinsbourne M (1992) Time and the observer: the where and when of consciousness in the brain. Behav Brain Sci 15:183–247
Fuchs T (2012) Das Gehirn – ein Beziehungsorgan. Eine phänomenologisch-ökologische Konzeption, 4th edn. Kohlhammer, Stuttgart
Guastello S, Koopmans M, Pincus D (eds) (2008) Chaos and complexity: recent advances and future directions in the theory of nonlinear dynamical systems psychology. Cambridge University Press, Cambridge
Kauffman S (1993) The origins of order – self-organization and selection in evolution. Oxford University Press, New York
Kruse P, Stadler M (eds) (1995) Ambiguity in mind and nature. Springer, Berlin
Noë A (2004) Action in perception. MIT Press, Cambridge
Port R, van Gelder TJ (eds) (1995) Mind as motion: explorations in the dynamics of cognition. MIT Press, Cambridge
Searle JR (1998) The rediscovery of mind. MIT Press, London
Storch M, Cantieni B, Hüther G, Tschacher W (2010) Embodiment, 2nd edn. Huber, Bern
Swenson R, Turvey MT (1991) Thermodynamic reasons for perception-action cycles. Ecol Psychol 3:317–348
Tschacher W, Dauwalder J-P (eds) (1999) Dynamics, synergetics, autonomous agents–nonlinear systems approaches to cognitive psychology and cognitive science. World Scientific, Singapore

Self-Organization and the City

Juval Portugali
ESLab (Environmental Simulation Lab), Department of Geography and the Human Environment, Tel Aviv University, Tel Aviv, Israel

Article Outline

Glossary
Definition of the Subject
Introduction
Complexity Theories of Cities: An Overview
Self-Organization and the City
Future Directions
Bibliography

Keywords

Self-organization; City; Planning; Urbanism; SIRN; Information adaptation

Glossary

Self-organization A property of open and complex systems that achieve their order spontaneously, that is, by means of "self-organization."

City A form of settlement that first emerged in the Near East (the core being Mesopotamia) some 5,500 years ago. Since its first appearance in Mesopotamia, it has diffused in space and time. With colonialism, the Western-European form of city has diffused to the entire world, suppressing on the way other forms of cities (e.g., in South America, East Asia, etc.). In the last few decades, the city has become the most dominant form of settlement: for the first time in human history, more than half of world population lives in cities.

Urbanism The term refers to the totality of life in cities: the interrelations between the social structure, culture, economy, politics, architecture, physical morphology, etc. associated with life in cities. The first appearance of cities is thus termed *the urban revolution*. Most students of urbanism would agree that twenty-first-century society is undergoing a major urban transformation; some describe it as a new urban revolution.

Planning Planning is, on the one hand, a basic cognitive capability of humans while, on the other, a profession and research domain termed interchangeably *city planning*, *urban and regional planning*, or *environmental planning*. City planners work and act in the context of planning law and administration, the aim of which is to regulate and control life in cities.

SIRN (synergetic inter-representation network) An approach to cognitive mapping and urban dynamics suggesting that cities emerge, maintain their order, and change again as a consequence of an ongoing interaction between cognitive maps that are constructed in the mind/brain of humans as internal representations and the city as a collective external representation. This ongoing interaction gives rise to a network; some of whose elements are in the mind/brain while others in the world.

Information deflation, inflation and adaptation A view suggesting that Shannon's notion of information is a property of closed systems and that in complex, self-organizing systems, one has to take into consideration the role of *semantic information*. Due to semantic information, the process of self-organization often entails *information deflation*; in some cases, it entails *information inflation*. The suggestion is that information deflation and inflation are two facets of the process of *information adaptation*.

Definition of the Subject

Self-organization is a central property of open and complex systems. While the concept had already appeared in the 1940s, its modern use was

A. Hutt, H. Haken (eds.), *Synergetics*,
https://doi.org/10.1007/978-1-0716-0421-2_471

Originally published in
R. A. Meyers (ed.), *Encyclopedia of Complexity and Systems Science*, © Springer Science+Business Media LLC 2017
https://doi.org/10.1007/978-3-642-27737-5_471-2

pioneered in the 1960s by people such as Haken (1983, 1987) with his theory of *synergetics*, Prigogine with his notion of *dissipative structures* (Nicolis and Prigogine 1977; Prigogine 1980; Prigogine and Stengers 1984), and others (see review in Chap. 3.1 Portugali (2000)). Such systems are typically in "a far from equilibrium condition" and exhibit phenomena of chaos, fractal structure, and the like. For a long time, the term "self-organization" was used also as an umbrella name for these theories; nowadays, it is common to refer to these theories as *complexity theories*.

The notions of self-organization and complexity originated in the sciences, specifically in physics, as a property of natural systems. However, as we shall see below, from the start, they were associated with the city – at the beginning, the city was used as a metaphor to convey the notion of "self-organization" (Nicolis and Prigogine 1977), while at a later stage, it was studied as a genuine self-organization system in its own sake (Allen 1981).

Most theories and methodologies of complexity developed in the last three decades have been applied also to the study of cities with the result that we now have a new domain of research that has already been termed (Portugali 2011, Portugali et al. 2012) *complexity theories of cities* (CTC). CTC now include a rich body of research on *fractal cities* (Batty and Xie 1999), *self-organization and the city* (Portugali 2000), *cities and complexity* (Batty 2005), cellular automata and agent base urban simulation models (Benenson and Torrens 2004), studies on cities from the perspective of Bak's self-organized criticality (Batty and Xie 1999), studies on cities as networks (Batty 2005), and much more. This growing body while enriching our understanding of cities and providing sophisticated tools to city planning also exposes problems that will become the challenges for the next generation of studies on complexity, self-organization, and the city.

Introduction

The title "Self-Organization and the City" enfolds *two notions* – "self-organization" and "city," *a thesis* suggesting that cities are complex self-organizing systems and an *inconsistency*, the view of cities as complex systems that achieve their order spontaneously contradicts the traditional view of cities as symbols of organized order and planning. From the title thus follow four questions: what is self-organization? What is a city? In what sense are cities self-organizing systems? What is the meaning of planning and design in a self-organizing system? In an *Encyclopedia of Complexity and System Sciences* such as this, there is no need to introduce the term self-organization beyond what has been said about it above; we are thus left with three introductory tasks, namely, to clarify the notion "city," elaborate the thesis that cities are self-organizing systems, and solve the contradiction between self-organization and planning or design in the realm of cities.

What Is a City?

There are two ways to answer this question: first, by looking at explicit attempts to define a city and, second, by exposing the way the different theories of cities explicitly describe, or implicitly perceive, a city.

Explicit Attempts to Define a City

The history of the many attempts to define "a city" is rather confusing: Whenever a definition was proposed, it was always possible to falsify it (in Popper's 1959 sense) by putting forward cities that do not comply with the definition. The main reason for the failure to define cities is that the various attempts to do so were always made with reference to what in cognitive science (Rosch 1999) is called *classical categories*, that is, groups composed of entities sharing some necessary and sufficient conditions that define them as a category and distinguish them from other categories. Students of urbanism have implicitly treated cities as classical categories, and yet, cities are not classical categories – they form a category due to what Wittgenstein (Wittgenstein 1953) has termed *family resemblance*. As a consequence, attempts to define them in terms of a classical category ended up with a failure (Portugali 2000).

A family resemblance category becomes a category not when its elements share some common denominators, but when they form a *network* of partial links and similarities. Further research and experiments have found that many family resemblance categories have a *core-periphery* structure, in the sense that some instances of the category are more *prototypical* of the category than others and they thus form its center, while the rest of the instances form the category's periphery (Johnson 1987; Lakoff 1987; Rosch 1999).

The city is a good example of a family resemblance category with a core-periphery structure. On the one hand, there are no common elements between the "first" cities of some 5,500 years ago and the cities of today except for the name. On the other hand, the first cities had space-time links and similarities with subsequent cities, which in turn had common elements with subsequent cities, and so on until the global cities of today. The result of this process is that cities form a huge space-time family resemblance network extending in time and space from the ancient cities of some 5,500 years ago to the cities of today. In this network, one can identify space-time moments during which certain cities became more characteristic or prototypical of the category than others. Such cities have temporarily captured the center of the category city, pushing to the periphery the rest of the instances, only to be replaced in subsequent space-time moments by other prototypical cities, other centers, and other peripheries. How does this huge network evolve in time and space? The answer is: "by means of self-organization" (Portugali 2000).

Images of Cities

This section discusses images of cities that are implicit or explicit in several of the urban theories. Only theories that facilitate subsequent discussion will be discussed.

The Economic City The city is portrayed as a center-periphery structure with several rings that come into being by an economic competition between land uses that differ in their spatial demand function (Fig. 1). The land uses with the highest and steepest *spatial demand curves* or *rent bid curves* (Alonso 1965; Isard 1956) capture the

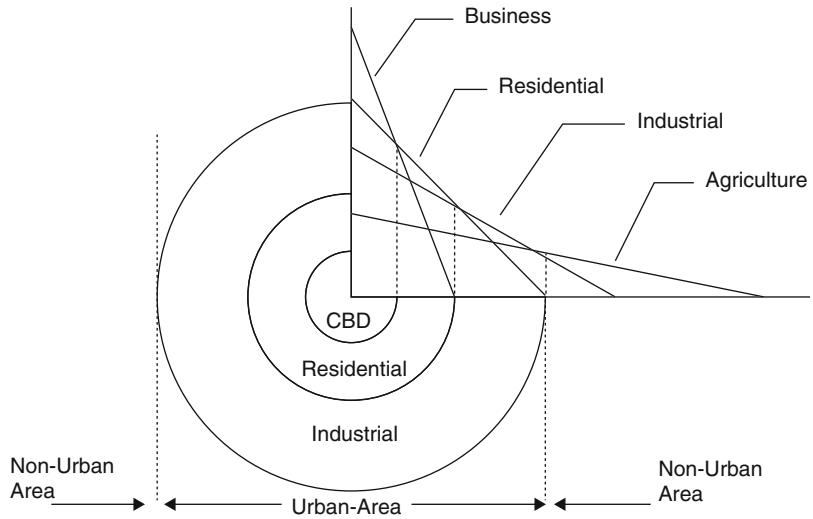

Self-Organization and the City, Fig. 1 Thünen's type of land use system as transformed into an urban land use system by location theory. Businesses are prepared to pay high rent at the center of the city, but are reluctant to "live" far from it. Their spatial demand curves (or rbc – rent bid curves) are thus the highest and steepest. Industrialists, in this exposition, are exactly the opposite, and residents are in between: they cannot afford to pay the high prices at the center, but are prepared to live far from it, and so on. Each land use thus occupies a ring were it can pay (bid for) the highest rent. Note that the principle of marginal utility which is implicit in Thünen's landscape here appears explicitly as the central economic principle

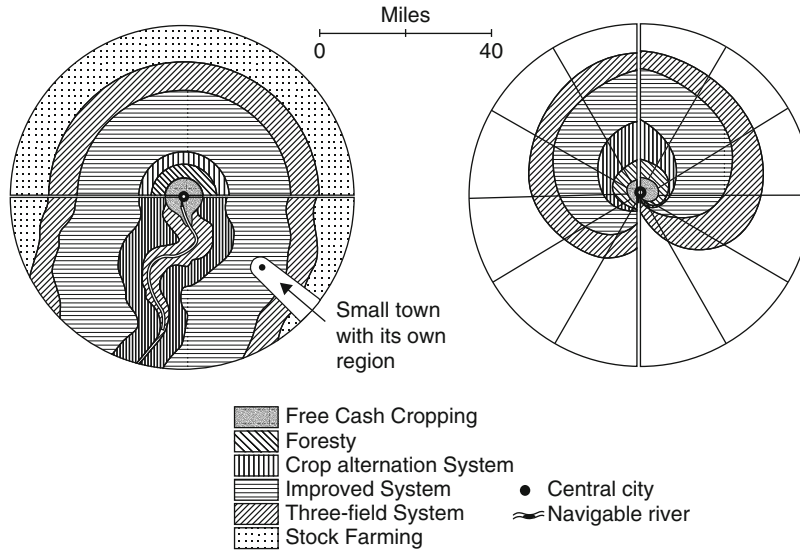

Self-Organization and the City, Fig. 2 The diagrams of Thünen's *isolated state*: *left*, *upper part of the diagram* "This shows the Isolated State in the shape it must take from the assumptions made in Section One. . .." *Left*, *lower part* "Here we see the Isolated State crossed by a navigable river. Here the ring of crop alternation become very much larger, stretching along the river . . . The effect of constructing a highway is similar, . . ." (Par. 385). *Right* "The diagram illustrates the effect of the Town grain price on the extension of the cultivated plain" (Par. 386) (Source: von Thünen 1826)

central ring – the most accessible area of the city – thus forming the central business district (CBD); the rest of the land uses occupy the peripheral rings. The origin of this city image is von Thünen's (von Thünen 1826) *isolated state* (Fig. 2): Originally formulated as a theory of agricultural land uses, it became the founding theory of all location theories including urban land use theories.

The City as a Central Place The city is perceived as a central place that mediates between the city's complementary region and other cities that form a hierarchical network of central places (Fig. 3). The origin of this view is Christaller's (Christaller 1933) *central place theory* that perceived the city as a central place for tertiary activities (a market place, transportation node, and administrative center). Lösch's (Lösch 1954) central place theory was more ambitious and complicated and portrayed the city as a central place for all production, consumption, transportation, and political activities (Fig. 4).

The City as a Node in a System of Cities The city here "looses" its autonomy in the sense that it is perceived as a node in a system of cities – no attention is paid to the city's role or function; the focus of interest is on the system as a whole. This view is due to Auerbach (Auerbach 1913) who already at the turn of the twentieth century showed that the rank-size distribution of cities obeys the power law. In a famous work from 1949, Zipf showed that this rank-size distribution typifies not only cities (Fig. 5) but a whole range of phenomena (Zipf 1949). Zipf's work provided a source of inspiration to a long list of subsequent studies on systems of cities (Pumain 2005).

The Ecological City As in the economic city, here too, the city is portrayed as a center-periphery ring structure. However, here, the city's structure emerges out of a competition between cultural and socioeconomic groups in a way similar to the competition between species in natural ecology. The various studies in this domain are termed *urban ecology*; their source of inspiration is the

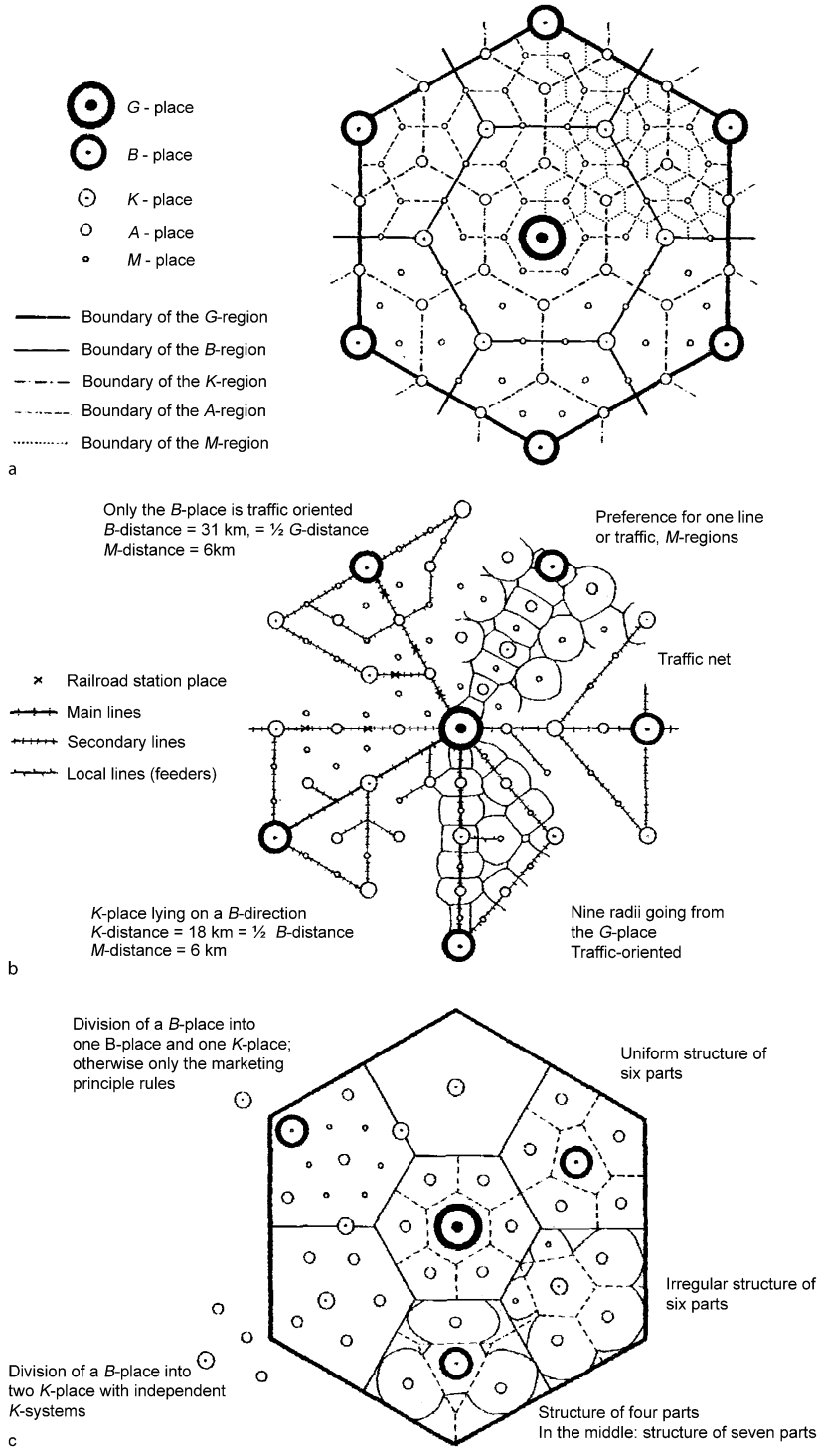

Self-Organization and the City, Fig. 3 Christaller's systems of central places according to the three locational principles. (**a**) The marketing regions in a system of central places. (**b**) A system of central places developed according to the traffic principle. (**c**) A system of central places developed according to the separation principle (Source: Figs. 2, 4, 6 in (Christaller 1933))

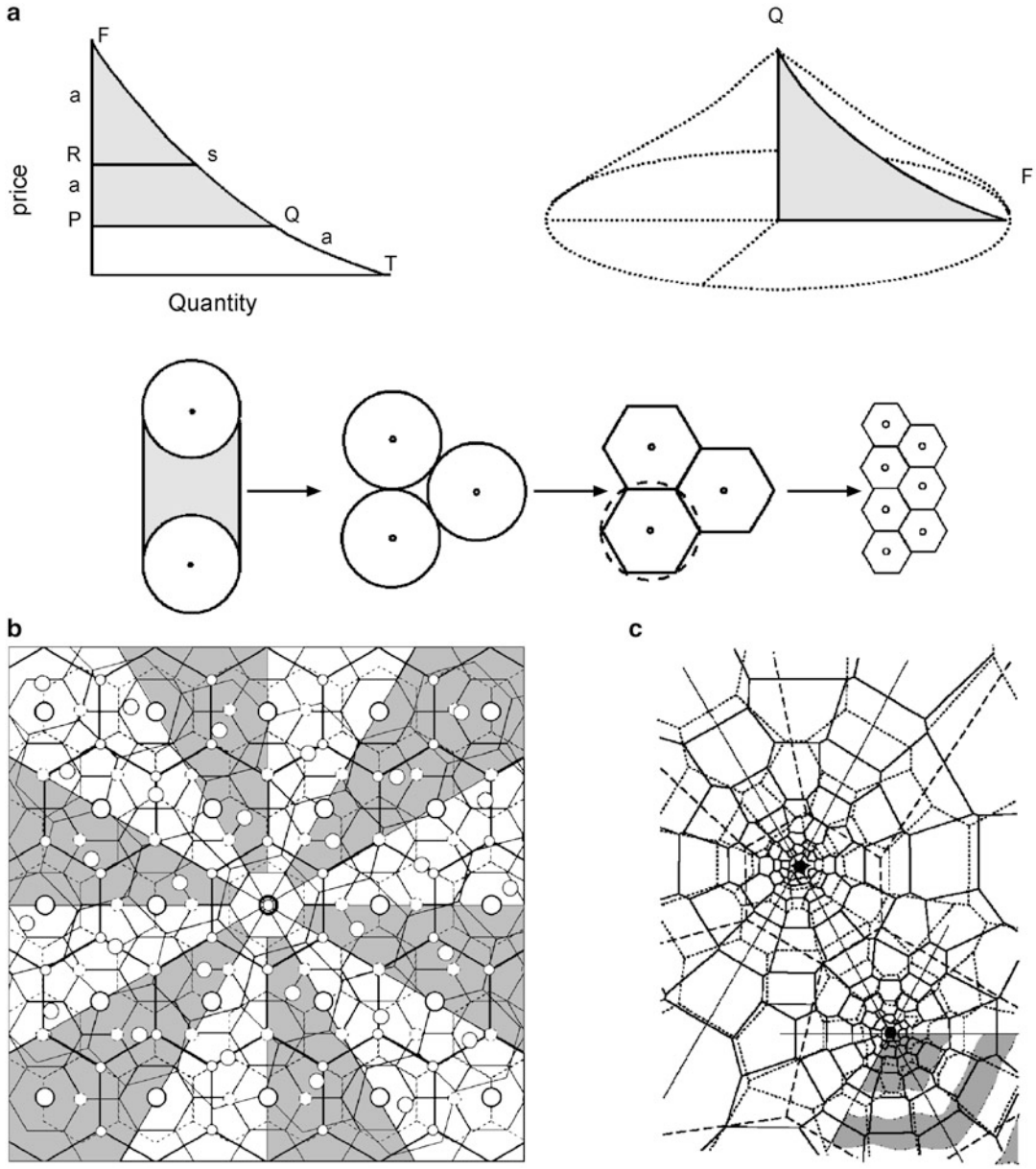

Self-Organization and the City, Fig. 4 (**a**) The derivation of Lösch's system of central places. *Top* the derivation of a *spatial demand cone* with its market area (*right*) out of an "ordinary" demand curve (*left*). *Bottom* development of market areas from the large circle to the final small hexagon (Source: Figs. 20–23 in Lösch 1954). (**b**) Lösch's derived system of central places with their market areas, divided into "city-poor," "city-rich" sectors (Source: Fig. 28 in Lösch 1954). (**c**) A Lösch system of central places modified by Isard (1956) so as to be consistent with the resulting population distribution

Chicago school of social ecology. Several urban landscapes were suggested; the most dominant one is Burgess' (1925, 1926, 1927) ring structure (Fig. 6).

The City as a Representation of Society The city is here perceived as a spatial representation of society as a whole. This image of the city emerged in the early 1970s as a consequence of

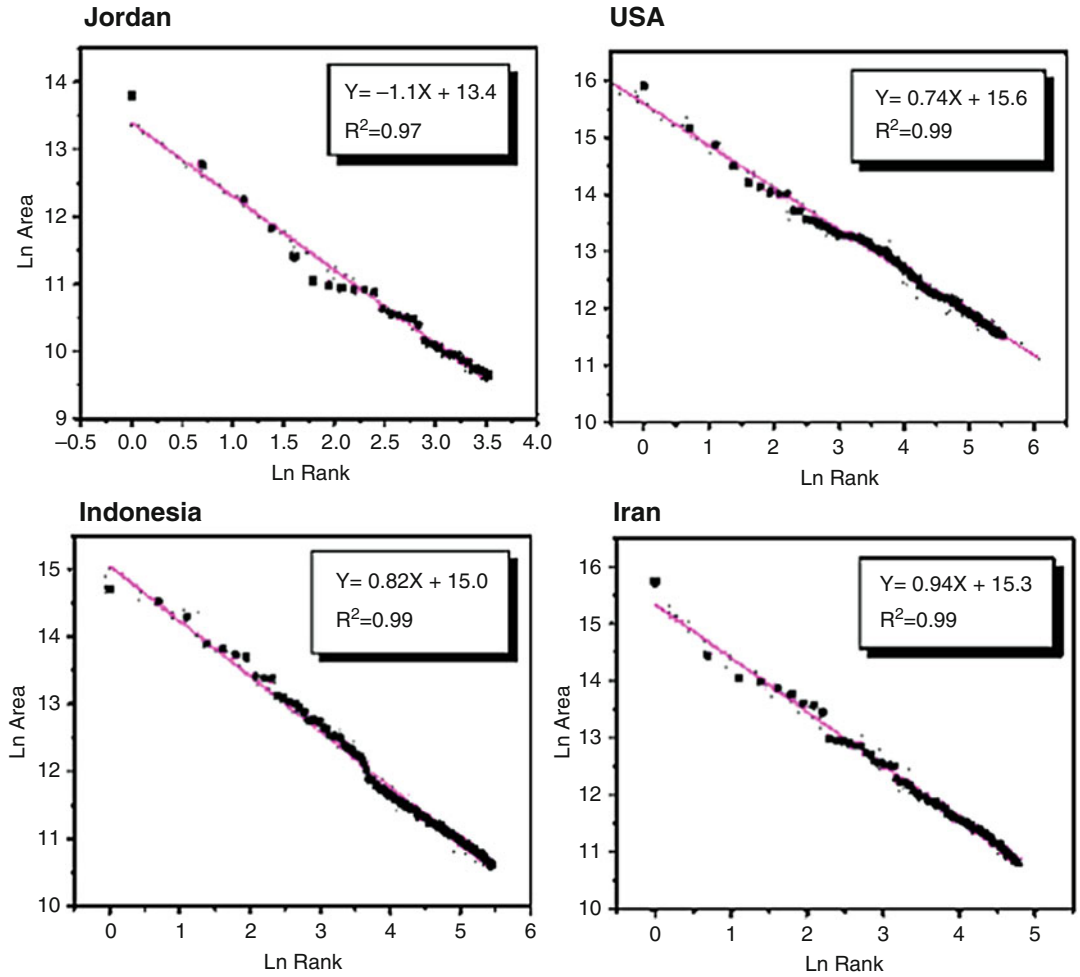

Self-Organization and the City, Fig. 5 Rank-size distribution of cities with more than 100,000 inhabitants in four different countries (Source: Fig. 2.7 in Blumenfeld-Lieberthal 2005)

a paradigm shift the study of cities underwent – from liberal social and economic theories to more radical ones with Marxism being the most dominant view. Two Marxist interpretations of the city can give the flavor of this approach. The first is Castells' (1977) view according to which the city is a spatial representation of the structure of society as perceived by structuralist-Marxist theory (Fig. 7). The second is Harvey's view according to which the city's landscape emerges, as a logical consequence, out of internal contradictions inherent in the capitalist *mode of production* that, according to this view, dominates world society of the twentieth and twenty-first centuries, namely, between forces of spatial agglomeration and processes of spatial dispersion. As illustrated in Fig. 8, this tension can be resolved only by *the urbanization of capital* (Gregory 1994; Harvey 1985).

The City as a Sociocultural Force The city is here perceived as a force that is shaping the life of the people living in it. In urban societies, it implies that the city is in fact shaping society. This view is due to the study of Wirth's (1938) *Urbanism as a Way of Life* and also of Park's study *The City* (1925). In 1970 Lefebvre has published a

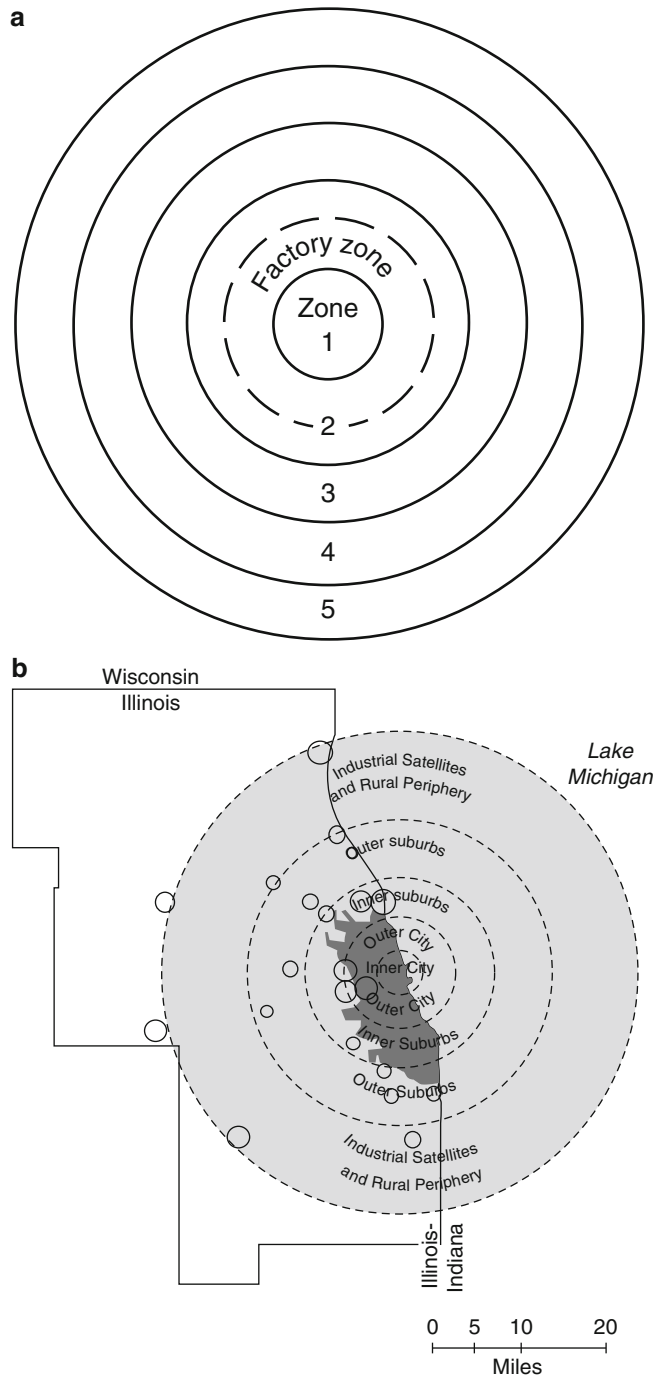

Self-Organization and the City, Fig. 6 (**a**) Burgess concentric zone model. (1) Central business district, (2) zone in transition, (3) zone of working men's homes, (4) residential zone, and (5) commuters' zone. (**b**) Regional differentiation of Chicago as commonly presented in several geographical textbooks (Source: Portugali 2000)

monograph *La Révolution Urbaine* suggesting from a Marxist point of view that society is reaching a stage of being completely urban so that urbanism is replacing industrialism as the major force of society (Lefebvre 1970).

The Postmodern City The city of the twenty-first century is described as the postmodern city (Portugali 2000): untamed, shrew, capricious, and ever-changing; actually it is not a city but a text written by millions of unknown writers, unaware

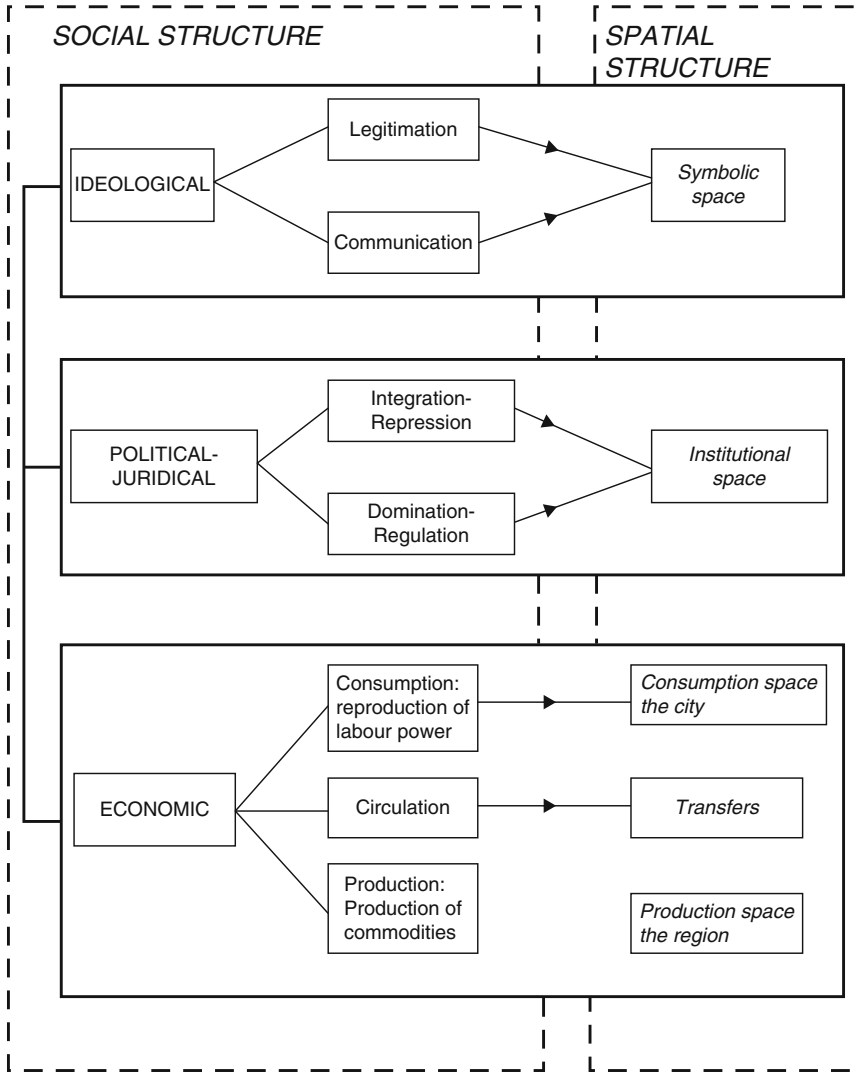

Self-Organization and the City, Fig. 7 The Marxist city as a spatial representation of social structure (Castells 1977) (Source: Gregory 1994)

that they are writers, read by millions of readers, each reading his or her own personal and subjective story in this ever-changing chaotic text, thus changing and recreating and further complicating it. Today's urbanism is a big "theater" at the center of whose stage we see a kaleidoscope of shapes, forms, high-tech science-fiction structures, cultures and subcultures, Italians, Chinese, Japanese, Jews, Indians, Gays, Lesbians. Yapese; nothing is stable; nothing is true nor matters for more than a second, not the Marxist urban categories, nor any other grand theory or truth; all must go, must move, and clear the way to the new next whatever it is.

The Self-Organizing City Strangely enough, an image of the city similar to the postmodern one is emerging out of complexity studies of cities. This is a seemingly similarity; however, a closer look reveals, first, that theories of complexity made a direct and explicit link to the views of cities as central places, to the studies on systems of cities, and to the ecological views on the city. Second is

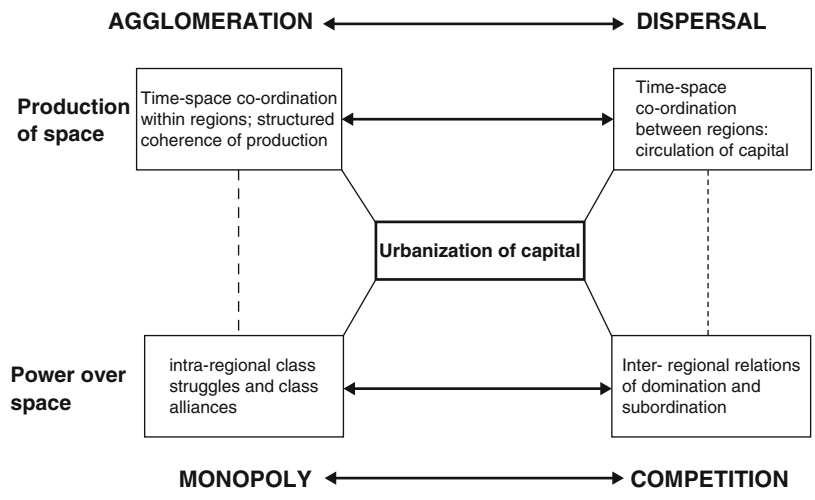

Self-Organization and the City, Fig. 8 The Marxist city as an outcome of basic tensions in the landscape of capitalism (Harvey 1985) (Source: Gregory 1994)

that the notion of self-organizing city has several important resemblances with modern social theory-oriented urban studies that perceive the city as the representation of society.

In What Sense Are Cities Self-Organized Systems?

Self-organization is a property of systems that are open and complex. No one plans such systems, no one fully controls them and yet they have order, rules, and organization, and all these emerge spontaneously by means of self-organization. A nice example of self-organization is provided by human languages (Chinese, Hebrew, English, etc.). Each such language is an open system; each is a complex system; each is a system that emerged out of synergetic interaction between a huge number of people (the "parts" of such systems); no one has ever fully controlled languages; no one has fully planned a language; and yet each of the human languages has order, rules, and organization, and all these emerged spontaneously by means of self-organization.

Similarly to human languages, each city is an artifact; each is an open system; each is a complex system; each city is a system that emerged out of interaction between a huge number of people; no one fully controls it; and yet it has order, rules, organization, and all these spontaneously by means of self-organization.

But cities are not languages. For one thing, their products are stand-alone objects such as buildings, roads, bridges, etc. that exist and survive independently of their producers. The products of languages are humans' voices and gestures that have no existence independent of their producers. Cities, in this respect, are akin to writing and texts – the external, stand-alone, representations of languages. The appearance of cities, some 5,500 years ago, hand in hand with writing, is, to my mind, not accidental.

A second difference concerns planning and design: There are no language planners, and the attempt to "plan" the international language of Esperanto ended in failure. But there are many city planners and designers – much more than appreciated in conventional planning theory. This is so because as recently suggested (Portugali 2011), planning is a basic cognitive capability of humans with the implication that each agent operating in the city (person, family, company) is a planner on a certain scale. In certain cases, because of the nonlinearities that typify the complexity of cities, the planned or designed action of a single individual might influence the city more than that of the official planners and their plans. Urban dynamics can thus be seen as an ongoing interaction between planners and their plans when none of them can fully determine the final form and structure of the city. They are all *participants* in a big city planning game (see Part III in Portugali 2000, 2011).

The Inconsistency Between Self-Organization and Planning

All theories of cities were associated with city planning. The basic idea is that the city is an

artifact and as such a product of humans' intentions and needs. Planning is needed in order to implement human needs and intentions in a rational way. The notion of complexity suggests that the city is a product of spontaneous self-organization; if this is so, who needs city planning? The answer to this inconsistency has already been given above: the plans produced by city planners, like those produced by "ordinary" urban agents, are *participants* in a big city planning game.

Complexity Theories of Cities: An Overview

The discussion in this section proceeds under the titles of eight "cities" that are related to general theories or specific methodologies. It starts with "dissipative cities" to indicate that Prigogine's was the first complexity theory applied to the study of cities.

Dissipative Cities

In their introduction to *Self-Organization in Non-equilibrium Systems*, Nicolis and Prigogine (1977) use the example of a city as a metaphor to convey to their fellow physicists what they mean by "self-organization."

> "An appropriate illustration would be a town that can only survive as long as it is a center for inflow of food, fuel . . . and sends out products and wastes."

Peter Allen (1981) – Prigogine's student – showed that towns and cities are not just metaphors, but genuine self-organizing systems. He did so by reformulating *central place theory* (above section "Images of Cities") in terms of Prigogine's theory (Note the resemblance between the hexagonal landscapes of *central place theory* and the hexagonal Bénard cells – one of the canonical experiments of the paradigm of self-organization).

Allen and co-workers' have developed a sequence of several models which elaborated their theoretical treatment of hierarchical landscapes of central places, first, with respect to systems of cities in a given region and later at the intra-urban scale in connection with a single city. At a later stage, they have also applied their models to real case studies of Brussels and the Belgian provinces (Sanglier and Allen 1989), see also (Prigogine 1980).

A typical model of Allan's starts with an infrastructure of localities in a region, each with its residents and jobs. The actors are individuals who migrate in order to get employment and employers who offer or take away jobs depending on the market's situation. The migration/interaction between localities and the introduction and extraction of economic activities (i.e., employment opportunities) create for each locality a kind of local "carrying capacity" and for the system as a whole nonlinearities and feedback loops which link population growth and manufacturing activities. An example for a simulated scenario produced by the model is Fig. 9. It starts (Fig. 9a) with a hypothetical region characterized by a rectangular lattice of homogeneous localities. Then, the mere play of chance factors, such as the place and time where different enterprises and migrations start, produces symmetry breakings which entail an uneven distribution of population, employment, and so on (Fig. 9b–d). The result is an evolutionary process by which new urban centers emerge, grow, and form the whole of the regional system of central places; as the system evolves, some old localities grow and others decline or even disappear, thus constructing the specific history of this region.

Allen and co-workers' approach exposes the similarity and difference between the "old" static approaches of Christaller and Lösch and the new treatment by means of self-organization. In both, economic activities and interactions give rise to cities as central places. However, while in the old formulations, the landscape reflects an equilibrium state which is the optimized sum of the properties of the various economic forces, the new landscape reflects a far-from-equilibrium situation in which the spatial hierarchical order among the central places is obtained, maintained, and then transformed, by means of interplay between interaction, fluctuations, and dissipation.

Synergetic Cities

Two main approaches of synergetics have been applied to the study of cities. The first is the master-equation approach that is a characteristic of Weidlich and co-workers studies in sociology,

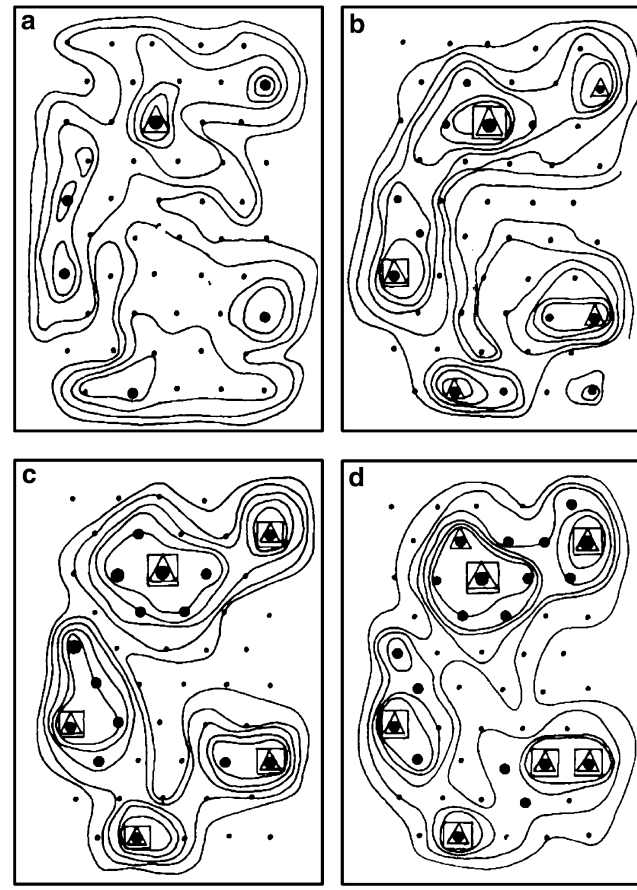

Self-Organization and the City, Fig. 9 Allen and Sanglier's simulated evolution of a dissipative system of cities (**a**) at time (t), $t = 4$, (**b**) at $t = 12$, (**c**) at $t = 20$, (**d**) at $t = 34$

economics, and urban dynamics (Weidlich and Haag 1983; Weidlich 1987, 1994, 1999). For many years, this was the main synergetic approach to cities, and most applications thus far have been within this conceptual frame (Haag et al. 1992; Pumain et al. 1987; Sanders 1992). The second, the pattern recognition approach, typifies the synergetics' treatment of pattern formation, cognition, pattern recognition, and brain activities, as developed in the last three decades by Haken and co-workers (1996). Since the 1990s, this approach has been applied to the study of cities as self-organizing systems (Haken and Portugali 1995; Portugali 2000, 2011).

Slow Cities and Fast Regions

One way to look at Haken's synergetics and its slaving principle is in terms of interplay between slow and fast processes:

> If in a system of nonlinear equations of motion for many variables these variables can be separated into slow ones and fast ones, a few of the slow variables . . . are predestined to become "order parameters" dominating the dynamics of the whole system on the macro-scale. (Weidlich 1999)

This perspective stands at the basis of Weidlich's and co-workers studies on socio-dynamics and cities (Weidlich and Haag 1983; Weidlich 1987, 1994, 1999). According to this perspective, fast and slow processes are easily identifiable in processes of settlement and urbanism. The fast ones typify the local micro-level of building sites, streets, subways, etc., whereas the slow processes typify the macro-level of whole regions which are often described as systems of cities. The relations between the slow and the fast processes are described by the slaving principle: on the one hand, the regional system

> serves as the environment and the boundary condition under which each local urban microstructure evolves. On the other hand, the . . . regional macrostructure is . . . the global resultant of many local structures. (Weidlich 1999)

This circular causality between the local and the global allows one to study global regional systems by assuming that local processes adapt to the slow regional ones and to study local urban processes by treating the regional context as given and of course to study the complex interplay between the local and the global. In all three cases, Weidlich has prescribed a four stages approach: stage 1 concerns the configuration space of the variables; stage 2 measures the utility of each configuration; stage 3 defines transition rates between configurations which are in fact utility differences; stage 4 derives stochastic or quasi-deterministic evolution equations for the system under consideration. The central evolution equation is the master equation which defines the probability that the configuration under examination is realized at a certain time.

The above theoretical procedure has been used to study the role of population pressure in "fast and slow processes in the evolution of urban and regional settlement structures." Figure 10 brings some results from these studies, in which the city capacity for building and development is related to population pressure. Figure 10a shows the evolving city capacity when the urban plain is uniform and Fig. 10b, when it is disturbed in one of its sites.

Pattern Formation and Pattern Recognition in the City

The paradigm of pattern recognition was derived by an analogy to the material process of pattern formation (Haken 1991). Haken and Portugali suggested that the synergetic pattern recognition paradigm is specifically attractive for the study of cities (Haken and Portugali 1995). The latter can be perceived as self-organizing systems which are both physical and cognitive: individuals' cognitive maps determine their location and actions in the city, and thus the physical structure of the city and the latter simultaneously affect individuals' cognitive maps of the city. In their preliminary mathematical model, Haken and Portugali construct the city as a hilly landscape which is evolving, changing, and moving as a consequence of the movement and actions of individuals (persons, families, households, firms, etc.). The latter give rise to the order parameters which compete and enslave the individual parts of the system and thus determine the structure of the city. The new feature of this exposition is that the order parameters enslave and thus determine two patterns (Fig. 11): one is the material pattern of the city, and the other is the cognitive pattern of the city – its cognitive map(s).

Chaotic Cities

Self-organization is often regarded as a theory about *Order Out of Chaos* (Prigogine and Stengers 1984), and yet, with a few exceptions (Dendrinos and Sonis 1990; Portugali 2000), chaotic behavior is rarely studied in cities. Most complexity studies of cities perceive cities as ordered structures which the theory of complexity explains just how their order state was created. According to Batty (see p. 29 in Batty (2005)), this is "because the required growth rates [for chaotic behavior to appear in cities] are far too large." My view is that this is due, firstly, to the tendency of most students of complexity to focus on the short-term dynamics of Western cities from which perspective cities are indeed structurally stable. However, when the focus of interest turns to the long-term rural-urban migration process in a country such as China or to the archeological record of the rise and fall of urban cultures (Portugali 2000; Portugali and Alfasi 2008), chaos suddenly appears. Looking at this *longue durée* (Braudel 1993) of cities, their evolution exhibits a very distinct and routinized path: a long period of "steady state," followed by a short period of strong fluctuations or chaos, from which the system reemerges to a new level of steady state and structural stability and so on (Fig. 12). As can be seen, the urban system moves from one structurally stable state to another, via bifurcations, when every evolutionary move is a transition from a microscopic chaotic state to an ordered, macro, steady state.

Secondly, this is due to the fact that phenomena of chaos and their role in cities during their short-term structurally stable periods have not as

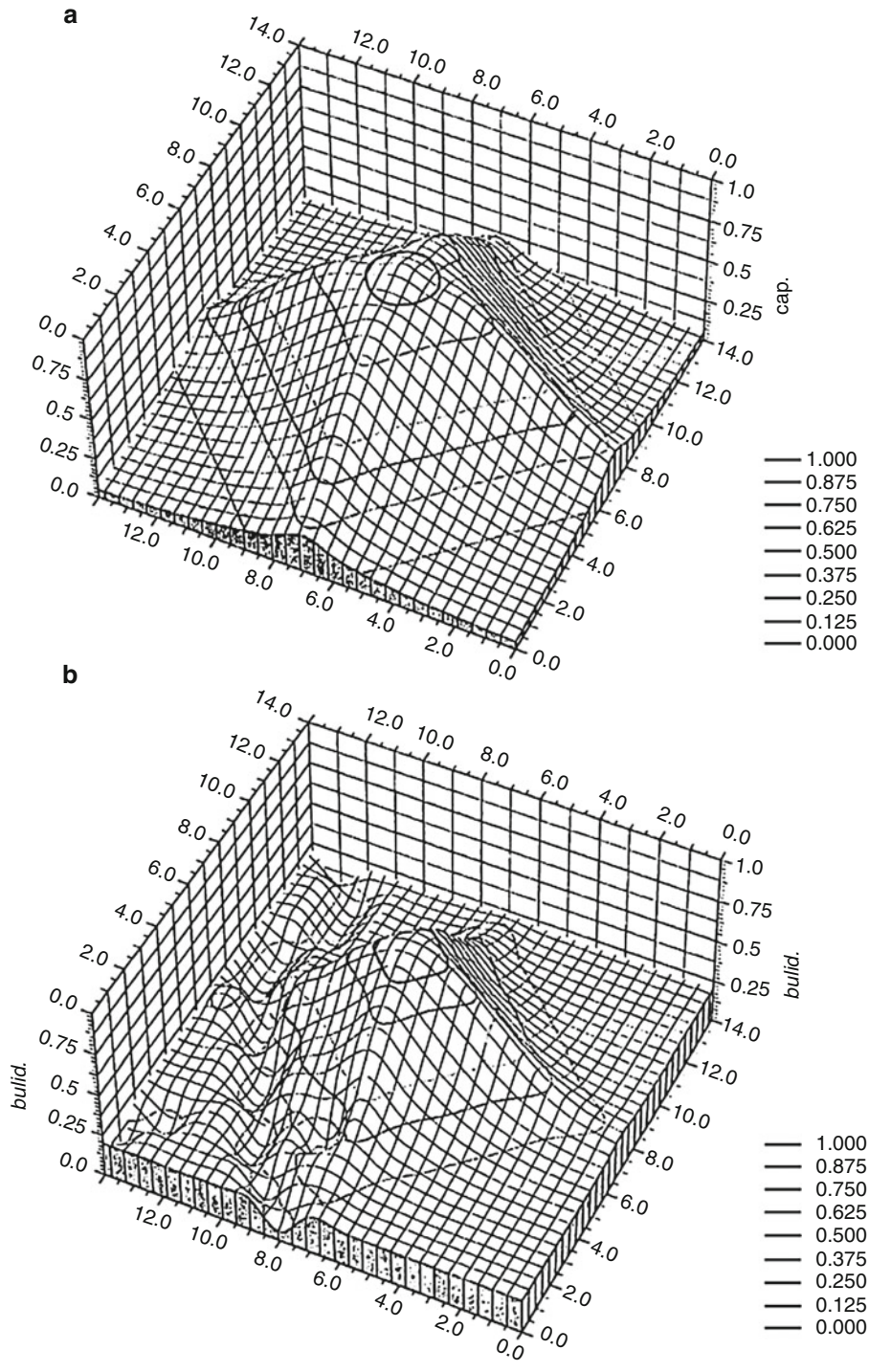

Self-Organization and the City, Fig. 10 Building and development under population pressure (Weidlich 1999). (**a**): on a uniform urban plain. (**b**): on an urban plain with disturbances

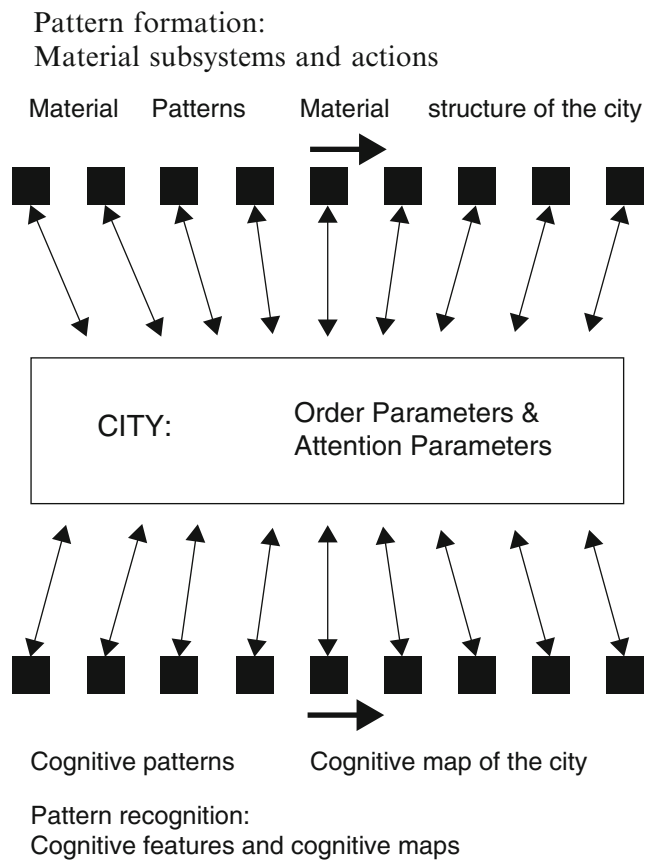

Self-Organization and the City, Fig. 11 The city as self-organizing systems which is at the same time both physical and cognitive. Its emerging order and attention parameters enslave the city's cognitive and material patterns (Source: Portugali 2000)

yet been fully studied. In a preliminary attempt to do so, it has been found that often, when the city as a whole evolves stably, a few local unstable chaotic areas are found captive within the otherwise stable city. This phenomenon has been termed *the captivity principle* with the suggestion that it might play a supplementary role to Haken's slaving principle (see Chap. 5.8 in Haken and Portugali 2015; Portugali 2000), namely, that these local islands of instability are needed in order to maintain the overall global stability of the city. Figure 15 below provides a hypothetical example simulated by means of cellular automata.

The play between chaos and order might show up also in the daily routines of cities. The movement of cars on the roads, or of pedestrians on pavements, is characterized by shifts between instable and stable motions and might thus be candidates for this kind of interpretation.

Fractal Cities

Mandelbrot's theory of fractals is based on the notions of *self-similarity* and the *fractal dimension* and on the idea that a rather simple iterative process might produce highly complex geometrical shapes. Using these principles, several scholars have demonstrated, first, that the complex geometries of urban form, growth, and evolution, on intra-urban and interurban regional scales, can be generated by means of a simple iterative process with a few and simple rules. Second, that many urban structures are self-similar and have fractal structure. The most comprehensive study in this domain is Batty and Longley's (1994) *Fractal Cities*, to which one can add studies on urban structure, on the fractal structure of transportation networks (Benguigui 1995), on the question "when and where is a city fractal?" (Benguigui et al. 2000) and more (for updated survey of studies, see Batty (2005)).

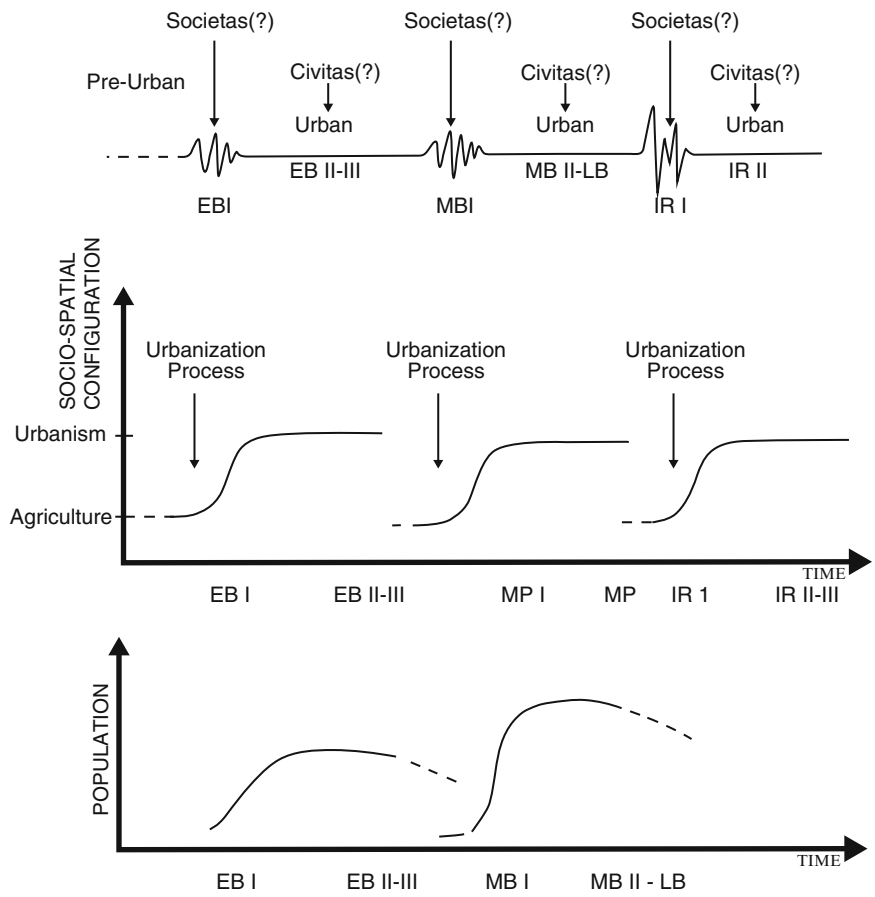

Self-Organization and the City, Fig. 12 The evolution of the settlement system in Palestine from the Early Bronze Age period to the Iron Age (Source: Portugali 2006a). *Top*: A description in terms of chaos and order. *Middle*: A description of the process as a rhythm between agriculture and urbanism, interrupted by global collapses of the urban system. *Bottom*: Calculated population changes in the Early Bronze and Middle Bronze periods (Source: Portugali 1994, 2000)

Figure 13 illustrates the evolving fractal structure of the Tel Aviv metropolitan area from 1935 onward.

Another important insight implied by fractal cities studies is that a city, or a system of cities, in a steady state does not mean equilibrium and stability, as is the case of Christaller's and Lösch's central place theories, for example, but rather a rich and complex evolution and change according to a given ordering principle.

Cellular Automata Cities

The attraction of cellular automata (CA) models to the study of cities is almost self-evident. Real cities are built of discrete spatial units such as houses, lots, city blocks, and the like. CA models are also built of discrete spatial units – the cells. In real cities, the properties of local spatial units (e.g., land value) are determined, to a large extent, in relation to their immediate neighbors; so are the properties of the cells in CA models. These resemblances, together with the mathematical simplicity of CA models, make them natural tools to simulate urban processes. In the last few years, CA urban simulation models are among the most popular approach to simulate the dynamic of cities (Batty 2005; Benenson and Torrens 2004; Portugali 2000).

One can divide the various models of CA cities into implicit and explicit self-organized CA cities. The first group refers to studies, the aim of which

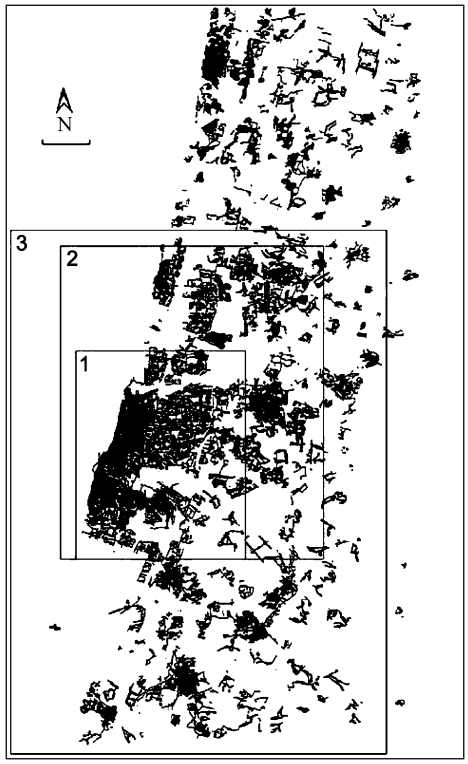

Self-Organization and the City, Fig. 13 The evolving fractal structure of the Tel Aviv metropolitan area from 1935 onward: the central parts 1 and 2 were fractal during the entire period, while their fractal dimension increased with time. The entire metropolitan area became fractal only after 1985. In 1991 the fractal dimension of the Tel Aviv metropolitan area was found to be 1.667 with error of 0.037 (Source: Benguigui 1995)

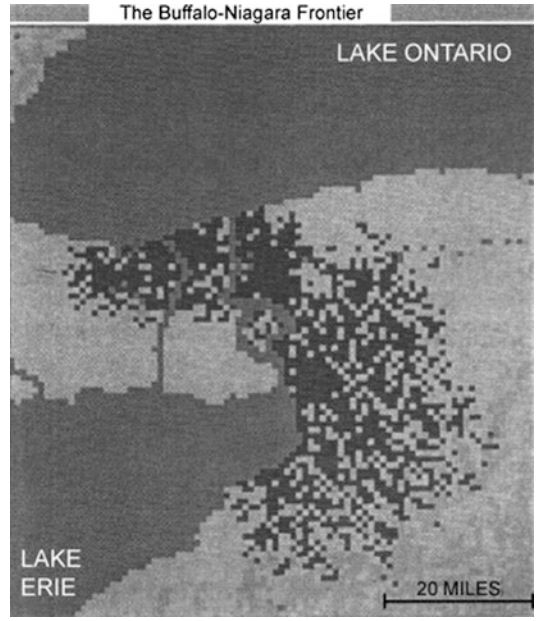

Self-Organization and the City, Fig. 14 Cellular automata simulation of the Buffalo-Niagara frontier (Source: Batty 1997)

is to use the simulation capabilities of the CA city in order to best-fit a certain simulated pattern to an existing one (Batty 2005). Figure 14 is an example. The general motivation here is to explain an existing or historical pattern, or alternatively to predict a future one for the purpose of planning. The fact that the model has properties of self-organization just adds more realism and sophistication to the simulation.

The second group concerns explicit self-organized CA cities. Here the central motivation is to use the model as means to investigate the self-organization properties inherent in cities and urbanism. For example, how micro decisions and behavior of individuals and firms, taken at the local scale, are related to the global behavior and structure of the city. Such models are essentially heuristic, and they regard the simulated CA city as essentially a learning device (Fig. 15).

Because of their iterative structure, CA models can be used as convenient tools to generate fractal structures (Batty 1997, 2005), and the insight they add to our understanding of cities is similar: an iterative process guided by a few simple rules can generate complex structures such as cities (Batty 2005).

AB and FACS Cities

CA is an efficient tool to model the relations between infrastructure objects of the city. Unlike infrastructure object, urban agents have aims and plans, can learn and move in the city, and see and know beyond their nearest neighbors. *Agent base* (AB) models that are built to imitate such cognitive entities were applied to the city dynamic too. An important source of inspiration here was Schelling's model that demonstrated how local and simple behavior of urban agents can give rise to complex residential segregation in cities – even when their tendency for segregation is minimal (Schelling 1974).

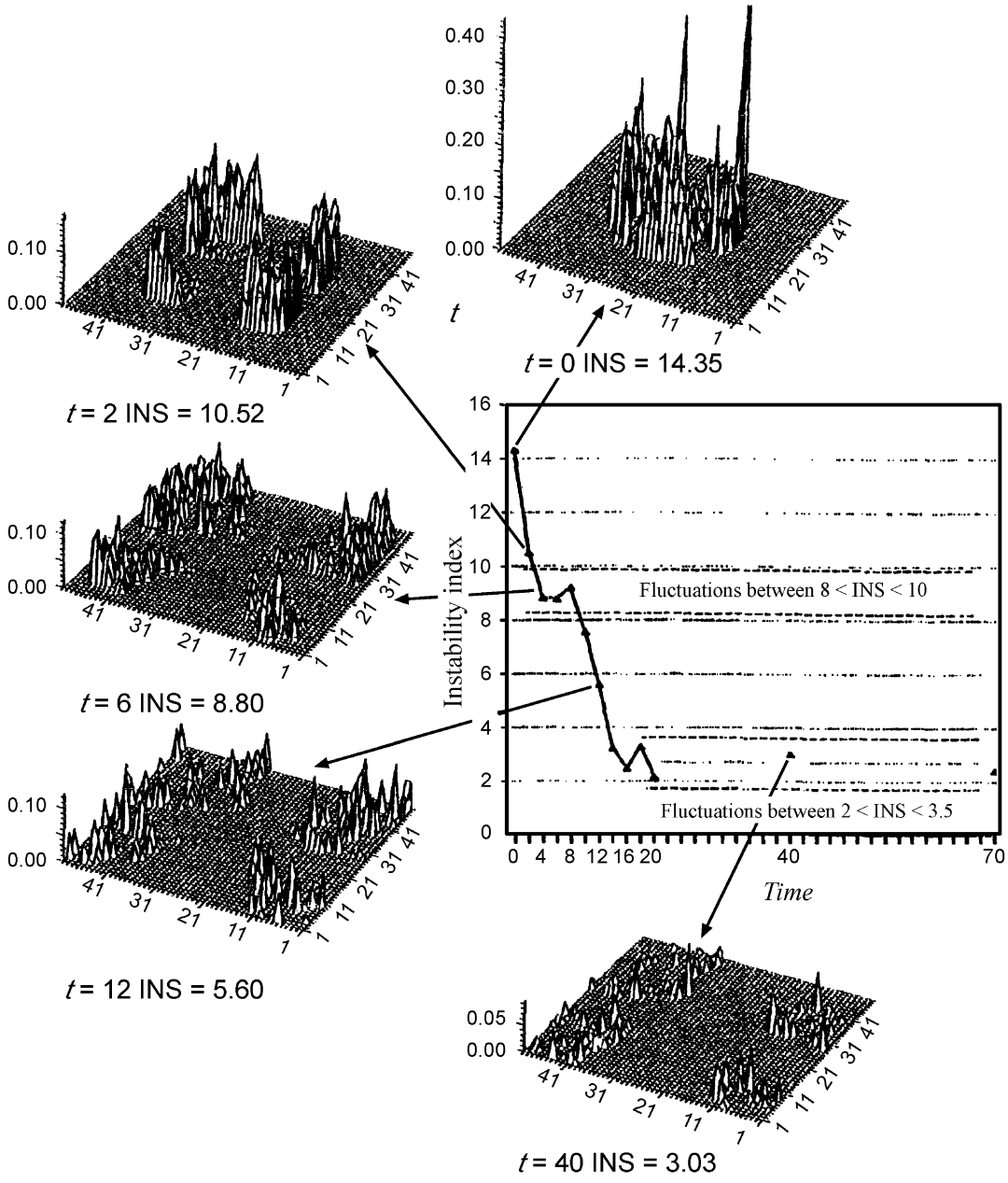

Self-Organization and the City, Fig. 15 Time evolution of consecutive stages of stability-instability surface (SIS) in the development of a city with 33% neutral Greens when the rest of the Greens and all the Blues are segregatives (Source: Portugali 2000)

Subsequent agent base studies have supported Schelling's finding (Batty 2005) and added that a small minority of agents with a tendency for segregation is sufficient to turn the whole city into a segregative structure (Portugali 2000).

Free agents on a cellular space (FACS) models combine CA and AB models (Portugali 2000, 2011). A typical such model is built as a superposition of a CA layer simulating the relationship between the city's infrastructure objects (buildings,

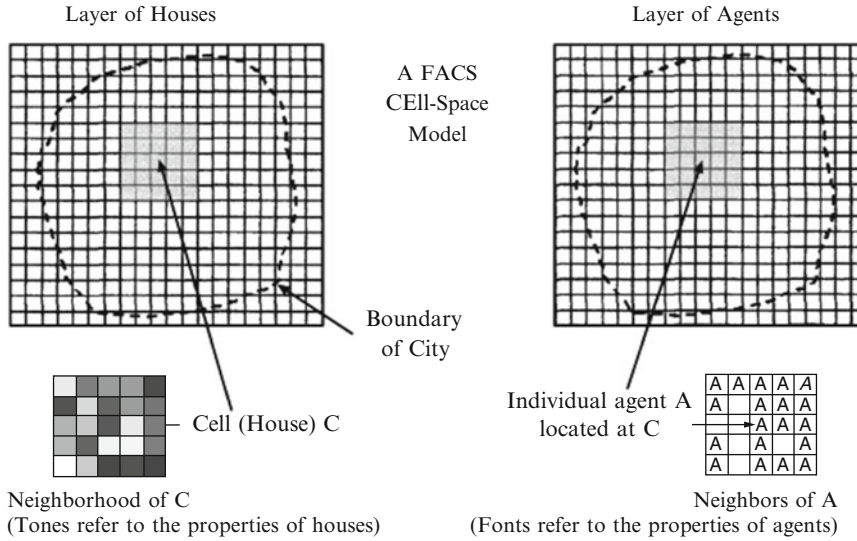

Self-Organization and the City, Fig. 16 A typical FACS model is constructed of two layers: a population layer of human agents describing the migratory and interaction activities of individuals (*right*), superimposed on a CA infrastructure describing the urban landscape (*left*) (Source: Portugali 2000)

roads, etc.) and AB layer that simulates the activities of the urban agents (Fig. 16). At each model iteration, new agent(s) come to the city with a certain intention in mind – say to find a house to live in. The agent then examines the available empty cells/buildings, ranks them according to its set of preferences, and picks the best one. Once the agent located itself in a certain cell, the CA dynamics starts: The properties of each cell are determined by reference to the properties of its neighbors and if the cell is occupied by a certain agent, by some mix between the properties of the agent and its neighbors. Figure 17 presents typical results.

Sandpile Cities

The sandpile, the canonical example of *self-organized criticality* (Bak et al. 1989; Bak and Chen 1991; Batty 2005; Batty and Xie 1999), has two incongruous features: the system is unstable in many of its local locations; nevertheless, its global state is absolutely robust: The local configurations of the sand change all the time because of the avalanches, while the statistical properties, such as the size distribution of the avalanches, remain essentially the same. Similarly to the sandpiles, cities appear volatile and fast moving at their local scales, while at their global scale, they appear absolutely robust (Batty 2005; Batty and Xie 1999). For example, the size distribution of many cities and systems of cities remains essentially the same under circumstances such as ongoing population growth (above section "Image of Cities").

Compared to the "grand" synergetic and dissipative cities, the sandpile city is a kind of a zooming in to the internal dynamics of self-organized cities in their steady state periods – when they are controlled by what in synergetics is called order parameters. Sandpile cities show how complex and rich is the internal dynamics of a city in steady state (Fig. 18).

Small World Cities

The notion *network* is implicit in all theories of complexity. Recently, Watts and Strogatz (1998) showed that complex networks have "small world" characteristics (Milgram 1967), and Barabasi and Alberst (Barabási and Réka 1999) demonstrated that complex networks are scale-free, thus following the *power law* that according to Barabási (2002) is a mark of self-organization.

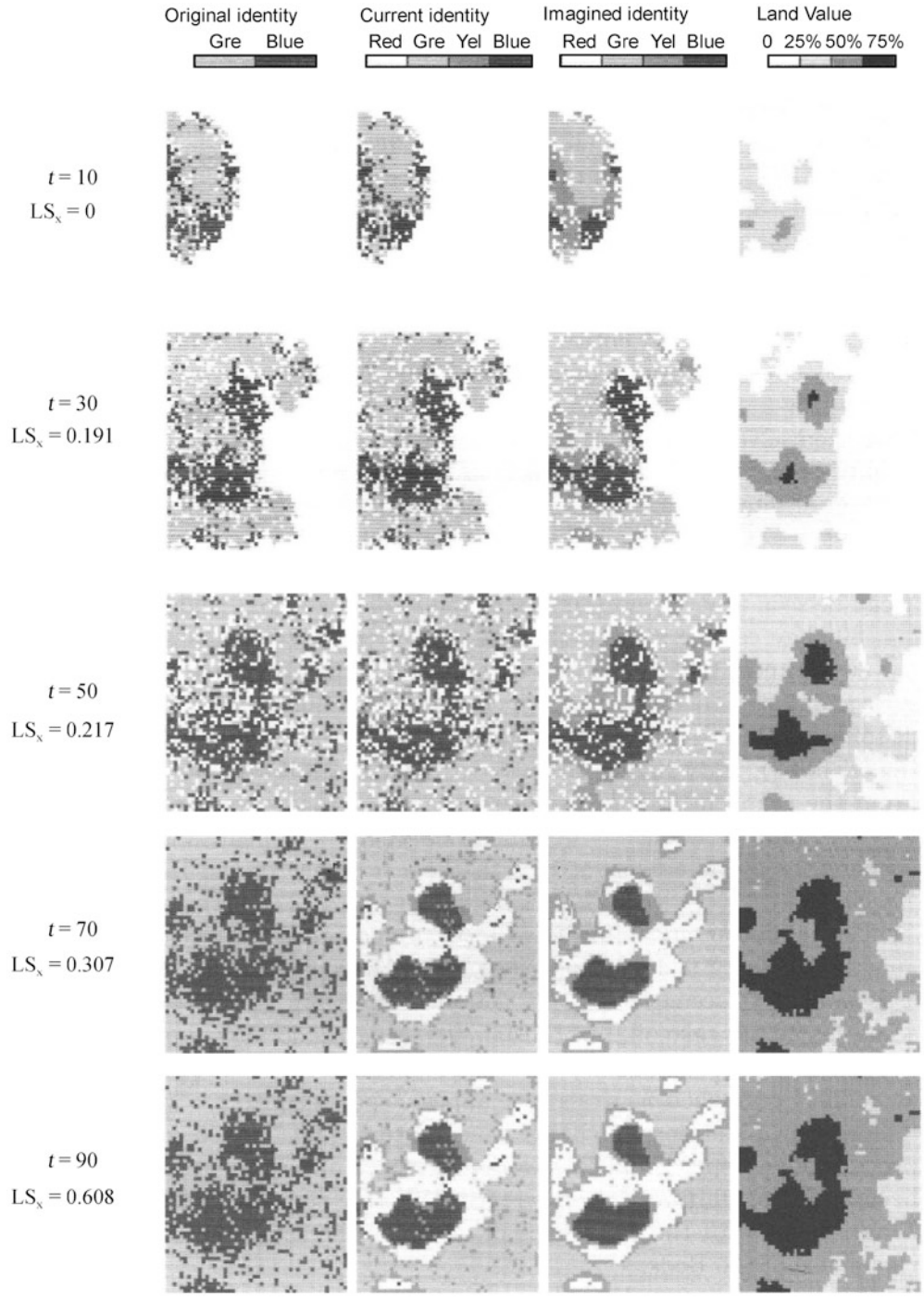

Self-Organization and the City, Fig. 17 Several snapshots from an evolving FACS city (Source: Portugali 2000)

The link to cities as complex systems was just natural: The view of systems of cities as networks characterized by the power law was indicated above. Single cities too were described as networks. Thus, Alexander's classic "a city is not a tree" (Alexander 1965) demonstrated that cities

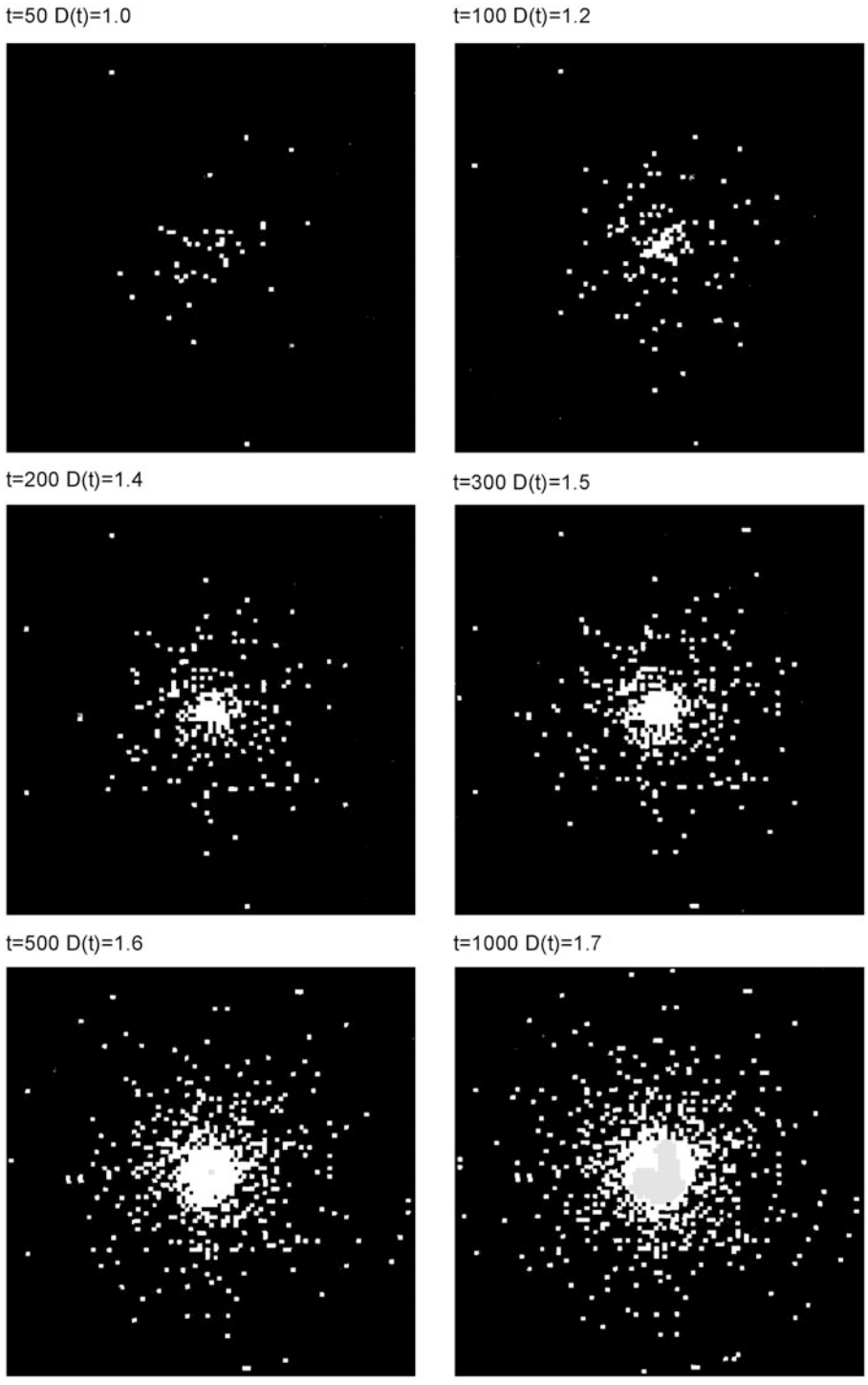

Self-Organization and the City, Fig. 18 Self-organized criticality: "Simulation of a hypothetical urban growth pattern in its critical level" (Source: Batty 2005)

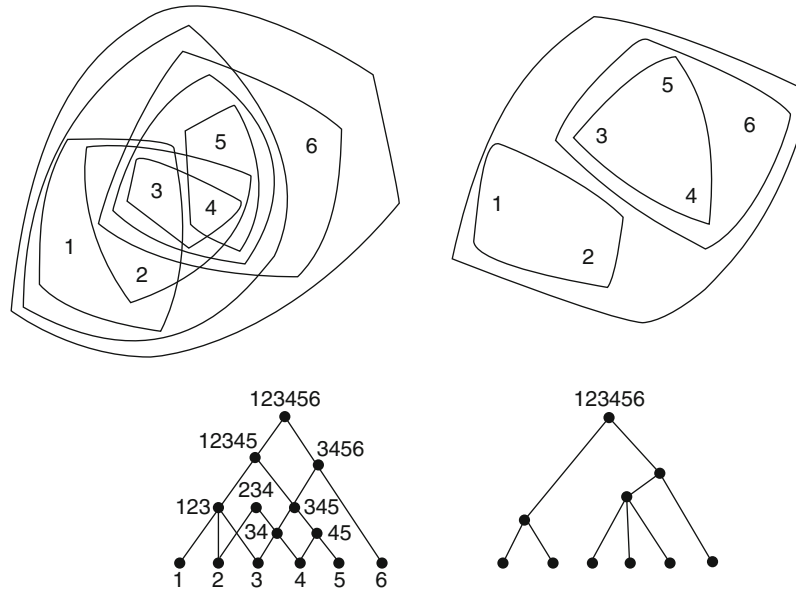

Self-Organization and the City, Fig. 19 A tree network (*right*) versus a semi-lattice network (*left*) (Source: Alexander 1965)

are typified not by a simple *tree network*, but by a complex *semi-lattice network* (Fig. 19). Alexander's view was recently reformulated in terms of the new science of networks (Salingaros 2005, 2006). Another example is Hillier's *space syntax* that analyzes the morphology of urban spaces in terms of networks (Hillier 1999; Hillier and Hanson 1984). Space syntax exposes the way society determines the urban morphology and the way the latter feeds back and reshapes society. The link between space syntax and network analysis has already produced several useful results (Dalton et al. 2003; Figueiredo and Amorim 2005; Hillier and Iida 2005; Porta et al. 2005; Ratti 2004).

In the domain of transportation, one can mention studies that characterize roads' traffic dynamics in terms of scale-free networks (Fig. 20) (Hu et al. 2006; Jiang 2007); the same was found for the transit system in Beijing (Wu et al. 2004), for pedestrian movement (Jian 2006), and for the canal networks of Venice (Blanchard and Volchenkov 2007). Andersson et al. (2003) showed that the market dynamics generates land values that can be represented as a growing scale-free network. Finally, Batty (2005) has suggested viewing cities and their dynamics from the combined perspectives of networks, fractals, self-organized criticality, and AB.

Self-Organization and the City

Self-Organization and the City is an ongoing project that explores the city as a complex system from two interrelated perspectives: Haken's (1983) synergetic theory of complex systems, in particular from the perspective of the pattern recognition paradigm (Haken 1983, 1987, 1993) and IRN – inter-representation nets (Portugali 1996a). The link between the two is termed SIRN – synergetic inter-representation nets. For details and bibliography, see Portugali (2011).

SIRN: Synergetic Inter-representation Networks

IRN commences with a distinction between cognitively *simple tasks* that can be performed by working memory (e.g., $\mathbf{2 \times 3 = 6}$) and *complicated tasks* (e.g., $\mathbf{257 \times 389 = 99{,}973}$) that are the result of the "magic number seven" that constraints our ability to process information in working memory (Miller 1956). One way to overcome this limitation is by means of IRN: We first externalize the task (write it down on a paper); then we solve part of it internally ($\mathbf{9 \times 7 = 63}$); externalize it again and so on in a sequence until the task is completed.

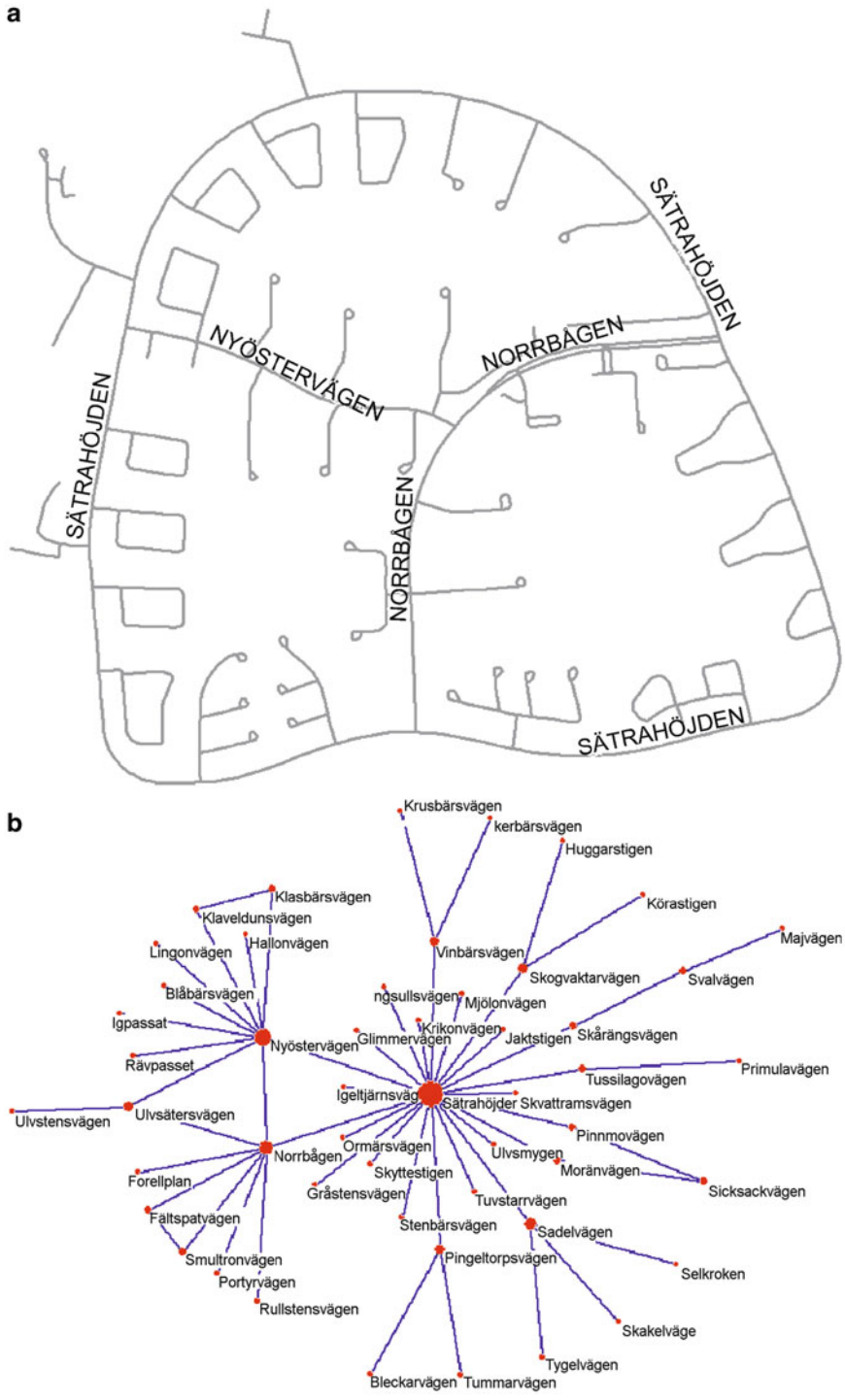

Self-Organization and the City, Fig. 20 A small street network (**a**) and its connectivity graph (**b**). Every node in **b** is labeled by the corresponding street name, and the size of nodes shows the degree of connectivity of individual streets (Source: Jian 2006)

Complex tasks refer to creative cognitive tasks, when a person writes, paints, designs, etc. Such a task often starts with a vague idea in mind that the person then externalizes by writing it down, painting it on a canvas, sketching it on a paper, etc. Here too, the process proceeds by interplay between internal and external representations, but with one important addition – it involves emerging properties. It is here were synergetics gets in and the process becomes SIRN. More specifically, the process might start with a preliminary internal idea (or external cue that entails internal idea) that the person then externalizes and so on. After a few internal-external iterations, an order parameter (in the sense of synergetics) emerges and enslaves subsequent iterations.

The development of the notion of SIRN was inspired by Bartlett's serial reproduction scenarios in his study *Remembering* (Bartlett 1932). A typical such scenario starts when a test person is shown a text or a figure and is asked to reproduce it out of memory (Fig. 21). The result is offered to a second person that is asked to do the same and so on. As shown by Bartlett, at the beginning, the reproductions change from person to person; however, at certain stage, they stabilize and become a *scheme*. Stadler and co-workers (Stadler and Kruse 1990) demonstrated that the scenarios proceed as synergetic self-organized process. The focus of interest in the above studies was on the way schemata are created. Haken and Portugali have used the Bartlett scenarios as illustration of the play between internal and external representations (Haken and Portugali 1996; Portugali 1996a).

It is important to emphasize, first, that external representations are media that enable communication between persons and the emergence of collective SIRNs – e. g., a brainstorm. Second, that internal and external representations are *generative* – once produced, they generate new ideas and properties not seen before in previous representations.

The Basic SIRN Model

Haken and Portugali (1996; Portugali 2011, Chap. 7) have cast the SIRN process into the formalism of synergetics. They started with Haken's (Haken 1991) "synergetic computer" (Fig. 22, *top*), composed as it is of an input layer with model neurons representing the initially given input activity, a middle layer representing the order parameters, and an output layer with neurons representing the final activity of each neuron. The first step is to look at this network from the side, as indicated by the arrow. The result is shown in Fig. 22, *bottom*, *left*. Adding to the latter external inputs and outputs, we arrive at our basic SIRN model (Fig. 22, *bottom*, *right*) that has two kinds of inputs, internal and external, and two kinds of outputs, again internal and external. The middle node symbolizes the order parameters that emerge out of the interaction between internal and external representations.

The basic SIRN model can be seen as symbolizing a self-organizing active agent that is subject to two flows of information: internal and external (Fig. 23). The first is coming from the mind/brain, in the form of ideas, fantasies, dreams, thoughts, and the like, while the second from the "world" – via the senses, the agent's body, and/or artifacts. The interaction between these two flows gives rise to an order parameter that governs the agent's action and behavior, as well as the feedback information flow to the agent's mind. "Action or behavior" may refer to a single individual executing exploratory behavior, reproducing texts or drawing, as well as to several individuals collectively reproducing a large-scale artifact such as a city. In an analogous fashion, the "feedback information flow" refers to the formation of internal representations, such as images or learned patterns. The order parameters are determined by a competition in line with the synergetics' pattern recognition paradigm noted above. Note that all the above steps (and below) can and have been performed by a computer so that the approach is entirely operational.

In order to apply the basic SIRN model to specific case studies, Haken and Portugali (1996) reformulated it in terms of three prototype submodels: the *intrapersonal*, the *interpersonal collective*, and the *interpersonal with a common reservoir* submodels (Fig. 24). The first refers to a solitary agent, the second to a sequential

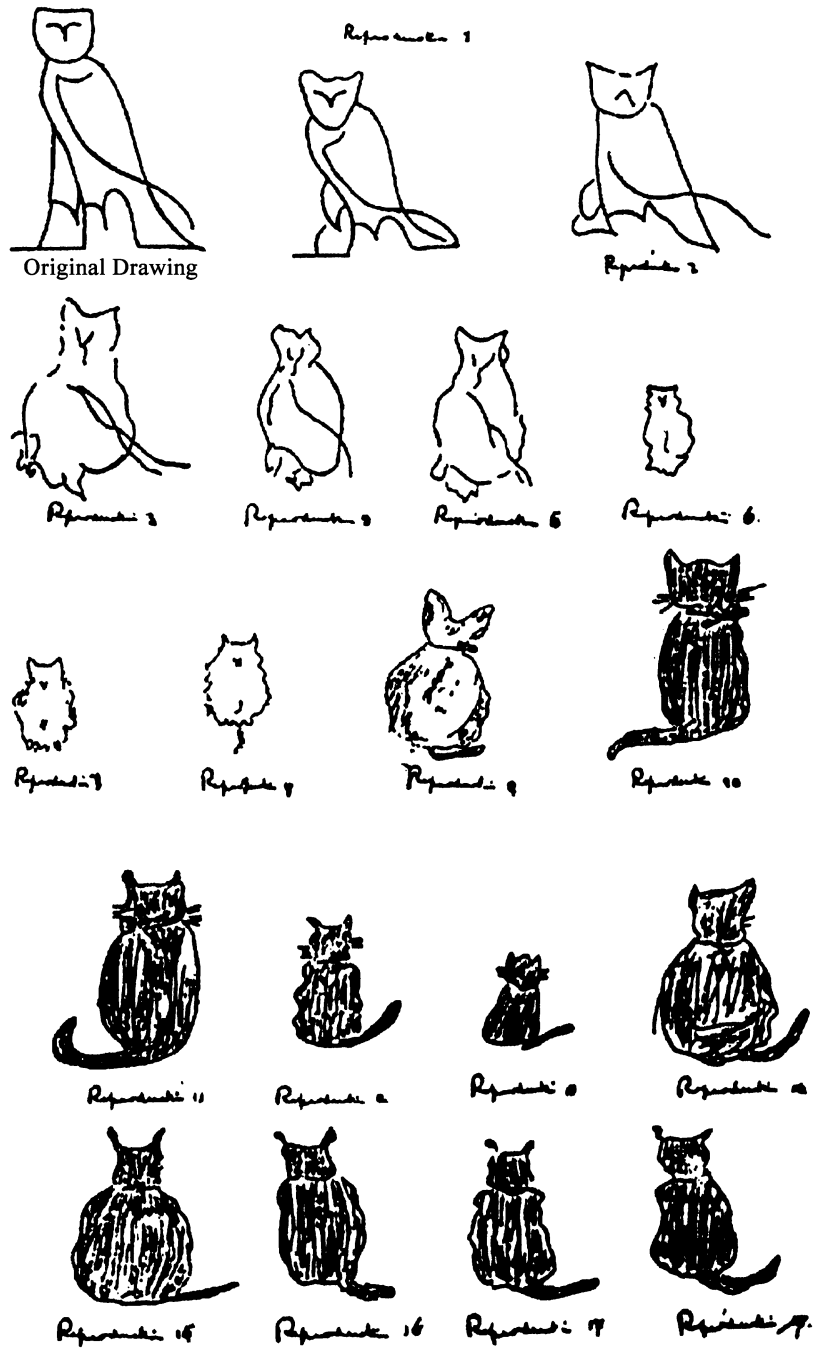

Self-Organization and the City, Fig. 21 A Bartlett's scenario of serial reproduction: an Egyptian "Mulak" (owl) transformed into a cat (see pp. 180–181 of Bartlett (1932))

dynamics of several agents, and whereas the third to a simultaneous interaction. The third submodel is, in fact, a theory of urban dynamic. The intrapersonal is typical to the way of an artist, for instance, develops her/his work (Fig. 25), whereas the interpersonal to the Bartlett scenario that provided a source of inspiration to IRN (above, Fig. 21).

In the first two submodels, the process depends fully on the biological memories of individuals. In

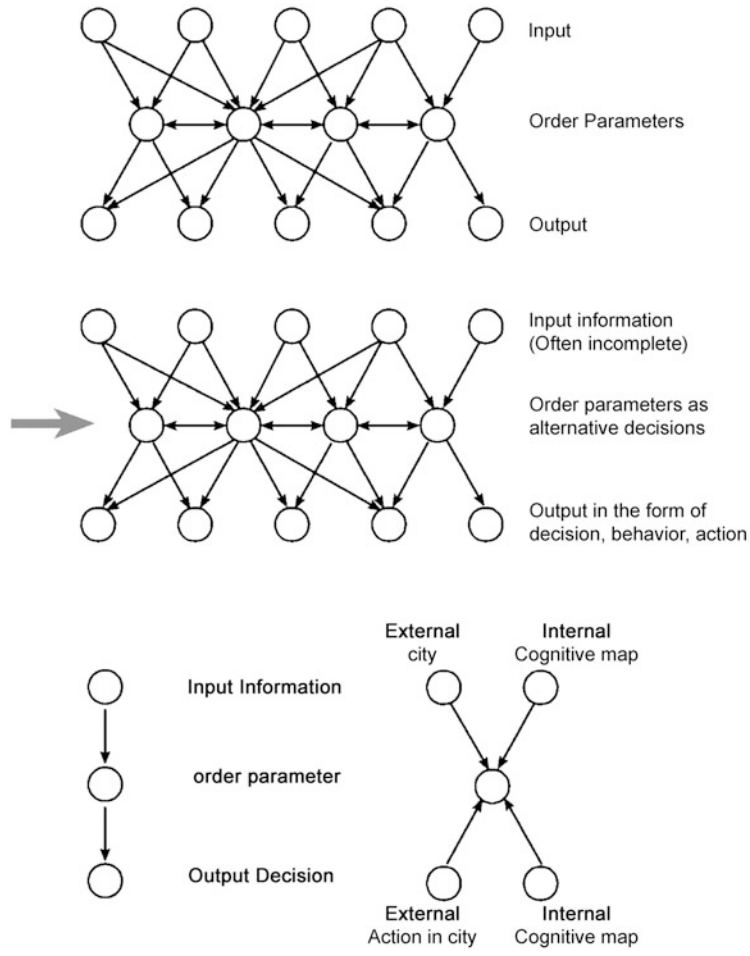

Self-Organization and the City, Fig. 22 The derivation of the SIRN model. See text

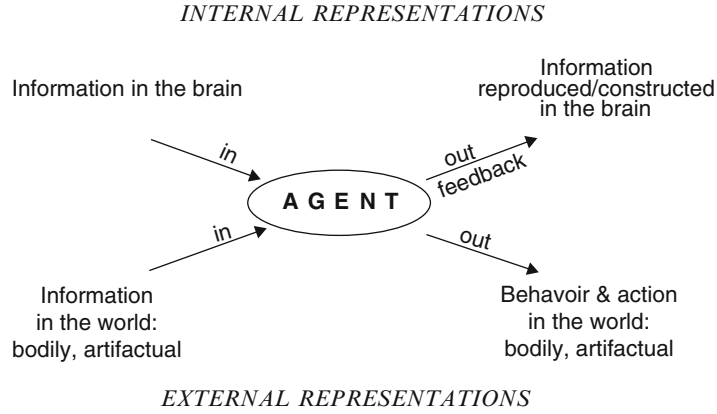

Self-Organization and the City, Fig. 23 The SIRN model symbolizes a self-organizing agent that is subject to two forms of information, internal and external, and is actively constructing two forms of information, again internal and external. Graphically, Fig. 23 corresponds to Fig. 22 (*bottom*, *right*) turned 180° on its NW-SE axis

the third submodel, the process depends partly on biological memories, as before, but partly also on externalized non-biological memory that we term a *common reservoir*. This common reservoir of external, artificial, and non-biological memory might take the form of texts, the Internet, buildings, or whole cities.

Figures 24 (*bottom*) and 26 illustrate graphically this public-collective SIRN submodel. Each individual agent is subject to internal input constructed by the mind/brain and external input which is the legible information coming from the common reservoir, that is, the city. The interaction between these two forms of input gives rise to a competition between alternative decision rules that ends up when one or a few decision rules "wins." The winning rule(s) is/are the order parameter(s) that enslave(s) the system. The emerging order parameter governs an external output, which in the case of a city is the agent's behavior and action in the city, and an internal output, which is an information feedback loop back to the agent's mind/brain.

Both the previous submodel and the present one involve a two-scale self-organization process: an individual local scale referring to each individual agent as a self-organizing system and a collective global scale, referring to the whole city as a self-organizing system. The individual agents by their action and behavior determine the city, which by means of its emerging order parameter(s) enslaves the minds of the individual agents. In the language of synergetics, this process is termed *circular causality*. In terms of social theory, it is close to notions of socio-spatial *reproduction* and *structuration*. Recent applications show that the common reservoir might be a non-biological externalized memory such as a city (Portugali 2000, 2002, 2003, 2004, 2011), a planning textual report or an urban planning policy emerging out of a discourse among the members of a planning team (Portugali and Alfasi 2008). Note that as in the previous model, here too, due to circular causality, as the process evolves, the subjective cognitive maps of the individual agents are becoming more similar to each other, and an inter-subjective, collective cognitive map emerges. Both private-subjective cognitive maps and public-collective ones are thus *constructions*.

The City Game

A simple and effective way to illustrate the SIRN view on the dynamics of cities is by means of a set of experiments termed *city games* (Portugali 1996a, 2011). A city game can be described as a group dynamics that involves some 40 to 70 participants. Their aim is to build a city on a floor, representing the site for a new city. Each player is given a 1:100 mock-up of a building and in his/her turn is asked to locate it in the virtual city on the floor, in what s/he considers as the best location for that building. In a typical game (Fig. 27a, b), the players observe the city as it develops and in the process also learn the spontaneously emerging order on the ground. It is typical in such games that, after a few initial iterations, an observable urban order emerges. The participants internalize this emerging order and tend to locate their buildings in line with it. As can be seen, the main features of such a game are the main ingredients of SIRN, namely, a sequential interplay between internal and external representations, the emergence of a collective complex city as an artifact, and a typical synergetic process of self-organization. Needless to say that the city game is not a 1:1 description of reality, but an illustration of the dynamics of cities as *dual* self-organizing systems.

Cognition and the City

SIRN is at once a theory of cognition, cognitive mapping, and urban dynamics. This emphasis on cognition is a direct consequence of complexity theory; a major achievement of complexity theory was to show how local behavior and interaction between urban agents give rise to the global structure of the city. The agent is thus the main and most important actor. Given this, one would assume that practitioners of complexity theory and urban simulation models will have an elaborated theory of agents' perception, behavior, decision-making, and action, especially so in light of the fact that a whole body of research on agents' behavior was readily available. I'm referring to studies on spatial cognition, spatial behavior, and cognitive mapping that were developed on the interface between cognitive science and urban studies (Golledge and Timmermans 1988; Kitchin and Freundschuh

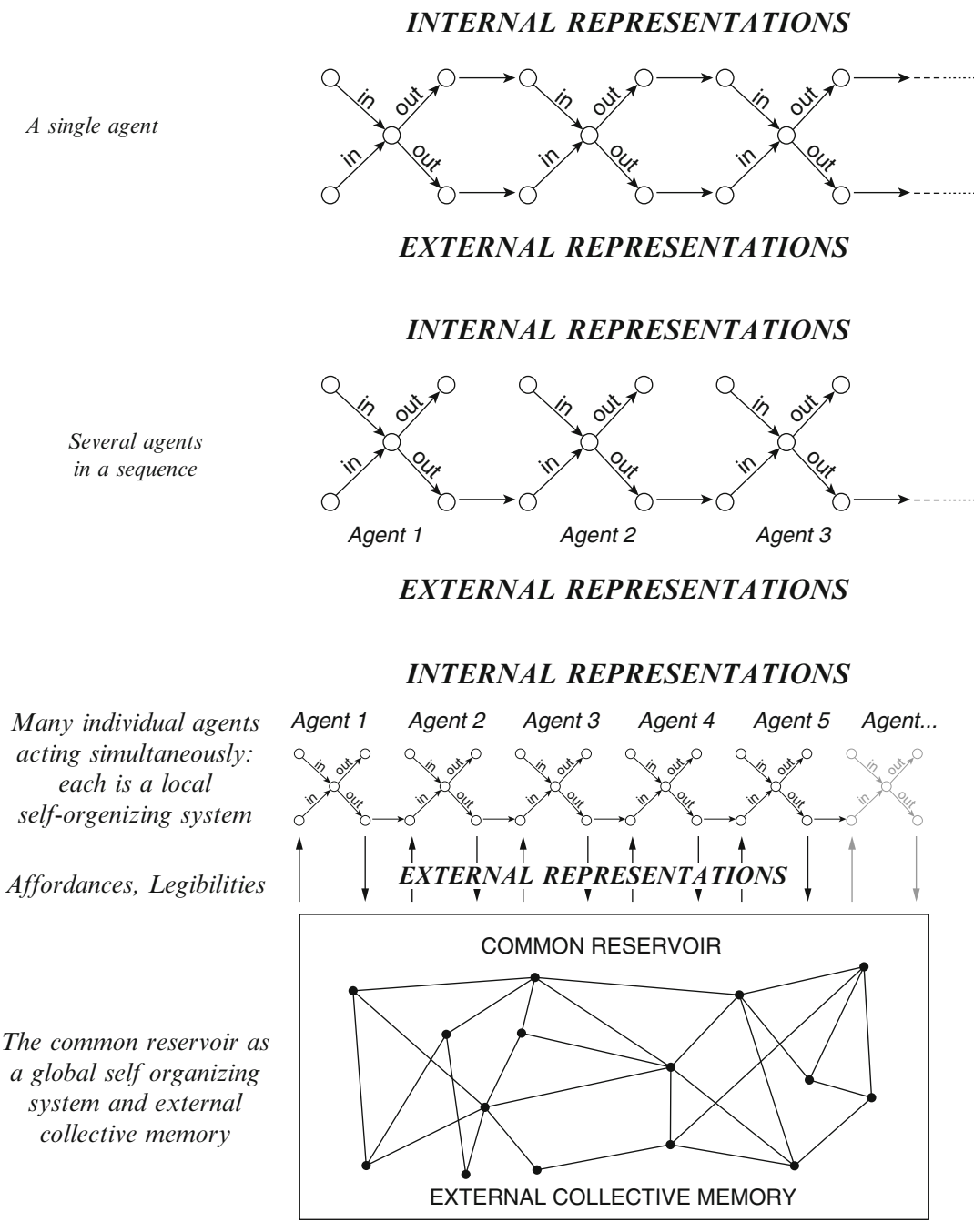

Self-Organization and the City, Fig. 24 *Top*: The intrapersonal SIRN submodel of a single person. *Middle*: The interpersonal submodel, serial reproduction of several persons. *Bottom*: The interpersonal with a common reservoir submodel. Note that in the intrapersonal submodel, information is transmitted via external and internal outputs, in the interpersonal via external output only (action and behavior), while in the third, submodel information and interaction between the agents are mediated by the common reservoir (e.g., a text, a city, the Internet, etc.) (Source: Portugali 2002)

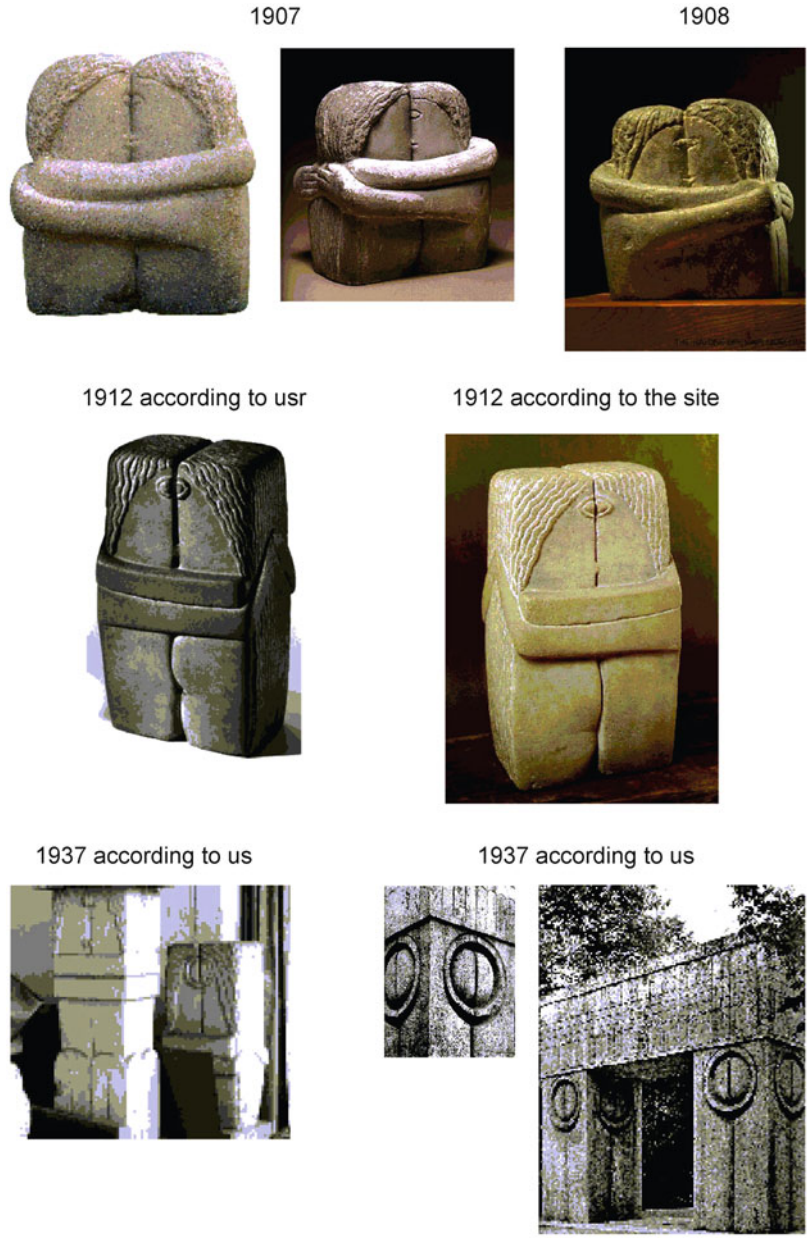

Self-Organization and the City, Fig. 25 "The Kiss" by Brancusi: from a figurative kiss in 1907 to the geometrical "Gate of the Kiss" in 1937, an intrapersonal SIRN process in sculpturing

2000; Portugali 1990, 1996b, 2004, 2005). And yet, with few exceptions such as SIRN, this body of theoretical and empirical studies is largely overlooked by students of complexity theory of cities. Researchers in this field tend to follow economists by assuming that individuals behave in space as simple "economic persons." The result is that the rather *simple* behavior of agents in the models contradicts the *complex* behavior revealed by studies on cognitive mapping and spatial behavior.

In *The Sciences of the Artificial*, Simon (1979) suggested that the observed complex behavior of human agents, guided as it is by aims, plans, intentions, needs, policies and so on, misleads us as it is only an external appearance of innately

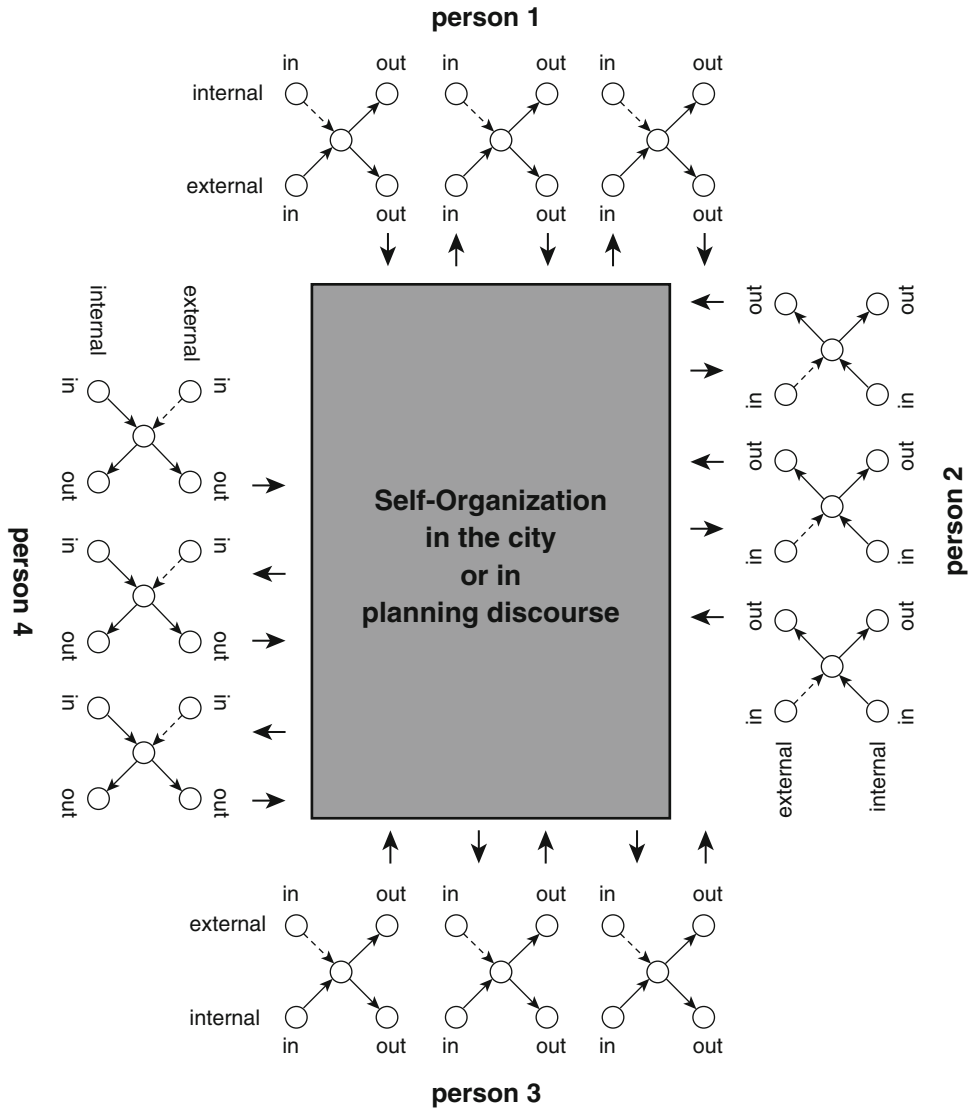

Self-Organization and the City, Fig. 26 Another conceptualization of the public-collective SIRN submodel. Each individual agent is subject to internal input – a cognitive map constructed by the mind/brain and external input – the legible information coming from the common reservoir, that is, the city of a planning team. The interaction between these two forms of input gives rise to a competition between alternative decision rules that ends up when one or a few decision rules "wins." The winning rule(s) is/are the order parameter(s) that enslave(s) the system. The emerging order parameter governs an external output, which in the case of a city is the agent's behavior and action in the city, and an internal output, which is an information feedback loop back to the agent's mind/brain

simple behaving entities: Similarly to simple animals, we humans as

> behaving systems, are quite simple. The apparent complexity of our behavior over time is largely a reflection of the complexity of the environment in which we find ourselves. (ibid. 53)

Most AB/CA urban simulation models are built in line with Simon's logic. They typically start with local interactions between agents having a few simple aim(s) "in mind." This interaction gives rise to an urban system, which from iteration to iteration becomes increasingly complex.

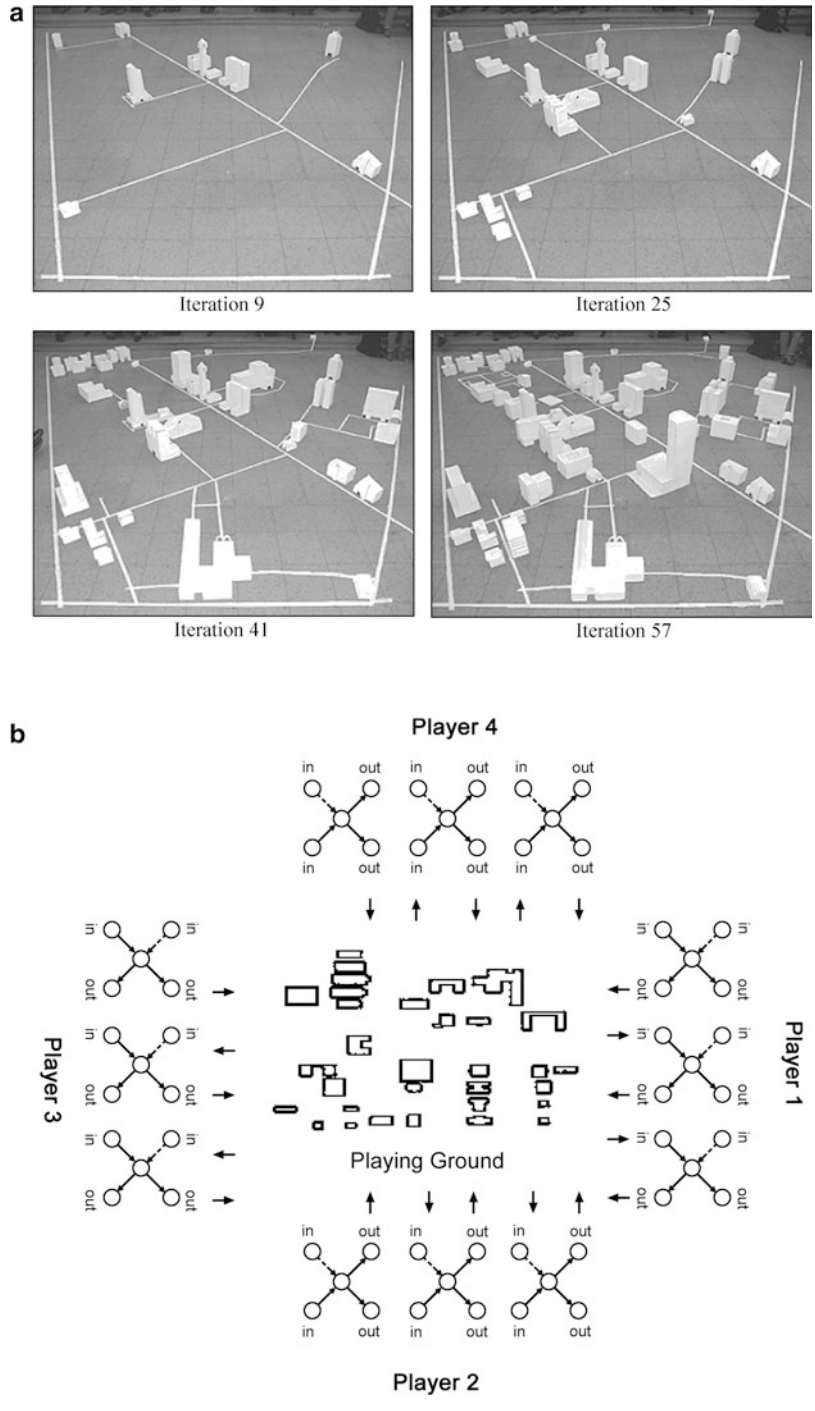

Self-Organization and the City, Fig. 27 (**a**) Four snapshots from a typical city game (at iterations 1, 15, 35, 57). (**b**) A conceptualization of the city game

Complexity is thus understood as a property of the whole global system, but not of its individual parts.

The efficiency of the *simple cause → complex effect* model is apparent. But there is a catch here: Several empirical studies, of animals' and humans' exploratory behavior, for example, falsify Simon's view (Portugali 2002, 2003, 2004). Furthermore, the property of the city as a *dual*

self-organizing system implies that the initial conditions of such complex systems are relatively large numbers of interacting parts, each of which is itself a complex system exhibiting complex behavior. Can there then be a science of cities that is not based on Simon's model? The answer is yes! To see how we shall look at the relations between self-organization and information.

Information Compression, Inflation, and Adaptation

Complexity is a property of systems that exchange matter and *information* with their environment and that their huge number of parts forms networks characterized by complex feedback and feedforward loops that allow intensive flow of *information* inside the system.

The notion *information* is associated with Shannon's theory of information (Shannon and Weaver 1959) that has played a seminal role in the development of system thinking. In Shannon's theory the notion of information is a pure quantity (usually measured by *bits*) devoid of any meaning. Such a concept of information makes sense only in closed systems where the number of possible states the system can take is finite and a priori known, hence the link between information and the notion of entropy, which is a property of closed systems. For example, the information conveyed by throwing a die is 2.5 bits, that is, the logarithm to the base of 2 of the six possible states the system can take. But the complex systems we are dealing with are by definition *open*. So what is the meaning of information in complex systems?

In *Information and Self-Organization*, Haken (1988) suggested that complex systems "self-organize," that is, "interpret," the information that comes from the environment. In other words, the meaning assigned to the message depends on the receiver (the receiving system) and not just on the message itself as in Shannon's theory. Haken (see p. 15 in 1990) has consequently suggested two forms of information: *semantic information* which is information *with* meaning versus *Shannonian information* which is "information with meaning exorcized." Haken further emphasizes that the process of self-organization implies "an enormous compression of information" (see pp. 25, 35, 151 in Haken (1988)).

Haken and Portugali (2003; Portugali 2011, Chaps. 8, 9) have studied information in the context of the city. They show that different elements of the city transmit different quantities of Shannonian information that can be practically measured by means of information *bits*, for example (Fig. 28). They further show that cognitive processes such as pattern recognition and categorization entail an enormous information compression, thus affecting the quantity of the Shannonian information conveyed by the city (ibid.) and that information compression is just one facet of the process – the other facet is *information inflation* (Haken and Portugali 2015): In certain urban situations, categorization might entail information compression while in others information inflation (Fig. 29). Information inflation and compression are thus two aspects of the process of *information adaptation* by which individuals and collectivities shape the city in a way that is adapted to the inhabitants' cognitive capabilities.

The notion information adaptation has far-reaching implications to the above discussion about the scientific method and the science of cities: Self-organization as information compression implies a *complex* → *simple* model and thus an alternative Simon's *simple* → *complex* model. The process of information inflation, on the other hand, is in line with Simons' model. These two models are thus two facets of a single process of information adaptation that in some cases requires inflations while in others compression. Complexity theory shows that whatever are the opening conditions (complex or simple), a scientific approach is possible.

CogCity

A central property of complex systems is the process of *circular causality* that typifies also the dynamics of cities: Thus, in the SIRN model, the interaction between the local/micro-urban agents gives rise to the global structure of the city, which then feeds back and prescribes the behavior, interaction and action of the agents, and so on. Guided by Simon's *simple* → *complex* model, standard urban simulation models have become excellent tools to simulate the first part of this loop – the

way local interactions give rise to a global structure – but they fail to describe the second, feedback part of the loop. CogCity (cognitive city) is a model that attempts to simulate the dynamic of cities as a process of circular causality (Portugali 2004, 2011, Chap. 18).

CogCity is essentially a FACS model (above section "AB and FACS Cities") with several additions that make it an explicit SIRN, cognitive, urban simulation model. It differs from standard AB/CA urban simulation models in that the latter are essentially bottom-up in their structure (Fig. 30, *left*). CogCity, per contra, is characterized by an ongoing interaction between top-down and bottom-up. Figure 30, *right*, describes a typical scenario: It starts

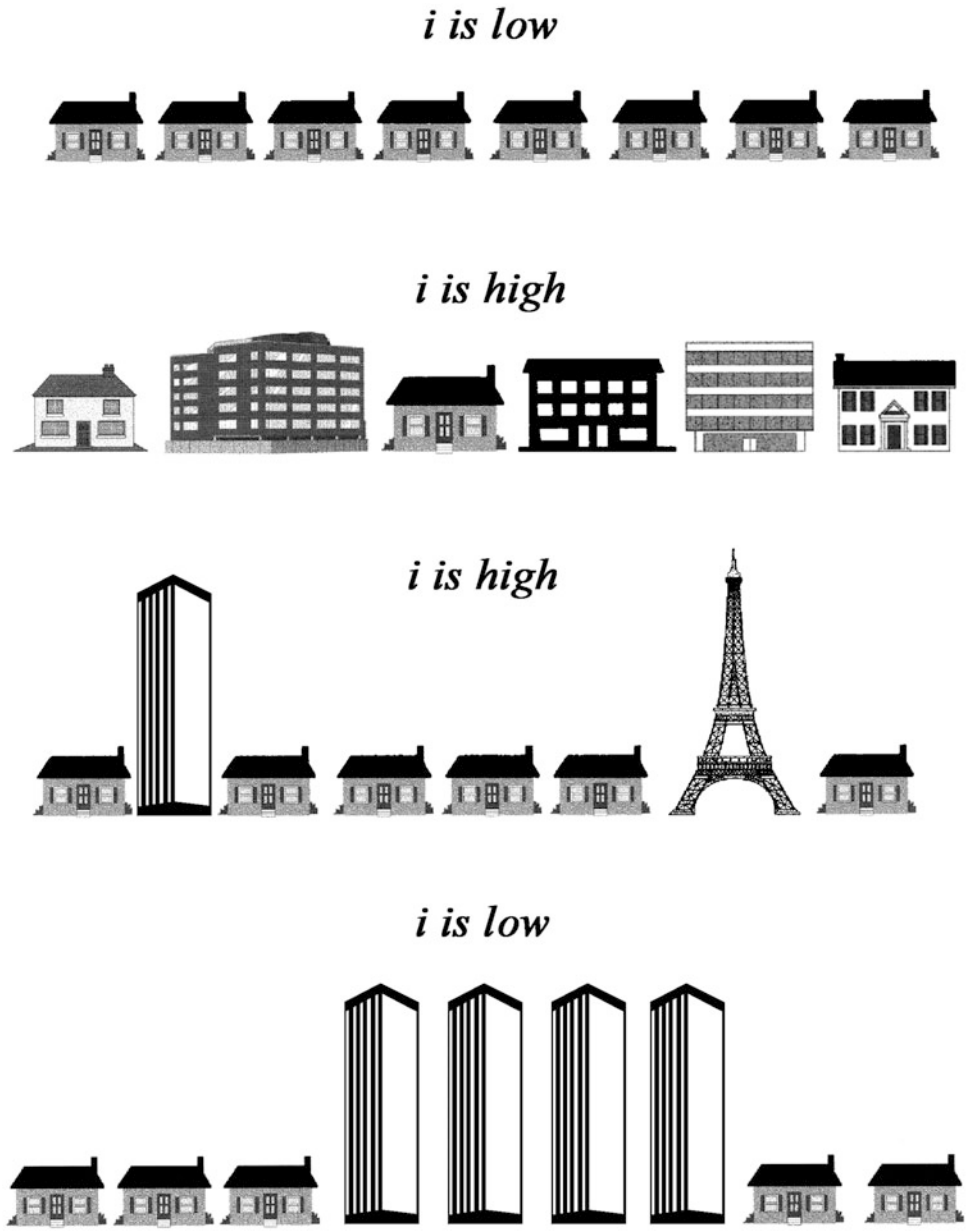

Fig. 28 (continued)

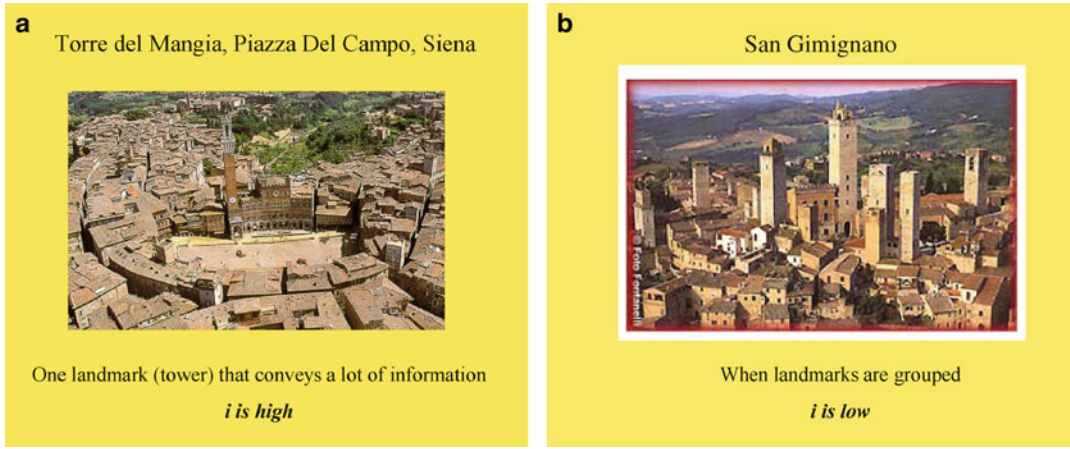

Self-Organization and the City, Fig. 28 Different configurations and categorizations of buildings convey different quantities of Shannonian information. When all buildings are similar, information (*i*) is low. When they are different, *i is high* but difficult to memorize. When landmarks are added *i is high*, provided that they are located apart from each other; otherwise, *i is low* (Source: Haken and Portugali 2003). (**a**) An example of a good landmark. (**b**) An example of a not very effective landmark

Self-Organization and the City, Fig. 29 If all buildings in the city are different from each other, categorization entails information compression, if they are similar – information inflation

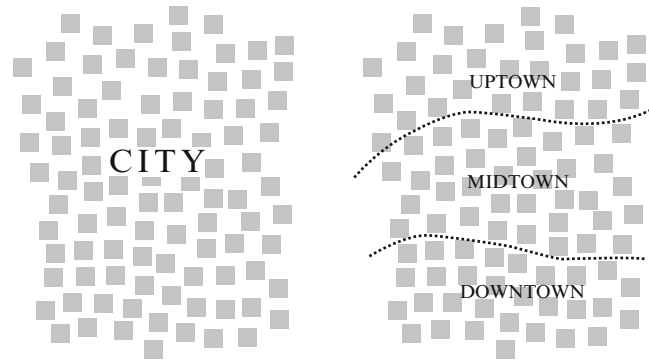

top-down when an agent arrives to the city with a global cognitive map in mind, compares it to the global structure of the city, and selects a local subarea. Now starts the bottom-up process: the agent selects the empty cells in that local area, evaluates the appropriateness of the cells and their nearest neighbors in light of its needs, and then takes a decision and action. In parallel, the properties of every cell are determined according to its relations to its nearest neighbors and so on.

In a regular AB/CA simulation, the process ends here: the global outcome is recorded and mapped as the output of this specific iteration and the model is ready for a new iteration. In a SIRN-CogCity model, the process continues and feeds back to the global structure of the city that allows the top-down process in the next iteration: Firstly, the state of the various central places is determined. Secondly, peripheries are determined around central places. Thirdly, areas are defined or redefined. Fourthly, subareas are redefined. Fifthly, given areas and subareas, the global state of the city as a whole and its rank-size structure, are defined. The latter changes redefine the local membership state of each cell in the various infrastructure objects and become the externally represented input for a new agent in the next iteration and so on in circular causality (Figs. 31, 32).

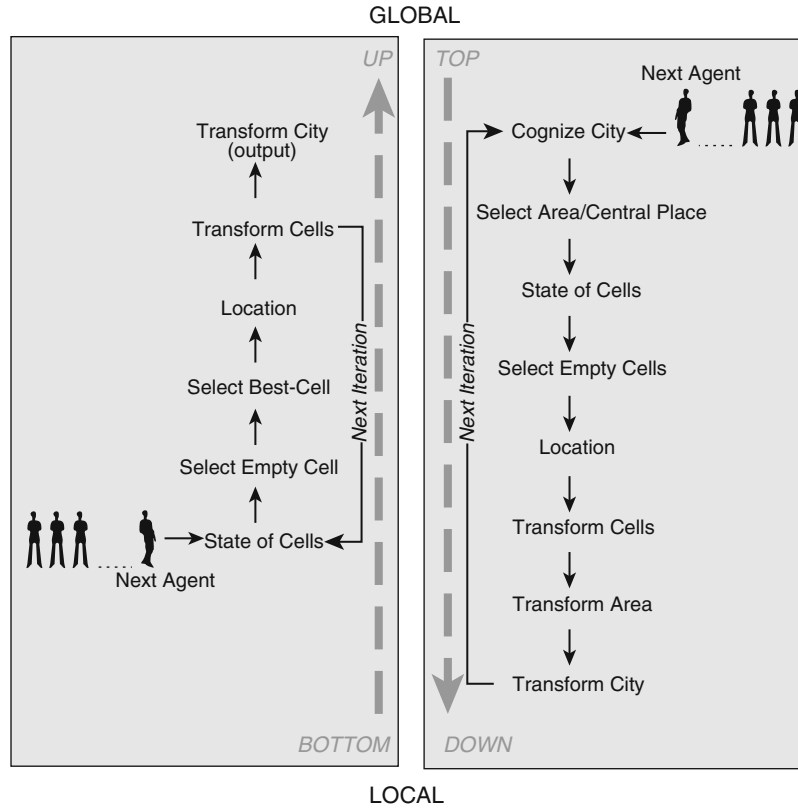

Self-Organization and the City, Fig. 30 A cognitive (*right*) vs non-cognitive (*left*) AB/CA urban simulation model (Source: Portugali 2004)

Planning and Design

Planning

The link between self-organization and cities is contradictory. Firstly, since cities were always regarded as symbols of planned action, walls, roads, castles, and fortresses indicated a central authority that is capable of planning. Secondly, since planning as means to achieve a controlled order diametrically opposes self-organization as the spontaneous emergence of order. This is a seemingly contradiction, however, since cities are *dual* self-organizing systems with the implication that every urban agent is a planner at a certain scale. This view is supported by psychology and cognitive science that consider planning as one of the basic cognitive capabilities of humans (Morris and Ward 2005).

Cognitive planning, that is, the ability to think, decide, and act ahead, must be based on information about the future which by definition is partial and insufficient – a situation that according to Haken typifies also the process of pattern recognition as conceptualized by synergetics. Based on this analogy, Haken (1998) described decision situation in the context of planning as in Fig. 33.

This decision situation raises the question of "How do people complement the unknown data?" According to Haken and Portugali, as in pattern recognition tasks here too, the unknown data is being supplied by means of associative memory (Haken 1998; Portugali 2000), conceptual cognitive maps (Portugali 2004, 2005), and decision heuristics (Portugali 2000; Tversky and Kahneman 1974, 1981). Table 1 specified several decision heuristics and their interpretation in the context of cities.

Haken and Portugali (2000) have further suggested that complex processes of decision-making in the context of city planning evolve according to their SIRN model. This suggestion was further elaborated by Portugali and Alfasi (Portugali and Alfasi 2008) who demonstrated

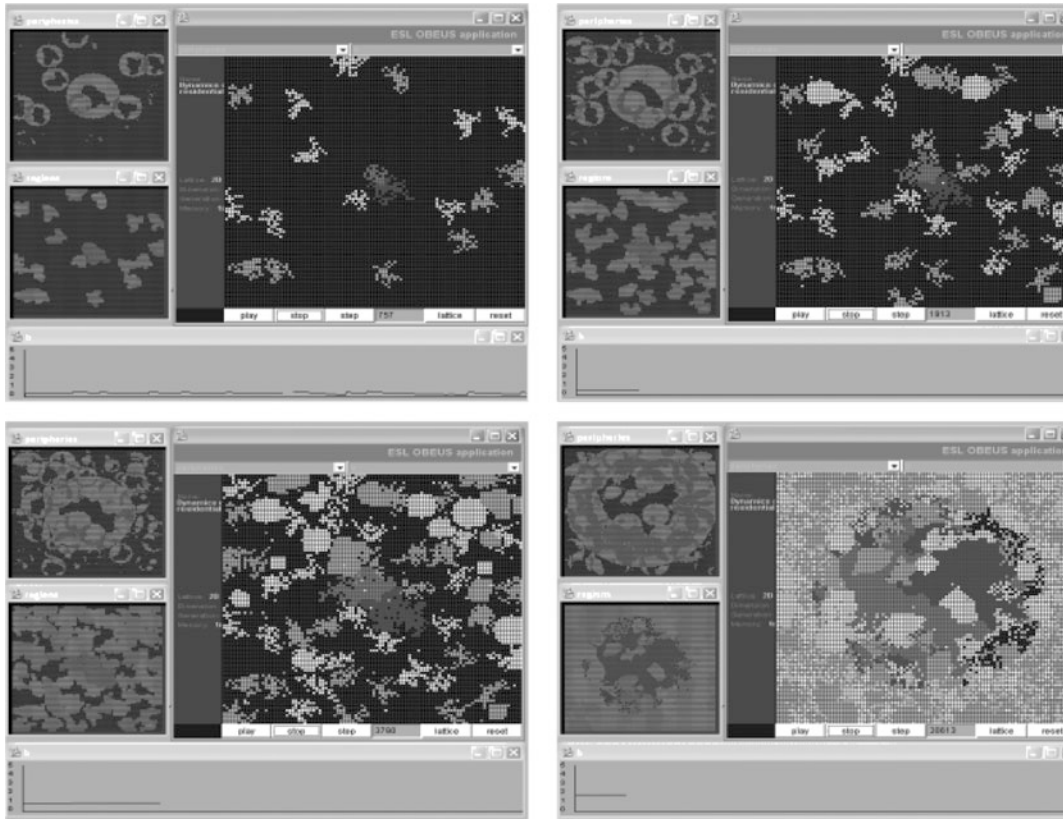

Self-Organization and the City, Fig. 31 Preliminary results from an evolving scenario simulated by CogCity: The central screen in each of the four snapshots shows the evolving spatial distribution of various kinds of agents, the *top left* screen the evolution of centers and subcenters, while the *bottom left*, the evolving cognitive maps of agents (Source: Portugali 2004)

empirically how the SIRN process practically takes place in the reality of *planning discourse* as it evolved among members of a planning team engaged in formulating urban policies concerning the development of the city of Beer Sheva, Israel (Fig. 34).

As a basic cognitive capability, planning is intimately associated with the fact that humans are social creatures – people tend to plan together (e.g., families, friends, firms, etc.). Some planning decisions are thus made solitarily while others collectively. Planning is also a profession that is closely linked to the central authorities of society (municipal, regional, national governments, etc.). We thus have three forms of planning – *solitary*, *collective*, and *professional*.

The notion that cities are complex self-organizing systems thus implies a novel view on planning the essence of which is, first, that all three forms of planning (solitary, collective, and professional) participate in the dynamic of cities. Second, that due to nonlinearities that typify cities as complex systems, the act of a single solitary planner might affect the evolution of a city more than the planning act of a professional planning team. (For an example, see Portugali (2006b)). Does that mean that due to self-organization, there is no need for city planning? Not at all! – It means that we have to adopt a new perception of *plans as participants* in the overall urban dynamics. It also means that we have to adopt a new perception of urban dynamics as a complex interaction between many plans at different scales, or more specifically, between solitary, collective, and professional planning agents, each with its specific plan.

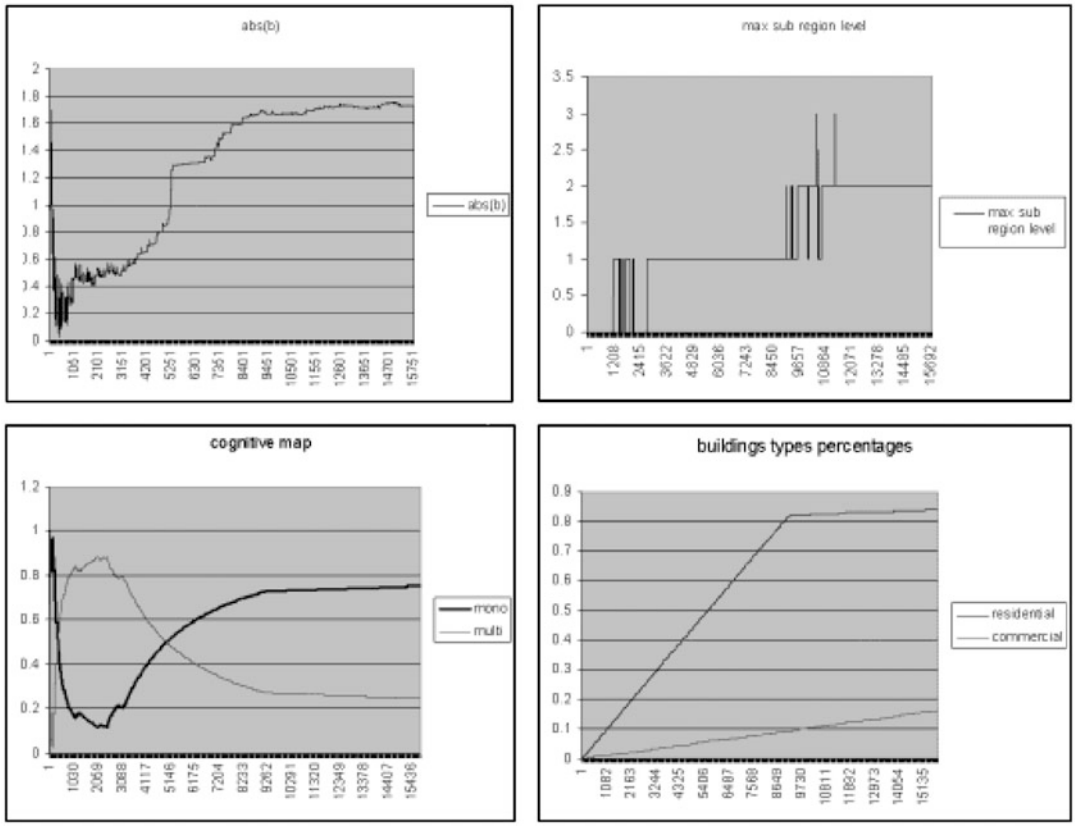

Self-Organization and the City, Fig. 32 Preliminary results from an evolving scenario simulated by CogCity – the graphs (Source: Portugali 2004)

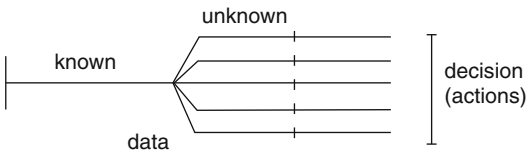

Self-Organization and the City, Fig. 33 Decisions in the city are characterized by insufficient data. In such a reality, the known data may be complemented in a variety of ways. Each of these ways might entail a different decision and action (Source: Haken 1998; Portugali 2000)

Design

As recently indicated by Stolk and Portugali (2016), the distinction between planning and design is far from being clear. Thus, for Rittel (a leading theoretician of planning and design), the two are synonymous (Protzen and Harris 2010, 2); for others, the two are different: Planning is more about urban policies, while design is more associated with the architectural form of cities. Still others point that planning is associated with procedures needed to reach a goal, while design with creativity and innovation. In the above-noted study, Stolk and Portugali, approaching the issue from Trope and Liberman (2010) *construal level theory*, suggest that while planning tends to start from the here and now and becomes more and more abstract as it proceeds to the future, design tends to start with a mental leap to an abstract future from which it then proceeds backward in order to arrive to the concrete here and now.

How do planners move from the here and now to the future and how designers, following the mental leap, move backward from the abstract future to the concrete here and now? The answer: by means of SIRN planning and design processes. The process with respect to planning was suggested and demonstrated above in connection

Self-Organization and the City, Table 1 Seven heuristics and their interpretation in the context of cities (for sources, see Portugali (2000))

Heuristic	Description	Urban interpretation
Similarity	The similarity of two items is expressed as a function of their common and distinctive features	The recognition of fundamental rules of urban composition, such as a grid layout, built form, or urban fabric, is performed through similarity
Representativeness	The probability that an object or event belongs to a particular class is judged by the degree to which the description is representative of a stereotype	Urban categories are identified on the basis of architectural stereotypes, such as church, skyscraper, boulevard, tower, park, arch, etc.
Availability	The probability of an event, or frequency of a class, is assessed by the ease with which instances or occurrences can be brought to mind or recalled	Availability would make universal symbols (such as Macdonald's signs, stop signs, etc.) more easily identified and recalled
Decision frame	The frame that a decision-maker formulates the problem (gain versus loss, etc.) is influenced by norms, habits, and personal characteristics of the decision-maker	Urban frames for decisions (congested versus free, public versus private, etc.) depend on the cultural code of each agent (e.g., a tourist, a taxi driver, a policeman, etc.)
Anchoring	The tendency of people to make estimates by starting from an initial base value that is adjusted to yield the final answer	City's internal representations can contain certain categories such as style, urban violence, town size, etc., which can be "fired on" early in the process of cognition; once switched on, it stays on and is only eventually reprocessed
Synergetic I: collective effects	When facing complex decision situations, people tend to rely on what other people are doing or saying	Drivers, pedestrians, and intra- and interurban immigrants tend to "follow the stream," that is, to take decisions in line with what others are doing
Synergetic II: attention parameter effect	When facing complex decision situations, people often employ several heuristics in a sequence. First, the attention parameter calls into using a heuristic. Then, when exhausted, another attention parameter heuristic emerges and so on	Intra- and interurban immigrants, for example, often start with a given location decision heuristic (say synergetic I); if it doesn't work, they switch to an alternative heuristic and so on

with planning discourse as illustrated above in Fig. 26 and below in Fig. 34 ; here we focus on design.

In several previous studies, we've developed a SIRN design process (Stolk and Portugali 2012; Tan and Portugali 2012; Portugali and Stolk 2014). Similarly to the general SIRN model, it starts from a *general SIRN design model* that symbolizes a self-organizing designer that is subject to two flows of information: internal and external. The interaction between these two flows gives rise to an order parameter that governs the designer's action and behavior that determine the resultant externally represented design and so on until the design process is completed. In line with the three SIRN submodels, we've developed three design submodels: The first, the *intrapersonal design* submodel, refers to a solitary designer; the second, the *interpersonal design* submodel, refers to a sequential dynamics of several designers, while the third, the *collective design* submodel, refers to a simultaneous interaction between many designers. An example of the first is design by means of sketching; an example of the second is the diffusion in space-time of design solutions while of the third is the design city game developed by Tan and Portugali (2012) and presented in Figs. 35 and 36.

In addition to the above three submodels, Portugali and Stolk (2014) suggest a fourth SIRN submodel – a *hybrid intrapersonal design model*. Here, in the SIRN interaction between

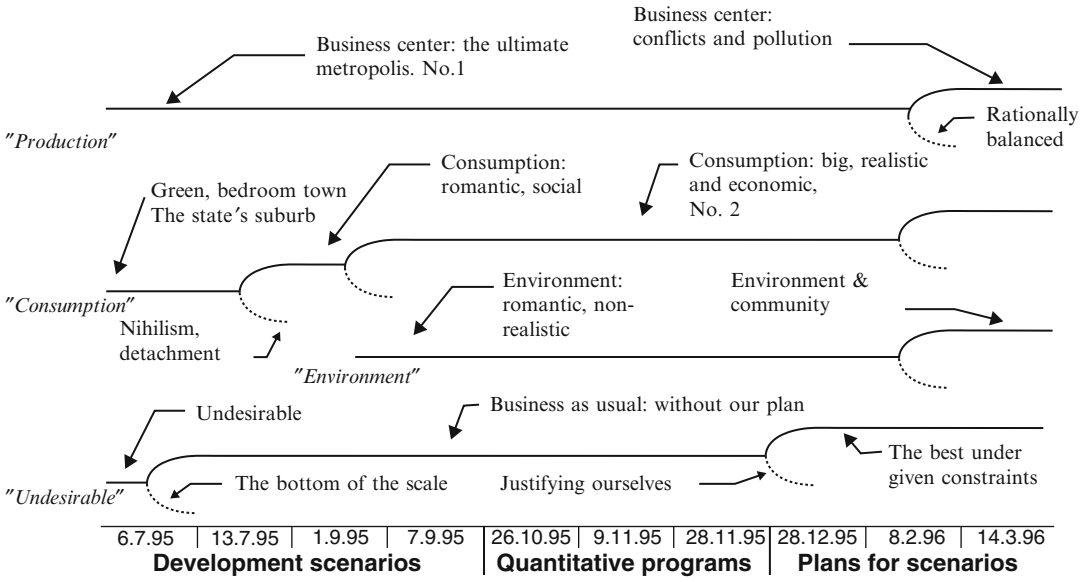

Self-Organization and the City, Fig. 34 Bifurcation diagram of the planning discourse. Each alternative is represented with a continuous line along the time axis (the x-axis). A *horizontal line* represents an order state during which the alternative scenario maintains a certain image and possesses certain attributes. Bifurcation points indicate a shift from one order state to another. The *broken lines* represent optional order states that were not actualized (Source: Portugali and Alfasi 2008)

Self-Organization and the City, Fig. 35 Several snapshots from the design city game as it developed in the area of Sportpark de Wierden, Almere Haven, and the Netherlands (Tan and Portugali 2012)

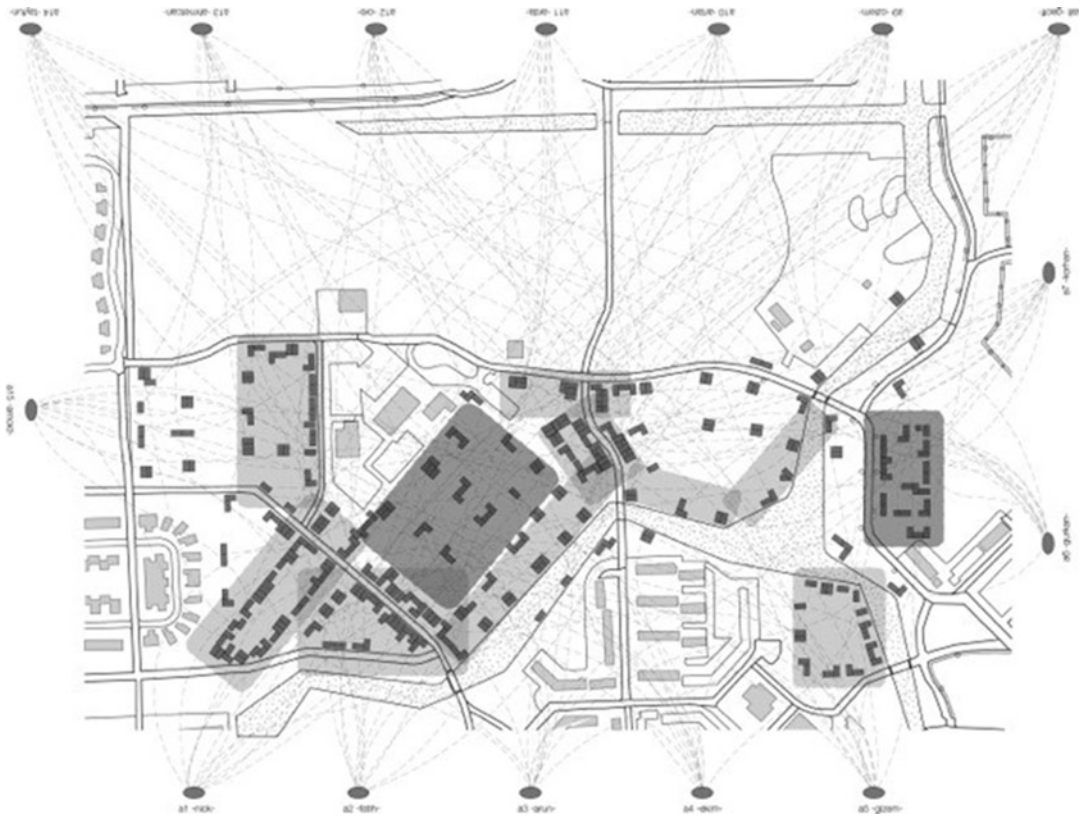

Self-Organization and the City, Fig. 36 The resultant outcome from the above design city game (Tan and Portugali 2012)

internal and external representations, the designer responds to external representations in the form of urban simulation models that inform the designer about the way his internally represented ideas affect the city as a whole.

A Self-Planned/Self-Designed City

Urban planning and design have two facets: on the one hand, they are related to the *process of planning and design* – the way city planners and designers are or should plan, while, on the other, to the structure of the *planning/design system*, the administrative framework within which they plan. The first refers to the planners or designers as individuals or groups, while the second to planning as a component in the form of governance that dominates a city or a country. The two are interrelated, however, since the discourse on how planning is or should be conducted affects the planning law and the latter, once it enforced, determines how planners practically plan.

Can there be a planning and design system that is built in line with the city as a self-organized complex system? The answer suggested here is positive: In a sequence of studies, Portugali and Alfasi have portrayed the principles of such self-planned city (Portugali 2000) and the way it can be applied to the reality of city planning law and structure of Israel (Alfasi and Portugali 2007; Portugali 2011, Chap. 16). The suggestion here is that this system can accommodate also the process of design. Similarly to current planning and design systems, it is a three-layer system: the legislative, the judiciary, and the executive. It differs from current systems in the following: First, its planning and design laws refer to the qualitative relations between the various city objects (Fig. 37) and not to land use plans that assume to determine top-down the urban landscape. This property makes it specifically appropriate to design. Second, it suggests a novel planning/design judicature composed of spatially distributed "planning/design courts" conducted by professionals

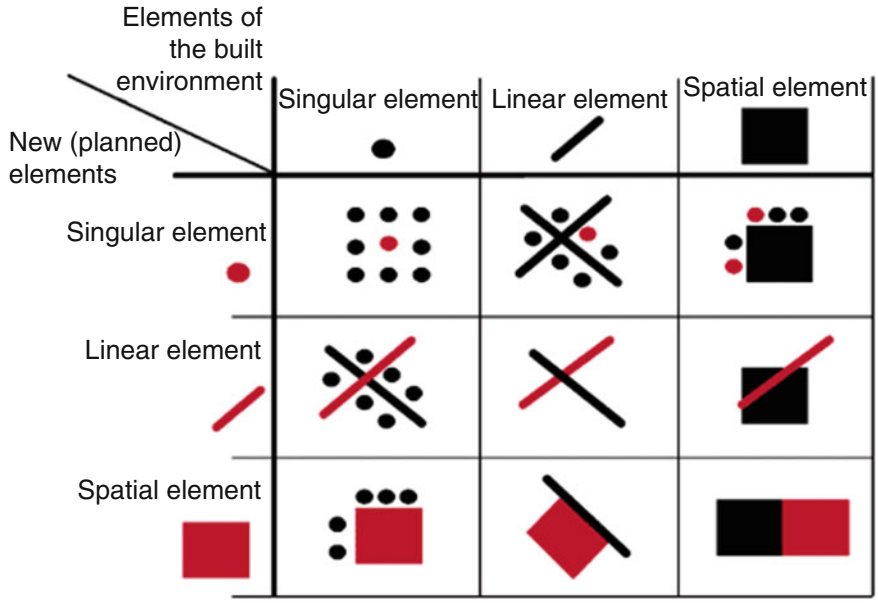

Self-Organization and the City, Fig. 37 Proposition for a new planning structure for a self-planned city: the interrelations between urban elements provide the basis for planning law. A singular urban element might be a building, a linear one might be a road, while an example for a spatial urban element is a park

who have specialized in law, planning and design. Their aim is to evaluate, accept or reject the plans or designs proposed by all planning and design agents – solitary, collective or professional. Third, it suggests a separation of authorities that doesn't exist today in standard planning and design administrations. Finally, it suggests a process of hermeneutic planning and design that enables phase transition and adaptation to new situations. Figure 38 describes the structure and operation of this self- organized planning-design system.

Prediction, Planning, Self-Organization and Cities

The first principle of the above planning-design system is that its planning-design laws refer to qualitative relations between the various city objects and not to land use plans. The reason is that land use plans are commonly based on predictions. This is problematic since prediction in the context of complex systems such as cities is associated with four fundamental properties. First, the nonlinearities that typify cities imply that one cannot establish predictive cause-effect relationships between some of the variables. Second, many of the triggers for change in complex systems have the nature of unpredictable mutations (Allen 1997), not because of the lack of data but because of their very nature. Third, unlike closed systems, in complex systems, the observer, with his/her predictions, is part of the system – a point made by Jantsch (Jantsch 1981) more than two decades ago and largely ignored since then. In such a situation, predictions are essentially feedforward loops, affecting the system and its future evolution with implications that include self-fulfilling and self-falsifying or self-defeating predictions (Portugali 2006b,2011, Chap. 4).

From the above follows a dilemma: complex systems are in essence unpredictable, and, yet, the current practices of planning as well as planning administration and law are based on the ability to predict. In a recent paper (ibid.), it was shown that this situation leads to planning paradoxes that are the result of phenomena of self-fulfilling and self-falsifying predictions. It was further shown that these phenomena are the result of the *feedforward* and *feedback loops* that are typical of complex systems in general and of cities and regions in particular. The existence of such loops is one of the properties that make systems complex. Such loops are responsible to the situation by which a prediction, a plan, or a

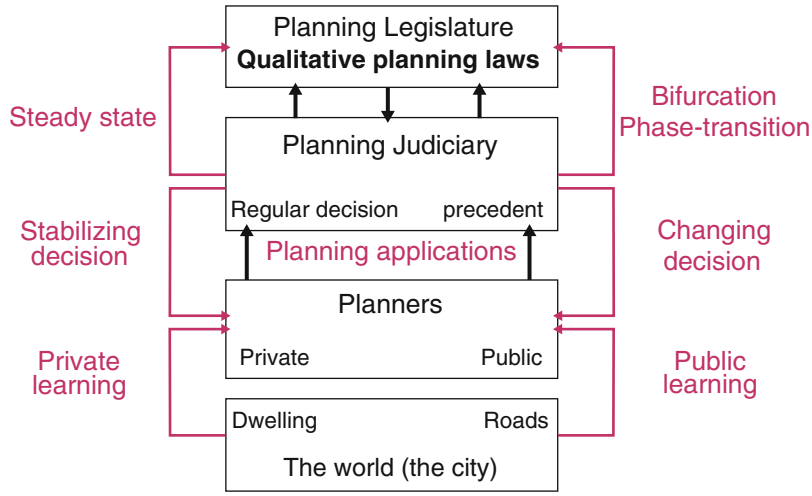

Self-Organization and the City, Fig. 38 Proposition for a new planning structure for a self-planned city: the system is built of private planners (the inhabitants of the city) and professional planners. Each of them might submit a plan to the planning judiciary. In the latter the "planning judge" takes decisions according to the planning law as determined by the planning legislature. Unlike the current structure, there is a clear separation of authorities

design, once produced, becomes a *participant* in the system's dynamic.

Another way to look at this issue is from the point of view of the distinction between Shannonian and semantic information (above, section "Information Compression, Inflation, and Adaptation"): Predictions and plans are essentially kinds of information transmission. One can thus speak of Shannonian prediction and semantic prediction. In the first, the outcome of the prediction is independent of the receiver(s), while in the second, it depends on the meaning attached to it by a receiver or receivers. A weather forecast is a good example for both: it has no effect on the climatic system, but it might affect the urban system – following the prediction people might behave in different ways that might entail phenomena of self-falsifying and self-fulfilling predictions as described above.

Planning and design theories have not as yet internalized the implications of complexity theory to city planning and design. For example, in the planning and decision support systems (PSS, DSS) that are currently discussed and built by proponents of the complexity paradigm, urban simulation models are assumed to function as sophisticated prediction devises (Brail 2006; Brail and Klosterman 2001; Geertman and Stillwell 2003). The result is a discrepancy that to my mind characterizes the domain of urban and regional planning as well as design: On the one hand, planning and design theories, as well as the structure of planning law, practice, and administration, are all based on the (usually implicit) assumption that cities are essentially predictable entities and that given sufficient data, information, and models, their future behavior is in essence predictable. On the other hand, current urban theory suggests that cities are complex, self-organizing, and nonlinear systems and that as a consequence their future behavior is in essence not predictable even if sufficient information and data are collected and available (Portugali 2000).

Urbanism

In section "Explicit Attempts to Define a City," we've defined the category "city" in terms of a family resemblance according to which a settlement becomes a "city" not by having some necessary and sufficient properties, but by being a member in a network of cities that has center, periphery, etc. This view is in line with cognitive science's approach to concepts and categories. In the latter, it is common also to distinguish between *basic level* categories and *superordinate* categories (Rosch et al. 1976). A "chair," for instance, is

a basic level category whereas "furniture" a superordinate. The suggestion here is that a *city* is a basic level category, whereas *urbanism* is a superordinate one, referring to the totality of cities ranging from their physical structure, architecture, economics, politics, social and cultural composition, and so on. The term "urban revolution" (coined by Childe (1950)) thus implies a major transformation in society with the basic level category "city" at its center.

Most complexity studies of cities have traditionally focused on specific aspects of cities – land use, morphology, transportation, social segregation, etc. – but not on the totality of city life which is what urbanism is all about. Why? Because they evolved mainly out of regional sciences' attempt to develop a scientific approach to cities and the consequent tendency to choose research issues that can be analyzed by reference to "real-world" data. The study of urbanism was thus left to the "soft" social theory approaches to cities (Castells 1977, 1996; Harvey 1985, 1996).

This is rather unfortunate because twenty-first century world society is undergoing a major transformation with urbanism at its center: Massive rural-urban migration and demographic processes entailed a situation by which cities such as Mexico City, Bombay (Mumbai), and Sao Paolo grew from 8.8 million, 6.2 million, and 8.3 million, respectively, in 1970 to over 20 million, over 16 million, and again over 18 million today; for the first time in human history, the number of people living in cities is crossing 50% of the world's population, and the process is still on. In the last few decades, we've witnessed the emergence of *world cities*, or *global cities*, that form the centers for the globalization process.

These quantitative processes are associated with several qualitative processes: a process of privatization leads to the decline of the welfare nation-state; the emergence of a civil society takes over many of the past duties and functions of the nationalist welfare state; the crucial problems of many (post)modern counties are no longer classical national problems (e.g., national self-determination, national boundaries, etc.), but rather the problems of cities. The events of September 11 and the ensuing wars in Afghanistan and the Middle East are tragic indications to the *urbanization of war*. Finally, the process of globalization is making some world cities more dominant than the states within which they exist, thus repressing the nation states.

All of the above indicates the more fundamental change: According to Lefebvre (1970), its essence is that urbanism is replacing industrialization as the dominant force in society. My view is that the essence of this change is that urbanism is challenging nationalism as the order parameter of modern society (Portugali 2006b).

Complexity and Urbanism

Complexity studies of cities, with their focus on the short-term dynamics of cities and of national systems of cities, are indeed highly advanced in terms of mathematical formalism and data analysis but rather anachronistic in terms of the issues studied; as such, they have so far said very little on the dramatic urban phenomena of the twenty-first century. Can they say more about the issue of urbanism? The answer is yes! And for several reasons, to my mind, the "deeper messages" of complexity theories is that they have discovered properties in matter hitherto assigned to life, art, and society (Portugali 1985). It is not surprising therefore that complexity theories, particularly synergetics, bear many similarities to social theory and philosophy, and, as a consequence, several of the notions that originated in the study of complex systems can be related to similar notions that originated in the domain of social theory (Portugali 2006a):

- Both are essentially systemic and even holistic.
- Both tend to conceptualize "development" and "evolution" in terms of abrupt changes rather than a smooth progression. In social theory, the common terms for an abrupt change are (social/political/cultural) "revolution" while in the language of complexity "bifurcations" and "phase transitions" (that reminds one of Gould's and Eldredge's, (1980) *punctuated equilibrium*).
- Synergetics' notion of "order parameter" is similar to social theory's notion of "mode of

production." Synergetics' notions of "enslavement" and "circular causality" are close to social theory's notions of "social reproduction" and "socio-spatial reproduction" (Giddens 1984; Lefebvre 1974).
- Complexity's view of systems in "a far from equilibrium condition" comes close to postmodernism's recent emphasis on viewing reality as ever-changing and transforming, hence the general popularity of notions such as "chaos" and "butterfly effect."

Several writers have already responded to these similarities from the perspective of the sciences, philosophy, media/cultural critics, and modern and postmodern social theory (Cilliers 1998; Johnson 2001; Kellert 1993; Portugali 2006a; Rasch and Wolfe 2000). A preliminary attempt has also been made to employ synergetics as a complexity theory of urbanism (Portugali 2000, 2006b), that is, to interpret the current changes in cities and urbanism in terms of synergetics along the following scenario: the combined force of rapid population growth, urban expansion, and technological change throughout the twentieth century acted as a control parameter. Toward the end of the twentieth century and at the beginning of the twenty-first century, we are witnessing a bifurcation and phase transition followed by a competition between the newly emerging *urban order parameter* and the old nationalist one. My personal view is that what we see emerging today out of this competition is not the replacement of nationalism as an order parameter by urbanism but the *urbanization of nationalism*.

Future Directions

Looking in retrospect at more than three decades of complexity theory studies of cities, one can now appreciate some of its major achievements: First, the link between cities and complexity theory gave urban studies a strong theoretical basis it never had before. The fact that complexity theory was applied to a large number of domains gave urban studies a wide context and many sources of inspiration. The fact that complexity theory comes with a rich and strong mathematical formalism gave urban studies a sound methodological background. The attempt to transform the study of cities into a science of cities is today closer than ever. Batty's (2013) *The New Science of Cities* is probably the first explicit comprehensive attempt toward such a science. How should the new science of cities develop is still an open question, however.

Complexity theory has given us a new insight to our understanding of the dynamics of cities. According to Batty (2005), the most important contribution is that complexity studies of cities have verified the intuitive views of Jane Jacobs (1961) and Alexander (1965), namely, that the complex entity "city," with its variety of different land uses, socio-spatially and culturally segregated communities, transportation networks, and all the rest, is an outcome of "bottom-up" processes: The local interaction between agents at local scale, conducted by very few and simple rules, gives rise to the complexity we term "city." My own view is that CTC have given us "a single and sound theoretical basis to a variety urban phenomena and properties that so far were perceived as independent of each other and thus interpreted by reference to different theoretical bases . . ." (Portugali 2011, 96).

At the same time, however, it must be admitted that the potential contribution of complexity theories to urbanism, planning, and urban design has yet to be realized. The complexity approach has indeed given the bottom-up views on the nature of cities a strong mathematical formalism that can be quantified by real data. But this focus on the local, the bottom-up, and the quantifiable was not without price: Cities and urbanism of the twenty-first century are in the midst of a dramatic transformation, new forms of cities are emerging – world cities, global cities, and megacities, and yet the vast majority of complexity studies still focus on the old traditional quantitative urban questions, leaving the qualitative grand urban issues to the "nonscientific" social theory oriented urban studies. Can complexity theories of cities contribute? The answer suggested above is yes! SIRN is one approach in this direction and the field is ripe for others.

The same applies to planning. In the literature on planning theory, it is common to make a distinction between *planning theory* versus *theory in*

planning (Faludi 1973), that is, between theories about how to plan and theories about urban and regional dynamics that planners can use during the planning process. Examining complexity theories of cities from this perspective, we see that they are very innovative with respect to theory in planning, but very conservative when it comes to theory of planning: The vast majority of studies simply ignore the implications of complexity to urban, regional, and environmental planning.

Why do we need a complexity theory of planning? The answer is twofold: First, standard planning theory was developed in the 1950s and 1960s hand in hand with what we consider today as anachronistic urban theory. Both are based on the (usually implicit) assumption that cities are in essence simple, mechanistic systems that given sufficient data and advanced technologies, their future behavior is predictable and hence controllable. As we've seen above, complexity theories tell us a different story: Cities are complex self-organized systems that are in essence unpredictable and controllable even if sufficient data and the most advanced technologies are at hand. From here follow a whole set of new and interesting questions: what is the role of planning in a complex system? Are all parts and components of the system unpredictable? In the above, we've suggested some preliminary answers – but new ones must still come.

Finally, it is important to mention the issue of extreme events in cities. The rapid processes of urbanization cities underwent in the last few decades and the "urbanization of war" made cities rather vulnerable areas in cases of extreme events. The question of how cities and their inhabitants behave and respond to extreme events is a pressing social issue that already started to capture the attention of students of complexity theory of cities and urbanism.

Bibliography

Alexander C (1965) A city is not a tree. *Architectural Forum*,Vol 122, No 1, April 1965, pp 58–62 (Part I), Vol 122, No 2, May 1965, pp 58–62 (Part II)

Alfasi N, Portugali J (2007) Planning rules for a self-planned city. Plann Theory 6(2):164–182

Allen PA (1981) The evolutionary paradigm of dissipative structures. In: Jantsch E (ed) The evolutionary vision. Westview Press, Boulder, pp 25–71

Allen PM (1997) Cities and regions as self-organizing systems: model of complexity. Routledge, London

Allen P, Sanglier M (1981) Urban evolution, self-organization and decision making. Environ Plan A 13:169–183

Allen PM, Strathern M (2004) Complexity: the integrated framework for integrated models of urban and regional systems. In: A talk delivered at a conference on The Dynamics of Complex Urban Systems, Monte Verita, 4–6 November 2004

Allen P, Sanglier M, Engelen G, Boon F (1985) Towards a new synthesis in the modeling of evolving complex systems. Environ Plann B Plann Des 12:65–84

Alonso W (1965) Location and land use. Harvard University Press, Cambridge, MA

Andersson C, Hellervik A, Lindgren K, Hagson A, Tornberg J (2003) Urban economy as a scale-free network. Phys Rev E 68(3):036124

Auerbach F (1913) Das Gesetz der Bevolkerungskoncentration. Petermanns Geogr Mitt 59:74–76

Bak P, Chen K (1991) Self-organized criticality. Sci Am 28:26–33

Bak P, Chen K, Creutz M (1989) Self-organized criticality in the game of life. Nature 342:780–782

Barabási A-L (2002) Linked: the new science of networks. Perseus, Cambridge

Barabási A-L, Réka A (1999) Emergence of scaling in random networks. Science 286:509–512

Bartlett FC (1932/1961) Remembering: a study in experimental and social psychology. Cambridge University Press, Cambridge

Batty M (1996) Urban evolution on the desktop: simulations using extended cellular automata. Unpublished paper, Centre for Academic Spatial Analysis, UCL

Batty M (1997) Cellular automata and urban form: a primer. J Am Plan Assoc 63(2):266–274

Batty M (2005) Cities and complexity: understanding cities with cellular automata, agent based models and fractals. MIT Press, Cambridge, MA

Batty M (2013) The new science of cities. MIT Press, Boston

Batty M, Longley P (1994) Fractal cities. Academic Press, London

Batty M, Xie Y (1994) From cells to cities. Environ Plann B Plann Des 21:531–548

Batty M, Xie Y (1999) Self-organized criticality and urban development. In: Portugali J (ed) Population, Environment and Society on the Verge of the 21st Century. Special issue of Discrete Dyn Nat Soc 3(2–3):109–124

Benenson I, Torrens PM (2004) Geosimulation: automata based modeling for urban phenomena. Wiley, London

Benguigui L (1995) A fractal analysis of the public transportation system of Paris. Environ Plan A 27:1147–1161

Benguigui L, Czamanski D, Marinov M, Portugali J (2000) When and where is a city fractal. Environ Plann B 27(4):507–519

Blanchard P, Volchenkov D (2007) Scale-free segregation in transport networks. arXiv:0710.1592

Blumenfeld-Lieberthal E (2005) Dynamics of urban morphology in the Tel-Aviv metropolitan area. Ph.D thesis, Technion, Haifa
Brail RK (2006) Planning support systems evolving: when the rubber hits the road. In: Portugali J (ed) Complex artificial environments, complexity series. Springer, Heidelberg, pp 307–317
Brail RK, Klosterman RE (eds) (2001) Planning support systems. ESRI Press, New York
Braudel F (1993) A history of civilizations (trans: Mayne R. Penguin Books, New York
Burgess B (1925) The growth of the city: an introduction to a research project. In: Park R, Burgess EW, McKenzie RD (eds) The city. Chicago University Press, Chicago, pp 47–62
Burgess EW (1926/1968) The urban community. Greenwood Press, New York
Burgess EW (1927) The determination of gradients in the growth of the city. Am Sociol Soc Publ 21:178–184
Castells M (1977) The urban question. MIT Press, Cambridge, MA
Castells M (1996) The rise of the network society. Blackwell Publishers, Malden
Childe VG (1950) The urban revolution. Town Plan Rev 21:3–17
Christaller W (1933/1966) Central places in southern Germany. Prentice Hall, Englewood Cliffs
Cilliers P (1998) Complexity and postmodernism. Routledge, London
Dalton N, Peponis J, Conroy-Dalton R (2003) To tame a TIGER one has to know its nature: extending weighted angular integration analysis to the description of GIS road-centerline data for large scale urban analysis. In: Hanson J (ed) Proceedings of the 4th International Space Syntax Symposium. University College London, London, pp 65.1–65.10
Dendrinos DS, Sonis M (1990) Chaos and socio-spatial dynamics. Springer, New York/Berlin
Faludi A (1973) A reader in planning theory. Pergamon Press, Oxford
Figueiredo L, Amorim L (2005) Continuity lines in the axial system. In: Van Nes A (ed) 5th International Space Syntax Symposium. TU Delft, Faculty of Architecture, Section of Urban Renewal and Management, Delft, pp 161–174
Garling T, Golledge RG (eds) (1993) Behavior and environment. North-Holland, Amsterdam/London/New York/Tokyo
Geertman S, Stillwell J (eds) (2003) Planning support systems in practice. Springer, Heidelberg
Giddens A (1984) The constitution of society: outline of the theory of structuration. University of California Press, Berkeley
Golledge RG, Timmermans H (eds) (1988) Behavioral modeling in geography and planning. Croom Helm, London/New York/Sydney
Gould SJ (1980) The panda's thumb. Norton, New York
Gregory D (1994) Geographical imaginations. Blackwell, Cambridge, MA
Haag G, Muntz M, Pumain D, Saint-Julien T, Sanders L (1992) Interurban migration and the dynamics of a system of cities. Environ Plan A 24:181–198
Haken H (1979) Pattern formation and pattern recognition – an attempt at a synthesis. In: Haken H (ed) Pattern formation by dynamical systems and pattern recognition. Springer, Berlin, pp 2–13
Haken H (1983) Synergetics, an introduction, 3rd edn. Springer, Berlin
Haken H (1987) Advanced synergetics: an introduction (2nd print). Springer, Berlin/New York
Haken H (1988/2000) Information and self-organization: a macroscopic approach to complex systems. Springer, Berlin
Haken H (1990) Synergetics of cognition. Springer, Berlin
Haken H (1991/2004) Synergetic computers and cognition. Springer, Berlin
Haken H (1993) Synergetics as a strategy to cope with complex systems. In: Haken H, Mikhailov A (eds) Interdisciplinary approaches to non-linear complex systems. Springer, Berlin
Haken H (1996) Principles of brain functioning: a synergetic approach to brain activity, behavior and cognition. Springer, Berlin
Haken H (1998) Decision making and optimization in regional planning. In: Beckmann MJ, Johansson B, Snickars F, Thord R (eds) Knowledge and networks in a dynamic economy. Springer, Berlin
Haken H, Portugali J (1995) A synergetic approach to the self-organization of cities. Environ Plann B Plann Des 22:35–46
Haken H, Portugali J (1996) Synergetics, inter-representation networks and cognitive maps. In: Portugali J (ed) The construction of cognitive maps. Kluwer, Dordrecht, pp 45–67
Haken H, Portugali J (2003) The face of the city is its information. Environ Psychol 23:385–408
Haken H, Portugali J (2015) Information adaptation: the interplay between Shannon information and semantic information in cognition. SpringerBriefs. Springer, Heidelberg/Berlin
Harvey D (1985) The urbanization of capital. Basil Blackwell, Oxford
Harvey D (1996) Justice, nature and geography of differences. Basil Blackwell, Oxford
Hillier B (1999) Space is the machine: a configurational theory of architecture. Cambridge University Press, Cambridge
Hillier B, Hanson J (1984) The social logic of space. Cambridge University Press, Cambridge
Hillier B, Iida S (2005) Network effects and psychological effects: a theory of urban movement. In: Cohn A, Mark D (eds) Spatial information theory, Lecture notes in computer science, vol 3603. Springer, Berlin, pp 473–490
Hu MB, Wang WX, Jiang R, Wu QS, Wang BH, Wu YH, (2006) Urban traffic dynamics: a scale-free network perspective. http://arxiv.org/abs/physics/0606086v1
Isard W (1956) Location and space economy. Published jointly by the Technology Press of Massachusetts Institute of Technology and Willey, New York

Jacobs J (1961) The death and life of great American cities. Harmondsworth, London: Penguin Books
Jantsch E (ed) (1981) The evolutionary vision. Westview Press, Boulder
Jian B (2006) Small world modeling for complex geographic environments. In: Portugali J (ed) Complex artificial environments: simulation, cognition and VR in the study and planning of cities. Springer, Berlin
Jiang B (2007) A topological pattern of urban street networks: universality and peculiarity. Physica A 384:647–655
Johnson M (1987) The body in the mind: the bodily basis of meaning, imagination, and reason. The University of Chicago Press, Chicago
Johnson S (2001) Media/cultural critics – postmodern complexity: Emergence. Scribner, New York
Kellert SH (1993) In the wake of chaos. University of Chicago Press, Chicago
Kitchin R, Freundschuh S (2000) Cognitive mapping: past, present and future. Outledge, London
Lakoff G (1987) Women, fire and dangerous things: what categories reveal about the mind. The University of Chicago Press, Chicago/London
Lefebvre H (1970) La Révolution Urbaine. Gallimard, Paris
Lefebvre H (1974) The production of space. English translation, 1995. Blackwell, Oxford
Lösch A (1954) The economics of location. Yale University Press, New Haven
Lynch K (1960) The image of the city. MIT Press, Cambridge, MA
Mandelbrot BB (1983) The fractal geometry of nature. Freeman, San Francisco
Milgram S (1967) The small world problem. Psychol Today 2:60–67
Miller GA (1956) The magic number seven, plus or minus two: some limits on our capacity for processing information. Psychol Rev 63(2):81–97
Morris R, Ward G (eds) (2005) The cognitive psychology of planning. Psychology Press, Hove/New York
Nicolis G, Prigogine I (1977) Self-organization in non-equilibrium systems: from dissipative structures to order through fluctuations. Wiley-Interscience, New York
Park RE (1925/1967) The city. Chicago University Press, Chicago
Protzen JP, Harris DJ (2010) The universe of design: Horst Rittel's theories of design and planning. London Routledge
Popper KR (1959) The logic of scientific discovery. Hutchinson, London
Porta S, Crucitti P, Latora V (2005) The network analysis of urban streets: a primal approach. http://arxiv.org/abs/physics/0506009
Portugali J (1985) Parallel currents in the natural and social sciences. In: Portugali J (ed) Links between natural and social sciences. A special theme issue. Geoforum 16(2):227–238
Portugali J (1990) Preliminary notes on social synergetics, cognitive maps and environmental recognition. In: Haken H, Stadler M (eds) Synergetics of cognition. Springer, Berlin, pp 379–392
Portugali J (ed) (1992) Geography, environment and cognition. A special theme issue. Geoforum 23(2)
Portugali J (1994) Theoretical speculations on the transition from nomadism to monarchy. In: Finkelstein I, Na'aman N (eds) From nomadism to monarchy. Yad Izhak Ben-zvi, Jerusalem, pp 203–217
Portugali J (1996a) Inter-representation networks and cognitive maps. In: Portugali J (ed) The construction of cognitive maps. Kluwer, Dordrecht/Boston/London, pp 11–43
Portugali J (ed) (1996b) The construction of cognitive maps. Kluwer, Dordrecht
Portugali J (2000) Self-organization and the city. Springer, Heidelberg
Portugali J (2002) The seven basic propositions of SIRN (Synergetic Inter-Representation Networks). Nonlinear Phenom Complex Syst 5(4):428–444
Portugali J (2003) SIRN (Synergetic Inter-Representation Networks), artifacts and snow's two cultures. In: Tschacher W, Dauwalder J-P (eds) Dynamical system approaches to embodied cognition. World Scientific, Singapore, pp 277–294
Portugali J (2004) Toward a cognitive approach to urban dynamics. Environ Plann B Plann Des 31:589–613
Portugali J (2005) Cognitive maps are over 60. In: Cohn AG, Mark DM (eds) COSIT 2005, LNCS, vol 3693. Springer, Berlin, pp 251–264
Portugali J (2006a) Complexity theory as a link between space and place. Environ Plan A 38:647–664
Portugali J (2006b) The scope of complex artificial environments. In: Portugali J (ed) Complex artificial environments: simulation, cognition and VR in the study and planning of cities. Springer, Heidelberg
Portugali J (ed) (2006c) Complex artificial environments: simulation, cognition and VR in the study and planning of cities. Springer, Heidelberg
Portugali J (2011) Complexity, cognition and the city. Springer, Berlin Heidelberg
Portugali J, Alfasi N (2008) An approach to planning discourse analysis. Urban Studies 45(2): 251–272
Portugali J, Haken H (1992) Synergetics and cognitive maps. In: Portugali J (ed) Geography, environment and cognition. A special issue. Geoforum 23(2):111–130
Portugali J, Benenson I, Omer I (1994) Socio-spatial residential dynamics: stability and instability within a self-organizing city. Geogr Anal 26(4):321–340
Portugali J, Benenson I, Omer I (1997) Spatial cognitive dissonance and sociospatial emergence in a self-organizing city. Environ Plann B Plann Des 27:263–285
Portugali J (2012) Complexity theories of cities: achievements, criticism and potentials. In: Portugali J et al. (eds) *Complexity Theories of Cities Have Come of Age*. Springer, Heidelberg, Berlin, pp 47–62
Portugali J, Tan E, Meyer VJ, Stolk EH (2012) Complexity theories of cities have come of age. Springer, Berlin Heidelberg

Portugali J, Stolk E (2014) A SIRN view on design thinking – An urban design perspective. *Environment and Planning B: Planning and Design* 41:829–846

Prigogine I (1980) From being to becoming. Freeman & Co, San Francisco

Prigogine I, Stengers I (1984) Order out of chaos. Bantam, New York

Pumain D (ed) (2005) Hierarchy in natural and social sciences, methodos series (hardcover). Springer, Heidelberg

Pumain D, Saint-Julien T, Sanders L (1987) Application of a dynamic urban model. Geogr Anal 19(2):152–166

Rasch W, Wolfe C (2000) Observing complexity. University of Mennesota Press, Minneapolis

Ratti C (2004) Space syntax: some inconsistencies. Environ Plann B Plann Des 31:487–499

Rosch E (1999) Reclaiming concepts. J Conscious Stud 6(11–12):61–77

Rosch E, Mervis C, Gray W, Johnson D, Boyes-Braem P (1976) Basic objects in natural categories. Cogn Psychol 8:382–439

Salingaros N (2005) Principles of urban structure. Techne Press, Amsterdam/Holland

Salingaros N (2006) A theory of architecture. Umbau-Verlag, Solingen

Sanders L (1992) Systems de Villes et Synergetique. Anthropos, Paris

Sanders L, Pumain D, Mathian H, Guerin-Pace F, Bura S (1997) SIMPOP: a multiagent system for the study of urbanism. Environ Plann B Plann Des 24:287–306

Sanglier M, Allen P (1989) Evolutionary models of urban systems: an application to the Belgian provinces. Environ Plan A 21:477–498

Schelling T (1974) On the ecology of micro-motives. In: Marris R (ed) The corporate society. Macmillan, London

Shannon CE, Weaver W (1959/1963) The mathematical theory of communication. University of Illinois Perss, Illinois

Simon H (1979) The science of the artificial. MIT Press, Cambridge, MA

Snow CP (1964) The two cultures and a second look. Cambridge University Press, Cambridge

Stadler M, Kruse P (1990) The self organization perspective in cognition research: historical remarks and new experimental approaches. In: Haken H, Stadler M (eds) Synergetics of cognition. Springer, Berlin, pp 32–52

Stolk EH, Portugali J (2012) A SIRN view on urban design – the case of Almere Hout. In: Portugali J, Tan E, Meyer VJ, Stolk EH (eds) Complexity theories of cities have come of age. Springer, Berlin Heidelberg

Stolk E, Portugali J (2016) A complexity-cognitive view on scale in urban design. In: Portugali J, Stolk E (eds) *Complexity, Cognition Urban Planning and Design*. Springer, Heidelberg, Berlin

Tan E, Portugali J (2012) The responsive city design game. In: Portugali J, Tan E, Meyer VJ, Stolk EH (eds) Complexity theories of cities have come of age. Springer, Berlin Heidelberg

Trope Y, Liberman N (2010) Construal-level theory of psychological distance. Psychol Rev 117:440–463

Tversky A, Kahneman D (1974) Judgement under uncertainty: heuristics and biases. Science 185:1124–1131

Tversky A, Kahneman D (1981) The framing of decision and psychology of choice. Science 211:4538

von Thünen JH (1826/1966) von Thünen's isolated state. An English translation (Hall P (ed)). Pergamon, Oxford

Watts DJ, Strogatz SH (1998) Collective dynamics of 'small-world' networks. Nature 393:440–442

Weidlich W (1987) Synergetics and social science. In: Graham R, Wunderlin A (eds) Lasers and synergetics. Springer, Berlin, pp 238–256

Weidlich W (1994) Synergetic modeling concepts for sociodynamics with application to collective political opinion formation. J Math Sociol 1(4):267–291

Weidlich W (1999) From fast to slow processes in the evolution of urban and regional settlement structures: the role of population pressure. In: Portugali J (ed) Population, Environment and Society on the Verge of the 21st Century. A special theme issue of Dis Dyn Nat Soc 3: 137–147

Weidlich W, Haag G (1983) Concepts and models of a quantitative sociology. Springer, Berlin/New York

Wirth L (1938) Urbanism as a way of life. Am J Sociol 64:1–24

Wittgenstein L (1953) Philosophical investigations (trans: Anscombe GEM). Blackwell, Oxford

Wu J, Gao Z, Sun H, Huang H (2004) Urban transit system as a scale-free network. Mod Phys Lett B 18(19–20):1043–1049

Zipf GK (1949) Human behaviour and the principle of least-effort. Addison-Wesley, Cambridge

Financial Market Dynamics: A Synergetic Perspective

Lisa Borland
Cerebellum Capital, San Francisco, CA, USA

Article Outline

Glossary
Introduction
Price Dynamics
Data
Stylized Facts of Markets
Financial Market Modeling
Predator-Prey, Many Interacting Agents, and Spin Models
Statistical Feedback Models
Multi-timescale Models
Cross-Sectional Dynamics
Simulations
Final Comments
Future Directions
Bibliography

Glossary

Econophysics An interdisciplinary research field where theories and methods originally developed by physicists are used to model financial markets and economic systems.

Market panic A state in which correlations among stock returns are very high together with highly elevated levels of the VIX Index.

Market volatility Market volatility is the uncertainty of price moves of a given market (rather than a single stock), such as the US stock market, which is well represented by the S&P 500 Index.

Stock returns The relative change in value of the price of a stock over a particular time horizon (e.g., 1 day or 1 year).

Stylized facts Statistical characteristics of financial time series that appear to be somewhat universal across asset classes and geographies. These include volatility clustering, long-range memory in absolute price returns, and the fat-tailed distribution of price returns that persist over horizons ranging from intraday to weeks.

The VIX Index Also known as the "fear" index, this represents a forward view of volatility or uncertainty in the market. It is computed from stock index option prices.

Volatility The risk or uncertainty of the magnitude of a stock's returns. Realized volatility can be calculated from the historical time series of stock returns over some past window, most commonly as the standard deviation of returns, but other proxies can be used such as the mean absolute value of returns.

Introduction

Over the past decades, the field of econophysics has become established as a subject area that connects concepts, ideas, and models stemming from physics to explain the underlying dynamics driving financial markets. In particular physicists have made advances in applying the fields of statistical physics and nonlinear dynamics to create models that explain some of the statistical and dynamic properties of financial markets. Underlying to many of these models are notions common to synergetics (Haken 1977), ranging from interacting agents and nonlinear feedback to predator-prey dynamics and spontaneous self-organization.

In reality, market researchers have access to historical price and volume time series for a collection of stocks. They analyze this data and try to understand the relationships and dynamics of this joint stochastic system either for the purpose of predicting future price changes or analyzing and predicting future risks. Traders and portfolio managers will use their inferences to construct

A. Hutt, H. Haken (eds.), *Synergetics*,
https://doi.org/10.1007/978-1-0716-0421-2_694

Originally published in
R. A. Meyers (ed.), *Encyclopedia of Complexity and Systems Science*, © Springer Science+Business Media LLC 2018
https://doi.org/10.1007/978-3-642-27737-5_694-1

desirable portfolios which they must construct by executing buys and sells in the market. But this in turn affects the market itself which feeds back into the historical data that they continue to analyze over time. Furthermore, at any instant, there is not just one trader interacting with the market but many, many thousands, across the globe and with their own unique objective. Their actions also feed back into the price formation process affecting the data that they then continue to analyze. In addition, news, external events, fundamental properties, and macroeconomic phenomena also get incorporated into the price. These interactions are sketched in Fig. 1, and it is clear to see that there are multiple feedback loops at play.

In this entry we'll provide an overview of financial market dynamics and some of the models that have been developed to describe them and conclude by going in depth for one example that stems directly from synergetics.

Price Dynamics

In my view the price of a stock is the macroscopic observable that emerges as a result of the microscopic interactions of many agents in an extremely complex system. At any given time, there is no such thing as a well-defined price of a stock. It is not as simple as when you go to the grocery store, and prices are clearly marked so a transaction can be planned and executed exactly. Instead, in financial markets, all across the globe at any moment in time, traders are submitting orders to buy and sell a certain amount of a stock; furthermore, their orders are not all sent to the same place but rather to one of several exchanges.

In addition each trader acts with their own view and utility on a spectrum of timescales; they base their buy or sell decisions on their individual information set for their own individual intent. Traders' views may depend on fundamental properties of the company whose stock is being traded, as well as general trends in the particular industry in question. Stock-specific events, such as mergers and acquisitions, have a big impact, as do world events, such as wars, terrorist attacks, and natural disasters. It is ultimately the collection and interaction of this supply and demand that drive the microscopic dynamics of price formation in conjunction of course with the rules of individual exchanges and regulations, which have evolved over the years and continue to do so. For example, in the United States in the mid-1990s, the NYSE and the Nasdaq were the only two exchanges where transactions could occur. Typical market participants were large institutions, and typical order sizes were in the thousands of shares. How quickly you got your order into the market was not

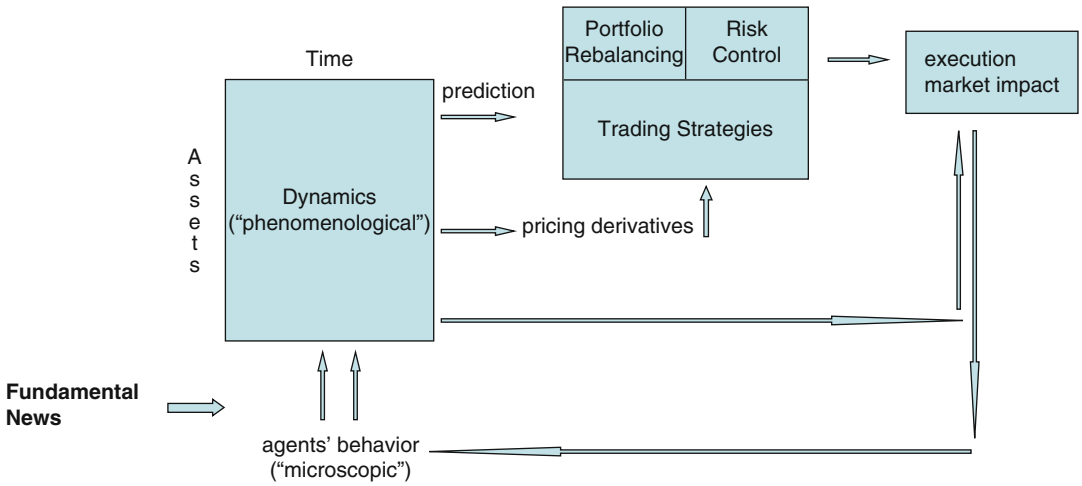

Financial Market Dynamics: A Synergetic Perspective, Fig. 1 The big picture: observed asset prices affect traders' decisions, which feed back into observed asset prices

an important factor. Today just some 20 years later, the market structure is quite different. The market is fragmented, consisting of several "dark pools" (where traders cannot see the orders of others) and 12 "lit" exchanges where traders can place their orders to buy or sell a given quantity of a stock at a given price. The orders on lit exchanges can be seen by market participants (hence the name). Typical order sizes are hundreds of shares, and institutional investors constitute a much smaller percentage since electronic trading has become accessible to anyone.

Trades can be organized into a so-called limit order book according to the price-time priority. An order has a time, price, size, and action (e.g., buy, sell, cancel, among others) associated with it. If two orders to buy come in with the same price, the one that came in first gets placed ahead in the order book queue. However if an order comes in to buy at a higher price, it goes ahead of the other orders regardless of when it entered the book. Orders to sell are handled in the same fashion. Size doesn't affect priority, and the different amounts available to be bought or sold at different prices constitute the full order book. At any given moment, at the top of the book, there is a best price to buy a certain amount and a best price to sell a certain amount. The difference between them is called the spread. If an order comes in that crosses the spread, a transaction will occur. As long as there is enough volume at the top of the book, then that is the price that the transaction will occur at; otherwise some of the orders will be filled at worse prices as the liquidity at deeper levels of the book gets consumed.

This illuminates the fact that there is no well-defined price. Is it the price to sell or the price to buy? Is it the mid of those? Is it some kind of volume-weighted mid, depending on how many orders to buy or sell at a given price? In practice, the last recorded transaction price is what is used here, but it is easy to see how this could be problematic if a stock doesn't trade very frequently.

Data

Over the past 20 years, the amount of financial data that is recorded has literally exploded. This is largely due to the explosion of electronic trading and its easy access to the community. Apart from the increased volume of algorithmic and electronic trading and the increased number of mainly electronic exchanges, other factors such as increased regulations for risk management and audit trails, decreased latencies, and higher time resolution also contribute to the exponential boom in data. There are also more traded instruments, new types of ETFs (exchange-traded funds which are essentially investable funds that themselves trade like stocks) and new derivative instruments. As an example of increased time stamp granularity, the TAQ (Trade and Quote) database which has been one of the main sources of transaction data for the NYSE, AMEX, and Nasdaq exchanges started out recording trades and quotes with times stamps marked at the second precision from 1993 to 2003. After that the data was collected at millisecond precision until 2015 and is currently marked at nanoseconds after a brief microsecond era. This is just one example showing the evolution of the importance of speed and the actual timescales that are now relevant. While in the past, only the price and volume at the top of the limit order book was available, the entire depth of the book can be constructed because every order on each of the many electronic exchanges are collected and consolidated.

Stylized Facts of Markets

The huge amounts of data started attracting the attention of physicists around the mid-1990s, and many of the early seminal papers dealt with uncovering and understanding properties of the empirical distribution of returns (or relative price changes). Returns of stocks can be calculated over different timescales τ, and when the distributions of these are plotted out, it is clear that they are far from Gaussian, but rather are well fit with power-law tails in such a way that the power-law behavior persists from timescales ranging from intraday to the order of a few weeks. On daily timescales, the exponent of the power law is about 3, often referred to as the cubic law of finance (Gopikrishnan et al. 1999; Gabaix et al. 2003). The kurtosis of these distributions decays in a regular fashion, roughly as $\tau^{-0.2}$ where τ is the

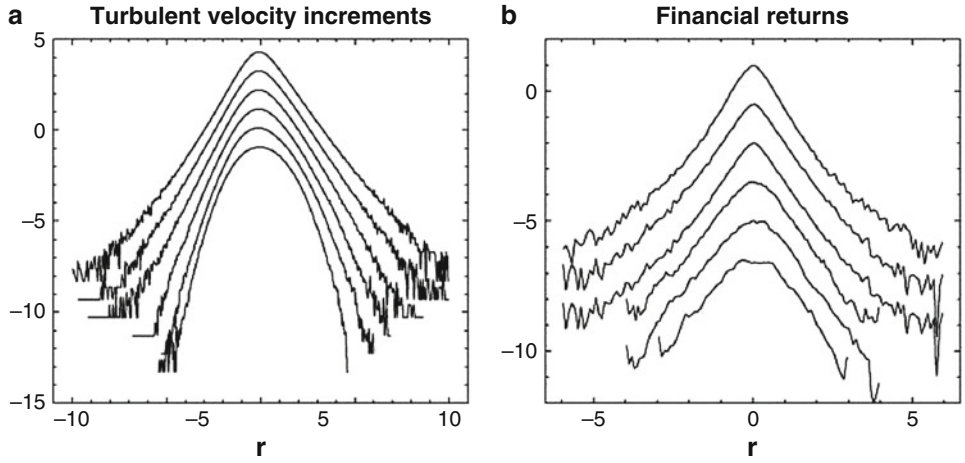

Financial Market Dynamics: A Synergetic Perspective, Fig. 2 The distribution of financial returns bear similarity to the distribution of velocity in turbulent systems. Small scales (top), larger scales (bottom). The y-axis is on a logarithmic scale, and curves are shifted for display purposes. In (**a**) r = velocity increments, and in (**b**) r = returns, in units of standard deviations

timescale over which returns are calculated (Bouchaud and Potters 2004). These distributions bear many similarities to those of turbulent systems (see Fig. 2).

Volatility (defined either as the standard deviation of returns over some past window or simply by a proxy such as the absolute value of returns) exhibits clustering behavior such that there appears to be regimes of higher or lower volatility, on all timescales (see Fig. 3). Furthermore, there is memory in volatility in the sense that the autocorrelation of absolute returns is very strong, decaying slowly as a power law. More subtle statistical features are inherent, such as a behavior analogous to the Omori law for earthquakes in that a large volatility shock will be followed by aftershocks at a certain rate. Furthermore, large negative returns are indicative of higher volatility, an effect known as the leverage effect (Bouchaud et al. 2001). Figure 3 beautifully illustrates some of these effects. It shows intraday prices for a few days surrounding May 6, 2010, the day of the so-called Flash Crash. After a large negative return, volatility increases and decays only slowly. Another interesting property of stock return time series is the presence of time-reversal asymmetry in the sense that future volatility conditioned on past observations is not symmetric (Lynch and Zumbach 2003). Finally, financial time series exhibits multi-fractal scaling of moments (see, e.g., Borland and Bouchaud 2012). All of these so-called stylized facts are not only observed for stock returns but also for other financial instruments such as commodities and currencies, and they are observed across geographies. Realistic market models should ideally capture the basics of these features for stock returns and volatility across time.

Financial Market Modeling

Modeling the intricate dynamics and microstructure of the limit order book is a field of study which has gotten some traction over the past decades. One of the most insightful and detailed studies attempting to understand the dynamics of price formation on this level, as well as the market impact of trading, has been done within the physics community, for example, by Bouchaud, Farmer, and Lillo (Bouchaud et al. 2004, 2009; Lillo et al. 2003). They reveal that the processing of supply and demand in markets has long-range memory and is also related to the origin of market fluctuations among many other interesting findings. Another interesting and rather intuitive model of the order book was developed by Cont et al. (2010) who formulated a stochastic equation for the mid-price based on the order book dynamics. More recently, some authors model the order

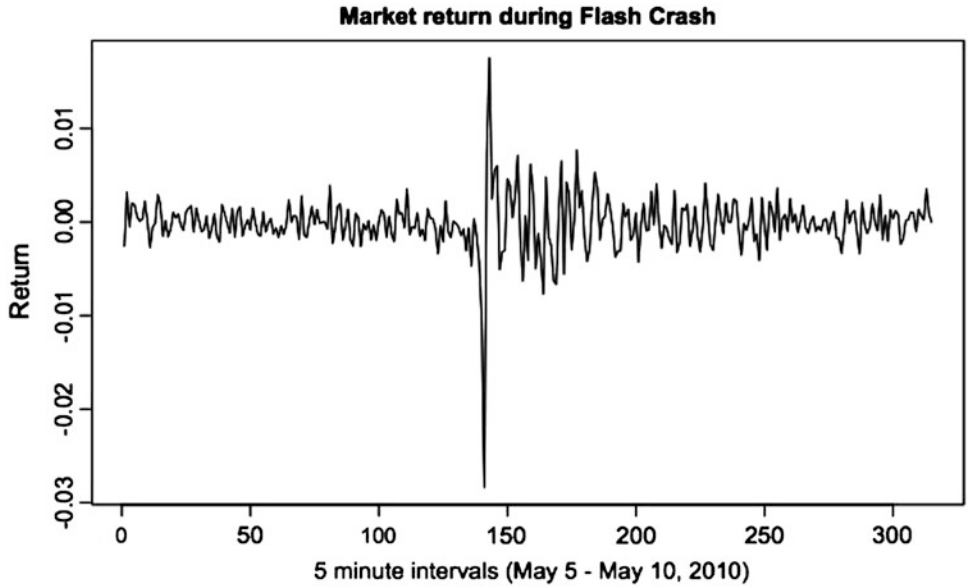

Financial Market Dynamics: A Synergetic Perspective, Fig. 3 A time series of market returns around the Flash Crash of May 6, 2010

flow dynamics of bids and ask via self-exciting Hawkes processes (Bacry and Muzy 2014; Alfonsi and Blanc 2015), leading to a nice framework where questions such as optimal trade execution, for example, can be studied. In spirit and in analogy to physics, these models eluded to above can be seen as microscopic models, based on underlying empirical observations of the actual order placement and execution process (viz., the order book). Ultimately though, the price once formed evolves as a stochastic process, and it is often more tractable to use a mesoscopic description which aims at describing the price process as a stochastic Langevin equation where the key feature is how to capture the volatility, or noise, that drives the process. This is the most important effect since stock price changes (or returns) from moment to moment are essentially unpredictable, so the deterministic part of the equation is less interesting. (Though of course, if you can predict it ever so slightly, you are in luck!)

For many years and in a large body of the financial literature, the random nature of price time series was modeled by most as a simple Brownian motion. The first to propose such a model was Bachelier in his thesis in 1900, which lays largely undiscovered until much later when Black and Scholes wrote their famous paper in 1973 based on a very similar model. They made important contributions in particular to the pricing of options, for which they received the Nobel Prize (Black and Scholes 1973) in 1997. Options are traded instruments that give the right, not the obligation, to buy a stock at a later date at a certain price, called the strike price. In Black and Scholes' work, the log price is assumed to follow a Gaussian distribution, and even today many trading assumptions and risk control notions are based off of that prior.

However, as we have seen, the Gaussian model of Black and Scholes is insufficient to describe the statistical properties of real financial time series data. Several alternative models have been proposed, and here we review some that fit well into the spirit of synergetics.

Predator-Prey, Many Interacting Agents, and Spin Models

The Lotka-Volterra equation is used to describe the positive and negative feedback loops between interacting species, where one preys on the other. It is also one of the first successful models for

describing the fact that wealth among members of the society follows a Pareto power-law distribution (and hence also that fluctuations in financial markets follow a power law) (Levy et al. 2000; Levy and Solomon 1997; Solomon 1998). That model also recovers realistic features of financial markets such as bubbles and crashes as well as volatility clustering.

The basic ingredients of the model are to introduce feedback between individual and collective wealth fluctuations of a collective set of traders. The central feedback loop consists in computing the market price of the stock as the sum of the individual wealths w_i invested in the stock by the traders and then determining fluctuations of a given trader's wealth as their previous wealth multiplied by the stock return. The basic idea of the model is that wealth at time $t + 1$ is proportional to wealth at time t multiplied by the random factor which corresponds to relative gains or losses over the last period. There is also a coupling of the individual's wealth to the global wealth of the society (e.g., things like social services). In addition, there is also competition between each individual and the other members of society, which plays the part of limiting growth of the average wealth to values that are sustainable for the current conditions and resources. The Solomon-Levy model leads to a power law for the distribution of individual wealth, namely:

$$P(w) \propto w^{-1-\eta} \tag{1}$$

where η is typically between -1 and -2. In Solomon (1998) the very interesting conclusion is drawn that any quantity which is a sum of random increments proportional to the wealths w_i will have fluctuations described by a Levy distribution of index β equal to the exponent η of the wealth power distribution. Since the individual investments are stochastically proportional to the investors' wealth, the stock market fluctuations will be described by a truncated-Levy distribution of index equal to the measured exponent $\eta = 1.4$ (which results in a tail index close to 3 as eluded to above when we talked about the cubic law of finance). This is an amazing and nontrivial result: based on simple notions of competition, local and global feedback of the wealth of members of society, a mechanism for describing the distribution of stock market fluctuations is designed.

Solomon and Levy's wealth equation is a mesoscopic description of the stock market which was written down by the authors as a description of the outcome of many simulation runs of their microscopic model (Levy et al. 2000). The microscopic model looks at individual investors with various ways of deciding how much stock to buy or sell at a given time. Simulations of that collective group of investors then gave rise to the dynamics of wealth fluctuations as described by their Lotka-Volterra equation.

Another approach of interacting agents was proposed by Lux and Marchesi (2000). Individual trading agents are simulated, including an explicit price formation process. Agents are modeled as different types of traders interacting in a speculative market: "noise traders" and "fundamentalists." Fundamentalists base their action on fundamental valuation of the stock. The noise traders base their trading decisions on price data and flows, which leads to herding behavior. They react to the recent past of the market and can have either positive or negative expectations of the future based on that past. The dynamic of the model is that traders compare profits gained by the noise traders and fundamentalists and then switch their own strategy to that which was more profitable in the recent past. Depending on whether traders want to buy or sell, supply or demand will be infused into the market, and the price will be adjusted according to the excess demand. In addition, the dynamics of the fundamental value of the stock follows a standard lognormal Brownian motion with uncorrelated Gaussian noise.

Lux and Marchesi formulate the state-dependent transition probabilities that describe, for each group of traders, the probability of switching to the other group. For noise traders there is also the internal switching between a pessimistic and optimistic view of the market. The price gets adjusted up or down based on supply and demand according to excess demand being either on the buy or sell side.

Based on these simple yet realistic dynamics, a theoretical analysis and simulations show that the most important features of real financial markets emerge as a consequence. They find that the

market is on average efficient in the sense that the price on average reflects a fundamental equilibrium. The amount of pessimistic and optimistic traders is roughly even, and in equilibrium both the noise traders and the fundamentalists do equally well. Though the system always tends toward a stable equilibrium, it exhibits autocorrelated fluctuations around that fundamental equilibrium and simulations of the model show on-off intermittency of fluctuations. This is very similar to the properties of real market fluctuations, where volatility shows memory and clustering.

Other classes of models are spin-based models in which analogies are made between the interactions and dynamics of spin systems and financial markets. Some interesting spin models have been proposed, for example, Cont and Bouchaud (2000), Chowdhury and Stauffer (1999), and Bornholdt (2001). These models can reproduce (under certain parameter settings) features such as the volatility clustering of financial markets.

Statistical Feedback Models

The above models are useful as frameworks to think about the dynamics of market participants and the emergence of the stylized facts one observes. For certain applications (e.g., risk management or the pricing of options), a slightly higher level view of price formation can be useful, namely, in terms of modeling the price itself as a stochastic process.

As mentioned above most of traditional mathematical finance is based on the Black-Scholes model which assumes a Brownian equation of motion for stock prices:

$$dS(t) = \mu S dt + S\sigma d\omega \tag{2}$$

where ω is drawn from a Gaussian distribution with zero mean and variance one. This type of model is very useful because it allows for the analytic calculation of many important quantities related to risk management and derivative instruments such as options. However, that model is too simple to capture all of the anomalous statistics observed in real financial time series. In an attempt to rectify that, several modifications to the standard Black-Scholes model of price returns have been proposed in the literature, and they all have in common that they somehow extend either the assumption of a constant volatility term σ in Eq. 2 or the source of the noise term ω. For example, there is the stochastic volatility model of Heston (1993) where σ itself is modeled as a mean reverting stochastic process and the Levy models where the noise ω is assumed to be drawn form a fat-tailed Levy distribution. Those models are a little more realistic than the standard model, but both have the shortcoming that they convolve too quickly to a Gaussian distribution, meaning that they do not capture the persistence of fat tails of return distributions over the timescales observed in reality, where returns over timescales ranging from seconds up to about 2 weeks or longer all still exhibit tails. One model which does really well in this sense (and also earned a Nobel Prize for Engle (Bollerslev et al. 1994)) is the GARCH model, which incorporates memory into σ. In fact, the memory of volatility is a key feature that reproduces many known stylized facts of financial price series.

Motivated among other things by this, we proposed a model (Borland 2002a, b; Borland and Bouchaud 2004) within the framework of nonextensive statistical physics (Tsallis 1988) in which the volatility term follows a statistical feedback process in the sense that it depends on the probability of past observations, explicitly:

$$dS = \mu S dt + \sigma S d\Omega \tag{3}$$

where

$$d\Omega = P(\Omega)\frac{1-q}{2}d\omega. \tag{4}$$

In this equation, P corresponds to the probability distribution of Ω, which simultaneously evolves according to the corresponding nonlinear Fokker-Planck equation (Tsallis and Bukman 1996; Borland 1998):

$$\frac{\partial P}{\partial t} = \frac{\partial P^{2-q}}{\partial \Omega^2}. \tag{5}$$

It can be solved exactly yielding:

$$P = \frac{1}{Z(t)}\left(1 - (1-q)\beta(t)\Omega(t)\right)^{\frac{1}{1-q}} \qquad (6)$$

The exact form of the coefficients Z and β are given in Borland (2002a, b). Equation 6 recovers a Gaussian in the limit $q \to 1$ while exhibiting power law tails for $q > 1$. In that case, our model is exactly equivalent to the Black-Scholes model.

The statistical feedback term P can be seen as capturing the market sentiment. Intuitively, this means that if the market players observe unusually high deviations of $\Omega(t)$ (which is essentially equal to the detrended and normalized log stock price) from the reference value $\Omega(0)$, then the effective volatility will be high because in such cases $P(\Omega)$ is small, and the exponent $1 - q$ is a negative number. Conversely, traders will react more moderately if Ω is close to its more typical or less extreme values. As a result, the model exhibits intermittent behavior consistent with that observed in the effective volatility of markets. In practice, q can be obtained empirically from a fit to the data. Remarkably, $q = 1.4$–1.5 fits very well to return distributions of very many financial instruments, corresponding to a tail index of about 3.

This non-Gaussian statistical feedback model allowed us to derive closed-form option pricing formulae (Borland 2002a, b; Borland and Bouchaud 2004) that fit very well to real market prices over many time horizons, and we used the model in real-life trading situations. For further reading about this topic, summarized successes, applications, and shortcomings of the model, we refer to Borland (2008).

Multi-timescale Models

In spite of the success at pricing options and other derivatives such as credit default swaps, as a model of real returns, the statistical feedback formulation has the drawback that returns relative to a particular initial time constituting the memory in the volatility; instead we took inspiration from that model and proposed that the volatility depends on returns over multiple timescales (Borland and Bouchaud 2012). The intuition is that different traders pay attention to different timescales. For example, some only care about returns on an intraday or daily level; others are more focused on monthly or whatever the rebalancing frequency is of their trades. Explicitly, this multi-timescale model can be written as:

$$\Delta y = \sigma_t \, \Delta\omega \qquad (7)$$

$$\sigma_t = \sigma_0 \sqrt{1 + \sum_{\tau=0}^{T} \frac{g}{\sigma_0^2 \tau_\alpha} \left(y_t - y_{t-\tau}\right)^2} \qquad (8)$$

where y denotes the logarithm of the stock price; hence Δy represents the change in log stock price and corresponds to stock returns. The parameters g and α can be calibrated to fit empirical data ($g = 0.85$ and $\alpha = 1.15$) (Borland and Bouchaud 2012), and σ_0 corresponds to the baseline volatility. ω represents uncorrelated standard Gaussian noise. This model is motivated by the statistical feedback model that we presented in Borland (2002a, b) and Borland and Bouchaud (2004) and is very similar to the FIGARCH models (Lynch and Zumbach 2003; Bollerslev et al. 1994). In fact, without the summation and setting $t - \tau = 0$, this equation can be shown to be of the same form as our statistical feedback model. That model has the advantage of analytic tractability for options pricing, whereas Eq. 7 doesn't allow for that. However, it can be simulated and shown to fit real data remarkably well, reproducing a slew of known stylized facts (Borland and Bouchaud 2012), including volatility clustering, the fat-tailed distributions of returns persistent over increasing timescales, time-reversal asymmetry of volatility, and multi-fractal scaling properties.

Cross-Sectional Dynamics

The models we discussed up to now have focused on capturing the time series properties of stock returns. In order to fully understand the joint stochastic process, the cross-sectional dynamics of stock returns, i.e., the dynamics of the correlation structure of markets, is also important. Understanding how the distribution of returns as well as

their correlations behaves during such times as the financial crisis in 2008 can be extremely important for managing financial risks. Several authors have studied these cross-sectional dynamics, such as Borland (2012), Preis et al. (2012), Kaizoji (2006), Lillo and Mantegna (2000), Munnix et al. (2012), Ferreira et al. (2015), Raffaelli and Marsili (2006), and Sornette (2002), but we shall delve into one model that fits right into the paradigm of synergetics (Borland 2012).

To set the stage, one should understand that financial markets go through different types of regimes (often referred to as "risk on" or "risk off") or, as in this paper, "panic" times or "normal" times. The VIX Index captures forward-looking expected volatility. In "panic" times, the VIX is very high, whereas in "normal" times, it is more moderate. Based on the VIX, one can for US markets categorize the periods 2008–2009 (the financial crisis), 2010 (the foreclosure crisis), and 2011 (the debt ceiling crisis) as periods of high uncertainty or panic. As discussed in Borland (2012) we showed that, during panic times, the dispersion (standard deviation) of stock returns cross sectionally increases, as does the time series volatility. However, the kurtosis (corresponding to the tails of the cross-sectional distribution) tends to decrease. In addition, correlations approach 1.

To further explore the correlation structure, or co-movement of stocks at a given time, we define the variable s:

$$s = \frac{s_{\text{up}} - s_{\text{down}}}{s_{\text{up}} + s_{\text{down}}} \tag{9}$$

where s_{up} is the number of stocks that has positive returns over a given interval and s_{down} is the number of stocks that has negative moves on that same interval (e.g., a day). If $s = 0$ then roughly the same number of stocks moved up as down, and the assumption is that the stocks had little co-movement and so were uncorrelated. If all stocks move together either up or down, the value of s will be +1 or −1, and the stocks will have high correlation. So, the following picture emerges: if $s = 0$ there is no correlation, and we are in a disordered state. However if $s \neq 0$ then there is correlation, and we are in an ordered state; in other words, in the spirit of synergetics, s is the order parameter of the system. This behavior of s under different market conditions can be seen in histograms calculated for data during periods of panic versus more normal periods. In normal times, s is unimodal, and in panic times we obtain a bimodal distribution (see Fig. 4).

We refer to these phenomena as statistical signatures of market panic: high time series volatility, high cross-sectional dispersion, low cross-sectional kurtosis, and a bimodal distribution of s. In order to create a model that replicates these signatures, we proposed in Borland (2012) a synergetic model where the variable s plays the same role as the magnetic moment in a ferromagnetic spin system. In the same way that the magnetic system will either be in an ordered or disordered state depending on the value of the temperature, the financial system will be in a correlated or uncorrelated state depending on the value of volatility.

Explicitly, the stock returns for each instrument across time is modeled by Eq. 7 (inserting $\Delta\omega^i = \omega_t^i\sqrt{\Delta t}$ according to the assumptions of Brownian noise):

$$\Delta y^i = \sigma_t^i \omega_t^i \sqrt{\Delta t} \tag{10}$$

with

$$\sigma_t^i = \sigma_0^i \sqrt{1 + \sum_{\tau=0}^{T} \frac{g}{\left(\sigma_0^i\right)^2 \tau^\alpha} \left(y_t^i - y_{t-\tau}^i\right)^2} \tag{11}$$

where y_i is the log stock price of the i-th stock and ω_t^i is a zero mean Gaussian noise with unit variance so that $\left\langle \omega_t^i \omega_{t'}^i \right\rangle = \delta_{tt'}$. For an ensemble of N stocks, we assume that the ω_t^i, $i = 1, \cdots, N$ are correlated proportional to $|s|$ across stocks, so $\left\langle \omega_t^i \omega_t^j \right\rangle = |s|$ for $i \neq j$ and 1 for $i = j$.

We hypothesize that s can be described by the Langevin equation

$$\frac{ds}{dt} = -as - bs^3 + F_t \tag{12}$$

with $a = \gamma(\sigma_c - \sigma_M)$, b a scaling parameter, and σ_c a critical volatility level, and σ_M is the market

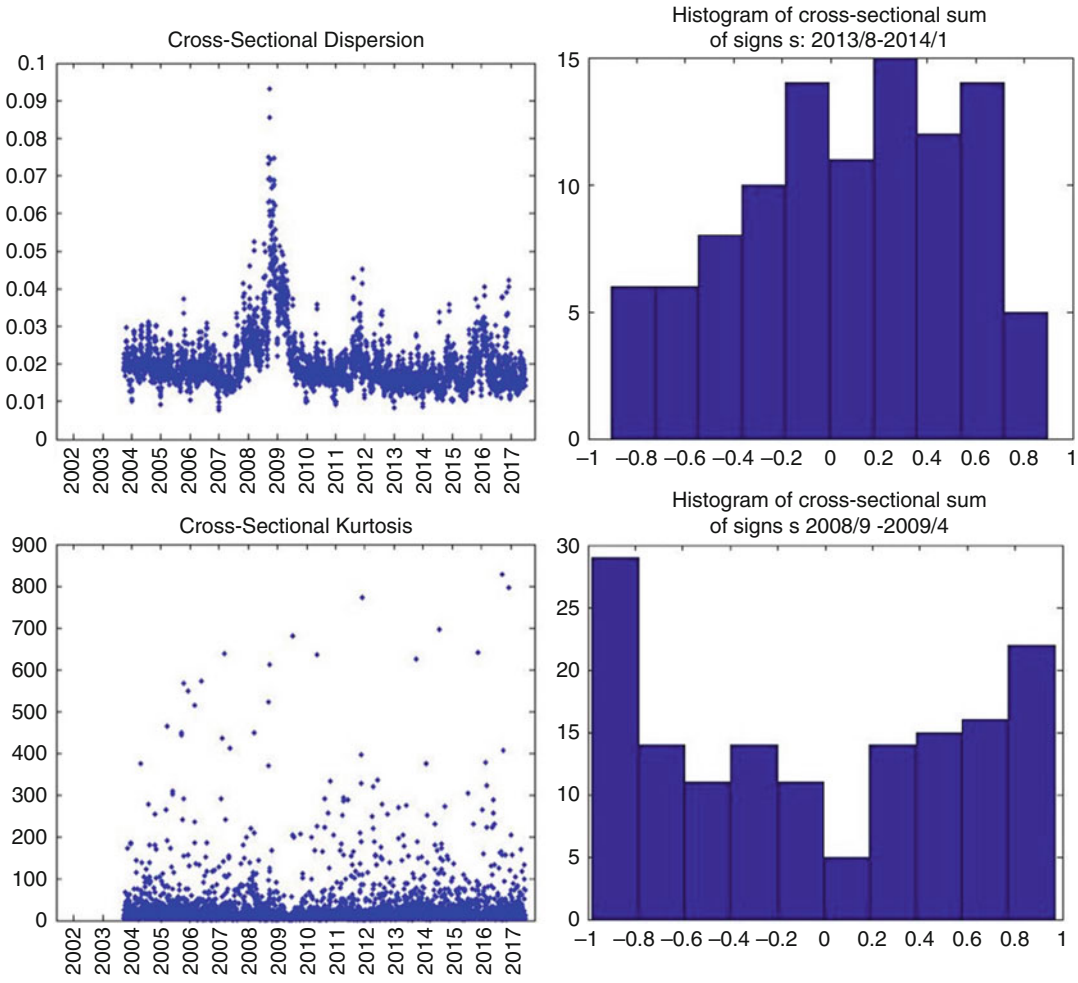

Financial Market Dynamics: A Synergetic Perspective, Fig. 4 Properties of cross-sectional stock returns in normal times, and times of panic (Borland 2012), calculated across the top 1000 stocks by market capitalization. "Panic" times are defined as periods of high uncertainty among investors, such as 2008–2009 (the financial crisis), 2010 (the foreclosure crisis), and 2011 (the debt-ceiling crisis)

volatility. In this model, s can be thought of as jiggling around in a potential well. The control parameter of the system is σ_M. When $\sigma_M < \sigma_c$, that well only has one minimum at 0, so $|s|$ fluctuates around that point. If $\sigma_M > \sigma_c$ the potential well attains two new minima at $\pm\sqrt{a/2b}$. $|s|$ becomes non-zero, and correlations are high: stocks tend to move up or down together in accordance, which is manifested in a bimodal distribution of s. We say that there is a phase transition as σ_M crosses above the critical value, since the collective behavior of the stocks is qualitatively very different. This type of phase transition model is based on the dynamics and theories of synergetic self-organizing systems. In particular, s can be seen analogous to the magnetic moment m in ferromagnetic systems, There, the system goes from the disordered to the ordered state as the temperature T (which is the control parameter) drops beneath a critical temperature T_c.

Hence, the parameter σ_M in the financial system plays a role similar to temperature in the magnetic system.

We model σ_t^i as in Eq. 11. Conditions for stability and values which calibrate to real returns are discussed extensively in Borland and Bouchaud (2012). The feedback in the model is controlled by g, and the power law memory in time is related to α.

The market volatility σ_M can increase to values larger than σ_c due to either (i) exogenous jumps (news, external fear) affecting all stocks so that σ_0 becomes $\sigma_0 + \sigma_{\text{shock}}$ or (ii) endogenous, idiosyncratic jumps which are more stock specific. In this paper we consider only exogenous jumps describing market-wide situations such as the Lehman Brothers collapse, although endogenous ones akin to the dynamics of the Flash Crash have been discussed in Borland and Hassid (2010).

Simulations

To simulate the joint cross-sectional dynamics of the market, the individual dynamics of $N = 500$ stocks are generated using Eqs. 10 and 11. The "market" is then defined as the equal weighted average of those stocks' returns. This is akin to how the *S&P* 500, which represents the US market, is composed of 500 stock returns (albeit weighted by market capitalization). Furthermore, market-wide exogenous shocks which correspond to external fear factors or general sentiment are applied to the base volatility σ_0. In previous papers we have injected artificial shocks, but for this contribution, we let the actual jumps in the VIX drive the external exogenous volatility shocks in the model such that if the VIX corresponds to a volatility greater than 0.25, it will induce a shock σ_{shock} to the system such that σ_0 becomes $\sigma_0 + \sigma_{\text{shock}}$.

The dynamics of each individual stock were generated using Eqs. 10 and 11. The parameters used were those determined in Borland and Bouchaud (2012), namely, the feedback parameter $g = 0.85$ and $\alpha = 1.15$. The base volatility was chosen at $\sigma_0 = 0.20$ which is the typical annualized volatility of a stock, and we allow $\sigma_{t0}^i = \sigma_0(1 + \varepsilon * \eta(t))$ where η is a zero mean white noise, and $\varepsilon = 0.2$ was chosen. We included $T = 300$ terms in the volatility feedback term. The time step for the simulations was chosen to $\Delta t = 1/252$, corresponding to 1 trading day (there are 252 trading days in a year). The noise σ_t^i driving each stock is drawn from a normal Gaussian distribution uncorrelated in time with 0 mean and unit standard deviation yet with a correlation across stocks driven by Eq. 12.

More explicitly, the correlations across stocks at a given time point were modeled according to the phenomenological equation (12) using $b = 0.01$ and $F_t = 0.1v$ where v is a standard Brownian noise. Given a value of s from this equation, the noise across stocks was then drawn from a correlated set of noises, with correlation equal to $\tanh|s|$. The mechanism for attaining that noise utilized the Cholesky decomposition technique. The critical volatility σ_c was chosen to be $\sigma_c = 0.4$ which is roughly twice the annualized standard deviation of market returns. At each time point in the simulation, individual stock paths are generated, and their mean is taken to represent the value of the market as a whole at that time point. The control parameter $\sigma_M = \sigma_0 + \sigma_{\text{shock}}$ feeds back into Eq. 12 thus affecting the correlation dynamics that defines the cross-sectional behavior of the 500 stocks in the simulation.

Figure 5 shows actual market returns in the time period 2003–2017, together with the VIX. Figure 6 shows simulated market returns, together with a plot of market volatility defined as the recent standard deviation of market returns. It is clear that the features follow the general profile of actual returns quite closely, and the simulated market volatility reflects the main features of the VIX (although remember these will not match exactly since the VIX is an index calculated from the implied volatility of options on the *S&P* 500). The simulation does have volatility spikes in 2008–2009, 2010, and 2011, as does the VIX. We also show a time series

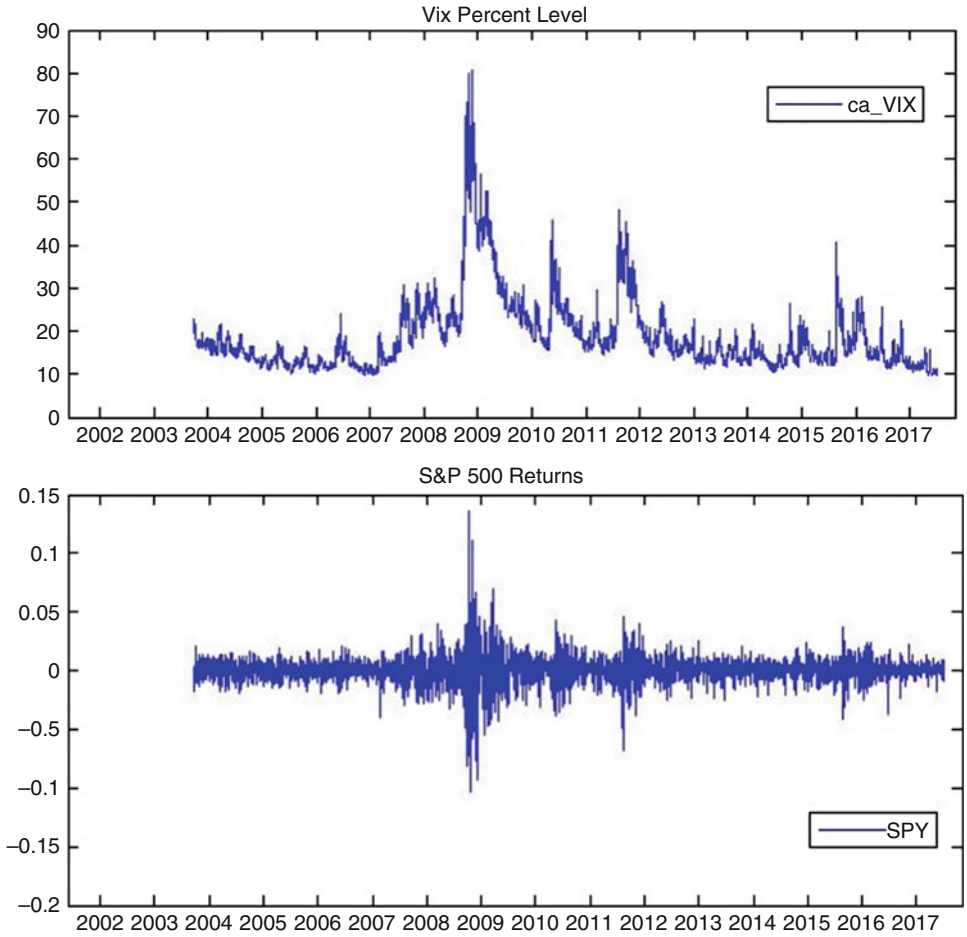

Financial Market Dynamics: A Synergetic Perspective, Fig. 5 The VIX volatility index and daily S&P 500 market returns

of 2 of the 500 simulated stock returns that constitute the market in aggregate. Individual stocks' price paths were generated by Eq. 11 and exhibit idiosyncratic periods of volatility clustering not apparent in the market, due to the multi timescale feedback aspect of the dynamics which is stock specific. In addition, cross-sectional dispersion of the simulated stock market increases in times of panic, while the kurtosis appears to dip in those periods. Finally, histograms of s are bimodal during the times of panic, and unimodal in normal times, just as in the real data. These cross-sectional properties are shown in Fig. 7. It is apparent that the model captures a similar behavior of cross-sectional features as in the real market data.

Final Comments

The multi-timescale collective feedback model we described for the joint stochastic process of a set of stocks over time agrees qualitatively with actual features seen in real markets, both across time and across stocks. Elements of synergetics enter the

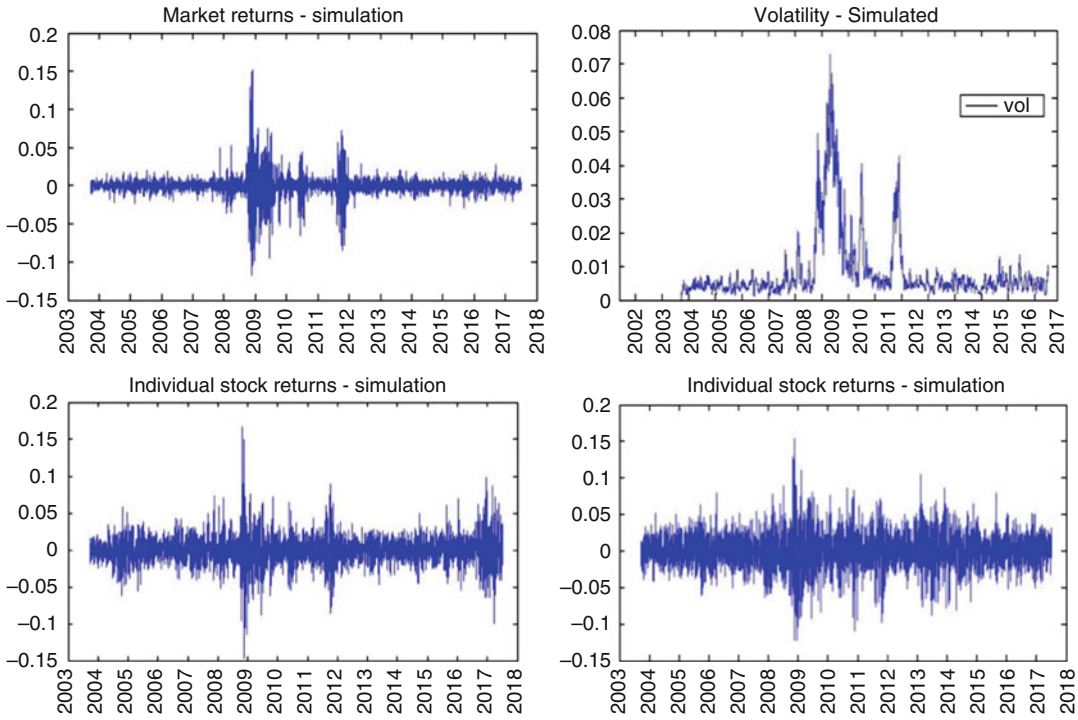

Financial Market Dynamics: A Synergetic Perspective, Fig. 6 The simulated market returns, together with two individual stocks' return time series. We also show simulated market volatility which can be compared to the VIX

model in various aspects. The correlation between stocks acts as the order parameter of the system, with the volatility, which is related to the collected external perception of panic or fear acting as the control parameter. Furthermore, the dynamics of each individual stock follows a feedback process that aims to capture the collective behavior of individual agents acting on different timescales. In addition, we have reviewed other more agent-based models that have been proposed within the physics and econophysics community that all have similar notions embedded, namely, that it is the interaction of individual market participants and the feedback with the overall macroscopic level of the financial system (be it via price, wealth, or volatility) that appear to lead to systems that reproduce many of the interesting anomalous statistics observed in real financial markets.

Future Directions

Financial markets are constantly evolving, producing ever-increasing sets of data, so the task of modeling the complexities driving their behavior will certainly remain a fruitful area of research for some time to come. Additionally, in spite of the success of the models we have discussed here when it comes to reproducing realistic market features and stylized facts, many financial practitioners still use the simpler notions consistent with a Black-Scholes-type Gaussian model of financial time series. One reason for this could be that many of the models have been developed within the field of econophysics, using concepts from physics, and are not yet incorporated in more traditional mathematical finance programs. An important area of further work would therefore

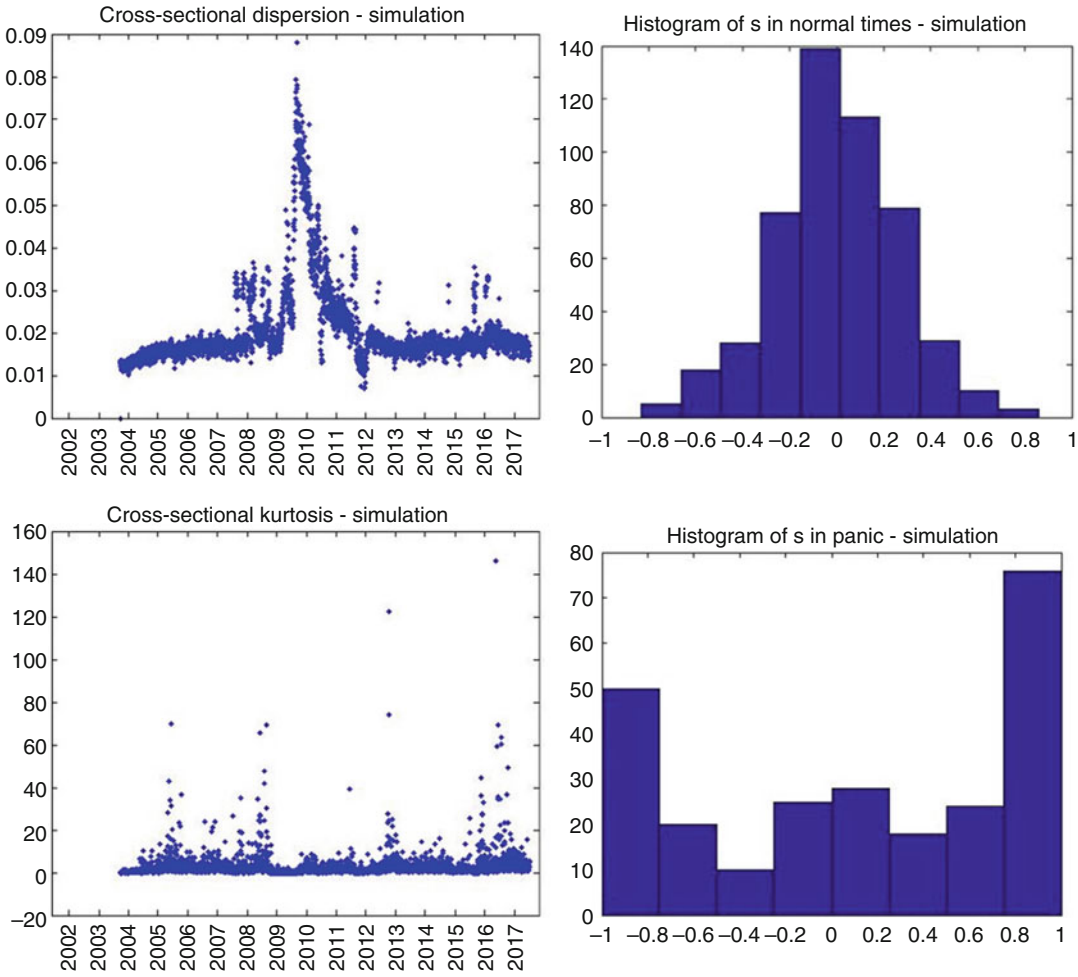

Financial Market Dynamics: A Synergetic Perspective, Fig. 7 Cross-sectional properties of the simulated 500 stock return paths comprising the simulated market

be to try and integrate some of the new insights that these models lend us into practical applications which can be used where real money is managed, in order to have better and more proactive tools both for price modeling and risk management.

Bibliography

Alfonsi A, Blanc P (2015) Dynamical optimal execution in a market-impact Hawkes price model. In: Finance and stochastics. Springer, Heidelberg, pp 1–36

Bacry E, Muzy J-F (2014) Hawkes model for price and trades high-frequency dynamics. Quant Finance 14(7):1147–1166

Black F, Scholes M (1973) The pricing of options and corporate liabilities. J Polit Econ 81:637–659

Bollerslev T, Engle RF, Nelson DB (1994) ARCH models. In: Engle RF, McFadden D (eds) Handbook of econometrics, vol 4. Elsevier Science, Amsterdam

Borland L (1998) Microscopic dynamics of the nonlinear Fokker-Planck equation: a phenomenological model. Phys Rev E 57(6):6634

Borland L (2002a) Option pricing formulas based on a non-Gaussian stock price model. Phys Rev Lett 89(9):098701

Borland L (2002b) A theory of non-Gaussian option pricing. Quant Finance 2:415–431

Borland L (2008) Non-Gaussian option pricing: successes, limitations and perspectives. In: Editors Claudia Riccardi, H. Eduardo Roman (eds) Anomalous fluctuation phenomena in complex systems: plasmas, fluids and financial markets. Research Signpost, India, pp 311–333

Borland L (2012) Statistical signatures in times of panic: markets as a self-organizing system. Quant Finance 12(9):1367–1379

Borland L, Bouchaud J-P (2004) A non-Gaussian option pricing model with skew. Quant Finance 4:499–514

Borland L, Bouchaud J-P (2012) On a multi timescale statistical feedback model for volatility fluctuations. J Invest Strateg 1:1–40

Borland L, Hassid Y (2010) Market panic on different time-scales. ArXiv e-prints 1010.4917

Bornholdt S (2001) Expectation bubbles in a spin model of markets: intermittency from frustration across scales. Int J Mod Phys C 12(05):667–674

Bouchaud J-P, Potters M (2004) Theory of financial risks and derivative pricing. Cambridge University Press, United Kingdom

Bouchaud J-P, Matacz A, Potters M (2001) Leverage effect in financial markets: the retarded volatility model. Phys Rev Lett 87(22):228701

Bouchaud J-P, Gefen Y, Potters M, Wyart M (2004) Fluctuations and response in financial markets: the subtle nature of random price changes. Quant Finance 4(2):176–190

Bouchaud J-P, Farmer JD, Lillo F (2009) How markets slowly digest changes in supply and demand. In: Thorsten Hens Klaus Schenk-Hoppe (ed) Handbook of financial markets: dynamics and evolution. Elsevier, North Holland, pp 57–160

Chalet D, Marsili M, Zhang Y-C (2013) Minority games: interacting agents in financial markets. OUP Catalogue, Oxford University Press, United Kingdom

Chowdhury D, Stauffer D (1999) A generalized spin model of financial markets. Eur Phys J B 8(3):477–482

Cont R, Bouchaud J-P (2000) Herd behavior and aggregate fluctuations in financial markets. Macroecon Dyn 4(02):170–196

Cont R, Stoikov S, Talreja R (2010) A stochastic model for order book dynamics. Oper Res 58(3):549–563

Ferreira P, Dionasio A, Movahed SMS (2015) Stock market comovements: nonlinear approach for 48 countries. arXiv.org [q-fin] arXiv:1502.05603

Gabaix X, Gopikrishnan P, Plerou V, Stanley HE (2003) A theory of power-law distributions in financial market fluctuations. Nature 423:267

Gopikrishnan P, Plerou V, Nunes Amaral LA, Meyer M, Stanley HE (1999) Scaling of the distribution of fluctuations of financial market indices. Phys Rev E 60:5305

Haken H (1977) Synergetics: an introduction. Springer, Berlin-Heidelberg-New York

Heston SL (1993) A closed-form solution for options with stochastic volatility with applications to bond and currency options. Rev Financ Stud 6:327–343

Kaizoji T (2006) Power laws and market crashes. Prog Theor Phys Suppl 162:165–172

Levy M, Solomon S (1997) New evidence for the power-law distribution of wealth. Physica A 242(1):90–94

Levy H, Levy M, Solomon S (2000) Microscopic simulation of financial markets: from investor behavior to market phenomena. Academic, Academic Press, New York

Lillo F, Mantegna R (2000) Variety and volatility in financial markets. Phys Rev E 62:6126–6134

Lillo F, Farmer JD, Mantegna RN (2003) Econophysics: master curve for price-impact function. Nature 421(6919):129–130

Lux T, Marchesi M (2000) Volatility clustering in financial markets: a microsimulation of interacting agents. Int J Theor Appl Finance 3(04):675–702

Lynch PE, Zumbach GO (2003) Market heterogeneities and the causal structure of volatility. Quant Finance 3(4):320–331

Munnix M, Shimada T, Schafer R, Leyvraz F, Seligman TH, Guhr T, Stanley HE (2012) Identifying states of a financial market. Sci Rep 2:644

Preis T, Kenett DY, Stanley HE, Helbing D, Ben-Jacob E (2012) Quantifying the behavior of stock correlations under market stress. Scientific Reports 2, 752

Raffaelli G, Marsili M (2006) Dynamic instability in a phenomenological model of correlated assets. J Stat Mech Theory and Experiment, Volume 2006, August 2006. 8001

Solomon S (1998) Stochastic Lotka-Volterra systems of competing auto-catalytic agents lead generically to truncated pareto power wealth distribution, truncated Levy-stable intermittent market returns, clustered volatility, booms and crashes. In: Decision technologies for computational finance. Springer US, Springer Science + Business Media B.V., Dordrecht. pp 73–86

Sornette D (2002) Why stock markets crash: critical events in complex financial systems. Princeton University Press, Princeton, NJ

Tsallis C (1988) J Stat Phys 52:479; Curado EMF, Tsallis C (1991) Possible generalization of Boltzmann-Gibbs statistics. J Phys A 24:L69; (1991) 24:3187; (1992) 25:1019

Tsallis C, Bukman DJ (1996) Anomalous diffusion in the presence of external forces. Phys. Rev. E 54, R2197(R)

Industrial Society's Natural Future

Hans G. Danielmeyer and Thomas Martinetz
Institut für Neuro- und Bioinformatik, Universität zu Lübeck, Lübeck, Germany

Article Outline

Introduction
Industry
Economy
Human Nature
Finance
Details
Outlook
Conclusion
Appendix
Bibliography

Major Terms

Unisex life expectancy life insurer's disaster-corrected national averages after birth.

Industrial evolution long-term envelope above all disasters of the leading nation's gross domestic products (GDPs), the real (inflation-corrected) value of goods and services produced per capita p.a.

National recoveries optimal paths with asymptotic convergence into the industrial evolution.

Human capacity individual combination of inherited and educated capacities; its average per capita value follows from equilibrium between all main variables.

Annual working time the official paid working time as part of the natural flow of time; a similar part is used for unpaid homework including reproduction; both yield with Sundays and 8 h of sleep per day the inevitable annual part of spare time required for enjoying affluence far above biologic needs.

Systems engineering optimizes annual working time for the GDP in line with technical progress.

Physical capital real per capita value of technical infrastructure; different for production and housing.

Synergetics understanding complex systems by deriving constructive relations between their subsystems; this chapter unites four academic disciplines with a unique family of six analytic solutions.

Introduction

The Cold War secured the world's longest time of relative peace and, on average, the best existential conditions. Yet the richest nations developed a precarious combination of new problems: population relevant increase of the life expectancy and decreasing endemic birth rates, diverging national and international distributions of incomes and wealth, coexistence of the largest private assets and public debts, loss of stable employment, saturation of economic growth, unemployed youth, and decreasing financial and political stability.

A civilization capable of visiting its moon should be able to understand and shape its planetary future. But the industrial society's four dynamic subsystems industry, economy, human nature, and finance seem to be too complex for understanding any one of them with quantitative forecasting quality.

On the other hand, macro-systems can acquire long-term stability by combining constructive properties of their subsystems. Fauna and flora exemplify this since primeval times. Self-organizing systems were generally treated by Hermann Haken. He coined the term synergetics for constructively interacting subsystems (Haken 1983). According to this theory, the macroscopic dynamics of a complex system can be captured by few characteristic variables obeying simple equations even when it operates close to instability.

A. Hutt, H. Haken (eds.), *Synergetics*,
https://doi.org/10.1007/978-1-0716-0421-2_704

Originally published in
R. A. Meyers (ed.), *Encyclopedia of Complexity and Systems Science*, © Springer Science+Business Media LLC 2018
https://doi.org/10.1007/978-3-642-27737-5_704-1

The homonymous Springer Series published extensions and applications quantifying order-disorder transitions from lasers in physics to networks in city planning. So far, most examples quantified a macro-system with two subsystems connected by the same academic discipline. In this chapter, we complete the natural theory of mankind's largest possible macro-system by unifying four subsystems that were separated by four academic disciplines. This explains why understanding the industrial society's nature with forecasting quality comes now so late compared with the natural sciences.

When four subsystems determine the dynamic success of their macro-system, there must exist at least four constructive relations between them. They must follow from the existing data. In 1987, we began collecting long-term data series without academic bounds from the eighteenth-century UK to the current G7 level nations. In 1991, we formed a small group of chief technical officers in the new PICMET community (Portland International Center for Management of Engineering and Technology) and organized an international research project for future business policy with Hitachi, Siemens, and other companies. It was jointly supported including staff participation by the European Commission and MITI (Japan's former Ministry of International Trade and Industry).

At first, we derived the dynamics of national recoveries from World War II and their convergence into a collective industrial evolution. This chapter includes all relevant data on the industrial society and completes its theoretical basis. Our analytic solutions for recovery from national disasters were new and relevant for national and business planning since no globally active company could neglect the world's largest and fastest growing national market. In particular, we predicted China's current change from fast exponential to slow linear growth and the currently observed saturation of G7 level growth to an asymptotically approached final state (Danielmeyer and Airaghi 1999).

For discussion and wider understanding, we supported a working group (Kümmel et al. 2000) that developed into the German Physical Society's current division "Physics of Socio-Economic Systems" (SOE). In its tenth year, we discovered the industrial society's intrinsic order with the identical time-dependence of the G7 level lifestyle's unisex life expectancy and the industrial evolution. The latter appeared for the first time as upper envelope of the best gross domestic products (GDPs), the national annual outputs of goods and services above all disasters since the eighteenth-century UK (Danielmeyer and Martinetz 2010). This bio-economic time-dependence was the final proof of our natural theory. It resolved immediately three mysteries of three disciplines: the current linearity of G7 level economic growth, the life insurer's current success with linear extrapolation of G7 level life expectancies, and the partial heritability of human longevity (Herskind et al. 1996).

In 2014, we adopted the so far newest results on national annual working times (Hubermann and Minns 2007). Their smooth decrease since 1800 from 96 to 39 h per week showed that systems engineering generates not only the technical infrastructure but implicitly also the annual spare time required for enjoying life far above biologic needs. Without it G7 level affluence would neither be demanded nor produced. As shown with the section on human nature, this spare time completed the theoretically required minimum number of six long-term variables for quantifying the industrial society's peaceful evolution. The latter's existence defines also every optimal recovery from unpredictable disasters. All variables and their corresponding data are plotted in the following sections.

We derived six simple constructive relations in and between the four subsystems. They have one unique family of six irreversible analytic solutions. Since individuals are biologically limited systems, the family saturates inevitably per capita. This excludes unlimited exponential growth per capita. The appendix offers an extension for small population growth or decline. As shown with all following plots, the solutions reproduce the industrial society's data from its start in the eighteenth-century UK to its current state without any fitting parameter.

This agreement will continue into the industrial society's asymptotic final state because all time constants are inherited as directly measured

constants of the human species. Such solutions are even without genetic stabilization very rare in nature and new to economy and finance. Their derivatives and analytic integrals are also valid solutions for the macro-system. This allows many cross-checks that lead to additional discoveries and explain details that were clearly observed but not understood to date. Not knowing the collective dynamics while managing the subsystems separately caused some of the new problems identified in this introduction's first paragraph. The other problems will turn out to be natural and inevitable.

All data shown are 5 to 10 year's averages of the annual data published by the national statistical offices or by specifically cited sources. Short-term fluctuations are hereby reduced to the plotted size of the data because we showed earlier that instabilities associated with the northern hemisphere's theoretical phenomenon of business cycles have a base period of 2Pi years but are damped down to half a cycle (Danielmeyer and Martinetz 2009). Thus, the following agreement with theory may give the impression that the data show simulations of the theory. This is definitely not the case. Finding and processing an order of magnitude higher volume of original data and converting inflation and exchange rates to US$ of 1991 or 2010 through two centuries with different national reference times took about half of this chapter's development time.

The entire database will be published in due time together with the Mathematica programs for all plots. The analytic solutions are plotted into their data. Only one data point per nation is required for locating every successful national recovery completely with respect to the industrial evolution. The appendix lists the natural and all national constants used for the plots.

The main text follows the subsystem's contribution to the natural theory. Industrial engineers do exactly what the theory describes. The economy is physically caught between human demand and industrial supply. Since these three subsystems are controlled by the laws of nature, the financial subsystem must follow them, not vice versa. The conclusion proposes a pragmatic solution for the problems associated with the financial subsystem's saturating or even negative interest rates because time runs out especially for Europe with half a billion individuals lacking a cohesive constitution.

The outlook offers a timely example for using all figures as benchmarks for long-term national planning. The latter is now possible in spite of unpredictable disasters because the industrial evolution is immune to them as long as innovation continues challenging human adaptability as the slowest and, therefore, dynamically decisive process.

Industry

Industrial engineers are renowned for the development, quality, efficiency, and reliability of the industrial society's technical infrastructure termed physical capital by economists. Less known but equally important is the fact that systems engineers design the annual working time required for producing the GDP with technical progress optimally and irreversibly into every production line. Machines are not just input factors. They organize and amplify annual working time with respect to human power, speed, and/or precision for producing the GDP.

That optimizing annual working time generates simultaneously the annual spare time was so far neglected because the latter has no direct economic value. But without this spare time, the G7 level affluence far above biologic needs could neither be enjoyed nor demanded and produced. The maximum sum of weekly working time w (t) and weekly spare time s(t) equals the agricultural 16 h 6 days per week without vacation. We use this maximum available active time of 96 h per week now as unit and dimension of $\epsilon = 1$ p. a. for measuring annual working and spare time. Then systems engineers split the flow of active time according to

$$w + s = \epsilon \equiv 1 \text{ p.a.} \tag{1}$$

Using this natural unit makes sense because the GDP contains the same unit and all real values are in the end created by human work, including

natural resources and physical capital. Figure 1 shows this inevitable tradeoff for the maximum available active time of 96 h per week:

We selected the data of the USA and Germany-West Germany-Germany from the comprehensive work of Hubermann and Minns as examples of the most stable and unstable industrial nation concerning political and territorial integrity. Strawe reported nearly the same data but contributed also the earliest official working time of 1823. It is still close to the agricultural and physical maximum of 96 h per week. The lowest annual working time is due to the Great Depression. Its decennium of declining employment ended for the USA with a nearly vertical step in 1941 due to its entry into World War II. In order to resolve this, we dropped our 5- to 10-year averaging for 1930 and the transition 1941/42. But even such a disruption left no long-term trace. This means technical progress is quite immune to disasters. Since there is no superior force providing such regularity over two centuries, there must exist some "invisible hand" as proposed already by the moral philosopher and customs officer Adam Smith in 1776 for his early vision of a self-stabilizing free market. The following sections show that this hand is generally provided with every individual's inherited and educated capacities.

Business administration measures labor with its cost or employment on the microeconomic level. But on the macroeconomic level, the cost of labor is a bad variable because as income it must essentially buy the GDP, and employment is no variable at all since nations try to keep it high. The section on details links this problem to macroeconomics' neoclassical paradigm.

Fortunately, systems engineers design the annual working time w(t) optimally into the technical infrastructure $k_w(t)$ of every production line. A priori there is no reason for assuming any nonlinearity beyond their product. Then an industrial nation's GDP per capita is generated with the simplest possible relation

$$y = wk_w. \tag{2}$$

The other part k_s is designed for housing and reproduction with a trade-off corresponding to Eq. 1 between generally unpaid homework and spare time. Their sum k(t) is the entire real (inflation corrected) per capita value of the national technical infrastructure. National statistics list all three parts as physical capital:

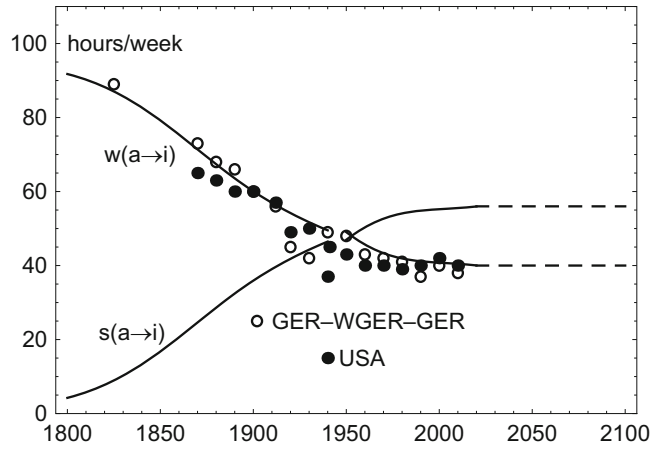

Industrial Society's Natural Future, Fig. 1 Systems engineers divide the flow of time into weekly working time (plot with data) and the spare time required for enjoying G7 level affluence. Sunday and sleeping time are neglected. ($a \rightarrow i$) indicates that the observed working time is actually a superposition of the agricultural and industrial working times as quantified with Eq. 4. Original data source: Strawe (1994) and Hubermann and Minns (2007)

$$k_w = \lambda\, k(t) = k - k_s. \qquad (3)$$

The appendix' Table 2 shows $\lambda = 0.45 \pm 0.02$ for Germany's recovery from World War II.

Initially, industry left agriculture in its poor state $y_o = \epsilon k_o$ with the maximum working time from Eq. 1 and, including crafts enterprise, up to 1.000 US$ in their present value for Germany's preindustrial GDP per capita. For the first time, their linear superposition

$$w_{a\to i}(t) = (y_o + y)/(k_o + k_w) \qquad (4)$$

is quantified for the entire transition from the agricultural to the industrial society as shown in Fig. 1. Considering today's G7 level contribution to the GDP of industrial food generation, processing, and distribution, the industrial society just absorbed agriculture as expressed with Eq. 4. The following section on the economy derives the analytic solutions for the industrial GDP and the physical capital needed for Eq. 4. Thus, the agreement seen in Fig. 1 without any fitting parameter between the data and Eqs. 2, 3, and 4 confirms using the simple product in Eq. 2 and the sum $\epsilon \equiv 1$ p.a. as natural unit for measuring working and spare time.

That systems engineers created not only technical progress but implicitly also the spare time required for enjoying and demanding affluence, and education far beyond biologic needs is decisive since these extensions allow mankind for the first time to reach its genetic limits. Asking systems engineers to be less successful with achieving technical progress, generating four of the industrial society's six main quantities, and optimizing the trade-off between working and spare time would jeopardize their professional ethics and the industrial society's physical sustainability.

Annual working time and physical capital generate the GDP with Eq. 2. The fourth quantity, annual spare time, could connect the GDP's supply with its demand when a real counterpart of k_w would exist for life at home that could amplify spare time for generating demand like k_w amplifies working time for supply. The next sections show that biology found a genetically safe and orders of magnitude cheaper solution for generating demand.

Economy

Production data are measured at the microeconomic level with the detailed costs of taxable added value tasks. Business administration integrates them to the company level. National statistical offices integrate them to the macroeconomic level, correct them for inflation to get the real (inflation-corrected) values, and reduce them to internationally comparable data for the real per capita values of the national GDP, physical capital, and labor. Then the data can be corrected for foreign trade imbalance and converted to the lead currencies US dollar and Euro. The new theory agrees with all data through two centuries for all successful recoveries, and the collective industrial evolution is the first quality proof of economic data collection and processing. Systematic mistakes of one per cent p.a. would have added up to unacceptable discrepancies between data and a new theory that has no fitting parameters.

Full agreement between theory and data requires also quantifying the economic equilibrium between national supply and demand, both to be independently determined. But for G7 level affluence, there are no added value parts for measuring and integrating demands. Individual demands overlap in time, with different and changing satisfaction, and without money's property of additivity. As already suspected by Jean-Baptiste Say in 1803, national demand and its theoretical equilibrium with supply cannot be quantified within the discipline of economics. The next section recalls how nature resolved this bio-economic problem.

This section must yield the industrial production variables for Eq. 4 with $k_w = \lambda k$ from Eq. 3. So far, macroeconomics used the fiscal depreciation rate γ_k for the physical decay rate. Then the annual maintenance cost is given by $\gamma_k k = \mu_k\, y$. This depreciation is tax deductible and immediately useable for new investment. In Japan, equipment bought for research and development could be completely written off in its year of purchase. When bought at year's end, this equipment was a tax- and maintenance-free Christmas bonus. Depreciation is generally used by national tax authorities for stimulating investment, employment,

and economic growth. Then the effective physical lifetime G of physical capital against technical obsolescence and aging through wear and tear is much larger than the fiscal lifetime $1/\gamma_k$. Even more important is the fact that G provides a memory for the level of technical progress at the year the annual addition $\dot{k}$ to k(t) is produced. Then the annual cost of maintaining its original purchase value is given by

$$k/G = \mu\, y. \tag{5}$$

It identifies the required part $\mu(t)$ of the GDP y(t). We named it capital function. G will be directly measured with Fig. 3. It yields for the USA, Germany, and Japan the same constant result $G = 25$ years. Due to its proximity to the generation gap, we named it generation constant.

Solving a problem with three unknowns requires three independent equations. Equation 5 excludes exponential growth because economies can only grow with an increasing capital coefficient $k/y = \mu\, G$, i.e., with $\dot{\mu} > 0$. This follows from the fact that technical progress can only be designed into the annual addition $\dot{k} = \mu G\dot{y} + \dot{\mu} G y$ of new physical capital, not into the GDP of finished products nor into the already accumulated physical capital. Since the latter must be maintained simultaneously, economic growth requires the annual flow

$$\dot{k} + k/G = \mu\, y + \mu G\dot{y} + \dot{\mu} G y \equiv \overline{\mu} y + \dot{\mu} G y \tag{6}$$

from the GDP. The fastest recovery from loss of $k(t)$ results when the maximum affordable value $\overline{\mu}$ of $\mu(t)$ is used throughout as "saving constant" for $k(t)$. Then the identity has with one equation

$$\mu(1 + G\dot{y}/y) = \overline{\mu} \tag{6a}$$

for two variables $\mu(t)$ and $y(t)$ still no general solution. But the initial and final states $k_o = \mu_o G y_o$ and $\overline{k} = \overline{\mu} G \overline{y}$ are now defined with the measurable and reported initial growth rate

$$\beta = (\overline{\mu}/\mu_o - 1)/G. \tag{7}$$

For the nations used as examples, all three parameters are listed in Table 1 of the appendix. Successful recovery and the initial growth rate depend on the level of technical progress given by μ_o at the time of the decision to recover with $\overline{\mu}$. Obtaining the latter from national statistics is explained in the appendix. Generally, it follows from β and $0.08 \le \mu_o \le 0.11$.

Equation 6a quantifies the continuous decrease of the growth rate with increasing capital coefficient $\mu_o G \le k/y \le \overline{\mu} G$. The industrial society's growth saturates inevitably because of the limited trade-off between saving for growth of physical capital and maintaining its accumulated level. When the capital function's increase $\dot{\mu} > 0$ is neglected, Eq. 7 is a solution of Eq. 6a, but exponential growth is just one of the ideal pure cases that are physically impossible.

The GDPs in Fig. 2 help now in discovering the natural solution for Eqs. 6 and 6a. The GDPs show two overlapping dynamics: one quantifies recovery from disasters, the other the ideal peaceful industrial evolution. Two interrupted recovery paths are dashed. The first shows how the USA caught up with the UK due to the Monroe Doctrine's separation of American and European global ambitions.

European global ambitions. The second shows that the first World War prevented Germany and Japan from catching up with the USA. This changed dramatically with their cooperation after World War II during the Cold War's peace on G7 soil.

Industrial Society's Natural Future, Table 1 National constants for recovery from national disasters

Nation range	GER <1938	GER and JAP >1949	KOR >1970	USA >1940	PR CHN >1980
$\overline{\mu}$	0.15	0.25	0.26	0.18	0.38
μ_o	0.08	0.08	0.08	0.08	0.11
β p. a.	0.035	0.09	0.09	0.05	0.10
Halftime τ	2005	1971	2010	1965	2045

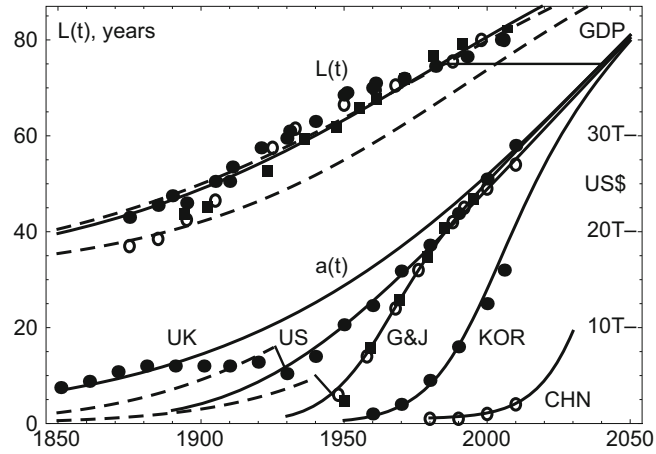

Industrial Society's Natural Future, Fig. 2 Average life expectancies after birth (upper left) and recoveries (lower right) of the USA (points), West Germany/Germany (squares), and Japan (circles). Successful recoveries converged into the industrial evolution a(t) established initially by the UK as only world power before its stagnation after 1880; South Korea's convergence is beyond halftime; China enters its long nearly linear path after its Cultural Revolution. Their scale in US$ 1000 of 1991 is adjusted to show both theoretical inflection points at the horizontal bar's ends from L(t) to a(t). Its constant length and their identical shape relative to their industrial change yield the industrial society's mean maximum life expectancy L(t). The dashed paths are explained in the text. Updated from Danielmeyer and Martinetz (2009). The early GDP data are from Mitchell's international tables (Mitchell 1988)

All successful recoveries of the general GDP y(t) converge into the collective industrial evolution $a(t)$ defined as envelope of the best per capita GDPs above all disasters. Although $a(t)$ represents the peaceful existential conditions, the suspected parallelism of a(t) and L(t) after their normalization to the same industrial increase suggests, and the next section confirms, that $a(t)$ is already dominated by demand because the mean life expectancy measures progress toward mankind's all-inclusive demand for longevity.

Since there exists no superior authority controlling five recoveries on three continents for five generations, the convergence must proceed without a parameter specifying the division of annual working time between recovery and evolution. Figure 2 shows a smooth transition from recovery into the evolution without overshoot. The only process that achieves this is the growth rate's linear division in proportion to the future gaps $a - y$ and $\overline{a} - a$ to be closed for recovery and evolution:

$$\dot{y}/y = \beta(1 - y/a) + (\dot{a}/a)(y/a). \qquad (8)$$

Then linearity must apply also to approaching asymptotically the final GDP $\overline{y} \equiv \overline{a} = 75.000$ US$ of 1991 (or, due to inflation, 110.000 US$ of 2010) p.a. per capita. This means for the industrial evolution's growth rate

$$\dot{a}/a = (1 - a/\overline{a})/E. \qquad (9)$$

Its solution

$$a = \overline{a}/\left(1 + e^{(T-t)/E}\right) \qquad (9a)$$

is known as logistic function. It is plotted in Fig. 2 as envelope of the best national GDPs above all disasters from the eighteenth-century UK to the G7 nations. We named $a(t)$ industrial evolution and its growth parameter $E = 62$ years evolution constant (Danielmeyer and Martinetz 2009). Its inflection point is at halftime in $T = 2040$ where $a = \overline{a}/2$. The fit is exact to one calendar year because of UK's early exponential path and the much later nearly constant slope at G7 level convergence. E follows according to Eq. 9 from the directly measured initial growth rate $1/E = 0.016$ p.a. Other properties of the logistic function will be discussed in the next section.

Equation 8 has with Eqs. 9 and 9a the simple solution $1/y = 1/a + (1/\overline{a})e^{\beta(\tau-t)}$ so that

$$y = \overline{a}/\left(1 + e^{(T-t)/E} + e^{\beta(\tau-t)}\right). \qquad (10)$$

A fast check is possible by inserting Eqs. 9a and 10 into this simple solution where both exponential terms of the same kind cancel separately. τ is the halftime of national recovery listed in the appendix' Table 1. $y(t)$ converges into a(t) for $t > \tau + 1/\beta$.

The GDP grows when the exponential terms in the denominator decrease. There is no alternative since every nominator of Eq. 10 consists of a component of the asymptotic final state. According to Eq. 7, the recovery term removes technical limits and obstacles. The next section shows that the slower evolutionary term removes human limits and obstacles. It follows that Adam Smith's accumulation of wealth introduced in 1776 is not the industrial society's goal. Its real goal is reaching the given human limits with technical and human cooperation by removing both kinds of obstacles as they appear after earlier obstacles are removed.

"As they appear" is for more than one kind of obstacle only possible with the unique structure of Eq. 10 where the exponential terms compete in the denominator. Financial wealth grows exponentially with the nominator. There the faster process would always win, and human maturation will be missed. Not knowing this fundamental difference caused the Great Depression after 1930 and the financial disaster after 2007. The next section shows why industrial engineering and human nature dominate the economy and finance.

Inserting the solution Eq. 10 and its time derivative into Eq. 6a yields with some patience and the identity $ce^{\gamma t} \equiv e^{\gamma(t+\Delta t)}$ for $\Delta t = \gamma^{-1} \ln c$ the solution

$$\mu = \overline{\mu} y_k / y \qquad (11)$$

for the capital functions plotted in Fig. 4. They agree automatically with their data because the original data shown for y(t) and k(t) agree with their data in Figs. 2 and 3. Discrepancies between the measured values of $\overline{\mu}$ from Eqs. 7 and 11 and the officially published values (see the appendix) disclose central planning and/or irregular reporting practices. They destroy also the

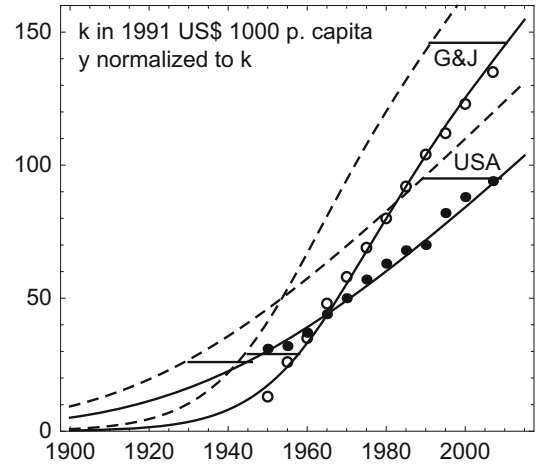

Industrial Society's Natural Future, Fig. 3 Time-shifts between GDP (dashed, taken from Fig. 2, normalized with the factor $\overline{\mu}G$) and physical capital (plots in data) for the USA and Germany and Japan disclose the generation and evolution constants G and E

parallelism expected theoretically between $\overline{\mu}Gy$ and k(t) in Fig. 3 for recovery and evolution.

The auxiliary function $y_k(t)$ is the direct result of the above patience. Its only difference to the GDP y(t) is that its exponential terms are delayed by

$$\Delta\tau_k = \beta^{-1} ln(1 + \beta G) \qquad (12)$$

and

$$\Delta T_k = E\, ln(1 + G/E) = 21 \text{ years}. \qquad (13)$$

Inserting Eqs. 11, 12, and 13 into Eq. 5 yields finally

$$k = \overline{\mu} G y_k = \overline{\mu} G \overline{a} / \left(1 + e^{(T+\Delta T_k - t)/E} + e^{\beta(\tau+\Delta\tau_k - t)}\right). \qquad (14)$$

Both time-shifts are measured with the length of the four bars in Fig. 3. The normalizing factor for comparing y(t) with k(t) is $\overline{\mu}G$. Well below halftime of recovery, the time-shifts for Eq. 12 are different (13 years with $\beta = 0.09$ p.a. for Germany, 16 years with $\beta = 0.05$ p.a. for the USA) but yield the same effective physical lifetime

$G = 25$ years for $k(t)$. This was the first measurement of this important time constant (compare its introduction with Eq. 5). Its proximity with the generation gap means that the industrial society respects implicitly the fairest intergenerational contract for maintaining the value of the inherited physical capital: Every generation renews it on average once during its time of responsibility.

The time-shifts observed here between the charging flow and the stored result k(t) are the analogue for irreversible processes of the phase shifts known from periodic processes. This essential information on the industrial society's reaction times was always hidden in the data. It was just not detectable with the exponential approximation because of the exponential function's physically impossible property of unlimited exchangeability between value and time.

The slight bends seen for Germany and Japan after 1980 are due to the convergence of y(t) into a(t) in Fig. 2. Beyond convergence the time-shifts are constant for 21 years (upper lines) and yield with G from Eq. 13, again the evolution constant $E = 62$ years known from UK's eighteenth-century growth rate.

Measuring the constancy of E through two centuries required patience beyond 2010 until the length of the upper lines in Fig. 3 was clear. The decisive role of systems engineers for creating and maintaining the industrial society's technical infrastructure could not have been confirmed earlier than 240 years after Boulton and Watt's first steam engine with acceptable efficiency for production lines.

Our first analytic solutions for the macroeconomic production variables show that real growth per capita requires removing two kinds of obstacles as they appear in recovering from disasters and the industrial evolution. Both reaction times are directly measured with the time delay of physical capital with respect to the GDP. Industrial engineering determines the supply of goods and services completely. The only parameter that can and must be nationally fixed is the saving constant $\overline{\mu}$ for physical capital. It determines time and speed of recovery and the technical infrastructure's final level. "As they appear" specifies one unique family of analytic solutions where the removal of both kinds of obstacles competes in the denominator. This structure favors the early innovators like the UK because the gap to be closed for catching up with industrial evolution was in the eighteenth century much smaller than China's and India's gap in the twenty-first century.

Human Nature

The preceding section described the first measurements of the industrial society's physical lifetimes and/or reaction times. They are measured in situ and are here to stay as effective time constants for every human civilization. This section shows that they are heritable, i.e., stabilized by the human genome, and that the industrial society's long-term future is predictable in spite of unpredictable disasters, as long as innovation challenges human adaptability as the slowest and dynamically decisive process. Then optimal medium-term recoveries from unpredictable disasters are also predictable because of the "optimality condition" of Eq. 8.

For long-term equilibrium, the supplied GDP must equal the demanded GDP. Annual spare time is the compatible and exactly known counterpart of annual working time. Then symmetry with the supply of Eq. 2 would require just a counterpart on the side of demand for physical capital on the side of supply.

In search of a permanently measurable quantity with the shape of a(t), we found in 2009 the mean G7 life expectancies L(t) at birth shown in Fig. 2. The lowest circles are caused by higher infant mortality due to Japan's later industrialization. The plot is the visually best fit through all other data assuming the simplest possible logistic dynamics with the industrial evolution's growth parameter E:

$$L - L_o = \left(\overline{L} - L_o\right) / \left(1 + e^{(T_L - t)/E}\right). \qquad (15)$$

Its parameters are $L_o = 30$ years, the life expectancy known as the medieval minimum for stable populations with average harvests, and the

asymptotically approached maximum mean life expectancy $\overline{L} = 118$ years. Since antiquity it was expected near 120 years. After two orders of magnitude growth of the GDP per capita, the G7 passed the inflection and halftime point of the mean life expectancy in $T_L =$ 1981. Rainer Ansorge found a robust numerical convergence to these parameters (Ansorge 2010).

Only a factor of 2.4 in the GDP is required for reaching on average the maximum mean life expectancy for the G7 level lifestyle. The life expectancy measures progress toward longevity, the all-inclusive top demand. Longevity is to a relevant extent heritable (Herskind et al. 1996). Life insurers eliminate all deaths due to identifiable national disasters, extrapolate the resulting mortalities and existential conditions, and obtain the insurable life expectancies $L(t)$ currently up to 115 years. With a(t) from Eq. 9a, the disaster-corrected existential conditions were for the first time quantitatively known. This allows replacing the life insurer's very complicated numerical approach with the simple analytic integral named bio-economic relation:

$$L = L_o + \left(\left(\overline{L} - L_o\right)/\overline{L}\overline{a}\right) \int_t^{t+\overline{L}} a(t)dt$$
$$\cong L_o + \left(\overline{L} - L_o\right)/\left(1 + e^{\left(T-\overline{L}/2-t\right)/E}\right). \quad (16)$$

Since $\overline{L} < 2E$, the approximation of the exact logarithmic integral with the logistic function is as good as observed in Fig. 2. The shift between both inflection points shown with the bar in Fig. 2 is theoretically given by the identity and measured as the bar's length with the result

$$T - T_L \equiv \overline{L}/2 = 59 \text{ years}. \quad (17)$$

Its extrapolated value $\overline{L} = 118$ years is now directly measured with its time-shift. This first measurement of the maximum unisex life expectancy will be reached in the twenty-second century.

The bio-economic relation Eq. 16 resolved three mysteries of three disciplines (Danielmeyer and Martinetz 2010): the current linearity of G7 level growth, the life insurer's success with linear extrapolation of the disaster-corrected mortality, and the fractional heritability of the life expectancy, because only the part adapted to within the generation gap can be heritable.

The lower dashed path for *L(t)* in Fig. 2 would theoretically result when integration and averaging would proceed over the life insurer's predicted mean life expectancy $L(t)$. But predictions cannot be embodied. Naturally embodied is the inherited maturation program from birth to the genetic limit $\overline{L}$ with the proportionality of Eq. 9 between the current growth rate and the future gap to be closed. Equation 9 includes what Eq. 16 quantifies: the human capacity to monitor, integrate, and average over the existential conditions, adapt to them with the partially inherited gains of the life expectancy, and report the final result with death. This master plan protects the genome from external manipulation because it allows maturation without external monitoring and control. The logistic function represents life's condition sine qua non.

Since only the part of longevity acquired within the generation gap can be passed on to the offspring, the industrial evolution extends over 16 generations instead of the one to four generations experienced individually during the industrial evolution. Now the industrial society can be quantitatively understood as the largest possible extension of the human maturation program for reaching mankind's given limits through social and technical cooperation. This natural goal explains why the industrial society can be developed at all, defended against unnatural goals, and quantified with the rigor of the natural sciences.

The mean life expectancy is already the integrated result of satisfying the relevant demands. A counterpart of physical capital, which amplifies spare time for generating demand like k_w amplifies working time for generating supply, is obviously not required for long-term equilibrium between demand and supply. In fact, biologic processes are subconsciously regulated on the molecular level with enzymes, hormones, and proteins. Conscious actions are controlled with only100 bits per second and electric signals that are synthesized with the brain's inherited and educated capacities.

This architecture for generating demand requires less than 100 Watts and comes by heritage for free. It is orders of magnitude more effective than the 6 kilowatts per capita required for generating and maintaining the G7 level lifestyle with the industrial society's technical infrastructure worth 10^5 US$ per capita.

On the other hand, the natural theory's data for spare time and the evolution constant E open a classical way for quantifying equilibrium between demand and supply. Figure 4 collects the operating costs as parts of the GDP of per capita leading nations during their so far best time:

The law and order costs (upper data) exclude all transfers but include all costs from the legislative to defense. They are proportional to the national population but beyond this not just proportional to the GDP but to the accumulated physical capital. The next section explains this result with the increasing social stress due to the nationally and internationally diverging distributions of incomes and wealth.

The educational data in Fig. 4 contain all national costs from kindergarten to university. Their doubling within 15 years was capitalism's answer to the "Sputnik Shock" caused in 1956 when socialism orbited the first satellites. The next section continues this track with the social consequences. Here we assume there exists an indestructible but appreciating combination h(t) named human capacity of educated and inherited capacities. We assume they organize and amplify annual spare time for enjoying and demanding G7 level affluence like $k_w(t)$ amplifies annual working time for supplying that affluence. With human capacity for demand, we avoid confusion with Gary Becker's human capital used in 1964 for quantifying the economic value of the work force. The human capacities' educated component can now be estimated with

$$h_e/E = va. \tag{18}$$

This defines in analogy to Eq. 5 a national parameter $v(t)$ named capacity function for maintaining the educational level. Accepting $\overline{v} = 0.07$ from Fig. 4 as final level yields $\overline{h}_e = \overline{v}E\overline{a} = 4.3\overline{a}/\epsilon$. This is a minimum because it does not include the parent's priceless education. The evolution constant E is the effective reaction time of the actually needed human capacity h_s that combines h_e and the inherited capacity.

Both capacities are per capita indestructible and, like knowledge, nonadditive since their contents can compete for making decisions. For long-term equilibrium between the evolutionary demand and supply, the formal value of h_s follows with the generation of a(t) according to Eq. 2 from

$$sh_s = a = wk_w. \tag{19}$$

Eliminating both times with Eq. 1 yields a form with all exponential terms in the nominator:

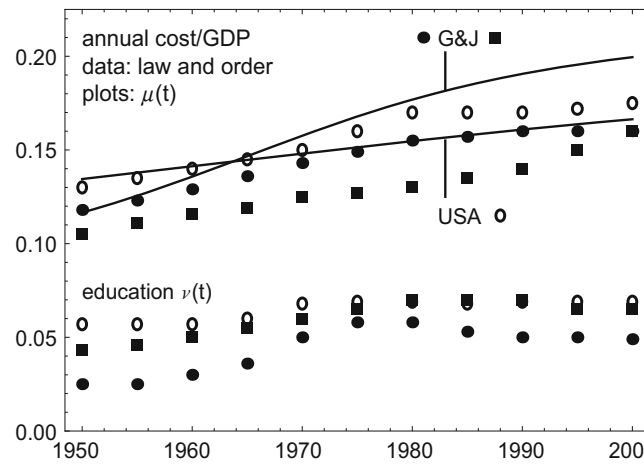

Industrial Society's Natural Future, Fig. 4 The costs of keeping Germany, Japan, and the USA just operational exceed one third of their GDPs. The plots are the capital functions of Eq. 11

$$\epsilon/a = 1/h_s + 1/k_w. \quad (20)$$

This relation has again the property that the obstacles can and must be removed as they appear because the value a/ϵ of the annual national output cannot be larger than the smaller of both storable quantities. For long-term equilibrium, $k_w/h_s = s/w$. Inserting $k_w = \lambda\mu Ga$ from Eqs. 2 and 5 yields finally for the evolutionary level

$$h_s = a/(\epsilon - 1/\lambda\mu G). \quad (21)$$

With $\lambda = 0.47$ from the appendix and $\overline{\mu} = 0.26$, Germany and Japan require $\overline{h}_s = 1.7\overline{a}/\epsilon$ for final equilibrium. The USA need a little more due to smaller saving and larger consumption. But even that is well below the final educational level $\overline{h}_e = 4.3\overline{a}/\epsilon$ from Eq. 18.

This first comparison between educated and required human capacity shows that G7 level nations installed implicitly a sufficient safety buffer against a limiting role of education for the industrial society's evolution except for Germany, as Fig. 4 and the Pisa Tests showed. It follows that human capacity's inherited part dominates and limits the industrial evolution. This agrees with the role of the bio-economic relation $L(a)$ of Eq. 16.

Equation 20 allows deriving the maximum part of the GDP left for education and consumption. a(t) saturates with increasing k_w, whereas the sum $b(t) = 2k/G \cong 4k_w/G$ of maintaining physical capital and law and order increases continuously as shown in Fig. 4. Differentiating $a(t) - b(t)$ with respect to k_w yields the maximum difference for $\hat{k}_w = (3/2)h_s$. The integers result from the square root 2/5 of 4/G. Eliminating s(t) in Eq. 19 with its trade-off Eq. 1 yields $w = \epsilon/\left(1 + \widehat{k}_w/h_s\right) = 0.4\epsilon$. Thereafter w(t) saturates as shown in Fig. 1 because the evolution's optimal industrialization must implicitly wait for the adaptation of h_s. Explicitly this means waiting for human demand, a situation that was experienced already in China when a nationwide housing project benefitted more speculators than tenants in 2010.

Since h_s is indestructible and $w(t)$ fixed by technical progress, destruction of the technical infrastructure down to $k_w \ll h_s$ destroys long-term equilibrium and reduces the GDP of Eq. 19 to the recovery GDP $y = wk_w$ of Eq. 3. Annual pay necessarily follows the national GDPs, but recovery can be much faster than starting from agriculture because h_s maintains its evolutionary level when $\overline{v}$ keeps its relative level. This explains the fast recoveries of West Germany, Japan, and South Korea in Fig. 2. China invited foreign experts and required joint ventures.

Human nature and industry dominate the economy with the division of time of Eq. 1, the bio-economic relation of Eq. 16, the optimality condition of Eq. 8, and the genetic constants G, E, and $\overline{L}$. The per capita saturation of G7 level growth observed with all four figures is theoretically confirmed against any defense. The theoretically prominent complications caused since 1923 with the neoclassical paradigm's fractional exponents are discussed in the section on details.

Finance

During the Cold War's best time of peaceful growth on G7 soil, the financial sector acquired a dominating influence over business, human life, and politics. The mission of the European and all national central banks is stabilizing the currency and, as supporting goal, stabilizing the growth and inflation rates near 2% each. This banking paradigm means stabilizing exponential growth forever. It is based on an empirical relation between inflation and employment called Phillips curve. Believing in it as a natural growth law (which it is not), central banks and national governments injected since 1980 trillions of US dollars into their economies for stopping saturation and recovering exponential growth per capita.

General banks take care of the people's savings, investments, and loans. For the banking paradigm's exponential growth, an interest rate of 4% p.a. would maintain saving competitive with investing into business. But since 2010 the interest on G7 level saving accounts is practically zero. This rate cannot be due to the generally quoted subprime mortgage disaster of 2007 because the following section on the outlook for Europe shows with Fig. 6 that this disaster left

hardly a trace in the medium-term growth of European nations.

Quoted are now external and internal risks from terrorism, refugees, tax havens, and protecting the Euro to rescuing banks, high bank leverages, interbank confidence, compliance, and consolidation pressure. But zero interest must have a deeper cause than management problems of a subsystem that depends on non-zero interest. After all, the business policy of the most powerful financial institution is fundamentally challenged by the total failure of the largest experiment carried out under this policy for nearly 40 years.

This failure follows with the rigor of the natural sciences from the constructive relations between the natural subsystems. The real cause of zero interest is that all main variables saturate per capita because individuals are limited systems per unit of time flow ϵ (Eq. 1), per annual supply due to $\overline{\mu}$ (Eqs. 6 and 6a) and law and order, and per annual demand due to $\overline{L}$. Saturation would also follow for education from pursuing the analogy to $\overline{\mu}$ for $\overline{v}$ introduced after Eq. 18. For peace on their soil, the average real per capita growth rates of G7 level GDPs will fall from now 0.9% p.a. to 0.4% in 2100. For the lower half of families with most of the children, the effective growth rate is already negative.

Since money is not subject to the laws of nature, it can theoretically grow exponentially with the principal in the nominator. This is perfectly fine for regular credits, but not for long-term policy. Not knowing this fundamental difference caused the financial problems listed in the introduction: financial instability, diverging distributions of incomes and wealth, coexistence of the largest public debts and private fortunes in history, and also zero interest. A recollection of the financial decisions made during the industrial society's best time for accumulating wealth helps understanding how the inequality problems came about and how they can be resolved.

Capitalism's answer to the Sputnik Shock shown in Fig. 4 consisted essentially of improving top education and research in the natural and engineering sciences. Together with the industrial reaction, the 15-year effort created the industrial society's largest technology push to date. This was a unique time of commitment, confidence, and optimism mainly in the USA, Japan, and Western Europe. Many high technology parks were built in the 1960s for direct cooperation between academia and industry. Some industrial labs followed AT&T Bell Labs' Area 1 policy of selecting worldwide postdocs for individual research hoping for discoveries that open new markets. Information theory and coding, solid-state electronics, optical communication, and software systems were invented there and developed in a cooperative spirit. In the end socialism lost its competitive power due to this technology push.

The courage of giving fresh postdocs 3 years of individual free research (no teams) with industrial effectiveness and without any other obligation requires a locus genii that takes time to develop with a steady flow of international top-level postdocs, on-the-job language and writing courses, free links to government and university labs, good library and laboratory services, direct relation to one permanently assigned patent attorney who applied within 2 weeks before conferences, tenure only for primus inter pares management having their own labs, an individual scientific career path to the associate executive director level, and ideally also a safe monopoly market of the parent company like national telecommunications for AT&T called "Ma Bell" by the people. 30,000 of a million AT&T employees worked at Bell Labs. ABB, Alcatel, GE, GM, Hitachi, IBM, Nokia, Philips, Siemens, Toshiba, and many other global companies followed suit and built new laboratories in technology parks far from the pressure of immediate manufacturing needs.

The contrast between great advances in science and engineering and a weak economy prompted the USA's first decision to end the US dollar's gold backing in 1971 in the hope of recovering exponential per capita growth. That was just-in-time because the second move came with printing money against the fourfold oil price hike of 1973–1975. Since the growth rate continued its decrease, the final move came in 1981 with cutting the top tax rate for the rich to 28% with the immediately criticized argument that the freed money would "trickle down" to the poor. With

due delay the UK, Japan, Germany, and many other nations followed suit.

Yet even such a tax cut could not increase the growth rate. Instead, pension funds and financial analysts discovered the opportunity to stimulate profit instead of growth by innovating managerial and financial processes. This started the divergence of executive incomes. Pension fund managers and financial analysts demanded fast return on investment and increasing shareholder value as top criteria for corporate policy. Cash-strapped communities were convinced to selling their infrastructure and leasing it back. Banks created unlimited derivatives just by different packaging and called them products. Hedge funds were invented and speculations against the Euro allowed. Bank leverages exceeded the factor 10.

This concerted effort prepared the stage for an uncontrolled monetarism. Finally, the subprime mortgage crisis culminated in the global banking disaster after the US government refused the Lehman Brother's bailout in 2007. With the expression "house poor," a new kind of poverty emerged. Since 1981 trillions of dollars or Euros were injected into G7 level nations for stimulating growth, after 2008 also for stabilizing the Euro and many European banks. The final coup was creating "bad banks" just for sweeping junk papers under the carpet.

As short-term result, the technology push had not enough time to materialize. Central sales and just completed research divisions were closed because their corporate mission prevented buying and selling manufacturing divisions. MBAs and lawyers replaced engineers and scientists in management and supervisory boards. This required a booming management consultant business because boards were professionally too narrow for a global market where technology became a commodity for locating factories in regions with cheap labor. Streamlining until every company looked simple enough for lean top management became a goal for management consulting also because it extended relations, sometimes ending with an attractive position.

The divergence of incomes was also driven by the consolidation of business from independent crafts and groceries to global industry and supermarket chains. This silent social revolution created the most powerful hierarchy in business. The shift from political to global business power is highly visible. Transnational trade agreements are the logic consequence. Some professionals had the chance of starting with the research boom in the USA and experiencing the full revolution during their careers by finishing in a streamlined European board.

But G7 level growth continued saturating, and instead of trickling down, the injected money found its way into the top decile's accounts. From 1942 to 1981, its share of the USA's annual income was stable at 34%, and then it grew nearly linearly to 51% in 2012 (Saez 2014). The worst consequence is that pension funds dry out fast with negligible growth and interest. Assuming the entire pension system consists of one big fund, its required per capita volume is

$$k^* = \sigma(p/z)y \tag{22}$$

(Danielmeyer and Martinetz 2009). Compared with the national physical capital of Eq. 5, this pension fund must be maintained with a capital coefficient of

$$\mu^* G^* = k^*/y = \sigma p/z. \tag{23}$$

For estimating the fund's required volume, assume it pays an interest rate of $z = 1\%$ p.a. above the rate of inflation for a really minimum pension level per individual of $\sigma = 0.1$ relative to the real GDP per capita. The retired fraction $p(t)$ of the population depends on its age distribution. A not too simple model calculation with a logistic tail for L(t) from Eq. 16 yields for this century $p = 0.6$ and 0.4 for an effective retirement age of 60 and for an increase in proportion to L(t) from 60 to 85 in 2100, respectively, when the mean life expectancy will be 107 years (Danielmeyer and Martinetz 2009). Taking the average value $p = 0.5$ yields in 2100 toward the end of this century a capital coefficient $\mu^* G^* = 5$ years for the required pension fund. For a real fund with $G^* = 25$ years, the capital function's value must be $\mu^* = 0.2$.

There is only one such fund per G7 level nation, namely, the total value of its physical capital. But that is already owned by the rich. For the USA, the top quintile owns 80 ± 5% of total wealth (Saez 2014). This means that even for a 1% growth rate above inflation and increasing retirement age, there will be no alternative to returning to a fair distribution of incomes and wealth and reviving the classical tax-based pension system. This example shows how simple and useful analytic solutions are compared to numerical approximations.

Now the highly profitable time of fast recovery is over and with it the main social ordering power for the first two generations after World War II. The social situation disclosed by Emmanuel Saez and Thomas Piketty in 2014 is quantitatively confirmed with an analytic theory that unites all dynamic subsystems of the industrial society for this century. So far, the consequence was the electorate's observed split into an international top class and a disappointed national majority.

The responsible governments allowed this social splitting consciously but without knowing the so far hidden fundamental cause. The resulting disorder can and must be corrected. The enormous subsidies for recovering exponential growth and rescuing banks were especially critical for the European Union because it lacks the uniting power of a common constitution.

Details

This natural theory could only be developed for per capita quantities because reproduction and immigration rates are unpredictable. In the long run, even very small monotonic changes spoil analytic solutions. However, by replacing G with $G_\pi = G/(1 + \gamma_\pi G)$, the theory accepts small and slowly changing population growth with rate γ_π. The impact of this approximation follows from three examples.

For poor nations, a population growth rate of γ_π= 4% p.a. all but excludes catching up with the G7 because that rate will exactly double the cost of just maintaining physical capital's value per capita. This can already be seen with Eq. 5 and its physical lifetime of $G = 25$ years. The PR of China knew why it stabilized its population with a tough but successful one child per family policy, but it must already correct it for preventing the projected decrease to 0.75 of the female to male ratio in the relevant age for reproduction.

Japan's population is expected to decrease for the foreseeable future with rate $\gamma_\pi \approx -1\%$ p.a. This will save with $G_\pi = 33$ years about 25% of the maintenance cost of physical capital compared to the case of constant population. Fortunately, the natural theory allows controlled retreat from untenable levels of affluence. The capital function must be reduced from 0.21 to 0.17. As observed, the real GDP decreases in spite of subsidizing growth with building.

The natural theory's second long-term requirement is using the annual working time with the unit of Eq. 1 as macroeconomic labor variable. So far economics used employment or cost of the work force. This lead in 1923 to the neoclassical production function $y = A(t)\ell^{\varphi}k^{1-\varphi}$ as theoretical workhorse. Since this is unlike Eq. 2 a static equation, all variables were assumed to grow with the same constant exponential growth rate except for the technical progress function A(t) with an estimated growth rate near 2% p.a. But no original producer can separate technical progress from the price of physical capital. Equation 2 leads to $\dot{w}/w = -\dot{k}/k$ for constant GDP. The relative value of new industrial physical capital increases in proportion to its saving of relative working time. This is the natural pricing rule for physical capital.

The sum of neoclassical exponents must be 1 because of dimensional coherence and scaling with population. Another so far silent reason for fractional exponents is that housing is included although it is designed for reproduction at home. Such exponents are physically wrong, and neoclassical production functions are underdetermined in spite of two fitting possibilities. The natural production function of Eq. 2 is completely determined without any fitting. This is one of the best examples for synergetics: finding simple solutions for seemingly insoluble problems by accepting that macro-systems exist only because they are stronger than the sum of its subsystems. Keeping micro- and macroeconomics together in one academic

discipline is easy when their natural differences are understood and accepted as inevitable.

Figure 5 shows Germany's predicted GDP with a parametric plot over the entire evolution. Its first 250 years before 1950 are now irrelevant. The predicted wide maximum is due to the industrial evolution's smooth dynamics. According to Eq. 13, it peaks 21 years after the industrial evolution's halftime in 2040. The evolution's definition with Eq. 9 can be directly read from the axis intersections of the dashed line for $\dot{a}/a$. Since $\dot{y}/y$ converges into it without overshoot, Eq. 10 describes the optimal path from the deepest level of destruction to the final level $\overline{a}$ without fitting parameter. This excludes the existence of a third kind of obstacle for the industrial society. The natural theory is complete.

The small detail's data are collected for Germany in Table 2 of the appendix. Their agreement with the investment peak of $\dot{k} = k(\dot{y}/y + \dot{\mu}/\mu)$ from Eq. 5 shows the advantage of analytic solutions. All derivatives and analytic integrals are also valid solutions for the system. We named the new phenomenon convergence crisis. The peak and economic growth are physically due to the term $\dot{\mu}Gy$ in Eq. 6. Just this term was neglected to date. The USA's smooth development was short of showing a peak because that appears only for $\beta > 0.05$ p.a.

Without having the real explanation, Japan coined the term "hollowing out" for its convergence crisis. Assuming that due to cheaper imports from China about 4% of its manufacturing was lost, Japan began immediately with injecting money into new housing and Tokyo office towers (dashed). By now it is clear that this classical policy could only deepen and extend the crisis. In Germany, employment collapsed

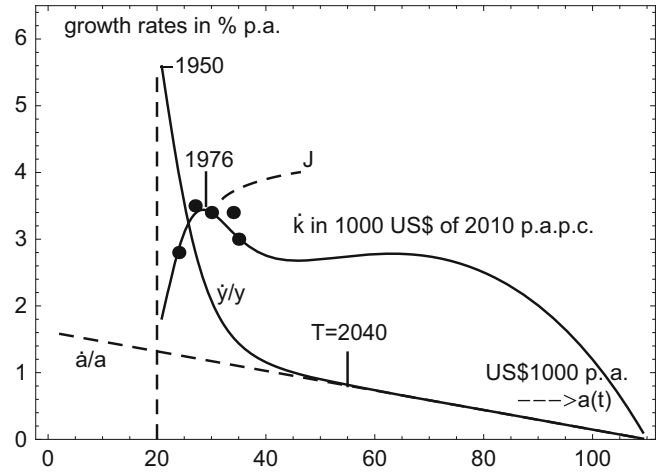

Industrial Society's Natural Future, Fig. 5 Parametric plots over the industrial evolution (Eq. 10) of its growth rate $\dot{a}/a$, West Germany's annual addition of physical capital (with data during its convergence crisis' peak from Table 2 in the appendix), and its rapidly decreasing growth rate after 1950 from Eq. 8. Both continue into Germany's evolutionary saturation

Industrial Society's Natural Future, Table 2 Data processing for West Germany's convergence crisis

Page	Quantity, unit	1960	1970	1980	1990	1993
46	Population P, millions	55.4	60.7	61.5	63.3	65.5
678	K, 10^9 DM of 1991	3291	5719	8479	10,989	11,975
678	K_w/K	0.42	0.44	0.45	0.45	0.46
678	ΔK_{in}	245	362	418	502	487
678	ΔK_{out}	38	73	131	188	210
$\dot{K}$	$\epsilon(\Delta K_{in} - \Delta K_{out})$	207	289	287	314	277
$\dot{k}$	$\dot{K}/P$ in 10^3 US$ of 2010	2.8	3.5	3.4	3.6	3.0

Source: Statistical Yearbook of Germany 1995, Metzger-Poeschl 1996

initially by 4%, but thereafter West Germany's 63 million people were saved by well-timed unification with 18 million East Germans and their huge demand for renewing their entire infrastructure with G7 level standards.

Table 1 of the appendix predicts the PR of China's convergence crisis from 2045 to 2055. Due to its longer linear path, China's peak will top Germany and Japan's peak by a factor 2 to 3. With a population of 1.6 billion instead of West Germany's 63 million, China's convergence crisis will cause the industrial society's largest imaginable financial and social disaster.

Outlook

Figure 6 shows the change Δk of net physical capital over the change Δy of the GDP between 2006 and 2014 for European nations. Both quantities were obtained from Eurostat's tables (eurostat.eu) for 2006 and 2014. Luxembourg and Norway grew exceptionally because they are dominated by finance and offshore oil, respectively. Such sectors have no special influence on the life expectancy because the latter requires balanced educational, medical, social, and technical progress. All other nations follow the natural theory's course (dashed) surprisingly well, not only the European G7 level nations. The UK's departure from industry started already with the oil price hike in 1973. Except for Ireland (ie), Spain (es), and Greece (gr), the subprime mortgage crisis left in the critical 8 years hardly a trace.

The top positions are occupied by Austria (at), Denmark (dk), and Sweden (se). These countries profited from Europe's recovery because their technical infrastructure survived World War II. The central G7 level group is quite homogeneous. The lower group consists mainly of nations that are still recovering from World War II because in the socialist block they could not benefit from the Cold War's Western boom.

Longer $\Delta k/\Delta y$-lines for the top nations should not be mistaken for stronger growth. Their average levels are in the denominator of both growth rates (besides the factor of 8) so that for equal growth rates, the top lines should have three times the length of the low group. Since the top lengths are much shorter, the entire continent's growth rate saturates.

Europe's future depends essentially on a functioning common market for a dozen G7 level nations, another dozen relatively poor and/or politically critical nations, and the Russian Federation. The latter is geographically invincible, has again global ambitions, and is with 150 million people the natural enemy of a strong European Union with 500 million people. The USA and China have also increasing internal problems, but they can defend themselves.

The European Union can no longer afford fighting the laws of nature by injecting tens of

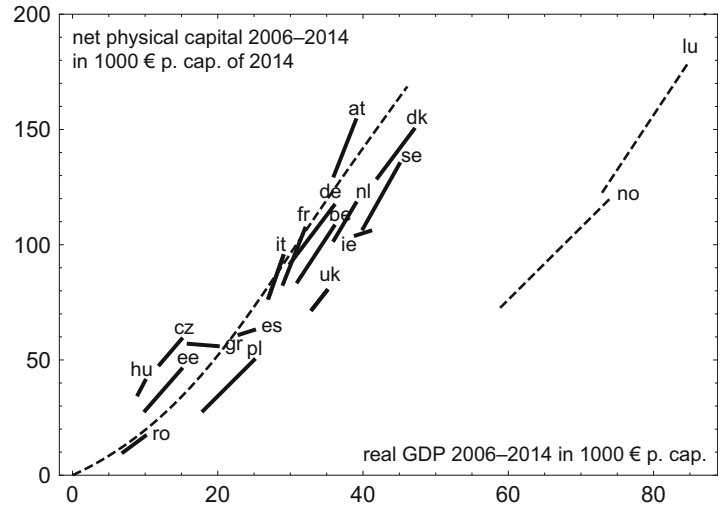

Industrial Society's Natural Future, Fig. 6 Full growth through the mortgage crisis of European nations identified by their e-mail code

billions of Euros per year without any possible success for increasing the growth rate. That money doesn't trickle down but ends up in top accounts and tax havens. Asking the most successful nations to be less successful would impede Europe's physical sustainability without solving the problems of the other nations and offend the professional ethics of systems engineers especially in Central Europe where the "ingenieur" derives from genius instead of engine.

All national media know that the European Union redistributes 90% of its budget also for integrating the poorer member states. The media must stop criticizing the 10% used for administrative tasks that all members would need separately with altogether much higher costs. Not the young but national media, languages, and governments are the obstacles to unification.

Reversing the divergence of incomes and wealth requires much more time than legislative periods permit. The evolution constant $E = 62$ years is the natural time horizon for sustainable planning because it is the reaction time for human maturation, mean life expectancy, and industrial evolution. This coincidence and proximity to $2L_o$ suggests that aging is due to a well-defined process involving parents and grandparents. Investing this time now with dedicated patience is Europe's last chance and challenge for survival in China's and North America's world.

Conclusion

The industrial society's theoretical base is now complete. Six simple constructive relations unite four subsystems and their associated academic disciplines with a unique family of six analytic solutions. They are completely determined by three inherited time constants of the human species and two national constants for the educational and technical infrastructure.

This progress was possible with the discovery of two directly correlated pairs of variables evolving from the eighteenth-century UK to the current G7 level nations nearly without a trace of financial and political disasters: the life insurer's disaster-corrected national predictions of the unisex life expectancy after birth and the envelope of the best real (inflation-corrected) GDPs per capita above all disasters named industrial evolution and the engineer's division of the annual flow of active time into annual spare time and paid and unpaid annual working time. Initially, agricultural and industrial annual working times overlap. Physical capital for paid work in production and housing for unpaid work in reproduction must be separated. The latter may allow quantifying the average home evolution. Then Gary Becker's pioneering work of 1964 could also be completed after half a century with quantitative forecasting power.

The best time for global development was the Cold War's peace on G7 soil. After 1950 the annual spare time became implicitly the main driver of growth into affluence far beyond biologic needs. After 1980 writing and copying software for robot manufacturing became so easy and cheap that employment shifted to stand-by jobs known from supervising chemical production. The cost of hard labor in classical disciplines became the cost of time across disciplines. School and university teaching adapted too late, especially in Europe.

Due to the Great Depression in the USA and the destruction of Germany and Japan in World War II, the per capita destructible physical capital showed two constant time delays relative to the normalized GDPs. Before the transition in the 1980s, three observed delays allowed the first measurement of the physical lifetime (25 years) of physical capital against technical obsolescence. After the transition, the delay allowed measuring the superposition of the physical capital's lifetime and the human reaction time (62 years) to improving existential conditions.

The corresponding effect between the industrial evolution's existential conditions and the industrial increase of the mean unisex life expectancy at birth resulted in the latter's constant precedence (59 years). Human life integrates and averages linearly over the existential conditions from life to death. This leads to a life expectancy whose relation to the industrial evolution is an invariant of the macro-system named bio-economic relation. This precedence equals half the final average life expectancy of 118 years.

All three time constants are encoded with the heritable human maturation program. They fix and limit the dynamics of all variables so that all data are reproduced without any fitting parameter. The implicit assumption that the industrial society's evolution can be optimized by any subsystem's independent reasoning or paradigm is refuted against any defense by the genetic power of human nature. The saving constant for physical capital is the dominant national parameter; it fixes the speed of recovery and the G7 level lifestyle. The national effort for education must just be large enough for challenging human adaptability to affluence to its inherited limit. These conditions provide forecasting power.

As overall result, the industrial evolution survived all unnatural policies nearly without a trace and became implicitly an extended projection of the individual maturation program. This formed the largest possible and sufficiently diversified macro-system. Longevity is the industrial society's uniting natural goal; Adam Smith's accumulation of wealth was a dividing spin-off. Reaching the genetic limits takes half a millennium instead of the maximum unisex life expectancy because only the part adapted to within the generation gap can be heritable. Without this projection and the partial heritability of longevity, the majority cannot reach the genetic limits of the human species.

Theoretically this natural goal is embodied in the unique structure of the analytic solutions. It allows the technical and human infrastructures to contribute independently to longevity by competing with different time constants in the denominator. Physically, economic growth is achieved by removal of technical and human obstacles as they appear during the industrial evolution.

When two competing exponential terms compete in the nominator, the faster will win, and human maturation is missed. Money can be exponentially printed in the nominator; it is not subject to and, therefore, not controlled by the laws of nature. Optimizing the financial subsystem without knowing its structural incompatibility with the natural subsystems caused the new financial and political problems of the G7 level nations listed in the introduction and explained in the section on finance. Realizing and respecting this difference is the key to surviving this century's saturation of G7 level economic growth.

The top demand's data come with the life expectancy free house. Everyone's learned capacity is individually entangled with human nature's priceless inherited capacity. The latter comes also free house. Together they allow discriminating positive, neutral, and negative contributions to longevity. Hereby billions of daily decisions achieve long-term equilibrium between demand and supply. No human institution has the power and diligence to mastermind the industrial evolution above all disasters in three continents with different cultures for half a millennium. Society's master plan is the human maturation program, and this is installed in every individual.

The seamless agreement without fitting parameter between data and theory in Figs. 1, 2, 3, 4, and 5 suggests that forcing different master plans onto society will fail like communism. Subsidizing the financial utopia of exponential growth per capita at G7 level must stop immediately because fighting the laws of nature is futile even for mankind's most powerful institutions. The currently available money should be saved from inflation by century projects that stabilize Europe and its relation with Africa. The same applies to North and South America. China agreed recently to its change from exponential to linear growth, but it must also agree to contain its convergence crisis immediately by reducing its growth rate even faster than predicted by the natural theory.

The natural theory's forecasting power reduces the macro-system's apparent complexity and the risk of long-term social planning decisively. The divergence of the distributions of wealth and income can and must be reversed. The national pension systems can and must be stabilized not for the next election but for the life insurer's predicted life expectancy. The section on finance showed against any defense that returning to tax-based pension systems is inevitable.

Jobs must be created for the young and for the lusty seniors because both groups are powerful voters. Reproducing couples need stable jobs. The G7 level employment challenge requires a level of social innovation that is only comparable

to the level of technical innovation. There can be no political stability without success on the job front with fair pay.

All nations have nearly the same final problems because (with the XY-difference) they are subject to the same maturation program. Beyond that, the new possibility of long-term planning raises the question what governments and their national and international institutions can actually contribute to the industrial society's long-term success. Most of their creative time was probably spent with preventing national and international disasters and repairing the damages when that failed. Finding socially uniting goals before mankind's biologic limits are practically reached is this century's top challenge.

Acknowledgment We thank Ron Kay (IBM San Jose/ICSI Berkeley) for 20 years of continuous encouragement through all parts of this work; our medical colleagues in Lübeck for lunchtime discussions on genetics and life expectancy; Hermann Haken, the Ph.D. thesis advisor of one of us in Stuttgart, for reviving discussions on synergetics after half a century; and Axel Hutt, the editor of this chapter, for suggesting ways how to close many gaps between theory and text. The Japanese-German Center Berlin helped understanding Monbusho's educational reports. Yasutsugu Takeda of Hitachi and George Metakides of the European Commission's Esprit Program supported this work with the only project that was to our knowledge jointly financed by Japan's former Ministry of International Trade and Industry and the European Commission (Danielmeyer and Airaghi 1999). Original 20 years at AT&T Bell Labs and Siemens AG allowed deep insights into innovation, systems engineering, and business administration.

Appendix

Natural Constants of the Human Species

$\epsilon = 1$ p.a, the calendar year's unit for measuring the annual flow of working and spare time

$E = 62$ years, evolution constant, effective reaction time of L(t), a(t), and $h(t)$

$G = 25$ years, generation constant, effective physical lifetime of $k(t)$

$L_o = 30$ years, mean minimum life expectancy for maintaining the medieval population

$\overline{L} = 118$ years, mean maximum life expectancy at time of birth for the G7 level life style

Main Variables of the Industrial Society

$y(t)$, gross domestic product (GDP) per capita, after recovery $\rightarrow a(t)$, industrial evolution

$k_w(t)$, national physical capital per capita in production; $k(t)$ includes the housing part

$h_e(t)$, educated part of human capacity h(t) per capita; $h_s(t)$ includes the inherited part

$L(t)$, mean G7 level life expectancy

$s(t)$, annual spare time

$w(t)$, annual working time

Evaluating National Policy

The fastest way is inserting the recent data of the nation to be tested into Figs. 1, 2, 3, 4, 5, and 6. This should yield the halftime τ and the initial growth rate β of the last recovery. National statistics show the total annual support $\dot{k} + k/G$ of Eq. 6 for physical capital as gross fixed capital formation ($GFCF$). Then the saving constant is given by $\overline{\mu} = GFCF(t)/y(t)$. When this ratio is not fairly constant, the economy is centrally planned (like China's). Starting central planning means endless central planning or a veritable revolution for a free (nearly self-ordering) society.

Bibliography

Ansorge R (2010) Stability concerning the time-dependence of the mean life expectancy with respect to relevant parameters. Hamburger Beiträge zur Angewandten Mathematik 10:1–8

Becker GS (1964) Human capital: a theoretical and empirical analysis with special reference to education, University of Chicago Press, 1993, Chicago

Danielmeyer HG, Airaghi A (1999) Chapter 1. In: Danielmeyer, Takeda Y (eds) The company of the future. Springer. ISBN 3-540-65861-0 Berlin, Heidelberg, New York (published also in Chinese)

Danielmeyer HG (2009) How will our grandchildren probably live? (in German). Focus (J Univ Luebeck) 26(2):22–27

Danielmeyer HG, Martinetz T (2009) An exact theory of the industrial evolution and national recovery, Technical Report SIIM-TR-A-09-05, pdf http://www.inb.uni-luebeck.de

Danielmeyer HG, Martinetz T (2010) The biologic stability of the industrial evolution. Eur Rev 18(2):263–268, pdf http://www.inb.uni-luebeck.de

Haken H (1983) Advanced synergetics: instability hierarchies of self-organizing systems and devices. Springer, Berlin, Heidelberg

Herskind AM, McGue M, Holm NV, Sørensen TI, Harvald AB, Vaupel JW (1996) The hereditability of human longevity: a population based study of 2872 Danish twin pairs born 1879–1900. Hum Genet 97:319–323

Hubermann MM, Minns C (2007) The times they are not changin': days and hours of work in old and new worlds 1870–2000. Explor Econ Hist 444:538–567

Kümmel R et al (2000) Economic growth – driving forces and constraints in the perspective of economics and the sciences, WE-Heraeus-Seminar No. 243, Physikzentrum Bad-Honnef (Germany)

Mitchell BR (1988) British historical statistics. Cambridge University Press, Cambridge (UK)

Piketty T (2014) Capital in the 21st century. The Belknap Press of Harvard University Press, Cambridge MA (USA), London

Saez E (2014) Income and wealth inequality: evidence and policy implications. https://eml.berkeley.edu/~saez/lecture_saez_chicago14.pdf

Say J-B (1803) Traité d'économie politique ou Simple Exposé de la manière dont se forment, se distribuent et se consomment les richesses. http://www.daupine.fr/CRJBS/traité.pdf

Smith A (1776) An inquiry into the nature and causes of the wealth of nations. Oxford University Press 1993, Oxford, New York

Strawe C (1994) Arbeitszeit, Sozialzeit, Freizeit. http://www.dreigliederung.de/essays/1994-12-001.htm

Index

A
Aboutness, intentionality, 344, 350
Action chains and child play, 330–334
Additive noise, 183
  delayed systems, 186
  neural mass network, 186
  non-delayed systems, 185
  synchronisation in spiking neural network, 192
Agent base (AB) city models, 373–374
Amplitude equations of BAB patterns, 309, 314–317
Analytical theories of turbulence, 108
Annual working time, 422, 425, 435
Arnold tongues, 57
Attractor, 5, 197, 199, 201, 211, 224, 227
Axisymmetric vortices, Lamb-Oseen vortex, 111

B
Behavior and synergetics, 309–339
Belousov-Zhabotinky reaction, 198
Berry-Robnik-Brody distribution, 143
Beta-range oscillatory activity, 223
Bifurcation theory, 2
Billiard systems, 143–145
Binding problem, 222
Black-Scholes model, 411
Brain activity and body (BAB) patterns, 309
Brain pacemaker, 2
  closed-loop DBS, 256
  coordinated reset stimulation, 240–246
  definition, 236
  mixed nonlinear delayed feedback, 251
  model-based development, 238
  multisite linear delayed feedback, 246–248
  nonlinear delayed feedback, 248–251
  plasticity, 253–256
  proportional–integro–differential feedback, 251–253
  self-organization processes, 236
  standard high-frequency stimulation, 238–240
Brody distribution, 143
Brownian equation of motion, 411
Buoyancy, 59–60
Bursting classifications, 201

C
Cahn-Hilliard equation, 78, 80
Cellular automata, 372–373
Center manifold theorem, 184
Chaotic dynamics in neural system, 2, 197, 211
Chaotic systems, 136, 146
Chapman-Kolmogorov equation, 125, 164–165
Chay model, 202, 206
China's convergence crisis, 437
City, 357
  adaptation, 388
  agent base (AB) models, 373–374
  cellular automata, 372–373
  as central place, 360
  chaotic, 369–371
  CogCity, 388–389
  cognition and, 383–388
  definition, 358–359
  design, 393–396
  dissipative, 367
  ecological city, 360–361
  fractal, 371–372
  free agents on a cellular space (FACS) models, 374–375
  images of, 359–360
  inflation, 388
  information compression, 388
  as node in system of cities, 360
  pattern formation and pattern recognition in, 369
  planning, 391–393
  postmodern, 364–365
  rank-size distribution of, 363
  as representation of society, 362–363
  sandpile, 375
  self-organization and, 361, 365–366
  self-planned/self-designed, 396–398
  slow, 368
  small world, 375–378
  as sociocultural force, 363–364
  synergetic, 367–368
  synergetic inter-representation networks (SIRN), 378–383
  urbanism, 398–399

A. Hutt, H. Haken (eds.), *Synergetics*,
https://doi.org/10.1007/978-1-0716-0421-2

Class-B lasers, 40
Class-C lasers, 40
Clinical psychology, 2, 263
Coarsening, 49, 62
CogCity, 388–389
Cognition, 343
Cognitive science, intentionality, 345
Cold War's peace, 438
Conditional probability distribution, 125
Conductance-based Plant model, 203
Continuity equation, 52–53
Control parameter, 5, 49
  movement coordination, 287
Coordinated reset (CR) stimulation, 235, 237, 238, 240–246
Correlation localization measure, 145
Critical point, threshold, onset, 49
Cross-sectional dynamics, 412, 413

D
Deep brain stimulation (DBS), 235
  closed-loop, 256
  high-frequency (HF), 236, 238
  novel stimulation techniques, 237
  permanent, 236
  setup, 237
Delayed feedback, 1, 235
Delayed systems, 186
Depreciation, 425
Desai-Zwanzig model, 152
Determinism, 309
Disjoining pressure, 60
  ultra-thin films gravitation, 74–75
Dissipative dynamics, patterns and interfaces
  definition, 85
  dynamics of defects, 90
  front interactions and coarsening, 94
  interface, 85
  interfaces of patterns, 96–97
  interfacial instabilities, 93–94
  modulated and distorted patterns, 88–89
  moving interfaces, 91–93
  nonlinear Schrödinger equation (NLS), 87
  open system isotropic, two dimensions, 86
  phase dynamics, 89–90
  stationary and propagating fronts, 91–93
  stationary pattern, 85–91
  structures built up of fronts, 94–96
  symmetry-breaking bifurcation, 86–87
  wave pattern, 85, 97–103
Drift-diffusion estimates, 166–167
Dynamical localization, 138
Dynamical system, 5
Dynamical systems based modeling (DSBM)
  benefits, 216
  description, 213
Dynamical systems theory, 343
Dynamic diseases, self-organization in clinical psychology, 264–265
Dynamic Takatsuji model, 171

E
Econophysics, 405
Electroencephalography (EEG), 2
Entropy localization measure, 145
Entropy principle, 17–18
Euler equations, 53, 109
European Union, 438
Evolution equations, 5

F
Faraday patterns, 57
Feedback systems, delayed, 32
Financial data, 407
Financial market, 3
Financial market modeling, 408
Fixed point, stable, 5
Fluctuating forces, 5
Fluid dynamics
  basic equation, 107
  pattern formation, 1
    Arnold tongues, 57
    basic equations of, 52–54
    Bénard, Henri, 50, 60
    buoyancy, 59–60
    Cahn-Hilliard equation, 78, 80
    coarsening, 62
    conserved order parameter fields, 73–80
    continuity equation, 52–53
    definition, 49–50
    disjoining pressure, 60
    disjoining pressure, ultra-thin films gravitation, 74–75
    eigenvalue problem, 64, 67
    Euler equations, 53
    Faraday, Michael, 50
    Faraday patterns, 57
    flat unstable liquid layer, 81
    Ginzbur–Landau equation, 64, 66
    gradient expansion, 69, 70
    gravity waves, 54–55
    hexagonal motion of fluid, 61
    incompressible fluids, 53
    incompressible irrotational fluids, 53
    instabilities, 56–57
    Korteweg stress, 79
    Landau coefficient, 68
    Laplace pressure and disjoining pressure, 56–57
    large-scale instability, 60
    linear stability analysis of flat surface, 56–57
    Lorenz, Edward, 51
    lubrication approximation, 74
    Marangoni effect, 60
    mechanisms of instability in fluids, 57–60

Navier–Stokes equations, 51, 53–54, 79
non-local order parameter equations, 69
nucleation, 76
numerical solutions, 55
order parameter equation, 52, 66–73
parametric excitation, 57
pattern formation, 60–63
phase field, 79
phase field models, 76–77
plane waves, 51
Prandtl number, 66
precursor film, 75
random dot initial condition, 72
Rayleigh number, 67
regular squares, 62
rolls, high Prandtl number, 62
self-organized fluid patterns, 81
shallow water equations, 55
small Reynolds number, 54
small scale instabilities, 60
spinodal dewetting, 75–76
surface deformation, 60
surface tension, 60
surface waves, 54–56
Swift-Hohenberg equation, 69
Swift-Hohenberg-Haken equation, 70, 71
"thick films" *vs.* "thin films," 61
thin film equation, 63
thin films, 74
time series, numerical integration, 77
transport equations, 54
Turing, Alan, 50
turing structures/turing instabilities, 65
types of instabilities, 63
wave instabilities, 65
turbulence, 1
axisymmetric vortices, Lamb-Oseen vortex, 111
basic hydrodynamic equations, 109
Chapman-Kolmogorov equation, 125
conditional probability distribution, 125
definition, 108
determinism and stochasticity, 115–117
development, 108
Euler's equation, 109
evolution equations, probability distributions, 116
existence and smoothness results, 111
fine structure of turbulence, 118
Fokker-Planck equation, 126, 127
functional equations, 116–117
hierarchy of moment equations, 116
increments, 118
integral scales, 118
Kolmogorov scales, 119
Kolmogorov's 4/5 law, 120–121
Lagrangian fluid dynamics, 128
Lagrangian formulation, incompressible fluid dynamics, 110
Lagrangian map, 113
Lamb-Oseen vortex equation, 112
length and time scales in turbulent flows, 118
longitudinal and transversal components, statistics of, 125–126
Lundgren spiral, 112
Markovian properties, 124–125
multiscale analysis, turbulent fields, 124–128
Navier-Stokes equation, 109
Newtonian fluids, 109
N-scale probability distribution, 125
Onsager's statistical theory, 114–115
path integral formulation, 117
pattern formation and routes to chaos, 113
phenomenological theories of turbulence, 121–124
point vortex motion, 113
random vortex distributions, 112–113
Reynolds equation and turbulence modeling, 117–118
sinews of turbulence, 112
statistical averages, 115–117
statistics of increments, 119–120
stretched vortices, 112
Taylor length and Taylor-based Reynolds number, 119–120
vortex solutions, Navier-Stokes equation, 111
vortex stretching term, 110
vorticity alignment, 112
vorticity formulation, incompressible fluid dynamics, 110
Fokker-Planck equation, 5, 126, 127
Free agents on a cellular space (FACS) models, 374–375
Free will, 309
Functionality, intentionality, 344, 350–351
Fundamentalists base, 410

G
GARCH model, 411
Generalized Langevin equation, 5
Generalized spike-wave patterns, 213
Gestalt theory, 2
Ginzbur–Landau equation, 64
G7 level growth, 422
Grasping of objects, with different sizes, 317–326
Gravity waves, 54–55
Great Depression, 424, 438
Gross domestic products (GDPs), 422
Group, 5
Growth per capita, 422

H
Haken-Kelso-Bunz (HKB) model, 287
Hamiltonian system, 134, 135
Hamilton operator, 5
Hartman-Grobman theorem, 214
Heisenberg picture in quantum mechanics, 5
Hodgkin-Huxley model, 199
Hopf bifurcation point, 228

I
Independent component analysis, 216
Industrial evolution, 422, 423, 425, 427, 429
Infinite boundaries, 14–15
Information deflation, inflation and adaptation, 357
Instability, 5
  fixed point, 9–12
  limit cycle, 12
  Tori, 12
Intentionality, 3, 343
  aboutness, 344, 350
  cognitive science, 345
  definition, 343–344
  functionality, 344, 350–351
  mental-likeness, 344, 351–352
  and representation, 346–347
  synergetics, 347–349
Interfaces, dissipative dynamics, 85
  definition, 85
  dynamics of defects, 90
  front interactions and coarsening, 94
  interfacial instabilities, 93–94
  modulated and distorted patterns, 88–89
  moving interfaces, 91–93
  nonlinear Schrödinger equation (NLS), 87
  open system isotropic, two dimensions, 86
  of patterns, 96–97
  phase dynamics, 89–90
  stationary and propagating fronts, 91–93
  stationary pattern, 85–91
  structures built up of fronts, 94–96
  symmetry-breaking bifurcation, 86–87
  wave pattern, 85, 97–103
Interfacial instabilities, dissipative dynamics, 93–94
Ito-Langevin equation, 159

K
Korteweg stress, 79
Kramers-Moyal expansion, 165–166
Kuramoto-Sakaguchi model, 229

L
Lamb-Oseen vortex, 111
Landau coefficient, 68
Langevin equation, 5
  linear Fokker-Planck equations, 159
Laser dynamics
  application of, 43
  definition, 31
Laser paradigm, 7
Leech heart interneuron model, 202, 205
Life expectancy, 430
Limit-cycle
  oscillations, 228
  stable, 5
Linear and nonlinear Fokker-Planck equations, 149
  Chapman-Kolmogorov equation, 164–165
  Desai-Zwanzig model, 152
  drift-diffusion estimates, 166–167
  dynamic Takatsuji model, 171
  Ito-Langevin equation, 159
  Kramers-Moyal expansion, 165–166
  Langevin equations, linear Fokker-Planck equations, 159
  linear nonequilibrium thermodynamics, 176–178
  liquid crystal model, 152–153, 172–174
  Markov property, 157
  martingales, 167–168
  nonextensive systems, 175–176
  nonextensive thermostatistics, 154–156
  second-order and higher-order statistics, 157–159
  semiclassical description of quantum systems, 174–175
  Shimizu-Yamada model, 170
  short-time propagator, 163–164
  strongly nonlinear, 159
  time-dependent solutions and first-order statistics, 156
  Vlasov-Fokker-Planck models, 153–154
  Winfree and Kuramoto model, 153
Linear Fokker-Planck equation, 2
Linear nonequilibrium thermodynamics, 176–178
Liquid crystal model, 152–153, 172–174
Logistic function, 427
Lotka Volterra equation, 409, 410

M
Magneto-and electroencephalography (M/EEG), 222
Marangoni effect, 60
Markovian properties, 124–125
Markov process, 149
Markov property, 157
Martingale process, 149
Mental-likeness, intentionality, 344, 351–352
Method of solution, synergetics, 9
Microscopic theory, 8
Mind-body problem, 343
Mixed-mode oscillations (MMOs), 198, 203
Mixed nonlinear delayed feedback, 251
Modeling framework, 334–338
Modulated and distorted patterns, 88–89
Movement coordination, 2
  asymmetry in mode of coordination, 300–301
  breaking and restoring symmetries, 297–300
  control parameter, 287
  coupling, 296–297
  definition, 287–288
  Haken-Kelso-Bunz (HKB) model, 287
  motor programs, 288
  order parameter, 287
  oscillator level, 293–296
  perturbations and fluctuations, 291–293
  phase transition, 287

relative phase, 289–291
stability, 291–293
transitions to anti-phase, 301–304
Moving interfaces, dissipative dynamics, 91–93
Multiplicative noise, 183
Multisite linear delayed feedback (MLDF), 246–248
Multi-timescale models, 412

N
Naturalization, 343
Natural patterns, 49
Navier-Stokes equation
compressible fluids, 53
fluid dynamics, pattern formation, 51, 53–54, 79
fluid dynamics, turbulence, 109
incompressible fluids, 54
Neural mass model, 224, 226, 232
Neural mass network, 186–194
Neuron models, chaos in, 201–206
Non-delayed systems, 185–187
Nonextensive systems, 175–176
Nonextensive thermostatistics, 154–156
Non-Gaussian statistical feedback model, 412
Nonlinear, 149
Nonlinear delayed feedback (NDF), 248–251
mixed, 251
Nonlinear dynamics, communication of patient and therapist, 267–271
Nonlinear Fokker-Planck equation, 2
Nonlinear Schrödinger equation (NLS), 87
Normal form, 5

O
Onsager's statistical theory, 114–115
extension to three dimensions, 115
two-dimensional turbulence, 114–115
Open system isotropic, two dimensions
dissipative dynamics, patterns and interfaces, 86
Order parameter, 5, 49, 235
movement coordination, 287
Order parameter equation
fluid dynamics, pattern formation, 52, 66–73
non-local, 69
Order parameter fields, conserved, 73–80
Oscillatory neural activity, 221

P
Pareto power-law distribution, 410
Pattern, 5
dissipative dynamics
definition, 85
dynamics of defects, 90
front interactions and coarsening, 94
interface, 85
interfaces of patterns, 96–97
interfacial instabilities, 93–94
modulated and distorted patterns, 88–89
moving interfaces, 91–93
nonlinear Schrödinger equation (NLS), 87
open system isotropic, two dimensions, 86
phase dynamics, 89–90
stationary and propagating fronts, 91–93
stationary pattern, 85–91
structures built up of fronts, 94–96
symmetry-breaking bifurcation, 86–87
wave pattern, 85, 97–103
Period-doubling, Chay model, 202
Peripheral physiological systems, synchronization patterns, 265–267
Phase dynamics, dissipative dynamics, 89–90
Phase oscillators, 229
Phase synchronisation, 2
neural systems
correlated behaviour and phase synchronisation, 224
effects of, 230–231
micro-and macroscopic views, 222–224
and oscillators, 229
from single cell dynamics to neural masses, 224–227
Phase transition, 287
Phenomenological synergetics, 8, 18–21
Phenomenological theories of fine structure, turbulence, 107
PICMET community, 422
Planning, 357
Plasticity, 253–256
Poincaré-Husimi function, 144
Poincaré mappings, 199–201
Principal component analysis, 216
Principle of uniform semiclassical condensation (PUSC), 141–142
Probability distribution function, 5
Proportional-integro-differential feedback (PIDF) stimulation, 237, 251–253

Q
Quadratic integrate-and-fire (QIF) neurons, 224
Quantum chaos, 1, 133
classically fully chaotic (ergodic) systems, 138–140
dynamical localization, 142–143
generic system, 140–143
PUSC, 141–142
quantum phase space, 141
spectral statistics, 142
Quantum-classical correspondence, 5, 13
Quantum dot (QD), 31
Quantum-dot lasers, 33
Quantum localization, 138
Quantum theoretical formulation, 13
Quantum-well (QW) lasers, 32, 35

R
Regular spatial and spatio-temporal patterns, 14
Relaxation oscillations (ROs), 33

S
Saddle-node (SN) bifurcation, 38
Schrödinger picture, quantum mechanics, 6
Second-order and higher-order statistics, 157–159
Self-organization, 1, 3, 6, 357
  clinical psychology
    dynamic diseases, 264–265
    in human change processes, 271–275
    nonlinear dynamics, communication of patient and therapist, 267–271
    self-organizing brain, 276–281
    synchronization patterns, peripheral physiological systems, 265–267
    synergetic navigation system, 275–276
  definition, 357–358
  and planning, 366–367
  processes, 236
Semantic synergetics, 8, 21–22
Semiclassical description of quantum systems, 174–175
Shilnikov chaos
  description, 214–215
  in epileptic seizures, 215–217
Shimizu-Yamada model, 170
SIRN (synergetic inter-representation network), 357
Skinner and determinism, 310–314
Slaving principle, 6, 49, 184, 212
Slow-fast decomposition, 199
Spatial coordinate (vector x), 6
Spectrum, 6
Sputnik Shock, 433
Stability of system, 6
Stable limit cycle, 227, 228
Standard high-frequency stimulation, 238–240
State vector, 6
Stationary and propagating fronts, 91–93
Stationary pattern, dissipative dynamics, 85–91
Structural science, 343
Structures built up of fronts, 94–96
Swift-Hohenberg equation, 49, 69
Swift-Hohenberg-Haken equation, 70, 71
Symmetry, 6
Symmetry-breaking bifurcation, 86–87
Synchronization, 235
  patterns, peripheral physiological systems, 265–267
Synergetic inter-representation network (SIRN), 357, 378–383
Synergetic navigation system, 275–276
Synergetics, 1, 3, 309, 421
  basic equations, 8–9
  definition, 6
  hierarchical structure, 8
  role in science, 6

T
TAQ (Trade and Quote) database, 407
Taylor length and Taylor-based Reynolds number, 119–120
Thomas-Fermi rule, 136, 138
Time-delayed feedback, 36
Time-dependent solutions and first-order statistics, 156
Tonic-spiking and bursting, 200
Torus bifurcation (TB), 203
Trajectory, 6
Transition routes, 201
Turbulence modeling and large eddy simulations, 107
Turbulent cascades, 107
Turing patterns, 49

U
Urbanism, 357, 398–399
  complexity and, 399–400

V
Vertical-cavity surface emitting lasers (VCSELs), 43
VIX volatility index, 416
Vlasov-Fokker-Planck models, 153–154
Volatility, 408
Vortex motions, 107
Vorticity formulation, incompressible fluid dynamics, 110

W
Walk-run transitions, 326–330
Wave chaos, 135, 147
  See also Quantum chaos
Wave pattern
  forced systems, 102–103
  plane waves, 97–98
  spiral and scroll waves, 98–100
  spiral patterns and turbulence, 100–102
Wilson-Cowan model, 227, 228
Winfree and Kuramoto model, 153
World War II, 422